

# THE JOURNAL OF PHYSICAL CHEMISTRY

Registered in U. S. Patent Office © Copyright, 1968, by the American Chemical Society

VOLUME 72, NUMBER 13 DECEMBER 16, 1968

## Temperature Dependence of Nuclear Magnetic Resonance Coupling Constants and Chemical Shifts of the Vinyl Halides and Some Vinyl Ethers

by Wallace S. Brey, Jr., Katherine Nasfay Scott,

Department of Chemistry, University of Florida, Gainesville, Florida 32601

and Donald R. Whitman

Case Western Reserve University, Cleveland, Ohio 44106 (Received July 17, 1968)

The temperature dependence of the nmr parameters of the vinyl halides and three vinyl ethers has been investigated. All spectra of the vinyl halides have been carefully analyzed by several computer programs, and consideration of line intensities as well as frequencies has been found necessary to resolve ambiguities in line assignments for vinyl chloride. Solvent studies suggest intramolecular effects to be more important than intermolecular effects in causing the temperature dependence. Proton-proton coupling constants have been found to be independent of the temperature, although proton-fluorine coupling constants decrease with increasing temperature. The temperature variations of the proton chemical shifts, which for vinyl halides parallel that of ethylene, have been interpreted in terms of the excitation of molecular vibrations. The temperature dependence of the chemical shifts of vinyl ethers is modified by the existence of rotational isomers about the oxygen-phenyl bond.

### I. Introduction

The nmr parameters of vinyl compounds give considerable information about the effects of both the substituent and the medium. Banwell and Sheppard<sup>1</sup> have found that, while the coupling constants in a vinylic system are dependent on the electron distribution within the  $\sigma$ -bond framework, the chemical shifts are largely dependent on the electron distribution in the  $\pi$ -electron system. Brügel, *et al.*,<sup>2</sup> have stated that the nmr spectra of vinyl compounds provide to date the best experimental method for checking the effects predicted by mesomeric and inductive theories. The electronegativity of the substituent has been correlated with the proton coupling constants,<sup>1,3-7</sup> whereas the chemical shifts have been related to the group dipole moment of the substituent.<sup>8-11</sup>

No regular relation has been found between the proton chemical shifts and the <sup>13</sup>C chemical shifts in vinyl compounds.<sup>12</sup> The proton chemical shifts and the <sup>13</sup>C-H coupling constants, however, appear to be linearly related in both vinylic and nonvinylic compounds.<sup>11,13-16</sup>

Deviations from this relationship have been used to determine the anisotropy effect of a number of substituents.<sup>14,16</sup> The *gem*-coupling constants in five

- (1) C. N. Banwell and N. Sheppard, *Mol. Phys.*, **3**, 351 (1960).
- (2) W. Brügel, T. Ankel, and F. Krückeberg, *Z. Elektrochem.*, **64**, 1121 (1960).
- (3) G. S. Reddy and J. H. Goldstein, *J. Chem. Phys.*, **35**, 380 (1961).
- (4) J. S. Waugh and S. Castellano, *ibid.*, **35**, 1900 (1961).
- (5) T. Schaefer, *Can. J. Chem.*, **40**, 1 (1962).
- (6) J. Feeney, A. Ledwith, and L. H. Sutcliffe, *J. Chem. Soc.*, 2021 (1962).
- (7) F. Hruska, G. Kotowycz, and T. Schaefer, *Can. J. Chem.*, **43**, 2827 (1965).
- (8) E. B. Whipple, J. H. Goldstein, and L. Mandell, *J. Chem. Phys.*, **30**, 1109 (1959).
- (9) A. A. Bothner-By and C. Naar-Colin, *J. Amer. Chem. Soc.*, **83**, 231 (1961).
- (10) G. S. Reddy, C. E. Boozer, and J. H. Goldstein, *J. Chem. Phys.*, **34**, 700 (1961).
- (11) R. E. Mayo and J. H. Goldstein, *J. Mol. Spectrosc.*, **14**, 173 (1964).
- (12) G. E. Maciel, *J. Phys. Chem.*, **69**, 1947 (1965).
- (13) E. B. Whipple, *et al.*, *J. Chem. Phys.*, **34**, 2136 (1961).

vinyl compounds have been found to vary with the dielectric constant of the solvent.<sup>17</sup>

Although a considerable amount of work has thus far been done to correlate the nmr parameters of vinyl compounds with the effects of the substituent and of the medium, the effect of temperature on these parameters has not been investigated. The present paper reports a study of the effect of temperature on these parameters in the vinyl halides and in a number of vinyl ethers. Some solvent and dilution studies were also made in order to discover if the temperature dependences were due to inter- or intramolecular effects. Carbon disulfide and trichlorofluoromethane were selected as solvents because of their large temperature range and chemical inertness.

The temperature dependence of the nmr spectra of vinyl ethers is of particular interest, because the infrared spectrum of vinyl 2-ethylhexyl ether indicates that there exist two rotational isomers due to restricted rotation about the O-C(vinyl) bond resulting from conjugation of the unshared electrons of the oxygen with the  $\pi$  electrons of the vinyl group.<sup>18</sup> In the nmr spectrum of this compound, no individual rotational isomers could be detected even at low temperatures, either because of too rapid interconversion rate or because of similar shielding in the two forms.<sup>6</sup> It was found in the present investigation that the temperature-dependent variation of the nmr parameters of the vinyl ethers could be interpreted in terms of changes in the relative populations of the rotational isomers and of changes in bonding.

In addition to vinyl 2-ethylhexyl ether, the temperature dependence of the spectra of phenyl vinyl ether and phenyl 2-vinoxyethyl ether,  $C_6H_5OCH_2CH_2OCH=CH_2$ , has also been investigated. In phenyl vinyl ether the shielding of the vinyl group in the two rotational isomers is expected to be rather different owing to the proximity of the anisotropic phenyl group.

## II. Experimental Section

The spectra of the carbon disulfide solutions of vinyl fluoride and of vinyl iodide were obtained on a Varian Model A-60A spectrometer at 60 MHz operating frequency. All the other spectra were obtained on a Varian Model DP-60 spectrometer at 56.4 or 60 MHz operating frequency.

The temperature of the sample could be varied using the Varian variable-temperature accessory. The sample was allowed to reach the desired temperature and then to equilibrate for at least 15 min before the recording of the spectrum was begun. The temperature during a given run was held constant to  $\pm 1^\circ$ . The sample temperature was monitored with a copper-constantan thermocouple. The thermocouple and probe had previously been calibrated using the known temperature dependence of the chemical shifts of methanol

and of ethylene glycol. The indicated temperatures are believed to be accurate to  $\pm 2^\circ$ .

The sample of vinyl iodide was synthesized by Dr. J. P. Tandon, formerly of this department. The other vinyl halides were commercially available compressed gases obtained from the Matheson Co. and from Peninsular ChemResearch. The 2-ethylhexyl vinyl ether was a commercial product from Carbide and Carbon Chemicals Corp. The other vinyl ethers were synthesized by Dr. R. E. Thompson, formerly of this department. All the samples were used as received. No impurity peaks were observed in the spectra.

Compounds were run both as neat liquids and as solutions. The latter were made up approximately by volume in a vacuum line. Each sample was then sealed in an nmr tube under vacuum. A tetramethylsilane (TMS) internal reference has been used in all the samples except neat vinyl iodide, the sample of which was not referenced.

The spectra were calibrated using audiofrequency modulation or the known chemical shift difference of the peaks in a TMS- $CDCl_3$  solution. All the values reported for the chemical shifts, coupling constants, and line positions represent the average of five to ten independent determinations. The indicated scatter in these values is the average deviation from the mean of these determinations. The intensities of the peaks were measured with a planimeter on spectra obtained at slow sweep rates.

## III. Results and Calculations

The nmr spectra of all the compounds investigated showed changes with temperature. The most prominent change is that of the combination lines in the vinyl chloride and vinyl iodide spectra. The spectra at 37 and  $-103^\circ$  of a 1:1 v/v solution of vinyl chloride in  $CS_2$  are reproduced in Figure 1. The lines in the spectrum have been numbered according to the ABC scheme of ref 2, which is equivalent to the ABX scheme of ref 19. As the temperature of vinyl chloride is decreased, the combination lines, lines 14 and 15, approach one another and decrease in intensity. Such changes in the combination lines, which have also been observed previously by Schaefer and Schneider<sup>20</sup> when the concentration of vinyl bromide was varied in

(14) J. H. Goldstein and G. S. Reddy, *J. Chem. Phys.*, **36**, 2644 (1962).

(15) G. S. Reddy and J. H. Goldstein, *J. Mol. Spectrosc.*, **8**, 475 (1962).

(16) G. S. Reddy and J. H. Goldstein, *J. Chem. Phys.*, **38**, 2736 (1963).

(17) V. S. Watts and J. H. Goldstein, *ibid.*, **42**, 228 (1965).

(18) M. L. Brey and P. Tarrant, *J. Amer. Chem. Soc.*, **79**, 6533 (1957).

(19) J. A. Pople, W. G. Schneider, and H. J. Bernstein, "High-Resolution Nuclear Magnetic Resonance," McGraw-Hill Book Co., Inc., New York, N. Y., 1959, pp 132-134.

(20) T. Schaefer and W. G. Schneider, *Can. J. Chem.*, **38**, 2066 (1960).

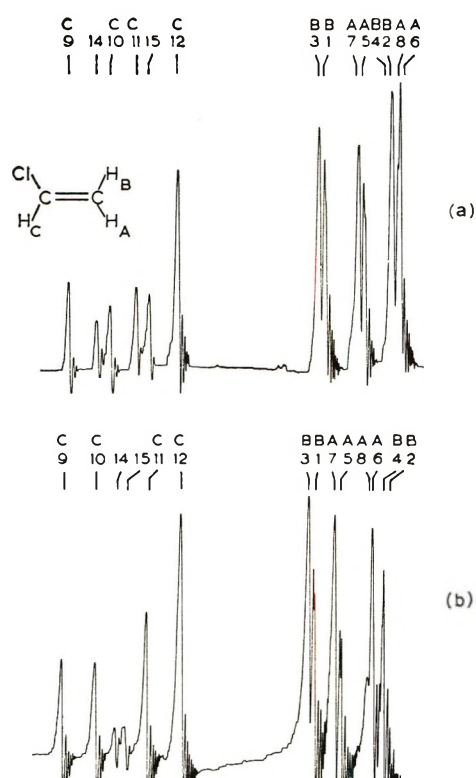


Figure 1. Spectrum of vinyl chloride at 56.4 MHz (1 volume of sample:1 volume of  $\text{CS}_2$ ): a,  $37^\circ$ ; b,  $-103^\circ$ .

benzene solutions, are due to changes in the relative chemical shifts of the two methylene protons.

Similar changes in the combination lines, lines 13 and 14, are observed for vinyl iodide both as a neat liquid and in  $\text{CS}_2$  solution. The spectra of vinyl iodide at  $32^\circ$  neat and in  $\text{CS}_2$  solution, have been reproduced in Figure 2. The numbering of the transitions and the designation of the protons is the same as in Figure 1. For vinyl iodide  $\text{H}_B$  is the X nucleus in an AXC approximation, and the combination lines of observable intensity now show up in the  $\text{H}_B$  region of the spectrum. Line 15, which is the  $\beta\alpha\beta \rightarrow \alpha\beta\alpha$  transition, is of non-observable intensity. For vinyl chloride,  $\text{H}_C$  is the X nucleus in the ABX approximation and line 13, the  $\beta\beta\alpha \rightarrow \alpha\alpha\beta$  transition, is of nonobservable intensity. As the temperature of either the neat liquid sample or the  $\text{CS}_2$  solution of vinyl iodide is decreased, the combination lines approach one another and decrease in intensity. In the neat liquid sample, the combination lines cross below  $10^\circ$  and recede on subsequent cooling. The relative positions and intensities of the combination lines in vinyl iodide are a function of the relative chemical shifts of protons  $\text{H}_A$  and  $\text{H}_C$ .

Several methods have been employed to obtain the chemical shifts and the coupling constants from the spectra. For all the spectra, the midpoint between the outer lines of the pattern assigned to a given proton was taken as a first approximation to the chemical shift. Next, for each vinyl halide spectrum, the positions of

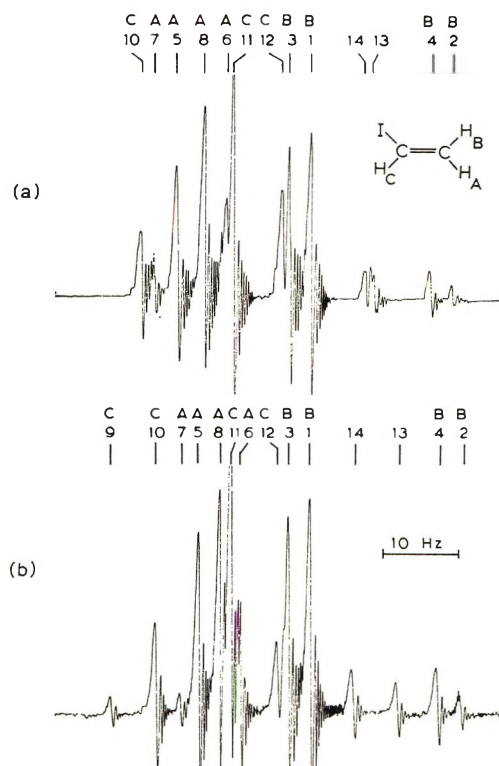


Figure 2. Spectrum of vinyl iodide at 60 MHz and  $32^\circ$ : a, neat; b, 1 volume of sample:2 volumes of  $\text{CS}_2$ .

the lines were measured relative to transition 12. These experimental line positions and the approximate spin parameters were then used by Whitman to calculate a set of coupling constants and chemical shifts for vinyl bromide and vinyl chloride at each temperature. The analysis consisted in using a computer program<sup>21</sup> to determine an assignment consistent with spacing and intensity sum rules, together with a least-squares procedure to obtain the set of spin energy levels most consistent with the observed transitions. Then the direct-analysis equations<sup>22</sup> were solved iteratively to find the spin parameters which reproduce these energy levels. An interesting consequence of this technique is the generation in some cases of more than a single set of spin parameters and line assignments, each of which reproduces the experimental line positions, but with very different intensities. As an illustration, the results of two different calculations, A and B, are reported in Tables I and II. Both calculations reproduce the least-squares line positions, but clearly only calculation A yields intensities in agreement with the experimental values. The computer line-assignment feature of the DRW program is advantageous for complex spectra. The generation of more than one set of spin parameters is a disadvantage of programs that fit only the line frequencies without at the same time fitting the line intensities.<sup>23</sup>

(21) D. R. Whitman, *J. Chem. Phys.*, **36**, 2085 (1962).

(22) D. R. Whitman, *J. Mol. Spectrosc.*, **10**, 250 (1963).

Table I: Example of Results of Calculations of Vinyl Chloride (One Volume of Sample to One Volume of CS<sub>2</sub> at -82° and 56.4 MHz)

Transition sequence	Relative line positions, Hz				Relative line intensities									
	Obsd	Least squares	Calculation A	Calculation B	Calculation C	Calculation D	Calculation E	Obsd	Calculation A	Calculation B	Calculation C	Calculation D	Calculation E	
I 9	-21.4 ± 0.5	-21.371	-21.372	-21.372	-21.47	-21.373	-21.373	0.4 ± 0.1	0.61	0.61	0.61	0.61	0.61	0.61
I 10	-15.3 ± 0.3	-15.219	-15.220	-15.220	-15.40	-15.221	-15.221	0.4 ± 0.1	0.57	0.14	0.58	0.57	0.14	0.14
I 14	-11.9 ± 0.4	-11.944	-11.945	-11.945	-11.88	-11.946	-11.946	0.2 ± 0.1	0.20	0.69	0.19	0.20	0.69	0.69
I 15	-9.4 ± 0.4	-9.420	-9.420	-9.421	-9.61	-9.421	-9.421	0.3 ± 0.1	0.21	0.78	0.20	0.21	0.78	0.78
I 15	-6.1 ± 0.2	-6.145	-6.146	-6.145	-6.09	-6.146	-6.146	0.9 ± 0.2	0.89	0.25	0.90	0.89	0.25	0.25
I 12	0.0	0.007	0.007	0.007	-0.02	0.007	0.007	1.6 ± 0.4	1.52	1.53	1.52	1.52	1.53	1.53
I 3	28.6 ± 0.6	28.557	28.557	28.556	28.50	28.557	28.557	1.6 ± 0.2	1.26	1.25	1.24	1.26	1.25	1.25
I 1	29.7 ± 0.7	29.681	29.681	29.681	29.74	29.682	29.682	1.4 ± 0.2	1.36	1.31	1.39	1.36	1.31	1.31
I 7	34.4 ± 0.8	34.356	34.356	34.355	34.29	34.357	34.357	1.4 ± 0.3	1.26	1.28	1.28	1.26	1.28	1.28
I 5	35.4 ± 0.8	35.480	35.481	35.480	35.53	35.483	35.482	0.9 ± 0.2	1.03	1.08	1.01	1.03	1.08	1.08
I 4	...	40.508	40.508	40.507	40.35	40.510	40.510	1.8 ± 0.3	0.21	0.09	0.23	0.21	0.09	0.09
I 2	41.7 ± 1.0	41.632	41.633	41.632	41.59	41.635	41.635	1.2 ± 0.1	1.49	1.46	1.47	1.49	1.46	1.46
I 8	43.7 ± 1.0	43.783	43.783	43.783	43.88	43.785	43.785	...	1.27	1.38	1.24	1.27	1.38	1.38
I 6	...	44.907	44.908	44.908	45.12	44.910	44.910	...	0.12	0.16	0.14	0.12	0.16	0.16

A set of spin parameters was obtained for each vinyl halide spectrum at each temperature by using the FREQUENT IV program of Bothner-By on the IBM 709. The input spin parameters were adjusted until all the calculated and observed line positions and intensities in a given spectrum agreed within experimental error. One result is given in calculation C, Tables I and II. For vinyl fluoride and vinyl iodide, up to three lines in some of the calculated spectra deviated from the observed line positions by 0.1-0.2 Hz beyond the experimental error. Undoubtedly, the agreement would be better if trial parameters to two decimal places were used; however, this did not appear to be justified by the accuracy of the data.

Finally, the LAOCN3 program, kindly supplied by Bothner-By and Castellano,<sup>24</sup> was used on the IBM 360 computer to calculate the spectra of vinyl chloride. Starting with a set of trial parameters, the LAOCN3 program iterates toward a set of adjusted parameters corresponding to the smallest least-squares deviation between observed and calculated line frequencies. The output of this program contains both the root-mean-square error after each cycle of adjustment and the probable error associated with the parameter sets. Depending on the choice of input parameters, and hence the line assignments, the LAOCN3 program may also yield more than one set of spin parameters which will fit the line frequencies but not necessarily the line intensities. This is illustrated by calculations D and E, Tables I and II. Using transition sequence II of Table I, the LAOCN3 program gives the results labeled calculation D, which are almost identical with the results of the DRW program, labeled A. Similarly, the two results using sequence I, labeled B and E, are almost identical with each other.

The final result of each of the three computer methods employed shows that the line assignment in vinyl chloride changes as the temperature is lowered. At 37°, the transition sequence is given by sequence I of Tables I and II. At lower temperatures, only by using sequence II of Table I can both line intensities and positions be reproduced. Such line-assignment changes are not obvious, since the observed line positions and line intensities do not change appreciably at the crossover point.

In addition, a very small change in parameters can give an alternate sequence. For example, using the relative chemical shifts and coupling constants  $\nu_A = 40.40$  Hz,  $\nu_B = 35.30$  Hz,  $\nu_C = -9.30$  Hz,  $J_{AB} = -1.50$  Hz,  $J_{AC} = 6.90$  Hz, and  $J_{BC} = 14.90$  Hz, one obtains transition sequence I. Changing  $\nu_A$  to 40.20 Hz but keeping all the other parameters the same will give sequence II. Examination of the energy-level diagrams

(23) S. Castellano and J. S. Waugh, *J. Chem. Phys.*, **34**, 295 (1961).

(24) A. A. Bothner-By and S. Castellano, LAOCN3, Mellon Institute, Pittsburgh, Pa.

**Table II:** Method of Calculation, Transition Sequence, and Nmr Parameters Used to Obtain the Results in Table I

Calculation	Method	Transition sequence	$\nu_A^a$ Hz	$\nu_B^a$ Hz	$\nu_C^a$ Hz	$J_{AB}^a$ Hz	$J_{AC}^a$ Hz	$J_{BC}^a$ Hz
A	DRW	II	38.055	35.241	-9.252	-1.383	6.989	14.648
B	DRW	I	38.853	34.557	-9.367	-1.404	8.868	12.790
C	FREQUINT IV	II	38.00	35.30	-9.30	-1.50	6.90	14.80
D	LAOCN3	II	38.057	35.242	-9.253	-1.383	6.990	14.649
E	LAOCN3	I	38.855	34.559	-9.368	-1.404	8.868	12.791

<sup>a</sup> Designation of the protons is the same as in Figures 1-7.

obtained for the two sets of parameters shows that the small change in the chemical shift of  $H_A$  has interchanged the  $\beta\alpha\alpha$  energy level with the  $\alpha\beta\alpha$  energy level, while changing the values of the other energy levels by only  $\pm 0.1$  Hz. This results in an interchange of the appropriate transition frequencies without an appreciable change of the line-frequency values and the line intensities. This particular example illustrates the point<sup>25</sup> that when the best solution is near the energy-level crossover point, the spectrum is hard to analyze unless the starting parameters are sufficiently close to the best solution.

From Tables I and II, it can be seen that the lines for which intensity changes on altering the transition sequence are significant are 10, 11, 14, and 15. At  $37^\circ$  and at  $-65^\circ$  and below, the relative intensities of these four lines are quite different, so it is not difficult to select the proper transition sequence. At temperatures below  $37^\circ$  but above  $-65^\circ$ , the intensities of the four lines are rather similar, and the choice of the correct transition sequence is not as clear-cut. Here the probable error of the parameter sets, from the LAOCN3 program, was most helpful. If it is possible to vary simultaneously several of the parameters in a particular way, such that a good fit with the observed spectrum is retained, then the probable error in that particular set of parameters will be quite large.<sup>24</sup> For vinyl chloride the *cis* and *trans* coupling constants, and to a lesser extent the *cis* and *trans* chemical shifts, have shown large probable errors in the temperature range in question. In this range, the set of adjusted parameters and line assignment has been selected as the best which gave good agreement with the line intensities and also the smallest probable error in the parameter sets, although this choice did not always yield the smallest root-mean-square error in line positions. On this basis, the correct line assignment below  $37^\circ$  is given by sequence II.

Both the approximate and the computer-obtained chemical shifts of the vinyl halides have been plotted against the sample temperature. The slopes of the approximate and computer-obtained plots are identical within experimental error, except for neat vinyl iodide below  $-30^\circ$ , where there is an overlap of peaks and a reliable estimate of the approximate chemical shift could not be made.

Since the approximate and computer-obtained parameters for the vinyl halides had the same temperature dependence, computer-obtained nmr parameters have not been calculated for the vinyl ethers. The approximate values of the chemical shifts are an even better approximation in the case of the vinyl ethers than in the case of the vinyl halides, since the vinyl ethers have a more nearly first-order spectrum.

The room-temperature spin parameters of the vinyl halides and the vinyl ethers in the various solutions are summarized in Table III. These values are in reasonable agreement with those quoted in the literature.<sup>1-3,5-7,11,13,14,17,20,26-29</sup>

A plot of the proton chemical shifts of vinyl bromide against the sample temperature is shown in Figure 3. In Figure 4, the proton chemical shifts of vinyl chloride in  $CFCl_3$  solution and in  $CS_2$  solution have been plotted against the temperature. The lines have been drawn through the  $CFCl_3$  solution points. There is considerably more scatter in the points of the  $CS_2$  solution, but the temperature dependence of vinyl chloride does not appear to be different in the two solvents. The chemical shift *vs.* the temperature plots for vinyl fluoride and vinyl iodide are curved, as can be seen from Figures 5 and 6. For the vinyl ethers the approximate chemical shift *vs.* temperature plots are straight lines; figures for these have not been included. The slopes of the chemical shift plots at  $25^\circ$  are summarized in Table IV, which also contains for each compound the range of temperatures investigated. The slopes of the plots for a given compound have been found to be independent of the medium. Figure 7 shows the temperature dependence of the H-F coupling constants of vinyl fluoride.

#### IV. Discussion

*A. General Features of the Spectra.* The most striking feature of the spectra is the increased chemical

(25) T. Yamamoto and S. Fujiwara, *Bull. Chem. Soc. Jap.*, **39**, 333 (1966).

(26) C. N. Banwell and N. Sheppard, *Proc. Roy. Soc.*, **A263**, 136 (1961).

(27) E. B. Whipple and Y. Chiang, *J. Chem. Phys.*, **40**, 713 (1964).

(28) R. A. Hoffman and B. Gestblom, *J. Mol. Spectrosc.*, **13**, 221 (1964).

(29) G. J. Martin and M. L. Martin, *J. Chim. Phys.*, **61**, 122 (1964).

Table III: Chemical Shifts and Coupling Constants of the Vinyl Protons

Compd	Solvent	Concn (volume of sample: volume of solvent)	Temp, °C	Chemical shifts ( $\tau$ ) <sup>a</sup>			Coupling constants, <sup>a</sup> Hz		
				H <sub>A</sub>	H <sub>B</sub>	H <sub>C</sub>	J <sub>AB</sub>	J <sub>AC</sub>	J <sub>BC</sub>
Vinyl fluoride	CS <sub>2</sub>	Satd	40	5.601 ± 0.003	5.263 ± 0.003	3.476 ± 0.003	-3.2 ± 0.1 <sup>b</sup>	4.6 ± 0.1 <sup>b</sup>	12.6 ± 0.1 <sup>b</sup>
Vinyl chloride	CS <sub>2</sub>	1:1	21	4.63 ± 0.04	4.54 ± 0.04	3.76 ± 0.04	-1.4 ± 0.1	7.0 ± 0.2	14.7 ± 0.1
	CS <sub>2</sub>	1:3	37	4.66 ± 0.03	4.57 ± 0.03	3.78 ± 0.03	-1.5 ± 0.1	6.9 ± 0.1	14.8 ± 0.1
	OFCI <sub>2</sub>	1:1	37	4.651 ± 0.004	4.552 ± 0.004	3.761 ± 0.004	-1.4 ± 0.1	7.0 ± 0.2	14.8 ± 0.2
Vinyl bromide	CS <sub>2</sub>	1:1	37	4.084 ± 0.005	4.206 ± 0.005	3.576 ± 0.005	-1.7 ± 0.1	7.2 ± 0.1	15.0 ± 0.1
	CS <sub>2</sub>	1:2	37	4.071 ± 0.005	4.215 ± 0.005	3.589 ± 0.005	-1.7 ± 0.1	7.2 ± 0.1	15.0 ± 0.1
	OFCI <sub>2</sub>	1:1	37	4.055 ± 0.005	4.181 ± 0.005	3.569 ± 0.005	-1.7 ± 0.1	7.2 ± 0.1	15.0 ± 0.1
Vinyl iodide	None	...	32	...	...	...	-1.5 ± 0.1	7.8 ± 0.1	15.9 ± 0.1
	CS <sub>2</sub>	1:2	40	3.427 ± 0.003	3.745 ± 0.003	3.420 ± 0.003	-1.5 ± 0.1	8.0 ± 0.1	15.9 ± 0.1
Vinyl 2-ethylhexyl ether	None	...	32	6.15 ± 0.01 <sup>d</sup>	5.94 ± 0.01 <sup>d</sup>	3.60 ± 0.04 <sup>d</sup>	1.6 ± 0.2 <sup>d</sup>	6.9 ± 0.3 <sup>d</sup>	14.1 ± 0.6 <sup>d</sup>
Phenyl 2-vinoxyethyl ether	None	...	32	...	5.86 ± 0.01 <sup>d</sup>	3.59 ± 0.04 <sup>d</sup>	1.9 ± 0.1 <sup>d</sup>	6.8 ± 0.1 <sup>d</sup>	14.0 ± 0.1 <sup>d</sup>
	CS <sub>2</sub>	1:5	30	...	5.88 ± 0.01 <sup>d</sup>	3.60 ± 0.01 <sup>d</sup>	2.0 ± 0.1 <sup>d</sup>	6.8 ± 0.1 <sup>d</sup>	14.0 ± 0.1 <sup>d</sup>
Phenyl vinyl ether	None	...	32	5.74 ± 0.02 <sup>d</sup>	5.32 ± 0.02 <sup>d</sup>	3.52 ± 0.02 <sup>d</sup>	1.4 ± 0.1 <sup>d</sup>	6.0 ± 0.1 <sup>d</sup>	13.4 ± 0.2 <sup>d</sup>

<sup>a</sup> Designation of the protons is the same as in Figures 1-7. <sup>b</sup> The proton-fluorine couplings are:  $J_{AX} = 51.8$  Hz,  $J_{BX} = 19.6$  Hz, and  $J_{CX} = 84.4$  Hz. <sup>c</sup> Sample was not referenced with internal TMS. <sup>d</sup> Approximate spin parameters. <sup>e</sup> Could not be determined. The spectral positions of H<sub>A</sub> and of the OCH<sub>2</sub>CH<sub>2</sub>O group overlap at 56.4 MHz.

Table IV: Temperature Dependence of the Vinyl Proton Chemical Shifts

Compd	10 <sup>4</sup> × temp coeff <sup>a</sup> (at +25°), ppm/deg			Temp limits, °C
	H <sub>A</sub> <sup>b</sup>	H <sub>B</sub> <sup>b</sup>	H <sub>C</sub> <sup>b</sup>	
Vinyl fluoride <sup>c</sup>	+8.0	+5.2	+5.4	-89, 40
Vinyl chloride	+6.5	+3.9	+2.8	-121, 37
Vinyl bromide	+6.0	+2.8	+2.8	-120, 37
Vinyl iodide	+9.8	+5.7	+5.5	-108, 50
Vinyl 2-ethylhexyl ether	+1.0	-3.8	+6.2	-57, 105
Phenyl 2-vinoxyethyl ether	... <sup>d</sup>	-5.5	+3.5	-44, 92
Phenyl vinyl ether	+2.5	+6.1	-5.0	-32, 92

<sup>a</sup> A positive temperature coefficient indicates a shift to a higher field with increased temperature. <sup>b</sup> Designation of the protons is the same as in Figures 1-7. <sup>c</sup> The temperature coefficients of the proton-fluorine couplings are:  $J_{AX} = -2.1 \times 10^{-2}$  Hz/deg,  $J_{BX} = -0.9 \times 10^{-2}$  Hz/deg, and  $J_{CX} = -1.8 \times 10^{-2}$  Hz/deg. <sup>d</sup> Overlapped by the OCH<sub>2</sub>CH<sub>2</sub>O peaks at 56.4 MHz.

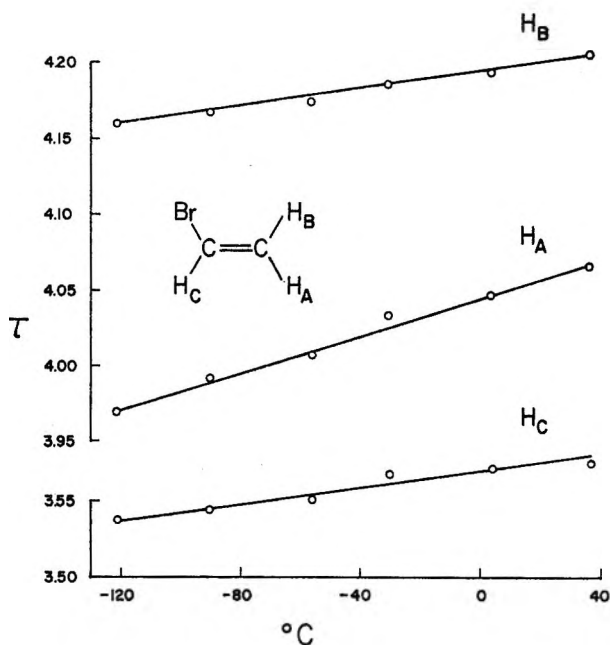


Figure 3. Temperature dependence of the vinyl bromide chemical shifts, in ppm on the  $\tau$  scale (1 volume of sample: 1 volume of CS<sub>2</sub>).

shift difference between the methine proton and the methylene protons for the series of substituents  $I < Br < Cl < F < O$ . The large shielding of the methylene protons in vinyl fluoride and in the vinyl ethers has been observed previously<sup>2,4,6,30</sup> and has been attributed to the lone pair conjugation of the substituent with the vinylic system, which results in high electron density in the  $\beta$  position. For a number of vinyl compounds, Banwell and Sheppard<sup>1</sup> have found a linear

(30) R. T. Hobgood, G. S. Reddy, and J. H. Goldstein, *J. Phys. Chem.*, **67**, 110 (1963).

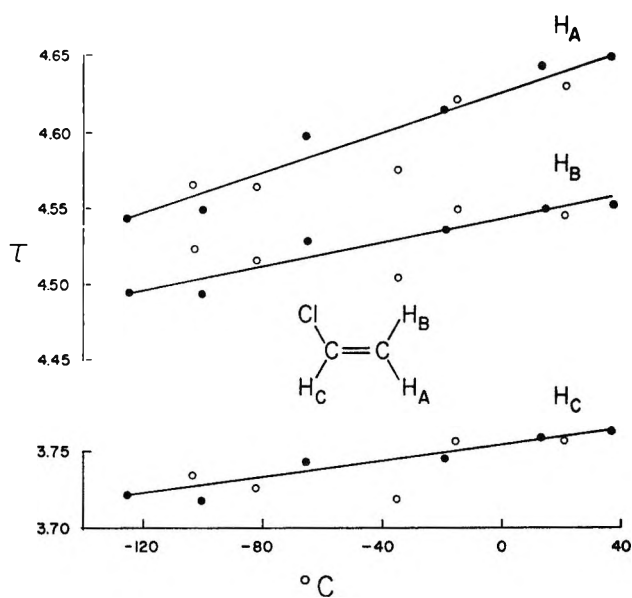


Figure 4. Temperature dependence of the vinyl chloride chemical shifts, in ppm on the  $\tau$  scale: ●, 1 volume of sample:1 volume of  $\text{CFCl}_3$ ; ○, 1 volume of sample:1 volume of  $\text{CS}_2$ .

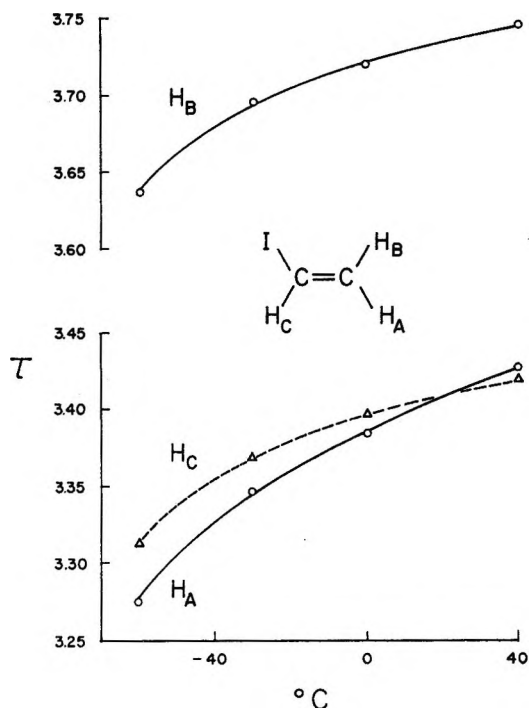


Figure 5. Temperature dependence of the vinyl iodide chemical shifts, in ppm on the  $\tau$  scale (1 volume of sample:2 volumes of  $\text{CS}_2$ ).

relationship between the  $\sigma_R$  parameter,<sup>31</sup> the resonance contribution to the Hammett-type  $\sigma$  constant, and the chemical shift difference between the methine proton and the methylene protons. In the present work, it was found that vinyl iodide, which has not been included by Banwell and Sheppard, fits this relationship nicely. Thus, for vinyl iodide, the strongly nonfirst-

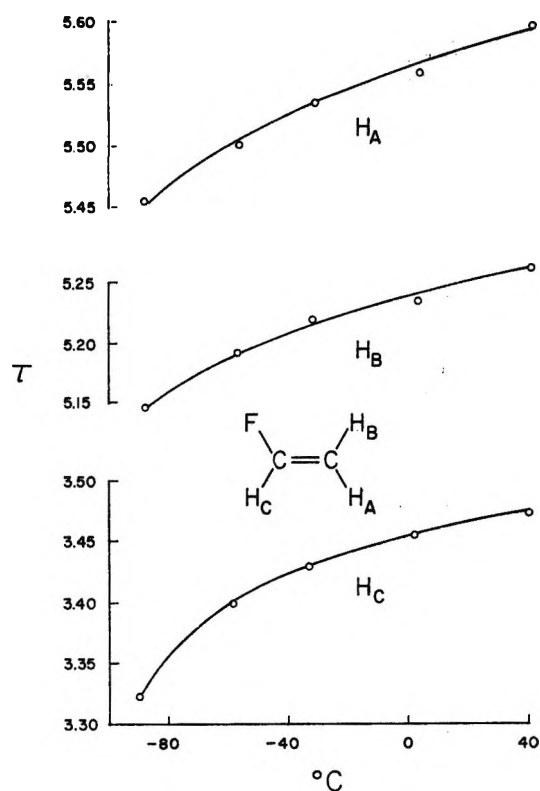


Figure 6. Temperature dependence of the vinyl fluoride chemical shifts, in ppm on the  $\tau$  scale (saturated in  $\text{CS}_2$ ).

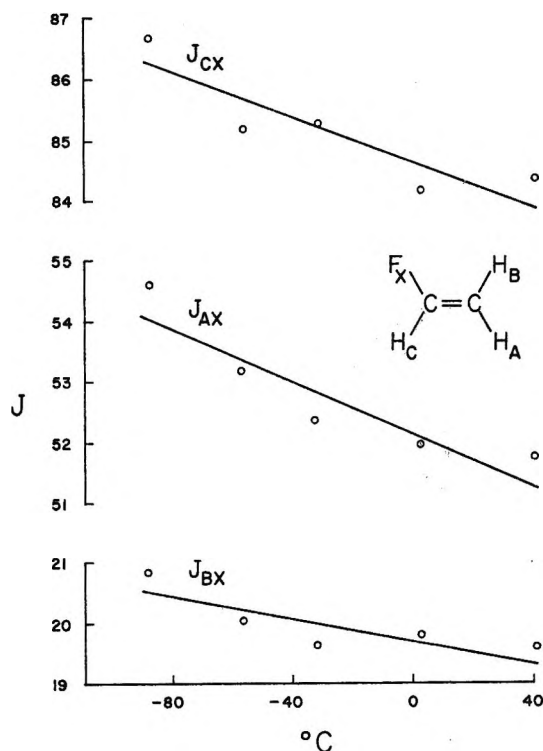


Figure 7. Temperature dependence of the vinyl fluoride H-F coupling constants, in hertz (saturated in  $\text{CS}_2$ ).

(31) R. W. Taft, Jr., *J. Amer. Chem. Soc.*, **79**, 1045 (1957).

order spectrum which results from the small chemical shift difference between the protons can be attributed to the lessened mesomeric contribution of iodine as compared with the other halogens.

*B. Temperature Dependence of the Vinyl Coupling Constants.* The proton coupling constants for all the compounds studied are independent of temperature within the experimental error of the measurements. On the other hand, all H-F coupling constants in vinyl fluoride decrease with increasing temperature. Excitation of out-of-plane molecular vibrations, if it affects the coupling constant, would clearly be expected to reduce the vicinal H-H coupling constants, according to the well-known variation of this type of constant with the dihedral angle,<sup>32</sup> in which the maximum value occurs for 0 or 180°. Furthermore, based on the work of Abraham and Cavalli<sup>33</sup> and of Williamson,<sup>34</sup> it appears that H-F couplings in many cases tend to depend upon geometry in a way parallel to the H-H coupling dependence.

It may be pointed out that the H-F coupling constants measured here are larger in magnitude than those between two hydrogen atoms and that therefore a variation corresponding to an equal fractional change in magnitude can be observed more easily than for the H-H couplings. However, comparisons show that a change in the H-H *trans* or *cis* coupling constants of magnitude proportional to those observed for the H-F constants could easily be seen. The present results for vinyl fluoride thus demonstrate that there is an essential difference between the factors influencing these two types of coupling constants, since, in a single molecule, their dependences upon temperature are dissimilar.

*C. Temperature Dependence of the Vinyl Proton Chemical Shifts.* The temperature dependence of shifts observed in the present work is severalfold greater than that observed by Petrakis and Sederholm<sup>35</sup> for their gaseous samples, which, with the exception of HBr, were hydrocarbons. Either effects of the condensed phase or the effects of the substituent, or both, could cause the greater temperature dependence.

Vinyl chloride shows the same temperature dependence in CS<sub>2</sub> solution and in CFC<sub>3</sub> solution. More importantly, both phenyl 2-vinoxyethyl ether and vinyl iodide show the same temperature dependence as neat liquids and as CS<sub>2</sub> solutions. Thus the main factor influencing the temperature dependence is probably not the solvent effect, since it is unlikely that the interactions among the very polar solute molecules and that between solute and solvent would result in the same temperature dependence. Intramolecular changes appear to be a more consistent explanation.

Furthermore, for the compounds in this study for which dilution with CS<sub>2</sub> was tried, all three proton resonances shift upfield on dilution. Thus, for protons with positive temperature dependence of chemical shift,

dilution has the same effect as raising the temperature; for protons with a negative temperature dependence of chemical shift, dilution has the same effect as lowering the temperature. If solute-solute interactions, rather than intramolecular effects, were the principal cause of the temperature dependence of the chemical shifts, one would expect dilution and increase in temperature to change the chemical shift in the same direction.

Considering first the vinyl halides, the proton shielding is observed to increase with increasing temperature. Petrakis and Sederholm<sup>35</sup> attribute the positive shielding dependence of ethylene to the excitation of the twisting mode about the double bond, which reduces the double-bond character of the C-C bond but increases the electron density about the protons. In vinyl halides, all three out-of-plane vibrations contain contributions from the twisting coordinate, so that the twisting mode cannot be assigned to any one of these vibrations. For vinyl fluoride and vinyl bromide, the highest frequency out-of-plane vibration is predominantly made up of the twisting coordinate.<sup>36,37</sup> For vinyl chloride and vinyl iodide, no comparable normal-coordinate analyses have been carried out, but it seems reasonable that for these compounds too the highest frequency out-of-plane vibration is largely composed of the twisting coordinate. For ethylene, the twisting mode has a frequency of 1027 cm<sup>-1</sup>.<sup>38</sup> For the vinyl halides even the highest frequency out-of-plane vibrations range from 931 to 946 cm<sup>-1</sup>.<sup>36,37,39,40</sup> Thus while quantitative calculations could not be carried out for the vinyl halides, the larger, positive temperature dependence of the chemical shifts in these compounds is well accounted for by the lower frequency of the vibrations.

In each of the vinyl halides, the proton, H<sub>A</sub>, which is *trans* to the substituent, shows the largest shift to higher field upon increase of temperature. In addition to the effect of the twisting vibrations, which should shield all the protons to about the same extent, there are several other factors which must be considered as contributing to this result. In the out-of-plane vibrational modes mostly easily excited—those with the smaller vibrational frequencies and also, by chance, those with small contributions from the twisting motion—the amplitudes of the displacements of H<sub>A</sub> are much larger than those of the displacements of the other

(32) M. Karplus, *J. Chem. Phys.*, **30**, 11 (1959).

(33) R. J. Abraham and L. Cavalli, *Mol. Phys.*, **9**, 67 (1965).

(34) K. L. Williamson, *et al.*, *J. Amer. Chem. Soc.*, **88**, 5678 (1966).

(35) L. Petrakis and C. H. Sederholm, *J. Chem. Phys.*, **35**, 1174 (1961).

(36) J. R. Scherer and W. J. Potts, *ibid.*, **31**, 1691 (1959).

(37) J. R. Scherer and W. J. Potts, *ibid.*, **30**, 1527 (1959).

(38) B. L. Crawford, Jr., J. E. Lancaster, and R. G. Inskeep, *ibid.*, **21**, 678 (1953).

(39) S. Narita, S. Ichinohe, and S. Enomoto, *ibid.*, **31**, 1151 (1959).

(40) P. Torkington, *Proc. Roy. Soc.*, **A206**, 17 (1951).



hydrogens. However, out-of-plane motions in a  $\pi$ -bonded molecule reduce that part of the shielding which originates in the anisotropy of the  $\pi$  cloud.<sup>35,41</sup> Considering only this type of anisotropy, excitation of such vibrations could not explain the observed larger temperature coefficient for  $H_A$ .

On the other hand, there is expected to be a downfield shift, associated with the anisotropy of the carbon-hydrogen bond, which increases with increasing vibration and thus opposes the effect of twisting motion. In the point-dipole approximation, the neighbor anisotropy effect varies inversely with the cube of  $R$ , the distance between the dipole and the proton affected.<sup>42</sup> That this effect is smallest for  $H_A$  is illustrated by styrene, for which the anisotropic susceptibility correction for the phenyl group decreases in the order  $H_C > H_B > H_A$ .<sup>43</sup> For Cl, Br, and I, the susceptibility difference ( $\Delta\chi = \chi_{||} - \chi_{\perp}$ ) is such as to cause shielding.<sup>14,16</sup> Excitation of out-of-plane vibrations increases the distance from the halogen to the hydrogen nucleus, and thus an increase in temperature decreases the shielding, tending to offset the effect of the twisting motion, but to an extent which is smallest for  $H_A$ .

The difference between the temperature coefficients of  $H_A$  and  $H_B$  increases in the order  $Cl < Br < I$ . This increasing difference results from the increasing anisotropy of the C-X bond. Spiesicke and Schneider<sup>44</sup> have found a similar correlation between the anisotropy of the substituent and the chemical shift of  $^1H$  and  $^{13}C$ . On their plot of chemical shift *vs.* electronegativity of X in a series of compounds  $CH_3X$  and  $CH_3CH_2X$ , these authors found that the deviation from linearity increased in the order  $Cl < Br < I$ . Deviations from the linear relationship between the proton chemical shifts and the  $^{13}C$ -H coupling constants have been used to estimate the anisotropy of the substituent.<sup>14,16</sup> For methyl and ethyl halides, the anisotropy corrections to the proton shifts at 40 MHz were -15, -25, and -35 Hz for Cl, Br, and I, respectively.

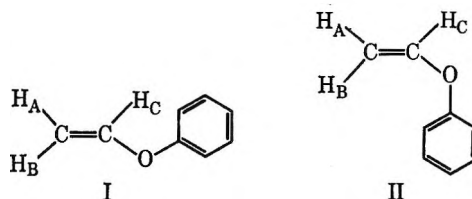
In the present work, it was found that the individual temperature coefficients in the vinyl halides do not follow a regular trend with substitution: all of these parameters have a minimum value for either vinyl chloride or vinyl bromide. This suggests additional contributions to the temperature dependence from the competing inductive and mesomeric effects of the substituent.

For the vinyl ethers, the pattern of chemical shift variation with temperature is dependent upon the structure of the group attached to the oxygen atom. The temperature dependence of the nmr parameters of phenyl 2-vinoxyethyl ether is much more similar to that of vinyl 2-ethylhexyl ethyl ether than to that of phenyl vinyl ether. Apparently, the temperature dependence is more influenced by what is attached

immediately to the ether oxygen than by whether a phenyl group is present or not. This is strong evidence that the temperature dependence is due to intramolecular changes, rather than to changes in the preferred mutual orientation between neighboring molecules when an aromatic ring is present.<sup>45</sup>

In the vinyl ethers the temperature coefficients of the chemical shift of  $H_A$  are unusually small. The temperature coefficient of  $H_B$  in both alkyl vinyl ethers is negative. Both of these temperature dependences are associated with a decreased mesomeric effect of the oxygen with increasing temperature. Increased molecular vibrations, including torsional oscillations about the C-O bond at elevated temperature, tend to reduce conjugation in the O-C-C grouping, and this, in turn, reduces the charge transferred to the carbon-bearing  $H_A$  and  $H_B$  and decreases their shielding. This effect would be expected to be greater for the vinyl ethers than for the vinyl halides.

In phenyl vinyl ether, both  $H_B$  and  $H_C$  have temperature coefficients which are of opposite sign from the corresponding temperature coefficients in the other two vinyl ethers.  $H_B$  and  $H_C$  are the two hydrogens most affected by the anisotropy of the phenyl group. Increased temperature is expected to shift the equilibrium between rotational isomers toward more of form II.



Since the phenyl group is undoubtedly tilted out of the plane of the vinyloxy group, as is indicated by molecular models, this would tend to shield  $H_B$  and deshield  $H_C$ , which is what is observed. Thus while the equilibrium constant for the equilibrium between rotational isomers in vinyl ethers cannot be calculated from the present data, the qualitative behavior of the temperature dependences of the nmr parameters gives evidence for the existence of these isomers.

*Acknowledgment.* The authors wish to thank the University of Florida Computing Center and its personnel for help with the FREQUENT IV and LAOCN3 computations.

(41) J. A. Pople, W. G. Schneider, and H. J. Bernstein, ref 19, pp 176-179.

(42) H. M. McConnell, *J. Chem. Phys.*, **27**, 226 (1957).

(43) C. E. Johnson, Jr., and F. A. Bovey, *ibid.*, **29**, 1012 (1958).

(44) H. Spiesicke and W. G. Schneider, *ibid.*, **35**, 722 (1961).

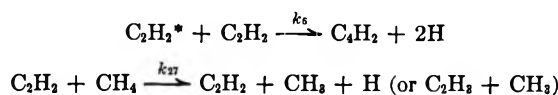
(45) W. G. Schneider, *J. Phys. Chem.*, **66**, 2653 (1962).

# The Acetylene-Photosensitized Reaction of Methane at 1470 Å

by Seiki Takita, Yuji Mori, and Ikuzo Tanaka

Laboratory of Physical Chemistry, Tokyo Institute of Technology, Ohokayama, Meguro-ku, Tokyo, Japan  
(Received January 5, 1968)

Acetylene photosensitization in the acetylene-methane system at 1470 Å has been observed. The reaction mechanism of the acetylene photolysis has also been studied. In the acetylene system the main products are ethylene and diacetylene. In the acetylene-methane system ethane and propylene are also produced in amounts related to the pressure of methane. The pressure dependences of the disproportionation and recombination reactions of vinyl radicals have been discussed. It is found that the occurrence of the disproportionation reaction is about three times the occurrence of the recombination reaction. With the result of the isotopic analyses of ethylene formed in the C<sub>2</sub>H<sub>2</sub>-CD<sub>4</sub> and C<sub>2</sub>D<sub>2</sub>-CH<sub>4</sub> systems, the ratio of the acetylene-photosensitized reactions is estimated. For



we obtained  $k_s/k_{27} \cong 10^2$ .

## 1. Introduction

It has been shown that the absorption spectrum of acetylene below 2000 Å has a sharply banded structure.<sup>1-3</sup> This means that the excited state of acetylene has a significant lifetime. A few investigations of acetylene photolysis in the vacuum ultraviolet region have been carried out.<sup>4-6</sup> Koyano, *et al.*,<sup>5</sup> reported the chemiionization reaction of Lyman α (1216 Å)-excited acetylene. Stief, *et al.*,<sup>6</sup> who observed the C<sub>2</sub> Swan band in the photolysis of acetylene with Xe or Kr resonance lines, strongly suggested the production of a long-lived excited state of acetylene.

In the present work we discuss the acetylene photosensitization of methane as well as the radical reactions in the acetylene photolysis. The main products are ethylene and diacetylene in the acetylene system. Ethane and propylene are also produced in the acetylene-methane system. All products except diacetylene disappear when a small amount of nitric oxide is added in the reaction system. Isotopic analyses were made of the ethylene and ethane formed in the C<sub>2</sub>H<sub>2</sub>-CD<sub>4</sub> and C<sub>2</sub>D<sub>2</sub>-CH<sub>4</sub> systems.

## 2. Experimental Section

*A. Light Source.* The Xe resonance lines were excited in an air-cooled electrodeless discharge operated by an Ito-Chotampa 2450-Mc microwave generator. The lamp having Ba getter in the side arm was filled with 0.5 Torr of Xe and 4 Torr of Ne. The lamp emitted resonance radiation at 1470 Å (8.4 eV) and at 1295 Å (9.6 eV). The intensity at 1295 Å was about 2% of the intensity at 1470 Å, which was estimated as 10<sup>15</sup> quanta/sec, and was considered to be unimportant. LiF was used as a window and was attached with Picein.

*B. Materials.* Acetylene and methane were obtained from Takachiho Co., and both gases contained ethane and ethylene as impurities. Acetylene was purified by a gas chromatograph provided with a 2-m silica gel column at 70°. Methane was trapped on silica gel which was packed in U trap and cooled to liquid N<sub>2</sub> temperature. The silica gel was then warmed to room temperature and the methane was collected. The purified gases contained no impurity within the sensitivity of a gas chromatograph with a flame ionization detector, made by Hitachi Co. The purified acetylene had a minimum purity of 99.999%. Methane-*d*<sub>4</sub> was obtained from Merck Sharp & Dohme Ltd. of Canada and was purified in the same manner as the CH<sub>4</sub>. Methane-*d*<sub>4</sub>, after purification, contained less than 2% CD<sub>3</sub>H. Acetylene-*d*<sub>2</sub> was made from CaC<sub>2</sub> crystals and D<sub>2</sub>O. To remove impurities, the CaC<sub>2</sub> was placed into a quartz tube and heated to 800° under high vacuum for 2 days. Then the CaC<sub>2</sub> was cooled to 77°K and mixed with D<sub>2</sub>O. Acetylene-*d*<sub>2</sub> purified by a gas chromatograph provided with a 2-m silica gel column at 30° contained less than 2% C<sub>2</sub>HD. Xe, Ne, and nitric oxide, obtained from Takachiho Co., were used without further purification.

*C. Procedure.* The entire experimental apparatus was mercury free. The reaction system of about 200 cm<sup>3</sup> volume was isolated by a metal valve with Teflon packing to prevent the adsorption of products. Other

- (1) W. C. Price, *Phys. Rev.*, **47**, 444 (1935).
- (2) P. G. Wilkinson, *J. Mol. Spectry.*, **2**, 387 (1958).
- (3) T. Nakayama and K. Watanabe, *J. Chem. Phys.*, **40**, 558 (1964).
- (4) M. Zelikoff and L. M. Aschenbrand, *ibid.*, **24**, 1034 (1956).
- (5) I. Koyano, I. Tanaka, and I. Omura, *ibid.*, **40**, 2734 (1964).
- (6) L. J. Stief, V. J. Decarlo, and R. J. Mataloni, *ibid.*, **42**, 3113 (1965).

stopcocks were greased with Apiezon T grease. The LiF window of 15-mm diameter was sealed to the reaction cell with Picein. The window of the lamp was brought as close as possible to the window of the reaction cell and N<sub>2</sub> gas was allowed to flow between the two windows to prevent light absorption by air. The reaction gas was circulated by a magnetic fan. The acetylene pressure was measured by an oil manometer and the methane pressure was measured by a metal Bourdon gauge.

The light was completely absorbed at an acetylene pressure higher than 2 Torr. The extinction coefficient of methane at 1470 Å is  $\leq 0.1 \text{ atm}^{-1} \text{ cm}^{-1}$ . The reaction time was 5 min in the acetylene (2 Torr)-methane system, but in the acetylene system it was prolonged in proportion to the acetylene pressure. The conversions in these reactions were less than 1.2% and the photolysis of the products can be ignored. This is proven by Figure 1. All condensable products at 77°K were analyzed by a gas chromatograph with a

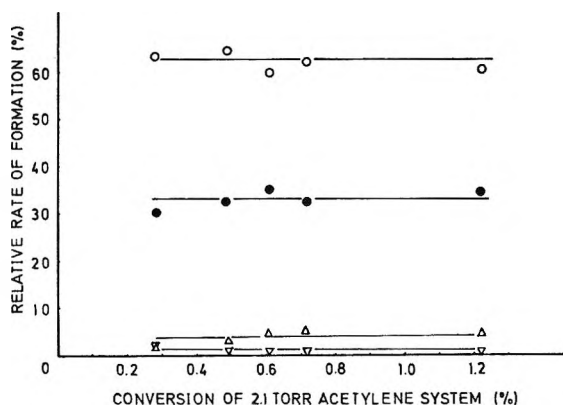


Figure 1. Relative rate of formation of each product against the conversion in 2.1 Torr acetylene system: O, C<sub>4</sub>H<sub>2</sub>; ●, C<sub>2</sub>H<sub>4</sub>; ▽, 1,3-C<sub>4</sub>H<sub>6</sub>; △, C<sub>4</sub>H<sub>4</sub>.

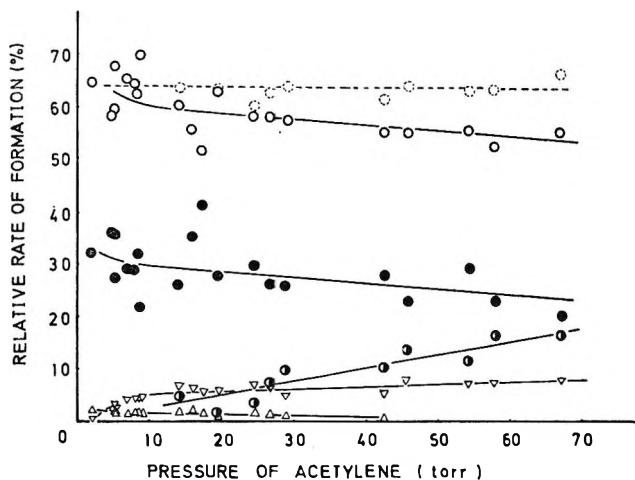


Figure 2. Relative rate of formation of each product against the pressure of acetylene: O, C<sub>4</sub>H<sub>2</sub>; ●, C<sub>2</sub>H<sub>4</sub>; ▽, 1,3-C<sub>4</sub>H<sub>6</sub>; ⊙, C<sub>6</sub>H<sub>6</sub>; △, C<sub>4</sub>H<sub>4</sub>; ○, C<sub>4</sub>H<sub>2</sub> (in this case C<sub>6</sub>H<sub>6</sub> is omitted).

flame ionization detector except in the C<sub>2</sub>H<sub>2</sub>-CD<sub>4</sub> system, where isotopic analyses of the isolated ethylene and ethane were carried out. Noncondensable products at 77°K were not detected, and polymer was never analyzed though its formation was distinguishable especially in the acetylene system.

### 3. Results and Discussion

A. *Acetylene System.* In this system the products were ethylene, diacetylene, vinylacetylene, 1,3-butadiene, benzene, and polymer. Hydrogen was not analyzed quantitatively. The relative rate of formation of each product vs. acetylene pressure is shown in Figure 2. In Figure 3 the pressure dependency of the quantum yield for diacetylene formation, which is estimated from Table I, is shown.

Table I<sup>a</sup>

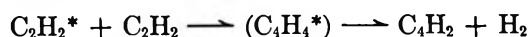
Expt no.	P, pressure of acetylene, Torr	Yield of C <sub>4</sub> H <sub>2</sub> , %	Av yield of C <sub>4</sub> H <sub>2</sub> , % (at 2.1 Torr)	P/2.1, Torr	$\varphi_P/\varphi_{2.1}$
A1	2.1	1.41	0.94	1.0	1.9
A2	24.1	0.16		11.3	
A3	2.1	0.47		1.0	
A4	18.0	0.13	0.42	8.4	2.6
A5	2.1	0.36		1.0	
A6	5.1	0.23	0.35	2.4	1.6
A7	2.1	0.33		1.0	
B1	2.1	0.73	0.50	1.0	1.9
B2	40.1	0.05		18.7	
B3	2.1	0.26		1.0	
B4	49.7	0.02	0.20	23.2	2.3
B5	2.1	0.15		1.0	
C1	2.1	1.44	0.88	1.0	2.9
C2	62.6	0.08		28.9	
C3	2.1	0.32		1.0	
D1	2.1	0.93	0.75	1.0	2.2
D2	12.9	0.28		6.0	
D3	2.1	0.57		1.0	

<sup>a</sup> If the successive three experiments are carried out, the pressure dependency of the quantum yield of diacetylene can be estimated, though the transmission of the window of the reaction cell decreases by the formation of polymer during the reaction. The experiment at P Torr of acetylene was always carried out between two experiments at the standard acetylene pressure (2.1 Torr), and the yield of diacetylene at the standard pressure should be averaged. The reaction times of all experiments were 5 min.  $\varphi_P$  means the yield of C<sub>4</sub>H<sub>2</sub> at P Torr of acetylene.

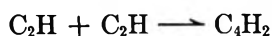
All products except diacetylene disappeared when a small amount of NO was added. Since C<sub>2</sub>H<sub>2</sub><sup>\*</sup> and maybe C<sub>2</sub>H<sub>2</sub><sup>\*</sup> too, is hardly scavenged under this condition, it is most probable to assume that diacetylene is formed from the reaction of C<sub>2</sub>H<sub>2</sub><sup>\*</sup> and C<sub>2</sub>H<sub>2</sub> or the reaction of C<sub>2</sub>H and C<sub>2</sub>H<sub>2</sub>.

(7) A. M. Tarr, O. P. Strausz, and H. E. Gunning, *Trans. Faraday Soc.*, 61, 1946 (1965).

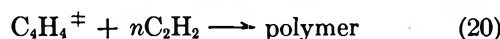
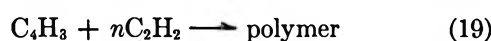
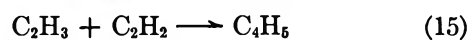
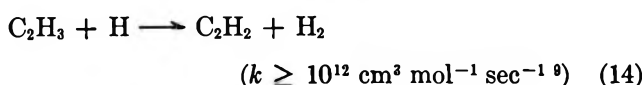
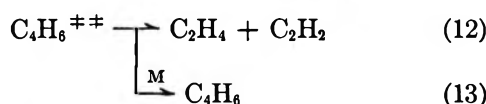
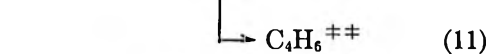
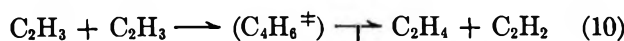
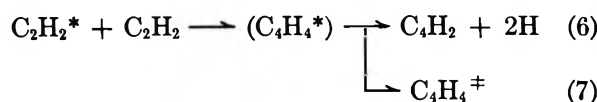
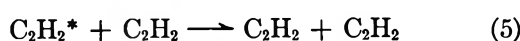
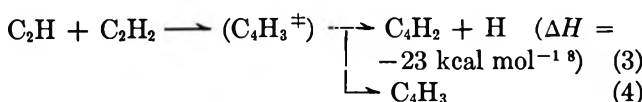
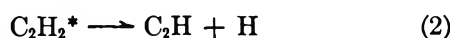
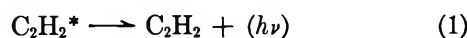
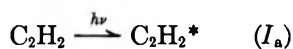
In Figure 2, the fraction of diacetylene is almost constant against the pressure of acetylene (if we neglect the product of benzene, the fraction would be constant as indicated by the dotted line in Figure 2). This means that the formation of diacetylene must be accompanied by the formation of corresponding intermediates which give ethylene, 1,3-butadiene, and vinylacetylene—probably the hydrogen atoms. Therefore, the reactions which may give diacetylene



can be excluded in our reaction scheme. The formation of diacetylene by the recombination reaction



is also not probable, because the reaction between  $\text{C}_2\text{H}$  and  $\text{C}_2\text{H}_2$  is very fast.<sup>8</sup> From these considerations the following reaction scheme may be reasonable.



By the steady-state treatment, we obtain

$$R_{\text{C}_4\text{H}_2} = \frac{I_a}{k_1 + k_2 + (k_5 + k_6 + k_7)[\text{C}_2\text{H}_2]} \left\{ \frac{k_2 k_3}{k_3 + k_4} + k_6 [\text{C}_2\text{H}_2] \right\} \quad (21)$$

where  $I_a$  means the light absorption by acetylene.

When acetylene pressure is low enough, the approximation may be preferable that

$$k_1 + k_2 \gg (k_5 + k_6 + k_7)[\text{C}_2\text{H}_2] \quad (22)$$

Then

$$R_{\text{C}_4\text{H}_2}^1 \cong \frac{k_2 k_3 I_a}{(k_1 + k_2)(k_3 + k_4)} \quad (23)$$

If acetylene pressure is high enough

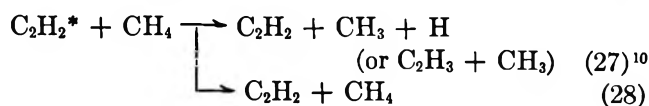
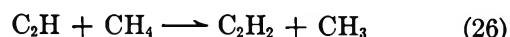
$$(k_5 + k_6 + k_7)[\text{C}_2\text{H}_2] \gg k_1 + k_2 \quad (24)$$

Then

$$R_{\text{C}_4\text{H}_2}^h \cong \frac{k_6 I_a}{k_5 + k_6 + k_7} \quad (25)$$

Therefore eq 21 is consistent with Figure 3 if  $R_{\text{C}_4\text{H}_2}^h > R_{\text{C}_4\text{H}_2}^1$ . Thus we suggest that reactions 3 and 6 are the important processes for the formation of diacetylene. Since the rate of formation of vinylacetylene does not increase with increasing total pressure in both the acetylene system and the acetylene-methane system, vinylacetylene should not be formed from the stabilization of  $\text{C}_4\text{H}_4^\ddagger$  but rather from reaction 17.

*B. C<sub>2</sub>H<sub>2</sub> (2.1 Torr)-CH<sub>4</sub> System.* In this system, not only the products obtained in the acetylene system but also ethane and propylene were detected, and the following reactions should be added to the reaction scheme of eq 1-20.

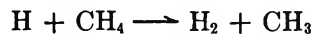
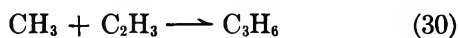


(8) J. N. Bradley and G. B. Kistiakowsky, *J. Chem. Phys.*, **35**, 264 (1961).

(9) G. G. Volpi and F. Zocchi, *ibid.*, **44**, 4010 (1966).

(10) Assuming the reaction  $\text{C}_2\text{H}_2^* + \text{CH}_4 \rightarrow \text{C}_2\text{H}_2 + \text{CH}_3 + \text{H}$ , we discuss two cases, one where  $\text{CH}_2$  has rather low energy as is produced by the decomposition of  $\text{CH}_2\text{N}_2$  and the other where  $\text{CH}_2$  is highly excited methylene as is produced in the photolysis of methane at 1236 Å. Produced methylene radicals react as follows:  $\text{CH}_2 + \text{CH}_4 \rightarrow \text{C}_2\text{H}_5^*$ . In the former case, 50% of  $\text{C}_2\text{H}_5^*$  is stabilized and gives ethane at 26 mm of methane: J. A. Bell and G. B. Kistiakowsky, *J. Amer. Chem. Soc.*, **84**, 3417 (1962). Therefore  $\text{CH}_2$  cannot be the precursor of the methyl radical in our experimental conditions. This is not consistent with the data that the yield of propylene increases with increasing the methane pressure.

In the latter case,  $\text{C}_2\text{H}_5^*$  decomposes into  $\text{C}_2\text{H}_4$  and  $\text{H}_2$ : P. Ausloos, R. Gorden, Jr., and S. G. Lias, *J. Chem. Phys.*, **40**, 1854 (1964). The yield of ethylene is almost pressure independent. In this case ethylene-*d*<sub>4</sub> should be produced in the  $\text{C}_2\text{H}_2$ - $\text{CD}_4$  system, but we could not find any ethylene-*d*<sub>4</sub>. Therefore in our experiment the reaction  $\text{C}_2\text{H}_2^* + \text{CH}_4 \rightarrow \text{C}_2\text{H}_2 + \text{CH}_3 + \text{H}_2$  is not important.



$$(\Delta E^\ddagger = 7.8 \text{ kcal mol}^{-1}) \quad (31)$$

Figure 4 shows the relative rate of formation of each product against the methane pressure. The yield of ethylene does not increase with increasing methane pres-

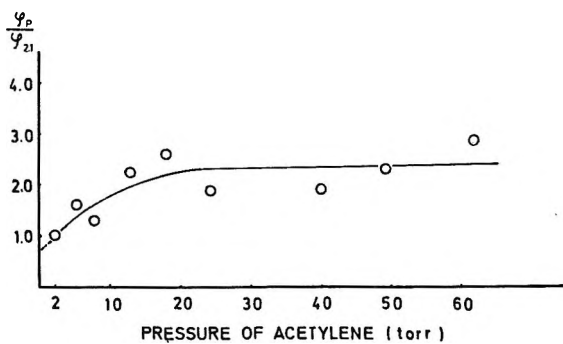


Figure 3. The pressure dependence of the quantum yield ratio ( $\varphi_P/\varphi_{2.1}$ ) of diacetylene.

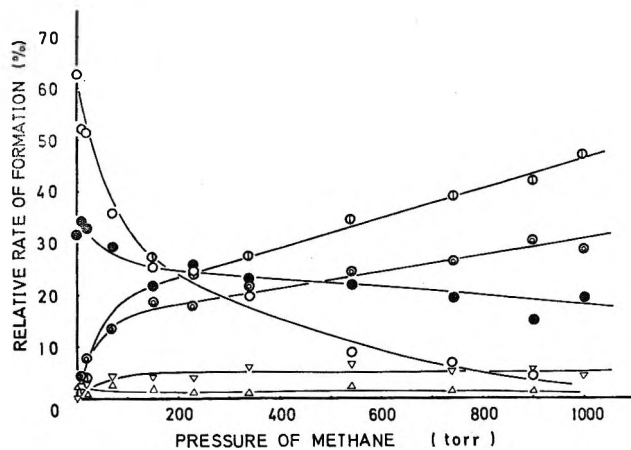


Figure 4. Relative rate of formation of each product against the pressure of methane: O,  $\text{C}_4\text{H}_2$ ; ●,  $\text{C}_2\text{H}_4$ ; ○,  $\text{C}_2\text{H}_6$ ; ⊙,  $\text{C}_3\text{H}_6$ ; ▽, 1,3- $\text{C}_4\text{H}_6$ ; △,  $\text{C}_4\text{H}_4$ .

sure but rather it decreases. Therefore the following reaction is not important.



The importance of reaction 29 (the recombination of methyl radicals) in the formation of ethane is verified by isotopic analysis of ethane, where  $\text{C}_2\text{D}_6$  was the only product of ethane produced in the  $\text{C}_2\text{H}_2\text{-CD}_4$  system. From processes 10–13, 16, and 17

$$R_{\text{C}_2\text{H}_4+1,3-\text{C}_4\text{H}_6} = (k_{10} + k_{11})[\text{C}_2\text{H}_3]^2 + (k_{16} + k_{17})[\text{C}_4\text{H}_5][\text{C}_2\text{H}_3] \quad (33)$$

Since the yield of 1,3- $\text{C}_4\text{H}_6$  was much smaller than that of  $\text{C}_4\text{H}_4$  in the 2.1 Torr acetylene system,  $k_{16}$  should be

negligible compared with  $k_{17}$ . Moreover, vinylacetylene did not increase with increasing the pressure of the reaction system (Figures 2 and 4). Therefore  $k_{16}$  can be ignored in eq 33. Then

$$(k_{10} + k_{11})[\text{C}_2\text{H}_3]^2 \cong$$

$$R_{\text{C}_2\text{H}_4+1,3-\text{C}_4\text{H}_6} - k_{17}[\text{C}_4\text{H}_5][\text{C}_2\text{H}_3]$$

$$(k_{10} + k_{11})[\text{C}_2\text{H}_3]^2 \cong R_{\text{C}_2\text{H}_4+1,3-\text{C}_4\text{H}_6} - R_{\text{C}_4\text{H}_4} \quad (34)$$

On the other hand, the rates of formation of ethane and propylene are given as

$$R_{\text{C}_2\text{H}_6} = k_{29}[\text{CH}_3]^2 \quad (35)$$

$$R_{\text{C}_3\text{H}_6} = k_{30}[\text{CH}_3][\text{C}_2\text{H}_3] \quad (36)$$

From eq 34–36

$$\frac{\sqrt{(R_{\text{C}_2\text{H}_4+1,3-\text{C}_4\text{H}_6} - R_{\text{C}_4\text{H}_4})R_{\text{C}_2\text{H}_6}}}{R_{\text{C}_3\text{H}_6}} \cong \frac{\sqrt{k_{29}(k_{10} + k_{11})}}{k_{30}} \quad (37)$$

The left-hand side of eq 37 is plotted in Figure 5. This equation indicates that if our reaction scheme is complete, the ratio  $[(R_{\text{C}_2\text{H}_4+1,3-\text{C}_4\text{H}_6} - R_{\text{C}_4\text{H}_4})R_{\text{C}_2\text{H}_6}]^{1/2}/R_{\text{C}_3\text{H}_6}$  should be independent of the methane pressure. However, the ratio in Figure 5 is not exactly constant and decreases slightly in proportion to the methane pressure. This implies that there might be another reaction process, in addition to our scheme, but it cannot be important because the gradient of the slope is not large (Figure 5).

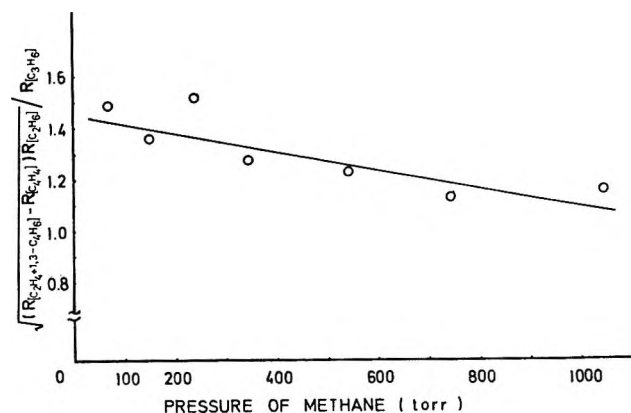


Figure 5. The plots of  $[(R_{\text{C}_2\text{H}_4+1,3-\text{C}_4\text{H}_6} - R_{\text{C}_4\text{H}_4})R_{\text{C}_2\text{H}_6}]^{1/2}/R_{\text{C}_3\text{H}_6}$  against the pressure of methane.

*C. Disproportionation and Recombination Reactions of Vinyl Radicals.* The fact that the yield of 1,3-butadiene depends on the total pressure in the system is shown in both Figure 2 and Figure 4. This pressure dependency is mainly caused by the third-body effect in reaction 13, because reaction 16 can be ignored as was discussed before. As for ethylene and 1,3-buta-

(11) R. Klein, *et al.*, *J. Chem. Phys.*, **30**, 58 (1959).

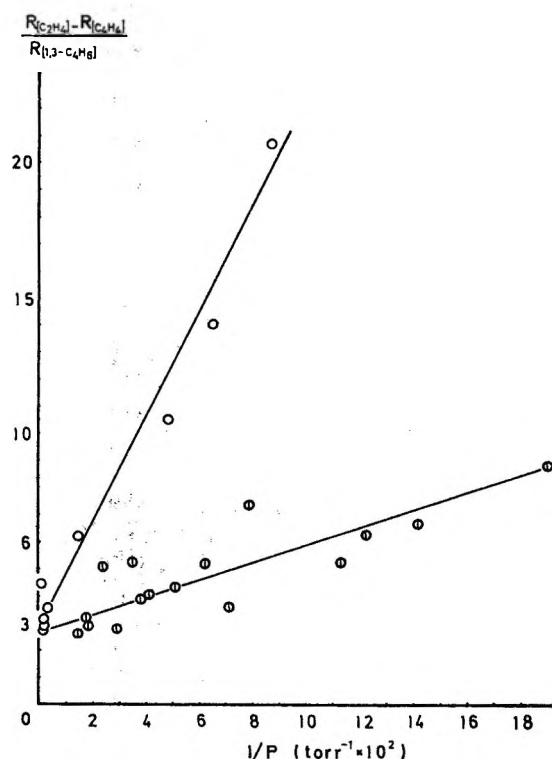


Figure 6. The plots of  $(R_{C_2H_4} - R_{C_4H_4})/R_{1,3-C_4H_6}$  vs. reciprocal of total pressure of the reaction system:  $\odot$ , acetylene system;  $\circ$ , acetylene (2.1 torr)-methane system.

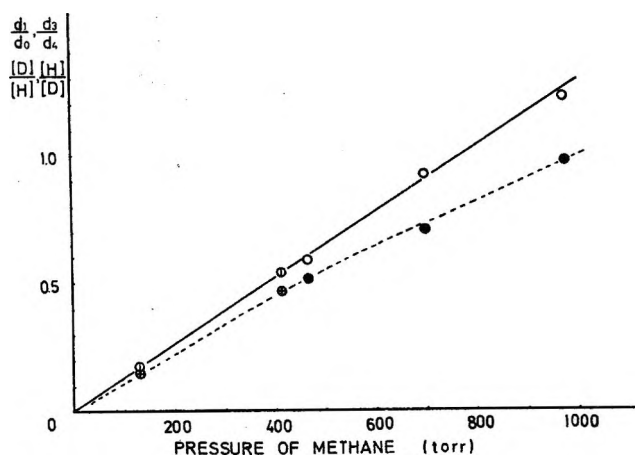


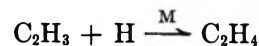
Figure 7. The plots of  $d_1/d_0$ ,  $d_3/d_4$ ,  $[D]/[H]$ , and  $[H]/[D]$  against the pressure of methane:  $\odot$ ,  $d_1/d_0$ ;  $\circ$ ,  $d_3/d_4$  ( $d_0$ ,  $d_1$ ,  $d_3$ , and  $d_4$  mean  $C_2H_4$ ,  $C_2H_3D$ ,  $C_2HD_3$ , and  $C_2D_4$ , respectively);  $\oplus$  ( $[D]/[H]$ ) and  $\bullet$  ( $[H]/[D]$ ) were calculated from eq 45.  $d_0$ ,  $d_1$  (in the  $C_2H_2-CD_4$  system) and  $d_4$ ,  $d_3$  (in the  $C_2D_2-CH_4$  system) were the major products, and other deuterated ethylenes were hardly detected.

diene formed from reactions 10–13 and 17, the steady-state approximation leads to

$$\frac{R_{C_2H_4} - R_{C_4H_4}}{R_{1,3-C_4H_6}} = \frac{k_{12}}{k_{13}} \left( 1 + \frac{k_{10}}{k_{11}} \right) \frac{1}{[M]} + \frac{k_{10}}{k_{11}} \quad (38)$$

In Figure 6 the value of  $(R_{C_2H_4} - R_{C_4H_4})/R_{1,3-C_4H_6}$  is plotted against the reciprocal of third-body pressure.

From the intercept of Figure 6 we get  $k_{10} \cong 3k_{11}$  and from the slope we can see that, in reaction 13, acetylene is about seven times more effective than methane as the deactivator. This figure also indicates that the reaction



is not important.

*D. Isotopic Analysis of Ethylene Formed in  $C_2H_2-CD_4$  (or  $C_2D_2-CH_4$ ) System.* Using the result of the isotopic analysis of the ethylene produced in the reaction system  $C_2H_2-CD_4$  (or  $C_2D_2-CH_4$ ), the ratio  $[d_1]/[d_0]$  (or  $[d_3]/[d_4]$ ) was plotted against the methane pressure in Figure 7;  $d_1$  and  $d_0$  mean the  $C_2H_3D$  and  $C_2H_4$ , respectively. For the system  $C_2H_2-CD_4$  the steady-state treatment leads to

$$\begin{aligned} \frac{d[H]}{dt} &= k_2[C_2H_2^*] + k_3[C_2H][C_2H_2] + \\ & 2k_6[C_2H_2^*][C_2H_2] - k_9[H][C_2H_2] - \\ & k_{14}[H]\{[C_2H_3] + [C_2H_2D]\} - k_{31}[H][CD_4] = 0 \end{aligned}$$

$$[H] = \frac{k_2[C_2H_2^*] + k_3[C_2H][C_2H_2] + 2k_6[C_2H_2^*][C_2H_2]}{k_9[C_2H_2] + k_{14}\{[C_2H_3] + [C_2H_2D]\} + k_{31}[CD_4]} \quad (39)$$

$$\begin{aligned} \frac{d[D]}{dt} &= k_{27}[C_2H_2^*][CD_4] - k_9[D][C_2H_2] - \\ & k_{14}[D]\{[C_2H_3] + [C_2H_2D]\} - k_{31}[D][CD_4] = 0 \end{aligned}$$

$$[D] = \frac{k_{27}[C_2H_2^*][CD_4]}{k_9[C_2H_2] + k_{14}\{[C_2H_3] + [C_2H_2D]\} + k_{31}[CD_4]} \quad (40)$$

$$\begin{aligned} \frac{d}{dt}[C_2H] &= k_2[C_2H_2^*] - \\ & (k_3 + k_4)[C_2H][C_2H_2] - k_{26}[C_2H][CD_4] = 0 \end{aligned}$$

$$[C_2H] = \frac{k_2[C_2H_2^*]}{\{(k_3 + k_4)[C_2H_2] + k_{26}[CD_4]\}} \quad (41)$$

From eq 39 and 40, we get

$$\begin{aligned} \frac{[C_2H_2D]}{[C_2H_3]} &= \frac{[D]}{[H]} = \\ & \frac{k_{27}[C_2H_2^*]}{k_2[C_2H_2^*] + k_3[C_2H][C_2H_2] + 2k_6[C_2H_2^*][C_2H_2]} [CD_4] \end{aligned} \quad (42)$$

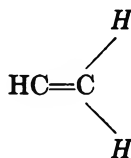
Substituting eq 41 for  $[C_2H]$  into eq 42

$$\begin{aligned} \frac{[C_2H_2D]}{[C_2H_3]} &= \frac{[D]}{[H]} = \\ & \frac{k_{27}}{k_2 \left( 1 + \frac{k_3[C_2H_2]}{(k_3 + k_4)[C_2H_2] + k_{26}[CD_4]} \right) + 2k_6[C_2H_2]} \times \\ & [CD_4] \end{aligned} \quad (43)$$

$1 > k_3[\text{C}_2\text{H}_2]/\{(k_3 + k_4)[\text{C}_2\text{H}_2] + k_{26}[\text{CD}_4]\}$  and eq 43 is modified to

$$\frac{k_{27}}{k_2 + 2k_6[\text{C}_2\text{H}_2]}[\text{CD}_4] > \frac{[\text{D}]}{[\text{H}]} > \frac{1}{2} \frac{k_{27}}{k_2 + k_6[\text{C}_2\text{H}_2]}[\text{CD}_4] \quad (44)$$

If there is no isotope effect in the formation of the ethylene, we can express  $[d_1]/[d_0]$  with  $[\text{H}]$  and  $[\text{D}]$  by making a simple probability calculation based on the assumption that one of the italic hydrogens in



should be transferred. Thus

$$\frac{[d_1]}{[d_0]} = \frac{[\text{D}]}{[\text{H}]} + \frac{[\text{D}]}{2[\text{H}] + [\text{D}]} = \frac{[\text{D}]}{[\text{H}]} \left( 1 + \frac{1}{2 + \frac{[\text{D}]}{[\text{H}]}} \right) \quad (45)$$

From eq 45 and the data of  $[d_1]/[d_0]$ , the ratio  $[\text{D}]/[\text{H}]$  was calculated and was also plotted in Figure 7. From the slope of the curve of  $[\text{D}]/[\text{H}]$  in Figure 7 and eq 44, we have

$$\frac{k_{27}}{k_2 + 2k_6[\text{C}_2\text{H}_2]} > \frac{1}{1000} > \frac{1}{2} \frac{k_{27}}{k_2 + k_6[\text{C}_2\text{H}_2]} \quad (46)$$

After some approximations shown in the Appendix, the ratio  $k_6/k_{27}$  was estimated as

$$k_6/k_{27} \cong 10^2 \quad (47)$$

### Appendix

When the acetylene pressure is low, eq 21 may be written as

$$R_{\text{C}_2\text{H}_2} \cong \frac{k_2 k_3 I_a}{(k_3 + k_4)(k_1 + k_2)} + \frac{k_6 I_a [\text{C}_2\text{H}_2]}{k_1 + k_2} \quad (\text{A-1})$$

This means that the yield of diacetylene in Figure 3 should increase linearly at low pressure of acetylene. Then the intercept which is extrapolated to 0.7 in Figure 3 gives the value which is close to

$$\frac{k_2 k_3 I_a}{(k_1 + k_2)(k_3 + k_4)} / \frac{I_a}{k_1 + k_2 + 2.1(k_6 + k_8 + k_7)} \left\{ \frac{k_2 k_3}{k_3 + k_4} + 2.1k_6 \right\} \quad (\text{A-2})$$

Therefore if we can neglect  $k_6$  and  $k_7$  compared to  $k_8$

$$\frac{k_2 k_3}{(k_1 + k_2)(k_3 + k_4)} / \frac{1}{k_1 + k_2 + 2.1k_8} \left\{ \frac{k_2 k_3}{k_3 + k_4} + 2.1k_6 \right\} \cong 0.7 \quad (\text{A-3})$$

As the yield of diacetylene is always nearly equal to two times the total yield of ethylene, 1,3-butadiene, and vinylacetylene in the acetylene system, reaction 4 may be unimportant in comparison with reaction 3. Then

$$\frac{k_3}{k_3 + k_4} \cong 1 \quad (\text{A-4})$$

From relations A-3 and A-4

$$\frac{k_2}{k_1 + k_2} / \frac{1}{k_1 + k_2 + 2.1k_8} \{k_2 + 2.1k_6\} \cong 0.7 \quad (\text{A-5})$$

On the other hand, when the pressure of acetylene is high enough, we have the following relation from eq 25 and Figure 3

$$\frac{k_6 I_a}{k_5 + k_6 + k_7} / \frac{I_a}{k_1 + k_2 + 2.1k_8} \left\{ \frac{k_2 k_3}{k_3 + k_4} + 2.1k_6 \right\} \cong 2.5 \quad (\text{A-6})$$

If we can neglect  $k_5$  and  $k_7$  again compared with  $k_6$ , eq A-6 is reduced to a simple relation using eq A-4

$$(k_1 + k_2 + 2.1k_6)/(k_2 + 2.1k_6) \cong 2.5 \quad (\text{A-7})$$

Therefore

$$k_1 \cong 1.5(k_2 + 2.1k_6) \quad (\text{A-8})$$

From relations A-5 and A-8, we get

$$k_2 \cong 3k_6 \quad (\text{A-9})$$

Then using the relations 46 and A-9, we obtain

$$1.5 \times 10^2 > \frac{k_6}{k_{27}} > 1.0 \times 10^2 \quad (\text{A-10})$$

## Crystal Structure of the Zeolite Nickel Faujasite

by D. H. Olson

*Mobil Research and Development Corporation, Central Research Division, Princeton, New Jersey 08540*  
(Received February 1, 1968)

The crystal structure of vacuum-dehydrated, nickel-exchanged natural faujasite has been determined using single-crystal X-ray techniques. The nickel exchange and subsequent dehydration have considerably modified the zeolite framework. Nickel(II) occupies two-thirds of the SI sites and in these sites attains near-perfect octahedral coordination with framework oxygens (Ni-O, 2.29 Å). The remaining nickel ions are distributed in four additional unique positions. Two of these positions are in the region of the SI' site and the other two are in SII and SII' sites. A trace of residual water may play a major role in determining the nickel ion distribution.

### Introduction

The catalytic importance of zeolites X and Y has prompted numerous investigations into the physical and chemical nature of these crystalline aluminosilicates. The role played in catalysis by cations associated with the zeolite framework is also of interest and has received considerable attention.<sup>1,2</sup> Knowledge of the position of the cations in the zeolites is necessary to ascertain their role in catalytic reactions. The cation positions of nickel(II) in vacuum-dehydrated, nickel-exchanged natural faujasite have been determined using single-crystal X-ray techniques. The cation site selectivity agrees with esr<sup>3</sup> and ir<sup>4</sup> studies of related transition metal zeolites. Also, the framework has undergone striking modification to accommodate the nickel ions.

### Experimental Section

The faujasite crystal used in this study was chipped from a mineral specimen from Kaiserstuhl, Bavaria. The crystal was batch exchanged at 90° for 60 days. The exchange solution, 1.0 M in nickel(II), was prepared using a 3:1 ratio of the chloride and acetate salts of nickel(II). At 25° the pH of the solution was 5.9. Following exchange, the pale green crystal was washed thoroughly and ground to a 0.01 cm radius sphere using a Bond-type<sup>5</sup> crystal-grinding apparatus. The crystal was placed in a glass capillary (0.01 mm thick walls), which was part of a simple glass system that could be connected directly to a high-vacuum line. The crystal was dehydrated by heating, while evacuating, to 400° over a 2-hr period, followed by evacuation for 7 hr at 400° and 10<sup>-6</sup> torr. After the system had cooled to room temperature, the crystal, which had turned dark brown during calcination, was sealed in the evacuated capillary.

The diffraction symmetry and systematic extinctions of nickel faujasite are consistent with the space group Fd3m assigned by Bergerhoff, *et al.*,<sup>6</sup> for natural faujasite. The lattice parameter,  $a = 24.410(5)$  Å, was determined by double-scanning diffractometry<sup>7</sup> on a

Siemens goniometer equipped with a General Electric Eulerian cradle, and the intensity data were collected using the moving crystal-moving counter technique<sup>8</sup> with nickel-filtered copper radiation. Background counts (1 min) were taken at each end of a 4°, 4-min scan. The 706 unique reflections with a 2θ cutoff at 140° were measured. The intensity data were corrected for absorption and Lorentz polarization factors. The error in the net intensity was calculated using

$$\Delta I = \{(\text{total counts}) + 2(\text{total background counts}) + [0.05(\text{total counts})]^2 + [0.06(\text{total background counts})]^2\}^{1/2}$$

and the corresponding standard error in the observed structure factor was found by applying the method of finite differences<sup>9</sup>

$$\sigma(F) \cong Lp^{-1/2}[(I + \Delta I)^{1/2} - I^{1/2}]$$

Following the data collection, the crystal was analyzed for Ni, Mg, Ca, Al, and Si, using microprobe techniques. Since the Si content appeared to be in error, the Si:Al ratio reported by Bergerhoff, *et al.*,<sup>6</sup> and Baur<sup>10</sup> for natural faujasite was used to calculate the unit cell contents. The excellent agreement found for the average Si(Al)-O distances for this structure

- (1) P. E. Pickert, J. A. Rabo, E. Dempsey, and V. Schomaker, *Proc. Int. Congr. Catal., 3rd, Amsterdam, 1964*, 1, 714 (1965).
- (2) R. L. Mays and P. E. Pickert, in "Molecular Sieves," Society of Chemical Industry, London, 1968, p 112.
- (3) T. I. Barry and L. A. Lay, *J. Phys. Chem. Solids*, **27**, 1821 (1966).
- (4) C. L. Angell and P. C. Schaffer, *J. Phys. Chem.*, **70**, 1413 (1966).
- (5) W. L. Bond, *Rev. Sci. Instrum.*, **22**, 344 (1951).
- (6) G. Bergerhoff, W. H. Baur, and W. Nowacki, *Neues Jahr Mineral. Montash.*, 193 (1958).
- (7) H. W. King and L. F. Vassamillet, *Advan. X-Ray Anal.*, **5**, 78 (1961).
- (8) T. C. Furnas, Single Crystal Orienter Instruction Manual, General Electric Co., Milwaukee, Wis., 1957.
- (9) D. E. Williams and R. E. Rundle, *J. Amer. Chem. Soc.*, **86**, 1660 (1964).
- (10) W. H. Baur, *Amer. Mineral.*, **49**, 697 (1964).



and for natural faujasite<sup>10</sup> supports this method of calculation. The unit cell composition,  $\text{Ni}_{27}\text{Ca}_4(\text{AlO}_2)_{58}(\text{SiO}_2)_{134}$ , shows a slight cation excess, which may be an indication of the limit of accuracy of the analysis.

### Solution of the Structure

Least-squares refinement<sup>11</sup> of a set of faujasite framework parameters from an earlier study,<sup>12</sup> plus estimated cation positional and population parameters, resulted in  $R$  (omitting  $F = 0$  values) = 0.069. The structure factors in this refinement were computed using the Hartree-Fock-Slater (HFS) ionic scattering factors computed by Hanson and Pohler.<sup>13</sup> The atoms were assumed to be in the following ionic forms:  $\text{O}^-$ ,  $\text{Si}^{2+}$ ,  $\text{Al}^+$ , and  $\text{Ni}^{2+}$ . Scattering factors for  $\text{Si}^{2+}$  were obtained by interpolating between Si and  $\text{Si}^{3+}$  form factors. For the tetrahedral atom site,  $\text{Si}^{2+}$  and  $\text{Al}^+$  form factors were combined in accordance with the Si:Al ratio of natural faujasite.<sup>6,10</sup> The calculations at this point included allowances for anisotropic thermal motion. A difference map showed scattering matter within the sodalite cage, in addition to electron density accounted for by partial occupancy of nickel in SI.<sup>14</sup> From the threefold interatomic distance  $\text{Ni}(3)\text{-O}(2) = 2.20 \text{ \AA}$ , a peak at  $x = y = z = 0.207$  (SII') was assigned to nickel ion Ni(3). Since its true identity was uncertain, a peak at  $x = y = z = 0.081$  was accounted for using partial occupancy of oxygen and was labeled O(w1). A very small peak at  $x = y = z = 0.161$  was assumed to be oxygen, O(w2), on the basis of the  $\text{Ni}(3)\text{-O}$  distance of  $2.0 \text{ \AA}$ . Since this peak has an electron density value just slightly above the difference map background level,  $0.4 \text{ electron/\AA}^3$ , its existence is uncertain. The population and positional parameters of these additional sodalite cage atoms were adjusted, using a succession of difference maps. The difference map in Figure 1, which is based upon a model that excludes the additional sodalite cage atoms, shows the O(w1), O(w2), and Ni(3) peaks. This difference plot also shows a peak at  $x = 1/8$ , the center of the sodalite cage. With a model that included O(w1) and Ni(3), this peak decreased to less than half the height shown, and the O(w2) peak height remained unchanged. Consequently, the peak at  $x = y = z = 1/8$  was judged to be insignificant. Including O(w1), O(w2), and Ni(3) atoms in the model and computing two more least-squares cycles reduced  $R$  (omitting  $F = 0$  values) to 0.046 and  $R$  (all data) to 0.059. Final positional and thermal parameters and a structure factor listing are given in Tables I-III, respectively. Interatomic distances and angles were computed using ORFFE<sup>15</sup> and are given in Tables IV and V.

Plots of  $(\Delta F)^2w$  vs.  $F$  and  $(\sin \theta)/\lambda$  revealed that the  $(\Delta F)^2w$  were nearly constant over the range of  $F$  and  $(\sin \theta)/\lambda$ . The constancy of  $(\Delta F)^2w$  implies that the weighting scheme employed is satisfactory.<sup>16</sup> In addition to checking the weighting scheme, in the last few

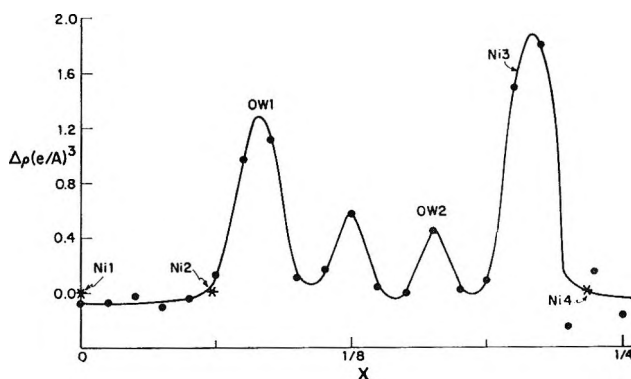


Figure 1. Difference plot,  $\Delta\rho(xxx)$  vs.  $x$  (fractional).

least-squares cycles anomalous dispersion corrections were included in the calculation of the structure factors, and the secondary extinction multiplier<sup>17</sup> was refined. Neither of the latter corrections appreciably changed the  $R$  value or the standard deviations of the variables, which indicates that anomalous dispersion and secondary extinction were not seriously affecting the observed intensity data.

### Discussion of the Structure

The nickel exchange and subsequent vacuum calcination produced a general loss of regularity in the zeolite framework. This loss may be seen by comparing the framework, interatomic distances, and angles of nickel-exchanged natural faujasite and hydrated natural faujasite (Table VI). Further comparison (Table VI) reveals substantial reorientation of the tetrahedra, as is reflected in the  $3.7^\circ$  change in the mean value of the  $\text{Si}(\text{Al})\text{-O-Si}(\text{Al})$  angle—and even more in the  $10.5^\circ$  average deviation from the mean for nickel faujasite, compared with a  $1.7^\circ$  average deviation for hydrated faujasite.<sup>10</sup> Although a similar loss of regularity is observed in dehydrated  $\text{CaX}$  and  $\text{SrX}$ ,<sup>18</sup> it is much more pronounced for nickel faujasite. This difference is ascribed to the relatively high polarizing power of the nickel ion (ionic radii for  $\text{Ni}^{2+}$ ,  $\text{Ca}^{2+}$ , and  $\text{Sr}^{2+}$  are

(11) W. R. Busing, K. O. Martin, and H. A. Levy, ORFLS, Oak Ridge National Laboratory, Oak Ridge, Tenn., 1962.

(12) D. H. Olson, G. T. Kokotailo, and J. F. Charnell, *J. Colloid Interface Sci.*, in press.

(13) H. P. Hanson and R. F. Pohler, *Acta Crystallogr.*, **21**, 435 (1966).

(14) The site designations used here are those introduced by Pickert, *et al.*<sup>1</sup> SI is in the center of the hexagonal prism; SI' is adjacent to SI and in the sodalite cage; SII' is in the sodalite cage and is adjacent to the supercage six ring; and SII is in the supercage adjacent to SII'.

(15) W. R. Busing, K. O. Martin, and H. A. Levy, ORFFE, Oak Ridge National Laboratory, Oak Ridge, Tenn., 1964.

(16) D. W. J. Cruickshank, D. Pilling, A. Bujosa, F. M. Lovell, and M. R. Truter in "Computing Methods and the Phase Problem in X-Ray Crystal Analysis," R. Pepinsky, J. M. Robertson, and J. C. Speakman, Ed., Pergamon Press Inc., New York, N. Y., 1961, p 32.

(17) W. H. Zachariasen, *Acta Crystallogr.*, **16**, 1139 (1963).

(18) D. H. Olson, Mobil Research and Development Corp., unpublished research.

**Table I:** Final Fractional Coordinates<sup>a</sup> and Estimated Standard Deviations

Atom	Set	$P^b$	$x$	$y$	$z$
Si(Al)	i	1.000	-0.05333 (3)	0.03554 (3)	0.12268 (3)
O(1)	h	1.000	0.10812 (8)	-0.10812 (8)	0.00000
O(2)	g	1.000	-0.00345 (9)	-0.00345 (9)	0.14528 (11)
O(3)	g	1.000	0.18759 (8)	0.18759 (8)	-0.03171 (11)
O(4)	g	1.000	0.16780 (8)	0.16780 (8)	0.31574 (12)
Ni(1)	c	0.660 (6)	0.00000	0.00000	0.00000
Ni(2)	e	0.096 (8)	0.0543 (15)	0.0543 (15)	0.0543 (15)
Ni(3)	e	0.06 (2)	0.2074 (20)	0.2074 (20)	0.2074 (20)
Ni(4)	e	0.199 (4)	0.2334 (2)	0.2334 (2)	0.2334 (2)
O(w1)	e	0.18 (6)	0.081 (5)	0.081 (5)	0.081 (5)
O(w2)	e	0.06 (6)	0.161 (10)	0.161 (10)	0.161 (10)

<sup>a</sup> Origin at  $\bar{3}m$ . <sup>b</sup> Population parameter.

**Table II:** Vibration Tensor Components and Estimated Standard Deviations ( $\text{\AA}^2$ )

Atom	$U_{11}$	$U_{22}$	$U_{33}$	$U_{12}$	$U_{13}$	$U_{23}$
Si(Al)	0.0283 (5)	0.0222 (5)	0.0219 (5)	0.0007 (3)	-0.0022 (3)	-0.0033 (4)
O(1)	0.046 (1)	0.046 (1)	0.044 (2)	-0.004 (2)	-0.008 (2)	-0.008 (2)
O(2)	0.047 (1)	0.047 (1)	0.043 (2)	0.011 (2)	0.000 (1)	0.000 (1)
O(3)	0.046 (1)	0.046 (1)	0.048 (2)	0.009 (2)	-0.004 (1)	-0.004 (1)
O(4)	0.043 (1)	0.043 (1)	0.060 (2)	0.015 (2)	0.004 (1)	0.004 (1)
Ni(1)	0.039 (1)	0.039 (1)	0.039 (1)	0.001 (1)	0.001 (1)	0.001 (1)
Ni(2)	0.348 (51)	0.348 (51)	0.348 (51)	0.281 (50)	0.281 (50)	0.281 (50)
Ni(3)	0.019 <sup>a</sup>					
Ni(4)	0.069 (3)	0.069 (3)	0.069 (3)	0.025 (3)	0.025 (3)	0.025 (3)
O(w1)	0.038 <sup>a</sup>					
O(w2)	0.038 <sup>a</sup>					

<sup>a</sup> Isotropic  $U$ .

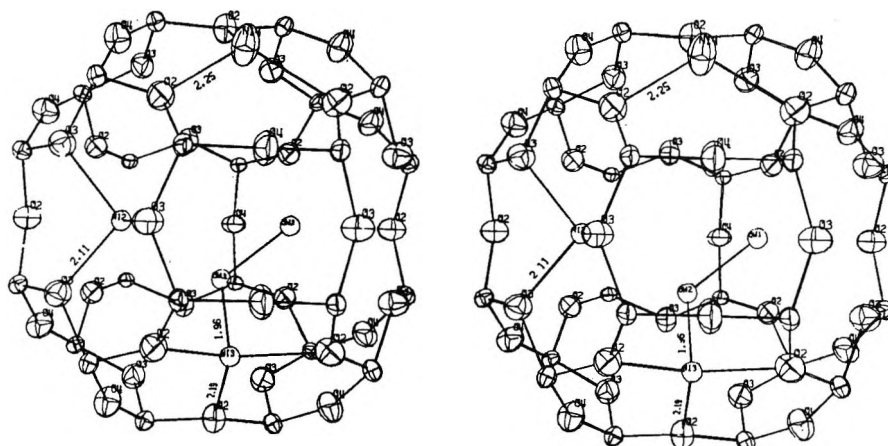


Figure 2. Stereoscopic view of the sodalite cage atom distribution of nickel faujasite. Because of the partial occupancy of the nonframework atom sites, not all symmetry related sites are filled.

0.78, 0.99, and 1.13 $\text{\AA}$ , respectively). Smith, *et al.*, have also found a decrease in regularity upon dehydration of calcium chabazite.<sup>19,20</sup>

One result of the loss of regularity in nickel faujasite can be seen in Figure 2.<sup>21</sup> The large Si(Al)-O(4)-Si(Al) angle, 158.3 $^\circ$ , results in a relatively short O(4)-O(4) distance, 2.96 $\text{\AA}$ , across the sodalite cage four-

membered ring (compare with the 3.52- $\text{\AA}$  distance in hydrated faujasite).<sup>10</sup> Except for interactions be-

(19) J. V. Smith, *Acta Crystallogr.*, **15**, 835 (1962).

(20) J. V. Smith, F. Rinaldi, and L. S. Dent Glasser, *ibid.*, **16**, 45 (1963).

(21) Computer drawn using ORTEP: C. K. Johnson, ORTEP, Oak Ridge National Laboratory, Oak Ridge, Tenn., 1964.

Table III: Observed and Calculated Structure Factors for Nickel Faujasite

H	K	FOBS	FCAL	H	K	FOBS	FCAL	H	K	FOBS	FCAL	H	K	FOBS	FCAL
••••L =	0	••••••		7	1	415	404	21	9	1140	1159	20	4	304	310
4	0	18C6	1649	9	1	279	253	23	9	507	518	22	4	828	848
8	0	1671	1682	11	1	2014	2065	25	9	731	734	24	4	246	144
12	0	3081	3245	13	1	292	279	27	9	126	116	26	4	533	536
16	0	3816	3860	15	1	319	249	11	11	4641	4536	28	4	208	139
20	0	633	670	17	1	2509	2491	13	11	1319	1202	6	6	843	839
24	0	2521	2540	19	1	1696	1772	15	11	871	861	8	6	582	588
28	0	123	118	21	1	1103	1057	17	11	686	668	10	6	663	720
2	2	3407	3417	23	1	1446	1410	19	11	0	42	12	6	947	928
6	2	1231	1202	25	1	260	174	21	11	1922	1966	14	6	2441	2470
10	2	300	274	27	1	154	156	23	11	1968	1979	16	6	713	716
14	2	2080	2100	29	1	166	24	25	11	307	292	18	6	191	51
18	2	267	245	3	3	3226	3147	27	11	704	689	20	6	1651	1664
22	2	1425	1410	5	3	1346	1370	13	13	1512	1490	22	6	907	899
26	2	553	489	7	3	1145	1094	15	13	619	583	24	6	663	647
4	4	2207	2109	9	3	2180	2096	17	13	767	723	26	6	531	518
8	4	3630	3596	11	3	761	772	19	13	419	450	28	6	289	277
12	4	118	83	13	3	552	531	21	13	354	363	8	8	1469	1464
16	4	1909	1948	15	3	920	906	23	13	214	112	10	8	2008	2006
20	4	255	177	17	3	445	439	25	13	613	589	12	8	724	716
24	4	52	65	19	3	290	186	15	15	632	570	14	8	316	238
28	4	504	481	21	3	606	676	17	15	152	107	16	8	716	658
6	6	3605	3613	23	3	398	473	19	15	682	685	18	8	1168	1192
10	6	1173	1185	25	3	937	914	21	15	497	475	20	8	158	188
14	6	278	293	27	3	258	277	23	15	0	103	22	8	1107	1079
18	6	1732	1728	29	3	111	66	25	15	173	218	24	8	235	145
22	6	2080	2068	5	5	257	129	17	17	540	524	26	8	158	15
26	6	772	768	7	5	1324	1318	19	17	0	55	28	8	89	107
8	8	3934	3966	9	5	308	302	21	17	139	219	10	10	237	192
12	8	2115	2174	11	5	1330	1342	23	17	533	497	12	10	278	280
16	8	573	575	13	5	957	976	17	19	0	93	14	10	288	210
20	8	3524	3604	15	5	1032	1041	21	19	61	51	16	10	191	89
24	8	641	700	17	5	961	945	21	21	281	263	18	10	0	62
28	8	999	963	19	5	247	238	••••L =	2	••••••		20	10	1154	1111
10	10	4190	4133	21	5	1572	1560	2	2	1211	1240	22	10	870	863
14	10	1527	1554	23	5	902	854	4	2	242	338	24	10	344	314
18	10	459	385	25	5	157	49	6	2	621	605	26	10	177	149
22	10	3097	3139	27	5	0	95	8	2	2432	2432	12	12	745	769
26	10	298	304	29	5	287	290	10	2	902	960	14	12	1511	1526
12	12	6615	6707	7	7	839	810	12	2	185	216	16	12	290	224
16	12	602	541	9	7	2242	2226	14	2	521	496	18	12	227	247
20	12	659	640	11	7	1262	1263	16	2	864	836	20	12	560	576
24	12	990	1113	13	7	770	798	18	2	1281	1313	22	12	318	362
14	14	499	606	15	7	338	376	20	2	1254	1260	24	12	408	407
18	14	550	585	17	7	331	350	22	2	154	172	26	12	748	752
22	14	567	519	19	7	962	873	24	2	1526	1545	14	14	1243	1240
26	14	1188	1193	21	7	558	594	26	2	611	604	16	14	905	884
16	16	1219	1218	23	7	310	302	28	2	915	922	18	14	0	40
20	16	493	494	25	7	41	91	4	4	89	71	20	14	954	932
24	16	574	542	27	7	824	795	6	4	3259	3187	22	14	698	694
18	18	414	437	9	9	892	840	8	4	743	746	24	14	685	710
22	18	0	36	11	9	0	30	10	4	465	504	26	14	114	83
20	20	245	256	13	9	1601	1595	12	4	1322	1294	16	16	842	859
••••L =	1	••••••		15	9	556	545	14	4	363	327	18	16	577	570
3	1	3634	3583	17	9	892	904	16	4	347	411	20	16	234	265
5	1	1401	1314	19	9	1506	1528	18	4	720	702	22	16	470	495

tween oxygens of the same tetrahedron, 2.96 Å is the shortest oxygen-oxygen distance in the nickel faujasite structure. Such short distances are of interest because they indicate favorable sites for hydrogen bonding. Infrared evidence has established the existence of framework hydroxyls in various cationic forms of synthetic faujasites.<sup>22</sup> Although hydrogen bonding of these OH groups has not been established, framework distortions of the type found here have resulted in oxy-

gen-oxygen distances favorable for such bonding. The next shortest oxygen-oxygen distance, 3.25 Å, is between two O(3)'s of the SI six ring (Figure 3); it results in an unusually small SI port diameter of 0.96 Å (computed assuming a hard-sphere model and a 1.40 Å radius for oxygen). This port size may be compared

(22) C. L. Angell and P. C. Schaffer, *J. Phys. Chem.*, **69**, 3463 (1965).

Table III (Continued)

H	K	FOBS	FCAL	H	K	FOBS	FCAL	H	K	FOBS	FCAL	H	K	FOBS	FCAL
24	16	170	114	15	11	1266	1267	16	8	1320	1331	15	7	379	335
18	18	350	298	17	11	436	412	18	8	0	66	17	7	2837	2859
20	18	482	504	19	11	583	595	20	8	1252	1211	19	7	794	800
22	18	97	97	21	11	1390	1364	22	8	395	344	21	7	275	242
20	20	433	434	23	11	124	77	24	8	0	133	23	7	732	741
****L = 3*****				25	11	812	827	26	8	45	228	25	7	208	35
3	3	989	1027	27	11	213	271	28	8	721	704	27	7	559	538
5	3	3596	3535	13	13	2044	2032	10	10	988	991	9	9	1959	1883
7	3	2172	2048	15	13	489	513	12	10	216	165	11	9	299	300
9	3	430	430	17	13	493	543	14	10	232	198	13	9	1553	1590
11	3	1690	1675	19	13	0	97	16	10	554	549	15	9	1250	1250
13	3	1537	1554	21	13	1226	1201	18	10	231	223	17	9	291	176
15	3	1518	1553	23	13	0	113	20	10	305	299	19	9	647	659
17	3	194	201	25	13	376	367	22	10	312	282	21	9	716	713
19	3	986	978	15	15	846	859	24	10	0	21	23	9	79	141
21	3	1313	1290	17	15	434	357	26	10	404	416	25	9	786	788
23	3	1169	1198	19	15	985	959	12	12	736	747	27	9	354	296
25	3	78	47	21	15	105	197	14	12	16	87	11	11	2318	2325
27	3	807	844	23	15	386	475	16	12	488	486	13	11	462	470
29	3	412	422	25	15	205	177	18	12	670	704	15	11	556	553
5	5	110	119	17	17	194	147	20	12	1041	1008	17	11	1675	1695
7	5	1945	1921	19	17	833	828	22	12	0	5	19	11	155	168
9	5	176	182	21	17	475	484	24	12	148	49	21	11	0	226
11	5	161	134	23	17	237	206	26	12	293	230	23	11	714	681
13	5	477	505	19	19	193	233	14	14	1124	1158	25	11	125	153
15	5	1822	1821	21	19	511	534	16	14	324	324	27	11	986	937
17	5	760	818	****L = 4*****				18	14	1399	1383	13	13	509	525
19	5	1225	1224	4	4	293	283	20	14	151	60	15	13	1816	1772
21	5	105	88	6	4	61	14	22	14	688	733	17	13	848	825
23	5	259	267	8	4	2183	2132	24	14	165	29	19	13	256	282
25	5	924	974	10	4	896	985	16	16	1624	1651	21	13	0	98
27	5	243	208	12	4	2073	2173	18	16	277	207	23	13	543	438
29	5	0	61	14	4	226	174	20	16	1158	1150	25	13	582	574
7	7	282	314	16	4	268	241	22	16	55	61	15	15	695	757
9	7	362	213	18	4	1735	1817	24	16	322	210	17	15	1248	1178
11	7	519	496	20	4	991	973	18	18	543	554	19	15	738	748
13	7	1779	1820	22	4	811	812	20	18	287	281	21	15	554	514
15	7	822	806	24	4	419	441	22	18	568	562	23	15	715	696
17	7	604	590	26	4	57	69	20	20	0	51	25	15	304	311
19	7	1022	1011	28	4	257	269	****L = 5*****				17	17	2454	2407
21	7	827	854	6	6	4095	4059	5	5	7999	7979	19	17	552	579
23	7	1038	1007	8	6	1391	1425	7	5	1253	1343	21	17	59	131
25	7	418	360	10	6	116	59	9	5	2157	2192	23	17	598	573
27	7	653	596	12	6	142	15	11	5	1447	1486	19	19	429	427
9	9	1442	1410	14	6	1364	1370	13	5	1300	1331	21	19	0	7
11	9	2642	2649	16	6	0	160	15	5	889	873	****L = 6*****			
13	9	532	522	18	6	1108	1077	17	5	4356	4459	6	6	5866	5780
15	9	0	24	20	6	239	267	19	5	180	207	8	6	132	41
17	9	1996	2005	22	6	1051	1042	21	5	1086	1097	10	6	509	532
19	9	253	99	24	6	218	141	23	5	0	48	12	6	1001	981
21	9	465	429	26	6	269	184	25	5	643	649	14	6	1333	1370
23	9	821	803	28	6	215	219	27	5	1567	1570	16	6	5668	5905
25	9	165	253	8	8	1279	1245	7	7	2239	2140	18	6	597	582
27	9	568	619	10	8	171	160	9	7	195	226	20	6	617	545
11	11	365	364	12	8	328	248	11	7	900	872	22	6	1292	1306
13	11	1231	1217	14	8	0	119	13	7	1757	1799	24	6	187	22

with the 1.56 Å port diameter computed for hydrated faujasite.<sup>10</sup> In general, it is seen that the framework has undergone considerable modification upon exchange and subsequent dehydration. Moreover, this modification is much more pronounced than might be inferred from the 1% decrease in lattice parameter.

A summary of the nonframework atom distribution is given in Table VII. Assignment of the scattering matter found in nonframework positions is based upon

interatomic distances and electron count. The O(w2) assignment is based upon the 2.0 (2) Å Ni(3)-O(w2) distance, which is acceptable for a nickel-oxygen bond. O(w2) is believed to be derived from residual water. It should be pointed out again that the existence of O(w2) is uncertain because of its low occupancy factor. However, X-ray studies of CaX and SrX<sup>18</sup> dehydrated under similar conditions also show scattering matter in this position, which adds support to the O(w2) assign-

Table III (Continued)

H	K	FOBS	FCAL	H	K	FOBS	FCAL	H	K	FOBS	FCAL	H	K	FOBS	FCAL	H	K	FOBS	FCAL
26	6	567	591	25	7	1114	1157	22	10	810	797	17	17	460	489	21	17	606	610
28	6	2917	2905	27	7	0	75	24	10	151	160	19	17	271	267	19	19	425	517
8	8	435	408	9	9	653	591	26	10	164	232	21	17	646	586	****L = 12*****			
10	8	308	301	11	9	1521	1531	12	12	642	678	19	19	508	488	12	12	2307	2391
12	8	761	802	13	9	155	203	14	12	717	702	21	19	361	396	14	12	360	341
14	8	2333	2313	15	9	1160	1112	16	12	922	920	****L = 10*****				16	12	1333	1303
16	8	593	650	17	9	1477	1427	18	12	507	434	10	10	1197	1084	18	12	76	18
18	8	0	26	19	9	195	47	20	12	336	222	12	10	2371	2460	20	12	476	536
20	8	256	304	21	9	253	201	22	12	0	30	14	10	33	39	22	12	229	247
22	8	206	79	23	9	354	308	24	12	621	667	18	10	549	580	24	12	1064	1115
24	8	63	123	25	9	696	700	26	12	117	103	20	10	616	566	14	14	1459	1527
26	8	1027	1050	27	9	107	166	14	14	182	70	22	10	525	466	16	14	259	155
28	8	319	305	11	11	404	384	16	14	458	464	24	10	419	422	18	14	240	320
10	10	569	517	13	11	478	484	18	14	893	913	26	10	458	411	20	14	72	3
12	10	2247	2233	15	11	1663	1695	20	14	253	233	12	12	1051	1062	22	14	277	180
14	10	415	444	17	11	1230	1193	22	14	699	777	14	12	1046	975	16	16	778	773
16	10	740	759	19	11	0	24	24	14	148	133	16	12	240	175	18	16	237	241
18	10	267	268	21	11	499	539	16	16	988	991	18	12	127	63	20	16	462	463
20	10	862	830	23	11	66	5	18	16	105	92	20	12	270	97	22	16	180	127
22	10	252	222	25	11	351	413	20	16	336	351	22	12	1929	1880	18	18	554	482
24	10	674	644	13	13	0	10	22	16	393	349	24	12	481	426	20	18	389	368
26	10	312	246	15	13	0	76	18	18	608	569	14	14	373	429	****L = 13*****			
12	12	732	711	17	13	230	160	20	18	219	290	16	14	376	399	13	13	1474	1429
14	12	168	110	19	13	299	325	22	18	364	401	18	14	311	334	15	13	C	134
16	12	514	519	21	13	572	567	20	20	273	210	20	14	1153	1190	17	13	1195	1201
18	12	788	744	23	13	156	130	****L = 3*****				22	14	79	15	19	13	627	654
20	12	99	44	25	13	187	246	9	9	504	459	24	14	585	617	21	13	722	685
22	12	959	913	15	15	954	1003	11	9	2008	2024	16	16	363	315	23	13	88	23
24	12	334	274	17	15	476	524	13	9	1646	1653	18	16	381	344	15	15	56	106
26	12	321	338	19	15	472	477	15	9	489	469	20	16	292	224	17	15	361	283
14	14	2482	2617	21	15	202	206	17	9	1154	1167	22	16	600	607	19	15	430	418
16	14	706	671	23	15	625	590	19	9	374	451	18	18	511	471	21	15	145	138
18	14	482	509	17	17	1397	1447	21	9	929	860	20	18	228	129	17	17	C	121
20	14	1226	1231	19	17	440	454	23	9	1077	1072	****L = 11*****				19	17	462	491
22	14	815	778	21	17	216	168	25	9	409	465	11	11	5796	6002	****L = 14*****			
24	14	355	320	23	17	315	292	11	11	991	1040	13	11	899	919	14	14	1052	1033
16	16	560	577	19	19	1435	1476	13	11	571	555	15	11	184	243	16	14	1219	1198
18	16	2092	2059	21	19	0	27	15	11	712	693	17	11	955	926	18	14	542	550
20	16	158	60	****L = 8*****				17	11	576	560	19	11	535	588	20	14	C	88
22	16	934	909	8	8	3540	3593	19	11	399	329	21	11	1679	1647	22	14	1007	1032
24	16	255	221	10	8	189	210	21	11	200	179	23	11	1888	1874	16	16	194	138
18	18	566	489	12	8	3226	3250	23	11	100	108	25	11	318	251	18	16	538	576
20	18	574	508	14	8	260	222	25	11	563	535	13	13	691	625	20	16	170	178
22	18	117	115	16	8	2383	2407	13	13	1086	1076	15	13	0	62	18	18	268	290
20	20	191	189	18	8	927	915	15	13	682	643	17	13	561	530	****L = 15*****			
****L = 7*****				20	8	551	555	17	13	318	301	19	13	903	981	15	15	863	942
7	7	2261	2239	22	8	263	145	19	13	258	176	21	13	0	89	17	15	175	58
9	7	1771	1739	24	8	176	70	21	13	373	370	23	13	891	900	19	15	419	415
11	7	1041	1048	26	8	0	75	23	13	106	49	15	15	551	579	17	17	785	799
13	7	255	276	10	10	2042	2083	25	13	704	727	17	15	784	752	19	17	535	522
15	7	478	456	12	10	221	86	15	15	1000	1058	19	15	604	655	****L = 16*****			
17	7	765	807	14	10	1467	1461	17	15	766	714	21	15	0	7	16	16	2177	2156
19	7	0	106	16	10	441	482	19	15	145	53	23	15	164	158	18	16	283	257
21	7	121	192	18	10	255	308	21	15	440	464	17	17	523	538	****L = 17*****			
23	7	0	86	20	10	191	128	23	15	299	320	19	17	215	207	17	17	2642	2787

ment. Scattering matter at  $x = y = z = 0.081$  (SI') in nickel faujasite gives further support. The corresponding O(w2) scattering matter in CaX and SrX<sup>18</sup> is coordinated to SI' cations in addition to bonding to the SII' cation. However, the small ionic radius of nickel(II) does not allow it to coordinate effectively to both the SII' O(w2) and the three SI' O(3) framework oxygen atoms. Thus it appears that nickel ions take up two site SI' positions, with the site furthest from the framework oxygen atoms (O(w1) scattering matter) being occupied when a residual water oxygen atom occupies site SII'. Assuming O(w1) scattering matter to be nickel(II) ions, the Ni-O(w2) and Ni-O(3) distances are 2.0 (3) and 2.8 (1) Å, respectively; the 2.8-Å

distance implies only weak, long-range interactions between nickel and the three O(3) oxygen atoms. The 3:1 ratio of O(w1):O(w2) electron density is also in agreement with the assignment of O(w1) scattering matter to the nickel ion and the O(w1)-O(w2) interaction to an Ni-O bond. It should be kept in mind that the low occupancy factors for Ni(3), Ni(O(w1)), and O(w2) do not require simultaneous occupancy of these sites. However, without simultaneous occupancy, the existence of scattering matter in these sites is difficult to explain.

The total equivalents of located cations, 48, is 10 short of the 58 equiv of aluminum/unit cell (O(w1) was assumed to be a nickel ion). This difference may be

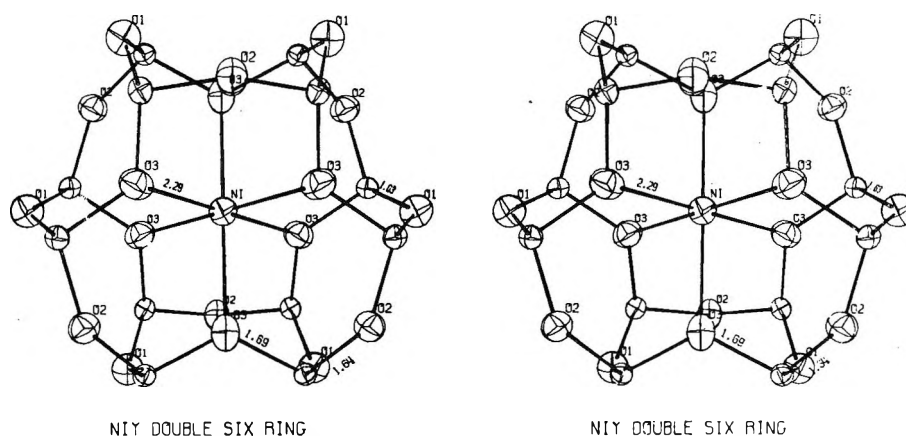


Figure 3. Stereoscopic view of the hexagonal prism atom distribution in nickel faujasite.

**Table IV:** Framework Interatomic Distances and Angles for Nickel Faujasite

Distances, Å		Angles, deg	
Si(Al)-O(1)	1.633 (1)	Si(Al)-O(1)-Si(Al)	129.7 (2)
Si(Al)-O(2)	1.641 (1)	Si(Al)-O(2)-Si(Al)	138.4 (2)
Si(Al)-O(3)	1.695 (2)	Si(Al)-O(3)-Si(Al)	125.1 (2)
Si(Al)-O(4)	1.613 (1)	Si(Al)-O(4)-Si(Al)	158.3 (2)
Av 1.646		Av 137.9	
O(1)-O(2)	2.713 (3)	O(1)-Si(Al)-O(2)	111.9 (1)
O(1)-O(3)	2.654 (3)	O(1)-Si(Al)-O(3)	105.8 (1)
O(1)-O(4)	2.687 (1)	O(1)-Si(Al)-O(4)	111.7 (1)
O(2)-O(3)	2.674 (2)	O(2)-Si(Al)-O(3)	106.6 (1)
O(2)-O(4)	2.643 (2)	O(2)-Si(Al)-O(4)	108.6 (1)
O(3)-O(4)	2.746 (3)	O(3)-Si(Al)-O(4)	112.2 (1)
Av 2.686		Av 109.5	

**Table V:** Nonframework Atom Interatomic Distances and Angles for Nickel Faujasite

	Distances, Å
Ni(1)-O(3)	2.289 (3)
Ni(2)-O(3)	2.12 (3)
Ni(2)-O(2)	2.984 (8)
Ni(3)-O(2)	2.20 (4)
Ni(3)-O(4)	2.98 (4)
Ni(3)-O(w2)	2.0 (2)
Ni(4)-O(2)	2.260 (3)
Ni(4)-O(4)	3.028 (3)
O(w1)-O(w2)	2.0 (3)
	Angles, deg
O(3)-Ni(1)-O(3) (3) <sup>a</sup>	90.4 (1)
O(3)-Ni(1)-O(3) (3̄) <sup>a</sup>	89.6 (1)
O(3)-Ni(2)-O(3) (3) <sup>a</sup>	100.0 (20)
O(2)-Ni(3)-O(w2)	101.0 (20)
O(2)-Ni(3)-O(2) (3) <sup>a</sup>	116.0 (20)
O(2)-Ni(4)-O(2) (3) <sup>a</sup>	111.4 (2)

<sup>a</sup> Denotes symmetry operation applied to the first oxygen atom of the triplet.

**Table VI:** Comparison of the Nickel Faujasite and the Hydrated Faujasite<sup>a</sup> Framework<sup>b</sup>

	Nickel faujasite	Hydrated faujasite
Si(Al)-O, Å	1.646 (0.025)	1.647 (0.005)
O-O, Å	2.686 (0.029)	2.689 (0.020)
∠O-Si(Al)-O, deg	109.5 (2.5)	109.5 (1.2)
∠Si(Al)-O-Si(Al), deg	137.9 (10.5)	141.6 (1.7)

<sup>a</sup> Reference 10. <sup>b</sup> All values are mean values; values in parentheses are the average deviations from the mean.

**Table VII:** Summary of the Nonframework Atom Distribution in Nickel Faujasite

Species <sup>a</sup>	Site	P	No./sodalite cage
Ni(1)	SI	0.66	1.32
Ni(2)	SI'	0.10 <sup>b</sup>	0.40 <sup>b</sup>
Ni(3)	SII'	0.06	0.24
Ni(4)	SII	0.20	0.80
O(w1)(Ni) <sup>c</sup>	SI'	0.18 (0.06)	0.72 (0.24)
O(w2)	SII'	0.06	0.24

<sup>a</sup> Assigned on the basis of internuclear distances and electron count. <sup>b</sup> Unrealistically large thermal parameters for this atom introduce uncertainty in this value. <sup>c</sup> Computed as O<sup>-</sup>, numbers in parentheses give values assuming nickel ion occupancy.

due to hydronium ion exchange that resulted from the acidic exchange solutions. It is also possible that a small amount of framework aluminum was removed during the 2-month contact with the exchange solution. Acid leaching of aluminum is well known in the zeolite clinoptilolite.<sup>23</sup>

In site I, nickel attains near-perfect octahedral coordination with the six O(3) oxygens (Figure 3). Relative to their positions in natural faujasite, in which this

(23) R. M. Barrer and M. B. Makki, *Can. J. Chem.*, **42**, 1481 (1964).

site is vacant, all six O(3) oxygens have shifted 0.50 Å toward Ni(1) and the center of the double six ring—a striking demonstration of the ability of the aluminosilicate framework to adjust to changes in cation position. The Ni(1)–O(3) distance, 2.29 Å, is an average value that includes O(3) oxygen positions for SI sites containing no nickel ions. This fact is illustrated by the O(3) thermal ellipsoids, which are elongated in the Ni–O direction. Finding the nickel ion on both sides of the supercage six ring may be due to the presence of the residual water, O(w2), and the resultant Ni(3)–O(w2) bond formation.

Although the nickel ions prefer SI sites, they are distributed among four, and possibly five, different sites, with no site completely filled. This distribution agrees with conclusions drawn by Barry and Lay.<sup>3</sup> From esr studies of manganese in mixed cation X zeo-

lites, these authors found manganese(II) distributed in a number of sites and concluded that Mn<sup>2+</sup> does not have very strong site preference.

Also, from ir studies of CO adsorbed on various cationic forms of zeolite Y, Angell and Schaffer<sup>4</sup> found that Ni<sup>2+</sup> and Co<sup>2+</sup> ions have no overwhelming preference for site I. Although site I has the highest occupancy in nickel faujasite (66%), it is not fully occupied. In this respect, *i.e.*, a lack of high site preference, transition metal zeolites differ from calcium in zeolite Y, which prefers site SI,<sup>24</sup> and rare earth ions in zeolites X and Y, which prefer SI' sites.<sup>11,25,26</sup>

(24) R. P. Dodge, unpublished research. (See ref 1.)

(25) J. V. Smith, J. M. Bennett, and E. M. Flanigen, *Nature*, **215**, 241 (1967).

(26) D. H. Olson, G. T. Kokotailo, and J. F. Charnell, *ibid.*, **215**, 270 (1967).

## The Dielectric Behavior of Aqueous Solutions of Bovine Serum

### Albumin<sup>1</sup> from Radiowave to Microwave Frequencies

by Edward H. Grant,

*Department of Physics, Queen Elizabeth College, London, England*

Susan E. Keefe,

*Physics Department, Guy's Hospital Medical School, London, England*

and Shiro Takashima

*Electromedical Division, Moore School of Electrical Engineering, University of Pennsylvania, Philadelphia, Pennsylvania (Received February 5, 1968)*

The purpose of the work described in this paper was to investigate the dielectric behavior of the protein bovine serum albumin. The investigation was made to try and solve some of the problems that had arisen from measurements obtained by other workers in the radiowave and microwave frequency range. To do this, measurements were made over as wide a concentration, temperature, and pH range as possible. It was confirmed that there was a subsidiary dispersion in the frequency range 200–2000 MHz, and the possible molecular interpretation of the dispersion is discussed. It can be concluded that this dispersion is probably due to water bound to the protein. By assuming a dielectric mixture theory the variation of the amount of bound water with concentration and pH is estimated.

#### Introduction

From dielectric measurements made by Oncley<sup>2</sup> and Buchanan, Haggis, Hasted, and Robinson<sup>3</sup> on egg albumin at megacycle and microwave frequencies, respectively, it has been suggested that a further dielectric dispersion may occur between the two principal dispersion regions (Figure 1). This extra dispersion ( $\delta$  region) for egg albumin was observed by Grant<sup>4</sup>

and was followed by similar work on BSA.<sup>5</sup> Prior to these studies the first direct observation of this sub-

(1) In this paper, bovine serum albumin will be abbreviated as BSA.

(2) J. L. Oncley, *Chem. Rev.*, **30**, 433 (1942).

(3) T. J. Buchanan, G. H. Haggis, J. B. Hasted, and B. G. Robinson, *Proc. Roy. Soc.*, **A213**, 379 (1952).

(4) E. H. Grant, *Nature*, **196**, 1194 (1962).

(5) E. H. Grant, *J. Mol. Biol.*, **19**, 133 (1966).

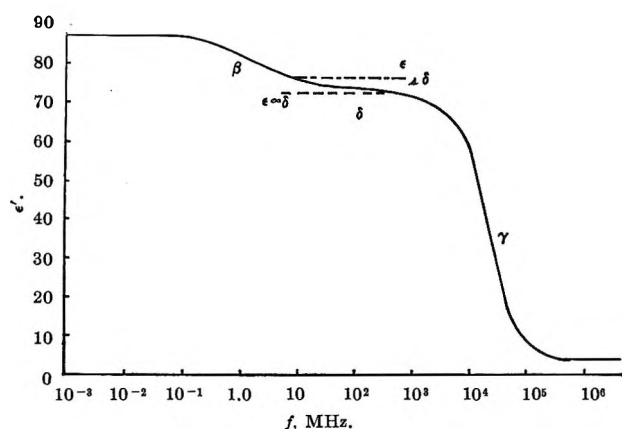


Figure 1. A typical dielectric dispersion curve for a protein solution.

secondary dispersion region for any protein had been made by Schwan<sup>6</sup> for haemoglobin. However, the egg albumin and BSA work suffered by being restricted to one or two concentrations only, and the haemoglobin studies were carried out at one temperature only. Therefore, it was decided to investigate the  $\delta$  region further. The present paper shows results taken over wider frequency and temperature ranges for five different concentrations of BSA and also indicates the effect of a variation in the pH of the solution.

In order to extend the frequency range for the purpose of obtaining a full analysis, the present results were used in conjunction with those taken by Buchanan, *et al.*, at microwave frequencies. This means that results of the dielectric constant ( $\epsilon'$ ) are available for the 7 g/dl solution over the frequency range 50 kHz to 24 GHz and 50 kHz to 2000 MHz for the remainder.

In this paper it will be shown that the results confirm the general propositions of a previous paper<sup>5</sup> but that modifications have been made to the detailed conclusions drawn.

### Experimental Section

**Apparatus.** The measurements were made between 50 and 200 kHz on a low-frequency bridge which was designed by Schwan<sup>7</sup> and between 500 kHz and 200 MHz with a Boonton RX meter, Type 250 A. At 100 kHz and 1 MHz checks were made with 7 g/dl BSA solution using a Wayne Kerr B201 transformer ratio arm bridge, and in both cases agreement was obtained to within 1%. At these frequencies it was not possible to measure the dipolar contribution to  $\epsilon''$  with any accuracy, owing to the high ionic conductivity.

In the frequency range 190–2000 MHz, measurements were carried out using coaxial line apparatus similar to that described by Buchanan and Grant.<sup>8</sup> From the observations made on the standing wave pattern set up in a short-circuited coaxial line cell containing the BSA solution, values of the dielectric constant ( $\epsilon'$ ) and dielectric loss ( $\epsilon''$ ) were calculated. A description

of the modified apparatus will form the basis of a future paper.<sup>9</sup>

**Materials.** The protein used was supplied by the Armour Pharmaceutical Company, Eastbourne, England (Lot No. KBO472), and the figure quoted for the dimer content was 1–5%. This figure is comparatively low for a commercial product but values as low as 1% have been reported<sup>10</sup> for the Armour product. Conductivity water was used as the solvent, and the concentration of the solution was found from the ultraviolet absorption spectrum at 215 and 225 m $\mu$ . The pH of the solution was varied by dialyzing the BSA solution with a buffer solution of tris(hydroxymethylaminomethane) in hydrochloric acid or sodium carbonate and sodium bicarbonate until the required pH was obtained. The pH of the solution was measured on a direct-reading pH meter.

### Results

The dielectric decrement ( $\delta\epsilon'$ ) and the absorption increment ( $\delta\epsilon''$ ) for a protein solution at each temperature and frequency were defined by the equations

$$\Delta\epsilon' = c\delta\epsilon' = \epsilon'_w - \epsilon' \quad (1)$$

and

$$\Delta\epsilon'' = c\delta\epsilon'' = \epsilon''_D - (\epsilon''_w)_{cor} \quad (2)$$

where  $\epsilon'_w$  is the dielectric constant of pure water at the appropriate wavelength and  $c$  is the concentration in grams of protein per 100 ml of solution. The parameter  $(\epsilon''_w)_{cor}$  is the dielectric loss of water, corrected for the volume of the protein molecules, and is given by

$$(\epsilon''_w)_{cor} = \frac{(100 - c\bar{v})}{100} \epsilon''_w \quad (3)$$

where  $\epsilon''_D$  is the total dipolar contribution to the dielectric loss and  $\bar{v}$  is the partial specific volume. In these experiments  $\bar{v}$  was taken to be 0.73 cm<sup>3</sup>/g at 25°.<sup>11</sup> Owing to the high errors in  $\delta\epsilon''$  (discussed previously<sup>12</sup>), all the quantitative deductions about the  $\delta$  dispersion parameters have been made from values of  $\epsilon'$ .

Values of  $\epsilon'$  were obtained for five different concentrations of BSA solution from 7 to 34 g/dl in the temperature range from 2.5 to 25°, and the variation of  $\epsilon'$  with log frequency ( $f$ ) in the two extreme cases is shown in Figures 2 and 3,<sup>13</sup> respectively. The variation

(6) H. P. Schwan, *Advan. Biol. Med. Phys.*, **5**, 191 (1957).

(7) H. P. Schwan and K. Sittel, *Trans. Amer. Inst. Elec. Engrs.*, **72**, 114 (1953).

(8) T. J. Buchanan and E. H. Grant, *Brit. J. Appl. Phys.*, **6**, 65 (1955).

(9) S. E. Keefe and E. H. Grant, to be submitted for publication.

(10) H. A. Peterson and J. F. Foster, *J. Biol. Chem.*, **240**, 2503 (1965).

(11) M. J. Hunter, *J. Phys. Chem.*, **70**, 3285 (1966).

(12) E. H. Grant, *Ann. N. Y. Acad. Sci.*, **125**, 478 (1965).

(13) Individual results will be supplied on request.



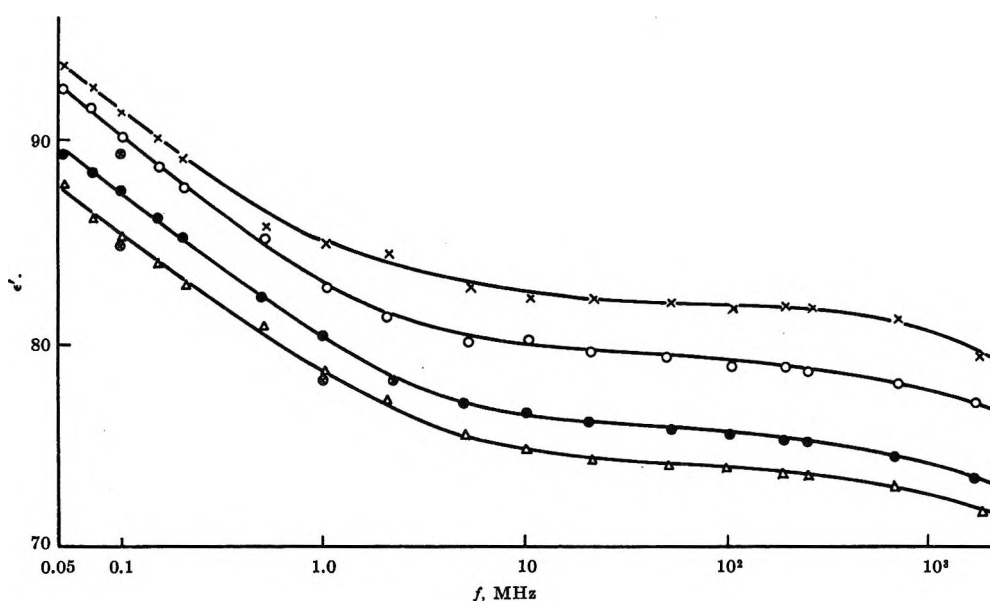


Figure 2. The variation of  $\epsilon'$  with frequency for a 7 g/dl BSA solution (pH 5.07):  $\otimes$ , measured on a B201 bridge at 25 or 10°;  $\times$ , 2.5°;  $\circ$ , 10°;  $\bullet$ , 20°;  $\triangle$ , 25°. (Errors in  $\epsilon'$  ( $\pm 1\%$ ) have been omitted for clarity.)

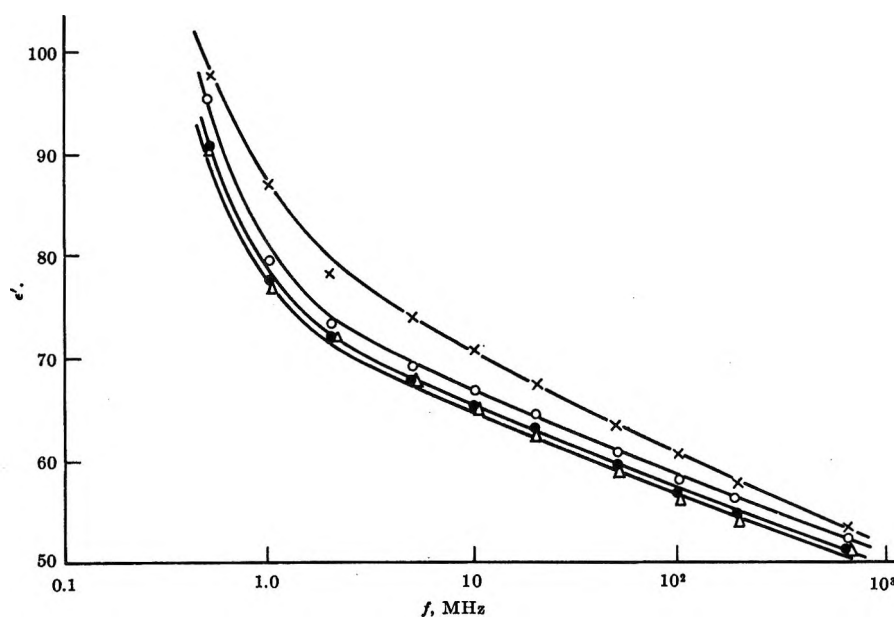


Figure 3. The variation of  $\epsilon'$  with frequency for a 34 g/dl BSA solution (pH 5.07):  $\times$ , 2.5°;  $\circ$ , 10°;  $\bullet$ , 20°;  $\triangle$ , 25°. (Errors in  $\epsilon'$  ( $\pm 1\%$ ) have been omitted for clarity.)

of  $\Delta\epsilon'$  with concentration was found to be similar at all frequencies; Figure 4 shows the shape of the curve at 700 MHz. The dielectric element decreases with temperature at all concentrations, the curves for the 7 g/dl solution being shown in Figure 5.

In order to obtain information on the behavior of solutes in water, it is necessary to calculate from the known values of  $\epsilon'$  and  $\epsilon''$  the following parameters for each dispersion. These are the relaxation wavelength,  $\lambda_s$  (or relaxation frequency,  $f_s$ ); the dielectric constant at the low-frequency end of each dispersion,  $\epsilon_s$ ; the dielectric constant at the high-frequency end

of each dispersion,  $\epsilon_\infty$ ; and  $\alpha$ , which is a measure of the spread of relaxation times. It is convenient to use the wavelength notation ( $\lambda_s$ ) in the microwave region and the frequency notation ( $f_s$ ) in the radiofrequency range.

With a protein solution there are three dispersions and consequently there will be three sets of values of  $\epsilon_s$ ,  $\epsilon_\infty$ ,  $\lambda_s$  (or  $f_s$ ), and  $\alpha$ , so each parameter will be allotted a further subscript  $\beta$ ,  $\delta$ , or  $\gamma$  when referring to an actual dispersion.

These dispersions will now be considered individually, starting with the  $\gamma$  dispersion. The  $\gamma$  dispersion has been studied by Buchanan, *et al.*,<sup>3</sup> who made measure-

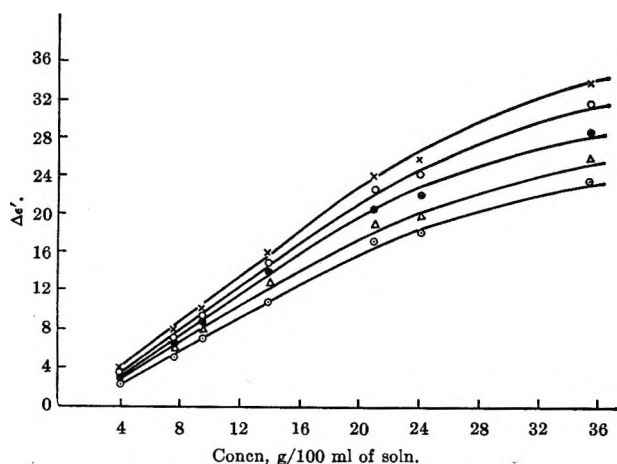


Figure 4. The variation of dielectric decrement with solute concentration at 700 MHz:  $\times$ , 2.5°;  $\circ$ , 10°;  $\bullet$ , 20°;  $\Delta$ , 30°;  $\circ$ , 40°. (Errors in  $\Delta\epsilon'$  ( $\pm 8\%$ ) have been omitted for clarity.)

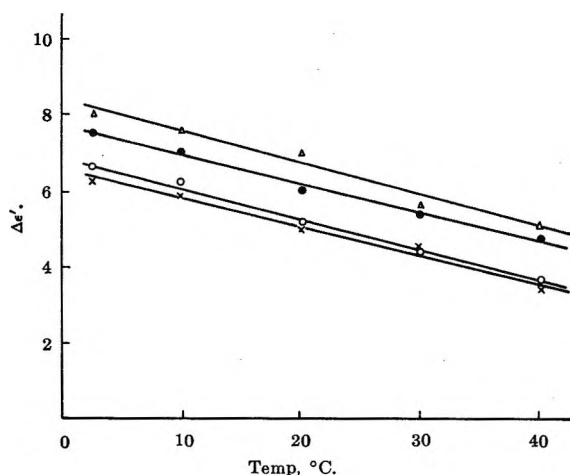


Figure 5. The variation of dielectric decrement with temperature for a 7 g/dl BSA solution:  $\Delta$ , 2000 MHz;  $\bullet$ , 700 MHz;  $\circ$ , 25 MHz;  $\times$ , 190 MHz. (Errors in  $\Delta\epsilon'$  ( $\pm 8\%$ ) have been omitted for clarity.)

ments of  $\epsilon'$  and  $\epsilon''$  at 1.264, 3.175, and 9.22 cm. To obtain all the dielectric parameters a range of values of  $\lambda_s$  and  $\alpha$  was initially calculated for the  $\gamma$  dispersion by using their values of  $\epsilon'$  and  $\epsilon''$  in the equation

$$\frac{\lambda\epsilon''}{\epsilon' - \epsilon_\infty} = \lambda\left(\frac{\lambda_s}{\lambda}\right)^{1-\alpha} \left[ 1 - \left(\frac{\lambda_s}{\lambda}\right)^{1-\alpha} \frac{\alpha\pi}{2} \right] \quad (4)$$

and hence obtaining the most probable value of  $\alpha$  and  $\lambda_s$ . This equation was derived by Grant, *et al.*,<sup>14</sup> assuming the Cole-Cole dielectric theory.<sup>15</sup> It was assumed that  $\epsilon_\infty$  for free water is 4.5,<sup>14</sup> which when corrected for the volume occupied by the protein molecules gave a value of 4.4 for  $\epsilon_{\infty\gamma}$ . Buchanan, *et al.*, concluded that their results were consistent with a dispersion having a single relaxation time and  $\epsilon_\infty = 5.5$ , but subsequently Grant<sup>16</sup> suggested a distribution of relaxation times in conjunction with a lower value of  $\epsilon_\infty$ .

In view of recent work on water<sup>17</sup> which supports a lower value of  $\epsilon_\infty$ , the best interpretation of the results of Buchanan, *et al.*, is to assume that  $\alpha = 0.02$  and  $\epsilon_\infty = 4.4$ . The reason for disagreement with earlier work is probably the overlap of the  $\delta$  dispersion, which would not have been apparent to the earlier workers since the existence of the  $\gamma$  dispersion was not recognized.

$\epsilon_{s\gamma}$  was then calculated from the equation

$$\epsilon_s = \epsilon' + \epsilon'' \cot(1 - \alpha) \frac{\pi}{2} + \frac{2\epsilon''^{1/2}}{(\epsilon' - \epsilon_\infty)[1 - \cos(1 - \alpha)\pi] - \epsilon'' \sin(1 - \alpha)\pi} \quad (5)$$

which has been derived from the Cole-Cole equation by Aaron and Grant.<sup>18</sup>

Assuming a Cole-Cole distribution

$$\epsilon' = \epsilon_\infty + \frac{(\epsilon_s - \epsilon_\infty) \left[ 1 + \left(\frac{f}{f_s}\right)^{1-\alpha} \sin \frac{\alpha\pi}{2} \right]}{1 + 2 \sin \frac{\alpha\pi}{2} \left(\frac{f}{f_s}\right)^{1-\alpha} + \left(\frac{f}{f_s}\right)^{2(1-\alpha)}} \quad (6)$$

it follows that at the point of inflexion of the dispersion curve, *i.e.*, when the frequency of the measurement ( $f$ ) is equal to the relaxation frequency ( $f_s$ ), that

$$\frac{d\epsilon'}{d(\ln f)} = \frac{-(\epsilon_s - \epsilon_\infty)(1 - \alpha)}{2 \left( 1 + \sin \frac{\alpha\pi}{2} \right)} \quad (7)$$

and

$$\epsilon' = \frac{\epsilon_s + \epsilon_\infty}{2} \quad (8)$$

The relatively large experimental errors in  $\epsilon'$  and the range of frequency over which the measurements have been taken make it difficult to extrapolate the  $\beta$  dispersion curve to give an accurate value of  $\epsilon_{s\beta}$ . Therefore, the parameters for the  $\beta$  dispersion were found by substituting the experimental values of  $\epsilon'$  and  $\lambda$  into eq 6 and finding the best fit with the use of eq 7 and 8. By this means  $\epsilon_{\infty\beta}$ ,  $\epsilon_{s\beta}$ ,  $\alpha_\beta$ , and  $f_{s\beta}$  were determined.

This approach should be compared with the previous work of Moser, *et al.*,<sup>19</sup> and Oncley,<sup>2</sup> who analyzed their dispersion curves in terms of a superposition of two single relaxation times rather than a distribution of relaxation times. In the case of Oncley's work, very dilute solutions were employed (thereby minimizing

(14) E. H. Grant, T. J. Buchanan, and H. F. Cook, *J. Chem. Phys.*, **25**, 156 (1957).

(15) K. S. Cole and R. H. Cole, *ibid.*, **9**, 341 (1941).

(16) E. H. Grant, *Phys. Med. Biol.*, **2**, 17 (1957).

(17) E. H. Grant and R. Shack, *Brit. J. Appl. Phys.*, **18**, 1807 (1967).

(18) M. W. Aaron and E. H. Grant, *ibid.*, **18**, 957 (1967).

(19) P. Moser, P. Q. Squire, and C. T. O'Konshi, *J. Phys. Chem.*, **70**, 744 (1966).

the effect of intermolecular attractions), and with Moser, *et al.*, the dielectric measurements were all extrapolated to infinite dilutions and the analyses were carried out with the extrapolated values.

Since in the present case the concentration of macromolecules is high enough to permit molecular interaction, it is not surprising that a satisfactory explanation of the results can be obtained by assuming a distribution of relaxation times, although for small to moderate distribution the Cole-Cole function and the superposition of two Debye functions approximate to any given situation equally well. Therefore, there is no variance between the present and previous methods of analysis, and, of course, in all cases the reliability of the extrapolated values depends upon the correctness of the assumed theory. In Table I the errors quoted in connection with the listed parameters are of experimental origin only and take no cognizance of the fact that it may be possible to fit the parts better by some other (as yet unknown) form of dispersion curve.

Since the parameters for the  $\beta$  and  $\gamma$  dispersions were calculated, this fixes the parameters for the  $\delta$  dispersion, since  $\epsilon_{\infty\beta} = \epsilon_{s\delta}$  and  $\epsilon_{s\gamma} = \epsilon_{\infty\delta}$ , and therefore  $\alpha_\delta$  and  $f_{s\delta}$  can be calculated from eq 7 and 8.

The suggested parameters for a 7 g/dl BSA solution at 25° are shown below in Table I.

**Table I:** Dispersion Parameters for 7 g/dl BSA at 25°

Dispersion region	$\epsilon_0$ ( $\pm 0.5$ )	$\epsilon_\infty$ ( $\pm 0.5$ )	$(f_s)$ , MHz	$\alpha$
$\beta$	88.2	75.9	0.3	$0.3 \pm 0.1$
$\delta$	75.9	71.0	250	$0.7 \pm 0.1$
$\gamma$	71.0	4.4	20,000	$0.02 \pm 0.01$

So far the results given here have all been for solutions having a pH of approximately 5, which is near the isoelectric point. Measurements were also made on solutions of BSA of concentration approximately 7 g/dl at frequencies of 250, 700, and 2000 MHz in the temperature range of 2.5–40° for three other pH values. The decrement values referred to unit concentration for these solutions are shown in Table II. The dielectric behavior of the buffer solution was measured to see if the addition of the salt had any effect on the value of  $\epsilon'$  as compared with pure water. The change was found to be negligible in the case of  $\epsilon'$ , but the dielectric loss was found to be higher due to the increase in conductivity.

## Discussion

The  $\delta$  dispersion region lies between the  $\beta$  and  $\gamma$  regions, which therefore suggests that its molecular origin is connected with the relaxation of molecules having an activation free energy of rotation between that of

**Table II:** Variation of  $\delta\epsilon'$  with pH

Frequency, MHz	Temp., °C	$\delta\epsilon'$ ( $\pm 0.07$ )			
		pH			
		5.07	7.85	8.8	9.8
250	2.5	0.93	0.75	0.73	0.75
	10	0.83	0.87	0.74	0.72
	20	0.70	0.7	0.7	0.58
	30	0.57	0.64	0.71	1.22
	40	0.44	0.52	0.48	1.58
700	2.5	1.05	0.97	0.81	0.94
	10	0.94	0.85	0.88	0.86
	20	0.87	0.85	0.87	0.77
	30	0.77	0.72	0.7	0.7
	40	0.70	0.58	0.52	0.38
2000	2.5	1.2	0.76	0.88	0.03
	10	1.12	0.52	0.93	0.31
	20	1.0	1.04	0.68	0.99
	30	0.78	0.85	0.79	0.68
	40	0.67	0.59	0.65	0.76

the protein and free water. It had been suggested previously by Schwan<sup>6</sup> for haemoglobin and by Grant<sup>12</sup> for egg albumin that the origin of this dispersion was the relaxation of bound water, and this proposal will now be further examined.

The term bound water is taken to mean water bound to the protein molecules by bonds of greater strength than the water-water bond existing in pure water. If the bound-water hypothesis is correct, the quantity of bound water (or water of hydration,  $w$ ) present must accord with a reasonable molecular picture, and, subject to the stated assumptions, this will now be shown to be so by the following analysis.

The estimation of hydration from dielectric results has the disadvantage that a dielectric mixture formula must be chosen, and the uncertainty in the choice of this can lead to some error. In the initial studies of Buchanan, *et al.*,<sup>3</sup> the following equation was used

$$\epsilon' - \epsilon_{\text{water}} = \frac{K\rho}{1 - \rho} (\epsilon_{\text{solute}} - \epsilon') \quad (9)$$

where  $\rho$  is the volume concentration of the solute and  $K$  is a constant depending upon the shape of the solute particle. This expression was based on the equation originally derived by Fricke<sup>20</sup>

$$\frac{\epsilon' - \epsilon_1}{\epsilon' + x\epsilon_1} = \rho \frac{\epsilon_2 - \epsilon_1}{\epsilon_2 + x\epsilon_1} \quad (10)$$

where  $\epsilon_1$  and  $\epsilon_2$  refer to the solvent and solute, respectively, and  $x$  is another constant depending upon particle shape. The value of  $x$  is 2 for a spheroid and decreases for both prolate and oblate ellipsoids. When  $\epsilon_2/\epsilon_1$  is small compared with unity, eq 10 reduces to eq 9 and  $K = (1/x)(1 + x)$ ; otherwise

(20) H. Fricke, *Phys. Rev.*, **24**, 575 (1924).

$$K = [(1 + x)/x] + (\epsilon_2/\epsilon_1)$$

The above approach depends on the assumption that the system under consideration corresponds to a suspension of macroscopic particles in a continuum, and it has been pointed out previously by Grant<sup>5</sup> that there is no good reason why this *a priori* assumption should be made for a protein solution. To take the other extreme, if the dielectric constant of the mixture is related to the components in relation to their volume proportions, then

$$\epsilon' - \epsilon_1 = \rho(\epsilon_2 - \epsilon_1) \quad (11)$$

The interesting point to notice, however, is that provided  $\rho$  is small ( $<0.15$ ) all these equations, eq 9–11, can be written in the form

$$\epsilon' - \epsilon_1 = k\rho(\epsilon_2 - \epsilon_1) \quad (12)$$

where  $k$  would range between 1 and about 1.8 for most protein molecules. (For higher values of  $\rho$  the value of  $k$  becomes increasingly dependent on  $\rho$ .) In the particular case of BSA, recent work<sup>19</sup> has shown that this molecule is a prolate ellipsoid with an axial ratio of 3, from which it follows that the maximum value of  $k$  is 1.6. The minimum value of  $k$  is 1, which corresponds to the case where eq 11 is assumed to hold.

Values of  $k$  less than 1 are not anticipated, since this would mean that  $\epsilon_2 > \epsilon_1$ , which, in turn, would require existence of strongly hydrated particles, with the bound water taking a dielectric constant too high to be consistent with the present analysis. As is clear from Table III a high value for the dielectric constant of the bound water must be coupled with a high value of  $k$ .

**Table III:** Variation of the Hydration and Static Dielectric Constant of Bound Water with  $k$  near the Isoelectric Point (pH 5.07)

$k$	$w$ , g/g of protein	$\epsilon_{sB}$
1.0	0.64	114 ± 15
1.1	0.51	128 ± 20
1.2	0.41	148 ± 25
1.3	0.33	170 ± 35
1.4	0.24	212 ± 50
1.5	0.18	264 ± 75

The purpose of the above discussion is to emphasize the fact that in our view there is no way, at present, of deciding which is the correct mixture formula appropriate to the case of a protein solution, although there is every expectation that it will take the form of eq 12. In the subsequent analysis two representative values of  $k$  will be chosen and the dielectric parameters will be calculated for each case.

Reverting to the symbols defined earlier in the paper, the following may be written

$$100\delta\epsilon' = k[\bar{v}(\epsilon'_w - \epsilon'_p) + w(\epsilon'_w - \epsilon'_B)] \quad (13)$$

where  $w$  is the weight of the bound water per unit weight of protein and  $\epsilon'_p$ ,  $\epsilon'_w$ , and  $\epsilon'_B$  are the permittivities of the protein, free water, and bound water, respectively.

It is also assumed that the contributions of the bound water and protein to  $\epsilon_\infty$  at the high-frequency end of the  $\delta$  dispersion are due to their atomic and electronic polarizations only and are assumed to have values of 4.4 and 4.0, respectively, the precise magnitudes being unimportant. At the low-frequency end of the  $\delta$  dispersion, eq 13 becomes

$$100\delta\epsilon_{s\delta} = k[\bar{v}(\epsilon'_w - 4) + w(\epsilon'_w - \epsilon_{sB})] \quad (14)$$

where  $\epsilon_{sB}$  is the dielectric constant of bound water at frequencies well below its dispersion. A similar equation can be written for  $\delta\epsilon_{\infty\delta}$ ; hence when  $\epsilon_{s\delta}$  and  $\epsilon_{\infty\delta}$  are both known (as in the case of 7 g/dl BSA solution having a pH of 5.07), a range of values of  $w$  and  $\epsilon_{sB}$  at 25° can be found as shown in Table III.

In order to calculate the variation of hydration with pH, these values of  $k$  and  $w$  were then substituted into eq 13, and the value of the dielectric constant of the bound water ( $\epsilon'_B$ ) at a given temperature and frequency was calculated at pH 5.07. It was then assumed that  $\epsilon'_B$  and  $k$  remained constant as the pH changed, and the quantity of bound water was then calculated by substituting different values of  $\delta\epsilon'$ , corresponding to changes in pH and frequency, into eq 13.

In Table IV is shown the variation of  $\epsilon'_B$  at 25° with frequency, and Table V shows the change of  $w$  with pH at this temperature for values of  $k = 1.1$  and 1.3. It is worth remarking that Moser, *et al.*,<sup>19</sup> obtained  $w = 0.64$  for BSA by combining measurements made in the  $\beta$  dispersion with birefringence results. Taking this value in conjunction with the present data gives a value of 114 for the static dielectric constant of bound water corresponding to a  $k$  factor of 1 (Table III).

In order to investigate the variation of  $w$  with concentration, it would be necessary to have the values of

**Table IV:** Variation of  $\epsilon'_B$  with Frequency at 25° for Two Values of  $k^a$

Frequency, MHz	$\epsilon'_B$ ( $\pm 20\%$ )	
	$k$	
	1.1	1.3
$\ll f_{s\delta}$	128	170
250	71.6	95.2
700	42.0	54.2
2000	29.6	38.2
$\gg f_{s\delta}$	4.4	4.4

<sup>a</sup> Relaxation frequency ( $f_{s\delta}$ ) of  $\sim 250$  MHz; distribution parameter ( $\alpha_\delta$ ) of  $\sim 0.6$ .

**Table V:** Variation of the Hydration ( $w$ ) with pH at 25° for Two Values of  $k$  (Calculated from Measurements at Three Frequencies)

Frequency, MHz	$w$ ( $\pm 0.2$ ), g/g of protein							
	$k = 1.1$				$k = 1.3$			
	pH	pH	pH	pH	pH	pH	pH	pH
	5.07 <sup>a</sup>	7.85	8.8	9.8	5.07 <sup>a</sup>	7.85	8.8	9.8
250	0.52	0.8 <sup>b</sup>	...	...	0.32	0.23	0.1	...
700	0.52	0.42	0.45	0.3	0.32	0.20	0.22	...
2000	0.52	0.64	0.25	0.4	0.32	0.44	0.1	0.21

<sup>a</sup> Values of  $w$  at pH 5.07 calculated from  $\epsilon_s - \epsilon_\infty$  values.

<sup>b</sup> Error of  $\pm 0.8$ .

$\epsilon'$  at all concentrations over the complete frequency range 0.05–24,000 MHz. In the absence of any measurements in the  $\gamma$  dispersion region for concentrations other than 7 g/dl, it was only possible to obtain a rough estimate of the variation of  $w$  with concentration, and this was done as follows. The variation of  $\Delta\epsilon'$  with concentration was found to be very similar at all frequencies, and Figure 4 shows the general shape of the curve at 700 MHz. The marked change in the slope at a concentration of about 22 g/dl solution indicates a decrease in  $\delta\epsilon'$  at higher concentrations, but as there was no definite variation with frequency of this change it was difficult to predict any change of  $\epsilon_s - \epsilon_\infty$  with concentration. From eq 7 it can be seen that if  $\alpha$  were to remain constant with concentration, the slope of the  $\epsilon'$  against the  $\log f$  curves at the point  $f = f_s$  for any concentration would be proportional to  $\epsilon_s - \epsilon_\infty$ . Also it can be shown from eq 13 that  $\delta\epsilon_\infty - \delta\epsilon_s$  is proportional to the quantity of bound water ( $w$ ), assuming that  $\epsilon_{sB}$  is constant with concentration.

Values of slope per unit concentration for five different concentrations are tabulated below in Table VI. It can be seen that an abrupt change in  $\epsilon_s - \epsilon_\infty$  occurs at approximately the same concentration as the change in slope in Figure 4, suggesting a sudden increase in the amount of bound water at this concentration (between 21 and 23%). This should be compared with a similar transition observed by Schwan<sup>6</sup> for haemoglobin where the change in slope occurred at around 10%.

The variation of  $w$  with temperature could not be calculated owing to lack of data, but the corresponding curve for  $\Delta\epsilon'$  with temperature is shown in Figure 5.

**Table VI:** The Variation of  $\epsilon_s - \epsilon_\infty$  with Concentration Assuming a Constant Spread Parameter  $\alpha$ 

Concn, g/dl	Slope/ $c \propto (\epsilon_s - \epsilon_\infty)$
7	0.063 $\pm$ 0.007
14	0.065 $\pm$ 0.004
20.5	0.061 $\pm$ 0.003
23	0.126 $\pm$ 0.004
34	0.12 $\pm$ 0.003

The amount of bound water for BSA in solution near its isoelectric point was found to vary from 0.18 to 0.64 g/g of protein, depending on the mixture formula chosen, and this range is in agreement with other workers. Both Fisher<sup>21</sup> and Chatterjee and Chatterjee<sup>22</sup> have summarized the values of  $w$  obtained for BSA by 15 different methods and show that  $w$  lies in the range 0.1–0.6 g/g of protein. This result, taken in conjunction with the present work, reinforces our proposal that the  $\delta$  dispersion is due to the relaxation of bound water.

The values of  $\epsilon'_B$  in Tables III and IV should be compared with Schwan's<sup>23</sup> proposal for the dielectric behavior of water bound to haemoglobin. Schwan found that  $\epsilon'_B$  falls from about 90 to around 5, but the latter value is approached at frequencies as low as 2000 MHz. In our case  $\epsilon_{sB}$  is over 100, and at 2000 MHz the value of  $\epsilon'_B$  is still considerably above the infinite-frequency value. Schwan also remarks that a wider distribution of relaxation times exists for bound water, as compared with free water, and this observation is supported by the present work, assuming that BSA and haemoglobin are comparable cases. The magnitude of the values of  $\epsilon'_B$  indicated in Tables III and IV may appear high for the ordinary water substance, but it should be remembered that the dielectric constant of an associated liquid depends not only on the molecular dipole moment but also on local molecular interaction as well. These are unknown for water bound to BSA and would be expected to be different from the situation existing in pure liquid water. A closer parallel may exist between bound water and ice when the dielectric constant exceeds 130 at  $-66^\circ$ .<sup>24</sup> It is also interesting to notice that Takashima<sup>25</sup> found that the dielectric constant of water bound to protein crystals exceeds 200.

The variation of bound water with the pH of the solution is shown in Table V when no significant trends are observed. As far as we are aware, no previous measurements on the dielectric behavior of protein solutions at different pH values have been carried out at the high-frequency end of the  $\beta$  dispersion.

## Conclusions

The parameters found for the  $\beta$  dispersion agree fairly well with those found by Moser, *et al.*,<sup>19</sup> who made measurements on BSA at 25° between 1 KHz and 10 MHz. They obtained values of 0.17 and 350 KHz for the low-frequency increment and relaxation frequency, respectively, compared with the corresponding present value of 0.14 and 250 KHz. The disagreement in the former parameter is likely to be due to the

(21) H. F. Fisher, *Biochim. Biophys. Acta*, **109**, 544 (1965).

(22) A. Chatterjee and S. N. Chatterjee, *J. Mol. Biol.*, **11**, 432 (1965).

(23) H. P. Schwan, *Ann. N. Y. Acad. Sci.*, **125**, 366 (1965).

(24) R. P. Auty and R. H. Cole, *J. Chem. Phys.*, **20**, 1309 (1952).

(25) S. Takashima, *J. Polym. Sci.*, **62**, 233 (1962).

fact that Moser, *et al.*, used defatted material. In the case of the relaxation frequency, our result refers to a 7 g/dl solution, whereas the previous value was obtained by extrapolating the dielectric parameters to infinite dilution; precise agreement is therefore not to be expected. With regard to the high-frequency decrement, Moser, *et al.*, quote 0.60 as compared with our 0.35, which is probably due to our use of the Cole-Cole function (rather than two Debye functions) as the best representation of the  $\beta$  dispersion. However, there would still appear to be some unresolved difference present which must await further work for explanation; experimentally the region around 10 MHz is one of the most difficult to investigate.

For the  $\gamma$  dispersion it was found that the results were not consistent with a single relaxation time (*i.e.*,  $\alpha = 0$ ) as has been suggested by Buchanan, *et al.*,<sup>3</sup> but were more compatible with a small distribution with  $\alpha = 0.02$ . A large degree of overlap between the  $\delta$  and  $\gamma$  dispersion is also indicated.

The results clearly confirm the existence of the  $\delta$  dispersion and are compatible with the suggestion that it is due to the rotation of the bound water. However, it has been pointed out previously by Schwan<sup>6</sup> that the polar side chains could also relax in this frequency region, and the present measurements cannot be taken to disprove this. Although at the beginning of this re-

search it had been hoped that it would be possible to account unambiguously for the  $\delta$  dispersion in molecular terms, this has not been proved to be the case. Measurements on very pure proteins of known structure will have to be carried out to illuminate the situation further, and future progress will also depend on some theoretical advancement being made on the question of the appropriate mixture formula.

*Acknowledgments.* The authors wish to thank Professor C. B. Allsopp of Guy's Hospital Medical School and Professor H. P. Schwan of the University of Pennsylvania for providing the facilities which enable the experimental work to be carried out. Acknowledgment is also due to Dr. W. L. G. Gent and Mr. F. A. Huthwaite for valuable discussions and technical assistance, respectively. We are also indebted to Mr. G. Pugh of the Borough Polytechnic for advice in connection with the use of the computer. This work formed part of a research program leading to the Ph.D. degree of the University of London for S. E. K., and it is a pleasure to thank the Science Research Council for a research studentship. We also thank the Central Research Fund of London University and the Science Research Council for equipment grants, and we acknowledge the support by Grants NSFGB-855, NIH-HE-01253, and NONR-551-(52).

## Multicomponent Equilibria in Exchange of Substituents between the Dimethylsilicon and Dimethylgermanium Moieties

by Kurt Moedritzer, Leo C. D. Groenweghe, and John R. Van Wazer

Central Research Department, Monsanto Company, St. Louis, Missouri 63166 (Received February 6, 1968)

Scrambling equilibria of the substituents Cl, Br, and I (system I) and Cl, Br, I, and  $\text{OC}_6\text{H}_5$  (system II) between the dimethylsilicon and dimethylgermanium moieties have been studied by quantitative proton nuclear magnetic resonance spectroscopy. The experimental data have been evaluated in terms of sets of the minimum number of equilibrium constants, which in turn have been used to compute theoretical equilibrium distributions. As a result of preferential affinities for silicon *vs.* germanium, certain species do not appear at equilibrium.

Although a few studies by various authors deal with redistribution equilibria involving the exchange of more than two different kinds of substituents on a given central moiety, we believe that there has not been a report prior to this one of the situation where more than two kinds of substituents were scrambled between more

than one kind of polyfunctional moiety. The work reported herein was undertaken as part of a broad study of equilibrium-controlled structural chemistry, and it demonstrates the fact that reactions involving as many as 20 different product species may be treated quantitatively. The goal of the broad study is to be able to

handle in detail any equilibrium-controlled situation on either an *a priori* or an *a posteriori* basis. This paper presents part of the mathematics needed for the quantitative treatment and gives experimental data which will be used in a future theoretical summation aimed at establishing the basis for *a priori* predictions.

Previous studies of simple redistribution<sup>1</sup> equilibria in systems based on either dimethylsilicon or dimethylgermanium as well as competition studies of the exchange of pairs of substituents<sup>2,3</sup> between dimethylsilicon and dimethylgermanium moieties prompted the present investigation of the competition equilibria involving three and four different kinds of substituents between these two moieties. The reason for selecting dimethylsilicon and dimethylgermanium as the central moieties in this work lies in the availability from previous studies of pertinent equilibrium constants which are required for the calculations presented in this paper and which due to inherent reasons could not be determined from the experimental data described herein.

### Experimental Part

**Starting Materials.** The dimethyldihalogermanes<sup>4</sup> and dimethyldibromosilane<sup>5</sup> were prepared according to methods of the literature. Dimethyldiphenoxygermane was made from dimethyldibromogermane, phenol, and triethylamine in benzene (bp 135° at 0.6 mm). Dimethyldichlorosilane was purchased from Alfa Inorganics, Inc., Beverly, Mass., and was redistilled before use.

**Sample Preparation and Data Acquisition.** For the first system studied in this paper (system I) the samples were prepared by sealing various proportions of four of the five components,  $(\text{CH}_3)_2\text{SiCl}_2$ ,  $(\text{CH}_3)_2\text{SiBr}_2$ ,  $(\text{CH}_3)_2\text{GeCl}_2$ ,  $(\text{CH}_3)_2\text{GeBr}_2$ , and  $(\text{CH}_3)_2\text{GeI}_2$ , in 5 mm o.d. nmr tubes and heating at 120°. As seen from the nmr patterns obtained in 1-day intervals, equilibrium was attained in 5.5 days at this temperature. The final equilibrium data were obtained after having held the samples for 14.5 days at this temperature. Samples of the second system of this paper (system II) were studied in a similar manner. They were prepared from various proportions of the four components,  $(\text{CH}_3)_2\text{SiCl}_2$ ,  $(\text{CH}_3)_2\text{SiBr}_2$ ,  $(\text{CH}_3)_2\text{GeI}_2$ , and  $(\text{CH}_3)_2\text{Ge}(\text{OC}_6\text{H}_5)_2$ . Equilibrium was reached in less than 9 days at 120°, with the final equilibrium data having been measured after 17.5 days at this temperature.

Quantitative equilibrium data were obtained from the electronically integrated peak areas of the methyl protons of the dimethylsilicon or dimethylgermanium moieties of the respective compounds at equilibrium using a Varian A-60 spectrometer. Typical nmr spectra are shown in Figure 1, from which it can be seen that, in spite of the complicated nature of the spectral patterns, the individual resonances are well resolved. Weighted-average equilibrium constants<sup>6</sup> were calculated using a computer program for the IBM 7044.

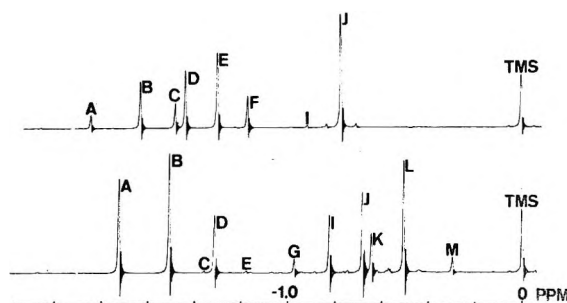


Figure 1. Proton nmr spectra of equilibrated samples: top spectrum, experiment 1 of Table II; bottom spectrum, experiment 1 of Table III. The lettering of the peaks refers to the assignments in Tables II and III.

**Computer Program.** The following discusses the computer logic used to obtain the equilibrium composition of systems in which several substituents undergo exchange between one or more different central moieties. It is possible to write a more efficient program using the presently available convergence techniques. The case of four kinds of monofunctional substituents reorganizing on two kinds of polyfunctional central moieties is described in detail. The logic for other systems (including the exchange of several substituents on a single central moiety) may readily be derived therefrom.

Let Q and M be the two different central moieties on which the substituents T, X, Y, and Z exchange sites. Let, furthermore,  $q_{i,j,k,l}$  and  $m_{i,j,k,l}$  denote the concentration of the compounds  $\text{QT}_i\text{X}_j\text{Y}_k\text{Z}_l$  and  $\text{MT}_i\text{Z}_j\text{Y}_k\text{Z}_l$ , respectively. In the case of the compounds  $\text{QT}_i\text{X}_j\text{Y}_k\text{Z}_l$ ,  $i + j + k + l = \nu$ , and in the case of the compounds  $\text{MT}_i\text{X}_j\text{Y}_k\text{Z}_l$ ,  $i + j + k + l = \mu$ , where  $\nu$  and  $\mu$  are the number of exchangeable sites on the Q and M moieties, respectively. Furthermore, let the stoichiometry be defined by

$$R_1 = [\text{X}]/([\text{Q}] + [\text{M}]) \quad (1)$$

$$R_2 = [\text{Y}]/([\text{Q}] + [\text{M}]) \quad (2)$$

$$R_3 = [\text{Z}]/([\text{Q}] + [\text{M}]) \quad (3)$$

$$R_4 = [\text{Q}]/([\text{Q}] + [\text{M}]) \quad (4)$$

The equilibrium constants used are of the form corresponding to the formation of a compound from two other ones each containing all but one of the substituents of that compound. Such reactions are exemplified by reactions 5 and 6

(1) K. Moedritzer, *Advan. Organometal. Chem.*, **6**, 171 (1968).

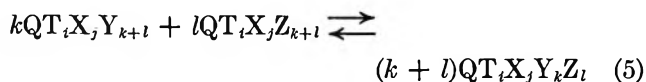
(2) K. Moedritzer and J. R. Van Wazer, *J. Inorg. Nucl. Chem.*, **28**, 957 (1966).

(3) J. R. Van Wazer, K. Moedritzer, and L. C. D. Groenweghe, *J. Organometal. Chem.*, **5**, 420 (1966).

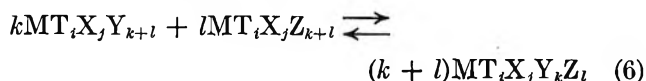
(4) K. Moedritzer, *ibid.*, **6**, 282 (1966).

(5) K. Moedritzer and J. R. Van Wazer, *ibid.*, **6**, 242 (1966).

(6) L. C. D. Groenweghe, J. R. Van Wazer, and A. W. Dickinson, *Anal. Chem.*, **36**, 303 (1964).



where  $i + j + k + l = \nu$  and



where  $i + j + k + l = \mu$ .

The equilibrium constants for these reactions are represented as  ${}^{\text{Q}}K_{i,j,k,l}$  and  ${}^{\text{M}}K_{i,j,k,l}$ , respectively. (This notation does not specify exactly from which two components the formation occurs except when two of the subscripts in the equilibrium constant equal zero in which case the reagents are the two pertinent end-member compounds, *i.e.*, Q compounds having one of the set  $i, j, k, l$  being equal to  $\nu$  or M compounds where one of the set equals  $\mu$ ).

Equilibrium constants between compounds containing different central moieties are chosen to have the form

$$K_{\text{I}} = \frac{m_{\mu,0,0,0}{}^{\nu} q_{0,\nu,0,0}{}^{\mu}}{m_{0,\mu,0,0}{}^{\nu} q_{\nu,0,0,0}{}^{\mu}} \quad (7)$$

$$K_{\text{II}} = \frac{m_{\mu,0,0,0}{}^{\nu} q_{0,0,\nu,0}{}^{\mu}}{m_{0,0,\mu,0}{}^{\nu} q_{\nu,0,0,0}{}^{\mu}} \quad (8)$$

$$K_{\text{III}} = \frac{m_{\mu,0,0,0}{}^{\nu} q_{0,0,0,\nu}{}^{\mu}}{m_{0,0,0,\mu}{}^{\nu} q_{\nu,0,0,0}{}^{\mu}} \quad (9)$$

The iterative computer procedure consists of a Fibonacci<sup>7,8</sup> search method on the natural logarithm of the ratios of the end-member molecules,  $\tau_1 = q_{0,\nu,0,0}/q_{\nu,0,0,0}$ ;  $\tau_2 = q_{0,0,\nu,0}/q_{\nu,0,0,0}$ ; and  $\tau_3 = q_{0,0,0,\nu}/q_{\nu,0,0,0}$ , which are allowed to vary between  $-88$  and  $+88$  to accommodate the IBM 7044 computer overflow limitations. The first Fibonacci value in this range is taken for  $\ln \tau_1$ ,  $\ln \tau_2$ , and  $\ln \tau_3$ , from which the ratios of the corresponding end members containing the other central moiety, M, are obtained

$$\ln \tau_1' = \ln \frac{m_{0,\mu,0,0}}{m_{\mu,0,0,0}} = \frac{\mu \ln \tau_1 - \ln K_{\text{I}}}{\nu} \quad (10)$$

The remaining ratios of end members may readily be calculated; *e.g.*

$$\ln \frac{q_{0,\nu,0,0}}{q_{0,0,\nu,0}} = \ln \tau_1 - \ln \tau_2 \quad (11)$$

Setting  $q_{\nu,0,0,0} = m_{\mu,0,0,0} = 1$ ,  $q_{0,\nu,0,0}$  and  $m_{0,\mu,0,0}$  are calculated from  $\tau_1$  and  $\tau_1'$ , respectively, and the compounds with two different substituents are obtained as exemplified for  $q_{i,j,0,0}$  where  $i + j = \nu$

$$\ln q_{i,j,0,0} = \ln q_{i+j,0,0,0} + \frac{j \ln \tau_1 + \ln {}^{\text{Q}}K_{i,j,0,0}}{i+j} \quad (12)$$

The concentrations of all the other compounds can be calculated in a similar fashion. All concentrations are normalized to sum to unity and to satisfy the param-

eter  $R_1 = [Q]/([Q] + [M])$  by adjusting the starting values of  $q_{\nu,0,0,0}$  and  $m_{\mu,0,0,0}$ . Then the calculated values of  $R_1$ ,  $R_2$ , and  $R_3$  represented by  $R_1^0$ ,  $R_2^0$ , and  $R_3^0$ , respectively, may be obtained.

When  $R_3^0$  turns out to be larger or smaller than  $R_3$ ,  $\ln \tau_3$  is increased or decreased, respectively, to the next Fibonacci value in the series, and all concentrations involving the substituent Z are reevaluated to obtain a new  $R_3^0$ , which process is repeated until a satisfactory agreement between  $R_3$  and  $R_3^0$  is obtained. Then  $\ln \tau_2$  is altered in a similar fashion to adjust for  $R_2^0$ , and the search on  $\ln \tau_3$  is started all over again. When  $R_2$  and  $R_3$  are satisfactorily close to  $R_2^0$  and  $R_3^0$ ,  $\ln \tau_1$  is adjusted and  $\ln \tau_2$  and  $\ln \tau_3$  are searched as above, which is repeated until all three composition parameters,  $R_1^0$ ,  $R_2^0$ , and  $R_3^0$ , reach the desired values at which time an acceptable solution has been obtained.

Although it has not been proven that this procedure should always lead to the proper solution, *i.e.*, that  $R_1^0$ ,  $R_2^0$ , and  $R_3^0$  each vary monotonically with  $\tau_1$ ,  $\tau_2$ , and  $\tau_3$ , respectively, the program has never failed to do so in the many cases tested.

The constant

$${}^{\text{Q}}K_{i,j,k,l} = \frac{q_{i,j,k,l}{}^{k+l}}{q_{i,j,k+l,0}{}^k q_{i,j,0,k+l}{}^l} \quad (13)$$

may be defined from the constants of the form

$${}^{\text{Q}}K'_{i,j,k,l} = \frac{q_{i,j,k-1,l+1} q_{i,j,k+1,l-1}}{q_{i,j,k,l}{}^2} \quad (14)$$

by the relationship

$${}^{\text{Q}}K_{i,j,k,l} = \prod_{m=1}^k {}^{\text{Q}}K'_{i,j,m,k+l-m}{}^{-m} \prod_{m=1}^{l-1} {}^{\text{Q}}K'_{i,j,k+m,l-m}{}^{-k(l-m)} \quad (15)$$

Using the usual experimental data, the primed constants may be calculated with much higher accuracy than the unprimed ones, and the unprimed constants calculated therefrom thus have a smaller experimental error. Therefore, the first step in the computer program is to apply eq 15.

## Results and Conclusions

*Three-Substituent System.* Scrambling involving three kinds of monofunctional substituents on a single difunctional central moiety results<sup>9</sup> at equilibrium in the presence of no more than six compounds, three containing two like substituents and three containing two different substituents. A quantitative description of all equilibria for the central moiety being  $(\text{CH}_3)_2\text{Ge}$

(7) R. E. Billman and S. E. Deyfrus, "Applied Dynamic Programming," Princeton University Press, Princeton, N. J., 1962, p 152.

(8) J. Kiefer, *Proc. Amer. Math. Soc.*, **4**, 502 (1953).

(9) K. Moedritzer, and J. R. Van Wazer, submitted for publication in *J. Chem. Soc.*



Table I: Equilibrium Constants<sup>a</sup>

	System I <sup>b</sup>		System II <sup>c</sup>	
	Q = (CH <sub>3</sub> ) <sub>2</sub> Si (at 120°)	Q = (CH <sub>3</sub> ) <sub>2</sub> Ge (at 35°)	Q = (CH <sub>3</sub> ) <sub>2</sub> Si (at 120°)	Q = (CH <sub>3</sub> ) <sub>2</sub> Ge (at 35°)
$K_1 = [\text{QCl}_2][\text{QBr}_2]/[\text{QBrCl}]^2$	0.31 ± 0.02	0.26 ± 0.01	0.30 ± 0.02	0.29 ± 0.07
$K_2 = [\text{QCl}_2][\text{QI}_2]/[\text{QClI}]^2$	(0.40) <sup>d</sup>	0.58 ± 0.05	(0.40) <sup>d</sup>	(0.67) <sup>e</sup>
$K_3 = [\text{QBr}_2][\text{QI}_2]/[\text{QBrI}]^2$	(0.45) <sup>e</sup>	0.31 ± 0.02	(0.45) <sup>e</sup>	0.33 ± 0.02
$K_4 = [\text{QCl}_2][\text{Q(OPh)}_2]/[\text{QCl(OPh)}]^2$	...	...	0.11 ± 0.01	(0.24) <sup>f</sup>
$K_5 = [\text{QBr}_2][\text{Q(OPh)}_2]/[\text{QBr(OPh)}]^2$	...	...	0.16 ± 0.04	(0.15) <sup>f</sup>
$K_6 = [\text{QI}_2][\text{Q(OPh)}_2]/[\text{QI(OPh)}]^2$	...	...	(0.12) <sup>g</sup>	(1.33) <sup>f</sup>
			System I (at 120°)	System II (at 120°)
$K_{\text{I}} = [\text{Me}_2\text{SiBr}_2][\text{Me}_2\text{GeCl}_2]/[\text{Me}_2\text{SiCl}_2][\text{Me}_2\text{GeBr}_2]$			(2.9 × 10 <sup>-4</sup> ) <sup>g</sup>	(2.9 × 10 <sup>-4</sup> ) <sup>g</sup>
$K_{\text{II}} = [\text{Me}_2\text{SiBr}_2][\text{Me}_2\text{GeI}_2]/[\text{Me}_2\text{SiI}_2][\text{Me}_2\text{GeBr}_2]$			(5.0 × 10 <sup>3</sup> ) <sup>g</sup>	(5.0 × 10 <sup>3</sup> ) <sup>g</sup>
$K_{\text{III}} = [\text{Me}_2\text{SiBr}_2][\text{Me}_2\text{Ge(OPh)}_2]/[\text{Me}_2\text{Si(OPh)}_2][\text{Me}_2\text{GeBr}_2]$			...	(6.6 × 10 <sup>-7</sup> ) <sup>h</sup>

<sup>a</sup> Weighted-average values and their standard errors. The constants with the corresponding standard errors given were determined from the experimental equilibrium data; the others listed in parentheses are literature values which were used in the computer calculations. <sup>b</sup> Dealing with the exchange of Cl, Br, and I between (CH<sub>3</sub>)<sub>2</sub>Si and (CH<sub>3</sub>)<sub>2</sub>Ge. <sup>c</sup> Dealing with the exchange of Cl, Br, I, and OPh between (CH<sub>3</sub>)<sub>2</sub>Si and (CH<sub>3</sub>)<sub>2</sub>Ge. <sup>d</sup> Reference 1. <sup>e</sup> Reference 2. <sup>f</sup> From a study of the equilibrium in the exchange of Cl, Br, I, and OPh on (CH<sub>3</sub>)<sub>2</sub>Ge. <sup>g</sup> Estimated. <sup>h</sup> Unpublished results.

and the substituents Cl, Br, and I is given by the three equilibrium constants of the form of  $K_1$ ,  $K_2$ , and  $K_3$  in Table I. In addition to these, equilibria involving compounds having the same set of exchangeable substituents but a central moiety different from the first one will be controlled by a similar set of three constants. Thus for the second central moiety, (CH<sub>3</sub>)<sub>2</sub>Si, and the same set of exchangeable substituents, an additional set of constants of the form of  $K_1$ ,  $K_2$ , and  $K_3$  are needed for quantitative characterization of all equilibria involving only this moiety.

The sorting of exchangeable substituents between two kinds of central moieties generally is expressed in terms of intersystem equilibrium constants involving pairs of exchangeable substituents. Since there are three different kinds of exchangeable substituents in the present system, one could write three intersystem equilibrium constants dealing with the sorting of Cl vs. Br, Br vs. I, and Cl vs. I between the two central moieties. However, two such constants of the form of  $K_{\text{I}}$  and  $K_{\text{II}}$  in Table I are sufficient, since the third constant involving the sorting of Cl vs. I may be calculated from the former two.

Thus the 12 possible different compounds expected at equilibrium are determined by a total of 8 equilibrium constants. The experimental data in Table II show, however, that of these 12 expected species, only 9 are seen at equilibrium in the mixtures studied. The absence of (CH<sub>3</sub>)<sub>2</sub>SiI<sub>2</sub>, (CH<sub>3</sub>)<sub>2</sub>SiBrI, and (CH<sub>3</sub>)<sub>2</sub>SiClI at equilibrium is a result of the nonrandomness of the intersystem equilibrium constants  $K_{\text{I}}$  and  $K_{\text{II}}$  in Table I—a situation which favors a distribution of the low atomic weight halogens on silicon and of the high atomic weight halogens on germanium. To some extent, this depends also on the over-all composition.

Owing to the absence at equilibrium of certain species, reliable values for all eight equilibrium constants could not be determined. As seen in Table I, these are  $K_2$  and  $K_3$  for the silicon part of the equilibria and the intersystem constants  $K_{\text{I}}$  and  $K_{\text{II}}$ . Therefore, when utilizing the computer program for the calculation of the theoretical equilibrium-distribution data corresponding to the experimental composition parameters  $R_1$ ,  $R_2$ ,  $R_3$ , and  $R_{\text{I}}$  from the minimum-number set of equilibrium constants, the values for  $K_2$  and  $K_3$  (for the silicon part) and  $K_{\text{I}}$  and  $K_{\text{II}}$  were obtained from previous separate studies.<sup>1,2</sup> These values are listed in parentheses in Table I.

Good agreement is observed in Table II for the experimental and theoretical equilibrium concentrations as well as for all of the  $R$  values calculated from the ingredients of the mixture and as obtained from the experimental data based on the assignments of Table II. The observed proton nmr chemical shifts of the compounds seen at equilibrium are also listed in Table II. The six experiments shown in this table correspond to different proportions of the reagents, with the resulting stoichiometry for each experiment being defined by composition parameters (mole ratios) given at the bottom of the table.

*Four-Substituent System.* A similar treatment of the scrambling equilibria of the four exchangeable substituents Cl, Br, I, and OC<sub>6</sub>H<sub>5</sub> on the dimethylgermanium moiety leads to a maximum of four species containing like substituents and six species containing mixed substituents with the equilibria in this system determined by the six equilibrium constants of the form of  $K_1$  to  $K_6$  in Table I. Analogously, the presence of dimethylsilicon moieties in the equilibria gives the ten corresponding silicon compounds, which are determined

**Table II:** Experimental and Calculated Equilibrium Data at 120° (in Mole Percentages) for the System Involving the Exchange of Cl, Br, and I on the (CH<sub>3</sub>)<sub>2</sub>Si and (CH<sub>3</sub>)<sub>2</sub>Ge Moieties

Signal	Chemical shift <sup>a</sup>	Assignment	Experiment no.					
			1	2	3	4	5	6
A	-1.85	(CH <sub>3</sub> ) <sub>2</sub> GeI <sub>2</sub>	3.3 <sup>b</sup> (3.4) <sup>c</sup>	9.6 (9.3)	9.8 (10.0)	5.3 (5.9)	9.2 (9.0)	2.8 (2.7)
B	-1.63	(CH <sub>3</sub> ) <sub>2</sub> GeBrI	12.3 (12.5)	22.8 (22.7)	15.5 (16.8)	10.0 (10.1)	15.6 (15.9)	9.6 (9.4)
C	-1.48	(CH <sub>3</sub> ) <sub>2</sub> GeClI	7.4 (6.6)	0.9 (0.4)	6.6 (5.5)	11.2 (10.8)	7.7 (6.9)	10.7 (10.2)
	...	(CH <sub>3</sub> ) <sub>2</sub> SiI <sub>2</sub>	... (0.0)	... (0.0)	... (0.0)	... (0.0)	... (0.0)	... (0.0)
D	-1.44	(CH <sub>3</sub> ) <sub>2</sub> GeBr <sub>2</sub>	13.6 (14.4)	17.9 (17.3)	8.2 (8.9)	4.5 (5.5)	8.2 (8.7)	10.1 (10.2)
E	-1.30	(CH <sub>3</sub> ) <sub>2</sub> GeBrCl	20.8 (20.1)	1.2 (0.8)	8.4 (7.7)	16.1 (15.6)	10.3 (10.1)	30.1 (29.3)
	...	(CH <sub>3</sub> ) <sub>2</sub> SiBrI	... (0.0)	... (0.6)	... (0.0)	... (0.0)	... (0.0)	... (0.0)
F	-1.17	(CH <sub>3</sub> ) <sub>2</sub> GeCl <sub>2</sub>	8.7 (7.4)	... (0.0)	3.4 (1.8)	12.9 (11.7)	4.2 (3.0)	22.7 (22.1)
	...	(CH <sub>3</sub> ) <sub>2</sub> SiClI	... (0.1)	... (1.0)	... (0.2)	... (0.1)	... (0.1)	... (0.0)
G	-1.06	(CH <sub>3</sub> ) <sub>2</sub> SiBr <sub>2</sub>	... (0.0)	9.9 (9.2)	0.1 (0.1)	... (0.0)	... (0.0)	... (0.0)
I	-0.91	(CH <sub>3</sub> ) <sub>2</sub> SiBrCl	1.9 (1.4)	22.2 (22.1)	4.5 (3.1)	1.2 (0.8)	3.0 (2.3)	0.3 (0.3)
J	-0.76	(CH <sub>3</sub> ) <sub>2</sub> SiCl <sub>2</sub>	32.1 (34.2)	15.7 (16.7)	43.7 (46.0)	38.9 (39.5)	41.7 (44.0)	13.8 (15.7)

Composition parameter	Experiment no.					
	1	2	3	4	5	6
R <sub>1</sub> ≡ [Cl]/([Si] + [Ge])	1.113 <sup>d</sup> (1.117) <sup>e</sup>	0.576 (0.557)	1.120 (1.137)	1.297 (1.321)	1.134 (1.128)	1.155 (1.141)
R <sub>2</sub> ≡ [Br]/([Si] + [Ge])	0.628 <sup>d</sup> (0.622) <sup>e</sup>	0.991 (1.018)	0.456 (0.449)	0.376 (0.363)	0.457 (0.453)	0.595 (0.602)
R <sub>3</sub> ≡ [I]/([Si] + [Ge])	0.259 <sup>d</sup> (0.263) <sup>e</sup>	0.433 (0.429)	0.424 (0.417)	0.327 (0.316)	0.409 (0.417)	0.251 (0.259)
R <sub>t</sub> ≡ [Si]/([Si] + [Ge])	0.357 <sup>d</sup> (0.340) <sup>e</sup>	0.496 (0.478)	0.494 (0.483)	0.404 (0.401)	0.464 (0.447)	0.161 (0.141)

<sup>a</sup> In parts per million relative to internal tetramethylsilane as measured in experiment 3. <sup>b</sup> From the nmr peak areas. <sup>c</sup> Calculated from the constants for system I in Table I and for *R* values calculated from the ingredients. <sup>d</sup> From the ingredients of the mixture. <sup>e</sup> Calculated from the experimental nmr data.

by another set of six equilibrium constants of the form of  $K_1$ – $K_6$  for silicon. Relating the sorting of the four exchangeable substituents between dimethylsilicon and dimethylgermanium are six intersystem constants, one for each different pair of substituents. Of these, however, only three are independent ones, from which the other three may be calculated. We selected the constants represented by  $K_I$ ,  $K_{II}$ , and  $K_{III}$  in Table I as the three independent ones. Thus at equilibrium in this system, there may be as many as 20 different species, the relative concentrations of which are determined by the 15 equilibrium constants of Table I.

Again, only 5 of the 15 equilibrium constants in Table I (system II) could be determined from the experimental data in Table III, owing to the high degree of non-randomness in the sorting of substituents between dimethylsilicon and dimethylgermanium. Therefore, the theoretical mole percentage concentrations listed in parentheses in Table III were calculated using previously determined values for the required additional ten equilibrium constants which could not be obtained from the present experimental data. Also for this system at equilibrium, good agreement between experimental and calculated concentrations is observed.

As seen from the experimental data in Table III, the distribution of the substituents between the silicon and germanium moieties is similar to the first system discussed in this paper. The low atomic weight halogens favor the dimethylsilicon moieties at equilibrium, and the high atomic weight halogens favor the dimethylgermanium moieties, with the phenoxy groups favoring

the dimethylsilicon moiety. As a result of this preference, species containing Si–I bonds do not appear at equilibrium, *e.g.*, (CH<sub>3</sub>)<sub>2</sub>SiI<sub>2</sub>, (CH<sub>3</sub>)<sub>2</sub>SiBrI, (CH<sub>3</sub>)<sub>2</sub>SiClI, and (CH<sub>3</sub>)<sub>2</sub>SiI(OC<sub>6</sub>H<sub>5</sub>). Similarly, compounds having Ge–O bonds are not favored at equilibrium, *e.g.*, (CH<sub>3</sub>)<sub>2</sub>Ge(OC<sub>6</sub>H<sub>5</sub>)<sub>2</sub>, (CH<sub>3</sub>)<sub>2</sub>GeCl(OC<sub>6</sub>H<sub>5</sub>), (CH<sub>3</sub>)<sub>2</sub>GeBr(OC<sub>6</sub>H<sub>5</sub>), and (CH<sub>3</sub>)<sub>2</sub>GeI(OC<sub>6</sub>H<sub>5</sub>). Also (CH<sub>3</sub>)<sub>2</sub>GeCl<sub>2</sub> at equilibrium appears in only small amounts.

## Discussion

The rates of equilibration for analogous germanium compounds generally are much faster than for silicon compounds. This means that during the equilibration process the germanium species in the systems described in this paper are at equilibrium at all times. The rate-determining steps are substitutions on silicon, processes which have been found previously to be quite slow, particularly the reactions involving phenoxy groups.<sup>10</sup> Therefore, it appears that of the equilibrium constants in Table I the ones involving germanium moieties only correspond to the temperature of the nmr probe, since upon quenching of the samples to room temperature, the germanium species will attain the equilibrium corresponding to that temperature. The transfer of substituents from germanium to silicon and *vice versa* generally has been found to be relatively slow at room temperature.<sup>11</sup> This means that, upon quenching and

(10) K. Moedritzer and J. R. Van Wazer, *J. Inorg. Nucl. Chem.*, **29**, 1571 (1967).

(11) K. Moedritzer and J. R. Van Wazer, *Inorg. Chem.*, **5**, 547 (1966).

**Table III:** Experimental and Calculated Equilibrium Data (in Mole Percentages) for the System Involving the Exchange of Cl, Br, I, and OC<sub>6</sub>H<sub>5</sub> on the (CH<sub>3</sub>)<sub>2</sub>Si and (CH<sub>3</sub>)<sub>2</sub>Ge Moieties

Signal	Chemical shift <sup>a</sup>	Assignment	Experiment no.				
			1	2	3	4	5
A	-1.79	(CH <sub>3</sub> ) <sub>2</sub> GeI <sub>2</sub>	15.6 <sup>b</sup> (15.8) <sup>c</sup>	10.4 (10.9)	24.3 (23.5)	25.1 (24.0)	8.5 (8.8)
B	-1.57	(CH <sub>3</sub> ) <sub>2</sub> GeBrI	19.8 (18.7)	13.5 (12.6)	18.5 (16.5)	22.8 (21.5)	14.3 (14.0)
	...	(CH <sub>3</sub> ) <sub>2</sub> SiI <sub>2</sub>	... (0.0)	... (0.0)	... (0.0)	... (0.0)	... (0.0)
C	-1.43	(CH <sub>3</sub> ) <sub>2</sub> GeClI	0.9 (0.5)	0.3 (0.2)	0.3 (0.1)	4.4 (3.5)	6.0 (4.9)
D	-1.38	(CH <sub>3</sub> ) <sub>2</sub> GeBr <sub>2</sub>	8.4 (7.3)	5.7 (4.8)	4.7 (3.8)	7.0 (6.4)	7.8 (7.5)
	...	(CH <sub>3</sub> ) <sub>2</sub> SiBrI	... (0.1)	... (0.3)	... (0.6)	... (0.0)	... (0.0)
E	-1.25	(CH <sub>3</sub> ) <sub>2</sub> GeBrCl	0.8 (0.5)	1.4 (0.2)	1.0 (0.1)	3.2 (2.7)	8.7 (6.8)
	...	(CH <sub>3</sub> ) <sub>2</sub> GeI(OC <sub>6</sub> H <sub>5</sub> )	... (0.0)	... (0.0)	... (0.0)	... (0.0)	... (0.0)
F	-1.11	(CH <sub>3</sub> ) <sub>2</sub> GeCl <sub>2</sub>	... (0.0)	... (0.0)	... (0.0)	0.4 (0.3)	2.6 (1.8)
	...	(CH <sub>3</sub> ) <sub>2</sub> SiClI	... (0.2)	... (0.4)	... (0.5)	... (0.0)	... (0.0)
	...	(CH <sub>3</sub> ) <sub>2</sub> GeBr(OC <sub>6</sub> H <sub>5</sub> )	... (0.0)	... (0.0)	... (0.0)	... (0.2)	... (0.3)
G	-1.02	(CH <sub>3</sub> ) <sub>2</sub> SiBr <sub>2</sub>	2.1 (2.6)	8.1 (8.1)	10.5 (11.4)	... (0.0)	... (0.0)
H	-0.90	(CH <sub>3</sub> ) <sub>2</sub> GeCl(OC <sub>6</sub> H <sub>5</sub> )	... (0.0)	... (0.0)	... (0.0)	0.8 (0.1)	0.5 (0.2)
	...	(CH <sub>3</sub> ) <sub>2</sub> SiI(OC <sub>6</sub> H <sub>5</sub> )	... (0.2)	... (0.2)	... (0.4)	... (0.0)	... (0.0)
I	-0.87	(CH <sub>3</sub> ) <sub>2</sub> SiBrCl	10.1 (10.5)	23.3 (22.5)	15.2 (15.6)	... (0.8)	... (0.8)
J	-0.72	(CH <sub>3</sub> ) <sub>2</sub> SiCl <sub>2</sub>	13.5 (12.7)	19.5 (18.8)	7.2 (6.4)	4.4 (5.9)	11.0 (12.4)
K	-0.68	(CH <sub>3</sub> ) <sub>2</sub> SiBr(OC <sub>6</sub> H <sub>5</sub> )	6.5 (7.4)	6.1 (7.0)	8.7 (10.2)	1.3 (1.4)	0.3 (0.9)
	...	(CH <sub>3</sub> ) <sub>2</sub> Ge(OC <sub>6</sub> H <sub>5</sub> ) <sub>2</sub>	... (0.0)	... (0.0)	... (0.0)	... (0.0)	... (0.0)
L	-0.53	(CH <sub>3</sub> ) <sub>2</sub> SiCl(OC <sub>6</sub> H <sub>5</sub> )	19.0 (20.1)	12.0 (13.0)	8.3 (9.4)	21.3 (23.4)	30.8 (32.6)
M	-0.31	(CH <sub>3</sub> ) <sub>2</sub> Si(OC <sub>6</sub> H <sub>5</sub> ) <sub>2</sub>	3.2 (3.3)	0.8 (1.0)	1.1 (1.4)	9.4 (9.7)	9.4 (9.0)

Composition parameter	Experiment no.				
	1	2	3	4	5
R <sub>1</sub> ≡ [Cl]/([Si] + [Ge])	0.572 <sup>d</sup> (0.578) <sup>e</sup>	0.741 (0.760)	0.387 (0.392)	0.431 (0.393)	0.737 (0.732)
R <sub>2</sub> ≡ [Br]/([Si] + [Ge])	0.572 <sup>d</sup> (0.582) <sup>e</sup>	0.684 (0.719)	0.733 (0.738)	0.394 (0.413)	0.378 (0.389)
R <sub>3</sub> ≡ [I]/([Si] + [Ge])	0.512 <sup>d</sup> (0.519) <sup>e</sup>	0.355 (0.346)	0.652 (0.674)	0.730 (0.774)	0.365 (0.373)
R <sub>4</sub> ≡ [OC <sub>6</sub> H <sub>5</sub> ]/([Si] + [Ge])	0.344 <sup>d</sup> (0.319) <sup>e</sup>	0.221 (0.197)	0.229 (0.192)	0.445 (0.422)	0.521 (0.504)
R <sub>1</sub> ≡ [Si]/([Si] + [Ge])	0.572 <sup>d</sup> (0.544) <sup>e</sup>	0.712 (0.698)	0.560 (0.510)	0.412 (0.364)	0.557 (0.515)

<sup>a</sup> In parts per million relative to internal tetramethylsilane as measured in experiment 3. <sup>b</sup> From the nmr peak areas. <sup>c</sup> Calculated from the constants for system II in Table I and from *R* values calculated from the ingredients. <sup>d</sup> From the ingredients of the mixture. <sup>e</sup> Calculated from the experimental nmr data.

immediately obtaining the nmr spectra, the equilibria with regard to the distribution of the substituents between silicon and germanium will correspond to the temperature at which the samples were held for equilibration, which in the present case is 120°. Since equilibration of these substituents on silicon at room temperature in the absence of catalysts<sup>1</sup> does not proceed at all, the equilibria between the silicon species also represent the situation at 120°.

The results reported here exemplify the usual situation<sup>12</sup> in which the values of an equilibrium constant (for a substituent-exchange reaction in a set of reactions in which all chemical species are accounted for) are seen to vary by only a small amount with environmental changes, while nmr chemical shifts may show appreciable variations. Thus not only do the values of a given constant not change appreciably in the various experiments listed in Table II and III, but also, as shown in Table I, there is no distinguishable difference between values of the same constant measured in the two different systems studied here. Moreover, the results obtained here agree with values<sup>13</sup> of the same equilibrium constant as measured in the exchange of only two kinds of substituents on a single kind of polyfunctional moiety.

From a quantum-mechanical viewpoint,<sup>14</sup> it is not surprising that there are noticeable changes in the nmr chemical shifts with variation in molecular environment, while equilibrium constants for substituent exchange are virtually unaffected. Since hydrogen nmr shifts are mainly attributable to the paramagnetic terms, the predominant operator for this property involves the expectation value of  $1/r$ . Since the hydrogen atoms are positioned in the outer regions of the molecule, this slowly declining  $(1/r)$  function is expected to be affected by neighboring molecules. On the other hand, the energy changes induced by atom or group

(12) See K. Moedritzer, *Advan. Organometal. Chem.*, **6**, 171 (1968), and J. R. Van Wazer and K. Moedritzer, *Angew. Chem. Int. Ed.*, **5**, 341 (1966), for reviews.

(13) In ref 2, it is shown that, for Q = (CH<sub>3</sub>)<sub>2</sub>Si at 120°, K<sub>1</sub> = 0.31 ± 0.03, and for Q = (CH<sub>3</sub>)<sub>2</sub>Ge at 35°, K<sub>1</sub> = 0.30 ± 0.02, K<sub>2</sub> = 0.67 ± 0.07, and K<sub>3</sub> = 0.35 ± 0.01. K. Moedritzer and J. R. Van Wazer, *Inorg. Chem.*, **7**, 2105 (1968), have also shown that for Q = (CH<sub>3</sub>)<sub>2</sub>Si at 150°, K<sub>4</sub> = 0.16 ± 0.01 and K<sub>5</sub> = 0.14 ± 0.01. K. Moedritzer and J. R. Van Wazer, *J. Organometal. Chem.*, **13**, 145 (1968), have shown that, for exchange of the appropriate monofunctional substituents between the CH<sub>3</sub>Ge< and (CH<sub>3</sub>)<sub>2</sub>Ge< moieties, K<sub>5</sub> = 0.24 ± 0.01 and K<sub>6</sub> = 1.61 ± 0.05, for Q = (CH<sub>3</sub>)<sub>2</sub>Ge at 35°.

(14) *Ab initio* calculations are now being interpreted in our laboratories to elucidate both of the matters touched upon in the reference paragraph.

substitutions to the most part come from quite deep within the molecule so that they are little perturbed by the presence of neighboring molecules.

The equilibrium constants in Table I make up one complete minimum-number set of the constants required for the complete mathematical determination of all equilibria in these systems. Of course, any other set of constants which satisfies the conditions of totally determining all equilibria in these systems may be chosen. From any such properly chosen set of constants, any other equilibrium not expressed specifically by that set may be calculated from it.

From the three intersystem equilibrium constants  $K_I$ ,  $K_{II}$ , and  $K_{III}$ , the following additional intersystem constants have been calculated

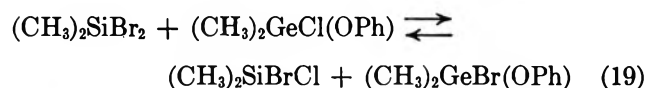
$$K_{IV} = \frac{[(CH_3)_2SiI_2][(CH_3)_2Ge(OPh)_2]}{[(CH_3)_2Si(OPh)_2][(CH_3)_2GeI_2]} = \frac{K_{III}}{K_{II}} = 1.3 \times 10^{-10} \quad (16)$$

$$K_V = \frac{[(CH_3)_2SiCl_2][(CH_3)_2Ge(OPh)_2]}{[(CH_3)_2Si(OPh)_2][(CH_3)_2GeCl_2]} = \frac{K_{III}}{K_I} = 2.3 \times 10^{-8} \quad (17)$$

$$K_{VI} = \frac{[(CH_3)_2SiI_2][(CH_3)_2GeCl_2]}{[(CH_3)_2SiCl_2][(CH_3)_2GeI_2]} = \frac{K_I}{K_{II}} = 5.8 \times 10^{-8} \quad (18)$$

Whereas  $K_{IV}$  and  $K_V$  have not been measured previously,  $K_{VI}$  has been found in a separate study<sup>2</sup> to have a value of  $1.2 \times 10^{-6}$ .

Another example for these kinds of calculations is the equilibrium constant for the reaction of eq 19



$$K_{VII} = \frac{[(CH_3)_2SiBrCl][(CH_3)_2GeBr(OPh)]}{[(CH_3)_2SiBr_2][(CH_3)_2GeCl(OPh)]} = \sqrt{{}^{Ge}K_4/{}^{Si}K_1} {}^{Ge}K_5 K_I = 1.3 \times 10^2 \quad (20)$$

The value of  $K_{VII}$  shows that the equilibrium of eq 19 lies well to the right.

*Acknowledgment.* We wish to thank Raymond E. Miller for valuable experimental assistance.

## The Thermal Decomposition of Solid Hexaamminecobalt(III)

### Azide. The Cobalt(II) Reaction

by T. B. Joyner

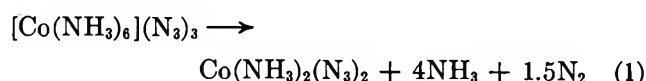
Chemistry Division, Naval Weapons Center, China Lake, California 93555 (Received February 19, 1968)

The rates of decomposition of solid hexaamminecobalt(III) azide to cobalt(II) complexes have been measured, and the kinetic parameters have been determined. Under low ammonia pressures an apparent activation energy of ca. 46 kcal/mol is close to the values obtained for the analogous reactions of azidopentaamminecobalt(III) azide and *cis*- and *trans*-diazidotetraamminecobalt(III) azide, suggesting a reaction mechanism common throughout the series. Under higher ammonia pressures (50–200 torr), the hexaammine is unique in showing a lower apparent activation energy of ca. 32 kcal/mol. This may indicate a reaction path unavailable to the substituted compounds.

#### Introduction

The ability of solid hexaamminecobalt(III) azide to decompose to either CoN or cobalt(II) has been established, and the rather complicated relationship between the reactions has been qualitatively discussed.<sup>1</sup> This paper considers the kinetics of the cobalt(II) reaction. The CoN reaction, with its interesting induction period,

will be dealt with separately. The cobalt(II) reaction



(1) T. B. Joyner and F. H. Verhoek, *Inorg. Chem.*, **2**, 334 (1963).

is complex with labile products (a series of cobalt(II) ammine azides have been identified<sup>2</sup>) and a marked sensitivity to ammonia. Despite consequent difficulties, rate data have been obtained over a reasonable range of experimental conditions and analysis is possible. The results are of particular value in relation to similar studies with the substituted azidopentaamminecobalt(III) azide<sup>3</sup> and *cis*- and *trans*-diazidotetraamminecobalt(III) azide.<sup>4,5</sup>

### Experimental Section

**Preparation.** Preparation and purification have been described.<sup>1</sup> The cobalt(II) reaction is most reliably demonstrated by powders. The data presented here were obtained from two independent preparations labeled A and B. Briefer studies with four other preparations confirmed the findings. Microscopic examination and nonrotated X-ray powder patterns indicated crystal sizes in the range of 0.1–1  $\mu$ . The samples were stored in opaque vacuum desiccators over P<sub>2</sub>O<sub>5</sub>. The reaction occurs in larger crystals,<sup>1</sup> but its course is erratic and complicated by the competitive CoN reaction; hence there was no serious effort to obtain kinetic data from such samples. Conversely, powders rarely show the CoN reaction, although explosions are a problem.

**Procedure.** The experimental techniques have been discussed.<sup>6</sup> In brief, the usual run used a *ca.* 10-mg sample with the reaction followed by pressure increase, *ca.* 75 torr for eq 1. As before, "normal" runs were made with the system initially evacuated and the solid exposed to only its own products, while "ammonia" runs involved an initial pressure of added ammonia. Normal runs with 5- and 20-mg samples indicated that sample size influenced the rate only through the pressure of the self-generated ammonia. With proper alterations in the system volume, there was no significant change in reaction rates. The studies were conducted within 4 weeks of sample preparation, with check runs to establish that no kinetically significant aging had occurred.

**Products.** The solids were identified by X-ray powder patterns. The early findings<sup>2,6</sup> were confirmed and extended. Very careful observations of the reaction vessel revealed a small number of tiny (0.01–0.05 mm in length) transparent crystals just above the hot zone. These were collected, with difficulty, in a partially congealed droplet of a commercial rubber cement suspended on a glass capillary. Powder patterns identified ammonium azide. Although the crystals are a very minor constituent of the products, their presence indicates a heretofore unreported reaction. Additionally, runs under 400 torr of ammonia and low temperatures (120° or less) are anomalous and appear to yield mixtures containing at least one unidentified component.

### Results

The cobalt(II) reaction has been described briefly.<sup>1</sup>

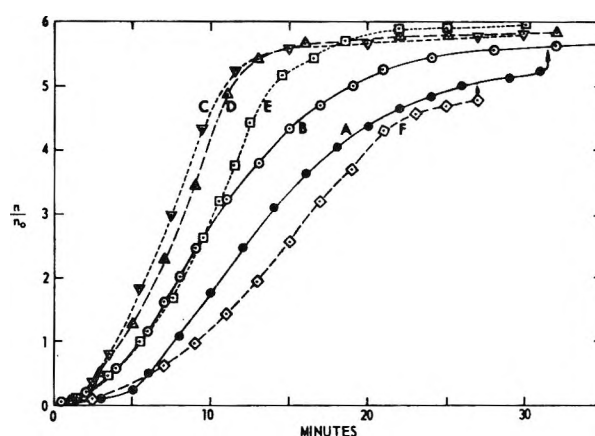


Figure 1. Decomposition of powdered  $[\text{Co}(\text{NH}_3)_6](\text{N}_3)_3$  (preparation A) at 140°. Initial ammonia pressures in torr: curve A, 0; curve B, 11; curve C, 50; curve D, 100; curve E, 200; curve F, 400. The solid arrows indicate explosions.

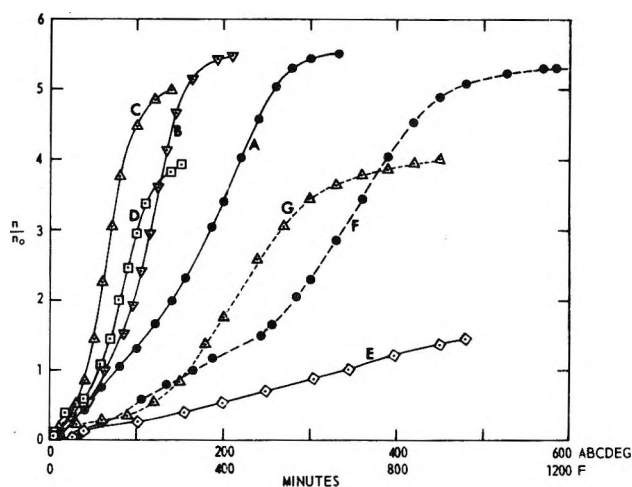
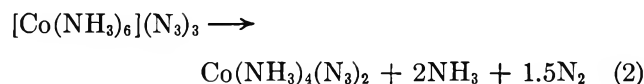


Figure 2. Decomposition of powdered  $[\text{Co}(\text{NH}_3)_6](\text{N}_3)_3$  at low temperatures. Initial ammonia pressure in torr for 120° runs: curve A, 0; curve B, 50; curve C, 100; curve D, 200; curve E, 400 (preparation B). Ammonia pressures in torr for 110° runs: curve F, 0; curve G, 100. With the exception of curve E all runs were with preparation A.

Figures 1 and 2 more fully illustrate its temperature and ammonia dependence, with  $n/n_0$ , the moles of gas evolved per mole of original compound, plotted against time. In many respects the decomposition resembles the analogous reactions of the substituted compounds.<sup>3–5</sup> In all cases the investigation is seriously hindered by the narrow range of conditions within which the reaction may be studied. Above 150° it is too fast. Even at lower temperatures explosions are frequent and, at the least, interfere with the collection

- (2) T. B. Joyner and F. H. Verhoek, *Inorg. Chem.*, **1**, 557 (1962).
- (3) T. B. Joyner, *J. Phys. Chem.*, **69**, 1723 (1965).
- (4) T. B. Joyner, *ibid.*, **71**, 3431 (1967).
- (5) T. B. Joyner, *ibid.*, **72**, 703 (1968).
- (6) T. B. Joyner and F. H. Verhoek, *J. Amer. Chem. Soc.*, **83**, 1069 (1961).

of data. (Efforts to avoid explosions cause the abrupt terminations of some curves—for instance, Figure 2, curve D.) Moderate ammonia pressures (50–200 torr) accelerate the reaction, tend to inhibit explosions, and produce the most symmetrical curves. Greater pressures lead to decreasing gas evolution and higher amines of cobalt(II), notably a green compound presumed to be a tetraammine.<sup>2</sup> This would call for an ideal stoichiometry of



although in fact the green compound is usually observed in mixtures with the diammine. Low temperatures (120°) and high ammonia (400 torr) drastically curtail both rate and gas evolution.

The above observations are generally typical of the substituted compounds. The major difference in the reaction of the hexaammine is a greater willingness to follow eq 1 to completion. For instance, with preparation A at 140° the normal run (Figure 1, curve A) goes to near completion, whereas substituted compounds usually explode after the evolution of only about 1 mol of gas.<sup>3-5</sup> The 11-torr ammonia run (Figure 1, curve B) generally parallels the normal curve but commences somewhat earlier. The 50–200-torr runs (curves C–E) are faster, but at 400 torr (curve F) a decrease in gas evolution and rate is observed. Preparation-B curves are similar but with slight differences in rate, an expected consequence of variations in crystal size and shape.

At 120 and 110° (Figure 2) there is again an acceleration by moderate ammonia but with some reduction in gas evolution. Runs D and G show stoichiometries close to eq 2 and yield the green compound. With preparation A the normal runs go to completion (curves A and F). Preparation B is somewhat more prone to conversion to the CoN reaction. Normal and 50-torr runs followed the cobalt(II) path to  $n/n_0 = ca. 2.5$  and then converted to the CoN reaction and went quickly to completion. The 100-torr runs are similar to those of preparation A. The 400-torr, 120° run (included in Figure 2 as curve E) shows a great curtailment in rate and gas evolution. A powder pattern taken after 440 min and an  $n/n_0$  of only 1.4 showed a mixture of the green tetraammine and an unidentified compound, suggesting that decompositions under these conditions are not comparable with the usual cobalt(II) reaction. A similar situation was noted for the substituted compounds.

The difference in the reactions of the hexaammine and the substituted compounds is most apparent at the lower temperatures. This is illustrated by the relationships of the normal and 100-torr ammonia runs for the hexaammine and the azidopentaammine. At 140° the ammonia runs are faster. At 110° the hexaam-

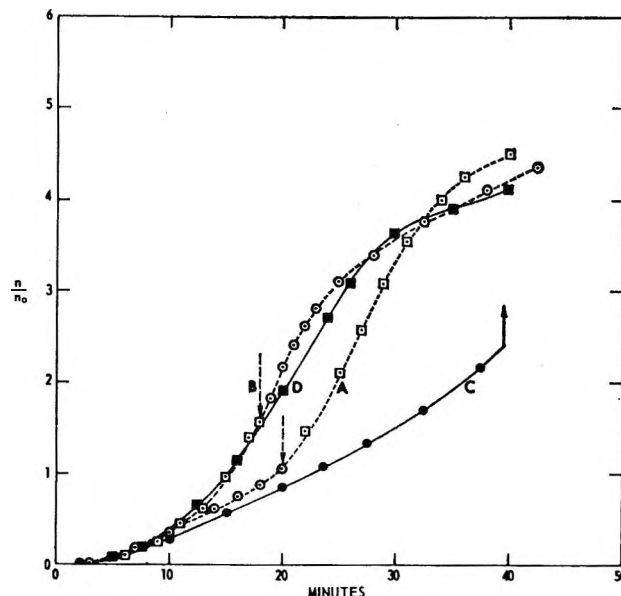


Figure 3. Decomposition of powdered  $[\text{Co}(\text{NH}_3)_6](\text{N}_3)_3$  (preparation B) at 130°: curve A, initially normal run altered (dashed arrow) to conditions appropriate for a 100-torr ammonia run; curve B, 100-torr ammonia run altered (dashed arrow) to conditions appropriate for a normal run; curve C, normal run; the solid arrow indicates an explosion; curve D, 100-torr ammonia run.

mine maintains this order (Figure 2 curves F and G). Conversely, an azidopentaammine normal run reached  $n/n_0 = 1.1$  at 990 min, and a much slower 100-torr run reached only  $n/n_0 = 0.8$  at 11,400 min (ref 3, Figure 1). Both runs converted to the CoN reaction.

Since the normal and ammonia reactions of the hexaammine differ in both rate and curve shape, it is of interest to see if early growth patterns can persist and effect the reaction after a change in conditions. Experiments at 130° were commenced as normal or 100-torr ammonia runs, and at about 25% completion altered to the reverse conditions by either opening to a small volume containing the necessary ammonia or briefly venting to an appropriate evacuated volume. The initially normal run (Figure 3, curve A) showed an immediate acceleration to the rate of a 100-torr ammonia run. The results are less clear for the reverse case. A 100-torr ammonia run vented to a pressure approximately correct for a normal run at 25% completion (curve B), maintained the relatively fast ammonia rate for a time, and then tapered off to a rather asymmetric curve only slightly different from a 100-torr run carried to completion.

Several 100-torr ammonia runs at 120 and 140° were interrupted at 25, 50, and 70% completion and cooled for up to 30 min. The rates after reinitiation were comparable with uninterrupted runs. Some efforts were made to isolate the solid and to determine the ratio of evolved ammonia and nitrogen. The experiments are difficult. The cobalt(II) compounds are labile to ammonia absorption, loss, and explosion. Also, the ac-

curacy of the estimations (made by vacuum line manipulations and the differences in total gas, total ammonia, and added ammonia) is impaired by the large excess of ammonia. The inaccuracy, most serious when the evolved gas is small, has led to some suspicions of an anomalous low initial nitrogen evolution.<sup>3</sup> Later studies appear to contradict this. While some reservations should probably be maintained, it is now believed that the ratio of the evolved gases remains essentially constant during a run.

### Discussion

The kinetic analysis follows previous papers.<sup>3-5</sup> The reduction is again assumed rate controlling, with relatively rapid equilibration of the cobalt(II) amines responsible for the decreased gas evolution under added ammonia and lower temperatures.

*Ammonia Runs.* The curves can be described by the Avrami-Erofeev or Prout-Tompkins equations<sup>7</sup>

$$[-\ln(1 - \alpha)]^{1/3} = k_{AE}t + c_{AE} \quad (3)$$

$$\ln[\alpha/(1 - \alpha)] = k_{PT}t + c_{PT} \quad (4)$$

where  $\alpha$  is the fraction reacted,  $t$  is the time, and  $k$  and  $c$  are constants. Over-all, the former is the more successful.<sup>8</sup> Both yield similar values for the temperature dependence. Figure 4 gives illustrative curves, Table I reports rate constants. In general, eq 3 and 4 give good fits for more than 85% of a run. Rarely an anomalous (and unexplained) early region ( $\alpha < 0.3$ ) leads to broken curves with the constants from the final 70% correlating with the other runs. Since rates are often very dependent upon the early nucleation, the anomalous runs may simply be slow in attaining the usual growth pattern.

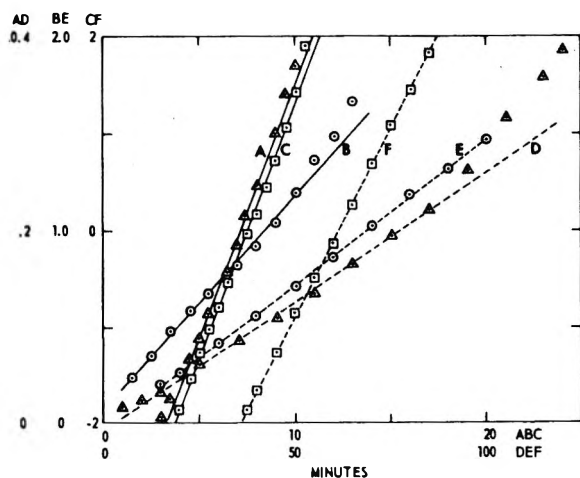


Figure 4. Illustrative kinetic treatments: curve A, 140°, normal run treated by eq 5,  $\alpha$ ; curve B, 140°, 100-torr run, eq 3,  $[-\ln(1 - \alpha)]^{1/3}$ ; curve C, 140°, 100-torr run, eq 4,  $\ln[\alpha/(1 - \alpha)]$ ; curve D, 120°, normal run, eq 5,  $\alpha$ ; curve E, 120°, 100-torr run, eq 3,  $[-\ln(1 - \alpha)]^{1/3}$ ; curve F, 120°, 100-torr run, eq 4,  $\ln[\alpha/(1 - \alpha)]$ . The ordinate plots the functions of  $\alpha$  as given in the equations and listed above.

Table I: Rate Constants for the Cobalt(II) Reaction

Temp, °C	Initial NH <sub>3</sub> pressure, torr	10 <sup>4</sup> k <sub>i</sub> , sec <sup>-1</sup>	10 <sup>4</sup> k <sub>AE</sub> , sec <sup>-1</sup>	10 <sup>4</sup> k <sub>PT</sub> , sec <sup>-1</sup>
Preparation A				
150	0	40.9	22.9	58.2
140	0	8.66	7.63	36.4
140	0	7.85	7.45	37.2
140	0	7.92	7.97	40.1
130	0	1.84	2.49	13.2
130	0	1.84	2.61	12.7
120	0	0.493	1.06	4.70
110	0	0.0961	0.313	1.36
140	11		7.20	36.5
150	50		32.3	150
140	50		16.9	84.7
130	50		5.70	29.1
120	50		1.68	8.48
150	100		32.6	146
140	100		15.8	81.1
130	100		5.48	30.7
120	100		1.94	10.9
110	100		0.693	3.41
150	200		31.9	147
140	200		11.8	62.3
130	200		4.79	23.7
120	200		1.68	9.72
140	400		8.50	42.8
Preparation B				
150	0	30.0		
140	0	7.37	11.3 <sup>a</sup>	56.4 <sup>a</sup>
130	0	1.79		
120	0	0.447		
110	0	0.118		
95	0	0.0119		
150	50		45.6	224
140	50		19.7	94.1
130	50		6.03	32.3
120	50		(1.92) <sup>b</sup>	(7.31) <sup>b</sup>
150	100		38.1	184
140	100		19.2	89.3
130	100		6.62	32.9
120	100		2.55	12.9
110	100		0.733	3.54
150	400		20.8	115
140	400		10.9	66.6
130	400		3.97	18.8

<sup>a</sup> With the exception of the 140° run, explosions or conversion to the CoN reaction prevent satisfactory treatment of the later portions of normal runs with preparation B. <sup>b</sup> Converted to the CoN reaction at  $\alpha = 0.4$ . The constant is estimated from the early data.

The constants for the 50–200-torr runs show no great dependence on ammonia. The 400-torr data are

(7) P. W. M. Jacobs and F. C. Tompkins in W. E. Garner, "Chemistry of the Solid State," Butterworth and Co., Ltd., London, 1955, Chapter 7.

(8) Although the equations are based on different models,<sup>7</sup> in practice distinction is often difficult depending (particularly) on the very early and late portions of the reaction where such inherent features as particle sizes and shapes, surface conditions, and nucleation sites and rates may give anomalous growth patterns.

somewhat lower, with the drastic curtailment preventing analysis of the 120° run. The 11-torr run gives broken plots by either eq 3 or 4. Its resemblance to a normal run is reflected in the constants for  $\alpha > 0.5$ , although the initial regions do not show the linearity of normal runs (see below).

Arrhenius plots yield the data of Table II. With preparation A the 50–200-torr runs give apparent activation energies in good mutual agreement (*ca.* 32 kcal/mol) and significantly lower than the results (46–54 kcal/mol) of comparable analyses for the substituted compounds.<sup>3–5</sup> With preparation B the 100-torr runs agree, but the 50- and 400-torr data are limited. Conversion of the 50-torr, 120° run to the CoN reaction restricts the data to  $\alpha < 0.4$ . A rate constant can be estimated but was not used in obtaining the apparent

**Table II:** Apparent Activation Energies ( $E_a$ ) and Preexponentials ( $A$ )

Initial NH <sub>3</sub> pressure, torr	Treatment	$E_a$ , kcal/mol	Log $A$ sec <sup>-1</sup>
Preparation A			
0	Eq 5 <sup>a</sup>	47.7	22.16
0	Eq 3 <sup>b</sup>	33.9	14.85
50	Eq 3	33.0	14.62
100	Eq 3	31.6	13.88
200	Eq 3	32.2	14.12
0	Eq 4 <sup>b</sup>	31.8	14.43
50	Eq 4	32.1	14.84
100	Eq 4	30.8	14.13
200	Eq 4	30.1	13.73
Preparation B			
0	Eq 5 <sup>a</sup>	43.8	20.04
50	Eq 3	33.9	15.19
100	Eq 3	32.1	14.19
50	Eq 4	32.9	15.34
100	Eq 4	31.8	14.73

<sup>a</sup> Applied to  $\alpha < 0.5$ . <sup>b</sup> Applied to  $\alpha > 0.5$ .

activation energy. The curtailment of the reaction at 120° limits the 400-torr data to three points which roughly parallel the 100-torr constants but do not justify calculation of an apparent activation energy.

*Normal Runs.* Normal runs have rather asymmetric curves with quite linear early regions ( $\alpha < 0.3$ ). A similar linearity with the substituted compounds was treated by

$$\alpha = k_1 t + c_1 \quad (5)$$

Centering eq 5 on  $\alpha = 0.15$  gives the constants of Tables I and II and an apparent activation energy of  $46 \pm 4$  kcal/mol (with the high uncertainty due to the rather approximate treatment). To establish that the difference from ammonia runs was not an artefact of the analysis, efforts were made to treat the initial regions

of the latter by eq 5. The curvature prevented a satisfactory fit; however, the essentially equivalent treatment of Jacobs and Kureishy<sup>9</sup> applied to intervals of  $\alpha$  of 0.05 in the range  $\alpha = 0-0.20$  confirmed the lower apparent activation energy of ammonia runs.

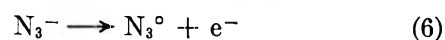
The value of 46 kcal/mol is close to the apparent activation energies of the substituted compounds. With the latter, early explosions ended the normal runs. The more complete hexaammine curves can be analyzed with either eq 3 or 4 giving good fits for the deceleratory region ( $\alpha > 0.5$ ). The apparent activation energy (34 kcal/mol) is typical of ammonia runs, a reasonable consequence of the *ca.* 25 torr of ammonia evolved by  $\alpha = 0.5$ .

### Conclusions

With substituted compounds the qualitative resemblance and similar apparent activation energies, 46–54 kcal/mol for normal *and* ammonia runs, made it reasonable to assume the same mechanism throughout the series. With the hexaammine the qualitative similarity persists, and, moreover, the early stages of normal runs have a 46-kcal/mol apparent activation energy. In contrast, however, added ammonia leads to a lower apparent activation energy, suggesting the possibility of a path unavailable to the substituted compounds.

It should be emphasized that the conclusions are based on a comparison of a series of compounds. Although rate constants of solid-state reactions may be very complex quantities,<sup>7</sup> the similarity in the apparent activation energies is obvious and useful. It argues, in particular, against mechanisms requiring very different paths for the various compounds. Such differences might have been suggested by the diversity in composition, cation, and crystal structure and the possibility that the substituted complexes with a coordinated azide of considerable covalent character<sup>10</sup> might react differently from the hexaammine with only ionic azides.

Although analysis of the companion CoN reaction is intended prior to summary discussions of the two systems, it is advantageous to suggest here a mechanism for the cobalt(II) reaction capable of explaining both the similar apparent activation energies and the exceptional case of the hexaammine under ammonia. As with azide decompositions generally,<sup>11,12</sup> it seems reasonable to expect a rate-controlling step of the type



without being specific as to the detailed nature of the products. (These exist in or on solids with many possibilities for their environment and structure; usually

(9) P. W. M. Jacobs and A. R. T. Kureishy, *J. Chem. Soc.*, 4718 (1964).

(10) G. J. Palenik, *Acta Crystallogr.*, 17, 350 (1964).

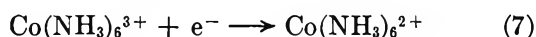
(11) D. A. Young, "Decomposition of Solids," Pergamon Press Inc., New York, N. Y., 1966, Chapters 4, 5.

(12) P. Gray, *Quart. Rev.*, 17, 441 (1963).

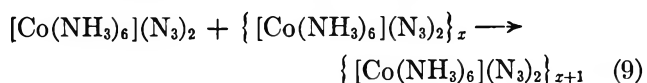
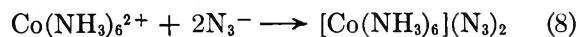


promotion to conduction or exciton bands is assumed.) Although the location of eq 6 is unknown, an interesting hypothesis associates it with the cobalt(II) product (an azide, of course, capable of further reaction) or with the reactant-product interface.

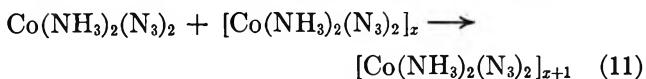
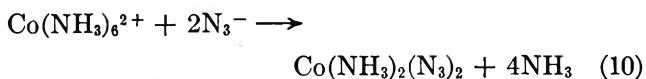
Following reduction of the cation



ligand rearrangement and crystallization of diazido-diamminecobalt(II) will eventually occur. However, with the hexaammine an intermediate is possible. Hexaamminecobalt(II) differs only slightly in size from the original hexaamminecobalt(III).<sup>13</sup> Its azide salt, although labile to ammonia loss or explosion, is known at room temperature.<sup>2</sup> Since the cations are similar and the hexaamminecobalt(II) will be generated in proximity to azide ions, it is possible that little rearrangement would be necessary for the formation of a hexaamminecobalt(II) azide phase. This may be represented by



with eq 9 emphasizing the formation of a phase. Under experimental conditions hexaamminecobalt(II) azide is not a final product and so must ultimately yield the diammine

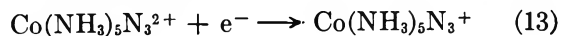


Nitrogen may result from



Added ammonia should favor the hexaamminecobalt(II) azide. A greater concentration of ammonia at the reaction site<sup>14</sup> might retard reactions 10 and 11 and so lead to a transient phase, growing at the reactant interface and losing ammonia and forming diazidodiamminecobalt(II) at its rear, of some duration and depth. With no added ammonia reaction 10 may occur before a transient phase could be organized. Thus the reactant may be in contact with diazidodiamminecobalt(II) when ammonia pressures are low and hexaamminecobalt(II) azide when they are higher. If the rate-controlling step is correctly associated with the cobalt(II) phase, different apparent activation energies are plausible.

Although diazidodiamminecobalt(II) occurs throughout the series (providing the common path), the transient phase is unlikely for the substituted compounds. Counterparts of eq 7, for instance



yield species which would have to first form the hexaamminecobalt(II) ion and then crystallize its azide salt. This is unlikely under the experimental conditions and is in marked contrast to hexaamminecobalt(III) where the transient phase is a natural outcome of the initial reduction. Thus there is a path unique for hexaamminecobalt(III) azide under added ammonia.

The model can explain the runs of Figure 3. The initially normal run (curve A), upon addition of ammonia, might quickly build up sufficient hexaamminecobalt(II) azide to assume the rate of ammonia runs. In the opposite case, the initial ammonia reaction would have established a transient phase of some depth. Despite the ammonia decrease at  $\alpha = 0.25$ , this phase might persist for some time, growing at its front with the rate of an ammonia run but suffering an increased ammonia loss at its rear. (It is tempting to associate the slight bulge in curve B with this loss; however, the effect is small and should be noted with caution.) Only with the destruction of the transient phase would the reactant learn of the altered conditions and finally revert, as observed, to a rate more nearly typical of a normal run.

Ammonia affects the reactions of substituted compounds without seriously altering the apparent activation energies. A plausible explanation involves the lability of the ammonia-cobalt(II) azide system and its complexity (at room temperature) in the diammine region.<sup>2</sup> If the complexity persists at higher temperatures, association of eq 6 with the ammonia-dependent cobalt(II) phases offers opportunities for effects on rate. These involve the lower amines which, unlike hexaamminecobalt(II) azide, would be common throughout the series including the hexaamminecobalt(III) reaction under the early low pressures of normal runs.

While the cobalt(II) reaction has been quite well defined, some problems remain. A minor reaction yields ammonium azide. The ammonium ion implies loss of a second ammonia to unidentified products. The curtailment in rate at low temperatures and high ammonia has been established but not studied. The decomposition of the cobalt(II) products, prior to the explosions which prevent detailed study, is slow. This is understandable even though eq 6 is associated with the cobalt(II) phase. The cobalt(III) reactant is important as a recipient of the electron. Its exhaustion forces alternate reactions (to be discussed subsequently) leading ultimately to Co(0) or CoN.

(13) M. T. Barnet, B. M. Craven, H. C. Freeman, N. E. Kime, and J. A. Ibers, *Chem. Commun.*, 307 (1966).

(14) The problem of the ammonia at the site is difficult. The reaction occurs in or on a solid, beneath solid products, and with the local environment influenced by the evolved gases and adsorption of ammonia. Thus formation and crystallization of products, diffusion of gases, the physical nature of the solids, and other conceivable factors may influence the reaction. Clearly the effective ammonia need not be simply related to the measured pressure. This forced the fairly extensive studies under ammonia.

# New Method for Determining Magnetic Susceptibility and Magnetic Moment

by Toshio Ikeda and Hisashi Yoshioka

Department of Chemistry, Shizuoka University, Shizuoka, Japan (Received March 4, 1968)

A new method was presented for the determination of the magnetic susceptibility of a liquid by measuring the time of flow of the liquid through the capillary of a viscometer in the presence of an external, heterogeneous magnetic field. This viscometer method was used on aqueous solutions of some of the chlorides of the transition group elements and was found to give reproducible and accurate results, to within  $\pm 0.5\%$  of the true magnetic susceptibilities and moments.

The magnetic susceptibility, measurable by various methods, is one of the most fundamental quantities characterizing the magnetic properties of matter.<sup>1</sup> Most of the available methods can be reduced to the measurement of the magnetic force acting on the sample. A new method will be reported here for determining the magnetic susceptibility by using a capillary viscometer. This method is seemingly quite different from the usual ones; however, it can be considered, in principle, to be an alternative of the Gouy balance method or of the Quincke method, using a watch in place of a chemical balance or scale.

## Principle

When a capillary viscometer of the Ostwald type is placed in a magnetic field so that its globular part may come within the homogeneous magnetic field near the center of the pole gap of an electromagnet, while its capillary part, fixed in the direction of gravity, is drawn through the heterogeneous magnetic field, the liquid in the viscometer is forced through the capillary by gravity and the magnetic force acting on the liquid passing through this region of heterogeneous magnetic field. The Hagen-Poiseuille expression for the time,  $t$ , of flow of a liquid of a certain volume,  $v$ , through the capillary of the viscometer is

$$\frac{1}{t} = \frac{\pi r^4}{8lv\eta} (\rho gh - \frac{1}{2}\kappa H^2) \quad (1)$$

where  $r$  and  $l$  are, respectively, the radius and the length of the capillary of the viscometer, while  $h = l \cos \theta$ ,  $\theta$  being an angle between the directions of gravity and the capillary axis of the viscometer (in the present case,  $\theta = 0$ );  $\rho$  and  $\eta$  are the density and the viscosity coefficients, respectively, of the liquid in the presence of an external magnetic field,  $g$  is the acceleration of gravity, and  $\kappa$  represents the volume magnetic susceptibility of the liquid.  $H$  is the local magnetic field in the liquid medium in the region of the homogeneous magnetic field near the center of the pole gap of the magnet. In

the case of para- and diamagnetic substances,  $H$  may be approximated by the external applied magnetic field. If the time of flow of a liquid of the same volume,  $v$ , through the capillary of the viscometer in the same system in the absence of an external magnetic field is given by  $t_0$ , one may write

$$(1/t_0) - (1/t) = \kappa H^2 / 2\rho gh t_0 \quad (2)$$

because the dimensional change (regarding  $r$ ,  $l$ , and  $v$ ) of the viscometer due to the magnetostrictive effect is practically negligible, and further because there is some experimental evidence that the density and viscosity of aqueous solutions, irrespective of their magnetic nature, are practically unaffected by a magnetic field of the strength used here. Equation 2 is the basic equation for calculating the magnetic susceptibility. As is clear in eq 2, the liquid is identified as paramagnetic or diamagnetic according to whether the time,  $t$ , is longer or shorter, respectively, than  $t_0$ . It is of course possible, using eq 2, to calculate the value of  $\kappa$  if the time,  $t$ , is measured at one convenient magnetic field strength; however, it is equally important to prove the validity of the linear relation, eq 2, over a wide range of magnetic field strengths.

## Experimental Section

**Material.** Kosō Guaranteed reagent grade manganese chloride, ferrous chloride, cobaltous chloride, and nickel chloride, once recrystallized from water (except for the ferrous chloride), were each dissolved in pure water to make the concentration 1 or 2  $M$ . In the case of ferrous chloride, it was dissolved in hydrochloric acid to prevent it from hydrolyzing.

**Magnet.** A Bitter type 500-kg electromagnet (water-cooling type) of Tokyo Denki Seiki Co. was used. The magnet pole pieces of 60-mm cross-sectional diameter were set at a separation of 21 mm. The magnet was operated with the aid of a stabilized

(1) *E.g.*, P. W. Selwood, "Magnetochemistry," Interscience Publishers, New York, N. Y., 1943.

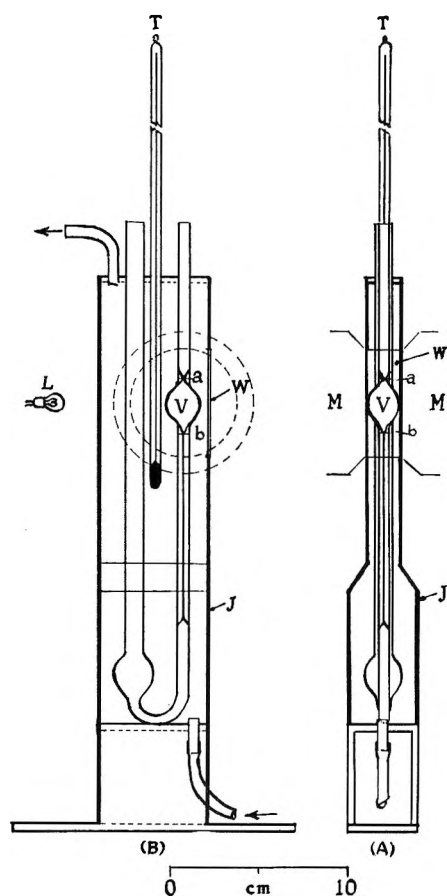


Figure 1. Experimental setup (front view, A, and side view, B: V, Ostwald viscometer; a, b, mark lines; W, glass window; M, magnet; J, cabinet made of polyvinyl chloride; T, mercury thermometer; L, lamp.

dc source at a current up to 28 A, corresponding to a magnetic field of 20 kG. The magnetic field was calibrated with a Toshiba HM-3 Hall element magnetic field meter at the center of the pole gap and was found to be homogeneous within the central region of the pole (about 30 mm in diameter) having a relative fluctuation of  $10^{-4}$ .

**Viscometer.** A viscometer of the Ostwald type, equipped with a thermostat jacket, was fixed between the pole gap of magnet so that its globular part could enter the homogeneous magnetic field near the center of the pole gap of magnet and its capillary could extend out of the magnetic field through the heterogeneous region of field, in the direction of gravity. Figure 1 shows the experimental arrangement, where V is an Ostwald viscometer fixed upright in a water jacket of a rectangular polyvinyl chloride cabinet to which a glass window, W, is attached at the level of the upper globular part of the viscometer so that two mark lines, a and b, cut on the viscometer may be seen in the counterlight of a miniature electric bulb set behind the cabinet.

**Measuring.** The time of flow of the liquid was measured with a stopwatch to an accuracy of 0.1 sec at two

temperatures, 25 and 35°, the temperature being controlled within  $\pm 0.05^\circ$  by circulating thermostated water around the viscometer.

### Results and Discussion

Some typical results are represented in Figures 2 and 3. In all cases one finds a perfectly linear relation passing through the origin. The results may be expressed in the experimental formula

$$\sqrt{|(1/t_0) - (1/t)|} = \alpha H \quad (3)$$

where  $\alpha$  is a function of temperature and concentration, characteristic of the liquid. The values of  $\alpha$  are listed in Table I. In comparing eq 3 with eq 2, one finds

$$|\kappa| = 2\rho g h t_0 \alpha^2 \quad (4)$$

by which the calculations of Table I were carried out.

**Calculation of Magnetic Moments and Susceptibilities.** If the Wiedemann's additivity law is applied,

Table I: Paramagnetic Properties of Ions of the Transition Group Elements in Aqueous Solutions as Determined by the Viscometer Method ( $\beta = 0.9273 \times 10^{-20}$  erg/G,  $l = 10.6$  cm, and  $g = 979.8$  cm/sec<sup>2</sup>)

Salt	Temp, °C	C, M	$\rho$ , g/ml	$10^6 \alpha$ , sec <sup>-1/2</sup> G <sup>-1</sup>	$t_0$ , sec	$\mu_{eff}$ ( $\beta$ )
MnCl <sub>2</sub>	25	1.0115	1.099	1.455	286.7	5.87
	25	2.023	1.196	1.733	383.3	5.88
	35	1.009	1.096	1.583	234.1	5.87
FeCl <sub>2</sub>	35	2.018	1.193	1.874	310.9	5.83
	25	1.052 <sup>a</sup>	1.122	1.300	298.1	5.33
	25	2.105 <sup>b</sup>	1.244	1.502	425.1	5.39
CoCl <sub>2</sub>	35	1.049 <sup>c</sup>	1.119	1.416	244.7	5.34
	35	2.100 <sup>d</sup>	1.241	1.639	346.4	5.39
	25	0.241	1.025	0.580	233.2	4.87
	25	0.481	1.052	0.860	248.4	4.86
	25	0.722	1.080	1.038	265.1	4.86
	25	0.962	1.107	1.185	284.7	4.94
	25	1.203	1.133	1.270	303.5	4.97
	25	1.444	1.159	1.332	326.7	4.94
	25	1.684	1.185	1.396	350.7	4.99
	25	1.925	1.211	1.421	377.6	4.97
NiCl <sub>2</sub>	35	0.240	1.022	0.637	191.2	4.93
	35	0.480	1.049	0.958	203.3	4.96
	35	0.720	1.077	1.154	217.2	4.97
	35	0.960	1.104	1.282	233.6	4.95
	35	1.200	1.130	1.402	248.1	5.00
	35	1.440	1.156	1.460	266.3	4.96
	35	1.680	1.182	1.515	286.4	4.98
	35	1.920	1.208	1.548	307.2	4.97
	25	0.464	1.053	0.506	249.5	3.32
	25	0.929	1.107	0.748	290.3	3.40
25	1.393	1.161	0.841	331.9	3.32	
25	1.858	1.212	0.882	388.6	3.29	
35	0.463	1.050	0.573	204.5	3.41	
35	0.926	1.104	0.827	237.3	3.45	
35	1.389	1.158	0.903	271.0	3.28	
35	1.853	1.209	0.961	316.0	3.28	

<sup>a</sup> [Cl<sup>-</sup>] = 2.792 N. <sup>b</sup> [Cl<sup>-</sup>] = 5.584 N. <sup>c</sup> [Cl<sup>-</sup>] = 2.784 N. <sup>d</sup> [Cl<sup>-</sup>] = 5.569 N.

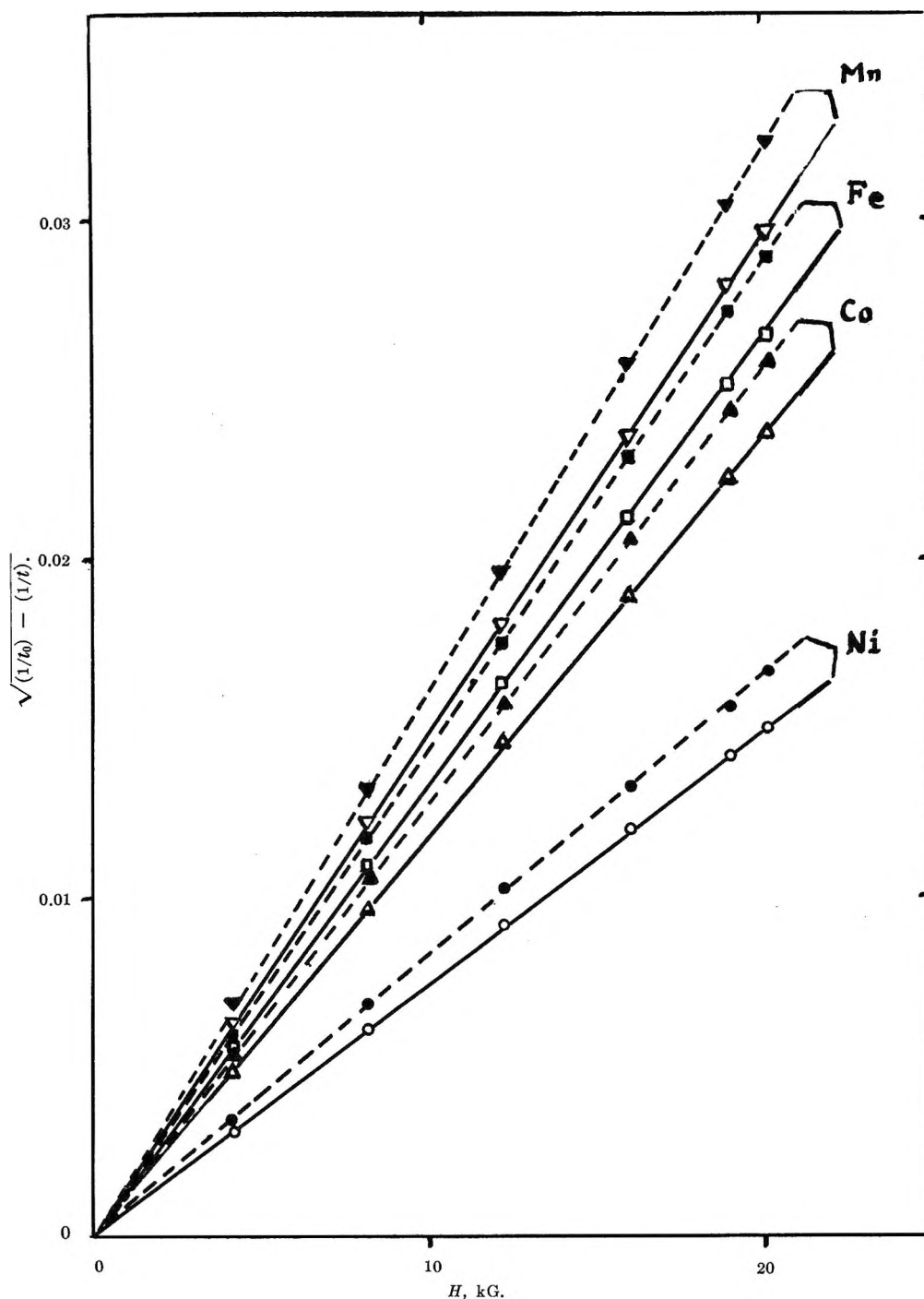


Figure 2. Relationship between the reciprocal time of flow of aqueous salt solutions of the transition group elements and the external magnetic field at 25° (—) and 35° (---): ▼, 1.009 *M* MnCl<sub>2</sub>; ▽, 1.0115 *M* MnCl<sub>2</sub>; ■, 1.049 *M* FeCl<sub>2</sub>; □, 1.052 *M* FeCl<sub>2</sub>; ▲, 0.960 *M* CoCl<sub>2</sub>; △, 0.962 *M* CoCl<sub>2</sub>; ●, 0.926 *M* NiCl<sub>2</sub>; and ○, 0.929 *M* NiCl<sub>2</sub>.

the volume magnetic susceptibility,  $\kappa$ , of an aqueous solution of a chloride of the type,  $MCl_n$ , at a concentration of  $C$  (*M*) may be expressed as

$$1000\kappa = \{1000\rho - C[(M) + n(Cl)]\}\chi_w + C(M)\chi_+ + nC(Cl)\chi_- \quad (5)$$

where  $\chi_w$ ,  $\chi_+$ , and  $\chi_-$  are the mass magnetic susceptibilities of water, cation  $M^{n+}$ , and the chloride ion, respectively;  $\rho$  is the density of the solution, and (*M*) and

(*Cl*) represent the atomic weights of cation  $M^{n+}$  and the chloride ion, respectively. In the present work, the magnetic susceptibility,  $\chi_+$ , of a paramagnetic cation,  $M^{n+}$ , was obtained from the observed magnetic susceptibility,  $\kappa$ , of the solution of a paramagnetic salt,  $MCl_n$ , by eliminating the contributions from the chloride ions in  $MCl_n$  solution by using the volume magnetic susceptibility of hydrochloric acid, whose chloride ion concentration was equivalent to that of the solution of

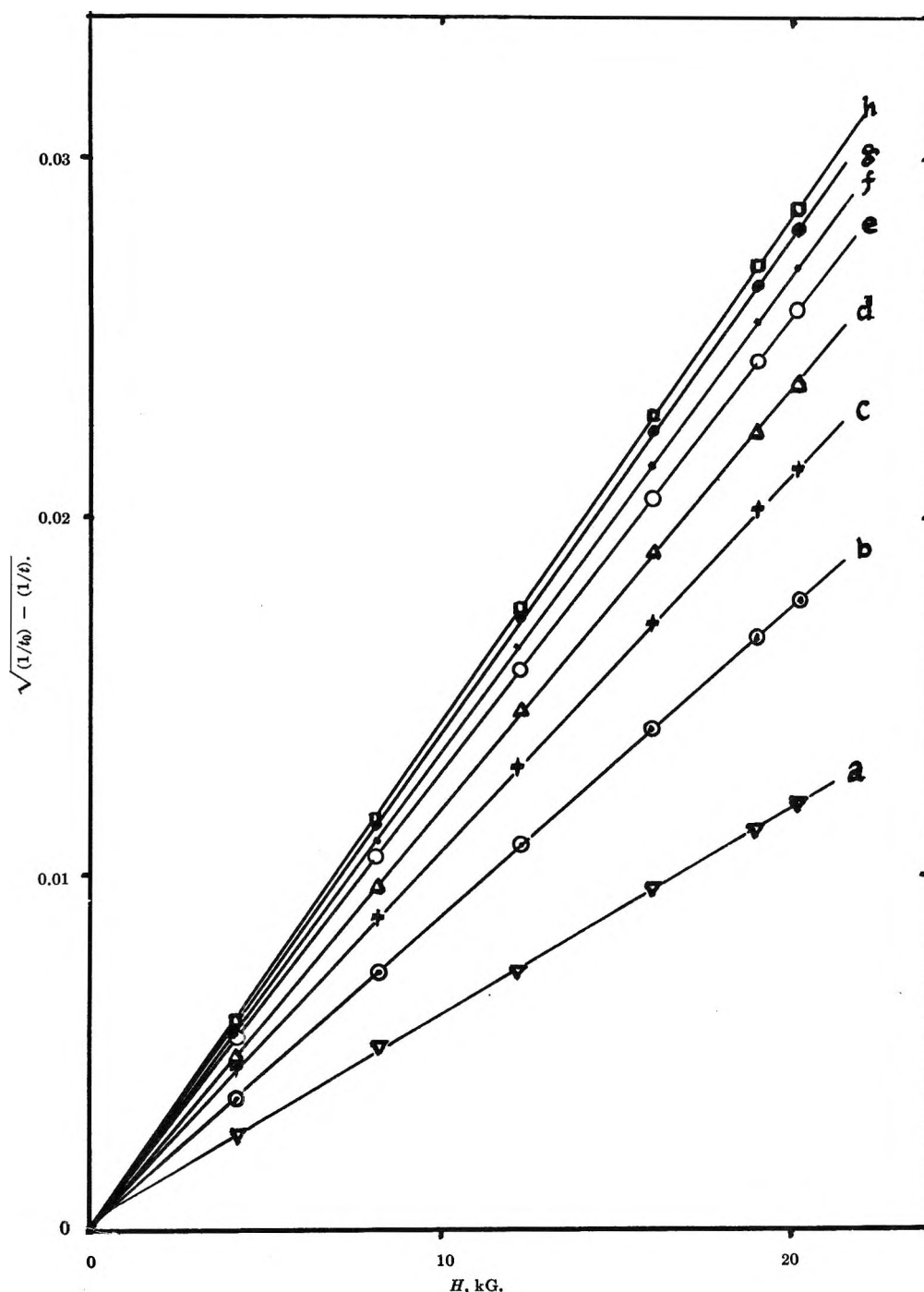


Figure 3. Concentration dependence of the reciprocal time of flow of aqueous solution of  $\text{CoCl}_2$  at  $25^\circ$  vs. the external magnetic field: a, 0.241 M; b, 0.481 M; c, 0.722 M; d, 0.962 M; e, 1.203 M; f, 1.444 M; g, 1.684 M; h, 1.925 M.

$\text{MCl}_n$ . Using eq 5, the Curie-Langevin equation for the molar magnetic susceptibility of the paramagnetic cation,  $\text{M}^{n+}$ , may be expressed as

$$\begin{aligned}
 (\text{M})\chi_+ &= \frac{N\beta^2\mu_{\text{eff}}^2}{3kT} = \\
 &\frac{1000}{C} [(\kappa - \kappa') - (\rho - \rho')\chi_w] + \\
 &[(\text{M}) - n(\text{H})]\chi_w + n(\text{H})\chi_{\text{H}^+} \quad (6)
 \end{aligned}$$

where  $\mu_{\text{eff}}$  denotes the effective magnetic moment in the Bohr magneton unit ( $\beta = 0.9273 \times 10^{-20}$  erg/G);  $N$ ,  $k$ , and  $T$  have their usual significance, and  $(\text{H})$  denotes the atomic weight of hydrogen. The mass magnetic susceptibility of water,  $\chi_w$ , is known by Auer<sup>2</sup> to be  $-0.72224 \times 10^{-6}$  g<sup>-1</sup> at  $25^\circ$  and  $-0.72286 \times 10^{-6}$  g<sup>-1</sup> at  $35^\circ$ . The symbols  $\rho'$  and  $\kappa'$  represent the density and the volume magnetic susceptibility, respec-

(2) H. Auer, *Ann. Physik*, **18**, 593 (1933).

tively, of hydrochloric acid at a concentration  $nC$ . Here the value of  $\kappa'$  for a given concentration  $C'$  was estimated for convenience by using the empirical equation  $\kappa' = \kappa_w + aC'$ , where the constant,  $a$ , was found by the present viscometer method, the density data, and Auer's values of mass magnetic susceptibility of water,  $-1.41 \times 10^{-8}$  and  $-0.23 \times 10^{-8} \text{ ml}^{-1} \text{ mol}^{-1}$  at 25 and 35°, respectively. Finally,  $\chi_{\text{H}^+}$ , denotes the mass magnetic susceptibility of the hydrogen ion,  $\text{H}^+$ , due to its nuclear magnetic moment, which contributes an insignificant amount,  $10^{-10}/\text{g-ion}$ , to the calculation of eq 6. In the case of ferrous chloride, an additional correction must be made for the contribution from the excessive hydrochloric acid that had been previously added for the prevention of hydrolysis.

The effective magnetic moments of some ions of the transition group elements were calculated by the aid of eq 4 and 6, and the results are listed in Table I. Here, the diamagnetic correction for the cation itself was not made. The values of  $\mu_{\text{eff}}$  found are reproducible within  $\pm 0.5\%$ , independent of concentration and temperature of the solution, and match the literature values (Table II). However, here as in many literature values, the deviation of  $\mu_{\text{eff}}$  from the spin-only value is considerable, except for  $\text{Mn}^{2+}$ .

**Table II:** Effective Bohr Magnetron Number,  $\mu_{\text{eff}}$ , for Ions of the Transition Group Elements in Aqueous Solutions

Ion	$\mu_{\text{eff}}$			Spin only
	This work	Selwood <sup>a</sup>	Van Vleck <sup>b</sup>	
$\text{Mn}^{2+}$	$5.87 \pm 0.01$	5.2-5.96 5.4-6.0	5.2-5.96	5.92
$\text{Fe}^{2+}$	$5.36 \pm 0.02$	5.0-5.5 (2.5)	5.33	4.90
$\text{Co}^{2+}$	$4.95 \pm 0.02$	4.4-5.2	4.6-5.0	3.87
$\text{Ni}^{2+}$	$3.34 \pm 0.04$	2.9-3.4	3.23	2.83

<sup>a</sup> Reference 1, p 99. <sup>b</sup> J. H. Van Vleck, "The Theory of Electric and Magnetic Susceptibilities," Oxford University Press, London, 1932, p 285.

On the other hand, the mass magnetic susceptibility,  $\chi$ , of the solution can be calculated when one takes into

consideration the relation  $\kappa = \rho\chi$  for eq 2. Some examples of this direct determination of  $\chi$  at several magnetic field strengths are represented in Table III. The results, including the magnetic moments, are reasonably consistent, except for those obtained from experiments performed at the lowest magnetic field.

**Table III:** The Mass Magnetic Susceptibility,  $\chi$ , of an Aqueous Solution of  $\text{CoCl}_2$  and the Effective Bohr Magnetron Number,  $\mu_{\text{eff}}$ , of  $\text{Co}^{2+}$  Determined at Different Magnetic Field Strengths ( $\beta = 0.9273 \times 10^{-20} \text{ erg/G}$ )

$H$ , G	$C = 1.203 M$ , $\rho = 1.133 \text{ (at } 25^\circ)$			$C = 1.200 M$ , $\rho = 1.130 \text{ (at } 35^\circ)$		
	$t$ , sec	$10^6\chi$ , $\text{g}^{-1}$	$\mu_{\text{eff}}$ ( $\beta$ )	$t$ , sec	$10^6\chi$ , $\text{g}^{-1}$	$\mu_{\text{eff}}$ ( $\beta$ )
0	303.5	...	...	248.1	...	...
4,160	306.3	10.81	5.08	250.2	9.93	4.96
8,200	314.1	10.37	4.98	256.2	9.77	4.90
12,270	328.3	10.42	4.99	267.3	9.91	4.95
16,050	348.0	10.31	4.97	283.0	9.94	4.96
19,050	369.9	10.28	4.96	300.3	9.95	4.96
20,150	380.3	10.28	4.96	308.2	9.93	4.96

These studies show that this viscometer method can give results reproducible to within  $\pm 0.1\%$ ; however, the accuracy of this method depends primarily on the accuracy of the determined  $h$  or  $l$ . Since it is technically difficult to measure  $l$ , the length of the capillary of the viscometer, directly using a scale with an accuracy of  $\Delta l \lesssim \pm 0.5 \text{ mm}$  because of the shape of the capillary endings of viscometer, it is difficult to keep the relative deviation of  $\kappa$  below  $\pm 0.5\%$  in the present work, where  $l$  is measured to be 10.6 cm.<sup>3</sup> On the other hand, the sensitivity of this method can be increased by decreasing  $h$  or by increasing  $\theta$ , the deflection angle of the capillary axis of the viscometer, from 0° to a value near 90°; in this case, however, the slightest uncertainty in measuring  $\theta$  would bring a considerable error into the final results.

(3) Of course, it may be possible to determine the effective value of  $h$  for the measuring by using viscometer data based on pure water and taking Auer's value of susceptibility as the standard for eq 4. In the present work, it was found that  $t_0 = 220.7 \text{ sec}$  and  $\alpha^2 = -0.1578 \times 10^{-12} \text{ sec}^{-1} \text{ G}^{-2}$  for pure water at 25°, which gives an effective value of  $h = 10.58 \text{ cm}$ .

## Statistical Theory for the Equilibrium Distribution of Rigid Molecules in Inert Porous Networks. Exclusion Chromatography

by J. Calvin Giddings, Eugene Kucera, Christopher P. Russell, and Marcus N. Myers

*Department of Chemistry, University of Utah, Salt Lake City, Utah 84112 (Received March 8, 1968)*

The principles of statistical mechanics are used to formulate a general expression for the partitioning of molecules between bulk fluid and inert, solid porous networks. This subject is of particular relevance to gel filtration and permeation chromatography and to other membrane methods used for separating macromolecules. The theory is first applied to a model in which rigid molecules, ranging in shape from spherical to thin rod, partition in various pores of simple shape and in distributions of such pores. The rigid-molecule model is applicable to many species, *e.g.*, the DNA's, of biological interest. In order to simulate better the behavior of real networks, the theory is developed for random porous networks. From one of these, the random-plane model, we get a simple exponential partitioning law and find that a new parameter, the *mean external length*,  $\bar{L}$ , uniquely determines the partitioning of all rigid molecules. The latter finding is tested for the simple networks, also, to see if the properties of  $\bar{L}$  are in any sense universal. It is found that  $\bar{L}$  better characterizes partitioning in the examined systems than previously proposed parameters such as radius of gyration, equivalent hydrodynamic radius, and molecular weight.

### Introduction

Many macromolecular separation techniques rely on a differential penetration of molecules into porous materials. Various membrane techniques such as ultrafiltration and differential dialysis, along with the powerful gel-exclusion methods of chromatography,<sup>1,2</sup> are foremost examples. The equilibrium distribution coefficient of macromolecules between bulk liquid and these porous networks must be known in order to characterize the systems.

Many model systems and empirical rules have been used to obtain equations for the dependence of the partition coefficient on molecular and pore dimensions.<sup>3</sup> The theoretical models have generally been limited to simple molecules, *e.g.*, spheres, and to simple pore networks. In the first rigorous treatment of such a model, Porath treated an equivalent spherical molecule in conical pores.<sup>4</sup> He correctly recognized that the volume "available" to a penetrating molecule was less than that of the cone because of finite molecular radius. An altogether different pore network was treated by Laurent and Killander,<sup>5</sup> who used an equation by Ogston<sup>6</sup> to determine the partitioning of a sphere in a network of random rods. By contrast, the only rigorous treatment of nonspherical molecules is that by Casassa for flexible polymer chains in various simple pores.<sup>7</sup>

Perhaps the most generally accepted principle of exclusion chromatography is that by Flodin,<sup>8</sup> who assumed microregions of excluded volume which increase with molecular size. This principle, as it stands, is valid only for spherical molecules; its proper extension, as we discuss here, revolves around excluded volume in general configuration space.

It is clear on theoretical grounds that a macromole-

cule will be partially excluded even from pores so large that there is no physical barrier to penetration. This partial exclusion is due to a statistical or configurational entropy phenomenon. Thus a rod-shaped macromolecule near a wall is not entirely free to rotate; certain angular configurations are forbidden because they entail a partial overlap, Figure 1. In this case exclusion is essentially a surface effect (a viewpoint especially emphasized here), deriving from the steric constraints which any surface will impose on nearby molecules. The loss of entropy resulting from these constraints, and thus the partial exclusion from such regions, is magnified in porous media because of the relatively large surface area.

Central to chromatographic applications is the assumption that migration rate is a function of partitioning *equilibrium*. (Transport properties are assumed to enter only when considering peak dispersion.) The close relationship between equilibrium and migration has been discussed elsewhere.<sup>9</sup> Occasionally migration is attributed to nonequilibrium.<sup>10</sup> However, the evidence that most chromatographic migration is an "equi-

- (1) J. Porath and F. Flodin, *Nature*, **183**, 1657 (1959).
- (2) J. C. Moore, *J. Polym. Sci., Part A*, **2**, 835 (1964).
- (3) R. L. Pecsok and D. Saunders, *Separation Sci.*, **1**, 613 (1966).
- (4) J. Porath, *Pure Appl. Chem.*, **6**, 233 (1963).
- (5) T. C. Laurent and J. Killander, *J. Chromatogr.*, **14**, 317 (1964).
- (6) A. G. Ogston, *Trans. Faraday Soc.*, **54**, 1754 (1958).
- (7) E. F. Casassa, *Polym. Lett.*, **5**, 773 (1967).
- (8) P. Flodin, Ph.D. Dissertation, University of Uppsala, Uppsala, Sweden, 1962.
- (9) J. C. Giddings, "Dynamics of Chromatography. Part 1. Principles and Theory," Marcel Dekker, Inc., New York, N. Y., 1965.
- (10) G. K. Ackers, *Biochemistry*, **3**, 723 (1964).

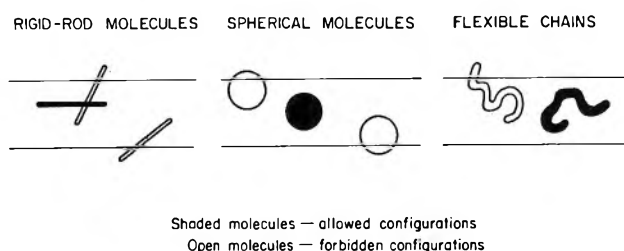


Figure 1. Illustration of allowed and forbidden configurations.

librium" phenomenon is very strong. The arguments favoring the equilibrium concept are: (1) partition coefficients obtained by chromatographic (usually glpc) means are generally in excellent agreement with those obtained by static methods; (2) peak elution volumes are usually flow independent; and (3) on fundamental theoretical grounds, a large departure from equilibrium is totally incompatible with the narrow peaks obtained from good chromatographic systems. It is, of course, conceivable that a few "ink-bottle" pores might reach equilibrium only slowly with respect to outside concentration. If their volume is small, no effect beyond minor tailing will be observed. If some pores are totally closed off or cannot be reached by the molecules in any sequence of configurations, their volume is not to be counted. If nonequilibrium should become a strong factor, which is conceivable under certain conditions, it would immediately reveal itself through excessive peak spreading and poor resolution.<sup>9</sup>

### General Equilibrium Theory

*General Formulation.* Like other kinds of thermodynamic equilibrium, the present case can be most generally related to molecular and external interactions through the formalism of statistical mechanics. Thus the equilibrium partition constant  $K$  is the ratio of partition functions for molecules within the pores and within the bulk liquid, respectively, and is consequently the ratio of the two configuration integrals

$$K = \frac{\iiint \text{drd}\psi \text{d}\lambda \exp[-\epsilon_p(\mathbf{r}, \psi, \lambda)/kT]}{\iiint \text{drd}\psi \text{d}\lambda \exp[-\epsilon_b(\lambda)/kT]} \quad (1)$$

Generalized coordinates  $\mathbf{r}$ ,  $\psi$ , and  $\lambda$  describe molecular position, orientation, and conformation (free internal variables), respectively. Coordinate  $\mathbf{r}$ , which here specifies the location of the molecular center of gravity, extends completely over an element of the porous network having unit free volume and over a unit volume of the bulk liquid, respectively. (The finite slope of the repulsive interaction between molecule and pore wall makes the definition of "free volume" theoretically and experimentally imprecise. In practice it is well defined and reasonably accessible to measurement. More satisfying theoretically would be a partition coefficient whose network concentration was defined in reference to the total network volume, the free as well

as restricted regions, *i.e.*,  $\mathbf{r}$  restricted to unit network volume. In any case,  $K$  is uniquely defined once free volume is specific and can be easily transformed.)

We now approximate the energies in "porous" and "bulk" configurations,  $\epsilon_p$  and  $\epsilon_b$ , respectively, as additive sums of appropriate terms. In the bulk liquid we will have an energy  $\epsilon_M$  due to intramolecular interactions (thus depending upon conformation coordinate  $\lambda$ ) and an energy  $\epsilon_{MN}$  due to intermolecular interactions; thus  $\epsilon_b = \epsilon_M + \epsilon_{MN}$ . (We omit solute-solvent interaction terms, except as they influence  $\epsilon_M$  and  $\epsilon_{M_p}$ , below, since they are equal in and out of the pore.) Within the porous network there is, in addition, an energy term,  $\epsilon_{M_p}$ , stemming from interactions between the macromolecule and the pore walls; thus  $\epsilon_p = \epsilon_M + \epsilon_{MN} + \epsilon_{M_p}$ . Substitution of these expressions back into eq 1 provides a reasonably general framework for such equilibrium applicable to both rigid and flexible molecules. The following treatment will entail various assumptions leading to the calculations central to this paper.

First we arbitrarily impose a restriction to linear isotherms (the limiting  $K$  as we approach infinite dilution), for which we may write  $\epsilon_{MN} = 0$ . This limit is of the form

$$K = \frac{\iiint \text{drd}\psi \text{d}\lambda \exp[-\epsilon_M(\lambda)/kT] \exp[-\epsilon_{M_p}(\mathbf{r}, \psi, \lambda)/kT]}{\iiint \text{drd}\psi \text{d}\lambda \exp[-\epsilon_M(\lambda)/kT]} \quad (2)$$

*Rigid Molecules.* We next assume that all "accessible" conformations are energetically equal or that only a single conformation exists (rigid molecule), such that  $\epsilon_M = 0$ . We further assume that a "hard-wall" potential can be used to describe  $\epsilon_{M_p}$ . This means that the geometrical extension of pore walls and macromolecule must be approximated by distinct and discontinuous (although perhaps complex) boundaries, the overlap of which leads to  $\epsilon_{M_p} = \infty$  and the disengagement of which yields  $\epsilon_{M_p} = 0$ . Such a potential function does not account for adsorptive forces; however, the latter represents a separate phenomenon outside the scope of this treatment (although accounted for above).

Since  $\epsilon_{M_p}$  is discontinuous in configuration space, restricted to the two values zero and infinity, the Boltzmann factor,  $\exp(-\epsilon_{M_p}/kT)$ , is likewise discontinuous. Its value is 1 for all molecular configurations free from wall overlap and 0 for overlapping configurations. We now generalize our treatment of the Boltzmann factor to accommodate random pores.

In describing the behavior of real porous materials it is desirable to introduce pores whose dimensions are fixed by random planes, rods, etc. In such cases the location of a pore wall is not definite but is fixed by a probability density function. We may imagine an



ensemble of random-pore networks with pore walls so distributed. A molecule of given configuration (fixed  $\mathbf{r}$ ,  $\psi$ ,  $\lambda$ ) will fail to intersect a pore wall in a certain fraction of the pore networks. This fraction, of course, will equal the ensemble average,  $\langle \exp(-\epsilon_{MP}/kT) \rangle$ . We now introduce the parameter  $q(\mathbf{r}, \psi, \lambda)$ , which can be taken as the latter ensemble average and which can be alternately defined as the probability that a molecule of given configuration is *not* intersected by a pore wall. Clearly for random pores  $q$  may range continuously from 0 to 1; for uniform pores it must be 0 or 1. (The use of an ensemble average to treat random-pore networks can actually be introduced into eq 1 and carried through the subsequent equations. However, only in the "hard-wall" approximation is  $q$ , defined as an ensemble average of the Boltzmann factor, equivalent to the alternate definition of  $q$  as the probability of no intersection with pore walls.)

With the above treatment of the molecule-pore interaction term,  $\epsilon_{MP}$ , and the condition that  $\epsilon_M = 0$ , eq 2 reduces to the simple form

$$K = \frac{\iiint d\mathbf{r} d\psi d\lambda q(\mathbf{r}, \psi, \lambda)}{\iiint d\mathbf{r} d\psi d\lambda} \quad (3)$$

which shows  $K$  to be the configuration-space average of  $q$ .

In view of the probabilistic interpretation of  $q$ , we see that the present case, reduced to its most fundamental aspects, revolves around the probability that two arbitrary surfaces intersect one another. The two surfaces describe the physical boundaries of the molecule and the pore network, respectively.

Clearly the restraints imposed by any fixed pore wall will cause a local reduction in concentration near the wall. Local concentration will increase as one moves away from the wall, finally reaching bulk value when the distance from the center of gravity to the wall exceeds that from the center of gravity to the farthest extreme of the molecule (so that  $q = 1$  for all orientations and conformations at that position). This phenomenon is described by a local partition coefficient,  $\kappa$ , the relative density of centers of gravity as a function of position  $\mathbf{r}$ .

$$\kappa(\mathbf{r}) = \frac{\iint d\psi d\lambda q(\mathbf{r}, \psi, \lambda)}{\iint d\psi d\lambda} \quad (4)$$

We define also another local partition coefficient,  $\kappa'$ , which is the distribution coefficient for molecules with fixed conformation and orientation

$$\kappa'(\psi, \lambda) = \frac{\int d\mathbf{r} q(\mathbf{r}, \psi, \lambda)}{\int d\mathbf{r}} \quad (5)$$

Our present calculations deal mainly with rigid molecules which lack internal degrees of freedom. In this case eq 3 reduces to

$$K = \frac{\iint d\mathbf{r} d\psi q(\mathbf{r}, \psi)}{\iint d\mathbf{r} d\psi} = \frac{\int d\mathbf{r} \kappa(\mathbf{r})}{\int d\mathbf{r}} = \frac{\int d\psi \kappa'(\psi)}{\int d\psi} \quad (6)$$

These forms will be used to obtain  $K$  for subsequent models.

The above formulation can be interpreted thermodynamically with enthalpy and entropy terms acquired in the usual way. We note that the model leading to eq 3 permits only monoenergetic configurations; enthalpy effects are therefore absent. In this case, the standard free energy change is simply  $\Delta G^\circ = -T\Delta S^\circ$ . The entropy term, of course, is equivalent to  $\Delta S^\circ = R \ln(\Omega/\Omega_0)$ , where  $\Omega/\Omega_0$  is the ratio of accessible microscopic configurations or states within the free pore volume compared with those in an equal volume of bulk liquid. The ratio  $\Omega/\Omega_0$  is clearly the ratio of configuration integrals and is equal to  $K$ . We conclude that the dominant effect in this kind of equilibrium relates to changes in configurational entropy. A similar conclusion has been reached for the case of flexible polymer chains by Casassa.<sup>7</sup>

### Uniform-Pore Networks

In this case we assume a porous network composed of identical, simple pores. We need, fortunately, deal with only one of them, this being representative of all. The coordinate system is fixed to this pore and the above integrations applied. Nonintersection coefficient  $q$  is either 0 or 1, depending upon the configuration, all other values being ruled out by the fixed geometry.

*Molecules of Spherical Shape.* Rotational states can be ignored here, reducing the complexity to that of integration over the positional coordinate only. The local partition coefficient will be  $\kappa = 0$  if the sphere center is closer to the nearest wall than its radius  $L_0/2$ ; otherwise  $\kappa = 1$ .

First, consider pores of infinite length and circular cross section ("circular" pores) with diameter  $d_0$ . (Following this, all pore dimensions will be represented by lower case symbols and molecular dimensions will be represented by capitals. See the list of Principal Symbols at end of text.) We have

$$\begin{aligned} \kappa &= 1 \quad (\text{for } 0 \leq r \leq (d_0 - L_0)/2) \\ \kappa &= 0 \quad (\text{for } (d_0 - L_0)/2 \leq r \leq d_0/2) \end{aligned} \quad (7)$$

Applying eq 6, in the next to last form, we find  $K$  as the ratio of two circular areas, one with diameter  $d_0 - L_0$  and one with diameter  $d_0$

$$\begin{aligned} K &= [1 - (L_0/d_0)]^2 = [1 - (L_0s/4)]^2 \quad (L_0 < d_0) \\ K &= 0 \quad (L_0 \geq d_0) \end{aligned} \quad (8)$$

Quantity  $s$  is the surface area per unit of free volume or the reciprocal "hydraulic radius." Henceforth, pore size will be represented by  $s$ . Quantity  $L_0s$  is simply a dimensionless size ratio (of molecules to pores). We

will find that this kind of dimensionless parameter is crucial to all partition equations.

Similarly, for an infinite pores with rectangular sides  $d_0$  and  $d_1$

$$K = \left[ 1 - \frac{L_0 s}{2(1+p)} \right] \left[ 1 - \frac{p L_0 s}{2(1+p)} \right] \quad (L_0 \leq d_0) \quad (9)$$

where  $p = d_1/d_0$  and  $d_0 \leq d_1$ . For brevity we omit now separate expressions for the totally excluded cases,  $K = 0$ ; for small pores in this instance. This occurs when  $d_0 \leq L_0$ . Interestingly, eq 9 reduces to eq 8 as  $p \rightarrow 1$ ; i.e., square and circular pores of equal  $s$  have identical partitioning for spherical molecules.

When pores exist between infinite parallel plates we have

$$K = 1 - (L_0 s/2) \quad (L_0 \leq 2/s) \quad (10)$$

and when they are spherical cavities

$$K = [1 - (L_0 s/6)]^3 \quad (L_0 \leq 6/s) \quad (11)$$

In the latter case we must rationalize the need for ingress and egress (see later).

More difficult is the case of an infinite pore of elliptical cross section. We give this result for completeness

$$K = 1 + \frac{\alpha^2}{p} - \frac{4\alpha}{\pi} E\left(\frac{\pi}{2}, \frac{(p^2 - 1)^{1/2}}{p}\right) \quad \left(\alpha < \frac{1}{p} \leq 1\right) \quad (12a)$$

and

$$K = \frac{2}{\pi} \arcsin \left[ p \left( \frac{1 - \alpha^2}{p^2 - 1} \right)^{1/2} \right] + \frac{\alpha^2}{p} \arcsin \left[ \frac{1}{\alpha} \left( \frac{1 - \alpha^2}{p^2 - 1} \right)^{1/2} \right] - \frac{4\alpha}{\pi} \left\{ E\left[\frac{\pi}{2}, \frac{(p^2 - 1)^{1/2}}{p}\right] - E\left\{ \arcsin \left[ \frac{1}{\alpha} \left( \frac{\alpha^2 p^2 - 1}{p^2 - 1} \right)^{1/2} \right], \frac{(p^2 - 1)^{1/2}}{p} \right\} \right\} \quad \left(\frac{1}{p} < \alpha \leq 1\right) \quad (12b)$$

where  $E(\alpha, x)$  is the elliptical integral of the second kind,  $p = d_1/d_0$ , the ratio of the long and short axes of the elliptical cross section, and  $\alpha = L_0/d_0 = p L_0 s/(1+p)$ . These expressions reduce to eq 8 and 10 as  $p$  approaches 1 and  $\infty$ , respectively.

*Rigid Molecules with Rotational Symmetry.* When molecules with an axis of symmetry occupy pores of infinite length and constant cross section, eq 6 (last expression) reduces to the specific form

$$K = \frac{\int_0^{\pi/2} d\theta \int_0^\pi d\phi \kappa'(\theta, \phi) \sin \theta}{\int_0^{\pi/2} d\theta \int_0^\pi d\phi \sin \theta} \quad (13)$$

where  $\theta$  is the angle between the principal axes of pore and molecule and  $\phi$  is the azimuth.

The first step in dealing with this integral is the evaluation of  $\kappa'(\theta, \phi)$ , eq 5. This quantity can be calculated as the fraction of the pore cross section accessible to the "area" projected onto that cross section by the arbitrarily oriented molecule. For instance, a thin rod of length  $L_1$  will project a line of length  $L_1 \sin \theta$ . If the cross section is circular, the center of such a line (of fixed  $\theta$ ) can "explore" the fractional area

$$\kappa' = \frac{16}{\pi d_0^2} \int_0^{1/2 [d_0^2 - L_1^2 \sin^2 \theta]^{1/2}} \{ [(d_0^2/4) - r^2]^{1/2} - L_1 \sin(\theta/2) \} dr \quad (L_1 \sin \theta \leq d_0) \quad (14)$$

where quantity  $\kappa'$  is zero for  $L_1 \sin \theta \geq d_0$ .

Since  $\kappa'$  is not dependent on  $\phi$  in circular pores,  $K$  is simply

$$K = \frac{\int_0^{\pi/2} d\theta \kappa' \sin \theta}{\int_0^{\pi/2} d\theta \sin \theta} = \int_0^{\pi/2} d\theta \kappa' \sin \theta \quad (15)$$

The expressions for this integral appear in eq 18.

By the same method, substituting new parameters  $\alpha = L_0/d_0$  and  $\beta = L_1/d_0$  and variable  $\zeta = r/(L_0/2)$ , we obtain of an ellipsoid of revolution in a cylindrical pore the integral

$$K = \iint d\theta d\zeta \sin \theta (1 - \zeta^2)^{1/2} \times \left( 1 - \frac{(\alpha^2 - \beta^2) \cos^2 \theta + \beta^2}{\{\alpha^2 \zeta^2 + [(\alpha^2 - \beta^2) \cos^2 \theta + \beta^2](1 - \zeta^2)\}^{1/2}} \right) \times \left( 1 - \frac{\alpha^2 [(\alpha^2 - \beta^2) \cos^2 \theta + \beta^2]}{\{\alpha^2 \zeta^2 + [(\alpha^2 - \beta^2) \cos^2 \theta + \beta^2](1 - \zeta^2)\}^{3/2}} \right) \quad (16)$$

where integration limits for  $\theta$  in the interval  $(0, \pi/2)$  and  $\zeta$  in  $(0, 1)$  are such that both multiplicands in parenthesis are positive and

$$0 < 1 - \frac{\alpha^2}{\{\alpha^2 \zeta^2 + [(\alpha^2 - \beta^2) \cos^2 \theta + \beta^2](1 - \zeta^2)\}^{1/2}}$$

For the case of the rectangular pore we obtain

$$K = \frac{2}{\pi} \iint d\theta d\phi \sin \theta \times \{ 1 - [\alpha^2 + (\beta^2 - \alpha^2) \sin^2 \theta \sin^2 \phi]^{1/2} \} \times \left\{ 1 - \frac{1}{p} [\alpha^2 + (\beta^2 - \alpha^2) \sin^2 \theta \cos^2 \phi]^{1/2} \right\} \quad (17)$$

where integration limits for  $\theta$  in  $(0, \pi/2)$  and  $\phi$  in  $(0, \pi/2)$  are again such that both multiplicands are

positive. Unfortunately, these integrals cannot be expressed in terms of elementary functions; numerical evaluation is necessary, even for a flat disk ( $\beta = 0$ ). For a thin rod ( $\alpha = 0$ ), we get the following equations for a cylindrical pore

$$K(\beta) = 1 - \frac{4}{3\pi\beta} \left[ (1 - \beta^2)E\left(\frac{\pi}{2}, \beta\right) - (1 - \beta^2)F\left(\frac{\pi}{2}, \beta\right) \right] \quad (\beta \leq 1) \quad (18a)$$

$$K(1) = 1 - \frac{8}{3\pi} \doteq 0.151 \quad (\beta = 1) \quad (18b)$$

$$K(\beta) = 1 - \frac{4}{3\pi} \left[ (1 + \beta^2)E\left(\frac{\pi}{2}, \frac{1}{\beta}\right) - (\beta^2 - 1)F\left(\frac{\pi}{2}, \frac{1}{\beta}\right) \right] \quad (\beta \geq 1) \quad (18c)$$

where  $F(\alpha, x)$  is the elliptical integral of the first kind. For a rectangular pore, we have

$$K(\beta, p) = 1 - \frac{1+p}{2p}\beta + \frac{2\beta^2}{3\pi p} \quad (\beta \leq 1) \quad (19a)$$

$$K(\beta, p) = \frac{1}{2\beta} - \frac{\beta}{2p} + \frac{2\beta^2}{3\pi p} + \frac{\beta}{\pi p} \arccos \frac{1}{\beta} - \frac{1}{3\pi p} (\beta^2 - 1)^{1/2} [2\beta + (1/\beta)] \quad (1 \leq \beta \leq p) \quad (19b)$$

$$K(\beta, p) = K'' = \frac{1}{2\beta} + \frac{p}{2\beta} + \frac{2\beta^2}{3\pi p} - 1 + \frac{\beta}{\pi p} \arccos \frac{1}{\beta} + \frac{\beta}{\pi} \arccos \frac{p}{\beta} - \frac{1}{3\pi p} (\beta^2 - 1)^{1/2} [2\beta + (1/\beta)] - \frac{1}{3\pi p} (\beta^2 - p^2)^{1/2} \left( 2\beta + \frac{p^2}{\beta} \right) \quad (p \leq \beta \leq (1 + p^2)^{1/2}) \quad (19c)$$

$$K(\beta, p) = K'' + \frac{2}{\pi} \arcsin \left[ \frac{p^2(\beta^2 - p^2 - 1)}{(\beta^2 - p^2)(1 + p^2)} \right]^{1/2} + \frac{2}{\pi} \arcsin \left[ \frac{\beta^2 - p^2 - 1}{(\beta^2 - 1)(1 + p^2)} \right]^{1/2} - \frac{1}{\pi} \left( \frac{p}{\beta} + \frac{\beta}{p} \right) \arcsin \left( \frac{\beta^2 - p^2 - 1}{\beta^2 - p^2} \right)^{1/2} - \frac{1}{\pi} \left( \beta + \frac{1}{\beta} \right) \arcsin \left[ \frac{p^2(\beta^2 - p^2 - 1)}{\beta^2 - p^2} \right]^{1/2} + \frac{\beta}{3\pi p} \left( 2 + \frac{p^2}{\beta^2} + \frac{1}{\beta^2} \right) (\beta^2 - p^2 - 1)^{1/2} \quad ((1 + p^2) \leq \beta) \quad (19d)$$

Equations 16 and 17, apply specifically to the partitioning of ellipsoids of revolution in several pore

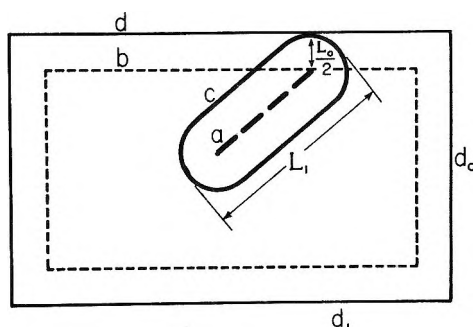


Figure 2. Illustration of equivalent configurations for treating capsule-shaped molecules. The allowed and forbidden configurations for thin-rod molecule a in pore b are identical with those for capsule-shaped molecule c in pore d.

types. However, from a special case of these results, eq 18 and 19 for infinitely thin rods ( $\alpha = 0$ ), we can generate solutions for a whole new class of molecular models. The latter appear easier to deal with than the ellipsoids, and thus will have considerable utility in our present studies.

We begin with the limiting case of an infinitely thin rod, eq 18 and 19. We then add to this rod a layer of radius  $L_0/2$  extending in all directions, so that we generate a capsule-shaped molecule (hemispheres capping each end of a right-angle cylinder). Simultaneously, we enlarge the pore diameter by  $L_0$ . Clearly each configuration possible before this operation is still possible after it; each one forbidden before is forbidden afterward. This is illustrated in Figure 2. The configuration integral for a single pore is identical in the two cases, but since the free volume has been increased, the configuration integral (and thus  $K$ ) is decreased in like proportion.

The desired operation is achieved mathematically in two steps. First we substitute  $p'$  and  $\beta'$  for  $p$  and  $\beta$  in eq 18 and 19. These new quantities are defined by

$$\beta \longrightarrow \beta' = \frac{L_1 - L_0}{d_0 - L_0} \quad (20a)$$

$$p \longrightarrow p' = \frac{d_1 - L_0}{d_0 - L_0} \quad (20b)$$

Second, we multiply  $K(\beta')$  or  $K(\beta', p')$  from eq 18 or 19 such that

$$K = \frac{(d_0 - L_0)^2}{d_0^2} K(\beta') \quad (21)$$

or

$$K = \frac{(d_0 - L_0)(d_1 - L_0)}{d_0 d_1} K(\beta', p') \quad (22)$$

for cylindrical or rectangular pores, respectively. We express  $\beta'$  and  $p'$  in terms of the dimensionless parameters  $M = L_0/L_1$ ,  $p = d_1/d_0$ , and  $sL_1$ . For cylindrical pores

$$\beta' = \frac{(1 - M)sL_1}{2 - MsL_1} \quad (23)$$

while for rectangular pores

$$\beta' = \frac{p(1 - M)sL_1}{2(1 + p) - pMsL_1} \quad (24a)$$

and

$$p' = \frac{2p(1 + p) - pMsL_1}{2(1 + p) - pMsL_1} \quad (24b)$$

For a thin rod, of course,  $M = 0$ , while for a sphere  $M = 1$ .

**Distribution of Uniform Pores.** Most porous media are characterized by a considerable dispersion in pore size. One means of accounting for this is to assume pores of a given shape where a density function  $f(s)$  represents the size distribution. Thus the fraction of pore volume whose surface:volume ratio lies between  $s$  and  $s + ds$  is  $f(s)ds$ . The over-all  $K$  is then simply a sum or integral of the component distribution coefficients for each kind of pore

$$K = \int_0^\infty K'(s'L)f(s') ds' \quad (25)$$

where  $L$  is the characteristic length of a molecule. The obvious generalization is to assume various kinds of pores, each with its own density function  $f_i(s)$  and distribution coefficient  $K_i'(sL)$

$$K = \sum_i \int_0^\infty K_i'(s'L)f_i(s') ds' \quad (26)$$

Here, of course,  $\sum_i \int_0^\infty f_i(s') ds' = 1$ , while the surface area per unit volume is  $s = \sum_i \int_0^\infty s'f_i(s') ds'$ .

### Theory of Partitioning in Random Pores

As shown above, an element of nonuniformity and randomness can be introduced into the porous network by choosing density functions,  $f_i(s)$ , corresponding to a broad range of pore shapes and sizes. However, in general, this approach appears to us as unduly artificial and cumbersome, unless specific knowledge is available relative to the size and shape distribution. Otherwise, one must be arbitrary in the choice of pore shapes and size distribution. While the approach below is not entirely free from such objections, it is at once more direct and provides simpler results for less well-characterized systems. Rather remarkably, the results in some cases are simpler and of broader scope than those for the most elementary of uniform pores.

We have pursued the thesis that exclusion is a surface-overlap phenomenon. Therefore a random-pore network may be thought of as an initially free volume partitioned into pores by surfaces of random location and orientation. If a molecule of given configuration in the free space is intersected by one or more of the

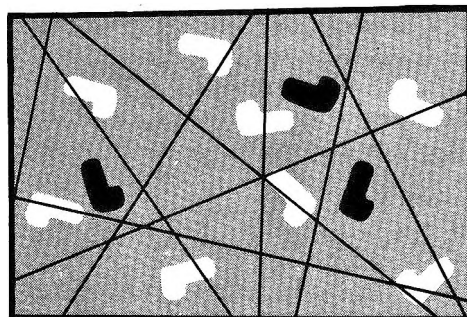


Figure 3. The randomly positioned bodies represent molecules initially in equilibrium in *bulk* fluid. Those molecules (unshaded) cut by the superimposed random surfaces are excluded from the hypothetical pore network created by those surfaces. The partition coefficient  $K$  is the ratio of the number of uncut (shaded) molecules to the total.

inserted surfaces, that macromolecule represents a forbidden state which is automatically excluded from the porous network ( $q = 0$ ). This is illustrated in Figure 3.

The theoretical problem of random pores can be generally handled by the formalism of the last section, which deals with the probability of such intersection. It is only necessary to evaluate  $q(\mathbf{r}, \psi, \lambda)$  in the various cases in order that the integrations can be applied.

If the porous medium is homogeneous (but not necessarily isotropic),  $q$  loses its dependence on  $\mathbf{r}$  and thus equals the local partition coefficient,  $\kappa'$ , defined by eq 5. If it is isotropic,  $q$  is independent of  $\psi$ . If the molecule is rigid,  $q$ , as before, does not depend upon  $\lambda$ . All such cases and combinations of cases have relevance for particular systems.

Frequently it is useful to imagine a porous network composed of several independent systems of surfaces. In this case  $q = q_1q_2 \dots q_n$ , and the partition coefficient, eq 3, is of the form

$$K = \frac{\iiint d\mathbf{r} d\psi d\lambda \Pi q_i(\mathbf{r}, \psi, \lambda)}{\iiint d\mathbf{r} d\psi d\lambda} \quad (27)$$

The simplest model network is constructed of infinite parallel planes randomly positioned along the  $x$  axis with mean spacing  $\bar{d}_x$ . Let  $L_x(\psi, \lambda)$  equal the molecular projection onto the  $x$  axis when in a certain configuration. The configuration-dependent partition coefficient,  $\kappa'(\psi, \lambda) = q(\psi, \lambda)$ , for this homogeneous, anisotropic medium follows the Poisson distribution

$$\kappa' = q = \exp(-L_x/\bar{d}_x) = \exp(-sL_x/2) \quad (28)$$

When integrated (averaged) over angle and conformational coordinates, this yields  $K$ . However, there is no universal integrated form; in general, we are left with an integral expression whose complexity increases with that of the molecular geometry. Molecules of spherical shape, with  $L_x = L_0$  (the sphere diameter), are subject to the simplest treatment. In this case

$$K = \exp(-sL_0/2) \quad (29)$$

which is roughly comparable with eq 10 for a sphere between equally spaced planes.

We now consider a network constructed from  $n$  systems of random, parallel planes, each with an arbitrary orientation and mean spacing  $\bar{d}_i$ . Our molecule of fixed configuration projects a length  $L_i$  along the axis normal to the  $i$ th system of planes. For each plane system there is a unique  $q_i = \exp(-s_i L_i/2)$ , following eq 28. For  $\kappa' = q = \prod q_i$ , we have

$$q = \prod_n \exp(-s_i L_i/2) = \exp(-\sum_n s_i L_i/2) = \exp(-s \sum_n L_i w_i/2) \quad (30)$$

where  $w_i (\sum_n w_i = 1)$  describes the angle-dependent distribution of surfaces. This expression can be modified readily to account for a continuous angular distribution of planes. Equation 30 is to be substituted back into eq 27 to get  $K$ .

We now consider an isotropic network of random planes (the *random-plane model*). For this we make all weighting factors equal,  $w_i = 1/n$ , and let  $n$  approach infinity. We further stipulate that all plane orientations are equally represented. In this limit

$$q = \exp(-s\bar{L}/2) \quad (31)$$

where  $\bar{L}$  is the mean length of projection of the molecule along the various axes. While  $L_i$  is a function of molecular orientation  $\psi$ ,  $\bar{L}$  is not by virtue of the continuous isotropic condition. The partition coefficient from eq 27 now becomes

$$K = \frac{\int d\lambda \exp[-s\bar{L}(\lambda)/2]}{\int d\lambda} \quad (32)$$

and one need only average over conformational states to arrive at  $K$ .

For rigid molecules we have

$$K = \exp(-s\bar{L}/2) \quad (33)$$

This equation is valid for molecules of any shape, no matter how complex. It is the first rigorous equation with a definable size parameter covering all fixed molecular geometries. Quantity  $\bar{L}$  is the crucial dimension. Two molecules of equal  $\bar{L}$  will partition identically in such a network despite any conceivable difference in shape. We call  $\bar{L}$  the *mean external length*, reflecting the fact that only the extreme groups of the molecule affect its partitioning behavior. Internal shielded groups have no effect.

The simple and yet universal nature of the (above)  $K$  expression for the random-plane model is of considerable interest. The fact that it is valid for a random network having many odd pore shapes suggests that it may at once reflect the characteristics of many kinds of pores. In the Results section we will investigate how

well  $\bar{L}$  characterizes partitioning in other pore networks.

We note that the random-plane model entails philosophical ingress and egress problems. This will likely not detract from the basic surface-overlap effect and thus the nature of the  $K$  vs.  $s$  relationship. This problem does not exist in the two-dimensional random-plane model. However, the anisotropy of this model causes considerable complication and prevents the extraction of a simple length parameter, although it can be shown that  $\bar{L}$  serves as a rough approximation here also. Only with spheres do the two models yield identical results.

A treatment analogous to the above can be used when the random elements are not plane surfaces. For instance, if the network is composed of randomly positioned thin rods or fibers pointed along the  $x$  axis, the local partition coefficient of eq 28 becomes

$$\kappa' = q = \exp(-A_x/\bar{a}_x) \quad (34)$$

Where  $A_x$  is the *area* of the molecule projected on a plane normal to the  $x$  axis and  $\bar{a}_x$  is the mean cross section occupied by the rigid fiber, a term analogous to mean spacing  $\bar{d}_x$  for planes.

In the isotropic random-fiber case, using  $q = \prod q_i$  as in the random-plane model, we get the simple analog of eq 33

$$K = \exp(-\bar{A}h) \quad (35)$$

where  $\bar{A}$  is the projection,  $A_x$ , averaged over all directions in space and  $h$  is the fiber length per unit volume.

If the fiber diameter,  $l_0$ , is not negligible by comparison with the dimension of the molecule, the general result is somewhat more complicated. First  $A_x$  must be interpreted as the molecule's projected area *plus* the area generated by rolling a circle of diameter  $l_0$  around the perimeter of the projection of the molecule. Second,  $\kappa'$  and  $K$  become equilibrium constants in reference to unit network volume, not just unit *free* volume. Thus each expression must be multiplied by  $1/f'$ , where  $f'$  is the porosity of the network. With these changes the equations are still valid.

The above expression, like eq 33 for random planes, is valid for any molecular shape. Parameter  $\bar{A}$  replaces  $\bar{L}$  as a general measure of partitioning. Unfortunately  $\bar{A}$  is more difficult to evaluate if the fiber diameter,  $l_0$ , is finite. Also length parameter  $h$  replaces area parameter  $s$ , reflecting the altered nature of the assumed network.

In the special case involving spherical molecules of diameter  $L_0$  and fibers of finite diameter  $l_0$ , eq 35 reduces to

$$K = (1/f') \exp[-\pi h(L_0 + l_0)^2/4] \quad (36)$$

which equation forms the basis of the Laurent-Killander-Ogston theory of exclusion chromatography mentioned earlier. (This equation is also valid in the one-dimensional, anisotropic case.) The use of a random-

fiber (or brush-pile) model is physically reasonable for true gels where molecular chains define the pore network.<sup>11</sup>

*Equations for  $\bar{L}$  for Various Molecules.* Since we wish to investigate the characterizing properties of the mean external length,  $\bar{L}$ , we present equations for  $\bar{L}$  for several molecular types. We also give, for completeness, equations for  $\bar{A}$  (applicable in the case of thin fibers,  $l_0 = 0$ ). Quantity  $L_1$  is the length of the molecule along the axis of revolution and  $L_0$  is the equatorial diameter, in accord with our earlier usage.

For prolate ellipsoids of revolution ( $L_1 > L_0$ ), we have

$$\bar{L} = \frac{L_0^2}{2(L_1^2 - L_0^2)^{1/2}} \ln \frac{(L_1^2 - L_0^2)^{1/2} L_1}{L_0} + (L_1/2) \quad (37)$$

$$\bar{A} = \frac{\pi L_0}{4} \left[ \frac{L_1^2}{(L_1^2 - L_0^2)^{1/2}} \arcsin \frac{(L_1^2 - L_0^2)^{1/2}}{L_0} + L_0 \right] \quad (38)$$

For oblate ellipsoids ( $L_1 < L_0$ )

$$\bar{L} = \frac{L_0^2}{2(L_0^2 - L_1^2)^{1/2}} \arcsin \frac{(L_0^2 - L_1^2)^{1/2}}{L_0} + (L_1/2) \quad (39)$$

$$\bar{A} = \frac{\pi L_0}{4} \left[ \frac{L_1^2}{(L_0^2 - L_1^2)^{1/2}} \ln \frac{(L_0^2 - L_1^2)^{1/2} + L_0}{L_1} + L_0 \right] \quad (40)$$

For capsule-shaped molecules (two hemispheres capping a right-angle cylinder), we have the simple expressions

$$\bar{L} = \frac{L_0 + L_1}{2} \quad (41)$$

$$\bar{A} = \frac{\pi}{4} L_0 L_1 \quad (42)$$

For torus ("doughnut"-) shaped molecules or for molecules generated by rotating the capsule form about an axis normal to its polar axis

$$\bar{L} = \frac{\pi}{4} L_0 + \left(1 - \frac{\pi}{4}\right) L_1 \quad (43)$$

We do not give the  $\bar{A}$  expression for this last case since, as a complicated double integral (one being elliptical), it is too involved for practical use.

## Results

The foregoing equations are used below to construct curves showing the dependence of partition coefficient  $K$  on molecular size  $L$  and surface area per unit pore volume  $s$ . Further on in this section we will apply such curves to determine the validity of using various molecular length parameters to characterize partitioning.

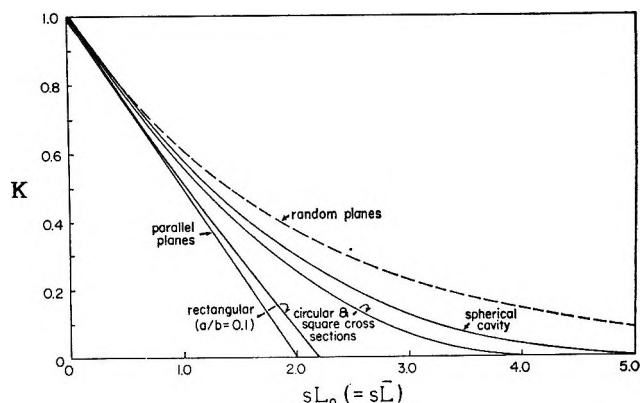


Figure 4. Values of  $K$  for spherical molecules of diameter  $L_0$  in various types of pores.

*Nature of the Partitioning Curves.* Figure 4 applies to spherical molecules in various pore types. The curves differ considerably from pore to pore, except that as sphere diameter  $L_0$  becomes small,  $K$  approaches unity along a common curve. Examination of the pertinent equations shows that all curves converge to  $K = 1 - (sL_0/2)$  as  $sL_0 \rightarrow 0$ . In this region wall curvature and corners become unimportant; the "probe" or spherical molecule is sufficiently small that nearly all elements of surface appear to it as plane areas. The slope of the curve further to the right clearly relates to selectivity, indicating that various pores have different separating characteristics. This subject will be examined in a later paper.

Figure 5 gives the corresponding plots for thin-rod molecules. The general features are similar in the two figures, except that there are several crossing points and a generally decreased tendency to intersect  $K = 0$  short of  $sL \rightarrow \infty$ . As rod length  $L_1$  becomes small, the curves converge to  $K = 1 - (sL_1/4)$ .

The general proximity of the various curves in Figures 4 and 5 and their common shape show that parameter  $s$  is reasonably good for characterizing pore size. The obvious exception to this would be media with pores defined by molecular chains (*e.g.*, the brush-pile model). The latter are not considered in this section.

The range between the spherical and thin-rod extremes can be explored, as outlined in the Theory section, by adding a layer of given radius to a thin rod. In this way,  $K$  depends on the relative thickness of the resulting "capsule"-shaped molecule, where shape is characterized by  $M = (\text{diameter})/(\text{length}) = L_0/L_1$ . In Figure 6 we plot  $K$  against  $sL_1$  at various  $M$  values. These curves all pertain to long pores of circular cross section ("circular" or "cylindrical" pores). The latter yield fairly typical results, as previously made evident in Figures 4 and 5. For a given  $L_1$ , penetration into the pores increases as the molecules become thinner

(11) B. Gelotte and J. Porath in "Chromatography," E. Heftmann, Ed., 2nd ed, Reinhold Publishing Corp., New York, N. Y., 1967.

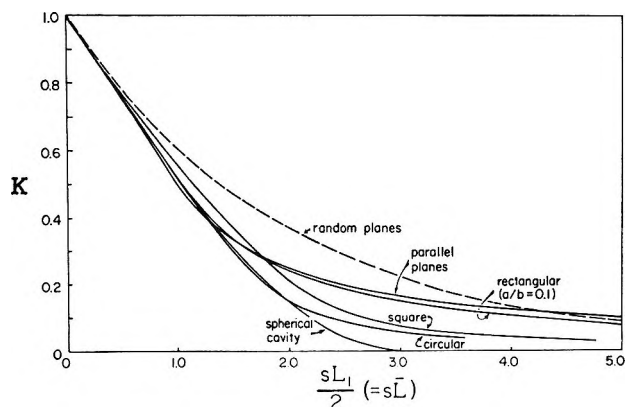


Figure 5. Values of  $K$  for thin rods of length  $L_1$  in various pores.

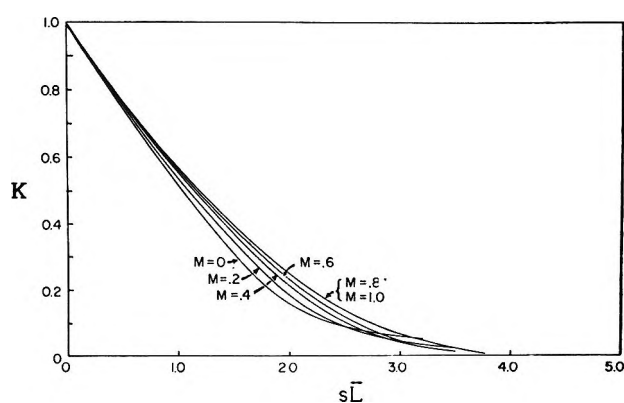


Figure 7. Plots of  $K$  against  $s\bar{L}$  for molecules with various  $M$  values in circular pores.

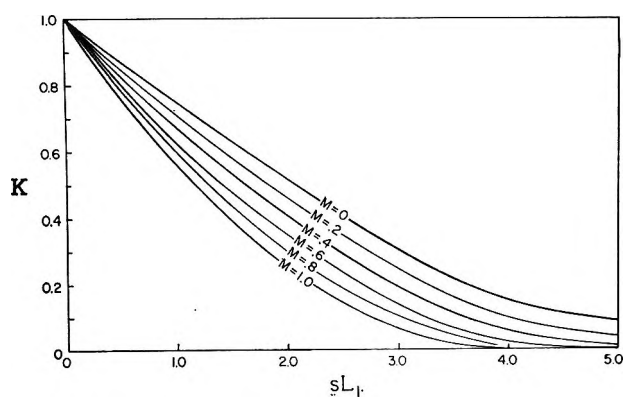


Figure 6. Plots of  $K$  against  $sL_1$  for molecules of various width to length ratios,  $M$ , in circular pores.

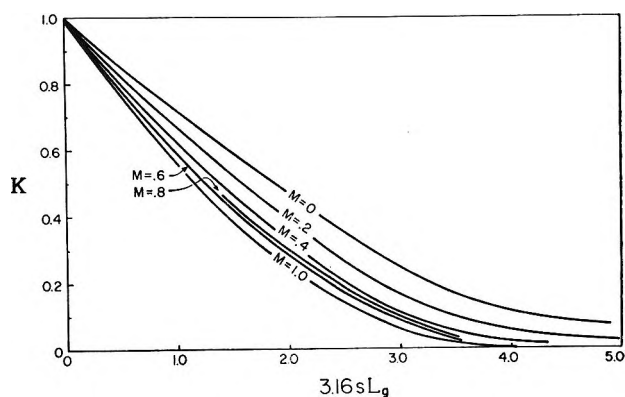


Figure 8. Plots of  $K$  against  $3.16sL_g$  for capsule-shaped molecules of variable shape in circular pores.

( $M$  smaller), and thus their probability of wall overlap decreases. Quantity  $K$  differs by more than twofold over most of this plot for two molecules of equal maximum length  $L_1$ , but with opposite extremes of relative thickness,  $M$ . Clearly,  $L_1$  does not characterize the partitioning very well when different molecular shapes are present.

*A Comparison of Parameters to Characterize Partitioning.* We have alluded to the possible value of the mean external diameter,  $\bar{L}$ , as a parameter to characterize the partitioning of diverse molecules. In the random-plane model, as we have shown,  $\bar{L}$  completely characterizes the partitioning of rigid molecules no matter how complex the molecular shape. We must determine if  $\bar{L}$  has any correlating ability in other pore networks. In Figure 7 we consider the same pore network (pores of circular cross section) and molecules as in Figure 6 but plot  $K$  against  $s\bar{L}$  instead of  $sL_1$ . The closeness of the curves (*i.e.*, the relative small differences in  $K$  at a given value of  $\bar{L}$  with constant  $s$ ) demonstrates that  $\bar{L}$  is a good measure of partitioning in this pore network also. It is superior to  $L_1$ , as shown by the narrow band between the extreme curves in Figure 7 compared with the broad band of Figure 6.

In the early history of gel filtration chromatography, the radius of gyration,  $L_g$ , was implied to be a crucial partitioning parameter.<sup>4</sup> In Figure 8 we show  $K$  vs.  $3.16sL_g$  for the same group of molecules and circular pores. The constant coefficient,  $3.16$  ( $\approx 10^{1/2}$ ), is fixed to make the curve for spherical molecules ( $M = 1$ ) coincide with that of Figures 4, 6, and 7 (also Figures 9–11). Density is assumed constant. The band between the extreme curves ( $M = 0$  and 1) is narrower than that for the  $K$ - $sL_1$  plots (Figure 6), but severalfold wider than the band for the  $K$ - $s\bar{L}$  plots. However, for  $M > 0.4$ ,  $L_g$  provides very good correlation.

The same comparison can be made using "dumbbell" molecules. This example is chosen for its mathematical convenience in making additional comparisons. Recall that our molecules have two hemispheres capping a right-angle cylinder. The cylinder can be replaced by a thin, rigid connecting rod of negligible mass. It is obvious that such a change will not alter the partition coefficient, since any molecular configuration previously overlapping the wall must continue to do so, etc. Also parameter  $\bar{L}$  will remain unchanged. Thus the  $K$  vs.  $s\bar{L}$  plots yield the same narrow band shown in Figure 6. The radius of gyration depends very much on this shape change; when this is calculated and the

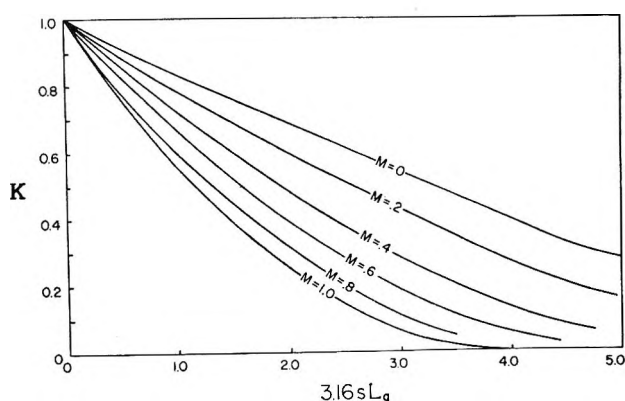


Figure 9. Plots of  $K$  against  $3.16 sL_g$  for "dumbbell" molecules of variable  $M$  in circular pores.

$K$  vs.  $3.16 sL_g$  plots are constructed, Figure 9 results. The band is broader than before (Figure 8). This calculation points to a basic flaw in the radius of gyration as a principal partitioning parameter. First, it receives a contribution from interior groups, even completely shielded groups, which clearly have no influence on partitioning in any kind of exclusion system. (Fortunately the exterior groups are weighted more heavily.) Second, it has a spurious dependence on local mass, a relevant consideration if regional density differences exist in the system, *e.g.*, the viruses whose outer shells are chemically unlike the enclosed DNA.

Similar objections apply to the use of molecular weight (or molar volume) as a correlating parameter. Within a fixed family of macromolecules (*e.g.*, all spheres or all random chain polymers of a given kind), molecular weight (along with most other imaginable size parameters) will adequately specify partitioning. However, such parameters are questionable in comparing different classes of macromolecules and thus in predicting the behavior of one class from data collected for a different class. This is illustrated in Figure 10, where we examine the effect of the volume-related parameter  $L_v$ , the diameter of a sphere whose volume equals that of the given molecule.

More recently the equivalent hydrodynamic radius or diameter has been proposed for the characterization of partitioning.<sup>12</sup> While this parameter is relatively difficult to calculate for odd-shaped molecules, it is easily measured through viscosity experiments. In order to test this parameter, we have used an equation by Perrin for the friction coefficient of prolate ellipsoids of revolution.<sup>13</sup> We have then assumed that the hydrodynamic behavior of a prolate ellipsoid can be approximated by that of a "capsule"-shaped particle of equal length and girth. In this way we are able to construct approximate partitioning curves which show the effect of equivalent hydrodynamic diameter,  $L_h$ , Figure 11. This figure shows that  $L_h$  well characterizes the partitioning in the range  $M = 0.4-1.0$ . For

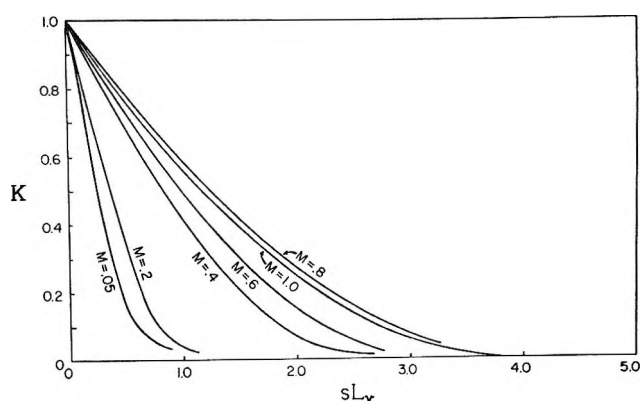


Figure 10. Plots of  $K$  against  $sL_v$  in circular pores.

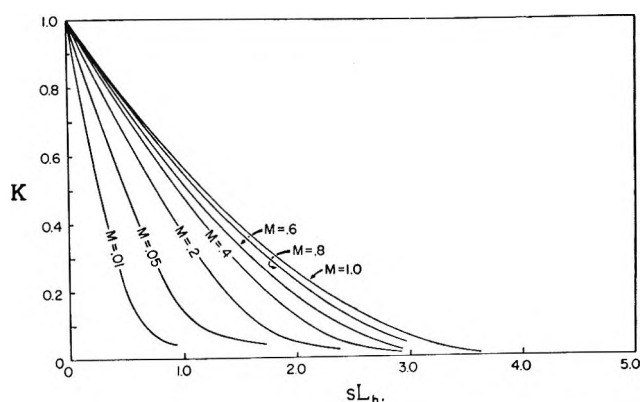


Figure 11. Plots of  $K$  vs.  $sL_h$  for various  $M$  values in circular pores.

"thinner" molecules ( $M < 0.4$ ), the correlation becomes increasingly unsatisfactory.

The foregoing results show that the mean external length,  $\bar{L}$ , is somewhat more satisfactory than other commonly used parameters in characterizing partitioning in the random-plane and circular-pore models. The next most successful parameter appears to be the radius of gyration. These two measures are tested side by side in one more model network, that consisting of uniform, parallel planes, in order to gain a modicum of confidence that the above conclusion is broadly applicable. In Figures 12 and 13, analogous to Figure 7 and 8 except for the change in pore geometry, we show the relevant calculations. Clearly  $\bar{L}$  is less successful than before (Figure 7). (Still another plot, for rectangular pores, suggests that the divergence of curves in Figure 12 is unusually large. This is not shown here.) Figure 13 shows the radius of gyration plots (this correlation is also worse than before (Figure 8) and less satisfactory than that provided by  $\bar{L}$ ).

We conclude that  $\bar{L}$  is somewhat more successful than other molecular size parameters proposed for character-

(12) H. Benoit, Z. Grubisic, P. Rempp, D. Decker, and J. G. Zilliox, *J. Chim. Phys.*, **63**, 1507 (1966).

(13) F. Perrin, *J. Phys. Radium*, [7] **5**, 497 (1934).



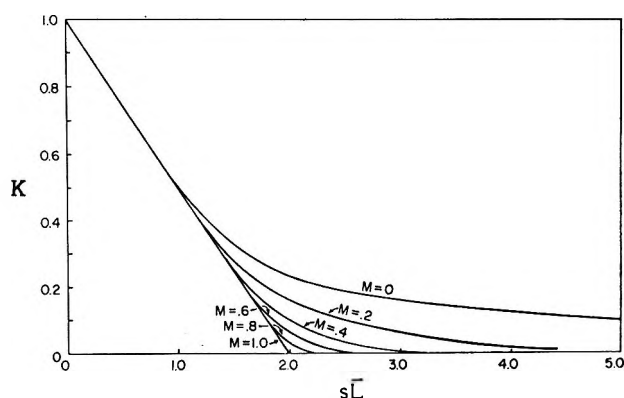


Figure 12. Plots of  $K$  against  $s\bar{L}$  for molecules with various  $M$  values in uniform, parallel planes.

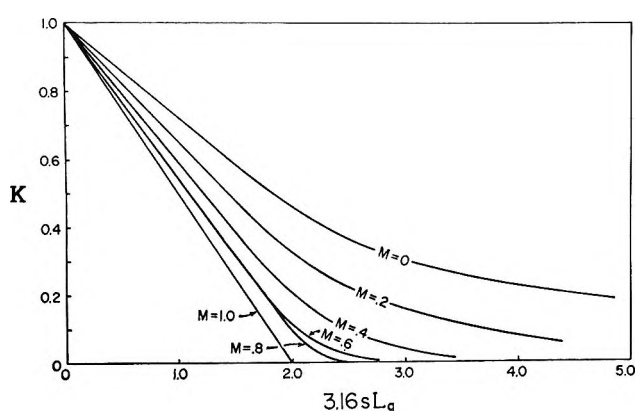


Figure 13. Plots of  $K$  against  $s\bar{L}$  for capsule-shaped molecules of variable shape in uniform, parallel planes.

izing partitioning in a group of model pore networks and, therefore, will possibly best characterize partitioning in real porous media. The fact that  $\bar{L}$  rigorously fulfills this function only for a random-pore model suggests that the randomness of real porous systems would not impair our ability to make such correlations.

### Conclusion

The general theory of macromolecular partitioning in inert porous media is rather easily formulated, eq 1. The true difficulty comes in reasonably characterizing the laboratory system, in evaluating the integrals applicable to that system, and then in finding a reasonable common grounds for a wide range of systems.

It is likely impossible to characterize rigorously the partitioning of various complex macromolecules in arbitrary and irregular porous media by any single or simple group of measurable parameters. Each unique bump or fold in the pore wall will contribute its own singular effect to the exclusion of a given molecule. If we sacrifice the description of such detailed interactions, we will perhaps be able to divide our systems into rough classes which can be approximated by various models, such as those used here. This procedure presupposes that a given pore network or group

of molecules can be clearly associated with a given model or models. In this approximation partitioning is characterized by simple parameters, but it remains only an approximation. However, microscopic porous networks are notoriously random, suggesting that little additional sacrifice in accuracy would usually attend the common grouping of most systems and the attempt to find a parameter or group of parameters to approximate the behavior of all.

The latter approach is suggested here. Results with various models confirm that the dimensionless parameter  $s\bar{L}$  reasonably characterizes partitioning. This term, conveniently, is the direct product of the molecular parameter  $\bar{L}$  and the network parameter,  $s$ .

The choice of  $s$  to represent the porous network is made because (1)  $s$ , as the reciprocal hydraulic radius, is a reasonable common denominator for the behavior of different pore types, (2) surface area is the most general and well-defined measure of pore size, and (3) the exclusion phenomenon is basically a geometrical surface effect, depending primarily upon surface area and only secondarily upon the more subtle details of surface configuration and curvature. We recognize that the secondary effects may be far from negligible. For instance, surface-roughness corrections will be necessary when the probe molecule which measures surface area and the partitioning macromolecule "see" different surface areas.

Parameter  $\bar{L}$  is suggested strictly by the theory of random pores bounded by plane surfaces. It has quite generally, of course, the main attributes which describe the tendency of a molecule to overlap with surfaces.

Assuming that  $s\bar{L}$  characterizes a system according to some known function,  $\bar{L}$  for the macromolecule can be rather easily obtained from measured  $K$  values. This dimension, being an average length, would help confirm structural or size hypotheses or aid in choosing between alternate conformations in solution. It promises to be simpler in application than the hydrodynamic radius, since the latter is difficult to relate theoretically to complex structures.

This approach would have many of the advantages that accompany the measurement of other physical parameters by chromatographic means, including the achievement of solute purification simultaneous with the measurement process.<sup>14</sup>

*Acknowledgment.* This investigation was supported by Public Health Service Research Grant GM10851-11 from the National Institutes of Health. E. K. acknowledges a Public Health Service Postdoctoral Research Fellowship award.

### Appendix. Principal Symbols

*General Coordinates.*

$\mathbf{r}$  Positional vector

(14) J. C. Giddings and K. L. Mallik, *Ind. Eng. Chem.*, **59**, 18 (1967).

$\psi$	Orientation "vector"	$\bar{A}$	Mean area of projection
$\lambda$	Conformational "vector"		
$r$	Radial coordinate	<i>Pore.</i>	
$\theta, \phi$	Polar and azimuthal angle	$d_0$	Width or diameter of pore cross section
		$d_1$	Length of pore cross section
		$\bar{d}_x$	Mean spacing between planes perpendicular to the $x$ axis
		$p$	$d_1/d_0$
		$s$	Pore surface per unit free volume
		$f, f_i$	Distribution in pore size
		$f'$	Porosity
		<i>Fiber.</i>	
		$\bar{a}_x$	Mean area per fiber parallel to the $x$ axis
		$h$	Fiber length per unit volume
		$l_0$	Fiber diameter
		<i>Molecule pore.</i>	
		$\alpha$	$L_0/d_0$
		$\beta$	$L_1/d_0$
		$\beta'$	$(L_1 - L_0)/(d_0 - L_0)$
		$p'$	$(d_1 - L_0)/(d_0 - L_0)$
<i>Physicochemical Parameters.</i>			
$\epsilon_D, \epsilon_b, \epsilon_M, \epsilon_{MN}, \epsilon_{MP}$	Energies		
$K$	Partition coefficient		
$\kappa$	Local partition coefficient		
$\kappa'$	Partition coefficient for molecules with given orientation and conformation		
$q, q_i$	Nonintersection probabilities		
<i>Molecule.</i>			
$L_1$	Polar length		
$L_0$	Equatorial diameter		
$\bar{L}$	Mean external diameter		
$L_x$	Length of projection of a molecule into the $x$ axis		
$M$	$L_0/L_1$		
$A_x$	Area of projection into the plane perpendicular to the $x$ axis		

## Electromotive Force Studies in Aqueous Solutions at Elevated Temperatures. X. The Thermodynamic Properties of HCl-KCl, HCl-RbCl, HCl-CsCl, HCl-MgCl<sub>2</sub>, HCl-CaCl<sub>2</sub>, HCl-SrCl<sub>2</sub>, and HCl-AlCl<sub>3</sub> Mixtures<sup>1</sup>

by M. H. Lietzke and H. A. O'Brien, Jr.<sup>2</sup>

Department of Chemistry, University of Tennessee, Knoxville, Tennessee, and Chemistry Division, Oak Ridge National Laboratory, Oak Ridge, Tennessee (Received March 11, 1968)

The activity coefficient of HCl in HCl-KCl, HCl-RbCl, HCl-CsCl, HCl-MgCl<sub>2</sub>, HCl-CaCl<sub>2</sub>, HCl-SrCl<sub>2</sub>, and HCl-AlCl<sub>3</sub> mixtures has been studied as a function of total ionic strength, temperature, and composition of the mixture. At constant temperature and ionic strength the logarithm of the activity coefficient of HCl in the mixtures varies linearly with the ionic strength fraction of salt, in conformity with Harned's rule. The activity coefficients of the salts in the mixtures were calculated by using the parameters describing this variation and those for the variation of the activity coefficients of the respective salts with ionic strength in the pure salt solutions. The corresponding parameters for four systems previously studied are also given to correct certain inconsistencies between those values and the parameters reported in this paper.

In previous papers in this series the thermodynamic properties of HCl-NaCl,<sup>3</sup> HCl-BaCl<sub>2</sub>,<sup>4</sup> HCl-LaCl<sub>3</sub>,<sup>5</sup> and HCl-GdCl<sub>3</sub><sup>6</sup> mixtures were described. The present paper extends these studies to mixtures of HCl with KCl, RbCl, CsCl, MgCl<sub>2</sub>, CaCl<sub>2</sub>, SrCl<sub>2</sub>, and AlCl<sub>3</sub>. In all of this work measurements of the emf of the cell Pt-H<sub>2</sub> ( $p = 1$ )|HCl( $m_2$ ), MCl<sub>x</sub>( $m_3$ )|AgCl, Ag, where MCl<sub>x</sub> is the appropriate metal chloride, have been com-

pared with measurements of the osmotic or activity coefficient of the salt to calculate the thermodynamic

(1) Research sponsored by the U. S. Atomic Energy Commission under contract with the Union Carbide Corp.

(2) This paper is based on a dissertation by H. A. O'Brien, Jr., presented to the Department of Chemistry of the University of Tennessee in partial fulfillment of the requirements for the Ph.D. degree, 1968.

**Table I:** Observed Values of the Emf in Volts for the Cell Pt-H<sub>2</sub> (*p* = 1)|HCl (*m*<sub>2</sub>), KCl (*m*<sub>3</sub>)|AgCl (Ag and Deviations<sup>a</sup> of the Emf Values Calculated from Smoothed Activity Coefficients)

<i>m</i> <sub>2</sub>	<i>m</i> <sub>3</sub>	Temp, °C					
		25	60	90	125	150	175
0.1242	0.3671	0.3107 (-5)	0.2984 (+10)	0.2816 (0)	0.2584 (-3)	0.2389 (-10)	...
0.2526	0.2399	0.2915 (-2)	0.2772 (+7)	0.2601 (+11)	0.2349 (+11)	...	...
0.3585	0.1105	0.2830 (+2)	0.2666 (-7)	0.2465 (-28)	0.2212 (-17)	0.2008 (-3)	0.1793 (+23)
0.2468	0.7388	0.2750 (-4)	0.2574 (+2)	0.2389 (+1)	...	...	...
0.4987	0.4838	0.2555 (+2)	0.2360 (-2)	0.2167 (+3)	0.1889 (-6)	0.1676 (-6)	0.1461 (+8)
0.7366	0.2460	0.2444 (+12)	0.2244 (+1)	0.2028 (-10)	0.1757 (+4)	...	...

<sup>a</sup> The deviations are given in parentheses after each reported emf as the observed emf values less the values calculated from smoothed activity coefficients. Thus a positive deviation indicates that the emf reported here is algebraically larger.

**Table II:** Observed Values of the Emf in Volts for the Cell Pt-H<sub>2</sub> (*p* = 1)|HCl (*m*<sub>2</sub>), RbCl (*m*<sub>3</sub>)|AgCl (Ag and Deviations<sup>a</sup> of the Emf Values Calculated from Smoothed Activity Coefficients)

<i>m</i> <sub>2</sub>	<i>m</i> <sub>3</sub>	Temp, °C					
		25	60	90	125	150	175
0.1211	0.3723	0.3126 (-5)	...	0.2828 (+12)	0.2596 (+16)	0.2385 (-5)	0.2190 (+9)
0.2445	0.2322	0.2949 (+2)	0.2780 (-4)	0.2583 (-21)	0.2341 (-8)	0.2123 (-19)	0.1907 (-9)
0.3689	0.1237	0.2824 (+3)	0.2659 (+9)	0.2488 (+16)	...	...	...
0.2450	0.7222	0.2682 (0)	0.2500 (-18)	0.2338 (-16)	0.2143 (-6)	...	...
0.4884	0.5000	...	0.2340 (+23)	0.2166 (+35)	0.1860 (-24)	0.1704 (+11)	...
0.7168	0.2243	0.2442 (+4)	0.2232 (-5)	0.2016 (-16)	0.1739 (-19)	...	...

<sup>a</sup> See footnote a, Table I.

**Table III:** Observed Values of the Emf in Volts for the Cell Pt-H<sub>2</sub> (*p* = 1)|HCl (*m*<sub>2</sub>), CsCl (*m*<sub>3</sub>)|AgCl (Ag and Deviations<sup>a</sup> of the Emf Values Calculated from Smoothed Activity Coefficients)

<i>m</i> <sub>2</sub>	<i>m</i> <sub>3</sub>	Temp, °C					
		25	60	90	125	150	175
0.1136	0.3554	0.3136 (-2)	0.3003 (+2)	0.2844 (+3)	0.2622 (+14)	0.2416 (-1)	...
0.2330	0.2491	0.2938 (+1)	0.2788 (+8)	0.2609 (+5)	0.2366 (+14)	0.2156 (+11)	0.1913 (-5)
0.3504	0.1296	0.2809 (-12)	0.2641 (-18)	0.2449 (-26)	0.2197 (-15)	0.1981 (-16)	0.1751 (-11)
0.2190	0.6730	0.2778 (+9)	0.2602 (+15)	0.2390 (+9)	...	...	...
0.4433	0.4667	0.2571 (-4)	0.2381 (+3)	0.2170 (-6)	0.1911 (+8)	0.1699 (+10)	0.1469 (+10)
0.6820	0.2500	0.2436 (-15)	0.2241 (-7)	0.2024 (-15)	0.1744 (-11)	0.1519 (-13)	0.1287 (-6)

<sup>a</sup> See footnote a, Table I.

properties of both HCl and the salt in the HCl-MCl<sub>2</sub> mixtures.

### Experimental Section

The experimental apparatus and the preparation of the electrodes and solutions were the same as described previously.<sup>7</sup> In the case of the HCl-KCl, RbCl, and CsCl mixtures the measurements were carried out in the temperature range 25–175°, while in the case of the HCl-MgCl<sub>2</sub>, CaCl<sub>2</sub>, SrCl<sub>2</sub>, and AlCl<sub>3</sub> mixtures the measurements were extended only to 60°. Solutions of total ionic strength approximately 0.5 and 1.0 were used in which the ratio of HCl to MCl<sub>2</sub> was varied. No drift of emf with time was observed after the cells attained equilibrium. In general, the values were more reproducible in the solutions containing a higher frac-

tion of acid, and values taken at the same temperature were reproducible, with few exceptions, to at least ±0.5 mV.

### Results and Discussion

The treatment of the results in the case of the systems studied in the present paper was the same as that followed in the study of the HCl-NaCl mixtures.<sup>3</sup> Each emf value was corrected to 1.00 atm of hydrogen pres-

- (3) M. H. Lietzke, H. B. Hupf, and R. W. Stoughton, *J. Phys. Chem.*, **69**, 2395 (1965).
- (4) M. H. Lietzke and R. W. Stoughton, *ibid.*, **70**, 756 (1966).
- (5) M. H. Lietzke and R. W. Stoughton, *ibid.*, **71**, 662 (1967).
- (6) M. H. Lietzke and R. W. Stoughton, *ibid.*, **72**, 257 (1968).
- (7) R. S. Greeley, W. T. Smith, Jr., R. W. Stoughton, and M. H. Lietzke, *ibid.*, **64**, 652 (1960).

**Table IV:** Observed Values of the Emf in Volts for the Cell Pt-H<sub>2</sub> (*p* = 1)|HCl (*m*<sub>2</sub>), MgCl<sub>2</sub> (*m*<sub>3</sub>)|AgCl (Ag and Deviations<sup>a</sup> of the Emf Values Calculated from Smoothed Activity Coefficients)

<i>m</i> <sub>2</sub>	<i>m</i> <sub>3</sub>	Temp. °C		
		25	40	60
0.1237	0.1206	0.3177 (-8)	0.3132 (-1)	0.3054 (-5)
0.2509	0.0816	0.2973 (+11)	0.2919 (+19)	0.2820 (+8)
0.3761	0.0322	0.2821 (-13)	0.2757 (-8)	0.2655 (-13)
0.2518	0.2376	0.2805 (-3)	0.2748 (+4)	0.2653 (-1)
0.4998	0.1522	0.2589 (-4)	0.2515 (-4)	0.2407 (-7)
0.7614	0.0710	0.2448 (+7)	0.2374 (+15)	0.2253 (+9)

<sup>a</sup> See footnote a, Table I.

**Table V:** Observed Values of the Emf in Volts for the Cell Pt-H<sub>2</sub> (*p* = 1)|HCl (*m*<sub>2</sub>), CaCl<sub>2</sub> (*m*<sub>3</sub>)|AgCl (Ag and Deviations<sup>a</sup> of the Emf Values Calculated from Smoothed Activity Coefficients)

<i>m</i> <sub>2</sub>	<i>m</i> <sub>3</sub>	Temp. °C		
		25	40	60
0.1219	0.1181	0.3182 (-2)	0.3143 (+7)	0.3068 (+2)
0.2463	0.0757	0.2969 (+2)	0.2910 (-3)	0.2816 (-12)
0.3400	0.03583	0.2874 (-2)	0.2821 (+9)	0.2728 (+7)
0.2436	0.2393	0.2829 (-3)	0.2774 (+9)	0.2669 (-1)
0.4775	0.1556	0.2613 (-5)	0.2540 (-2)	0.2428 (-7)
0.7291	0.07612	0.2462 (0)	0.2391 (+11)	0.2263 (-1)

<sup>a</sup> See footnote a, Table I.

**Table VI:** Observed Values of the Emf in Volts for the Cell Pt-H<sub>2</sub> (*p* = 1)|HCl (*m*<sub>2</sub>), SrCl<sub>2</sub> (*m*<sub>3</sub>)|AgCl (Ag and Deviations<sup>a</sup> of the Emf Values Calculated from Smoothed Activity Coefficients)

<i>m</i> <sub>2</sub>	<i>m</i> <sub>3</sub>	Temp. °C		
		25	40	60
0.1210	0.1245	0.3175 (-6)	0.3141 (+8)	0.3062 (0)
0.2469	0.0824	0.2961 (-6)	0.2910 (+4)	0.2815 (-4)
0.3672	0.0403	0.2857 (+17)	0.2777 (+6)	0.2673 (0)
0.2443	0.2552	0.2801 (-10)	0.2750 (+7)	0.2651 (+4)
0.4899	0.1581	0.2596 (-4)	0.2527 (+5)	0.2400 (-13)
0.5991	0.0767	0.2559 (-5)	0.2482 (-2)	0.2364 (-7)

<sup>a</sup> See footnote a, Table I.

sure by subtracting  $(RT/2\mathcal{F}) \ln f_{H_2}$ , where the hydrogen fugacity,  $f_{H_2}$ , was taken equal to the hydrogen pressure. The corrected emf values,  $E$ , at each ionic strength were then plotted as a function of temperature, and the values were corrected to round values of temperature. These values are given in Tables I-VII.

The activity coefficient  $\gamma_{\pm}$  of HCl at each temperature and set of concentrations in the mixtures was evaluated by using the Nernst equation and previous values<sup>8</sup> of the standard potential,  $E^{\circ}$ , of the Ag-AgCl electrode. In this equation  $m_2$  and  $m_3$  are the molalities

$$E = E^{\circ} - \frac{RT}{\mathcal{F}} \ln [m_2(m_2 + xm_3)] - \frac{2RT}{\mathcal{F}} \ln \gamma_{\pm} \quad (1)$$

of HCl and the appropriate salt, respectively, while  $T$  is the absolute temperature,  $R$  is the gas constant, and  $\mathcal{F}$  is the Faraday. The factor  $x$  has a value of 1 for the systems involving univalent salts, 2 for the systems involving divalent salts, and 3 for the HCl-AlCl<sub>3</sub> system.

Plots of  $\ln \gamma_{\pm}(\text{HCl})$  vs. the ionic strength fraction of salt were made at each temperature and total ionic strength for each of the systems. In all cases the plots were linear within experimental error and within the deviations of the ionic strength from the "constant value" in conformity with Harned's rule, as previously observed in the case of the HCl-NaCl mixtures.

*Expressions for  $\gamma_{\pm}$  of HCl and MCl in the Mixtures.* The activity coefficients of HCl were smoothed as to HCl and MCl<sub>2</sub> concentrations and temperature in the same manner as described previously.<sup>3</sup> Hence the logarithm of the activity coefficient of the HCl was assumed to be given by

$$\begin{aligned} \ln \gamma_2 = & -s\rho^{1/2}\sqrt{I}/(1 + 1.5\sqrt{I}) + \\ & 2I \left[ B_{22} + \left( \frac{B_{23}}{j} - B_{22} \right) X_3 \right] + \\ & 3I^2 \left[ C_{222} + 2 \left( \frac{C_{223}}{j} - C_{222} \right) X_3 + \right. \\ & \left. \left( C_{222} + \frac{C_{233}}{k} - \frac{2C_{223}}{j} \right) X_3^2 \right] \quad (2) \end{aligned}$$

while the corresponding equation for the salt was assumed to be

$$\begin{aligned} \ln \gamma_3 = & -s\rho^{1/2}\sqrt{I}/(1 + 1.5\sqrt{I}) + \\ & f_1 I \left[ \frac{B_{33}}{j} + \left( B_{23} - \frac{B_{33}}{j} \right) X_2 \right] + \\ & f_2 I^2 \left[ \frac{C_{333}}{k} + 2 \left( \frac{C_{233}}{j} - \frac{C_{333}}{k} \right) X_2 + \right. \\ & \left. \left( \frac{C_{333}}{k} + C_{223} - \frac{2C_{233}}{j} \right) X_2^2 \right] \quad (3) \end{aligned}$$

where  $s$  is the Debye-Hückel limiting slope,  $\rho$  is the density of water, and  $I$  is the total ionic strength. In these equations  $B_{ij}$  and  $C_{ijk}$  are interaction coefficients, the subscript 2 referring to the acid (HCl) and the subscript 3 to the salt.  $X_2$  and  $X_3$  are the ionic strength fractions of acid and salt, respectively, in the mixtures. Values of the remaining symbols,  $f_1$ ,  $f_2$ ,  $j$ , and  $k$ , the values of which depend upon the valence of the salt in the mixture, are listed in Table VIII. Since, as noted previously, Harned's rule seems to apply for the acid in the mixtures, the coefficient of the  $X_3^2$  term in eq 2 is zero; i.e.,  $C_{222} + (C_{233}/k) - (2C_{223}/j) = 0$ , for all the systems reported in this paper.

(8) M. H. Lietzke and R. W. Stoughton, *J. Phys. Chem.*, **68**, 3043 (1964).

**Table VII:** Observed Values of the Emf in Volts for the Cell Pt-H<sub>2</sub> (*p* = 1)|HCl (*m*<sub>2</sub>), AlCl<sub>3</sub> (*m*<sub>3</sub>)|AgCl (Ag and Deviations<sup>a</sup> of the Emf Values Calculated from Smoothed Activity Coefficients)

<i>m</i> <sub>2</sub>	<i>m</i> <sub>3</sub>	Temp., °C								
		25	30	35	40	45	50	55	60	
0.1188	0.0586	0.3243 (+5)	0.3229 (+3)	0.3214 (+3)	0.3199 (+4)	0.3182 (+4)	0.3166 (+5)	...	...	
0.2469	0.0374	0.3003 (+8)	0.2961 (-17)	0.2947 (-12)	0.2944 (+5)	0.2919 (+1)	0.2897 (+1)	...	...	
0.3783	0.0165	0.2835 (-1)	0.2814 (-2)	0.2795 (+1)	0.2770 (-1)	0.2729 (-21)	0.2699 (-23)	...	0.2671 (+3)	
0.2500	0.1221	0.2866 (+4)	0.2847 (+4)	0.2828 (+5)	0.2802 (0)	0.2786 (+7)	0.2763	...	0.2708 (+2)	
0.5014	0.0807	0.2614 (-3)	0.2594 (-1)	0.2573 (+1)	0.2548 (+1)	0.2520 (0)	0.2491 (-3)	0.2461 (-5)	...	
0.7581	0.0386	0.2447 (-4)	0.2419 (-8)	0.2395 (-6)	0.2374 (0)	...	...	...	0.2258 (+3)	

<sup>a</sup> See footnote a, Table I.**Table VIII:** Values of *f*<sub>1</sub>, *f*<sub>2</sub>, *j*, and *k* to be used in Eq 2 and 3

Salt type	<i>f</i> <sub>1</sub>	<i>f</i> <sub>2</sub>	<i>j</i>	<i>k</i>
MCl	2	3	1	1
MCl <sub>2</sub>	4/3	2	3	9
MCl <sub>3</sub>	1	3/2	6	36

The coefficients *B*<sub>*ij*</sub> and *C*<sub>*ijk*</sub> are, of course, temperature dependent. If the coefficients are expressed as

$$B_{iq} = B'_{iq} + B''_{iq}/T;$$

$$C_{ijq} = C'_{ijq} + C''_{ijq}/T \quad (4)$$

they are consistent with temperature-independent excess free enthalpies and entropies, *i.e.*, excess over the molality and Debye-Hückel parts. If the coefficients are expressed as

$$B_{iq} = B'_{iq} + (B''_{iq}/T) - B'''_{iq} \log T \quad (5)$$

and

$$C_{ijq} = C'_{ijq} + (C''_{ijq}/T) + C'''_{ijq} \log T \quad (5')$$

then they give rise to excess enthalpies varying linearly with temperature and excess entropies varying linearly with  $\ln T$ . It was found that when eq 2 was used to describe the variation of  $\ln \gamma \pm (\text{HCl})$  in the HCl-KCl, HCl-RbCl, and HCl-CsCl mixtures, it was possible to express the *B*<sub>*12*</sub> as in eq 5 and the *C*<sub>*112*</sub> as in eq 4. Convergence difficulties in the least-squares fit were encountered when an attempt was made to use both eq 5 and 5'. This probably means that in the ionic strength range studied (to 1.0 *m*) the contribution of the *B* terms is much more important than that of the *C* terms (hence the difficulty in determining as many parameters in the *C* coefficients). This same behavior was reported in the case of the HCl-NaCl mixtures.<sup>3</sup>

In the case of HCl-MgCl<sub>2</sub>, HCl-CaCl<sub>2</sub>, HCl-SrCl<sub>2</sub>, and HCl-AlCl<sub>3</sub> mixtures, the emf measurements were made only from 25 to 60°. This narrower temperature range did not permit the estimation of as many parameters describing the temperature dependence of the coefficients. Hence in the study of these mixtures both the *B*<sub>*12*</sub> and *C*<sub>*112*</sub> coefficients were expressed as in eq 4.

The values of *B*'<sub>*22*</sub>, *B*''<sub>*22*</sub>, *B*'''<sub>*22*</sub>, *B*'<sub>*23*</sub>, *B*''<sub>*23*</sub>, *B*'''<sub>*23*</sub>, *C*'<sub>*222*</sub>, *C*''<sub>*222*</sub>, *C*'<sub>*223*</sub>, and *C*''<sub>*223*</sub> were obtained directly by the least-squares fit of eq 2, while the values of *C*'<sub>*233*</sub> and *C*''<sub>*233*</sub> were obtained by the application of Harned's rule, *C*<sub>*222*</sub> + (*C*<sub>*233*</sub>/*k*) - (2*C*<sub>*223*</sub>/*j*) = 0. The additional parameters needed for calculating the  $\ln \gamma_3$  values (eq 3), namely, the coefficients *B*<sub>*33*</sub> and *C*<sub>*333*</sub> for the pure salt solutions, were evaluated by the method of least squares using activity coefficient data<sup>9</sup> on these solutions at 25°.

The parameters for calculating the various *B* and *C* coefficients are given in Table IX. The parameters for the HCl-NaCl, HCl-BaCl<sub>2</sub>, HCl-LaCl<sub>3</sub>, and HCl-GdCl<sub>3</sub> systems previously studied are also given to correct certain inconsistencies in the published values;

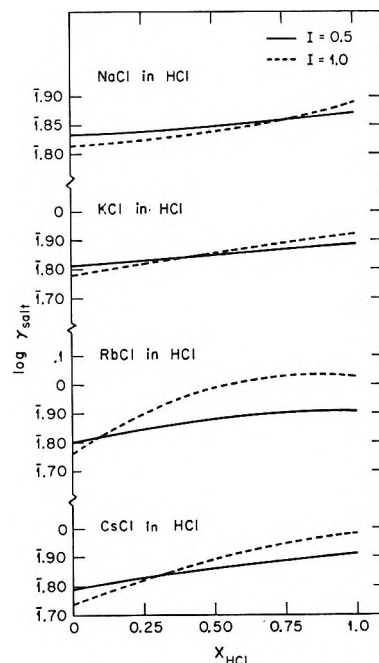


Figure 1. Plots of  $\log \gamma(\text{salt})$  vs. ionic strength fraction of HCl at 25° for HCl-NaCl, HCl-KCl, HCl-RbCl, and HCl-CsCl mixtures.

(9) R. A. Robinson and R. H. Stokes, "Electrolyte Solutions," Academic Press, New York, N. Y., 1955, Appendix 8.10.

**Table IX:** Parameters of the  $B$  and  $C$  Coefficients (Eq 2 and 3) on a Common Logarithm Basis

	HCl-NaCl	
$B'_{22} = 1.86790$	$B''_{22} = -59.3857$	$B'''_{22} = -0.283880$
$B'_{23} = 2.72578$	$B''_{23} = -121.853$	$B'''_{23} = -0.39708$
$B_{33} = 0.0061030$ (at 25°)		
$C'_{222} = 0.0258302$	$C''_{222} = -6.73533$	
$C'_{223} = 0.0132623$	$C''_{223} = -4.90705$	
$C'_{233} = 0.0006944$	$C''_{233} = -3.07877$	
$C_{333} = 0.00260143$ (at 25°)		
	HCl-KCl	
$B'_{22} = 4.21977$	$B''_{22} = -171.663$	$B'''_{22} = -0.627825$
$B'_{23} = 6.26286$	$B''_{23} = -319.157$	$B'''_{23} = -0.908563$
$B_{33} = -0.0149227$ (at 25°)		
$C'_{222} = 0.0351923$	$C''_{222} = -13.3788$	
$C'_{223} = -0.00654506$	$C''_{223} = 1.58631$	
$C'_{233} = -0.0482824$	$C''_{233} = 16.55142$	
$C_{333} = 0.00389896$ (at 25°)		
	HCl-RbCl	
$B'_{22} = 4.81120$	$B''_{22} = -220.359$	$B'''_{22} = -0.706169$
$B'_{23} = 9.90811$	$B''_{23} = -591.959$	$B'''_{23} = -1.40034$
$B_{33} = -0.0253282$ (at 25°)		
$C'_{222} = 0.00171577$	$C''_{222} = 0.268611$	
$C'_{223} = -0.152656$	$C''_{223} = 58.8894$	
$C'_{233} = -0.307028$	$C''_{233} = 117.510$	
$C_{333} = 0.00607747$ (at 25°)		
	HCl-CsCl	
$B'_{22} = 3.98135$	$B''_{22} = -163.200$	$B'''_{22} = -0.589402$
$B'_{23} = 7.18090$	$B''_{23} = -376.183$	$B'''_{23} = -1.03797$
$B_{33} = -0.0428693$ (at 25°)		
$C'_{222} = 0.0125601$	$C''_{222} = -7.27713$	
$C'_{223} = -0.00513225$	$C''_{223} = 4.67404$	
$C'_{233} = -0.0228246$	$C''_{233} = 16.6252$	
$C_{333} = 0.00781711$ (at 25°)		
	HCl-MgCl <sub>2</sub>	
$B'_{22} = 0.109829$	$B''_{22} = -16.3675$	
$B'_{23} = 0.412489$	$B''_{23} = -103.858$	
$B_{33} = 0.301615$ (at 25°)		
$C'_{222} = -0.0581506$	$C''_{222} = 17.5945$	
$C'_{223} = -0.231623$	$C''_{223} = 73.4094$	
$C'_{233} = -0.8663826$	$C''_{233} = 282.1059$	
$C_{333} = -0.131846$ (at 25°)		
	HCl-CaCl <sub>2</sub>	
$B'_{22} = 0.0393685$	$B''_{22} = 3.52212$	
$B'_{23} = -0.0802115$	$B''_{23} = 70.8553$	
$B_{33} = 0.134729$ (at 25°)		
$C'_{222} = -0.00766993$	$C''_{222} = 3.64253$	
$C'_{223} = 0.0598873$	$C''_{223} = -24.0431$	
$C'_{233} = 0.4283532$	$C''_{233} = -177.0414$	
$C_{333} = 0.003627376$ (at 25°)		
	HCl-SrCl <sub>2</sub>	
$B'_{22} = 0.191441$	$B''_{22} = 45.6564$	
$B'_{23} = -0.198303$	$B''_{23} = 97.6033$	
$B_{33} = 0.104545$ (at 25°)		
$C'_{222} = -0.0978938$	$C''_{222} = 33.1445$	
$C'_{223} = -0.0403692$	$C''_{223} = 14.2616$	
$C'_{233} = 0.638829$	$C''_{233} = -212.7309$	
$C_{333} = 0.006354318$ (at 25°)		

Table IX (Continued)

HCl-BaCl <sub>2</sub>		
$B'_{22} = 2.64886$	$B''_{22} = -98.6722$	$B'''_{22} = -0.397120$
$B'_{23} = 11.1291$	$B''_{23} = -510.7983$	$B'''_{23} = -1.638268$
$B_{33} = 0.1707873$ (at 25°)		
$C'_{222} = 0.0321406$	$C''_{222} = -10.2650$	
$C'_{223} = 0.0633759$	$C''_{223} = -22.16523$	
$C'_{233} = 0.09099$	$C''_{233} = -40.60638$	
$C_{333} = 0.06586335$ (at 25°)		
HCl-AlCl <sub>3</sub>		
$B'_{22} = 0.0685392$	$B''_{22} = -3.96990$	
$B'_{23} = -0.497682$	$B''_{23} = 244.765$	
$B_{33} = 0.514398$ (at 25°)		
$C'_{222} = -0.621122$	$C''_{222} = 18.9971$	
$C'_{223} = -0.0227609$	$C''_{223} = -7.55938$	
$C'_{233} = 1.629084$	$C''_{233} = -774.6082$	
$C_{333} = 0.00607768$ (at 25°)		
HCl-LaCl <sub>3</sub>		
$B'_{22} = 2.52103$	$B''_{22} = -87.0994$	$B'''_{22} = -0.380853$
$B'_{23} = 29.1766$	$B''_{23} = -1596.85$	$B'''_{23} = -4.17835$
$B_{33} = 0.290756$ (at 25°)		
$C'_{222} = 0.0303565$	$C''_{222} = -9.44179$	
$C'_{223} = -0.0602743$	$C''_{223} = 19.8402$	
$C'_{233} = -1.816124$	$C''_{233} = 577.9868$	
$C_{333} = 0.03092964$ (at 25°)		
HCl-GdCl <sub>3</sub>		
$B'_{22} = 2.41185$	$B''_{22} = -67.2133$	$B'''_{22} = -0.372759$
$B'_{23} = 28.8136$	$B''_{23} = -1598.56$	$B'''_{23} = -3.99226$
$B_{33} = 0.375081$ (at 25°)		
$C'_{222} = 0.0663522$	$C''_{222} = -21.9425$	
$C'_{223} = -0.225857$	$C''_{223} = 22.6755$	
$C'_{233} = -5.09896$	$C''_{233} = 1062.04$	
$C_{333} = -0.680408$ (at 25°)		

some were given on a common logarithm basis and some on a natural logarithm basis. Since plots of the logarithm of the activity coefficient of HCl in all the mixtures studied in this work vary linearly with the ionic strength fraction of the salt in the mixtures and are similar to those for the HCl-NaCl,<sup>3</sup> HCl-BaCl<sub>2</sub>,<sup>4</sup> HCl-LaCl<sub>3</sub>,<sup>5</sup> and HCl-GdCl<sub>3</sub>,<sup>6</sup> mixtures, they are not shown here. Instead, it is interesting to compare the activity coefficient behavior of HCl in the various acid-salt mixtures containing 0.5 ionic strength fraction of salt at total ionic strengths of 0.5 and 1.0. In all cases the  $\log \gamma(\text{HCl})$  values at  $I = 0.5$  are lower (more negative) than the corresponding value at  $I = 1.0$  at 25° and higher (more positive) at 175°. The crossover points seem to be a function of the valence type of the salt. In the case of the HCl-alkali metal chloride mixtures the crossover points fall in the range 100–125°; with the HCl-alkaline earth chlorides the crossover point is about 90°; and in the HCl-trivalent metal chlorides mixtures the crossover point is about 60°. Hence the higher the valence type of the salt the lower is the crossover temperature.

Figures 1–3 show how the  $\log \gamma(\text{salt})$  varies with total ionic strength and fraction of acid at 25° for the

various mixtures. In all cases the  $\log \gamma$  values are lower at  $I = 1.0$  in the pure salt solutions and then, with the exception of the HCl-BaCl<sub>2</sub> and HCl-LaCl<sub>3</sub> mixtures, cross the  $I = 0.5$  curve. The following additional observations can be made concerning the activity coefficient behavior of the salt in the mixtures.

1. In the case of the HCl-NaCl mixtures (Figure 1), both curves are concave upward. In the HCl-KCl system the plots are linear; that is, both the HCl and the KCl obey Harned's rule in the HCl-KCl mixtures at 25°. In the HCl-RbCl and the HCl-CsCl mixtures the  $\log \gamma(\text{salt})$  vs.  $X(\text{HCl})$  plots are concave downward. Note that in the HCl-RbCl mixtures the activity coefficient of the RbCl becomes greater than unity at high fractions of acid in solutions of total ionic strength 1.0.

2. In the case of the HCl-alkaline earth chloride mixtures (Figure 2), the activity coefficient curves are concave downward in the HCl-MgCl<sub>2</sub> mixtures and concave upward in the remaining systems.

3. In the HCl-AlCl<sub>3</sub> and HCl-GdCl<sub>3</sub> systems, the  $\log \gamma(\text{salt})$  plots at  $I = 1.0$  cross the plots at  $I = 0.5$ ; both sets of curves are concave upward. There is no crossover in the  $\log \gamma(\text{salt})$  plots for the HCl-LaCl<sub>3</sub> mix-

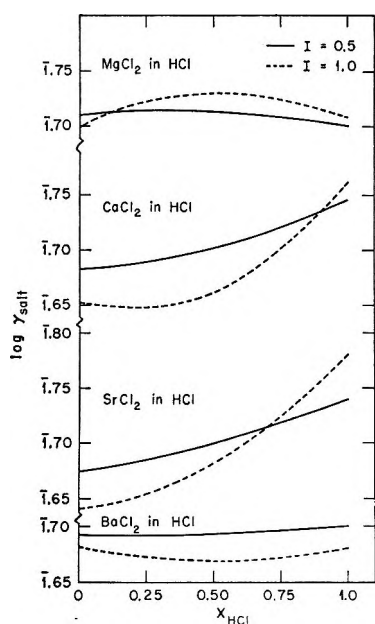


Figure 2. Plots of  $\log \gamma(\text{salt})$  vs. ionic strength fraction of HCl at 25° for HCl-MgCl<sub>2</sub>, HCl-CaCl<sub>2</sub>, HCl-SrCl<sub>2</sub>, and HCl-BaCl<sub>2</sub>.

tures and the curves are concave downward. The activity coefficient behavior of the AlCl<sub>3</sub> thus more closely resembles that of GdCl<sub>3</sub> than of LaCl<sub>3</sub> in the corresponding HCl-salt mixtures. This behavior is not qualitatively unexpected since Al(III) is the least basic and La(III) the most basic of the three metal ions.

Values of the emf,  $E$ , were calculated, using the previously determined  $E^\circ$  values and the  $B$  and  $C$  values for the smoothed activity coefficients (Table IX), for each experimental point in each of the systems. The algebraic difference between the observed  $E$  values and those calculated are given below the observed  $E$  values in Tables I-VII.

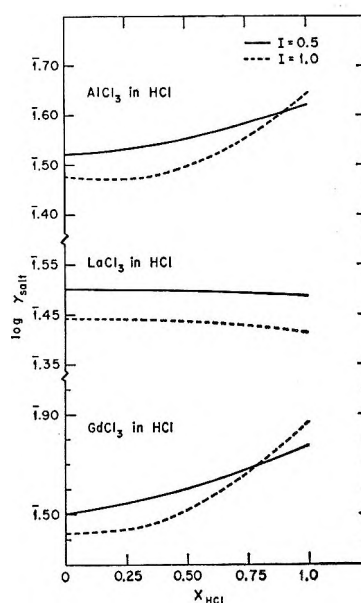


Figure 3. Plots of  $\log \gamma(\text{salt})$  vs. ionic strength fraction of HCl at 25° for HCl-AlCl<sub>3</sub>, HCl-LaCl<sub>3</sub>, and HCl-GdCl<sub>3</sub> mixtures.

The relationship between the  $B$  and  $C$  coefficients as defined by eq 2 and 3 and the  $\alpha$  coefficient of Harned's rule as well as the expressions for the partial molal free energy,  $\bar{G}_q$ , the partial molal enthalpy,  $\bar{H}_q$ , and the partial molal entropy,  $\bar{S}_q$ , for component  $q$  may be calculated using the expressions previously reported<sup>10</sup> in the study of the HBr-KBr and the HCl-LaCl<sub>3</sub><sup>5</sup> mixtures.

*Acknowledgment.* The authors wish to express their sincere appreciation to Dr. R. W. Stoughton for helpful suggestions concerning this work.

(10) M. H. Lietzke and R. W. Stoughton, *J. Phys. Chem.*, **67**, 2573 (1963).



# Phase Transformations in the Praseodymium Oxide–Oxygen System: High-Temperature X-Ray Diffraction Studies

by D. Arthur Burnham and LeRoy Eyring

Department of Chemistry, Arizona State University, Tempe, Arizona 85281 (Received March 19, 1968)

High-temperature X-ray diffraction was used to study the stability regions of the intermediate phases in the praseodymium–oxygen system. The isobaric studies of the  $\text{PrO}_x\text{-O}_2$  system, in which the reaction path was traced in reduction on heating and then in oxidation on cooling, confirmed that single phases existed in regions indicated by previous tensimetric studies and that two phases existed in regions showing hysteresis in the isobaric studies. X-Ray isothermal studies, made to examine hysteresis effects, indicated that hysteresis loops encompassed diphasic regions and that the composition of the end members of the diphasic gap was virtually constant. An attempt to interpret and rationalize these results in terms of coherent intergrowth is made with examples of somewhat similar behavior in other systems.

## Introduction

Recently, phase-analysis data from many sources on the praseodymium oxide–oxygen system have been reviewed and combined with extensive isobaric studies to yield a plausible phase diagram and a reasonable interpretation of phase transformations in this elaborate oxide system.<sup>1</sup> Figure 1 is a temperature–composition projection of the  $\text{PrO}_x\text{-O}_2$  phase diagram thus derived showing the existence of several ordered intermediate phases of narrow composition range belonging to a homologous series,  $\text{Pr}_n\text{O}_{2n-2}$ , and at higher temperatures two immiscible phases covering nearly the entire composition range of  $\text{PrO}_x$ ,  $1.5 \leq x \leq 2.0$ .

In addition to providing information establishing the phase relationships shown in Figure 1, the isobaric studies of Hyde, *et al.*,<sup>1</sup> proved to be a rich source of detailed information concerning the route of transformation between the phases including hysteresis behavior. The latter had been revealed earlier in the isothermal investigations of Ferguson, *et al.*,<sup>2</sup> and especially Faeth and Clifford.<sup>3</sup>

The present investigations continue an effort to understand the relationship between nonstoichiometry and ordered intermediate phases in oxides and the nature of hysteresis in chemical systems.

The high-temperature X-ray diffraction studies reported here were undertaken to compare phase relationships observed by this technique with those obtained principally by tensimetric measurements and with X-ray results from quenched samples and also to procure an X-ray diffraction history of events during excursion of a hysteresis loop. Such studies should provide valuable additional information concerning the nature of hysteresis for which the ideas of a domain structure have been convincingly advanced.<sup>1</sup>

## Experimental Part

Diffraction traces were produced using a Norelco

diffractometer. Copper radiation ( $\lambda_{\alpha_1} = 1.54051$ ,  $\lambda_{\alpha_2} = 1.54433$ , and  $\lambda_{\beta} = 1.3921$ ) was produced by a Philips X-ray diffraction unit. A scan rate of  $0.5^\circ (2\theta)/\text{min}$  was used. The Bragg reflection angles were read directly as  $2\theta$  values at the center of the diffraction peaks which were determined in the following manner. Horizontal chords were drawn at regular intervals across the upper two-thirds of the peak profile. A line was drawn through the midpoints of each of the chords. The angle where this line intersected the peak envelope was recorded as the peak center. The diffraction angles and assigned Miller indices for a given phase were then punched on IBM computer cards.

The lattice parameters were determined by a least-squares analytical treatment with the aid of a CDC 3400 computer. The program, which allowed cell-constant computation for any crystal system and provided a convenient method of incorporating correction terms for various experimental errors, was kindly provided by Mueller, Heaton, and Miller, Argonne National Laboratory.<sup>4</sup>

*The High-Temperature X-Ray Furnace.* A high-temperature furnace and sample holder were constructed using the basic design of Mauer and Bolz.<sup>5</sup> The design was modified as required to solve the specific problems of this research as described below.

The collimated X-ray beam entered the furnace

(1) B. G. Hyde, D. J. M. Bevan, and L. Eyring, *Phil. Trans. Roy. Soc. London, Ser. A*, **259**, 583 (1966).

(2) R. E. Ferguson, E. D. Guth, and L. Eyring, *J. Amer. Chem. Soc.*, **76**, 3890 (1954).

(3) P. A. Faeth and A. F. Clifford, *J. Phys. Chem.*, **67**, 1453 (1963).

(4) M. H. Mueller, L. Heaton, and K. T. Miller, *Acta Crystallogr.*, **13**, 828 (1965).

(5) F. A. Mauer and L. H. Bolz, National Bureau of Standards Report 3148, U. S. Government Printing Office, Washington, D. C., 1953; F. A. Mauer and L. H. Bolz, National Bureau of Standards Report 4685, U. S. Government Printing Office, Washington, D. C., 1956.

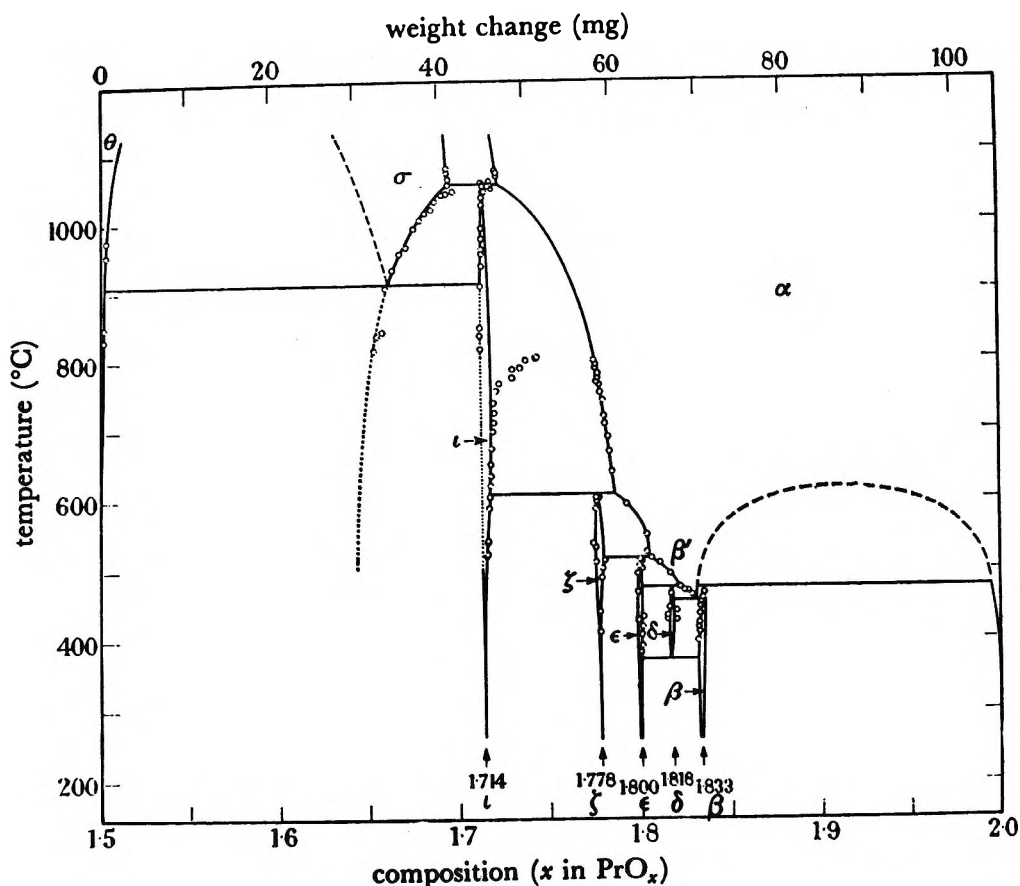


Figure 1. Projection of the praseodymium oxide phase diagram on the temperature-composition plane. Experimental points are indicated and dashed lines indicate assumed extensions. (See ref 1, p 589.)

through a beryllium window. The beryllium windows, each covering  $83^\circ$  of arc, sealed the furnace chamber, permitting X-ray diffraction patterns to be obtained while the sample was being heated in a controlled atmosphere.

A support for the specimen plate, made from recrystallized alumina, was mounted in a slot in the furnace tube. The portion of the tube above the support was cut away to admit and exit the X-ray beam. Closely spaced heater wires were wound directly underneath the specimen plate. In addition, there was an inner alumina core concentrically located in the furnace tube and cut so that it fitted around the support. Part of the heater wire was closely wound on the inner core. This construction was designed to reduce radiation loss and minimize temperature gradients.

To reduce temperature gradients further, an auxiliary shield heater was inserted above the sample. Platinum-rhodium heater wire was wound on a crescent-shaped alumina core forming a convex arc relative to the sample. This geometrical arrangement maintained a source of heat above the sample and left a window for passage of X-rays up to  $50^\circ \theta$ .

The sacrifice of the high-angle reflection was justified in this instance, since the composition of the oxide under study is so temperature sensitive.

The primary heater element of the diffractometer furnace was made from platinum-10% rhodium wire of 0.033-in. diameter and was capable of producing temperatures of  $1400^\circ$  even in oxidizing atmospheres. The shield heater element was a 0.015-in. diameter wire of the same alloy. The electrical feedthroughs were Kovar glass high-voltage terminals.

Each heating element was controlled by a separate variable transformer supplied by a voltage-stabilized source. Voltage settings for the main heater and the shield heater were adjusted to provide a balance between heat loss from the sample surface and heat gain from the shield heater. Proper settings were obtained from a series of calibration graphs, plotting the change in temperature for a given main power setting against increased power settings for the shield heater. The temperatures increased sharply when more power than necessary for a heat balance was supplied to the shield heater. The points where the slope of these plots changed was interpreted as the setting where balanced heating occurred.

A vacuum system and oxygen source were used to adjust the furnace chamber pressure in the interval ranging from 1 atm to  $10^{-5}$  mm. Gas pressures above 1 mm were measured manometrically; pressures at the low end of the range were indicated by an ion gauge.

An isopropyl alcohol-Dry Ice-cooled trap integrated with the system maintained a low vapor pressure of water. A 6-l. ballast flask was included in the system so that pressures would be virtually independent of the furnace temperature.

The temperature of the sample was indicated by a platinum-platinum-10% rhodium thermocouple. The 0.010-in. thermocouple leads entered the furnace chamber through a Conax fitting. The thermocouple junction was placed in a groove cut in the alumina support plate and was covered with alumina cement. This positioned the thermocouple junction immediately below and in contact with the specimen plate.

Two features in the design of the diffraction apparatus created difficulties in temperature determination: the large size of the sample surface exposed ( $\sim 1 \text{ cm}^2$ ) and the slot openings for incident and diffracted X-ray beams. The thermocouple was calibrated *in situ* using silver powder and the lattice-expansion data of Simmons and Balluffi.<sup>6</sup> The calibration curve showed a maximum low of  $2^\circ$  at  $200^\circ$ , crossed over zero correction at  $350^\circ$ , and was  $20^\circ$  high at  $800^\circ$ . An average correction of  $-3^\circ/100^\circ$  was used for samples with similar thermal conductivity and emissivity.<sup>7</sup>

**Sample Preparation and Procedure.** Samples of praseodymium oxide (99.999% rare earth purity), obtained from American Potash and Chemical Corp., Lindsay Division, were heated to  $850^\circ$  for 12 hr in air to remove adsorbed water and  $\text{CO}_2$  and was stored in a desiccator over magnesium perchlorate. Portions were ground in an agate mortar and were applied in a toluene suspension to a specimen plate ( $1 \times 2 \text{ cm}$ ) cut from Alundum reaction boats and ground to a uniform 0.020-in. thickness. The toluene quickly evaporated leaving a thin but uniform and adherent sample layer. The thinness of the sample reduced the temperature difference through the oxide and prevented sample buckling.

The sample was observed to warp and buckle at higher temperatures when it was supported on platinum sheet; therefore, although Alundum had thermal conductivity properties inferior to platinum, it was selected for the experiments. Diffraction patterns of rare earth oxide samples on Alundum substrates were identical with those on platinum, even at temperatures up to  $1050^\circ$ .

After preparation, the specimen plate was placed on the center of the alumina support in the diffractometer furnace. It was customary to record a diffraction pattern of the sample before any adjustment of pressure or temperature was made.

Isobaric studies were made on oxide samples by taking diffractometer traces of the specimen at various temperature settings, first in reduction on the heating cycle and then in oxidation on cooling. Traces were made when thermal equilibrium was achieved following each new temperature setting. In order to study the

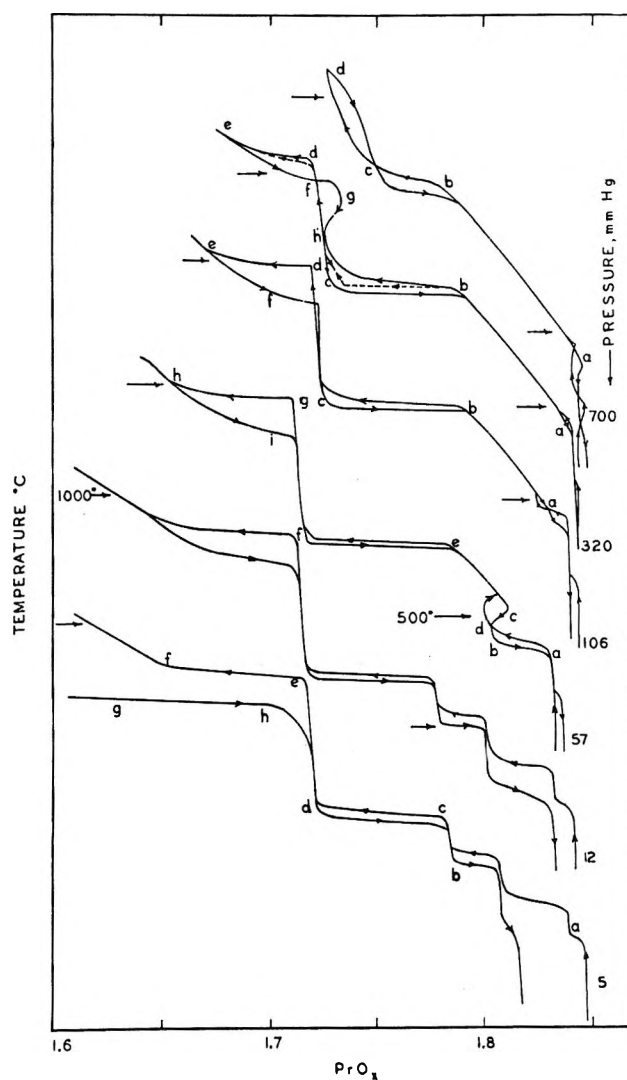


Figure 2. Selected isobaric runs in the praseodymium oxide-oxygen system at normal pressures of 700, 320, 106, 57, 12 and 5 torr. (See ref 8, p 2049.)

stability regions of the intermediate phases, a series of runs in the pressure range from 1 atm down to 3 mm of oxygen pressure were made. The isobaric data were supplemented with one isothermal run. The isobars and isotherms obtained from thermogravimetric analyses<sup>1,8</sup> served as guides for establishing appropriate environmental conditions of temperature and oxygen pressure. Figures 2 and 3 show the isobaric and isothermal data of Kordis and Eyring on very pure material.<sup>8</sup>

### Experimental Results

**Isobaric Studies in the Praseodymium Oxide-Oxygen System. Reduction-Oxidation Cycle at an Oxygen Pressure of 3-4 mm.** A preliminary run at 3-4 mm

- (6) R. O. Simmons and R. W. Balluffi, *Phys. Rev.*, **119**, 600 (1960).  
 (7) F. A. Mauer and L. H. Bolz, "Advances in X-Ray Analysis," W. M. Mueller, Ed., Plenum Press, New York, N. Y., 1961, p 229.  
 (8) J. Kordis and L. Eyring, *J. Phys. Chem.*, **72**, 2044 (1968).

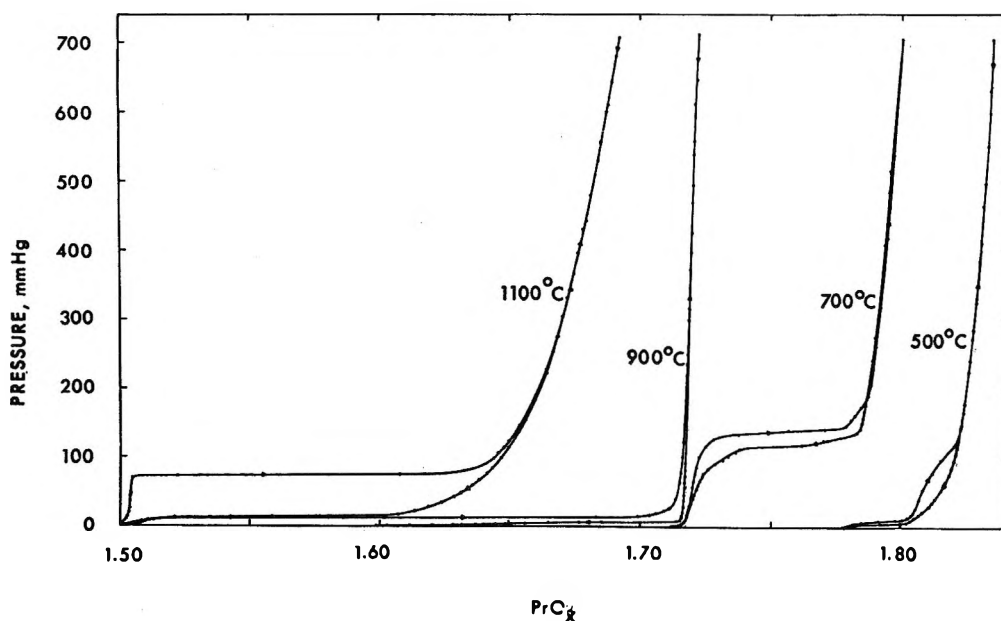


Figure 3. Isothermal runs of the praseodymium oxide-oxygen system at 1000, 900, 700 and 500°. (See ref 8, p 2050.)

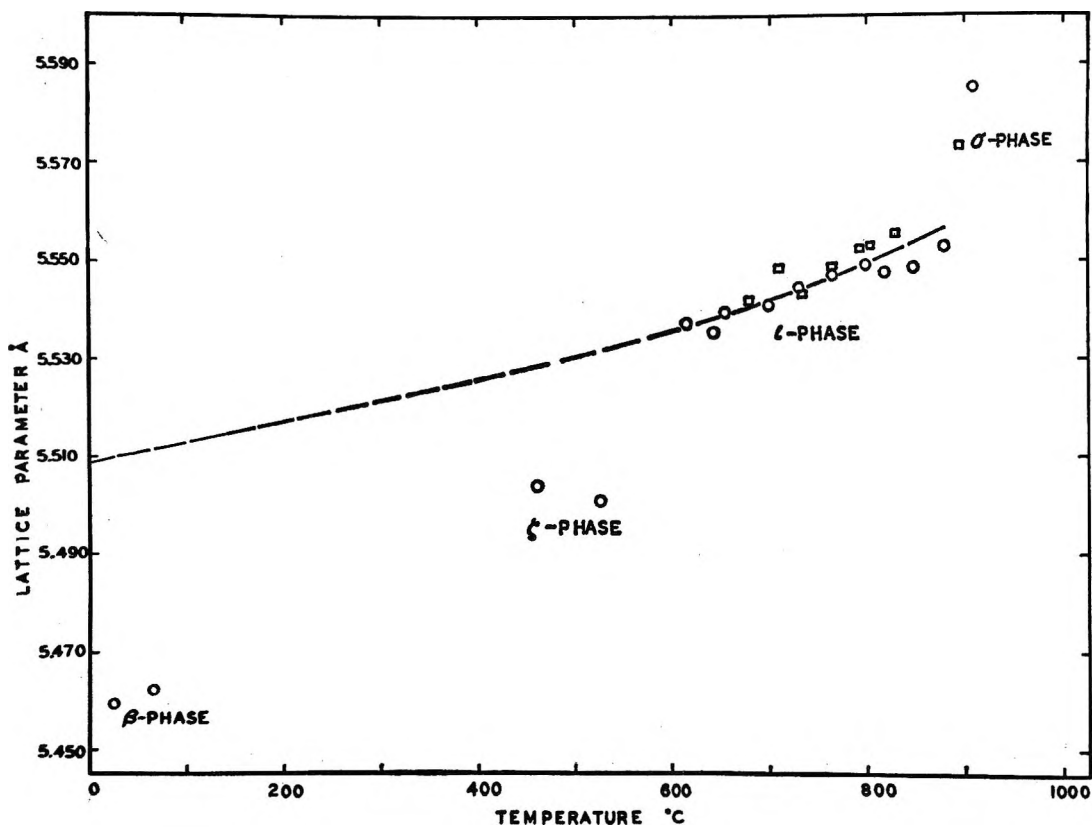


Figure 4. Lattice parameters of praseodymium oxide crystals as a function of temperature. An isobaric reduction (O)-oxidation (□) cycle at oxygen pressures of 3-4 torr. The dashed curve is a quadratic least-squares fit of the data.

of pressure showed the feasibility of observing phase transformations by following the changes in cell symmetry and lattice parameter during an oxidation-reduction cycle. Most of the measurements were of the  $\iota$  phase ( $\text{PrO}_{1.714}$ ) and the bcc  $\sigma$  phase ( $\text{PrO}_{1.674}$ ) at

elevated temperatures (see Table I and Figure 1 for phase designation). The lattice parameter *vs.* temperature plot for this run is shown in Figure 4.

The sample of praseodymium oxide at the initiation of the heating cycle was composed entirely of the  $\beta$

**Table I:** Lattice Parameters of the Ordered Phases at 25°

Phase	Obsd lattice parameters, Å	Lit. value, Å <sup>a</sup>
$\beta$	$a = 5.468 \pm 0.002$ (fcc)	$a = b = 5.466$ $c = 5.461$ $\alpha = \beta = \gamma \simeq 90.08^\circ$ (triclinic)
$\epsilon$	$a = 5.481 \pm 0.002$ (fcc)	$a = b = c = 5.4820 \pm 0.0005$ $\alpha = \beta = 90.28^\circ$ $\gamma = 90.09^\circ$ (triclinic)
$\zeta$	$a = 5.487 \pm 0.004$ (fcc)	$a = 5.478 \pm 0.001$ $b = 5.482 \pm 0.001$ $c = 5.496 \pm 0.001$ $\alpha = 90.15^\circ$ $\beta = 90.50^\circ$ $\gamma = 90.91^\circ$ (triclinic)
	$a = 5.510 \pm 0.002$ $\alpha = 89.68^\circ \pm 0.02$ (rhombic)	$a = 5.5096 \pm 0.0005$ $\alpha = 89.63^\circ$ (rhombic)

<sup>a</sup> J. O. Sawyer, B. G. Hyde, and L. Eyring, *Bull. Soc. Chim. Fr.* 1190 (1965).

phase ( $\text{PrO}_{1.833}$ ). Guinier powder diagrams of the  $\beta$  phase which show splitting of the strong lines and many weaker superstructure lines were tentatively indexed as a triclinic pseudocell based on a fluorite cell of  $\text{PrO}_2$ .<sup>9</sup> The relatively strong superstructure lines and splitting of the fluorite-type reflections which characterizes the Guinier powder patterns of the  $\beta$  phase are not seen in the diffractometer trace. This is not surprising, since annealing periods of  $\sim 100$  days were required to resolve the broad fluorite-type reflections in the Guinier patterns.<sup>9</sup> Diffractometer traces did show definite peak broadening but lacked the resolution required to index the patterns except on the basis of fcc symmetry.

The first diffraction pattern taken during the heating cycle (521°) was apparently that of the  $\zeta$  phase ( $\text{PrO}_{1.778}$ ). The presence of the  $\zeta$  phase at 521° is in agreement with the 5-mm isobar shown in Figure 2 (path b-c). Guinier diagrams of the  $\zeta$  phase at room temperature show the cell symmetry to be triclinic:<sup>9</sup> the  $\langle 111 \rangle$  reflection is split into four lines of equal intensity, while the  $\langle 200 \rangle$  reflection is split into three lines of equal intensity. The diffractometer does not resolve these reflections into components which would indicate symmetry lower than fcc. Broadened peaks and an abrupt change in cell edge dimension distinguishes the  $\zeta$  phase trace from the  $\beta$ -phase pattern.

By the time a temperature of 614° was reached, the cell had changed to the rhombohedral  $\iota$  phase and the cell edge had increased 0.03 Å.

In the diffractometer trace of the  $\iota$  phase, the  $\langle 220 \rangle$

reflection of the fluorite-type cell is split into two components of equal intensity, while the  $\langle 200 \rangle$  reflection remains singularly sharp. The observed peak splitting and peak width, both for these reflections and in the high-angle region, are in accord with those expected from a rhombohedral distortion of a fluorite cubic cell.<sup>9</sup> Ten lattice parameters were computed from the diffractometer data in the temperature interval 614–880°. Referring to Figure 2, it is seen that the presence of the  $\iota$  phase in this temperature interval is in accord with the stability range indicated by path d-e of the 5-mm isobar.

In Figure 4, a line drawn to represent a least-squares fit of the  $\iota$ -phase lattice parameters to a quadratic equation (temperature is the independent variable) and extrapolated to 25° gives a parameter that agrees with literature values (see Table I).

Perhaps it should be noted that in isobaric runs the lattice parameter responds to changes both in temperature and composition increasing with the former and decreasing with increase of the latter. Since reduction occurs on heating, the effects are additive in both directions. This gives rise to moderate slopes for single phases of narrow composition range as seen for the  $\iota$  phase in Figure 4 and steeper slopes for the  $\sigma$  or  $\alpha$  phases of variable composition as seen in later isobars.

The diffraction pattern taken after a temperature jump to 909° showed a further increase in lattice parameter of 0.03 Å and a cell symmetry characteristic of the bcc C-type sesquioxide which has been designated as the  $\sigma$  phase. The heating cycle was stopped at this temperature.

At 831° on the cooling cycle, the rhombohedral reflections dominated the diffraction trace. The  $\sigma$  phase present distorted the rhombohedral pattern because of superimposition of the mainline reflections of two phases. The  $\iota$ -phase reflections were clearly distinguishable, but there were insufficient numbers of bcc reflections resolved for lattice-parameter computation. Six more points between 803 and 678° were observed during the oxidation cycle. The temperature at which  $\sigma$  reflections disappeared could not be ascertained because of the presence of the strong rhombohedral reflections. The  $\iota$ -phase lattice parameters from the reduction and oxidation cycles were compared, and no significant differences were observed.<sup>10</sup>

*Reduction-Oxidation Cycle at an Oxygen Pressure of 45–50 mm.* The sample for this run was probably exposed to moist air during preparation, as evidenced by the presence of fluorite-type  $\text{PrO}_2$  in what was thought to be pure  $\beta$  phase. After heating the sample under vacuum to 270°, all  $\text{PrO}_2$  was reduced to  $\beta$  (see Figure 5). The oxygen pressure over the sample

(9) J. O. Sawyer, E. G. Hyde, and L. Eyring, *Bull. Soc. Chim. Fr.*, 1190 (1965).

(10) X-Ray data are available (D. A. Burnham, *Dissertation Abstr.*, 27B, 3058 (1967)).

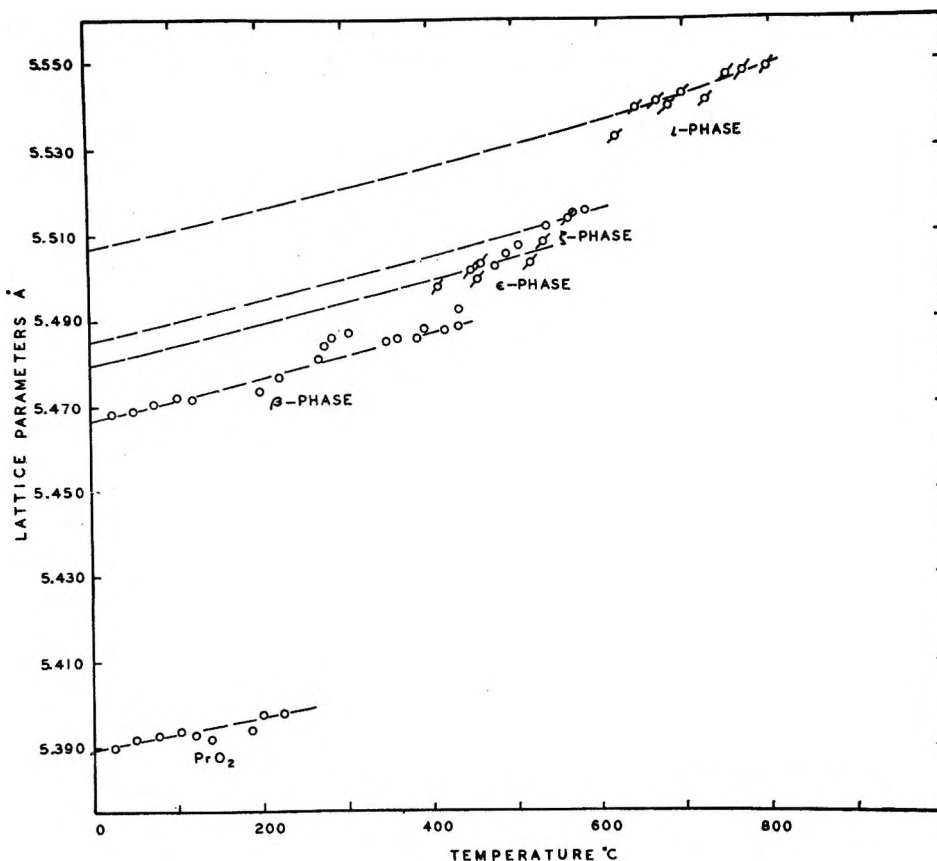


Figure 5. Lattice parameters of praseodymium oxide crystals as a function of temperature. Two isobaric reduction runs (O,  $\circ$ ) at oxygen pressures of 45–50 torr. The dashed curves are quadratic least-squares fits to the parameters.

was then adjusted to 45 mm and the heating cycle was resumed.

Between 270 and 450°, the  $\beta$  phase existed as a single phase. The  $\epsilon$  phase ( $\text{PrO}_{1.80}$ ) was found at 462°—its presence shown only by the abrupt change in lattice parameter (0.01 Å). Between 518 and 536°, another lattice-parameter change occurred. The small increase (0.005 Å) made phase identification difficult, but it did correspond to the expected transition  $\epsilon \rightarrow \zeta$  ( $\text{PrO}_{1.778}$ ). Between 594 and 616°, a third lattice-parameter jump occurred (0.02 Å), accompanied by a symmetry change from face-centered cubic (fcc) to a rhombohedral cell, indicating the phase transition  $\zeta \rightarrow \iota$  ( $\text{PrO}_{1.714}$ ). Additional data up to 918° indicated only thermal expansion of the  $\iota$  single phase.

The diffraction patterns of the  $\iota$  phase were indexed on a hexagonal basis so that the  $a:c$  axial ratio could be calculated. A plot of the ratio against temperature showed that the hexagonal  $\iota$  phase had a virtually constant ratio of 1.071 over its entire range of existence (>300°). A least-squares fit of the data was made, and the standard deviation of the axial ratios was found to be 0.002 and the maximum deviation 0.004. Since the composition change is small under these conditions, it is apparent that thermal expansion is essentially isotropic for  $\iota$  phase.

Above 918° the rhombohedral phase was reduced to

the bcc  $\sigma$  phase. The changes in the diffraction pattern observed during the  $\iota \rightarrow \sigma$  transition were the same as in the previous isobar: the main reflections sharpened considerably and the extra lines of the bcc phase appeared and the lattice parameter increased 0.02 Å.

The lines drawn through data points in Figure 5 represent lattice parameters for each single phase. It should be stated that the least-squares fit was prejudiced, since at least one room temperature lattice parameter (quenched sample) was used in each calculation.

*A Reduction-Oxidation Cycle at an Oxygen Pressure of 100 mm.* The cell constants from this run are plotted in Figure 6. A line representing a least-squares fit of thermal expansion data, drawn through all the constants from room temperature to 469°, and an extrapolated value of  $5.486 \pm 0.003$  Å was obtained at 25°. This compared with the triclinic cell edge reported by Sawyer, *et al.*,<sup>9</sup> for the  $\epsilon$  phase,  $a = 5.482 \pm 0.001$  Å. Apparently the  $\epsilon$  phase was obtained in the low-temperature vacuum treatment and remained up to above 500°.

Between 502 and 635°, four cell constants were obtained with lattice parameters greater than expected for thermal expansion of a phase of narrow composition range. Also, the diffractometer peaks had

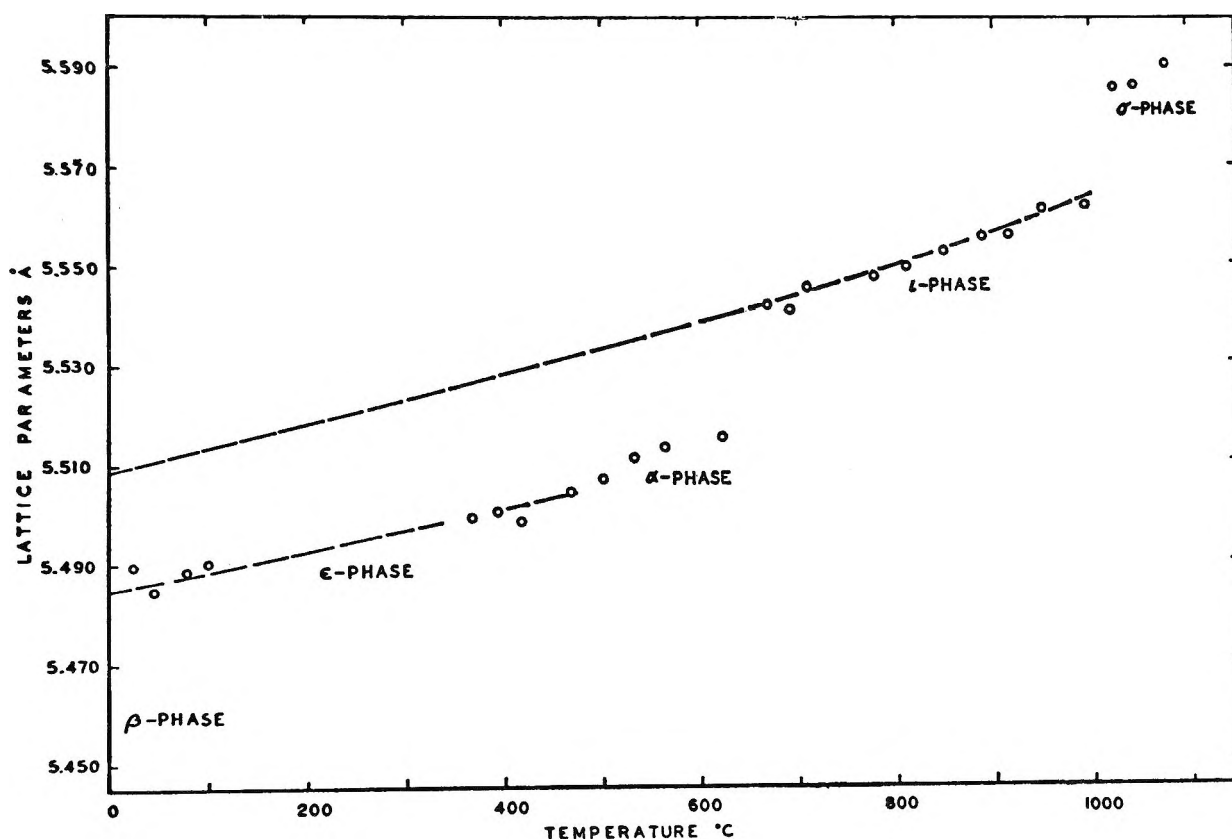


Figure 6. Lattice parameters of praseodymium oxide crystals as a function of temperature. Isobaric reduction at an oxygen pressure of 100 torr. The dashed curves are quadratic least-squares fits of the data.

sharpened significantly. The change corresponded to the thermogravimetric analysis isobaric data where a break from the  $\epsilon$  phase to the  $\alpha$  phase (disordered high-temperature phase of variable composition) occurs. This is represented by the path a-b of the 106-mm isobar shown in Figure 2. At 670°, the cell symmetry had changed to the rhombohedral  $\iota$  phase and the cell constant suddenly increased  $\sim 0.025$  Å. This temperature corresponded to the initiation of the diphasic region  $\alpha \rightarrow \iota$  represented by the path b-c on the tga isobar. The diphasic region, which has a range of existence of only 15° according to the tga diagram, was bypassed. From 670 to 993°, only the  $\iota$  phase was observed. Changes in the O/Pr ratio of this phase, even over this extended temperature range, are only 0.005, so that the change in the  $\iota$  lattice parameters was due primarily to thermal expansion. According to room temperature X-ray diagrams, a change of 0.005 in O/Pr corresponds to an edge dimension change of  $\sim 0.002$  Å.<sup>1</sup>

At 1025° there was a transition to body-centered cubic symmetry and an increase in lattice parameter of 0.025 Å. This phase change corresponded to the  $\iota \rightarrow \sigma$  transformation represented by the path d-e in Figure 2. The remaining points up to 1077° show marked compositional changes of the  $\sigma$  phase in addition to thermal expansion. This expansion closely resembles that of the  $\alpha$  phase.

*Reduction-Oxidation Cycles at Oxygen Pressures of 320 and 700 mm.* X-Ray isobaric studies at oxygen pressures of 320 mm showed essentially the same features as the 700-mm isobar. The X-ray data are plotted in Figure 7. From room temperature to 430°, diffraction patterns showed only the  $\beta$  phase. Between 478 and 701°, five diffraction patterns of the fcc  $\alpha$  phase were obtained. These were characterized not only by the sharpness of the pattern but also by the rapidly increasing lattice parameters, indicative of the compositional change expected for this phase.

The lattice parameters of the sample, at 700 mm, along the "α slope" gave lower values by  $\sim 0.008$  Å than the corresponding data in the 320-mm isobar. At the same temperature, the  $\alpha$  composition differs by 0.02 O/Pr between 320 and 700 mm of oxygen pressure. According to room temperature X-ray data, this composition interval corresponds to a cell dimension change of 0.008 Å.

High-temperature diffraction studies were made of the  $\alpha \rightarrow \iota$  conversion at 700 mm of oxygen pressure. At 863° the  $\alpha$  phase predominated, but the  $\iota$  phase increased as the temperature was raised, as shown by the change in intensity of the reflections. The  $\iota$  phase present continued to change composition, as indicated by the shift in its diffraction pattern. At 992°, the highest temperature achieved, the  $\alpha$  phase was still visible, but at this temperature  $\iota$  phase predominated.

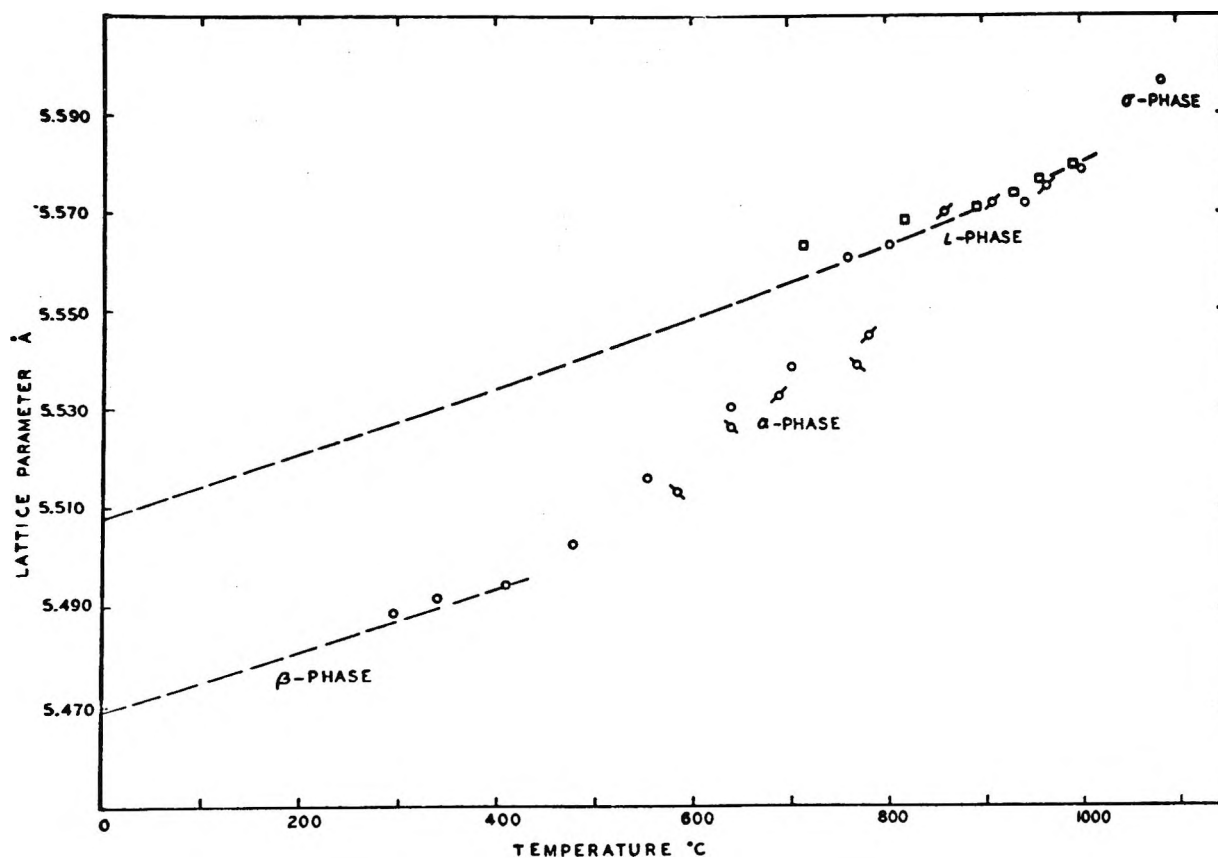


Figure 7. Lattice parameters of praseodymium oxide crystals as a function of temperature. A reduction path was made at 700 torr (○) and twice at 700 torr (◊ and ◑) and an oxidation path was made at 320 torr (◻). The dashed curves are quadratic least-squares fits of the data.

The X-ray results correspond to the reduction curve of the tga 700-mm isobar shown in Figure 2 and the interpretation given by Hyde, *et al.*<sup>1</sup> The X-ray patterns indicated that at 320 mm of pressure the  $\alpha \rightarrow \iota$  transition was completed at 760°.

The predominance of  $\iota$  phase of the normal lattice parameters in the  $\alpha \rightarrow \sigma$  transition at 650 mm suggested that whereas the bulk sample did not reduce readily and completely to  $\iota$  as seen in the isobars perhaps the thin X-ray sample did. Therefore, an isobaric run on the thermal balance at 700 mm was started but was stopped at 870° where it was allowed to soak for several days. The temperature during this period was cycled at  $\pm 5^\circ$  with a period of about 20 min and was allowed to make an excursion of  $-20$  to  $30^\circ$  over the period of about 5 days. The sample composition under these conditions was observed to cycle in phase with the temperature showing reversibility for these small variations in stress, but no drift toward  $\iota$  composition was observed during the experiment beyond that caused by temperature increase. There is no reason, therefore, to believe that the isobars do not reflect the composition of the thin X-ray samples.

The tga 320-mm isobar (Figure 2) shows a crossover of the vertical part of the reduction curve by the cooling curve in oxidation, indicating a composition greater

than experienced in this temperature range in reduction. Lattice parameters measured at various temperatures along this oxidation curve showed no abnormal behavior in the rhombohedral phase. Evidently, the amount of  $\alpha$  phase present was too small to be detected by the diffractometer.

The sharper order-disorder transition ( $\iota \rightarrow \sigma$ ) between 1052 and 1083° was examined carefully and was observed to be diphasic all the way as  $\sigma$  grows at the total expense of  $\iota$ . A sample left overnight in the middle of the range did not change perceptibly in its diffraction characteristics.

*An Isothermal Reduction-Oxidation Cycle at 699°.* The isothermal study was conducted to examine by high-temperature X-ray diffraction the hysteresis loops manifest in isothermal tensimetric studies.<sup>2,3</sup> For purposes of comparison, the temperature-composition isotherms of praseodymia reported by Kordis and Eyring<sup>8</sup> are shown in Figure 3.

The  $\beta$  phase reduced to the  $\iota$  phase under vacuum conditions at 700°. Diffraction traces were made at each pressure setting, first in oxidation and then in reduction. X-Ray patterns at 10 and 90 mm showed only the  $\iota$  phase. At 130 mm of pressure, the first signs of distortion of the rhombohedral pattern were observed, indicating the presence of the  $\alpha$  phase. Traces



at 140, 160, and 200 mm showed increased distortion as the amount of  $\alpha$  increased, but  $\iota$  remained the major phase. At 300 mm, the rhombohedral reflections were no longer detectable; the fcc symmetry of the  $\alpha$  phase remained.

The pressure was lowered to 147 mm for the first setting in reduction. Both the rhombohedral and fcc phases were seen; the fcc reflections distorted the  $\iota$  pattern. The two phases were also found at 125 and 95 mm of pressure. The diphasic region existed at lower pressures in reduction than observed in oxidation. In addition there was a shift in the hysteresis loop upward in pressure. If the temperature were higher than thought by 10° this difference could be explained.

The cell dimensions of the  $\iota$  phase remained constant, regardless of the pressure setting. It was difficult to judge how the composition of the  $\alpha$  phase varied over the 300 mm of pressure range, since complete patterns were not obtained for this phase in diphasic regions. However, large composition changes would have caused perceptible movement of the fcc reflections in the X-ray diagrams. It appears that the compositional changes observed in the tensimetric studies<sup>2,3</sup> are changes in the relative amounts of the constituent phases in which each phase maintains virtually constant composition.

**Thermal Expansion.** The determination of the coefficient of thermal expansion is easily made once the lattice parameters for a given phase have been determined as a function of temperature. The thermal expansion data are reported in Table II as linear expansion coefficients. The lattice parameters used in the calculations were taken from curves representing a least-squares fit of the data. Thermal expansion data were not calculated for phases with extended variable composition.

**Table II:** Thermal Expansion Data

Oxide	Phase	Linear coeff of expansion ( $\times 10^6$ )	Temp. °C
PrO <sub>1.833</sub>	$\beta$	9.9	400
PrO <sub>1.80</sub>	$\epsilon$	9.5	500
PrO <sub>1.778</sub>	$\zeta$	9.7	580
PrO <sub>1.714</sub>	$\iota$	9.6	900
PrO <sub>1.5</sub>	$\phi$ (C type)	8.7	900
PrO <sub>1.5</sub>	$\theta$ (A type)	9.9 ( <i>a</i> axis) 20.7 ( <i>c</i> axis)	900

## Discussion

The X-ray diffraction studies at high temperatures are consistent with the phase diagram shown in Figure 1 which was largely deduced from isobaric tensimetric curves such as those shown in Figure 2. In all instances where single phases were expected from the

previous work, single phases were observed in these X-ray studies.

In the interpretation of the tensimetric curves, *nearly* horizontal lines were viewed as two-phase regions in spite of their small slope. These regions were seen to be diphasic by high-temperature X-ray diffraction. For example, in the  $\iota \rightarrow \sigma$  transition which occurred over a 50° interval from 1052° at 320 mm of pressure, the  $\sigma$  phase grew at the expense of  $\iota$  as the temperature increased. Long waiting periods did not change the diffraction patterns.

All regions which exhibited hysteresis in the tensimetric work had been interpreted as two-phase regions, even though they showed bivariant behavior of appreciable magnitude in one of their branches (called pseudophases<sup>1</sup>). This dissymmetry was evident in the X-ray results for both isobaric and isothermal studies. It was of interest to examine these regions in particular by X-ray diffraction.

The  $\alpha \rightarrow \iota$  transition at 700–1000° is of special concern. Because of the shape of the curve (b–d Figure 2), the compositions involved, and the occurrence of hysteresis, it had been concluded that in reduction  $\alpha$  converts rapidly but incompletely to  $\iota$  at about 850° and that some  $\alpha$  persists even at 1000°. This was confirmed by X-ray diffraction.

The  $\alpha \rightarrow \iota$  pseudophase has some special kind of stability toward small temperature fluctuations, as indicated in the Experimental Results described above. Such "phases" are observed when closely related structures transform with a loss of symmetry, especially when a disorder–order transformation occurs (*i.e.*,  $\alpha \rightarrow \iota$  or  $\sigma \rightarrow \iota$ ).

This behavior is explicable in terms of coherent intergrowth of domains of related phases.<sup>1</sup> The domains are perhaps of the order of 5–20 unit cells in extent, which would make them at most about 100 Å in linear dimension. If such domains were oriented at random or under severe strain, they should be amorphous or at least have very broad lines with poor resolution. Actually, two phases are observed in region c–d, Figure 2, in reduction at 700 mm, and each phase gives quite sharp reflections. The  $\iota$  phase has a lattice parameter which shows only the normal expansion with temperature, while the  $\alpha$  phase observed is seen to reduce its composition but still persists at 992°. The X-ray results would be consistent with the domain ideas only if the small domains are arranged in phase on the grid of the coherent heterogeneous matrix of the crystal in such a way that the diffracted beam is reinforced as though they were actually contiguous in crystallites of at least 500 Å in linear dimension.

Crystallites larger than 500 Å in linear dimension would not be expected to have the anomalous stability or to exhibit the hysteresis phenomena observed.

Recently, Andersson, *et al.*,<sup>11</sup> observed that the mixed oxide W<sub>4</sub>Nb<sub>26</sub>O<sub>77</sub> reported by others is an ordered

intergrowth of the adjoining compounds  $WNb_{12}O_{33}$  and  $W_3Nb_{14}O_{44}$ . They reported that its structure contains two distinct structural elements, one characteristic of each of the adjoining compounds each finite in two dimensions but infinite in the other. They further suggested that ranges of homogeneity in such systems may be due to disordered intergrowth allowing the variation in composition. Wadsley<sup>12</sup> had earlier described naturally occurring nonstoichiometric hydrated vanadium oxide minerals as intergrowths of two distinct structures.

It is suggested that coherent intergrowth is responsible for the behavior of these oxide materials, and studies of these regions are being continued both by tensimetric and X-ray methods.

*Acknowledgment.* It is our pleasure to acknowledge the support of the U. S. Atomic Energy Commission which made this work possible.

(11) S. Andersson, W. G. Mumme, and A. D. Wadsley, *Acta Crystallogr.*, **21**, 802 (1966).

(12) A. D. Wadsley in "Nonstoichiometric Compounds," L. Mandelcorn, Ed., Academic Press, New York, N. Y., 1964, p 98.

## High-Temperature X-Ray Diffraction Studies of the Terbium Oxide–Oxygen and Mixed Cerium Terbium Oxide–Oxygen Systems

by D. Arthur Burnham, LeRoy Eyring, and J. Kordis

*Department of Chemistry, Arizona State University, Tempe, Arizona 85281 (Received March 19, 1968)*

High-temperature X-ray diffraction was used to study the stability regions of the intermediate phases in the terbium oxide–oxygen and the mixed cerium terbium oxide–oxygen systems and to clarify the nature of chemical hysteresis and "pseudophase" phenomena in such systems. These isobaric X-ray diffraction studies of the terbia system confirmed the major features of the phase diagram gained from previous tensimetric work. Also, in both isothermal and isobaric studies the presence of hysteresis was confirmed. It was shown that hysteresis loops encompassed diphasic regions and that the composition of the ordered phases of narrow homogeneity range in diphasic regions remained virtually constant with temperature. X-Ray diffraction traces also showed that the pseudophases seen in oxidation were diphasic mixtures of the same two phases seen in reduction. In the ternary system ( $Ce_{0.2}Tb_{0.8}O_x$ ) studied, no diphasic regions were observed. The resolution found in X-ray patterns of terbia, which distinguished the different phases, was lost when ceria was admixed. Line broadening in the X-ray diffraction patterns was thought to be a combination of incipient phase transition of the terbia in the mixed oxide and variations in homogeneities of the crystallites because of the presence of cerium.

### Introduction

The terbium oxide–oxygen system has recently been studied by Hyde and Eyring<sup>1</sup> using an isobaric technique which proved to be powerful in the clarification of phase relationships in the  $PrO_x$  system.<sup>2</sup> The isobaric runs together with other results on the  $TbO_x-O_2$  and related systems were considered in detail. Figure 1 shows a partial phase diagram of the system as derived from the isobars.

Kordis and Eyring have repeated some of the isobaric and isothermal tensimetric studies on the  $TbO_x-O_2$  system with a sample of greater purity (99.999%) than had previously been available.<sup>3</sup> Some results of these experiments are shown in Figures 2 and 3. In addition, they made extensive tensimetric studies of the

$Ce_yTb_{1-y}O_x-O_2$  system.<sup>4</sup> Some of the isobaric results of the  $Ce_{0.2}Tb_{0.8}O_x-O_2$  are shown in Figure 4.

Both the  $TbO_x-O_2$  and  $Ce_yTb_{1-y}O_x-O_2$  systems show complex tensimetric behavior. The former affords an additional example (to that of the  $PrO_x-O_2$  system<sup>2</sup>) of intermediate phases of narrow composition range ( $Tb_nO_{2n-2}$ ) separated by two phase regions and undergoing hysteresis and "pseudophase" formation. The mixed-oxide system exhibits incipient behavior in an analogous way; however, in addition, there appears

(1) B. G. Hyde and L. Eyring, in "Rare Earth Research. III," L. Eyring, Ed., Gordon and Breach, New York, N. Y., 1966, p 623.

(2) B. G. Hyde, D. J. M. Bevan, and L. Eyring, *Phil. Trans. Roy. Soc. London*, **A259**, 583 (1966).

(3) J. Kordis and L. Eyring, *J. Phys. Chem.*, **72**, 2030 (1968).

(4) J. Kordis and L. Eyring, *ibid.*, **72**, 2044 (1968).

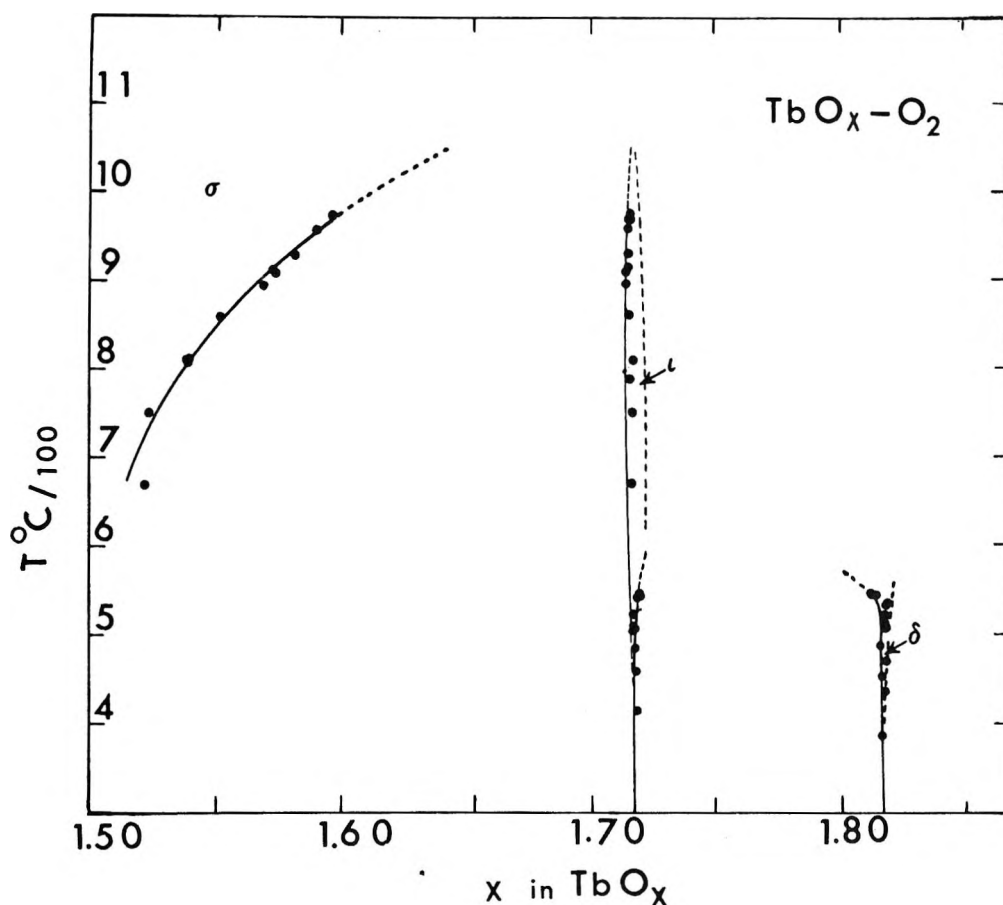


Figure 1. Projection of the terbium oxide phase diagram on the temperature-composition plane. The experimental points are shown. (See ref 1, p 634.)

a nonstoichiometric phase analogous to the  $\alpha$  phase of the  $\text{PrO}_x\text{-O}_2$  system.

High-temperature X-ray diffraction studies of the  $\text{PrO}_x\text{-O}_2$  system have been carried out<sup>5</sup> to provide yet another window through which to view the complicated behavior of that system. Similarly, high-temperature X-ray measurements were undertaken in the  $\text{TbO}_x$  and  $\text{Ce}_y\text{Tb}_{1-y}\text{O}_x$  systems to elaborate on the tensimetric studies.

#### Experimental Procedures

The high-temperature furnace, sample holder, and techniques used in the X-ray diffraction studies have already been described.<sup>5</sup> The lattice parameters were determined by a least-squares analytical treatment with the aid of a Control Data Corporation 3400 computer.<sup>6</sup> The same sample of  $\text{Ce}_{0.2}\text{Tb}_{0.8}\text{O}_x$  was employed as by Kordis and Eyring<sup>4</sup> in their tensimetric studies.

#### An Isobaric Study in the Terbium Oxide-Oxygen System

*Reduction-Oxidation Cycle at an Oxygen Pressure of 10 mm.* Figure 2 indicates the tensimetric behavior to be expected of a cyclic run in the approximate vicinity of the 10 mm of oxygen isobar selected for X-ray study. The three phases observed in this investigation

had different cell symmetries and lattice spacing differences greater than 0.03 Å. The lattice parameters are plotted in Figure 5. A tabulation of the known  $\text{TbO}_x$  phases is given in Table I.

The triclinic  $\delta$  phase ( $\text{TbO}_{1.818}$ ) is found to be the stable form at lower temperatures. The  $\delta$ -phase X-ray patterns were indexed on the basis of the triclinic cell suggested by Baenziger, *et al.*<sup>7</sup> The cell parameters calculated for this cell at 25°, based on a least-squares fit of  $\delta$ -phase lattice parameters to a quadratic equation (temperature is the independent variable), are  $a = b = c = 5.287 \pm 0.005$  Å,  $\alpha = \beta = 90.58^\circ$ , and  $\gamma = 90.00^\circ$ .

The  $\delta$  phase was stable up to 469°. Between 469° and 490°, a transition to the  $\iota$  phase ( $\text{TbO}_{1.714}$ ) occurred. The relative amounts of two phases over this extended temperature range were constant for any given temperature—the peak profile did not change after 2–4 hr (no further change was observed after 48 hr of standing). The transition to the  $\iota$  phase was complete

(5) D. A. Burnham and L. Eyring, *J. Phys. Chem.*, **72**, 4415 (1968).

(6) M. H. Mueller, L. Heaton, and K. T. Miller, *Acta Crystallogr.*, **13**, 828 (1965).

(7) N. C. Baenziger, H. A. Eick, H. S. Schuldt, and L. Eyring, *J. Amer. Chem. Soc.*, **83**, 2219 (1961).

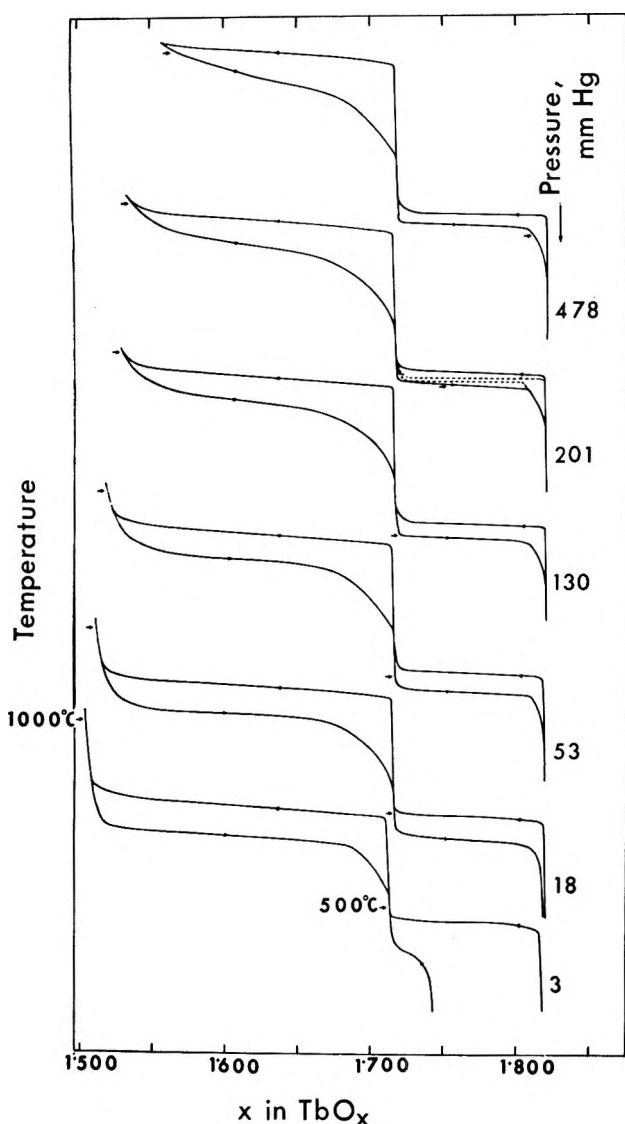


Figure 2. Selected isobaric runs in the terbium oxide-oxygen system at normal pressures of 478, 201, 130, 53, 18, and 3 torr. (See ref 3, p 2034.)

at 505°. Between 505 and 753°, 13 lattice parameters were indexed on the basis of a rhombohedral pseudocell described by Baenziger, *et al.*,<sup>7</sup> and were consistent with the change expected for thermal expansion of a single phase of narrow composition range. The cell parameters at 25°, based on an extrapolated value from a least-squares fit of the  $\iota$ -phase lattice parameters, are:  $a = 5.319 \pm 0.004 \text{ \AA}$  and  $\alpha = 89.71^\circ$ . This compares with the cell constants  $a = 5.319 \pm 0.001 \text{ \AA}$  and  $\alpha = 89.41^\circ$  reported by Baenziger, *et al.*<sup>7</sup>

The diffraction patterns of the  $\iota$  phase indexed on a hexagonal basis gave an  $a:c$  ratio by a least-squares fit of 1.072, which was virtually constant over the entire temperature range.

Between 787 and 833°, the  $\iota \rightarrow \sigma$  phase transition occurred. Reduction of the  $\sigma$  phase was followed by X-ray diffraction to 940° before the oxidation cycle was begun.

Hysteresis loops in the terbium oxide-oxygen system are larger than the corresponding ones of the praseodymium oxide-oxygen system. The  $\sigma$  phase exists at a lower temperature in oxidation than is the case in reduction. Samples were equilibrated until there was no further change in the X-ray patterns. X-Ray diffraction indicated a single phase pattern of  $\sigma$  at 810°, but at 743° the  $\iota$  phase appeared. At 702°, a complete diffraction trace showed the principal phase to be  $\iota$ , but  $\sigma$  was still evident. Further cooling eliminated any trace of the  $\sigma$  phase. The diphasic region existed over a 100–150° range in oxidation and only over a 60–70° range in reduction. At any point in the temperature range, the relative proportion of the two phases remained constant both times. Diffraction patterns taken after 24 hr of standing at temperature and compared with the initial traces showed no further change.

The  $\iota$  phase was observed down to 448° as a single phase. The thermal expansion curve of the  $\iota$  phase in oxidation is identical with that of the reduction curve. By 390° the  $\iota \rightarrow \delta$  phase transition had not occurred. The temperature was well below that seen for the diphasic region in reduction. The sample was then cooled rapidly to room temperature, and the diphasic region was bypassed. At room temperature, the pattern was that of the triclinic  $\delta$  phase.

#### An Isobaric Study of the Mixed Cerium Terbium Oxide-Oxygen System

*Reduction-Oxidation Cycle at an Oxygen Pressure of 10 mm.* For purposes of comparison, the temperature-composition isobars of the  $\text{Ce}_{0.2}\text{Tb}_{0.8}\text{O}_x\text{-O}_2$  system obtained from tga studies reported by Kordis and Eyring<sup>4</sup> are included (see Figure 4). The resolution of the strong peaks that distinguished the different phases in the terbium oxide system was lost when cerium was admixed. In general, the quality of the diffractometer traces was poor. The low-angle peaks were reasonably sharp, but the  $\text{K}\alpha$  doublets of the high-angle peaks were unresolved. Long annealing times caused no perceptible improvement in the quality of the diffraction patterns. It was not possible to detect any phase transformations by change in cell symmetry. The lattice parameters calculated were all expressed in terms of the face-centered cubic lattice dimensions. The probable errors for the cell dimensions were high and the random scattering of data points rather large.

The high-temperature X-ray studies reveal an irregular lattice parameter expansion curve, as shown in Figure 6. Up to 406°,  $\text{Ce}_{0.2}\text{Tb}_{0.8}\text{O}_x$  followed an expansion curve expected for a single phase of narrow composition. From 406 to 550°, the lattice parameters increased rapidly. A portion of an isobar at an oxygen pressure of 215 mm was studied by X-ray diffraction methods to see if the temperature range for which this rapid cell expansion occurred could be extended. The

Table I: Some Properties of Phases in the Terbium-Oxygen System

Oxide	Color	Lattice type	Lattice parameters, Å	Equil conditions			Ref
				Temp, °C	Atm	Pressure	
TbO <sub>1.500</sub>	White	bcc (C)	$a = 10.729$ $a = 10.7281 \pm 0.0005$ $a = 10.752 \pm 0.006$	750	H <sub>2</sub>	1 atm	<i>a, b</i> <i>c</i> <i>d</i>
TbO <sub>1.500</sub>	White	Monoclinic (B)	$a = 13.92$ $b = 3.536$ $c = 8.646$ $\beta = 100.2^\circ$	1960	N <sub>2</sub>	1 atm	<i>a, c</i>
TbO <sub>1.500</sub>		Hexagonal (A)	$a = 3.84$ $c = 6.13$	2200	H <sub>2</sub>	1 atm	<i>e</i>
TbO <sub>1.715</sub>	Brown	Rhombohedral Pseudocell	$a = 6.509 \pm 0.002$ $\alpha = 99^\circ 21' \pm 0.5'$ $a = 5.319 \pm 0.001$ $\alpha = 89.41^\circ$	813	Air	1 atm	<i>a, c</i>
TbO <sub>1.809</sub>	Dark brown	Triclinic	$a = b = c = 5.286 \pm 0.001$ $\alpha = b = 89.35^\circ$ $\gamma = 90^\circ$	790	O <sub>2</sub>	300 atm	<i>a, c</i>
TbO <sub>1.823</sub>	Dark brown	Rhombohedral	$a = 5.283 \pm 0.001$ $\alpha = 89.68^\circ$	332	O <sub>2</sub>	1970 atm	<i>a, c</i>
TbO <sub>1.96</sub>	Dark brown	fcc (F)	$a = 5.220 \pm 0.001$ $a = 5.213 \pm 0.002$	350	[O] [O]	Discharge tube <3 mm of O <sub>2</sub>	<i>a, c</i> <i>f</i>
TbO <sub>2</sub>	Dark red	fcc (F)	$a = 5.220 \pm 0.003$  $a = 5.220$	200  162	H <sub>2</sub> O HCl CH <sub>3</sub> COOH HClO <sub>4</sub> H <sub>2</sub> O	Air  306 atm	<i>g</i> <i>h</i> <i>a</i>

<sup>a</sup> J. B. MacChesney, H. J. Williams, R. C. Sherwood, and J. F. Potter, *J. Chem. Phys.*, **44**, 596 (1966). <sup>b</sup> S. J. Schneider and R. S. Roth, *J. Res. Nat. Bur. Std.*, **A64**, 309 (1960). <sup>c</sup> N. C. Baenziger, H. A. Eick, H. S. Schuldt, and L. Eyring, *J. Amer. Chem. Soc.*, **83**, 2219 (1961). <sup>d</sup> V. B. Glushkova and A. G. Boganov, *Izv. Akad. Nauk SSSR, Ser. Khim.*, 1131 (1965). <sup>e</sup> M. Foëx, J. P. Traverse, and J. P. Contures, *Compt. Rend.*, **260**, 3670 (1965). <sup>f</sup> D. M. Gruen, W. C. Koehler, and J. J. Katz, *J. Amer. Chem. Soc.*, **73**, 1475 (1951). <sup>g</sup> G. Brauer and B. Pfeiffer, *J. Less-Common Metals*, **5**, 171 (1963). <sup>h</sup> A. F. Clifford, "Rare Earth Research, II," R. S. Vorres, Ed., Gordon and Breach, New York, N. Y., 1964, p 35.

lattice parameters in the 215-mm isobar were all smaller (greater oxygen content) than the corresponding data in the 10-mm isobar. In the isobaric curves it was also observed that at a given temperature the mixed oxide composition (oxygen content) increases with the oxygen pressure as indeed would be expected.

Returning to a consideration of the 10-mm isobar, the X-ray data for temperatures between 550 and 900° showed a smooth expansion curve, but with a greater lattice-parameter change than observed for the  $\iota$  phase of pure terbia. This was interpreted as indicative of a continual compositional change in this temperature zone. There was definite peak broadening as this temperature range was traversed. However, the peaks did not have the resolution of components or splitting necessary for identification of a crystal symmetry lower than face-centered cubic. At temperatures above 900°, the diffraction peaks narrowed, but no extra lines indicating the presence of a body-centered phase were observed.

It can be seen in Figure 6 that the X-ray data for the oxidation cycle were similar to those in reduction. It is clear from the 392 isobar (Figure 4) that the system is reversible through the  $\delta$ ,  $\alpha$ , and  $\alpha\iota$  regions ( $\alpha\iota$  signifies the pseudophase between the  $\alpha$  and  $\iota$  phases). This would suggest that there is in fact only a single phase in the whole of this composition interval and that a  $\alpha$ - $\alpha\iota$  two-phase region seen in the PrO<sub>x</sub>-O<sub>2</sub> is nonexistent. The X-ray results seem to confirm this difference also.

### Isothermal Studies in the Terbium Oxide-Oxygen System

*Reduction-Oxidation Cycle at 497°.* At 1 atm of oxygen pressure only the triclinic  $\delta$  phase was observed. The first pressure adjustment from 1 atm to 70 mm had reduced the oxide sample to the rhombohedral  $\iota$  phase. Further reduction of pressure in five intervals of 10 mm down to pump vacuum each produced nearly identical diffraction patterns, in every case the  $\iota$

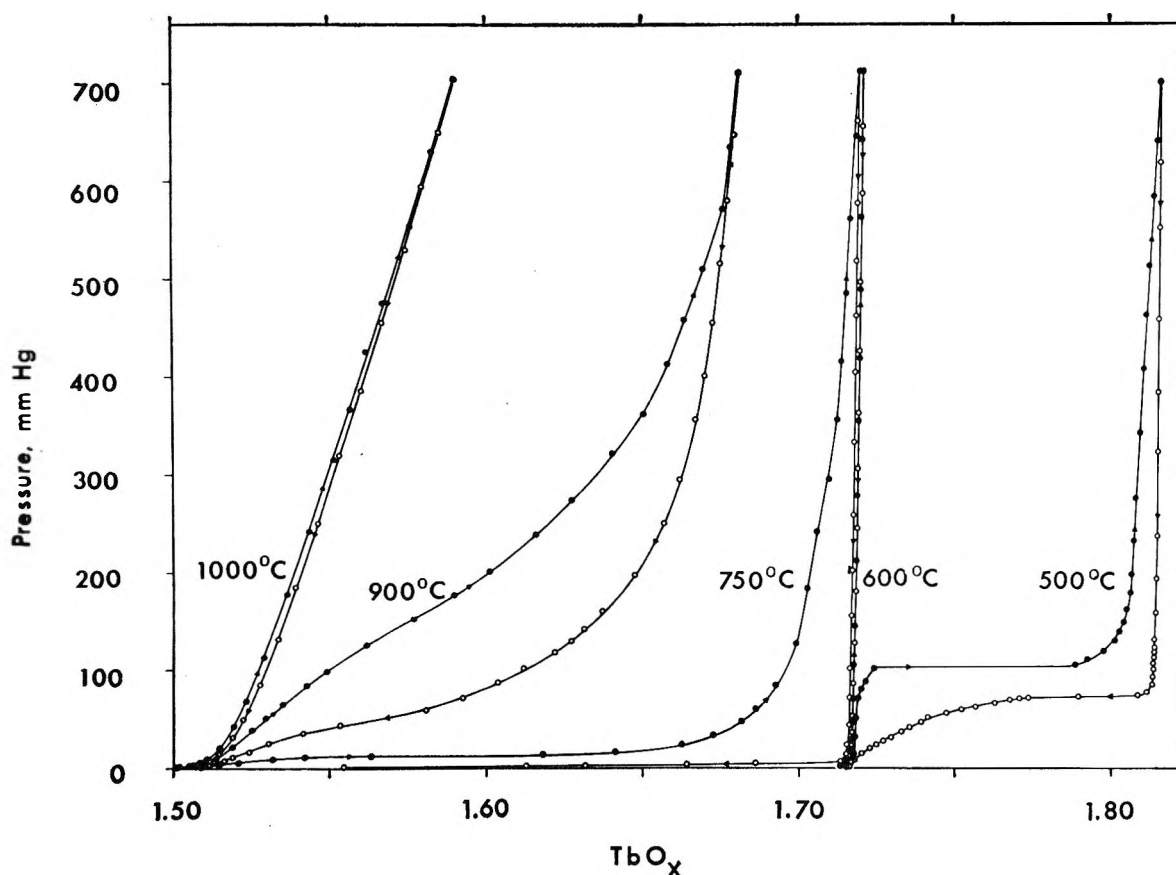


Figure 3. Isothermal runs of the terbium oxide-oxygen system at 1000, 900, 750, 600, and 500°. (See ref 4, p 2046.)

phase. From pump-vacuum conditions the oxygen pressure was increased in intervals of 25 mm. At 300 mm the triclinic  $\delta$  phase appeared but  $\iota$  was still the predominant phase. These observations agree none too well with the 500° isotherm in Figure 3; hence a further X-ray isotherm was run at the nominally lower temperature below.

*Reduction-Oxidation Cycle at 473°.* When the pressure was adjusted to 1 atm of oxygen and the sample brought to thermal equilibrium for the run, only the  $\delta$  phase was present. A series of pressure reductions was made to 100 mm and only the triclinic cell was seen. The rhombohedral  $\iota$  phase first appeared at 90 mm of oxygen pressure, and the amount of this phase increased as further reductions in pressure were made. At pump vacuum, complete reduction to  $\iota$  had occurred.

In the oxidation cycle, the triclinic system did not show on the X-ray patterns until adjustment was made to an oxygen pressure of 120 mm. At 150 mm only the triclinic cell was observed.

The results of this isothermal run more nearly correspond to the tga diagram for the 500° cycle (see Figure 3). Hence the importance of fine temperature control and its precise measurement in the traversal of diphasic regions is emphasized.

*Reduction-Oxidation Cycle at 902°.* The start of the

reduction cycle in the high-temperature diffractometer furnace was made at an oxygen pressure of 150 mm where the X-ray pattern showed that there was a mixture of the  $\iota$  and  $\sigma$  phases. At 100 and 30 mm of pressure the rhombohedral phase was still detected in the presence of the  $\sigma$  phase, but only the  $\sigma$  phase remained when the reduction process was continued to vacuum conditions.

On the oxidation path, the first observation was made at 100 mm where only the  $\sigma$  phase was seen. The reaction  $\sigma \rightarrow \iota$  was still in progress at a pressure of 200 mm, but at 300 mm if  $\sigma$  was present the amount was too small to be seen. If these results are compared with the tga 900° isotherm shown in Figure 3, it is apparent that the  $\iota$  phase is more dominant than would be expected. This seems to be characteristic of diagrams of the  $\sigma\iota$  pseudophase as also observed in the isobars.

*Thermal Expansion.* A least-squares fit of the lattice-parameter data on the several oxide phases yields the coefficients of expansion listed in Table II. No composition change is assumed to occur over the temperature range in which measurements were made.

## Discussion

It is possible to generalize to some extent from the experience gained in these experiments and those dis-

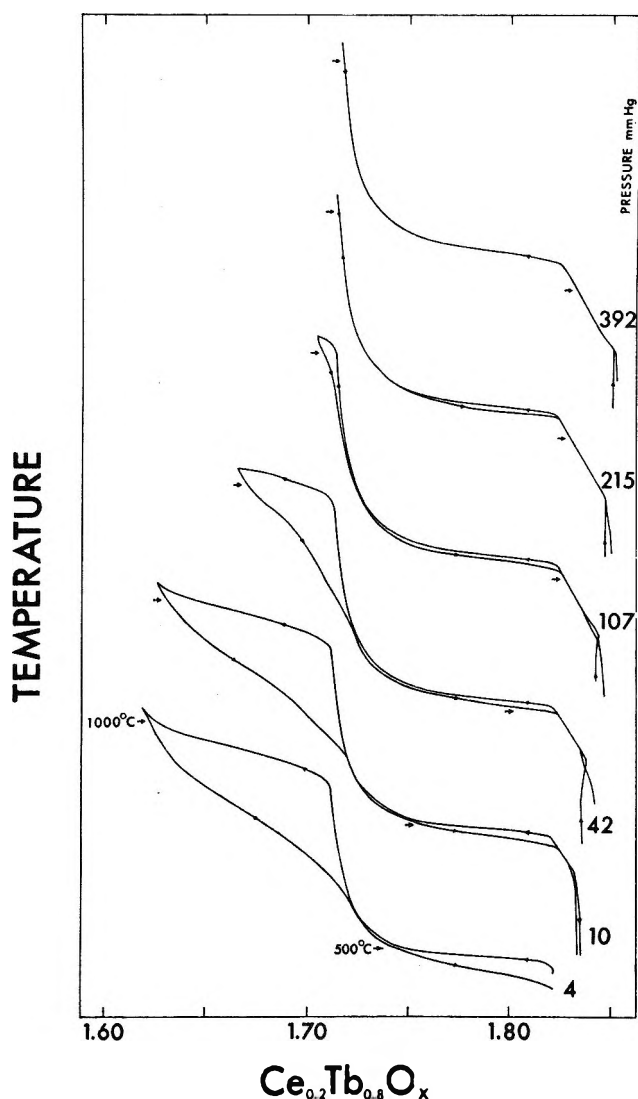


Figure 4. Selected isobaric runs in the mixed  $\text{Ce}_{0.2}\text{Tb}_{0.8}\text{O}_x\text{-O}_2$  system at nominal oxygen pressures of 392, 215, 107, 42, 10, and 4 torr. (See ref 3, p 2035.)

Table II

Phase present	Linear coeff of expansion ( $\times 10^6$ )	Temp. °C
$\text{TbO}_{1.812}$ ( $\delta$ )	9.0	400
$\text{TbO}_{1.714}$ ( $\iota$ )	8.5	793
$\text{Ce}_{0.2}\text{Tb}_{0.8}\text{O}_{1.812+\delta}$	8.9	400

cussed earlier.<sup>5</sup> High-temperature X-ray diffraction mirrors the tensimetric behavior of the oxide systems studied. Single-phase regions of narrow composition range seen in pressure, temperature, composition measurements appear as singly diffracting materials with almost no shift in lattice parameter except normal thermal expansion. In all cases where hysteresis or pseudophase behavior had been seen in the tensimetric work, two phases were seen in the X-ray diffraction

patterns. Furthermore, the appearance of two phases was skewed with regard to reduction or oxidation, a pattern consistent with the tensimetric hysteresis loops.

The hysteresis loops were always distorted by a relative retardation in the half of the loop traversed when the symmetry was reduced in the transition. For example, when the cubic (disordered)  $\sigma$  phase transforms to  $\iota$ , the diphasic temperature range is expanded leading to the formation of the pseudophase, whereas the reverse part of the cycle is relatively crisp. The X-ray diffraction shows this very well. When  $\iota$  transforms to  $\delta$  phase, the tensimetric work indicates pseudophase formation at  $\text{TbO}_{1.80}$  which was not seen by X-ray diffraction perhaps because of the too small composition change between  $\text{TbO}_{1.80}$  and  $\text{TbO}_{1.818}$ .

In the ternary system ( $\text{Ce}_{0.2}\text{Tb}_{0.8}\text{O}_x$ ) studied, no diphasic regions were observed. The resolution found in X-ray patterns of terbia, which distinguished the different phases, was lost when cerium was admixed. The diffraction patterns showed changes in peak width that varied with composition. The line broadening in the X-ray diffraction patterns was thought to be a combination of incipient phase transition of the terbia in the mixed oxide and inhomogeneities of the crystallites because of the presence of cerium.

Convincing arguments have been used to show an agreement between observed isothermal hysteresis loops and the properties of a theoretical model of hysteresis based on the existence of domains.<sup>8</sup> The energy that stabilizes the presence of domains of two coexisting phases results from surface effects and strain. There is coherence between the reactant and product since there is a close structural relationship between phases. The domain concept expressed in other terms becomes the microheterogeneity hypothesis of Ariya, *et al.*<sup>9,10</sup> The pseudophases appear when microdomains of two different phases become interlocked. There is an epitaxial relationship between microdomains which makes destruction of the cooperative arrangement difficult.

According to Ariya's estimate, the microdomains range from 5 to 10 unit cells in linear dimensions. The X-ray patterns of diphasic regions where hysteresis was evident showed sharp diffraction peaks for two phases and with no apparent anomalies. Normally, X-ray powder methods require larger crystallite ( $\sim 0.1 \mu$ ) for sharp diffraction patterns.

If the microdomains were part of a coherent polycrystalline mass with random orientation with respect to one another, each microdomain would give independent reflections, and diffraction peak broadenings

(8) P. A. Faeth and A. F. Clifford, *J. Phys. Chem.*, **67**, 1453 (1963).

(9) S. M. Ariya and M. P. Morozova, *Zh. Obshch. Khim.*, **28**, 2617 (1958); *J. Gen. Chem. USSR*, **28**, 2647 (1958).

(10) S. M. Ariya and Yu. G. Popov, *Zh. Obshch. Khim.*, **32**, 2077 (1962); *J. Gen. Chem. USSR*, **32**, 2054 (1962).

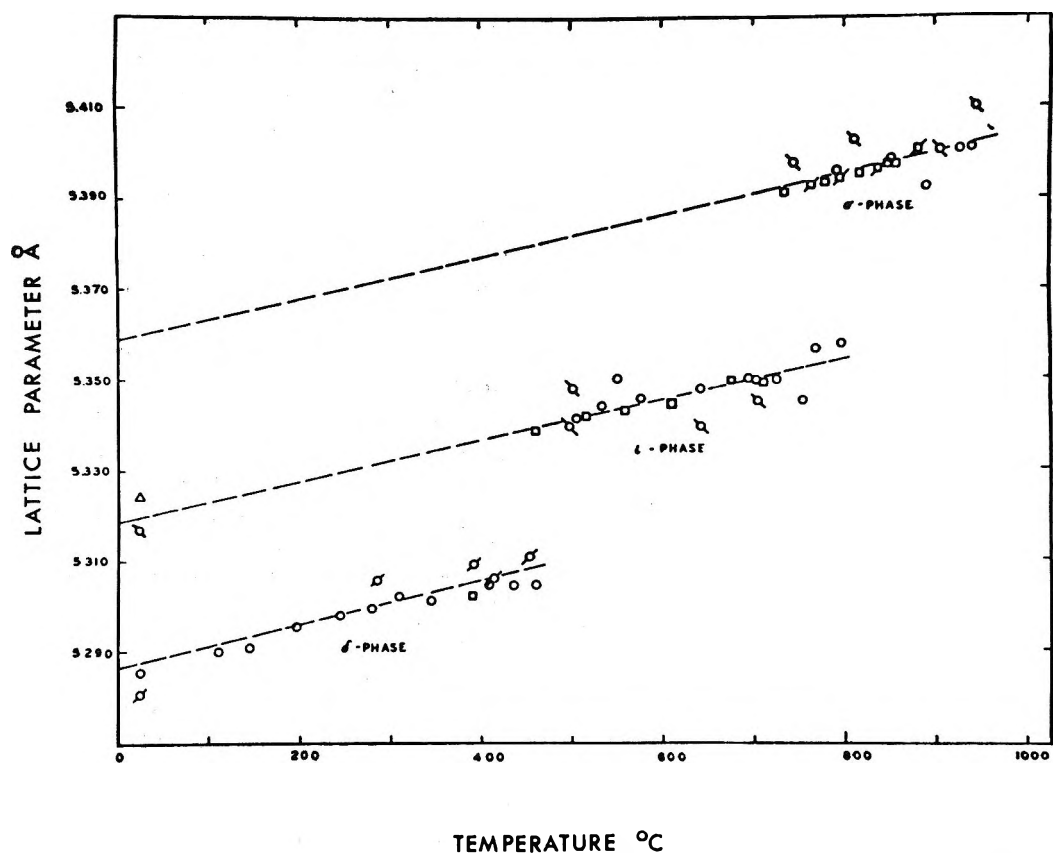


Figure 5. Lattice parameters of terbium oxide crystals as a function of temperature. Isobaric reduction ( $\circ$ ,  $\oslash$ )–oxidation ( $\square$ ,  $\sqsupset$ ,  $\oslash$ ) cycles at an oxygen pressure of 10 torr. The dashed curves are quadratic least-squares fits to the data.

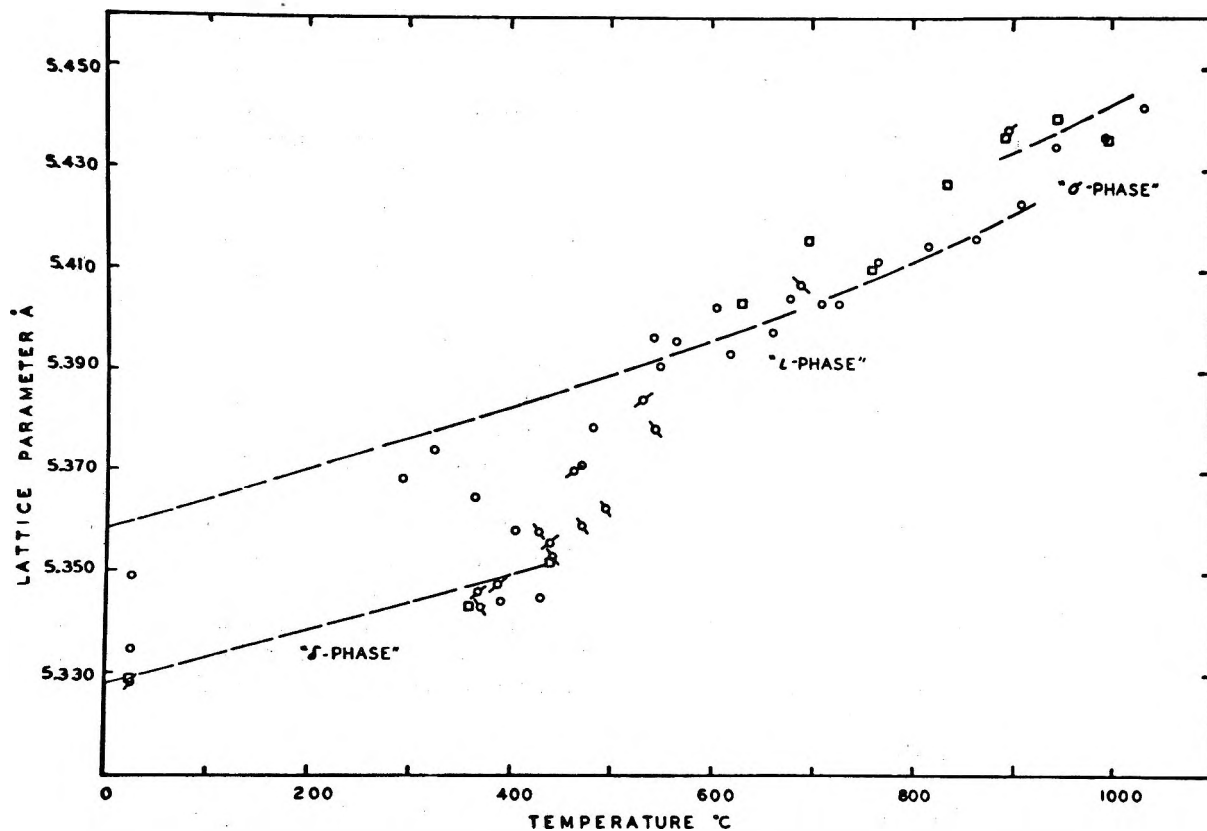


Figure 6. Lattice parameters of  $\text{Ce}_{0.2}\text{Tb}_{0.8}\text{O}_z$  crystals as a function of temperature. Isobaric reduction ( $\circ$ ,  $\oslash$ )–oxidation ( $\square$ ) cycles at 10 torr and a reduction ( $\oslash$ ) run at 215 torr. The dashed curves are quadratic least-squares fits to the data.



would be characteristic of the shape and size of each unit.<sup>11</sup>

It is possible that microdomains could be so oriented with respect to each other that reflections from all planes in the "crystal" are in phase with each other. There are examples of intergrowth of similar substances in a single crystal. Evans and Mrose<sup>12</sup> showed in their work on hydrated vanadium oxide minerals an intergrowth of two phases on a microscopic scale. The two phases were members of a homologous series  $H_{2n-2}V_nO_{3n-2}$ : haggite,  $n = 4$  and "phase B,"  $n = 6$ . Both have monoclinic symmetry and cell dimensions that differ only along the  $a$  axis and the angle  $\beta$ . The superimposed X-ray patterns observed were sharp.

Because of the similarity in structure between the oxide phases studied in this work, there is coherence between microdomains which apparently permits sharp X-ray diffraction. The implication is that reflections from the coherent microdomains remain in phase, the

diffraction pattern showing all the characteristics of larger crystallites.

A recent study of mixed tungsten niobium oxides by Andersson, *et al.*,<sup>13</sup> suggests that a range of composition would result from disordered intergrowth of constituent phases in a way analogous to ordered intergrowth between two adjacent homologous phases in the system.

The nature of intergrowth in rare earth oxides will be quite different and should be investigated further by  $p$ ,  $t$ ,  $x$  and high-temperature X-ray methods.

*Acknowledgment.* We acknowledge with pleasure the support of the United States Atomic Energy Commission.

(11) N. F. M. Henry, H. Lipson, and W. A. Wooster, "The Interpretation of X-Ray Diffraction Photographs," Macmillan and Co. Ltd., New York, N. Y., 1961, p 212.

(12) H. T. Evans and M. E. Mrose, *Amer. Mineral.*, **45**, 1144 (1960).

(13) S. Andersson, W. A. Mumme, and A. D. Wadsley, *Acta Crystallogr.*, **21**, 802 (1966).

## Anomalous Temperature Dependence of Kinetic Carbon

### Isotope Effects and the Phenomenon of Crossover

by Thomas T.-S. Huang, William J. Kass, Warren E. Buddenbaum, and Peter E. Yankwich<sup>1</sup>

*Noyes Laboratory of Chemistry, University of Illinois, Urbana, Illinois 61801 (Received March 25, 1968)*

The effects of diagonal and off-diagonal stretching force constant variations on the temperature-dependent and temperature-independent factors in the intramolecular isotopic rate constant ratio for the decomposition of oxalic acid-<sup>13</sup>C have been explored. Crossover (change in sense with respect to unity) of the temperature-dependent factor is not observed when the reaction coordinate consists of a single internal coordinate displacement. When a zero frequency is achieved by employing one large off-diagonal force constant (two elements in the reaction coordinate), crossover is observed only if the basic diagonal force field is asymmetric at one or more isotopic bonds. If the reaction coordinate contains three or more elements (two or more non-zero off-diagonal force constants are employed), anomalies of temperature dependence can be generated with symmetric diagonal force fields. Two new techniques for study of the effects of systematic variation of the composition of the reaction coordinate are introduced and/or applied.

#### Introduction

The early calculations of Urey<sup>2</sup> showed that in a number of cases equilibrium constants of isotopic exchange reactions change with temperature from a region in which  $K$  is greater than unity to one in which it is less than unity, or the reverse. This phenomenon, which has since become known as *crossover*, has been established experimentally for <sup>13</sup>C only in the carbon dioxide-calcite and carbon dioxide-dolomite gas-solid exchange systems.<sup>3</sup> Crossover is found rather infrequently in Urey's tabulations. However, recently,

Stern, Spindel, and Monse<sup>4</sup> have observed frequent occurrence of crossover and of more complex anomalies of temperature dependence in extensive calculations of small-molecule isotope exchange reactions of <sup>18</sup>O and <sup>16</sup>N. For comparison with results to be reported here,

(1) Presented in part before the Fifth International Symposium on Stable Isotopes, Leipzig, Oct 1967.

(2) H. C. Urey, *J. Chem. Soc.*, 562 (1947).

(3) D. A. Northrup and R. N. Clayton, *J. Geol.*, **74**, 174 (1966).

(4) M. J. Stern, W. Spindel, and E. U. Monse, *J. Chem. Phys.*, **48**, 2908 (1968).

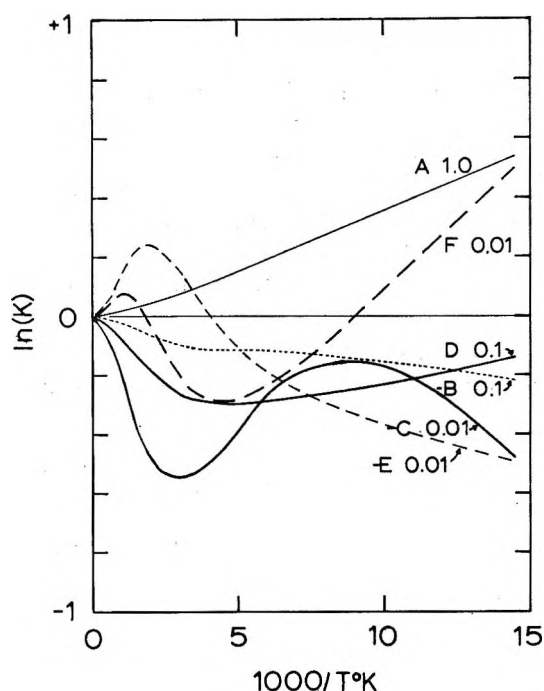


Figure 1. Types of temperature dependence of isotope exchange equilibrium constants observed by Stern, Spindel, and Monse.<sup>4</sup> Letters are their type designations; numbers are the value of  $+1$  on the common ordinate scale. For positive values of  $\ln K$  the heavy isotope concentrates in the first-named species: A,  $\text{H}^{16}\text{NO}_2\text{-}^{16}\text{NO}$ ; -B, *cis*- $\text{H}^{18}\text{ONO-N}^{18}\text{O Cl}$ ; -C, *cis*- $\text{HON}^{18}\text{O-N}^{18}\text{O Br}$ ; D,  $\text{F}^{18}\text{ONO}_2\text{-N}^{18}\text{O}^+$ ; -E,  $^{16}\text{NOF-}^{16}\text{NO}_2^-$ ; F, *cis*- $\text{H}^{18}\text{ONO-N}^{18}\text{OO}$ .

certain of their *type* results have been replotted in Figure 1.

Wolfsberg and Stern<sup>5,6</sup> pointed out the complex manner by which thermal excitation of vibration contributes to an isotope effect and alluded to the fact that the contributions of the excitation terms could result in complex temperature dependences, and they showed<sup>6</sup> how certain force constant changes, between isotopic reactant and transition state, could produce a secondary deuterium kinetic isotope effect almost temperature independent over a range of  $200^\circ$ . However, there has been no computational exploration in search of crossover or other anomalies of temperature dependence of kinetic isotope effects of  $^{13}\text{C}$  or other second-row atoms.

We write an isotopic rate constant ratio in the form

$$k/k' = (\text{TIF})(\text{TDF}) \quad (1)$$

The temperature-independent factor (TIF) arises in the reaction coordinate and is the  $T = \infty$  limit of  $k/k'$ , while the temperature-dependent factor (TDF) arises in the genuine vibrations of the normal molecules and activated complexes. There is no factor like TIF in an isotope exchange equilibrium constant; therefore, additional possibilities for crossover exist in isotope rate effects because the senses with respect to unity of TIF and TDF are not necessarily the same. That is, a

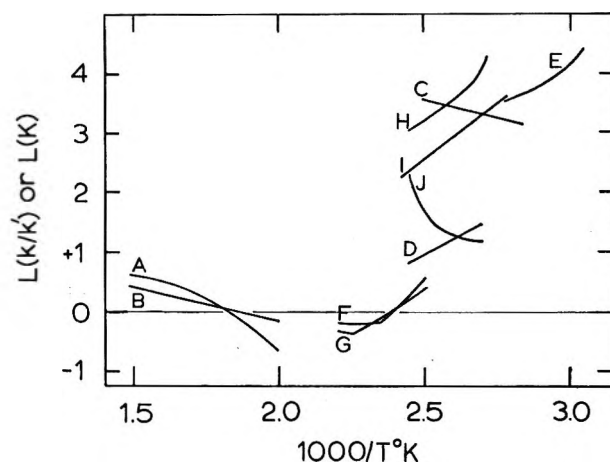
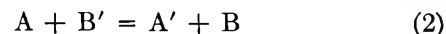


Figure 2. Crossover and large temperature dependence anomalies in  $^{13}\text{C}$  isotope effects: gas-solid isotope exchange: A,  $\text{CO}_2\text{-dolomite}$ ;<sup>3</sup> B,  $\text{CO}_2\text{-calcite}$ ;<sup>3</sup> decomposition rate effects, intermolecular: C, oxalic acid, in dioxane;<sup>10</sup> D, oxalic acid in glycerine;<sup>11</sup> E, malonic acid in sulfuric acid;<sup>12</sup> decomposition rate effects, intramolecular: F, oxalic acid- $h_2$ , gas phase;<sup>8</sup> G, oxalic acid- $d_2$ , gas phase;<sup>9</sup> H, malonic acid in quinoline;<sup>13</sup> I, malonic acid in dioxane;<sup>14</sup> J, oxalic acid in glycerine.<sup>11</sup>  $L(x) = 100 \ln x$ .

kinetic isotope effect might have associated with it a TDF of "normal" temperature dependence (*e.g.*, Stern, Spindel, and Monse's type A) and yet exhibit crossover because TIF lay on the opposite side of unity.

Some of the available experimental results on kinetic carbon isotope effects cannot be satisfyingly explained unless the occurrence of crossover is postulated,<sup>7</sup> but crossover has actually been observed only in the intramolecular  $^{13}\text{C}$  isotope effects in the gas-phase decompositions of oxalic acid- $h_2$ <sup>8</sup> and oxalic acid- $d_2$ .<sup>9</sup> These rate results and the equilibrium data of Northrup and Clayton are plotted together in Figure 2.<sup>10-14</sup>

*Rationale and Objectives of This Investigation.* An isotope exchange reaction may be written in the form



Calculation of its equilibrium constant involves knowledge of and/or assumptions concerning two molecular

(5) M. Wolfsberg and M. J. Stern, *Pure Appl. Chem.*, **8**, 225 (1964).

(6) M. Wolfsberg and M. J. Stern, *ibid.*, **8**, 325 (1964).

(7) P. E. Yankwich and W. E. Buddenbaum, *J. Phys. Chem.*, **71**, 1185 (1967).

(8) G. Lapidus, D. Barton, and P. E. Yankwich, *ibid.*, **70**, 3135 (1966).

(9) G. Lapidus, D. Barton, and P. E. Yankwich, *ibid.*, **70**, 1575 (1966).

(10) T. T.-S. Huang and P. E. Yankwich, unpublished experiments.

(11) W. A. Buddenbaum, M. A. Haleem, and P. E. Yankwich, *J. Phys. Chem.*, **71**, 2929 (1967).

(12) P. E. Yankwich, R. L. Belford, and G. Fraenkel, *J. Amer. Chem. Soc.*, **75**, 832 (1953).

(13) P. E. Yankwich and R. L. Belford, *ibid.*, **76**, 3067 (1954); E. M. Grigg, *Aust. J. Chem.*, **9**, 252 (1956).

(14) P. E. Yankwich and R. M. Ikeda, *J. Amer. Chem. Soc.*, **82**, 1891 (1960).

geometric configurations and two force fields. Stern, Spindel, and Monse<sup>4</sup> have dissected Urey's condition<sup>2</sup> for the occurrence of crossover in such an equilibrium, showing that a crossover may occur when a *large vibrational frequency with small isotope shift* in species A is paired with a *small vibrational frequency with large isotope shift* in species B. Alternate addition to A and B of frequencies of increasing magnitude but isotope shifts of decreasing size may yield additional crossovers, all this within the harmonic approximation. These workers studied all the possible <sup>13</sup>O and <sup>15</sup>N exchange reactions among 14 small-molecule species, employing for each the best force field available. They found no correlation between the occurrence of temperature dependence anomalies in the equilibrium constant and the structures of the molecules, and, similarly, they found that examination of the actual frequency distributions of the molecules did not provide a means for predicting the type of temperature behavior.

Formally, the situation for kinetic isotope effects is similar. In the case of an *intermolecular* isotope effect, with A regarded as the normal molecules and B as the transition state, the analogy is particularly close (differing only in there being one less genuine vibrational frequency in B, that giving rise to TIF) and one might expect crossovers and other anomalies of temperature dependence to occur in  $k/k'$ , though perhaps with lesser frequency because of the usually assumed similarities between normal molecules and activated complexes. The situation is quite different when an *intramolecular* isotope effect is considered, for in the calculation of the appropriate rate constant ratio only the geometry and force field of B are involved; there is no pairing possible between two different species (such as A and B) of large and small frequencies with small and large isotope shifts.

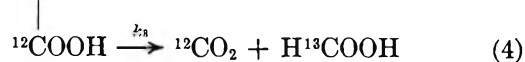
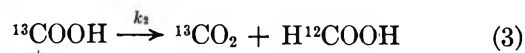
The investigation reported here is of intramolecular isotope rate effect calculations for a simplified model of the decomposition of oxalic acid-<sup>13</sup>C. This system was selected because: (a) crossover in the temperature dependence of  $k/k'$  has been observed experimentally and (b) it affords with a minimum number of atoms a maximum in kinds of bond isotopy situations (the C—C bond is always isotopic in both activated complexes; the C=O and C—O bonds, while isotopic in both complexes, may have different force constants in the two; and the O—H bonds are never isotopic).

To decrease the possibility of temperature-dependence anomalies being generated and thus increase their significance if observed, low-frequency variation and isotope shift contributions to  $k/k'$  from bends, wags, and torsions were minimized by maintaining the associated force constants at fixed values; only stretching force constants were treated as parameters.

### Description of Calculations and Methods

*Notation.* The isotopic rate constant ratio calcu-

lated was  $k_2/k_3$  in the notation of Lindsay, McElcheran, and Thode.<sup>15</sup>



The ordinate in all graphs is  $L(x) = 100 \ln x$ , the logarithmic form effecting the convenient separation  $L(k/k') = L(\text{TIF}) + L(\text{TDF})$ .

*Vibrational Frequency Calculation.* The normal-mode vibrational frequencies (harmonic approximation) were calculated via Wilson's<sup>16</sup> FG matrix method on an IBM 7094 digital computer; Schachtschneider's<sup>17</sup> original programs were modified<sup>18</sup> for this application.

*Geometry and Basic Force Fields.* The geometry assumed for oxalic acid was based on the results of Shibata and Kimura,<sup>19</sup> except for the OH bond length and COH bond angle which derive from the data for formic acid obtained by Lerner, Dailey, and Friend.<sup>20</sup> The molecule is assumed planar with carbonyl groups *trans*; hydroxyl hydrogens are in juxtaposition with opposite carbonyl oxygens.<sup>21–24</sup>

Values of the diagonal force constants,  $F_{ii}$ , were based on various literature sources<sup>16,17,25</sup> or were set by us at "reasonable" values.<sup>26</sup> All off-diagonal or interaction force constants,  $F_{ij}$ , were set equal to zero. The unsymmetric force field,  $U$ , was obtained from the symmetric force field,  $S$ , by changes in  $F_{11}$ ,  $F_{55}$ , and  $F_{77}$ , equivalent to  $1/2$  unit changes in bond order, the related changes in internal displacement coordinates being in imitation of a particular three-element reaction coordinate. Values of the input parameters are shown in Table I.

*The Potential Function, Reaction Coordinate, and Associated Frequency,  $\nu_1$ .* General methods, reported in an

(15) J. G. Lindsay, D. E. McElcheran, and H. G. Thode, *J. Chem. Phys.*, **17**, 589 (1949).

(16) E. B. Wilson, Jr., J. C. Decius, and P. C. Cross, "Molecular Vibrations," McGraw-Hill Book Co., Inc., New York, N. Y., 1955.

(17) J. H. Schachtschneider and R. G. Snyder, *Spectrochim. Acta*, **19**, 117 (1965).

(18) Certain modifications were kindly provided us by Professors M. Wolfsberg and M. J. Stern; others were developed in our laboratory by L. B. Sims and W. E. Buddenbaum.

(19) S. Shibata and M. Kimura, *Bull. Chem. Soc. Jap.*, **27**, 485 (1954).

(20) R. G. Lerner, B. P. Dailey, and J. P. Friend, *J. Chem. Phys.*, **26**, 680 (1957).

(21) Changes in geometry within limits of physical and chemical reasonableness produce relatively small changes in calculated kinetic isotope effects.<sup>6,22</sup> The balance between effects of geometric and force field changes has been detailed by Stern and Wolfsberg.<sup>23,24</sup>

(22) P. E. Yankwich and A. E. Veazie, *J. Amer. Chem. Soc.*, **80**, 1835 (1958).

(23) M. J. Stern and M. Wolfsberg, *J. Chem. Phys.*, **45**, 2618 (1966).

(24) M. J. Stern and M. Wolfsberg, *ibid.*, **45**, 4105 (1966).

(25) L. Jensorsky, *Z. Chem.*, **3**, 453 (1963).

(26) Although the details of our findings will depend on the force constant values, none of the general observations are modified by the modest alteration of the selected values within limits appropriate for the oxalic acid normal molecule.

**Table I:** Values of Input Parameters<sup>a,b</sup>

Coordinate	No. ( <i>i</i> )	$F_{ii}$ <sup>d</sup>	
		<i>S</i> field	<i>U</i> field
C <sub>1</sub> —C <sub>2</sub> <sup>c</sup>	1	4.5	2.25
C <sub>2</sub> =O	2	12.0	12.0
C <sub>1</sub> =O	3	12.0	12.0
C <sub>2</sub> —O	4	5.0	5.0
C <sub>1</sub> —O	5	5.0	7.5
O <sub>2</sub> —H	6	7.0	7.0
O <sub>1</sub> —H	7	7.0	3.5
O=C—O	8, 9	1.08	1.08
O=C—C	10, 11	0.71	0.71
O—C—C	12, 13	0.77	0.77
C—O—H	14, 15	0.70	0.70
C—C(=O)—O	16, 17	0.60	0.60
H—O—C—C	18, 19	0.30	0.30
O—C—C=O	20, 21	0.30	0.30

<sup>a</sup> Masses are in atomic mass units. <sup>b</sup> Bond distances (Ångströms): C—C, 1.54; C—O, 1.37; C=O, 1.22; O—H, 0.96; bond angles (degrees): O=C—O, 125; O=C—C, 122; C—O—H, 108. <sup>c</sup> C<sub>1</sub> will appear in the CO<sub>2</sub> product. <sup>d</sup> Stretching force constants are in mdyn/Å; bend, wag, and torsion force constants (tabulated in that order) in mdyn Å.

earlier publication from this laboratory,<sup>27</sup> have been developed for forcing some arbitrary vibration of the activated complex

$$\mathbf{X}_1 = \mathbf{R}_1 \mathbf{S} \quad (5)$$

where  $\mathbf{S}$  is a column of some complete set of internal displacement coordinates,  $S_j$ , to be a normal mode with preselected frequency  $\nu_1$ . The necessary condition is that  $\mathbf{F}$  satisfy the relation

$$\mathbf{F}\mathbf{G}(\mathbf{R}_1)^\dagger = \lambda_1(\mathbf{R}_1)^\dagger \quad (6)$$

where  $\mathbf{R}_1$  is an eigenvector of  $\mathbf{F}\mathbf{G}$ ; once  $\mathbf{F}$  satisfies eq 6, there will exist an eigenvector of  $\mathbf{F}$  which is closely related to  $\mathbf{R}_1$ . If this column vector is  $(\mathbf{A}_1)^\dagger$ , then

$$\mathbf{F}(\mathbf{A}_1)^\dagger = (F^0)_{11}(\mathbf{A}_1)^\dagger \quad (7)$$

where  $(F^0)_{11}$  can be regarded as the force constant for the motion  $\mathbf{X}_1$  ( $\mathbf{Q}_1$  in the more common notation), which for  $\nu_1$  imaginary (or zero) is identified as the reaction coordinate. For the special case  $\nu_1 = 0$ , the two versions of the reaction coordinate are related simply by

$$\mathbf{R}_1 = c\mathbf{A}_1\mathbf{G}^{-1} \quad (8)$$

where  $c$  is a constant.

Generally,  $\mathbf{R}_1$  and  $\mathbf{A}_1$  are similar, but among the advantages of an exploratory investigation *via*  $\mathbf{A}_1$  is that the number of its nonzero elements, for  $\nu_1 = 0$ , never exceeds the number of diagonal force constants,  $F_{ii}$ , employed in the computation of the  $F_{ij}$  required to generate the zero frequency (or one, if a single stretching force constant is set to zero). This property makes it convenient to develop the transition state either by writing  $\mathbf{A}_1$  and then calculating the few required  $F_{ij}$

(variant *RC*: the reaction coordinate restricts the force field) or by selecting values for a few  $F_{ij}$  according to some rule (*vide infra*) and then observing the resultant simple  $\mathbf{A}_1$  (variant *FF*: the force field restricts the reaction coordinate).

This paper reports results obtained *via* the *RC* and *FF* variants of the  $\mathbf{A}_1$  approach, with  $\nu_1 = 0$ ; a similar study employing the  $\mathbf{R}_1$  approach is in progress and will be reported elsewhere.

**Types of Calculation.** We report below the results of four kinds of calculations, the principal differences among them being the complexity of the reaction coordinate and the method for achieving a value of zero for the  $\nu_1$  associated with it: type I: one nonzero element in  $\mathbf{A}_1$ , one  $F_{ii} = 0$ , *S* and *U* fields (variants *RC* and *FF* are the same); type II: one geometric mean  $F_{ij} = \pm (F_{ii}F_{jj})^{1/2} \neq 0$ , two nonzero elements in  $\mathbf{A}_1$ , ( $A_{1i}$  and  $A_{1j}$ ), *S* and *U* fields, variant *FF*; type III: three nonzero elements in  $\mathbf{A}_1$  ( $A_{1k}$ ), three  $F_{ij} \neq 0$  (which are linear combinations of the  $F_{kk}$ ), *U* field, variant *RC*; type IV: two (or three)  $F_{ij} = \pm \alpha_{ij}(F_{ii}F_{jj})^{1/2} \neq 0$ ,  $i$  common,  $\sum(\alpha_{ij})^2 = 1$ , three (or four) nonzero elements in  $\mathbf{A}_1$ , ( $A_{1i}$  and the  $A_{ij}$ ), *U* field, variant *FF*.

## Results and Discussion

**Type I Calculations.** The values of  $L(\text{TDF})$  obtained by setting one  $F_{ii} = 0$  in the *U* field are plotted

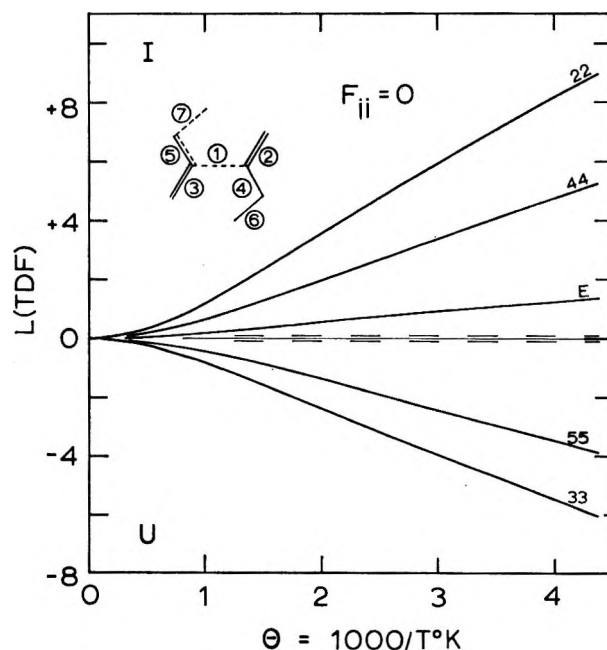


Figure 3.  $L(\text{TDF})$  vs.  $\theta$  (type I calculations, *U* field). Data for  $F_{11}$ ,  $F_{66}$ , or  $F_{77} = 0$  are too close to those for *E* to show on this scale. The light broken lines are the limits of  $L(\text{TDF})$ . (For both the *S* and *U* fields,  $L(\text{TDF})$  values are: 11, 0; 22, +0.0835; 33 = -22; 44 = +0.0980; 55 = -44; 66 = +0.0092; 77 = -66.)

(27) W. E. Buddenbaum and P. E. Yankwich, *J. Phys. Chem.*, **71**, 3136 (1967).

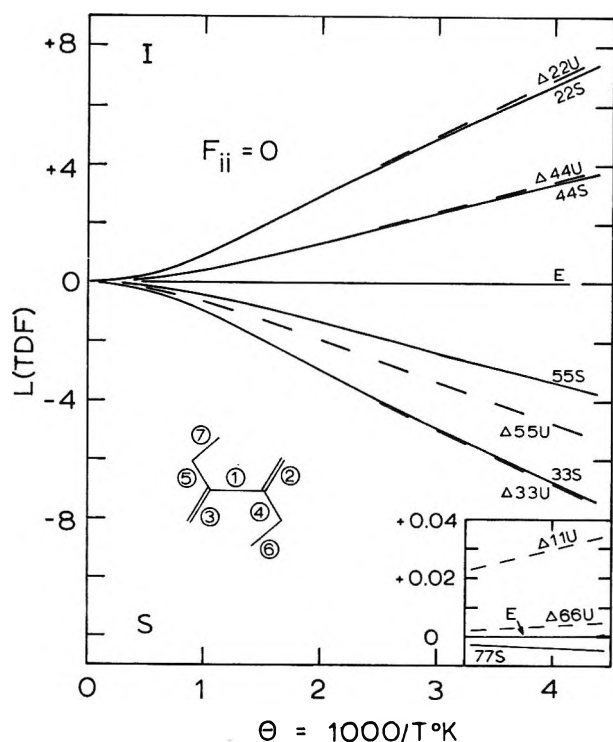


Figure 4.  $L(\text{TDF})$  vs.  $\theta$  (type I calculations,  $S$  field): —,  $S$ -field results; ---,  $\Delta iiU = iiU - EU$ .  $L(\text{TIF})$  limits are the same as in Figure 3. 66S and  $\Delta 66U$  coincide, as do 77S and  $\Delta 77U$ . In the inset, the ordinates are displaced and are 100 $\times$  main scale; abscissas are unchanged.

vs.  $\theta = 1000/T^\circ\text{K}$  in Figure 3; similar results for the  $S$  field appear in Figure 4. The graph marked  $E$  in each case is based on a calculation for the whole force field; that is, it is the plot of  $L(K_{\text{eq}}) = L(E)$  for the isotope exchange reaction.



All of these results are of Stern, Spindel, and Monse's type A (see Figure 1); they exhibit what anyone would call "normal" temperature dependence. There are no crossovers in  $L(\text{TDF})$ ; because the signs of  $L(\text{TIF})$  and  $L(\text{TDF})$  are always the same, there are no crossovers in  $L(k/k')$ . However, as  $L(k/k')$  becomes large, the plot of  $L(\text{TDF})$  may show slight concavity toward  $L(E)$ , as is the case for 22 (*i.e.*,  $F_{22} = 0$ ) in Figures 3 and 4. This is what one would expect for a model exhibiting a distribution of high and low vibrational frequencies, and such a frequency mix effect can be understood most easily in terms of the behavior with changing  $u$  ( $u = h\nu/kT$ ) of the Bigeleisen-Mayer<sup>28</sup> separative-effect function,  $G(u)$ . Because the  $L(\text{TIF})$  obtained with this type of calculation are so small and the regions of near linearity of  $L(\text{TDF})$  vs  $\theta$  so extensive, all of these results conform between  $\theta = 1$  and 4 (at least) with the linear relation between  $L(\text{TDF})_{\text{mean } \tau}$  and  $\Delta L(\text{TDF})_{T_1, T_2}$ ,<sup>29,30</sup> in turn, that relation can be derived from any of the several " $\bar{\gamma}$ " relations of Bigeleisen and Wolfsberg.<sup>31</sup>

Comparison of similar  $S$  and  $U$  data exposes some small effects of the asymmetry of the  $U$  force field which arise in the actual dependence of  $\bar{\gamma}$  on the reaction coordinate<sup>32,33</sup> through differences among the applicable subsets of the elements of  $\mathbf{G}$ . The relative sensitivities of  $L(\text{TDF})$  to the zeroed  $F_{ii}$  are listed in Table II; the calculation is of  $y_{ii} = [L(\text{TDF})_{ii} - E/F_{ii}]_{\theta=4}$ . Except for the case of  $F_{55}$ , where the difference arises directly from the change in its value between the  $S$  and  $U$  fields, the asymmetry effects reflected in the differences between  $\Delta iiU$  and  $iiS$ <sup>34</sup> arise in the shifts in value of  $y_{ii}(S)$  to  $y_{ii}(U)$ ; further, differences in the magnitudes of related  $y$ 's account for the unsymmetrical disposition of related  $iiU$  with respect to  $EU$  (*e.g.*, for the difference in magnitudes of  $\Delta 22U$  and  $\Delta 33U$ ).

Table II: Sensitivity of  $L(\text{TDF})$  to the Zeroed  $F_{ii}$  at  $\theta = 4$

$ii$	$y_{ii}(S)$	$y_{ii}(U)$
11	+0.0000	+0.0131
22	+0.5590	+0.5743
33	-0.5590	-0.5637
44	+0.6746	+0.6908
55	-0.6746	-0.6304
66	+0.00054	+0.00054
77	-0.00054	-0.0011

Although these asymmetry effects for type I calculations are so small as to be merely curiosities, we show later that different techniques for defining the reaction coordinate and obtaining  $\nu_1 = 0$  increase their magnitude, as well as that of  $L(\text{TIF})$ , so that they contribute significantly to the sizes of certain anomalies of temperature dependence.

*Type II Calculations.*  $A_{1i}$  and  $A_{1j}$  are the only nonzero elements in the reaction coordinate eigenvector when the condition  $\nu_1 = 0$  is obtained by including  $F_{ij} = \pm(F_{ii}F_{jj})^{1/2}$  in  $\mathbf{F}$ , which is diagonal otherwise;<sup>35</sup> here,  $F_{ij} = +$  implies asymmetric motion and  $F_{ij} = -$  implies symmetric motion in the coordinates  $S_i$  and  $S_j$ ,<sup>36-38</sup> and

(28) J. Bigeleisen and M. G. Mayer, *J. Chem. Phys.*, **15**, 261 (1947).

(29) P. E. Yankwich and H. S. Weber, *J. Amer. Chem. Soc.*, **78**, 564 (1956).

(30) P. E. Yankwich and R. M. Ikeda, *ibid.*, **81**, 1532 (1959).

(31) J. Bigeleisen and M. Wolfsberg, *Advan. Chem. Phys.*, **1**, 15 (1958); eq II.16, II.29, II.30.

(32) A. J. Kresge, N. N. Lichtin, K. N. Rao, and R. E. Weston, Jr., *J. Amer. Chem. Soc.*, **87**, 437 (1965).

(33) W. E. Buddenbaum, W. G. Koch, and P. E. Yankwich, *J. Phys. Chem.*, **70**, 673 (1966).

(34) For brevity, this style of reference will be employed hereinafter in several situations distinguishable from the context. Here, the phrase is to be read: "... between the plots vs.  $\theta$  of the difference [ $L(\text{TDF})$  for  $F_{ii} = 0$ ,  $U$  field] - [ $L(\text{TDF})$  for  $K_{\text{eq}}$ ,  $U$  field] and [ $L(\text{TDF})$  for  $F_{ii} = 0$ ,  $S$  field]."

(35) H. S. Johnston, W. A. Bonner, and D. J. Wilson, *J. Chem. Phys.*, **26**, 1002 (1957).

**Table III:** Values of  $F_{ij}$  and  $L(\text{TIF})$ , Type II Calculations

$ij$	$F_{ij}^a$ (S field)	$L(\text{TIF})^b$		$F_{ij}^a$ (U field)	$L(\text{TIF})$	
		$F_{ij} = +$	$F_{ij} = -$		$F_{ij} = +$	$F_{ij} = -$
12	7.3485	+0.2563	-0.1540	5.1962	+0.1854	-0.1265
13	7.3485	-0.2563	+0.1540	5.1962	-0.1854	+0.1265
14	4.7434	+0.3138	-0.1538	3.3541	+0.2490	-0.1419
15	4.7434	-0.3138	+0.1538	4.1079	-0.2092	+0.1297
16	5.6125	-0.0269	+0.0285	3.9686	-0.0195	+0.0204
17	5.6125	+0.0269	-0.0285	2.8062	+0.0267	-0.0285
23	12.0000	0	0	12.0000	0	0
24	7.7460	+0.2077	+0.0106	7.7460	+0.2077	+0.0106
25	7.7460	-0.0456	-0.0471	9.4868	-0.0308	-0.0292
26	9.1652	+0.1008	+0.0512	9.1652	+0.1008	+0.0512
27	9.1652	+0.0835	+0.0617	6.4807	+0.0780	+0.0501
34	7.7460	+0.0456	+0.0471	7.7460	+0.0456	+0.0471
35	7.7460	-0.2077	-0.0106	9.4868	-0.2160	-0.0044
36	9.1652	-0.0835	-0.0617	9.1652	-0.0835	-0.0617
37	9.1652	-0.1008	-0.0512	6.4807	-0.1008	-0.0387
45	5.0000	0	0	6.1237	+0.0242	+0.0164
46	5.9161	+0.0792	+0.1076	5.9161	+0.0792	+0.1077
47	5.9161	+0.0829	+0.1027	4.1833	+0.0749	+0.1013
56	5.9161	-0.0829	-0.1027	7.2457	-0.0787	-0.1020
57	5.9161	-0.0791	-0.1077	5.1235	-0.0627	-0.1081
67	7.0000	0	0	4.9498	-0.0030	-0.0032

<sup>a</sup> This quantity with positive sign is the  $(F_{ij})_0$  employed in calculations of types III and IV; *vide infra*. The round-off error in these values is  $\pm 0.0001$ . <sup>b</sup>  $F_{ij}$  in mdyne/Å;  $L(\text{TIF}) = 100 \ln (\text{TIF})$ .

$$A_{1i}/A_{1j} = \pm (F_{ji}/F_{ii})^{1/2} \quad (10)$$

The results of calculations of  $L(\text{TDF})$  for  $F_{ij} = +$ , S field, are shown in Figure 5; the values of the  $F_{ij}$  and  $L(\text{TIF})$  are collected in Table III. There are no crossovers in  $L(\text{TDF})$  or in  $L(k/k')$ ,  $L(\text{TIF})$  having always the same sign as  $L(\text{TDF})$ . An imperfect division of the  $L(\text{TDF})$  plots into magnitude classes can be made on the basis of the results shown in Figure 3 for type I calculations. Assign to each  $i$  or  $j$  an  $L(\text{TDF})$  directive effect number  $\delta_i$ , as shown in Table IV; then, the slope of the plot of  $L(\text{TDF})_{ij}$  vs.  $\theta$  ( $= 1000^\circ \text{K}/T$ ) is roughly proportional to  $\delta_i + \delta_j$ , with the following exceptions: (a) 16<sup>34</sup> and 17 are sign reversed, as are 25 and 34, and (b) 25 and 34 are too small. No similar classification is possible for  $L(\text{TIF})$ , though its sign is predicted correctly with exception (a) just noted.

Like the graphs in Figures 3 and 4, all in Figure 5 are Stern, Spindel, and Monse's type A. It should be

**Table IV:** Directive Effect Numbers,  $\delta_i$ 

$i$	$\delta_i$
1	1 (potentiator) <sup>a</sup>
2	+2
3	-2
4	+1
5	-1
6	+0
7	-0

<sup>a</sup> +1 with  $\delta_j = +$ ; -1 with  $\delta_j = -$ .

noted that the nonzero values of  $L(\text{TDF})$  where  $i$  and  $j$  are nonadjacent coordinates (*i.e.*, having no atom in common, *e.g.*, 36) would not be predicted from the first-order high-temperature approximation<sup>31,39</sup> because such  $G_{ij}$  are zero; however, the elements of  $\mathbf{G}^{-1}$  entering the exact calculation are not subject to this limitation.

The graphs in Figure 6 are the S-field results for  $F_{ij} = -$  instead of +; there are no crossovers in  $L(\text{TDF})$ . Where  $i$  and  $j$  are adjacent and isotopic coordinates,<sup>40</sup>  $L(\text{TDF})$  has a sign which is the reverse of that which obtains when  $F_{ij} = +$ , and it is decreased in magnitude;  $i6(-)$  is the same as  $i7(+)$ , and  $i7(-)$  the same as  $i6(+)$ ; there are no other significant effects on  $L(\text{TDF})$ . In Table III one sees that all of the  $L(\text{TIF})$  change in magnitude with the sign change in  $F_{ij}$ , but only for those in the group 1*j* does sign reversal take place; because of this, there are small crossovers (near

(36) The general relation is  $F_{ij} = \pm ([F_{ii} - (F^0)_{ii}][F_{jj} - (F^0)_{jj}])^{1/2}$ , or, in terms of the curvature parameter  $d$  of Willi and Wolfsberg,<sup>37,38</sup>  $(F^0)_{ii}[F_{ii} + F_{jj} - (F^0)_{ii}] = F_{ii}F_{jj} - (F_{ij})^2 = d \leq 0$ , where  $d < 0$  corresponds to curvature in the potential barrier and  $v_i = ni$ . As  $n$  increases from zero, elements in  $\mathbf{A}_1$  other than  $A_{1i}$  and  $A_{1j}$  assume relatively small nonzero values; however, in a manner sensitive to the identity of  $i$  and  $j$ , there may be quite significant effects of these  $A_{1k}$  on both  $L(\text{TIF})$  and  $L(\text{TDF})$  for values of  $n$  as small as a few hundred  $\text{cm}^{-1}$ .

(37) A. V. Willi and M. Wolfsberg, *Chem. Ind.*, 2097 (1964).

(38) A. V. Willi, *Can. J. Chem.*, **44**, 1889 (1966).

(39) J. Bigeleisen, "Proceedings of the International Symposium on Isotope Separation, Amsterdam, 1957," North Holland Publishing Co., Amsterdam, Netherlands, 1958, pp 121-157.

(40) This condition arises because the isotope functions as the sensor of relative motion only in adjacent coordinates.

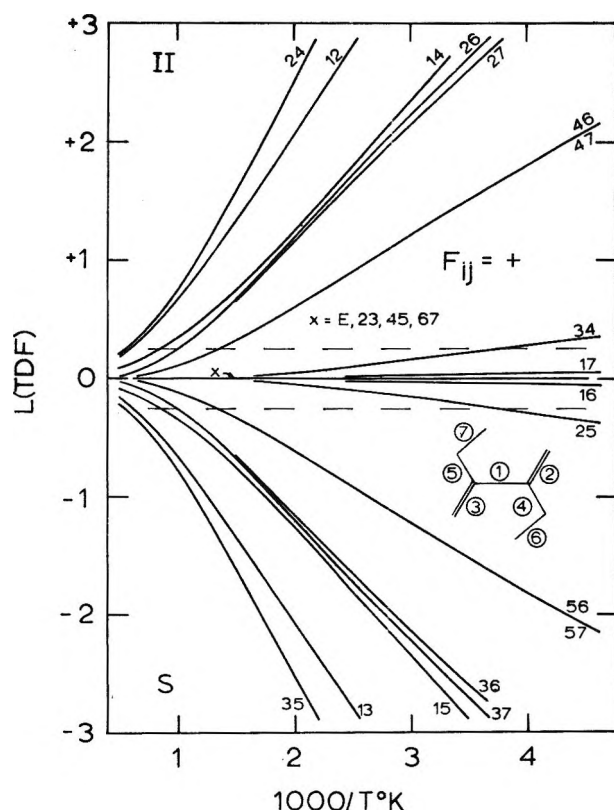


Figure 5.  $L(\text{TDF})$  vs.  $\theta$  (type II calculations,  $S$  field,  $F_{ij} = +$ ). The light broken lines are the limits of  $L(\text{TIF})$ . For 46 and 47 (as well as 56 and 57) the results differ slightly but by less than the thickness of the curve at the largest values of  $\theta$  indicated; the values for 46 are the higher.

$\theta = 0.1, 10^4 \text{ }^\circ\text{K}$  in  $L(k/k')$  for 24 and 35 (and the graphs of these show strong low-temperature curvature toward  $E$ ).

Figure 7 is a collection of  $L(\text{TDF})_{ij}$  vs.  $\theta$  for  $F_{ij} = +$ ,  $U$  field. The asymmetry of the force field has resulted in crossovers in  $L(\text{TDF})$  for 36, 37, 56, and 57; the crossover region is shown with an expanded ordinate scale for these four and for  $E$  in Figure 8a. Some of these crossovers disappear and others come into being when  $L(\text{TDF})$  and  $L(\text{TIF})$  are added to form  $L(k/k')$ ; these effects are noted in the caption to Figure 7. The values of  $L(\text{TIF})$ , as expected, are the same for the situation  $U(+)$  as for  $S(+)$ , except where  $i$  or  $j = 1, 5$ , or  $7$ ; there are no sign reversals and, usually, where there is a change in value,  $L(\text{TIF})$  for  $U(+)$  is the lower in absolute magnitude, the exceptions being 35 and two which were zero with  $S(+)$ , 45 and 67. Because the values of  $F_{11}$ ,  $F_{55}$ , and  $F_{77}$  are different in the  $S$  and  $U$  fields, all cases where  $i$  or  $j = 1, 5$ , or  $7$  correspond to somewhat different eigenvectors in  $S(+)$  and  $U(+)$ ; therefore, effects of the  $U$ -field asymmetry must be derived from consideration of those few  $ij$  which do not contain those coordinates. The reaction coordinate is unaffected by the force field asymmetry in 23, 24, 26, 34, 36, and 46. Figure 8c contains plots for these  $ij$  of  $\Delta\Delta L(\text{TDF})_{ij}$ , which is  $ijU(+)$  -  $EU$  -  $ijS(+)$ ,<sup>41</sup> the

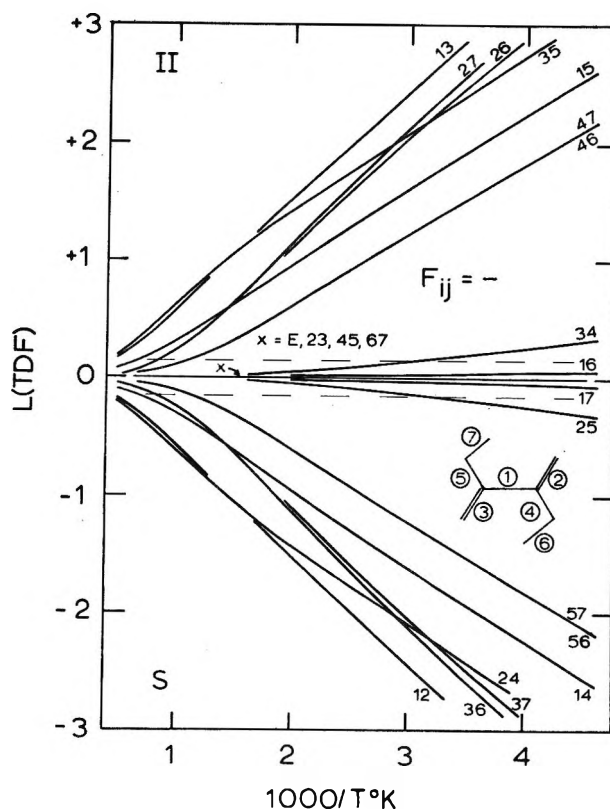


Figure 6.  $L(\text{TDF})$  vs.  $\theta$  (type II calculations,  $S$  field,  $F_{ij} = -$ ). The light broken lines are the limits of  $L(\text{TIF})$ . Between 46 and 47, the values for 47 are the higher (56 and 57 similarly).

difference between the two force fields of the deviation of  $ij$  from its corresponding  $E$ . Where  $ijS(+)$  is of appreciable magnitude, at least 0.3 at  $\theta = 4$ , these differences are small (1-5% of  $L(\text{TDF})$ ); in the case of 23, however, the entire deviation from  $E$  arises in the asymmetry of the  $U$  force field. In no other case is the effect of desymmetrizing the force field sufficiently large to alter the basic shape of any of the curves with respect to that of  $E$ , and if  $F_{ij}$  is not changed in value there is no important change down to  $200^\circ\text{K}$  in the relative position of  $ij$  and  $E$ .

Certain of the features of the crossovers demonstrated thus far are worthy of consideration in the context of laboratory experiments. First, the angles of intersection with the  $L(\text{TDF}) = 0$  line are all much lower than would seem to be required in explanation of some of the experimentally observed anomalies of temperature dependence (curves A, F, and G, Figure 2). Partly, this is because the calculated crossovers occur at relatively high temperatures, above which the fractionation effects are small. The angle of incidence might well increase if the crossover temperature were lowered, though a lower crossover temperature does not guarantee a larger high-temperature extremum.

Results for  $U$ -field calculation, with  $F_{ij} = -$ , are dis-

(41)  $ES = 0$ .

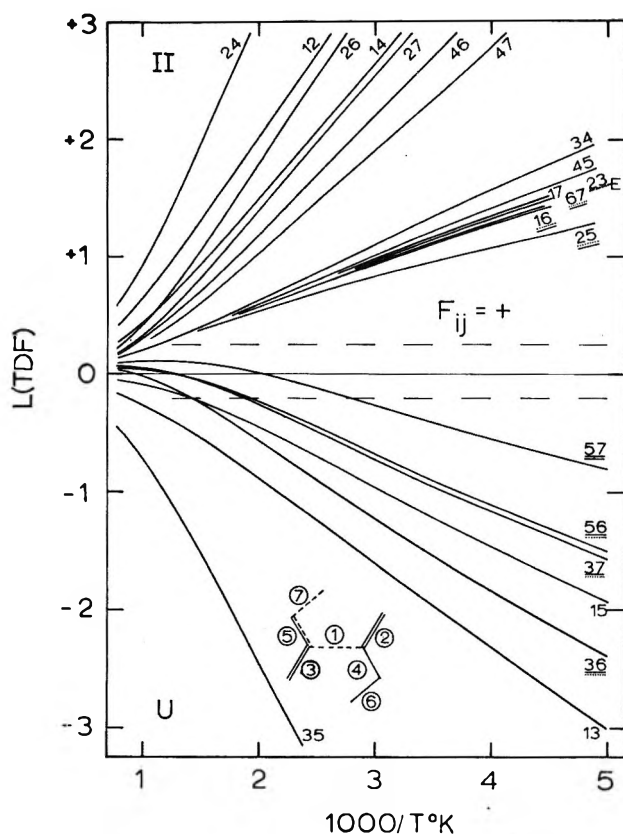


Figure 7.  $L(\text{TDF})$  vs.  $\theta$  (type II calculations,  $U$  field,  $F_{ij} = +$ ). The light broken lines are the limits of  $L(\text{TIF})$ . The short heavy dashes near  $E$  indicate the position of that graph in the central clump of curves. The double underlines refer to the occurrence of crossover:  $\cdots$ , absent,  $\text{---}$ , present; the upper underline refers to  $L(\text{TDF})$ , the lower underline to  $L(k/k')$ . (For example,  $\underline{\underline{\cdots}}$  is read: There is no crossover in  $L(\text{TDF})$ , but, because  $L(\text{TDF})$  and  $L(\text{TIF})$  have opposite sign, in the case of  $25$ , there is a crossover in  $L(k/k')$ .)

played in Figure 9; the crossover region is enlarged in Figure 8b, and the plots of  $\Delta\Delta L = ijU(-) - EU - ijS(-)$  are shown in Figure 8d. The character of these results, except for effects which at present would be likely to be undetectable experimentally, is generally as expected from the discussion above of the sequelae of changing the force field from  $S$  to  $U$  and/or the sign of  $F_{ij}$  from plus to minus; however, the number of intersections of  $ij$  curves is greater than in Figure 7.

The input parameters selected for the  $S$  force field were appropriate to the situation in the normal molecule; this has been the approach in the few published kinetic isotope effect calculations of type II.<sup>35, 37, 38, 42-44</sup> The failure of the  $S$  field to yield crossovers or any other kind of temperature dependence anomaly led us to alterations of the diagonal force field reflective of the changes in bond order which might be expected at the transition state. The  $U$  field which resulted is, of course, as arbitrary as any other; however, though the effects of further force field variations are suggested by comparison of the  $S$ -field and  $U$ -field results, a few of these were subjected to direct test. Some of the results

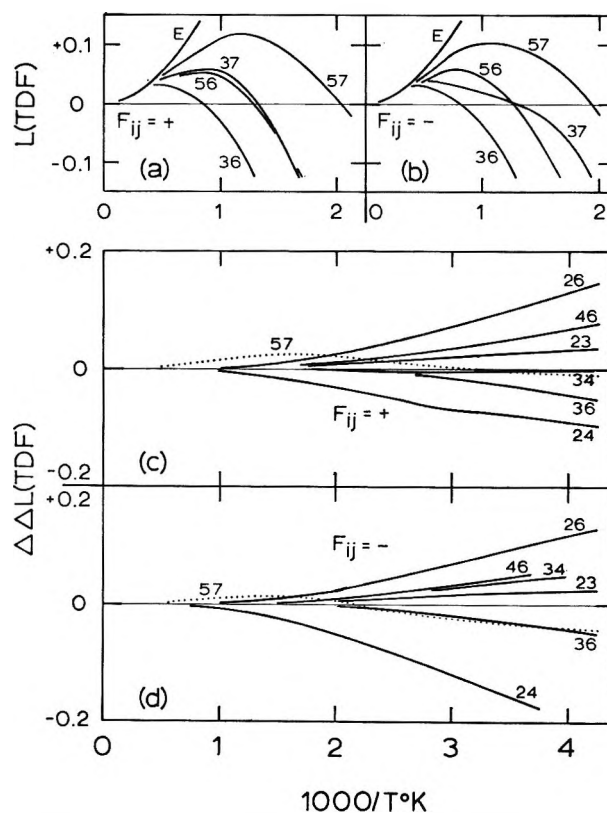


Figure 8.  $L(\text{TDF})$  vs.  $\theta$  (type II calculations with  $U$  field): (a)  $F_{ij} = +$ , (b)  $F_{ij} = -$ .  $\Delta\Delta L(\text{TDF}) = ijU - EU - ijS$  vs.  $\theta$  (type II calculations with  $U$  field): (c)  $F_{ij} = +$ , (d)  $F_{ij} = -$ . The results for  $57$  are shown because of its interesting change of sign with temperature.

of these additional computations are collected in the parts of Figure 10. The selection of  $ij = 15, 17$ , and  $57$  was made because their components  $F_{ij}$  are different in force fields  $S$  and  $U$ ;  $F_{55}$  was selected for variation because it is associated with the bond-order changes between  $S$  and  $U$ ,  $F_{22}$  because it is not.

Because the coordinate  $S_2$  is in none of the selected  $ij$ , variation of  $F_{22}$  has no effect on any of the  $L(\text{TIF})$ ; as expected,  $L(\text{TIF})$  is shifted for  $15$  and  $57$  when  $F_{55}$  is changed.  $L(E)$ , which is not shown, lies very close to the curves marked  $17(12)$  and  $17(7.5)$ ; thus its position and variation can be inferred accurately. Consideration of the results collected in Figures 5-7, 9, and 10, checked by many additional calculations which are not detailed here, leads to the general statements in Table V concerning the effects of diagonal force constant variations on  $L(E)$  and the factors of  $L(k/k')$ . To a first approximation, such effects are additive,<sup>31</sup> but with increasing  $F_{ij}$ , the effect of unit increase decreases,<sup>45</sup> as

(42) P. E. Yankwich and P. D. Zavitsanos, *J. Phys. Chem.*, **68**, 1275 (1964).

(43) P. E. Yankwich and P. D. Zavitsanos, *Pure Appl. Chem.*, **8**, 287 (1964).

(44) P. E. Yankwich and P. D. Zavitsanos, *J. Phys. Chem.*, **69**, 918 (1965).

(45) For example, at  $\theta = 4$ ,  $\Delta L(E)/\Delta F_{22} = -0.398$  if  $F_{22} = 12$ , but  $-0.336$  if  $F_{22} = 18$ .



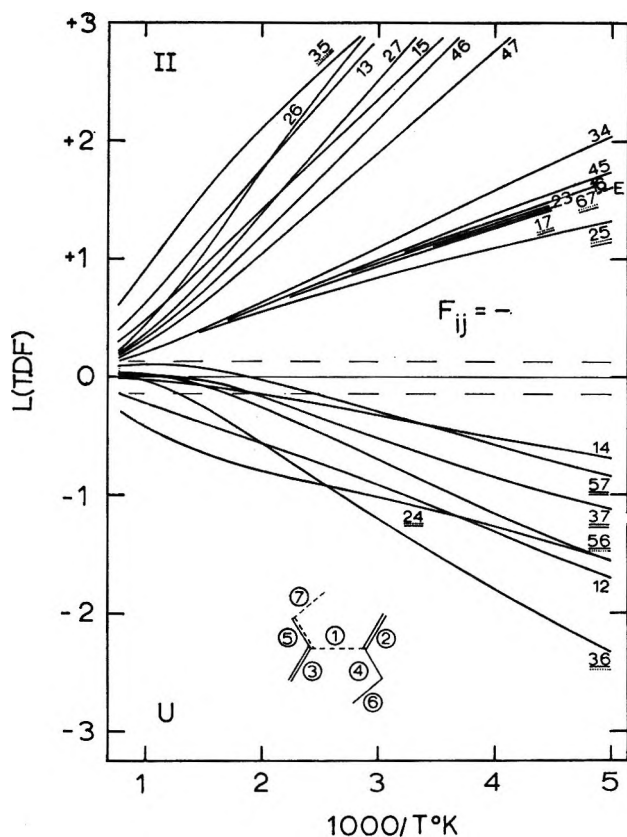


Figure 9.  $L(\text{TDF})$  vs.  $\theta$  (type II calculations,  $U$  field,  $F_{ij} = -$ ). (See the caption to Figure 7 for an explanation of the underlines.)

**Table V:** Indicators for Effects on  $L(E)$ ,  $L(\text{TIF})_{ij}$ , and  $L(\text{TDF})_{ij}$  of Diagonal Force Constant Variations:  $\Delta F_{kk} = +^{a,b}$

$k$	Indicator for		$\Delta L(\text{TDF})_{ij}$
	$\Delta L(E)$	$\Delta L(\text{TIF})_{ij}$	
1	0	$1j, +\delta_j$ if $F_{ij} = +$ ; $-\delta_j$ if $F_{ij} = -$ ; other $ij, 0$	As TIF
2	$-\delta_2$	$i$ or $j = 2, -\delta_2$ ; other $ij, 0$	$-\delta_2$
3	$-\delta_3$	$i$ or $j = 3, -\delta_3$ ; other $ij, 0$	$-\delta_3$
4	$-\delta_4$	$i$ or $j = 4, -\delta_4$ (for $24, +\delta_4$ ); other $ij, 0$	$-\delta_4$
5	$-\delta_5$	$i$ or $j = 5, -\delta_5$ (for $35, +\delta_5$ ); other $ij, 0$	$-\delta_5$

<sup>a</sup> The indications for sign of  $\Delta L$  are correct, but for magnitude are only approximate. The rules for the very small effects when  $k = 6$  or  $7$  are complex. <sup>b</sup> Example:  $\Delta F_{22} = +, -\delta_2 = -2$  (Table IV). According to the above, this force constant alteration lowers  $L(E)$  and all  $L(\text{TDF})_{ij}$ ;  $L(\text{TIF})_{ij}$  is lowered if  $i$  or  $j = 2$ ; it is unaffected otherwise.

expected from the behavior of the vibrational excitation factor, EXC, defined by Wolfsberg and Stern.<sup>5</sup> This makes it possible to generate  $ij$  curves having closely similar properties but which correspond to different reaction coordinates, such as  $15(8)$  and  $57(10)$  in Figure 10a. On the other hand, when the elements of two  $ij$  differ in the manner of their isotopy, the

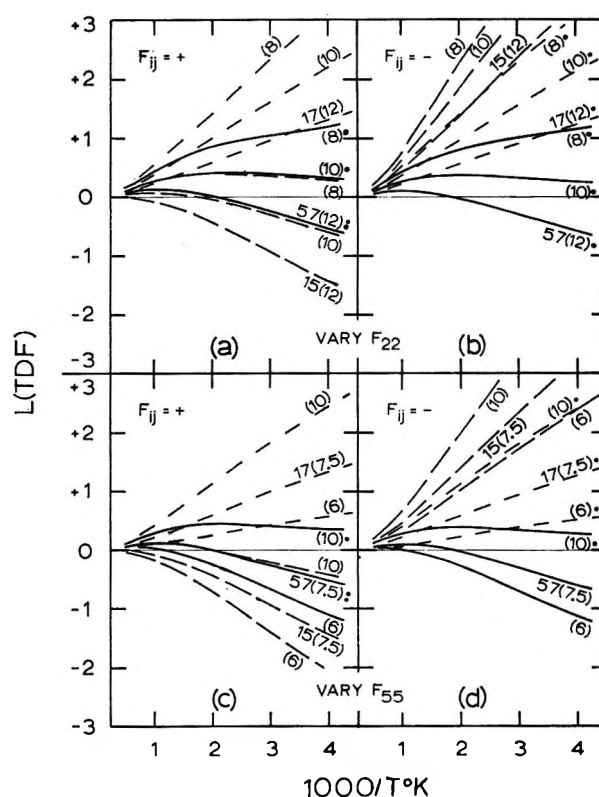


Figure 10. Effects of certain  $F_{ii}$  variations on  $L(\text{TDF})$  vs.  $\theta$  for selected  $ij$  (type II calculations,  $F_{ij} = +$  or  $-$ ): —,  $ij = 57$ ; ---,  $ij = 17$ ; - - - ,  $ij = 15$ . Basic force field is  $U$ ;  $F_{ii}$  is shown in parentheses;  $ij$  is shown for  $U$ -field value of  $F_{ii}$ . The number of heavy dots following the curve label is the number of crossovers in  $L(k/k')$ .

$L(\text{TDF})$  curves can be made to intersect, as do  $57(10)$  and  $17(6)$  in Figure 10c.

Fundamentally, all of the various  $ij$  curves have similar shape (except  $24$  and  $35$  with  $F_{ij} = -$ , *vide supra*), and intersections among those related to a given  $E$  are rare; therefore, if two  $ij$  curves are to traverse a given span of  $\theta$  with significantly different slopes, they must be related to different  $E$  (*i.e.*, to significantly different and internally noncompensating diagonal force fields). Even for modest variations in the force field, calculations of type II exhibit over a limited range of  $\theta$  (and for most experiments the span of  $\theta$  is only  $0.4$ – $0.7$ ) considerable variety of temperature dependence. For example, if they were experimental observations between  $\theta = 2.5$  and  $3.5$ , certain of the curves in Figure 10a would be described as follows:  $17(8)$ , large isotope effect (IE) with normal temperature dependence (TD);  $57(8)$ , moderate IE with abnormally small TD normal in sign;  $57(10)$ , moderate IE with TD abnormal in sign and magnitude;  $15(10)$ , moderate IE with TD normal in sign but abnormally large; and  $15(12)$ , large IE with TD somewhat larger than normal.

Results obtained from type II calculations are characterized by rather small values of  $L(\text{TIF})$ ; this approach thus suffers certain limitations on the variety of

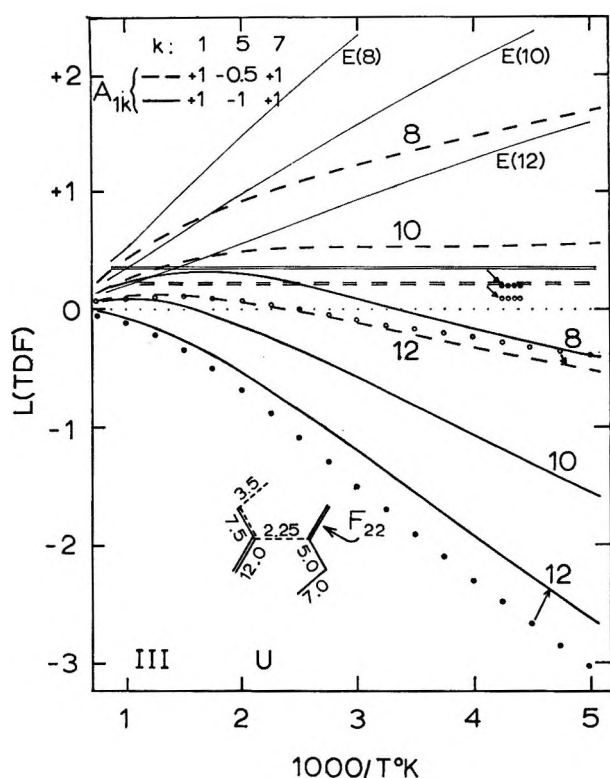


Figure 11:  $L(\text{TDF})$  vs.  $\theta$  (type III calculations,  $U$  field, with  $F_{22}$  varied; numbers adjacent to curves are values of  $F_{22}$ ; other  $F_{ij}$  have  $U$ -field values shown): —,  $K(E)$ ; - - -,  $A_1 = A_{11}:A_{15}:A_{17} = +1: -0.5: +1$ ; —,  $A_1 = A_{11}:A_{15}:A_{17} = +1: -1: +1$ ;  $\circ \circ \circ$ ,  $\bullet \bullet \bullet$ , tests of the  $ij$  additivity relationship for the two  $A_1$  with  $F_{22} = 12$ ;  $\circ \circ \circ \circ$  and  $\bullet \bullet \bullet \bullet$ , calculated  $-L(\text{TIF})$ . The light horizontal double lines are drawn at the positions of  $-L(\text{TIF})$  for these two  $A_1$ ; these double lines are "zero" if the ordinate scale is read as  $L(k/k')$ .

experimental observations it might be expected to explain. For example, among the results shown in Figure 2 those for systems F, G, and possibly D, might be reproduced *via* type II models; all of the others seem to require larger  $L(\text{TIF})$ 's than such models can yield.

**Type III Calculations.** The initial conditions in this type of calculation are that  $A_1$  consist of three elements,  $A_{1i}$ ,  $A_{1j}$ , and  $A_{1k}$ , and that  $\nu_1 = 0$ . In a calculation preliminary to the solution of the secular equation, the off-diagonal elements of  $F$  are obtained in terms of the  $F_{ii}$  (here three in number) related to the selected elements of  $A_1$ , which are  $F_{ii}$ ,  $F_{jj}$ , and  $F_{kk}$ ; the composition and values of these force constants are shown in Table VI.<sup>46</sup> The graphs in Figure 11 show the results for the  $U$  force field ( $F_{22} = 12$ ) and for two lower values of  $F_{22}$ ; in Figure 12, similar results are shown for  $F_{55}$  below, at (7.5), and above the  $U$ -field value.

The curves in Figures 7 and 9 show that the directive influences on  $L(\text{TDF})$ , with respect to  $L(E)$ , of the individual  $F_{ij}$  are as follows: 15, negative if  $F_{ij} = +$ ; 17, negative if  $F_{ij} = -$ , positive if  $F_{ij} = +$ ; and 57, negative if  $F_{ij} = +$ . Since the 17 effects are small, it is not surprising that the shapes of the curves in Figures

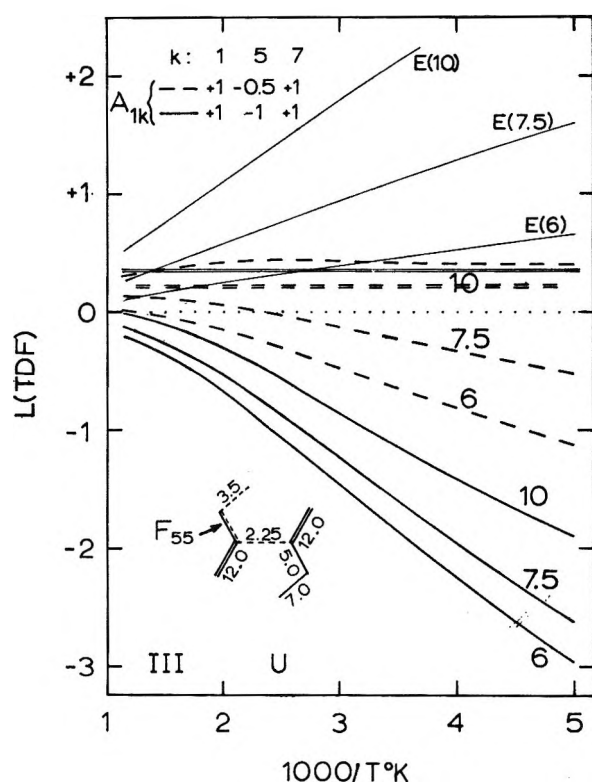


Figure 12.  $L(\text{TDF})$  vs.  $\theta$  (type III calculations,  $U$  field, with  $F_{55}$  varied; numbers adjacent to curves are values of  $F_{55}$ ; other  $F_{ij}$  have  $U$ -field values shown). Curve families designated as in Figure 11.

11 and 12 are very similar to those in Figure 7, where all  $F_{ij} = +$ . This similarity suggested to us a test of an additive relationship between the results for the component  $L(\text{TDF})_{ij}$  and the three-element  $L(\text{TDF})_{ijk}$ . The primary effect of the asymmetry of the  $U$  field with respect to the  $S$  field would be removed by considering all contributions in terms of the deviations from  $L(E)_v$ ; of course, one could not tell whether a "slight" failure of the additivity test arose in a secondary effect of asymmetry or in some other factor, such as incorrect selection of the linear combination coefficients, without a very much more detailed exploration. The linear combination function is

$$L(\text{TDF})_{ijk} - E = \sum \alpha_{ij} [L(\text{TDF})_{ij} - E] \quad (11)$$

In the notation employed earlier, and rearranged, eq 11 predicts the value for  $L(\text{TDF})_{157}$  to be

$$157 = \alpha_{15}(15) + \alpha_{17}(17) + \alpha_{57}(57) - E(\alpha_{15} + \alpha_{17} + \alpha_{57} - 1) \quad (12)$$

The curves plotted with open and solid circles in Figure 11 are  $L(\text{TDF})_{157}$  vs.  $\theta$ , calculated *via* eq 12 for the two reaction coordinates indicated; in these computations, with all  $F_{ij}$  at  $U$ -field values, the  $\alpha_{ij}$  are the ratios

(46) The coefficients of the diagonal force constants  $F_{nn}$  in the terms comprising the  $F_{ij}$  are  $(-1)^m (A_{1n})^2 / (2A_{1i}A_{1j})$ , where  $m = 1$  if  $n = i$  or  $j$ , but  $= 0$  if  $n = k$ .

**Table VI:** Composition and Values of  $F_{ij}$  for Type III Calculations

Composition	$F_{ij}$			$\alpha_{ij}$ ( $= (F_{ij})_0 / (F_{ij})_0^a$ )
	6	7.5 <sup>b</sup>	10	
$A_{11}:A_{15}:A_{17} = +1:-0.5:+1$				
$F_{15} = +1.0F_{11} + 0.250F_{65} - 1.0F_{77}$	0.25	0.625	1.25	0.1521
$F_{17} = -0.5F_{11} + 0.125F_{65} - 0.5F_{77}$	-2.125	-1.938	-1.625	0.6905
$F_{67} = -1.0F_{11} + 0.250F_{65} + 1.0F_{77}$	2.75	3.125	3.75	0.6099
$A_{11}:A_{15}:A_{17} = +1:-1.0:+1$				
$F_{15} = +0.5F_{11} + 0.500F_{65} - 0.5F_{77}$	2.375	3.125	4.375	0.7607
$F_{17} = -0.5F_{11} + 0.500F_{65} - 0.5F_{77}$	0.125	0.875	2.125	0.3118
$F_{67} = -0.5F_{11} + 0.500F_{65} + 0.5F_{77}$	3.625	4.375	5.625	0.8539

<sup>a</sup> The  $(F_{ij})_0$  are the single-parameter values listed in Table III; these  $\alpha_{ij}$  are for  $F_{65} = 7.5$ . <sup>b</sup> Since  $S_2$  is not part of the reaction coordinate in these calculations, these values of  $F_{ij}$  are employed for any value of  $F_{22}$  (Figure 11).

of the individual  $F_{ij}$  shown in Table VI to the  $F_{ij}$  which yielded  $\nu_1 = 0$  in the calculations of type II (Table III). The agreement for  $L(\text{TDF})$  is fair, but the analog of eq 12 for  $L(\text{TIF})$  does not predict the value of the temperature-independent factor nearly so well. Earlier we argued that the comparative rarity of intersections among the various  $ij$  curves obtained for type II calculations was due to the fact that fundamentally all such were of the same shape; the same argument accounts for the failure of any of the  $ij$  graphs to intersect that for  $E$ . The intersection near  $\theta = 1.75$  of the calculated and "predicted"  $ijk$  plots and the failure of the additivity relation to predict  $L(\text{TIF})$  both suggest that graphs in similar regions of the  $L(\text{TDF})$  vs.  $\theta$  field of type II and type III functions may actually have slightly different shape and that other selections of  $ijk$  and  $A_1$  might yield, at least, an intersection of  $L(\text{TDF})_{ijk}$  and  $L(E)$ . Earlier, temperature independence of a large kinetic isotope effect has been assumed to arise in a large TIF; intersection of  $L(\text{TDF})_{ijk}$  and  $L(E)$  would provide an alternate basis for such a situation. (In fact, neither a zero frequency<sup>4</sup> nor nonzero  $F_{ij}$ 's<sup>6</sup> are necessary for a plateau in TDF.)

*Type IV Calculations.* When  $\nu_1 = 0$  and  $A_1$  has  $n$  nonzero elements, the several  $F_{ij}$  for calculations of type III are obtained from the  $n$  simultaneous equations

$$\mathbf{F}(\mathbf{A}_1)^\dagger = \mathbf{0} \quad (13)$$

If  $n > 3$ , the number of  $F_{ij}$  is greater than  $n$  and certain of them become parameters, along with all of the  $F_{ii}$ .<sup>27</sup> The set of nonzero parameters can be limited conveniently to the  $F_{ii}$  by the requirement that some  $i$  be common in the nonzero  $F_{ij}$  related to the elements of  $A_1$ . Then the  $i$ th equation of the set of  $n$  from eq 13 is

$$\sum_j F_{ij}A_{1j} = 0 \quad (14)$$

(and has  $n$  nonzero elements), while the remaining equations  $j$ ,  $n - 1$  in number, are

$$F_{ij}A_{1i} + F_{jj}A_{1j} = 0 \quad (15)$$

Let the subscript 0 indicate a value appropriate to a type II calculation, which employs but one  $F_{ij}$  to achieve  $\nu_1 = 0$ . Then

$$(F_{ij})_0^2 = (F_{ii})_0(F_{jj})_0 \quad (16)$$

and, since

$$(F_{ij})_0 = -(A_{1j}/A_{1i})_0(F_{jj})_0 = -(A_{1i}/A_{1j})_0(F_{ii})_0 \quad (17)$$

we have

$$(A_{1j}/A_{1i})_0^2 = (F_{ii})_0/(F_{jj})_0 \quad (18)$$

For each  $j \neq i$ , eq 15 and 16 may be combined to yield

$$(F_{ij})_0/(F_{ij})_0 = (A_{1j}/A_{1i})_0/(A_{1j}/A_{1i})_0 = \alpha_{ij} \quad (19)$$

where  $\alpha_{ij}$  has been defined for an earlier purpose (Table VI).

When the  $n - 1$  equations  $j$  are substituted into the  $i$ th equation, we have

$$(F_{ii})_0 - \sum_{j \neq i} (F_{jj})_0(A_{1j}/A_{1i})_0^2 = 0 \quad (20)$$

or

$$\sum_{j \neq i} [(F_{jj})_0/(F_{ii})_0](A_{1j}/A_{1i})_0^2 = 1 \quad (21)$$

When the ratios of diagonal force constants are replaced by eq 18, we obtain the useful result

$$\sum_{j \neq i} [(A_{1j}/A_{1i})_0^2/(A_{1j}/A_{1i})_0^2] = \sum_{j \neq i} (\alpha_{ij})^2 = 1 \quad (22)$$

Equations 19 and 22 furnish the basis for calculations of type IV.

Type IV and type III calculations differ in character primarily in that completely independent selection of the several elements of  $A_1$  is possible in the latter but not in the former. The more limited type IV calculations are the more convenient for exploratory purposes.

Some of the significant features of results obtained via calculations of type IV are displayed in Figure 13; the elements of  $A_1$  are identified and values of the several  $\alpha_{ij}$  are listed in Table VII. Part a of the figure

Table VII: Reaction Coordinates Used for Figure 13; Type IV Calculations

Reaction coordinate	<i>i</i>	<i>j</i>	<i>k</i>		$\alpha_{ij}$	$\alpha_{ik}$	$\alpha_{il}$	$L(\text{TIF})^a$
A1	5	1	3	7	+0.707	+0.500	+0.500	-0.1895
A2					-0.707	+0.500	+0.500	+0.0768
A3					+0.707	+0.500	-0.500	-0.1630
A4					+0.707	-0.500	+0.500	-0.3890 (-0.4201) <sup>a</sup>
B1	3	1	5	7	+0.500	+0.707	+0.500	-0.1557
B2					+0.500	-0.707	+0.500	-0.4768 (-0.4181)
B3					+0.500	+0.707	-0.500	-0.0975
C1	7	1	2	5	+0.500	+0.707	+0.500	+0.0152
C2					+0.500	-0.707	+0.500	+0.3217
C3					+0.500	+0.707	-0.500	-0.2312 (-0.2881)
C4					-0.500	+0.707	+0.500	+0.0044
D	1	2	3	5	+0.500	+0.500	+0.707	-0.1538
G	3	1	5		+0.707	-0.707		-0.4042
H	5	1	3		+0.707	-0.707		-0.3985 (-0.4166)
J	1	3	5		-0.707	+0.707		(-0.1062)
L(0.4)	4	1	2		+0.400	-0.917		(+0.3004)
L(0.6)					+0.600	-0.800		(+0.3958)
L(0.8)					+0.800	-0.600		(+0.4156)

<sup>a</sup> Where the basic force field is *S*, the value is shown in parentheses.

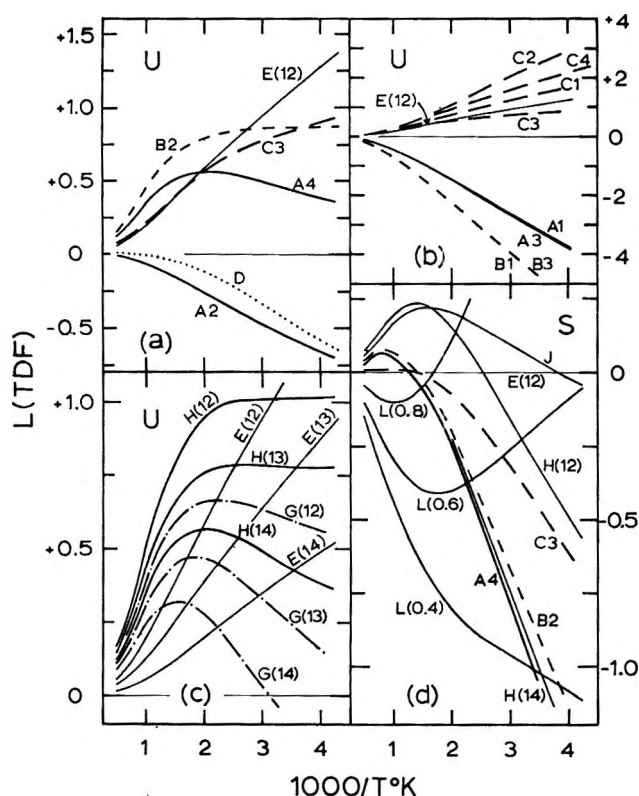


Figure 13.  $L(\text{TDF})$  vs.  $\theta$  (type IV calculations): (a) several four-element reaction coordinates, *U* field; (b) effects of changing sign of one  $F_{ij}$ , all three of which were + for the base reaction coordinates A1, B1, and C1, *U*-field; (c) effects of variation of  $F_{22}$  (all other  $F_{ij}$  at *U*-field values) on *E* crossovers of results for reaction coordinates G and H; values of  $F_{22}$  shown in parentheses; (d) effects of reaction coordinate variations on the production of crossovers in computations employing the *S* force field.

contains plots of  $L(\text{TDF})_{ijkl}$  vs.  $\theta$  for several four-element reaction coordinates; the *U* force field was em-

ployed. In these examples the  $\alpha_{ij}$  have various signs, as do the  $F_{ij}$  derived therefrom; if  $A_{1i}$  is taken always to be positive, the signs of the several  $A_{1j}$ , etc., are opposite to those of the related  $\alpha_{ij}$ , as required by eq 15. Two kinds of crossover are illustrated: A4 will cross the  $L(\text{TDF}) = 0$  line at very low temperatures (indicating that this kind of result can be obtained *via* calculations of type IV as well as those of types II and III); B2 and C3 cross the equilibrium constant curve,  $E(12)$ , an important feature not previously observed.<sup>47</sup> The type of plateau exhibited by B2 is similar to those generated in some type III calculations (Figures 11 and 12) but differs in that the isotope effect is larger because of the crossover of *E*; the plateau for reaction coordinate D is an extreme example of the type found earlier for  $(F_{67})_0 = +$  and  $-$  (in type II calculations, Figures 7 and 9) but differs in that the high-temperature isotope effect is practically zero out to  $\theta = 1.2$ . Because all of the  $L(\text{TIF})$ 's for the examples in Figure 13a are opposite in sign to the  $L(\text{TDF})$ 's,  $L(k/k')$  for these coordinates will exhibit an additional crossover at high temperatures. Comparison of the  $L(\text{TIF})$  values in Tables III and VII reveals that those obtained for type IV calculations are often larger in absolute magnitude than those for type II. We have observed that, all other things being equal,  $L(\text{TIF})$  increases in size with the number of  $F_{ij}$  employed to achieve  $\nu_1 = 0$ ; although the signs and approximate magnitudes of  $L$

(47) Calculations of type III can be made to yield crossovers with respect to *E*, though no results of that kind are among the results reported here. The fundamental shapes of type II curves are such that crossing of *E* cannot occur with them within the limitations of force field variation imposed on this study. Were the limitation " $F_{ij} = 0$  except where required to produce  $\nu_1 = 0$ " removed, it would be possible to generate *E* crossing with a kinetic isotope effect of normal temperature dependence (Stern, Spindel, and Monse's type A) through use of small  $F_{ij}$  in the force field for *E*.

(TIF) and  $L(\text{TDF})$  can be inferred from the type II results for the  $F_{ij}$  employed in a type IV calculation, this relation of  $L(\text{TIF})$  to the number of  $F_{ij}$  implies that simple additivity is not an adequate description of the relation among type II and type IV results (*vide infra*).

Part b of Figure 13 illustrates an interesting aspect of II-IV additivity failure. Results obtained in type II calculations for  $(F_{37})_0$  and  $(F_{57})_0$  are the same for  $(F_{ij})_0 = +$  or  $-$ , except at the highest temperatures. If II-IV additivity obtained, the results for reaction coordinates A1, B1, and C1 should be unaffected by a switch in sign of one of these off-diagonal force constants. A1 becomes A3 when  $F_{57}$  is switched from  $+$  to  $-$ , and B1 becomes B3 when  $F_{37}$  is switched from  $+$  to  $-$ ; in the case of both these pairs the effect of the sign switch is very small (shown by thickening of the curves at low temperatures). However, the reaction coordinates C2, C3, and C4 differ from C1 only in the change of sign of  $F_{57}$  from  $+$  to  $-$ , and in each case the effect of this switch is substantial on both  $L(\text{TDF})$  and  $L(\text{TIF})$ . The rationalization of these apparently divergent observations lies in the fact that in coordinates A and B the common element is 5 and 3, respectively, while in C it is element 7 (a nonisotopic coordinate); in type II calculations only very small shifts in  $L(\text{TDF})$  were observed when as  $(F_{17})_0$  was changed from  $+$  to  $-$ .

Part c of Figure 13 is a test of diagonal force constant effects on  $E$  crossovers for reaction coordinates G and H;  $F_{22}$  was varied. The maximum separation between  $ijk$  and  $E$  at high temperatures is little affected by the value of  $F_{22}$ , but the position of this maximum separation is shifted to higher temperature as  $F_{22}$  increases. Note that in several cases there are crossovers of  $L(\text{TDF}) = 0$  as well as of  $L(E)$ , and, since  $L(\text{TIF})$  and  $L(\text{TDF})$  are opposite in sign at high temperatures,  $L(k/k')$  will exhibit an additional crossover in that region in all cases.

Part d of Figure 13 is a test of the relation of the  $E$  crossover to the asymmetry of the  $U$  force field. These calculations were performed with the  $S$  force field, and it is apparent that  $E$  crossover does not depend for its origin on diagonal force field asymmetry. (The result for H(14) is included to show how a variety of reaction coordinates coupled with modest changes in force field can result in very similar  $L(\text{TDF})$  curves.)

Figure 14 shows the results of systematic changes in the signs of  $F_{ij}$  and  $F_{ik}$  for four reaction coordinates of similar composition and having equal absolute values of  $\alpha_{ij}$  and  $\alpha_{ik}$ . A few crossovers of  $L(E)$  are observed, but none of  $L(\text{TDF}) = 0$  within a temperature range convenient for experiment. These graphs provide an important test of the simple additivity relation, for eq 11 predicts that the plots for  $+-$  and  $-+$ <sup>48</sup> should be disposed symmetrically with respect to  $E$ ; in no case is this relation even approximated.

The simplest situation in which the influence on

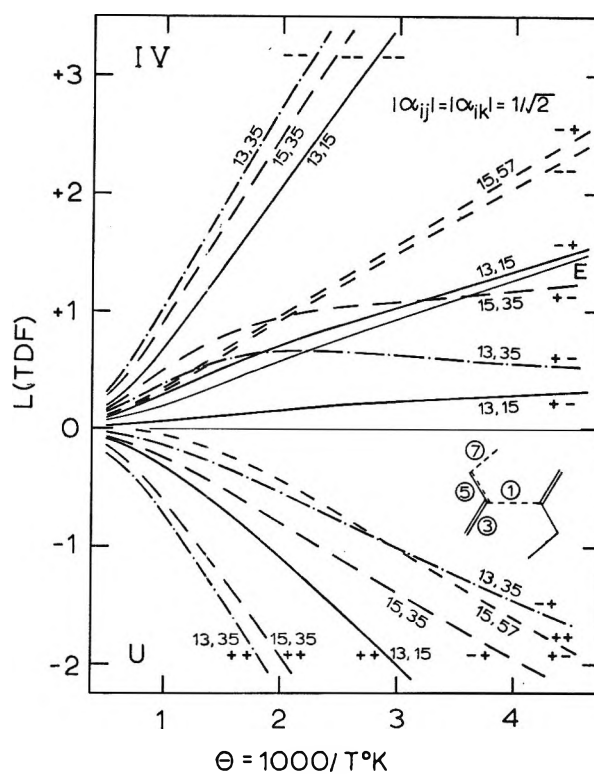


Figure 14.  $L(\text{TDF})$  vs.  $\theta$  (type IV calculations). Effects of systematic changes in the signs of the equally weighted  $F_{ij}$  and  $F_{ik}$  for four reaction coordinates. The sign pairs are for  $ij$  and  $ik$  placed in ascending numerical order.

calculated isotope effects of systematic variations in the elements of a type IV reaction coordinate can be studied occurs when  $A_1$  has three elements and two off-diagonal force constants,  $F_{ij}$  and  $F_{ik}$ , are varied from the minimum through zero to maximum values.<sup>49</sup> Because of the great significance of  $E$  crossing in type IV calculations, exploration of three-element  $A_1$  effects was limited to the  $S$  force field, in which any crossover is an  $E$  crossover.

The number of type IV calculations possible for this model is very large;<sup>50</sup> our discussion is restricted to those types of results which appear to occur with the greatest frequency. The first examples are the related triad (17, 57), (15, 17), and (15, 57); these differ only in the choice of the internal coordinate to be considered common,  $i$ , from the triplet (1, 5, 7). (This

(48) I.e.,  $F_{ij} = +, F_{ik} = -$  and  $F_{ij} = -, F_{ik} = +$ .

(49) The extremal values of these force constants are  $(F_{ij})_0, +$  and  $-$ , and  $(F_{ik})_0, +$  and  $-$ . For convenience, in the remainder of this discussion the symbol  $(F_{ij})_0$  will be taken to represent a positive magnitude. Then,  $\alpha_{ij}$  and  $F_{ij}$  always have the same sign; see eq 19.

(50) For the model and isotope effect studied here there are 105 different pairings of an  $ij$  and an  $ik$  possible. Use of the  $S$  force field converts 102 of these to pairs whose members are related simply to each by reversal of the sign of  $L(\text{TDF})$ . The calculations can be classified on the basis of the magnitude and sign of respective component type II  $L(\text{TDF})_{ij}$  and whether their signs change when  $F_{ij}$  is switched from positive to negative value (see Figures 5 and 6); however, the results of the calculations do not conform to such a classification scheme.

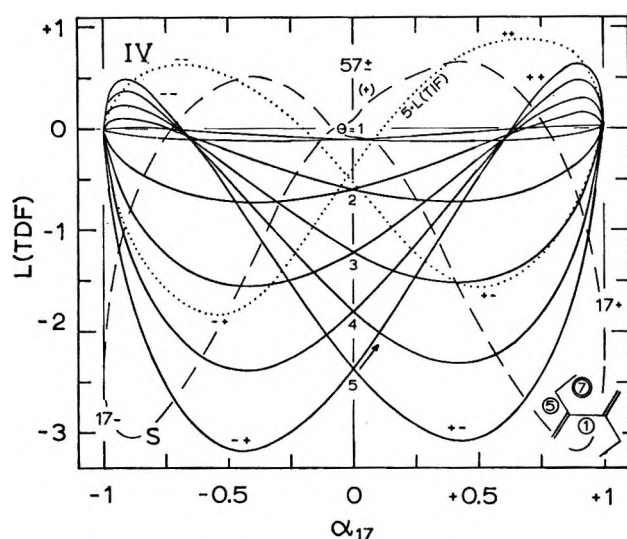


Figure 15.  $L(\text{TDF})$  vs.  $\alpha$  (type IV calculations). In this figure  $ij = 17$  and  $ik = 57$ ; the difference between  $(F_{57})_0 = +$  and  $-$  results is very small and is not shown. The following remarks apply to Figures 15–19: solid curves are  $L(\text{TDF})$  vs.  $\alpha_{ij}$  at various values of  $\theta$ ; the dotted curve is  $L(\text{TIF})$  vs.  $\alpha_{ij}$ ; the dashed curve is  $L(\text{TDF})$  vs.  $\alpha_{ik}$  at the low temperature  $\theta = 5$ . For the purposes of these figures,  $ij$  and  $ik$  are placed in ascending numerical order internally and with respect to each other; thus the symbol  $+ -$  means that in that region  $\alpha_{ij} = +$  (as is  $F_{ij}$ ) and  $\alpha_{ik} = -$  (as is  $F_{ik}$ ). The symbol  $(+)$  on the dashed curve indicates where one would find the  $\theta = 5$  point for  $\alpha_{ij} = +1$  were the abscissas  $\alpha_{ik}$  instead of  $\alpha_{ij}$ . In the bond diagram, the common coordinate  $i$  is double circled.

triplet was selected because the difference between the  $S$  and  $U$  fields resides in these  $F_{it}$ .

The results for calculations with  $ij = 17$ ,  $ik = 57$ , are shown in Figure 15. Equations 15, 19, and 22 permit one to follow the exchange of "motion" (relative to that in the *common* coordinate  $S_7$ ) between coordinates  $S_1$  and  $S_5$  as  $\alpha_{17}$  is varied. Suppose one starts at the point  $\alpha_{17} = 0$ ,  $\alpha_{57} = +1$  and follows the arrow into the " $++$  area" of the calculation, continuing around the isotherm to the starting point. Initially (see Table VIII) there is no motion in  $S_1$  ( $A_{11} = 0$ ), while that in  $S_5$  is at a maximum and antisymmetric with respect to that in  $S_7$  ( $A_{15} = -$ ). As we follow the curve, motion in  $S_1$  antisymmetric to that in  $S_7$  increases, passes through a maximum, decreases, and then is replaced by motion symmetric to that in  $S_7$  which follows the same course; correspondingly, the motion in  $S_5$  antisymmetric to that in  $S_7$  decreases, is replaced by motion symmetric with respect to that in  $S_7$  which reaches a maximum, then decreases, and is replaced by antisymmetric motion which reaches a maximum. In this calculation, coordinates 1 and 5 are both isotopic and one might expect the isotope effects at  $\alpha_{17} = -1, 0$ , and  $+1$  to be connected to each other without intervening extrema; this is obviously not the case.

Isotherms in Figure 15 are distorted 8's. There are two convergence regions, near  $|\alpha_{17}| = 0.6$ . Because

Table VIII: Exchange of "Motion" between Coordinates  $S_1$  and  $S_5$  in a Circuit of an Isotherm of the Map of the Type IV Calculation:  $ij = 17$ ,  $ik = 57$  (Figure 15)

"Area"	$\alpha_{17}$	$\alpha_{57}$	$A_{11}^a$	$A_{15}^a$	$A_{17}$
++	0	+1	0	-1.1832	+1
	+0.7071	+0.7071	-0.8819	-0.8366	+1
+-	+1	0	-1.2472	0	+1
	+0.7071	-0.7071	-0.8819	+0.8366	+1
--	0	-1	0	+1.1832	+1
	-0.7071	-0.7071	+0.8819	+0.8366	+1
-+	-1	0	+1.2472	0	+1
	-0.7071	-0.7071	+0.8819	-0.8366	+1
	0	+1	0	-1.1832	+1

<sup>a</sup> Normalized to  $A_{17} = +1$ .

these convergences lie so that  $L(\text{TDF}) < 0$ , the plateaus which they represent on plots of  $L(\text{TDF})$  vs.  $\theta$  are replaced by regions in which crossover occurs (at progressively higher temperatures) as  $|\alpha_{17}|$  increases.

Extrema are observed for  $L(\text{TIF})$  and for  $L(\text{TDF})$  at each temperature in each of the four sign "areas" of the calculation ( $++$ ,  $+-$ , etc.) but not at simply related values of  $\alpha_{17}$ . For such intermediate extrema to occur, it is apparently a sufficient, but not a necessary, condition that coordinates  $j$  and  $k$  have an isotopic atom in common.

Results for  $ij = 15$ ,  $ik = 17$ , are plotted in Figure 16. Because the data for  $F_{17} = +$  and  $F_{17} = -$  lie so close together, only those for  $F_{17} = +$  are plotted (except at  $\theta = 5$ ). There are two convergence regions in the complete set of curves, both very close to  $\alpha_{15} = 0$ . The  $17 +$  or  $-$  values of  $L(\text{TDF})_{17}$  are so small that the crossover regions are extremely narrow and would be of little importance to an attempt at matching a calculated crossover to an experimentally observed one.

The last calculations in this triad are those for  $ij = 15$ ,  $ik = 57$ , shown in Figure 17. (Again, results for  $F_{57} = -$  are not shown because they lie so close to those for  $F_{57} = +$ .) The convergence regions are now well displaced from  $\alpha_{15} = 0$ ; plateaus are observed near  $\alpha_{15} = -0.5$ , and the area of crossovers is broad, extending from  $\alpha_{15} = -0.28$  to  $-0.46$ . Near  $\alpha_{15} = +1$ ,  $L(\text{TDF})$  is practically independent of  $\alpha$ , but as  $\theta$  increases above 3.5 a minimum in the curves appears which moves to progressively lower values of  $\alpha$ .

Figure 18 displays graphs for the pair  $ij = 27$ ,  $ik = 57$ . Results of this type are cousins of the variety shown in Figure 15, the most important difference being that extrema in  $L(\text{TIF})$  and  $L(\text{TDF})$  are not observed at intermediate values of  $\alpha_{ij}$ . If the data for  $F_{57} = -$  had been plotted as well as those for  $F_{57} = +$ , two close pairs of convergences would have been shown. As in Figure 15, these pairs are well separated; as in Figure 17, the slopes of the curves near the areas

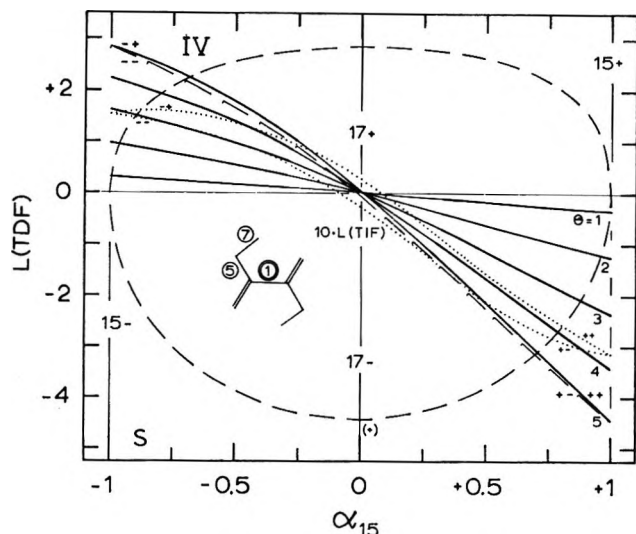


Figure 16.  $L(\text{TDF})$  vs.  $\alpha$  (type IV calculations,  $ij = 16$ ,  $ik = 17$ ). Results for  $F_{17} = -$  are shown only at  $\theta = 5$  (ticked dashes).

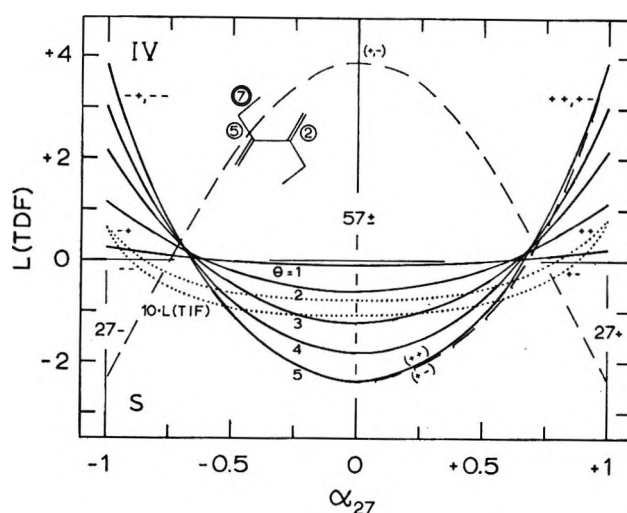


Figure 18.  $L(\text{TDF})$  vs.  $\alpha$  (type IV calculations,  $ij = 27$ ,  $ik = 57$ ). Results for  $F_{57} = -$  are shown only at  $\theta = 5$  and for the  $F_{27} = +$  case (ticked dashes).

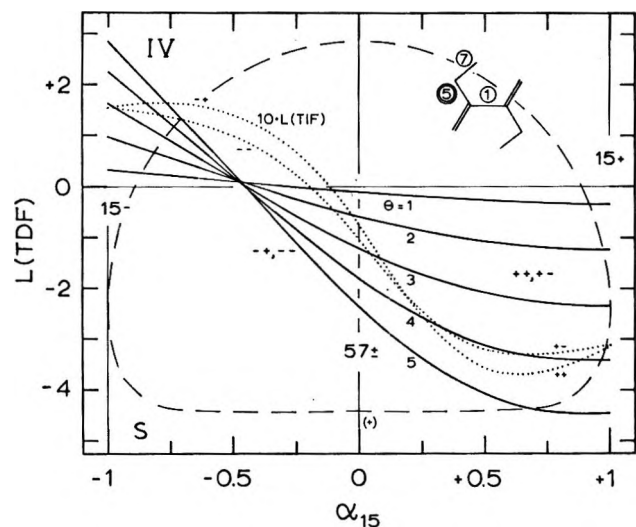


Figure 17.  $L(\text{TDF})$  vs.  $\alpha$  (type IV calculations,  $ij = 15$ ,  $ik = 57$ ). The difference between  $F_{57} = +$  and  $-$  results is very small and is not shown.

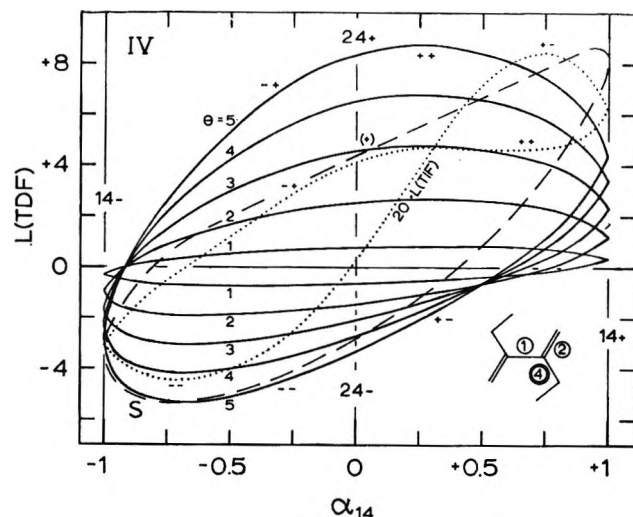


Figure 19.  $L(\text{TDF})$  vs.  $\alpha$  (type IV calculations,  $ij = 14$ ,  $ik = 24$ ).

of convergence is sufficiently high that crossover occurs only over a modest range of  $\alpha_{ij}$  values, here about 0.1 unit wide.

The only other type of results which appear to be frequent of occurrence and different from those displayed in Figures 15–18 is shown in Figure 19; the graphs in this figure are for  $ij = 14$ ,  $ik = 24$ . There are two convergence regions: that near  $\alpha_{14} = -0.9$  coincides with  $L(\text{TDF}) = 0$ , neither a plateau nor crossovers in plots of  $L(\text{TDF})$  vs.  $\theta$  would be observed for any negative value of  $\alpha_{14}$ ; the convergence near  $\alpha_{14} = +0.5$  does not include the lowest values of  $\theta$ , so both plateaus and crossovers would be observed over a rather wide range of  $\alpha_{14}$  (perhaps as wide as 0.3 unit). The  $L(\text{TIF})$  curve bears little resemblance to those for

$L(\text{TDF})$ , as was found also for data of the type shown in Figure 17.

### Conclusion

This research has explored the effects of diagonal and off-diagonal stretching force constant variations on the temperature-dependent and temperature-independent factors in the intramolecular isotopic rate constant ratio for the decomposition of oxalic acid- $^{13}\text{C}$ . These variations correspond to reaction coordinates which consist of up to four internal coordinate displacements; in all cases, the “vibrational” frequency associated with the reaction coordinate was taken as zero. Crossover (*i.e.*, change in sense with respect to unity as a function of temperature) in the temperature-dependent factor in  $k/k'$  is not observed when the reaction coordinate contains but a single element. Reaction

coordinates consisting of two elements (one nonzero off-diagonal force constant) yield crossover only if the basic diagonal force field is asymmetric at one or more isotopic bonds. Many of the details of the results for two-element reaction coordinates can be related to the results obtained with single-element reaction coordinates.

When the reaction coordinate contains three or more elements, crossovers in the temperature-dependent factor can be produced with symmetric diagonal force fields, as can "plateau" regions where the isotope effect is almost constant over a wide range of temperature. The details of such results, which require for their generation the use of two or more nonzero off-diagonal force constants, can be inferred only generally from those obtained with one such off-diagonal force constant value and therefore can be related to the results for single-element reaction coordinates only with difficulty. That is, with increasing complexity of the reaction coordinate, consideration of the isotope effect consequences of the motion to be those of a superposition of individual internal coordinate displacements becomes an increasingly inaccurate approximation.

This research has shown that crossover and other

anomalies of temperature dependence can be generated (in a model system chosen for its impediments to such generation) by reasonable adjustments of the transition state force field. Whether or not the results reported here constitute a demonstration that such anomalies are *prevalent* in kinetic isotope effects is a matter of judgement and can be established firmly only by exploration of the behavior of a number of different model systems. Intermolecular isotope effects may be expected to have different properties than intramolecular isotope effects. Further, the inclusion of bending force constants among the parameters varied should drastically alter the frequency with which anomalies of temperature dependence are observed. When the possibilities thus afforded are added to those expected from selection of an imaginary frequency (as opposed to a zero frequency) for the reaction coordinate motion,<sup>27</sup> the task of exploring even a single reaction is seen to be truly enormous, unless only four or five atoms are involved in the transition state. Methods for systematizing such exploration remain to be developed.

*Acknowledgment.* This research was supported by the U. S. Atomic Energy Commission, COO-1142-78.

## Solid-State Reactivity of Picric Acid and Substituted Hydrocarbons

by R. P. Rastogi<sup>1a</sup> and N. B. Singh

*Department of Chemistry, Gorakhpur University, Gorakhpur, U. P., India (Received April 18, 1968)*

The solid-state reactivity of picric acid + acenaphthene, picric acid +  $\beta$ -naphthylamine, and picric acid + pyrocatechol has been investigated. The results show that diffusion in the solid state is controlled by surface migration, in conformity with the earlier finding by Rastogi and Singh. It is found that molecules having a smaller size and molecules having greater symmetry are more favorable for surface migration.

### Introduction

Solid-state reactions between picric acid and naphthols, recently investigated by Rastogi and Singh,<sup>1b</sup> are a novel class of solid-state reactions, since the kinetics are controlled by surface migration. The rate of advance of the product layer when the reactants are kept adjacent to each other is given by

$$\xi^2 = 2k_i t e^{-p\xi} \quad (1)$$

where  $\xi$  is the thickness of the product layer at any time  $t$ , and  $k_i$  and  $p$  are constants. If A and B are the two reactants kept adjacent to each other and the reaction progresses in the direction of the arrow, the surface

migration of A would take place in the manner shown below



Using this model of surface diffusion, Rastogi and Singh<sup>1b</sup> have shown that

$$k_i = 4n\pi r^2 D_0 e^{-E/RT} \quad (2)$$

where  $D_0$  is the diffusion coefficient,  $E$  is the energy of

(1) (a) Visiting Professor, Department of Chemistry, Indiana University, Bloomington, Ind. (b) R. P. Rastogi and N. B. Singh, *J. Phys. Chem.*, **70**, 3315 (1966).



activation, and  $n$  and  $r$  are the number and radius of the particles of B, respectively. Very little is known about the mechanism of surface migration. The purpose of this paper is to get an insight into the nature of mechanism. Surface migration would be expected to be favored by symmetrical and planar molecules, since such molecules can move on the surface relatively easily as compared with unsymmetrical molecules, particularly when the surface is not perfectly smooth. The unsymmetric molecules would get entangled on the surface. In order to examine this point, the solid-state reactivity of acenaphthene,  $\beta$ -naphthylamine, and pyrocatechol, which have varying degrees of asymmetry, has been studied. The influence of the size of the molecules on solid-state reactivity has also been investigated. The results are reported in this article.

### Experimental Section

**Materials and Purifications.** Picric acid (BDH) was purified as described earlier.<sup>1b</sup> Acenaphthene was first distilled under vacuum and then recrystallized from absolute alcohol. The melting point of the purified sample was 94.2°. Pyrocatechol and  $\beta$ -naphthylamine were purified by successive recrystallization from distilled water. The melting points of the purified samples were 103.8 and 111.0°, respectively.

**Kinetic Study of the Solid-State Reaction.** The procedure employed for studying the kinetics of the solid-state reaction between (i) picric acid and acenaphthene, (ii) picric acid and  $\beta$ -naphthylamine, and (iii) picric acid and pyrocatechol was the same as described earlier.<sup>1b,2</sup> The kinetics were also studied when the reactants were separated by a known distance. Such a study could not be made for  $\beta$ -naphthylamine, since a negligible reaction occurred under such conditions. Six to seven runs were made for kinetic studies at each temperature and for a definite particle size.

Equation 1 fits the kinetic data when the reactants are in contact. On plotting  $\log(\xi^2/t)$  against  $\xi$ , a straight line is obtained. The parameters of eq 1 for different temperatures and for different particle size are

**Table I:** Influence of Temperature on  $k_i$  (Particle Size, above 150 mesh)

Reactants	Temp ( $\pm 1$ ), °C	$k_i$ , cm <sup>2</sup> /hr	$p$ , cm <sup>-1</sup>
Acenaphthene	25	$(2.50 \pm 0.00) \times 10^{-4}$	$35 \pm 8$
	35	$(3.33 \pm 0.14) \times 10^{-4}$	$22 \pm 8$
	45	$(7.92 \pm 0.00) \times 10^{-4}$	$14 \pm 8$
	55	$(1.47 \pm 0.06) \times 10^{-3}$	$14 \pm 8$
$\beta$ -Naphthylamine	35	$(2.44 \pm 0.07) \times 10^{-5}$	$55 \pm 1$
	55	$(7.92 \pm 0.00) \times 10^{-5}$	$57 \pm 1$
	65	$(1.25 \pm 0.02) \times 10^{-4}$	$57 \pm 1$
Pyrocatechol	45	$(1.54 \pm 0.28) \times 10^{-3}$	$19 \pm 2$
	55	$(2.34 \pm 0.06) \times 10^{-3}$	$14 \pm 2$
	65	$(5.47 \pm 0.13) \times 10^{-3}$	$15 \pm 2$

given in Tables I and II, respectively. These are the mean parameters obtained from six runs.

**Table II:** Influence of Particle Size on  $k_i$  ( $45 \pm 1^\circ$ )

Reactants	Particle size, mesh	$k_i$ , cm <sup>2</sup> /hr	$p$ , cm <sup>-1</sup>
Acenaphthene <sup>a</sup>	120-150	$2.23 \times 10^{-3}$	$13 \pm 1$
	170-200	$1.51 \times 10^{-3}$	$13 \pm 1$
	200-240	$1.14 \times 10^{-3}$	$16 \pm 1$
	240-270	$4.77 \times 10^{-4}$	$12 \pm 1$
Pyrocatechol <sup>a</sup>	100-120	$1.51 \times 10^{-3}$	$14 \pm 2$
	120-150	$1.34 \times 10^{-3}$	$21 \pm 2$
	170-200	$1.02 \times 10^{-3}$	$20 \pm 2$
	200-240	$4.35 \times 10^{-4}$	$18 \pm 2$

<sup>a</sup> The higher values of  $k$ , as compared with those reported in Table I are due to the fact that since in the latter case the particle size was above 150 mesh the material contained large numbers of particles finer than 270 mesh.

**Table III:** Kinetic Parameters When the Reactants are Kept Apart (Particle Size, above 150 mesh)

Reactants	Temp ( $\pm 1$ ), °C	$d$ , cm	$k$ , cm <sup>2</sup> /hr	$p'$ , cm <sup>-1</sup>
Acenaphthene	45	1.401	$5.6 \times 10^{-8}$	2.5
		0.825	$2.8 \times 10^{-5}$	
		0.467	$6.2 \times 10^{-5}$	
	55	0.218	$1.5 \times 10^{-4}$	2.0
		1.283	$3.0 \times 10^{-5}$	
		0.835	$5.7 \times 10^{-5}$	
65	0.567	$1.1 \times 10^{-4}$	1.3	
		0.253		$2.2 \times 10^{-4}$
		1.252		$1.5 \times 10^{-4}$
	0.909	$1.7 \times 10^{-4}$	1.3	
		0.617		$2.6 \times 10^{-4}$
		0.335		$3.8 \times 10^{-4}$
Pyrocatechol	45	0.810	$2.5 \times 10^{-5}$	2.3
		0.763	$3.3 \times 10^{-5}$	
		0.446	$6.1 \times 10^{-5}$	
	65	0.256	$9.6 \times 10^{-5}$	1.5
		1.496	$4.9 \times 10^{-5}$	
		1.226	$8.3 \times 10^{-5}$	
1.006	$10.6 \times 10^{-5}$	1.5		
	0.815		$12.5 \times 10^{-5}$	

When the reactants are separated by a distance  $d$ , the kinetic data are fitted by the equation

$$\xi^2 = kt + c \quad (3)$$

where  $k$  and  $c$  are constants.  $k$  is found to depend on  $d$  in the following manner

$$k = A'e^{-p'd} \quad (4)$$

where  $A'$  and  $p'$  are constants and  $d$  is the length of the air gap. When  $\log k$  is plotted against  $d$ , a straight line

(2) R. P. Rastogi, P. S. Bassi, and S. L. Chaddha, *J. Phys. Chem.*, **66**, 2707 (1962).

is obtained. The parameters of eq 4 are given in Table III.

When  $\log k_i$  is plotted against  $1/T$ , a straight line is obtained. The values of the energy of activation ( $E$ ), the free energy of activation for diffusion ( $\Delta G^*$ ), the entropy of activation for diffusion ( $\Delta S^*$ ), and the enthalpy of activation for diffusion ( $\Delta H^*$ ) are given in Table IV. From Table IV, it appears that except for  $\alpha$ -naphthol, the entropy of activation for diffusion in all cases is negative. This means that the entropy in the activated state is less than that in the initial state. In other words, the activated state is more ordered. It is evident that the vapor-phase diffusion would involve a disordered state and  $\Delta S^*$  would then be positive. This means that vapor-phase diffusion is not significant in the above reactions. This is also confirmed by the lower values of energy of activation as compared with the heat of sublimation.

**Table IV:** Energy of Activation, Enthalpy of Activation, Free Energy of Activation, and Entropy of Activation for Diffusion

Reactants	Particle size, mesh	$E$ , kcal/mol	$\Delta H^*$ , kcal/mol	$\Delta G^*$ , kcal/mol	$\Delta S^*$ , cal/mol deg
Acenaphthene	Above 150	11	11	12	-6
$\beta$ -Naphthylamine	Above 150	11	10	14	-13
Pyrocatechol	Above 150	10	9	13	-13
$\alpha$ -Naphthol <sup>a</sup>	Above 150	19	18	18	+18
$\beta$ -Naphthol <sup>a</sup>	Above 150	10	9	14	-14
Naphthalene <sup>b</sup>	100	11	10	17	-23
Phenanthrene <sup>b</sup>	100	8	8	23	-49
Anthracene <sup>b</sup>	100	6	5	23	-58

<sup>a</sup> See ref 1b. <sup>b</sup> R. P. Rastogi, P. S. Bassi, and S. L. Chaddha, *J. Phys. Chem.*, **67**, 2569 (1963).

We will now examine the dependence of  $k_i$  on particle size. If temperature is kept constant, it follows from eq 2 that

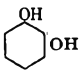
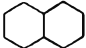
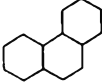
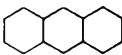
$$k_i = \theta r^2 \quad (5)$$

where  $\theta = 4n\pi D_0 e^{-E/RT}$ . It is found that  $k_i$  varies directly with the square of the radius of particle, since when  $k_i$  is plotted against  $r^2$  a straight line is obtained. This further confirms the fact that surface migration plays an important role in solid-state diffusion in the present case, in agreement with our earlier finding.<sup>1b</sup>

Table V shows how  $k_i$  depends on the size of reactant molecules. It appears that surface migration of bulky molecules is more difficult as compared with simpler molecules. This is expected.

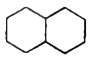
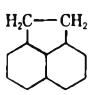
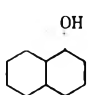
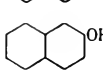
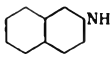
In order to understand the nature of surface migration, it is interesting to compare the values of  $k_i$  for molecules having different degrees of asymmetry. It would be easier for a flat molecule to drift on the surface. The asymmetry would depend on the dipole moment,

**Table V:** Influence of Molecular Size on  $k_i$  (Particle Size, 100 mesh;  $45 \pm 1^\circ$ )

Reactants	$k_i$ , cm <sup>2</sup> /hr	Ref
	$1.51 \times 10^{-3}$	a
	$4.68 \times 10^{-4}$	b
	$4.80 \times 10^{-6}$	b
	$2.39 \times 10^{-8}$	b

<sup>a</sup> This work. <sup>b</sup> R. P. Rastogi, P. S. Bassi, and S. L. Chaddha, *J. Phys. Chem.*, **67**, 2569 (1963).

**Table VI:** Dependence of  $k_i$  on Dipole Moment (Particle Size, above 150 mesh;  $35 \pm 1^\circ$ )

Reactants	Dipole moment, D	$k_i$ , cm <sup>2</sup> /hr	Ref
	0.00	$4.22 \times 10^{-4}$	a
	0.79	$3.35 \times 10^{-4}$	b
	1.91	$1.84 \times 10^{-4}$	c
	2.01	$6.74 \times 10^{-5}$	c
	2.12	$2.44 \times 10^{-5}$	b

<sup>a</sup> R. P. Rastogi, P. S. Bassi, and S. L. Chaddha, *J. Phys. Chem.*, **67**, 2569 (1963). <sup>b</sup> This work. <sup>c</sup> See ref 1b. <sup>d</sup> See ref 3.

and hence the values of  $k_i$  should decrease with an increase in the values of the dipole moment.<sup>3</sup> The trend of values recorded in Table VI justifies this conclusion.

In order to ascertain the extent of asymmetry in a molecule, the coordinates of the center of gravity of acenaphthene,  $\alpha$ -naphthol,  $\beta$ -naphthol, and  $\beta$ -naphthylamine with respect to the center of gravity of naphthalene as the origin were estimated. The line joining the carbon nuclei in 9 and 10 positions was taken as the  $y$  axis, whereas the plane of the naphthalene molecule was taken as the  $x$ - $y$  plane. The coordinates of the center of gravity are given in Table VII. It is clear from Table VII that as the asymmetry increases

(3) A. L. McClellan, "Tables of Experimental Dipole Moments," W. A. Freeman and Co., San Francisco, Calif., 1963.

**Table VII:** Coordinates of the Center of Gravity

Molecules <sup>a</sup>	<i>x</i>	<i>y</i>	<i>z</i>
Naphthalene	0.00	0.00	0.00
Acenaphthene	0.00	0.550	0.00
$\alpha$ -Naphthol	0.089	0.371	0.00
$\beta$ -Naphthol	0.397	0.115	0.00
$\beta$ -Naphthylamine	0.403	0.150	$\approx 0.00$

<sup>a</sup> The data for bond distances and bond angles were taken from structure reports (N. V. A. Oosthoek's Uitgevers Mij, Utrecht, 1948-1957). For the purpose of calculation the first four molecules are considered to be planar.

the value of  $k_i$  decreases. In the case of  $\alpha$ -naphthol,  $\beta$ -naphthol, and  $\beta$ -naphthylamine the shift of the center of gravity  $r$  ( $r = \sqrt{x^2 + y^2 + z^2}$ ) is 0.381, 0.413,

and 0.432, respectively. The values of  $k_i$  also show this sequence, showing thereby that the asymmetry of the molecules plays an important role in the solid-state reaction where surface migration plays a predominant role.

From the above study, surface migration may be pictured as follows. The surface of the reactant which diffuses into the other is in a state of disturbance. The molecules at the surface have a tendency to vaporize. However, they sometimes find it easier to drift on the surface. The tendency of surface migration is affected by the asymmetry of the molecules. In a similar manner, bulky molecules have a smaller tendency for surface migration.

*Acknowledgment.* N. B. S. is thankful to the Council of Scientific and Industrial Research for supporting the investigation.

## Adsorption Characteristics of Water-Soluble Polymers. I.

### Poly(vinyl alcohol) and Poly(vinylpyrrolidone) at the Aqueous-Air Interface

by J. E. Glass

Research and Development Department, Union Carbide Corporation, Chemicals and Plastics, South Charleston, West Virginia 25303 (Received April 24, 1968)

Relatively little is known about the interfacial characteristics of adsorbed macromolecules. This article relates part of a general investigation into the interfacial behavior of water-soluble polymers. The surface tension of two classes of water-soluble polymers, poly(vinyl alcohol) and poly(vinylpyrrolidone), were studied as a function of concentration, time, temperature, and molecular weight. The investigation of polymeric alcohols, with varying degrees of acetylation, showed the surface activity function to be relatable to the polymer's cohesive energy density. A linear relationship was not observed between hydrocolloids of different chemical structure. This observation is discussed with respect to the contributing factors of a polymer's total cohesive energy density and surface tension parameters. The surface activities of vinyl alcohol-vinyl acetate (11-12%) copolymers are observed to have negligible to slightly positive temperature coefficients. In contrast to this, a poly(vinyl alcohol) material with less than 1% acetylation is observed to exhibit a strongly exothermic adsorption behavior. Examination of vinylpyrrolidone polymers reveals that both high and low molecular weight species also possess negative surface activity-temperature coefficients. Employing an exponential, Fickian model, equilibrium values and diffusion coefficients were calculated from the time dependence of the surface activity measurements. Thermodynamic parameters of adsorption were determined from the equilibrium values.

#### Introduction

Models pertaining to the solution theory<sup>1-3</sup> of macromolecular adsorption have been suggested over the past 20 years. (There are numerous publications dealing with the statistical mechanics of isolated, interfacial macromolecules. References to earlier works are given in ref 1-3.) The adsorbate has been analyzed as an isolated species<sup>1-3</sup> and as an entity capable of interfacial interactions.<sup>4-8</sup>

In connection with the theoretical treatment of the adsorption phenomena, there has been rather extensive publication of data covering adsorption from solution at solid interfaces.<sup>9-18</sup> The facts established from such polymer adsorption studies have been reviewed by Stromberg,<sup>16</sup> Patat,<sup>17</sup> and Silberberg.<sup>18</sup> (Numerous studies have been made of macromolecular adsorption at solid interfaces. Reference to data prior to 1964 may be found in three<sup>16-18</sup> reviews on this subject.) Investigations have provided similar data with respect to spread<sup>19</sup> films. In contrast to these areas, little is known about the surface tension characteristics of synthetic polymer<sup>20-26</sup> solutions.

This study deals with the relatively neglected area of macromolecular adsorption at the aqueous-air interface. The investigation is involved with the determination of the thermodynamic parameters of adsorption, the number of polymer segments present in the interfacial region (the Gibbs excess functions), and the relative inter-

facial intrinsic diffusion coefficients. As such, it is a study of the surface activity of water-soluble polymers as a function of concentration, time, temperature, and molecular weight.

- (1) A. Silberberg, *J. Chem. Phys.*, **48**, 2835 (1968).
- (2) F. L. McCrackin, *ibid.*, **47**, 1980 (1967).
- (3) C. A. J. Hoeve, *ibid.*, **44**, 1505 (1966).
- (4) M. L. Huggins, *Makromol. Chem.*, **87**, 119 (1965); *J. Amer. Chem. Soc.*, **86**, 3535 (1964).
- (5) J. Llopis and J. A. Subirana, *J. Polym. Sci.*, **60**, 113 (1962).
- (6) T. Kawai, *ibid.*, **35**, 401 (1959).
- (7) J. T. Davies, *J. Colloid Sci. Suppl.*, **1**, 9 (1954).
- (8) L. Ter Minassia-Saraga and I. Prigogine, *Mém. Serv. Chim. État (Paris)*, **38**, No. 2, 109 (1953).
- (9) G. J. Howard and P. McConnell, *J. Phys. Chem.*, **71**, 2974, 2981, 2991 (1967).
- (10) G. Steinberg, *ibid.*, **71**, 292 (1967).
- (11) I. R. Miller, *J. Polym. Sci., Part C*, **16**, 1433 (1967).
- (12) F. W. Rowland and F. R. Eirich, *ibid., Part A-1*, **4**, 2033, 2401 (1966).
- (13) C. Thies, *J. Phys. Chem.*, **70**, 3783 (1966).
- (14) B. J. Fontana, *ibid.*, **70**, 1801 (1966).
- (15) R. R. Stromberg, D. J. Tutas, and E. Passaglia, *ibid.*, **69**, 3955 (1965).
- (16) R. R. Stromberg, "Treatise on Adhesion and Adhesives," Vol. 1, R. L. Patrick, Ed., Marcel Dekker, Inc., New York, N. Y., 1967, Chapter 3.
- (17) F. Patat, E. Killmann, and C. Schliebener, *Fortschr. Hochpolym. Forsch.*, **3**, 332 (1964).
- (18) A. Silberberg, *J. Phys. Chem.*, **66**, 1884 (1962).
- (19) For a review of this area, see G. L. Gaines, "Insoluble Monolayers at Liquid-Gas Interfaces," Interscience Publishers Inc., New York, N. Y., 1966.

### Experimental Section

Surface tension measurements were conducted at 25, 50, and 70° ( $\pm 0.1^\circ$ ) using the drop-weight method. A stalagmometer with a ground-glass tip was employed. The tip of the apparatus was enclosed in a glass container with a vertical side arm for pressure equilibration. The readings were taken in a constant-temperature bath. A Hallikainen temperature-control unit was employed. The apparatus was cleaned with chromic acid and distilled water prior to each determination. After the initial cleaning the stalagmometer was rinsed with the aqueous polymer solution to be investigated. This procedure allowed for adsorption of polymer molecules onto the glass surface previous to the actual determination. The data were calculated using the correction factors of Harkins and Brown.<sup>27</sup> At least 20 drops were averaged for each determination. Nitrogen gas inlet and vacuum-outlet micrometer metering valves were employed with the stalagmometer in order to regulate the development of the drop's growth. Droplet lifetimes of 10, 30, and 60 sec were investigated. The precise lifetime could not be achieved in every determination; the readings were corrected to the exact times desired (10, 30, and 60 sec) by a Lagrangian interpolation. All of the values listed in the various tables of this report were calculated with an IBM 360 computer. The calculations were performed in a two-part program. Results from the first program are shown in the various figures. A second program, not incorporating very low concentration data, employed counter systems which facilitated calculation of the various Gibbs equilibrium isotherm parameters. When applicable, least-squares analysis was employed in the determination of each value. The experimental accuracy, depending upon the polymer's concentration and surface activity, varied from  $\pm 0.2$  to  $\pm 0.6$  dyn/cm. Owing to the experimental inaccuracies at low concentrations, the thermodynamic parameters of adsorption cannot be determined accurately at infinite dilution. It was necessary that these parameters be proportioned from the more reliable higher concentration data.

The interaction between the surface viscoelastic property of an aqueous polymer solution and the rate of drop formation affects only slightly the absolute nature of the surface tension determinations. This viscoelastic parameter is presently under investigation. Preliminary evidence, at the low concentrations employed in this study, indicates that it does not affect the relative nature nor the significance of the findings. This observation is supported by the agreement of parts of this study with the studies on poly(vinyl alcohol) *via* the pendant-drop method<sup>24</sup> and also by the studies of polyethylene glycol *via* the capillary-rise method<sup>20</sup> and *via* the ring-balance method<sup>21</sup> at higher concentrations (for the latter studies see the ensuing paper on the ethylene oxide polymers).

The polymers employed in these investigations were commercially obtained materials. They were dried to a constant weight and gave a negligible ash residue. Each of the polymeric materials was dissolved in distilled water which had been previously degassed with high-purity nitrogen. The molecular weight distribution of the poly(vinylpyrrolidone) samples (General Aniline and Film Corp.) was determined by sedimentation velocity measurements. The molecular weight distribution in this series of polymers was found to be greater than a random distribution. The weight-average molecular weight of the poly(vinyl alcohol) samples (Wacker-Chemie and the Du Pont Co.) was obtained from commercial literature.<sup>28</sup> The per cent hydrolysis of the polymeric alcohols was determined by a caustic acid titration procedure.

### Theoretical Model

An exponential model

$$\pi = \pi_{\infty} e^{-k/t} \quad (1)$$

where  $\pi$  is the surface pressure at time  $t$ ,  $\pi_{\infty}$  is the surface pressure at infinite time,  $k$  is a constant, and  $t$  is the time in seconds, was assumed for the adsorption of macromolecules at the aqueous-air interface. This model was based upon results obtained with the 88–89% hydrolyzed poly(vinyl alcohol) (PVA) solutions. Such a model is consistent with the PVA aging experiments observed previously *via* the pendant-drop technique.<sup>24</sup> With several polymer solutions a time dependence of the surface tension parameter was not observed. In these instances the values obtained were equated to equilibrium values. In order to obtain the finite time interval required to reach the exponential equilibrium value when a time dependence was observed, a rate of decrease in the surface tension with time function,  $\alpha$ , was selected

$$\alpha = \frac{d\pi/dt}{\pi} = 10^{-8} \quad (2)$$

A value of  $10^{-8}$  was selected for the rate-of-decrease function, since this value was found to give an approximate equilibrium time greater than that observed by

(20) E. L. Lovell and H. Hibbert, *J. Amer. Chem. Soc.*, **62**, 2144 (1940).

(21) A. Couper and D. D. Eley, *J. Polym. Sci.*, **3**, 345 (1948).

(22) A. Katchalsky and I. Miller, *J. Phys. Chem.*, **55**, 1182 (1951).

(23) C. Capitani and G. Righi, *Ind. Chim. Belge.*, **20**, Spec. No. 691, 695 (1955).

(24) H. L. Frisch and S. Al-Madfai, *J. Amer. Chem. Soc.*, **80**, 3561, 5613 (1958).

(25) K. Fukawa, T. Asakura, and H. Daimon, *Kobunshi Kagaku*, **18**, 596 (1961).

(26) S. Hayashi, C. Nakano, and T. Motoyama, *ibid.*, **21**, 300 (1964).

(27) W. D. Harkins and F. E. Brown, *J. Amer. Chem. Soc.*, **41**, 499 (1919).

(28) "Gelvatol: Polyvinyl Alcohol, Properties and Uses," Shawinigan Resins Corp., Technical Booklet, Springfield, Mass., 1964.

an independent technique<sup>29</sup> for surfactant molecules. This approximate equilibrium time, together with the Gibbs excess function calculated from the equation

$$\Gamma = -\frac{1}{RT} \frac{d\gamma}{d \ln c} \quad (3)$$

was employed in the equation

$$D = \frac{\left(\frac{\Gamma}{N}\right)^2}{t(\text{eq})} \quad (4)$$

where  $\Gamma$  is the surface excess concentration (mol/cm<sup>2</sup>),  $N$  is the concentration (mol/ml) in the bulk solution, and  $t(\text{eq})$  is the time required to reach a surface pressure equal to within  $10^{-8}$  the value at infinite time, for the calculation of the relative diffusion coefficients. Excess parameters calculated *via* the Silberberg modified adsorption equation<sup>18</sup> will be presented in a future paper. The diffusion model is a simplified form of the one first derived by Ward and Tordai.<sup>30</sup> The model has been shown to be adequate for a diffusion process to the mercury-aqueous interface in the reduction of cuprous ions<sup>31</sup> and for the interfacial diffusion of poly(methacrylic acid).<sup>32</sup> The concentration dependence is removed from the relative diffusion coefficients through the equation

$$D = D_0(1 + k_D C) \quad (5)$$

Modified empirical Schofield-Rideal and Henry's law equations were employed to evaluate thermodynamic parameters of adsorption. A similar approach had been reported by Cassel and Formstecher.<sup>33</sup> The modified equations employed are two approaches, suggested by Ross and Chen.<sup>34</sup> An analysis of the results based upon the macromolecular considerations of Flory and Huggins is being completed and will be reported in the near future.

## Results

The surface tension characteristics of aqueous poly(vinyl alcohol) solutions, *via* the pendant-drop method, had been previously examined by Al-Madfai and Frisch.<sup>24</sup> Their investigations were conducted at relatively high concentrations (0.5 and 1.0 wt %) and were concerned with the dependence of the surface tension parameter upon the age of the solution drop surface. These workers<sup>24</sup> suggested that the magnitude of the observed relaxation times shows diffusion to be the controlling factor to interfacial adsorption. Fukawa and coworkers,<sup>25</sup> employing a vertical-plate method, suggested that aging is not simply a diffusion process at high concentrations of PVA. The authors invoke a steric barrier by adsorbed macromolecules which inhibits further interfacial diffusion. Hayashi and coworkers<sup>26</sup> have shown, *via* the weight-drop procedure, that the surface activity of vinyl alcohol-vinyl acetate copolymers is related to the copolymer's chemical con-

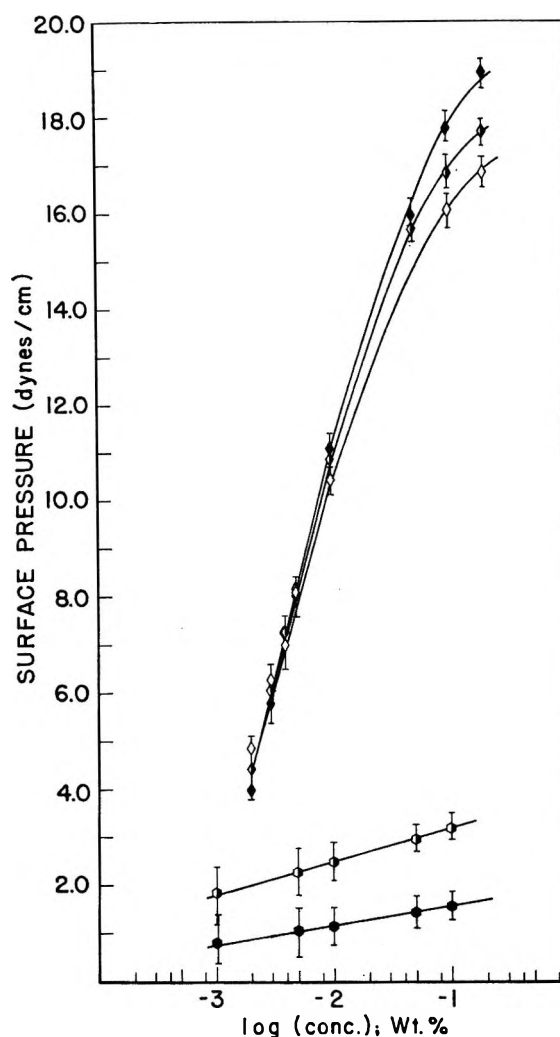


Figure 1. Surface activity-temperature dependence of poly(vinyl alcohol)-aqueous solutions:  $\diamond$ , 89.0% hydrolysis,  $1.3 \times 10^5$  weight-average molecular weight, 25°;  $\square$ , 89.0% hydrolysis,  $1.3 \times 10^5$  weight-average molecular weight, 50°;  $\bullet$ , 89.0% hydrolysis,  $1.3 \times 10^5$  weight-average molecular weight, 70°;  $\circ$ , 99.3% hydrolysis,  $1.2 \times 10^5$  weight-average molecular weight, 50°;  $\ominus$ , 99.3% hydrolysis,  $1.2 \times 10^5$  weight-average molecular weight, 70°.

stitution. This investigation indicated that block copolymers are more surface active than random vinyl alcohol-vinyl acetate copolymers.

The surface pressure values, relative intrinsic interfacial diffusion coefficients, and thermodynamic parameters of adsorption for the poly(vinyl alcohol) and poly(vinylpyrrolidone) families are given in Tables I-III. The temperature dependencies of the poly(vinyl alcohol) materials are shown graphically in Figure 1. The

(29) E. B. Greenhill, *Trans. Faraday Soc.*, **45**, 625 (1949).

(30) A. F. H. Ward and L. Tordai, *J. Chem. Phys.*, **14**, 453 (1946).

(31) P. Delahay and I. Trachtenberg, *J. Amer. Chem. Soc.*, **79**, 2355 (1957).

(32) I. R. Miller, *Trans. Faraday Soc.*, **57**, 301 (1961).

(33) H. Cassel and M. Formstecher, *Kolloid Z.*, **61**, 18 (1932).

(34) S. Ross and E. S. Chen, *Ind. Eng. Chem.*, **57**, No. 7, 40 (1965).

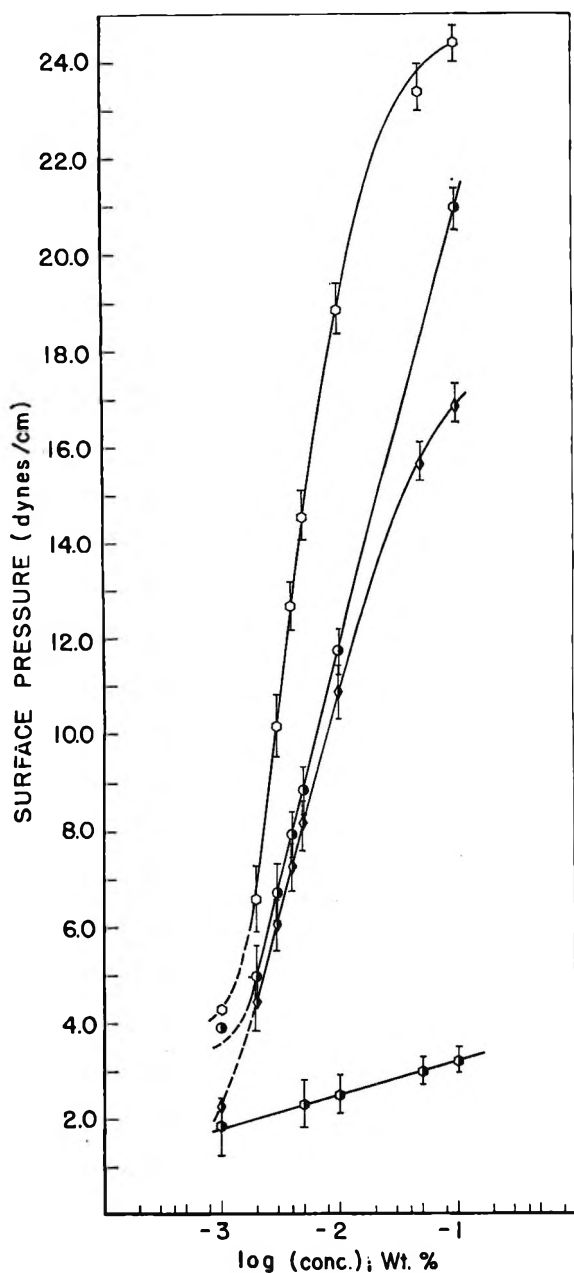


Figure 2. Surface activity-hydrolysis dependence of poly(vinyl alcohol)-aqueous solutions: ○, 77.5% hydrolysis,  $1.0 \times 10^5$  weight-average molecular weight, 25°; ●, 88.7% hydrolysis,  $1.0 \times 10^4$  weight-average molecular weight, 50°; ◆, 89.0% hydrolysis,  $1.3 \times 10^5$  weight-average molecular weight, 50°; ◼, 99.3% hydrolysis,  $1.2 \times 10^5$  weight-average molecular weight, 50°.

89% hydrolyzed vinyl alcohol-vinyl acetate copolymer displays a slightly endothermic adsorption characteristic. The 99% hydrolyzed polymeric alcohol exhibits a relatively strong exothermic behavior.

The effect of the copolymer's per cent hydrolysis on the solution's surface activity is shown in Figure 2. The effect of molecular weight, in the 89% hydrolysis range, also is shown in Figure 2. The lower the per cent hydrolysis the more surface active the vinyl alcohol copolymer. The 77% hydrolyzed material was not

investigated at 50° since the product precipitates from aqueous solution at approximately 46°. The 99% hydrolyzed polymeric alcohol was not investigated at 25° because it precipitates from solution on standing at room temperature.

The present investigations of low and high molecular weight, 88-89% hydrolyzed poly(vinyl alcohol) samples reveal data which contrast with those obtained by Al-Madfai and Frisch.<sup>24</sup> In their investigation of low molecular weight polymers, the higher molecular weight material exhibited the greater surface activity. A random-coil configuration, for such low molecular weight materials, would not be predicted.<sup>35-38</sup> A different adsorption rheology could account for the different surface activity-molecular weight dependence noted in the present work. The observed difference in this investigation is not due to a difference in intrinsic diffusion coefficients, since this parameter was found to be smallest for the lower molecular weight material. In independent coalescence studies of liquid drops, a real difference in the stabilizing behavior was evident between the low and high molecular weight polymeric alcohols. The low molecular weight material exhibited a strong interfacial aging characteristic with time, *i.e.*, a rigid gel-like film formed that could be siphoned from organic-aqueous interfaces. A cursory examination of methyl cellulose materials, which possess approximately the same surface tension characteristics, reveals that these materials also exhibit an aging effect at a liquid-liquid interface. The aging tendency of the low molecular weight methyl cellulose species was found to be greater at a given time interval than that noted for a correspondingly higher molecular weight material. This faster aging tendency of moderately surface active macromolecules probably reflects a greater reorientation ability of lower (to *ca.* 10,000) molecular weight species. As such this aging tendency may represent a change of monolayer state, *i.e.*, from a gaseous type to a liquid or condensed-liquid type monolayer. This type of reorientation and phase-change capability is presumably not significant for the more compact species (<10,000 mol wt). The initiation of such a phase change could account for a slightly greater segment density of the lower molecular weight species at room temperature.

The time dependence of the surface activity function for the 89% hydrolyzed vinyl alcohol-vinyl acetate copolymer is shown in Figure 3. A reproducible time dependence of the surface activity parameter could not be obtained for the 99% hydrolyzed material.

(35) H. Marzolph and G. V. Schulz, *Makromol. Chem.*, **13**, 120 (1954).

(36) P. Doty, J. C. Mitchell, and A. E. Woodward, *J. Amer. Chem. Soc.*, **79**, 3958 (1957).

(37) J. A. Faucher and R. W. Callard, unpublished results.

(38) R. D. Lundberg, F. E. Bailey, and R. W. Callard, *J. Polym. Sci., Part A-1*, **4**, 1563 (1966).

Table I: Adsorption Parameters of Poly(vinyl alcohols) at the Aqueous-Air Interface

Wt-av mol wt	% hy- drolysis <sup>a</sup>	Temp. °C	Concn		Surface pressure, <sup>b</sup> dyn/cm				Time required to reach equil, hr	Relative intrinsic diffusion coeff, (D <sub>0</sub> ), cm <sup>2</sup> /sec	Surface excess function (10 <sup>18</sup> Γ), mol/cm <sup>2</sup>	
			Wt %	M	10 sec	30 sec	60 sec	Equil <sup>c</sup>				
1.2 × 10 <sup>6</sup>	99.3	50		0.859 × 10 <sup>-8</sup>	...	...	...	1.82 <sup>d</sup>	...	...	0.108	
				0.430 × 10 <sup>-7</sup>	...	...	...	2.29	...	...		
				0.859 × 10 <sup>-7</sup>	...	...	...	2.49	...	...		
				0.430 × 10 <sup>-6</sup>	...	...	...	2.96	...	...		
				0.859 × 10 <sup>-6</sup>	...	...	...	3.19	...	...		
			70		0.850 × 10 <sup>-8</sup>	...	...	...	0.81 <sup>d</sup>	...	...	0.053
				0.425 × 10 <sup>-7</sup>	...	...	...	1.06	...	...		
				0.850 × 10 <sup>-7</sup>	...	...	...	1.16	...	...		
				0.425 × 10 <sup>-6</sup>	...	...	...	1.41	...	...		
				0.850 × 10 <sup>-6</sup>	...	...	...	1.58	...	...		
1.0 × 10 <sup>4</sup>	88.7	25	0.0020	0.199 × 10 <sup>-8</sup>	3.40	5.38	6.04	6.77	7.29	7.82 × 10 <sup>-18</sup>	1.57	
			0.0030	0.299 × 10 <sup>-8</sup>	4.51	6.83	7.57	8.40	6.93			
			0.0040	0.399 × 10 <sup>-8</sup>	5.21	7.84	8.69	9.62	6.88			
			0.0050	0.499 × 10 <sup>-8</sup>	5.98	8.66	9.51	10.43	6.55			
			0.0100	0.997 × 10 <sup>-8</sup>	8.29	11.23	12.11	13.06	5.92			
			0.1000	0.997 × 10 <sup>-6</sup>	18.07	19.90	20.39	20.88	3.34			
			50		0.198 × 10 <sup>-6</sup>	3.16	4.52	4.95	5.41	6.45	9.47 × 10 <sup>-18</sup>	1.62
				0.296 × 10 <sup>-6</sup>	4.27	6.12	6.69	7.32	6.45			
				0.395 × 10 <sup>-6</sup>	5.19	7.27	7.90	8.60	6.24			
				0.494 × 10 <sup>-6</sup>	6.01	8.18	8.84	9.55	5.98			
				0.988 × 10 <sup>-6</sup>	9.10	11.14	11.72	12.33	4.84			
				0.988 × 10 <sup>-6</sup>	18.26	20.41	20.99	21.58	3.59			
			70		0.196 × 10 <sup>-6</sup>	2.61	3.66	3.99	4.34	6.26	10.5 × 10 <sup>-18</sup>	1.66
				0.293 × 10 <sup>-6</sup>	3.95	5.38	5.82	6.28	5.99			
				0.391 × 10 <sup>-6</sup>	4.92	6.62	7.13	7.68	5.87			
				0.489 × 10 <sup>-6</sup>	5.68	7.59	8.16	8.77	5.80			
				0.978 × 10 <sup>-6</sup>	8.35	10.61	11.27	11.96	5.27			
				0.978 × 10 <sup>-6</sup>	18.21	20.37	20.95	21.54	3.60			
1.3 × 10 <sup>4</sup>	89.0	25	0.0020	0.160 × 10 <sup>-7</sup>	2.60	4.29	4.86	5.51	7.62	8.5 × 10 <sup>-16</sup>	1.44	
			0.0030	0.239 × 10 <sup>-7</sup>	3.51	5.60	6.29	7.06	7.34			
			0.0040	0.319 × 10 <sup>-7</sup>	4.26	6.55	7.29	8.12	7.05			
			0.0050	0.399 × 10 <sup>-7</sup>	4.93	7.30	8.05	8.88	6.74			
			0.0100	0.798 × 10 <sup>-7</sup>	7.16	9.66	10.41	11.22	5.89			
			0.1000	0.798 × 10 <sup>-6</sup>	13.26	15.48	16.09	16.72	4.23			
			50		0.160 × 10 <sup>-6</sup>	14.44	16.32	16.83	17.35	3.77	12.1 × 10 <sup>-16</sup>	1.61
				0.158 × 10 <sup>-7</sup>	2.74	4.01	4.41	4.84	6.63			
				0.237 × 10 <sup>-7</sup>	3.78	5.50	6.04	6.63	6.59			
				0.316 × 10 <sup>-7</sup>	4.48	6.55	7.21	7.92	6.64			
				0.395 × 10 <sup>-7</sup>	5.12	7.40	8.11	8.89	6.52			
				0.790 × 10 <sup>-7</sup>	7.40	10.06	10.87	11.74	5.97			
				0.395 × 10 <sup>-6</sup>	12.54	14.98	15.67	16.38	4.54	15.8 × 10 <sup>-16</sup>	1.66	
				0.790 × 10 <sup>-6</sup>	14.43	16.31	16.82	17.34	3.77			
				0.158 × 10 <sup>-6</sup>	16.25	17.38	17.68	17.98	2.80			
			70		0.156 × 10 <sup>-7</sup>	2.95	3.76	4.00	4.25			5.30
				0.235 × 10 <sup>-7</sup>	4.14	5.41	5.79	6.19	5.58			
				0.313 × 10 <sup>-7</sup>	4.97	6.52	6.98	7.47	5.61			
1.0 × 10 <sup>6</sup>	77.5	25		0.192 × 10 <sup>-7</sup>	2.87	5.56	6.56	7.73	8.74	5.20 × 10 <sup>-15</sup>	4.31	
				0.0030	0.288 × 10 <sup>-7</sup>	4.04	8.45	10.16	12.21			9.24
				0.0040	0.383 × 10 <sup>-7</sup>	5.30	10.65	12.68	15.09			8.99
				0.0050	0.479 × 10 <sup>-7</sup>	7.02	12.57	14.54	16.81			8.21
				0.0100	0.959 × 10 <sup>-7</sup>	14.05	17.79	18.86	20.00			5.22
				0.0500	0.479 × 10 <sup>-6</sup>	20.75	22.85	23.40	23.97			3.33
				0.1000	0.959 × 10 <sup>-6</sup>	22.51	24.02	24.41	24.80			2.73

<sup>a</sup> Mole per cent hydrolysis determined by a caustic acid titration procedure. <sup>b</sup>  $\pi = \gamma_0 - \gamma_{\text{soln}}$ . <sup>c</sup> Calculated from exponential model (eq 1). <sup>d</sup> Average values for 10-, 30-, and 60-sec data; a time dependence was not observed.



**Table II:** Thermodynamic Parameters of Poly(vinyl alcohol) Adsorption

Wt-av mol wt	% hydrolysis <sup>a</sup>	Temp, °C	$\Delta F$ , kcal/mol <sup>b</sup>	$\Delta H$ , cal/mol <sup>b</sup>	$\Delta S$ , eu <sup>b</sup>
$1.2 \times 10^5$	99.3	50	-13.0	...	...
		70	-13.3	-9240	11.7
$1.0 \times 10^4$	88.7	25	-10.7	...	...
		50	-11.7	348	37.3
$1.3 \times 10^5$	89.0	70	-12.4	105	36.5
		25	-12.1	...	...
$1.0 \times 10^5$	77.5	50	-13.2	376	42.1
		70	-14.1	172	41.5
		25	-12.3	...	...

<sup>a</sup> Per cent hydrolysis determined by a caustic acid titration procedure. <sup>b</sup> Thermodynamic functions determined from modified Gibbs equations.<sup>34</sup>

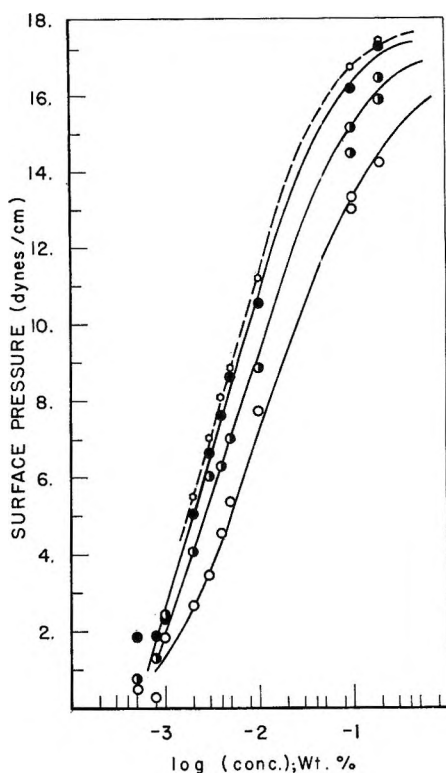


**Figure 3.** Surface activity-time dependence of 89.0% hydrolyzed poly(vinyl alcohol)-aqueous solutions (25°): ○, exponential equilibrium value; ○, 10 sec; ◐, 30 sec; ●, 60 sec.

Investigation of high and low molecular weight poly(vinylpyrrolidone) materials revealed a different type of adsorption isotherm. The data are shown with respect to their temperature and molecular weight dependence in Figure 4. The pyrrolidone polymers show slightly exothermic adsorption characteristics. No time dependence was observed. Data representative of the time studies and of the scatter in surface activity measurements are shown in Figure 5. It was

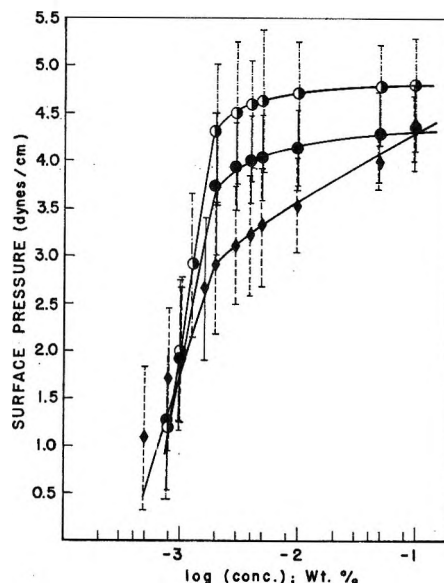


**Figure 4.** Surface activity of poly(vinylpyrrolidone)-aqueous solutions: ○,  $9.1 \times 10^5$  weight-average molecular weight, 50°; ●,  $9.1 \times 10^5$  weight-average molecular weight, 70°; ◆,  $2.5 \times 10^4$  weight-average molecular weight, 70°.

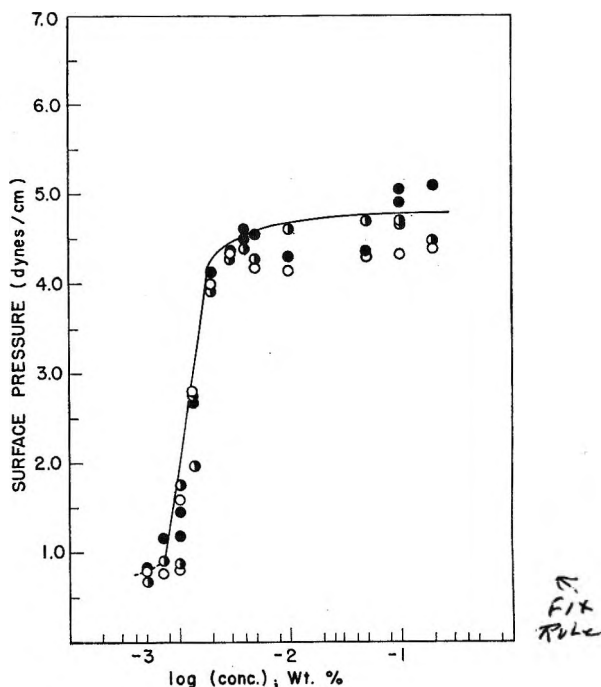


**Figure 5.** Scatter in poly(vinylpyrrolidone)-aqueous solution data ( $9.1 \times 10^5$  weight-average molecular weight, 50°): ○, 10 sec; ◐, 30 sec; ●, 60 sec.

difficult to obtain reproducible results in the pyrrolidone series.

The recent work of Assarsson<sup>39</sup> has revealed the pyrrolidone ring structure to be strongly hydrated. Little tendency toward migration to the interface would

(39) P. G. Assarsson, Ph.D. Thesis, Polytechnic Institute of Brooklyn, 1966, P. G. Assarsson, *Dissertation Abstr.*, 28B, 641 (1967).

Table III: Adsorption Parameters of Poly(vinylpyrrolidones) at the Aqueous-Air Interface

Wt-av mol wt	Temp, °C	Concn, <i>M</i>	Surface pressure (equil), <sup>a</sup> dyn/cm	Surface excess function (10 <sup>19</sup> Γ), mol/cm <sup>2</sup>	Thermodynamic parameters		
					Δ <i>F</i> , kcal/mol	Δ <i>H</i> , cal/mol	Δ <i>S</i> , eu
9.1 × 10 <sup>6</sup>	50	0.869 × 10 <sup>-9</sup>	1.21				
		0.109 × 10 <sup>-8</sup>	2.00				
		0.141 × 10 <sup>-8</sup>	2.91				
		0.217 × 10 <sup>-8</sup>	4.31				
		0.326 × 10 <sup>-8</sup>	4.50				
		0.434 × 10 <sup>-8</sup>	4.58	1.30	-14.4	...	...
		0.543 × 10 <sup>-8</sup>	4.62				
		0.109 × 10 <sup>-7</sup>	4.71				
		0.543 × 10 <sup>-7</sup>	4.78				
		0.109 × 10 <sup>-6</sup>	4.80				
	70	0.860 × 10 <sup>-9</sup>	1.26				
		0.107 × 10 <sup>-8</sup>	1.93				
		0.215 × 10 <sup>-8</sup>	3.74				
		0.322 × 10 <sup>-8</sup>	3.94				
0.430 × 10 <sup>-8</sup>		4.00	1.05	-15.3	-1030	41.6	
0.537 × 10 <sup>-8</sup>		4.04					
0.107 × 10 <sup>-7</sup>		4.14					
0.537 × 10 <sup>-7</sup>		4.29					
0.107 × 10 <sup>-6</sup>	4.35						
2.5 × 10 <sup>4</sup>	50	0.198 × 10 <sup>-7</sup>	1.38				
		0.316 × 10 <sup>-7</sup>	2.11				
		0.395 × 10 <sup>-7</sup>	2.46				
		0.632 × 10 <sup>-7</sup>	3.17				
		0.790 × 10 <sup>-7</sup>	3.45	0.58	-12.2	...	...
		0.119 × 10 <sup>-6</sup>	3.68				
		0.158 × 10 <sup>-6</sup>	3.77				
		0.198 × 10 <sup>-6</sup>	3.85				
		0.395 × 10 <sup>-6</sup>	3.97				
		0.198 × 10 <sup>-6</sup>	4.34				
	0.395 × 10 <sup>-6</sup>	4.46					
	70	0.196 × 10 <sup>-7</sup>	1.10				
		0.313 × 10 <sup>-7</sup>	1.72				
		0.391 × 10 <sup>-7</sup>	2.03				
		0.626 × 10 <sup>-7</sup>	2.67				
		0.782 × 10 <sup>-7</sup>	2.90	0.47	-12.9	-764	35.4
		0.117 × 10 <sup>-6</sup>	3.10				
		0.156 × 10 <sup>-6</sup>	3.22				
0.196 × 10 <sup>-6</sup>		3.31					
0.391 × 10 <sup>-6</sup>	3.53						
0.196 × 10 <sup>-6</sup>	3.98						
0.391 × 10 <sup>-6</sup>	4.14						

<sup>a</sup> A time dependence of the surface activity function was not discernible; values obtained were approximated to equilibrium conditions.

therefore be anticipated. In view of the Gibbs excess functions expected from cohesive energy density considerations, Assarsson's observations could account for the relatively low surface concentrations observed with pyrrolidone entities.

### Discussion

The Gibbs excess functions within the poly(vinyl alcohol) series are related to the increasing hydrophobic character of the molecular species. The hydrophobic character of the molecules is related to their solubilities

and therefore to the cohesive energy densities<sup>40</sup> of the macrostructures. The cohesive energy density function, since it reflects the negative potential energy of attraction, also will reflect the relative cohesive forces between macromolecules in the interfacial region; the lower the cohesive energy density, the greater will be the increase in the surface activity for a given amount

(40) J. H. Hildebrand and R. L. Scott, "The Solubility of Nonelectrolytes," 3rd ed, Reinhold Publishing Corp., New York, N. Y., 1950; J. H. Hildebrand and R. L. Scott, "Regular Solutions," Prentice-Hall Inc., Englewood Cliffs, N. J., 1962.

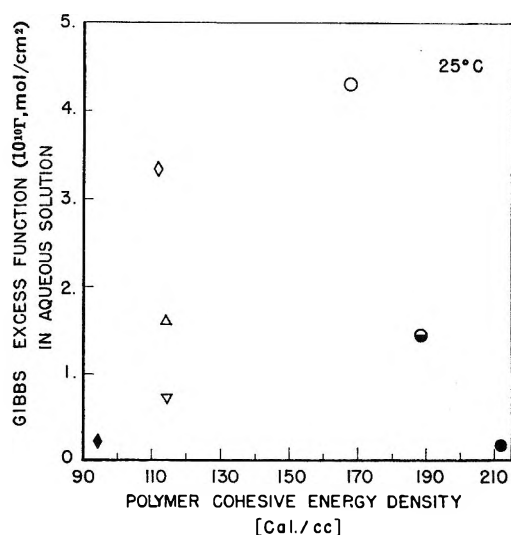


Figure 6. Surface concentration vs. total polymer cohesive energy density (cal/cc): poly(ethylene oxide): ◆, 400 number-average molecular weight; ◇,  $2.4 \times 10^6$  weight-average molecular weight; poly(vinylpyrrolidone): ▽,  $2.5 \times 10^4$  weight-average molecular weight; △,  $9.1 \times 10^6$  weight-average molecular weight; poly(vinyl alcohol): ○, 77.5% hydrolysis,  $1.0 \times 10^6$  weight-average molecular weight; ◐, 89.0% hydrolysis,  $1.3 \times 10^6$  weight-average molecular weight; ●, 99.3% hydrolysis,  $1.2 \times 10^6$  weight-average molecular weight.

of interfacial material. Taking these parameters as such within the poly(vinyl alcohol) and poly(vinylpyrrolidone) series, the Gibbs excess functions are not linearly related to the cohesive energy density (Figure 6) of the macromolecules. In order to substantiate further the nonlinearity of these parameters, data obtained with ethylene oxide polymers (see the ensuing article) are shown in Figure 6 with the poly(vinyl alcohol) and poly(vinylpyrrolidone) data. The nonlinearity is probably related to the complexities of the cohesive energy density<sup>41-43</sup> and surface tension<sup>44</sup> parameters. The molecular cohesive energy density function has been analyzed to be the summation of three independent factors: polar, nonpolar, and hydrogen bonding. A similar analysis has shown the surface tension of water to be a function of hydrogen bonding and dispersion force contributions. It is possible that the hydrogen bonding contributions to the surface tension and to the cohesive energy density of the system relate to bulk solubility and the tendency of the macromolecules toward interfacial migration. It also is likely that the nonpolar and polar contributions of the surface activity and the cohesive energy density parameters relate to the cohesive interactions of the adsorbed polymers in the interfacial region and, consequently, to the decrease in the surface tension at a given surface concentration. The effect of these contributing parameters would be a functional relationship of these various factors to the over-all surface activity of the aqueous polymer solutions. The co-

hesive energy density values shown in Figure 6 were calculated from molecular parameters obtained from a multiple regression analysis of over 500 compounds by Martin, Hoy, and Price.<sup>45</sup> The values in Figure 6 are total cohesive energy values. Procedures for the calculation, through the sum of Small's values,<sup>46</sup> of the individual contributing molar parameters (polar, nonpolar, and hydrogen bonding) to the cohesive energy density function are being developed in our laboratories.

The relative intrinsic interfacial diffusion coefficients calculated from the time dependence of the surface activity measurements are given in Table I for the vinyl alcohol-vinyl acetate copolymers. A wide variety of mechanistic interpretations may be given the interfacial adsorption of macromolecules. A discussion of the adsorption process is given in the following article with the interpretation of the poly(ethylene oxide) results.

As indicated by the adsorption free energy functions in Tables II and III, there is a substantial driving force for macromolecular interfacial adsorption. In general, the interfacial adsorption of macromolecular species results from a total increase in the entropy of the system. The total entropy change upon adsorption is the sum of two competing entropic factors indicated in eq 6. The configurational entropy,  $\Delta S_P$ , is

$$\Delta S_T = \Delta S_P + \Delta S_H \quad (6)$$

lost upon interfacial adsorption, inhibiting the adsorption process. The  $\Delta S_H$  term favors adsorption of the macromolecular species and is the dominant factor in adsorption. This term arises from three sources: (1) liberation of water molecules from the aqueous-polymer interface, (2) liberation of water molecules from the aqueous-air interface, and (3) from the total entropy of dilution of the bulk phase during the adsorption process.

It is evident from the data that the entropy term, with one exception, provides the impetus for adsorption at the aqueous-air interface. The higher the molecular weight of the polymer, the more favorable the entropy term. The vinyl alcohol-vinyl acetate copolymers are characterized by a relatively small endothermic adsorption process; entropic forces are the dominating factors in adsorption. In contrast to this, the polymeric alcohol with less than 1% acetylation is characterized by a rather dominant enthalpic term. These results

(41) R. F. Blanks and J. M. Prausnitz, *Ind. Eng. Chem., Fundam.*, **3**, 1 (1964).

(42) J. L. Gardon, *J. Paint Technol.*, **38**, 43 (1966).

(43) C. M. Hansen, *ibid.*, **39**, 104, 505, 511 (1967).

(44) F. M. Fowkes, *J. Phys. Chem.*, **66**, 382 (1962); F. M. Fowkes, "Contact Angle, Wettability and Adhesion," *Advances in Chemistry Series*, No. 43, American Chemical Society, Washington, D. C., 1964, p 99.

(45) R. L. Martin, K. L. Hoy, and B. A. Price, unpublished results.

(46) P. A. Small, *J. Appl. Chem.*, **3**, 71 (1953).

are consistent with the well-known solubility characteristics of polymeric alcohols. The solubilization of polymeric alcohols with low acetylation content is an endothermic process; *i.e.*, it is necessary to supply heat in order to disrupt the intermolecular hydrogen bonding that exists in the bulk polymer. The low acetylated polymer on standing at room temperature will precipitate from aqueous solution. The enthalpy parameter indicates that with increasing acetylation the hydroxyl functions of the polymer are more easily hydrogen bonded by the solvent water molecules. The breakage of this solvation facilitates an endothermic adsorption process. It is exceedingly difficult, however, to solvate the low acetylated material. The high degree of intermolecular hydrogen bonding in the low acetylated species facilitates a more compact macromolecular configuration. This compact structure does not provide an efficient means for obtaining a high interfacial segment density. The small entropy parameter associated with the adsorption supports a compact adsorption configuration for this high molecular weight polymer.

Data from the investigation of poly(vinylpyrrolidone) solutions, Figures 4 and 5, are characterized by relatively poor experimental accuracy. Analysis of the data (Table III) indicates a negative temperature coefficient for both high and low molecular weight species. The exothermic adsorption behavior of pyrrolidone polymers indicates that an intermolecular interaction is competing effectively with the intramolecular hydrogen bonding of the polymer by aqueous solvent molecules.

A decrease in the polymer's hydrodynamic volume would be expected to give both a more favorable

total entropy factor and an increased interfacial segment density. This prediction would be valid for a material whose adsorption is characterized by a high loop density distribution. In an effort to evaluate this hypothesis organic additive-poly(vinylpyrrolidone) systems were investigated. Previous investigations<sup>47</sup> have shown that certain additives can either expand or contract the hydrodynamic volume of vinylpyrrolidone polymers in aqueous solution. Investigation of these organic-polymer complexes did not reveal any noticeable change in the surface activity function attributable to the polymer's hydrodynamic volume. The question of the relationship between a polymer's hydrodynamic volume and its surface activity is considered in more detail in the poly(ethylene oxide) studies related in the following paper.

In summary, the data contained in this report indicate that the surface activities of polymer-aqueous solutions are nonlinear with respect to the polymer's cohesive energy density. This may be related to the complexities of the surface activity and cohesive energy density parameters. The driving force for adsorption of a water-soluble polymer at the aqueous-air interface arises from an entropic contribution. One exception to this observation is noted with a 99% hydrolyzed poly(vinyl alcohol). In this latter case the driving force for adsorption arises predominately from an enthalpic contribution. It is suggested in this case that a high degree of internal hydrogen bonding results in a coiled structure which negates any substantial entropic contribution to the adsorption process.

(47) P. Molyneux and H. P. Frank, *J. Amer. Chem. Soc.*, **83**, 3169, 3175 (1961).

## Adsorption Characteristics of Water-Soluble Polymers. II.

### Poly(ethylene oxide) at the Aqueous-Air Interface<sup>1</sup>

by J. E. Glass

Research and Development Department, Union Carbide Corporation, Chemicals and Plastics,  
South Charleston, West Virginia 25303 (Received April 24, 1968)

The surface tension characteristics of poly(ethylene oxide) derivatives were examined as a function of concentration, time, temperature, and molecular weight. The effects of the polymer's adsorption rheology and the degree of alkyl substitution upon the surface tension of ethylene oxide derivatives were also examined. A high ( $10^6$ ) molecular weight material exhibits a slightly positive surface activity-temperature coefficient. The adsorption characteristics, as a function of concentration and time, remain approximately constant in the  $10^4$  to  $10^6$  molecular weight range. Below a molecular weight range of  $10^4$  the surface activities of the aqueous solutions exhibit a marked dependence upon polymer molecular weight; *i.e.*, the surface tension values decrease with decreasing degree of polymerization. In contrast to the high molecular weight material, an ethylene oxide polymer of 400 molecular weight exhibits exothermic adsorption characteristics. The marked surface activity dependence is characterized by a decreasing entropy factor and by an increasingly compact rheological structure. Both factors are independently associated with the polymer's decreasing molecular weight. An examination of alkyl-substituted triethylene glycol derivatives supports the above conclusions and provides insight into the adsorption rheology of poly(ethylene oxides). Contrary to previous investigations, this study indicates that all ethylene oxide adducts from the trimeric to the  $2.4 \times 10^6$  molecular weight polymer have portions of their structures oriented out of the interfacial region. The surface activity of ethylene oxide copolymers, as a function of concentration, reveals unique polynomial behaviors. These adsorption characteristics are interpreted as the first observed reorientations, by surface tension measurements, of interfacially adsorbed macromolecules.

#### Introduction

In studies of reactions related to carbohydrates and polysaccharides, Lovell and Hibbert<sup>2</sup> studied the surface activity of aqueous poly(ethylene glycol) solutions *via* the capillary-rise method. This extensive investigation neglected the effects of polymer adsorption on the glass-capillary interface and the variation of contact angle with polymer molecular weight. The study observed the surface tension parameter as a function of concentration and molecular weight. Couper and Eley,<sup>3</sup> employing the ring-balance procedure, recorded the aqueous surface tensions of four poly(ethylene glycols), ranging in molecular weight from 1000 to 6000. Both investigations were inconclusive in elucidating the principles governing the behavior of polymeric glycols.<sup>4</sup> Lovell and Hibbert postulated that poly(ethylene oxide) entities with greater than 18 ethoxide units tended to orient out of the interface as in the case of fatty acids. Couper and Eley proposed that the adsorbed ethoxide macromolecules lie approximately flat at the aqueous surface. The data obtained in the present investigation strongly indicate that *all* poly(ethylene oxide) entities, ranging from the trimeric to the polymeric species of  $2.4 \times 10^6$  molecular weight, have portions of their structures oriented out of the interfacial region.

The present investigation was concerned with determining surface concentrations, thermodynamic and rheological aspects of adsorption, reorientational ability

of adsorbed species, and relative interfacial intrinsic diffusion coefficients of poly(ethylene oxide) derivatives.

#### Experimental Section

The experimental details of this investigation are described in the preceding paper. Except for four materials the poly(ethylene oxide) derivatives studied were commercially obtained samples. The 10,000 and the methoxyl-initiated 13,000 poly(ethylene oxide) polymers and the diethyl- and dimethyltriethylene glycol derivatives were laboratory-prepared samples. The molecular weight distributions of all high molecular weight poly(ethylene oxide) derivatives were found to be broader than a random distribution. The triethylene glycol materials were rectified by distillation on a Nestor-Faust spinning band column. Vpc analysis of the distilled trimeric entities showed the commercial materials to be of excellent purity. The dimethyl and diethyl derivatives contained approximately 2% impurity. The impurity judged by its retention time was the parent compound, triethylene glycol. The vpc analyses were determined on a Carbowax 20M column using a flame ionization detector.

(1) Presented in part at the 155th National Meeting of the American Chemical Society, San Francisco, Calif., April 1968.

(2) E. L. Lovell and H. Hibbert, *J. Amer. Chem. Soc.*, **62**, 2144 (1940).

(3) A. Couper and D. D. Eley, *J. Polym. Sci.*, **3**, 345 (1948).

(4) A. Katchalsky and I. Miller, *J. Phys. Chem.*, **55**, 1182 (1951).

Table I: Adsorption Parameters of Poly(ethylene oxides) at the Aqueous-Air Interface

Wt-av mol wt	Temp, °C	Concn		Surface pressure, dyn/cm				Time required to reach equil, hr	Relative intrinsic diffusion coeff ( $D_0$ ), cm <sup>2</sup> /sec	Surface excess function ( $10^{19}r$ ), mol/cm <sup>2</sup>
		Wt %	$M$	10 sec	30 sec	60 sec	Equil			
$2.4 \times 10^6$	25	0.0009	$0.374 \times 10^{-9}$	0.64	3.42	5.20	7.91	13.94	$4.85 \times 10^{-12}$	2.99
		0.0010	$0.415 \times 10^{-9}$	0.84	3.92	5.77	8.48	13.37		
		0.0013	$0.540 \times 10^{-9}$	1.18	5.11	7.37	10.62	13.02		
		0.0020	$0.831 \times 10^{-9}$	2.08	7.18	9.79	13.34	11.97		
		0.0030	$0.125 \times 10^{-8}$	4.31	8.75	10.44	12.46	9.05		
		0.0040	$0.166 \times 10^{-8}$	6.16	9.45	10.51	11.70	7.04		
		0.0050	$0.208 \times 10^{-8}$	7.30	9.75	10.48	11.26	5.79		
		0.0100	$0.415 \times 10^{-8}$	9.30	10.17	10.40	10.64	3.22		
		0.0500	$0.208 \times 10^{-7}$	10.04	10.38	10.46	10.55	1.97		
		0.1000	$0.415 \times 10^{-7}$	10.13	10.42	10.49	10.57	1.81		
	50	0.371	$0.371 \times 10^{-9}$	0.94	2.17	2.67	3.30	9.85	$9.21 \times 10^{-12}$	3.61
		0.412	$0.412 \times 10^{-9}$	1.07	2.73	3.45	4.36	10.40		
		0.535	$0.535 \times 10^{-9}$	1.52	4.20	5.41	6.96	10.83		
		0.823	$0.823 \times 10^{-9}$	2.61	6.70	8.48	10.73	10.44		
		0.124	$0.124 \times 10^{-8}$	4.70	8.55	9.94	11.54	8.33		
		0.165	$0.165 \times 10^{-8}$	6.99	9.73	10.57	11.48	6.19		
		0.206	$0.206 \times 10^{-8}$	8.79	10.29	10.71	11.13	4.27		
		0.412	$0.412 \times 10^{-8}$	10.12	10.78	10.95	11.13	2.70		
	70	0.412	$0.412 \times 10^{-7}$	10.69	11.04	11.13	11.21	1.91	$10.9 \times 10^{-12}$	3.60
		0.407	$0.407 \times 10^{-9}$	1.82	3.63	4.31	5.12	8.93		
		0.530	$0.530 \times 10^{-9}$	2.61	5.41	6.49	7.78	9.18		
		0.815	$0.815 \times 10^{-9}$	4.10	8.37	10.00	11.95	9.09		
		0.122	$0.122 \times 10^{-8}$	6.25	10.02	11.28	12.69	7.39		
		0.163	$0.163 \times 10^{-8}$	8.77	10.83	11.42	12.03	4.94		
		0.204	$0.204 \times 10^{-8}$	10.08	11.08	11.34	11.61	3.30		
		0.407	$0.407 \times 10^{-8}$	10.92	11.27	11.36	11.45	1.93		
	0.407	$0.407 \times 10^{-7}$	11.14	11.42	11.49	11.56	1.71			
	$4.3 \times 10^{6c}$ $1.3 \times 10^4$ (methoxyl initiated)	25	0.0005	$0.383 \times 10^{-7}$	1.26	3.86	5.11	6.76	11.40	$7.44 \times 10^{-10}$
0.0006			$0.460 \times 10^{-7}$	1.70	4.84	6.28	8.16	11.01		
0.0007			$0.537 \times 10^{-7}$	2.19	5.70	7.24	9.19	10.52		
0.0008			$0.614 \times 10^{-7}$	2.71	6.49	8.07	10.03	10.04		
0.0009			$0.690 \times 10^{-7}$	3.36	6.95	8.33	9.99	9.18		
0.0010			$0.767 \times 10^{-7}$	4.17	8.06	9.51	11.21	8.74		
0.0020			$0.153 \times 10^{-6}$	9.11	9.98	10.22	10.45	3.26		
0.0030			$0.230 \times 10^{-6}$	9.58	10.14	10.28	10.43	2.56		
0.0050			$0.383 \times 10^{-6}$	9.78	10.22	10.34	10.46	2.28		
0.0100			$0.767 \times 10^{-6}$	9.90	10.29	10.39	10.49	2.12		
0.1000			$0.767 \times 10^{-6}$	10.09	10.39	10.47	10.54	1.83		
$1.0 \times 10^4$			25	0.0005	$0.499 \times 10^{-7}$	1.00	3.97	5.60	7.90	
	0.0006	$0.598 \times 10^{-7}$		1.38	4.93	6.78	9.31	12.13		
	0.0007	$0.698 \times 10^{-7}$		1.75	5.72	7.69	10.34	11.72		
	0.0008	$0.798 \times 10^{-7}$		2.20	6.46	8.46	11.06	11.16		
	0.0009	$0.897 \times 10^{-7}$		2.69	7.17	9.15	11.69	10.65		
	0.0010	$0.997 \times 10^{-7}$		3.27	7.67	9.49	11.74	9.93		
	0.0020	$0.199 \times 10^{-6}$		8.70	9.47	9.67	9.87	3.12		
	0.0030	$0.299 \times 10^{-6}$		9.00	9.58	9.73	9.88	2.69		
	0.0050	$0.499 \times 10^{-6}$		9.12	9.63	9.77	9.90	2.52		
	0.0100	$0.997 \times 10^{-6}$		9.17	9.67	9.79	9.92	2.46		
	0.1000	$0.997 \times 10^{-6}$		9.29	9.72	9.83	9.95	2.30		
	$1.0 \times 10^3$	25		0.0010	$0.997 \times 10^{-6}$	2.29	2.80 <sup>d</sup>	2.91	4.33	$3.21 \times 10^{-20}$
0.0020			$0.199 \times 10^{-6}$	2.94	3.57	3.71	4.24			
0.0030			$0.299 \times 10^{-6}$	3.41	4.00	4.14	3.87			
0.0040			$0.399 \times 10^{-6}$	3.72	4.31	4.44	3.71			
0.0050			$0.499 \times 10^{-6}$	3.99	4.55	4.67	3.50			
0.0100			$0.997 \times 10^{-6}$	4.76	5.32	5.44	3.22			
0.0200			$0.199 \times 10^{-4}$	5.52	5.92	6.01	2.55			
0.0500			$0.499 \times 10^{-4}$	6.16	6.36	6.40	1.71			

Table I (Continued)

Wt-av mol wt	Temp, °C	Concn		Surface pressure, dyn/cm				Time required to reach equil, hr	Relative intrinsic diffusion coeff ( $D_0$ ), cm <sup>2</sup> /sec	Surface excess function ( $10^{10}\Gamma$ ), mol/cm <sup>2</sup>
		Wt %	$M$	10 sec	30 sec	60 sec	Equil			
$4.0 \times 10^5$	50		$0.988 \times 10^{-6}$				2.94 <sup>b</sup>			
			$0.198 \times 10^{-6}$				3.60			
			$0.296 \times 10^{-6}$				4.05			
			$0.395 \times 10^{-6}$				4.37			
			$0.494 \times 10^{-6}$				4.61	...	...	0.410
			$0.988 \times 10^{-6}$			...	...	5.37		
			$0.198 \times 10^{-4}$					6.12		
			$0.494 \times 10^{-4}$					6.80		
	25	0.0020	$0.499 \times 10^{-6}$	0.54	0.79 <sup>a</sup>	0.86	5.97			
		0.0030	$0.748 \times 10^{-6}$	0.65	1.04	1.14	6.56			
		0.0040	$0.997 \times 10^{-6}$	0.76	1.23	1.35	6.63			
		0.0050	$0.125 \times 10^{-4}$	0.86	1.36	1.50	6.57	$2.63 \times 10^{-22}$	0.239	
		0.0100	$0.249 \times 10^{-4}$	1.17	1.77	1.93	6.22			
		0.0500	$0.125 \times 10^{-3}$	2.18	2.71	2.83	4.51			
		0.1000	$0.249 \times 10^{-3}$	2.72	3.08	3.16	3.39			
		0.2000	$0.499 \times 10^{-3}$	3.58	3.45	3.42	1.89			
		50		$0.494 \times 10^{-6}$				0.78 <sup>b</sup>		
				$0.741 \times 10^{-6}$				0.98		
	$0.988 \times 10^{-6}$					1.11				
	$0.124 \times 10^{-4}$		...	...	1.21	...	...	0.174		
	$0.247 \times 10^{-4}$				1.52					
	$0.124 \times 10^{-3}$				2.29					
	$0.247 \times 10^{-3}$				2.62					
70		$0.494 \times 10^{-6}$				2.94				
		$0.489 \times 10^{-6}$				0.67 <sup>b</sup>				
		$0.733 \times 10^{-6}$				0.82				
		$0.978 \times 10^{-6}$				0.92				
		$0.122 \times 10^{-4}$	...	...	1.01	...	...	0.132		
		$0.244 \times 10^{-4}$			1.27					
		$0.122 \times 10^{-3}$			1.89					
	$0.244 \times 10^{-3}$			2.14						
	$0.489 \times 10^{-3}$			2.56						

150.17 (triethylene glycol)<sup>d</sup>

<sup>a</sup> No difference was noted in values obtained at drop rates of 30 and 60 sec. <sup>b</sup> A time dependence of the surface pressure was not discernible; values obtained were approximated to equilibrium conditions. <sup>c</sup> See Table IV. <sup>d</sup> See Table III.

### Theoretical Model

The exponential, Fickian model employed to calculate the adsorption parameters of water-soluble polymers is described in the preceding paper.

### Results

The data obtained in the adsorption studies of ethylene oxide materials are presented in Tables I-IV. Representative data are plotted in Figures 1-6. The adsorption isotherms at 25 and 70° for the  $2.4 \times 10^6$  molecular weight poly(ethylene oxide) material are shown in Figures 1 and 2. The time-dependent isotherms resemble the time-dependent characteristics of undecanoic acid<sup>5</sup> and octyl alcohol.<sup>6,7</sup> The extreme curvature differences of the 10-, 30-, and 60-sec readings in the  $10^{-3}$  wt % concentration range invalidates the use of the exponential model over the complete iso-

therm. In the linear Gibbs region the exponential model appears valid for the calculation of equilibrium surface pressures. As illustrated in Figures 1 and 2 the higher the temperature the smaller the difference between the surface pressure-time measurements. This results in a smaller "kink" in the calculated equilibrium curve. The same observation is noted when one decreases the weight-average molecular weight from  $10^6$  to  $10^4$ . Except for the small time-dependent variations, the adsorption isotherms are similar in appearance over the molecular weight range from  $10^4$  to  $10^6$ .

It will be noted from the data that the  $2.4 \times 10^6$

(5) D. G. Dervichian, *Kolloid Z.*, **146**, 96 (1956).

(6) C. C. Addison, *Phil. Mag.*, **36**, 73 (1945).

(7) R. S. Hansen and T. C. Wallace, *J. Phys. Chem.*, **63**, 1085 (1959).

**Table II:** Thermodynamic Parameters of Poly(ethylene oxide) Adsorption

Wt-av mol wt	Temp, °C	$\Delta F$ , kcal/mol <sup>a</sup>	$\Delta H$ , cal/mol <sup>a</sup>	$\Delta S$ , eu <sup>a</sup>
$2.4 \times 10^6$	25	-14.4	...	...
	50	-15.6	568	50.2
	70	-16.7	569	50.3
$4.3 \times 10^6$	25	-13.3	...	...
$1.3 \times 10^4$ (methoxyl initiated)	25	-11.5	...	...
$1.0 \times 10^4$	25	-11.5	...	...
$1.0 \times 10^3$	25	-9.4	...	...
400	50	-10.2	-37	31.6
	25	-7.9	...	...
	50	-8.4	-1460	21.5
150.17 (triethylene glycol)	70	-8.8	-1910	20.1
	25	-3.9	...	...

<sup>a</sup> Thermodynamic functions determined from modified Gibbs equations (S. Ross and E. S. Chen, *Ind. Eng. Chem.*, **57**, No. 7, 40 (1965)).

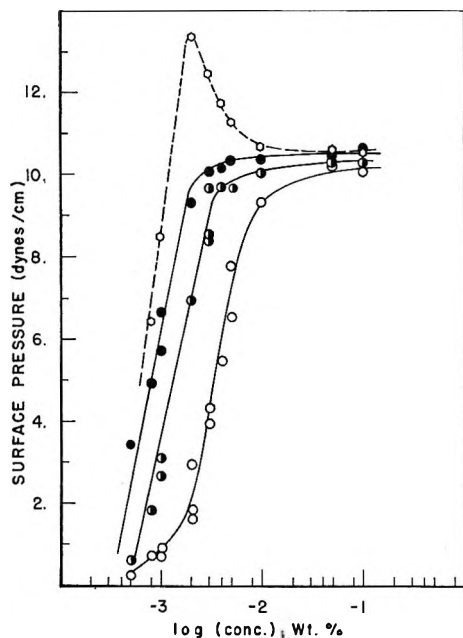


Figure 1. Surface activity-time dependence of  $2.4 \times 10^6$  weight-average molecular weight poly(ethylene oxide)-aqueous solutions (25°):  $\circ$ , exponential equilibrium;  $\odot$ , 10 sec;  $\bullet$ , 60 sec.

molecular weight polymer possesses a positive temperature coefficient in its surface activity functions. The low molecular weight (number-average molecular weight of 400) material has a negative coefficient. It also is evident that there is a marked decrease in the surface pressure parameter with decreasing polymer molecular weight. This latter effect is shown graphically in Figure 3.

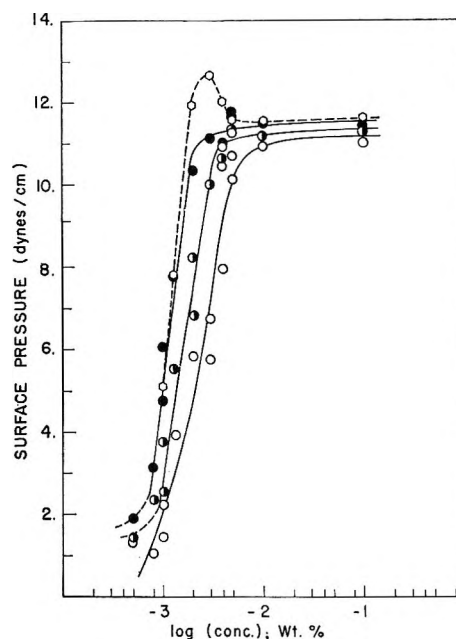


Figure 2. Surface activity-time dependence of  $2.4 \times 10^6$  weight-average molecular weight poly(ethylene oxide)-aqueous solutions (70°):  $\circ$ , exponential equilibrium value;  $\odot$ , 10 sec;  $\bullet$ , 60 sec.

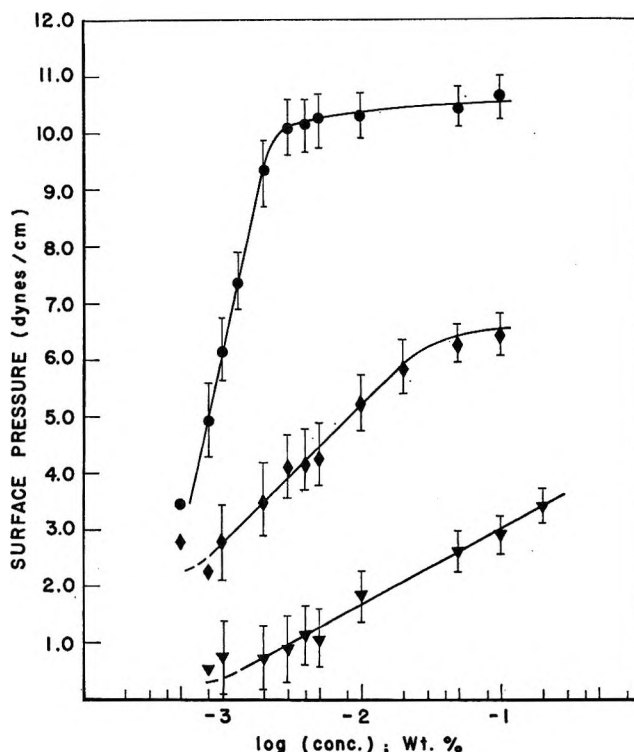


Figure 3. Surface activity-molecular weight dependence of poly(ethylene oxide)-aqueous solutions (25°, 60-sec. data):  $\bullet$ ,  $2.4 \times 10^6$  weight-average molecular weight;  $\blacklozenge$ ,  $1.0 \times 10^3$  number-average molecular weight;  $\blacktriangledown$ , 400 number-average molecular weight.

The time dependence of the surface pressure function for the trimeric materials is not discernible *via* the weight-drop method (the materials are of low



**Table III:** Adsorption Characteristics of Triethylene Glycol Derivatives (Aqueous Solutions, 25°)

Compd	Concn		Surface pressure (30 sec), dyn/cm	Surface excess function ( $10^{10}\Gamma$ ), mol/cm <sup>2</sup>	Free energy <sup>a</sup> of adsorption ( $\Delta F$ ), kcal/mol	Cohesive energy density of bulk material, cal/ml		
	Wt %	<i>M</i>				Non-polar	Polar	Total
Triethylene glycol	1.0000	$0.664 \times 10^{-2}$	1.53	0.668	-3.87	77.60	67.00	144.60
	2.0000	$0.133 \times 10^{-1}$	2.52					
	5.0000	$0.332 \times 10^{-1}$	4.39					
Triethylene glycol, monomethyl ether	1.0000	$0.607 \times 10^{-2}$	3.44	1.15	-4.40	71.57	44.22	115.78
	2.0000	$0.121 \times 10^{-1}$	5.29					
	5.0000	$0.304 \times 10^{-1}$	8.14					
Triethylene glycol, monoethyl ether	1.0000	$0.559 \times 10^{-2}$	5.30	1.40	-4.70	65.77	37.33	103.22
	2.0000	$0.112 \times 10^{-1}$	7.59					
	5.0000	$0.280 \times 10^{-1}$	10.93					
Triethylene glycol, dimethyl ether	1.0000	$0.559 \times 10^{-2}$	6.30	1.46	-4.80	62.88	17.47	80.28
	2.0000	$0.112 \times 10^{-1}$	8.61					
	5.0000	$0.280 \times 10^{-1}$	12.09					
Triethylene glycol, diethyl ether	1.0000	$0.483 \times 10^{-2}$	11.50	1.82	-5.25	62.88	17.47	80.28
	2.0000	$0.967 \times 10^{-2}$	14.63					
	5.0000	$0.242 \times 10^{-1}$	18.80					

<sup>a</sup>  $\Delta F$  determined from modified Gibbs equations (S. Ross and E. S. Chen, *Ind. Eng. Chem.*, **57**, No. 7, 40 (1965)); 30-sec values approximated as equilibrium conditions.

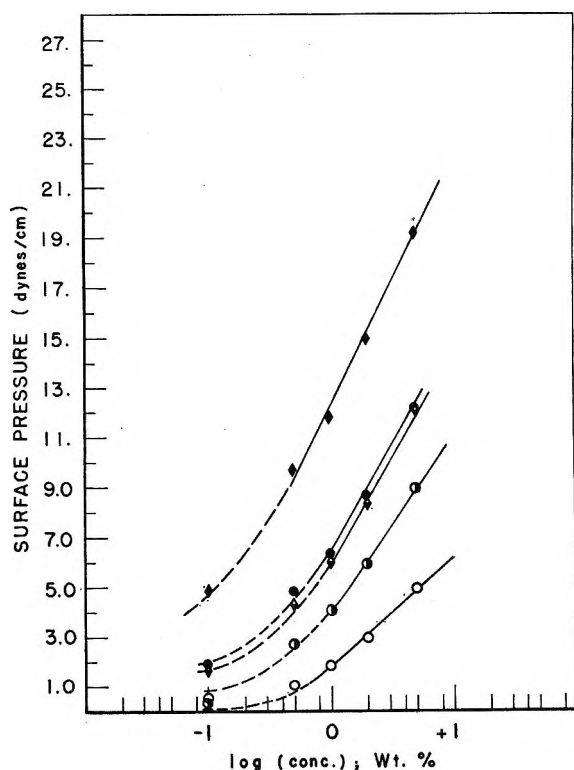


Figure 4. Adsorption characteristics of triethylene glycol derivatives (25°, 30-sec data): O, R = H, R' = H; ◐, R = CH<sub>3</sub>, R' = H; ◑, R = C<sub>2</sub>H<sub>5</sub>, R' = H; ●, R = CH<sub>3</sub>, R' = CH<sub>3</sub>; ◔, R = C<sub>2</sub>H<sub>5</sub>, R' = C<sub>2</sub>H<sub>5</sub>.

molecular weight and the concentrations employed are high). The  $\Gamma$  functions denoted in Table III were determined at a drop life of 30 sec and were approximated

to equilibrium values. The cohesive energy density parameters of the triglycol materials also are listed in Table III. The adsorption isotherms are shown in Figure 4.

The investigation of high molecular weight ethylene oxide copolymers (Table IV) reveals rather interesting results. In these investigations, comonomer units of 1-butylene, propylene, and styrene oxide were incorporated with the ethylene oxide structure. It is evident from Figure 5 that the copolymer structures exhibit rather unusual polynomial behaviors. Instead of leveling to a relatively constant surface pressure at higher concentrations, the three copolymers exhibit a steady increase in surface pressure. These increases in surface pressure can be interpreted as reorientations of the copolymers to allow the more hydrophobic segments to reposition themselves within the interfacial region. A time-dependent reorientational effect was not observed using the weight-drop method; this phenomenon will be investigated *via* the pendant-drop technique. The relative cohesive energy values of the hydrophobic comonomer units reflect, to a first approximation, the increases in surface pressure observed. Owing to variation of the comonomer content with each sample and the lack of information with respect to the relative block or random nature of the comonomer structures, further analysis of the data is not attempted. The time dependence of one of the copolymers is illustrated in Figure 6. The molecular weight values listed in Table IV for the copolymers are approximations; they were obtained through the use of viscosity measurements with the

Table IV: Adsorption Parameters of Poly(ethylene oxide) Copolymers at the Aqueous-Air Interface (25°)

Comonomer structure	% structure <sup>a</sup> in ethoxide polymer	Approx <sup>b</sup> wt-av mol wt	Concn		Surface pressure, dyn/cm				Time required to reach equil, hr	Surface excess function (10 <sup>18</sup> Γ), mol/cm <sup>2</sup>
			Wt %	M	10 sec	30 sec	60 sec	Equil		
None	...	4.3 × 10 <sup>5</sup>	0.0008	0.186 × 10 <sup>-8</sup>	0.96	3.46	4.76	6.54	12.16	3.33
			0.0009	0.209 × 10 <sup>-8</sup>	1.11	3.98	5.47	7.53	12.16	
			0.0010	0.232 × 10 <sup>-8</sup>	1.28	4.47	6.10	8.34	12.03	
			0.0020	0.464 × 10 <sup>-8</sup>	4.27	8.18	9.63	11.32	8.68	
			0.0030	0.696 × 10 <sup>-8</sup>	8.15	9.74	10.18	10.65	4.55	
			0.0040	0.928 × 10 <sup>-8</sup>	9.27	10.11	10.33	10.56	3.18	
			0.0050	0.116 × 10 <sup>-7</sup>	9.67	10.29	10.46	10.62	2.70	
			0.0100	0.232 × 10 <sup>-7</sup>	10.26	10.63	10.73	10.83	2.05	
			0.0500	0.116 × 10 <sup>-6</sup>	10.52	10.87	10.96	11.05	1.94	
			0.1000	0.232 × 10 <sup>-6</sup>	10.60	10.90	10.98	11.05	1.80	
Propylene oxide	7.7	1.5 × 10 <sup>5</sup>	0.0005	0.332 × 10 <sup>-8</sup>	0.95	2.92	3.87	5.12	11.41	3.63
			0.0008	0.532 × 10 <sup>-8</sup>	1.80	5.44	7.17	9.45	11.31	
			0.0010	0.665 × 10 <sup>-8</sup>	2.43	6.72	8.66	11.16	10.85	
			0.0016	0.106 × 10 <sup>-7</sup>	5.81	9.22	10.38	11.24	8.51	
			0.0020	0.133 × 10 <sup>-7</sup>	8.35	10.24	10.77	11.33	4.85	
			0.0030	0.199 × 10 <sup>-7</sup>	9.60	10.99	11.37	11.76	3.95	
			0.0040	0.266 × 10 <sup>-7</sup>	10.17	11.43	11.77	12.12	3.68	
			0.0050	0.332 × 10 <sup>-7</sup>	10.48	11.75	12.09	12.44	3.64	
			0.0100	0.665 × 10 <sup>-7</sup>	11.24	12.88	13.33	13.79	3.97	
			0.0500	0.332 × 10 <sup>-6</sup>	15.65	18.09	18.75	19.44	4.09	
0.1000	0.665 × 10 <sup>-6</sup>	19.00	22.06	22.90	23.77	4.16				
1-Butylene oxide	3.4	2.6 × 10 <sup>5</sup>	0.0005	0.192 × 10 <sup>-8</sup>	0.48	1.86	2.62	3.67	12.54	4.19
			0.0008	0.307 × 10 <sup>-8</sup>	1.12	4.40	6.19	8.70	12.56	
			0.0009	0.345 × 10 <sup>-8</sup>	1.38	5.09	7.06	9.78	12.30	
			0.0010	0.383 × 10 <sup>-8</sup>	1.61	5.69	7.79	10.68	12.09	
			0.0020	0.767 × 10 <sup>-8</sup>	5.22	9.60	11.18	13.01	8.40	
			0.0030	0.115 × 10 <sup>-7</sup>	9.31	10.83	11.25	11.68	4.19	
			0.0040	0.153 × 10 <sup>-7</sup>	10.07	11.33	11.66	12.01	3.68	
			0.0050	0.192 × 10 <sup>-7</sup>	10.55	11.73	12.04	12.36	3.50	
			0.0100	0.383 × 10 <sup>-7</sup>	11.87	13.19	13.55	13.91	3.50	
			0.0500	0.192 × 10 <sup>-6</sup>	16.38	19.13	19.89	20.67	4.24	
0.1000	0.383 × 10 <sup>-6</sup>	19.58	23.56	24.67	25.84	4.63				
Styrene oxide	1.3	4.6 × 10 <sup>5</sup>	0.0005	0.108 × 10 <sup>-8</sup>	0.49	1.74	2.40	3.31	12.17	3.94
			0.0008	0.173 × 10 <sup>-8</sup>	1.04	4.11	5.80	8.17	12.62	
			0.0010	0.217 × 10 <sup>-8</sup>	1.65	5.30	7.09	9.49	11.62	
			0.0016	0.347 × 10 <sup>-8</sup>	4.03	9.11	9.62	11.98	10.21	
			0.0020	0.434 × 10 <sup>-8</sup>	6.39	9.64	10.69	11.84	6.90	
			0.0030	0.650 × 10 <sup>-8</sup>	8.90	10.49	10.93	11.38	4.36	
			0.0040	0.867 × 10 <sup>-8</sup>	9.50	10.70	11.02	11.35	3.71	
			0.0050	0.108 × 10 <sup>-7</sup>	9.85	10.82	11.08	11.34	3.29	
			0.0100	0.217 × 10 <sup>-7</sup>	10.55	11.23	11.41	11.58	2.68	
			0.0500	0.108 × 10 <sup>-6</sup>	12.85	14.11	14.45	14.79	3.30	
0.1000	0.217 × 10 <sup>-6</sup>	15.04	16.77	17.23	17.70	3.54				

<sup>a</sup> Determined with a Varian HR 100 nmr spectrometer (100°, 4% solution in heptadeuteriodimethylformamide). <sup>b</sup> Approximate weight-average molecular weight obtained through application of viscosity measurements with Mark-Houwink parameters for homopolymer.

Mark-Houwink parameters determined for the homopolymer. Since the molecular weights are approximations, no thermodynamic parameters or relative diffusion coefficients are reported for these materials.

### Discussion

The 25° data obtained in these investigations strongly complement those previously determined by the capil-

lary-rise method.<sup>2</sup> In the initial stage of this study, a ring-balance method was employed; this procedure was noted to give erratic results at low concentrations. In the previous ring-balance measurements<sup>3</sup> of the 4000 and 6000 molecular weight polyethylene glycols, an inflection was not observed in the adsorption isotherms, and consequently, the calculations were not based upon the Gibbs linear region. The omission of

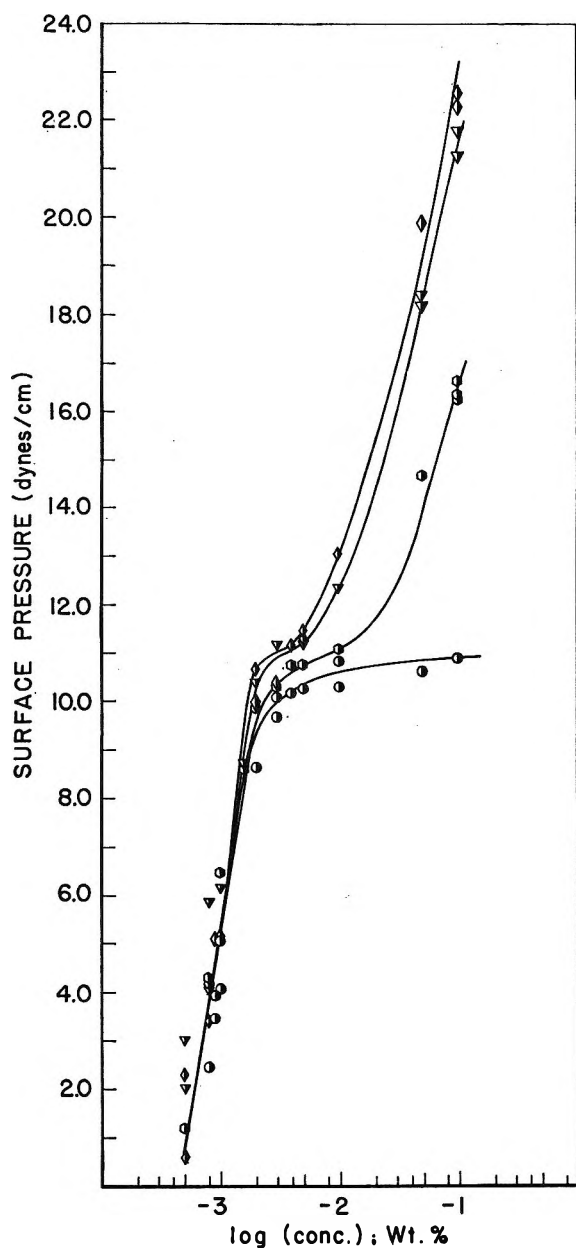


Figure 5. Adsorption characteristics of ethylene oxide copolymers (25°, 10<sup>5</sup> weight-average molecular weight, 30-sec data): ○, poly(ethylene oxide) homopolymer; □, 1.3 mol % styrene oxide copolymer; ▽, 7.7 mol % propylene oxide copolymer; ◇, 3.4 mol % 1-butylene oxide copolymer.

the correct Gibbs parameters led to the conclusion that there were no interfacial orientation effects for poly(ethylene oxide) entities.

In an effort to discern the adsorption rheology of very low molecular weight ethylene oxide adducts, a series of alkyl-substituted derivatives of triethylene glycol were investigated. The data shown in Table III indicate that even the trimeric species is not completely adsorbed in the interfacial region. An average of 1.82 of the 3 hydrophobic segments are adsorbed. This conclusion can be deduced by applying simple models to the data given in Table III. Comparison of various

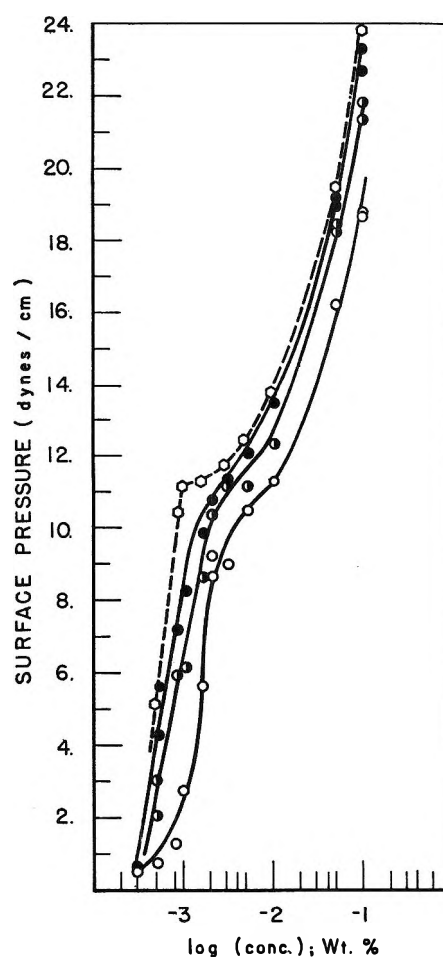


Figure 6. Surface pressure-time dependence of ethylene oxide-propylene oxide (7.7 mol %) copolymer-aqueous solutions (25°): ○, exponential equilibrium value; ○, 10 sec; ◐, 30 sec; ●, 60 sec.

adsorption models with the data either over- or underestimates the adsorption capabilities of the lesser alkylated derivatives. In brief, if any of the five triethylene glycol derivatives investigated could be expected to adsorb in a flat zig-zag manner, it would be the diethyl ether material. Assuming that the five hydrophobic segments of this compound are completely adsorbed, one can deduce, from the observed Gibbs excess functions, that an average of 1.82 of the 3.00 hydrophobic segments of triethylene glycol are interfacially adsorbed. Analysis of this nature is more informative than correlation<sup>2</sup> of molecular volumes with Gibbs excess function areas, since it provides a relative and consequently more accurate method of deducing adsorption rheology. The data indicate that even with the low molecular weight trimeric species, a poly(ethylene oxide) adduct does not lie in a flat zig-zag fashion at the aqueous-air interface.

As discussed in the preceding article, variations in the surface activity of solutes are most likely related to the variety of factors contributing to the surface tension and solubility parameters. A listing of the polar

and nonpolar contributions to the cohesive energy density parameters of the triethylene glycol materials is given in Table III. They are not very informative with respect to interfacial analysis because the hydrogen bonding component (and its associated hydration) is not listed. The contributions to the cohesive energy density by the hydrogen bonding capability of the solutes are not available at this time. Since all non-ionic, water-soluble materials are soluble by virtue of the hydrogen bonding phenomenon, this parameter is vital to an understanding of the surface activity of solutes in aqueous solution.

The adsorption of macromolecules from the bulk of the solution can be depicted as occurring in two stages: (1) diffusion from the bulk of the solution to the sub-surface phase and (2) movement from the subsurface phase to the surface layer with possible orientation of the adsorbing species. Lovell and Hibbert<sup>2</sup> observed (capillary-rise method) that 8 hr was required to obtain equilibrium for dilute solutions of poly(ethylene glycols). At the relatively high concentrations of 0.5 and 1.0% wt (pendant-drop method), 20 min was required<sup>8</sup> for equilibration of ethylene oxide-propylene oxide block copolymers in tetralin solutions. These values agree in magnitude with the equilibrium times calculated from the empirical and theoretical models employed in this report.

The variations of the relative intrinsic interfacial diffusion coefficients with temperature agree with what would be predicted for bulk diffusion rates; *i.e.*, the coefficients increase with increasing temperature. For high molecular weight materials the diffusion times determined by the exponential, Fickian model approximate values close to bulk parameters. The diffusion times can, of course, be altered to fit the bulk diffusion parameters by adjusting the rate of decrease factor,  $\alpha$  (eq 2 in the preceding paper). From analysis of the diffusion coefficients (Table I), it is evident that the calculated values are in contrast to the data obtained in bulk solutions; *i.e.*, the interfacial diffusion coefficients are smaller for the lower molecular weight entities. In an attempt to interpret this abnormality three factors may be considered to influence the adsorption phenomenon; they are (1) steric hindrance by the adsorbed molecules already in the interfacial region to the adsorption of additional species, (2) cohesive interaction between the adsorbing molecule and those already adsorbed, and (3) a desolvation energy barrier for the adsorbing species. There is definitely a cohesive interaction between adsorbing and adsorbed molecules at the aqueous-air interface; this is determined *via* Schofield-Rideal analysis of the data. This analysis is not discussed in this paper. Large macromolecular species in the interfacial region can also be anticipated to offer steric hindrance to the adsorption of incoming polymeric entities. The results anticipated from both arguments would suggest a

reversal in the diffusion coefficients; *i.e.*, lower molecular weight polymers would have larger diffusion constants. The third possible consideration, a desolvation energy barrier for the adsorbing species, has been proposed<sup>9-11</sup> in studies concerned with the adsorption characteristics of low molecular weight compounds.

The data presented in Table III indicated that the hydroxyl end groups influence the surface activity of the trimeric species. In a cursory examination of poly(ethylene oxide) data at room temperature, a relationship between an increasing surface activity and decreasing importance of the hydroxyl end groups might be postulated. Such a postulate would also approximate a mechanism to explain the decrease in diffusion coefficients. Although appealing, the desolvation mechanism is not consistent with the data of these investigations. This mechanism would not explain the difference in diffusion coefficients of the high molecular weight species. No substantial difference in the hydration characteristics of the high molecular weight materials would be expected. The thermodynamic parameters derived from the temperature-dependence studies also negate such a relationship. For example, it is untenable to propose that the hydroxyl end groups influence the exothermic adsorption process of the 400 molecular weight species.

It is therefore concluded that the variation in the observed diffusion coefficients arises from a difference in the relative driving force for adsorption. The only plausible alternative explanation for the observed trend in interfacial diffusion rates is an interaction between drop rate and surface viscoelastic properties of the aqueous polymer solutions. An investigation of the surface viscoelastic properties is currently under study in our laboratories. Preliminary results indicate that it is not a significant factor in the calculated diffusion coefficients.

The thermodynamic data clearly point to a surface activity-entropy relationship. A decrease in the entropy factor with decreasing polymer molecular weight results in a decreased surface pressure. Frisch and Simha<sup>12</sup> have postulated that the surface pressure function will decrease with decreasing polymer molecular weight. This prediction was based upon the increasing significance of a configurational entropy loss with decreasing polymer molecular weight. In a later paper, Frisch<sup>8</sup> obtained experimental support for this concept. The thermodynamic data presented in Table II, together with the data previously obtained by

(8) H. L. Frisch and S. Al-Madfaï, *J. Amer. Chem. Soc.*, **80**, 3561, 5613 (1958).

(9) C. M. Blair, Jr., *J. Chem. Phys.*, **16**, 113 (1948).

(10) C. C. Addison and S. K. Hutchinson, *J. Chem. Soc.*, 3387, 3395 (1949).

(11) F. H. Garner and P. Mina, *Trans. Faraday Soc.*, **55**, 1616 (1959).

(12) H. L. Frisch and R. Simha, *J. Chem. Phys.*, **27**, 702 (1957).

Callard and Faucher,<sup>13</sup> adequately explain the adsorption characteristics without invoking a configurational entropy factor. Above a molecular weight of 6000, Callard and Faucher observed that the viscosity-molecular weight exponential parameter was 0.78; below a molecular weight of 6000, the constant was 0.29. Their findings indicate that the low molecular weight species is a very compact structure. This compact structure is relatively inefficient in providing a high interfacial segment density. The trimeric species is more efficient in providing interfacial segments than is the nonameric species (the 400 molecular weight material). If as surmised above the trimeric species has an average of 1.82 adsorbed segments, a compact spheroidal nonameric species is even less efficient (<10%) in providing hydrophobic segments for interfacial adsorption.

The relative inefficiency of a compact adsorbing species was demonstrated in the preceding paper with a low acetylated poly(vinyl alcohol) material. In the high molecular weight polymeric alcohol the decreasing entropy parameter is obtained, at approximately constant polymer molecular weight, by varying the acetate content. In both the lower molecular weight poly(ethylene oxide) and the high molecular weight, low acetylated poly(vinyl alcohol), the adsorbing species is a rather compact structure which cannot provide a substantial number of interfacial segments. The decrease in the surface activity is not related to an increasingly competitive configurational entropy term since the relative entropy loss of a contracted solution structure would be minimal.

Contraction in the hydrodynamic volume of a polymer molecule could be expected to affect favorably the entropy of adsorption and provide, in an interfacially adsorbed looped structure, a higher interfacial segment density. The addition of inorganic electrolytes to aqueous solutions of poly(ethylene oxide) derivatives has been shown<sup>14</sup> to decrease the hydrodynamic volume of poly(ethylene oxide) derivatives. Multivalent anions are very effective in decreasing the polymer's hydrodynamic volume; monovalent electrolytes are less effective. In these investigations it has been observed that the addition of potassium sulfate (0.36 *M*) results in a 2.0 dyn/cm increase in the surface pressure (0.1 wt %, 25°) of the  $2.4 \times 10^6$  molecular weight species. Equivalent or higher concentrations of potassium chloride do not effect a notable increase in the surface pressure of poly(ethylene oxide) solutions. The change in surface pressure noted by the addition of potassium sulfate is observed despite a competing electrolyte effect. Although the multivalent electrolyte decreases the polymer's hydrodynamic volume, the Mark-Houwink viscosity-molecular weight parameters indicate that the contraction of a high molecular

weight species is much less than that noted for the low molecular weight entities without electrolyte addition. The increase in surface pressure through the addition of inorganic electrolytes was achieved at polymer concentrations in excess of that required for complete surface coverage. The increase in surface pressure could be achieved only if the adsorbed species is characterized by a high degree of unadsorbed segments (a looped adsorption rheology).

In summary, it has been shown that all ethylene oxide adducts from the trimeric to the  $2.4 \times 10^6$  molecular weight polymer have portions of their structures oriented out of the interfacial region; poly(ethylene oxide) derivatives are not adsorbed in a completely flat zig-zag interfacial arrangement at the aqueous-air interface. The surface activity of poly(ethylene oxide) solutions is observed to decrease below a molecular weight of  $10^4$ . This molecular weight range corresponds to the transition region for random coil formation of poly(ethylene oxide) molecules in solution. The driving force for adsorption is entropic for the high molecular weight ( $10^6$ ) polymer; enthalpic contributions play a significant role in the adsorption of a lower molecular weight (400) material. A decrease in the degree of polymerization results in a diminishing entropy of adsorption. It is suggested that the marked surface activity-molecular weight dependence results not only from a decreasing entropy term but also from an increasingly compact rheological structure. In the 400 number-average molecular weight species, rheological compactness permits approximately 10% of the hydrophobic segments to interfacially adsorb, whereas with the trimeric entity approximately 70% of available segments are adsorbed. Finally, reorientational effects were observed in high molecular weight ethylene oxide copolymers.

The studies described in this and in the preceding paper represent part of an investigation to determine the factors governing the surface behavior of water-soluble polymers. The data obtained in these investigations are presently being interpreted in terms of the polymer solution theories of Huggins and Flory in terms of the more empirical Schofield-Rideal and van der Waals-Gibbs modified equations,<sup>15</sup> and *via* Silberberg's modified adsorption equation.<sup>16</sup> The analyses are being completed and will be reported in the near future.

(13) R. W. Callard and J. A. Faucher, unpublished data, quoted by F. E. Bailey and J. V. Koleske in "Nonionic Surfactants," Vol. 1, M. J. Schick, Ed., Marcel Dekker, Inc., New York, N. Y., 1967, p 803.

(14) F. E. Bailey, Jr., and R. W. Callard, *J. Appl. Polym. Sci.*, **1**, 56 (1959).

(15) S. Ross and E. S. Chen, *Ind. Eng. Chem.*, **57**, No. 7, 40 (1965).

(16) A. Silberberg, *J. Phys. Chem.*, **66**, 1884 (1962).

# Absorptions and Fluorescences of 2-Phenylnaphthalene, 2'-Methyl-2-phenylnaphthalene, and 1-Fluoro-2-phenylnaphthalene. Spectroscopic Evidence for the Equilibrium Conformation of the Lowest Excited States<sup>1</sup>

by Homer E. Holloway, Robert V. Nauman, and James H. Wharton

Department of Chemistry, Louisiana State University, Baton Rouge, Louisiana 70803 (Received April 29, 1968)

The absorption and fluorescence characteristics of 2-phenylnaphthalene and two of its derivatives, 2'-methyl-2-phenylnaphthalene and 1-fluoro-2-phenylnaphthalene, are reported. In the case of 2-phenylnaphthalene a gap of  $1770\text{ cm}^{-1}$  is observed between the absorption and the fluorescence emission. Comparison of this gap with those observed from 2'-methyl-2-phenylnaphthalene ( $610\text{ cm}^{-1}$ ) and 1-fluoro-2-phenylnaphthalene ( $510\text{ cm}^{-1}$ ) suggests that the shift is due in part to a Stokes shift associated with rotation during the lifetime of the excited state ( $\sim 1290\text{ cm}^{-1}$ ) and in part to solvent stabilization of the excited state ( $\sim 480\text{ cm}^{-1}$ ). Comparison of the solution absorption and solution fluorescence with the crystal absorption indicates that in the equilibrium ground state molecules of 2-phenylnaphthalene in solution are distributed about an angular conformation while in the lowest excited state the molecules are distributed about a planar or near-planar conformation. The data indicate that the mean conformation of 2'-methyl-2-phenylnaphthalene is angular in both the equilibrium ground and lowest excited states and that of 1-fluoro-2-phenylnaphthalene is planar in both the equilibrium ground and excited states. Significant and unusual temperature effects are observed in the spectrum of 2'-methyl-2-phenylnaphthalene. The conformations of eight other derivatives of 2-phenylnaphthalene are derived from similar analyses of their spectra.

The influence of the steric effect on the ultraviolet absorption spectra of polynuclear aromatic hydrocarbons has been the subject of numerous theoretical and experimental papers.<sup>2-7</sup> Unfortunately most of these studies have been carried out on biphenyl for which no structure can be observed in the solution absorption spectrum or have been carried out under conditions which limit the observation of structure. These featureless spectra preclude a critical test of theory and in addition do not encourage further experimentation.

The spectra of the 2-phenylnaphthalenes show distinct electronic transitions with some vibrational structure, and significant temperature effects are observable. In addition the spectra provide considerable information concerning the conformations and the energy effects associated with changes in conformation. Thus the 2-phenylnaphthalenes constitute a much superior testing ground for theoretical models of composite polynuclear aromatics.

## Experimental Section

**Purification of Solvents.** Phillips pure grade 3-methylpentane and isopentane were purified in the following manner. The commercial solvents were repeatedly washed with fuming sulfuric acid, then rinsed consecutively with distilled water, saturated sodium carbonate solution, and distilled water again, were dried

over magnesium sulfate for 24 hr, and were distilled at a rate of 10 drops/min through a 2-ft column filled with glass beads. These solvents were considered to be satisfactory when the absorption characteristics of unsaturated impurities had been eliminated and there was no detectable solvent emission with maximum spectrometer sensitivity. Gas chromatographic analysis showed that the purified 3-methylpentane contained 20% 2-methylpentane.

**Preparation and Purification of Compounds. 2-Phenylnaphthalene.** Commercial grade 2-phenylnaphthalene contains an anthracene as an impurity which could not be completely removed. Pure synthetic 2-phenylnaphthalene was prepared by the following method. Di-2-naphthoyl peroxide was prepared by the procedure described by Kharasch and Dannley.<sup>8</sup> The peroxide was allowed to react with benzene as

(1) Adapted from the Ph.D. dissertation of H. E. Holloway, Louisiana State University, 1967.

(2) R. N. Jones, *J. Amer. Chem. Soc.*, **67**, 2127 (1945).

(3) R. A. Friedel, M. Orchin, and L. Reggel, *ibid.*, **70**, 199 (1948).

(4) H. Suzuki, *Bull. Chem. Soc. Jap.*, **32**, 1340 (1959).

(5) Y. Gondo, *J. Chem. Phys.*, **41**, 3928 (1964).

(6) R. Grinter, *Mol. Phys.*, **11**, 197 (1966).

(7) A. Golebiewski and A. Parczewski, *Theor. Chim. Acta*, **7**, 171 (1967).

(8) M. S. Kharasch and R. L. Dannley, *J. Org. Chem.*, **10**, 410 (1945).

described by Hey and Walker.<sup>9</sup> The solid product was fractionally sublimed giving large plates of 2-phenylnaphthalene which melted at 104°.

**1-Fluoro-2-phenylnaphthalene.** This compound was prepared from 2-phenylnaphthalene by a four-step reaction sequence. 1-Amino-2-phenylnaphthalene was prepared by the procedure outlined by Hey and Lawton.<sup>10</sup> The 1-amino-2-phenylnaphthalene was diazotized by NaNO<sub>2</sub> in a 49% hydrofluoric acid solution at 0.5°. To the diazotized mixture was added NaBF<sub>4</sub> which precipitated the diazonium fluoroborate. The yellow precipitate was separated by filtration, was washed with methanol and ether, and then was dried under vacuum. The product was decomposed by heating, and 1-fluoro-2-phenylnaphthalene was obtained as the product. The 1-fluoro-2-phenylnaphthalene was separated from the reaction mixture by steam distillation. Four crystallizations from ethanol gave white needles which melted at 60°. Carbon-hydrogen analysis confirmed the empirical formula of the compound.

**2'-Methyl-2-phenylnaphthalene.** This compound was prepared by the procedure outlined by Friedel, Orchin, and Reggel.<sup>11</sup> The crude reaction product was purified by four crystallizations from methanol followed by two fractional sublimations. The purified sample melted at 46.0–46.5°.

**Apparatus and Methods.** The absorption spectra of 2-phenylnaphthalene, 2'-methyl-2-phenylnaphthalene, and 1-fluoro-2-phenylnaphthalene were measured with a Cary Model 14 spectrophotometer. 3-Methylpentane was used as the solvent for all compounds when the absorption spectra were measured at room temperature, and a 1:6 mixture of 3-methylpentane-isopentane was used to form rigid glassy solutions at 77°K. The latter solvent forms a very transparent glass that does not shatter the 1-cm<sup>2</sup> quartz cells when they are cooled in liquid nitrogen.

The fluorescence emission spectra were measured with the Cary Model 14 spectrophotometer which was operated in the single-beam mode. The emitting sample was placed at the normal site of the visible light source. The sample holder was designed in such a manner that the emitting sample is located at the focal point of the visible optical system and that front-surface excitation was obtained. The samples were excited by use of a specially designed Cary Model 15 monochromator that was coupled with a 450-W xenon light source. The emissions were all measured from solutions of rigid glassy 3-methylpentane at 77°K. All emissions were excited at 2800 Å (35,710 cm<sup>-1</sup>). No photolytic effects were observed in the low-temperature emission spectra.

### Spectra and Analysis

The room-temperature absorption spectra of 2-phenylnaphthalene, 2'-methyl-2-phenylnaphthalene, and 1-fluoro-2-phenylnaphthalene are shown in Figure 1.

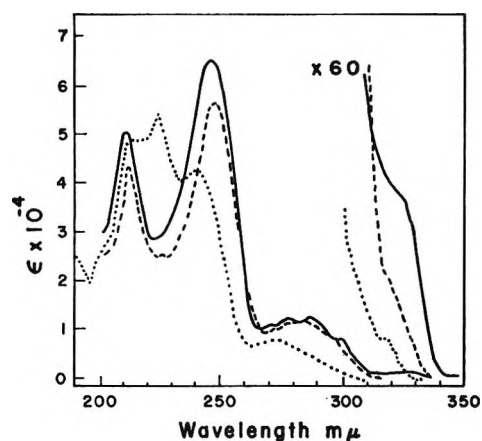


Figure 1. Room-temperature absorption spectra of 2-phenylnaphthalene (-----), 1-fluoro-2-phenylnaphthalene (—), and 2'-methyl-2-phenylnaphthalene (·····), (solvent, 3-methylpentane).

The electronic transitions are identified by Clar's notation as  $\alpha \sim 320 \text{ m}\mu$ ,  $\rho \sim 287 \text{ m}\mu$ ,  $\beta \sim 250 \text{ m}\mu$ , and  $\beta' \sim 212 \text{ m}\mu$ . The three spectra are similar with respect to transition energies; however, significant and varying degrees of inhomogeneous broadening are readily apparent. If one assumes that near-equal absorption intensities should be observed for the same absorption band in each compound, then the degree of inhomogeneous broadening must increase in the order 1-fluoro-2-phenylnaphthalene < 2-phenylnaphthalene < 2'-methyl-2-phenylnaphthalene. The observed broadening is best interpreted by assuming that there is superposition of the spectra of isomers; these conformers are molecules that differ with respect to the angle between the phenyl and naphthyl ring planes. In view of this interpretation one might conclude that the extent of inhomogeneous broadening observed in the absorption spectrum depends only on the breadth of the molecular distribution with respect to angle in the ground electronic state. This assumption neglects the potential function associated with conformation in the excited states. The latter point is extremely important to a discussion of band widths and contours and is a subject of discussion in another paper.<sup>12</sup>

Figure 2 shows the absorption spectrum and the fluorescence spectrum of 2-phenylnaphthalene in a rigid glassy 1:6 mixture of 3-methylpentane-isopentane at 77°K. The long-wavelength crystal absorption at room temperature is also shown. The absorption and emission frequencies are given in Table I. The low-temperature solution absorption spectrum shows

(9) D. H. Hey and W. E. Walker, *J. Chem. Soc.*, 2217 (1940).

(10) D. H. Hey and S. E. Lawton, *ibid.*, 378 (1940).

(11) R. A. Friedel, M. Orchin, and L. Reggel, *J. Amer. Chem. Soc.*, **70**, 203 (1948).

(12) H. E. Holloway, R. V. Nauman, and J. H. Wharton, *J. Phys. Chem.*, **72**, 4474 (1968).

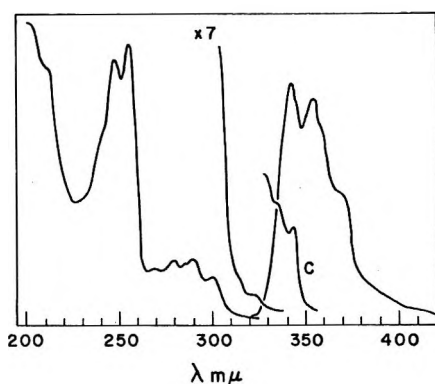


Figure 2. Absorption and fluorescence spectra (77°K) of 2-phenylnaphthalene (solvent, 1:6 3-methylpentane-isopentane). Room-temperature crystal absorption (C).

**Table I:** Absorption and Emission Frequencies of 2-Phenylnaphthalene, 2'-Methyl-2-phenylnaphthalene, and 1-Fluoro-2-phenylnaphthalene (Solvent, 1:6 3-Methylpentane-Isopentane (77°K))

Band	—2-Phenyl— naphthalene		2'-Methyl-2-phenyl- naphthalene		1-Fluoro-2-phenyl- naphthalene	
	$\lambda$ , Å	$\bar{\nu}$ , cm <sup>-1</sup>	$\lambda$ , Å	$\bar{\nu}$ , cm <sup>-1</sup>	$\lambda$ , Å	$\bar{\nu}$ , cm <sup>-1</sup>
(a) Absorption						
$\alpha$	3225	31,010	3215	31,100	3265	30,630
			3180	31,450	3200	31,250
			3070	32,570	3125	32,000
$\rho$	3010	33,220	2930	34,130	3010	33,220
	2890	34,600	2825	35,400	2890	34,600
	2780	35,970	2730	36,630	2780	35,970
$\beta$	2680	37,310	2640	37,880	2680	37,310
	2550	39,220	2500	40,000	2530	39,530
$\beta'$	2465	40,570	2430	41,150	2460	40,650
	2120	47,170	2130	46,950	2115	47,280
(b) Fluorescence Emission						
	3420	29,240	3280	30,490	3320	30,120
	3545	28,210	3335	29,985	3480	28,740
	3680	27,170	3455	28,940	3660	27,320
	3825	26,140	3585	27,890	3870	25,840
			3725	26,850		

considerably more structure than the room-temperature solution spectrum.

The first vibrational band of the  $\alpha$  transition is observed at 3225 Å (31,010 cm<sup>-1</sup>). Increasing the concentration intensifies this weak band, but the spectrum does not show any longer wavelength bands. However, if the solubility of 2-phenylnaphthalene is exceeded (as evidenced by a cloudy glass), additional bands beginning at 3430 Å (29,150 cm<sup>-1</sup>) are observed. These longer wavelength bands coincide with those observed from a polycrystalline sample. These results are analogous to those observed for the similar molecule biphenyl for which it is known that the molecules are planar in the crystal.<sup>13</sup> These comparisons and the fact that substituted 2-phenylnaphthalenes that cannot as-

sume the planar conformation do not show the red shift convince us that in crystalline 2-phenylnaphthalene the molecules are planar. The band at 31,010 cm<sup>-1</sup> in the solution spectrum is assigned to be the 0-0 band<sup>14</sup> of the  $\alpha$  transition for the molecule in solution and that at 29,150 cm<sup>-1</sup> is assigned to be the 0-0 band of the  $\alpha$  transition for the molecule in the crystalline matrix. The 1860-cm<sup>-1</sup> red shift of the crystal spectrum from the solution spectrum is attributed to a change from a nonplanar molecule in solution to a planar molecule in the crystal. In glassy solution at 77°K the electronic transition is interpreted to be a transition from a nonplanar equilibrium ground state to a nonplanar Franck-Condon excited state, while in the crystal the transition is interpreted to be from a planar ground state to a planar Franck-Condon excited state.

The 0-0 band of the fluorescence emission from rigid glassy solution is observed at 3420 Å (29,240 cm<sup>-1</sup>) and is red shifted 1770 cm<sup>-1</sup> from the position of the 0-0 band in absorption. The observed shift could be attributed to a failure to find other bands in absorption or fluorescence emission, stabilization of the Franck-Condon excited state by solvent interaction, a Stokes shift associated with a distance coordinate, and a Stokes shift associated with the angular coordinate or a combination of these effects. Since our arguments depend critically upon the absorption measurements, the measurements were carried out with a 0-0.1 absorbance scale and the base line was measured and subtracted. Thus the assignment of the 0-0 band in the solution absorption is believed to be correct. In addition, the Franck-Condon contour of the fluorescence emission does not show the characteristics of a forbidden origin. This is a strong indication that the first band measured in emission is the 0-0 band and that the 1770-cm<sup>-1</sup> shift is not the result of a Stokes shift due to a displacement of the excited-state potential function along a distance coordinate away from that of the ground state. Thus by elimination the shift between emission and absorption is attributed to a Stokes shift associated with the angular coordinate and in part to stabilization of the excited state by solvent interaction.

Comparison of the fluorescence emission from rigid glassy solution with the room-temperature crystal absorption shows a partial mirror image relationship. The vibrational frequency measured in the fluorescence (1030 cm<sup>-1</sup>) compares favorably with the vibrational frequency measured in the crystal absorption (920

(13) A. Hargreaves and S. H. Rizer, *Acta Crystallogr.*, **15**, 365 (1962).

(14) Here and in the discussion that follows, the term 0-0 band is used in the experimental sense of being the lowest energy band in absorption and the highest energy band in emission. In cases where the zero-point energy falls at different conformations for the ground and excited state, the experimental value of the 0-0 band energy must lose significance.



$\text{cm}^{-1}$ ); the ground-state vibrational frequency is higher as is normally observed. The 0-0 band of the fluorescence emission is  $90 \text{ cm}^{-1}$  to the blue of the 0-0 band of the crystalline absorption. Solvent considerations indicate that the crystalline transitions should be red shifted from those in the hydrocarbon solvent for the same conformation of the solute molecule in each environment. The vibrational similarity and near coincidence of the 0-0 bands between the crystal absorption spectrum and the solution fluorescence spectrum, as opposed to a  $1770\text{-cm}^{-1}$  shift between the 0-0 bands of solution absorption spectrum and solution fluorescence spectrum, indicate that the equilibrium conformation of the lowest excited state of 2-phenylnaphthalene in rigid glassy solution closely approaches the conformation of the molecule in the crystalline state.

Consistent with these observations is the interpretation that for the equilibrium ground state in solution the molecules of 2-phenylnaphthalene are distributed about an angular conformation and that for the equilibrium excited state the molecules are distributed about a planar or near-planar conformation. The shift between absorption and emission is believed to be composed of a Stokes shift due to rotation from the angular to the planar conformation during the lifetime of the excited state and in part to solvent stabilization of the excited state.

Further support of our analysis is given by the absorption spectra and fluorescence emission spectra of 2'-methyl-2-phenylnaphthalene and 1-fluoro-2-phenylnaphthalene. These spectra are shown in Figures 3 and 4, respectively, and the absorption and emission frequencies are given in Table I.

For 2'-methyl-2-phenylnaphthalene the shift between the 0-0 band of the  $\alpha$  transition and the 0-0 band of the fluorescence emission spectrum is only  $610 \text{ cm}^{-1}$ , as compared with  $1770 \text{ cm}^{-1}$  in the case of 2-phenylnaphthalene. Both the absorption spectrum and fluorescence spectrum are blue shifted relative to those of 2-phenylnaphthalene, and bands at longer wavelengths than those from glassy solution are not observed in the crystal absorption spectrum as they are in the case of 2-phenylnaphthalene. Thus the steric interaction between 2'-methyl and either 1- or 3-hydrogen is evidently the predominate consideration in the balance between steric repulsion and resonance stabilization. Rotation in the excited state is effectively blocked and very little Stokes shift is observed. The data also indicate that the molecules in solution are distributed about an angular conformation in which the average angle between ring planes is greater than that in the case of 2-phenylnaphthalene and that the equilibrium excited-state conformation is very near that of the equilibrium ground state.

A dramatic temperature effect occurs in the absorption spectrum of 2'-methyl-2-phenylnaphthalene, especially in the region of the  $\beta$  and  $\beta'$  bands. The

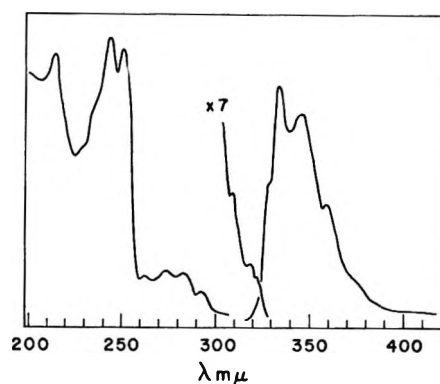


Figure 3. Absorption and fluorescence spectra ( $77^\circ\text{K}$ ) of 2'-methyl-2-phenylnaphthalene (solvent, 1:6 3-methylpentane-isopentane).

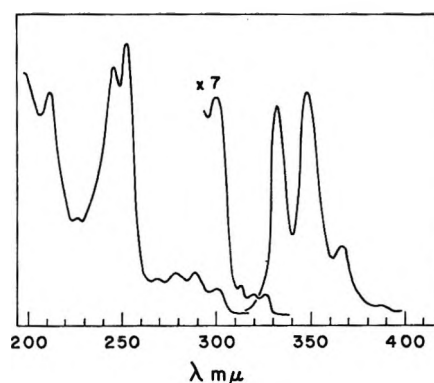


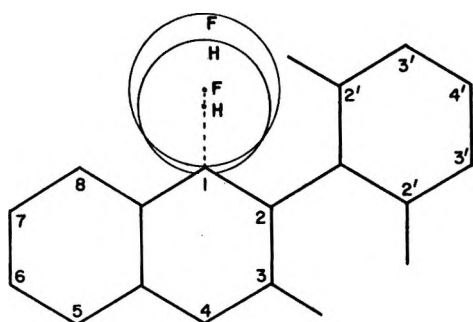
Figure 4. Absorption and fluorescence spectra ( $77^\circ\text{K}$ ) of 1-fluoro-2-phenylnaphthalene (solvent, 1:6 3-methylpentane).

apparent band at  $2250 \text{ \AA}$  in the room-temperature absorption spectrum disappears in the low-temperature spectrum; this band may result from the overlap of the  $\beta'$  band with  $\beta$  bands of the various conformers. The  $\beta$  and  $\beta'$  bands in this compound have very unusual contours in the room-temperature spectrum. In the low-temperature spectrum the  $\beta$  band is somewhat broader than normal and two maxima appear. Comparison with the  $\beta$  band of 2-phenylnaphthalene indicates that these two maxima may correspond to the different conformational isomers which are expected for 2'-methyl-2-phenylnaphthalene.

The room-temperature and low-temperature absorption spectra of 1-fluoro-2-phenylnaphthalene are much sharper than those of either 2-phenylnaphthalene or 2'-methyl-2-phenylnaphthalene. The spectrum is red shifted relative to that of 2-phenylnaphthalene, and the shift between the 0-0 band of the  $\alpha$  transition and that of the fluorescence spectrum is only  $510 \text{ cm}^{-1}$ . These data again indicate that the absorbing and emitting molecules are very similar. Replacement of the 1 hydrogen with a fluorine is believed to remove a hydrogen-hydrogen repulsion and substitute a weak hydrogen-fluorine attraction. Support for the contention is obtained by comparing the approximate  $\text{CF}\cdots\text{H}$  struc-

**Table II:** Ground- and Lowest Excited State Conformations of 2-Phenylnaphthalene Derivatives

Compd	Ground state	Excited state	Temp effect
2-Phenylnaphthalene	Angular	Planar	Small
2'-Methyl-2-phenylnaphthalene	Angular	Angular	Large
1-Fluoro-2-phenylnaphthalene	Planar	Planar	Small
1-Chloro-2-phenylnaphthalene	Planar	Planar	Medium
1-Bromo-2-phenylnaphthalene	Near planar	Planar	Large
6-Bromo-2-phenylnaphthalene	Angular	Planar	Small
2'-Fluoro-2-phenylnaphthalene	Near planar	Planar	Small
2'-Chloro-2-phenylnaphthalene	Near planar	Planar	Medium
2'-Bromo-2-phenylnaphthalene	Angular	Angular	Large
4'-Chloro-2-phenylnaphthalene	Near planar	Planar	Small
4'-Bromo-2-phenylnaphthalene	Near planar	Planar	Small

**Figure 5.** Geometry of 2-phenylnaphthalenes and the numbering system.

ture of 1-fluoro-2-phenylnaphthalene (Figure 5) with the valence angle and bond distance for hydrogen bonding with fluorine. The  $CF\cdots H$  angle ( $\sim 115^\circ$ ) and  $F\cdots H$  distance ( $\sim 1.6 \text{ \AA}$ ) are very close to the  $HF\cdots H$  angle ( $120^\circ$ ) and  $F\cdots H$  distance ( $1.34 \text{ \AA}$ ) observed in crystalline hydrogen fluoride.<sup>15</sup>

The experimental data indicate that in solution molecules of 1-fluoro-2-phenylnaphthalene are distributed about a planar configuration in both the equilibrium ground state and lowest excited state.<sup>16</sup>

### Discussion

The high quality of the materials prepared for this study indicates that the experimental results are not the result of ubiquitous impurities. On the other hand, the analysis and/or interpretation of these experimental results may contain artifacts. Because of the complexity of these molecular systems most of the individual interpretations seem indefensible. However, the consistency of the analysis from system to system indicates strongly that our main attitudes are correct. These attitudes are that the conformation in both the equilibrium ground state and equilibrium excited state are determined by the balance between steric and resonant effects. The tendency toward planarity increases in the excited states because of increased resonance considerations. The magnitude of the steric effect gives rise to three situations. These are a

planar ground and planar excited state (weak repulsive or attractive steric effects, 1-fluoro-2-phenylnaphthalene), an angular ground state and planar excited state (intermediate steric effects, 2-phenylnaphthalene), and an angular ground state and an angular excited state (strong steric effects, 2'-methyl-2-phenylnaphthalene). The magnitude of the shifts observed and the transition energies are then indirect measures of the steric and resonant effects. The interpretations are not as simple and direct as one would like because contributions from solvent stabilization, substitutional shifts, and a lack of structure in some systems make comparison difficult.

The shift associated with solvent stabilization of the excited state can be estimated from the shifts observed from systems in which the conformations of the ground and excited states are indicated to be essentially the same. The average shift observed in these cases is  $480 \text{ cm}^{-1}$ . Thus the  $1770\text{-cm}^{-1}$  shift observed in the 2-phenylnaphthalene case is broken down into  $1290 \text{ cm}^{-1}$  due to rotation in the excited state and  $480 \text{ cm}^{-1}$  due to solvent stabilization of the excited state. The solvent shift may seem quite large; however, the lowest excited state of 2-phenylnaphthalene is calculated to have a dipole moment of 9 D.<sup>12</sup> Thus the solvent shift is not unreasonable. The gap between the crystal absorption and crystal fluorescence of 2-phenylnaphthalene has been measured to be  $420 \text{ cm}^{-1}$ . This also supports the order of magnitude given for the solvent stabilization of the excited state.

Intuitively it seems that the glassy matrix should block or at least partially block the rotational relaxa-

(15) Y. K. Syrkin and M. E. Dyatkina, "Structure of Molecules and the Chemical Bond," Interscience Publishers, New York, N. Y., 1950, p 276.

(16) The fact that the fluorescence from 1-fluoro-2-phenylnaphthalene is  $880 \text{ cm}^{-1}$  to the blue of that from 2-phenylnaphthalene was of some concern. However, for 1-chloro-2-phenylnaphthalene we find the fluorescence only  $200 \text{ cm}^{-1}$  to the blue of that of 2-phenylnaphthalene. The shift between absorption and emission is only  $440 \text{ cm}^{-1}$ . Thus we conclude the blue shift for the 1-fluoro compound results from an inductive effect of the fluoro group. The data from the bromo derivative also support this conclusion.

tion in the excited state. The emissions have been measured from more rigid alcoholic glasses and there is evidence that these solvents do partially block the rotational relaxation. In these solvents the bulk of the emission red shifts but shoulders are found at higher energy than in glassy 3-methylpentane. The relaxation in any solvent is dependent upon the excitation energy. For example, in the measurements reported herein the emissions were excited at a 12-kcal/mol higher energy than the origin in absorption. Thus during the process of internal conversion and vibrational relaxation of the stretching modes considerable local heating of the matrix occurs. In view of this the effective temperature in the microscopic region surrounding the solute molecule is unknown during the time of relaxation. Since there is no significant shift between the room-temperature and 77°K fluorescence emission in the 3-methylpentane solvent, we conclude that this

rigid matrix does not block the relaxation process under the conditions of excitation used in these studies.

In all, 2-phenylnaphthalene and ten of its derivatives have been studied. A summary of the results is given in Table II. The temperature effect given is considered large if major changes occur in the relative intensities of the electronic absorption bands as temperature decreases and small if relative intensities of the electronic transitions are unaffected by temperature changes in the range 77–300°K.

*Acknowledgment.* H. E. H. gratefully acknowledges the support of the National Science Foundation in the form of a Science Faculty Fellowship and appointments to two Summer Research Participation Programs for College Teachers. We thank one of the referees for unusually close attention to experimental details that permitted us to improve our illustrations and clarify some of the discussion.

# The Electronic Structure and Spectra of 2-Phenylnaphthalene. Ground- and Excited-State Potential Energies as Functions of Molecular Conformation<sup>1</sup>

by Homer E. Holloway, Robert V. Nauman, and James H. Wharton

*Department of Chemistry, Louisiana State University, Baton Rouge, Louisiana 70803 (Received April 29, 1968)*

The potential energy as a function of molecular conformation of the ground electronic state of 2-phenylnaphthalene is considered to be the sum of the steric repulsion energy between nonbonded hydrogens and the  $\pi$  delocalization energy. The computation of the steric repulsion energy as a function of molecular conformation has been based on a model which includes both the van der Waals repulsion energy and the molecular deformation energy. The delocalization energy has been computed as a function of conformation by semiempirical SCF-MO methods. For the ground electronic state the equilibrium conformation is predicted to be that with an angle of  $30^\circ$  between ring planes. The theoretical electronic spectrum has been computed by the semiempirical SCE-MO-CI method as a function of molecular conformation. The theoretical spectrum for the  $30^\circ$  conformation is found to be in excellent agreement with the experimental spectrum. The potential energy as a function of molecular conformation of the excited electronic states has been estimated from the steric repulsion energy developed for the ground-state and the delocalization energies computed from the results of the configuration interaction calculations. A planar equilibrium conformation is predicted for the lowest excited state. The computations predict that thermal equilibration of the lowest excited state should give rise to a Stokes shift between the absorption and fluorescence spectrum of  $920\text{ cm}^{-1}$ . This agrees favorably with the experimental value of  $1290\text{ cm}^{-1}$ . The extent of inhomogeneous broadening of the absorption spectrum as a function of temperature predicted from the ground- and excited-state potential functions has been found to be in good agreement with experimental observations. Finally, the dramatic temperature effect observed for the  $\beta$  band of 2'-methyl-2-phenylnaphthalene is qualitatively explained in terms of the potential functions of 2-phenylnaphthalene.

In the preceding paper the spectra of the 2-phenylnaphthalenes have been analyzed in some detail.<sup>2</sup> Considerable information about the conformations and the energy effects associated with changes in conformation was deduced from comparisons of the experimental spectra. In addition, there were observed significant temperature effects which could be interpreted only qualitatively by consideration of the experimental data alone.

Here we describe our efforts to compute the energy effects associated with changes in conformation of 2-phenylnaphthalene and to interpret quantitatively the temperature effects observed in the absorption spectrum. Even a semiquantitative agreement between experiment and theory requires rather accurate computations of the change in ground-state energy with conformation and of the change in excited-state energies with conformation.

Since  $\sigma$ - $\pi$  separability is probably not a good approximation for twisted composite polynuclear aromatics and since the  $\sigma$  framework is important to the steric effects in the untwisted conformations, it would seem that a full  $\sigma$ - $\pi$  computation is necessary. However, the equilibrium conformation of 2-phenylnaphthalene approaches the planar conformation and hence the  $\pi$ - $\pi$  interaction makes the greatest contribution to the "delocalization" energy in this range of conformation. In addition, the  $\sigma$ - $\sigma$  interaction can be included as an empirical, nonbonded hydrogen repulsion in which both

the van der Waals repulsion and the molecular distortion are included in the steric repulsion energy. Thus in the case of 2-phenylnaphthalene the latter approach is expected to give better results than those that can currently be obtained from a full  $\sigma$ - $\pi$  computation.

## Methods

*Electronic Energy States.* As a guide to the interpretation of the electronic spectrum of 2-phenylnaphthalene, a computation based upon a configuration interaction model of the Pariser-Parr-Pople type<sup>3</sup> using SCF-MO's as basis functions has been carried out. Since the computation consisted of a straightforward application of the method, only the empirical parameters and basic assumptions are recapitulated. The input data were based on the structure shown in Figure 1 in which  $sp^2$  hybridization is assumed and all bond lengths are taken to be  $1.40\text{ \AA}$ , except the interannular bond which is assumed to be  $1.48\text{ \AA}$ . The latter distance is based on the fact that the central bond in planar biphenyl has been measured to be  $1.50\text{ \AA}$ <sup>4</sup> and the interannular bond in 2-phenylnaphthalene should be slightly shorter.

(1) Adapted from the Ph.D. dissertation of H. E. Holloway, Louisiana State University, 1967.

(2) H. E. Holloway, R. V. Nauman, and J. H. Wharton, *J. Phys. Chem.*, **72**, 4468 (1968).

(3) R. G. Parr, "Quantum Theory of Molecular Electronic Structure," W. A. Benjamin, Inc., New York, N. Y., 1963.

(4) A. Hargreaves and S. H. Rizer, *Acta Crystallogr.*, **15**, 365 (1962).

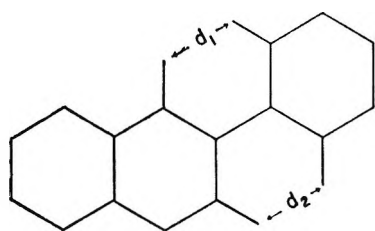


Figure 1. Geometry of 2-phenylnaphthalene ( $d_1$  and  $d_2$  distances between nonbonded hydrogens).

The empirical parameters were  $\beta_{uv}^0 = -2.39$  eV for adjacent carbons in the ring skeletons,  $\beta_{uv}^0 = 0$  for nonadjacent carbons,  $\beta_{2,11} = [S_{2,11}(1 - S_{2,11})/S^0(1 - S^0)] \beta^0 \cos \theta$  for the bonded carbons between rings,<sup>5</sup>  $\gamma_{\mu\mu} = 11.08$  eV, and  $\gamma_{\mu\nu} = 14.397/(1.300 + R_{\mu\nu})$  eV/Å.<sup>6</sup>

Calculations were made for the 0, 30, 45, 90° conformations. In the configuration interaction model for each conformation 25 singly excited configurations ( $\Psi_j^{-1}\Psi_k$ ) and the ground-state configuration were used. The computations were carried out with an IBM 7040 digital computer using a program written by Bloor and Gilson.<sup>7</sup>

**Steric Effects.** Numerous authors have considered the steric effect in overcrowded molecules, especially in the case of biphenyl. Adrian<sup>8</sup> has applied the "perfect-pairing" approximation of valence bond theory to a rigid molecular model. Goodwin and Morton-Blake<sup>9</sup> developed a simple nonbonded H-H potential function by empirically fitting a function consisting of the Hückel molecular orbital resonance stabilization energy combined with an assumed form for the steric repulsion energy to the experimentally measured equilibrium conformation; again, a rigid model was assumed. Golebiewski and Parczewski<sup>10</sup> developed a method for calculating the most stable conformation by minimizing the combined delocalization energy and the steric repulsion energy. The steric repulsion energy included the van der Waals repulsion energy and the molecular strain energy. This division of the steric repulsion energy into two contributions appears to offer a better rationale than does that based on the rigid molecule; however, these authors did not develop a potential function relating the steric repulsion to the molecular conformation. In addition, the authors used the hard-sphere model for van der Waals repulsions developed by Coulson and Senet<sup>11</sup>; this model was later criticized by Coulson and Haigh.<sup>12</sup> In the paper by Coulson and Haigh an extensive evaluation of steric interaction between nonbonded hydrogens has been made, and 14 H-H van der Waals potential functions have been examined. These authors conclude that atoms are "softer" than they had been assumed to be.

In the evaluation of the steric effect in 2-phenylnaphthalene, it is assumed that the steric potential function of biphenyl will closely approach that of 2-phenylnaph-

thalene. The merits of this assumption will be discussed as the magnitudes of the various interaction terms are evaluated. Thus the analysis is in fact that for biphenyl. A general theory for the quantitative evaluation of the steric repulsive energy of planar biphenyls has been given by Westheimer and Mayer<sup>13</sup> and has been applied to a calculation of rates of racemization by Westheimer.<sup>14</sup> In this method the total steric repulsion energy is given by

$$E_s = \frac{1}{2} \sum_i a_i q_i^2 + U(d_1) + U(d_2) \quad (1)$$

where  $a_i$  is the force constant associated with the displacement  $q_i$  along the normal coordinate and  $U(d)$  is the van der Waals repulsion between nonbonded hydrogens separated by the distance  $d_1$  or  $d_2$ . The distances  $d_1$  and  $d_2$  are given by the equations

$$d_1 = d_{10} + \sum_i b_i q_i \quad (2)$$

$$d_2 = d_{20} + \sum_i b_i' q_i \quad (2')$$

In these equations  $d_{10}$  and  $d_{20}$  are the separations between the nonbonded hydrogen pairs in the undistorted planar molecule. In the case of biphenyl,  $d_{10}$  and  $d_{20}$  are equal. The constants  $b_i$  and  $b_i'$  are geometric factors which relate the increase in  $d_1$  and  $d_2$  to the magnitude of the displacements. The minimum value of  $E_s$  with respect to all possible variations in the normal coordinates that influence  $d_1$  and  $d_2$  is found by solving the set of equations given by

$$\left( \frac{\partial E_s}{\partial q_i} \right)_{q_j \neq q_i} = 0 = \frac{1}{2} \frac{\partial}{\partial q_i} \sum_j a_j q_j^2 + \frac{\partial}{\partial q_i} U(d_1) + \frac{\partial}{\partial q_i} U(d_2) \quad (3)$$

The van der Waals potential function used was that given by Muller<sup>15</sup> and is

$$U(d) = -\frac{2818.1}{(d/a_0)^6} + 63,335e^{-2.645d/a_0} \text{ kcal/mol} \quad (4)$$

in which  $d$  is expressed in angströms and  $a_0 = 0.529$  Å. This equation was selected because (1) it was derived to

(5) Reference 3, p 100.

(6) N. Mataga and K. Nishimoto, *Z. Phys. Chem. (Frankfurt)*, **13**, 140 (1957).

(7) J. E. Bloor and B. R. Gilson, "Closed-Shell SCF-LCAO-MO," Quantum Chemistry Program Exchange QCPE-71.1, Indiana University, Bloomington, Ind., 1966.

(8) F. J. Adrian, *J. Chem. Phys.*, **28**, 608 (1958).

(9) T. H. Goodwin and D. A. Morton-Blake, *Theor. Chim. Acta*, **1**, 458 (1963).

(10) A. Golebiewski and A. Parczewski, *ibid.*, **7**, 171 (1967).

(11) C. A. Coulson and S. Senet, *J. Chem. Soc.*, 1813 (1955).

(12) C. A. Coulson and C. W. Haigh, *Tetrahedron*, **19**, 527 (1963).

(13) F. H. Westheimer and J. E. Mayer, *J. Chem. Phys.*, **14**, 733 (1946).

(14) F. H. Westheimer, *ibid.*, **15**, 252 (1947).

(15) A. Muller, *Proc. Roy. Soc.*, **A154**, 624 (1936).

agree with the observed splittings in the infrared spectra that arise from the intermolecular force fields caused by overcrowding and (2) it appears to be one of the potential functions that can be considered to be consistent with the experimental results in the analysis of Coulson and Haigh.

The vibrational force constants used are given in Table I. With the exception of the C-C interannular stretch, the force constants are those used by Westheimer in the case of 2,2'-dibromo-4,4'-dicarboxybiphenyl. The force constant corresponding to the interannular stretch was calculated by means of an assumed linear relation between bond order and the stretching force constant. Carbon-carbon single and double bonds and benzene bonds were used as reference points.

**Table I:** Values of the Force Constants,  $a_i$

Vibration	$a_i$
Interannular stretch	$6.1 \times 10^6$ dyn/cm
C-C-H bend	$0.86 \times 10^{-11}$ dyne cm/radian <sup>2</sup>
C-H stretch	$5.0 \times 10^6$ dyn/cm
Benzene ring	
1 <sup>a</sup>	$45.9 \times 10^6$ dyn/cm
6 + 8	$13.7 \times 10^6$ dyn/cm
(6 + 8)*	$450 \times 10^6$ dyn/cm
12	$46.2 \times 10^6$ dyn/cm
14	$138 \times 10^6$ dyn/cm
19	$74.6 \times 10^6$ dyn/cm

<sup>a</sup> The notation corresponds to that of Westheimer's normal-coordinate analysis.

In the case of planar undeformed biphenyl the bond lengths have been taken to be the following: C-H, 1.08 Å; ring C-C, 1.40 Å; and interannular C-C, 1.48 Å. The bond angles were taken to be 120°. The choice of 1.48 Å for the interannular bond length was based upon the bond distance measured for biphenyl in the vapor<sup>16</sup> where steric repulsion is absent. The distortion of the molecule is assumed to be sufficiently small that second- and higher order terms relating the H-H distance to the magnitude of the vibration in question can be neglected. Only three of the ring vibration normal-coordinate force constants (6 + 8, 6 + 8\*, and 12) and the corresponding geometric factors have been used. Analysis shows that the remainder of the force constants are so large or that the geometric factors are so small that the rings are essentially undistorted in these modes and thus the distortion energy is negligible. The geometric factors  $b_i$  and  $b_i'$  are given in Table II.

Table III gives the displacements, the energy associated with the displacements, and the total steric repulsion energy for planar biphenyl. The data show that the C-H stretch can be neglected and that the strain energy involving ring distortions is quite small (0.49 kcal/mol) as expected.

**Table II:** Geometric Factors,  $b_i, b_i'$

Vibration	$b_i$	$b_i'$
Interannular stretch	1.00	
C-C-H bend	$1.08 \times 10^{-8}$ cm/radian	
C-H stretch	-0.50	
Benzene rings		
6a + 8a	1.25	1.30
(6a + 8a)*	2.55	5.00
12	1.60	1.60

**Table III:** Contributions to the Steric Repulsion Energy of Planar Biphenyl

Vibration	Displacement ( $q_i$ )	Energy, kcal/mol
A. Model Including Ring Distortions		
Interannular stretch	0.022 Å	0.21
C-C-H bend	0.084 radian	1.76
C-H stretch	0.004 Å	0.02
(6a + 8a)	0.008 Å	0.12
(6a + 8a)*	0.002 Å	0.28
12	0.004 Å	0.09
$2U(d)$ ( $d = 2.04$ Å)		3.00
		5.48
B. Model Neglecting Ring Distortions		
Interannular stretch	0.0235 Å	0.24
C-C-H bend	0.0901 radian	2.01
$2U(d)$ ( $d = 2.018$ Å)		3.30
		5.55

In view of the small contributions of the ring distortions to the change in distance between nonbonded hydrogens and to the interaction energy, the calculation was repeated and the ring distortions and C-H stretch were neglected. These results are given in Table III. Neglect of the ring distortions severely alters the contribution of the C-C-H bend to the total energy but does not increase the total interaction energy significantly. Thus, because of the stiffness of the benzene rings, their distortions can be neglected in considering the total steric repulsion energy; however, the error in the individual contributions is apt to be quite large. The predicted 0.0235-Å stretch of the C-C interannular bond combined with the assumed 1.48 Å bond length for undeformed biphenyl gives 1.5035 Å for the interannular bond length in the planar molecule, a result that is in excellent agreement with experiment.<sup>4</sup> In addition, the predicted 2.08-Å nonbonded hydrogen distance is in fair agreement with the 1.97-Å distance estimated from experiment.<sup>17</sup>

(16) A. Almendinger and O. Bastiansen, *Kgl. Norske Videnskab. Selskabs Skrifter*, 4 (1958).

(17) See ref 12, p 543.

With the assumption that ring distortions can be neglected, biphenyl serves as a good model for 2-phenylnaphthalene, provided that the assumption that  $d_{10} = d_{20}$  is justifiable in the case of 2-phenylnaphthalene and that  $d$  for 2-phenylnaphthalene and  $d$  for biphenyl are equal. Analysis of the bond orders of planar 2-phenylnaphthalene indicates that  $d_{10} \cong 1.79 \text{ \AA}$  and  $d_{20} \cong 1.81 \text{ \AA}$ , while  $d_0$  for biphenyl was  $1.80 \text{ \AA}$ . Thus a slight bending ( $\sim 0.003$  radian) of the C-C-C angles at the interannular bond would tend to make these distances equal and would involve very little strain energy (0.001 kcal/mol). Thus the steric repulsion energy of planar biphenyl should be applicable to 2-phenylnaphthalene.

If one considers only the interannular stretch and the C-C-H bends to be modes to relieve the van der Waals interaction, then calculation of the total repulsive energy as a function of the angle between planes is considerably reduced in complexity. The calculation involves fixing the molecule at various angles, calculating the corresponding  $d_0$  which is given by

$$d_0 = (12.50 - 9.24 \cos \theta)^{1/2} \quad (5)$$

and minimizing the repulsive energy. It is assumed that the hydrogens are displaced from each other along a line joining their undisplaced positions. The distortion involves both the in-plane and out-of-plane bending constants. The out-of-plane bending constant is  $0.39 \times 10^{-11} \text{ dyn cm/radian}^2$ .<sup>18</sup> The computation was made for the 0, 10, 20, 30, 40, and 60° conformations. The resulting repulsive potential function is given by the upper curve ( $E_s$ ) in Figure 2.

**Resonance Energy.** Several semiempirical methods commonly used to calculate increased resonance stabilization due to twist have been examined. Most of these methods include as the major contribution the function

$$E_\pi(\theta) = 2\rho_{rs}\beta_{rs} \cos^2 \theta \quad (6)$$

in which  $p_{rs}$  is the  $\pi$  bond order,  $\beta_{rs}$  is the resonance integral, and  $\theta$  is the angle between planes. Bond orders have been calculated by a variety of methods, while  $\beta_{rs}$  is generally selected to agree with the thermochemical data and an experimental picture of relatively free rotation. If the attitudes previously applied to biphenyl are applied to 2-phenylnaphthalene, the potential function obtained for the ground state indicates the planar conformation to be the most stable. In addition, the potential function shows very little energy variation. Thus there is predicted a broad molecular distribution which when combined with the transition energies calculated as a function of  $\theta$  suggests that the electronic absorption bands should be extremely broad. Both the planar ground-state conformation and extremely broad bands are in complete discord with the experimental results. Without adjusting  $\beta$  to an unrealistically small value and changing  $\beta$  between ground

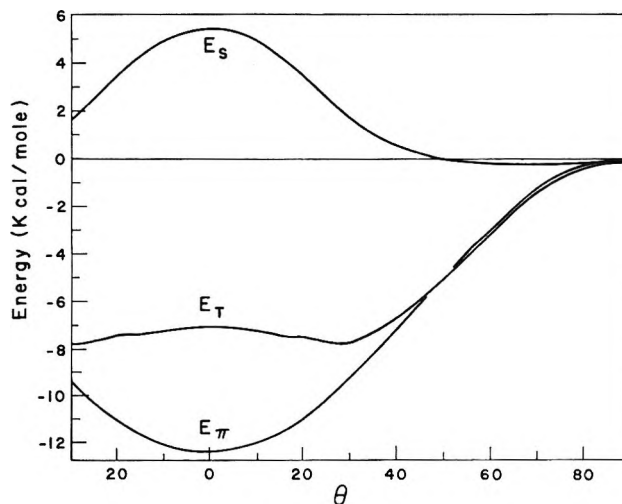


Figure 2. Potential energy as a function of conformation for the ground electronic state ( $E_s$ , steric repulsion energy;  $E_\pi$ , delocalization energy;  $E_T$ , total energy).

and excited states, the empirical methods developed for biphenyl are not applicable to 2-phenylnaphthalene.

It seems more nearly consistent to use the same model to predict resonance stabilization energies that has been used to calculate state energies. Pople<sup>19</sup> has successfully used the SCF method to calculate ground-state resonance energies without making a significant adjustment of  $\beta$ . Hence, the energy of delocalization across the interannular bond gained by untwisting the molecule is given by

$$E_\pi(\theta) = 2 \sum_{i=1}^8 E_i(\theta) - 2 \sum_{i=1}^8 E_i\left(\frac{\pi}{2}\right) \quad (7)$$

$E_i(\theta)$  is the energy eigenvalue of the  $i$ th SCF-MO at a given  $\theta$ . The function obtained is shown as the lower curve ( $E_\pi$ ) in Figure 2. A second-order correction to this function results from the variation in interannular bond length with the variation in angle between planes. This effect requires that the resonance stabilization plus steric repulsion should be minimized in one step. However, our  $\beta$  vs. bond length function is essentially invariant to the 0.02  $\text{\AA}$  bond stretch predicted by the steric interaction.

For the  $j$ th excited state the energy of delocalization across the interannular bond gained by untwisting the molecule is given by

$$E_{\pi,j}(\theta) = E_\pi(\theta) + \alpha_j(\theta) - \alpha_j\left(\frac{\pi}{2}\right) \quad (8)$$

in which  $\alpha_j(\theta)$  is the transition energy for the  $\theta$  conformation calculated from the configuration interaction model.

(18) R. C. Lord and D. H. Andrews, *J. Phys. Chem.*, **41**, 149 (1937).

(19) J. A. Pople, *Trans. Faraday Soc.*, **49**, 1375 (1953); A. Brickstock and J. A. Pople, *ibid.*, **50**, 901 (1954).

## Results and Discussion

**Ground-State Potential Function.** The ground-state potential function ( $E_r$ ) is shown in Figure 2 and is the sum of  $E_\pi(\theta)$  and  $E_\sigma(\theta)$ . The minimum energy is predicted at  $\theta = 30^\circ$ . In the range  $-40^\circ < \theta < 40^\circ$  the function is relatively flat but is predicted to rise rather sharply above  $40^\circ$ . These results are consistent with the intuitive prediction that the equilibrium conformation of 2-phenylnaphthalene should exhibit a greater tendency toward planarity than does biphenyl; the equilibrium angle in biphenyl has been determined to be  $42^\circ$ .<sup>16</sup> In addition the results are consistent with the analysis of the electronic absorption spectra of 2-phenylnaphthalene. The absorption spectra indicate that the equilibrium conformation in the ground state is angular; spectra of molecules in rigid hydrocarbon glasses are being compared with computational predictions for molecules in the gas phase. The minimal portion of the potential function is so broad that one must work at low temperatures in order to observe sharper spectra that result from a narrow distribution of molecules; low vapor pressure with the resulting need for long path lengths that lead to appreciable scattering prohibits the observation of vapor spectra at low temperatures. Consequently, the undesirable but necessary alternative of observing the spectra of 2-phenylnaphthalene in solution was adopted.

The predicted molecular distributions at 300 and 77°K, in which classical Boltzmann statistics are assumed, are shown in Figure 3. At room temperature a substantial population of the planar conformation is indicated, while at 77°K essentially no population of the planar conformation is indicated. Even at high temperature the molecular distribution is essentially confined to the region of  $\pm 40^\circ$ . However, in the computation of the steric repulsion energy and the delocalization energy  $\sigma$ - $\pi$  separability was assumed, and in the case of molecules like 2-phenylnaphthalene  $\sigma$ - $\pi$  separability may be a rather poor approximation for the  $90^\circ$  conformation. Thus at high angles the model assuming separate  $\sigma$ - $\sigma$  (steric repulsion function) interaction and separate  $\pi$ - $\pi$  (delocalization function) must be a poor approximation. On the other hand, as  $\theta$  approaches zero,  $\sigma$ - $\pi$  separability is a much better approximation. Consequently, the contour of the potential function is considered to be a good approximation below  $\theta = 45^\circ$ .

**Electronic Energy States.** Figure 4 is a graphical representation of the bonding MO's of the subsystems and shows the mixing of the localized MO's that occurs as the molecule approaches the planar conformation. The solid line implies that a great deal of subsystem character ( $>90\%$ ) is retained by the indicated MO's in the planar composite system. Dotted lines imply very little contribution, while the dashed lines imply extensive delocalization. As indicated, the major effect arises from the mixing of the  $B_1$  orbital of benzene with

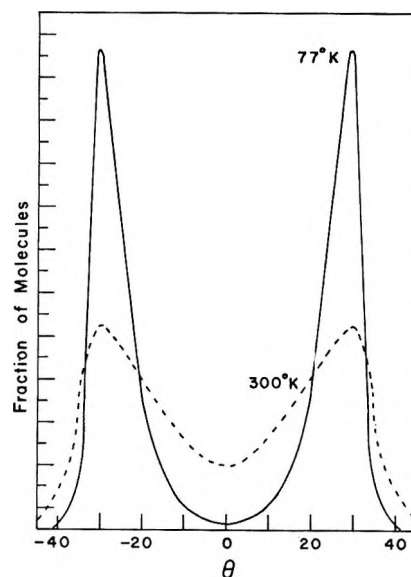


Figure 3. Molecular distribution functions for the ground electronic state at 77 and 300°K.

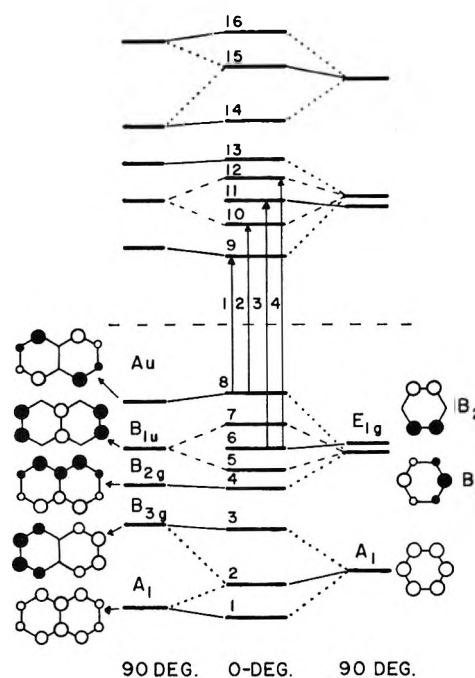


Figure 4. A correlation diagram for the molecular orbital energy levels of planar and twisted 2-phenylnaphthalene. The solid lines indicate the subsystem MO's that make the greatest contribution (greater than 90%) to the delocalized MO's while the dotted lines indicate the minor contributors. The dashed lines indicate that the subsystem MO's make essentially equal contributions to the delocalized MO's. Configurational excitations are denoted by arrows 1-4. Excitations 1 and 3 show no charge-transfer characteristics, while excitations 2 and 4 show partial charge-transfer characteristics.

the  $B_{1u}$  orbital of naphthalene. The MO's of 2-phenylnaphthalene can be classified as delocalized (5 and 7), partially localized (1, 2, 3, 4, and 8), and localized (6).



Table IV: Transition Energies and Transition Moments

Band <sup>a</sup>	Wave function	Conformations									
		90°		45°		30°		0°		Exptl <sup>c</sup>	
		$\Delta E^b$	$M$	$\Delta E$	$M$	$\Delta E$	$M$	$\Delta E$	$M$	$\Delta E$	$\epsilon$
$\alpha$	$\Psi_7^{-1}\Psi_9 - \Psi_8^{-1}\Psi_{10}$	4.26	0.0	4.16	0.0	4.11	0.0	4.00	0.0	4.21	$\sim 4 \times 10^2$
$\rho$	$\Psi_8^{-1}\Psi_9$	4.50	0.80	4.40	0.75	4.35	0.80	4.29	0.90	4.33	$1.25 \times 10^4$
$\beta$	$\Psi_7^{-1}\Psi_9 + \Psi_8^{-1}\Psi_{10}$	5.74	2.24	5.17	2.00	5.03	2.02	4.93	2.02	4.98	$5.7 \times 10^4$
$\beta'$	$\Psi_7^{-1}\Psi_{10}$	6.44	1.11	5.95	0.77	5.85	0.69	5.77	0.61	5.85	$4.1 \times 10^4$
...	$\Psi_6^{-1}\Psi_9 - \Psi_8^{-1}\Psi_{11}$	6.10	0.0	6.04	0.75	6.00	0.76	5.97	0.84	...	...
...	$\Psi_5^{-1}\Psi_9 - \Psi_8^{-1}\Psi_{12}$	5.97	0.0	6.07	1.07	6.06	1.16	6.05	1.18	...	...
...	$\Psi_4^{-1}\Psi_9 - \Psi_8^{-1}\Psi_{13}$	6.27	0.05	6.29	0.49	6.29	0.47	6.29	0.45	...	...
...	$\Psi_6^{-1}\Psi_{11}$	6.19	0.35	6.52	0.58	6.57	0.42	6.92	0.54	...	...
...	$\Psi_6^{-1}\Psi_{10} - \Psi_7^{-1}\Psi_{11}$	7.12	0.0	6.73	1.06	6.69	1.08	6.67	1.11	...	...
...	$\Psi_6^{-1}\Psi_{10} - \Psi_7^{-1}\Psi_{12}$	7.00	0.0	6.94	0.51	6.93	0.52	6.59	0.17	...	...

<sup>a</sup> Clar's notation. <sup>b</sup>  $\Delta E$  in electron volts. <sup>c</sup> Experimental values from  $\lambda_{\max}$  of the room-temperature-solution spectrum.

Thus three types of nonpolar configurational excited states and three types of polar configurational excited states (charge transfer of varying extents) are included in the configuration interaction model. Consideration of only first-order configurational interaction indicates that the  $\alpha$  and  $\beta$  transitions involve polar excited states (delocalized to partially localized), while the  $\rho$  transition involves a nonpolar excited state (partially localized to partially localized). Higher excited states include a great deal of charge-transfer character, giving rise to extensive charge-transfer mixing in the configuration interaction calculation.

The transition energies and transition moments obtained from the configuration interaction computation are given in Table IV along with the experimental results. For all conformations with  $\theta$  less than  $45^\circ$ , the calculated spectrum is in satisfactory agreement with the experimental results. The calculation for the  $30^\circ$  conformation agrees best with the experimental results; however, this agreement must be considered to be fortuitous because of the limited accuracy of the computation. It is significant that the calculated and measured spectra are in agreement in the range of  $\theta$  predicted to be pertinent by the ground-state potential function.

According to the configuration interaction model, the energy of the  $\alpha$  and  $\rho$  transitions is not extremely sensitive to the angular conformation, while the energy of the  $\beta$  transition is predicted to be very sensitive to the conformation. This is interpretable in terms of mixing the charge-transfer excited states ( $\Psi_6^{-1}\Psi_9 - \Psi_8^{-1}\Psi_{11}$  and  $\Psi_5^{-1}\Psi_9 - \Psi_8^{-1}\Psi_{12}$ ) with the state corresponding to the  $\beta$  transition.

The experimental spectrum is compared with the calculated spectrum in Figure 5. Only those transitions which are computed to have nonzero transition moments (except the  $\alpha$  transition) are included in the calculated spectrum. As observed, the calculated spectrum is in excellent agreement with the experimental spectrum for the  $\alpha$ ,  $\rho$ , and  $\beta$  transitions. The measured

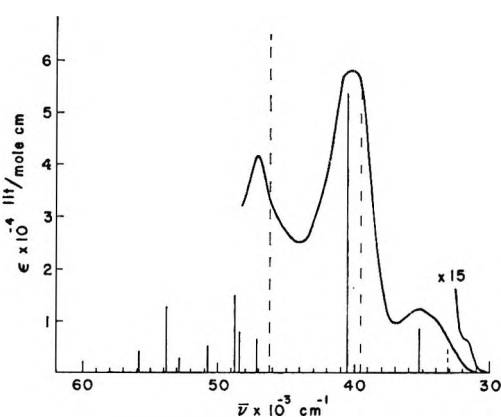


Figure 5. Comparison of the theoretical spectrum of the  $30^\circ$  conformation with the experimental spectrum. Calculated transitions (solid lines and short dashed line) are those of Table IV in the order of increasing energy. Lengths of solid lines are proportional to the transition moment squared, while the  $\alpha$  transition is dashed to indicate a transition moment of zero. The tall vertical dashed lines show the calculated upper and lower limits for the energy of the  $\beta$  transition ( $90$  and  $0^\circ$  conformations, respectively).

intensity of the  $\beta'$  transition is considerably higher than that predicted by the transition moment of the  $\Psi_7^{-1}\Psi_{10}$  transition. This indicates that a better interpretation of the band labeled  $\beta'$  is the superposition of the  $\Psi_7^{-1}\Psi_{10}$ ,  $\Psi_6^{-1}\Psi_9 - \Psi_8^{-1}\Psi_{11}$ , and  $\Psi_5^{-1}\Psi_9 - \Psi_8^{-1}\Psi_{12}$  transitions. The sum of the squares of the corresponding transition moments gives a good account of the intensity observed for the  $\beta'$  band. The tall vertical dashed lines in Figure 5 indicate the range of energies calculated for the  $\beta$  transition as the conformation is changed from  $90$  to  $0^\circ$ . The calculations indicate that no conformation has other allowed transitions in this range.

*Stokes Shift.* The potential functions for the ground state and first three excited states are shown in Figure 6. The excited-state potential functions are the sum of the delocalization energy (eq 8) computed for each excited state and the steric repulsion energy calculated for the ground state. Use of the ground-state steric repulsion

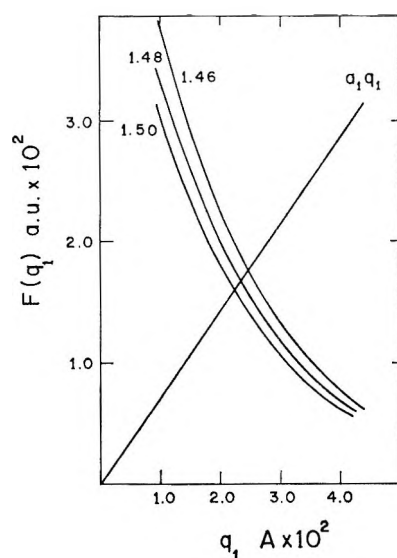


Figure 7. Graphical solutions for the displacement along the interannular bond length corresponding to minimum steric repulsion energy for bond lengths of 1.46, 1.48, and 1.50 Å in undeformed planar biphenyl.

between absorption and fluorescence than do the other resonance integrals. In addition the predicted ground- and excited-state conformations are acceptable. This analysis indicates that the theoretical results are not ultrasensitive to the value of the resonance integral between rings and that the best over-all results would be probably obtained with  $\beta \sim 2.00$  eV.

The sensitivity of the steric repulsion computation to changes in assumed coordinates has been investigated by varying the interannular bond distance for the undeformed molecule from 1.46 to 1.50 Å. The positions  $q_i^\circ$  corresponding to the minimum energies are found by solving the system of equations defined by eq 3. For the stretching of the interannular bond length this equation takes the form

$$a_i q_i^\circ = \frac{2\partial U}{\partial q_1} = F_1 d(q_i^\circ) \quad (11)$$

for the planar molecule. Graphically, the solution is shown in Figure 7 using interannular bond lengths of 1.46, 1.48, and 1.50 Å for the undeformed molecule. Inspection shows that the  $q_i^\circ$  and  $F_i(q_i^\circ)$  which enter into the energy are not very sensitive to the assumed interannular bond length. In Table VI the results of the total steric repulsion calculation are given for the planar molecule as a function of bond length. The results show that slight relaxations of the stretching and bending modes give rise to essentially constant non-

bonded hydrogen distances at very little cost in energy. Further analysis shows that the steric repulsion curves for the different interannular bond lengths rapidly converge as the angle between rings increases. The implication is that within reasonable limits the solutions to the steric contribution do not critically depend upon the assumed coordinates.

Table VI: Sensitivity of the Results to the Parameters. Variation of Interannular Bond Length

Undeformed bond length, Å	Equil bond length, Å	H-H distance, <sup>a</sup> Å	Steric energy <sup>b</sup>
1.46	1.4848	2.0101	6.18
1.48	1.5035	2.0181	5.50
1.50	1.5223	2.0269	5.03

<sup>a</sup> Nonbonded hydrogen distance for the planar molecule.

<sup>b</sup> Steric energy for the planar conformation in kilocalories per mole.

## Conclusions

The agreement between the experimental observations and theoretical predictions in the case of 2-phenylnaphthalene is extremely gratifying. This is especially true since our parameters have been taken from similar molecular systems. It seems possible within the framework of the computation to obtain a much better fit between experiment and theory by empirical methods. Perhaps this will be a worthwhile endeavor when more experimental data become available.

The initial success in the theoretical analysis of 2-phenylnaphthalene indicates that a combined theoretical-experimental attack on the spectra of the 1- and 2'-substituted 2-phenylnaphthalenes will provide considerable insight into the nature of intramolecular interactions. Thus far, 12 derivatives of 2-phenylnaphthalene have been synthesized and are currently being studied.

*Acknowledgment.* We wish to thank Dr. Jimmie McDonald for measuring the vapor spectrum of 2-phenylnaphthalene. H. E. H. gratefully acknowledges the support of the National Science Foundation in the form of two appointments to Summer Research Participation Programs for College Teachers and a Science Faculty Fellowship. We are especially grateful to one of the referees who made comments that showed deep understanding and suggested methods for improving and clarifying the discussion.

## Heterogeneous Activation in Thermal Unimolecular Reaction<sup>1a</sup>

by Kenneth M. Maloney<sup>1b</sup> and B. S. Rabinovitch

Department of Chemistry, University of Washington, Seattle, Washington 98105 (Received May 22, 1968)

The contribution of simple heterogeneity to the observed rate of reaction for thermal unimolecular systems has been examined. The equation of continuity was solved with appropriate boundary conditions. It is shown for spherical reactors that the magnitude of heterogeneous activation-deactivation effects is a function of the reactor size, the degree of falloff, temperature, and collision cross section. The variation of the concentration of activated substrate molecules as a function of the radial distance,  $r$ , of the pressure and collision diameter of the reactant and of the specific reaction rate of the reactant is illustrated, along with the behavior of a heterogeneity function  $H(E)$ ' that ranges between the limits of zero (no heterogeneity) and unity (complete heterogeneity). Application is made to the ethyl isocyanide thermal isomerization.

### Introduction

Homogeneous thermal unimolecular gas-phase reactions are frequently studied in a spherical reactor as a function of pressure and temperature. It is desirable that the contribution of heterogeneity to the observed rate be quantitatively assessed. Hudson and Heicklen<sup>2</sup> (HH) have made an important contribution to the treatment of this problem. They examined the steady-state solution of the nonhomogeneous differential equation

$$D\nabla^2 C(r) + R'(r) - k_v C(r) = 0 \quad (1)$$

subject to the boundary conditions

$$-D \frac{dC(r_0)}{dr} = k_w C(r_0) \quad (r = r_0) \quad (2)$$

and

$$C(r) = \text{finite} \quad (r = 0) \quad (3)$$

where  $C(r)$  is the concentration of reacting molecules at radial distance  $r$ ,  $D$  is the diffusion coefficient,  $R'(r)$  is the rate of homogeneous production or introduction of reactant molecules,  $k_v$  is the first-order rate constant for homogeneous reaction,  $r_0$  is the radius of the spherical vessel, and  $k_w$  is the velocity constant for the heterogeneous wall reaction. Condition 2 takes into account reaction at the wall; condition 3 ensures a solution at  $r = 0$  and is introduced because eq 1 has a singularity.

The solution of eq 1 for a sphere was given by HH, for  $R'(r)$  a constant, as

$$\frac{DC(r)}{R'r_0^2} = \frac{1}{K_v} - \frac{(K_w/K_v) \sinh \{K_v^{1/2} r/r_0\} / (K_v^{1/2} r/r_0)}{[\cosh \{K_v^{1/2}\} + (K_w - 1) \sinh \{K_v^{1/2}\} / K_v^{1/2}]} \quad (4)$$

where  $K_v = k_v r_0^2 / D$  and  $K_w = k_w r_0 / D$ , and

$$\frac{R_v}{R_w} = \frac{K_v}{3K_w} + \frac{K_v/3}{K_v^{1/2} \coth \{K_v^{1/2}\} - 1} - 1 \quad (5)$$

where  $R_v$  and  $R_w$  were defined by HH to be the total homogeneous and heterogeneous rates, respectively. Equation 1 may be made very general, but some applications to a range of energy states (see below) will necessitate its restatement in the form of a set of equations that span the range of energy states.

### Equation of Continuity for Activation-Deactivation

HH considered as an illustration the simple but important example of activation and deactivation of excited molecules. In this case,  $C(r)$  becomes  $C_E^*(r)$ , the concentration of activated molecules in unit range of energy at  $E$ ;  $R'$  becomes  $R_E'$ , the rate of homogeneous activation of molecules of reactant  $C_A$  to states at  $E$ , and may be taken as independent of  $r$ ;  $k_v$  is the specific rate constant for collisional deactivation in the gas phase; and  $k_w$  is a similar quantity for wall deactivation. HH did not actually use their detailed formulation in their considerations but instead simply compared the rates of collision at the wall and in the gas phase. As is shown formally below, their comparison corresponds to the limiting low-pressure situation for which  $k_v C_E^*(r) \simeq 0$  in eq 6 and  $k_w C_E^*(r_0) = 0$  in eq 7 and which leads to eq 11.

We are interested in this illustration in connection with the evaluation of the contribution of wall activation in an experimental study of unimolecular isocyanide isomerization. While the simplified procedure is valid for the limiting low-pressure unimolecular case, the assessment of the contribution due to heterogeneity in general, *i.e.*, in the falloff region, necessitates the detailed solution of the equation of continuity. This must be done for a range of energy states, since the specific reaction rate constant  $k_E$  is a function of energy. Equation 1 of HH is formally modified as

(1) (a) This work was supported by the National Science Foundation; (b) abstracted from the Ph.D. thesis of K. M. Maloney, University of Washington, 1968.

(2) J. L. Hudson and J. Heicklen, *J. Phys. Chem.*, **71**, 1518 (1967).

$$D\nabla^2 C_E^*(r) + k_v B(E) C_A^2 - k_v C_E^*(r) C_A - k_E C_E^*(r) = 0 \quad (6)$$

where  $B(E)$  is the appropriate equilibrium distribution expression, and the second term represents  $R_E'$ ;  $k_v$  is now defined to be the specific rate constant for gas-phase collisions;  $k_E$  is the specific rate constant for the reaction. Only the most common case of a spherical reactor is examined, but these considerations can readily be extended to the cylindrical case with use of the development of HH. The reactant concentration  $C_A$  may be taken as constant. Equation 6 has implicit in it the strong-collision assumption. We rewrite the boundary condition 2 as

$$C_E^*(r) = C_E^*(r_0) \quad (r = r_0) \quad (7)$$

$C_E^*(r_0)$  is evaluated from the subsidiary condition

$$-D \frac{dC_E^*(r_0)}{dr} = k_w C_E^*(r_0) - W_E \quad (r = r_0)$$

where the wall activation parameter,  $W_E$ , is defined as

$$W_E = \bar{c} B(E) C_A / 4 = k_w B(E) C_A$$

and the strong-collision properties of the wall are again assumed. Any other assumption than this upper limiting case for wall contribution would make the computations unnecessarily involved for present purposes.

Evaluation of eq 6 subject to boundary conditions 3 and 7 leads to the following solution which is written in a form which may be readily compared with eq 4

$$\frac{DC_E^*(r)}{r^2} = \frac{R_E'}{K_{vE}} - \frac{[(K_w/K_{vE})r_0 R_E' - W_E] \sinh \{K_{vE}^{1/2} r/r_0\} (K_{vE}^{1/2} r)^{-1}}{\cosh \{K_{vE}^{1/2}\} + (K_w - 1) \sinh \{K_{vE}^{1/2}\} (K_{vE}^{1/2})^{-1}} \quad (8)$$

It is useful to write the solution in another form

$$C_E^*(r) = \frac{R_E'}{k_{vE}} + \frac{[C_E^*(r_0) - R_E'/k_{vE}] \sinh \{K_{vE}^{1/2} r/r_0\} r_0 r^{-1}}{\sinh \{K_{vE}^{1/2}\}}$$

where

$$C_E^*(r_0) = \left[ \frac{R_E'}{k_{vE}} + \frac{W_E r_0 \sinh \{K_{vE}^{1/2}\}}{D(K_{vE}^{1/2} \cosh \{K_{vE}^{1/2}\} - \sinh \{K_{vE}^{1/2}\})} \right] \times \left[ 1 + \frac{K_w \sinh \{K_{vE}^{1/2}\}}{(K_{vE}^{1/2} \cosh \{K_{vE}^{1/2}\} - \sinh \{K_{vE}^{1/2}\})} \right]^{-1}$$

where  $K_E = k_E r_0^2 / D$ ,  $k_{vE} = k_v C_A + k_E$ , and  $K_{vE} = K_v + K_E$ .  $K_v$  no longer retains the meaning given in connection with eq 4, since  $k_v$  has been redefined in eq 6,

and is given by  $k_v r_0^2 C_A / D$ . The total rate of chemical reaction for molecules in unit range at  $E$ ,  $R_{TE}$ , is

$$R_{TE} = 4\pi k_E \int_0^{r_0} C_E^*(r) r^2 dr = 4\pi r_0^3 k_E \left\{ \frac{R_E'}{k_{vE}} + \left( \frac{C_E^*(r_0) - R_E'/k_{vE}}{K_{vE} \sinh \{K_{vE}^{1/2}\}} \right) \times (K_{vE}^{1/2} \cosh \{K_{vE}^{1/2}\} - \sinh \{K_{vE}^{1/2}\}) \right\} \quad (9)$$

The net contribution of heterogeneous activation to the reaction,  $R_{wE}$ , is therefore  $R_{wE} = R_{TE} - R_{vE}$ , and the homogeneous rate in the absence of any wall effects is

$$R_{vE} = 4\pi k_E \int_0^{r_0} C_E^*(ss) r^2 dr = 4\pi k_E C_E^*(ss) r_0^3 / 3 \quad (10)$$

where  $C_E^*(ss) = [k_v C_A / (k_v C_A + k_E)] B(E) C_A$  and  $C_E^*(ss)$  is the steady-state concentration that would prevail in the absence of heterogeneity. The above definitions differ from ref 1. In the low-pressure limit, with the use of the appropriate modifications of eq 6-8, the total rate of reaction,  $R_{TE}$ , is the total rate of activation

$$R_{TE} = 4\pi k_E \int_0^{r_0} C_E^*(r) r^2 dr = 4\pi r_0^3 k_v B(E) C_A^2 / 3 + 4\pi r_0^2 k_w B(E) C_A \quad (11)$$

which in effect is the relation used by HH in their example and which applies for  $k_v C_A \ll k_E$  (*i.e.*,  $p \rightarrow 0$ ).

### Contribution of Heterogeneity to Unimolecular Reaction Rate

We define heterogeneity (as it refers to activation-deactivation at the wall) in a general manner applicable to any pressure region in which a unimolecular reaction may be studied. For a given system, the contribution  $H$  to the total rate of reaction due to heterogeneity is measurable in terms of the excess of the total rate of reaction in the reactor volume in question over the corresponding homogeneous rate, *i.e.*, the rate of reaction in a volume of the same size which is part of a reactor of infinite extent. Then

$$H(E) = \langle C_E^*(r) \rangle - C_E^*(ss)$$

and

$$H(E)' = 1 - C_E^*(ss) / \langle C_E^*(r) \rangle$$

$\langle C_E^*(r) \rangle$  is the average concentration of excited molecules ( $\langle C_E^*(r) \rangle = \int_0^{r_0} C_E^*(r) r^2 dr / \int_0^{r_0} r^2 dr$ ). The quantity  $H(E)'$  is defined for convenience to range between the limits of zero (no contribution due to heterogeneity) and unity (100% heterogeneous activation).

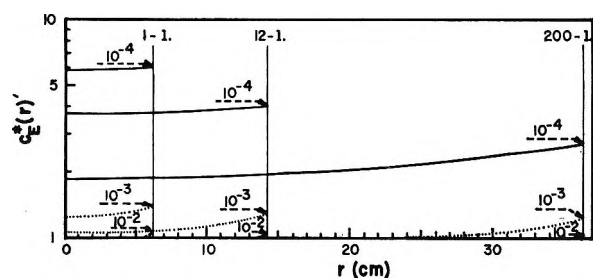


Figure 1. Concentration profiles of  $C_E^*(r)'$  vs.  $r$  for 1-, 12-, and 200-l. reactors, respectively, with  $k_E$  equal to the gas kinetic collision frequency at  $10^{-3}$  mm for a collision diameter,  $\sigma$ , of  $4.0 \text{ \AA}$  ( $k_E = 5.83 \times 10^3 \text{ sec}^{-1}$ ). Calculations have been made at  $260^\circ$ . Pressures begin at  $10^{-4}$  mm and increase by factors of 10 to a pressure of  $10^{-2}$  mm, above which  $C_E^*(r)$  becomes equal to  $C_E^*(ss)$  at all values of  $r$  and  $C_E^*(r)'$  equals unity everywhere: —,  $10^{-4}$  mm; ····,  $10^{-3}$  mm; ---,  $10^{-2}$  mm. These symbols are also used in subsequent figures. The vertical lines at 6.20, 14.20, and 36.28 cm represent  $r_0$  for the several reactors. The heads of the horizontal dashed arrows indicate the limiting concentration  $C_E^*(r_0)'$  at each pressure.

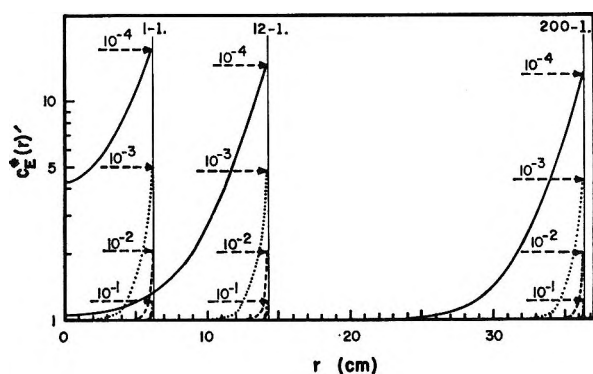


Figure 2. Concentration profiles of  $C_E^*(r)'$  vs.  $r$  for  $k_E$  corresponding to  $10^{-1}$  mm with  $\sigma = 4.0 \text{ \AA}$  ( $k_E = 5.83 \times 10^5 \text{ sec}^{-1}$ ). The calculation has been extended to  $10^{-1}$  mm (---). At  $10^{-4}$  mm, the system is in the second-order region.

The behavior of  $C_E^*(r)$  has been calculated at  $260^\circ$  from eq 8 for several vessels at three values of  $k_E$  (equal to the collision frequency  $\omega$  at  $10^{-3}$ ,  $10^{-1}$ , and 10 mm), and for  $\sigma_A = 4$  and  $7 \text{ \AA}$ , and for a typical mass,  $m_A = 60$  (Figures 1-4).  $C_E^*(r)'$  is the reduced concentration  $C_E^*(r)$  in units of  $C_E^*(ss)$ . These values of  $k_E$  and  $\sigma$  are representative of those of interest in conventional thermal systems. If  $k_E \gg \omega(10 \text{ mm})$ , then the falloff behavior occurs at such high pressures that the wall effects characteristic of lower pressure studies do not enter; if  $k_E < \omega(10^{-3} \text{ mm})$ , then a significant degree of falloff is not observable and such a system only can be examined close to the "high-pressure" region.

An important aspect of the behavior of  $C_E^*(r)'$  is not only the magnitude of the limiting value  $C_E^*(r_0)'$ , which increases with decreasing pressure and with increasing value of  $k_E$ , but also the distance  $r_h$  at which

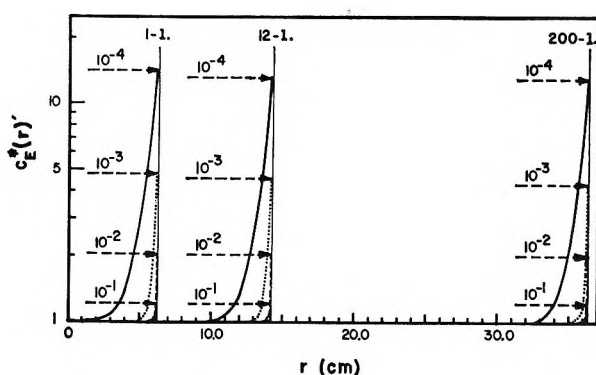


Figure 3. Here  $\sigma$  has been increased to  $7.0 \text{ \AA}$  but otherwise the calculation is for the same conditions as in Figure 2, except that the system reaches the second-order condition at  $10^{-3}$  mm. The decreased effect of heterogeneity relative to Figure 2 is evident.

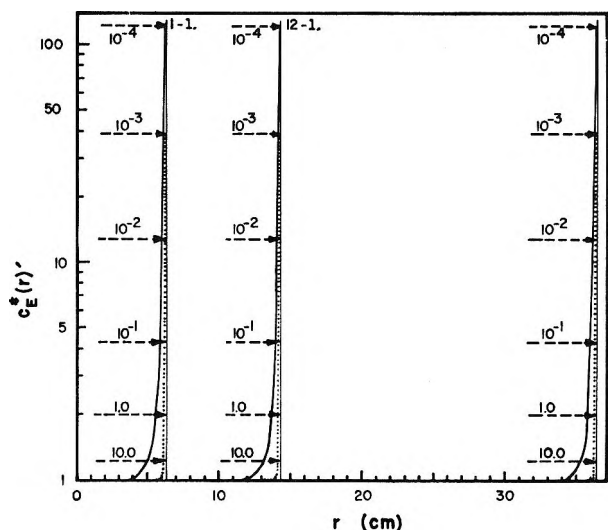


Figure 4. Concentration profiles of  $C_E^*(r)'$  vs.  $r$  for  $k_E$  corresponding to 10 mm with  $\sigma = 4.0 \text{ \AA}$  ( $k_E = 5.83 \times 10^7 \text{ sec}^{-1}$ ). For all pressures above  $10^{-3}$  mm the proximity of  $C_E^*(r)'$  to unity everywhere, except at  $r = r_0$ , is such that graphical representation of the area under the curves cannot be shown; the heads of the dashed arrows, however, indicate the limiting concentration  $C_E^*(r_0)'$  in each instance. Above 10 mm  $C_E^*(r)'$  becomes unity. The system is in the second-order region at all pressures.

the quantity  $C_E^*(r) - C_E^*(ss)$  first becomes greater than zero. As the value of  $k_E$  increases, for a given pressure and reactor size,  $r_h$  approaches closer to  $r_0$  and the change in  $C_E^*(r_0)'$  becomes very large. This behavior is for the reason that the rate of wall activation is independent of  $k_E$ , while  $C_E^*(ss)$  varies inversely with  $k_E$ ; also, as  $k_E$  increases, the activated molecules react before they can diffuse any appreciable distance from wall, and the concentration perturbation at the wall is not propagated inward.

Figure 5 illustrates the variation of  $H(E)'$  as a function of pressure in 1-, 12-, and 200-l. reactors, respectively, for the several  $k_E$  and collision diameters.

When  $C_E^*(r)$  becomes equal to  $C_E^*(ss)$  for all  $r$ ,  $H(E)' = 0$ . The arrow markers designate the respective threshold pressures below which each reaction (with characteristic rate constant  $k_E$ ) is in its own second-order region; the arbitrary but practical criterion was adopted that  $k_E > 100 (k_v C_A + 3k_w/r_0)$  for second-order behavior. For each reaction, the magnitude of  $H(E)'$  at values of the pressure below the markers depends simply on the relative rates of wall and homogeneous collision (activation) of A. At pressures above threshold, collisional deactivation as well as activation of  $A_E^*$  can occur at the wall so that the net rate of wall activation is reduced. It should be understood from the nature of Lindemann falloff that no effect on the

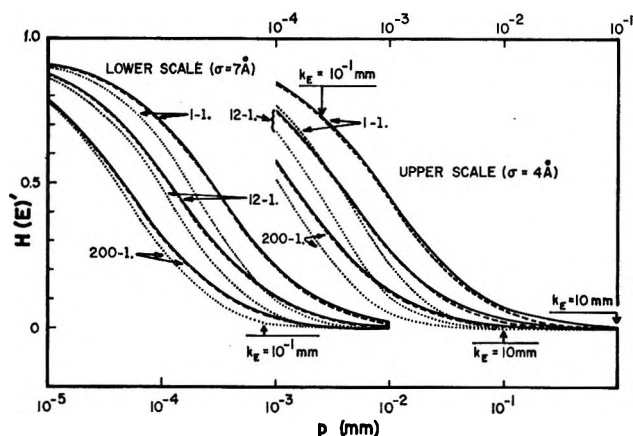


Figure 5. Summary plots of  $H(E)'$  vs. pressure for  $\sigma = 4.0$  and  $7.0 \text{ \AA}$ . These plots illustrate the dependence of heterogeneity on pressure, reactor volume,  $k_E$ , and collision cross section. The top scale is for the  $4.0\text{-\AA}$  case and the bottom scale is for the  $7.0\text{-\AA}$  case. That portion of each respective curve to the left of the arrows (positioned at the top of the figure for the  $4.0\text{-\AA}$  case and at the bottom of the figure for the  $7.0\text{-\AA}$  case) corresponds approximately to the second-order region for the values of  $k_E$  in question. The pressures at which the curves for the lowest  $k_E$  (corresponding to  $10^{-3} \text{ mm}$ ) enter the second-order region are below  $10^{-4} \text{ mm}$ .

observed rate constant due to "heterogeneity" may raise it above  $k_\infty$  for the reaction in its high-pressure equilibrium region—even though all activation were to take place at the wall. By contrast, the heterogeneity effect is a maximum for a given reaction when it is in the second order.

The  $H(E)'$  curves given in Figure 5 were calculated for the assumed collision diameters of 4 and  $7 \text{ \AA}$ . For the former case the homogeneous collision rate is reduced by one-third, all curves are moved to higher (by a factor of 3) pressures, and wall effects are enhanced.

The correct form (but not quantitative magnitude) of the pressure dependence of wall effects may be readily seen from the formulation of a simplified ratio of rates in terms of Lindemann-type expressions

$$R_T(E)/R_v(E) \propto \frac{\frac{r_0}{3}k_v C_A + k_w}{k_w + \frac{r_0}{3}(k_v C_A + k_E)} \bigg/ \frac{k_v C_A}{k_v C_A + k_E}$$

where  $R_T(E)/R_v(E)$  is the ratio of total rate in an energy range at  $E$  (due to the homogeneous plus heterogeneous contributions) to the rate if only the first contribution were to enter. Then

$$R_T(E)/R_v(E) \sim \left[ 1 + \frac{k_w}{\frac{r_0}{3}k_v C_A} \right] \left[ \frac{1}{1 + \frac{k_w}{\frac{r_0}{3}(k_v C_A + k_E)}} \right] \quad (12)$$

and

$$H(E)' \sim 1 - [R_v(E)/R_T(E)]$$

The first factor in the ratio of eq 12 describes the relative importance of wall and homogeneous collisions; the second factor relates to the region of falloff in question, in the form of the relative importance of total and homogeneous rates of removal of activated molecules. For  $k_w \ll r_0 k_v C_A / 3$ , the wall effect is unimportant and the ratio approaches unity and  $H' = 0$ ; for  $k_E \gg (k_v C_A, 3k_w/r_0)$ , the ratio has the full value of the first term, corresponding to maximum wall effect in the second-order region; for  $k_E \ll k_v C_A$ , the system is in the high pressure and the ratio is unity and  $H(E)' = 0$ , independent of the importance of  $k_w$ ; and for  $3k_w/r_0 \gg k_E \gg k_v C_A$ , as the pressure of the system decreases the second factor decreases more slowly than the first factor increases and  $H'$  goes to unity—also, the observed first-order rate constant is in this circumstance equal to  $k_\infty$ .

The simplification that entered the formulation of eq 12 was the (implicit) premature spatial averaging of  $C_E^*(r)$  and its replacement by an (unspecified) average.

Figures 1-5 provide a sufficient illustration of the dependence of  $H(E)'$  on various parameters so that semiquantitative estimates of  $H(E)'$  may be readily made for other systems. The variation of  $H'$  with temperature enters through the dependence of  $D$  and of the range of  $k_E$  on  $T$ , as well as of  $C_A$  if pressure is kept constant. In the second-order region,  $H(E)'$  does not vary with  $T$  if  $C_A$  is kept constant. In the falloff region, increase of  $T$  leads to increase of  $H(E)'$ . The magnitudes of these effects are illustrated in Figure 6 for the case of a 12-l. vessel, with  $k_E = 10^{-1} \text{ mm}$  and  $\sigma = 4 \text{ \AA}$ . An actual system in which the average effective value of  $k_E$ , and the region of falloff, changes with temperature is more complex, but the expected variation of  $H(E)'$  over a considerable range of temperature is not large.

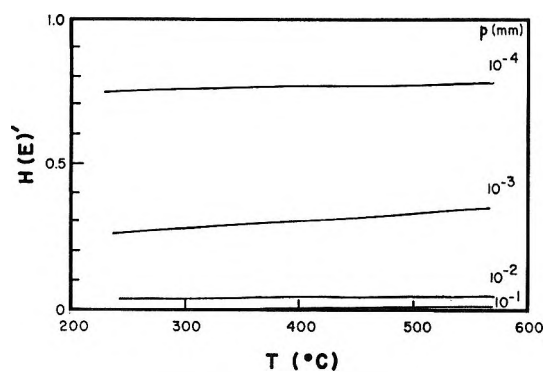


Figure 6. Illustration of the variation of  $H(E)'$  with temperature in a 12-l. vessel at several constant pressures for  $k_E = 0.1$  mm and  $\sigma = 4 \text{ \AA}$ . The rate of change of  $H(E)'$  with temperature passes through a maximum with decreasing pressure. The variation of  $H(E)'$  at  $10^{-4}$  mm, which is in the second-order region, is due to the variation of  $C_A$  with temperature at constant pressure.

### The Cyclopropane Reaction

As a practical example, HH considered the cyclopropane isomerization data which had been obtained by one of us;<sup>3</sup> they used the limiting second-order formulation for a pressure of  $1.53 \times 10^{-3}$  mm in a 12-l. reactor at  $500^\circ$ . The reduced rate,  $k/k_\infty$ ,<sup>4</sup> under these conditions is  $6 \times 10^{-3}$ , which corresponds to a reaction order of<sup>5</sup> 1.75. One may estimate<sup>5</sup> that a representative value of  $k_E$  for this system is  $5 \times 10^5 \text{ sec}^{-1}$  at the degree of falloff in question. The limiting calculation given by HH overestimated the heterogeneous contribution by only  $\sim 15\%$ .

### Illustration: Ethyl Isocyanide Isomerization

Owing to the increased molecular complexity of ethyl isocyanide as compared with methyl isocyanide,<sup>6</sup> the accessibility of the second-order thermal region decreases significantly and makes rate measurements in the pressure regions where heterogeneity becomes important unavoidable.

The effect of heterogeneity was calculated for this system for the several reactor volumes (0.5–200 l.), temperatures (190, 231, and  $260^\circ$ ), and pressures used. The Marcus–Rice<sup>7</sup> formulation was used to generate  $k_E$  at  $50\text{-cm}^{-1}$  intervals.<sup>8</sup> The corresponding hetero-

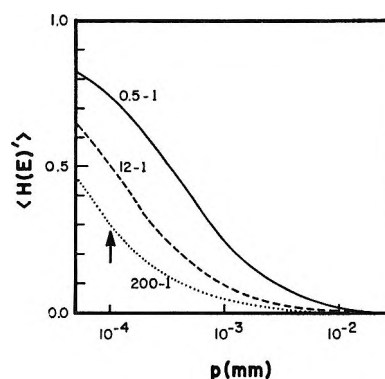


Figure 7. Variation of the average heterogeneity function,  $\langle H(E)' \rangle$ , with pressure for the ethyl isocyanide system at  $231^\circ$  in three reactors. The arrow shows the pressure below which the reaction would be effectively in the second-order region in the largest vessel for the case  $\sigma = 7 \text{ \AA}$ ; if  $\sigma$  were less,  $\langle H(E)' \rangle$  would be increased.

geneity functions  $H(E)'$  were calculated and averaged over the distribution function for the reacting molecules

$$\langle H(E)' \rangle = \int_{E_0}^{\infty} H'(E) \frac{k_E}{\omega + k_E} B(E) \times \\ dE / \int_{E_0}^{\infty} \frac{k_E}{\omega + k_E} B(E) dE$$

Summary plots of  $\langle H(E)' \rangle$  vs. pressure at the central temperature of  $230.9^\circ$  for the 0.5-, 12-, and 200-l. reactors with  $\sigma_A = 7 \text{ \AA}$  are given in Figure 7. Simple heterogeneity is estimated to become important below  $5 \times 10^{-2}$  mm in the 12-l. reactor and below  $1.5 \times 10^{-3}$  mm in the 200-l. reactor. The experimental results are in reasonable agreement.<sup>8</sup>

(3) B. S. Rabinovitch, P. W. Gilderson, and A. T. Blades, *J. Amer. Chem. Soc.*, **86**, 2994 (1964).

(4) E. W. Schlag and B. S. Rabinovitch, *ibid.*, **82**, 5996 (1960).

(5) D. C. Tardy and B. S. Rabinovitch, *J. Chem. Phys.*, **48**, 1282 (1968).

(6) F. W. Schneider and B. S. Rabinovitch, *J. Amer. Chem. Soc.*, **84**, 4215 (1962).

(7) R. A. Marcus and O. K. Rice, *J. Phys. Colloid Chem.*, **55**, 894 (1951).

(8) K. M. Maloney and B. S. Rabinovitch, submitted for publication.

# The Experimental Evaluation of $k_{\infty}$ in Unimolecular Reaction Systems<sup>1</sup>

by I. Oref and B. S. Rabinovitch

Department of Chemistry, University of Washington, Seattle, Washington 98105 (Received June 17, 1968)

Empirical methods described in the literature for the extrapolation of lower pressure data to  $k_{\infty}$  in thermal unimolecular reaction systems are examined. A systematic procedure is proposed wherein the plot of  $k^{-1}$  vs.  $p^{-\alpha_L}$  is extrapolated;  $\alpha_L$  is a parameter to be found from the data. Illustration of the method with experimental data is provided.

## Introduction

There are several procedures by which the high-pressure limiting unimolecular rate constant  $k_{\infty}$  may be evaluated from rate data which do not extend to sufficiently high pressure. The most common of these, the extrapolation of  $k^{-1}$  vs.  $p^{-1}$ , is rooted in historical precedent<sup>2</sup> and is not based on any currently accepted theoretical concepts. We propose here a systematic method by which  $k_{\infty}$  may be estimated from lower pressure data; the characteristics of this method are discussed and are related to the (empirical) methods which are conventionally employed for this purpose.

Two general approaches may be used for the evaluation of  $k_{\infty}$ , one "theoretical" and the other practical and empirical. The extrapolation to  $k_{\infty}$  by the "theoretical" method may be made by fitting some rate function, such as that of Slater (S),<sup>2a</sup> Rice, Ramsperger, and Kassel,<sup>2b</sup> Marcus and Rice,<sup>3</sup> or the quasi-theoretical form of Powell<sup>4</sup> to the curvature of the observed rate constant-pressure plot in the region in question. Obviously, the difficulty here is the accuracy and reliability of the fit obtained, else the problem posed were solved; in fact, even when experimental data do range all the way to  $k_{\infty}$ , the experimental curvature, *e.g.*, as expressed by Kassel's  $s$ , can be determined only roughly from typical data, *e.g.*,  $\Delta s = \pm 1$  or 2. When the data do not extend to the high-pressure limit, or only extend over a limited range, it can be very difficult to establish the appropriate magnitude of Kassel's  $s$  or Slater's  $n$  (and hence of the range of  $k/k_{\infty}$  involved) because the same range of slopes of the plot of  $\log k$  vs.  $\log p$ , from unity to zero, is traversed by all systems, whatever  $s$  or  $n$ , and because of the insensitivity of the functions. Hence, for incomplete data that may extend only over a limited range, the error in evaluation of the curvature increases and the value so obtained for  $k_{\infty}$  may be very inaccurate. In practice, this procedure has been scarcely used; its characteristics follow from standard statistical analysis and this note will not deal further with these other than to give some indirect insight below into the errors that may be generated.

The empirical procedures are very simple and easy to perform; they involve plotting the data in some form,

usually  $k^{-1}$  vs.  $p^{-1}$  (Hinshelwood, H) or  $k^{-1}$  vs.  $p^{-0.5}$  (Schlag and Rabinovitch, SR).<sup>5</sup> The H plot is especially inaccurate because for most systems the plot approaches the ordinate in a near-asymptotic manner and the intercept is extremely difficult to evaluate; this extrapolation tends always to give an underestimate of  $k_{\infty}$ . The SR plot usually has less curvature than the H plot; it may give rise to an overestimate (usually) or underestimate of  $k_{\infty}$ , depending on the curvature of the fall-off data, *i.e.*, on the true value of  $n$  or  $s$  which characterizes the data. We wish now to examine the problems of extrapolation and the nature and relation between the various procedures. We suggest an extension of these methods by which  $k_{\infty}$  can be determined in a more general way if the empirical method is chosen.

## Rationale of Procedure

Consider the plot,  $k^{-1}$  vs.  $p^{-\alpha}$ , where  $0 < \alpha < 1$ . This graphical form when applied to a given set of experimental data will be found to be concave upward or downward depending on the value of  $\alpha$  used. However, for every set of data there is an  $\alpha_L$  which will roughly linearize the plot,  $k^{-1}$  vs.  $p^{-\alpha_L}$ . We have systematically evaluated  $\alpha_L$  with the use of the Slater quantity  $I_n(\theta)$  to generate  $k/k_{\infty}$ . The function  $I_n(\theta)$  was chosen because of its simple form: for this function the fall-off "curvature" of the dependence of  $k$  on  $p$  depends only on a single parameter  $n$ , by contrast with RRK<sup>2</sup> or RRKM<sup>3</sup> treatments. The Slater function does not necessarily give *precisely* the same shape as experimental data, but then neither does any theory, *e.g.*, RRKM, even though more soundly based.

(1) This work was supported by the National Science Foundation.

(2) (a) N. B. Slater, "Theory of Unimolecular Reactions," Cornell University Press, Ithaca, N. Y., 1959; (b) L. S. Kassel, "Kinetics of Homogeneous Gas Reactions," Chemical Catalog Co., New York, N. Y., 1932.

(3) R. A. Marcus and O. K. Rice, *J. Phys. Colloid Chem.*, **55**, 894 (1951); R. A. Marcus, *J. Chem. Phys.*, **20**, 359 (1952).

(4) R. E. Powell, *ibid.*, **30**, 724 (1959).

(5) E. W. Schlag and B. S. Rabinovitch, *J. Amer. Chem. Soc.*, **82**, 5996 (1960); B. S. Rabinovitch and K. W. Michel, *ibid.*, **81**, 5065 (1959).



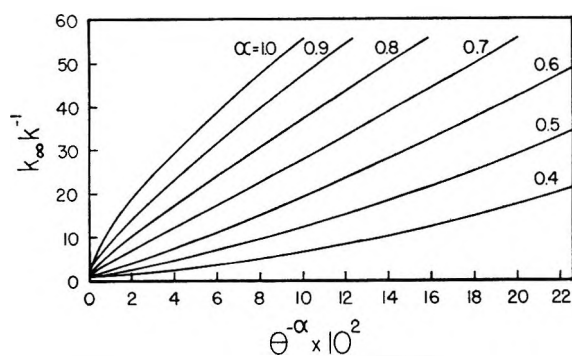


Figure 1. Plot of the inverse function  $I_n(\theta)^{-1}$  vs.  $\theta^{-\alpha}$ , for the case  $n = 11$  and for various values of  $\alpha$ ;  $\alpha_L = 0.65$ .

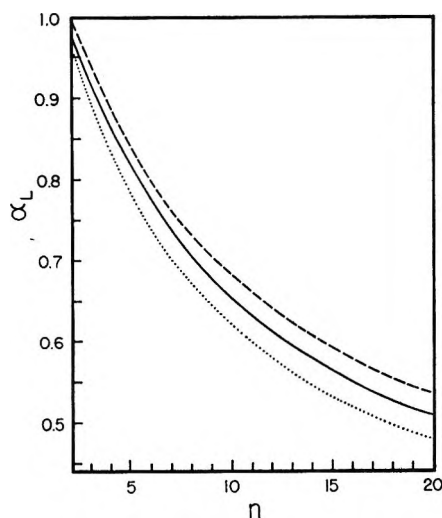


Figure 2. Variation of  $\alpha_L$  with  $n$  for various ranges of  $k/k_\infty$ : —, 0.05–0.99; ----, 0.05–0.5; ····, 0.1–0.99.

Figure 1 presents sample plots of  $k_\infty k^{-1}$  vs.  $\theta^{-\alpha}$  for the case of  $I_{11}(\theta)$ . It is seen that the curvature of the plot varies with the value of  $\alpha$ ; for  $\alpha = 0.65$ , the plot is approximately a straight line. As shown in Figure 2,  $\alpha_L$  is a strong function of the value of  $n$ ; but  $\alpha_L$  is also a weak function of the range of  $k_\infty k^{-1}$ . Figure 2 illustrates that  $\alpha_L$  varies weakly with the proximity to unity, and with the range of the values of  $I_n(\theta)$  from which it is deduced, for the sample cases  $I_n(\theta) = 0.05$ – $0.99$ ,  $I_n(\theta) = 0.5$ – $0.99$ , and  $I_n(\theta) = 0.05$ – $0.5$ . For actual experimental data,  $n$  varies by at least one or two units over a wide range of falloff and consequently the best fit to the data should also vary on that account. This variability in  $\alpha_L$  forebodes the error engendered (whether by the present method or by the “theoretical” fitting discussed first) by long extrapolation or by inaccurate or narrow range of data. It transpires that an experimental system of conventional accuracy must be close to the first-order region before any accurate conclusion regarding  $k_\infty$  can be reached. With this limitation, a procedure may be proposed for the evaluation of  $k_\infty$ : the quantity is found by extrapolation of the plot of  $k^{-1}$  vs.  $p^{-\alpha_L}$ ;  $\alpha_L$  may be evaluated by the

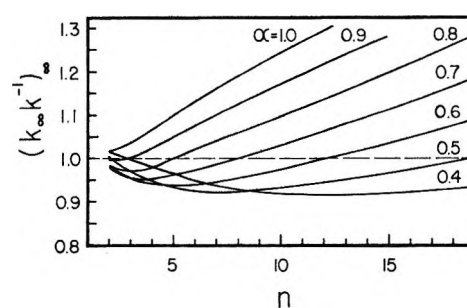


Figure 3. Plot of the value of the extrapolated intercept of  $I_n(\theta)^{-1}$  as a function of  $n$ , for various values of  $\alpha$ . The range of  $k/k_\infty$  used was 0.05–0.99.

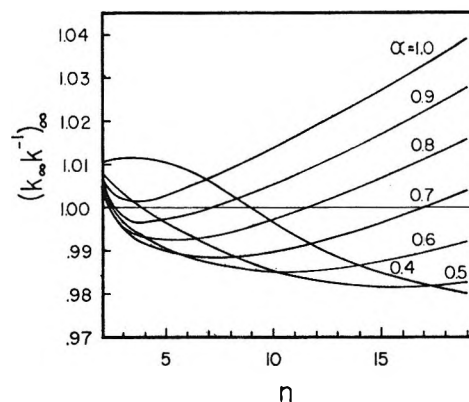


Figure 4. Similar to Figure 3 but for a range of  $k/k_\infty$  from 0.5 to 0.99.

weighted linear regression of  $k^{-1}$  on  $p^{-\alpha}$ ; a faster, and in many cases satisfactory, alternative would be evaluation of  $\alpha_L$  by graphical trial and error. Before illustrating the application of this procedure to experimental systems, it is desirable, first, to examine more generally the extrapolation of the Slater expression in order to illustrate the behavior to be expected for “ideal” data.

The inverse Slater function, treated as a set of experimental data, was plotted vs.  $\theta^{-\alpha}$  for a range of  $n$  and  $\alpha$ . The value of the intercept,  $(k_\infty k^{-1})_\infty$ , was in each case found by fitting the  $k_\infty k^{-1}$  vs.  $\theta^{-\alpha}$  plot by least squares with a fourth-order and a tenth-order polynomial in  $\theta^{-\alpha}$ . The choice of order was arbitrary, but the two series gave agreement and both give a good fit to  $I_n(\theta)$ . Figures 3 and 4 indicate the results of the extrapolation based on the fourth-order polynomial. They illustrate the kind of improvement in the evaluation of  $k_\infty$  to be expected when the “data” emphasize a range closer to  $k_\infty$  (Figure 4 relative to Figure 3); errors in the evaluation of  $\alpha_L$  become unimportant, as is to be expected. Not shown is another set of intercept estimates evaluated as a function of  $n$  for the limited range 0.05–0.5 of  $k/k_\infty$ : the errors are notably enhanced, especially for lower values ( $<15$ ) of  $n$ . We observe that a particular  $\alpha$  can give rise to an over- or under-estimate of the value of  $k_\infty$  whose deviation depends on the  $n$  value

**Table I:** Evaluation of  $k_\infty$  from Experimental Data by Extrapolation Based on  $\alpha_L$ 

System	$T, ^\circ\text{C}$	$k_\infty$ (re-ported), <sup>a</sup> $10^{-6} \text{ sec}^{-1}$	No. of data points	$k/k_\infty$ range of data	$pw = 0$		$pw = 1$		$pw = 2$	
					$\alpha_L$	$k_\infty, 10^{-6} \text{ sec}^{-1}$	$\alpha_L$	$k_\infty, 10^{-6} \text{ sec}^{-1}$	$\alpha_L$	$k_\infty, 10^{-6} \text{ sec}^{-1}$
$\text{CH}_3\text{NC}^6$	199.4	7.50	50	0.99-0.012	0.77	9.55	0.78	8.23	0.78	8.22
	230.4	92.5	99	0.99-0.0016	0.92	42.5	0.90	66.5	0.89	93.5
	259.8	767	49	0.27-0.0018	0.89	282	0.88	418	0.88	419
	199.4		14	0.74-0.098	0.78	7.51				
	230.4		14	0.89-0.66	0.47	103				
	199.4		14	0.99-0.74	0.94	7.61				
	230.4		14	0.99-0.89	0.64	94.7				
$c\text{-C}_3\text{H}_6^7$	500	61.7	43	0.96-0.081	0.58	58.0	0.57	60.1	0.57	60.1
			14	0.60-0.24	0.58	53.9				
			14	0.91-0.60	0.45	68.3				
$\text{N}_2\text{O}_2^7$	27	0.29 <sup>b</sup>	16	0.424-0.008	0.77	0.08	0.72	0.15	0.71	0.18

<sup>a</sup> This estimate of  $k_\infty$  is the one given by the original workers<sup>6</sup> in the case of  $\text{CH}_3\text{NC}$  and by Johnston and White<sup>7</sup> for the other systems.

<sup>b</sup> Given as 0.23 by Powell;<sup>4</sup> units of  $\text{sec}^{-1}$ .

of the system. Finally, the H plot, which is ideal for  $n = 1$ , is particularly inaccurate and yields an underestimate of  $k_\infty$  in every case; the SR value  $\alpha = 0.5$  is more accurate and is more appropriate for the higher  $n$  values usually encountered (ideally  $n = 18$ ), but it leads generally to overestimation of  $k_\infty$ .

Application of the method was made to experimental data for methyl isocyanide,<sup>6</sup> nitrogen pentoxide,<sup>7</sup> and cyclopropane.<sup>7</sup> Table I summarizes the values of  $\alpha_L$ ,  $w$ ,  $pw$ , and  $k_\infty$  obtained for the isocyanide and cyclopropane systems over both the total and partial range of the reported data;  $w$  is a weighting factor defined as  $k/k_{\text{max}}$ , where  $k_{\text{max}}$  is the largest measured value of  $k$ , and which is intended to emphasize the higher pressure data;  $pw$  is the power to which  $w$  may be raised and which increases the weight of the higher pressure points. It is apparent that the data may be accurately and reliably extrapolated for the evaluation of  $k_\infty$  only when the data are reasonably close to  $k_\infty$ . For the 260° isocyanide data, which extend only to  $k/k_\infty = 0.27$ ,  $k_\infty$  was originally fixed<sup>6</sup> by use of the measured value of  $E_a$  and the observed values of  $k_\infty$  at lower temperatures. These data provide an illustration of the possible errors in extrapolation of actual data to  $p = \infty$ ; it is inappropriate to give much weight to data for which  $k/k_\infty < 0.1$ . The case  $pw = 0$  corresponds to unsuitable weighting;  $pw = 2$  is suitable for the present illustration, but the suitability of a particular weighting factor will in general depend on the range and detail of the actual data. This remark also applies to the fitting of "theoretical" functions.

A variation of the procedure described above would be to find an average intercept by the use of several values of  $\alpha$ ; e.g.,  $\alpha = 0.5$  and 1 may be used<sup>8</sup> and the intercepts of the two plots averaged. However, it is apparent from Figures 3 and 4 that an uncritical averaging of intercepts could lead to larger rather than smaller

errors. As a matter of fact, for data which correspond to large  $n$  values it would be better to use only the intercept derived from the SR curve, rather than to average it with the value obtained from an H plot. A better way of proceeding by this method would be to use the values of  $\alpha$  which bracket  $\alpha_L$ . For  $\alpha > \alpha_L$ , the plot of  $k^{-1}$  vs.  $p^{-\alpha}$  is concave downward; for  $\alpha < \alpha_L$ , the plot is concave upward; these plots could, in one possible procedure, be made to yield identical intercepts.<sup>8</sup> The possible advantage, if any, of this method over the first is simply the avoidance of the evaluation of  $\alpha_L$ . Trial application was made to the methyl isocyanide, nitrogen pentoxide, and cyclopropane experimental systems, with  $pw = 0$ . The data were fitted by a least-squares procedure to fourth-order polynomials with use of Grant's reduction method<sup>9</sup> to solve the normal equation and to obtain the coefficients of the polynomial. In each case, three plausibly disparate values of  $\alpha$  were guessed; no effort was made to optimize the range of  $\alpha$ . The large variation of the intercept with  $\alpha$  found (Table II), and which exceeds that suggested by Figures 3 and 4, reflects the influence of experimental error. Inasmuch as the choices for  $\alpha$  are arbitrary, simple averaging of intercepts is here an unsatisfactory procedure.

By way of contrast, the Slater curve for  $n = 3$  was again represented by a fourth-order polynomial (this choice of  $n$  is close to the experimental value,  $n = 4-5$ , for  $\text{CH}_3\text{NC}$ ). Good agreement within a few per cent was found between the individual intercepts for various  $\alpha$ , and also between the average intercept and the theoretical value. This emphasizes the fact that the

(6) F. W. Schneider and B. S. Rabinovitch, *J. Amer. Chem. Soc.*, **84**, 4215 (1962).

(7) H. S. Johnston and J. R. White, *J. Chem. Phys.*, **22**, 1969 (1954).

(8) L. F. Loucks and K. J. Laidler, *Can. J. Chem.*, **45**, 2795 (1967).

(9) F. B. Holdebrand, "Introduction to Numerical Analysis," McGraw-Hill Book Co., Inc., New York, N. Y., 1956.

**Table II:** Application of "Averaging Method" to Experimental Systems

System	$T$ , °C	No. of data points	Range of $k/k_{\infty}$	$\alpha$	$\alpha_L$	$k(\text{reported})$ , $10^{-5} \text{ sec}^{-1}$	Intercept, $10^2 \text{ sec}$	$k(\text{av})$ , $10^{-5} \text{ sec}^{-1}$
CH <sub>3</sub> NC	199.4	50	0.99-0.012	0.60	0.77	7.50 <sup>e</sup>	6.2	8.8
				0.80			10.6	
				0.99			17.1	
	230.4	99	0.99-0.0016	0.60	0.92	92.5 <sup>e</sup>	0.92	61 <sup>a</sup>
				0.80			1.31	
				0.99			2.56	
	259.8	49	0.27-0.0018	0.60	0.89	767 <sup>e</sup>	0.116	375
				0.80			0.162	
				0.99			0.513	
o-C <sub>3</sub> H <sub>6</sub>	500	43	0.96-0.08	0.40	0.58	61.7 <sup>e</sup>	1.45	63
				0.50			1.58	
				0.60			1.71	
N <sub>2</sub> O <sub>5</sub>	27	16 <sup>b</sup>	0.43-0.008	0.60	0.71	0.29 <sup>c</sup>	3.48 <sup>c</sup>	0.13 <sup>c</sup>
				0.80			7.85	
				0.99			12.0	
Slater ( $n = 3$ )	...	15	1-0.03	0.60	0.83	(1.00)	1.10	1.03
				0.80			1.04	
				0.99			0.947	

<sup>a</sup> Higher order polynomial or a value of  $pw > 0$  improves the fit notably; the low value reflects the extreme range of  $k/k_{\infty}$  being fitted.  
<sup>b</sup> Smoothed values. <sup>c</sup> Units of  $\text{sec}^{-1}$  and sec.

fluctuations of the experimental data in real systems contribute heavily to errors and difficulty in the estimation of  $k_{\infty}$ .

It has been as much our purpose in this note to clarify the problems of data extrapolation, and particularly to emphasize the doubtful conclusions that obtain from long extrapolation of even good data, as it has been

to suggest a particular procedure. We are not advocating the exclusive use of the empirical method. We conclude that evaluation of  $k_{\infty}$  from lower pressure isothermal experimental data is a somewhat insecure bootstraps operation in which both "theoretical" and empirical procedures may be usefully employed to explore the vagaries of the data.

## Infrared Vibrational Properties of GeF<sub>2</sub>

by J. W. Hastie, R. Hauge, and J. L. Margrave

Department of Chemistry, Rice University, Houston, Texas 77001 (Received May 29, 1968)

Infrared vibrational spectra for GeF<sub>2</sub> have been observed both in the gas phase and in solid neon and argon matrices. Fundamental frequencies of  $\nu_1 = 692 \text{ cm}^{-1}$  and  $\nu_3 = 663 \text{ cm}^{-1}$  were found and a bond angle of  $94 \pm 4^\circ$  was determined using isotope shift measurements. A third prominent absorption, at  $676 \text{ cm}^{-1}$ , can be attributed to the presence of the dimer, (GeF<sub>2</sub>)<sub>2</sub>. The molecular parameters for GeF<sub>2</sub> are compared with those of SiF<sub>2</sub> and CF<sub>2</sub>.

### Introduction

Recently the stability of molecular GeF<sub>2</sub> over its condensed phase at low pressures has been established.<sup>1</sup> The absence of definite vibrational and geometrical information has, however, hindered the establishment of accurate thermodynamic data, *via* the third law through use of free energy functions, for this new species. Two other group IVa difluorides, CF<sub>2</sub> and SiF<sub>2</sub>, now have well-established spectroscopic, structural, and thermodynamic properties.<sup>2-7</sup> Although SiF<sub>2</sub> and CF<sub>2</sub> have proven to be generally very similar, there are some notable exceptions, such as an apparent instability of Si<sub>2</sub>F<sub>4</sub> as compared with C<sub>2</sub>F<sub>4</sub>. It is then of considerable interest to characterize GeF<sub>2</sub> to the same extent as that achieved for CF<sub>2</sub> and SiF<sub>2</sub> with a view to understanding better the nature of the bonding in these species. GeF<sub>2</sub> also provides a useful intermediate case between the expected predominantly covalent nature of SiF<sub>2</sub> and the ionic nature of SnF<sub>2</sub>.

As a part of this program of characterization of group IV difluorides, the ir spectra of GeF<sub>2</sub> vapors were studied. By analogy with the bent (100.9°) SiF<sub>2</sub> molecule, GeF<sub>2</sub> should have three active vibrational frequencies in the ir region. One of these, the  $\nu_2$  bending frequency, has been established from recent measurement<sup>8</sup> of a progression involving this frequency for the ground (<sup>1</sup>A<sub>1</sub>) and first excited (<sup>1</sup>B<sub>1</sub>) electronic states. A  $\nu_2$  value of  $263 \pm 5 \text{ cm}^{-1}$  was determined. Also a considerable number of populated bending states were observed, *e.g.*, at least ten in the ground electronic state. This fact, coupled with there being five significant isotopes of Ge, suggests the ir vibrational spectra might be broad and ill defined at the temperatures required ( $\sim 150^\circ$ ) to vaporize GeF<sub>2</sub>. Hence, it was decided to observe the spectra at low temperatures by trapping the species in inert gas matrices at liquid helium temperature. Normal gas-phase spectra were also recorded in order to analyze the matrix shift effect.

### Experimental Section

**Apparatus.** The gas cell (Figure 1) was constructed with optics arranged so that double-beam spectra

could be recorded, thus eliminating the severe problem of atmospheric absorptions in the ir spectra.

For the matrix-trapping apparatus a liquid He cryostat with the following essential features was designed. The cold window (CsI) was seated onto a copper block using indium metal as a thermal seal. The temperature of this block could be controlled to 1°K over the range 4.2–100°K by use of either gas or liquid flow inlet valves to the block or alternatively by adjustment of the flow rate through an outlet valve. The temperature of the block was measured with both a Cu-constantan thermocouple and a standard resistance thermometer. The window temperature was probably several degrees higher than that recorded from the cold block.

The molecular beam furnace consisted of a Pt-resistance heating coil and the sample was contained in a boron nitride Knudsen cell. The temperature of this cell was measured by using a Pt–Pt–10% Rh thermocouple. A pumping system capable of producing a pressure of  $10^{-7}$  torr without use of liquid helium was used. The presence of liquid helium reduced the pressure to  $10^{-8}$  torr.

High-purity rare gas samples, after passing over a liquid N<sub>2</sub> cooled surface, were introduced *via* two 1/8 in. in diameter nozzles at a 45° angle to the cold window. The sample molecular beam was introduced normal to the window and hence little or no premixing of the matrix and sample material occurred. After

- (1) K. F. Zmbov, J. W. Hastie, R. Hauge, and J. L. Margrave, *Inorg. Chem.*, **7**, 608 (1968).
- (2) K. F. Zmbov, J. W. Hastie, R. Hauge, and J. L. Margrave, *Proc. Int. Symp. High Temp. Technol., 3rd. Asilomar, Conf. Grounds, Calif.*, in press. Published as supplied to *J. Pure Appl. Chem.*
- (3) F. X. Powell and D. R. Lide, Jr., *J. Chem. Phys.*, **45**, 1067 (1966).
- (4) V. M. Rao, R. F. Curl, Jr., P. L. Timms, and J. L. Margrave, *ibid.*, **43**, 2557 (1965).
- (5) D. C. Milligan, D. E. Mann, M. E. Jacox, and R. A. Mitsch, *ibid.*, **41**, 1199 (1964).
- (6) K. C. Herr and G. C. Pimentel, *Appl. Opt.*, **4**, 25 (1965).
- (7) V. M. Khanna, R. Hauge, R. F. Curl, and J. L. Margrave, *J. Chem. Phys.*, **47**, 5031 (1967).
- (8) R. Hauge, V. M. Khanna, and J. L. Margrave, *J. Mol. Spectrosc.*, **27**, 143 (1968).

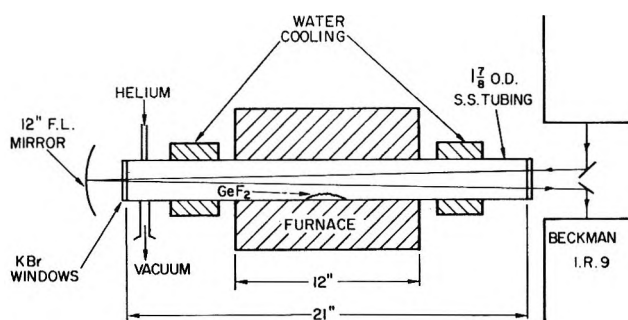


Figure 1. Schematic of gas cell apparatus.

matrix formation, the window could then be rotated normal to the ir light beam. A Beckman IR-9 spectrometer which covers the spectral region 400–4000  $\text{cm}^{-1}$  was used with both the gas cell and the matrix-trapping apparatus.

### Procedure

For the gas-phase experiment, several grams of GeF<sub>2</sub> was prepared in the usual manner by reaction of GeF<sub>4</sub> with Ge metal at 300° and distilled for collection at room temperature. Mass spectrometric analysis indicated no volatile impurities in the degassed, pure white crystalline material. The sample was contained in a nickel boat at the center of the gas cell. An atmosphere of several torr pressure of dry argon was also introduced into the gas cell to help prevent condensation of material on the KBr windows.

GeF<sub>2</sub> was vaporized at temperatures up to about 150° and spectra were recorded. Thus the growth of spectral peaks with both increasing and decreasing temperature, and hence sample concentration, allowed the unequivocal identification of the GeF<sub>2</sub> vapor spectra. By allowing the vapor to condense on the end windows, one could also obtain spectra for solid GeF<sub>2</sub>.

The matrix-trapping experiments were also carried out on vapor generated at 150°, and the matrix-forming conditions were as follows. From known vapor pressure data<sup>1</sup> at 150° the total salt pressure within the Knudsen cell was in the region of 10<sup>-1</sup> to 10<sup>-2</sup> torr. With the Knudsen orifice at 0.13 mm in diameter, this pressure range would result in an effusion rate of between 10<sup>-5</sup> and 10<sup>-6</sup> mol of GeF<sub>2</sub>/hr. The geometry of the apparatus ensures that only 0.5–1% of the effusing material reaches the cold window, and hence the rate of mass transfer to the window is 10<sup>-7</sup> to 10<sup>-8</sup> mol/hr. Inert gas flow rates corresponding to 10<sup>-3</sup> mol/hr were used. However, as the pressure of the vacuum chamber rose to nearly 10<sup>-4</sup> torr, with these flow rates not all of the inert gas was effectively trapped on the window. Assuming that only 10% of the inert gas directed at the window was trapped would produce a matrix GeF<sub>2</sub> to rare gas mole ratio in the range of 10<sup>3</sup> to 10<sup>4</sup>, indicating effective molecular isolation. A matrix-forming period of 30 min was usually sufficient to produce a

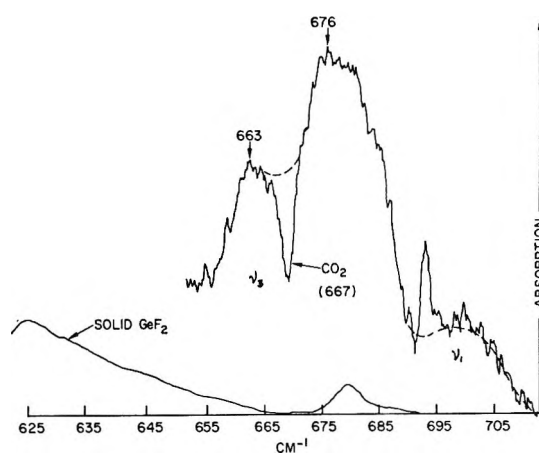


Figure 2. Gas-phase ir absorption over liquid GeF<sub>2</sub>.

suitable spectrum of GeF<sub>2</sub>. Background spectra were recorded on matrices formed under the same conditions of inert gas flow rate and Knudsen cell (empty) temperature, and no significant absorption features were noted.

### Results and Discussion

A typical temperature-dependent spectrum observed in the gas phase over liquid GeF<sub>2</sub> is indicated in Figure 2. The atmospheric CO<sub>2</sub> absorption, produced by adjusting the reference beam of the spectrometer to be slightly out of balance with the sample beam, was used as a calibration point. The known<sup>9</sup>  $\nu_3$  absorption of GeF<sub>4</sub> was also noted, thus verifying the known tendency of GeF<sub>2</sub> to disproportionate.<sup>1</sup> In fact, this disproportionation was a limiting factor in the generation of high GeF<sub>2</sub> pressures, and hence only weak spectra, as shown by Figure 2, could be observed. The spectrum has a great similarity to that obtained<sup>7</sup> previously for SiF<sub>2</sub>, and on this basis can be initially interpreted as an overlapping of the fundamental  $\nu_1$  and  $\nu_3$  absorptions of GeF<sub>2</sub>. The matrix-trapped results will be seen to allow a more definite interpretation.

The results of matrix trapping in neon at near liquid helium temperatures are indicated by the spectrum of Figure 3, which was entirely reproducible. That is, destroying the matrix by heating to over 60°K and re-depositing a new one reproduced the results. A band in the region of 800  $\text{cm}^{-1}$  may be readily assigned as the known  $\nu_3$  frequency<sup>9</sup> of GeF<sub>4</sub> which should be centered about 800  $\text{cm}^{-1}$ . The broad absorption shown in Figure 3 over the range 640–580  $\text{cm}^{-1}$  but extending to lower wave numbers compares with the solid GeF<sub>2</sub> absorption shown in Figure 2. Its ill-defined maximum is shifted in the matrix to lower energy by about 27  $\text{cm}^{-1}$ . The remaining three absorptions may be correlated with the main features found in the gas phase. If one allows for a matrix shift of about 8  $\text{cm}^{-1}$  to lower

(9) K. Nakamoto, "Infrared Spectra of Inorganic and Coordination Compounds," John Wiley & Sons, Inc., New York, N. Y., 1963.

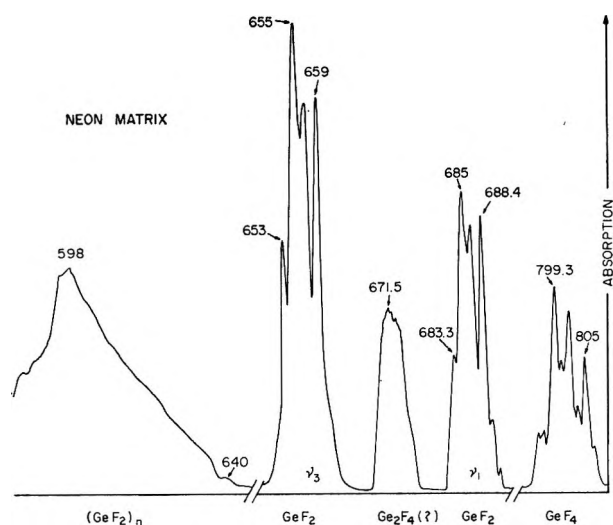


Figure 3. Ir absorption spectrum of  $\text{GeF}_2$  matrix isolated in neon at  $\sim 5^\circ\text{K}$ .

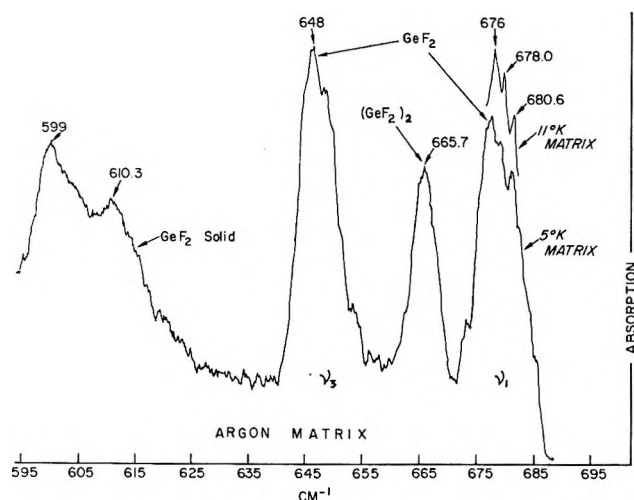


Figure 4. Ir absorption spectrum of  $\text{GeF}_2$  matrix isolated in argon at  $\sim 5^\circ\text{K}$ .

energies, the spectra of Figures 2 and 3 may be superimposed. Spectra of  $\text{GeF}_2$  in argon matrices, as indicated in Figure 4, showed a more pronounced shift of about  $15\text{ cm}^{-1}$  to lower wave numbers. It is of interest to note that an identical matrix shift was found<sup>7</sup> for  $\text{SiF}_2$  in argon. The negligibly small shift observed for the  $\nu_3$  frequency of  $\text{GeF}_4$ , which is nonpolar, supports the contention that frequency shifts are mainly a function of the dipole moments of the species for a particular matrix.

The extremely reproducible fine structure shown by several of the peaks in Figure 3 is interpreted as being the normal Ge isotope structure, rather than the often observed matrix splitting effect, for the following reasons. First, the effect could be reproduced using difference matrix-forming conditions, such as rare gas-to- $\text{GeF}_2$  concentration and window temperature. Second, the relative intensity of the fine structure absorptions

agrees with the known isotopic distribution in natural Ge, allowing for small changes due to overlap resulting from the instrumental resolution limit. The fact that the neon matrices allowed better resolution than argon is attributed to an annealing effect arising, since the matrix temperature, relative to the melting point of the rare gas solid, is effectively higher for neon than argon. This effect was verified by noting an improved resolution in argon matrices with increasing temperature, as shown in Figure 4.

Species containing two or more Ge atoms would probably not give rise to absorptions with clearly resolved isotope structure and on this basis the  $671.5\text{-cm}^{-1}$  absorption of Figure 3 is assigned to the  $\text{Ge}_2\text{F}_4$  species. Dimeric and higher polymeric species are known from mass spectrometric evidence<sup>1</sup> to exist in equilibrium with  $\text{GeF}_2$  in the Knudsen cell, and the polymeric bands are not necessarily the result of poor matrix isolation. The ill-defined absorption around  $598\text{ cm}^{-1}$  (shown in Figure 3) may readily be correlated with solid  $\text{GeF}_2$  as shown in Figure 2. Further supporting evidence for the dimer assignment is the fact that solid  $\text{GeF}_2$  also produces an absorption in the same region (see Figure 2). Solid  $\text{GeF}_2$  is considered to have a structure that involves Ge-F bridging, as is molecular  $\text{Ge}_2\text{F}_4$ , and hence both could conceivably give rise to an ir absorption of similar energy.<sup>1</sup>

The remaining absorptions must be assigned as the  $\nu_3$  and  $\nu_1$  stretches of  $\text{GeF}_2$ . It is of note that these two well-defined features do not appear in the solid  $\text{GeF}_2$  spectrum shown in Figure 2. With the contention that the fine structure of these two absorptions is attributable to Ge isotopes, an isotope-shift determination can be made. The isotope assignments are listed in Table I, and the frequency separation of the  $^{70}\text{Ge}$  and  $^{76}\text{Ge}$  difluoride species could be reproduced for different scans and different matrices to  $\pm 0.05\text{ cm}^{-1}$ , *i.e.*, of the order of less than 1% error. Using this separation, and the well-known relation between bond angle ( $2\alpha$ )

Table I: Isotope Separations for Ge-Containing Species

Ge isotope	% natural abundance	$\text{GeF}_2$ $\text{cm}^{-1}$				$\text{GeF}_4$ $\text{cm}^{-1}$	
		$\nu^{a,c}$	$\Delta\nu$	$\nu^{b,d}$	$\Delta\nu$	$\nu$	$\Delta\nu$
70	20.5	658.9 <sup>e</sup>		688.5		805.0	
			2.1		2.0		3.0
72	27.4	656.8		686.5		802.0	
			1.8		1.5		2.7
73	7.8	...		...		...	
74	36.5	655.0		685.0		799.3	
			2.0		1.7		2.6
76	7.8	653.0		683.3		796.7	

<sup>a</sup>  $\nu_{70} - \nu_{76} = 5.9\text{ cm}^{-1}$ . <sup>b</sup>  $\nu_{70} - \nu_{76} = 5.2\text{ cm}^{-1}$ . <sup>c</sup> For  $(658.9/653.0)^2$ ,  $2\alpha = 94 \pm 2^\circ$  ( $\nu_3$ ). <sup>d</sup> For  $(688.5/683.3)^2$ ,  $2\alpha = 82 \pm 3^\circ$  ( $\nu_1$ ). <sup>e</sup> Absolute error  $\pm 1\text{ cm}^{-1}$ ; relative error  $\pm 0.1\text{ cm}^{-1}$ .

**Table II:** Molecular Parameters of Some Group IVa Difluorides<sup>a</sup>

Molecule	$\nu_1$ , cm <sup>-1</sup>	$\nu_2$ , cm <sup>-1</sup>	$\nu_3$ , cm <sup>-1</sup>	$k_1$ mdyn/Å	$k_8/l^2$ , mdyn/Å	$k_{12}$ mdyn/Å	Angle, <sup>c</sup> deg	$r_{MX}$ , <sup>d</sup> Å	$D_{X-MX}$ , <sup>b</sup> kcal/mole	$k_1 r_{MX} / D_{X-MX}$ , <sup>e</sup> 10 <sup>-7</sup> dyn-cm
CF <sub>2</sub>	1222	668	1102	4.54	2.21	<i>g</i>	104.9	1.30	108	1.56 ± 0.07
SiF <sub>2</sub>	855	345	872	4.90	0.456	0.18	100.9	1.595	150	1.49 ± 0.06
GeF <sub>2</sub>	692 <sup>f</sup>	263	663 <sup>f</sup>	4.07	0.319	0.22	94 ± 4	1.73 ± 0.05	109	1.85 ± 0.1

<sup>a</sup> The frequency data for CF<sub>2</sub> are from Milligan, *et al.*,<sup>5</sup> and Herr, *et al.*<sup>6</sup> The SiF<sub>2</sub> data are from Khanna, *et al.*<sup>7</sup> <sup>b</sup> These data are summarized by Zmbov, *et al.*<sup>2</sup> <sup>c</sup> Bond angles and internuclear separations for CF<sub>2</sub> and SiF<sub>2</sub> are from Powell, *et al.*,<sup>8</sup> and Rao, *et al.*,<sup>4</sup> respectively. <sup>d</sup>  $r_{MX}$  for GeF<sub>2</sub> estimated by comparison with the diatomic species (J. W. C. Johns and R. F. Barrow, *Proc. Phys. Soc.*, **A71**, 476 (1958)). <sup>e</sup> The term is considered to indicate particular bond types and has been successfully applied to similarly bonded molecules for the prediction of dissociation energies (G. R. Somayajulu, *J. Chem. Phys.*, **33**, 1541 (1960)). <sup>f</sup> Values for the different isotopes of GeF<sub>2</sub> are not listed as a larger uncertainty exists in determining the matrix shift from the ill-defined gas-phase spectrum. <sup>g</sup> The more general force field calculation leads to an imaginary value of  $k_{12}$  and hence only the simple valence field approximation was used.

and antisymmetric stretch frequency ( $\nu_3$ ), the following bond angles were calculated.<sup>10</sup> Assuming the lower frequency absorption to be  $\nu_3$  resulted in a calculated angle of 94 ± 2°, while the higher frequency absorption gave only 82 ± 3°. The only added uncertainties involved in these bond angle calculations are the anharmonic corrections to the frequencies which may be neglected as this effect has been shown<sup>11</sup> to be small in similar bond angle determinations on SO<sub>2</sub> and SeO<sub>2</sub>. As CF<sub>2</sub> and SiF<sub>2</sub> have bond angles of 104.9 and 100.9°, respectively, the calculated value of 94 ± 2° for GeF<sub>2</sub> appears very reasonable. On the other hand, it is extremely unlikely that GeF<sub>2</sub> should have a bond angle less than 90°, as complete separation of s<sup>2</sup> and p<sup>2</sup> valence orbitals in Ge would produce a 90° angle. On this basis it appears that the lower frequency should be assigned as  $\nu_3$  and the higher one as the symmetric stretch  $\nu_1$ . Generally the more intense absorption can be attributed to  $\nu_3$ , and this is also the case for GeF<sub>2</sub>. The most realistic measure of the GeF<sub>2</sub> gas-phase bond angle is 94 ± 4°, although the data can be reproduced to better than ± 2° for the angle in neon and argon matrices.

### Valence Force Constants and Bonding

A number of attempts have been made to relate valence force constants to other molecular parameters, such as bond dissociation energies and internuclear separations, particularly within discrete groups of the periodic table (*e.g.*, p 459, ref 12). It will therefore be useful to apply some of these relationships to the MF<sub>2</sub> species of group IVa.

The valence force assumption, which seems to apply well for the majority of triatomic C<sub>2v</sub> symmetry molecules,<sup>12</sup> enables the molecular potential energy to be expressed in terms of a stretching and a bending force constant,  $k$  and  $k_8/l^2$ , respectively. For a more general valence force field,  $k$  is a function of  $k_1$  and  $k_{12}$  where  $k_{12}$  is a bond-bond interaction parameter and  $k_1$  is the simple stretching force constant. The basic equations relating these constants to the molecular parameters

and fundamental frequencies are conveniently listed by Herzberg.<sup>13</sup> This type of force constant determination does not require any internuclear separation parameters (which are not yet experimentally known for GeF<sub>2</sub>) for its calculation.

The evaluated force constants for CF<sub>2</sub>, SiF<sub>2</sub>, and GeF<sub>2</sub> are listed in Table II, together with other known molecular constant data. The smallness of  $k_{12}$  as compared with  $k_1$  indicates the validity of the valence bond approach for this set of molecules. Furthermore, the force constants for SiF<sub>2</sub> compare well with those obtained previously<sup>7</sup> by normal coordinate analysis.

The similarity in the variation of  $D_{X-MX}$  with the known  $D_{X-X}$  variation, in particular the maximum stability shown when X is bonded to a second row atom, might be attributed to similar effects, *i.e.*, a marked increase in the relative contribution of London forces to the bond energies in going from below to above the first octet in the periodic table.<sup>14</sup> This effect is also necessarily reflected in the  $k_1 r_{MX} / D_{X-MX}$  values as shown in Table II. There appears to be a qualitative dependence of the quantity  $k_1 r_{MX} / D_{X-MX}$  on the MX electronegativity difference which may be more quantitatively established when data become available for other similar species. The internuclear separations for C-F and Si-F in the triatomic species are within 0.03 Å of those for the diatomic species, and this was the basis for estimating the triatomic distance in GeF<sub>2</sub> of 1.73 Å as compared with the known diatomic value of 1.74 Å. Also the similarity in the diatomic and triatomic internuclear separations is in good accord with the observed small values of  $k_{12}$  and the Linnet and Hoare relation<sup>15</sup> between these quantities.

The need for extra data is apparent before a better

(10) G. Herzberg, "Infrared and Raman Spectra," D. Van Nostrand Co., Inc., Princeton, N. J., 1945.

(11) J. W. Hastie, R. Hauge, and J. L. Margrave, *J. Inorg. Nucl. Chem.*, in press.

(12) G. Herzberg, "Spectra of Diatomic Molecules," 2nd ed, D. Van Nostrand Co., Inc., Princeton, N. J., 1950.

(13) As may be seen on p 187 of ref 10.

(14) K. S. Pitzer, *J. Chem. Phys.*, **23**, 1735 (1955).

understanding of the trends thus far observed can be made, and further experiments in progress in this laboratory concern the other group IVa triatomic fluorides and chlorides.

Free energy functions for  $\text{GeF}_2(\text{g})$  have been calculated from the molecular parameters and frequencies given in Table II and are presented elsewhere.<sup>2</sup>

*Acknowledgments.* This work was supported by the United States Atomic Energy Commission and by the Robert A. Welch Foundation.

(15) J. W. Linnet and M. J. Hoare, *Trans. Faraday Soc.*, **45** 844 (1949).

## Thermodynamics of Binary Solutions of Nonelectrolytes with 2,2,4-Trimethylpentane. III. Volumes of Mixing with Cyclohexane (10–80°) and Carbon Tetrachloride (10–80°)<sup>1,2</sup>

by Elmer L. Washington and Rubin Battino<sup>3</sup>

*Department of Chemistry, Illinois Institute of Technology, Chicago, Illinois 60616 (Received May 29, 1968)*

Precise measurements of the volume of mixing of the two binary systems of cyclohexane–isooctane (2,2,4-trimethylpentane) and carbon tetrachloride–isooctane were made using a novel dilatometer over the range 10–80°. The volume of mixing for the cyclohexane–isooctane systems was extremely small and was either positive or negative depending on the temperature and composition. Generally, the deviations from ideality decreased with increase in temperature. The volume of mixing for the carbon tetrachloride system increased with an increase in temperature. At 80° the volumes of mixing for equimolar mixtures of isooctane with cyclohexane and carbon tetrachloride are  $-0.002$  and  $0.201 \text{ cm}^3 \text{ mol}^{-1}$ , respectively. At 10° these quantities are  $-0.008$  and  $0.184 \text{ cm}^3 \text{ mol}^{-1}$ . The coefficients of thermal expansion were determined for each of the systems. Three theoretical treatments of the volume of mixing were examined.

### Introduction

This paper reports a continuation of studies of binary solutions of nonelectrolytes with 2,2,4-trimethylpentane (isooctane).<sup>4–8</sup> The volume change on mixing (volume of mixing) for solutions of nonelectrolytes is of interest for two basic reasons. First, it is necessary to know the volumes of mixing to convert experimental data obtained from constant-pressure processes to mixing at constant volume.<sup>9,10</sup> Second, precise data on volumes of mixing can be used to test theories of solution and the liquid state.<sup>11–13</sup> Wood and Gray<sup>14</sup> demonstrated the importance of the volume dependence of the thermodynamic functions for solutions of nonelectrolytes.

### Apparatus and Experimental Procedure

*Description of the Dilatometer.* The dilatometer is shown in Figure 1. The position of the four sets of markings separated by the three bulbs and the capacity of the bulbs were chosen so that a 10° rise in temperature would bring the meniscus of the mercury (which confines the solvent or solution in the lower chamber)

from one set of markings to the next. The dilatometer is calibrated by the use of water confined by mercury. Once the dilatometer has been calibrated, the extent of

(1) Presented in part at the 152nd National Meeting of the American Chemical Society, New York, N. Y., Sept 1966.

(2) This contribution contains material taken from a thesis by E. L. Washington, presented to the Graduate School, Illinois Institute of Technology, in partial fulfillment of the requirements for the degree of Doctor of Philosophy.

(3) Department of Chemistry, Wright State University, Dayton, Ohio 45431.

(4) R. Battino, *J. Phys. Chem.*, **70**, 3408 (1966); R. Battino and G. W. Allison, *ibid.*, **70**, 3417 (1966).

(5) R. Battino, *J. Phys. Chem.*, **72**, 4503 (1968).

(6) S. E. Wood and O. Sandus, *ibid.*, **60**, 801 (1956).

(7) S. E. Wood, O. Sandus, and S. Weissman, *J. Amer. Chem. Soc.*, **79**, 1777 (1957).

(8) S. Weissman and S. E. Wood, *J. Chem. Phys.*, **32**, 1153 (1960).

(9) G. Scatchard, *Trans. Faraday Soc.*, **33**, 160 (1937).

(10) R. L. Scott, *J. Phys. Chem.*, **64**, 1241 (1960).

(11) I. A. McClure, J. E. Bennett, A. E. P. Watson, and G. C. Benson, *ibid.*, **69**, 2759 (1965).

(12) G. C. Benson and J. Singh, *ibid.*, **72**, 1345 (1968).



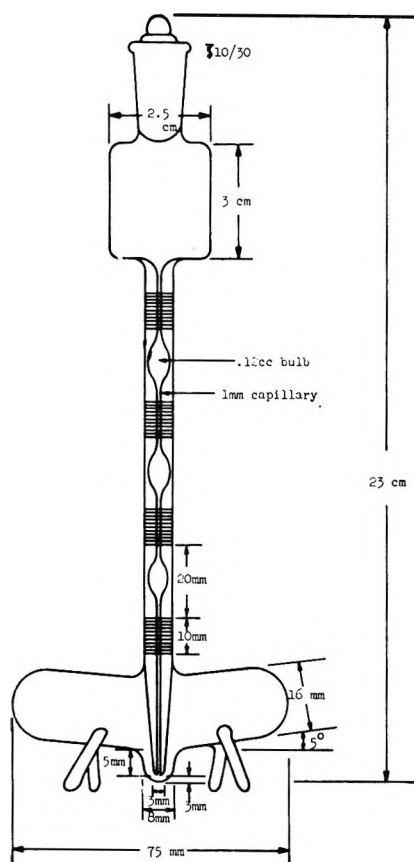


Figure 1. Dilatometer.

dilatation at four temperatures (about  $10^\circ$  apart) can be determined strictly by reading the position of the mercury meniscus. Several readings at slightly different temperatures can also be made at one set of markings. After the mercury level has reached the uppermost set of markings, sufficient mercury is removed (and weighed) to bring the level to the lowest set of markings; then levels can be read at three additional  $10^\circ$  intervals. Features of the dilatometer are that it is loaded with degassed solvents, few weighings are required, a wide range of compositions is possible, and the compositions of the mixtures are determined directly by weighing.

The dilatometer was fabricated from Pyrex glass No. 7740. The lower chamber is made from 16 mm o.d. tubing and has a capacity of about  $11 \text{ cm}^3$ . Precision-bore capillary tubing of 1-mm i.d. had three bulbs of approximately  $0.12\text{-cm}^3$  capacity blown into it. The etchings were spaced exactly at 1-mm intervals over a distance of 1 cm. Mercury heights in the capillary are read to  $\pm 0.02 \text{ mm}$  with a cathetometer. The expansion chamber at the top of the dilatometer is fitted with a ground-glass cap.

All liquids used including mercury are introduced into the dilatometer by means of chambers patterned after the one shown in Figure 2. In all cases the liquids are first degassed. The dilatometer connects to the

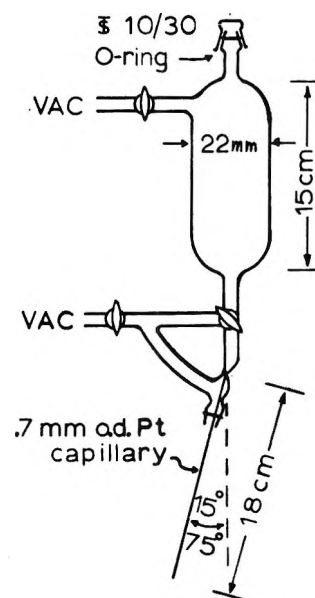


Figure 2. Delivery section of the vacuum line.

delivery section at the O-ring seal joint and the 0.7 mm o.d. platinum capillary extends to just above the bottom of the dilatometer. The different chambers had delivery sections tilting upward away from the vertical either at  $15$  or  $75^\circ$ . Mercury and the first solvent of a mixture use the  $75^\circ$  angle, and water and the second solvent of a mixture use the  $15^\circ$  angle.

The dilatometer was calibrated by first filling it completely with mercury and then displacing about  $9 \text{ cm}^3$  of the mercury with water. Excess mercury is removed (using a weight pipet shown in Figure 3) so that the mercury confining the water will appear at the lowest set of markings at the lowest temperature used. The platinum capillary on the weight pipet is lowered into the vertically held dilatometer, and mercury is removed by applying suction at the ground glass joint on the weight pipet. The volume of the dilatometer as a function of the temperature is obtained from the weights and densities of water and mercury. The volume,  $V_i(t, h)$ , at temperature  $t$  was fitted to the equation  $V_i(t, h) = V_i^0(t_{ref}) + b_i h_i + (1.02 \times 10^{-4}) \cdot (t - t_{ref})$ . In this equation  $t_{ref}$  is  $16.0$ ,  $45.3$ , or  $74.4^\circ$ ; the term  $V_i^0(t_{ref})$  is the volume at  $t_{ref}$  for the  $i$ th set of markings at  $h_i = 0$ ;  $h_i$  is the specific height reading for one of the four sets of markings;  $b_i$  is the slope (change of  $V_i$  with  $h_i$ ) for the  $i$ th set of markings; and  $t$  is the temperature at which  $V_i$  is measured. The values of  $b_i$  and  $V_i^0(t_{ref})$  were determined by a least-squares technique from measurements of  $h_i$  and  $V_i(t)$  at a given  $t_{ref}$  for each set of markings. A derived value of the coefficient of expansion of Pyrex glass agreed

(13) W. B. Streett and L. A. K. Staveley, *J. Chem. Phys.*, **47**, 2449 (1967).

(14) S. E. Wood and J. A. Gray, *J. Amer. Chem. Soc.*, **74**, 3733 (1952); also see ref 7.

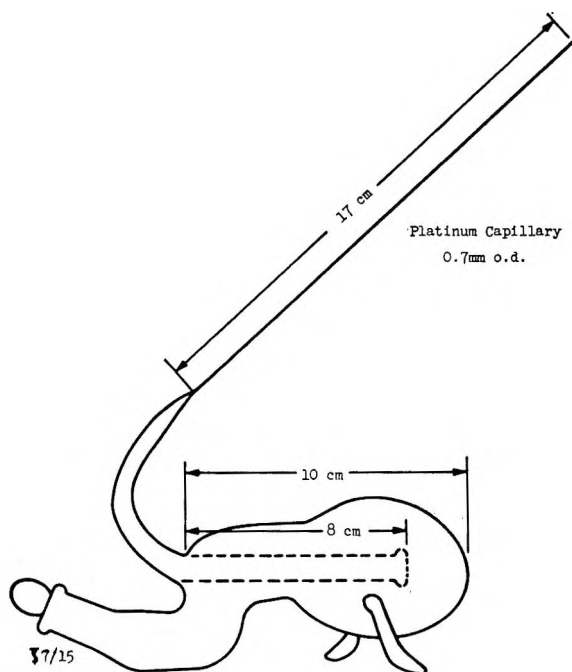


Figure 3. Mercury pipet.

within experimental error with literature values. The over-all reproducibility in  $V_i(t, h)$  was found to be within  $\pm 0.0003 \text{ cm}^3$ , which corresponds to an error of  $\pm 0.003 \text{ cm}^3 \text{ mol}^{-1}$  in the volume of mixing.

For mixtures the dilatometer is first filled with mercury. Then the first solvent is added, displacing some of the mercury. After appropriate weighings the second solvent is added, also displacing some of the mercury. No attempt is made to keep the solvents separated since we are measuring the density of a solution of known composition as a function of temperature. The different angles of loading were chosen so as to displace mercury readily without having the solvents slip past the mercury into the capillary. After the dilatometer is filled, the mercury meniscus in the capillary is first set at the lowest set of markings at  $10^\circ$ . The position of the meniscus is then read at approximately  $10^\circ$  intervals up to  $80^\circ$ , after removal of mercury as necessary. The compositions of the solutions were determined directly by weighing. The water thermostat was controlled to  $\pm 0.002^\circ$ , and temperatures were measured to  $\pm 0.003^\circ$  with a platinum resistance thermometer calibrated at the triple point of water and the freezing point of benzoic acid (using cells calibrated by the National Bureau of Standards). Washington<sup>15</sup> gives a complete description of the techniques used in making these measurements.

**Purification of Materials.** The isooctane used was Phillips Petroleum pure grade, 99 mol % minimum. The carbon tetrachloride was Fisher's 99 mol % certified solvent. These materials were further purified by distillation in a 6-ft vacuum-jacketed distilling column. Subsequently, they were vacuum distilled from  $\text{CaH}_2$

into Pyrex glass ampoules for storage. Each ampoule contained about  $40 \text{ cm}^3$  of solvent. The density of the isooctane was determined to be  $0.68778 \text{ g cm}^{-3}$  at  $25^\circ$  in comparison to  $0.68774$ ,<sup>6,8</sup>  $0.68775$ ,<sup>16</sup>  $0.68776$ ,<sup>17</sup> and  $0.68779 \text{ g cm}^{-3}$ .<sup>18</sup> The density of the degassed isooctane as determined with the dilatometer in this work was  $0.68788 \text{ g cm}^{-3}$  at  $25^\circ$ . Hence a difference of  $0.00010 \text{ g cm}^{-3}$  is evident between the degassed sample and the air-saturated sample, in excellent agreement with the value of  $0.00011 \text{ g cm}^{-3}$  obtained by Wood and Sandus.<sup>6</sup>

The density of the carbon tetrachloride was  $1.58444 \text{ g cm}^{-3}$  at  $25^\circ$ . This value for the density is somewhat higher than the value of  $1.58430 \text{ g cm}^{-3}$  measured 1 year earlier on the freshly purified carbon tetrachloride. There was a definite change in the density during the storage period. However, all of the volume-of-mixing determinations were made using the higher density solvent. It is extremely doubtful that this relatively small change in density will significantly affect the volume of mixing results. As indicated by McLure and Swinton, "excess volumes of mixing are usually little affected by small amounts of impurity."<sup>19</sup> Other reported values are  $1.58429$ <sup>14</sup> and  $1.58461 \text{ g cm}^{-3}$ .<sup>20</sup> The mean value of Timmerman's<sup>21</sup> more recent values is  $1.58448 \text{ g cm}^{-3}$  at  $25^\circ$ . The density of the carbon tetrachloride used in this work is in good agreement with this latter value. The density of the carbon tetrachloride without air was found to be  $0.00023 \text{ g cm}^{-3}$  higher than the air-saturated density at  $25^\circ$ , in comparison with  $0.00019$ <sup>14</sup> and  $0.00021 \text{ g cm}^{-3}$ .<sup>22</sup>

The cyclohexane was Phillips Petroleum research grade, which needed no additional purification. The density of the air-saturated cyclohexane was  $0.77388 \text{ g cm}^{-3}$  at  $25^\circ$  in comparison with  $0.77387$ ,<sup>17</sup>  $0.77381$ ,<sup>14</sup>  $0.77379$ ,<sup>23</sup> and  $0.77383 \text{ g cm}^{-3}$ .<sup>24</sup> A difference of  $0.00005 \text{ g cm}^{-3}$  was found in comparing the density of the degassed cyclohexane with air-saturated cyclohexane; Wood and Austin<sup>23</sup> reported  $0.00002 \text{ g cm}^{-3}$ .

The final resistivity of the purified water used in this

(15) E. L. Washington, Ph.D. Dissertation, Illinois Institute of Technology, Chicago, Ill., 1966.

(16) C. B. Kretschmer, J. Nowakowska, and R. J. Wiebe, *J. Amer. Chem. Soc.*, **70**, 1785 (1948).

(17) D. B. Brooks, F. L. Howard, and H. C. Crafton, *J. Res. Nat. Bur. Stand.*, **24**, 33 (1940).

(18) "Selected Values of Properties of Hydrocarbons," National Bureau of Standards Circular C461, U. S. Government Printing Office, Washington, D. C., 1947.

(19) I. McLure and F. L. Swinton, *Trans. Faraday Soc.*, **61**, 421 (1965).

(20) J. A. Larkin and M. L. McGlashan, *J. Chem. Soc.*, 3425 (1961).

(21) J. Timmerman, "Physico-Chemical Constants of Pure Organic Compounds," Elsevier Publishing Co., Amsterdam, The Netherlands, 1950.

(22) S. E. Wood and J. P. Brusie, *J. Amer. Chem. Soc.*, **65**, 1891 (1943).

(23) S. E. Wood and A. E. Austin, *ibid.*, **67**, 480 (1945).

(24) G. Scatchard, S. E. Wood, and J. M. Mochel, *J. Phys. Chem.*, **43**, 119 (1939).

work was usually about 0.95 megohm cm. The mercury was triply distilled. The specific volume of the mercury was calculated from the formula (valid from 0 to 100°) given by Scheel and Blankenstein,<sup>25</sup> and the density of mercury at 0° derived from the above equation was found to be in excellent agreement with the table published by Bigg.<sup>26</sup> The density of the water was calculated from the Tilton and Taylor equation.<sup>27</sup> The Tilton and Taylor equation is not valid above 45°, and Wood and Gray<sup>14</sup> fitted corrections determined by White<sup>28</sup> to provide density values in the range 45–85°. All values were converted to g cm<sup>-3</sup> by the factor 0.999973 ml cm<sup>-3</sup>.

### Experimental Results

The specific volumes of isooctane, carbon tetrachloride, cyclohexane, and the binary mixtures of isooctane with the latter two were determined over the whole range of composition at 25° and at each 10° interval from 10 to 80°. They were fitted by the method of least squares to an equation of the form

$$v = a + bt + ct^2 + dt^3 \quad (1)$$

where  $v$  is the specific volume and  $t$  is the temperature in degrees Centigrade. The values of the coefficients  $a$ ,  $b$ ,  $c$ , and  $d$ , which are functions of the composition, are given in Tables I and II. The standard deviations given in the last column of these tables are for the differences between the specific volumes calculated from eq 1 and the experimental values.

**Table I:** Coefficients of the Specific Volume Equations for Isooctane + Cyclohexane

$X_1^a$	$a$	$10^b$	$10^c$	$10^d$	Std dev ( $10^6 \Delta v$ )
0.00000	1.41203	1.6046	2.267	11.16	1.4
0.15731	1.39311	1.5825	2.342	10.03	1.7
0.17347	1.39100	1.5816	2.289	10.48	1.2
0.27523	1.37753	1.5760	2.143	10.91	2.9
0.41586	1.35774	1.5551	2.163	10.43	2.1
0.50321	1.34453	1.5429	2.180	9.74	2.4
0.51154	1.34317	1.5488	1.981	11.24	2.2
0.66476	1.31824	1.5278	1.995	10.19	2.5
0.68365	1.31489	1.5202	2.107	9.27	2.2
0.74900	1.30346	1.5049	2.220	8.27	2.4
0.82880	1.28863	1.4898	2.192	8.35	2.0
0.90212	1.27439	1.4747	2.174	8.22	1.3
1.00000	1.25451	1.4414	2.287	7.64	1.6

<sup>a</sup>  $X_1$  is the mole fraction of cyclohexane.

The percentage increase in the volume of mixing was calculated by means of the relation

$$100\Delta V^M/V^0 = 100v(Z_1d_1 + Z_2d_2) - 100 \quad (2)$$

where  $100\Delta V^M/V^0$  is the per cent increase in the volume of mixing at constant temperature and pressure,

**Table II:** Coefficients of the Specific Volume Equations for Isooctane + Carbon Tetrachloride

$X_3^a$	$a$	$10^b$	$10^c$	$10^d$	Std dev ( $10^6 \Delta v$ )
0.00000	1.41203	1.6046	2.267	11.16	1.4
0.12601	1.28269	1.4624	2.053	10.16	1.8
0.26927	1.14797	1.3145	1.809	9.25	1.3
0.37516	1.05582	1.2118	1.694	8.16	2.1
0.43881	1.00324	1.1520	1.636	7.49	2.2
0.53509	0.92719	1.0724	1.408	7.50	0.9
0.70463	0.80329	0.9359	1.172	6.49	0.7
0.78383	0.74923	0.8742	1.111	5.77	0.3
0.83075	0.71824	0.8418	1.027	5.57	1.2
0.88638	0.68244	0.7994	0.999	5.16	0.8
1.00000	0.61239	0.7228	0.832	4.88	1.6

<sup>a</sup>  $X_3$  is the mole fraction of carbon tetrachloride.

$d_1$  and  $d_2$  are the densities of the pure liquids,  $Z_1$  and  $Z_2$  are the volume fractions of the pure liquids, and  $v$ , the specific volume of the solution, was calculated from eq 1. The values so obtained were fitted to the general equation

$$100\Delta V^M/V^0 = Z_1Z_2(\alpha + \beta Z_1 + \gamma Z_1^2) \quad (3)$$

where the constants  $\alpha$ ,  $\beta$ , and  $\gamma$  are temperature dependent. Values  $\alpha$ ,  $\beta$ , and  $\gamma$  for the two systems are given in Table III. Subscript 1 refers to cyclohexane, 2 to isooctane, and 3 to carbon tetrachloride. The over-all error in the molar volume of mixing,  $\Delta \bar{V}^M$ , is  $\pm 0.003$  cm<sup>3</sup> mol<sup>-1</sup>. Table IV shows  $\Delta \bar{V}^M$  for both systems at 25°. Mole fractions,  $X$ , may be calculated from volume fractions by  $X_1 = Z_1\bar{V}_2^0/[\bar{V}_1^0 - Z_1(\bar{V}_1^0 - \bar{V}_2^0)]$ .

The thermal expansion coefficients,  $\alpha = (\partial V/\partial T)_p/V$ , for the pure liquids in the temperature range 10–80° are given by

$$\alpha_1 = 1.1478 \times 10^{-2} + (2.46 \times 10^{-5})t + (9.80 \times 10^{-8})t^2 \quad (4)$$

$$\alpha_2 = 1.1340 \times 10^{-2} + (2.12 \times 10^{-5})t + (1.48 \times 10^{-7})t^2 \quad (5)$$

$$\alpha_3 = 1.1791 \times 10^{-2} + (1.48 \times 10^{-5})t + (1.62 \times 10^{-7})t^2 \quad (6)$$

The agreement with Wood, *et al.*,<sup>14</sup> is excellent. At 25° the coefficients of thermal expansion are: cyclohexane, 0.001215; isooctane, 0.001196; and carbon tetrachloride, 0.001226.

Graphs of the relative volume of mixing *vs.* the vol-

(25) K. Scheel and F. Blankenstein, *Z. Physik.*, **31**, 202 (1925).

(26) P. H. Bigg, *Brit. J. Appl. Phys.*, **15**, 1111 (1964).

(27) L. W. Tilton and J. K. Taylor, *J. Res. Nat. Bur. Stand.*, **18**, 205 (1937).

(28) J. White, Ph.D. Thesis, Yale University, 1944.

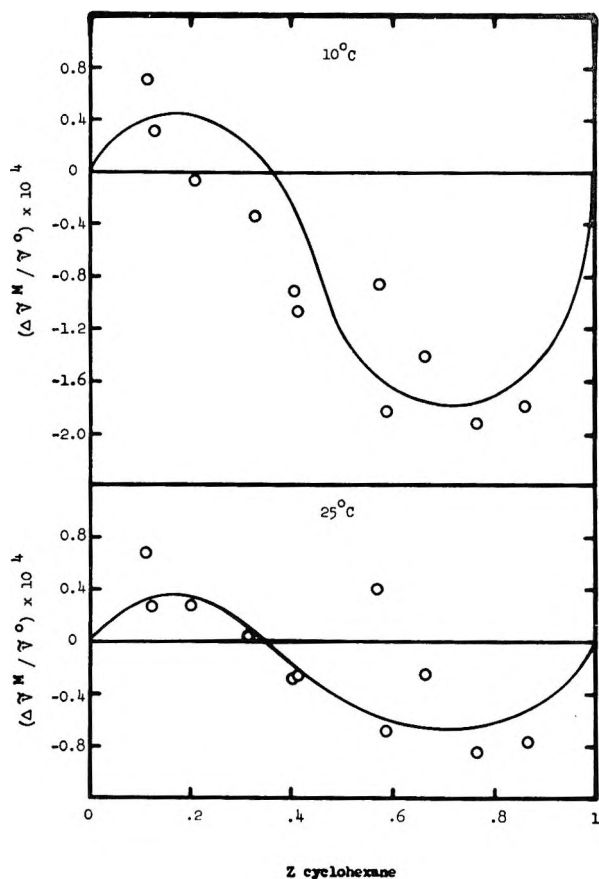


Figure 4. The relative volume of mixing,  $\Delta\bar{V}^M/\bar{V}^0$ , of the cyclohexane-isooctane system at 10 and 25° vs. the volume fraction of cyclohexane.

Table III: Coefficients for Eq 3

$t, ^\circ\text{C}$	Cyclohexane + isooctane		Carbon tetrachloride + isooctane		
	$10^2\alpha$	$\beta$	$\alpha$	$\beta$	$\gamma$
10	5.58	-0.230	0.809	-0.781	0.612
20	5.57	-0.154	0.816	-0.764	0.594
25	5.06	-0.122	0.822	-0.771	0.603
30	4.55	-0.094	0.828	-0.767	0.597
40	3.53	-0.050	0.845	-0.762	0.582
50	2.46	-0.018	0.870	-0.785	0.594
60	1.28	0.004	0.896	-0.798	0.582
70	0.00	0.016	0.926	-0.820	0.579
80	-1.41	0.021	0.962	-0.844	0.563

ume fraction of cyclohexane are given in Figure 4. The S-shaped curves and the nearly ideal behavior were unexpected for this system. The results at 25° are in good agreement with those obtained by Battino.<sup>4</sup> At higher temperatures the volume change on mixing is essentially zero. Relative volumes for the carbon tetrachloride-isooctane system are given in Figure 5. The relative volume is found to be symmetrical around the equal volume axis and increases with an increase in temperature. These results are also in good agreement with those obtained by Battino<sup>5</sup> at 25°.

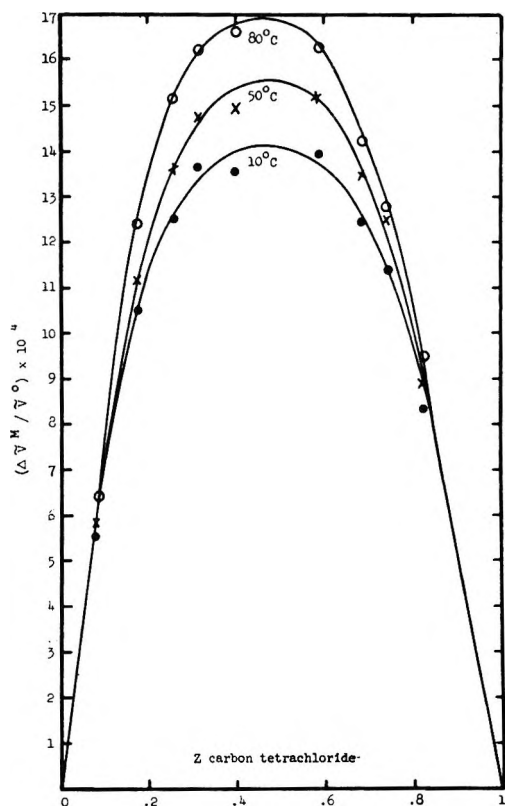


Figure 5. The relative volume of mixing,  $\Delta\bar{V}^M/\bar{V}^0$ , of the carbon tetrachloride-isooctane system at 10, 50, and 80° vs. the volume fraction of carbon tetrachloride.

Table IV: Volumes of Mixing at 25°

Cyclohexane + isooctane			Carbon tetrachloride + isooctane		
$Z_1$	$\Delta\bar{V}^M$	$100\Delta\bar{V}^M/\bar{V}^0$	$Z_1$	$\Delta\bar{V}^M$	$100\Delta\bar{V}^M/\bar{V}^0$
0.10893	0.010	0.006	0.07774	0.086	0.055
0.12083	0.004	0.003	0.17725	0.155	0.105
0.19915	0.004	0.003	0.25982	0.178	0.127
0.31797	0.000	0.000	0.31373	0.188	0.138
0.39879	-0.004	-0.003	0.40223	0.180	0.139
0.40680	-0.003	-0.002	0.58241	0.168	0.143
0.56493	0.005	0.004	0.67947	0.142	0.127
0.58595	-0.009	-0.007	0.74158	0.128	0.118
0.66148	-0.003	-0.003	0.82018	0.088	0.083
0.76020	-0.010	-0.009			
0.85786	-0.009	-0.008			

### Comparison of Theoretical and Experimental Results

To understand the volume of mixing, it is helpful to consider three different theoretical approaches. They are: (1) Flory's<sup>29,30</sup> reduced equation of state approach as derived from a simple partition function; (2) Prigogine's<sup>31</sup> corresponding state approach; and

(29) P. J. Flory, *J. Amer. Chem. Soc.*, **87**, 1833 (1965).

(30) A. Abe and P. J. Flory, *ibid.*, **87**, 1838 (1965); P. J. Flory and A. Abe, *ibid.*, **86**, 3563 (1964).

**Table V:** Parameters for the Pure Liquids for the Flory Calculation

Liquid	$t_i$ , °C	$\bar{V}^0$ , cm <sup>3</sup> mol <sup>-1</sup>	$10^3\alpha$ , deg <sup>-1</sup>	$\gamma$ , cal cm <sup>-3</sup> deg <sup>-1</sup>	$\bar{v}$	$v^*$ , cm <sup>3</sup> mol <sup>-1</sup>	$T^*$ , °K	$P^*$ , cal cm <sup>-3</sup>
Cyclohexane	10	106.81	1.174	0.280	1.2709	84.04	4686	128
	25	108.74	1.215	0.255	1.2901	84.29	4726	127
	80	116.84	1.407	0.179	1.3699	85.29	4858	119
Isooctane	10	163.15	1.157	0.191	1.3671	128.76	4729	86.8
	25	166.05	1.196	0.179	1.2863	129.09	4767	88.3
	80	178.26	1.398	0.133	1.3682	130.29	4868	87.9
Carbon tetra- chloride	10	95.33	1.196	0.298	1.2748	74.78	4643	137
	25	97.08	1.226	0.273	1.2922	75.13	4705	136
	80	104.31	1.401	0.191	1.3688	76.21	4866	126

**Table VI:** Comparison of Observed and Calculated Excess Quantities for the Flory Calculation and the Scatchard-Hildebrand Equation

	$t_i$ , °C	$r_1/r_2$	$s_1/s_2$	$X_{12}$ , cal cm <sup>-3</sup>	$\theta_2$	$\bar{v}_M$ , calcd	$\bar{v}^0$	$\Delta\bar{V}^E$ , cm <sup>3</sup> mol <sup>-1</sup>		
								Calcd <sup>a</sup>	Obsd	Calcd <sup>b</sup>
Cyclohexane + Isooctane										
$X_1$	10	0.653	1.15	1.73	0.57	1.2707	1.2686	0.225	-0.008	0.318
	25	0.653	1.15	1.34	0.57	1.2892	1.2878	0.145	0.007	0.351
	80	0.655	1.15	0.69	0.57	1.3704	1.3689	0.160	-0.002	0.516
Carbon Tetrachloride + Isooctane										
$X_3$	10	0.581	1.20	2.28	0.59	1.2728	1.2699	0.291	0.184	0.503
	25	0.582	1.20	1.89	0.59	1.2905	1.2885	0.208	0.188	0.557
	80	0.585	1.20	0.98	0.59	1.3700	1.3648	0.168	0.201	0.816

<sup>a</sup> Flory calculation. <sup>b</sup> Scatchard-Hildebrand equation.

(3) Scatchard and Hildebrand's<sup>32,33</sup> approach *via* regular solutions.

The volume of mixing for the cyclohexane-isooctane system affords a severe test of any theory. In addition to the volume of mixing being very small, it also changes sign around the equimolar axis, depending on the temperature under consideration. Calculations for this system were made at a mole fraction of 0.5 at 10, 25, and 80°. Similar calculations were made for the carbon tetrachloride-isooctane system. The volume of mixing for the latter system does not display an unusual composition dependence.

Flory's approach<sup>29,30</sup> is a statistical thermodynamic one using a reduced equation of state. The data for these calculations are presented in Table V. In this table,  $\bar{V}^0$  is the molar volume,  $\alpha$  is the coefficient of thermal expansion,  $\gamma$  is  $(\partial P/\partial T)_V$  or the thermal pressure coefficient (calculated from  $\gamma = \alpha/\beta$ , where  $\beta$  is the coefficient of compressibility),  $\bar{v}$  is a reduced volume calculated from

$$\bar{v}^{1/3} - 1 = (\alpha T/3)/(1 + \alpha T) \quad (7)$$

$\bar{T}$  is a reduced temperature calculated from the reduced equation of state

$$\bar{T} = (\bar{v}^{1/3} - 1)/\bar{v}^{1/3} \quad (8)$$

$v^*$  is given by  $\bar{V}^0/\bar{v}$  and is the hard-core volume per

mole,  $T^* = T/\bar{T}$  and is the characteristic temperature, and  $P^* = \gamma T \bar{v}^2$  and is the characteristic pressure.

The data for the mixtures are given in Table VI. To simplify the calculations Flory defined the molecular element or segment to be in correspondence for the two species such that  $r_1$  and  $r_2$  (where  $r$  is the number of elements or segments per molecule) are in the ratio of the respective molar core volumes  $v_1^*$  and  $v_2^*$  or  $r_1/r_2 = v_1^*/v_2^*$ . Also,  $s_1$  and  $s_2$  (where  $s$  is the number of intermolecular contact sites per segment) are in the ratio of the molecular surface areas of contact per segment. For our calculations both molecules in each system were taken to be spherical such that the equation  $s_1/s_2 = (r_1/r_2)^{-1/3} = (v_1^*/v_2^*)^{-1/3}$  could be used. The segment fraction per mole,  $\phi_2$ , is  $\phi_2 = 1 - \phi_1 = r_2 X_2 / (r_1 X_1 + r_2 X_2)$  and the site fraction,  $\theta_2$ , is defined as  $\theta_2 = \phi_2 s_2 / (\phi_1 s_1 + \phi_2 s_2)$ . The interaction parameter  $X_{12}$  was calculated from  $X_{12} = P_1^* [1 - (s_1/s_2)^{1/2} (P_2^*/P_1^*)^{1/2}]$ .<sup>2</sup> The interaction parameter was empirically adjusted both by Flory<sup>30</sup> and Benson and Singh,<sup>12</sup> but we did not follow this route in the calculation.

The reduced volume for the mixture,  $\bar{v}_M$ , was calculated by first calculating a reduced temperature for the mixture

$$\bar{T}_M = \left( \frac{\phi_1 P_1^* \bar{T}_1 + \phi_2 P_2^* \bar{T}_2}{\phi_1 P_1^* + \phi_2 P_2^*} \right) / \left( 1 - \frac{\phi_1 \theta_2 X_{12}}{\phi_1 P_1^* + \phi_2 P_2^*} \right)$$

The "ideal" reduced volume for the mixture,  $\bar{v}^0$ , is given by  $\bar{v}^0 = \phi_1\bar{v}_1 + \phi_2\bar{v}_2$ . The "ideal" reduced temperature,  $\bar{T}^0$ , was calculated by using  $\bar{v}^0$  in eq 8. The excess reduced volume,  $\bar{v}^E$ , is then given by  $\bar{v}^E = (\bar{v}^0)^{2/3}(\bar{T} - \bar{T}^0)/[4/3 - (\bar{v}^0)^{1/3}]$ .  $\bar{v}_M$  is then given by  $\bar{v}_M = \bar{v}^0 + \bar{v}^E$  and values of  $\bar{v}_M$  and  $\bar{v}^0$  are presented in Table VI. The excess molar volume,  $\Delta V^E$ , is then calculated from

$$\Delta V^E = (X_1v_1^* + X_2v_2^*)(\bar{v}_M - \bar{v}^0) \quad (9)$$

Columns nine and ten in Table VI compare the experimental excess molar volumes with those calculated from eq 9. The agreement is excellent for the carbon tetrachloride-isooctane system. Indeed, there is better agreement here than for similar systems cited by Abe and Flory.<sup>30</sup> In contrast, the agreement for the cyclohexane-isooctane system is good where we defined "good" as being within 0.1–0.2 cm<sup>3</sup> mol<sup>-1</sup>. Considering the near ideality of this system and the assumptions in the theory, the agreement must still be considered a success for the theory. We found no irregularities in the composition dependence calculated from the Flory theory for the cyclohexane-isooctane system. The calculations are quite sensitive to the  $\alpha$ 's which are used. This sensitivity is the reason for the small discrepancies in the  $\Delta\bar{V}^E$  calculated in this work and those calculated by Battino.<sup>4,5</sup>

Calculations based on Prigogine's theory<sup>31</sup> were found to be inadequate for both systems. Undoubtedly, the failure of this approach is related to the  $r^*$  values for the pure components differing by more than 10%.<sup>3</sup>

The volume of mixing from regular-solution theory is defined as<sup>32,33</sup>

$$\Delta\bar{V}^E = (\alpha T/\delta^2)(X_1\bar{V}_1^0 + X_2\bar{V}_2^0)(\delta_1 - \delta_2)^2 Z_1 Z_2 \quad (10)$$

where  $\alpha$  is the thermal expansion coefficient;  $\delta$ ,  $\delta_1$ , and  $\delta_2$  are the solubility parameters for the solution, pure component 1, and pure component 2, respectively; and  $Z_1$  and  $Z_2$  are the volume fractions. The values of  $\delta_1$  and  $\delta_2$  were taken from Hildebrand and Scott's monograph.<sup>33</sup> The value of  $\delta$  was taken as the mean value of  $\delta_1$  and  $\delta_2$ . These parameters were assumed to be independent of temperature. This assumption was thought to be partially justified in that we were calculating differences. Hildebrand and Scott<sup>33</sup> have indicated that "for the kind of approximate agreement

which is all one can expect, it suffices to have self-consistent values of  $\delta$  for the various components at one temperature even though the experimental measurement is at quite a different temperature." Values of  $\delta$  (cal<sup>1/2</sup> cm<sup>-3/2</sup>) for cyclohexane, isooctane, and carbon tetrachloride at 25° are 8.2, 6.9, and 8.6, respectively.

The volume of mixing as calculated from eq 10 is presented in the last column of Table VI. For comparison, the observed volume of mixing is also listed. It is evident that the agreement with experiment is poorer than in the case of the Flory calculation.

Hildebrand and Dymond<sup>34</sup> have derived a new equation relating the partial molal volumes to solubility parameters and  $(\partial E_1/\partial V)_T$

$$(\bar{V}_2 - \bar{V}_2^0)(\partial E_1/\partial V)_T = \bar{V}_2^0(\delta_2 - \delta_1)^2 \quad (11)$$

Equation 11 was applied to equimolar mixtures of the two systems under investigation. The calculated and observed values for  $\bar{V}_2 - \bar{V}_2^0$  are given in Table VII. The agreement is poor. As pointed out by Hildebrand and Dymond,<sup>34</sup> the agreement would be greatly improved if the solubility parameter for isooctane were 7.8 or 7.9 instead of 6.9. This discrepancy is typical for several other systems involving isooctane.

**Table VII:** Comparison of Observed and Calculated Values of  $\bar{V}_2 - \bar{V}_2^0$

Solute	$(\partial E_1/\partial V)_T$ , cal cm <sup>-3</sup>	$\bar{V}_2 - \bar{V}_2^0$	
		Exptl	Calcd (eq 11)
C <sub>6</sub> H <sub>12</sub>	75.4	0.02	3.73
CCl <sub>4</sub>	81.0	0.19	5.92

*Acknowledgment.* The authors are deeply indebted to Professor Scott E. Wood for many helpful discussions. The support of the Petroleum Research Fund (Grant No. 975-A3) is gratefully acknowledged.

(31) I. Prigogine, "The Molecular Theory of Solution," North-Holland Publishing Co., Amsterdam, The Netherlands, 1957.

(32) J. H. Hildebrand and R. L. Scott, "Solubility of Non-Electrolytes," 3rd ed, Reinhold Publishing Corp., New York, N. Y., 1950.

(33) J. H. Hildebrand and R. L. Scott, "Regular Solutions," Prentice-Hall, Inc., Englewood Cliffs, N. J., 1962.

(34) J. H. Hildebrand and J. Dymond, *J. Chem. Phys.*, **46**, 624 (1967).

## Thermodynamics of Binary Solutions of Nonelectrolytes with 2,2,4-Trimethylpentane. IV. Vapor-Liquid Equilibrium

### (35–75°) and Volume of Mixing (25°) with Carbon Tetrachloride<sup>1</sup>

by Rubin Battino

Department of Chemistry, Wright State University, Dayton, Ohio 45431 (Received May 29, 1968)

The vapor-liquid equilibrium in the 2,2,4-trimethylpentane-carbon tetrachloride system was measured isothermally at 10° intervals in the range 35–75° and over the entire range of composition. The volume of mixing was measured at 25° and the maximum was 0.218 cm<sup>3</sup> mol<sup>-1</sup>. The excess thermodynamic functions were calculated for the conditions of mixing at constant pressure and were found to be positive over the entire range of composition and temperature studied and small in magnitude (at 40° maxima are  $\Delta\bar{G}_p^E = 35.0$  cal mol<sup>-1</sup>,  $\Delta\bar{H}_p^E = 44$  cal mol<sup>-1</sup>, and  $\Delta\bar{S}_p^E = 0.23$  cal mol<sup>-1</sup> deg<sup>-1</sup>). The excess Gibbs function decreases slightly with increasing temperature, but the other functions are independent of temperature within experimental error. The constant volume thermodynamic functions are almost identical with the constant pressure functions. Good agreement was found with a theoretical treatment proposed by Flory and coworkers.

#### Introduction

The present paper continues the study of the thermodynamics of binary solutions with isooctane (2,2,4-trimethylpentane). The benzene-isooctane system was studied by Wood and Sandus<sup>2</sup> and Weissman and Wood.<sup>3</sup> The cyclohexane-isooctane system was studied by Battino,<sup>4</sup> Battino and Allison,<sup>5</sup> and Washington and Battino.<sup>6</sup> The volume of mixing for the carbon tetrachloride-isooctane system in the range 10–80° was measured in part III.<sup>6</sup> In this paper we report the isothermal vapor-liquid equilibrium (35–75°) at 10° intervals and the volume of mixing at 25°, both over the entire range of composition. The excess thermodynamic functions were calculated for the conditions of mixing at constant pressure and were found to be positive over the entire range of composition and temperatures studied.

Isooctane has been chosen as the component of interest because it shows one of the smallest orientation effects in the pure liquid phase for a common liquid. The difference in the heat capacity at constant volume of the pure substance in the liquid and ideal gas states is a good measure of the intermolecular orientation in the pure liquid. Wood, Sandus, and Weissman<sup>7</sup> calculated this difference for isooctane (1.0 cal mol<sup>-1</sup>), cyclohexane (4.7 cal mol<sup>-1</sup>), benzene (4.9 cal mol<sup>-1</sup>), and carbon tetrachloride (3.4 cal mol<sup>-1</sup>). In view of the rather ideal nature of mixtures of isooctane with cyclohexane,<sup>4–6</sup> it was of interest to determine the nature of mixtures of isooctane with carbon tetrachloride.

#### Experimental Procedure

**Materials.** The isooctane used was the same as that

described in a previous paper<sup>4</sup> (hereafter referred to as I) and had a density of 0.68780 g cm<sup>-3</sup> at 25°. The carbon tetrachloride used was Fisher Certified 99 mol % and this material, which had a density of 1.58437 g cm<sup>-3</sup> at 25°, was used without further purification in the vapor-liquid equilibrium measurements. For the volume-of-mixing measurements the carbon tetrachloride was purified by repeated distillation in a 6-ft packed column followed by a vacuum distillation from CaH<sub>2</sub>. The density of this material was 1.58430 g cm<sup>-3</sup> at 25°. This compares with the following values from the literature all at 25° and in grams per cubic centimeter: 1.58429,<sup>8</sup> 1.58461,<sup>9</sup> 1.58429,<sup>10</sup> 1.58414,<sup>11</sup> 1.58426,<sup>12</sup> 1.58437,<sup>13</sup> 1.58436,<sup>14</sup> and 1.58425.<sup>15</sup> The water

- (1) R. Battino, presented in part at the 155th National Meeting of the American Chemical Society, San Francisco, Calif., April 1968.
- (2) S. E. Wood and O. Sandus, *J. Phys. Chem.*, **60**, 801 (1956).
- (3) S. Weissman and S. E. Wood, *J. Chem. Phys.*, **32**, 1153 (1960).
- (4) R. Battino, *J. Phys. Chem.*, **70**, 3408 (1966).
- (5) R. Battino and G. W. Allison, *ibid.*, **70**, 3417 (1966).
- (6) Part III: E. L. Washington and R. Battino, *ibid.*, **72**, 4496 (1968).
- (7) S. E. Wood, O. Sandus, and S. Weissman, *J. Amer. Chem. Soc.*, **79**, 1777 (1957).
- (8) J. A. Barker, I. Brown, and F. Smith, *Discussions Faraday Soc.*, **44**, 142 (1953).
- (9) J. A. Larkin and M. L. McGlashan, *J. Chem. Soc.*, 3425 (1961).
- (10) S. E. Wood and J. A. Gray, *J. Amer. Chem. Soc.*, **74**, 3729 (1952).
- (11) G. Scatchard, S. E. Wood, and J. M. Mochel, *ibid.*, **61**, 3206 (1939).
- (12) G. Scatchard, S. E. Wood, and J. M. Mochel, *ibid.*, **62**, 712 (1940).
- (13) G. Scatchard and L. B. Ticknor, *ibid.*, **74**, 3724 (1952).
- (14) J. H. Hildebrand, B. B. Fisher, and H. A. Benesi, *ibid.*, **72**, 4348 (1950).

and mercury used were identical with the materials described in part I.

**Apparatus.** The volume of mixing at 25° was determined using the same apparatus and procedure as in I. The vapor-liquid equilibrium measurements were carried out in the same manner as in I. The vapor pressure of pure isooctane, which was used in the reference still, was calculated from<sup>16</sup>  $\log P(\text{torr}) = 6.81984 - [1262.490/(221.271 + t)]$ . The vapor pressure of pure carbon tetrachloride was measured and fitted to the following equation by a least-squares technique:  $P(\text{torr}) = 9.775 + 3.7046t - 0.01378t^2 + 0.001210t^3$ . The standard deviation of the fit was  $\pm 0.23$  mm, and the pressures calculated from this equation agreed to an average deviation of  $\pm 0.33$  mm with ref 11 and  $\pm 2.22$  mm with ref 15. To be self-consistent in the calculations, the vapor pressures of carbon tetrachloride used in this paper were all calculated using the equation cited above.

## Results

**Volume of Mixing.** Table I shows the composition, density, and relative volume of mixing at 25° for the

**Table I:** Densities of Carbon Tetrachloride-Isooctane Mixtures at 25°

Carbon tetrachloride— $X_1$ $Z_1$		$d$ , g cm <sup>-3</sup>	$-10^3 \Delta V^M / V_0$		$\Delta(\Delta V^M / V_0)$
			Obsd	Calcd	
0.00000	0.00000	0.68780	0.00	0.00	0.00
0.12325	0.07595	0.75540	0.66	0.67	-0.01
0.13074	0.08083	0.75972	0.72	0.70	0.02
0.24110	0.15666	0.82728	1.16	1.15	0.01
0.25016	0.16323	0.83315	1.18	1.18	0.00
0.34368	0.23440	0.89669	1.40	1.45	-0.05
0.45447	0.32755	0.97983	1.66	1.62	0.04
0.47281	0.34399	0.99459	1.61	1.64	-0.03
0.55905	0.42571	1.06764	1.70	1.65	0.05
0.57956	0.44628	1.08615	1.61	1.64	-0.03
0.67131	0.54425	1.17391	1.54	1.53	0.01
0.69237	0.56821	1.19541	1.50	1.49	0.01
0.77751	0.67141	1.28808	1.27	1.28	-0.01
0.79698	0.69654	1.31066	1.22	1.21	0.01
0.89745	0.83652	1.43665	0.76	0.76	0.00
1.00000	1.00000	1.58430	0.00	0.00	0.00

carbon tetrachloride-isooctane system. The data were fit by a least-squares technique to a function of the volume fraction,  $Z$ , and a function of the mole fraction,  $X$ . Subscript 1 refers to carbon tetrachloride

$$\frac{\Delta V^M}{V_0} = Z_1 Z_2 (0.01034 - 0.01130 Z_1 + 0.00672 Z_1^2) \quad (1)$$

$$\Delta \tilde{V}^M = X_1 X_2 (1.045 - 0.538 X_1 + 0.350 X_1^2) \quad (2)$$

The reproducibility of these measurements is  $\pm 0.003$  cm<sup>3</sup> mol<sup>-1</sup>. The maximum  $\Delta \tilde{V}^M$  is 0.218 cm<sup>3</sup> mol<sup>-1</sup> at a volume fraction of carbon tetrachloride of 0.35.

The composition of the vapor and liquid phases for

the vapor-liquid equilibrium measurements were determined from density measurements (to  $\pm 0.00002$  g cm<sup>-3</sup>) at 25°. The resultant error in determining the composition from the density measurements is  $\pm 0.00002$  in the mole fraction and this is the error in the compositions listed in Table I. (The high precision in the composition is due to the very large difference in the density of the two components.)

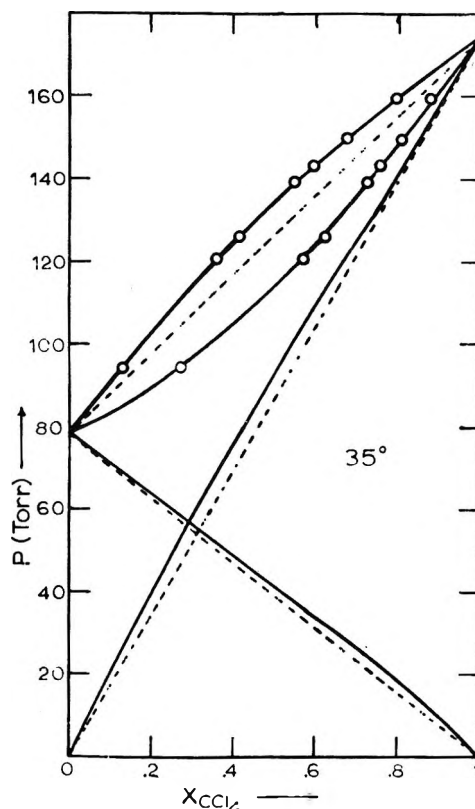


Figure 1. The vapor-liquid equilibrium at 35°.

**Vapor-Liquid Equilibria.** In Table II the results of the vapor-liquid equilibria measurements at the five temperatures investigated are presented;  $X_1$  is the composition (of carbon tetrachloride) in the liquid phase,  $Y_1$  is that in the vapor phase, and  $P$  is the total pressure. The remaining columns will be discussed later. The values in parentheses were not considered sufficiently reliable to incorporate in the calculations of the thermodynamic properties but were left in the table for purposes of comparison. The results for 35° are shown in Figure 1. The system shows small positive deviations from the (dashed) Raoult's law lines at all temperatures investigated.

(15) R. R. Dreisbach, "Physical Properties of Chemical Compounds. II," *Advances in Chemistry Series*, No. 22, American Chemical Society, Washington, D. C., 1961.

(16) "Selected Values of Properties of Hydrocarbons," National Bureau of Standards Circular C461, U. S. Government Printing Office, Washington, D. C., 1947.



Table II: Vapor-Liquid Equilibria<sup>a</sup>

$X_1$	$Y_1$	Dev in $Y_1$	$P$ , mm	Dev in $P$	$\Delta\bar{G}_p^E$ , cal mol <sup>-1</sup>	Dev in $\Delta\bar{G}_p^E$	$dP/dY_1$ (obsd)	Dev in $dP/dY_1$
35°								
0.1287	0.2714	-0.0034	94.17	-0.21	12.54	0.11	0.0904	-0.0016
0.3597	0.5703	-0.0055	120.43	-0.32	31.19	1.29	0.1378	-0.0045
0.4140	0.6210	-0.0048	126.04	-0.31	33.66	1.09	0.1477	-0.0046
0.5493	0.7281	-0.0027	139.23	-0.07	37.17	1.18	0.1676	-0.0037
0.5948	0.7590	-0.0025	143.11	-0.24	36.32	0.37	0.1712	-0.0042
0.6726	0.8087	-0.0017	149.78	-0.17	34.49	0.24	0.1756	-0.0037
0.7963	0.8788	-0.0036	159.58	-0.15	28.03	1.15	0.1649	-0.0117
45°								
0.1278	0.2633	-0.0002	142.45	-0.01	11.36	0.05	0.1329	-0.0002
(0.3137)	(0.5221)	(0.0042)	(173.13)	(-0.16)	(22.31)	(-2.81)	(0.1935)	(0.0039)
0.4350	0.6350	0.0000	191.76	0.17	31.72	0.59	0.2215	0.0002
0.5636	0.7352	0.0009	209.20	-0.04	33.15	-0.59	0.2470	0.0017
0.7227	0.8371	0.0004	228.75	-0.13	29.56	-0.57	0.2571	0.0011
0.8299	0.8980	-0.0017	240.54	-0.46	22.02	-0.43	0.2395	-0.0099
55°								
0.1264	0.2547	0.0026	208.91	0.21	9.69	-0.47	0.1895	0.0027
0.3076	0.4997	-0.0013	250.46	-0.11	23.12	0.37	0.2588	-0.0018
(0.4288)	(0.6280)	(0.0069)	(276.64)	(0.31)	(25.58)	(-3.02)	(0.3175)	(0.0136)
0.5601	0.7297	0.0041	302.17	0.26	29.75	-1.67	0.3501	0.0118
0.7177	0.8300	-0.0003	329.39	-0.25	28.10	-0.36	0.3534	-0.0016
0.8276	0.8972	0.0007	346.88	-0.51	20.04	-1.28	0.3525	0.0053
65°								
0.1248	0.2473	0.0060	298.19	0.45	7.41	-1.60	0.2650	0.0092
0.3054	0.4929	0.0041	354.81	0.42	19.39	-1.25	0.3603	0.0082
(0.4252)	(0.6213)	(0.0116)	(390.33)	(0.97)	(21.57)	(-4.61)	(0.4409)	(0.0319)
0.5505	0.7117	-0.0009	423.47	0.29	29.99	0.95	0.4512	-0.0031
0.7159	0.8273	0.0014	463.79	0.08	26.00	-0.62	0.4909	0.0096
0.8294	0.8959	0.0000	489.13	-0.07	19.74	-0.10	0.4734	0.0000
75°								
0.1250	0.2367	0.0028	416.75	1.22	8.85	0.84	0.3505	0.0069
0.3060	0.4813	0.0011	492.30	1.49	20.26	1.57	0.4717	0.0044
(0.4397)	(0.6146)	(-0.0003)	(545.36)	(2.55)	(27.76)	(3.39)	(0.5503)	(0.0016)
0.5518	0.7083	0.0006	584.87	1.52	28.20	1.46	0.6058	0.0049
0.7146	0.8215	-0.0003	638.04	0.67	25.62	0.86	0.6366	-0.0015
0.8319	0.8954	-0.0004	673.13	-0.01	18.49	0.17	0.6240	-0.0059

<sup>a</sup> The following are the average deviation and the standard deviation, respectively, for various terms:  $Y_1$ , 0.0020, 0.0027;  $P$ , 0.36, 0.55;  $\Delta\bar{G}_p^E$ , 0.79, 0.93;  $dP/dY_1$ , 0.0046, 0.0057.

### Thermodynamic Functions

The excess chemical potentials are defined by

$$\Delta\mu_1^E = \mu_1 - \mu_1^0 - RT \ln X_1 \quad (3)$$

where the standard states are the pure components. They were calculated from

$$\Delta\mu_1^E = RT \ln (PY_1/P_1^0X_1) + (\beta_{11} - \bar{V}_1^0)(P - P_1^0) + \delta(1 - Y_1)^2P + (\bar{V}_1 - \bar{V}_1^0)(1 - P) \quad (4)$$

By changing the subscripts, eq 3 and 4 are used to calculate  $\Delta\mu_2^E$ . In these equations  $P$  is the total vapor pressure,  $P^0$  is the vapor pressure of the pure component,  $X$  and  $Y$  are the mole fractions of the liquid and vapor

phases, respectively,  $\bar{V}_1$  and  $\bar{V}_1^0$  are the partial molar volumes of the component in solution and the molar volume of the pure component, respectively,  $\beta_{11}$  is the second virial coefficient, and  $T = 273.15 + t$ . The term  $\delta$  is defined by  $\delta = 2\beta_{12} - \beta_{11} - \beta_{22}$ . In the derivation of eq 4 the equation of state for the vapor was the virial equation used to the second virial coefficient. The last term in eq 4 corrects the chemical potentials from the experimental pressures to 1 atm. The change in the thermodynamic functions for mixing at constant pressure were calculated for the change of state in which  $X_1$  mol of carbon tetrachloride at 1 atm of pressure and the chosen temperature  $T$  and  $X_2$  mol of iso-octane at the same conditions are mixed to form 1 mol of solution under the identical conditions.

The second virial coefficients were calculated using Berthelot's equation, a procedure justified by many workers.<sup>17,18</sup> The second virial coefficients are given by

$$\beta_{ii} = B_{ii} - (A_{ii}/T^2) \quad (5)$$

where  $A = 27RT_c^3/64P_c$  and  $B = 9RT_c/128P_c$ . For carbon tetrachloride the equation  $\beta_{11} = 71.4 - [(13.25 \times 10^7)/T^2]$  was found from  $T_c = 556.25^\circ\text{K}$  and  $P_c = 44.98$  atm. For isooctane the equation  $\beta_{22} = 123.2 - [(21.89 \times 10^7)/T^2]$  was found from  $T_c = 544.30^\circ\text{K}$  and  $P_c = 25.5$  atm. The experimental virial coefficients for carbon tetrachloride measured by Lambert, *et al.*,<sup>17</sup> fit the above equation within their experimental error; those measured by Francis and McGlashan<sup>19</sup> were more negative; and those measured by Bottomley and Remington<sup>20</sup> were less negative. The term  $\beta_{12}$  was calculated by assuming the combining laws

$$B_{12} = (1/8)(B_{11}^{1/3} + B_{22}^{1/3})^3$$

and

$$A_{12} = (A_{11}A_{22})^{1/2}$$

Since we used a computer to calculate the excess chemical potentials according to eq 4, we decided to test the effect of varying the various terms in the equation on the numerical value of  $\Delta\mu_1^E$ . For this purpose we selected the data at  $55^\circ$  for  $X_1 = 0.5601$  for which  $\Delta\mu_1^E = 37.76$  cal mol<sup>-1</sup>. In terms of the properties measured, it appears from Table III that the calculation of  $\Delta\mu_1^E$  is most sensitive to variations in the total pressure.

**Table III:** Effect on  $\Delta\mu_1^E$  (37.76 cal mol<sup>-1</sup>) of Variations in  $P$ ,  $P_1^0$ ,  $X_1$ ,  $Y_1$ ,  $\beta_{11}$ ,  $\delta$ ,  $T$ ,  $\bar{V}_1^0$ , and  $\bar{V}_1 - \bar{V}_1^0$  at  $X_1 = 0.5601$  and  $55^\circ$

Term	Variation	$\Delta(\Delta\mu_1^E)$ , cal mol <sup>-1</sup>	Term	Variation	$\Delta(\Delta\mu_1^E)$ , cal mol <sup>-1</sup>
$P$	+0.1 mm	0.21	$\beta_{11}$	+10 cm <sup>3</sup>	0.02
	+1.0 mm	2.11		+100 cm <sup>3</sup>	0.23
$P_1^0$	+0.1 mm	0.17	$\delta$	+10 cm <sup>3</sup>	0.01
	+1.0 mm	1.71			
$X_1$	+0.0001	0.12	$T$	+0.1°	0.01
	+0.0010	1.16		+1.0°	0.11
$Y_1$	+0.0001	0.09	$\bar{V}_1^0$	+1.0 cm <sup>3</sup>	0.00
	+0.0010	0.89	$\bar{V}_1 - \bar{V}_1^0$	+1.0 cm <sup>3</sup>	0.00

The molar excess change of the Gibbs free energy on mixing at constant pressure was calculated from  $\Delta\bar{G}^E = X_1\Delta\mu_1^E + X_2\Delta\mu_2^E$ . The experimentally determined values of  $\Delta\bar{G}^E$  are given in Table II, and these values were smoothed by fitting the equation

$$\Delta\bar{G}^E = X_1X_2[a + b(X_1 - X_2)] \quad (6)$$

The coefficients  $a$  and  $b$  in this equation were fit by least squares as a function of temperature, and the resulting equations are

$$a = 174.13 - 0.9368t \quad (7)$$

$$b = 41.18 - 0.0038t \quad (8)$$

The deviations ( $\Delta\bar{G}_p^E(\text{exptl}) - \Delta\bar{G}_p^E(\text{calcd})$ ) between the experimental and the smoothed values of  $\Delta\bar{G}_p^E$  are given in Table II, and the standard deviation is  $\pm 0.93$  cal mol<sup>-1</sup>. These smoothed values were used to back-calculate  $Y_1$  and  $P$  with the use of eq 6–8 for each experimental point. The deviations from the experimental values are in columns three and five of Table II and are judged to be satisfactory.

The Redlich–Kister test for thermodynamic consistency requires that

$$\int_0^1 (\Delta\mu_1^E - \Delta\mu_2^E) dX_1 = 0 \quad (9)$$

The data for  $75^\circ$  are shown in Figure 2, where the circles are the experimental points. The solid line was determined by a least-squares fit of the experimental points, and the dashed line was determined from the smoothed values (eq 6–8). The dashed line must satisfy eq 9, since eq 6 must satisfy the Gibbs–Duhem relation on which the Redlich–Kister method is based. Table IV summarizes the results obtained for this test. The areas were determined by weighing cutouts. For comparison the ratio of the areas was determined (column four) for shifting the curves one standard deviation (third column) for the least-squares fit for the experimental points. The  $35^\circ$  data appear to be poor, but the remainder are quite satisfactory.

**Table IV:** Summary of Redlich–Kister Test

$t$ , °C	(+)/(–) <sup>a</sup>	$\sigma$ , cal	(+)/(–) <sup>b</sup> + $\sigma$
35	0.67	5.0	0.79
45	0.92	4.8	1.08
55	1.15	9.7	0.80
65	1.34	5.6	1.12
75	1.13	2.1	1.00

<sup>a</sup> Ratio of plus to minus areas. <sup>b</sup> Ratio when  $\Delta\mu_1^E - \Delta\mu_2^E$  is increased by  $\sigma$ .

Weissman and Wood<sup>3</sup> proposed a more stringent point-by-point test for thermodynamic consistency.

(17) J. P. Lambert, G. A. H. Roberts, J. S. Rowlinson, and V. J. Wilkinson, *Proc. Roy. Soc.*, **A196**, 113 (1949).

(18) G. Scatchard and F. G. Satkiewicz, *J. Amer. Chem. Soc.*, **86**, 130 (1964).

(19) P. G. Francis and M. L. McGlashan, *Trans. Faraday Soc.*, **51**, 593 (1955).

(20) G. A. Bottomley and T. A. Remington, *J. Chem. Soc.*, 3800 (1958).

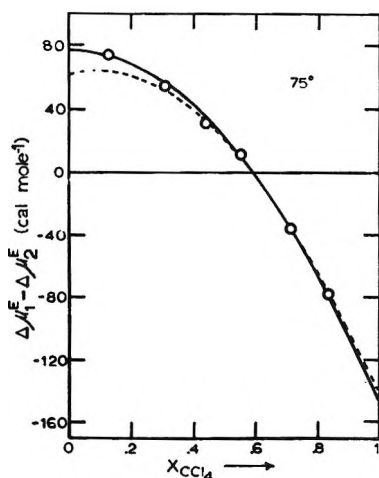


Figure 2. The Redlich-Kister plot for 75° data.

In their method the slopes  $dP/dY_1$  for the experimental and smoothed values are compared. These slopes are calculated from

$$\frac{dP}{dY_1} = \frac{(Y_1 - X_1)[(RT/Y_1Y_2) - 2\delta P]}{(RT/P) + X_1\beta_{11} + X_2\beta_{22} + (X_1Y_2^2 + X_2Y_1^2)\delta - \bar{V}_1} \quad (10)$$

In Table II the eighth column gives the experimental values of  $dP/dY_1$  and the last column gives the deviations of the calculated values from them. The agreement between the observed and calculated values at each temperature are: 35°, 3.3%; 45°, 1.2%; 55°, 1.5%; 65°, 1.5%; and 75°, 0.8%. The agreement is best at 75° and poorest at 35°, but the agreement is excellent when it is observed that this sensitive test is comparing slopes.

Table V gives the excess thermodynamic functions for mixing at constant pressure at 40, 55, and 70° and for every 0.1 mol fraction. These values were calculated from the smoothed data (eq 6-8). Since the constants  $a$  and  $b$  in eq 6 were found to be linear functions of the temperature within experimental error, both  $\Delta\bar{H}_p^M$  and  $\Delta\bar{S}_p^E$  are independent of the temperature. A check in the literature on systems comparable with the one investigated here show that it is not at all unusual for calorimetrically determined heats of mixing to have a negligible temperature dependence. The values of the thermodynamic functions are all positive over the entire range of composition and at all temperatures investigated. The change in the Gibbs free energy decreases slowly with an increase in temperature. Figure 3 shows the thermodynamic functions at 40°. The differences between the change in the thermodynamic functions on mixing at constant pressure and on mixing at constant volume were calculated according

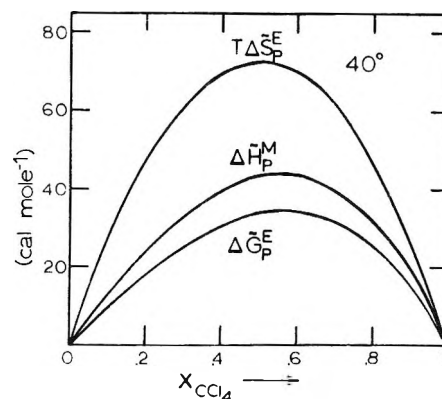


Figure 3. The excess thermodynamic functions at 40°.

**Table V:** Excess Thermodynamic Functions in Calories per Mole

$X_1$	$\Delta\bar{G}_p^E$			$\Delta\bar{H}_p^M$	$\Delta\bar{S}_p^E$	$\Delta\bar{E}_v^M$
	40°	55°	70°			
0.1	9.3	8.1	6.8	13	0.084	26 <sup>a</sup>
0.2	17.9	15.7	13.4	24	0.150	49
0.3	25.3	22.3	19.4	33	0.196	67
0.4	30.8	27.5	24.1	40	0.225	80
0.5	34.2	30.7	27.1	44	0.234	88
0.6	34.8	31.4	28.0	44	0.225	89
0.7	32.2	29.2	26.2	40	0.197	83
0.8	25.8	23.5	21.3	32	0.150	67
0.9	15.3	14.0	12.7	19	0.085	40

<sup>a</sup>  $\Delta\bar{E}_v^M$  is calculated from the Scatchard-Hildebrand equation.

to equations developed by Scatchard<sup>21</sup> and were found to be negligible for the free energy (about 0.03 cal mol<sup>-1</sup>) and nonnegligible for the entropy ( $\Delta\bar{S}_p^E - \Delta\bar{S}_v^E = 0.040$  cal mol<sup>-1</sup> deg<sup>-1</sup> at 40°) and the energy ( $\Delta\bar{H}_p^M - \Delta\bar{E}_v^E = 12$  cal mol<sup>-1</sup> at 40°).

### Discussion

Calculations were carried out for testing three theories of solutions. The corresponding states average potential model was found to be not applicable owing to the disparity in the size of the molecules. The Scatchard-Hildebrand approach yielded some satisfactory correlations, and the Flory approach yielded some excellent correlations.

The energy of mixing at constant volume can be calculated from the Scatchard-Hildebrand equation

$$\Delta\bar{E}_v^M = (X_1\bar{V}_1^0 + X_2\bar{V}_2^0)(\delta_1 - \delta_2)^2 Z_1 Z_2 \quad (11)$$

The  $\delta$ 's are solubility parameters and we used the following values for them at 40, 55, and 70°: carbon tetrachloride, 8.41, 8.21, and 8.01 and isooctane, 6.71, 6.55, and 6.38. The values of  $\Delta\bar{E}_v^M$  were calculated for each mole fraction at the three temperatures, but since the values only change 4 cal in this range, the average value

(21) G. Scatchard, *Trans. Faraday Soc.*, **33**, 160 (1937).

**Table VI:** Parameters for the Pure Liquids for the Flory Calculation

Liquid	$t$ , °C	$v$ , cm <sup>3</sup> mol <sup>-1</sup>	$10^3\alpha$ deg <sup>-1</sup>	$\gamma$ , cal cm <sup>-3</sup> deg <sup>-1</sup>	$\bar{v}$	$v^*$ , cm <sup>3</sup> mol <sup>-1</sup>	$T^*$ , °K	$P^*$ , cal cm <sup>-3</sup>	$C$ , cm <sup>3</sup> mol <sup>-1</sup>
Carbon tetra- chloride	25	97.08 <sup>a</sup>	1.229 <sup>a</sup>	0.273 <sup>b</sup>	1.2927	75.10	4697	136	1.09
	40	98.91 <sup>a</sup>	1.265 <sup>a</sup>	0.248 <sup>b</sup>	1.3113	75.43	4752	133	1.06
	70	102.88 <sup>a</sup>	1.363 <sup>a</sup>	0.205 <sup>b</sup>	1.3536	76.00	4836	129	1.02
Isooctane	25	166.06 <sup>c</sup>	1.197 <sup>c</sup>	0.179 <sup>d</sup>	1.2868	129.05	4760	88.4	1.21
	40	169.14 <sup>c</sup>	1.243 <sup>c</sup>	0.166 <sup>e</sup>	1.3072	129.39	4792	88.8	1.21
	70	175.85 <sup>c</sup>	1.361 <sup>c</sup>	0.141 <sup>e</sup>	1.3533	129.94	4845	88.6	1.20

<sup>a</sup> S. E. Wood and J. A. Gray, *J. Amer. Chem. Soc.*, **74**, 3729 (1952). <sup>b</sup> G. A. Holder and E. Whalley, *Trans. Faraday Soc.*, **58**, 2095 (1962). <sup>c</sup> S. E. Wood and O. Sandus, *J. Phys. Chem.*, **60**, 801 (1956). <sup>d</sup> A linear extrapolation of the 40 and 70° values. <sup>e</sup> W. A. Felsing and G. M. Watson, *J. Amer. Chem. Soc.*, **65**, 780 (1943), using the values for the coefficient of compressibility as calculated by S. Weissman and S. E. Wood, *J. Chem. Phys.*, **32**, 1153 (1960).

**Table VII:** Comparison of Observed and Calculated Excess Quantities for the Flory Calculation for an Equimolar Mixture

$t$ , °C	$X_{12}$ , cal cm <sup>-3</sup>	$\theta_2$	$\Delta H^M$ , cal mol <sup>-1</sup>		$\bar{v}$		$V^E$ , cm <sup>3</sup> mol <sup>-1</sup>		$TS^R$ , cal mol <sup>-1</sup>		$TS^E$ , cal mol <sup>-1</sup>		
			Calcd	Obsd	Calcd	Obsd	Calcd	Obsd	Calcd <sup>e</sup>	Calcd <sup>d</sup>	Calcd <sup>e</sup>	Calcd <sup>f</sup>	Obsd
25	1.88	0.59	44	44	1.2914	1.2890	0.245	0.216 <sup>a</sup>	12	-4	33	18	70
40	1.49	0.59	36	44	1.3108	1.3087	0.215	0.192 <sup>b</sup>	10	-3	33	20	73
70	1.14	0.59	27	44	1.3549	1.3535	0.154	0.190 <sup>b</sup>	9	0	33	24	80

<sup>a</sup> This work. <sup>b</sup> See ref 6. <sup>c</sup> From  $\bar{v}$ (calcd) and  $\Delta S_{\text{comb}} = \Delta S_{\text{id}}$ . <sup>d</sup> From  $\bar{v}$ (obsd) and  $\Delta S_{\text{comb}} = \Delta S_{\text{id}}$ . <sup>e</sup> From  $\bar{v}$ (calcd) and  $\Delta S_{\text{comb}} = -R[X_1 \ln \phi_1 + X_2 \ln \phi_2]$ , where  $\phi$  is the segment fraction (see ref 4 or 22). <sup>f</sup> From  $\bar{v}$ (obsd) and  $\Delta S_{\text{comb}} = -R[X_1 \ln \phi_1 + X_2 \ln \phi_2]$ .

is given in Table V. It is noteworthy that for the cyclohexane–isooctane system<sup>4</sup> the experimental  $\Delta \bar{G}_p^E$  was about 9 cal mol<sup>-1</sup> vs. a calculated  $\Delta \bar{E}_v^M$  of 55 cal mol<sup>-1</sup>. Thus the increase in the calculated values of  $\Delta \bar{E}_v^M$  for the two systems is comparable with the increase in the experimental values of  $\Delta \bar{G}_p^E$ . The volume change on mixing can also be calculated from the Scatchard–Hildebrand approach. As in the case of the cyclohexane–isooctane<sup>4</sup> system, we found much better agreement using the experimentally determined  $\Delta \bar{G}_p^E$  than those calculated from eq 11.

The statistical thermodynamic approach using a reduced equation of state which was proposed by Flory and coworkers<sup>22</sup> gave such excellent results for the cyclohexane–isooctane system<sup>4</sup> that we were very interested in using it for the current system. The calculations were carried out as indicated<sup>4,22</sup> using the parameters given in Table VI. The comparison of observed and calculated excess quantities is given in Table VII. The agreement for the heats of mixing is quite outstanding. The excess entropy,  $S^E$ , is related to the residual entropy,  $S^R$ , by

$$S^E = S^R + \Delta S_{\text{comb}} - \Delta S_{\text{id}} \quad (12)$$

where  $\Delta S_{\text{id}} = -R(X_1 \ln X_1 + X_2 \ln X_2)$  and  $\Delta S_{\text{comb}}$

is the combinatorial entropy appropriate to the system concerned. We calculated  $\Delta S_{\text{comb}}$  from

$$\Delta S_{\text{comb}} = -R(X_1 \ln \phi_1 + X_2 \ln \phi_2) \quad (13)$$

although this equation has been criticized for overcorrecting for disparities in molar volumes. The agreement between the calculated and experimental excess entropies is not very good, the calculated values being almost identical with those calculated in I. The agreement between the calculated and experimental volumes of mixing is outstanding. Abe and Flory<sup>22b</sup> also found very good agreement for volumes of mixing for a variety of systems. Benson and Singh<sup>23</sup> found that the Flory theory correlated fairly well the excess enthalpy and excess volume for some aromatic–alicyclic systems.

*Acknowledgment.* The support of the Petroleum Research Fund Grant No. 975-A3 for part of this work is gratefully acknowledged.

(22) (a) P. J. Flory, *J. Amer. Chem. Soc.*, **87**, 1833 (1965); (b) A. Abe and P. J. Flory, *ibid.*, **87**, 1838 (1965); (c) P. J. Flory and A. Abe, *ibid.*, **86**, 3563 (1964); (d) R. A. Orwoll and P. J. Flory, *ibid.*, **89**, 6814 (1967); (e) R. A. Orwoll and P. J. Flory, *ibid.*, **89**, 6822 (1967).

(23) G. C. Benson and J. Singh, *J. Phys. Chem.*, **72**, 1345 (1968).

Steric Effect in the Radiolysis of *cis*- and *trans*-1,2-Dimethylcyclohexane<sup>1</sup>

by Manfred K. Eberhardt

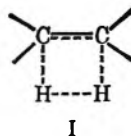
*Puerto Rico Nuclear Center,<sup>2</sup> Rio Piedras, Puerto Rico, and Institut für Radiochemie der Technischen Hochschule Munich, Munich, Germany (Received May 31, 1968)*

The radiolysis of *cis*- and *trans*-1,2-dimethylcyclohexane in the liquid phase was studied from  $2 \times 10^{20}$  to  $16 \times 10^{20}$  eV/ml at a dose rate of  $8.3 \times 10^{18}$  eV/ml hr. The main products are H<sub>2</sub>, 1,2-dimethylcyclohexene, 2,3-dimethylcyclohexene, 3,4-dimethylcyclohexene, 4,5-dimethylcyclohexene, octene-2, dimeric products, and isomerization. The *trans* compound shows a greater decrease in  $G(\text{olefin})$  with increasing dose than the *cis* isomer. Iodine ( $2 \times 10^{-2}$  M) reduces  $G(\text{H}_2)$  in the *trans*-1,2-dimethylcyclohexane from 3.54 to 2.36 ( $\Delta(G(\text{H}_2)) = 1.18$ ) but in the *cis* isomer the  $G(\text{H}_2)$  is only reduced from 3.70 to 3.05 ( $\Delta(G(\text{H}_2)) = 0.65$ ). Our results suggest that the difference of unscavengeable hydrogen between the two isomers,  $3.05 - 2.36 = 0.69$ , is due to molecular hydrogen elimination in the *cis*-1,2-dimethylcyclohexane and that tertiary axial hydrogens lead preferentially to the formation of scavengeable hydrogen atoms. A similar behavior was observed with *cis*- and *trans*-decalin. Evidence for opening and reclosure of the cyclohexane ring is presented.

## Introduction

The radiolysis of cyclohexane has been the subject of intense investigation.<sup>3</sup> Despite this there appears to be considerable controversy about the relative yields of different hydrogen precursors as well as the nature of these precursors. There are at least two precursors for hydrogen formation, one which is affected by radical scavengers and quenchers of excited states and one which is unaffected by these additives. The decrease in  $G(\text{H}_2)$  by radical scavengers has generally been attributed to the scavenging of thermal hydrogen atoms.<sup>4</sup> The formation of H<sub>2</sub> from cyclohexane by molecular detachment has been investigated simultaneously by two groups of workers by irradiating mixtures of C<sub>6</sub>H<sub>12</sub> and C<sub>6</sub>D<sub>12</sub>. From the isotopic composition of the hydrogen produced, Nevitt and Remsberg<sup>5</sup> concluded that no more than 25% of the total H<sub>2</sub> was formed by direct unimolecular detachment. Dyne and Jenkinson<sup>6</sup> arrived at a  $G(\text{H}_2 \text{ molecular})$  between 0.5 and 1.0.

In the present work we were mainly concerned with the mechanism of the molecular detachment process. Such a process appears to be impossible from the chair conformation of cyclohexane in the ground state in which the hydrogens on two adjacent carbon atoms are not eclipsed and therefore cannot form a four-center transition state.



A transition state like I is only possible in the boat form or flexible form of cyclohexane. It therefore appeared to us that the amount of molecular detachment should be dependent on the configuration of a cyclohexane derivative. We have therefore studied the radiolysis of *cis*- and *trans*-1,2-dimethylcyclohexane.

## Experimental Section

**Materials.** *cis*-Dimethylcyclohexane and *trans*-1,2-dimethylcyclohexane (puriss. *cis*-1,2-grade) were obtained from EGA Chemie Steinheim bei Heidenheim, Brenz, Germany. The purity was checked by vpc analysis. The only significant impurity was less than 1% of the other isomer. *cis*-Decalin and *trans*-decalin were puriss. grade (Schuchardt and Co., Munich). The decalin contained traces of tetralin, which was removed by shaking with fuming sulfuric acid followed by distillation *in vacuo*.

**Radiation.** Irradiations were carried out with a <sup>60</sup>Co source. The dose rate was determined with the Fricke dosimeter, using a value of 15.6 for  $G(\text{Fe}^{3+})$ . The dose rate was  $8.3 \times 10^{18}$  eV/ml hr. The total dose varied from  $0.4 \times 10^{20}$  to  $16 \times 10^{20}$  eV/ml.

**Analysis.** Hydrogen was analyzed by vpc using a 10-ft molecular sieve column at 50°. The hydrogen was detected with a thermal conductivity detector using argon as the carrier gas. The monomeric liquid products were analyzed by vpc on a 15-ft Carbowax 20M column at 65° and a flow rate of 25 ml of He/min. For detection a hydrogen flame detector was used. The peaks have been identified by comparison with standard samples. 3,4-Dimethylcyclohexene and 4,5-dimethylcyclohexene were not separated under our conditions. The dimeric products were analyzed using

(1) Presented at the 155th National Meeting of the American Chemical Society, San Francisco, Calif., March 1968.

(2) The Puerto Rico Nuclear Center is operated by the University of Puerto Rico for the U. S. Atomic Energy Commission under Contract AT-(40-1)-1833.

(3) J. W. T. Spinks and R. J. Woods, "An Introduction to Radiation Chemistry," John Wiley & Sons, Inc., New York, N. Y., 1964, pp 319-325.

(4) L. J. Forrestal and W. H. Hamill, *J. Amer. Chem. Soc.*, **83**, 1535 (1961).

(5) T. D. Nevitt and L. P. Remsberg, *J. Phys. Chem.*, **64**, 969 (1960).

(6) P. J. Dyne and W. M. Jenkinson, *Can. J. Chem.*, **38**, 539 (1960).

**Table I:** Main Products in the Radiolysis of *cis*- and *trans*-1,2-Dimethylcyclohexane

Isomer	Irradiation time, hr <sup>a</sup>	$G(H_2)$	$G(\text{cis-1,2-dimethylcyclohexane})$	$G(\text{trans-1,2-dimethylcyclohexane})$	$G(\text{olefin})$	$G(\text{dimer})$	$G(\text{octene-2})$	$G(\text{isomer})$	$D/C$
<i>cis</i>	5	3.69							
	24	3.62	1.1	0.9	0.47	0.4	0.48	2.2	6.1
	48	3.62	1.05	0.85	0.47	0.5	0.35	1.95	
	96	3.35	1.2	0.68	0.41	0.53	0.4	1.6	
	192	3.21	0.85	0.52	0.35	0.69	0.4	1.4	
<i>trans</i>	5	3.60							
	24	3.58	1.0	0.73	0.4	0.53	0	0.9	4.0
	48	3.49	0.86	0.62	0.33	0.68	...	0.65	
	96	3.59	0.63	0.52	0.29	0.86	..	0.62	
	192	3.24	0.42	0.38	0.22	0.78	..	0.56	

<sup>a</sup> Irradiation at a dose rate of  $8.3 \times 10^{18}$  eV/ml hr.

the same column as for the low-boiling products, but the temperature was raised to 150°.

### Results

The main products in the radiolysis of *cis*- and *trans*-1,2-dimethylcyclohexane are  $H_2$ , 1,2-dimethylcyclohexene, 2,3-dimethylcyclohexene, 3,4-dimethylcyclohexene, 4,5-dimethylcyclohexene, octene-2, dimeric products, and isomerizations (*cis*→*trans* and *trans*→*cis*). The  $G$  values of these products and their dose dependence are summarized in Table I. The different dimers have not been determined individually because of the multitude of different positional and configurational isomeric dimers, which have not been characterized to date. The  $G(\text{olefin})$  values from *trans*-1,2-dimethylcyclohexane show a greater dependence on dose than the *cis* compound. Table II shows some results of iodine-containing solutions of *cis*- and *trans*-1,2-dimethylcyclohexane as well as *cis*- and *trans*-decalin. The *trans* isomers produce about twice as much scavangeable hydrogen as do the *cis* isomers.

**Table II:** Effect of Iodine on  $G(H_2)$  in the Radiolysis of *cis*- and *trans*-1,2-Dimethylcyclohexane and *cis*- and *trans*-Decalin

Compd	Concn of $I_2$ , $M$	$G(H_2)$	$\Delta(G(H_2))$
<i>cis</i> -1,2-Dimethylcyclohexane	0	3.70	
	$1 \times 10^{-2}$	3.35	
	$2 \times 10^{-2}$	3.05	0.65
<i>trans</i> -1,2-Dimethylcyclohexane	0	3.54	
	$1 \times 10^{-2}$	2.45	
<i>cis</i> -Decalin	$2 \times 10^{-2}$	2.36	1.18
	0	4.3	
	$1 \times 10^{-2}$	3.95	
<i>trans</i> -Decalin	$2 \times 10^{-2}$	3.58	0.72
	0	4.65	
	$1 \times 10^{-2}$	3.52	
	$2 \times 10^{-2}$	2.93	1.72

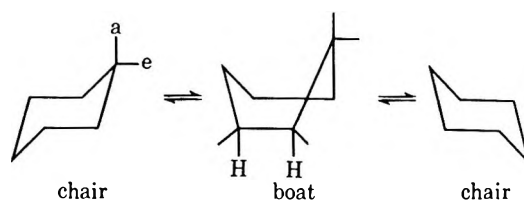


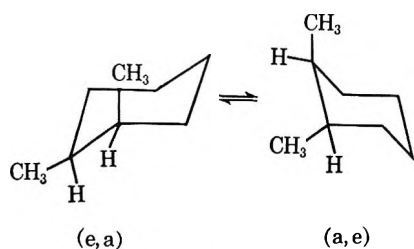
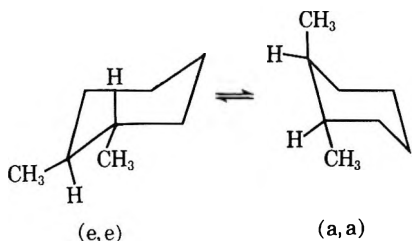
Figure 1. Conformations of cyclohexane.

### Discussion

In order to understand our results, let us first consider the stereochemistry of cyclohexane and the two 1,2-dimethylcyclohexanes.<sup>7</sup> Cyclohexane has two types of carbon-hydrogen bonds, equatorial bonds which lie in the plane of the cyclohexane ring and axial bonds which are either above or below the plane of the ring (see Figure 1).

Unimolecular hydrogen detachment is impossible from the chair conformation in the ground state. In the excited state, however, the true chair conformation may be slightly distorted in such a way as to allow unimolecular elimination. Since nothing is known about the structure of the excited state, we will try to rationalize our experimental results by considering only the ground state configuration. The *cis*-1,2-dimethylcyclohexane (Figure 2) has one axial and one equatorial methyl group, whereas the *trans*-1,2-dimethylcyclohexane exists in two conformational forms. The diequatorial form and diaxial form are readily interconvertible. The diaxial form (a, a) has four butane-gauche interactions, corresponding to an interaction energy of  $4 \times 0.9 = 3.6$  kcal/mol, whereas the diequatorial form (e, e) has only one such interaction. (See Figure 3.) The energy difference between the two conformers is therefore  $3.6 - 0.9 = 2.7$  kcal/mol. From the relationship  $\Delta F = -2.3 RT \log K$  it follows

(7) E. L. Eliel, "Stereochemistry of Carbon Compounds," McGraw-Hill Book Co., Inc., New York, N. Y., 1962, p 204 ff.

Figure 2. Conformations of *cis*-1,2-dimethylcyclohexane.Figure 3. Conformations of *trans*-1,2-dimethylcyclohexane.

that 99% of the molecules are in the diequatorial form at room temperature.

The *cis*-1,2-dimethylcyclohexane (Figure 2) can also exist in two conformations. Since the two forms have the same potential energy, half of the molecules exist in one form and half in the other. Since flipping from one chair conformation to another transforms all axial bonds into equatorial bonds and *vice versa*, twisting of the chair of *cis*-1,2-dimethylcyclohexane in such a way as to allow unimolecular detachment is energetically more favorable than in the *trans* isomer. We suggest therefore that the difference of unscavengeable hydrogen between the two isomers ( $3.05 - 2.36 = 0.69$ ) is due to molecular  $H_2$  detachment in the *cis*-1,2-dimethylcyclohexane. Okabe and McNesby<sup>8</sup> reported a different mechanism for molecular  $H_2$  formation. In the gas-phase photolysis of  $CH_3CD_3$  they found that molecular hydrogen is formed by splitting off two hydrogens from the same carbon atom. It appears doubtful whether these results obtained in the gas phase can be related to the present work in the liquid phase. Elimination of two hydrogens from the same carbon atom would not be expected to give different amounts of molecular hydrogen from *cis*- and *trans*-1,2-dimethylcyclohexane.

A  $2 \times 10^{-2} M$  solution of iodine in *trans*-1,2-dimethylcyclohexane shows a decrease in  $G(H_2)$  which is about twice as big as the decrease in the *cis* isomer. From this observation we conclude that axial tertiary carbon-hydrogen bonds lead preferentially to the formation of thermal hydrogen atoms. This surprising result prompted us to look for other examples of this kind. Table II shows the results of iodine solutions of *cis*- and *trans*-decalin. We find again a much greater decrease in  $G(H_2)$  in the *trans*-decalin than in the *cis*-decalin.

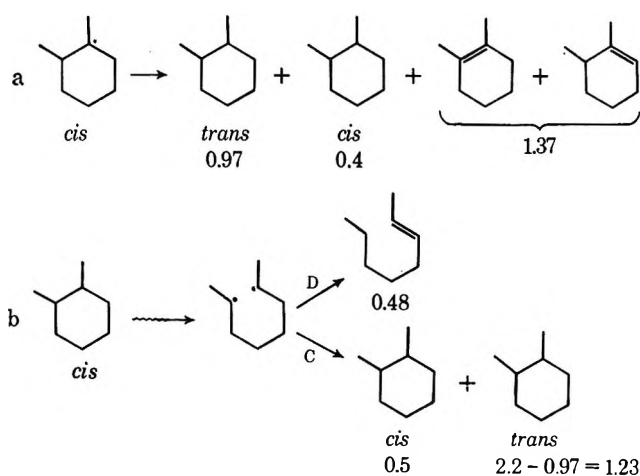


Figure 4. Isomerization reactions of *cis*-1,2-dimethylcyclohexane. For reaction a,  $trans:cis = 2.2/0.9$  (see Table I).  $G(\text{ring opening and reclosing}) = 2 \times (1.23 + 0.5) = 3.46$ ;  $G(\text{ring C-C bond breaking}) = 3.46 + 0.48 = 3.94$ .

Additional evidence for the formation of molecular hydrogen in the radiolysis of *cis*-1,2-dimethylcyclohexane can be obtained by examining the  $D/C$  disproportionation (combination) ratios (see Table I). The  $D/C$  ratio for *t*-butyl radicals has been reported as 4.4–4.6.<sup>9–11</sup> The same ratio was found in the radiolysis of methylcyclohexane by Freeman,<sup>12</sup> who concluded from this observation that there is no molecular hydrogen formation from methylcyclohexane. The  $D/C$  ratio for *trans*-1,2-dimethylcyclohexane is about the same as for methylcyclohexane and *t*-butyl radicals, but *cis*-1,2-dimethylcyclohexane has a  $D/C$  of 6.1, which suggests molecular hydrogen formation. This is in agreement with the iodine scavenger experiments.

In the radiolysis of cyclohexane a lot of carbon-hydrogen bond breaking but little carbon-carbon bond breaking has been observed. This surprising fact has been explained by a cage effect, but direct experimental proof of this has been missing. Opening and reclosing of the cyclohexane ring can of course not be observed in unsubstituted cyclohexane. In the case of *cis*- and *trans*-1,2-dimethylcyclohexane, however, ring opening and reclosing can lead to isomerization. These isomerization reactions and their  $G$  values are shown in Figure 4.

The disproportionation of tertiary 1,2-dimethylcyclohexyl radicals can lead to isomerization; *i.e.*, a radical derived from *cis*-1,2-dimethylcyclohexane can disproportionate to give an olefin plus a *trans* isomer and

(8) H. Okabe and J. R. McNesby, *J. Chem. Phys.*, **34**, 668 (1961).

(9) J. W. Kraus and J. P. Calvert, *J. Amer. Chem. Soc.*, **79**, 5921 (1957).

(10) W. J. Moore, *J. Chem. Phys.*, **17**, 1325 (1949).

(11) R. N. Birrell and A. F. Trotman-Dickenson, *J. Chem. Soc.*, 4218 (1960).

(12) G. R. Freeman, *J. Chem. Phys.*, **36**, 1535 (1962).

*vice versa*. The amount of this isomerization, however, cannot be greater than the amount of olefin formation from these tertiary radicals, *i.e.*, 1.37 ( $0.9 \pm 0.47$ ) for the formation of the *trans* from the *cis* isomer. We found, however, a *G* value for the formation of *trans*-1,2-dimethylcyclohexane of 2.2. There is only one other possibility for the isomerization of the *cis* isomer to the *trans* isomer and that is by opening and reclosing of the cyclohexane ring. This mechanism also explains the formation of octene-2 by intramolecular disproportionation. Intramolecular disproportionation and combination has been suggested previously by Freeman<sup>12</sup> in the radiolysis of methylcyclohexane. Our results provide experimental proof of such an opening and

reclosing of the cyclohexane ring. Isomerization following ring opening can only take place if a carbon-carbon bond between or adjacent to the methyl groups is broken but not if any of the other three carbon-carbon bonds of the cyclohexane ring are broken. Assuming equal probability for breaking of the six ring carbon-carbon bonds, we arrive at an estimated *G* value for ring opening and reclosing of 3.46, which is about equal to the *G* value for carbon-hydrogen bond breaking.

*Acknowledgment.* The author wishes to thank Professor Dr. H.-J. Born for his generous support of this work and Dr. H. Heusinger for helpful discussions.

## Photoelectric Effects in Thin and Bilayer Lipid Membranes in Aqueous Media

by H. T. Tien

Department of Biophysics, Michigan State University, East Lansing, Michigan 48823 (Received May 31, 1968)

When a beam of intense white light is directed onto one side of a lipid membrane constituted from photoactive pigments at a water-oil-water biface, certain photoelectric phenomena are produced. In this paper the experimental findings on the open-circuit photovoltage and the photoconductivity of the membrane are described. Possible explanations for the observed phenomena are discussed. The significance of these observations in relation to photosynthesis and other light-induced processes where membranous structures are believed to be essential is considered.

### Introduction

The high degree of orderliness and lamellar organization of chloroplasts in nature have been inferred from numerous studies.<sup>1-4</sup> These studies have led to the suggestion by Bassham and Calvin<sup>5</sup> that a crystalline lattice containing chlorophyll molecules and other compounds may be involved in the photosynthetic apparatus. They further suggested that such an organized structure of light-sensitive pigments may possess photoconductive properties resembling those of organic semiconductors. That the photoconductivity may exist in chlorophylls had been suggested earlier by Katz.<sup>6</sup> Investigations carried out by Eley,<sup>7</sup> Nelson,<sup>8</sup> and others<sup>9-11</sup> using thin films or compressed disks of chlorophylls and their related compounds have indeed demonstrated the existence of photoinduced electrical effects. In a number of publications, Arnold and co-workers<sup>12</sup> have observed semiconductive properties in chloroplast and chromatophore preparations. It should be mentioned that all these experiments were carried out either *in vacuo* or a *dry* state. Although these earlier investigations are significant in their own right, two im-

portant questions remain to be answered. (i) Can the photosynthetic pigments be organized in the form of

- (1) R. Sager and G. E. Palade, *Exp. Cell Res.*, **7**, 584 (1954).
- (2) A. J. Hodge, J. D. McLean, and F. V. Mercer, *J. Biophys. Biochem. Cytol.*, **1**, 605 (1955).
- (3) E. Steinman and F. S. Sjöstrand, *Exp. Cell Res.*, **8**, 15 (1955).
- (4) For further references, see (a) E. Rabinowitch, *Discussions Faraday Soc.*, **27**, 161 (1959); (b) J. B. Thomas, "Primary Photo-processes in Biology," North-Holland Publishing Co., Amsterdam, The Netherlands, 1965, pp 127-135.
- (5) J. A. Bassham and M. Calvin, "The Path of Carbon in Photosynthesis," Prentice-Hall, Inc., Englewood Cliffs, N. J., 1957, Chapter 12.
- (6) E. Katz, "Photosynthesis in Plants," Iowa State College Press, Ames, Iowa, 1949, p 287.
- (7) D. D. Eley, *Nature*, **162**, 819 (1948).
- (8) R. C. Nelson, *J. Chem. Phys.*, **27**, 864 (1957).
- (9) D. R. Kearns, G. Tollin, and M. Calvin, *ibid.*, **32**, 1020 (1960).
- (10) A. Terenin, E. Putzeiko, and I. Akimov, *Discussions Faraday Soc.*, **27**, 83 (1959).
- (11) B. Rosenberg and J. F. Camiscoli, *J. Chem. Phys.*, **35**, 982 (1961).
- (12) (a) W. Arnold and H. K. Sherwood, *Proc. Nat. Acad. Sci. U. S.*, **43**, 105 (1957); (b) W. Arnold and R. K. Clayton, *ibid.*, **46**, 769 (1960); (c) W. Arnold and H. K. Maclay, *Brookhaven Symp. Biol.*, **11**, 1 (1959).



thin membrane, preferably of the order of molecular thickness ( $\sim 100$  Å) which is assumed to exist in the native state, in an *aqueous* environment? (ii) In case such ultrathin membranes could be formed, would they exhibit light-induced electrical phenomena, such as photovoltaic effect and photoconductivity? The present work has been initiated with the aforementioned questions in mind.

Recently, techniques have been developed for the formation of ultrathin membranes from a variety of surface-active materials including brain proteolipids, phospholipids, synthetic surfactants, and oxidized cholesterol. These ultrathin membranes ( $<90$  Å thick) in aqueous media have been termed variously as bimolecular, black, or bilayer lipid membranes (henceforth abbreviated BLM). The BLM have been extensively investigated and shown to be the closest approach to natural membrane models.<sup>13</sup> From various physical properties together with the previously deduced arguments, the structure of the BLM is considered to be liquid crystalline and lamellar in organization.<sup>14</sup> In view of these facts, the recent formation of BLM from photosynthetic pigments has now permitted investigations of the effect of light on these BLM.<sup>15</sup> The present paper reports the photoelectric phenomena exhibited by these membranes separating two aqueous solutions, which hitherto have not been known.

### Experimental Details

**1. Apparatus.** The experimental setup for the measurement of the photovoltaic effect and photoconductivity is shown in Figure 1. The inner chamber of the cell assembly was made from a Teflon beaker (10 ml). A small hole (1.86 mm) was first punched through the wall of the beaker. A recessed groove was then machined out around the wall of the opening (see insert, Figure 1), which served as a reservoir for the lipid solution. The outer chamber was made of Pyrex glass, a portion of which was flattened to facilitate both the illumination and the observation of the membrane. The illumination of the membrane was provided by a tungsten lamp (500 W) which was installed in a lamp housing (Wild Heerbrugg Instruments, Inc.). The front aperture of the lamp housing was fitted with a quartz collector, a heat-absorbing filter, a gray filter, and two colored glass filters. A Keithley electrometer (610B) and a high-speed picoammeter (Keithley Model 416) were used to measure the photovoltage, the photoconductivity, and the resistance of the membrane. A selected voltage from a calibrated source could also be applied to the electrodes placed across the membrane which separated the two aqueous phases. Either a pair of saturated calomel or platinum electrodes was used. In certain cases, current-voltage curves of BLM in 0.1 M KI (made with water saturated with iodine) were measured with a controlled potential polarographic analyzer (EUA-19, Heath Co.). The temperature of the cell was

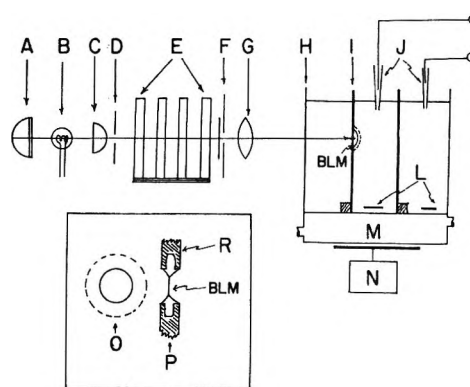


Figure 1. Schematic diagram of experimental setup for measurement of photo-emf, photoconductivity, and dark conductivity of thin and bilayer lipid membranes: A, concave mirror; B, 500-W tungsten lamp; C, quartz collector; D, field diaphragm; E, filter carrier assembly; F, shutter; G, focusing lens; H, Pyrex glass chamber; I, Teflon chamber; J, electrodes; L, stirring bars; M, water jacket; N, magnetic stirrer; BLM, bilayer lipid membrane (or thin lipid membrane). Lower insert shows an enlarged view of the aperture in the Teflon chamber: O, front view, P, cross section (side view); R, Teflon support.

controlled by a water jacket (joined at the bottom of the cell assembly), and the aqueous solutions were stirred magnetically. To control the exciting light, a shutter was interposed in the light path which was used both for timed and instantaneous illumination.

**2. Lipid Solutions.** All membranes (black and thin layer) were formed from a mixture of photosynthetic pigments dissolved in an alkane solvent. The pigments purchased from commercial sources were used without further purification. For BLM formation, a solution of chlorophyll (3.5%) and xanthophyll (5.2%) in *n*-octane (w/v) was used. Also used in this study were fresh pigments obtained from spinach leaves according to the procedure of Strain and Svec.<sup>16</sup> No apparent differences in the photoelectric effects of the membrane were observed between the fresh and commercial preparations.

**3. Procedure.** Most membranes studied were formed in 0.1 M KCl. The experimental techniques employed in the BLM formation have been previously described.<sup>13,17</sup> For thin layer membrane studies, a large drop of lipid solution (which usually would not thin spontaneously) was introduced to the opening in the Teflon chamber. The membranes during the formation stages were observed under green light at 40 $\times$  magnifi-

(13) For a review, see H. T. Tien and A. L. Diana, *Chem. Phys. Lipids*, **2**, 55 (1968).

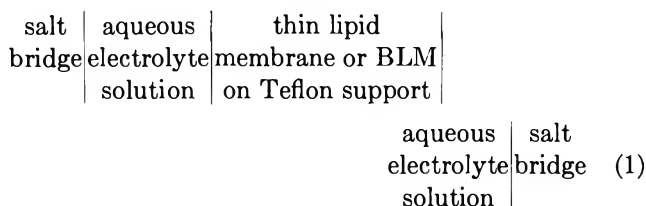
(14) H. T. Tien, *J. Theor. Biol.*, **16**, 97 (1967).

(15) H. P. Ting, W. A. Huemoller, S. Lalitha, A. L. Diana, and H. T. Tien, *Biochim. Biophys. Acta*, **163**, No. 4 (1968).

(16) H. H. Strain and W. A. Svec in "The Chlorophylls," L. P. Vernon and G. R. Seely, Ed., Academic Press, New York, N. Y., 1966, p 21.

(17) P. Mueller, D. O. Rudin, H. T. Tien, and W. C. Wescott, *J. Phys. Chem.*, **67**, 534 (1963).

cation. All measurements were carried out with the cell assembly in a shielded enclosure to reduce spurious electrical effects. The electrodes, apart from the tips immersed in the aqueous solution, were covered with black rubber tubing and were well shielded from the light. Using the usual notation, the cell may be written as



When the membrane was illuminated without imposing any external voltage, a light-induced emf was generated, which was measured by the electrometer and recorded. Both the dark and photocurrents of the membrane were measured by applying a small voltage (usually 10 mV) across the membrane. In certain cases, the photocurrent was also measured without dark current flowing. Action spectrum for the photovoltaic effect was obtained by use of monochromator (Bausch and Lomb Model 33-86-02) in place of the carrier assembly (see Figure 1). All experiments were carried out at  $22 \pm 1^\circ$ .

## Results

1. *Black or Bilayer Lipid Membranes (BLM) and Thin Lipid Membranes.* In the present investigation two types of lipid membranes were used. Although they are termed "membranes," it should be understood that they are formed *in situ* on a hydrophobic support immersed in an aqueous solution. In the case of BLM, the black area is surrounded by a thick layer known as the Plateau-Gibbs border, which is hundreds of thousands times thicker than the black membrane.<sup>18</sup> The thicknesses of BLM and thin lipid membranes used were, respectively, about 100 Å and 0.1 cm. The black area in the BLM constituted usually about 25% of the total area in contact with the aqueous solution. In 0.1 M KCl, the dark resistance of the BLM was about  $2 \times 10^5$  ohm-cm<sup>2</sup>. However, in 0.1 M KI + I<sub>2</sub> the membrane resistance was one order of magnitude lower.

As illustrated in Figure 1, the aqueous solutions in the two compartments are connected through the aperture (marked "BLM") in the Teflon chamber when the membrane is not present. When a BLM or a thin lipid membrane is formed in the aperture, two aqueous solution-membrane interfaces or a *biface* is created. The word "biface" is used here to stress the intimate nature of the two coexisting interfaces whose significance will be made clear in the course of the discussion of the results. Since the electrical resistance of the membrane (henceforth referring to either BLM or thin lipid membrane, unless otherwise stated) is several orders of magnitude higher than the bathing media, the aqueous solution on each side of the membrane serves essentially as

an electrical contact between the membrane and the external measuring instruments (see eq 1). We can therefore define the polarity of the biface following the established convention in electrochemistry. For a driven cell the cathode is the side of the biface where electrons enter or the site of reduction, and the other side of the biface is where the oxidation takes place. An exact opposite nomenclature is used for a generating cell in which the anode of course has a positive polarity.

2. *Light-Induced Photo-emf.* In the absence of an external electric field, a photovoltage was detected when one side of the membrane was illuminated. For a BLM constituted from chloroplast pigments separating two 0.1 M KCl solutions, the observed photo-emf was about a few millivolts. Three typical photovoltage recordings are shown in Figure 2. It can be seen that the rise portion of the curve consists of two distinct steps and is very reproducible. The initial rise is rapid ( $\sim 0.1$  sec or less). The measurement of the rise time of the light-induced voltage was limited by the rise time of the recorder used. The second rise portion of the curve is seen to be much slower, which did not show sign of saturation as long as the exciting light was incident on the membrane. In contrast, the time course of the light-induced voltage in a thin lipid membrane exhibited a greater tendency to saturation (see Figure 3). Typical light-induced voltages in thin lipid membranes obtained in three different runs are, respectively, 20 mV (in about 3 min), 27.5 mV (in about 4 min), and 23.5 mV (in about 5 min).

3. *Light Intensity and Open-Circuit Photo-emf.* The measured photovoltages as a function of light intensity of a thin lipid membrane are shown in Figure 4. These values were obtained after the membrane had been illuminated for 60 sec. Following the convention stated earlier (Results, section 1), the sign of the illumi-

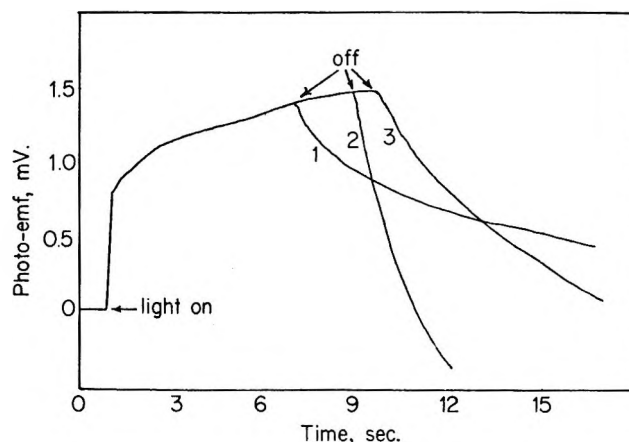


Figure 2. Light-induced voltages in a BLM constituted from a mixture of photosynthetic pigments in *n*-octane. Curves from three different runs are superimposed.

(18) H. T. Tien, *J. Gen. Physiol.*, [2] 52, 125 (1968).

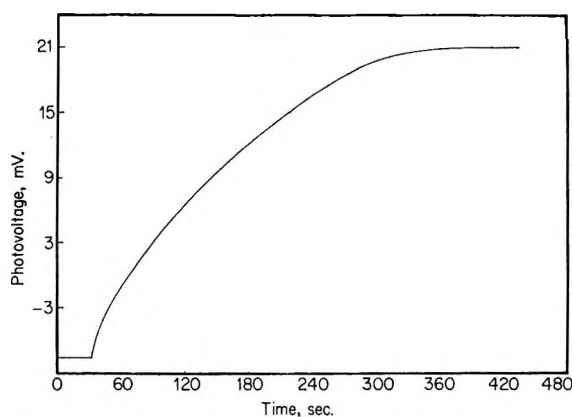


Figure 3. Light-induced voltages in a thin lipid membrane ( $\sim 0.1$  cm thick) formed from spinach chloroplast pigments in *n*-octane.

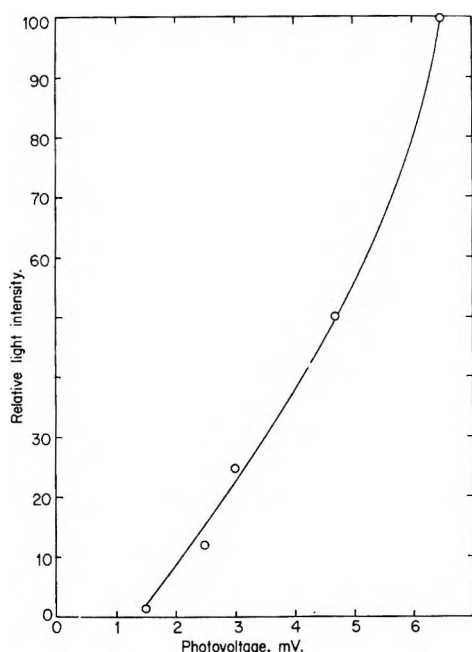


Figure 4. Open circuit photovoltage vs. light intensity for a thin lipid membrane prepared from spinach chloroplast pigments in *n*-octane. Readings were taken after 1 min of illumination.

nated side of biface was negative. Observations were also made with bands of light which had been isolated with optical-glass filters. Little photo-emf was detected when using green light ( $500\text{--}550\text{ m}\mu$ ). A small voltage ( $\sim 1\text{--}2\text{ mV}$ ) was induced with blue light ( $400\text{--}550\text{ m}\mu$ ). The greatest effect was observed when yellow light ( $500\text{--}800\text{ m}\mu$ ) was used to illuminate the membrane. It is worth noting that the voltage induced by yellow light required an induction period of about 20 sec. The maximum photo-emf obtained in the last case was about 5 mV after the membrane had been illuminated for about 5 min. Attempts were also made to obtain the action spectrum of the membrane for the photovoltaic effect. Preliminary results indicated that the

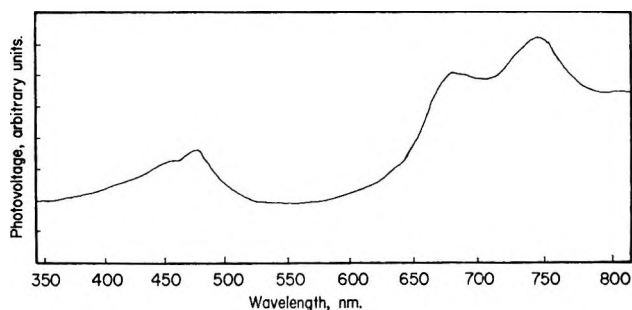


Figure 5. Action spectrum of a thin lipid membrane of spinach chloroplast pigments in 0.1 *N* KCl.

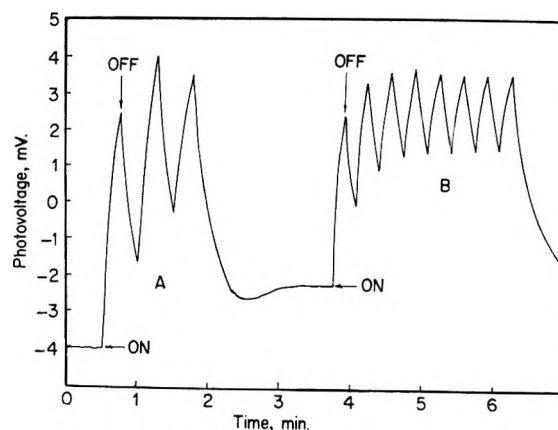


Figure 6. Variation of open circuit voltage in response to illumination of a thin lipid membrane separating two aqueous phases: region A, alternate 15-sec illumination and darkness; region B, alternate 10-sec illumination and darkness.

peak responses occurred at  $475$ ,  $680$ , and  $745\text{ m}\mu$ , which corresponded very roughly with the peaks of absorption spectrum for the same pigments in the bulk solution. The action spectrum of the photovoltaic effect of a thin lipid membrane is shown in Figure 5.

4. *Effect of Alternate Illumination and Darkness on Membrane Photovoltage.* Figure 6 shows typical responses of a thin lipid membrane to illumination cycles. Region A of Figure 6 was obtained by illuminating the membrane for 15 sec, followed by an equal period of darkness. In region B, the period between the illumination and darkness was of 20-sec duration. Similarly, the kinetics of changes for a BLM (25% black) on two different time cycles are shown in Figure 7. There are two distinct steps which can be clearly seen when the exciting light is switched on. On the other hand, the decay curves exhibit no such complicated time course in either thin lipid membranes or BLM.

5. *Light-Induced Current.* Figure 8 shows the measured current response as a function of time for a typical BLM (curve A) and for a thin lipid membrane (curve B). In the case of BLM, the black area in contact with the aqueous solution was about 25% of the total area. The current flowing through the membrane was mea-

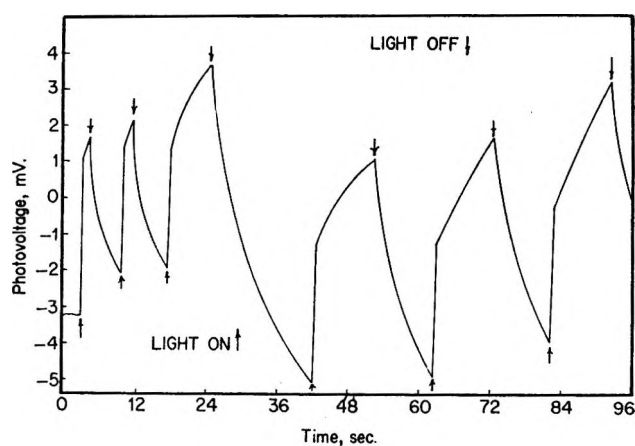


Figure 7. Photovoltaic effect of a black lipid membrane produced from chloroplast pigments (spinach leaves) in *n*-octane. The curve illustrates membrane voltage *vs.* time in response to photoactive light.

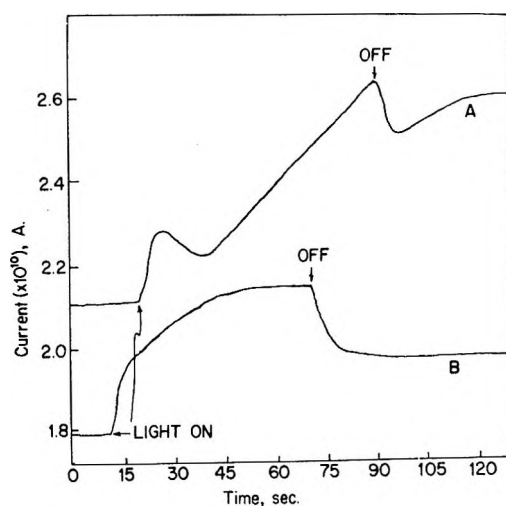


Figure 8. Typical behavior of light-induced current *vs.* time: curve A, BLM with 10 mV applied; curve B, thin lipid membrane under 50 mV of external voltage.

sured with a picoammeter and was recorded continuously during the run. The dark currents in both cases reached their final values very shortly after the voltage was applied across the membrane *via* the electrodes. Upon illumination with exciting light, the time course of BLM was complex. The photocurrent at first increased for a few seconds and then decreased and was then followed by another rise. For several BLM observed, it was found that the second rise in current resulted invariably in membrane rupture when the total current was about 2–3 times the dark current value. However, if the exciting light was switched off during the second phase, the current dropped briefly and rose to a new steady value as can be seen in Figure 8 (curve A). In contrast, thin lipid membranes formed from the same pigment solution displayed no such peculiar time course (see Figure 8, curve B). In the latter case, both the rise and decay followed an exponential course. It is of

significance to note that, in either BLM or thin lipid membranes, the dark current after illumination was substantially higher than the dark current prior to exposure to exciting light. It seems probable that there might be effects superimposed upon that due to photochemical reaction in the membrane or at the solution-membrane interface.

6. *Dark and Photocurrent as a Function of Applied Voltage.* Both the dark and photocurrent of a thin lipid membrane were measured as a function of increasing applied voltage. The results were obtained with the illuminated side of the biface at either positive or negative potential. The results of a typical run for a thin lipid membrane are presented in Figure 9. In the range of field strength examined, both the dark and photocurrents were ohmic up to 100 mV. The slight asymmetry in the case of dark current is probably not significant, since a slight concentration difference or electrode potential difference could exist across the membrane. The ratio of negative-positive currents was constant as a function of applied voltage and did not seem to level off at higher voltages. The ratio of photo-

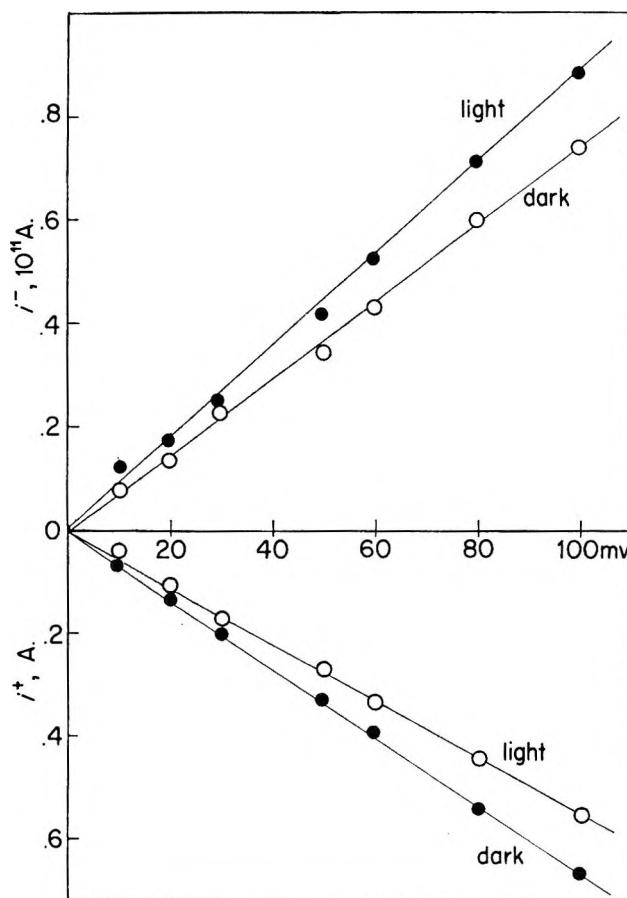


Figure 9. Variation of dark and photocurrent as a function of applied voltage. The upper curves were obtained with the side of biface facing photoactive light at positive potential; the lower curves are the illuminated side of biface at negative potential. A thin lipid membrane ( $\sim 0.1$  cm thick) was used.

currents ( $i^-/i^+$ ) was about 1.6. However, for a case of BLM studied, it was found that the photoconductivity of the membrane was less than the dark conductivity, irrespective of whether the illuminated side was at a positive or negative potential.

## Discussion

1. *The Physical State and Molecular Organization of the Membrane.* The general organization of the bimolecular or black lipid membranes has been considered previously.<sup>14</sup> The evidence at hand favors a liquid crystalline structure in which the hydrophilic portion of the molecule is situated at the aqueous solution-membrane interface. The interior of the BLM is believed to be similar to that of liquid hydrocarbon saturated with water. The experimental facts in support of this picture come from the following lines of evidence: (a) the liquid nature of the BLM can be demonstrated by the fact that a BLM may be probed with a fine object (thin wire or hair) which can be moved within the membrane and then withdrawn without rupturing the membrane; (b) the "hydrocarbonlike" interior is deduced from the materials used, (c) recent water permeability studies have shown that to a first approximation the BLM may be considered as a continuous liquid hydrocarbon layer of less than 100 Å thick (the permeability coefficient for water of such a layer would be expected to be about 35  $\mu$ /sec as estimated from the solubility and diffusion data);<sup>19</sup> (d) the dc resistance of the BLM is about  $10^8$  ohm-cm<sup>2</sup>. This corresponds to a bulk resistivity of about  $10^{14}$  ohm-cm. The resistivity of most wet liquid hydrocarbons is of the same order of magnitude; and (e) the dielectric breakdown strength of the BLM is usually in the range of  $10^5$  to  $10^6$  V/cm, which again corresponds closely to that of a long-chain liquid hydrocarbon. In view of these facts, it seems reasonable to consider that the interior of the BLM is essentially a thin, continuous layer of liquid hydrocarbon with dissolved water.

Although the exact chemical composition of the BLM and thin lipid membranes under study is not known, the rough correspondence between the absorption spectrum of the lipid solution used and the action spectrum for the photovoltaic effect (Figure 5) provides very good evidence that the membranes are composed of the principal photoactive pigments of the spinach chloroplasts. In the discussion which follows, the most important photosynthetic pigment chlorophyll (or Chl) will be chosen as a typical pigment. From the structural viewpoint, the chlorophyll molecule can be considered as a so-called amphipathic compound, in that one part of the molecule is hydrophilic and the other hydrophobic. Therefore, on the basis of energetics at the water-oil-water biface,<sup>14,18</sup> the molecules in the BLM should be oriented in such a way that the phytol groups extend inward and can be held by van der Waals forces, while the polar groups (*i.e.*, porphyrin plates) are lo-

cated at the aqueous solution-membrane interface. However, owing to the presence of dissolved water in the membrane, it is also conceivable that some of the Chl molecules might adopt orientations other than the one just described. The absorption peak in Figure 5 in the long-wave region around 745 m $\mu$  suggests that the pigments in the membrane are highly organized to give the absorption shift. This fact appears to be consistent with the absorption spectra of crystalline chlorophyll films and monolayers at air-water interfaces.<sup>20-22</sup> The bifacial tension of the membrane obtained recently is about 3-4 dyn/cm. This implies that those chlorophyll molecules situated at the biface in the membrane are tightly compressed together.<sup>15</sup> It seems likely therefore that the porphyrin plates of the molecules would be oriented more or less perpendicularly to the biface. On the basis of this information, it is estimated that the average area occupied per porphyrin group is much less than 75 Å<sup>2</sup>.

2. *The Origin of the Observed Light-Induced Phenomena in the Present Membrane System.* Since all photoelectric effects probably owe their origin to one basic phenomenon of the generation of charge carriers under illumination, the observed effects may be explained if we can provide some answers to the two most important questions: (i) that of the mechanism of charge generation in the membrane upon exposure to light and (ii) that of the mechanism of charge transport. In view of the preliminary and qualitative nature of the data, only a speculative explanation will be given at this time. Theoretical considerations are reserved for discussion in later publications when more quantitative data become available.

In explaining the photovoltaic effect in the BLM, the charge-injection scheme suggested by Kallmann and Pope<sup>23</sup> may be used. From the nature of the experimental arrangement indicated in eq 1, it may be argued that a greater number of excited pigment molecules will be produced at the illuminated side of the biface. The excited molecular state may exist in the form of an exciton as a result of absorption of photoactive radiation. For reasons not yet known, an exciton thus produced is capable of not only moving around from the site of generation but also of dissociating into an electron and a positive hole. This resulting charge separation is believed to be responsible for the observed photo-emf in the membrane. For a thin lipid membrane ( $\sim 0.1$  cm thick) which possesses a "bulk phase" (this is also true for a BLM owing to the presence of the Plateau-Gibbs border around the black area), the so-called Dember

(19) P. Schatzberg, *J. Polym. Sci.*, **10**, 87 (1965).

(20) E. E. Jacobs, A. S. Holt, R. Kromhout, and E. Rabinowitch, *Arch. Biochem. Biophys.*, **72**, 495 (1957).

(21) H. J. Trurnit and G. Colmano, *Biochim. Biophys. Acta*, **30**, 434 (1958).

(22) G. L. Gaines, Jr., W. D. Bellamy, and A. G. Tweet, *J. Chem. Phys.*, **41**, 2572 (1964).

(23) H. Kallmann and M. Pope, *J. Chem. Phys.*, **32**, 300 (1960).

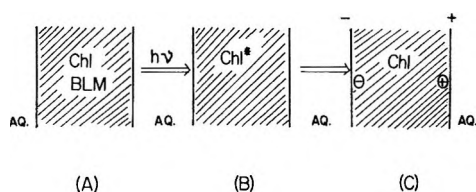


Figure 10. Scheme for light-induced phenomena in lipid membranes constituted from chloroplast pigments in an alkane solvent separating two aqueous solutions (Chl, chloroplast pigments as typified by chlorophyll; AQ, aqueous solution;  $h\nu$ , photoactive light;  $\text{Chl}^*$ , an excited chlorophyll molecule): this is an illustration of a BLM (or a thin lipid membrane) at a water-oil-water biface; B, upon absorption of photoactive light, an excited species is formed, which may be an exciton; C, the excited species or exciton is then dissociated into an electron,  $-$ , and a positive hole,  $+$ , (this event causes the biface to be charged as indicated by the positive and negative signs). Hatched areas represent either thin lipid membranes or bilayer (black) lipid membranes (BLM). See the details in the text.

effect may also be operative for the light-induced voltage.<sup>24</sup> Here, a thin lipid membrane (or the Plateau-Gibbs border in a BLM) is pictured as similar to that of a homogeneous semiconductor. Upon absorption of exciting light, a concentration gradient of charge carriers is produced across the biface. If we assume that the electrons and holes thus produced have different mobilities and lifetimes, a separation of charges in the membrane will result, hence the observed photovoltaic effect. As is mentioned in section 3 of the Results, the illuminated side of the biface becomes negative, which implies that a larger concentration of holes must be present at the "dark" side of the aqueous solution-membrane interface. The sequence of events leading to a spatial charge separation in a lipid membrane constituted from photoactive pigments is illustrated in Figure 10.

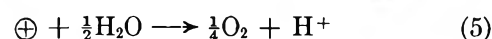
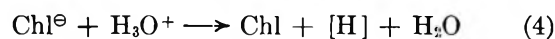
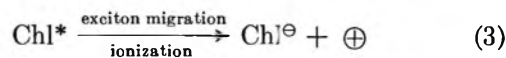
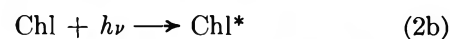
The question as to what is the mechanism by which charge carriers move through the lipid membrane is partially answered by the nature of postulated carriers (holes and electrons). However, it is known that BLM constituted from materials other than photoactive pigments are also capable of charge transport.<sup>13</sup> In these cases, it is generally accepted that the conducting species are ions present in the membrane and in the bathing solution. It would appear therefore that the lipid membranes formed from photoactive pigments must be capable of ionic conduction as well. At present, it is not known to what extent the charges are being transported by ions in the membrane since, even in the dark, it is conceivable that some electrons and holes could be generated thermally or by an external field. In the case of electronic conduction, it should be mentioned that the charges may be conducted in the membrane *via* the conjugated double bonds of the carotenes and xanthophylls which are abundantly present in the

extracted chloroplast pigments used in the present work.

3. *Significance of the Present Findings in Relation to Natural Membranes.* It is of immediate interest that the present membrane models offer a unique opportunity to the study of membrane-associated phenomena in the biological systems. Two outstanding examples are photosynthesis and related phenomena,<sup>25,26</sup> and the visual process.<sup>26,27</sup> In both of these cases membranous structures are known to play a crucial role. In the case of photosynthesis, the primary event is believed to be the conversion of light energy into chemical energy that can be utilized by the green plant. The molecular construct of this important energy transducer is not known but has been postulated by many investigators.<sup>28,29</sup> As mentioned in the Introduction, the photosynthetic pigments in the chloroplast are highly organized in two-dimensional lamellar layers, as revealed by electron microscopy. Further, it is believed that the close packing of pigment molecules in the organized arrays is essential for efficient energy transfer. The present findings demonstrate that an ultrathin membrane of lamellar structure constituted from chloroplast pigments in an aqueous environment can indeed function as an energy-transducing system. The present Chl-BLM behaves like a photocell whose maximum power output is estimated from the available data to be about  $10^{-13}$  W (at the light intensity used).

In connection with the primary event, a further question may be asked concerning the fate of electrons and holes produced in the lipid membrane, as depicted in Figure 10C. The following scheme is suggested along the lines previously proposed by Bassham<sup>30</sup> and by Calvin.<sup>28</sup> The observed facts may be expressed formally in terms of the following steps

photoactive pigments (ground state) +  $h\nu \longrightarrow$



The explanation of these equations is as follows. In eq 2 the photoactive pigment as typified by chlorophyll is excited by light. The excited molecule is ionized by an

(24) F. Gutmann and L. E. Lyons, "Organic Semiconductors," John Wiley & Sons, Inc., New York, N. Y., 1967, p 516.

(25) For references see *Brookhaven Symp. Biol.*, **19**, 303 (1967).

(26) W. D. McElroy and B. Glass, Ed., "Light and Life," The Johns Hopkins Press, Baltimore, Md., 1961.

(27) G. Wald, *Science*, **162**, 238 (1968).

(28) M. Calvin, *Brookhaven Symp. Biol.*, **11**, 160 (1959).

(29) A. A. Benson, *J. Amer. Oil Chem. Soc.*, **43**, 265 (1966).

(30) J. A. Bassham, *Brookhaven Symp. Biol.*, **11**, 26 (1959).

unknown mechanism (possibly *via* exciton migration), leading to the production of a free electron and a positive hole. Since the illuminated side is negative with respect to the "dark" side, it is suggested that the separated electron is localized at the aqueous solution-membrane interface (possibly in the porphyrin ring), as shown in Figure 10. Equations 4 and 5 represent in essence the photolysis of water using the highly organized lipid membrane structure as a barrier to separate the products of oxidation and reduction. This grossly oversimplified scheme is adapted merely as a convenient working hypothesis for further work. (See the paragraph below and ref 31). One would predict therefore from eq 5 that oxygen would be liberated at the site where hole discharge takes place. Experiments are being conducted to test whether O<sub>2</sub> evolution will occur using these lipid membranes.

In conclusion, it should be mentioned that a number of provocative formulations of the primary photo-physical and photochemical processes in photosynthesis have been proposed. The presently widely accepted scheme has its origin traceable to the conception of Van Niel.<sup>31</sup> The various current models call for the cooperation of two light quanta of different energy absorbed by separate pigment systems.<sup>32-38</sup> Whether we can make use of the BLM and the thin lipid membranes formed from the chloroplast pigments together with other relevant constituents to test these formulations and to give further insight into the photosynthetic process remain to be demonstrated.

### Summary

(1) It is shown that lipid membranes constituted

from photoactive pigments exhibit both the photo-voltaic effect and photoconductivity in aqueous solution.

(2) It is suggested that the charge carriers produced by exciting light are in the form of electrons and holes.

(3) In these membranes the mode of conduction is both ionic and electronic.

(4) It is pointed out that the present membrane system is a useful model in the understanding of visual process, photosynthesis, and related phenomena in which membranes are known to be important.

(5) A scheme is proposed to account for the fate of photogenerated electrons and holes in the membrane. The membrane, considered as a photocell, should be capable of effecting photolysis of water.

*Acknowledgment.* This work was supported by a National Institutes of Health Research grant (GM-14971).

(31) C. B. Van Niel in "Photosynthesis in Plants," J. Franck and F. W. Loomis, Ed., Iowa State College Press, Ames, Iowa, 1949, pp 437-495.

(32) R. Emerson and E. Rabinowitch, *Plant Physiol.*, **35**, 477 (1960).

(33) R. Hill and F. Bendall, *Nature*, **186**, 136 (1960).

(34) L. N. M. Duysens, J. Amesz, and B. M. Kamp, *ibid.*, **190**, 510 (1961).

(35) M. Losada, F. R. Whatley, and D. I. Arnon, *ibid.*, **190**, 606 (1961).

(36) H. T. Witt, A. Mueller, and B. Bumberg, *ibid.*, **191**, 194 (1961); **194**, 854 (1962).

(37) C. S. French, *Carnegie Inst. Washington*, **61**, 345 (1962).

(38) J. C. Goedheer, *Biochim. Biophys. Acta*, **66**, 61 (1963).

# A Kinetic Study of the Reaction of Water and *t*-Butyl

## Alcohol with Sodium in Liquid Ammonia<sup>1</sup>

by Robert R. Dewald and Richard V. Tsina<sup>2</sup>

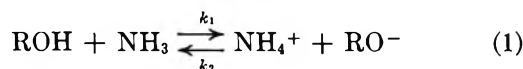
Department of Chemistry Tufts University, Medford, Massachusetts 02155 (Received June 3, 1968)

The reaction of two weak acids, water and *t*-butyl alcohol, with sodium in liquid ammonia has been studied conductometrically at  $-33.9^\circ$ . The kinetic data are consistent with the general mechanism:  $\text{ROH} + \text{NH}_3 \xrightleftharpoons[k_2]{k_1}$

$\text{NH}_4^+ + \text{RO}^-$  and  $\text{NH}_4^+ + \text{e}_{\text{am}}^- \xrightarrow{k_3} \text{NH}_3 + 0.5\text{H}_2$ , where R is *t*-butyl and H. For *t*-butyl alcohol,  $k_1$  was found to be  $(2.5 \pm 0.7) \times 10^{-6} M^{-1} \text{sec}^{-1}$  and  $k_2/k_3 = 1.3 \pm 0.3$ . The values found for water were  $k_1 = (7 \pm 2) \times 10^{-6} M^{-1} \text{sec}^{-1}$  and  $k_2/k_3 = 0.55 \pm 0.16$ . The bimolecular rate constant,  $k_3$ , is estimated to be  $(4 \pm 2) \times 10^6 M^{-1} \text{sec}^{-1}$  at  $-33.9^\circ$ .

### Introduction

Alcohols react readily with solutions of alkali metals in liquid ammonia with the evolution of hydrogen and the formation of alkoxides.<sup>3,4</sup> Kraus and White,<sup>4</sup> in work of a qualitative nature, reported that the reaction between sodium and ethanol in liquid ammonia was vigorous at first but rapidly slowed down, with the result that after 2.5 hr the reaction had gone to only 70% completion. They noted that extensive precipitation occurred. Later, Kelly, *et al.*,<sup>5</sup> reported kinetic data for the ethyl alcohol-sodium ammonia system. Using ammonia labeled with tritium, these workers followed the progress of the reaction by monitoring the volume and activity of the evolved gas ( $\text{H}_2$  and HT). They found that the reaction was initially first order in EtOH and zero order in Na. Between 25 and 50% completion, the reaction order was found to be indefinite, but during the last 50%, the reaction was slower and followed second-order kinetics, first order in both metal and alcohol. Only one set of characteristic data, however, was reported. Recently, Jolly<sup>6,7</sup> evaluated these data using a Powell plot based on the presumed mechanism



where R is ethyl. If the ammonium ion concentration is at a low steady-state value, the rate law

$$\frac{-d(\text{e}_{\text{am}}^-)}{dt} = \frac{k_1 k_3 (\text{e}_{\text{am}}^-) (\text{NH}_3) (\text{ROH})}{k_2 (\text{RO}^-) + k_3 (\text{e}_{\text{am}}^-)} \quad (3)$$

is obtained. Jolly found that the mechanism, (1) and (2), was at least qualitatively compatible with the data reported. The best Powell plot fit to the data was obtained by setting  $k_1 = 8 \times 10^{-3} \text{sec}^{-1}$  and  $k_2/k_3 = 6 \times 10^3$ . It was found initially,<sup>6</sup> however, that in the region

$f = 0.10\text{--}0.40$ , where  $f$  is the fraction of the reaction, the experimental points deviated unaccountably from the theoretical curve, but the fit was later<sup>7</sup> considerably improved when the formation of a complex between ethanol and the ethoxide ion was introduced. Jolly<sup>7</sup> pointed out that this assumption is quite arbitrary. One might further note that Kelly, *et al.*, employed relatively large concentrations of ethyl alcohol (0.2–0.4 *M*) and sodium (0.2–1.0 *M*), since fairly large amounts of gas were needed in order to perform an accurate analysis. The observations of Chablay<sup>3</sup> and Kraus<sup>4</sup> lead one to suspect that some precipitation of sodium ethoxide probably occurred,<sup>7</sup> the effect of which on the observed reaction kinetics is not *a priori* predictable.

We have studied the reaction kinetics of sodium with the two weak acids, water and *t*-butyl alcohol, with the aim of obtaining kinetic data in a system in which precipitation was not occurring. Water has been shown to react readily with sodium-ammonia solutions.<sup>8</sup> Pleskov<sup>9</sup> reported that solutions of sodium in liquid ammonia may be employed as a rapid method for the determination of small quantities of water. The ob-

(1) Presented in part before the Physical Chemistry Division at the 154th National Meeting of the American Chemical Society, Chicago, Ill., Sept 1967.

(2) This paper is part of a thesis submitted to Tufts University in partial fulfillment of the requirements for the degree of Doctor of Philosophy.

(3) E. Chablay, *Ann. Chim. (Rome)*, **8**, 145 (1917).

(4) C. A. Kraus and G. F. White, *J. Amer. Chem. Soc.*, **45**, 768 (1923).

(5) E. J. Kelly, H. V. Secor, C. W. Keenan, and J. F. Eastham, *ibid.*, **84**, 3611 (1962).

(6) W. L. Jolly, "Non-Aqueous Solvent Systems," T. C. Waddington, Ed., Academic Press, New York, N. Y., 1965, p 39.

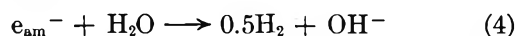
(7) W. L. Jolly, *Advances in Chemistry Series*, No. 50, American Chemical Society, Washington, D. C., 1965, p 27.

(8) W. C. Fernelius and G. W. Watt, *Chem. Rev.*, **29**, 195 (1937).

(9) V. A. Pleskov, *Zavodskaya Lab.*, **6**, 177 (1937); *Chem. Abstr.*, **31**, 61351 (1937).



served reaction, which is almost certainly due to solvated electrons,  $e_{am}^-$ , can be written



in which NaOH precipitates readily.<sup>10</sup> Chablay<sup>3</sup> noted that tertiary alkoxides are more soluble than secondary or primary alkoxides. Consequently it was felt that precipitation might best be avoided by using *t*-butyl alcohol as one of the weak acids in this study. By employing low reactant concentrations, we have successfully avoided precipitation during the course of the reaction.

### Experimental Section

Ammonia (Matheson) was condensed *in vacuo* in a trap containing sodium metal. The blue solution was stored in this trap in contact with an iron magnet until the extent of the autodecomposition reaction



was considerable. About half of the ammonia was distilled into a second trap which had been evacuated and flamed until the pressure stabilized at less than  $2 \times 10^{-6}$  torr. The ammonia was then distilled back into the trap containing the sodium. The blue solution was next frozen with liquid nitrogen and degassed. The second trap was again evacuated and flamed. The cycle of distilling back and forth, freezing, degassing, and flaming was repeated at least five times. The ammonia was then stored in contact with sodium, distilling enough for one or two experiments into the second trap just prior to use. Sodium (United Mineral and Chemical Co.) was distilled twice *in vacuo* and was stored in Pyrex capillaries. Ammonium bromide (Fisher reagent) samples were prepared by placing the salt in break-seal tubes which were sealed off under vacuum after evacuation to about  $10^{-6}$  torr.

The reaction of the two weak acids with sodium was followed conductometrically in an apparatus similar to that described elsewhere.<sup>11</sup> The reaction vessel was constructed of Pyrex and had a calibrated bulb for volume determination. The conductance cell<sup>11</sup> and break-seal tubes containing samples of the reactant and solid  $NH_4Br$  were sealed onto two side arms. The electrodes were either gold-plated platinum or in a few cases gold-plated tungsten. The cells were calibrated with standard KCl solutions using the data of Jones and Bradshaw.<sup>12</sup> Either a high-precision ac bridge similar to that described elsewhere<sup>13</sup> or a Wayne Kerr Universal bridge B 221A was used. The procedure followed in measuring the resistance of the solution is also described elsewhere.<sup>11</sup>

The *t*-butyl alcohol (Fisher Certified) was first distilled through a 3-ft packed column, and the middle fraction was introduced into a trap. The alcohol was next degassed by repeated freezing and evacuation. It was then distilled *in vacuo* into a second trap into

which sodium metal had been distilled. After the sodium had completely reacted, the alcohol was degassed by repeated freezing and pumping. The alcohol was distilled into tared break-seal tubes which were then sealed off under high vacuum and weighed. Water samples (starting with doubly distilled conductance water) were also prepared as described above, except the sodium metal was omitted. During the course of our investigation it became apparent that very small quantities of water would be necessary for some experiments (around  $5 \times 10^{-6}$  mol or less). These samples were prepared by equilibrating the water reservoir at an appropriate, thermostated temperature with evacuated bulbs of known volume on the vacuum line. The contents of the bulbs were then transferred to break-seal tubes, held at liquid nitrogen temperature, and then sealed under high vacuum.

The procedure followed for the sodium-ammonia solution preparation in the Pyrex apparatus is described elsewhere.<sup>11</sup> We feel that this technique is instrumental in removing traces of water from the walls of the apparatus as well as dissolved  $H_2$  gas from the solution. After the blue solution had been thoroughly degassed, the apparatus was disconnected from the vacuum line and immersed in a refrigerated bath at  $-33.9 \pm 0.2^\circ$  (Dow Corning No. 200 silicone fluid was used as the bath liquid.) The resistance of the sodium-ammonia solution was subsequently monitored as a function of time for approximately 1 hr to ensure stability. Next, the break-seal containing the *t*-butyl alcohol or water sample was broken, the solution was mixed, and the resistance of the mixture was followed as a function of time.

Bright platinum electrodes were found to be unsuitable for making measurements after either the alcohol or water was added to the sodium-ammonia solution, probably because of contamination of the electrodes by hydrogen evolved during the reaction. The gold-plated electrodes, however, were found to be quite suitable for taking conductance measurements in the reacting systems. This observation is consistent with the findings of Windwer and Sundheim<sup>14</sup> in a study of the solutions of the alkali metals in ethylenediamine.

In the experiments with *t*-butyl alcohol, after the reaction rate became negligible (unbleached solution), the evolved  $H_2$  gas was pumped through three liquid nitrogen traps using mercury leveling bulbs and was collected in a calibrated gas buret in which the volume and pressure of the gas were measured. During the

(10) M. Skossarewsky and N. Tchitchinadze, *J. Chem. Phys.*, **14**, 11 (1916).

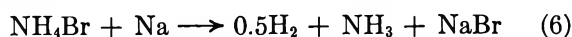
(11) R. R. Dewald and J. H. Roberts, *J. Phys. Chem.*, **72**, 4224 (1968).

(12) G. Jones and B. C. Bradshaw, *J. Amer. Chem. Soc.*, **55**, 1780 (1933).

(13) G. E. Smith, Ph.D. Thesis, Michigan State University, 1963.

(14) S. Windwer and B. R. Sundheim, *J. Phys. Chem.*, **66**, 1254 (1962).

pumping, the blue solution was frozen and kept at liquid nitrogen temperature. Next, solid ammonium bromide was added, *via* a break-seal, to the blue solution, and the remainder of the H<sub>2</sub> gas was collected. Finally, the total amount of metal could be determined from the stoichiometry of the reactions



in which R is *t*-butyl. The initial sodium concentration, as determined from the evolved H<sub>2</sub>, was in good agreement with the value determined from the initial resistance of the sodium-ammonia solution.

In this work, the conductivity measured for the reacting mixture was taken to be due to sodium alone, and the contribution to the conductance by either of the weak acids was considered to be negligible. Support for this procedure is apparent from the following data: for a 10<sup>-2</sup> M solution of water in liquid ammonia at -33.9°, the specific conductance<sup>15</sup> is 2.45 × 10<sup>-7</sup> ohm<sup>-1</sup> cm<sup>-1</sup> compared with 1.06 × 10<sup>-4</sup> ohm<sup>-1</sup> cm<sup>-1</sup> for a 10<sup>-4</sup> M sodium-ammonia solution<sup>11</sup> at the same temperature. Similarly, the contribution to the total conductivity due to alkoxides and hydroxides<sup>10</sup> produced was considered negligible in the initial phase of the reaction from which data were used in calculating rate constants. Conductance-concentration data obtained in this laboratory<sup>11</sup> for sodium-ammonia solutions were used in the calculations.

## Results

*a. The Reaction of *t*-Butyl Alcohol with Sodium in Liquid Ammonia.* Table I contains a summary of the results obtained from the reaction of sodium with *t*-butyl alcohol in liquid ammonia at -33.9°. Figure 1 shows three sodium concentration *vs.* time plots. It should be noted that the alcohol is present in excess. As shown in Figure 1, the sodium reacts rapidly at first and then the reaction rate levels off to an almost negligible change with time, even though the solution

**Table I:** Kinetic Data for the Reaction of Sodium with *t*-Butyl Alcohol in Liquid Ammonia at -33.9°

Run no.	10 <sup>6</sup> k <sub>1</sub> , M <sup>-1</sup> sec <sup>-1</sup>	k <sub>2</sub> /k <sub>3</sub>	10 <sup>2</sup> [Na], M	10 <sup>2</sup> [(CH <sub>3</sub> ) <sub>3</sub> COH], M
11B	3.3	1.1	6.07	5.14
28C	1.7	1.8	0.882	1.54
30C	3.8	1.5	1.34	4.57
102A	1.7	1.3	5.69	4.43
104A	1.7	0.78	5.46	2.14
113A	3.1	1.6	0.657	1.85
114A	2.1	1.2	1.13	1.74
142A	2.3	0.97	0.405	0.805
Av	2.5 ± 0.7 <sup>a</sup>	1.3 ± 0.3 <sup>a</sup>	...	...

<sup>a</sup> Average error.

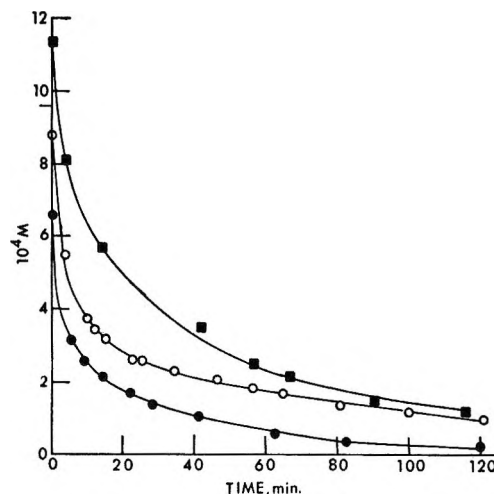


**Figure 1.** Sodium concentration, *M*, *vs.* time plots for the reaction of sodium with *t*-butyl alcohol at -33.9° in liquid ammonia: ■, run 114A; ○, run 28C; ●, run 113A.

remained blue. Other experiments using different initial concentrations gave similar results.

When sodium amide was present, as determined by following the conductance of a decomposing sodium solution (for 24 hr), no large drop in the initial sodium concentration was observed upon addition of the alcohol. In this experiment the initial concentrations were about 1.2 × 10<sup>-3</sup>, 4.2 × 10<sup>-4</sup>, and 2.66 × 10<sup>-3</sup> M sodium, sodium amide, and *t*-butyl alcohol, respectively. No precipitation was observed during the course of the reaction of sodium with *t*-butyl alcohol in any of the experiments. This observation is consistent with the reported greater solubility of tertiary alkoxides.<sup>3</sup>

*b. The Reaction of Water with Sodium in Liquid Ammonia.* Table II lists the kinetic data obtained for the reaction of sodium with water in liquid ammonia. It can be seen that the range of concentrations covered is indeed very large. In experiments 31C, 45B, and 46B (high concentrations) precipitation was

**Table II:** Kinetic Data for the Reaction of Sodium with Water in Liquid Ammonia at -33.9°

Run no.	10 <sup>6</sup> k <sub>1</sub> , M <sup>-1</sup> sec <sup>-1</sup>	k <sub>2</sub> /k <sub>3</sub>	10 <sup>4</sup> [Na], M	10 <sup>4</sup> [H <sub>2</sub> O], M
29B	4.0	0.63	0.400	0.268
38B	5.6	0.87	0.175	0.116
34C	6.5	0.49	0.714	0.118
35C	8.0	0.32	0.535	0.0757
27B	12	0.21	1.53	0.123
46B	<i>a</i>	0.76	82.3	89.3
45B	<i>a</i>	0.58	28.7	275
31C	<i>a</i>	0.55	84.7	18.8
Av	7 ± 2 <sup>b</sup>	0.55 ± 0.16 <sup>b</sup>	...	...

<sup>a</sup> Data insufficient to calculate *k*<sub>1</sub>. <sup>b</sup> Average error.

(15) R. R. Dewald and R. V. Tsina, unpublished work.

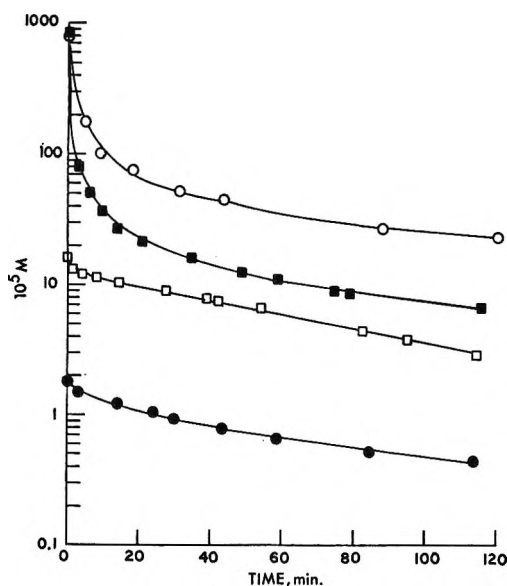
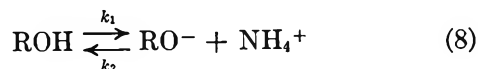


Figure 2. Semilogarithmic plots of sodium concentration,  $M$ , vs. time for the reaction of sodium with water at  $-33.9^\circ$  in liquid ammonia:  $\circ$ , run 46B;  $\blacksquare$ , run 31C;  $\square$ , run 27B;  $\bullet$ , run 38B.

observed during the course of the reaction. Owing to the rapid initial slope change in the above three experiments, the data were insufficient to calculate  $k_1$ , although reasonable values of  $k_2/k_3$  could be obtained. The five runs, 25C, 27B, 29B, 34C, and 38B, proceeded without observable precipitation and were used in calculating both  $k_1$  and  $k_2/k_3$ . Figure 2 shows examples of semilogarithmic plots of the sodium concentration vs. time for the reaction of sodium with water in liquid ammonia at  $-33.9^\circ$ .

## Discussion

For both weak acids, water and *t*-butyl alcohol, the kinetic data can be best explained in terms of reactions 1 and 2. This mechanism is similar to that suggested for other systems as outlined by Russell.<sup>16</sup> For the scheme



in which  $k_1$  pertains to a pseudo-first-order step, if the concentration of  $\text{NH}_4^+$  is small so that at any time

$$\frac{-d(\text{ROH})}{dt} = \frac{-d(e_{\text{am}}^-)}{dt} = \frac{2d(\text{H}_2)}{dt} \quad (10)$$

the rate expression becomes

$$\frac{-d(e_{\text{am}}^-)}{dt} = \frac{k_1 k_3 (\text{ROH})(e_{\text{am}}^-)}{k_2 (\text{RO}^-) + k_3 (e_{\text{am}}^-)} \quad (11)$$

Equation 11 may be rewritten in the form<sup>17</sup>

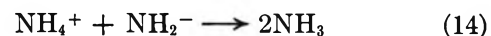
$$\frac{dx}{dt} = \frac{40k_1(a-x)(b-x)}{b-x + (k_2/k_3)x} \quad (12)$$

in which  $a = (\text{ROH})_i$ ,  $b = (e_{\text{am}}^-)_i$ ,  $x = (\text{ROH})_i - (\text{ROH}) = (\text{RONa})$ , and 40 is the molar concentration of the solvent, ammonia, in the pseudo-first-order step, eq 8. Ingold, *et al.*,<sup>17</sup> have shown that when  $V_2$  and  $V_3$  ( $V_n$  is the velocity of step  $n$ ) are similar and  $(\text{RO}^-)_i = 0$ , eq 12 may be integrated to yield

$$40k_1t = \left[ 1 - \frac{a(k_2/k_3)}{a-b} \right] \ln \frac{a}{a-b} + \left[ \frac{b(k_2/k_3)}{a-b} \right] \ln \frac{b}{b-x} \quad (13)$$

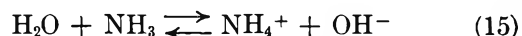
The above expression was used to evaluate  $k_1$  and  $k_2/k_3$  for the *t*-butyl alcohol-sodium and water-sodium runs in Tables I and II. It might be noted, however, that Ingold, *et al.*,<sup>17</sup> have pointed out that eq 13 is not very sensitive to the choice of  $k_2/k_3$ , a choice of 1.0 in some of their data being about as good as a choice of 1.2. The values of  $k_2/k_3$  obtainable by this method therefore cannot be expected to be reliable to better than about 20%. Our precision ranges from 23% in the case of *t*-butyl alcohol experiments to 29% in the case of water experiments. In the latter case, the low concentrations needed to avoid precipitation are probably responsible for the somewhat higher imprecision.

For the case of the partly decomposed sodium solution in which a substantial quantity of amide ion was initially present, it would be expected that the ammonium ion concentration would be small since



is known to proceed far to the right.<sup>18</sup> In this experiment a slow initial rate for the disappearance of sodium was observed upon addition of the alcohol. The slow reaction rate in this case would seem to substantiate the proposed two-step mechanism.

The equilibrium constant for the ammonolysis



in wet ammonia at  $-33.9^\circ$  is unreported. We performed a conductance experiment<sup>15</sup> in which known quantities of water vapor were added to carefully purified ammonia (as determined from its conductivity), raising the water concentration from  $3.56 \times 10^{-5} M$  to a final value of  $8.69 \times 10^{-3} M$ . We were able to estimate an equilibrium constant at  $-33.9^\circ$  for reaction 15 of about  $(4 \pm 2) \times 10^{-12}$ , which is comparable with the value estimated at  $25^\circ$  by Clutter and Swift.<sup>19</sup>

(16) G. R. Russell in "Techniques of Organic Chemistry," S. L. Friess, E. S. Lewis, and A. Weissberger, Ed., Vol. 8, Interscience Publishers, New York, N. Y., 1961, Part 1, p 383.

(17) E. D. Hughes, C. K. Ingold, S. Patai, and Y. Pocker, *J. Chem. Soc.*, 1230 (1957).

(18) H. Smith, "Organic Reactions in Liquid Ammonia," Interscience Publishers, New York, N. Y., 1960, p 39.

This result allows us to calculate a tentative value for the rate constant,  $k_3$ , of reaction 2. We find, using the  $k_1$  and  $k_2/k_3$  averages tabulated for the water-sodium reaction in Table II, a value of  $k_3 = (4 \pm 2) \times 10^6 M^{-1} \text{sec}^{-1}$  at  $-33.9^\circ$  in liquid ammonia. We may compare this result with the results found for the comparable reaction of the hydrated electron,  $e_{\text{aq}}^-$ , with the ammonium ion in water at zero ionic strength, as summarized by Rabani.<sup>20</sup> The rate constants reported vary from  $1.1 \times 10^6$  to  $1.8 \times 10^6 M^{-1} \text{sec}^{-1}$  at ambient (presumably) temperature. Our estimate of  $k_3$  appears to be in agreement with the work in the aqueous system<sup>20</sup> and is also consistent with the rate of the reaction between cesium and ethylenediammonium ions in ethylenediamine.<sup>21</sup>

Our kinetic data for the reaction of the two weak acids with sodium in liquid ammonia support the conclusion that the mechanism for reaction 4 is reactions 1 and 2.<sup>22</sup> The average values of  $k_1$  and  $k_2/k_3$  determined in the present work are in generally poor agreement with the comparable constants deduced from the data of Kelly, *et al.*,<sup>5</sup> by Jolly.<sup>6,7</sup> We feel that this

discrepancy may be due to unavoidable precipitation occurring when ethyl alcohol and sodium react at the concentrations employed by the former workers. We are now reinvestigating the kinetics of the reaction of ethyl alcohol with sodium in liquid ammonia. Also, the value reported in this work for the rate constant of the ammonium ion-solvated electron reaction is within the range of the stopped-flow method, and an effort is now being made in this laboratory to measure this constant directly.

*Acknowledgment.* This research was supported by the National Science Foundation under Grant No. GP 6239.

(19) D. R. Clutter and T. J. Swift, *J. Amer. Chem. Soc.*, **90**, 601 (1968).

(20) J. Rabani, *Advances in Chemistry Series*, No. 50, American Chemical Society, Washington, D. C., 1965, p 242.

(21) L. H. Feldman, R. R. Dewald, and J. L. Dye, *Advances in Chemistry Series*, No. 50, American Chemical Society, Washington, D. C., 1965, p 163.

(22) R. R. Dewald and R. V. Tsina, *Chem. Commun.*, 647 (1967).

## Vaporization Equilibria in the Sodium Chloride-Zinc Chloride System

by Donald W. Rice and N. W. Gregory

*Department of Chemistry, University of Washington, Seattle, Washington 98105 (Received June 5, 1968)*

Partial pressures of zinc chloride and of species of the form  $\text{Na}_x\text{ZnCl}_{2+x}$  in equilibrium with condensed mixtures of NaCl and  $\text{ZnCl}_2$ , and with pure NaCl(s), have been derived from effusion and transpiration data. Evidence is found for the existence of the solid-state compound  $\text{Na}_2\text{ZnCl}_4$ , for which values of  $\Delta H_f^\circ = -299 \pm 3 \text{ kcal mol}^{-1}$  and  $\bar{S}^\circ = 95 \pm 4.5 \text{ cal deg}^{-1} \text{ mol}^{-1}$  at  $625^\circ\text{K}$  are derived. In the presence of NaCl(s), partial pressures of the complex in the vapor phase, assumed to be  $\text{NaZnCl}_3(\text{g})$ , are only *ca.* 1% of those of  $\text{ZnCl}_2$  at  $600^\circ$ .

Relatively little is known about the zinc chloride-sodium chloride binary system. A melting point study by Nikonowa, Pawlenko, and Bergman indicates the existence of only one solid-state intermediate compound,  $\text{Na}_2\text{ZnCl}_4$ , with an incongruent melting point around  $410^\circ$ .<sup>1</sup> Its crystal structure has not been determined. Dijkhuis and Ketelaar studied NaCl-ZnCl<sub>2</sub> melts by emf methods at  $600^\circ$  and found that deviations from the ideal Temkin model appeared to be a maximum around  $X_{\text{NaCl}} = 0.59$ ; they suggested that this dissymmetry may be due to complex ion formation.<sup>2</sup> Ellis reported evidence from Raman studies for  $\text{ZnCl}_3^-$  and  $\text{ZnCl}_4^{2-}$  in KCl-ZnCl<sub>2</sub> melts.<sup>3</sup> Markov and Volkov observed that the volume change on mixing liquid NaCl

and  $\text{ZnCl}_2$  is negative for mole fractions of NaCl less than 0.5 and suggested the formation of complex ions.<sup>4</sup> We now report a thermodynamic study of this system in which vaporization characteristics between  $300$  and  $600^\circ$  have been determined by effusion and transportation experiments.

### Experimental Section

The torsion effusion and Knudsen effusion apparatus,

(1) N. Nikonowa, S. P. Pawlenko, and A. G. Bergman, *Bull. Acad. Sci. URSS Classe Sci. Chim.*, 391 (1941).

(2) C. Dijkhuis and J. A. Ketelaar, *Electrochim. Acta*, **12**, 795 (1967).

(3) R. B. Ellis, *J. Electrochem. Soc.*, **113**, 485 (1966).

(4) B. F. Markov and S. V. Volkov, *Ukr. Khim. Zh.*, **29**, 945 (1963).

cells and calibration procedures,<sup>5,6</sup> and the quartz transpiration apparatus and method<sup>6,7</sup> have been described previously; only features unique to the present application will be mentioned here.

Argon, at *ca.* 1000 torr and at flow rates between 10 and 50 cm<sup>3</sup> min<sup>-1</sup>, served as the carrier gas in transpiration studies; partial pressures of the various components of the equilibrium vapor were independent of flow rate over this range. Argon was made to flow either directly over heated NaCl-ZnCl<sub>2</sub> mixtures or first over a sample of pure ZnCl<sub>2</sub>, in a compartment adjacent to the main reactor and heated by a separate furnace to introduce the desired partial pressure of ZnCl<sub>2</sub>, and then over a sample of pure NaCl. Ideal gas partial pressures in the equilibrium vapor were deduced from the relative numbers of moles of Zn, Na, and Ar in the condensed sample. The total zinc transported was determined by EDTA compleximetric analysis;<sup>8</sup> sodium was determined with a Beckman DU flame photometer. Because solutions to be analyzed contained only 0.1–3.0 ppm of sodium, considerable care was necessary to prevent contamination. The pressure of argon was measured manometrically; the number of moles of argon flowing through the reactor was determined by measuring the pressure of the quantity collected (in a liquid nitrogen cooled trap) after expansion into a calibrated volume.

Samples of Baker's Analyzed reagent grade ZnCl<sub>2</sub> and Mallinckrodt analytical reagent NaCl were vacuum dried, and the ZnCl<sub>2</sub> was vacuum sublimed prior to use. Mixtures were first melted under vacuum and then cooled slowly; the composition was verified by analysis for zinc and chloride (Mohr method). The solidified melts were ground and transferred to the transpiration reactor or to effusion cells in a drybox. X-Ray powder photographs were taken of samples in Pyrex or Lindemann glass capillary tubes, using a Debye-Scherrer camera and Cu K $\alpha$  radiation.

### Results and Discussion

The vapor pressures of zinc chloride above the prepared solid mixtures were derived from independent Knudsen and torsion effusion experiments between 315 and 400°. At a given temperature pressures were considerably less than the equilibrium vapor pressure of pure zinc chloride<sup>5</sup> and did not change as  $X_{\text{NaCl}}$ (bulk) was varied between 0.7 and 0.92. The torsion effusion and Knudsen data gave the same values (within experimental uncertainty, see Figure 1) for the pressure when it was assumed that the zinc effused as monomeric zinc chloride. Results showed no systematic dependence on cell orifice areas, which ranged between  $2 \times 10^{-3}$  and  $90 \times 10^{-3}$  cm<sup>2</sup>.

A least-squares treatment of all effusion data gave the equation

$$\log P_{\text{ZnCl}_2}(\text{torr}) = - (8195 \pm 275)T^{-1} + 10.57 \pm 0.40 \quad (1)$$

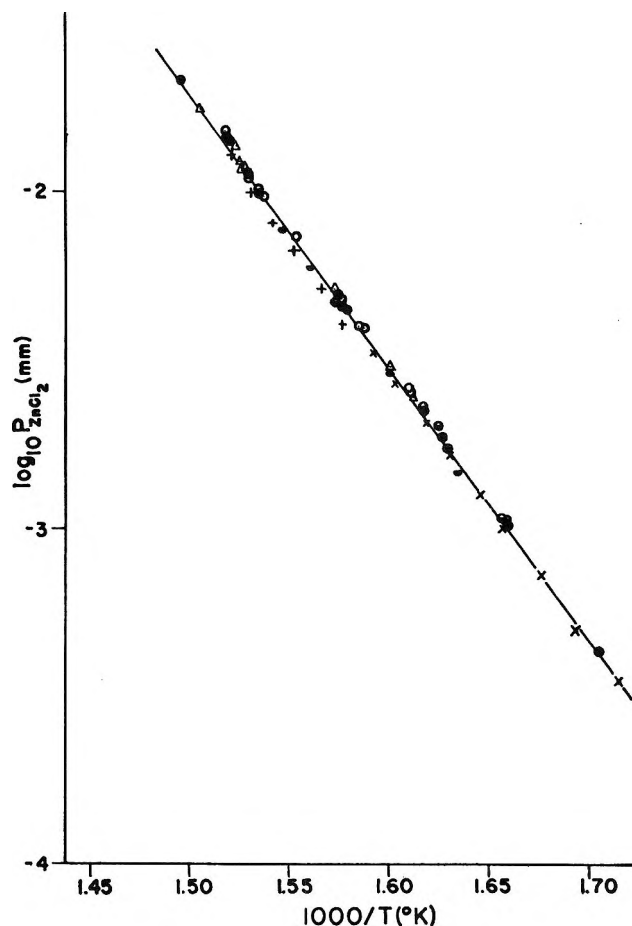


Figure 1. ZnCl<sub>2</sub> pressures above solid mixtures of NaCl and ZnCl<sub>2</sub> (eq 1 gives the solid line): Knudsen: cell 1,  $14.07 \times 10^{-3}$  – cm<sup>2</sup> orifice area; cell 2,  $2.24 \times 10^{-3}$  – cm<sup>2</sup> orifice area; torsion: cell 1,  $7.18 \times 10^{-3}$  – cm<sup>2</sup> total orifice area; cell 2,  $90.9 \times 10^{-3}$  – cm<sup>2</sup> total orifice area. For the data points,  $X_{\text{NaCl}}$  and cell, respectively: Knudsen: ●, 0.92, 1; ○, 0.83, 1; △, 0.74, 1 and 2; torsion: ◐, 0.92, 1; +, 0.74, 1; ×, 0.70, 2.

The data points and least-squares line are shown in Figure 1.

The observations are consistent with the conclusion, reached in the melting point study,<sup>1</sup> that the solid material in the cells was a mixture of Na<sub>2</sub>ZnCl<sub>4</sub> and NaCl. On this basis the mixtures had bulk mole fractions of Na<sub>2</sub>ZnCl<sub>4</sub> between 0.24 and 0.90. Since ZnCl<sub>2</sub> pressures were independent of the relative amounts of the two phases, the composition of these phases must have been the same in the different mixtures. Evidence for the composition of the complex solid was obtained from the following effusion experiment. An equimolar mixture of NaCl and ZnCl<sub>2</sub> was placed in a torsion cell

(5) D. W. Rice and N. W. Gregory, *J. Phys. Chem.*, **72**, 3361 (1968).

(6) See the Ph.D. thesis of D. W. Rice, University of Washington, Seattle, Wash., 1968.

(7) R. R. Richards and N. W. Gregory, *J. Phys. Chem.*, **68**, 3089 (1964).

(8) H. A. Flaschka, "EDTA Titrations," Pergamon Press Inc., New York, N. Y., 1959, p 75.

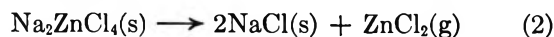
and brought to 288°. At this temperature the melting point diagram<sup>1</sup> indicates the presence of a liquid phase with  $X_{\text{NaCl}} \approx 0.45$  ( $X_{\text{ZnCl}_2} \approx 0.55$ ) in equilibrium with  $\text{Na}_2\text{ZnCl}_4(\text{s})$ . The effusion pressure of  $\text{ZnCl}_2$  was observed to be much higher than values represented by eq 1 and to remain constant at  $2.36 \times 10^{-3}$  torr for some time, as expected when both liquid and solid phases are present. When the pressure began to fall rapidly (the value predicted by eq 1 was just below the limit of reliable measurement), it was assumed that the liquid phase had disappeared. The apparatus was then cooled; analysis of the solid remaining in the cell gave  $X_{\text{NaCl}} = 0.654$ , which, within experimental error, is that expected for  $\text{Na}_2\text{ZnCl}_4$ , 0.666.

X-Ray powder patterns of samples of the various mixtures with  $X_{\text{NaCl}} \geq 0.7$  ( $X_{\text{ZnCl}_2} \leq 0.3$ ) showed the presence of at least one phase in addition to  $\text{NaCl}$ ;  $\text{NaCl}$  lines were at spacings expected for pure sodium chloride. The pattern characteristic of  $\text{ZnCl}_2(\text{s})$  was not observed. The 52 lines (Table I) not attributable to  $\text{NaCl}$  were the same in all samples and are believed characteristic of  $\text{Na}_2\text{ZnCl}_4$ . The pattern was too complex to permit an unambiguous assignment of crystal class and unit cell. An orthorhombic cell with  $a_0 = 5.68 \text{ \AA}$ ,  $b_0 = 10.0 \text{ \AA}$ , and  $c_0 = 14.1 \text{ \AA}$  gave a reasonable correlation of the spacings.

Table I:  $\text{Na}_2\text{ZnCl}_4$  X-Ray Powder Pattern

$\theta$ , deg	$1/d^2$ $\text{\AA}^{-2}$	$\theta$ , deg	$1/d^2$ $\text{\AA}^{-2}$	$\theta$ , deg	$1/d^2$ $\text{\AA}^{-2}$
6.45	0.0213	25.03	0.3031	35.10	0.5595
7.65	0.0300	25.83	0.3214	37.50	0.6273
8.45	0.0366	26.25	0.3311	39.03	0.6713
8.85	0.0401	27.38	0.3579	41.85	0.7534
9.43	0.0455	27.73	0.3666	42.20	0.7636
10.98	0.0614	28.20	0.3780	51.05	1.0236
11.95	0.0726	28.75	0.3915	52.08	1.0532
13.15	0.0876	29.30	0.4053	52.68	1.0704
14.68	0.1088	30.11	0.4261	58.05	1.2184
15.38	0.1191	30.60	0.4385	63.20	1.3483
17.13	0.1469	31.28	0.4564	63.90	1.3647
17.88	0.1596	31.85	0.4713	67.13	1.4368
19.13	0.1818	32.48	0.4882	69.13	1.4776
20.05	0.1989	32.85	0.4979	72.03	1.5312
20.68	0.2111	33.63	0.5192	73.28	1.5522
21.30	0.2234	34.12	0.5328	75.38	1.5844
24.30	0.2866	34.75	0.5498	76.80	1.6042
				82.50	1.6633

From these observations we conclude that eq 1 characterizes the equilibrium



The standard enthalpy and standard entropy changes (standard states chosen as pure solids and the perfect gas state at 1 atm, respectively) for reaction 2 at 625°K, obtained by the van't Hoff method (eq 1), are 37.5 ±

1.2 and  $35.2 \pm 1.3 \text{ cal deg}^{-1} \text{ mol}^{-1}$ , respectively; these results, together with standard values for  $\text{ZnCl}_2(\text{g})$ <sup>6</sup> and  $\text{NaCl}(\text{s})$ ,<sup>9</sup> give (at 625°K) a standard entropy for  $\text{Na}_2\text{ZnCl}_4(\text{s})$  of  $95 \pm 4.5 \text{ cal deg}^{-1} \text{ mol}^{-1}$  and  $\Delta H_f^\circ = -299 \pm 3 \text{ kcal mol}^{-1}$ .

*Association of Sodium Chloride and Zinc Chloride in the Vapor Phase.* In Knudsen experiments amounts of sodium in the condensates were detected which exceeded that expected from the sublimation of sodium chloride. Correction for the contribution of the sodium-containing species, which were only 0.1–1 mol % of the zinc, in the derivation of eq 1 was not necessary. To obtain sufficient amounts of sodium for an accurate determination, it was necessary to raise the temperature; effusion experiments above the melting point were unsuccessful because the liquid crept through the orifice. Transpiration experiments between 500 and 600° led to transport of sufficient quantities of sodium to permit determination by flame photometric methods with good precision.

The transpiration data are presented in Table II. The contribution (~10% maximum) from vaporization of sodium chloride was subtracted from the total amount of sodium collected;<sup>10,11</sup> the remainder was attributed to species such as  $\text{NaZnCl}_3(\text{g})$ . The specific

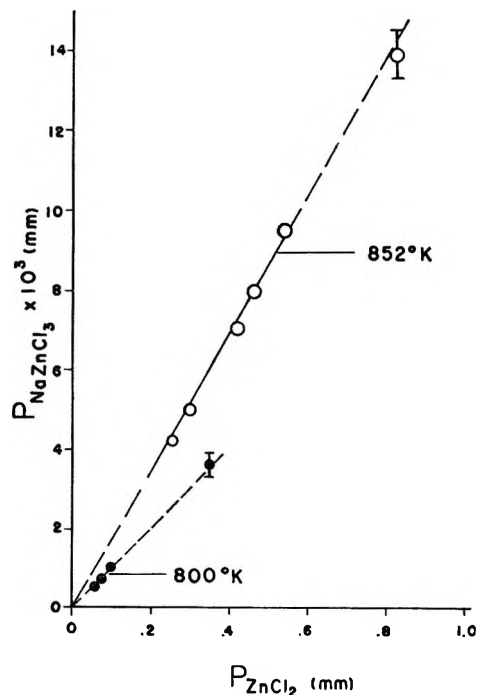


Figure 2. The apparent pressure of  $\text{Na}_2\text{ZnCl}_3$  vs. the pressure of  $\text{ZnCl}_2(\text{g})$ , in equilibrium with  $\text{NaCl}(\text{s})$ .  $\bullet$  and  $\circ$  represent the upper limit "saturation" values, obtained when both a melt and  $\text{NaCl}(\text{s})$  are present.

(9) K. K. Kelley and E. G. King, Bulletin 592, U. S. Bureau of Mines, U. S. Government Printing Office, Washington, D. C., 1961.

(10) J. E. Mayer and I. H. Wintner, *J. Chem. Phys.*, **6**, 303 (1938).

(11) T. A. Milne and H. M. Klein, *ibid.*, **33**, 1628 (1960).

Table II: Transpiration Results

Temp, °K	Flow rate, cm <sup>3</sup> /min	Ar pressure, mm	10 <sup>2</sup> [Ar], mol	10 <sup>2</sup> [Zn], mol	10 <sup>2</sup> [Na], mol	10 <sup>2</sup> [Na] (from NaCl), mol	P <sub>ZnCl<sub>2</sub></sub> , mm	10 <sup>3</sup> P <sub>NaZnCl<sub>2</sub></sub> , mm	10 <sup>3</sup> K <sub>3</sub>
Argon Passed over NaCl-ZnCl <sub>2</sub> (l) + NaCl(s) Mixtures									
847.2	51.0	973.4	12.35	9.92	16.0	0.572	0.780	12.1	15.5
850.2	52.8	944.7	11.10	9.45	15.7	0.592	0.805	12.8	15.9
851.1	21.5	993.7	5.473	4.54	7.33	0.287	0.820	12.8	15.6
800.0	15.3	1034.0	8.110	2.95	3.18	0.056	0.376	3.98	10.6
799.0	16.1	1033.0	10.94	3.69	4.10	0.074	0.348	3.80	10.9
773.7	15.3	1012.2	5.205	1.28	1.08	0.012	0.249	2.07	8.31
770.4	15.8	1019.0	12.86	2.81	2.33	0.025	0.222	1.82	8.20
799.2	50.6	990.0	21.09	7.98	7.75	0.149	0.374	3.57	9.54
767.9	47.8	974.0	26.00	5.69	4.20	0.045	0.213	1.56	7.32
Argon-ZnCl <sub>2</sub> Mixture Passed over Pure NaCl(s)									
852.2	55.0	968.4	18.55	10.3	19.3	1.01	0.539	9.52	17.7
851.7	52.5	964.0	25.47	12.2	22.4	1.40	0.463	7.95	17.2
852.7	53.9	965.1	17.89	7.78	14.1	1.00	0.420	7.02	16.7
852.9	54.0	941.0	25.70	8.18	15.3	1.50	0.299	5.04	16.9
853.4	54.8	960.5	15.93	4.20	8.00	0.930	0.253	4.29	17.0
799.0	49.0	955.0	36.41	2.21	2.45	0.267	0.0579	0.571	9.90
800.4	49.5	951.0	23.22	2.29	2.70	0.171	0.0940	1.04	11.0
798.7	50.1	891.0	15.34	1.27	1.43	0.117	0.0737	0.759	10.3

molecular form of the vapor complex has not been established. However, a series of experiments in which solid NaCl, at a fixed temperature, was allowed to equilibrate with various partial pressures of ZnCl<sub>2</sub> (all sufficiently small so no melt was formed) clearly demonstrated that the amount of sodium transported in complex molecules was proportional to the partial pressure of zinc chloride, Figure 2. This shows that complex molecular species containing more than one zinc atom per molecule were not present at significant concentrations. An effort to fix the sodium content of these molecules in a similar way was made by passing ZnCl<sub>2</sub>(g) over solid solutions of AgCl and NaCl. The activity of NaCl in such mixtures has been derived from emf measurements.<sup>12</sup> However, at large mole fractions of AgCl, a liquid phase was formed at temperatures needed to generate measurable amounts of the vapor-phase complex molecules; zinc chloride dissolved in this liquid and activities of sodium chloride were no longer known. At low mole fractions of AgCl, melt formation was avoided, but the activities of NaCl were not well enough established by the emf data to permit one to differentiate between, for example, a linear or square dependence of the pressure of the complex on the NaCl activity.

Hence, the question as to whether the correct molecular form of the complex is NaZnCl<sub>3</sub>, Na<sub>2</sub>ZnCl<sub>4</sub>, or a mixture of these and/or perhaps molecules with even larger amounts of NaCl, cannot be answered at present. Forms corresponding to M'MX<sub>3</sub> have been reported for the KCl-PbCl<sub>2</sub> and RbCl-PbCl<sub>2</sub> systems, although in neither is a 1:1 solid compound observed.<sup>13</sup> Evidence for this molecular form was based on vapor den-

sity experiments; however, the temperature (1345°K) was much higher than ours and these systems involve a different coordinating metal atom. Moss assumed without proof that the complex vapor molecules above KCl-ZnCl<sub>2</sub> mixtures have the form KZnCl<sub>3</sub>.<sup>14</sup> Bloom and Hastie pointed out the general lack of evidence to suggest the formation of significant amounts of alkali

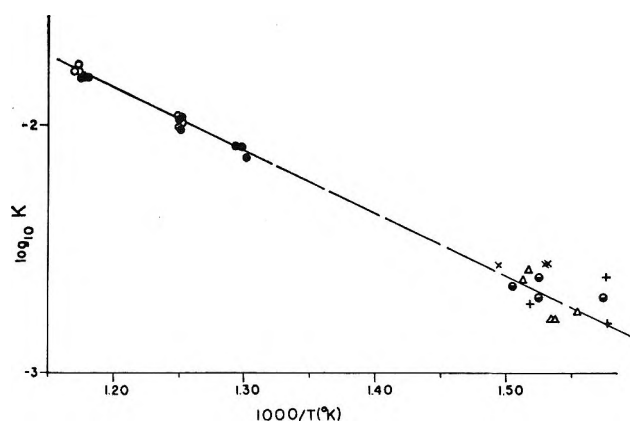


Figure 3. Apparent equilibrium constants for NaCl(s) + ZnCl<sub>2</sub>(g) → NaZnCl<sub>3</sub>(g). Transpiration: ●, argon over NaCl-ZnCl<sub>2</sub>(l) + NaCl(s); ○, argon-ZnCl<sub>2</sub>(g) over NaCl(s). X<sub>NaCl</sub> (Knudsen effusion, cell 1): +, 0.92; ×, 0.83; Δ, 0.73, ◐, 0.74.

(12) M. B. Panish, F. F. Blankenship, W. R. Grimes, and R. F. Newton, *J. Phys. Chem.*, **62**, 1325 (1958).

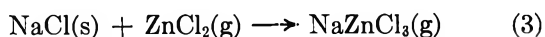
(13) K. Hagemark, D. Hengstenberg, and M. Blander, *ibid.*, **71**, 1819 (1967).

(14) H. I. Moss, Ph.D. Thesis, Indiana University, Bloomington, Ind., 1960.

(15) H. Bloom and J. W. Hastie, *Aust. J. Chem.*, **19**, 1003 (1966).

halide-metal halide binary vapor complex molecules with more than one alkali metal atom.<sup>16</sup>

Table II includes equilibrium constants evaluated on the basis of an assumed reaction



The temperature dependence of these constants is shown in Figure 3, together with values deduced from the effusion data. Considering the large uncertainty in the sodium determinations for small quantities obtained in the low-temperature effusion studies, the agreement between the two independent methods is quite good. Because the pressure of the complex is such a small fraction of the partial pressure of  $\text{ZnCl}_2$ , information concerning the molecular weight of the complex cannot be derived by comparison of effusion and transpiration data. The consistency of the two sets of data in no

way supports the assumption that  $\text{NaZnCl}_3$  is the dominant vapor form of the complex.

A least-squares treatment of the transpiration data, based on reaction 3, leads to the equation

$$\log K_3 = -(2593 \pm 250)T^{-1} + 1.261 \pm 0.315 \quad (4)$$

This relationship gives the line shown in Figure 3. Apparent thermodynamic properties of  $\text{NaZnCl}_3$  may be readily derived from eq 4; however, discussion of these values will be deferred until experimental evidence for the molecular form of the vapor is available. It may be noted that the association enthalpy of  $\text{NaCl(g)}$  and  $\text{ZnCl}_2(\text{g})$  ( $-42$  kcal) appears substantial, only *ca.* 6 kcal less, for example, than the dimerization enthalpy of  $\text{NaCl(g)}$  ( $-48$  kcal).

*Acknowledgments.* We acknowledge with thanks the financial support received from the National Science Foundation, GP-6608x.

## Reactions in the Cobalt-60 Irradiation of Pyridine and Methylpyridines

by J. J. Duvall and H. B. Jensen

*U. S. Department of the Interior, Bureau of Mines, Laramie Petroleum Research Center, Laramie, Wyoming 82070 (Received June 7, 1968)*

$\gamma$  Irradiation of nitrogen bases found in shale oil has been studied as a possible means of enhancing their value. Pyridine, 2-methylpyridine, 3-methylpyridine, 4-methylpyridine, and 2,6-dimethylpyridine were subjected to cobalt-60 irradiation with total dosages of  $2 \times 10^7$  to  $2 \times 10^8$  rads.  $G$  values for hydrogen, methane, acetylene, methylacetylene, and polymer, as determined by gas-liquid partition chromatography and mass spectroscopy, are reported. Products resulting from rupture of bonds external to the ring, rupture of ring bonds, aromatic substitution, and intramolecular rearrangement are reported. Respective examples of each of the above reactions on irradiation of 2-methylpyridine are the formation of methane, acetylene, 2,4-dimethylpyridine, and 3-methylpyridine. Possible reaction mechanisms are discussed. Dealkylation of methylpyridines occurred but not in significant amounts.

### Introduction

Shale oil contains relatively large amounts of nitrogen bases; thus, their investigation as a chemical source seems worthwhile. The nitrogen bases in naphtha-range shale oil products have been shown to be mostly  $\text{C}_2$ - $\text{C}_4$  alkylpyridines which have limited commercial value. Conversion of these alkyl-substituted pyridines to pyridine and methylpyridine would enhance the value of these nitrogen bases. One possible type of reaction for this conversion would be a  $\gamma$ -induced dealkylation. The obvious first step in such a study is to determine the effects of  $\gamma$  irradiation on pure compounds. This paper reports the action of  $\gamma$  irradiation from cobalt-60 upon pyridine, the three monomethylpyridines, and one dimethylpyridine.

Pyridine has been the subject of several  $\gamma$ -irradiation studies, but there is no mention of the  $\gamma$  irradiation of alkylpyridines. Pearce<sup>1,2</sup> found that the main product of the  $\gamma$  irradiation of pyridine was a polymer ( $G(\text{polymer}) = 3.14$ )<sup>3</sup> that was about one-third bipyridines ( $G(\text{bipyridine}) = 1.06$ ). Pearce also found small amounts of hydrogen ( $G(\text{H}_2) = 0.018$ ) and acetylene (no yield reported). In later work, Pearce and Ellison<sup>4</sup>

(1) C. K. Pearce, U. S. Department of Commerce, Clearinghouse for Federal Science and Technical Information, AD 286,058, Ft. Monmouth, N. J., 1962.

(2) C. K. Pearce, Department of Commerce, Clearinghouse for Federal Science and Technical Information, AD 605,430, Ft. Monmouth, N. J., 1964.

(3) The  $G$  value is the number of molecules changed per 100 eV of energy absorbed.



found that  $G(\text{polymer}) = 3.66 \pm 0.54$  and that the yield of bipyridines decreased with increasing dosage.

Klots and Johnsen<sup>5</sup> compared the effects of  $\gamma$  irradiation on pyridine with the effects of  $\gamma$  irradiation on benzene and reported  $G$  values as follows: polymer from pyridine, 3.48; polymer from benzene, 0.99; acetylene from pyridine, 0.0341; and acetylene from benzene, 0.0194. They concluded that pyridine was less stable than benzene to irradiation.

By radical yield, Antoine<sup>6</sup> also showed that pyridine was less stable than benzene to irradiation, and his  $G$  values for radical yield were 3.3 for pyridine and 0.78 for benzene. He reported the following  $G$  values for his pyridine irradiation work: polymer, 3.8;  $\alpha, \alpha'$ -bipyridyl, 1.1;  $C_2$  hydrocarbons, 0.045; hydrogen, 0.025; and hydrogen cyanide, 0.020.

We report  $G$  values for gases and residue and report a qualitative analysis of materials of similar molecular weight to the starting compound. These products suggest types of reactions that have occurred including ring rupture, aromatic substitution, and intramolecular rearrangement.

## Experimental Section

**Materials Irradiated.** Samples of pyridine (99.92 mol %),<sup>7</sup> 2-methylpyridine (99.91 mol %),<sup>8</sup> 3-methylpyridine (99.88 mol %),<sup>7</sup> and 4-methylpyridine (99.98 mol %)<sup>9</sup> were obtained from American Petroleum Institute (API) Research Project 52.

A sample of 2,6-dimethylpyridine was purified by preparative gas-liquid partition chromatography (glpc) using a 10% diglycerol column. The primary impurities removed by this preparative glpc step were 3-methylpyridine and 4-methylpyridine. The primary impurities left in the 2,6-dimethylpyridine were a second dimethylpyridine and 2-methylpyridine. The purity of the 2,6-dimethylpyridine used in the irradiation work was determined to be about 98%. In all of the starting materials, no impurities were apparent in glpc analysis with a thermal-conductivity detector.

**Sample Preparation.** Four samples of 5 ml of each of the pyridines were sealed under their own vapor pressure in glass ampoules equipped with break-seal tips. Care was taken to exclude air from coming into contact with the pyridine while it was being sealed in the break-tip ampoules.

**Irradiation.** The samples were irradiated at the Bureau of Mines Albany Metallurgical Research Center in Albany, Ore. This Center maintains a 100,000-Ci cobalt-60 source.<sup>10</sup> Each of the 20 5-ml ampoules was irradiated at a dose rate of  $1.44 \times 10^7$  rads/hr. One sample of each compound received a dosage of  $2.0 \times 10^7$  rads; one received three times this ( $6.0 \times 10^7$  rads); one received six times this ( $1.2 \times 10^8$  rads); and one received ten times this ( $2.0 \times 10^8$  rads). Ceric sulfate dosimetry was used to determine

the dose rate. A water bath maintained at  $30 \pm 2^\circ$  enclosed the samples during the irradiation.

**Analyses.** The irradiated samples were attached to a vacuum manifold and were fractionated into three materials: (1) compounds volatile at Dry Ice temperature (gases), (2) compounds volatile at room temperature but not volatile at Dry Ice temperature (liquids), and (3) compounds not volatile at room temperature (residues). The gases were transferred by a Toepler pump from the irradiation vessel through a Dry Ice trap to a buret where their volumes were measured. Quantitative analysis of the gases was accomplished by the use of glpc with a time-of-flight mass spectrometer as an adjunct for the positive identification of the gases. Hydrogen and methane were determined using a column of 5-Å molecular sieves and the other gases by use of a 35% dibenzyl ether column operated at  $40^\circ$ .

The liquids were qualitatively analyzed by glpc using a 15% Carbowax 20M column at  $150^\circ$  and a hydrogen-flame detector. Preparative glpc was used to concentrate the liquid products for identification by mass spectroscopy. Hydrogen cyanide was identified in the products from the irradiation of pyridine and 2-methylpyridine by an adaptation of the method of Fisher and Brown.<sup>11</sup>

The irradiation residues were examined by mass spectroscopy. An internal-standard method of mass spectral analysis<sup>12</sup> was used to determine the amounts of bipyridines and tripyridines present in the residue from the pyridine sample that had received the largest irradiation dosage.

## Results

All of the  $G$  values reported in this work are averages determined by weighing the results from a particular sample according to the ratios of total dosage reported earlier. For example, the  $G$  value from irradiation of pyridine to  $2 \times 10^8$  rads was given ten times the credence of that for the sample irradiated to  $2 \times 10^7$  rads.

**Gases.** Table I lists the gases identified from the irradiations and the  $G$  values of these gases. In addition to the gases listed in Table I, trace amounts of the

(4) C. K. Pearce and J. E. Ellison, Jr., *J. Phys. Chem.*, **70**, 1582 (1966).

(5) C. E. Klots and R. H. Johnsen, *ibid.*, **67**, 1615 (1963).

(6) F. Antoine, *Compt. Rend.*, **258**, 4742 (1964).

(7) R. V. Helm, W. J. Lanum, G. L. Cook, and J. S. Ball, *J. Phys. Chem.*, **62**, 858 (1958).

(8) R. V. Helm and others, U. S. Bureau of Mines, Laramie Petroleum Research Center, personal communication, 1967.

(9) J. C. Morris and others, U. S. Bureau of Mines, Laramie Petroleum Research Center, personal communication, 1967.

(10) S. D. Hill and F. E. Block, Bureau of Mines Report of Investigation 6465, Albany, Ore., 1964.

(11) F. B. Fisher and J. S. Brown, *Anal. Chem.*, **24**, 1440 (1952).

(12) R. T. Keen, R. A. Baxter, L. J. Miller, R. C. Shepard, and M. A. Rotheram, Atomic Energy Commission Research and Development Report NAA-SR-4356, Canoga Park, Calif., 1961.

**Table I:**  $G$  Values of Gaseous Products from the  $\gamma$  Irradiation of Pyridine and Methylpyridines

Gas	Pyridine	2-Methylpyridine	3-Methylpyridine	4-Methylpyridine	2,6-Dimethylpyridine
Hydrogen	$0.036 \pm 0.004^a$	$0.068 \pm 0.003$	$0.086 \pm 0.007$	$0.090 \pm 0.020$	$0.108 \pm 0.002$
Methane	$b$	$0.008 \pm 0.001$	$0.005 \pm 0.001$	$0.010 \pm 0.002$	$0.015 \pm 0.002$
Acetylene	$0.028 \pm 0.001$	$0.006 \pm 0.001$	$0.005 \pm 0.001$	$0.009 \pm 0.001$	$0.004 \pm 0.0002$
Methylacetylene	$<0.001$	$<0.001$	$0.002 \pm 0.001$	$0.003 \pm 0.001$	$0.002 \pm 0.0001$
	$0.065 \pm 0.004$	$0.083 \pm 0.004$	$0.099 \pm 0.007$	$0.113 \pm 0.023$	$0.129 \pm 0.001$

<sup>a</sup>  $\pm$  values are one standard deviation. <sup>b</sup> Not detected.

following gases were detected. From the irradiation of pyridine, butadiene and vinylacetylene were detected; from the methylpyridines, propylene was detected; and from all five compounds, ethylene and allene were detected.

**Liquids.** Those compounds which were not volatile at Dry Ice temperature but which were transferable at room temperature were examined qualitatively only and their compositions are listed on Table II. Hydrogen cyanide was quantitatively determined only in the products of the irradiation of pyridine and 2-methylpyridine. The  $G$ (hydrogen cyanide) from pyridine was  $0.010 \pm 0.007$ , and from 2-methylpyridine it was  $0.004 \pm 0.001$ . In the chromatograms of the liquid products there were no compounds with emergence times corresponding to acetonitrile, propionitrile, or acrylonitrile. Thus it was assumed that these compounds were not products of the irradiation. Note that in Table II some compounds are listed as both starting material and as products of a particular irradiation; identification of these compounds as products was through the increase in the size of the gas chromatographic peak, with increasing dosage, relative to other peaks in the chromatogram.

**Table II:** Liquid Products from the  $\gamma$  Irradiation of Pyridine and Methylpyridines

Product <sup>a</sup>	Pyridine	2-Methylpyridine	3-Methylpyridine	4-Methylpyridine	2,6-Dimethylpyridine
Pyridine		X <sup>b,c</sup>	X <sup>c</sup>	X	X <sup>c</sup>
2-MP			X	c	X <sup>c</sup>
3-MP		X			X
4-MP	c	X	d		X
2,3-DMP		X	X		
2,4-DMP		X		X	
2,5-DMP		X			X
2,6-DMP		d	c		
3,5-DMP			X		
2,3,6-TMP					X
2,4,6-TMP					X

<sup>a</sup> MP, methylpyridine; DMP, dimethylpyridine; TMP, trimethylpyridine. <sup>b</sup> X indicates that the compound is a product. <sup>c</sup> Present in starting material. <sup>d</sup> Obscured in gas chromatograph by main peak.

**Residues.** The weights of the residues were used to calculate  $G$  values for the appearance of the polymerized pyridine molecules as residue. These  $G$  values are given in Table III.

**Table III:**  $G$  Values for the Residue from the  $\gamma$  Irradiation of Pyridine and Methylpyridines

Compd	$G$ Value
Pyridine	$2.26 \pm 0.19^a$
2-Methylpyridine	$1.62 \pm 0.12$
3-Methylpyridine	$2.22 \pm 0.32$
4-Methylpyridine	$2.30 \pm 0.09$
2,6-Dimethylpyridine	$1.06 \pm 0.12$

<sup>a</sup>  $\pm$  values are one standard deviation.

Low-voltage mass spectra were obtained on all of the residues, and these spectra indicated that the residues were very complicated mixtures. Figure 1 is the low-voltage mass spectrum of the residue from the pyridine sample that received the largest total dosage and Figure 2 is the low-voltage mass spectrum of the residue from the 3-methylpyridine that received the largest dosage. The largest peaks in these spectra are those corresponding to the bipyridine, tripyridine, and tetrapyridine polymers. For pyridine the  $G$  values for dimer and trimer are  $G$ (bipyridine) = 0.25 and  $G$ (tripyridine) = 0.045. As shown in these two spectra, there are peaks corresponding to 2 amu greater than the dimer, 2 and 4 amu greater than the trimer, and 4 amu greater than the tetramer. The presence of these peaks in the mass spectra of the polymerized pyridines indicates that there are other reactions responsible for the polymer than just those resulting from radical recombination.

Analysis of the residues from the pyridine radiations by glpc showed that the bipyridine produced consisted almost entirely of 2,2'-bipyridine with no 4,4'-bipyridine or 3,3'-bipyridine present. In addition to the 2,2'-bipyridine, there was evidence of two other bipyridines present in these residues. Lack of easily available standards such as 2,3'-bipyridine and/or 2,4'-bipyridine prevented positive identification of these

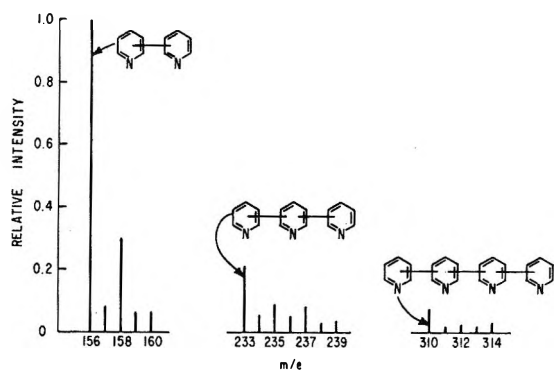


Figure 1. Selected peaks from the low-ionizing-voltage mass spectrum of the residue from the  $\gamma$  irradiation of pyridine.

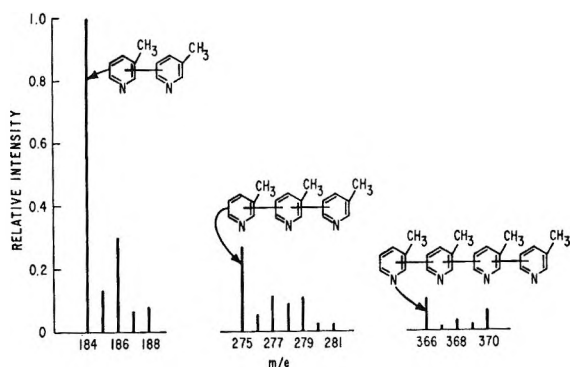
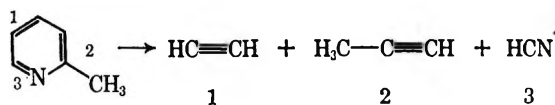


Figure 2. Selected peaks from the low-ionizing-voltage mass spectrum of the residue from the  $\gamma$  irradiation of 3-methylpyridine.

other bipyridines by glpc emergence times. Pearce and Ellison,<sup>4</sup> however, did report finding 2,2'-, 2,3'-, and 2,4'-bipyridines in the residue.

## Discussion

Examination of the gases produced by irradiation of the various alkyl-substituted pyridines indicates some of the reactions that occur. Thus the appearance of acetylene, methylacetylene, and hydrogen cyanide in the products from the irradiation of 2-methylpyridine is most easily explained by simple ring rupture



Each ring fragment is self-contained and no abstraction or addition of hydrogen is necessary to explain the products.

The formations of hydrogen and methane from the methylpyridines are the most important reactions from the standpoint of amount of gases produced. Methyl radicals are produced by the breaking of a ring carbon-substituent bond. The production of hydrogen radicals no doubt results from two reactions. The first would be by the breaking of a ring carbon-substituent bond;

the second reaction would be the production of hydrogen radicals from the substituent methyl groups. That there is nearly twice as much hydrogen produced from the monomethylpyridines than from pyridine is evidence for the production of hydrogen from the methyl substituents.

The two  $\alpha$  hydrogens of the pyridine ring are important ring hydrogens in the production of hydrogen from pyridines. If we assume that the  $G$  value of hydrogen from each of the  $\alpha$  hydrogens is 0.018, which is half of the total  $G$  value of hydrogen from pyridine itself, and if we assume a  $G$  value of 0.050 for the hydrogen production from the methyl group by subtracting 0.018 from the  $G$  value for 2-methylpyridine, we can calculate  $G(\text{hydrogen})$  values for 3-methylpyridine, 4-methylpyridine, and 2,6-dimethylpyridine. The calculated value for 3-methylpyridine would be 0.086, which is the determined value as shown in Table I. The calculated value for 4-methylpyridine would be 0.086, against the value of 0.090, and the value for 2,6-dimethylpyridine would be 0.100, against the value of 0.108 shown in Table I. Thus nearly all of the hydrogen produced from ring hydrogens is produced from the  $\alpha$  positions. Naturally the premise is not perfect owing to the effect that the substituent methyl groups have on electron distribution.

A methyl group appears to provide a protective effect as far as ring rupture is concerned. This protection is evidenced by the fact that the  $G$  values shown in Table I for acetylene plus methylacetylene production from the methylpyridines range from one-fourth to half as great as for the  $G$  value for acetylene in the unsubstituted pyridine. In addition, the amounts of methylacetylene from the methylpyridines are less than the amounts of acetylene. For example, 4-methylpyridine should produce equal amounts of acetylene and methylacetylene, but, as can be seen in Table I, three times as much acetylene as methylacetylene was produced. This suggests that in some cases the methyl group affords only temporary protection and that the pyridine nucleus was broken up after the methyl radical had departed.

The formation of the gases that occurred in minor amounts and that are not presented in Table I is more difficult to explain. Ethylene and propylene are probably produced by hydrogenation of acetylene and methylacetylene, respectively. Allene is probably produced by hydrogen rearrangement on methylacetylene. Vinylacetylene and butadiene from the unsubstituted pyridine may be precursors of acetylene, although no similar compounds are found in the irradiation of the methylpyridines.

The compounds found in the liquid fractions also indicate some of the reactions that occur during radiolysis of pyridines. The formation of dimethylpyridines from monomethylpyridines indicates that substitution of methyl radicals onto starting material occurs. An

example is the formation of 2,4-dimethylpyridine in the irradiation products of 2-methylpyridine.

The formation of 3-methylpyridine and 4-methylpyridine upon irradiation of 2-methylpyridine could occur in one of three ways: (1) intramolecular rearrangement of the excited molecule, (2) addition of a methyl radical to a product radical resulting from the loss of a methyl radical from the monomethylpyridine, and (3) loss of a methyl radical from a product dimethylpyridine molecule. The latter two processes seem unlikely when one considers the concentration of pyridine or dimethylpyridines formed, less than 0.01%. This leaves intramolecular rearrangement as the most likely process. Perhaps a  $\pi$  complex similar to those proposed by Dewar<sup>13</sup> is an intermediate product.

From the standpoint of amount of material reacted, the residue is the most important product in the irradiation of pyridine and the other methylpyridines. The polymers in the residue are formed either by free-radical aromatic substitution or by recombination of free radicals. Clouds of free radicals (spurs) are formed when energy is absorbed, and in these clouds recombination probably predominates. Pyridine free radicals are long lived, relative to other free radicals formed, and can migrate outside the cloud where aromatic substitution would be the predominant process.

The amount of polymer produced from pyridine and from the methylpyridines, like the amount of hydrogen produced, is related to the position of the methyl group upon the ring. This effect is illustrated in Figure 3. Methyl groups in the position  $\alpha$  to the nitrogen reduce the amount of residue produced, but methyl groups in the  $\beta$  and  $\gamma$  positions have little effect. These results are in agreement with Wheland<sup>14</sup> for free-radical substitution on pyridine and the results of other free-radical substitution reactions on pyridines.<sup>15,16</sup>

The result for  $G(\text{residue})$  for pyridine in this work is not in perfect agreement with the values reported earlier (see the Introduction). However, our  $G(\text{residue})$  for pyridine is in good agreement with the values for  $G(\text{residue})$  we obtained for the methylpyridines. Moreover, the way that the residue was separated, *i.e.*, by allowing all other material to transfer to a Dry Ice cooled trap and weighing material left behind, would suggest that  $G(\text{residue})$  values would be high rather than low because of pyridine not removed. The differences in  $G(\text{residue})$ , then, are probably due to the total dose that the samples received. The larger dose, with equal size samples, would yield a larger amount of residue, which should give greater accuracy in  $G(\text{residue})$  determinations. The total doses we used ranged from 4 to 400 times that reported elsewhere.<sup>1,2,4,5</sup>

It seems apparent that the pyridine free radical with the hydrogen missing from the position  $\alpha$  to the nitrogen is the most abundant for the following reasons: (1) all of the bipyridine formed is formed in the 2 position on at least one of the pyridine rings,<sup>4</sup> and (2) the hydrogen

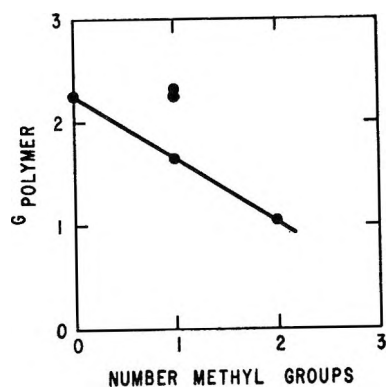


Figure 3. The effect of the number and position of methyl groups on polymer yield from the  $\gamma$  irradiation of pyridine and methylpyridines. The data points above the line represent 3-methylpyridine and 4-methylpyridine.

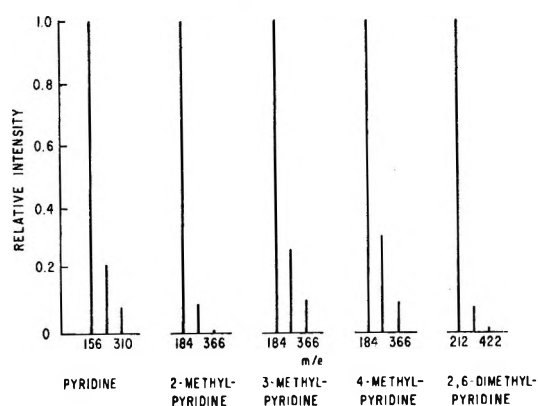


Figure 4. Dimer, trimer, and tetramer peaks from the low-ionizing-voltage mass spectra of the residues from the  $\gamma$  irradiation of pyridine and methylpyridines.

production is dependent on the position of the methyl group, as already mentioned.

Further evidence of the effect on residue formation of substitution on the  $\alpha$  position of the pyridine molecule is shown in the low-voltage mass spectrum in Figure 4. This figure shows the relationship between the amounts of bipyridines, tripyridines, and tetrapyridines. The peaks in these spectra are all normalized to the same height for the bipyridines. It can be seen that the amounts of tripyridines and tetrapyridines formed relative to the bipyridines in the case of 2-methylpyridine and 2,6-dimethylpyridine are considerably less than for the 3-methylpyridine and 4-methylpyridine. This suggests again that free-radical substitution is most important to the  $\alpha$  position in pyridine.

Hydrogenation of the pyridine ring can be used to explain the presence of substantial amounts of products

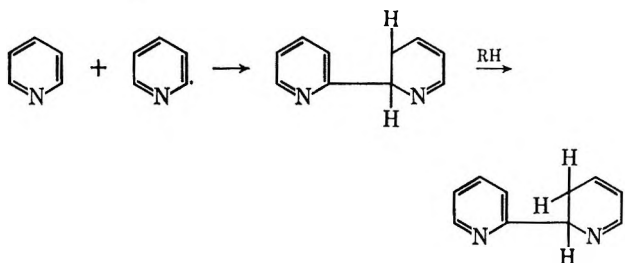
(13) M. J. S. Dewar, *Bull. Soc. Chim. Fr.*, C, 71 (1951).

(14) G. W. Wheland, "Resonance in Organic Chemistry," John Wiley & Sons, Inc., New York, N. Y., 1955, p 484.

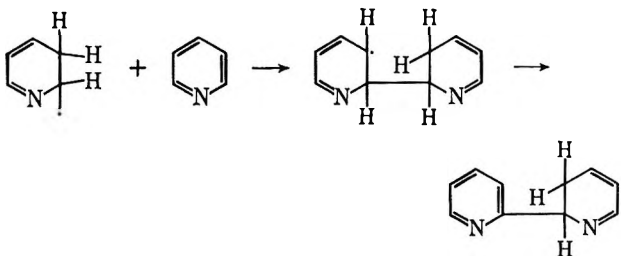
(15) D. H. Hey and E. W. Walker, *J. Chem. Soc.*, 2213 (1948).

(16) G. A. Swan and P. S. Timmons, *ibid.*, 4669 (1958).

with molecular weights of 158 (bipyridine plus 2 amu), 235 (tripyridine plus 2 amu), and 237 (tripyridine plus 4 amu) in the products of the irradiation of pyridine. These same type products are also in evidence in the case of the methylpyridines. This hydrogenation can occur in three ways: (1) direct addition of hydrogen to the bipyridine or tripyridine, (2) addition of a pyridine free radical to a pyridine molecule with the subsequent abstraction of a single hydrogen, as shown in the sequence

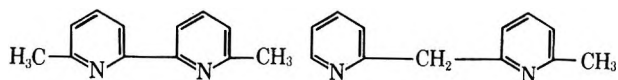


or (3) addition of a dihydropyridine free radical to a pyridine molecule with subsequent loss of a single hydrogen atom



The first possibility seems quite unlikely because of the small amount of bipyridine found in the products. The third way seems possible since it has been shown that a free radical is formed by the addition of a hydrogen atom as well by the loss of the hydrogen atom during irradiation of pyridine at  $-170^\circ$ .<sup>17-19</sup> However, in an analogous situation with benzene, the dihydrobenzene free radical was less stable than the phenyl radical, disappearing altogether from the esr spectrum at  $-50^\circ$ .<sup>20</sup> Because no dihydropyridine was found, the second possibility shown above must be regarded as the most important for the production of dihydrobipyridine. Both the dihydropyridine and the tetrahydrobipyridine would be expected as products if, indeed, dihydropyridine free-radical formation is important. A similar mechanism to the second possibility has been proposed to account for the production of cyclohexadienylbenzene in the irradiation of benzene.<sup>21</sup>

There are two main types of dimers, etc., that would be expected from irradiation of methylpyridines since hydrogen is produced from two sources—from ring hydrogens and from the methyl group. Both of these types would result from free-radical aromatic substitution on starting material. Other types described later are possible, but not probable, because of the



small amounts of free radicals compared with the large amounts of starting material.

One of the products that might be expected in the irradiation of the methylpyridines is that family of products called the 1,2-bisbipyridylethanes. As suggested previously, the methylpyridines probably yield "benzyl-" type radicals by loss of hydrogen. Samples of 1,2-bis(2-pyridyl)ethane and the corresponding ethylene and their 4-pyridyl analogs were available; however, no peaks in the gas chromatogram of the liquid or of the residue product had peaks corresponding to the emergence times of the known samples. This suggested that those "benzyl-" type free radicals formed did not combine to give ethane derivatives.

The hybrid molecule resulting from the recombination of a pyridyl radical and a "benzyl-" type radical was not detected, although the glpc emergence times of this kind of molecule could not be determined and it could well be that the peaks in the bipyridyl part of the chromatogram could be due to this type molecule. An example of such a molecule would be the recombination of the benzyl-type radical resulting from the loss of a hydrogen in the methyl group in 2-methylpyridine with the radical resulting from the loss of a hydrogen in the 6 position of 2-methylpyridine giving a 2-pyridyl-2'-(6-methylpyridyl)methane.

## Conclusions

Several types of reactions occur when pyridine and methylpyridines are subjected to  $\gamma$  irradiation. The pyridine nucleus is ruptured, as shown by the production of acetylene, hydrogen cyanide, and methylacetylene. Substitution reactions are the most prevalent reactions. The substitution reactions form bipyridines, tripyridines, tetrapyridines, and dimethylpyridines. The dimethylpyridines are formed from the monomethylpyridines by substitution reactions on the ring. Intramolecular rearrangements producing different monomethylpyridines from the starting material occur to a small extent. Thus 3-methylpyridine is formed from 2-methylpyridine. In general, the reactions that occur parallel those that occur when benzene compounds are irradiated, but the extent to which these reactions occur indicates that pyridines are less stable

(17) V. A. Sharpatyi, S. A. Safarov, and K. G. Yanova, *Dokl. Akad. Nauk. SSSR*, **147**, 863 (1962); *Proc. Acad. Sci. USSR, Chem. Sec.*, **147**, 1070 (1962).

(18) C. David, G. Geuskens, A. Verhasselt, P. Jung, and J. F. M. Oth, *Mol. Phys.*, **11**, 599 (1966).

(19) K. Tsuji, H. Yoshida, and K. Hayashi, *J. Chem. Phys.*, **45**, 2894 (1966).

(20) S. Ohnishi, T. Tonei, and I. Nitta, *ibid.*, **37**, 2402 (1962).

(21) M. K. Eberhardt, *J. Phys. Chem.*, **67**, 2856 (1963).

to irradiation than are the aromatic hydrocarbons. The most important product, by amount, is the residue. Dealkylation of methylpyridines is a relatively unimportant reaction, suggesting that production of pyridine from methylpyridines by  $\gamma$  irradiation alone would not be of significant value in enhancing the value of shale oil products.

*Acknowledgments.* The work upon which this report is based was done under a cooperative agreement between the Bureau of Mines, U. S. Department of the Interior, and the University of Wyoming. Reference to specific brand names is made for identification only and does not imply endorsement by the Bureau of Mines.

## The Chemical Model as Applied to Associated Liquid Solutions.

### The Ethanol-Heptane System

by R. W. Haskell,<sup>1a</sup> H. B. Hollinger, and H. C. Van Ness<sup>1b</sup>

Chemistry Department, Walker Laboratories, Rensselaer Polytechnic Institute, Troy, New York 12181  
(Received June 10, 1968)

The chemical model is developed for solutions where one component is associated. In essence, the idea is to consider the associated component (A) to consist of many species,  $A_1, A_2, \dots, A_r$ , which are in equilibrium according to reactions of the form  $A_1 + A_{j-1} = A_j$ . Based on this assumption, it is shown that for all of the presently used models the chemical contribution to the free energy of mixing is derivable from the ideal entropy of mixing (*i.e.*, in terms of mole fractions) for a multicomponent system or from Flory's expression for the entropy of a heterogeneous polymer and a monomeric solvent. In this development, it is found that the thermodynamic functions ( $G^E, H^E, S^E$ ) are indicators of the degree of association expressed as a chain size and also of the bond energies. Because of this connection, the success of a chemical model is shown to be sensitive to the size of  $r$  assumed in the above sequence. In particular, the case when  $r \rightarrow \infty$  and the equilibrium constants determine the concentrations of the various species is shown to be the best approach. A two-equilibrium constant (dimer constant and another which represents constants beyond the dimer) mole fraction model is found to give a good fit to the observed thermodynamic properties of the ethanol-heptane system up to the equimolar composition. Enthalpies and entropies of formation for the dimer were found to be about  $-8.5$  kcal/mol and  $-22.0$  cal/deg mol, respectively. Corresponding values for the linear species were found to be about  $-5.6$  kcal/mol and  $-11$  cal/deg mol. Also investigated is a comparison of the mole fraction and volume fraction formulations.

#### I. Introduction

A model which postulates chemical association, the chemical model, has been used extensively in the molecular interpretation of properties of certain classes of liquid solutions. We are especially interested in solutions containing one associating component A and one nonassociating component B, *e.g.*, an alcohol in a nonpolar solvent.<sup>2-6</sup> The associating component A is regarded as a collection of species  $A_1, A_2, \dots, A_r$  in equilibrium according to the reaction  $A_1 + A_{j-1} \rightleftharpoons A_j$ . By recognizing these chemical species we change our position from one of trying to describe strong interactions, which produce nonrandomness in the spatial distribution of the individual A molecules, to one of trying to describe weak interactions, which are ineffective in disturbing randomness in the spatial distribution of the assumed species.

The repulsive forces which one attributes to the interaction between a polymeric  $A_j$  molecule and other molecules may be represented to some extent by attributing a volume to the  $A_j$  molecule. This volume varies with the number  $j$  of A units involved. Since the advent of polymer theories based on volume fraction statistics, it has been natural to assume that volume fraction statistics are required for the statistical

(1) (a) Address all correspondence to the University of Utah, Salt Lake City, Utah; (b) Union Carbide Professor of Chemical Engineering, Rensselaer Polytechnic Institute.

(2) (a) O. Redlich and A. T. Kister, *J. Chem. Phys.*, **15**, 849 (1947); (b) C. B. Kretschmer and R. Wiebe, *ibid.*, **22**, 1697 (1954).

(3) A. C. P. Hwa and W. T. Ziegler, *J. Phys. Chem.*, **70**, 2572 (1966).

(4) H. Renon and J. M. Prausnitz, *Chem. Eng. Sci.*, **22**, 299 (1967).

(5) I. A. Wiebe and E. B. Bagley, *Ind. Eng. Chem., Fundamentals*, **6**, 209 (1967).

treatment of associated liquids and their solutions. Flory's equations for heterogeneous polymer solutions<sup>6</sup> have been carried over to the case of associated solutions. These treatments have been fairly successful in the description of vapor-liquid equilibria, not so successful in the description of enthalpy and entropy changes upon mixing, and unsuccessful in explanation of the temperature dependence of the thermodynamic functions.<sup>3,5</sup> It is possible that the volume fraction statistics are not completely suited to the treatment of associated solutions.

The purpose of this paper is to develop the chemical model from an expression for the entropy of mixing based on mole fraction statistics as applied to an ideal multicomponent system. The ethanol-heptane system is examined in detail because extensive thermodynamic data have been supplied by Van Ness, *et al.*<sup>7-9</sup> Dielectric<sup>10-12</sup> and spectroscopic (ir<sup>13-16</sup> and nmr<sup>17-19</sup>) evidence concerning the structure of alcohols and their solutions will also be examined. Finally a comparison will be made of the volume fraction and mole fraction models.

## II. Model Development

We take as our starting point the entropy of mixing for an ideal multicomponent system. The entropy of the mixture relative to a standard state in which the species are separated is (see Appendix I)

$$S^f = (\Delta S^m + S^0)^f = -R[n_B^f \ln x_B^f + \sum n_j^f \ln x_j^f] + \sum n_j^f s_j^0 + n_B^0 s_B^0 \quad (1)$$

where  $s_j^0$  is the molar entropy of pure  $j$ -mer. The superscript  $f$  denotes the final or equilibrium state of the mixture, and the superscript  $0$  indicates a pure species at the temperature and pressure of the mixture. Before mixing the components A and B, the entropy of the system is

$$S^i = (\Delta S^m + S^0)^i = -R[\sum n_j^i \ln x_j^i + \sum n_j^i s_j^0 + n_B^0 s_B^0] \quad (2)$$

where the superscript  $i$  denotes the initial or unmixed state containing the same species as the mixture at the same temperature and pressure. Thus the entropy of mixing for the binary system,  $\Delta S^m = S^f - S^i$ , is

$$\Delta S^m = -R[n_B^0 \ln x_B^f + \sum (n_j^f \ln x_j^f - n_j^i \ln x_j^i)] + \sum (n_j^f - n_j^i) s_j^0 \quad (3)$$

Equations 1 and 2 represent mixing processes in which there is no degradation of the polymer species. The chemical reaction which takes place in the actual mixing process is accounted for in (3) by the different mole numbers and mole fractions of the  $j$ -mers in the initial and final states. Equation 3 can be simplified by introducing the equilibrium constants (see Appendix II)

$$k_j = x_j/x_1^j \quad (4)$$

for the reactions described by  $jA_1 \rightleftharpoons A_j$ . Substitution of (4) into (3) yields

$$\Delta S^m = -R[n_B^0 \ln x_B^f + n_A^0 \ln (x_1^f/x_1^i)] - R\sum (n_j^f - n_j^i) \ln k_j + \sum (n_j^f - n_j^i) s_j^0 \quad (5)$$

where use has been made of the relation  $\sum j n_j = n_A^0$ . The second and third terms on the right side of (5) can be simplified further by using

$$g_j^0/T = -R \ln k_j = (h_j^0/T) - (s_j^0 - j s_1^0) \quad (6)$$

where  $h_j^0$  is the enthalpy change for the formation reaction  $jA \rightleftharpoons A_j$ . Putting (6) into (5), we find

$$\Delta S^m = -R[n_B^0 \ln x_B^f + n_A^0 \ln (x_1^f/x_1^i)] + \sum (n_j^f - n_j^i) h_j^0/T \quad (7)$$

The first term on the right side of (7) is  $\Delta G^m/T$ , which can be verified by using the integrated Gibbs equation ( $G = \sum n_j \mu_j$ ) to form

$$\Delta G^m = G^f - G^i = \sum (n_j^f \mu_j^f - n_j^i \mu_j^i) + n_B^0 (\mu_B^f - \mu_B^i) = n_A^0 (\mu_1^f - \mu_1^i) + n_B^0 (\mu_B^f - \mu_B^i) \quad (8)$$

and then inserting the appropriate formulas for the chemical potentials together with the equilibrium condition,  $j\mu_1 = \mu_j$ . Thus the second term on the right side of (7) represents the enthalpy change of mixing divided by the temperature.

An analysis similar to the one given above can be developed using Flory's expression for the entropy of mixing for a disoriented standard state

$$\Delta S^m = -R[\sum n_j \ln \phi_j + n_B \ln \phi_B] \quad (9)$$

or the more general equation based on the quasi-crystalline standard state.<sup>6</sup> In either case, it can be shown that the free energy of mixing is

- (6) P. J. Flory, *J. Chem. Phys.*, **12**, 425 (1944).
- (7) H. C. Van Ness, C. A. Soczek, G. L. Peloquin, and R. L. Machado, *J. Chem. Eng. Data*, **12**, 217 (1967).
- (8) H. C. Van Ness, C. A. Soczek, and N. K. Kochar, *ibid.*, **12**, 346 (1967).
- (9) F. Pardo and H. C. Van Ness, *ibid.*, **10**, 163 (1965).
- (10) G. Oster, *J. Am. Chem. Soc.*, **68**, 2036 (1946).
- (11) P. I. Gold and R. L. Perrine, *J. Chem. Eng. Data*, **12**, 4 (1967).
- (12) G. Oster and J. Kirkwood, *J. Chem. Phys.*, **11**, 175 (1943).
- (13) H. C. Van Ness, J. V. Van Winkle, H. H. Richtol, and H. B. Hollinger, *J. Phys. Chem.*, **71**, 1483 (1967).
- (14) N. D. Coggeshall and E. L. Saier, *J. Am. Chem. Soc.*, **73**, 5414 (1951).
- (15) U. Liddel and E. D. Becker, *Spectrochim. Acta*, **10**, 70 (1957).
- (16) M. Van Thiel, E. D. Becker, and G. C. Pimentel, *J. Chem. Phys.*, **27**, 95 (1957).
- (17) G. C. Pimentel and A. L. McClellan, "The Hydrogen Bond," W. H. Freeman and Co., San Francisco, Calif., 1960.
- (18) J. C. David, Jr., K. S. Pitzer, and C. N. R. Rao, *J. Phys. Chem.*, **64**, 1744 (1960).
- (19) C. M. Huggins, G. C. Pimentel, and J. N. Shooling, *ibid.*, **60**, 1311 (1956).

$$\Delta G^m/RT = [n_B^0 \ln \phi_B^f + n_A^0 \ln (\phi_1^f/\phi_1^i)] + \sum (n_j^i - n_j^f) \quad (10)$$

and the enthalpy of mixing is the second term on the right side of (7) multiplied by  $T$ .

The chemical model as developed above has some interesting general features. For example, thermodynamic properties can be expressed in terms of an average chain length  $J$  for the associated component

$$J = \frac{\sum j n_j}{\sum n_j} = \frac{n_A^0}{\sum n_j} \quad (11)$$

If  $J^i$  and  $J^f$  are the average chain lengths before and after mixing, then the enthalpy of mixing per stoichiometric mole of the mixture can be expressed as

$$\Delta H^m = x_A^0 \left[ \frac{1}{J^i} - \frac{1}{J^f} \right] H \quad (12)$$

where  $H$  is the energy of 1 mol of associative links,  $h_j^0 = (j - 1)H$ . It is assumed here that  $H$  is independent of  $j$ . Since  $J^i$  approaches unity in the limit of small  $x_A^0$ , the limiting value of  $\Delta H^m/x_A^0 x_B^0$  is given by

$$\left( \frac{\Delta H^m}{x_A^0 x_B^0} \right)_{x_A^0=0} = \left( \frac{1}{J^i} - 1 \right) H \quad (13)$$

In a highly associated liquid, such as ethanol,  $J^i$  may be so large that the right side of (13) is approximately  $-H$ . It should be noted that the left-hand side of (13) is given by the left intercept in Figure 1. Other physically significant intercepts which can be derived from (7) are

$$\begin{aligned} (G^E/RT x_A^0 x_B^0)_{x_A^0=0} &= \ln \gamma_A^0 = \ln x_1^i \\ (G^E/RT x_A^0 x_B^0)_{x_A^0=1} &= \ln \gamma_B^0 = \ln J^i \end{aligned} \quad (14)$$

where  $G^E = \Delta G^m - G^m(\text{ideal})$  is the excess free energy of mixing.

Another interesting feature of the mole fraction model is its prediction of a volume change on mixing. Unlike the volume fraction model, the mole fraction model does predict such a change, and the prediction agrees qualitatively with observed changes. The volume change can be interpreted as follows. Expressions 1 and 2 for the entropy can be regarded as expressions of  $S = k \ln W$ , where  $W$  is the number of ways to assign  $j$ -mers and solvent molecules to cells or lattice sites. Since the number of  $j$ -mers changes upon mixing, there must be a corresponding change in the number of available cells. Thus the volume change can be formulated as

$$\Delta V^m = v_c \sum (n_j^f - n_j^i) = v_c x_A^0 [(1/J^f) - (1/J^i)] \quad (15)$$

where  $v_c$  is the cell volume. Equation 15 has the same form as formula 12 for the heat of mixing. This similarity between the two properties is observed for the alcohol-normal hydrocarbon systems investigated by Van Ness and coworkers. (See Figure 2.)

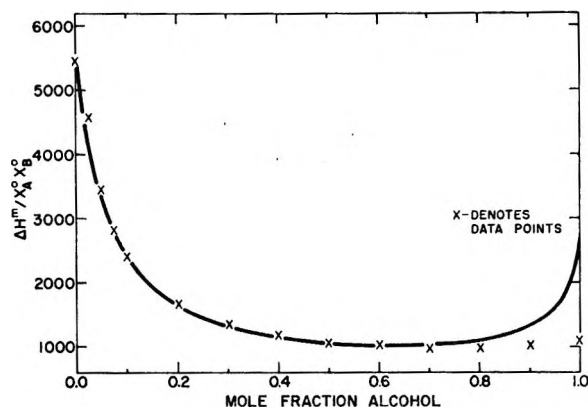


Figure 1. Theoretical (2K model) and experimental values of  $\Delta H^m/x_A^0 x_B^0$  for ethanol-heptane solutions at 333°K.

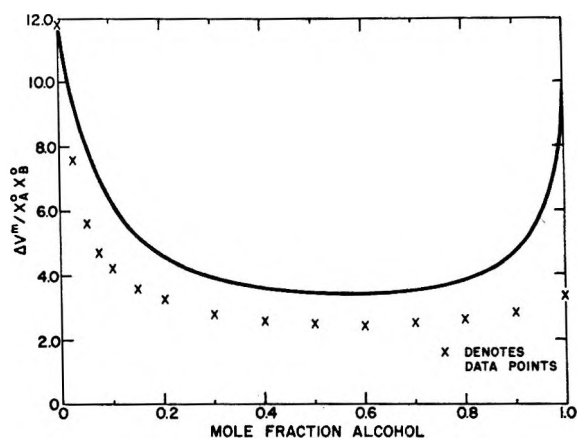


Figure 2. Theoretical (2K model) and experimental values of  $\Delta V^m/x_A^0 x_B^0$  for ethanol-heptane solutions at 333°K.

### III. Extent of Dissociation

From the discussion above we see that the changes of thermodynamic functions with mixing are completely determined for the mole fraction model by the dependence of  $x_1^i$ ,  $x_1^f$ , and  $x_B^f$  on the stoichiometric composition  $x_A^0$  and the equilibrium constants  $k_j$ . The equations to be solved are

$$\begin{aligned} \sum x_j^f + x_B^f &= 1 \\ \sum j x_j^f &= (x_A^0/x_B^0) x_B \\ k_j &= x_j^f / (x_1^f)^j, \quad j = 1, 2, 3, \dots \end{aligned} \quad (16)$$

The equilibrium constants are to be determined from experimental data. It is very difficult and not very profitable to determine all of the  $k_j$  values by curve fitting. On the other hand, it may be profitable to test various assumptions concerning the relative values of  $k_j$ . For example, if it is assumed that the free energy change for the addition of one A unit,  $A_1 + A_{j-1} \rightleftharpoons A_j$ , is independent of  $j$ , then it follows that  $k_j$  is  $K^{j-1}$ , where  $K$  is  $k_2$ , and there is only one adjustable parameter to be determined from the data. This case has been studied by Redlich and Kister.<sup>2a</sup> They let  $j$  go to in-



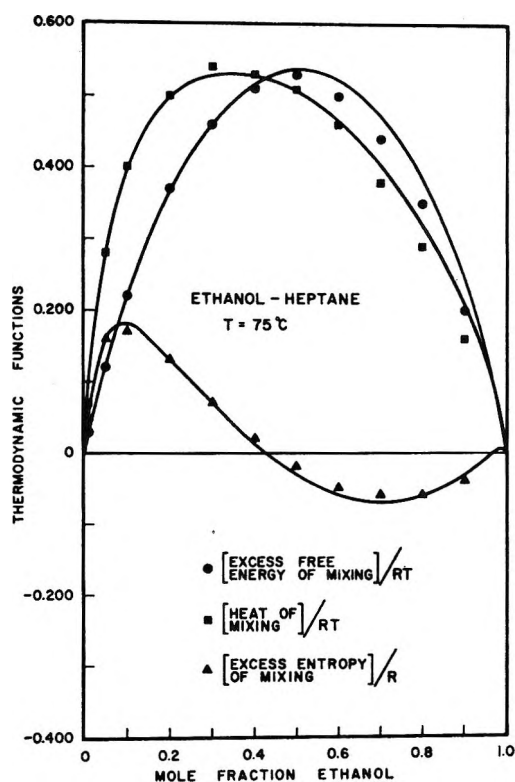


Figure 3. Theoretical (2K model) and experimental values of excess functions for ethanol-heptane solutions.

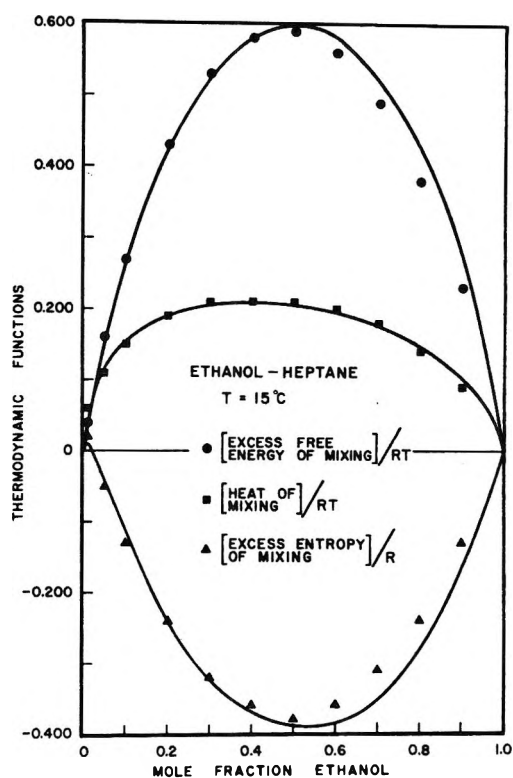


Figure 5. Theoretical (2K model) and experimental values of excess functions for ethanol-heptane solutions.

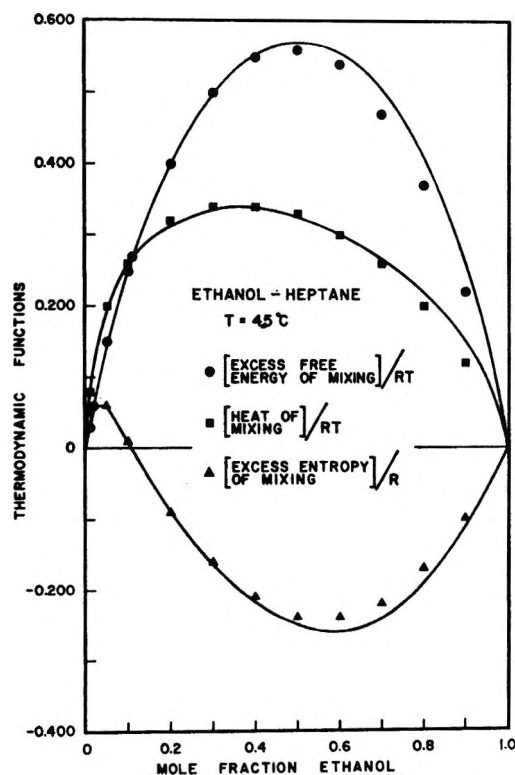


Figure 4. Theoretical (2K model) and experimental values of excess functions for ethanol-heptane solutions.

association model. As pointed out by Scatchard,<sup>20</sup> the continuous-association model of Redlich and Kister predicts thermodynamic functions which are symmetric about the equimolar composition. This kind of symmetry is not observed experimentally (see Figures 3-5) and we are led to ask whether or not there is something wrong with continuous-association models.

Let us consider models for which the extent of association is finite. Suppose  $r$  is the largest number of monomer units associated in a single chain. Then the largest  $j$ -mer is  $A_r$ , and  $r$  is the upper limit for the sums in (16). One of the interesting predictions of this model is the maximum value of  $G^E$ , which is sensitive to  $r$ . In the limit of infinite  $k_j$ , where  $G^E$  is maximized for fixed  $r$ , it is easy to solve eq 16 for  $G^E$  as a function of the stoichiometric composition (see Appendix III). If we maximize again, this time with respect to composition, we obtain the values listed in Table I. The experimental values of  $(G^E/RT)_{\max}$  for the ethanol- $n$ -heptane system range from 0.5 to 0.6 (see Figures 3-5), and these values are typical for low-molecular-weight alcohols in inert solvents. Looking at Table I we see that the predicted maxima for  $G^E$  reach up to experimental maxima only if the chain length  $r$  is of the order of 10 or greater. Clearly we cannot expect to describe the alcohol- $n$ -hydrocarbon systems on the basis of a mole fraction chemical model with just dimers and

finity in order to allow for association to an indefinite extent and to obtain what is called the continuous-

(20) G. Scatchard, *Chem. Rev.*, **44**, 7 (1949).

**Table I:** Estimation of Chain Length from the Maximum of the  $G^E$  Curve

Chain length, $r$	$(G^E/RT)_{\max}$	Compn ( $x_A^0$ ) at max	Chain length, $r$	$(G^E/RT)_{\max}$	Compn ( $x_A^0$ ) at max
2	0.223	0.400	15	0.571	0.466
4	0.387	0.427	21	0.594	0.472
6	0.459	0.442	50	0.647	0.485
8	0.501	0.450	100	0.668	0.493
10	0.529	0.456	$\infty$	0.692	0.500

trimers and other small polymers. Furthermore, if the  $k_j$  values are not infinite, as assumed for Table I, then the maximum chain length  $r$  must be even greater than indicated in order to bring  $G^E$  up to the level of experimental values. Thus it appears that we may as well let  $r$  go to infinity. In view of this result we are led to reconsider the continuous-association model. The symmetry of Redlich and Kister's model can be destroyed by altering the relation among the equilibrium constants  $k_j$ . Redlich and Kister used only one equilibrium constant as an adjustable parameter, and the introduction of additional parameters could certainly improve the model. On the other hand, this approach is fruitless unless there is a drastic improvement for a modest increase in the number of parameters.

We have found that the continuous association model with two independent equilibrium constants,  $k_2$  and  $k_3$ , is very successful in accounting for some of the properties of the ethanol-heptane system. It is convenient here to deal with the constants  $K_j$  for the reactions  $A_1 + A_{j-1} \rightleftharpoons A_j$ . We treat  $K_2 = k_2$  and  $K_3 = k_3/k_2$  as fitting parameters and assume that  $K_j = K_3$ ,  $j > 3$ . There are good physical grounds for separating  $K_2$  and  $K_3$  even if the other  $K_j$  terms are not independent. The evidence will be discussed following the development of the two-constant model.

#### IV. The Two-Constant Model

We have applied the two-constant model to the data of Van Ness and coworkers by determining the two equilibrium constants from  $G^E$  data. The fitting procedure is based on iteration equations for solving two simultaneous nonlinear equations in two unknowns.<sup>21</sup> The procedure can be described as follows.

We start with eq 16 which can be combined to form a cubic equation for the monomer mole fraction  $y = x_1^f$

$$K_3(K_3 - K_2)y^3 + [(K_3^2 + K_2)x_A^0 + 2(K_3 - K_2)]y^2 + (1 + 2K_3x_A^0)y - x_A^0 = 0 \quad (17)$$

The analogous equation for the initial monomer composition is a quadratic equation which has one physically significant root

$$x_1^i = \frac{1.0 + K_3 - [(1.0 + K_3)^2 - 4(K_3 - K_2)]^{1/2}}{2.0(K_3 - K_2)} \quad (18)$$

The mole fraction  $x_B^f$  can be determined from  $x_1^f$ ,  $K_2$ , and  $K_3$ . Thus the formula for  $G^E$

$$G^E(x_A^0, K_2, K_3) = RT \left[ x_A^0 \ln \frac{x_1^f}{x_1^i x_A^0} + x_B^0 \ln \frac{x_B^f}{x_B^0} \right] \quad (19)$$

can be used to calculate  $G^E$  at a particular composition from  $K_2$  and  $K_3$ . Alternatively, experimental data for  $G^E$  at two different compositions provides a determination of  $K_2$  and  $K_3$ . This is accomplished, following Singer, by introducing

$$g_i(K_2, K_3) = (RT)^{-1}[G^E(K_2, K_3, x_{A_i}^0) - G^E_1] \quad (20)$$

where the index  $i$  refers to a particular composition  $x_A^0$ , and  $G^E_i$  is the corresponding experimental value for  $G^E$ . The equations to be solved are  $g_1 = 0$  and  $g_2 = 0$ . The iteration formulas are

$$\begin{aligned} K_2^1 &= K_2 - D^{-1}[g_{23}g_1 - g_{13}g_2] \\ K_3^1 &= K_3 + D^{-1}[g_{22}g_1 - g_{12}g_2] \end{aligned} \quad (21)$$

where  $g_{ij}$  is the derivative of  $g_i$  with respect to  $K_j$ , and  $D$  is the determinant of the  $g_{ij}$  matrix. More detailed formulas and the iteration program are given elsewhere.<sup>22</sup>

It was found that the iteration procedure outlined above converges only for solutions containing less than 50 mol % alcohol. Values obtained for  $K_3$  were not sensitive to the composition pairs, but values for  $K_2$  were fairly sensitive. The following criteria were imposed in order to assess the reliability of the  $K_j$  values. (1) The values of  $K_2$  and  $K_3$  inserted into (19) must generate the  $G^E$  data. (2) The temperature dependence of the  $K_j$  values must satisfy the van't Hoff relation. (3) The  $K_j$  values together with the formation enthalpies, derived from the temperature dependence of the  $K_j$ , must provide a good fit of the  $\Delta H^m$  data.

It was possible to find  $K_j$  values that satisfied all of the requirements mentioned above, as illustrated in Figures 3-5. The following equations give the adjustable parameters

$$\ln \frac{K_j(T)}{K_j(T^0)} = \frac{[-H_j(T^0) + a_j T^0]}{R} \left( \frac{1}{T} - \frac{1}{T^0} \right) + \frac{a_j}{R} \ln \frac{T}{T^0} \quad (22)$$

$$H_j(T) = H_j(T^0) + a_j(T - T^0)$$

$K_2(T^0) = 53.88$ ,  $H_2(T^0) = -8850$  cal, and  $a_2 = 7.50$  cal deg<sup>-1</sup>;  $K_3(T^0) = 76.80$ ,  $H_3(T^0) = -5500$  cal, and  $a_3 =$

(21) J. Singer, "Elements of Numerical Analysis," Academic Press, New York, N. Y., 1964.

(22) R. W. Haskell, Ph.D. Thesis, Rensselaer Polytechnic Institute, Troy, N. Y., 1967; available from University Microfilms, Ann Arbor, Mich.

$-3.83 \text{ cal deg}^{-1}$ .  $T^0$  is  $288.15^\circ\text{K}$ .  $H_j$  is the enthalpy change for the reaction  $A_1 + A_{j-1} = A_j$ . Enthalpies and equilibrium constants are listed in Table II for

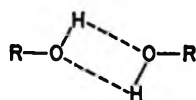
Table II: Two-Constant Model Fitting Parameters

$T$ , $^\circ\text{K}$	$K_2$	$K_3$	$H_2$ , kcal/mol	$H_3$ , kcal/mol
348.15	4.00	14.20	-8400	-5730
338.15	5.74	18.13	-8475	-5691
328.15	8.44	23.44	-8550	-5653
318.15	12.77	30.76	-8625	-5615
308.15	19.92	40.99	-8700	-5577
298.15	32.15	55.58	-8775	-5538
288.15	53.88	76.80	-8850	-5500

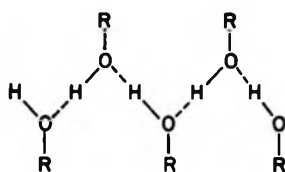
several temperatures. The temperature dependence of the enthalpies is quite small, but recognizing this temperature dependence leads to substantial improvements in fitting the model to the data. The value obtained for  $H_3$  suggests that one hydrogen bond is formed in the reaction. The value for the temperature coefficient  $a_3$  is reasonable if it is interpreted as a loss of heat capacity upon the formation of a bond. In the case of  $H_2$ , the value obtained suggests that the dimer is predominantly double bonded (see Figure 6a). This interpretation is supported by the increase of  $H_2$  with temperature (positive  $a_2$ ), which can be attributed to an increasing contribution from single-bonded dimers which would be expected at higher temperatures. The predominance of double bonds in dimers is also indicated by the values for the entropy changes  $S_2$  and  $S_3$  associated with the formation of dimers and the extension of higher polymers. The entropy changes can be calculated from

$$-RT \ln K_j = H_j - TS_j \quad (23)$$

We find the respective values for  $T$ ,  $S_2$  (eu), and  $S_3$  (eu): 288,  $-22.7$ ,  $-10.5$ ; 348,  $-21.3$ ,  $-11.2$ . These



(a) CYCLIC DIMER



(b) LINEAR POLYMER

Figure 6. Structures of some alcohol species.

values are reasonable when interpreted as entropy changes for the formation of single and double bonds.

## V. The Alcohol Structure

We have found that a two-constant model can account for the thermodynamic properties of ethanol-*n*-heptane mixtures over a substantial range of compositions and temperatures. The temperature dependence of the equilibrium constants suggests the existence of double-bonded dimers and higher polymers held together primarily by single bonds. In this section we will briefly review evidence from other sources concerning the structure of the alcohols.

There are considerable infrared data<sup>13-16</sup> for dilute alcohol solutions which show the existence of three absorption peaks corresponding to the hydroxyl stretching frequency of three apparently different hydroxyl environments or spectral species. These spectral species and their spectral characteristics are listed in Table III for ethanol. The important point in the present

Table III: Ir Spectral Species Observed in Dilute Alcohol Solutions

Spectral species	Wave number, $\text{cm}^{-1}$
Monomer	3630
Dimer	3500
Polymer	3350

discussion is the appearance of a dimer peak. It probably represents a cyclic structure (see Figure 6a) as argued by Van Ness, *et al.*,<sup>13</sup> since if it were an open-chain structure, it would presumably contribute to the spectral monomer and polymer absorption peaks. Further infrared evidence indicating the existence of small cyclic structures comes from the matrix isolation studies of Van Thiel, Becker, and Pimentel.<sup>16</sup> In this work a gas mixture of  $\text{N}_2$  and methanol was condensed onto a silver chloride window at  $20^\circ\text{K}$ . Several spectral species were observed as shown in Table IV. The designation of the various peaks involves interpretations, but it seems clear that these peaks represent

Table IV: Ir Spectral Species Observed in Matrix-Isolation Studies

Spectral species	Wave number, $\text{cm}^{-1}$
Monomer	3660
Dimer	3490
Trimer	3445
Tetramer	3290
Polymer	3250

short-chain structures in which the hydroxyl environment is different from that of a hydroxyl group participating in a linear-chain structure.

In agreement with the above conclusion is the evidence available from nuclear magnetic resonance spectra.<sup>17-19</sup> Here it has been possible to determine the dimer bond energy<sup>23</sup> by finding  $(\delta/x_A^0 x_B^0)_{x_A^0=0}$  at infinite dilution of the alcohol for several temperatures. For methanol and ethanol in  $\text{CCl}_4$ , the  $H_2$  values were found to be  $-9.4$  and  $-7.6$  kcal/mol, respectively.<sup>18</sup>

Some of the best evidence at present concerning the structure of the alcohols comes from dielectric constant measurements. Such measurements allow determination of Kirkwood's correlation parameter,<sup>24</sup>  $g$ . For the alcohols, we may represent  $g$  approximately by the formula

$$g = 1 + 2 \sum (\overline{\cos \gamma})_j \quad (24)$$

Here  $(\overline{\cos \gamma})_j$  represents the average cosine of the angle between a given dipole and its  $j$ th shell of neighbors. For the pure alcohols experimentally determined  $g$  values are in the range 2.8-3.2. Kirkwood found a  $g$  value of 2.6 for an infinite chain. In his calculation, rotation is allowed about the bond but bending is not. Figure 6b shows the type of structure assumed for the linear polymer upon which Kirkwood's calculation was based.<sup>25</sup>

Experimental results<sup>10-12</sup> for solutions of an alcohol in an inert solvent give the typical  $g$  vs.  $x_A^0$  curve shown in Figure 7. The value  $g = 1.0$  at infinite dilution means that there is no correlation between the dipole moments of the alcohol molecules; *i.e.*, the solution consists of monomers so greatly separated that the individual dipoles are randomly oriented. However, the  $g$  value quickly becomes less than unity with increasing alcohol concentration. According to (24), this can happen only when there is a tendency for the dipoles to be in an antiparallel orientation. From a chemical point of view this indicates the presence of cyclic structures.

As the alcohol mole fraction approaches 0.2,  $g$  approaches unity. This rise in  $g$  must result from an increase in the ratio of open-chain to closed-chain structures. At  $x_A^0 \cong 0.2$ ,  $g$  is again unity, and there must be a rough equivalence between the number of open- and closed-chain structures. It is interesting to notice that the chemical models predict average chain lengths of 2-6 as the temperature varies from 348 to 288°K at this composition. (See Figure 8.) These numbers are probably indicative of the size of cyclic structures to be found in the pure alcohol. As the alcohol concentration exceeds 0.2, the correlation parameter exceeds unity, indicating a predominance of open-chain structures. This predominance apparently reaches its maximum in the pure alcohol. It is interesting to note that lowering the temperature causes  $g$  to decrease in the low-concentration region and in-

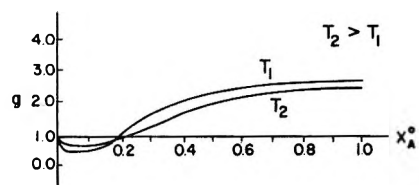


Figure 7. The correlation parameter for alcohol-inert solvent solutions.

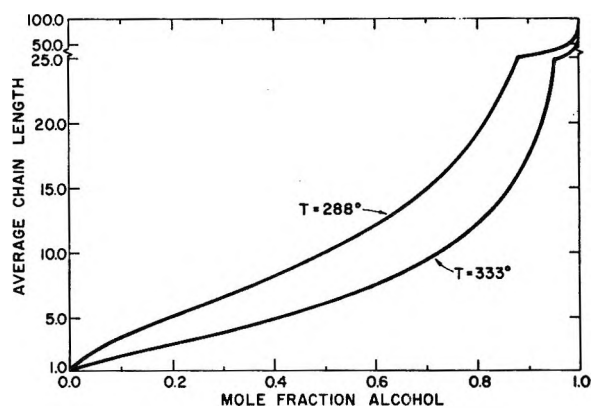


Figure 8. Theoretical chain lengths based on the 2K model for ethanol-heptane solutions.

crease in the high-concentration region. Apparently both open- and closed-chain structures become more stable.

The thermodynamic, spectroscopic, and dielectric evidence leads us to the following description of the alcohol structure. Near the boiling point it probably consists mostly of double-bonded dimers and open chains of, say, 10 segments on the average. At lower temperatures the average chain length increases and the cyclic size increases. At 288° the former may be 20 or 30, and the largest cyclic structures may be hexamers. We do not mean to imply by this that there are no small linear structures (2-6 segments) or no large cyclic structures (greater than 6 segments). However it would appear that the values of  $H_2$  and  $S_2$ , together with the correlation parameter values at low concentrations and also the above-mentioned spectroscopic evidence, strongly favor a large predominance of double-bonded dimers over the linear variety. As the number of segments becomes larger, entropy considerations make the existence of higher cyclics less likely. Average chain length considerations together with the composition value at which the correlation coefficient begins to exceed 1 would seem to indicate that cyclics beyond 6 segments are of insufficient concentration to affect the

(23) The slope of the chemical shift  $\delta$  (*i.e.*, the shift in the proton frequency measured from some standard such as a proton resonance in the methyl group) vs. composition at infinite dilution is obtained by extrapolating the measured shifts to infinite dilution.

(24) J. Kirkwood, *J. Chem. Phys.*, **7**, 911 (1939).

(25) L. Pauling, "Nature of the Chemical Bond," Cornell University Press, Ithaca, N. Y., 1945.

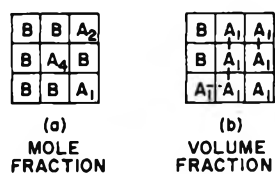


Figure 9. Two-dimensional representations of lattices for mole fraction and volume fraction statistics.

alcohol properties measurably in the temperature range studied. Indeed, the thermal properties of ethanol seem to be well represented by just allowing the dimer equilibrium constant to be different.<sup>26</sup> Thus it seems proper to conclude that the double-bonded dimer is the major cyclic at all temperatures but that dielectric constant values would require the inclusion of a few higher cyclics in the low-temperature range.

## VI. Mole Fractions and Volume Fractions

In this section we will compare the descriptions of the chemical models which are based on mole fraction statistics with those based on volume fraction statistics. The basic difference between the two types of descriptions can be illustrated by the cell diagrams in Figure 9. In both diagrams there are solvent molecules B, one monomer unit of alcohol A<sub>1</sub>, one dimer A<sub>2</sub>, and one tetramer A<sub>4</sub>. Notice that the mole fraction description attributes one cell to any *j*-mer whereas the volume fraction description attributes one cell to each formula molecule. If we imagine these species to be in chemical equilibrium, associating and disassociating, we can make the following comparisons. At infinite dilution of component A, only monomers are present; hence the two descriptions will be nearly equivalent. (If the molar volumes of A and B are equal, the descriptions are identical.) At infinite dilution of component B the two descriptions will be greatly different.

An example of the difference between the descriptions appears in the determination from the model of the limiting value of  $\Delta H^m/x_A^0 x_B^0$  at  $x_A^0 = 1$ . This is the right-hand intercept in Figure 1. The value is not so easily found as in the case of the left-hand intercept, which is given by (13). The value of the right-hand intercept depends on the details of the model and the relations assumed for the  $k_j$  values. On the other hand, the cell diagrams provide a means of approximating the intercept value. We assume that the intercept represents the enthalpy change for addition of a solvent molecule to a lattice containing only component A. In the case of the mole fraction description, this addition would nearly always prevent an associative reaction from occurring. In the case of the volume fraction description, this addition would only prevent about 1 out of *J* associative reactions from occurring since, roughly speaking, the solvent molecule will only be in the neighborhood of a reacting site (*i.e.*, end of chain neighbor) this fraction of the time. Thus

we expect the right-hand intercept to be about the same as the bond energy,  $-H^0$ , in the mole fraction description, and only a fraction of that value (of order  $-H^0/J$ ) in the volume fraction description. Exact derivations lead to the formulas listed in Table V. These expressions are all based on the one-constant model,  $k_j = K^{j-1}$ , for the evaluation of the sums in (11). It is interesting to note that the volume fraction relations explain at least qualitatively the appreciable increase of this intercept with temperature as noted by Van Ness and coworkers. Thus, as the temperature increases, the average chain length decreases and the intercept increases.

Table V: Right-Hand Intercept Expressions for Heat of Mixing

Description	$(\Delta H/x_A^0 x_B^0)_{x_A^0=1.0}$
Mole fraction	$[(1/J^i) - 1]H^0$
Volume fraction	
Disoriented std state	$\frac{-H^0}{PJ^i} \left( 1 - \frac{K}{(K+1) \ln(K+1)} \right)$
Quasi-crystalline std state	$\frac{-H^0}{2PJ^i} \left( 1 - \frac{1}{\sqrt{4K+1}} \right)$

Comparing the predictions shown in Table V with the experimental data, Figure 1, we find that the one-constant mole fraction model greatly overestimates the intercept. The two-constant model is better, as indicated in Figure 1, but it leaves much to be desired. It seems clear that for high alcohol concentrations the mole fraction description is bound to fail because it takes no account of the spatial extent of the associated species. In this range, the volume fraction description is undoubtedly a more accurate description. However, there are several difficulties with the volume fraction description; these are outlined below.

As noted by Wiehe and Bagley,<sup>5</sup> even when one allows for infinite association ( $k_{js} \rightarrow \infty$ ), one still finds difficulty in reaching the magnitude of  $G^E$  found experimentally.<sup>27,28</sup> Moreover, when the association constants are large,  $\Delta H^m$  is small, so that it is not possible (using the same parameters) to fit both  $\Delta H^m$  and  $\Delta G^E$  data. This difficulty is resolved by allowing the ratio of the molar volumes to become a fitting parameter or by including a physical interaction term of the Van Laar-Hildebrand-Scatchard form. The latter alternative leads to the models of Kretschmer and Wiebe<sup>2b</sup> and Renon and Prausnitz.<sup>4</sup> We have not

(26) A. V. Tobolsky and R. E. Thach, *J. Colloid Sci.*, **17**, 419 (1962).

(27) It is possible that part of the reason for the failure of the volume fraction model to achieve the proper magnitude is the fact that Flory's approximation of  $W$  in  $S = k \ln W$  overcounts.

(28) H. Tompa, "Polymer Solutions," Academic Press, New York, N. Y., 1956.

included a physical interaction term in the two-constant mole fraction model. Both Redlich and Kister<sup>2a</sup> and Stokes<sup>29</sup> found that the term does not account for more than a few calories in the mole fraction description. Furthermore, in practice, the term assumes the role of a curve-fitting parameter which takes up the slack between the chemical model predictions and observed data and thus tends to make all models appear reasonable.

Another difficulty with the volume fraction description enters because the model is a constant-volume model whereas most data are for constant pressure. Thus in applying the model one should transform the constant ( $T, P$ ) data into constant ( $T, V$ ) data. Only Kretschmer and Wiebe have considered this correction, which is significant with regard to  $\Delta H^m$  and  $\Delta S^m$  even though it can be neglected in the case of  $\Delta G^m$ .

Of the more recent volume fraction models we should also mention that of Hwa and Ziegler.<sup>3</sup> They considered a two-constant volume fraction model with a physical interaction term, but they did not make the correction due to a volume change, as mentioned above. They assumed that the dimer and higher polymer formation enthalpies were the same, and they did not try to satisfy the van't Hoff relation. These restrictions may partly explain the strong temperature dependence of their calculated bond energies for the ethanol-methylcyclohexane system (*i.e.*,  $-3590$  kcal at  $308^\circ\text{K}$ ,  $-1779$  kcal at  $273^\circ\text{K}$ , and  $-942$  kcal at  $248^\circ\text{K}$ ).

In summary, we have used an ideal-solution model of a multicomponent system to describe an alcohol-inert solvent solution. In particular we have determined two equilibrium constants (one for double-bonded dimers and the other for the linear-chain polymers) from the  $G^E$  data. We have used the van't Hoff relation to describe their temperature dependence and thereby determine the formation enthalpies and the heat of mixing. We have then tried to show that these formation enthalpies are consistent with data from other sources.

*Acknowledgment.* Acknowledgment is made to the donors of the Petroleum Research Fund, administered by the American Chemical Society, for partial support of this research.

## Appendix I

### Glossary of Symbols for Composition Variables

$n_B^0 = n_B^f = n_B^i$	Moles of solvent (not associated)
$n_j^f, n_j^i$	Moles of $j$ -mer in solution and associated component, respectively
$n^f = n_B + \sum n_j^f$	Total moles of solution
$n_A^0 = \sum j n_j^f = \sum j n_j^i$	Stoichiometric moles of associated component
$x_A^0 = \frac{n_A^0}{n_A^0 + n_B^0}$	Stoichiometric mole fraction
$x_j^f = n_j^f/n^f$	$j$ -Mer mole fraction in solution

$x_j^i = n_j^i/\sum n_j^i = x_j^f (x_A^0 = 1)$	$j$ -Mer mole fraction in pure alcohol
$X_j = v_j/v_B = jP$	Ratio of $j$ -mer to solvent molar volumes
$d^f = n_B^f + \sum X_j n_j^f$	
$d^i = \sum X_j n_j^f = d^f (x_A^0 = 1)$	
$\phi_j^f = X_j n_j^f/d^f$	$j$ -Mer volume fraction in solution
$\phi_j^i = X_j n_j^i/d^i$	$j$ -Mer volume fraction in the associated component
$\phi_B^f = n_B^f/d^f$	Solvent volume fraction

## Appendix II

Equation 4 follows from (1) and (2). Since (1) represents an athermal mixing process, we may write

$$(\Delta G^m)^f = -T(\Delta S^m)^f = RT(n_B^0 \ln x_B^f + \sum n_j^f \ln x_j^f)$$

Taking the partial derivatives of both sides with respect to  $n_j^f$  gives

$$\mu_j^f - \mu_j^0 = RT \ln x_j^f$$

Assuming chemical equilibrium, we have  $j\mu_1 = \mu_j$  which gives (4). This procedure applied to (2) gives

$$\mu_j^i - \mu_j^0 = RT \ln x_j^i$$

and similarly for the solvent using (1) we have

$$\mu_B^f - \mu_B^0 = RT \ln x_B^f$$

## Appendix III

We consider the case where the associated liquid contains the species  $A_1, A_2, \dots, A_r$ , but  $K \rightarrow \infty$ , so that the following approximations are possible

$$x_B^f + \sum x_j^f = x_B^f + x_r^f = 1 \quad (\text{A1})$$

$$\frac{\sum j n_j^f}{n^f} = r x_r^f = \frac{n_A^0}{n^f} = \frac{x_A^0 x_B^f}{n_B^0} \quad (\text{A2})$$

These equations can be solved to obtain

$$x_B^f = \frac{r x_B^0}{x_A^0 + r x_B^0} \quad (\text{A3})$$

$$x_r^f = \frac{x_A^0}{x_A^0 + r x_B^0} \quad (\text{A4})$$

Now the condition of equilibrium gives  $\mu_1 = (1/r)\mu_r$  so that  $G^f$  and  $G^i$  may be formulated in terms of the  $r$ -mer chemical potentials instead of the monomer chemical potentials. Therefore

$$G^f = \frac{n_A^0}{r} \mu_r^f + n_B^0 \mu_B^f \quad (\text{A5})$$

$$G^i = \frac{n_A^0}{r} \mu_r^i + n_B^0 \mu_B^i \quad (\text{A6})$$

so that for 1 stoichiometric mol of solution

$$\frac{\Delta G^m}{RT} = \frac{x_A^0}{r} \ln \frac{x_r^f}{x_r^i} + x_B^0 \ln x_B^f \quad (\text{A7})$$

(29) R. H. Stokes, unpublished data.

Now  $K \rightarrow \infty$  means  $x_r^i \rightarrow 1$  and thus the excess free energy is given by

$$\frac{G^E}{RT} = x_A^0 \ln \frac{(x_r^i)^{1/r}}{x_A^0} + x_B^0 \ln \frac{x_B^i}{x_B^0} \quad (\text{A8})$$

At the maximum value of  $G^E$  the activity coefficients of A and B are equal, so we have

$$\frac{(x_r^i)^{1/r}}{x_A^0} = \frac{x_B}{x_B^0} \quad (\text{A9})$$

Equations A3 and A4 may be combined with eq A9 to give the composition at the maximum. This calculation gives

$$x_A^0 = \frac{r}{r^c q}, \quad x_B^0 = \frac{1 - r^{-c}}{q} \quad (\text{A10})$$

where  $c = r/(r - 1)$  and  $q = 1 + [(r - 1)/r^c]$ . Equations A3 and A10 allow us to find the solvent activity coefficient as a function of the chain length. This relation is

$$(\gamma_B)_{\max} = \left( \frac{x_B^i}{x_B^0} \right)_{\max} = q \quad (\text{A11})$$

This gives us for  $(G^E/RT)_{\max}$  the equation

$$\left( \frac{G^E}{RT} \right)_{\max} = \ln (\gamma_B)_{\max} = \ln \left( 1 + \frac{(r - 1)}{r^c} \right)$$

Table I gives  $(G^E/RT)_{\max}$  and  $x_A^0$  for the various values of  $r$ .

## Ionic Polymerization under an Electric Field. XII. Living Anionic

### Polymerization of Styrene in the Binary Mixtures of

### Benzene and Tetrahydrofuran

by Norio Ise, Hideo Hirohara, Tetsuo Makino, and Ichiro Sakurada

Department of Polymer Chemistry, Kyoto University, Kyoto, Japan (Received June 11, 1968)

The anionic polymerization of the lithium salt of living polystyrene was investigated in the binary mixtures of benzene and tetrahydrofuran (THF) at 25° in the presence and absence of an electric field. The apparent propagation rate constant increased with increasing field strength and dielectric constant. The electric field did not affect the ion-pair propagation rate constant, whereas it increased the  $k_p''K^{1/2}$  term;  $k_p''$  is the free-ion propagation rate constant and  $K$  is the dissociation constant of the ion pair. The observed field effect was larger than that calculated by the Onsager theory on the second Wien effect. This discrepancy is discussed in terms of  $k_p''$ , which was found to increase with increasing field intensity. At a THF content of 60 vol %, the  $k_p''$  reached a limiting value of  $\sim 10^5 M^{-1} \text{sec}^{-1}$  when the field was intensified over 3 kV/cm. Evidence is presented which shows that the observed acceleration effect was not caused by the electroinitiation mechanism.

In previous papers, the influence of an electric field on polymerization reactions has been studied. The results have shown that cationic polymerizations can generally be accelerated, and the degree of polymerization of the polymers produced can be increased in the presence of a high-intensity electric field,<sup>1-6</sup> whereas free-radical polymerizations are not influenced.<sup>1</sup> Most recently it has been demonstrated that the monomer reactivity ratio in copolymerizations can also be affected by the field.<sup>7</sup> These field influences have been shown to coincide with the changes caused by an increase in the dielectric constant of the solvent. This agreement

supports our interpretation that the field effects observed are due to the field-facilitated dissociation<sup>8</sup> of the

(1) I. Sakurada, N. Ise, and T. Ashida, *Makromol. Chem.*, **82**, 284 (1964); **95**, 1 (1966).

(2) I. Sakurada, N. Ise, Y. Tanaka, and Y. Hayashi, *J. Polym. Sci., Part A-1*, **4**, 2801 (1966).

(3) I. Sakurada, N. Ise, and S. Hori, *Kobunshi Kagaku*, **24**, 145 (1967).

(4) I. Sakurada, N. Ise, and Y. Hayashi, *J. Macromol. Sci. Chem.*, **A1**, 1039 (1967).

(5) I. Sakurada, N. Ise, and Y. Tanaka, *Polymer*, **8**, 625 (1967).

(6) I. Sakurada, N. Ise, Y. Hayashi, and M. Nakao, *Kobunshi Kagaku*, **25**, 41 (1968).

growing chain ends. Though this interpretation appears reasonable, it lacks clear verification because of the intricate mechanism of the cationic polymerizations. Therefore, it is very interesting to study the field effect on much simpler systems.

As one such system, we have chosen a living anionic polymerization of styrene. This choice enables us to observe the field effect on the propagation step directly. In the present paper, the binary mixtures of benzene and tetrahydrofuran (THF) are used as solvents, and  $\text{Li}^+$ , which has been found to be strongly affected by solvents,<sup>9</sup> is chosen as the gegenion. This particular combination of living polymer-monomer-initiator-solvent has been studied by Bywater and Worsfold,<sup>10</sup> and the living anionic polymerizations in ethereal solvents have been investigated by the Syracuse and Mainz groups.<sup>11,12</sup> The propagation has been shown to proceed by two states of the growing chain ends, namely free ion and ion pair. The rate constant of free ions has been found to be much larger than that of ion pairs.

A brief description of the present work has been published earlier.<sup>13</sup>

## Experimental Section

*I. Purification of Reagents.* *A. Benzene.* Commercial benzene was washed by the usual method, refluxed over  $\text{CaH}_2$  for 1 week after drying, and distilled under nitrogen atmosphere onto a Na-K alloy. Using a high-vacuum line, the benzene was dried under violent stirring at room temperature, cooled down near to the melting point, and deaerated instantaneously. Several cycles of drying and deaeration were repeated and the benzene was distilled onto a Na mirror. After confirming the brightness of the Na mirror, the benzene was distilled into ampoules with break-seals which were adequately flamed, and the ampoules were sealed off from the vacuum line.

*B. Tetrahydrofuran.* A raw sample of THF was dried and distilled at atmospheric pressure in the same manner as the benzene. Then, on the vacuum line, the THF was brought into contact with the Na-K alloy. The deaeration was effected by cooling the THF to  $-78^\circ$  and then opening a cock to the vacuum line for about 10 min. Distillation into a trap at liquid nitrogen temperature did not occur. The adequately dried and deaerated THF showed a characteristic blue color.

*C. Styrene.* Commercially available styrene was washed and dried by the usual method and distilled onto  $\text{CaH}_2$  under reduced pressure. The styrene was then dried using a vacuum line and  $\text{CaH}_2$  was cooled to the melting point and deaerated. The styrene was then distilled onto the Na mirror. The distillation was repeated until the brightness of the mirror did not appear.

*II. Preparation of Living Polymer.* Following the

method described by Fujimoto, *et al.*,<sup>14</sup> *n*-butyl bromide was allowed to react with metal lithium in ether and then the solvent was replaced by benzene. Using the butyllithium thus prepared, poly(styryllithium) with an approximate degree of polymerization of 15 was prepared and used as the seed of the polymerization reaction.

*III. Polymerization Procedures and Apparatus.* As is well known, traces of oxygen, water, and carbon dioxide can inhibit living polymerization. In the preliminary experiments carried out under a nitrogen atmosphere in an open system, no reproducible results were obtained, and, in addition, the rate of polymerization was occasionally decreased by an application of an electric field.<sup>15</sup> Thereafter, a high-vacuum-line technique was always employed for purification of reagents and for polymerization.

Figure 1 shows our polymerization vessel. Ampoules A and B contained dilute and concentrated benzene solutions of the seed polymer, respectively, and ampoules C and D contained THF and a benzene solution of the monomer. The polymerization vessel was connected to the high-vacuum line, evacuated, flamed, and sealed off. Then the break-seal on ampoule B was crushed, and the whole vessel was rinsed with the concentrated solution of the living polymer. All the contents were then collected in container E and the vessel was washed by cooling the walls with a pad at Dry Ice-methanol temperature and condensing the benzene. From E the solvent was distilled into F, and E was

(7) I. Sakurada, N. Ise, Y. Hayashi, and M. Nakao, *Macromolecules*, **1**, 265 (1968).

(8) (a) M. Wien, *Ann. Phys.*, **83**, 327, 795 (1927); (b) M. Wien, *Phys. Z.*, **28**, 751, 834 (1927).

(9) D. N. Bhattacharyya, J. Smid, and M. Szwarc, *J. Phys. Chem.*, **69**, 624 (1965).

(10) S. Bywater and D. J. Worsfold, *ibid.*, **70**, 162 (1966).

(11) (a) D. N. Bhattacharyya, C. L. Lee, J. Smid, and M. Szwarc, *Polymer*, **5**, 54 (1964); (b) D. N. Bhattacharyya, C. L. Lee, J. Smid, and M. Szwarc, *J. Phys. Chem.*, **69**, 612 (1965); (c) M. van Beylen, D. N. Bhattacharyya, J. Smid, and M. Szwarc, *ibid.*, **70**, 157 (1966); (d) T. Shimomura, K. J. Tölle, J. Smid, and M. Szwarc, *J. Amer. Chem. Soc.*, **89**, 796 (1967); (e) T. Shimomura, J. Smid, and M. Szwarc, *ibid.*, **89**, 5743 (1967).

(12) (a) H. Hostalka, R. V. Figini, and G. V. Schulz, *Makromol. Chem.*, **77**, 240 (1964); (b) H. Hostalka and G. V. Schulz, *J. Phys. Chem.* (Frankfurt am Main), **45**, 286 (1965); (c) W. K. R. Barnikol and G. V. Schulz, *ibid.*, **47**, 89 (1965).

(13) I. Sakurada, N. Ise, H. Hirohara, and T. Makino, *J. Phys. Chem.*, **71**, 3711 (1967).

(14) T. Fujimoto, N. Ozaki, and M. Nagasawa, *J. Polym. Sci., Part A*, **3**, 2259 (1965).

(15) It appears highly plausible that an unremoved trace of water can be electrolyzed by the application of the field to produce oxygen which can inhibit the polymerization. Thus the presence of the electric field gives rise to a "negative" field effect as mentioned in the text. The negative field effect has also been observed for free-radical polymerization of methylmethacrylate,<sup>1</sup> when the monomer had been allowed to absorb water. In this connection, Khalestskii, *et al.*, have reported<sup>16</sup> the "retarding" influence of an electric field on radical polymerization. It appears to us that this influence is due to the electrolysis of foreign substances, since no detailed description of reagent purification was given.

(16) M. M. Khalestskii and B. I. Sukhoruker, *Vysokomol. Soedin.*, **3**, 1347 (1961).



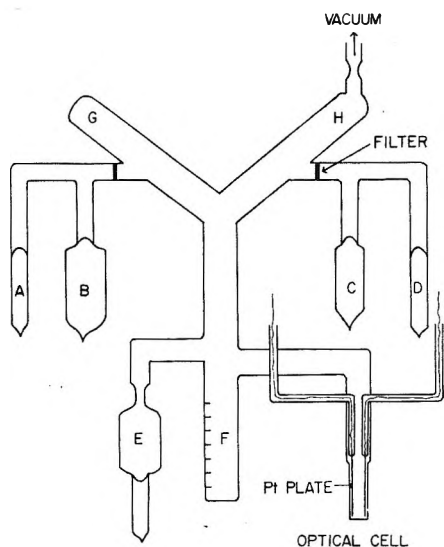


Figure 1. The apparatus used for kinetic studies of living polymerization under an electric field.

sealed off. The break-seals on ampoules A, C, and D were crushed, and, by turning the whole vessel upside down, the dilute solution of living polymer was admitted into G, and THF and the monomer solution into H. The apparatus was again turned upside down, the contents were vigorously shaken, and the mixture was allowed to collect in F. About 9 ml of the polymerizing solution was transferred into the attached optical cell, the cell was placed in a spectrophotometer, the recorder was switched on, and a high (dc) field was applied.

The quartz optical cell (optical path, 1 cm) was furnished with a pair of parallel platinum electrodes (cell constant,  $0.15 \text{ cm}^{-1}$ ). The spectrophotometer was an EPS-3T of Hitachi Manufacturing Co., Hitachi, Japan. The progress of polymerization was followed by monitoring the adsorption of styrene at  $291.5 \text{ m}\mu$ . The concentration of the living end was determined by measuring adsorption at  $335 \text{ m}\mu$  at regular intervals during the polymerization. The temperature of the optical cell was believed to be maintained at  $25 \pm 0.02^\circ$  by using a specially designed thermostated cell holder.

The spectrophotometric method was more appropriate for our purpose than the capillary flow technique, since a uniform electric field can be much more easily produced in the optical cell than in the capillary. By using spectrophotometry, the polymerization at concentrations of living ends lower than  $10^{-3} M$  could be investigated, as was noted earlier.<sup>11b</sup> At these concentrations, the polymerization proceeded fairly slowly. It can be claimed, therefore, that the field was applied during the whole course of polymerizations, though a stationary high field was set up about 15 sec later after the onset of the polymerization.

The initial monomer concentration of styrene was usually about 25 times that of the living end. The dielectric constants of the solvent mixtures were deter-

mined by using a capacitance bridge and a three-terminal guarded cell. The viscosity was determined with a Cannon-Ubbelohde viscometer.

The electric current caused by the application of the high field gives rise to two undesired phenomena, even though the current intensity was small. One is a temperature rise in the polymerizing solution. Under the present experimental conditions, calculations based on the assumption that the solution is adiabatic show that the maximum rise amounted to  $1.0^\circ$  in 30 sec, during which time most of the optical measurements were taken. According to control experiments performed without the cell holder mentioned above, a slow distillation of the solvent from the cell to F took place during a prolonged period. This was prevented by using a cell holder and by keeping the room temperature at about  $25^\circ$ . A second perplexing effect of the electric current is the electrolytical production of active propagating species or polymerization-initiating species. Since the elimination of this effect is most essential to our experiments, this matter will be discussed at length in the Discussion section.

## Results

The dielectric constant and viscosity of a series of mixtures of benzene and THF at  $25^\circ$  are given in Figure 2. The observed values of the pure liquids are in excellent agreement with the literature values. All of the polymerizations showed an internal first-order disappearance of styrene, as was observed previously.<sup>17</sup> The apparent propagation constant ( $k_p$ ) determined from our measurements is given as a function of the inverse half-power of the polystyryllithium concentration in Figure 3. According to Szwarc, *et al.*,<sup>11b</sup>

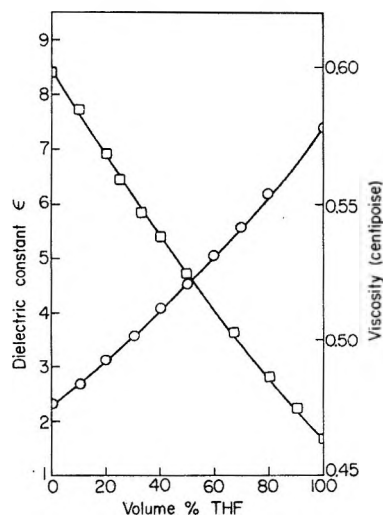


Figure 2. Dielectric constant (O), and viscosity (□) of THF-benzene mixtures at  $25^\circ$ .

(17) C. Geacintov, J. Smid, and M. Szwarc, *J. Amer. Chem. Soc.*, **84**, 2508 (1962).

the intercept of this plot gives the ion-pair propagation constant ( $k_p'$ ) and the slope is equal to  $k_p''K^{1/2}$ , where  $k_p''$  is the propagation constant of the free ion, and  $K$  is the dissociation constant of the ion pair.

The filled symbols and the blank ones in Figure 3 give the  $k_p$  values obtained in the presence of an electric field of 5 kV/cm and in its absence, respectively. Thus it is clear that the electric field increases the  $k_p''K^{1/2}$  values for THF contents of 30, 40, 50, and 60 vol %. On the other hand, the electric field has no influence on the  $k_p'$  values, which were 10.8, 19.0, 31, and 48  $M^{-1} \text{sec}^{-1}$  at THF contents of 30, 40, 50, and 60%, respectively.

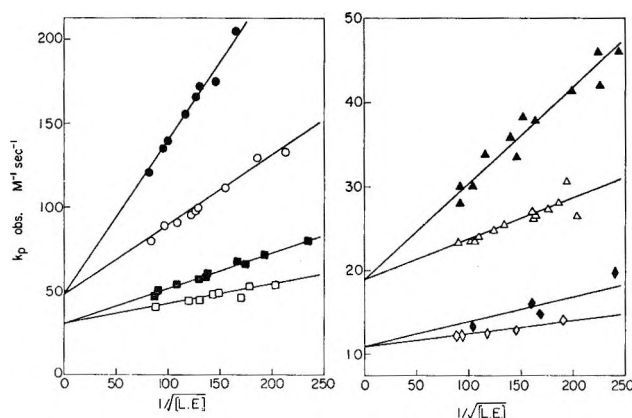


Figure 3. Dependence of the apparent propagation rate constant on poly(styryllithium) concentration at 25°. THF content (vol %): ●, ○, 60; ■, □, 50; ▲, △, 40; ◆, ◇, 30. The filled symbols are for 5 kV/cm, and the blank ones are for 0.

By combining the  $k_p''K^{1/2}$  values observed in the absence of the field and the  $K$  values (at 20°) reported by Bywater and Worsfold,<sup>10</sup> approximate values of  $k_p''$  can be estimated to be  $2 \times 10^4$ ,  $3 \times 10^4$ ,  $3.5 \times 10^4$ , and  $5 \times 10^4 M^{-1} \text{sec}^{-1}$  for THF contents of 30, 40, 50, and 60 vol %, respectively. These values are in good agreement with those reported earlier,<sup>10</sup> increasing with rising dielectric constant as was found earlier.<sup>10</sup>

At THF fractions of 10 and 20%, the  $k_p$  values were independent of the concentration of the living end both in the presence and absence of an electric field of 5 kV/cm. The  $k_p'$  values were 2.07 and 5.7  $M^{-1} \text{sec}^{-1}$  at 10 and 20%, respectively. No field effects on  $k_p$  and  $k_p'$  were observed.

Table I shows the field effects at various field strengths. The  $k_p''K^{1/2}$  values in the third column were determined based on the fact that  $k_p'$  is independent of the field strength.  $k_{p,E}''K_E^{1/2}/k_{p,0}''K_0^{1/2}$  is the ratio of the slopes of the  $k_p-1/\sqrt{[LE]}$  plot where  $[LE]$  is the concentration of the living end, with and without an electric field, which denotes the field-accelerating effect. It should be noted that the ratio increases with increasing field strength.

Table I: Field Effects at Various Field Strengths on the Living Anionic Polymerization of Styrene

THF vol fraction, %	Field strength, kV/cm	$k_p''K^{1/2}$ , $M^{-1/2} \text{sec}^{-1}$	$k_{p,E}''K_E^{1/2}/k_{p,0}''K_0^{1/2}$	$(K_E/K_0)^{1/2}$ (calcd)
40.0	0	0.05	1	1
	1.8	0.06	1.20	1.027
	4.0	0.09	1.80	1.056
	5.0	0.11	2.20	1.070
50.0	0	0.11	1	1
	1.0	0.12	1.09	1.012
	3.0	0.16	1.47	1.037
	5.0	0.20	1.82	1.061
	7.6	0.33	3.00	1.093
60.0	0	0.42	1	1
	0.5	0.46	1.09	1.006
	1.0	0.57	1.46	1.011
	2.0	0.77	1.83	1.022
	3.0	0.88	2.10	1.033
	5.0	0.91	2.16	1.055

## Discussion

It would be useful to mention at first the temperature effect on the apparent propagation rate constant ( $k_p$ ). According to Bywater and Worsfold,<sup>10</sup> the activation energy ( $E_{act}$ ) of the propagation process of the present system decreases with increasing THF content in the solvent. In the solvent mixtures, in which the field-accelerating effect was observed, the  $E_{act}$  value is believed to be smaller than 4 kcal. Thus the temperature rise due to the Joule effect, which amounts at the most to 1.0° under our experimental conditions, should increase the  $k_p$  value by 2%. The apparent increase in  $k_p$  resulting from the application of the field, on the other hand, is 55%, which greatly exceeds the temperature effect. Thus it was concluded that the observed field-accelerating effect is not due to the Joule effect.<sup>18</sup>

Next we turn to the possibility of the so-called electroinitiation mechanism.<sup>19</sup> Control experiments were carried out using monomer solutions containing no polystyryllithium. Application of an electric field (5 kV/cm) resulted in no change in the styrene absorption at 291.5  $m\mu$  and no living-end absorption at 335  $m\mu$ , even when approximately the same quantity of electricity was allowed to pass through the monomer solutions as in the case of polymerization. This fact rules out the possibility of the direct electron addition to the monomer by electrode reaction. Furthermore, it should be remarked that the time independence of the living-end concentration also excludes the possible role

(18) It is interesting to recall that in this laboratory field-accelerating effects were also observed for some cationic polymerizations which had negative apparent activation energies for their polymerization rates.

(19) See, for example: B. L. Funt, S. N. Bhadani, and D. Richardson, *J. Polym. Sci., Part A-1*, 2871 (1966); N. Yamazaki, S. Nakahama, and S. Kambara, *Polym. Lett.*, **B3**, 57 (1965).

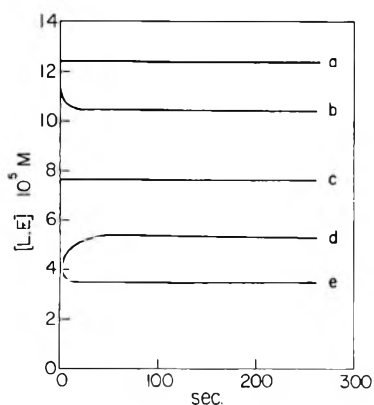


Figure 4. Time dependence of the concentration of living ends under an electric field at 25°C: a, d, e, polystyryllithium + monomer + solvent; b, c, polystyryllithium + solvent.

of the electroinitiation mechanism as follows. As curve a of Figure 4 shows, the living-end concentration in most cases stayed practically constant within the polymerization period. This implies that the living ends can be neither produced nor consumed by electrode reactions. The possibility that an equal amount of living ends can be produced at one electrode and simultaneously be consumed at the other can also be eliminated by curves b and c in Figure 4, which were obtained for polystyryllithium solution without monomers in the presence of the electric field (5 kV/cm). The results show that consumption, if it occurred at all, is only to a very small extent.

Furthermore, attention should be given to the fact that the field effect on the apparent propagation rate constant increases with decreasing living-end concentration (Figure 3), whereas the quantity of electricity being passed through the polymerizing solution, which is calculable from the field strength and current intensity, increases with increasing living-end concentration. By this experimental fact, we can assert that the observed field acceleration is not due to electrolytically initiated polymerization.<sup>20</sup>

It is to be noted further that the trend of decreasing of [LE] in the early stage of polymerization, as demonstrated by curves b and e, could be observed only when the high-vacuum line was clumsily handled so that the decrease was due to the introduction of retarding agents by electrolysis. We note that the increasing tendency demonstrated by curve d is associated with the decreasing trend of the specific conductivity<sup>22</sup> in the early stage of polymerization. The increase in [LE] was frequently observed when white precipitates were produced in *n*-BuLi solutions. Probably, an impurity (presumably LiBr) was reduced to metal lithium, from which a living anionic polymerization with two living ends started. When all of the LiBr was electrolyzed, [LE] reached a constant value. It should be noted that the  $k_p$  value was obtained from this constant value.

From the foregoing discussion, we conclude that the observed field-acceleration effect is not caused by the electroinitiation mechanism.<sup>23</sup> In previous papers<sup>1-7</sup> we ascribed the observed increase in the rate of cationic polymerizations to the second Wien effect, and we anticipated, as mentioned at the beginning of this paper, that the present anionic polymerization can be enhanced under an electric field as a result of this effect. As a matter of fact, the results show that the propagation rate constant was increased by the field. However, it should be noted that *the field influence was observed on the  $k_p''K^{1/2}$  term*. This situation invites some critical remarks on the mechanism of the field acceleration.

We confine ourselves to the field effect on  $K$ , namely, the second Wien effect. If the observed field effect is wholly attributed to the second Wien effect, the  $k_{p,E}''K_E^{1/2}/k_{p,0}''K_0^{1/2}$  given in the fourth column of Table I should be equal to  $K_E^{1/2}/K_0^{1/2}$ . According to the Onsager theory,<sup>24</sup> the field effect on the dissociation constant can be written

$$(K_E/K_0)^{1/2} = 1 + \frac{1}{2}b + \frac{1}{24}b^2 + \dots \quad (1)$$

where  $b = (9.636 \times 10^{-3})E/\epsilon T^2$  for 1:1-type electrolytes,  $E$  is the field intensity in kilovolts per centimeter, and  $\epsilon$  is the dielectric constant. The fifth column of Table I gives the  $(K_E/K_0)^{1/2}$  values calculated by eq 1. Evidently, the theoretical values are much smaller than the experimental ones given in the fourth column. This disagreement suggests first that the models and assumptions involved in the Onsager theory do not apply for the polymer systems. In this theory, the ions were assumed to be small metallic spheres. In our system, on the other hand, the living polymers having a degree of polymerization of about 15 at the onset of the polymerization exist in solvent containing benzene, which is a good solvent for polystyrene. Thus it is reasonable to assume a randomly coiled and partially free-draining model for the living polymers. This con-

(20) We recall here that the conductivity increase of weak-electrolyte solutions under high-intensity electric fields is independent of the pulse duration, if the latter is larger than the threshold value characteristic of electrolytes.<sup>21</sup> This independence supports the conclusion that the observed conductivity increase does not have its origin in the electrolysis but is due to the field-facilitated dissociation of the weak-electrolyte molecules, or the second Wien effect.

(21) H. C. Eckstrom and C. Schmelzer, *Chem. Rev.*, **24**, 367 (1939).

(22) The specific conductivity was obtained from the field strength and current intensity. Being determined by such an inaccurate method, it is not intended to develop a quantitative discussion of conductivity. We note, however, that a linear relation was obtained between the logarithm of the equivalent conductivity and that of the living-end concentration with a slope of  $-1/2$ , indicating the coexistence of free ions and ion pairs.

(23) Various evidence against the electroinitiation mechanism was discussed for cationic polymerizations.<sup>1-7</sup> Among them, the field influence on the monomer reactivity ratio in copolymerizations most definitely excluded the role of the electrolytical initiation,<sup>7</sup> since the reactivity ratio is determined solely by the propagation process.

(24) L. Onsager, *J. Chem. Phys.*, **2**, 599 (1934).

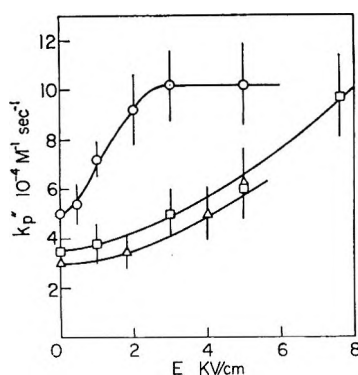


Figure 5. Field-intensity dependence of the free-ion rate constant at 25°. THF content (vol %): O, 60; □, 50; △, 40.

tradiates the metallic sphere model. Accordingly, the failure of the theory does not exclude the second Wien effect as a potential factor causing the observed field effect.<sup>25</sup>

The disagreement between theory and experiment may then be interpreted to imply that the free-ion rate constant ( $k_p''$ ) becomes larger with increasing field intensity, if the Onsager theory correctly accounts for the field-facilitated dissociation phenomenon taking place in the present system. By using the Onsager theory and the observed values of  $k_{p,E}''K_E^{1/2}/k_{p,0}''K_0^{1/2}$ ,  $k_{p,E}''$  was calculated and is shown in Figure 5 as a function of the field strength. In this calculation, the  $k_{p,0}''$  value was taken as  $5 \times 10^4$ ,  $3.5 \times 10^4$ , and  $3 \times 10^4 M^{-1} \text{sec}^{-1}$  for THF contents of 60, 50, and 40 vol %, respectively. It is seen from Figure 5 that  $k_{p,E}''$  increases with increasing field intensity. At a THF content of 60 vol %, the  $k_{p,E}''$  reaches a constant value of  $\sim 10^5 M^{-1} \text{sec}^{-1}$  above 3 kV/cm.

It has been suggested that the anionic growing chain ends of a free-ion type can be solvated by THF molecules *only weakly*.<sup>11b,d</sup> If this is true, it would be tempting to suggest that THF molecules can be removed by the applied electric field so that the desolvated growing ends become more accessible to monomers. Furthermore, the limiting value of  $k_{p,E}''$  ( $\sim 10^5 M^{-1} \text{sec}^{-1}$ ) might be ascribed to the "naked" growing ends. This interpretation appears to be supported by the experimental fact that  $k_{p,E}''$  values at lower THF contents (and hence at lower dielectric constants) increase more slowly with increasing field strength, as shown in Figure 5;<sup>26</sup> in other words, the lower the dielectric constant, the higher the field strength necessary to strip the THF molecules from the growing ends. This would be understandable if the solvation is primarily determined by the coulombic forces.

The desolvation theory seems to be acceptable at first sight. However, it is accompanied by the following defects. It should be pointed out that the intensity of the applied electric field ( $\sim 10^3 \text{ V/cm}$ ) is considerably lower than that due to a univalent ion, which may

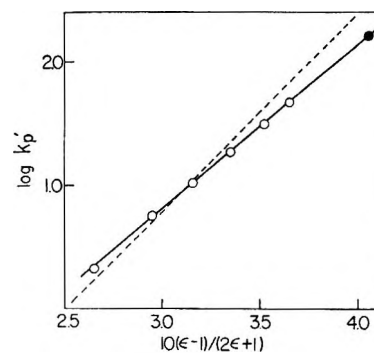


Figure 6. Dielectric constant dependence of the ion-pair rate constant at 25°: O, present work; ●, previous work;<sup>11b</sup> ---, previous work at 20°.<sup>10</sup>

amount to as much as  $10^7 \text{ V/cm}$  at 1-Å separation. The calculation by the Born<sup>27</sup> and Moelwyn-Hughes theories<sup>28</sup> shows that it is impossible to remove the solvent molecules from the growing chain ends by an external field, although the application of these theories to the present case is fairly questionable. Thus if desolvation is responsible for the observed increase in  $k_p''$ , forces other than coulombic ones must be predominant. This is inconceivable under the usual conditions.

From the foregoing discussion, it is clear that further studies are necessary in order to find out the true case for the observed field acceleration. High-precision conductivity measurements are urgently needed to judge the pros and cons of the interpretation in terms of the second Wien effect. Simultaneously, studies on the solvation state of the growing chain ends are also indispensable. Efforts along this line are currently being made in this laboratory.

These experiments show that the ion-pair propagation rate constant ( $k_p'$ ) is not affected by the electric field. The field intensity used in the present work was not high enough to vary the distance between charge centers of the ion pairs.

The Laidler-Eyring theory<sup>29</sup> on reaction rates between dipole molecules can be written

$$\frac{d \ln k}{d \left( \frac{\epsilon - 1}{2\epsilon + 1} \right)} = -\frac{1}{kT} \left( \frac{\mu_A^2}{r_A^3} + \frac{\mu_B^2}{r_B^3} - \frac{\mu_{\pm}^2}{r_{\pm}^3} \right) \quad (2)$$

where  $\mu$  and  $r$  are the dipole moment and radius, respectively, and A and B and  $\pm$  indicate the reactants and

(25) A most direct evidence for the Wien effect should be obtainable from the electric conductivity increase by the electric field. The conductivity determined as noted above was not, however, reliable enough to show the increase with increasing field.

(26) Experiments at field intensity higher than 8 kV/cm were impossible because of electric discharge in the optical cell.

(27) M. Born, *Z. Phys.*, **1**, 45 (1920).

(28) E. A. Moelwyn-Hughes, *Proc. Cambridge Phil. Soc.*, **45**, 477 (1948).

(29) K. J. Laidler and H. Eyring, *Ann. N. Y. Acad. Sci.*, **39**, 303 (1940).

critical complex, respectively. Figure 6 shows that eq 2 holds for the present systems. The filled circle, which denotes the result reported for 100% THF,<sup>11b</sup>

falls on the linear relation. The broken line in Figure 6 gives the results reported previously for 20%.<sup>10</sup> The agreement is fairly satisfactory.

## The Gibbs Free Energy of Transfer of the Alkali Perrhenates and Perchlorates between Pure Water and Pure Nitromethane

by G. R. Haugen

*Department of Thermochemistry and Chemical Kinetics, Stanford Research Institute, Menlo Park, California 94025*

and H. L. Friedman

*Department of Chemistry, State University of New York at Stony Brook, Stony Brook, New York 11790*  
(Received June 12, 1968)

Previously reported partition and salting-out experiments in the ternary system nitromethane, water, and electrolyte were combined with two series of new experiments to furnish the Gibbs free energy of transfer of each of the electrolytes between the various solvents. The determination of the partition of  $\text{CsClO}_4$  between the equilibrium water and nitromethane phases and the determination of the solubility of  $\text{LiReO}_4$  in nitromethane as a function of the concentration of added water are reported herein. The standard Gibbs free energies of formation at 25° of the ions Li, Na, K, Rb, Cs,  $\text{ClO}_4$ , and  $\text{ReO}_4$  in each of the solvents, of water saturated with nitromethane, of nitromethane saturated with water, and of pure nitromethane are reported. In addition, the standard Gibbs free energies of formation of the ions H, Cl, I,  $\text{Cr}(\text{NH}_3)_2(\text{SCN})_4$ , and  $\text{PF}_6$  in some of these solvents are reported. Both the electrostatic and nonelectrostatic contributions to the free energy of transfer of an ion from pure water to pure nitromethane tend to make this free energy more negative for larger ions. The Gibbs free energy of transfer of an electrolyte between pure water and pure nitromethane is accurately given by the Born charging processes. The specific solvation effects are apparently more noticeable in enthalpies and entropies of transfer than the free energies.

### Introduction

The changes in free energy, enthalpy, and entropy accompanying the solvation of a series of ions of similar structure are quantities that are fundamental to a molecular-level understanding of electrolyte solutions in the solvent. The changes in the same thermodynamic quantities accompanying the transfer of a series of ions from one solvent to another are also important. While more complicated than the solvation energies, the energetics of transfer have the advantage of being experimentally accessible for complex as well as for monatomic ions. A recent study of enthalpies of transfer from water to several aprotic solvents<sup>1</sup> illustrates what one may learn from such data, even with only a qualitative treatment.

The free energies of transfer are perhaps most directly determined by either emf cell measurements, including polarography, or by measurement of the ratio of the solubility of a salt in the two solvents, but it often happens that these methods are not applicable in a case of interest. The problem of obtaining accurate free

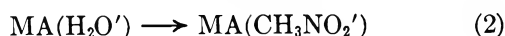
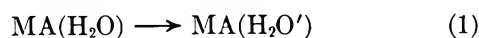
energy data in nonaqueous solvents is complicated by the increase in ion-ion interaction in the saturated salt solutions in these solvents and the difficulty of finding reversible electrodes that operate in these solvents. Furthermore, the systematic study of a group of similar ions is handicapped by the difficulty encountered in finding a series of salts with the right properties.

In a series of earlier publications<sup>2-4</sup> we have worked out an indirect, but rather general, method for determining free energies of transfer and applied it to the transfer of the alkali metal ions from water to nitromethane.

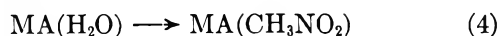
This method comprises the following steps for the

- (1) H. L. Friedman, *J. Phys. Chem.*, **71**, 1723 (1967).
- (2) G. R. Haugen and H. L. Friedman, *ibid.*, **60**, 1303 (1956).
- (3) H. L. Friedman and G. R. Haugen, *J. Amer. Chem. Soc.*, **76**, 2060 (1954).
- (4) G. R. Haugen and H. L. Friedman, *J. Phys. Chem.*, **67**, 1757 (1963).

transfer of the electrolyte MA from pure water to pure nitromethane at 25°



where  $\text{H}_2\text{O}'$  represents water saturated with nitromethane (1.99 mol of nitromethane/kg of water) and  $\text{CH}_3\text{NO}_2'$  represents nitromethane saturated with water (1.27 mol of water/kg of nitromethane). The standard free energy change,  $\Delta G_1$ , of the first process was determined by measuring the salting out of nitromethane by MA in aqueous solutions.<sup>2</sup> The standard free energy change,  $\Delta G_2$ , of the second process was determined by measurements of the partition of MA between aqueous and nitromethane phases in equilibrium.<sup>3</sup> The standard free energy change,  $\Delta G_3$ , of the third process was determined by measurements of the salting-out interaction of water and MA in nitromethane. The standard state of the electrolyte is defined as a hypothetical 1 *m* state in each case, but this is 1 mol of electrolyte/kg of water in the solvent range from  $\text{H}_2\text{O}$  to  $\text{H}_2\text{O}'$ , while it is 1 mol of electrolyte/kg of nitromethane in the solvent range from  $\text{CH}_3\text{NO}_2$  to  $\text{CH}_3\text{NO}_2'$ . The sum of these three processes is



so the desired standard free energy of transfer,  $\Delta G_4$ , is easily computed from these data.

As has been emphasized in the earlier work,<sup>1-4</sup> all of these standard free energy changes are additively constituted of ionic contributions, and this provides the possibility of an experimental check of the accuracy of the data for each process. For the present purpose, it also provides another advantage, namely, that different salts may be employed in the various processes in order to facilitate the experimental work, so long as there is a sufficiently complete body of data to enable all of the desired salt transfers to be constructed by means of the ionic additivity principle.

In the present paper two series of new experiments are reported: one to determine  $\Delta G_2$  for  $\text{CsClO}_4$  in order to obtain  $\Delta G_4$  for perchlorates, as well as perrhenates, and one to determine  $\Delta G_3$  for  $\text{LiReO}_4$ .

#### Measurement of $\Delta G_2$ for $\text{CsClO}_4$

The partition of  $\text{CsClO}_4$  was studied by equilibrating accurately known amounts of  $\text{CsClO}_4$ , water, and nitromethane at 24.92° and then analyzing each phase for  $\text{CsClO}_4$  by an application of a conductivity method.<sup>4,5</sup> After equilibration, the two phases were carefully separated, the denser nitromethane phase was sampled from the bottom of the equilibration vessel through a Teflon stopcock, thus preventing trapping of small quantities of the water phase. The error in the material balance ranged from 2% low to 2% high. This is a

satisfactory agreement, in view of the low concentration. The experimental partition coefficient ( $P = C_{\text{CH}_3\text{NO}_2}^2/C_{\text{H}_2\text{O}}^2$ , where  $C_{\text{CH}_3\text{NO}_2}$  is the concentration of  $\text{CsClO}_4$  in the nitromethane phase and  $C_{\text{H}_2\text{O}}$  is the concentration of  $\text{CsClO}_4$  in the water phase) is given in Table I.

**Table I:** Distribution of Cesium Perchlorate between Water and Nitromethane at 24.92° (Equilibrium Electrolyte Molalities and Partition Ratios)

$10^3 C_{\text{H}_2\text{O}}$ <i>m</i>	$10^4 C_{\text{CH}_3\text{NO}_2}$ <i>m</i>	$10^2 P$
7.848	10.95	1.947
7.610	10.50	1.904
1.510	1.998	1.751
5.818	8.155	1.965
1.189	1.586	1.779

The partition coefficient extrapolated to infinite dilution<sup>2,5</sup> was found to be  $1.83 \times 10^{-2}$ . This yields  $\Delta G_2 = 2.37$  kcal/mol for  $\text{CsClO}_4$ .

#### Determination of $\Delta G_3$ for $\text{LiReO}_4$

The material preparation and the measurement procedures have been described earlier.<sup>4</sup> A few additional measurements were made in order to reduce the uncertainties in interpretation.

The results of all of the determinations of the solubility  $e_s$  (the molality of the electrolyte in the saturated solution) in nominally dry nitromethane are shown in Table II. In consideration of the likely errors in the various measurements, we take  $1.0 \times 10^{-4}$  *m* as the best value (the average of the three lowest measurements). The dependence of the saturation molality,

**Table II:** Solubility of  $\text{LiReO}_4$  in Dry Nitromethane at 25°

Solubility, $\mu\text{m}$	Drying procedure								
	A <sup>a</sup>	B <sup>b</sup>	C <sup>c</sup>	D <sup>d</sup>	E <sup>e</sup>	F <sup>f</sup>	G <sup>g</sup>		
	213	156	151	97	93	109	288	250	189

<sup>a</sup> Solvent fractionally distilled at 1 atm in a steady-state column as described in ref 4, dry salt. <sup>b</sup> Solvent from A distilled from Drierite under high vacuum, dry salt. <sup>c</sup> Solvent from A distilled from  $\text{P}_4\text{O}_{10}$  at 1 atm, dry salt. <sup>d</sup> Solvent from A distilled from  $\text{P}_4\text{O}_{10}$  under high vacuum, dry salt. <sup>e</sup> Solvent from A; salt equilibrated with 0.3 *m*  $\text{H}_2\text{O}$  in nitromethane, then washed in dry solvent. <sup>f</sup> Solvent from A; salt equilibrated with 0.06 *m*  $\text{H}_2\text{O}$  in nitromethane, then washed with dry solvent. <sup>g</sup> Spectrograde solvent distilled from  $\text{P}_4\text{O}_{10}$  at 160 torr in 50-plate column; solubility determined both conductometrically and gravimetrically. The figure given is the average of four determinations agreeing within 5  $\mu\text{m}$ .

(5) G. R. Haugen, Ph.D. Thesis, University of Southern California, 1962.

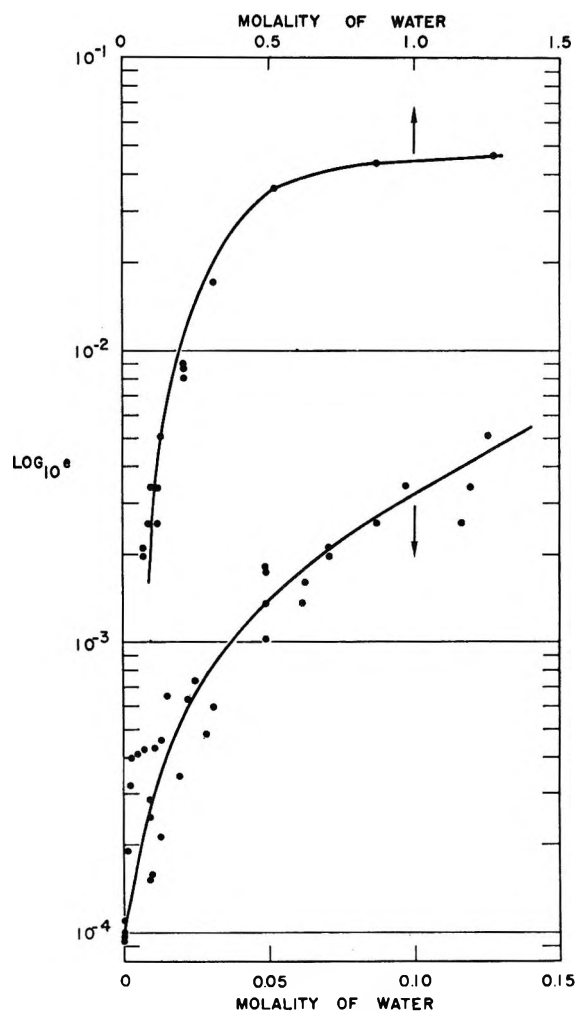


Figure 1. The solubility of  $\text{LiReO}_4$  in nitromethane as a function of added water concentration at  $25^\circ$ . The smooth curve through the data is employed in the calculations in the paper.

$e_s$ , on  $w$ , the molality of water in nitromethane, is shown in Figure 1. As in an earlier work,<sup>4</sup>  $e$  and  $w$  are both taken as the moles of solute per kilogram of nitromethane in these ternary mixtures. The scatter of the data is large compared with what has been achieved in other systems,<sup>4</sup> but the dependence of the solubility of the salt on the added water is much larger than in those other systems, so it seems worthwhile to proceed with an analysis of the data.

In view of the very large effect and the appearance of strong inflections in Figure 1, one may suspect that the interaction of  $\text{LiReO}_4$  with  $\text{H}_2\text{O}$  in nitromethane is more of a chemical effect involving definite stoichiometry than a medium effect as found in the other systems.<sup>4</sup> However, it is found that for a series of solutions of compositions  $e = 2 \times 10^{-4} m$  and  $w \leq 10^{-3} m$ , the equivalent conductance at  $25^\circ$  is well represented by the equation<sup>6</sup>

$$\Lambda = 111 + (1.3 \times 10^4)w \quad (5)$$

The linear dependence on  $w$  is characteristic of a

medium effect. Furthermore, the large value of  $\Lambda$  indicates that the electrolyte is completely dissociated. On the other hand, the graph of  $\Lambda$ , as a function of  $e$  for solutions with  $w = 0.84 m$ , is found to be similar to the conductance curve for aqueous  $\text{MgSO}_4$ , which would suggest that the electrolyte is about 50% associated at this value of  $w$  and  $e = 0.04 m$ . Such a small extent of association is hard to separate from activity coefficient effects.<sup>7</sup> The extent of association is expected to decrease with either increasing  $w$  or decreasing  $e$ , so the association is expected to be most important in the saturated solutions near  $w = 0.8 m$ . In case that the association takes effect over the whole range,  $0.2 m \leq w \leq 1.27 m$ , the variation of the free energy could be diminished by  $0.5 \text{ kcal/mol}$ .<sup>5</sup> However,  $\Delta G_3$  is determined in the limit of vanishing electrolyte molality; i.e., only the ion-water interaction contributes to the free energy,  $\Delta G_3$ .

For the interpretation of Figure 1, we need several results, obtained by Smith and Long<sup>8</sup> in their study of the system  $\text{LiReO}_4\text{-H}_2\text{O}$ . At  $25^\circ$  the solid phase in equilibrium with the saturated aqueous solution is  $\text{LiReO}_4 \cdot 2\text{H}_2\text{O}$ , and the solution is  $12.6 m$  in  $\text{LiReO}_4$ . Some other relevant results are summarized in Table III.

Table III:  $\text{LiReO}_4$  System at  $25^\circ$   
(Data of Smith and Long<sup>8</sup>)

	Activity of water at equil	$\Delta G^\circ$ , kcal/mol
$\text{LiReO}_4 \cdot 2\text{H}_2\text{O}(s) \rightarrow \text{LiReO}_4(aq) + 2\text{H}_2\text{O}(aq)$	0.50	-3.5 <sup>a</sup>
$\text{LiReO}_4 \cdot \text{H}_2\text{O}(s) + \text{H}_2\text{O}(l) \rightarrow \text{LiReO}_4 \cdot 2\text{H}_2\text{O}(s)$	0.32	-0.7
$\text{LiReO}_4(s) + \text{H}_2\text{O}(l) \rightarrow \text{LiReO}_4 \cdot \text{H}_2\text{O}(s)$	0.11	-1.3

<sup>a</sup> The osmotic coefficient of the saturated solution is 1.53, close to that of  $12.6 m \text{ LiNO}_3(aq)$ : R. A. Robinson and R. H. Stokes, "Electrolyte Solutions," Butterworth and Co. Ltd., London, 1955, p 504. It was assumed that  $\gamma_{\pm}$  is also the same as in  $12.6 m \text{ LiNO}_3(aq)$  (3.10), and  $\Delta G^\circ$  was calculated accordingly.

Now in Figure 1, as  $w$  ranges from 0 to  $1.27 m$ , the water activity,  $a_w$ , ranges from 0 to about 0.96, the latter estimated by applying Raoult's law to the aqueous phase in equilibrium with (wet) nitromethane. Therefore, the solid phase in equilibrium with the saturated solutions in Figure 1 ranges from  $\text{LiReO}_4$  at  $w = 0$  to  $\text{LiReO}_4 \cdot 2\text{H}_2\text{O}$  at  $w = 1.27 m$ . Were the solutions of water in nitromethane ideal, the transition from the

(6) We are grateful to Miss T. Sun for technical assistance with these measurements which were made at the IBM Research Center, Yorktown Heights, N. Y., and to Dr. V. R. G. Moorti for the measurements at large  $w$ , which were made at Stony Brook.

(7) E. A. Guggenheim, *Trans. Faraday Soc.*, **56**, 1159 (1960).

(8) W. T. Smith, Jr., and S. H. Long, *J. Amer. Chem. Soc.*, **70**, 354 (1948).

anhydrous salt to the monohydrate would occur at  $w = 0.1 m$ , and the transition from the mono- to the dihydrate would occur at  $w = 0.3 m$ . However, we know from the incomplete mixing of water and nitromethane at this temperature that the graph of  $a_w$  as a function of  $w$  must be convex upward, so each of these transitions occurs at a lower value of  $w$  than indicated above. The available data do not provide any very clear signals as to where the transitions are, so we have assumed that the first is at  $w = 0.05 m$  and the second is at  $w = 0.20 m$ . The results are not very sensitive to these assumptions.

From these considerations and those in the earlier work,<sup>4</sup> it follows that  $-\Delta G_3$  can be calculated as the sum of the three terms

$$I = \int_0^{0.05} (\partial\mu_e/\partial w)_{e=0} dw \quad (6)$$

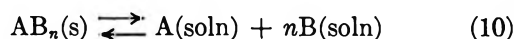
$$II = \int_{0.05}^{0.20} (\partial\mu_e/\partial w)_{e=0} dw \quad (7)$$

$$III = \int_{0.20}^{1.27} (\partial\mu_e/\partial w)_{e=0} dw \quad (8)$$

For term I, the general equation previously given<sup>4</sup> reduces to

$$I = -2RT \ln [e_s(w = 0.05)/e_s(w = 0)] = -3.14 \text{ kcal/mol} \quad (9)$$

For terms II and III, we need to consider equilibria of the form



for which we derive the equation<sup>9</sup>

$$(\partial\mu_A/\partial m_B)_{m_A} = \frac{S(\partial\mu_A/\partial \ln m_A)_{m_B} - n(\partial\mu_B/\partial m_B)_{m_A}}{1 - nm_A S} \quad (11)$$

where  $S$  is the experimentally observed (Figure 1) solubility interaction coefficient

$$S = -(\partial \ln m_A/\partial m_B)_{\mu, AB_n} \quad (12)$$

For the present problem, we identify A with the electrolyte and B with water. We then have

$$(\partial\mu_A/\partial \ln m_A)_{m_B} \sim 2RT \quad (13)$$

$$(\partial\mu_B/\partial m_B)_{m_A} \sim (RT/a_B)(\partial a_B/\partial m_B)_{m_A}$$

so in the notation used elsewhere in this paper, we have for eq 11

$$(\partial\mu_e/\partial w)_e = [2RTS - (nRT/a_w)(\partial a_w/\partial w)_e]/(1 - neS) \quad (14)$$

$$S \equiv -(\partial \ln e/\partial w)_{\mu, n\text{-hydrate}} \quad (15)$$

We make the additional assumption that the derivative at fixed  $e$  in eq 14 is the same as the derivative at  $e = 0$ , a reasonable approximation at the low values of

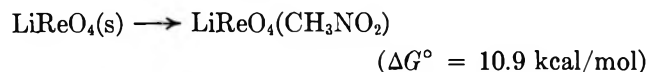
$e$  in these experiments provided that water-induced ion pairing is negligible. Now we can evaluate the integrals, defining II and III to get

$$II = -3.00 \text{ kcal/mol} \quad (16)$$

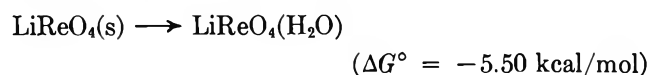
$$III = -3.00 \text{ kcal/mol} \quad (17)$$

The result is that for  $\text{LiReO}_4$  we have  $\Delta G_3 = 9.14$  kcal/mol and  $\Delta G_4 = 15.20$  kcal/mol where, for  $\Delta G_4$ , we have used the results of earlier work for  $\Delta G_1 + \Delta G_2$ .

We may also calculate  $\Delta G_4$  as the difference in the standard free energy of solution of  $\text{LiReO}_4(s)$  in dry nitromethane and in water. Estimating  $\gamma_{\pm}$  in the saturated solution in dry nitromethane as 0.97, we have



while from Table III we have



The result is  $\Delta G_4 = 16.4$  kcal/mol for  $\text{LiReO}_4$ .

#### $\Delta G_4$ Results

With the earlier measurements and the new data, we can compute  $\Delta G_4$  for the alkali perchlorates and perchlorates. The results are given in the second column of Table IV. They are not all independent determinations: in the computations of the steps  $\Delta G_1$ ,  $\Delta G_2$ , and  $\Delta G_3$  from the data, extensive use has been made of the fact that all these standard free energies of transfer comprise additive ionic contributions.

Another test of these results may be made by calculating  $\Delta G_4$  from the measured solubilities by means of the equation

$$\Delta G_4 = 2RT \ln [(m\gamma)_{\text{aq}}/(m\gamma)_{\text{nitromethane}}] \quad (18)$$

which is applicable when the solid phase in equilibrium with the saturated aqueous solution has the same composition as that in equilibrium with the saturated nitromethane solution. The  $m$  and  $\gamma$  are, respectively, the molal salt concentration and the mean ionic activity coefficient in the saturated solution. The required data are summarized in Table IV and the resulting  $\Delta G_4$  is given in the last column. The agreement between values of  $\Delta G_4$  determined by the two methods is excellent, except for  $\text{LiReO}_4$  and  $\text{NaReO}_4$ , the salts for which  $\Delta G_3$  is the most difficult to determine. It is also for these salts that the estimation of  $\gamma_{\pm}$  for the saturated

(9) Provided that the activity coefficient correction for the electrolyte in these systems is negligible, eq 11 is easily modified to take into account the association of the electrolyte:  $(\partial\mu_A/\partial m_B)_{m_A} = [(2RTS/\alpha\sqrt{1+4km_A}) - n(\partial\mu_B/\partial m_B)_{m_A}]/(1 - nm_A S)$ , where  $\alpha$  represents the degree of dissociation and  $k$  is the association constant (see ref 5 for the nonideal-solution case). As the electrolyte concentration approaches a low value, the effect of ion pairing diminishes with respect to the ion-water interaction, and the modified equation reduces to eq 14, providing that the observed slope,  $(\partial \ln e/\partial w)_{\mu, n\text{-hydrate}}$  for each hydrate is independent of electrolyte concentrations. Figure 1 demonstrates that this is apparently the case.



**Table IV:** Standard Free Energy of Transfer from Pure Water to Pure Nitromethane at 25°

Salt	$\Delta G_t$ (stepwise method) kcal/mol	Satd aqueous solution		Satd nitromethane solution		$\Delta G_t$ (solubility ratio method), kcal/mol
		$\epsilon$	$\gamma_{\pm}$	10%	$\gamma_{\pm}^a$	
LiReO <sub>4</sub>	15.2 ± 0.5	12.6	3.1 <sup>b</sup>	0.96	0.97	16.4 <sup>b</sup>
NaReO <sub>4</sub>	9.52 ± 0.3	5.05	0.64 <sup>c</sup> 0.39 <sup>d</sup>	0.43	0.43	10.4 10.1
KReO <sub>4</sub>	5.47 ± 0.2	0.0408	0.83 <sup>e</sup>	0.374	0.93	5.4
RbReO <sub>4</sub>	4.36 ± 0.2	0.0380	0.83 <sup>e</sup>	0.905	0.90	4.4
CsReO <sub>4</sub>	3.34 ± 0.2	0.0246	0.85	1.36	0.89	3.4
KClO <sub>4</sub>	5.11 ± 0.2	0.157	0.73	1.96	0.86	5.0
RbClO <sub>4</sub>	3.96 ± 0.2	0.0675	0.79	2.88	0.84	3.6

<sup>a</sup> All estimated by means of the Guntelberg equation:  $\ln \gamma_{\pm} = -A\sqrt{I}/(1 + \sqrt{I})$ , where  $A$  is the Debye-Hückel limiting-law coefficient for nitromethane. <sup>b</sup> This calculation is discussed in the section entitled Determination of  $\Delta G_t$  for LiReO<sub>4</sub>. <sup>c</sup> Assuming  $\gamma_{\pm}(\text{NaReO}_4) = \gamma_{\pm}(\text{NaClO}_4)$  at the same concentration. <sup>d</sup> Assuming  $\gamma_{\pm}(\text{NaReO}_4) = \gamma_{\pm}(\text{NaNO}_3)$  at the same concentration. <sup>e</sup> Assuming  $\gamma_{\pm}(\text{MReO}_4) = \gamma_{\pm}(\text{MClO}_4)$  at the same concentration.

solution of the salt in pure water (column 6, Table IV) is most uncertain. There are characteristic uncertainties in the determination by eq 18, which are different from those in the stepwise method, so the extent of agreement is good evidence that the stepwise method is reliable.

The Gibbs free energies of transfer allow the calculation of the standard free energies of formation of the various ions in each of the solvents studied, water saturated with nitromethane, nitromethane saturated with water, and pure nitromethane. All of our data in this series are summarized in this way in Table V. The choice of  $\Delta G_f^\circ(\text{Na}^+) = 0$  is arbitrary, but we do not have all the data needed for the usual  $\text{H}^+$  convention.

## Discussion

The transfer of the salt from pure water to pure nitromethane may be represented by the following steps: (1) removal of the charges of the ions in the solvent water, (2) transfer of the discharged ions from water to nitromethane, and (3) recharge of the ions in nitromethane.

Accordingly, the free energy of transfer,  $\Delta G_t$ , can be regarded as the sum of a mainly electrostatic term,  $\Delta G_{\text{es}}$ , corresponding to the combined effects of steps 1 and 3, and a nonelectrostatic term,  $\Delta G_{\text{nes}}$ , corresponding to the effect of step 2.

The nonelectrostatic term was identified with the free energy of transfer of the neutral species with the same atomic and electronic structures as the ions; the neutral species for the ions  $\text{ReO}_4^-$ ,  $\text{H}^+$ ,  $\text{Na}^+$ ,  $\text{K}^+$ ,  $\text{Rb}^+$ , and  $\text{Cs}^+$  were approximated by the following species:  $\text{OsO}_4$ ,  $\text{He}$ ,  $\text{Ne}$ ,  $\text{Ar}$ ,  $\text{Kr}$ , and  $\text{Xe}$ . In Figure 2, we compare  $\Delta G_{\text{es}}$  and  $\Delta G_{\text{nes}}$  defined in this way. It should be remarked that both terms increase as the alkali metal ion gets smaller, but the effect is much larger for  $\Delta G_{\text{es}}$ . The broken curve in Figure 2 represents the analogous decomposition of  $\Delta G_t + \Delta G_2$  into electrostatic and nonelectrostatic parts. Apparently, water in nitromethane

**Table V:** Standard Free Energy of Formation (kcal/mol) at 25°, Relative to  $\Delta G_f^\circ(\text{Na}^+) = 0$  (Hypothetical 1 *m* Standard States)

Ion	H <sub>2</sub> O <sup>a</sup>	10.6 wt	98.5 wt	CH <sub>3</sub> NO <sub>2</sub>
		% CH <sub>3</sub> NO <sub>2</sub> (H <sub>2</sub> O satd with CH <sub>3</sub> NO <sub>2</sub> )	% CH <sub>3</sub> NO <sub>2</sub> (CH <sub>3</sub> NO <sub>2</sub> satd with H <sub>2</sub> O)	
H <sup>+</sup>	62.59	62.40	61.89	...
Li <sup>+</sup>	-7.51	-7.49	-7.09	-1.83
Na <sup>+</sup> <sup>b</sup>	0.00	0.00	0.00	0.00
K <sup>+</sup>	-4.88	-5.00	-6.75	-8.93
Rb <sup>+</sup>	-4.86	-5.06	-7.46	-10.02
Cs <sup>+</sup>	-8.21 <sup>c</sup>	-8.43	-11.55	-14.39
ClO <sub>4</sub> <sup>-</sup>	60.02	59.81	65.30	69.17
ReO <sub>4</sub> <sup>-</sup>	-104.51 <sup>d</sup>	-104.81	-98.87	-94.99
Cl <sup>-</sup>	31.24	31.39	...	...
I <sup>-</sup>	50.25	...	70.5 <sup>e</sup>	...
Cr(NH <sub>3</sub> ) <sub>2</sub> (SCN) <sub>4</sub> <sup>-</sup>	...	<i>l</i> <sup>f</sup>	<i>l</i> <sup>f</sup> + 0.94	...
PF <sub>6</sub> <sup>-</sup>	...	<i>s</i> <sup>g</sup>	<i>s</i> <sup>g</sup> + 3.26 <sup>f</sup>	...

<sup>a</sup> Free energies in water are from "Selected Values of Chemical Thermodynamic Properties," National Bureau of Standards, Circular 500, U. S. Government Printing Office, Washington, D. C., 1952. <sup>b</sup>  $\Delta G_f^\circ(\text{Na}^+)$  defined as zero in each solvent. <sup>c</sup> H. L. Friedman and M. Kahlweit, *J. Amer. Chem. Soc.*, **78**, 4243 (1956). <sup>d</sup> G. E. Boyd, J. W. Cobble, and W. T. Smith, *ibid.*, **75**, 5784 (1953). <sup>e</sup> Estimated from the solubility data of D. T. Walden, *Z. Phys. Chem. (Leipzig)*, **A55**, 683 (1906). <sup>f</sup> Reported in Progress Report, Atomic Energy Commission Contract AT(11-1)-113, Project No. 2, Senior Investigator, Dr. H. L. Friedman, Department of Chemistry, University of Southern California, Los Angeles, Calif., 1953-1954. <sup>g</sup> Unknown values.

has the same effect on  $\text{Cs}^+$ ,  $\text{Rb}^+$ , and  $\text{K}^+$  but a much larger effect on  $\text{Na}^+$  and a still larger effect on  $\text{Li}^+$ . This very large effect on  $\text{Li}^+$  suggests selective solvation of the ion by water in nitromethane. However, as noted above, the conductivity measurements in mixtures of small amounts of water and LiReO<sub>4</sub> with nitromethane give no hint of a stoichiometric  $\text{Li}^+ - \text{H}_2\text{O}$  interaction.

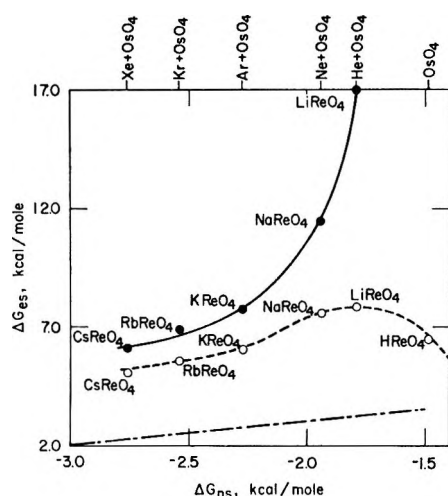


Figure 2. Correlation of electrostatic and nonelectrostatic free energies of transfer: —, transfer from water to pure nitromethane; ----, transfer from water to nitromethane saturated with water; - · - · -, line of unit slope. The abscissa values were calculated from the observed solubilities of the nonelectrolytes (H. L. Friedman, *J. Amer. Chem. Soc.*, **76**, 3284 (1954)).

It is of interest to see how well  $\Delta G_{es}$  is accounted for by the difference in the Born charging process in water and nitromethane. There is the usual problem in evaluating this term, an uncertainty as to what to use for the ionic radii. For this comparison, we follow the suggestion of Voet<sup>10,11</sup> that a solvent-characteristic term  $\Delta_+$  is to be added to the crystal radii of cations and another term  $\Delta_-$  is to be added to the crystal radii of anions. Then, using the  $\Delta_{+,-}$  values for water, derived by Latimer, Pitzer, and Slansky,<sup>11</sup> we find that  $\Delta G_{es}$  is accurately given by the appropriate combination of Born charging processes if in nitromethane we take  $\Delta_+ = 1.09 \text{ \AA}$  and  $\Delta_- = 0.00 \text{ \AA}$ , as shown in Figure 3.<sup>12</sup>

This good agreement allows little encouragement for looking for specific solvation effects in the data. Such effects are apparently much more noticeable in enthalpies and entropies of transfer than in free energies. However, the result that a larger  $\Delta_+$  is required in nitromethane than in water ( $\Delta_+ = 0.85 \text{ \AA}$ ) indicates that, aside from the dielectric constant effect, nitromethane is intrinsically a poorer solvent for cations than is water, whether because of the fact that the cation cannot get so close to the center of negative charge

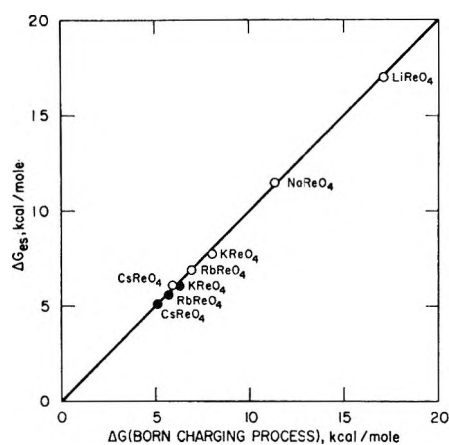


Figure 3. Comparison of the theoretical Born charging equation with the electrostatic portion of the observed free energy of transfer: O, the transfer between pure water and pure nitromethane (NM) ( $\Delta(\text{anion}) = 0.00$ ,  $\Delta(\text{cation}) = 1.09$ ); ●, the transfer between pure water and nitromethane saturated with water ( $\Delta(\text{anion}) = 0.10$ ,  $\Delta(\text{cation}) = 0.99$ ). The solid line represents the prediction of the Born charging equation,  $(z^2/2)\{[1 - (1/D_{H_2O})]\{[1/(R(+)) + \Delta_{H_2O}(+)]\} + [1/(R(-)) + \Delta_{H_2O}(-)]\} - [1 - (1/D_{NM})]\{[1/(R(+)) + \Delta_{NM}(+)] + [1/(R(-)) + \Delta_{NM}(-)]\}\}$ .

in nitromethane, the interpretation following from the discussion of  $\Delta_+$  given by Latimer, Pitzer, and Slansky, or because of other effects such as solvent basicity, which are gathered into the parameter  $\Delta_+$ .

The fact that the  $\Delta_-$  value found is less than that for water ( $0.10 \text{ \AA}$ ) is perhaps a clue that specific effects would be found in the free energies of transfer of a series of anions. The only comparison possible with the present data is for  $\text{ClO}_4^-$  and  $\text{ReO}_4^-$ ;  $\Delta G_4$  is  $0.4 \text{ kcal/mol}$  larger for the latter. This is opposite to the trend with size exhibited by the positive ions. This may be a manifestation of known effects in aqueous solution, for example,  $\text{ReO}_4^-$  being less a structure breaker than  $\text{ClO}_4^-$ ,<sup>13</sup> and it shows the importance of gathering more data on thermodynamics of transfer.

(10) A. Voet, *Trans. Faraday Soc.*, **32**, 1301 (1936).

(11) W. M. Latimer, K. S. Pitzer, and C. M. Slansky, *J. Chem. Phys.*, **7**, 108 (1939).

(12) The crystal radius of  $\text{ReO}_4^-$  is estimated from the Re-O bond length ( $1.84 \text{ \AA}$ ) and the van der Waals radius of oxygen ( $1.40 \text{ \AA}$ ) to be  $3.24 \text{ \AA}$ .

(13) M. Eisenstadt and H. L. Friedman, *J. Chem. Phys.*, **48**, 4445 (1967).

## Tracer Studies of Acid-Catalyzed Reactions. VIII. Langmuir Kinetics in Cycloalkane Isomerization over Silica-Alumina

by Joe W. Hightower and W. Keith Hall

Carnegie-Mellon University, Mellon Institute, Pittsburgh, Pennsylvania 15213 (Received June 12, 1968)

A series of static, microcatalytic, and steady-state flow experiments, designed to study the kinetics of cyclopropane and methylcyclopropane isomerization to olefins over silica-alumina, has demonstrated that the reactions may be reasonably well explained by a simple steady-state theory involving activation of the adsorbed cycloparaffin to a carbonium ion. The reaction orders varied between zero and first in different reactant pressure regions and increased toward unity as the temperature was increased. In general, the results could be explained by Langmuir-Hinshelwood kinetics. An isotopic-tracer technique was used to obtain information concerning the relative magnitude of the rate constants  $k_{-1}$  and  $k_2$  which determine the fate of the adsorbed surface complex, *i.e.*, the probability of its being desorbed as an unisomerized reactant or as an isomerized product molecule, respectively. Traditionally (Langmuir-Hinshelwood theory)  $k_{-1}$  has been assumed to be much larger than  $k_2$ , but for cyclopropane the two rate constants were about equal, and for methylcyclopropane  $k_2$  was considerably larger than  $k_{-1}$ . The treatment was therefore modified to agree with a simple picture in which cyclopropane is hydrogen bonded to an acidic hydrogen atom, becomes activated to a nonclassical carbonium ion, and either isomerizes or returns to the ground state.

### Introduction

Acids have long been known to catalyze the isomerization of cyclopropane and alkylcyclopropanes.<sup>1</sup> A number of oxides<sup>2</sup> are also catalysts for these reactions, and the activity of these solids has been attributed to their acidic nature. We<sup>3,4</sup> have recently used deuterium tracers to demonstrate that over silica-alumina the isomerization of both cyclopropane (CP) and methylcyclopropane (MCP) occurred *via* intermolecular hydrogen-transfer mechanisms, probably involving metastable ( $c\text{-C}_n\text{H}_{2n+1}^{\oplus}$ ) surface complexes. These surface species were formed not by direct interaction with Brønsted sites intrinsically present on the catalyst but by reaction of a substrate molecule with a proton supplied by a carbonaceous "residue" (coke) which was rapidly formed on its freshly pretreated surface. A similar picture, involving a *sec*-butyl carbonium ion complex, also explained all of the observations for interconversion of the *n*-butenes over silica-alumina.<sup>5-8</sup>

Whereas several investigators have clearly shown that the *n*-butene reactions over such catalysts are first order in reactant, the kinetics of the cyclopropanes have not been firmly established. Roberts<sup>2</sup> reported that no simple reaction order was followed during CP isomerization over several oxides. Bassett and Habgood<sup>9</sup> used a microcatalytic technique to demonstrate first-order kinetics over a relatively inactive sodium-X zeolite at high temperatures, and Larson, Gerberich, and Hall<sup>10</sup> suggested that similar behavior occurred over amorphous aluminosilicates at lower temperatures.

In order to gain a clearer insight into the kinetics of CP and MCP isomerization over silica-alumina, these reactions were studied in static, microcatalytic, and

steady-state flow reactors. It is the purpose of this communication to show that the results can be reasonably well explained by a Langmuir-Hinshelwood formulation. A tracer technique was used to evaluate the relative magnitudes of certain rate constants in the Langmuir-Hinshelwood equation which heretofore have not been amenable to experimental observation.

### Experimental Section

**Catalyst.** The Houdry M-46 silica-alumina (12.5% alumina) had a surface area of 270 m<sup>2</sup>/g and was ground and sieved to 40-60 mesh for all experiments. Pretreatment included slowly heating under vacuum to 530°, followed by calcining in O<sub>2</sub> and overnight evacuation at the same temperature. The catalysts were preconditioned by treatment with several charges or pulses of reactant at the desired reaction temperature until the conversion rates became reproducible.

- (1) C. R. Noller, "Chemistry of Organic Compounds," W. B. Saunders Co., Philadelphia, Pa., 1957, p 831.
- (2) R. M. Roberts, *J. Phys. Chem.*, **63**, 1400 (1959).
- (3) H. R. Gerberich, J. W. Hightower, and W. K. Hall, *J. Catalysis*, **8**, 391 (1967).
- (4) J. W. Hightower and W. K. Hall, *J. Am. Chem. Soc.*, **90**, 851 (1968).
- (5) J. W. Hightower, H. R. Gerberich, and W. K. Hall, *J. Catalysis*, **7**, 57 (1967).
- (6) J. W. Hightower and W. K. Hall, *J. Phys. Chem.*, **71**, 1014 (1967).
- (7) J. W. Hightower and W. K. Hall, *J. Am. Chem. Soc.*, **89**, 778 (1967).
- (8) J. W. Hightower and W. K. Hall, *Am. Inst. Chem. Engrs., Symposium Series*, **63**, 122 (1967).
- (9) D. W. Bassett and H. W. Habgood, *J. Phys. Chem.*, **64**, 769 (1960).
- (10) J. G. Larson, H. R. Gerberich, and W. K. Hall, *J. Am. Chem. Soc.*, **87**, 1880 (1965).

*Gases.* Cyclopropane was purchased from Ohio Chemical and Surgical Equipment Co., and MCP was an API standard sample. Perdeuteriocyclopropane and MCP were obtained from Merck Sharp and Dohme of Canada, Ltd. The latter was purified by glpc, and all reactants were twice distilled from  $-78$  to  $-195^\circ$  immediately before use. The Airco helium was passed through an activated charcoal trap thermostated at  $-195^\circ$ .

*Techniques.* The same 1.0-g catalyst sample held in a tubular reactor was used for both the microcatalytic and steady-state flow experiments. The catalyst bed filled loosely a 1-cm i.d. glass tube to a depth of about 2 cm. The temperature was maintained constant within  $\pm 0.5^\circ$  by means of a Thyatron regulated-resistance furnace above  $100^\circ$  and with a water bath below  $100^\circ$ . In the microcatalytic experiments, pulses of CP could be introduced by manipulation of stopcocks from a 5-cm<sup>3</sup> doser into a stream of helium flowing at various rates over the catalyst at 1 atm total pressure. The pulse size was varied by using different pressures of CP in the doser and then diluting the hydrocarbon with He. Products were collected in a trap thermostated at  $-195^\circ$  before being flashed into another helium stream which carried them into a 30 ft  $\times$  0.25 in. propylene carbonate on Chromosorb W glpc column at  $0^\circ$  for analysis.

In the steady-state flow experiments, He-CP mixtures were passed at a total pressure of 1 atm over the catalyst and through a constant-volume trap at room temperature. After steady-state conditions had been attained, the trap was by-passed and its contents were swept into the analytical glpc column. The partial pressure of the CP could be varied by means of a needle valve, but the *absolute* partial pressures could not be measured very accurately in these experiments. However, a measure of the *relative* partial pressure was obtained from the chromatographic data. Because the trap had a constant volume, the sum of the areas under the product propylene and CP peaks (sensitivities for the two compounds were essentially the same) was directly proportional to the initial pressure of CP; hence, the ratios of the total areas gave the *relative* initial CP pressures in any two experiments.

In the static experiments, 30 mg (for MCP) or 100 mg (for CP) of catalyst was placed in the bottom of a 20-mm o.d. tube which extended 4 in. below a 250-cm<sup>3</sup> spherical reactor; the total reactor volume was about 300 cm<sup>3</sup>. Measured amounts of reactants from a BET vacuum system were frozen into the reactor, which was then warmed rapidly to reaction temperature. Samples amounting to 1-5% of the total mixture were periodically removed for glpc analysis (a silver nitrate-ethylene glycol on firebrick column at  $0^\circ$  was used in addition to the propylene carbonate column for complete separation of the MCP products).

The same static reactor was used for the tracer ex-

periments, where the reactants were 1:1 mixtures of perdeuterio and lightweight materials. The separated products were trapped at  $-195^\circ$  and subjected to analysis for deuterium content at low ionizing voltages using a 6-in. radius Nuclide mass spectrometer. Under these conditions, fragmentation was less than 10%, and the usual corrections were made for naturally occurring <sup>13</sup>C, as well as for fragmentation.

*Treatment of Data. Static Experiments.* Adsorption isotherms (*vide infra*) of cyclopropane on silica-alumina indicated that the quantity of the reactant adsorbed was negligibly small compared with that in the gas phase of the reactor. For this reason the reaction could be followed accurately by observing concentration changes in the gas phase. To obtain an estimate of the *simple* reaction order  $n$  (of course the reaction might be more accurately described by a more complicated expression but over a limited pressure range  $n$  may be relatively constant), the equation

$$-\frac{dP}{dt} = kP^n \quad (1)$$

was transformed into one involving fractional conversion,  $x$ , and the initial partial pressure,  $P_0$ , by substituting  $P = P_0(1 - x)$ . The *initial* rate of conversion is

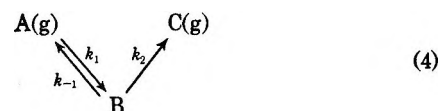
$$P_0 \left( \frac{dx}{dt} \right)_0 = kP_0^n \quad (2)$$

This equation was normalized for a given series of experiments (each at the same temperature using the same reproducible catalyst sample) to the lowest initial partial pressure,  $P_0^0$ , which yielded the fastest initial fractional conversion rate,  $(dx/dt)_0^0$ , as determined from aliquots of the gas phase. In logarithm form, a linear equation results, *viz.*

$$\log \left( \frac{P_0}{P_0^0} \right) = \frac{1}{n-1} \log \frac{(dx/dt)_0}{(dx/dt)_0^0} \quad (3)$$

whose slope is  $1/(n-1)$ .

According to the Langmuir-Hinshelwood hypothesis, the surface reaction of a single reactant can be formulated in terms of an adsorption isotherm<sup>11,12</sup> depicted in the scheme



Under steady-state conditions, *i.e.*, constant surface coverage  $\theta$ , the number of molecules being adsorbed ( $k_1P(1 - \theta)$ ) must equal the number being desorbed as

(11) C. N. Hinshelwood, "The Kinetics of Chemical Change," Oxford University Press, London, 1955.

(12) K. J. Laidler and I. M. Socquet, *J. Phys. Colloid Chem.*, **54**, 519 (1950).

reactants ( $k_{-1}\theta$ ) plus those reacting to form products ( $k_2\theta$ ). This assumption results in the equation

$$\theta = \frac{k_1 P}{k_{-1} + k_2 + k_1 P} \quad (5)$$

which becomes the normal Langmuir equation

$$\theta = \frac{KP}{1 + KP} \quad (6)$$

where the adsorption equilibrium constant  $K = k_1/(k_{-1} + k_2)$ . In the usual treatment  $k_{-1}$  is assumed to be much larger than  $k_2$ , and  $K$  then becomes the ratio  $k_1/k_{-1}$ . Note that inhibition by product has been assumed negligible in this treatment.

If the rate is proportional to coverage, *i.e.*

$$-(dP/dt) = k_2\theta \quad (7)$$

the reaction may be expressed in terms of initial fractional conversion rate  $(dx/dt)_0$  and initial pressure  $P_0$  by the linear equation

$$\frac{1}{(dx/dt)_0} = \frac{1}{k_2 K} + \frac{P_0}{k_2} \quad (8)$$

Again normalizing the results of a single series of experiments to the lowest initial pressure and the fastest initial fractional conversion rate, the equation becomes

$$\frac{(dx/dt)_0^0}{(dx/dt)_0} = \frac{1 + KP_0}{1 + KP_0^0} = \frac{1}{1 + A} + \frac{A}{1 + A} \left( \frac{P_0}{P_0^0} \right) \quad (9)$$

where  $A = KP_0^0$ . A plot of  $(dx/dt)_0^0/(dx/dt)_0$  vs.  $P_0/P_0^0$  should yield a straight line whose slope and intercept may be combined to give a value for  $K$  through the equation

$$K = \frac{\text{slope}}{P_0^0(\text{intercept})} \quad (10)$$

From its value,  $\theta$  may be calculated for any pressure from eq 6.

Once  $K$  has been evaluated, an integrated form of eq 7 may be used to relate the fractional conversion to time for a single reaction at initial pressure  $P_0$ , *viz.*

$$-2.303 \log(1 - x) - KP_0(1 - x) = k_2 K t - KP_0 \quad (11)$$

A straight line should be obtained when the entire left side of eq 11 is plotted against time.

*Steady-State Flow Experiments.* As with the static reactor, the reaction rates in the steady-state flow reactor were reduced to fractional conversion where  $(dx/dt)_0$  represents the initial, or differential, reaction rate obtained by plotting  $x$  vs. reciprocal flow rate for small values of  $x$ . The reactant partial pressure could be varied over a limited range and the *simple* reaction order,  $n$ , determined from plots according to eq 3.

In the Langmuir-Hinshelwood treatment, the normalized initial fractional conversion rates were plotted against  $P_0/P_0^0$  to determine the adsorption equilibrium constant  $K$  in eq 9. The extent of adsorption does not alter the definition of the fractional conversion rate determined from the gas phase in the steady-state reactions.

*Microcatalytic Experiments.* Data from the microcatalytic experiments could not be treated in the same way as data from the static and steady-state flow reactors because a significant fraction of each pulse was adsorbed on the catalyst. This caused pulse broadening and destroyed the simple relationship between fractional conversion and the gas-phase pressure.

The Langmuir-Hinshelwood scheme may be applied to the microcatalytic data in the following way. Let  $V$  ( $\text{cm}^3$ ) be the unfilled volume in a 1 cm long bed containing weight  $W$  (g) of catalyst. At low conversions, where the partial pressure of product is negligible compared with reactant, the molar concentration of adsorbed reactant  $Q$  (per g) is related to the pressure through the equation

$$Q = \frac{KQ_m P}{1 + KP} \quad (12)$$

where  $Q_m$  represents the specific monolayer capacity of the adsorbent and  $K$  is the equilibrium constant previously defined. The total number of moles,  $N$ , of reactant per 1-cm length of bed is then

$$N = \frac{PV}{RT} + \frac{KQ_m WP}{1 + KP} \quad (13)$$

If one assumes that the reaction rate is proportional to the amount of material adsorbed (*i.e.*, the surface reaction is rate controlling), the rate becomes

$$-\frac{dN}{dt} = k_2' Q W = \frac{k_2' K Q_m W P}{1 + KP} \quad (14)$$

Equation 13 may be differentiated to yield

$$\frac{dN}{dt} = - \left[ \frac{V}{RT} + \frac{KQ_m W}{1 + KP} - \frac{K^2 Q_m W P}{(1 + KP)^2} \right] \frac{dP}{dt} \quad (15)$$

which may be combined with eq 14 to give a complex equation relating  $dP/dt$  to the other variables. At low conversions where the microcatalytic reactor approximates a differential reactor,  $P \rightarrow P_0$  and

$$-\left( \frac{dP}{dt} \right)_0 = \frac{k_2' K Q_m W P_0}{\frac{V}{RT}(1 + KP_0) + K Q_m W - \frac{K^2 Q_m W P_0}{1 + KP_0}} \quad (16)$$

which at low pressures (where  $KP_0 \ll 1$ ) reduces to

$$-\left( \frac{dP}{dt} \right)_0 = \frac{k_2' K Q_m W P_0}{\frac{V}{RT} + K Q_m W} \quad (17)$$

and at high pressures ( $KP_0 \gg 1$ ) reduces to

$$-\left(\frac{dP}{dt}\right)_0 = \frac{k_2 Q_m W}{V/RT} \quad (18)$$

These equations can also be formulated in terms of fractional conversion by setting  $dx = -d(N/N_0)$ . Equation 13 gives  $N_0$  when  $P = P_0$ . Dividing the corresponding members of eq 14 by those of eq 13 yields the desired relationship, which for the initial conditions reduces to

$$\left(\frac{dx}{dt}\right)_0 = -\left[\frac{d(N/N_0)}{dt}\right]_0 = \frac{k_2 K Q_m W P_0}{(1 + KP_0) \frac{P_0 V}{RT} + K Q_m P_0 W} \quad (19)$$

and which can be inverted and rewritten as

$$\frac{1}{(dx/dt)_0} = \frac{1}{k_2'} + \frac{V}{k_2' K Q_m W R T} + \frac{P_0 V}{k_2 Q_m W R T} = D + E P_0 \quad (20)$$

where  $D = (1/k_2') + (V/k_2' K Q_m W R T)$  and  $E = V/k_2 Q_m W R T$ . For a given catalyst and temperature,  $D$  and  $E$  will be constants, and the initial rate will be a function only of  $P_0$ . Within a given series of experiments, then, the initial rates may be normalized to the lowest initial partial pressure,  $P_0^0$ , which corresponds to the fastest initial fractional conversion rate,  $(dx/dt)_0^0$ , viz.

$$\frac{(dx/dt)_0^0}{(dx/dt)_0} = \frac{D + E P_0}{D + E P_0^0} = \frac{D}{D + E P_0^0} + \frac{E P_0^0}{D + E P_0^0} \left(\frac{P_0}{P_0^0}\right) \quad (21)$$

Equation 21 is analogous to eq 9 derived for the static reactor. It must be remembered, however, that  $P_0$  is the initial partial pressure of the reactant *after* part of the pulse has been physically adsorbed.

**Tracer Experiments.** In the tracer experiments involving 1:1 mixtures of perdeuterio and lightweight molecules, the hydrogen atoms exchanged per molecule in the products were calculated<sup>7</sup> from

$$\text{(atoms exchanged)/(molecule)} = \sum_{i=0}^n i d_i + \sum_{i=n+1}^{2n} (2n - i) d_i \quad (22)$$

where  $n$  is the number of carbon atoms in the molecule, and  $d_i$  is the fraction of the molecules having  $i$  deuterium atoms.

## Results

The kinetics of cyclopropane isomerization were investigated over silica-alumina by observing the effect of varying the initial partial pressure in static, micro-

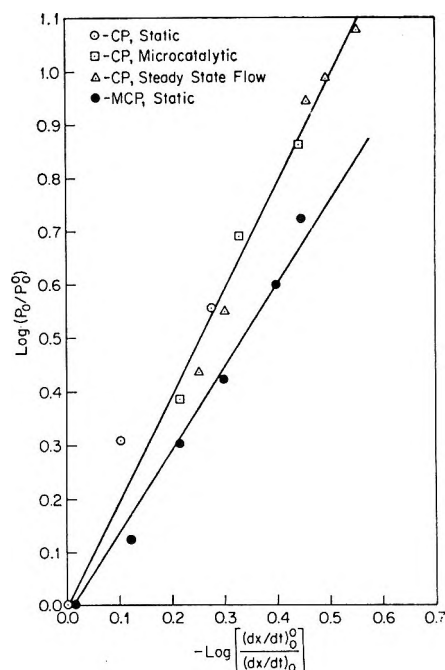


Figure 1. Plot showing the effect of initial partial pressure on initial reaction rate during cyclopropane and methylocyclopropane isomerization to olefins over silica-alumina. The slope is related to the simple apparent reaction order,  $n$ , through eq 3.

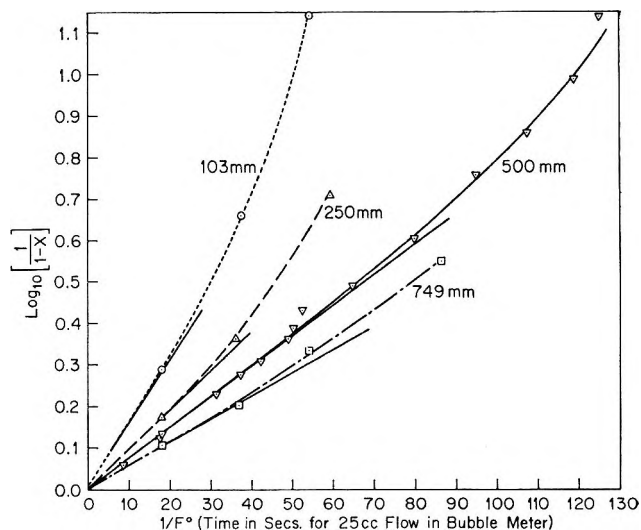


Figure 2. First-order plot of microcatalytic conversion of cyclopropane to propylene over silica-alumina for various pulse sizes at 150°; see eq 23.

catalytic, and steady-state flow reactors. In Figure 1 the relative initial rates have been plotted against relative initial pressures according to eq 3 to provide an estimate of the *simple* reaction order,  $n$ . Although such a plot is strictly applicable only for the static and steady-state cases, the microcatalytic results were included also. In this case, the initial pressures were assumed proportional to the pressure in the doser. The three sets of data for cyclopropane almost superim-

**Table I:** Effect of Reactant Partial Pressure on Reaction Rate during Cyclopropane and Methylcyclopropane Isomerization over Silica-Alumina (Langmuir Treatment)

Initial pressure, $P_0$ , mm	Rel initial pressure, $P_0/P_0^0$	Pressure in doser, mm	Calcd initial pressure, $P_0$ , mm	Calcd initial surface coverage, $\theta_0 = KP_0/(1 + KP_0)$	Rel initial rates, $(dx/dt)_0/(dx/dt)_0^0$	Calcd rel initial rates, $(1 + KP_0^0)/(1 + KP_0)$
Cyclopropane, Static Reactor, 150°						
27.6	1.00	...	...	0.37	1.00	1.00
56.1	2.03	...	...	0.54	0.79	0.72
101.7	3.68	...	...	0.68	0.53	0.50
Cyclopropane, Microcatalytic Reactor, 150°						
...	1.00	103	...	...	1.00	...
...	2.43	250	...	...	0.61	...
...	4.92	507	...	...	0.47	...
...	7.27	749	...	...	0.36	...
Cyclopropane, Flow Reactor, 150°						
...	1.00	...	6.8	0.13	1.00	1.00
...	2.73	...	18.6	0.28	0.56	0.58
...	3.54	...	24.1	0.34	0.50	0.53
...	8.78	...	59.7	0.56	0.35	0.36
...	9.68	...	65.8	0.58	0.32	0.34
...	11.87	...	80.7	0.63	0.28	0.30
Methylcyclopropane, Static Reactor, 50°						
53	1.33	...	...	0.45	0.75	0.89
106	2.65	...	...	0.62	0.51	0.61
40	1.00	...	...	0.39	1.00	1.00
212	5.30	...	...	0.77	0.36	0.38
53	1.33	...	...	0.45	0.75	0.89
159	3.98	...	...	0.71	0.40	0.47
40	1.00	...	...	0.39	0.97	1.00
80	2.00	...	...	0.56	0.61	0.72

posed and gave a reaction order of about 0.5 at 150°. The reaction order tended to increase toward unity at higher temperatures and to decrease as the temperature was lowered below 150°. A plot of data from static MCP isomerization at 50° is also included in Figure 1; for it  $n \approx 0.4$ .

In Figure 2 the results from the microcatalytic isomerization experiments have been plotted according to the first-order Bassett and Habgood equation<sup>9</sup>

$$kK' = \frac{F^0}{273RW} \ln \left( \frac{1}{1-x} \right) \quad (23)$$

for various pressures of cyclopropane in the 5.0-cm<sup>3</sup> doser;  $k$  is the reaction rate constant,  $K'$  an adsorption equilibrium constant,  $R$  the gas constant, and  $W$  the weight of catalyst. Had the kinetics been first order, all curves in Figure 2 would have superimposed; obviously, this was not the case. Furthermore, the curves deviated from linearity at high contact time in a direction consistent with the reactions being less than first order. It is thus apparent that the equation of Bassett and Habgood<sup>9</sup> cannot be used to fit our results.

After the first four to six pulses, the combined areas under propylene and cyclopropane peaks were propor-

tional to the pressure in the doser and equal to the cyclopropane area in the blank determination for each pressure. Since the data of Figure 2 were taken on "lined-out" catalysts, the observed deviations from the first-order law could not be attributed to a pressure-dependent process, *e.g.*, polymerization of product olefin. The straight lines drawn tangent to the curves at low conversion in Figure 2 represent the initial rates,  $(dx/dt)_0$ , which were normalized before recording in column 6, Table I.

All of the data for both CP and MCP have been plotted in Figure 3 according to the normalized Langmuir-Hinshelwood equations (eq 9 and 21), and the results are summarized in Table I. From the slope and intercepts of these plots, together with the absolute value of  $P_0^0$ , the adsorption equilibrium constant  $K$  could be calculated by eq 10. Since only in the static experiments were the absolute values of the initial pressure known, only in those cases could  $K$  be determined explicitly. For cyclopropane at 150°,  $K = 0.0212 \text{ mm}^{-1}$ ; for MCP at 50°,  $K = 0.0157 \text{ mm}^{-1}$ . However, since  $K$  is assumed to be a function only of the temperature according to Langmuir-Hinshelwood formulation, the value calculated in the static cyclopropane experiments should hold for the steady-state

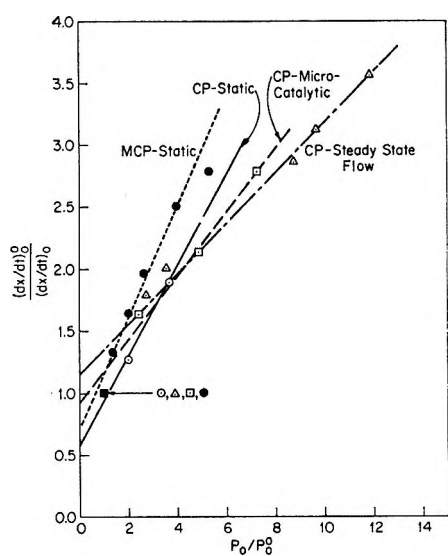


Figure 3. Langmuir-Hinshelwood plot relating initial reaction rate to initial partial pressure during cyclopropane and methylcyclopropane isomerization to olefins over silica-alumina; see eq 9 and 21.

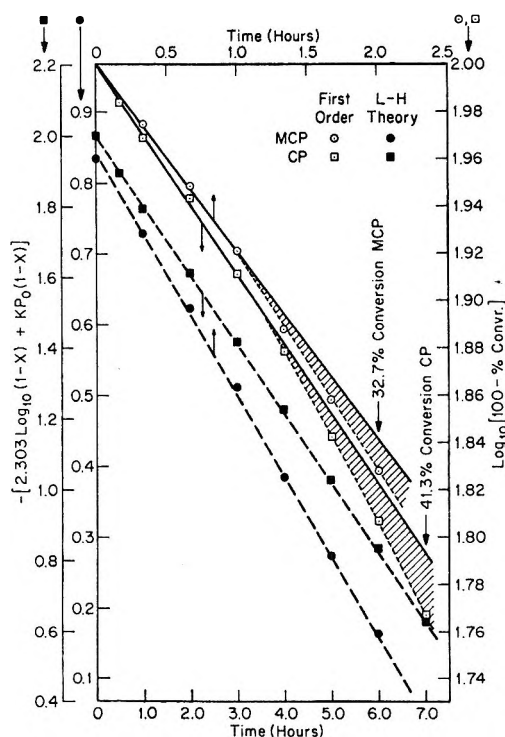


Figure 4. Langmuir-Hinshelwood and first-order plots contrasting fit of time-dependent data from cyclopropane and methylcyclopropane isomerization to olefins over silica-alumina; shaded areas indicate deviation from linearity on first-order plots.

flow experiments at the same temperature as well. With this assumption the absolute values for the initial pressures can be calculated; these results are shown in column 4, Table I. The highest calculated initial partial pressure (80.7 mm) in the flow experi-

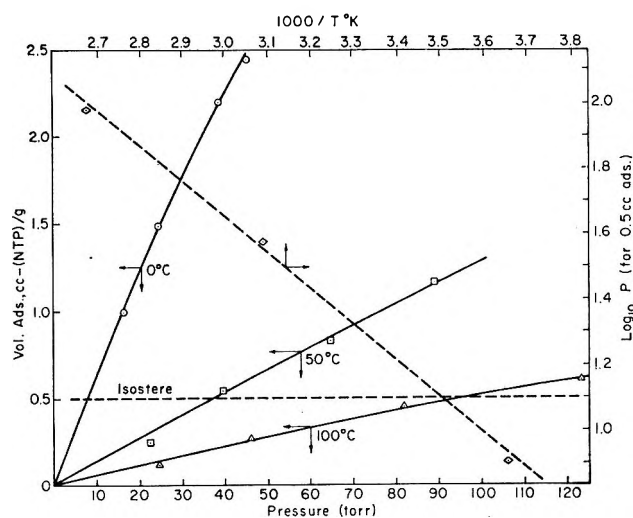


Figure 5. Adsorption of cyclopropane on silica-alumina. Isostatic heat is 5.5 kcal/mol.

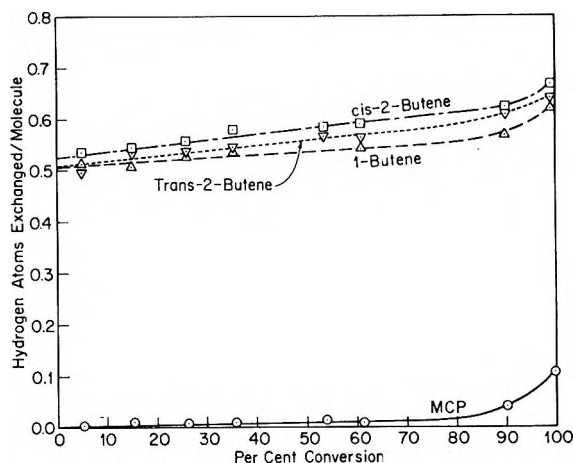


Figure 6. Exchange concentration curves for coisomerization of methylcyclopropane- $d_0, d_6$  over silica-alumina.

ment was in approximate agreement with a crude measurement which indicated about a 10:1 helium-cyclopropane reactant mixture; this would correspond to an initial partial pressure of about 76 mm. The initial surface coverage,  $\theta_0$ , may also be calculated from  $K$  and the  $P_0$  values may be calculated from eq 6; the values are given in column 5, Table I.

The same isomerization data (from a static reactor) have been plotted for both reactants in Figure 4 in accordance with both time-dependent eq 11 and the first-order law. Linear curves were obtained with both reactants for the Langmuir-Hinshelwood model, but significant deviations from linearity were observed when the same data were plotted on a strictly first-order basis. In another experiment the Langmuir-Hinshelwood plot for cyclopropane at 150° showed a small deviation from linearity above 80% conversion.

The volume of cyclopropane adsorbed on the catalyst was determined from the isotherms shown in Figure



5. The isosteric heat of adsorption at 0.5 cm<sup>3</sup> (NTP)/g was 5.2 ± 0.3 kcal/mol; Hall, Lutinski, and Gerberich<sup>13</sup> obtained a heat of adsorption of 5.5 kcal/mol from the variation of the chromatographic retention time with temperature in the same temperature region. Extrapolation of the data to 150° indicates that a pressure of over 200 mm would be required to cause 0.5-cm<sup>3</sup> adsorption on 1 g of catalyst. It was reported earlier that an irreversible "residue" amounting to about 1 cm<sup>3</sup> (NTP)/g formed on the surface under reaction conditions.<sup>10</sup> This would not, however, affect the pressure dependence.

The intercepts near 0.5 of the exchange concentration curves in Figure 6 indicate that the MCP isomerization reactions all involved an intermolecular exchange of one hydrogen atom.<sup>4,7,8</sup> Similar data for CP are presented in ref 10. Intermolecular scrambling among reactant molecules accompanied isomerization, but this process was much more extensive for CP than for MCP.

### Discussion

The results plotted in Figures 1 and 2 show that isomerizations of both CP and MCP to olefins over silica-alumina have apparent orders significantly less than unity. Furthermore, the apparent orders were not unique but are functions of temperature and pressure. These are characteristics of Langmuir-Hinshelwood behavior, and the reasonably straight lines in Figures 3 and 4 indicate that both the initial pressure and the time-dependent requirements of that theory are fairly well satisfied by the data. The deviations from linearity which appear in Figure 3 are outside experimental error, however, and may reflect variation in the heat of adsorption with surface coverage or effects of lateral intermolecular interactions on the surface, both being conditions which would violate Langmuir assumptions.

The data have been treated according to the simple Langmuir-Hinshelwood model, which assumes each adsorbed molecule may either react on or desorb from the surface. The product distributions for MCP isomerization reported earlier,<sup>3</sup> together with the present tracer results and those for CP,<sup>10</sup> suggest that B of eq 4 does not refer to the total adsorbed substrate but to a metastable (*c*-C<sub>n</sub>H<sub>2n+1</sub><sup>+</sup>) surface species, which is formed by interaction of a reactant molecule with a proton donated by a polymeric surface "residue."<sup>3,4</sup>

The heat of adsorption measured in Figure 5 (5.2 kcal/mol) is about equal to the heat of liquefaction of cyclopropane, suggesting that most of the adsorption is physical. In the microcatalytic experiments, a sizable fraction of each pulse was adsorbed on the catalyst. From the data of Figure 5, it is estimated that about 1 cm<sup>3</sup> was adsorbed when the cyclopropane pressure was 400 mm at 150°. Even if there were no spreading of the pulse between the doser and the reactor, the *P*<sub>0</sub> value used in eq 21 would be about 30% smaller than

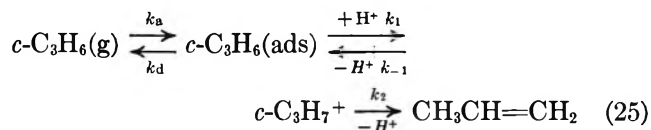
that originally measured in the doser. In principle, one could calculate the effective initial pressures after physical adsorption by applying the slope and intercept of the microcatalytic data in Figure 3 to eq 21; however, this would only be possible if the monolayer capacity *Q*<sub>m</sub> of the catalyst and the free volume *V* in the reactor bed were known accurately, *viz.*

$$P_0^0 = \frac{KQ_m WRT + V \left( \frac{\text{slope}}{\text{intercept}} \right)}{KV} \quad (24)$$

Furthermore, such a value would be only a crude estimate in a microcatalytic system because of the Gaussian shape of the pulse.<sup>14</sup> Therefore, we have simply assumed the pressure over the catalyst is proportional to the pressure in the doser.

This physical adsorption may be a type of hydrogen bonding similar to that which Liengme and Hall<sup>15</sup> observed in the interaction of ethylene with hydroxyl groups in zeolites. They showed that the system has characteristics of physical adsorption and suggested a mechanism by which the hydrogen-bonded complex could be thermally activated to a carbonium ion. The present data may be explained in the same way. This picture is strengthened by the recent work of Joris, Schleyer, and Gleiter,<sup>16</sup> who showed that cyclopropanes act as proton acceptors in hydrogen bonding.

If B is the carbonium ion, eq 5 should be replaced by, *e.g.*



According to this scheme, adsorption and desorption are very fast compared with carbonium ion formation. A simple steady-state treatment based on this model yields results which are formally identical with those already derived, *i.e.*

$$-dP/dt = k_2(c\text{-C}_3\text{H}_7^+) = k'KP/(1 + KP) \quad (26)$$

where  $k' = k_1k_2/(k_{-1} + k_2)$  and  $K = k_a/k_d$ . The chief difference is that values of *K* (and values of *θ*<sub>0</sub> and *P*<sub>0</sub> derived therefrom) may be taken as realistic estimates of the surface properties. Moreover, the selectivity ( $k_2/k_{-1}$ ) will not be the ratio of molecules which react to those which desorb. Rather, it will be the ratio of the metastable nonclassical carbonium ions of the type suggested by Baird and Aboderin<sup>17</sup> which de-

(13) W. K. Hall, F. E. Lutinski, and H. R. Gerberich, *J. Catalysis*, **3**, 512 (1964).

(14) W. A. Blanton, C. H. Byers, and R. P. Merrill, paper given at the 154th National Meeting of the American Chemical Society, Chicago, Ill., Sept 1967.

(15) B. V. Liengme and W. K. Hall, *Trans. Faraday Soc.*, **62**, 3229 (1966).

(16) L. Joris, P. von R. Schleyer, and R. Gleiter, *J. Am. Chem. Soc.*, **90**, 327 (1968).

compose to the olefin to those which return to the ground state without isomerization. This ratio can be estimated in coisomerization experiments of the type shown in Figure 6. With MCP, the scrambling of isotopes into the unreacted substrate was slow compared with isomerization; hence  $k_2/k_{-1} \gg 1$  and  $k' \approx k_1$ . With CP, these processes proceeded at a comparable rate;<sup>4,10</sup> hence  $k_2/k_{-1} \approx 1$  and  $k' \approx k_1/2$ .

The metastable carbonium ion has been pictured<sup>4</sup> as lying in a relatively shallow potential well near the top of the reaction coordinate. The selectivity thus depends upon the relative heights of the barriers between the carbonium ion and the olefin and between the ion and the reactant. With MCP, the latter is the highest so that the activation energy for the isomerization reaction may be identified with that for carbonium ion formation. With CP, it has been shown<sup>4,10</sup> that the activation energy for isotope scrambling is very nearly equal to that for isomerization (19 kcal/mol), suggesting the same conclusion but with the reservation that the two barriers have nearly the same height.

In the present work we have shown that our kinetic results conformed reasonably well to a simple Langmuir-Hinshelwood treatment. There is, however, an apparent discrepancy between the kinetic results and the physical adsorption data of Figure 5. Since the physical adsorption is much less than a monolayer under all reaction and adsorption conditions, it is possible to apply the monolayer Langmuir equation (eq 6) to the adsorption isotherms to obtain a value of  $KV_m$  at each temperature. In eq 6,  $\theta = V/V_m$ , where  $V_m$  is the monolayer capacity in  $\text{cm}^3$  (NTP)/g.  $V_m$  should be relatively insensitive to temperature and is probably about  $20 \text{ cm}^3/\text{g}$  (assuming each CP molecule covers  $25 \text{ \AA}^2$ ) or  $15 \text{ cm}^3/\text{g}$  (if CP molecules adsorb on surface hydroxyl groups whose concentration is  $1.5 \times 10^{14}/\text{cm}^2$ <sup>18</sup>).

Extrapolation of the  $K$  values obtained from the adsorption data in the  $0$ – $100^\circ$  temperature range to  $150^\circ$  yields  $2$ – $3 \times 10^{-4} \text{ mm}^{-1}$  which is two orders of magnitude lower than that obtained from the kinetic data. This means that the  $\theta$  values in Table I, which represent the coverage of active sites, are considerably larger than the  $\theta$  values calculated for physical ad-

sorption on the entire surface under comparable conditions. Hence, the hydrocarbon must be selectively adsorbed on a small portion of the surface, perhaps on Brønsted sites of sufficient acidity to effect proton transfer by thermal excitation and thereby catalyze the reaction. The apparent kinetic and adsorption inconsistency could be resolved if these sites were the  $\sim 1 \times 10^{13}/\text{cm}^2$  "residues" reported by Larson, *et al.*,<sup>10</sup> which act as sites for the reaction. For example, if the coverage at  $150^\circ$  and  $100 \text{ mm}$  is  $0.68$  (Table I), then the total adsorption on these sites should be about  $1 \text{ cm}^3$  (NTP)/g. The value estimated for these conditions from data of Figure 5 is about  $0.25 \text{ cm}^3$  (NTP)/g.

It must also be pointed out that the same kinetics can be equally well treated on the basis of a Freundlich isotherm

$$-\frac{dP}{dt} = kP^{1/r} \quad (27)$$

from which eq 3 can be written with  $n = 1/r$ . Figure 1 represents both treatments, and the  $r$  values calculated from the slope are  $1.9$  for CP and  $2.5$  for MCP. As with  $n$ ,  $r$  is not unique but decreases toward unity with increasing temperature.

Although both the Freundlich and Langmuir-Hinshelwood theories reasonably well fit the kinetic data, neither gives perfect agreement, but both offer an improvement in the fit of the data. We prefer the Langmuir-Hinshelwood development because it provides a mechanism to account for the tracer data. These findings demonstrate the utility of isotopic tracers in determining reaction mechanisms.

*Acknowledgment.* This work was sponsored by the Gulf Research & Development Co. as part of the research program of the Multiple Fellowship on Petroleum. The authors are grateful to Dr. H. W. Habgood for suggesting the theoretical treatment for the microcatalytic results.

(17) R. L. Baird and A. A. Aboderin, *J. Am. Chem. Soc.*, **86**, 252, 2300 (1964).

(18) W. K. Hall and F. E. Lutinski, *J. Catalysis*, **2**, 518 (1963).

## Cooperative Binding to a One-Dimensional Lattice.

### The Amylose-Iodine-Iodide Complex

by Friedemann W. Schneider,<sup>1</sup> Charles L. Cronan,

*Department of Chemistry, University of Southern California, Los Angeles, California 90007*

and Sunil K. Podder

*Department of Chemistry, University of California at Berkeley, Berkeley, California 94720 (Received June 12, 1968)*

Adsorption isotherms describing the cooperative binding of identical species to a linear lattice are calculated exactly for any chain length by the use of the matrix method. The cooperative energy of interaction  $w$  between first nearest neighboring species characterizes the shape, whereas the magnitude of the intrinsic association constant  $K_0$  for a species bound to one site describes the position of the isotherm in a semilogarithmic plot. In the limit of infinite chain length the isotherm is equivalent to the quasi-chemical approximation in one dimension which is thus shown to be exact. A curve-fitting method which permits a quick determination of the stacking coefficient  $K_{st}$  ( $=\exp(-w/RT)$ ) and  $K_0$  for experimental systems is discussed. As an example the binding isotherm of iodine-iodide in the helical cavity of amylose has been determined by equilibrium dialysis at  $10^{-2} M$  KI and  $20.0^\circ$ . For an effective chain length of 15 helical turns ( $n = 15$ ), the curve-fitting method is in good agreement with a nonlinear least-squares fit to the theoretical expression;  $K_{st} = 90 \pm 20$  ( $w = -2.62 \pm 0.15$  kcal/mol) and  $K_0 = (1.15 \pm 0.29) \times 10^4$ , the latter corresponding to  $\Delta F_0 = -5.43 \pm 0.15$  kcal/mol. Thus it is shown that the cooperativity in the linear amylose-iodine-iodide complex is moderate and that its main stability is derived from the intrinsic binding of a species to a helical turn.

#### Introduction

Cooperative structural changes between the helical and coiled forms of linear polypeptide chains have been described as quasi-one-dimensional phase transitions by Zimm and Bragg<sup>2</sup> who used the matrix method for the calculation of the partition function. The elementary steps occurring in the cooperative transition are monomolecular in nature. On the other hand, there are order-disorder transitions also of biological interest involving linear macromolecules whose elementary steps are bimolecular. Examples are the binding of small monomer molecules to linear macromolecules.<sup>3</sup>

This article presents a calculation of the equilibrium properties of a bimolecular cooperative order-disorder transition expressed in terms of a binding isotherm. Two statistical thermodynamic parameters characterize the calculated isotherms: the cooperative energy of interaction between first nearest neighbors of adsorbed species and the intrinsic association constant of an adsorbed species with its polymer site. The former is a measure of the sharpness of the isotherm, whereas the latter determines the relative position of the isotherm when the degree of saturation is plotted *vs.* the logarithm of the equilibrium concentration of free species. All sites are considered as equivalent, and all monomer species, whether bound or free, are of the same type. It is assumed that the bound species are localized; *i.e.*, they are placed in a periodic field representing the distribution of sites. The present matrix treatment is exact and valid for any chain length  $n$ . At infinite  $n$

it is shown to be equivalent to the quasi-chemical approximation in one dimension.<sup>4,5</sup> Using combinatorial methods Steiner<sup>6</sup> calculated one-dimensional adsorption isotherms including second nearest neighbor interactions. However, his expressions become very complicated especially for large  $n$  ( $\geq 15$ ) where the equations have to be solved numerically. On the other hand, the clarity and simplicity of the matrix method is much to be preferred for the present problem. Magee, Gibbs, and Zimm<sup>7</sup> calculated the temperature dependence of the degree of saturation  $\theta$  (their  $p = 1$ ) at constant concentration of free species and obtained  $\theta$  *via* the internal energy relationship which involves the graphical determination of slopes. A sample calculation given in their article is restricted to one set of thermodynamic parameters.

One of the main objectives of this paper is to furnish a reliable and direct method to determine the degree of cooperativity in one-dimensional adsorption. This is achieved by a curve-fitting method which compares

(1) To whom correspondence should be addressed.

(2) B. H. Zimm and J. K. Bragg, *J. Chem. Phys.*, **31**, 526 (1959).

(3) R. F. Steiner and R. F. Beers, Jr., "Polynucleotides," Elsevier Publishing Co., Amsterdam, The Netherlands, 1961.

(4) R. H. Fowler and E. A. Guggenheim, "Statistical Thermodynamics," Cambridge University Press, London, 1939.

(5) T. L. Hill, "An Introduction to Statistical Thermodynamics," Addison-Wesley Publishing Co., Inc., Reading, Mass., 1962.

(6) R. F. Steiner, *J. Chem. Phys.*, **22**, 1458 (1954)

(7) W. S. Magee, Jr., J. H. Gibbs, and B. H. Zimm, *Biopolymers*, **1**, 133 (1963).

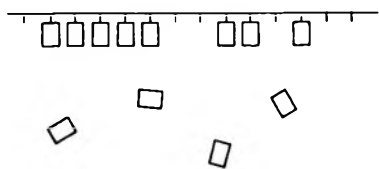


Figure 1. Schematic representation of a linear array of free and bound sites in equilibrium with "disordered" monomer in solution.

theoretical template curves with experimental isotherms for a given  $n$ . The cooperative energy of interaction is obtained from the shape, whereas the intrinsic binding constant is determined from the position of the isotherm using a semilogarithmic plot. An illustration is given for the amylose-iodine-iodide system at high iodide concentration. The "isosteric" heat of cooperative binding is a function of  $\theta$  and temperature, and it can be approximately determined experimentally by a Clausius-Clapeyron-type equation at constant  $\theta$ .

### Model and Statistical Weight Factors

The chainlike macromolecule consists of a linear array of equivalent and equidistant sites which can be either free or occupied by monomer species (Figure 1). Equilibrium exists between the ordered bound adsorbate and its "disordered" free-monomer concentration. There are two states for site  $i$ : it can either be free or occupied. Based on binary numbers the latter two states are indexed as 0 and 1, respectively. Since first nearest neighbor interactions are considered only, the probability of a given state  $k$  of site  $i$  depends upon the state  $l$  of the first neighboring site, the  $i - 1$  state, for example.

We can now write statistical weight factors  $M_{ik}$  as follows. For site  $i$  to be in an occupied state  $k$  and being preceded by site  $i - 1$  which is in a free state  $l$

$$M_{01} = K_0 m$$

where  $K_0$  is the intrinsic association constant per site and  $m = \exp(-\mu/RT)$ , where  $m$  is the concentration of free species in solution and  $\mu$  is their chemical potential. If an occupied site is preceded by an occupied site, there is a direct lateral "cooperative" interaction between the two neighboring species which leads to an additional term  $K_{st}$  and

$$M_{11} = mK_0 K_{st}$$

where  $K_{st} (=e^{-w/RT})$  is called the stacking coefficient,<sup>3</sup>  $w$  being the cooperative energy of interaction.

The statistical factor of a free site preceded by either a free or an occupied site is set equal to unity; *i.e.*,  $M_{00} = M_{10} = 1$ . This is to say that the statistical weight of a free site has been arbitrarily divided by the product of the internal partition functions of a free site in order to obtain the relative value of unity. Since we are interested in the thermodynamics of the order-

disorder transition, the use of relative statistical weights is justified.

### Partition Function

Following Zimm and Bragg<sup>2</sup> a statistical weight column vector  $a_i^+$  is defined which, for the case of first nearest neighbor interactions, consists of two components, one for each state of site  $i$ . The first component represents the statistical weight of all sites 1 to  $i$  where  $i$  is a free site, whereas the second component is the statistical weight of all sites 1 to  $i$  where  $i$  represents an occupied site. The vector  $a_i^+$  can be generated by defining a  $2 \times 2$  matrix operator  $M$  such that

$$a_i^+ = M^i \alpha^+$$

where

$$\alpha = \begin{pmatrix} 1 \\ 0 \end{pmatrix}$$

A row vector  $b_i$  is now introduced which contains the contributions of the remaining sites  $i + 1$  through  $n$

$$b_i = \omega M^{n-i}$$

where  $\omega = (1, 1)$ . The partition function is

$$Q = b_i \cdot a_i^+ = \omega M^n \alpha^+ \quad (1)$$

*i.e.*,  $Q$  represents the sum of all the components of the statistical weight vector  $a_n$ . An equivalent way of calculating  $Q$  is to start with the statistical weight vector for the first site which can be written down by inspection as

$$a_1 = \begin{pmatrix} 1 \\ K_0 m \end{pmatrix}$$

Then

$$Q = \omega M^{n-1} a_1$$

In order to calculate  $M^n$  the unsymmetrical matrix  $M$  is diagonalized, and the elements of the diagonal matrix,  $\Lambda$ , which are the eigenvalues of  $M$ , are then raised to the  $n$ th power

$$\Lambda^n = T^{-1} M^n T = \begin{pmatrix} \lambda_0^n & 0 \\ 0 & \lambda_1^n \end{pmatrix}$$

and

$$M^n = T \Lambda^n T^{-1}$$

where  $\lambda_0$  and  $\lambda_1$  are the eigenvalues of  $M$ .  $T$  is the transformation matrix and has the following form for the present mode of interactions

$$T = \begin{pmatrix} 1 & 1 \\ \lambda_0 - 1 & \lambda_1 - 1 \end{pmatrix}$$

and

$$T^{-1} = \frac{1}{\lambda_1 - \lambda_0} \begin{pmatrix} \lambda_1 - 1 & -1 \\ -\lambda_0 + 1 & 1 \end{pmatrix}$$

### Statistical Weight Matrix

The statistical weight matrix  $M$  can be written in terms of the statistical weight factors  $M_{ik}$  defined previously

$$M = \begin{pmatrix} 1 & 1 \\ K_0 m & K_0 m K_{st} \end{pmatrix}$$

Its eigenvalues are

$$\lambda_{0,1} = \frac{1}{2}[(1 + mK_0K_{st}) \pm \sqrt{(1 - mK_0K_{st})^2 + 4K_0m}] \quad (2)$$

The vectors  $b_i$  and  $a_i$  are now expressed in terms of eigenvalues

$$b_i = \frac{1}{\lambda_0 - \lambda_1} [\lambda_0^{n+1-i}(1 - \lambda_1) + \lambda_1^{n+1-i}(\lambda_0 - 1), \lambda_0^{n+1-i} - \lambda_1^{n+1-i}] \quad (3)$$

and

$$a_i = \frac{1}{\lambda_0 - \lambda_1} \left( \frac{\lambda_0^i(1 - \lambda_1) + \lambda_1^i(\lambda_0 - 1)}{(\lambda_0^i - \lambda_1^i)(\lambda_0 - 1)(1 - \lambda_1)} \right) \quad (4)$$

Substitution into eq 1 gives

$$Q = (1 - D)\lambda_0^{n+1} \left( 1 + \frac{D}{1 - D} R^{n+1} \right) \quad (5)$$

where  $D = (\lambda_0 - 1)/(\lambda_0 - \lambda_1)$  and  $R = \lambda_1/\lambda_0$ .

### Degree of Saturation and Isotherm

The usual way to calculate the degree of saturation in an exact fashion is to consider all eigenvalues of  $M$  by use of eq 5 and

$$\theta = \frac{1}{n} \left( \frac{\partial \ln Q}{\partial \ln K_0} \right)_{m,n}$$

Alternately, a simple expression for  $\theta$  is obtained by expressing the degree of saturation of a chain  $n$  as the ratio of the sum of all occupied sites  $i$  and the number of all available sites  $n$

$$\theta = \frac{1}{n} \sum_{i=1}^n p_i(\text{oc}) \quad (6)$$

where  $p_i$  is the probability that site  $i$  is occupied. As a consequence of eq 1

$$p_i(\text{oc}) = (b_{i,\text{oc}} a_{i,\text{oc}}) / Q \quad (7)$$

where  $b_{i,\text{oc}}$  and  $a_{i,\text{oc}}$  represent the second elements of  $b_i$  and  $a_i$  (eq 3 and 4), respectively. Substitution leads to

$$p_i(\text{oc}) = \frac{1}{Q} [D(1 - D)\lambda_0^{n+1}] \times (1 + R^{n+1} - R^{n-i+1} - R^i) \quad (8)$$

Since  $R < 1$

$$\theta = D \frac{1 + R^{n+1} - \frac{2R(1 - R^n)}{n(1 - R)}}{1 + \frac{D}{1 - D} R^{n+1}} \quad (9)$$

Equation 9 is similar to one obtained by Schwarz<sup>8</sup> for the helix-coil transition in polypeptides. Thus eq 9 represents the binding isotherm with the eigenvalues given in eq 2. For an infinite chain,  $n = \infty$ , the isotherm expression is identical with the quasi-chemical approximation<sup>4,5</sup> in one dimension which is thus seen to be exact. Since  $R^n \approx 0$  for  $n = \infty$ , eq 9 reduces to

$$\theta_{n=\infty} = D \quad (10)$$

Substitution and rearrangement leads to the more familiar form of the quasi-chemical approximation in one dimension

$$K_0 m = \frac{(\beta - 1 + 2\theta)}{(\beta + 1 - 2\theta)} e^{w/kT} \quad (11)$$

where  $\beta = [1 - 4\theta(1 - \theta)(1 - e^{-w/kT})]^{1/2}$ . The isosteric heat of adsorption depends upon  $\theta$  and temperature for the present one-dimensional cooperative system. For  $n = \infty$

$$\Delta H(\theta) = \Delta H(\theta = 0) - w \left( \frac{1 - 2\theta}{\beta} - 1 \right) \quad (12)$$

where  $\Delta H(\theta = 0)$  is the (temperature-independent) heat of adsorption at zero coverage.

### Discussion

A comparison between Zimm and Bragg's matrix operator<sup>2</sup> (for  $\mu = 1$ ) and the present one shows a direct analogy between the two cooperative systems; namely,  $s \doteq mK_0K_{st}$  and  $\sigma s \doteq mK_0$ , where  $\sigma$  is the nucleation parameter and  $s$  is the equilibrium constant for the addition of a helical turn to an already existing helix. This correspondence allows a similar discussion of the state of the macromolecule for the present case as that given by Zimm and Bragg for the helix-coil transition. The probabilities of the end site being occupied and of breaks in the stacks and the critical value of  $n$  at which stack formation starts for  $mK_0K_{st} > 1$  can be calculated in a similar fashion.

An important consequence of the present treatment is the relationship  $K_{st} = 1/\sigma$ . Thus in analogy to  $K_{st}$ , the  $\sigma$  parameter should show a temperature dependence; i.e.,  $\sigma = \exp(-w_\sigma/kT)$ . If  $w_\sigma$  represents a free energy rather than an enthalpy and  $\Delta H_\sigma = 0$ , then  $\sigma$  is entropy controlled and it is indeed temperature independent as assumed by Zimm and Bragg.<sup>2</sup> Very accurate data are necessary for such a distinction.

We have calculated a number of template isotherms from eq 9 and 10 as a function of  $K_{st}$  and  $n$  on a Honeywell 800 computer (Figures 2 and 3). The steepness

(8) G. Schwarz, Habilitationsschrift, Braunschweig, 1966.

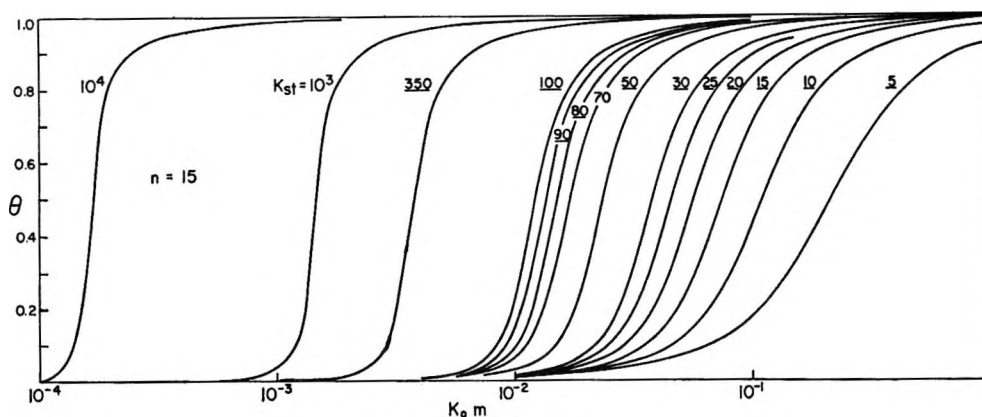


Figure 2. Binding isotherms for  $n = 15$ . Degree of saturation,  $\theta$ , as a function of  $K_0 m$  for various values of  $K_{st}$ .

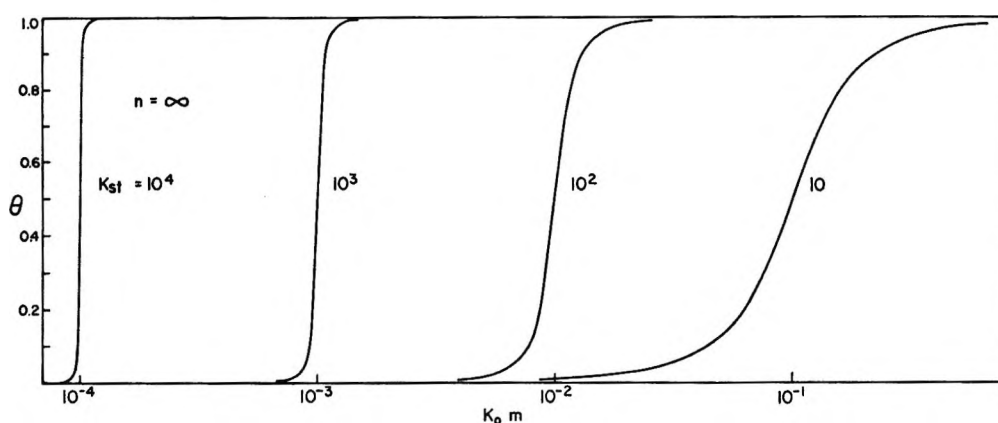


Figure 3. Binding isotherms for an infinite chain. Degrees of saturation as a function of  $K_0 m$  for various values of  $K_{st}$ .

of the isotherm increases for increasing  $K_{st}$  due to enhanced cooperativity. Likewise, for constant  $K_{st} > 1$  and increasing  $n$  the isotherm becomes steeper. Langmuir isotherms are obtained for  $K_{st} = 1$ , *i.e.*, when no interaction exists between bound species. For infinite chain and large  $K_{st}$  the average size of a stack at  $\theta = 0.5$  is equal to  $\sqrt{K_{st}}$ . The isotherm is then symmetrical with respect to the midpoint of the transition which occurs at  $mK_0K_{st} = 1$ . The coexistence of alternating stacks and regions of free sites is the very reason for the isotherms to be gradual rather than discontinuous.

For short chains,  $n \lesssim \sqrt{K_{st}}$ , at  $\theta \sim 0.5$ , approximately half of the chains are almost completely filled while the other half are completely empty. For this situation the system displays an "all-or-nothing" behavior. At the midpoint of the transition  $mK_0K_{st} \neq 1$  and the isotherm becomes nonsymmetrical.

#### Curve-Fitting Method

The calculated isotherms can be used as template curves in the form of a plot of  $\theta$  vs.  $\log(K_0 m)$ . Experimental curves of  $\theta_{\text{exptl}}$  vs.  $\log m_{\text{exptl}}$  at known  $n$  are compared with the above templates until an optimum fit of shape is obtained. The theoretical value of  $K_{st}$

is then assigned to the experimental isotherm and  $K_0$  is determined from the relative position of the isotherm along the  $\log(K_0 m)$  axis. Thus a quick and direct means is provided to determine the cooperative energy of interaction as well as the intrinsic association constant in one-dimensional adsorption. An application is given in the following.

#### The Amylose-Iodine-Iodide System

The adsorption isotherm of iodine-iodide in the helical cavity of amylose (DP (degree of polymerization)  $\simeq 900$ ) has been determined by equilibrium dialysis<sup>9</sup> at  $10^{-2} M$  KI and  $20.0^\circ$  (Figure 4) for an amylose concentration of  $4.45 \times 10^{-4} \text{ g/ml}$ . Spectrophotometric measurements of isotherms<sup>9-11</sup> at various iodide concentrations indicate that the bound species are of variable composition according to  $I_2-I_b^-$ , where  $b$  is a function of the over-all iodide concentration. At  $10^{-2} M$  KI  $b$  is approximately unity or slightly larger; *i.e.*,

(9) C. L. Cronan, M.S. Thesis, University of Southern California, 1968.

(10) F. W. Schneider and C. L. Cronan, Abstracts of Papers, Pacific Conference on Chemistry and Spectroscopy, Anaheim, Calif., Oct 1967, p 36.

(11) C. L. Cronan and F. W. Schneider, submitted for publication.

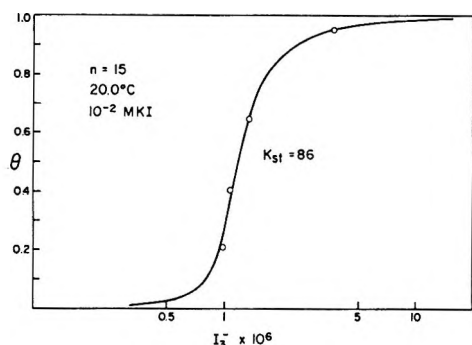


Figure 4. Binding isotherm of iodine-iodide in the helical cavity of amylose (DP = 900) as measured by equilibrium dialysis at  $10^{-2} M$  KI and  $20.0^\circ$ . The full line represents the least-squares fit of the theoretical isotherm (eq 9,  $n = 15$ ) to the experimental points for  $K_{st} = 86$  and  $K_0 = 1.20 \times 10^4$ . The visual fit,  $K_{st} = 90 \pm 20$ , is practically equivalent in shape and cannot be distinguished from the above isotherm.

the predominantly bound species is approximately  $I_3^-$  at  $10^{-2} M$  KI.<sup>11</sup>

The experiments were performed with dialysis tubing containing 20 ml of  $0.01 M$  KI with varying concentrations of  $I_2$  which was submerged in 80 ml of a  $0.0045\%$  amylose solution in  $0.01 M$  KI. Equilibrium was attained after 6 hr under constant magnetic stirring at  $20.0^\circ$ . The outer and inner solutions were analyzed spectrophotometrically on a Beckman DK2A spectrophotometer. The concentrations of free  $I_3^-$  and free  $I_2$  were calculated using  $\epsilon_{353 \text{ m}\mu} 26\,400$  and  $\epsilon_{288 \text{ m}\mu} 40,000$ <sup>12</sup> for  $I_3^-$  and  $K = 866 M^{-1}$  ( $20.0^\circ$ )<sup>13</sup> for the triiodide equilibrium in solution. The contribution of free  $I_2$  can be neglected spectrophotometrically owing to its low extinction coefficient ( $\epsilon_{353 \text{ m}\mu} 18$  and  $\epsilon_{288 \text{ m}\mu} 95$ <sup>12</sup>). A small correction determined from standard runs was applied to the concentration of bound iodine due to the reaction of  $I_2$  with the dialysis membrane. Difference spectra were taken using the free triiodide solution inside the dialysis tubing as a reference. The extinction coefficient of bound  $I_3^-$  was found to be  $\sim 38,500$  at  $640 \text{ m}\mu$ . The absorption spectrum of the complex itself, without superposition of the relatively strong bands of free  $I_3^-$  at  $288$  and  $353 \text{ m}\mu$ , is shown in Figure 5. The complex in this work shows an absorption band at  $\sim 343 \text{ m}\mu$ , a shoulder at  $\sim 460 \text{ m}\mu$ , and the blue band at  $607 \text{ m}\mu$  when  $\theta = 0.4$ . At almost complete saturation ( $\theta = 0.95$ ), the latter band is shifted toward a longer wavelength of  $\sim 625 \text{ m}\mu$ , probably due to the onset of a second adsorption process or the association of filled helices.<sup>11,14</sup> The latter process makes it somewhat difficult to determine precisely the limiting concentration of bound  $I_3^-$  at complete saturation. Spectrophotometric studies<sup>9-11</sup> indicate that at complete saturation approximately  $3.52 \times 10^{-5}$  mol of  $I_3^-$  was bound to the above anhydroglucose equivalent concentration of  $2.77 \times 10^{-4} N$ , which leads to a ratio of 8:1 anhydro-

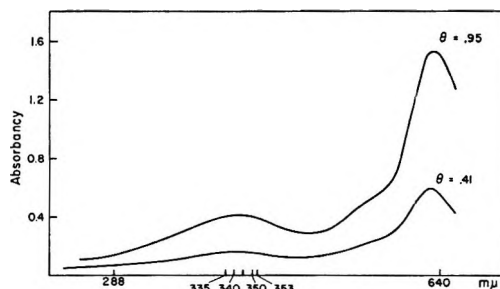


Figure 5. Difference spectrum of the amylose-iodine-iodide complex at  $10^{-2} M$  KI and  $20.0^\circ$ . Absorbance vs. wavelength in millimicrons (nonlinear scale). Notice the absence of an absorption band at  $288 \text{ m}\mu$ . For details see the text.

glucose molecules:bound  $I_3^-$  species, in good agreement with recent work.<sup>15</sup> The degree of saturation is calculated as the ratio of the concentration of bound  $I_3^-$  and the maximum concentration of bound  $I_3^-$  at complete saturation. It is clear from the nonsymmetric shape of the experimental isotherm (Figure 4) that the effective chain length is considerably less than the maximum possible value of  $n = 110-150$ , for which a nearly symmetrical isotherm is expected. On the basis of mechanochemical degradation studies of amylose, Szejtli, *et al.*,<sup>16</sup> have shown that an amylose-iodine complex of DP = 900 consists of approximately 7.6 helical segments, each segment having a number-average DP of about 118. If one converts this latter number to helical turns by use of the crystalline state value of 6 glucose residues/helical turn<sup>17</sup> or the above value of 8 glucose residues/turn in solution, then these helical segments consist of 15-20 helical turns each. If we assume that each turn of the helix acts as one adsorption site,<sup>17</sup> the value  $n \simeq 15$  is justified for use in the theoretical model. The concept of helical segments has been reaffirmed by Paulson's<sup>14</sup> electric field studies.

Application of the visual curve-fitting method to the experimental points (Figure 4) leads to  $K_{st} \simeq 90 \pm 20$  and  $K_0 = (1.15 \pm 0.29) \times 10^4$ , corresponding to  $w = -2.62 \pm 0.15 \text{ kcal/mol}$  and  $\Delta F_0 = -5.43 \pm 0.15 \text{ kcal/mol}$ , respectively. In order to provide a check of the visual best fit, an independent nonlinear least-squares fit of the experimental points to the theoretical expression (eq 9) was calculated on a Honeywell 800 computer.<sup>18</sup>

(12) A. D. Awtrey and R. E. Connick, *J. Amer. Chem. Soc.*, **73**, 1842 (1951).

(13) M. Davies and E. Gwynne, *ibid.*, **74**, 2748 (1952).

(14) C. M. Paulson, Ph.D. Thesis, University of California at Berkeley, 1965.

(15) S. R. Erlander, H. L. Griffin, and F. R. Senti, *Stärke*, **17**, 151 (1965).

(16) J. Szejtli, M. Richter, and S. Augustat, *Biopolymers*, **5**, 5 (1967), and references therein.

(17) R. S. Stein and R. E. Rundle, *J. Chem. Phys.*, **16**, 195 (1948).

(18) We thank Mr. Laszlo Engelman for the original nonlinear least-squares program and the University of Southern California Computer Science Laboratory for computing time.

A minimum in the standard deviation in  $\theta$  ( $\pm 0.040$ ) occurred for  $K_{st} = 86$  ( $\Delta F_{st} = -2.59$  kcal/mol) and  $K_0 = 1.20 \times 10^4$  ( $\Delta F_4 = -5.47$  kcal/mol), in good agreement with the values obtained from the curve-fitting method. Thus the one-dimensional adsorption model indicates that the degree of cooperativity for the complex at  $10^{-2}$  M KI is moderate and that the main source of the stability of the complex originates from the intrinsic binding of the species to one helical turn.

Reddy, *et al.*,<sup>19</sup> and Robin<sup>20</sup> suggested that the benzamide-triiodide complex, whose crystal structure they determined, can be used as a model for the solid amylose iodine-iodide complex on the basis of the close similarity of their electronic spectra. If the proposed equivalence is accepted then the helical cavity (diameter,  $\sim 6$  Å) of the crystalline amylose accommodates a single triiodide chain in which the  $I_3^-$  ions maintain their identity. In the linear chain, triiodide ions are bent by about  $3^\circ$  with respect to each other; their internal distance is  $\sim 2.92$  Å, and the distance of separation between adjacent  $I_3^-$  ions is 3.80 Å, as compared with the van der Waals distance of 4.6 Å. The resulting close-range dispersion forces are believed to be mainly responsible<sup>19,20</sup> for the attractive nearest neighbor interaction between the similarly charged  $I_3^-$  ions whose electrostatic repulsion must be compensated. Higher than first nearest neighbor interactions might become important owing to the long-range electrostatic interactions. A matrix treatment such as that of Baur and Nosa-

now<sup>21</sup> can be adapted to take such higher order interactions into account. On the other hand, the effective range of electrostatic forces is reduced at the relatively high ionic strength ( $10^{-2}$ ) used in this study.

Peticolas<sup>22</sup> described the sigmoid temperature dependence of the 600-m $\mu$  complex absorption band as being due to a helix-coil transition of the amylose backbone. The present work,<sup>9</sup> however, suggests that it is mainly due to the temperature dependence of the binding equilibrium. This view seems to be supported by temperature-jump studies<sup>10,11</sup> at  $10^{-2}$  M KI and  $20.0^\circ$ , which show concentration-dependent relaxation times in the millisecond region, as expected for bimolecular elementary processes which take place during binding. On the other hand, a pure helix-coil transition of short helices as above should occur in a fraction of 1  $\mu$ sec. Thus it is concluded that the amylose helix remains essentially intact during the binding process.

*Acknowledgment.* We thank Mr. P. K. Rawlings for performing the nonlinear least-squares calculations on a Honeywell 800 computer, and Miss Maymie Chenoweth, University of Southern California, for the enzymatic analysis of amylose solutions.

(19) J. M. Reddy, K. Knox, and M. B. Robin, *J. Chem. Phys.*, **40**, 1082 (1964), and references therein.

(20) M. B. Robin, *ibid.*, **40**, 3369 (1964).

(21) M. E. Baur and L. H. Nosanow, *ibid.*, **37**, 153 (1962).

(22) W. L. Peticolas, *Nature*, **197**, 898 (1963); *J. Chem. Phys.*, **40**, 1463 (1964).

## Kinetics of the Li(Hg)-Li<sup>+</sup> Reaction in Dimethyl Sulfoxide

by David R. Cogley and James N. Butler

*Tyco Laboratories, Inc., Waltham, Massachusetts 02154 (Received June 17, 1968)*

The electrode Li(Hg)-Li<sup>+</sup> has been studied in anhydrous LiCl-dimethyl sulfoxide (DMSO) solutions over the temperature range 20–34°. The standard rate constant, corrected for double-layer effects, of the Li(Hg)-Li<sup>+</sup> electrode in LiCl-DMSO solutions at 25° is  $(2.9 \pm 0.2) \times 10^{-5}$  cm/sec. The Tafel equation with cathodic transfer coefficient  $\alpha = 0.75 \pm 0.02$  is obeyed over the current density range  $10^{-5}$  to  $3 \times 10^{-3}$  A/cm<sup>2</sup>. The value of  $\alpha$  deduced from the concentration dependence of the apparent exchange current agrees with the value deduced from the Tafel equation. The enthalpy of activation at the reversible potential is 7.9 kcal/mol.

### Introduction

Recent interest in high-energy batteries has given considerable impetus to research on the deposition and dissolution of active metals which can be used as battery anodes.<sup>1</sup> However, the reactivity of lithium requires

that an electrolyte based on a nonaqueous aprotic solvent such as dimethyl sulfoxide (DMSO) be used.

(1) R. Jasinski, "High Energy Batteries," Plenum Press, New York, N. Y., 1966.



In an earlier paper<sup>2</sup> we reported exchange current values determined using a cell with two concentric pool electrodes. A transfer coefficient near 0.5 and an apparent exchange current of  $5.4 \times 10^{-4}$  A/cm<sup>2</sup> were deduced from the data for saturated (1.33 mol %) lithium amalgam in 0.5 M LiCl-DMSO. Because of the uneven current distribution on the electrodes, these results were somewhat in error. We report here the results of kinetic studies using a three-electrode cell with uniform current distribution and covering a range of concentrations and temperatures.

### Experimental Section

Lithium metal, 99.96% (Foote Mineral Co.), and triply distilled mercury (Doe and Ingalls) were used for the preparation of the amalgams by dissolution of lithium metal in mercury. Lithium chloride solutions were prepared by adding lithium chloride, 99.999% (Anderson Physics Laboratories), to DMSO (Fisher Chemical Co.), which had been dried with Linde Molecular Sieves and filtered through a 10–20  $\mu$  pore size glass frit. The water content of the solutions (analyzed by gas chromatograph) was less than  $1.5 \times 10^{-3}$  M (25 ppm).

Solutions and amalgams were prepared and the cell was assembled under argon in a drybox equipped with a vacuum transfer chamber and a gas-purification train (Vacuum Atmospheres Corp).

The cell is shown in Figure 1. The working electrode, W, counter electrode, C, and reference electrode, R, are amalgams of identical composition. W is a cylindrical pool, C is an annulus, and R is a sheath of amalgam on a flat-ended piece of nickel wire sealed in glass. The design achieves the following objectives: (1) to provide uniform current density over the surface of the working electrode in the presence of low-conductance nonaqueous electrolytes; (2) to minimize inter-electrode capacitance, thereby allowing measurements on a microsecond time scale; (3) to utilize materials compatible with lithium amalgams; (4) to provide for thermostating and sealing the cell against atmospheric contamination; and (5) to prevent diffusion of unwanted reaction products from the counterelectrode to the working electrode.

In order to provide uniform current distribution over its surface, the working electrode was placed at the bottom end of the cylindrical Pyrex cell, approximately four cell diameters away from the annular counterelectrode. Uniformity of the current density was tested experimentally by positioning the reference electrode above the center of the working electrode and then above the working electrode near the side wall. Values of current calculated from the Tafel equation and observed overpotential values indicate that values of the current density at the sloping (edge) region of the working electrode are 4% lower than at the center. Since approximately 80% of the working electrode

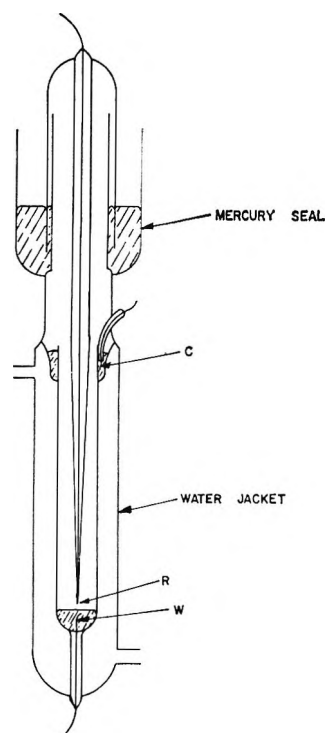


Figure 1. Cell for transient measurements with lithium amalgam electrodes.

area is within the flat region, the error caused by differences in calculated and real current densities is less than 1% if the reference electrode is positioned above the flat (center) portion of the working electrode (which it was for our exchange current determinations).

In order to minimize decomposition of amalgams and electrolytes and to avoid catalysis of the electrode reaction, the cell was constructed of Pyrex glass (which is low in leachable heavy metals). The working electrode and counterelectrode leads were 10-mil platinum wire sealed through the Pyrex glass in such a manner as to avoid contact with the DMSO electrolyte.

A secondary reference half-cell (*e.g.*, Ag|AgClO<sub>4</sub>-DMSO) with a liquid junction was avoided, since this would be a possible source of foreign ions and the determination of such a potential is unnecessary for the kinetic information we sought. The reference electrode consisted of a 20-mil nickel wire sealed in soft glass drawn to a 30-mil diameter. It was necessary to degas the nickel wire in a quartz tube under vacuum at 800° for 1 hr prior to making this seal in order to avoid gas bubbles in the soft glass. The sealed nickel wire was carefully sawed on a glass saw to yield a flat exposed nickel surface. Then the remainder of the reference electrode glass blowing was completed. The last step was to evacuate and seal the reference electrode.

After 1 week, the electrodes which had been prepared

(2) D. R. Cogley and J. N. Butler, *J. Electrochem. Soc.*, 113, 1074 (1966).

were tested with a Tesla coil; those which had leaked were discarded. Just prior to the experiment, the reference electrode was amalgamated by cathodization at approximately 1 mA/cm<sup>2</sup> in 1 M LiCl–DMSO followed by immersion in mercuric acetate–DMSO solution (the concentration was half that of saturation). This was repeated several times. The potential of reference electrodes prepared in this manner was 950 ± 50 mV positive of a lithium metal rod in LiCl–DMSO solution for cells which were not stirred during electrode cathodization or cycling. The thermodynamic value for a Li(s)|LiCl–DMSO|Li(Hg, satd) cell is 943 mV.<sup>3</sup> The reference electrodes were examined on a metallograph after rinsing in dilute aqueous acid, and the surface appeared granular and shiny, with a typical grain size of approximately 10<sup>-3</sup> cm. This is evidence of a thin amalgam layer on the nickel surface, with a roughness factor of perhaps 5–10. The potential drift of the amalgamated nickel substrate reference electrode was less than 2 mV/hr. This was well within our requirement of 50 μV for the pulse period of 25 msec.

Nickel was chosen in preference to platinum as a reference electrode substrate because amalgamation and cathodization experiments indicated that solvent decomposition apparently occurred on Pt wires cathodized as described above. It was impossible to achieve a stable potential with a Pt wire in LiCl–DMSO solutions except at potentials more than 1.5 V positive of the lithium metal.

After being filled with solution and amalgam, the cell was sealed (Figure 1), removed from the drybox, and thermostated by means of the water jacket.

Rectangular wave form current pulses were derived from a Wavetek function generator, Model 112, coupled with shunting resistors and diodes. The current was determined by observing the *IR* drop across a resistor in series with the cell. The potential response of the working electrode was monitored with an Analog Devices operational amplifier; its input impedance was greater than 10<sup>10</sup> ohms and its rise time was less than 0.5 × 10<sup>-6</sup> sec. The output of the operational amplifier was used to drive the oscilloscope, Tektronix Type 561A with a 3A7 differential preamplifier and a 2B67 time base. The 3A7 preamplifier was calibrated with a bias box and a Fluke high-impedance differential voltmeter which was calibrated against an Eppley standard cell. The 2B67 time base was calibrated with a Tektronix Type 180A Time-Mark generator. Details of the pulsing circuit not included in this article are given elsewhere.<sup>4</sup>

## Results and Discussion

Oscilloscope traces of the potential–time response of the working electrode and the *IR* drop across a resistor of known value were read by means of a Vernier scale and a magnifying glass with cross hairs. These readings were converted to overpotential and current values by

a simple computer program, employing the proper scaling factors and calibration values for the oscilloscope scales involved.

The change in potential of the working electrode during the passage of a galvanostatic pulse was assumed to be the sum of (1) concentration polarization, (2) *IR* drop between the working and reference electrodes and (3) electron-transfer overpotential. For the experiments reported here values of concentration polarization were calculated<sup>5</sup> and found to be less than 1% of the total change in potential in all cases. At the beginning of each galvanostatic pulse a clear discontinuity in the potential–time curve was observed and this was assumed to be the *IR* drop between the working and reference electrodes. The potential–time curves leveled off during the galvanostatic pulse, usually within 15 msec. This “steady-state value of the potential” minus the *IR* drop was taken to be the electron-transfer overpotential.

A second computer program was used to do a least-squares fit on the data in the form of the Allen and Hickling<sup>6</sup> equation given by Delahay<sup>7</sup> as

$$\ln \left[ \frac{I}{1 - \exp\left(\frac{nF\eta}{RT}\right)} \right] = \ln I_a^0 - (\alpha nF\eta/RT) \quad (1)$$

The quantity on the left-hand side of the equation is treated as the ordinate and  $\eta$  is treated as the abscissa. The slope yields  $\alpha$ , and the intercept at  $\eta = 0$  gives the apparent exchange current. Dividing the exchange current values (amperes),  $I_a^0$ , by the electrode area, 0.71 cm<sup>2</sup>, we obtain the exchange current density values  $i_a^0$ .

The standard exchange current density is defined as the apparent exchange current density corrected to unit activity (molar scale) of Li(Hg) and Li<sup>+</sup> and is given by

$$i_s^0 = i_a^0 \left( \frac{\text{Li(Hg)}_s}{\text{Li(Hg)}} \right)^\alpha \left( \frac{\text{Li}^+_s}{\text{Li}^+} \right)^{1-\alpha} \quad (2)$$

The true exchange current density is defined as the standard exchange current density corrected for double-layer effects (assuming lack of specific adsorption of Li<sup>+</sup> on Hg) and is given by

$$i_t^0 = i_s^0 \exp[-(\alpha n - z)F\phi_z/RT] \quad (3)$$

(3) D. R. Cogley and J. N. Butler, *J. Phys. Chem.*, **72**, 1017 (1968).

(4) “Study of the Kinetics of Lithium in Aprotic Solvents,” Final Report of Contract AF19(628)5525, Air Force Cambridge Research Laboratories, Hanscom Field, Bedford, Mass., Sept 1968.

(5) P. Delahay, “New Instrumental Methods in Electrochemistry,” John Wiley & Sons, Inc., New York, N. Y., 1954, p 180.

(6) P. L. Allen and A. Hickling, *Trans. Faraday Soc.*, **53**, 1626 (1957).

(7) P. Delahay, “Double Layer and Electrode Kinetics,” John Wiley & Sons, Inc., New York, N. Y., 1965, p 163.

Table I: Experimental Current, *I*, and Overpotential,  $\eta$ , Values

Conditions	Temp, °C	<i>I</i> , mA	$\eta$ , mV	Conditions	Temp, °C	<i>I</i> , mA	$\eta$ , mV
0.00904 M Li(Hg), 0.0631 M LiCl	20.33	0.0105	-2.85	0.1219 M Li(Hg), 0.210 M LiCl	25.00	0.0292	-0.9514
		0.0215	-5.75			0.0580	-1.90
		0.0599	-14.89			0.0580	-1.90
		0.1007	-22.49			0.146	-4.65
		-0.0106	3.20			0.146	-4.64
		-0.021	6.10			0.311	-5.12
		-0.0494	15.89			0.595	-16.32
		-0.0494	16.50			0.595	-16.39
		-0.0962	35.80			1.542	-34.37
						1.542	-34.34
	25.00	-0.0118	2.90	-0.0292	0.94		
		-0.0242	6.30	-0.0292	0.95		
		-0.0574	15.43	-0.1445	5.08		
		-0.1057	30.85	-0.1445	5.06		
		0.01125	-2.77	0.00904 M Li(Hg), 2.104 M LiCl	25.00	-0.0214	3.66
		0.02572	-6.15			-0.0485	8.43
		0.0657	-13.80			-0.0485	8.44
		0.109	-22.99			-0.1058	20.61
		0.109	-21.36			-0.208	46.38
		34.40	0.01597			-2.55	-0.208
0.0314	-4.65		-0.374			91.03	
0.0314	-4.63		-0.374			91.47	
0.0820	-11.58		-1.135			207.2	
0.0820	-11.64		-1.135			206.8	
-0.0157	2.57		-2.927	319.5			
-0.0310	5.12		-2.927	320.1			
0.388	-39.07		0.0503	-7.29			
0.388	-39.56		0.0503	-7.28			
1.067	-65.62		0.1276	-16.87			
1.067	-65.66	0.1276	-16.88				
1.136	-69.58	0.299	-32.42				
1.136	-68.79	0.299	-32.55				
		0.299	-33.2				

The heterogeneous rate constant (cm/sec) is given by

$$k_s^0 = \frac{i_s^0 \times 10^3}{nF} \quad (4)$$

or, corrected for double-layer effects

$$k_t^0 = \frac{i_t^0 \times 10^3}{nF} \quad (5)$$

Experimental values of  $\eta$  and *I* are given in Table I and the least-squares values of  $I_a^0$  and  $\alpha$  are given in Table II.

In Figure 2 we present a plot of  $\eta(\text{obsd})/\eta(\text{calcd})$  vs.  $\log I$  for the Li(Hg)-LiCl data. The scatter is low and mass-transfer polarization is not evident. The experimental data fit the Tafel equation well.

Assuming  $\alpha = 0.75$  and electrode area  $0.71 \text{ cm}^2$ , we compute the values given in Table III.

Values of excess charge, *q*, at the amalgam surface were obtained by graphical integration of the double-layer capacity vs. potential curve for 1 M LiPF<sub>6</sub>.<sup>8</sup> The values for LiPF<sub>6</sub> are expected to be quite similar to those for LiCl at highly negative potentials. The

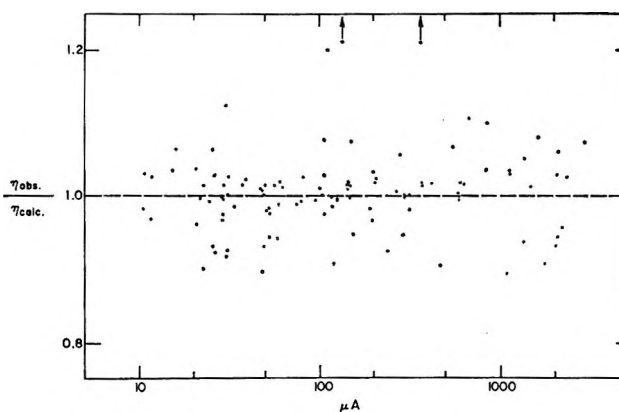


Figure 2. Ratio of observed overpotential to calculated overpotential vs.  $\log I$ . Arrows indicate points which lie off scale.

double-layer capacity has been shown to be nearly independent of the solute species at potentials negative of the point of zero charge, and we were thus able to obtain approximate values for *q*.  $\phi_2$  (V) is related to *q* (C/cm<sup>2</sup>) by the equation

(8) R. Payne, *J. Amer. Chem. Soc.*, **89**, 489 (1967).

**Table II:** Transfer Coefficient and Apparent Exchange Current Values for the Li(Hg)/LiCl-DMSO Couple

Run	[Li(Hg)], M	Activity coeff <sup>a</sup>	[LiCl], M	Activity coeff <sup>b</sup>	Temp, °C	$\alpha^c$	$10^4 I_a^0$ , A <sup>c</sup>
A1	0.00904	1.005	0.0631	0.621	20.33	0.74 ± 0.03	0.89 ± 0.02
					25.00	0.72 ± 0.03	1.07 ± 0.02
					34.40	0.77 ± 0.02	1.66 ± 0.04
A2	0.1219	1.061	0.210	0.515	25.00	0.74 ± 0.02	7.79 ± 0.09
A3	0.00904	1.005	2.104	0.372	25.00	0.763 ± 0.003	1.61 ± 0.03

<sup>a</sup> Reference 3. <sup>b</sup> G. Holleck, D. R. Cogley, and J. N. Butler, unpublished results. <sup>c</sup> Least-squares fit to Allen-Hickling plot.

**Table III:** Exchange Current and Rate Constant Values at 25° Calculated for  $\alpha = 0.75 \pm 0.02$ 

Run	$10^4 i_a^0$ , A/cm <sup>2</sup>	$q$ , $\mu\text{C}/\text{cm}^2$	$\phi_2$ , V	$10^4 k_t^0$ , A/cm <sup>2</sup>	$10^4 k_s^0$ , cm/sec	$10^4 k_e^0$ , cm/sec
A1	11.3 ± 0.3	-20.20	-0.148	2.7 ± 0.4	11.9 ± 0.3	2.8 ± 0.4
A2	8.9 ± 0.3	-20.54	-0.118	2.8 ± 0.2	9.2 ± 0.3	2.9 ± 0.2
A3	8.6 ± 0.6	-20.56	-0.063	4.4 ± 0.2	8.5 ± 0.6	4.6 ± 0.6

$$q = 2 \left( \frac{RT \epsilon \epsilon_0 C}{2\pi} \right)^{1/2} \sinh \left( \frac{zF\phi_2}{2RT} \right) \quad (6)$$

From the calculated values of  $k_t^0$  for runs A1 and A2, we see that values determined at quite different concentrations agree well. This may be taken as evidence that the proper value of  $\alpha$  was used in the computation and thus that the reaction is a simple electron-transfer process and that adsorption of the reacting species at the double layer did not occur. The  $k_t^0$  value calculated from run A3 is substantially higher than for the other runs. This may be accounted for by adsorption of lithium ion at the double layer in solutions of high lithium chloride concentration.

An Arrhenius plot of  $I_a^0$  vs.  $10^3/T$  is given in Figure 3 for run A1. The enthalpy of activation<sup>9</sup> calculated from the equation

$$\Delta H_0^\ddagger = -R \left( \frac{\partial \ln I_a^0}{\partial (1/T)} \right) \quad (7)$$

is 7.9 kcal/mol.

There are no other investigations of electrode kinetics in nonaqueous solutions with which our results can be

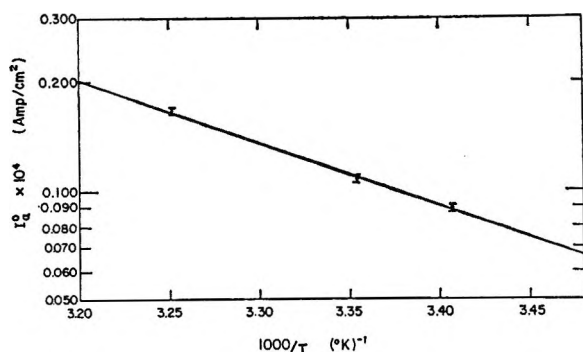


Figure 3. Arrhenius plot of  $\log I_a^0$  vs. reciprocal temperature.

compared. The lithium-lithium ion reaction in DMSO appears to be quite different in its energetics from the same reaction in water, where the rate constant is 100 times faster.<sup>10</sup> The enthalpy of activation observed in DMSO is similar to that for slow reactions such as hydrogen evolution and heavy metal ion deposition in aqueous solutions. These results indicate that there is a considerable enthalpy barrier in the transition state as well as the expected entropy of activation resulting from reorientation of solvent molecules.

*Acknowledgment.* This research was supported by the U.S. Air Force Cambridge Research Laboratories, Office of Aerospace Research, under Contract AF 19-(628)-5525, but does not necessarily reflect endorsement by the sponsor.

### Symbols

$\Delta H_0^\ddagger$	Real enthalpy of activation at the reversible potential, kcal/mol (eq 7)
$\alpha$	Cathodic transfer coefficient
$I$	Current, amperes
$n$	Equivalents per mole
$F$	Faraday constant, 96,500 C/equiv
$\eta$	Overpotential, volts
$R$	Gas constant, 8.314 J/mol deg
$T$	Absolute temperature, degrees Kelvin
$I_a^0$	Apparent exchange current, amperes (eq 1)
$i_a^0$	Apparent exchange current density, A/cm <sup>2</sup>
$i_s^0$	Standard exchange current density, A/cm <sup>2</sup> (eq 2)
$s$	Subscript s refers to reagents in standard state (unit activity on the molar scale)
$i_t^0$	True (corrected for double-layer effects) exchange current density, A/cm <sup>2</sup> (eq 3)
$z$	Units of charge on species reacting at the double layer
$\phi_2$	Helmholtz potential at the double layer, volts (eq 6)

(9) J. N. Agar, *Discussions Faraday Soc.*, 1, 81 (1947).

(10) H. Imai and P. Delahay, *J. Phys. Chem.*, 66, 1683 (1962).

$k_s^0$	Standard heterogeneous rate constant, cm/sec (eq 4)	$\epsilon$	Dielectric constant, 46.6 for DMSO
$k_t^0$	True heterogeneous rate constant, cm/sec (eq 5)	$\epsilon_0$	Permittivity of free space ( $1.1128 \times 10^{-5}$ )
$q$	Excess surface charge at the double layer, C/cm <sup>2</sup> (eq 6)	$C$	Electrolyte concentration

## The Molybdenum(VI)-Catalyzed Oxidation of Hydrazine

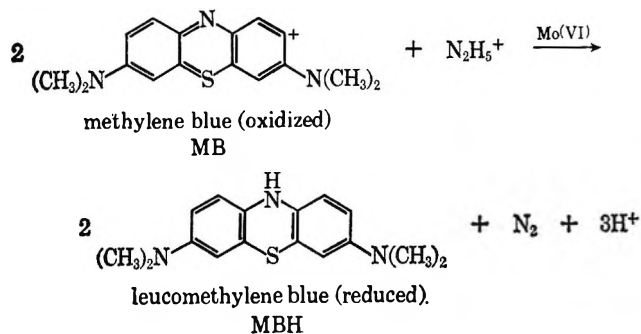
### by Methylene Blue

by T. Huang<sup>1</sup> and J. T. Spence

Chemistry Department, Utah State University, Logan, Utah 84321 (Received June 17, 1968)

The Mo(VI)-catalyzed oxidation of  $N_2H_5^+$  by methylene blue (MB) has been studied at pH 1.60. The reaction was found to be kinetically pseudo first order, with the rate dependent on Mo(VI) and  $N_2H_5^+$  concentrations and independent of MB concentration. The rate constant and activation parameters are essentially identical with those for the oxidation of  $N_2H_5^+$  by Mo(VI). To obtain information on the catalyzed reaction, the oxidation of  $Mo^{V_2}$  by MB has also been studied and has been found to proceed at a much faster rate than the catalyzed oxidation of hydrazine and with first-order kinetics, again independent of MB concentration. The results for the catalyzed oxidation of  $N_2H_5^+$  have been interpreted in terms of a slow oxidation of  $N_2H_5^+$  by Mo(VI) giving Mo(IV), followed by a fast oxidation of Mo(IV) by MB to regenerate Mo(VI). Small quantities of Mo(V) and MB radical, which are probably formed by competing reactions of Mo(IV) with Mo(VI) and the subsequent reaction of Mo(V) and MB, were detected by esr. A mechanism for the reaction involving Mo(IV), Mo(V), and MB radical as reactive intermediates is proposed.

Molybdenum is involved in the biological processes of nitrate reduction<sup>2</sup> and nitrogen fixation.<sup>3</sup> In the case of nitrate reductase and with other molybdenum enzymes such as xanthine oxidase, flavin is also a necessary cofactor, and it appears that the metal ion may participate in electron transfer between substrate and flavin. As a model for such reactions, the molybdenum(VI)-catalyzed oxidation of hydrazine to  $N_2$  by methylene blue (methylene blue is similar to flavins in its structure and redox properties) has been investigated.



The oxidation of  $N_2H_5^+$  by methylene blue (MB) in the presence of Mo(VI) has been used as an analytical method for the estimation of hydrazine, but little is known of the mechanism of the reaction.<sup>4</sup> Recent work

in this laboratory has shown that Mo(VI) oxidizes  $N_2H_5^+$  under the proper conditions and the mechanism of the reaction has been investigated.<sup>5</sup> The results of that study indicate Mo(VI) is a two-electron oxidant, giving  $N_2$  and  $Mo^{V_2}$  as products (the  $Mo^{V_2}$  is probably produced *via* Mo(IV) as an intermediate). This suggested that the oxidation with MB proceeds by a similar mechanism, with the Mo(IV) or Mo(V) being reoxidized to Mo(VI) by the dye. This has been confirmed by a kinetic study of the reaction and by an investigation of the oxidation of  $Mo^{V_2}$  by MB.

### Results

**Kinetics of the Mo(VI)-Catalyzed Reaction.** Straight lines and consistent values of the rate constant could only be obtained from the kinetic data when the reaction was treated as first order in  $N_2H_5^+$  and zero order in MB, according to the rate expression

(1) Abstracted from the Ph.D. dissertation of T. Huang, Utah State University, 1968.

(2) A. Nason, "The Enzymes," Vol. 7, P. D. Boyer, H. Lardy, and K. Myrback, Ed., Academic Press Inc., New York, N. Y., 1958, p 507.

(3) L. E. Mortenson, J. A. Morris, and I. R. Kennedy, Abstracts of Papers, American Society for Microbiology, Bacteriological Proceedings, 68th Annual Meeting, Detroit, Mich., 1968, p 133.

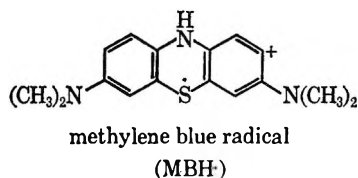
(4) R. Lang, *Z. Anal. Chem.*, **128**, 165 (1948).

(5) T. Huang and J. T. Spence, *J. Phys. Chem.*, **72**, 4198 (1968).

$$\frac{-d[\text{MB}]}{dt} = k_1'[\text{N}_2\text{H}_5^+]$$

Upon integration this gives the standard first-order rate equation. Additional kinetic data were collected at various temperatures and the activation energy and entropy were obtained from an Arrhenius plot.  $\Delta F^\ddagger$  for the reaction was calculated from Eyring's rate equation. The rate constants, obtained from the slopes of the first-order kinetic plots, and the activation parameters are found in Table I; typical plots are given in Figure 1.

An esr analysis of the reaction mixture showed the presence of two signals at very low concentrations, with  $g$  values of 1.94 and 2.00, respectively. These were attributed to Mo(V) monomer and methylene blue radical (MBH $\cdot$ ).<sup>5</sup>



*Kinetics of the Oxidation of Mo<sup>V</sup><sub>2</sub> by Methylene Blue.* Since the catalyzed reaction was found to be first order in N<sub>2</sub>H<sub>5</sub><sup>+</sup> and zero order in MB, it seemed likely that the dye is reduced in a fast step by either the Mo(IV) or Mo(V) formed by the reduction of Mo<sup>V</sup><sub>2</sub> by N<sub>2</sub>H<sub>5</sub><sup>+</sup>. Unfortunately, Mo(IV) is unstable in solution and its compounds are difficult to obtain. Mo<sup>V</sup><sub>2</sub>, on the other hand, is readily prepared by reduction of Mo(VI)<sup>6</sup> and a study of its oxidation by MB was made in order to obtain more information concerning the mechanism of the Mo(VI)-catalyzed reduction of N<sub>2</sub>H<sub>5</sub><sup>+</sup> by the dye.

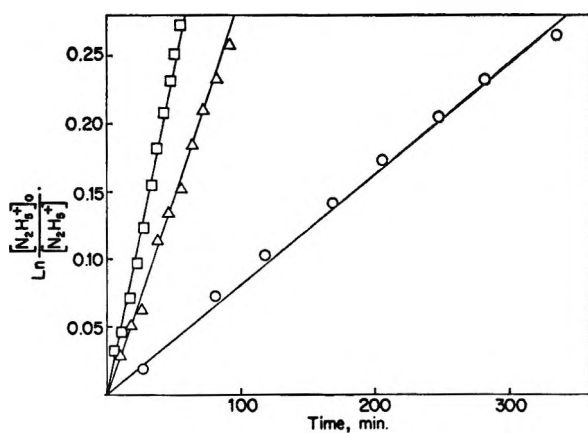


Figure 1. First-order kinetic plots for Mo(VI)-catalyzed oxidation of N<sub>2</sub>H<sub>5</sub><sup>+</sup> by MB: O, [Mo(VI)] = 4.91 × 10<sup>-4</sup> M, [N<sub>2</sub>H<sub>5</sub><sup>+</sup>]<sub>0</sub> = 1.91 × 10<sup>-4</sup> M, [MB]<sub>0</sub> = 9.86 × 10<sup>-6</sup> M, 50°; Δ, [Mo(VI)] = 4.98 × 10<sup>-4</sup> M, [N<sub>2</sub>H<sub>5</sub><sup>+</sup>]<sub>0</sub> = 2.00 × 10<sup>-4</sup> M, [MB]<sub>0</sub> = 1.000 × 10<sup>-4</sup> M, 70°; □, [Mo(VI)] = 4.91 × 10<sup>-4</sup> M, [N<sub>2</sub>H<sub>5</sub><sup>+</sup>]<sub>0</sub> = 1.82 × 10<sup>-4</sup> M, [MB]<sub>0</sub> = 9.75 × 10<sup>-6</sup> M, 80°. Phosphate buffer, pH 1.60, μ = 0.22 M.

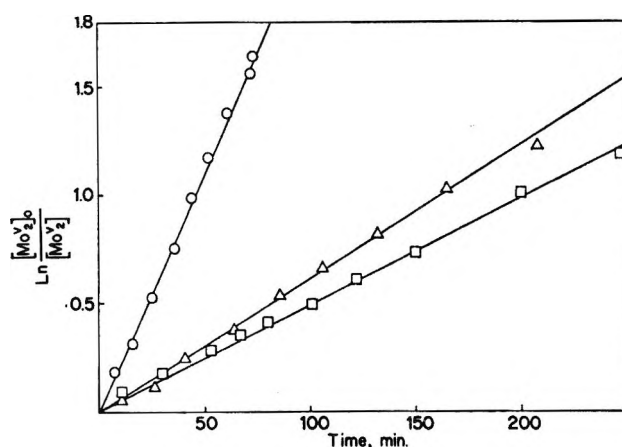
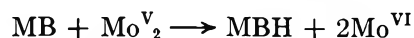


Figure 2. First-order kinetic plots for oxidation of Mo<sup>V</sup><sub>2</sub> by MB: O, [Mo<sup>V</sup><sub>2</sub>]<sub>0</sub> = 1.39 × 10<sup>-4</sup> M, [MB]<sub>0</sub> = 1.34 × 10<sup>-4</sup> M, 40°; □, [Mo<sup>V</sup><sub>2</sub>]<sub>0</sub> = 1.79 × 10<sup>-4</sup> M, [MB]<sub>0</sub> = 1.07 × 10<sup>-4</sup> M, 25°; Δ, [Mo<sup>V</sup><sub>2</sub>]<sub>0</sub> = 1.29 × 10<sup>-4</sup> M, [MB]<sub>0</sub> = 1.29 × 10<sup>-4</sup> M, 30°. Phosphate buffer, pH 1.60.

When Mo<sup>V</sup><sub>2</sub> was added to an anaerobic solution of MB at 70° and pH 1.60, the blue color disappeared entirely within 10 min, indicating essentially complete reduction to the leuco form. The temperature was therefore lowered to 25°, where the kinetics could be conveniently followed. The stoichiometry was checked by adding a twofold excess of Mo<sup>V</sup><sub>2</sub> to a known concentration of dye and then measuring the remaining Mo<sup>V</sup><sub>2</sub> spectrophotometrically at 289 mμ after the methylene blue was essentially completely reduced. The results confirmed the stoichiometric equation



The order of the reaction was found by plotting the data using various rate laws and found to be first order in Mo<sup>V</sup><sub>2</sub>, with the rate independent of MB concentration, according to the rate expression

$$\frac{-d[\text{MB}]}{dt} = k_1''[\text{Mo}^{\text{V}}_2]$$

This gives the standard first-order equation upon integration, which was plotted to obtain the rate constants (Figure 2). Additional runs were made at different temperatures, allowing the activation energy to be obtained from an Arrhenius plot. The results are summarized in Table II.

### Discussion

Previous work in this laboratory has shown that the oxidation of Mo<sup>V</sup><sub>2</sub> by I<sub>2</sub> and O<sub>2</sub> is first order in Mo<sup>V</sup><sub>2</sub>, with the rate being independent of oxidant concentration,<sup>6</sup> as was found in the present study of the oxidation with MB. It therefore seemed likely that the oxidation by the dye proceeds by the same mechanism as the oxidation by I<sub>2</sub> and O<sub>2</sub>. A comparison of the first-order

(6) E. P. Guymon and J. T. Spence, *J. Phys. Chem.*, **71**, 1616 (1967).

**Table I:** Mo(VI)-Catalyzed Oxidation of  $N_2H_5^+$  by MB at pH 1.60 and  $\mu = 0.22 M$ 

Run	$10^4[Mo(VI)]_0$ <i>M</i>	$10^4[N_2H_5^+]_0$ <i>M</i>	$10^4[MB]_0$ <i>M</i>	Temp, °C	$10^3k_1',^a$ min <sup>-1</sup>	$k_2',^b$ M <sup>-1</sup> min <sup>-1</sup>
1	4.91	1.91	0.986	50	0.825 ± 0.01	1.68
2	4.91	1.88	0.450	60	1.42 ± 0.02	2.89
3	4.98	2.00	1.000	70	2.90 ± 0.03	5.83
4	4.91	1.82	0.466	80	5.20 ± 0.06	10.6

<sup>a</sup> All rate constants are averages of two runs. <sup>b</sup>  $k_2' = k_1'/[Mo(VI)]$ .  $E_a = 14.7$  kcal/mol,  $\Delta S^\ddagger = -6.9$  eu,  $\Delta F^\ddagger = 16.4$  kcal/mol (calculated from  $k_2'$  at 70°).

**Table II:** Oxidation of  $MoV_2$  by MB

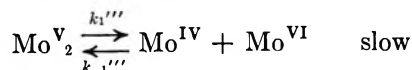
Run	$10^4[MoV_2]_0$ <i>M</i>	$10^4[MB]_0$ <i>M</i>	pH	$\mu$ , <i>M</i>	Temp, °C	$10^3k_1'',^a$ min <sup>-1</sup>
1	2.48	1.27	1.60	0.22	25	5.20
2	1.79	1.07	1.60	0.22	25	4.90
3	2.50	1.72	1.60	0.22	25	5.50
4	2.50	1.85	1.60	0.22	25	5.30
5	1.86	1.36	1.60	0.22	25	5.00
6	1.29	1.29	1.60	0.22	30	6.40 ± 0.30
7	1.29	1.29	1.60	0.22	35	14.8 ± 0.3
8	1.39	1.34	1.60	0.22	40	22.2 ± 0.5
9	1.29	1.29	1.65	0.22	30	5.90 ± 0.15

<sup>a</sup> For runs 6–9,  $k_1''$  values are averages of duplicates.  $E_a = 23.4 \pm 0.2$  kcal/mol.

rate constants and the activation energies for the reactions gives strong support for this, since they are the same order of magnitude:  $MoV_2$  oxidation by  $I_2$ :  $k = 2.72 \times 10^{-3}$  min<sup>-1</sup>, pH 1.65, 30°,  $\mu = 0.51 M$ ,  $E_a = 24.3$  kcal/mol;<sup>6</sup>  $MoV_2$  oxidation by MB:  $k_1'' = 5.90 \times 10^{-3}$  min<sup>-1</sup>, pH 1.65, 30°,  $\mu = 0.22 M$ ,  $E_a = 23.4$  kcal/mol.

The difference between the two constants might be due to the difference in ionic strength, since a negative salt effect was observed in the oxidation by  $I_2$ .<sup>6</sup> It is also possible MB forms a weak complex with  $MoV_2$  which could affect the rate somewhat.

It therefore seems likely the oxidations proceed by a similar mechanism, which was proposed to involve the dissociation of  $MoV_2$  into  $Mo(IV)$  and  $Mo(VI)$  as the rate-controlling step in the  $I_2$  oxidation ( $Mo(V)$  monomer as the reactive intermediate was ruled out in the oxidation of  $MoV_2$  by  $I_2$  on the basis that its rate of formation from the dimer, as measured by esr, is too slow to account for the over-all rate)<sup>6</sup>



From this mechanism, which is identical with that for the  $I_2$  oxidation with MB replacing  $I_2$  in the second step, the disappearance of MB may be written

$$-d[MB]/dt = k_2'''[MB][Mo(IV)] \quad (1)$$

Applying the steady-state assumption to  $Mo(IV)$  and substituting the resulting expression into eq 1

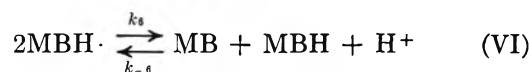
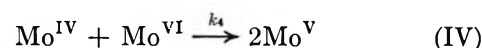
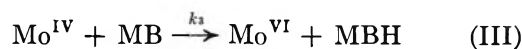
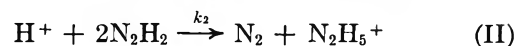
$$\frac{-d[MB]}{dt} = \frac{k_1''''k_2''''[MB][MoV_2]}{k_{-1}''''[Mo(VI)] + k_2''''[MB]} \quad (2)$$

If  $k_2''''[MB] \gg k_{-1}''''[Mo(VI)]$

$$\frac{-d[MB]}{dt} = k_1''''[MoV_2]$$

This is identical with the experimental rate law.

Taking into account all of the data reported here and the results of the investigation of the oxidation of  $N_2H_5^+$  by  $Mo(VI)$ ,<sup>5</sup> the following mechanism is proposed for the  $Mo(VI)$ -catalyzed oxidation of  $N_2H_5^+$  by MB.



Reaction I is rate controlling and is identical with the rate-controlling step in the oxidation of  $N_2H_5^+$  by

Mo(VI).<sup>5</sup> Therefore, the rate constants for the two over-all reactions should be the same. When the experimental rate constant for the catalyzed reaction,  $k_1'$  (Table I), is divided by the Mo(VI) concentration, the new constant  $k_2'$  is identical, within the experimental error, with that obtained in the oxidation by Mo(VI).<sup>5</sup>

$$\frac{-d(\text{MB})}{dt} = k_1'[\text{N}_2\text{H}_5^+] = k_2'[\text{N}_2\text{H}_5^+][\text{Mo(VI)}]$$

$$k_1' = k_2'[\text{Mo(VI)}]$$

For the Mo(VI)-catalyzed oxidation of  $\text{N}_2\text{H}_5^+$  by MB:  $k_2' = 5.83 \pm 0.06 \text{ M}^{-1} \text{ min}^{-1}$ , pH 1.60,  $\mu = 0.22$ ,  $70^\circ$ ,  $E_a = 14.0 \text{ kcal/mol}$ . For the oxidation of  $\text{N}_2\text{H}_5^+$  by Mo(VI):  $k = 5.87 \pm 0.05 \text{ M}^{-1} \text{ min}^{-1}$ , pH 1.60,  $\mu = 0.22$ ,  $70^\circ$ ,  $E_a = 14.3 \text{ kcal/mol}$ . Furthermore, the activation energies are seen to be essentially identical. Thus, the experimentally observed first-order reaction is actually pseudo first order, since the Mo(VI) concentration remains constant.

In this mechanism, reactions II<sup>7</sup> and III are fast, while reaction IV accounts for the presence of a small amount of Mo(V) monomer (as detected by esr). Since the monomer is known to dimerize readily,<sup>8</sup> and no dimer was observed, either reaction IV is much slower than reaction III or the monomer reacts quickly with MB to form MBH· radical, as in reaction V, followed by a rapid disproportionation of the radical according to equilibrium VI (such disproportionations are well known<sup>9</sup>), thus accounting for the small  $g = 2.00$  esr signal observed. Alternatively, if reaction V does not occur, the radical could still arise by equilibrium VI. That equilibrium VI actually exists was demonstrated by the observation of a small esr signal at  $g = 2.00$  in a solution of MB that had been partially reduced by dithionite under the reaction conditions.

The experimental rate law is obtained from the mechanism by the following treatment. The disappearance of MB may be written

$$\frac{-d[\text{MB}]}{dt} = k_3[\text{Mo(IV)}][\text{MB}] + k_5[\text{MB}][\text{Mo(V)}] + k_{-6}[\text{MB}][\text{MBH}](\text{H}^+) - k_6[\text{MBH}\cdot]^2 \quad (3)$$

Mo(IV), Mo(V), and MBH· are reactive intermediates and the steady-state assumption may be applied to each, which readily gives the expression

$$\frac{-d[\text{MB}]}{dt} = k_1[\text{Mo(VI)}][\text{N}_2\text{H}_5^+] \quad (4)$$

Since  $[\text{Mo(VI)}]$  is constant, this gives the pseudo-first-order experimental rate law

$$\frac{-d[\text{MB}]}{dt} = k_1'[\text{N}_2\text{H}_5^+] \quad k_1' = k_1[\text{Mo(VI)}]$$

The results suggest that Mo(IV) may be involved in

enzymatic reactions, in which case it would probably be stabilized by binding to the protein or coenzyme. This would account for the low percentage of total molybdenum detectable as Mo(V) (using esr) for reduced xanthine oxidase,<sup>10</sup> provided the ligand field of the enzyme is sufficiently distorted to lift the degeneracy of the  $t_{2g}$  orbitals of Mo(IV). Studies of model complexes of Mo(IV) with biologically important ligands to test this possibility are planned.

### Experimental Section

**Chemicals.** Methylene blue chloride, obtained from Hartman-Ledden Co., was used without further purification since recrystallization gave a product with  $\epsilon$  identical with that of the unrecrystallized material. Molybdenum(VI) and  $\text{MoV}_2$  stock solutions were prepared and standardized as previously described.<sup>6</sup> Materials for all buffers were reagent grade. Dithionite, used for reduction of MB, was obtained from J. T. Baker Co. All solutions were prepared from doubly distilled  $\text{H}_2\text{O}$ , since small amounts of  $\text{Cu}^{2+}$  and  $\text{Fe}^{3+}$  catalyze the autodecomposition of  $\text{N}_2\text{H}_4$ . Hydrazine sulfate solutions were prepared from Fisher Co. reagent and analyzed according to the method of Watt and Chrisp.<sup>11</sup> Helium (99.99%), used for deaeration, was obtained from J. T. Baker Co.

The kinetics of the oxidation of  $\text{N}_2\text{H}_5^+$  and  $\text{MoV}_2$  by MB were determined by following the disappearance of the dye at 609  $m\mu$ , using a quartz spectrophotometer cell which could be evacuated and filled anaerobically from a reaction vessel under He.<sup>6</sup> After filling, the cell was sealed and placed in a constant-temperature bath. Readings were made periodically in a Beckman DU spectrophotometer equipped with a constant-temperature compartment. The concentrations of  $\text{MoV}_2$  and  $\text{N}_2\text{H}_5^+$  were calculated from the stoichiometric relationships. In the stoichiometric determinations,  $\text{MoV}_2$  was measured spectrophotometrically at 289  $m\mu$  after all of the MB had been reduced to the leuco form. All reactions were run in phosphate buffer,  $\mu = 0.22 \text{ M}$ .

For esr measurements, samples were removed from the reaction vessel with a gastight syringe, transferred anaerobically to a quartz esr tube, frozen in liquid nitrogen, and measured in a Varian V-4500-10 X-band esr spectrometer equipped with 100-kc field modulation.

Rate constants and activation parameters were obtained from the slopes of the appropriate plots, using the method of least squares. The  $g$  values were ob-

(7) W. C. E. Higginson, "The Oxidation of Hydrazine in Aqueous Solution," Special Publication No. 10, The Chemical Society, London, 1957.

(8) J. T. Spence and M. Heydanek, *Inorg. Chem.*, **6**, 1489 (1967).

(9) W. M. Clark, "Oxidation-Reduction Potentials of Organic Systems," Williams and Wilkins Co., Baltimore, Md., 1960, p 184.

(10) H. Beinert and W. H. Orme-Johnson, "Magnetic Resonance in Biological Systems," A. Ehrenberg, B. G. Malmstrom, and T. Vanngard, Ed., Pergamon Press Ltd., London, 1967, p 221.

(11) G. W. Watt and J. D. Chrisp, *Anal. Chem.*, **24**, 2006 (1952).



tained by comparison with quinhydrone in alkaline ethanol.

*Acknowledgment.* Thanks are expressed to the U. S.

Public Health Service (Grant GM-08347, National Institute of General Medical Sciences) for financial support.

## The Fluorescence of Protonated Azulenoid Systems

by R. C. Dhingra and J. A. Poole

*Department of Chemistry, Temple University of the Commonwealth System of Higher Education, Philadelphia, Pennsylvania 19122 (Received June 20, 1968)*

The emissive behavior of protonated Hafner's hydrocarbons (*viz.*, 3,5-dimethylcyclopenta[*ef*]heptalenium, 3,5-dimethyl-8-phenylcyclohepta[*cd*]pentalenium, and 4-methylpentaleno[2,1,6-*def*]heptalenium ions) and of certain protonated 1-substituted azulenes (*viz.*, 1-trifluoroacetyl, 1-nitro, and 1-carboxy derivatives) have been examined in fluid solution at room temperature. Naphth[2,1,8-*cde*]azulene was also investigated and it was observed to emit anomalously. The fluorescence of the protonated species was normal except in two cases, where the emission originated from a high-energy singlet state.

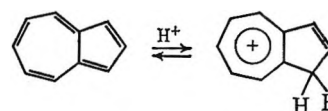
In a previous publication<sup>1</sup> we reported some of our experimental results concerning the anomalous emissive behavior of certain substituted, *peri*-condensed, non-alternant Hafner's hydrocarbons. Subsequently, we observed the conservation of this anomalous emissive property in 1-trifluoroacetylazulene, 1-nitroazulene, and in 1-azuloic acid. In each case the emission was observed to originate from a high-energy singlet state.<sup>2</sup> While inquiring into the extent of molecular modification required for elimination of the anomaly, we initiated an experimental investigation of the properties of the protonated species, in absorption and in emission.

### Experimental Section

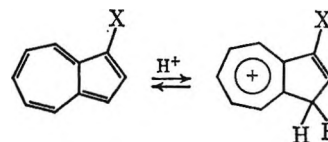
Details can be found in ref 1 and 2. All absorption spectra were taken either in Spectrograde cyclohexane as the solvent or 60% sulfuric acid (except for the 4-methylpentaleno[2,1,6-*def*]heptalene, where perchloric acid was employed, and naphth[2,1,8-*cde*]azulene, where concentrated sulfuric acid was required for protonation). Emission spectra were taken using fluorometric grade methylcyclohexane as the solvent. In all cases the temperature was  $23.5 \pm 1^\circ$ . It was generally observed that the ions exhibited more intense luminescence than the corresponding nonprotonated species.

### Results and Discussion

In the case of azulene, it is known<sup>3</sup> that reversible monoprotonation occurs to form the azulonium ion structure

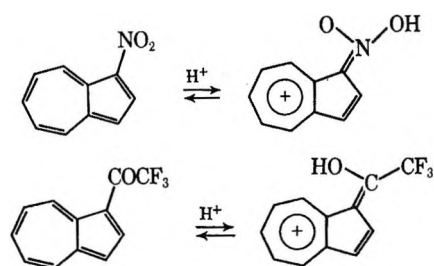


Concerning certain substituted azulenes, Meuche and Heilbronner have reported<sup>4</sup> that protonation of 1-nitroazulene in trifluoroacetic acid-sulfuric acid produced only the *aci* compound, the conjugate acid carrying the acidic proton on the nitro group rather than on the carbon atom in position 3. Similarly, Schulze and Long<sup>5</sup> have shown that in 100% sulfuric acid, reversible, monoprotonation of certain 1-substituted azulenes occurs. For the  $-\text{CH}_3$ ,  $-\text{Cl}$ , and  $-\text{CN}$  derivatives, the protonation occurs at position 3, forming the vinyltropylium-like ion structure



However, for  $-\text{NO}_2$  and  $-\text{COCF}_3$  the evidence indicated that only the *aci* compounds were produced, by oxygen protonation

- (1) R. C. Dhingra and J. A. Poole, *J. Chem. Phys.*, **48**, 4829 (1968).
- (2) R. C. Dhingra and J. A. Poole, *Chem. Phys. Lett.*, **2**, 108 (1968).
- (3) S. S. Danyluk and W. G. Schneider, *J. Amer. Chem. Soc.*, **82**, 997 (1960).
- (4) D. Meuche and E. Heilbronner, *Helv. Chim. Acta*, **45**, 1965 (1962).
- (5) J. Schulze and F. A. Long, *J. Amer. Chem. Soc.*, **86**, 322 (1964).



In the case of 1-azuloic acid, the conclusions were somewhat uncertain, and it is not clear how much protonation occurs at the 3 position. In the case of the three benzazulenes, Meier, Meuche, and Heilbronner reported<sup>6</sup> protonation on the five-carbon ring.

The results quoted above concern the immediately formed species; in certain cases other tautomeric forms are produced after some time has elapsed.

Our results on the protonation of Hafner's hydrocarbons are illustrated in Figure 1. It is clear that only the 4-methylpentaleno[2,1,6-*def*]heptalene (shown at the bottom of the figure) emits anomalously after protonation. This may be due to the fact that only in this case is an azulene moiety preserved upon protonation. Such protonation is expected to occur at a position on a five-membered ring (see, for example, the calculation of charge densities in a paper by Rosowsky, *et al.*<sup>7</sup>).

Figure 2 illustrates our results for the 1-substituted azulenes, and it is evident that the emission is normal in each case. Treibs and Scholz<sup>8</sup> reported the emission of a number of ions of the azulonium-type structure. Although they did not report the emitting level, a comparison with the available absorption spectra<sup>9</sup> indicates that the emission was normal.

In addition, we investigated the spectral properties of naphth[2,1,8-*cde*]azulene.



The synthesis and absorption spectrum of this compound have been described by Gardner, *et al.*<sup>10</sup> Heilbronner, *et al.*,<sup>11</sup> have carried out calculations of the energy levels and compared them with the experimentally observed spectra.

The absorption and emission spectra of this compound in methylcyclohexane and concentrated sulfuric acid are illustrated in Figures 3 and 4. The compound dissolves in concentrated sulfuric acid, giving a purple solution, from which, upon dilution, the hydrocarbon can be recovered. It can be seen that anomalous emission is exhibited in either solvent.

Therefore, it appears that protonation of a five-membered ring, or of an oxygen-carrying substituent on a five-membered ring, is sufficient to suppress the anomalous emission exhibited by these compounds.

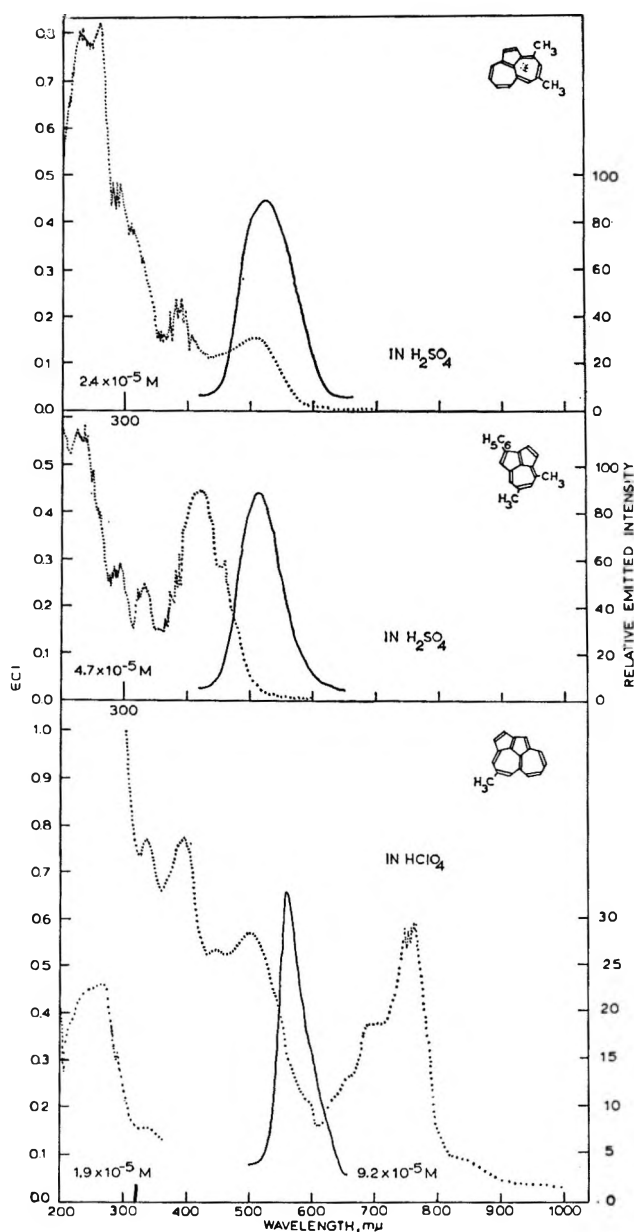


Figure 1. Absorption (····) and emission (—) spectra of substituted Hafner's hydrocarbons taken in fluid solution at room temperature, with concentrated acid as solvent. The exciting line is indicated in each case by a short vertical line in the short-wavelength region of the spectrum. The emission spectra were taken under the following experimental conditions: top:  $1.1 \times 10^{-3} M$ , sensitivity 30, 0.01 mm; middle:  $0.6 \times 10^{-3} M$ , sensitivity 30, 0.3 mm; bottom:  $2.5 \times 10^{-4} M$ , sensitivity 50, 0.001 mm. The compound names are: top, 3,5-dimethylcyclopenta[*ef*]heptalene; middle, 3,5-dimethyl-8-phenylcyclohepta[*cd*]pentalene; bottom, 4-methylpentaleno[2,1,6-*def*]heptalene.

(6) W. Meier, D. Meuche, and E. Heilbronner, *Helv. Chim. Acta*, **45**, 2628 (1962).

(7) A. Rosowsky, H. Fleischer, S. T. Young, R. Partch, W. H. Saunders, Jr., and V. Boekelheide, *Tetrahedron*, **11**, 121 (1960).

(8) W. Treibs and M. Scholz, *Z. Phys. Chem. (Leipzig)*, **214**, 118 (1959).

(9) E. Heilbronner, "Azulenes, Non-Benzenoid Aromatic Hydrocarbons," D. Ginsburg, Ed., Interscience Publishers, New York, N. Y., 1959, pp 251-252.

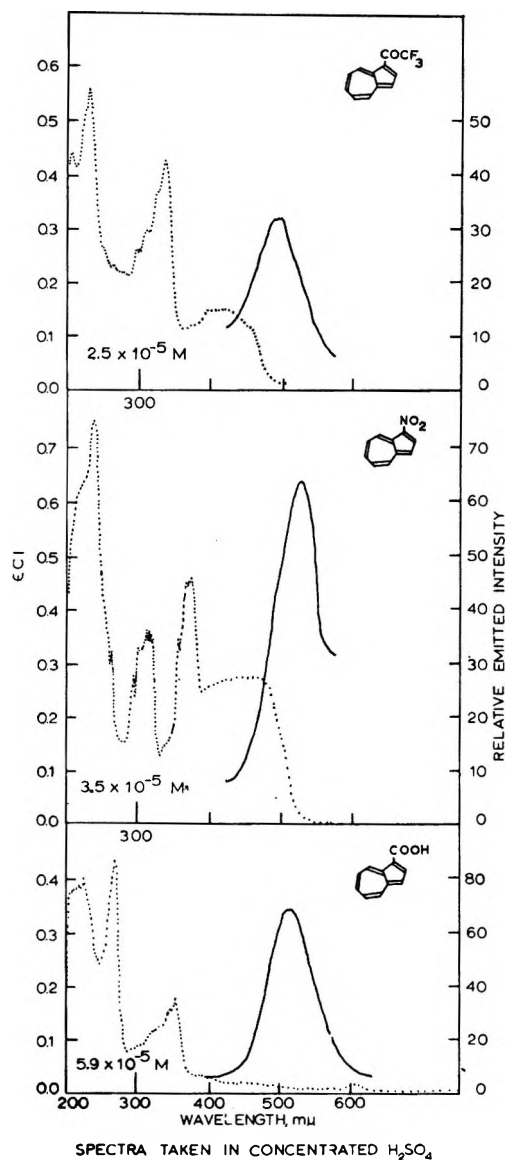


Figure 2. Absorption ( $\cdots$ ) and emission ( $-$ ) spectra of certain 1-substituted azulenes taken in fluid solution at room temperature, with 60% sulfuric acid as the solvent. The exciting line is indicated in each case by a short vertical line in the short-wavelength region of the spectrum. The emission spectra were taken under the following experimental conditions: 1-trifluoroacetylazulene:  $9.8 \times 10^{-4} M$ , sensitivity 50, 0.001 mm; 1-nitroazulene:  $6.9 \times 10^{-4} M$ , sensitivity 50, 0.003 mm; 1-azuloic acid:  $4.0 \times 10^{-4} M$ , sensitivity 30, 0.01 mm.

Exceptions to this occurred with *peri*-condensed systems containing four rings.

If one examines the data on the  $S_2$ - $S_1$  energy gap for the alternant (benzenoid) hydrocarbons compiled by Platt and coworkers,<sup>12</sup> the small gap for naphthalene is fairly typical. For the anomalously fluorescent non-alternants and substituted azulenes, the corresponding gap for azulene, which is large, seems to be typical. As can be seen from Table I, the energy gaps for the protonated species are similar whether or not anomalous emission is observed. In any case, the separation is of

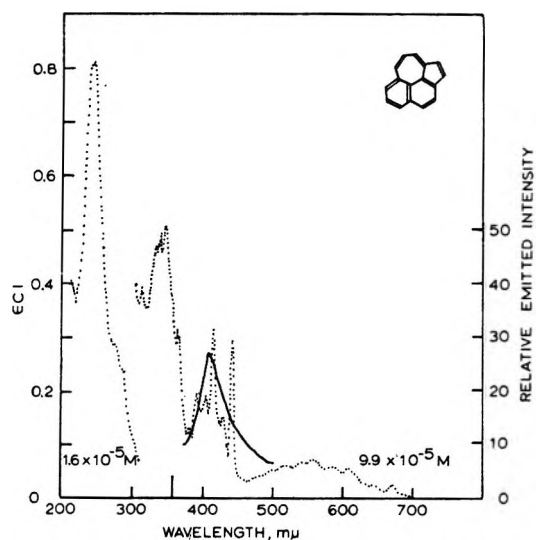


Figure 3. Absorption ( $\cdots$ ) and emission ( $-$ ) spectra of naphth[2,1,8-*cde*]azulene taken in fluid solution at room temperature, with methylcyclohexane as the solvent. The exciting line was 355  $m\mu$  and is indicated by a short vertical line in the short-wavelength region of the spectrum. The emission spectrum was taken under the following conditions:  $2.4 \times 10^{-4} M$ , sensitivity 50, 0.001 mm.

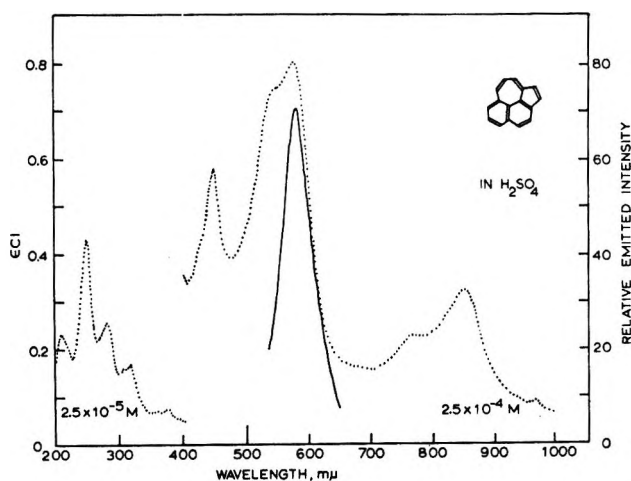


Figure 4. Absorption ( $\cdots$ ) and emission ( $-$ ) spectra of naphth[2,1,8-*cde*]azulene taken in fluid solution at room temperature, with concentrated sulfuric acid as the solvent. The exciting line was 500  $m\mu$  and is indicated by a vertical line in that region of the spectrum. The following experimental conditions were employed for observing the emission:  $7.5 \times 10^{-5} M$ , sensitivity 30, 0.003 mm.

the order of 6500-7500  $cm^{-1}$  for cases exhibiting anomalous emission as compared with 1300  $cm^{-1}$  in the case of naphthalene.

(10) P. D. Gardner, C. E. Wulfman, and C. L. Osborn, *J. Amer. Chem. Soc.*, **80**, 143 (1958).

(11) P. Baumgartner, E. Weltin, G. Wagniere, and E. Heilbronner, *Helv. Chim. Acta*, **48**, 751 (1965).

(12) J. R. Platt, *et al.*, "Systematics of the Electronic Spectra of Conjugated Molecules," John Wiley & Sons, Inc., New York, N. Y., 1964.

**Table I:**  $S_1-S_0$  and  $S_2-S_1$  Experimental Energy Spacings Corresponding to Maxima in the Absorption Spectra<sup>a</sup>

Compd or ion	$\Delta E(S_1-S_0)$	$\Delta E(S_2-S_1)$	Ref
Azulene <sup>b</sup>	15,800	13,700	<i>c</i>
Naphthalene	34,800	1,300	<i>d</i>
Naphth[2,1,8- <i>cde</i> ]azulene <sup>b</sup>	17,725	6,450	<i>e</i>
Azulenium	28,400	10,200	<i>f</i>
Benz[ <i>a</i> ]azulenium	25,850	11,300	<i>f</i>
Benz[ <i>e</i> ]azulenium	22,600	4,825	<i>f</i>
Benz[ <i>f</i> ]azulenium	25,850	6,550	<i>f</i>
Heptalenium	24,200	9,575	<i>f</i>
3, 5-Dimethylcyclopenta[ <i>ef</i> ]-heptalenium	19,608	6,708	<i>e</i>
3, 5-Dimethyl-8-phenylcyclohepta[ <i>cd</i> ]pentalenium	25,000	5,303	<i>e</i>
4-Methylpentaleno[2,1,6- <i>def</i> ]-heptalenium <sup>b</sup>	13,330	7,503	<i>e</i>
Naphth[2,1,8- <i>cde</i> ]azulenium <sup>b</sup>	11,110	6,444	<i>e</i>
1-Trifluoroacetylazulenium	23,810	6,493	<i>e</i>
1-Nitroazulenium	21,978	4,689	<i>e</i>
1-Carboxyazulenium	22,222	5,349	<i>e</i>

<sup>a</sup> The energy gap is given in  $\text{cm}^{-1}$ . <sup>b</sup> These substances emit anomalously. <sup>c</sup> J. E. Bloor, *Can. J. Chem.*, **43**, 3026 (1965). <sup>d</sup> I. B. Beriman, "Handbook of Fluorescence Spectra," Academic Press, New York, N. Y., 1965. <sup>e</sup> This work. <sup>f</sup> See ref 6.

The fluorescent behavior of substances which violate Kasha's rule<sup>13</sup> is of some interest because the phenome-

non bears a direct relation to the general problem of intramolecular nonradiative transitions, especially internal conversions and intersystem crossing. Similarly, the fact that the radiative process is observed from excited electronic states above the first excited singlet means that for these substances the experimental lifetime of the emitting state has been increased due to the elimination or considerable reduction of nonradiative downward transformations. Such high-energy storage mechanisms are important and worth further investigation both from experimental and theoretical points of view.<sup>14,15</sup>

*Acknowledgments.* The authors wish to thank Professor P. D. Gardner, Department of Chemistry, University of Utah, for the generous gift of a sample of naphth[2,1,8-*cde*]azulene. Similarly, we acknowledge Professor K. Hafner, Institut für Organische Chemie, Technische Hochschule Darmstadt, and Professor A. G. Anderson, Jr., Department of Chemistry, University of Washington, for gifts of samples of the compounds illustrated in Figure 1 and for 1-nitroazulene, respectively.

(13) M. Kasha, *Discussions Faraday Soc.*, **9**, 14 (1950).

(14) J. E. Bloor, *Can. J. Chem.*, **43**, 3026 (1965).

(15) I. B. Beriman, "Handbook of Fluorescence Spectra," Academic Press, New York, N. Y., 1965.

## Standard Potentials of Potassium Electrodes and Activity Coefficients and Medium Effects of Potassium Chloride in Ethanol-Water Solvents<sup>1</sup>

by Aloys J. Dill, Leonard M. Itzkowitz, and Orest Popovych<sup>2</sup>

*Department of Chemistry, Brooklyn College of the City University of New York, Brooklyn, New York 11210*  
(Received June 21, 1968)

Standard potentials of the potassium electrode and mean ionic activity coefficients of KCl were determined at 25° from emf measurements on potassium amalgam-silver chloride cells in ethanol-water mixtures containing 100.0, 92.3, 80.3, 60.2, 40.0, 20.3, and 15.0 wt % ethanol. Changes in the standard free energy of KCl upon transfer from water to each of the above nonaqueous media have been calculated. Variation of  $E^\circ_K$  with the solvent was interpreted in terms of ionic medium effects.

As part of an extensive study to determine the effect of the medium on the properties of electrolytes in ethanol-water mixtures, we measured the emf of potassium amalgam-silver chloride cells using dropping



amalgam electrodes containing approximately 0.02

wt % potassium. From emf measurements obtained on cell I with amalgams of accurately known composition, we derived the standard potentials of the po-

(1) Taken in part from the Ph.D. thesis of A. J. Dill, The City University of New York, July 1967.

(2) To whom inquiries should be addressed.

tassium electrode,  $E^\circ_K$ , as well as the activity coefficients and the medium effects for potassium chloride over the entire range of ethanol-water solvents. To date, activity coefficients of potassium chloride have not been reported for ethanol or for any of the ethanol-water mixtures. Values of  $E^\circ_K$  are known only for 100% ethanol<sup>3</sup> and, of course, for water.

### Experimental Section

**Materials.** USP 95% ethanol was purified by double fractionation, collecting 2.5 l. of a 5-l. charge. The final distillate had a density of 0.8067 g/ml at 25°, corresponding to 92.3 wt % ethanol. USP absolute alcohol was purified in a similar manner, after a preliminary 12-hr refluxing over magnesium ethoxide. The purified 100% ethanol had a specific conductance of  $10^{-8}$  mho  $\text{cm}^{-1}$  and a density of 0.7851 g/ml at 25°. Literature values are 0.7850<sup>4</sup> and 0.7851 g/ml.<sup>5</sup> Reagent grade potassium chloride was doubly recrystallized from deionized water and then was fused.

**Preparation of Solutions.** Ethanol-water mixtures were prepared to the approximate composition from 95% ethanol and distilled water, and their exact composition in weight per cent ethanol was then calculated from duplicate determinations of density and interpolated literature data on composition *vs.* density.<sup>4,5</sup> Stock solutions in all the solvents except pure ethanol were prepared by dissolving weighed amounts of potassium chloride. In absolute ethanol, a saturated solution was prepared and analyzed for chloride gravimetrically by precipitation as silver chloride.

**Preparation of Electrodes.** The silver-silver chloride electrodes were of the thermal electrolytic type prepared by the procedure described by Bates.<sup>6</sup> The electrodes used agreed with each other to better than 0.05 mV. Potassium amalgam containing approximately 0.02 wt % potassium was prepared by electrolysis of 1 N KOH. The electrolysis was carried out in a vessel which functioned as a separatory funnel, so that the amalgam could be drawn off from the KOH solution. Mercury served as the cathode and a platinum wire served as the anode. Dry nitrogen was bubbled through the mercury during the electrolysis in order to stir the amalgam. After the electrolysis proceeded for the required period of time, the amalgam was drawn off into an evacuated vessel for storage. All further transfers of the amalgam took place under an atmosphere of dry hydrogen. The percentage of potassium in the amalgam was determined by decomposition in hot standard sulfuric acid and back-titration with a standard base. In use, the amalgam contained in the reservoir was dropped through a 1-cm length of polarographic capillary at a rate which varied from about one drop per second to about one drop every 5 sec. This capillary was fastened to the electrode assembly by means of a Teflon tubing connector, so as to facilitate replacement if it became clogged during a run. The

spent amalgam dropped through the solution into the trap at the bottom of the electrode compartment, where it was isolated from the bulk of the solution. Isolation of the spent amalgam was necessary to prevent reaction with the solvent. The reference electrode compartment was separated from the amalgam compartment by a sintered glass disk, to prevent hydrogen used for deaeration of the solution from reaching the silver chloride electrode. Electrical contact with the amalgam was made by a platinum wire sealed into the neck of the electrode assembly.

**Measurements.** The 0.02% potassium amalgam was transferred to the dropping-electrode assembly under an atmosphere of dry hydrogen. The solution was placed in both electrode compartments and the cell was assembled. The assembled cell was placed in a water bath at 25.00°, controlled to better than  $\pm 0.01^\circ$  by a Yellow Springs Instrument Co. Model 72 proportional temperature controller. The actual temperature of the bath was verified by means of a certified National Bureau of Standards thermometer. Each silver-silver chloride electrode used was stored overnight in the KCl solution in which it was to be used for emf measurements. The hydrogen used for deaeration was first passed through a Deoxo catalytic purifier and then through a presaturation tower containing the pure solvent. The potential of cell I was measured when the amalgam drops were fully formed. Readings at about 10-min intervals were taken after the cell had been in the water bath for about 15 min. When consecutive readings agreed to about 0.2 mV, the potential was taken as final. Generally only three or four readings were necessary to reach a stable potential, which remained practically unchanged when equilibration was continued for an additional 0.5 hr. The measurements were carried out with an Electro Scientific Instruments Model 330 potentiometric dc voltmeter, which has an accuracy of 10 ppm of the reading. A certified Eppley Laboratories standard cell was used to check the standard cell in the instrument.

### Results and Discussion

**Activity Coefficients.** The potential  $E_I$  of cell I at 25° is given by

$$E_I = E^\circ_I + 0.05916 \log a_{K(Hg)} - 0.05916 \log (a_{K}a_{Cl}) \quad (1)$$

where  $E^\circ_I = E^\circ_{AgCl} - E^\circ_{K(Hg)}$  referred to  $E^\circ_H = 0$  in the given solvent and  $a_{K(Hg)}$  is the activity of potas-

(3) N. A. Izmaylov, "Electrochemistry of Solutions," Kharkov University Press, Kharkov, USSR, 1959, p 732.

(4) J. R. Graham, G. S. Kell, and A. R. Gordon, *J. Amer. Chem. Soc.*, **79**, 2352 (1957).

(5) N. S. Osborne, E. C. McKelvey, and H. W. Bearce, *J. Wash. Acad. Sci.*, **2**, 95 (1912).

(6) R. G. Bates, "Determination of pH," John Wiley & Sons, Inc., New York, N. Y., 1964, p 281.

sium in the amalgam. For purposes of evaluating activity coefficients of KCl, the term involving  $a_{K(Hg)}$  is combined with  $E_I^\circ$  resulting in the equation

$$E_I = E^{\circ'} - 0.05916 \log (a_{K}a_{Cl}) \quad (2a)$$

where

$$E^{\circ'} = E_I^\circ + 0.05916 \log a_{K(Hg)} \quad (2b)$$

Substituting molar concentrations and activity coefficients for activities and accounting for incomplete dissociation, we solve for the mean molar activity coefficient of KCl,  $f_{\pm}$

$$\log f_{\pm} = \frac{E^{\circ'} - E_I}{0.1183} - \log (\alpha C_{KCl}) \quad (3)$$

where  $\alpha$  is the degree of dissociation of KCl. The latter was calculated from the association constants of KCl available in the literature<sup>7</sup> for those ethanol-water mixtures where ionic association is appreciable. An estimate of the activity coefficient,  $f_{\pm}$ , which is needed for the above calculation, was made from the Debye-Hückel equation in which the ion-size parameter for a given solvent was chosen by interpolation of the values of  $d_j$  given by Hawes and Kay.<sup>7</sup> While  $d_j$  is not the best choice for use in the Debye-Hückel equation,  $\alpha$  is, fortunately, not a sensitive function of  $f_{\pm}$ . Experimental values of  $E_I$ ,  $C_{KCl}$ , and the calculated values of  $\alpha$  are given in Table I.

In order to evaluate  $E^{\circ'}$ , eq 3 is rearranged with the usual assumption that for purposes of extrapolation  $\log f_{\pm}$  can be expressed as a function of ionic strength  $I$

$$E_I + 0.1183 \log (\alpha C_{KCl}) = E^{\circ'} + 0.1183AI^{1/2} \quad (4)$$

From a plot of the left-hand side of eq 4 vs.  $I^{1/2}$ ,  $E^{\circ'}$  is obtained by extrapolation to zero ionic strength. According to the Debye-Hückel law, the function in eq 4 should be linear in very dilute regions, with any deviations from linearity occurring at higher concentrations of KCl. That the reverse is observed in some of our sets of data can be attributed to the well-known<sup>8</sup> corrosion of amalgam electrodes, which becomes appreciable at low electrolyte concentrations and in alcohol-rich media. For this reason one or two data points at the lowest concentrations of KCl (of the order of  $10^{-3} M$ ) were excluded from our calculations in some of the solvents (those points are designated in Table I with a footnote). The remaining data were analyzed with the aid of eq 4 using the method of least-squares programmed on an IBM 1620 computer. The FORTRAN program yielded the intercept  $E^{\circ'}$  and the slope  $0.1183A$  of the best straight line representing our experimental points and evaluated the activity coefficients of KCl at even concentrations. At any ionic strength in the region studied here, the activity coefficient can be calculated from  $-\log f_{\pm} = AI^{1/2}$ . The constants of the linear extrapolation,  $E^{\circ'}$  and  $A$ , and the cor-

Table I: Emf-Molarity Data

$10^3 C_{KCl}$	$\alpha$	$E_I$ , V	$10^3 C_{KCl}$	$\alpha$	$E_I$ , V
100.0% Ethanol			92.3% Ethanol		
0.6266	...	2.0293 <sup>a</sup>	2.8490	0.944	2.0206
0.6278	...	2.0264 <sup>a</sup>	5.0880	0.918	1.9978
1.2532	0.932	2.0024	6.1050	0.909	1.9908
1.5665	0.921	1.9955	7.1230	0.901	1.9850
1.5700	0.921	1.9950	8.1400	0.893	1.9791
1.8798	0.911	1.9860	9.1580	0.886	1.9750
1.8830	0.911	1.9869	10.750	0.877	1.9697
2.5064	0.893	1.9753	60.2% Ethanol		
2.5110	0.893	1.9766	30.010	0.962	2.0947
3.1330	0.877	1.9661	40.010	0.955	2.0828
3.1390	0.877	1.9656	50.010	0.949	2.0732
80.3% Ethanol			60.020	0.943	2.0656
17.998	0.924	2.0347	70.020	0.938	2.0591
23.998	0.912	2.0226	80.020	0.934	2.0533
29.997	0.902	2.0139	90.020	0.930	2.0484
35.996	0.893	2.0067	100.03	0.926	2.0438
41.996	0.886	2.0010	20.3% Ethanol		
47.995	0.879	1.9959	5.0840	1	2.1187 <sup>a</sup>
53.995	0.873	1.9915	10.168	1	2.1295
40.0% Ethanol			20.336	1	2.1508
1.0040	1	2.2939 <sup>a</sup>	50.840	1	2.1937
2.0080	1	2.2700	81.344	1	2.2268
5.0200	1	2.2267	101.68	1	2.2575
10.040	1	2.1938	15.0% Ethanol		
50.200	1	2.1200	5.1150	1	2.1349 <sup>a</sup>
100.40	1	2.0893	10.230	1	2.1447
			20.460	1	2.1662
			51.150	1	2.2088
			81.840	1	2.2417
			102.30	1	2.2731

<sup>a</sup> These data points were excluded from the least-squares analysis.

Table II: Results of Linear Extrapolation of Experimental Data Using Eq 4

Wt % ethanol	Range of $10^3 I, M$	$A$	$A_{DH}$	$E^{\circ'}$ , V (std dev)
100.0	1-3	3.06	2.96	1.6445 ( $\pm 0.00097$ )
92.3	2.7-9	2.45	2.51	1.7019 ( $\pm 0.0004$ )
80.3	16-47	1.01	1.90	1.8087 ( $\pm 0.0001$ )
60.2	30-100	0.556	1.24	1.9020 ( $\pm 0.0003$ )
40.0	5-100	0.569	0.872	1.9503 ( $\pm 0.0006$ )
20.3	5-100	0.404	0.649	1.9865 ( $\pm 0.0004$ )
15.0	5-100	0.440	0.606	2.0012 ( $\pm 0.0003$ )

responding theoretical Debye-Hückel limiting slopes,  $A_{DH}$ , are compiled in Table II.

The dielectric constants for the calculation of  $A_{DH}$  were interpolated from Akerlof's data.<sup>9</sup>

(7) J. S. Hawes and R. L. Kay, *J. Phys. Chem.*, **69**, 2420 (1965).

(8) K. Bräuer and H. Strehlow, *Z. Phys. Chem.* (Frankfurt am Main), **17**, 336 (1958).

(9) G. Akerlof, *J. Amer. Chem. Soc.*, **54**, 4125 (1932).

It seems that the Debye-Hückel limiting law may be valid for the KCl solutions in 100 and 92.3% ethanol, where ionic strengths never reach  $10^{-2} M$ . For the remaining solvents, the experimental values of  $A$  are lower than their counterparts in the limiting law. The discrepancies between experimental and theoretical values of the activity coefficients can be reduced somewhat by expressing the latter with the aid of Debye-Hückel equation in the form  $-\log f_{\pm} = AI^{1/2}/(1 + BdI^{1/2})$  using the same literature values<sup>7</sup> for the ion-size parameter  $d$  as in the estimation of  $\alpha$ , but the improvement is insufficient. Conversely, when experimental values of  $f_{\pm}$  are introduced in the above equation, the corresponding calculated  $d$ 's vary with ionic strength. Evidently, for those solutions where the experimental slopes,  $A$ , are effectively lower than the limiting slopes, our apparently linear relationships,  $-\log f_{\pm} = AI^{1/2}$ , are merely approximations of some more complex functions of  $I$ . Following a recent suggestion<sup>10</sup> to express the emf of a reversible cell as a polynomial in  $I^{1/2}$ , we rewrite eq 4 as

$$y \equiv E_1 + 0.1183 \log (\alpha C_{\text{KCl}}) = E^{\circ'} + 0.1183A_1I^{1/2} + 0.1183A_2I + 0.1183A_3I^{3/2} + \dots \quad (5)$$

This amounts to adding higher powers of  $I^{1/2}$  to the expression for the activity coefficient

$$-\log f_{\pm} = A_1I^{1/2} + A_2I + A_3I^{3/2} + \dots \quad (6)$$

Using a polynomial curve-fitting program for those sets of data which did not follow the Debye-Hückel limiting law, we obtained the following constants for eq 5 at the ethanol concentrations indicated

$$y = 1.9993 + 0.1183(0.6286I^{1/2} - 0.4495I) \quad (15.0\%) \quad (7a)$$

$$y = 1.9836 + 0.1183(0.6847I^{1/2} - 0.6692I) \quad (20.3\%) \quad (7b)$$

$$y = 1.9478 + 0.1183(0.8757I^{1/2} - 0.8002I) \quad (40.0\%) \quad (7c)$$

$$y = 1.8901 + 0.1183(1.475I^{1/2} - 2.3922I) \quad (60.2\%) \quad (7d)$$

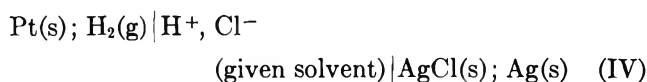
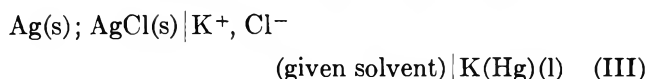
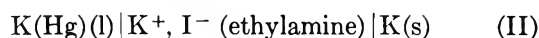
$$y = 1.8108 + 0.1183(0.8076I^{1/2} - 0.6900I) \quad (80.3\%) \quad (7e)$$

No significant improvement was achieved by extending this calculation to higher polynomials in  $I^{1/2}$ . The previously claimed<sup>10</sup> theoretical validity of eq 5 is corroborated here to some extent by the fact that the coefficients  $A_1$  in eq 7a-e are in most cases closer to the Debye-Hückel limiting slopes than the corresponding parameters from the linear extrapolation. Values of  $E^{\circ'}$  derived from the polynomials are within 1-2 mV of

their straight-line counterparts for all solvents except 60.2% ethanol. For this composition, a plot of  $y$  vs.  $I^{1/2}$  curves appreciably throughout the concentration range, so that a linear extrapolation represents a poor approximation here.

In their analysis of emf measurements with potassium and rubidium amalgam electrodes in methanol, Bräuer and Strehlow<sup>8</sup> drew attention to the corrosion (decomposition) of the amalgams due to a reaction with the solvent and outlined a method of correcting for it. The decomposition of amalgam increases the activity of the alkali metal ion in solution and reduces the activity of the metal in the amalgam phase by a corresponding amount. It manifests itself in plots of  $-\log f_{\pm}$  vs.  $I^{1/2}$  and of  $y$  vs.  $I^{1/2}$  as a curvature in the most dilute regions with a slope steeper than that predicted by the Debye-Hückel limiting law. The correction proposed by Bräuer and Strehlow ascribes all deviation from the limiting slope in dilute regions ( $C < 0.01 M$ ) to amalgam corrosion. Whereas this approach seems plausible for their data in methanol, which do follow the limiting law at  $C \geq 0.01 M$ , it cannot be applied to ours, where the experimental slopes,  $A$ , are less than the theoretical. Even for 60.2% ethanol, in which the extrapolation *via* eq 4 showed an appreciable curvature, the correction was found to be inapplicable, as it led to negative values for that parameter which is supposed to represent an increase in potassium ion activity due to corrosion. Only the few isolated points in the most dilute solutions which we rejected did curve away from the otherwise linear plots of eq 4 and appeared to be examples of amalgam decomposition. In our work, amalgam decomposition was probably minimized by the use of hydrogen gas to purge the apparatus overnight prior to each run and to saturate the solutions continuously before and during the measurements. Hydrogen counteracts amalgam corrosion not only through deaeration but also by mass action.

*Standard Potentials of Potassium.* In any solvent which interacts with potassium metal, the standard potential of the potassium electrode,  $E^{\circ}_{\text{K}}$ , is arrived at by adding the standard potentials of the cells



Lewis and Keyes<sup>11</sup> measured the potential of cell II using an amalgam containing 0.2216 wt % potassium. Since the potential of a cell of this type is independent

(10) D. Sen, D. A. Johnson, and R. N. Roy, *J. Phys. Chem.*, **71**, 1523 (1967).

(11) G. N. Lewis and F. G. Keyes, *J. Amer. Chem. Soc.*, **34**, 119 (1912).

both of the concentration of electrolyte and of the nature of solvent (provided the solvent does not interact with potassium metal), its standard potential at 25° is given by

$$E^{\circ}_{\text{II}} = E - 0.05916 \log a_{\text{K(Hg)}} \quad (8)$$

A table of activities of potassium in amalgams as a function of mole fraction is given by Armbruster and Crenshaw.<sup>12</sup> From this table we interpolate the value of  $a_{\text{K(Hg)}} = 0.02412$  for the Lewis and Keyes amalgam (mole fraction of potassium, 0.011267). Combining this activity with the measured potential of cell II,  $E_{\text{II}} = -1.0478$  V (corrected to the absolute voltage standard), we obtain from eq 5,  $E^{\circ}_{\text{II}} = -0.9521$  V. Similarly, values of  $E^{\circ}_{\text{I}}$  were computed from those of  $E^{\circ}$  via eq 2b by interpolating activities for our amalgams from the data of Armbruster and Crenshaw.<sup>12</sup> Since cell III is the reverse of cell I,  $E^{\circ}_{\text{III}} = -E^{\circ}_{\text{I}}$ . The standard potential of cell IV was interpolated for our exact solvent compositions from the available literature data.<sup>13-17</sup>

The activities of our amalgams and the standard potentials  $E^{\circ}_{\text{I}}$  and  $E^{\circ}_{\text{K}}$  are listed in Table III. Standard potentials on the molal scale were calculated from those on the molar scale and the density of the solvents.<sup>4,5</sup>

$$E^{\circ}(\text{molal}) = E^{\circ}(\text{molar}) - 0.1183 \log d_0 \quad (9)$$

As a double check on the activity of our amalgams and on the entire experimental procedure, we determined  $E^{\circ}_{\text{I}}$  in water from measurements on five of the amalgams to be  $2.1931 \pm 0.0005$  V (molar scale). The standard potential of potassium in water derived from it is  $-2.9230$  V (molal scale). Literature values are  $-2.9234$ <sup>12</sup> and  $-2.926$  V.<sup>18</sup> On the other hand, values of  $E^{\circ}_{\text{I}}$  in 100% ethanol are reproducible only to a few millivolts, as they are subject to additional errors resulting from the preparation and analysis of saturated solutions of KCl. The standard potential of potassium

in anhydrous ethanol determined in this study does not agree well with the literature value of  $-2.847$  V.<sup>3</sup> The  $E^{\circ}$  of potassium is more positive in ethanol-water mixtures than in either of the pure solvents. A possible interpretation of this phenomenon in terms of medium effects for the potassium ion and for the proton is offered in the next section.

*Medium Effects.* The medium effect  ${}_m\gamma_i$ , usually expressed in logarithmic form, is a measure of the difference between the standard free energy of solute  $i$  in water ( ${}_wG^{\circ}_i$ ) and in the given nonaqueous solvent ( ${}_sG^{\circ}_i$ ).

$${}_sG^{\circ}_i - {}_wG^{\circ}_i = RT \ln {}_m\gamma_i \quad (10)$$

In recent years, considerable attention has been devoted to medium effects of single ions, with the aid of which it is possible, in principle, to correlate ion-activity scales and standard emf series in different solvents and to evaluate liquid-junction potentials at aqueous-non-aqueous interphases. Several new extrathermodynamic methods have been proposed for the estimation of medium effects for single ions,<sup>19-22</sup> and the field has been partially reviewed.<sup>19-25</sup>

Thermodynamically allowed combinations of ionic medium effects are useful not only as starting points for estimation of their individual values but also as a means of testing the internal consistency of the latter. Two such combinations can be calculated from the  $E^{\circ}$  values determined in this study at 25°

$$\log {}_m\gamma_{\text{K}} + \log {}_m\gamma_{\text{Cl}} = \frac{{}_wE^{\circ}_{\text{I}} - {}_sE^{\circ}_{\text{I}}}{0.05916} \quad (11)$$

and

$$\log {}_m\gamma_{\text{K}} - \log {}_m\gamma_{\text{H}} = \frac{{}_sE^{\circ}_{\text{K}} - {}_wE^{\circ}_{\text{K}}}{0.05916} \quad (12)$$

Table III: Standard Potentials and Medium Effects at 25°

Wt % ethanol	10 <sup>3</sup> a <sub>K(Hg)</sub>	E° <sub>I</sub> , M	E° <sub>I</sub> , M	sE° <sub>K</sub>	Log	Log
					mγ <sub>K</sub> + log mγ <sub>Cl</sub>	mγ <sub>K</sub> - log mγ <sub>H</sub>
100.0	1.136	1.8187	1.831 <sub>1</sub>	-2.865	6.121	0.987
92.3	1.328	1.8721	1.8831	-2.757	5.242	2.803
80.3	1.909	1.9696	1.9787	-2.799	3.626	2.099
60.2	2.282	2.0464 <sup>a</sup>	2.0526	-2.830	2.377	1.574
40.0	2.206	2.1075	2.1111	-2.8687	1.388	0.918
20.3	1.377	2.1558	2.1575	-2.9021	0.6034	0.353
15.0	1.325	2.1714	2.1728	-2.9136	0.3448	0.159
0.0	...	2.1931 <sup>b</sup>	2.1932	-2.9230	0.0000	0.000

<sup>a</sup> Here, the  $E^{\circ}$  from the polynomial expression (eq 7d) was used in calculating  $E^{\circ}_{\text{I}}$ . For all other compositions values of  $E^{\circ}$  used are those from Table II. <sup>b</sup> An average was determined on five amalgams.

(12) M. H. Armbruster and J. L. Crenshaw, *J. Amer. Chem. Soc.*, **56**, 2525 (1934).

(13) J. A. V. Butler and C. M. Robertson, *Proc. Roy. Soc.*, **A125**, 694 (1929).

(14) H. S. Harned and D. S. Allen, *J. Phys. Chem.*, **58**, 191 (1954).

(15) A. Patterson and W. A. Felsing, *J. Amer. Chem. Soc.*, **64**, 1478 (1942).

(16) P. Seguela and J. Pariaud, *Compt. Rend.*, **253**, 1565 (1961).

(17) H. Taniguchi and G. J. Janz, *J. Phys. Chem.*, **61**, 688 (1957).

(18) K. Bräuer and H. Strehlow, *Z. Phys. Chem.* (Frankfurt am Main), **17**, 346 (1958).

(19) R. Alexander and A. J. Parker, *J. Amer. Chem. Soc.*, **89**, 5549 (1967).

(20) M. Alfenaar and C. L. De Ligny, *Rec. Trav. Chim. Pays-Bas*, **86**, 929 (1967).

(21) J. F. Coetzee and J. J. Campion, *J. Amer. Chem. Soc.*, **89**, 2513 (1967).

(22) O. Popovych, *Anal. Chem.*, **38**, 558 (1966).

(23) See ref 6, Chapters 7, 8.

(24) R. G. Bates in "The Chemistry of Non-Aqueous Solvents," Vol. I, J. J. Lagowski, Ed., Academic Press, New York, N. Y., 1966, Chapter 3.

(25) H. Strehlow in ref 24, Chapter 4.



where subscripts *s* and *w* indicate that the  $E^\circ$  was determined in the given nonaqueous solvent and in water, respectively, and is based on the standard state in the corresponding solvent. The combinations of the medium effects are compiled in the last two columns of Table II. The quantity  $\log m\gamma_K - \log m\gamma_H$  represents the difference in the standard free energy change experienced by potassium ions and by protons upon transfer from water to a given ethanol-water mixture. If we had a way of apportioning this difference between the two ions, we could estimate the very useful medium effects for the proton  $\log m\gamma_H$ . Values of  $\log m\gamma_H$  throughout the ethanol-water range would enable us to correlate pH scales in water and in ethanol-water mixtures by referring all of them to a single aqueous standard. Model calculations of the solvation energy of ions focus mainly on the electrostatic component of the energy and apply poorly to the proton, where basicity of solvent undoubtedly makes a major contribution. On the other hand, a successful model has been developed by Stokes<sup>26</sup> for the free energy of hydration of ions with a noble gas structure. This model, which accounts both for dielectric saturation in the vicinity of the ion and for increase in its radius due to hydration, was employed here to calculate the electrostatic standard free energy of potassium ions,  $G_{el}^\circ$ , in water and in ethanol-water mixtures

$$G_{el}^\circ \text{ (kcal/mol)} = 166 \left[ \frac{2.8}{9r_c(r_c + 2.8)} + \frac{D^{-1}}{r_c + 2.8} \right] \quad (13)$$

where the crystallographic radius of the potassium ion,  $r_c$ , was taken to be 1.33 Å,  $D$  is the macroscopic dielectric constant of the medium, 2.8 Å represents the increase in radius of the ion due to hydration, and 9 is the value assigned to the effective dielectric constant in the hydration layer. Omission of the "neutral" part of the solvation energy of potassium ions from the calculation of its medium effects amounts to adopting the "zero-energy assumption," which applies when the energy change experienced by a neutral molecule upon transfer from its gaseous standard state to its solution standard state is just that resulting from the accompanying change in volume. It has been demonstrated<sup>27</sup> that the zero-energy assumption is superior to the alternative "inert gas assumption" for the evaluation of hydration energies of individual ions. In the inert gas assumption, the neutral part of solvation energy of an ion is equated to the solvation energy of an inert gas molecule of the same size and may vary appreciably with solvent.

As shown in Table IV, the medium effect of the potassium ion calculated from the Stokes model increases steadily with increasing ethanol content, exhibiting the expected rise in solvation energy of an ion with de-

Table IV: Calculated Single-Ion Medium Effects for Potassium and the Proton

Wt % ethanol	$\log m\gamma_K - \log m\gamma_H$	$\log m\gamma_K$ (calcd from Stokes <sup>26</sup> model)	$\log m\gamma_H$ (by difference)
92.3	2.803	0.711	-2.092
80.3	2.099	0.525	-1.574
60.2	1.574	0.305	-1.269
50.0	1.22 <sup>a</sup>	0.225	-1.00
40.0	0.918	0.160	-0.758
30.0	0.625 <sup>a</sup>	0.106	-0.519
20.3	0.353	0.0651	-0.288
15.0	0.159	0.0456	-0.113

<sup>a</sup> Interpolated.

creasing dielectric constant of solvent. In contrast, the medium effect for the proton is negative throughout the ethanol-water range and decreases with increasing alcohol content. This means that in ethanol-water mixtures the proton exists in a lower energy state than in pure water, or that the mixtures are more basic than water. An independent corroboration for this conclusion can be derived from the behavior of the Hammett acidity function,  $H_0$ , in ethanol-water solvents. For a nonaqueous solution of acid HA at an analytical molality  $m_{HA}$  and with a degree of dissociation  $\alpha$ , the relationship between the medium effect of the proton and the  $H_0$  is

$$\log m\gamma_H = -H_0 - \log m_{HA} - \log \alpha - \log s\gamma_H + \log \frac{s\gamma_{BH^+}}{s\gamma_B} + \log \frac{m\gamma_{BH^+}}{m\gamma_B} \quad (14)$$

where subscript *s* denotes the salt-effect activity coefficients and  $BH^+$  and  $B$  are the acidic and basic forms of the Hammett (amine) indicator, respectively. Because medium effects are generally known to attain values orders of magnitude greater than salt effects, it is necessary to have some prior indication that the ratio  $m\gamma_{BH^+}/m\gamma_B$  is likely to be close to unity before accepting the  $H_0$  function as an approximate measure of hydrogen ion activity in a given solvent. According to a calculation by Strehlow,<sup>28</sup> the electrostatic component of  $m\gamma_{BH^+}$  in alcohol solvents is indeed close to unity, while it is also reasonable to expect that its neutral component would tend to cancel with  $m\gamma_B$ . If one then applies the usual assumption that the salt-effect ratio  $s\gamma_{BH^+}/s\gamma_B$  also deviates little from unity, the  $H_0$  function can serve as a basis for estimating  $\log m\gamma_H$ .

Braude and Stern<sup>28</sup> reported that for HCl solutions in mixtures of ethanol, dioxane, and acetone with water, the function  $-H_0$  passes through a minimum at approximately equimolar solvent composition and then

(26) R. H. Stokes, *J. Amer. Chem. Soc.*, **86**, 979 (1964).

(27) R. M. Noyes, *ibid.*, **84**, 513 (1962).

(28) E. A. Braude and E. S. Stern, *J. Chem. Soc.*, 1976 (1948).

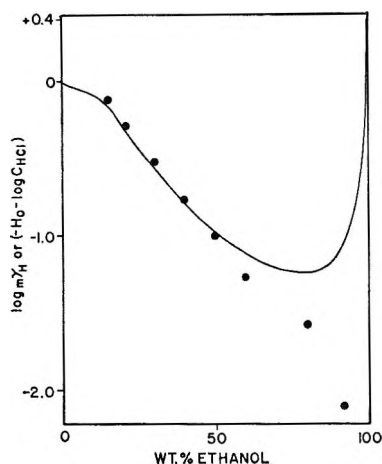


Figure 1. Comparison of calculated medium effects for the proton with the  $-H^0$  acidity function<sup>29</sup> in ethanol-water mixtures. The solid curve represents  $(-H^0 - C_{\text{HCl}})$  from the data of Braude and Stern.<sup>28</sup> Filled circles are values of  $\log m\gamma_{\text{H}}$  estimated in this study.

rises steeply in the region of the pure solvents. Their conclusion was that water is more basic in mixtures with other solvents than it is in the pure liquid state. This increase in the effective proton affinity of the water molecules is believed to be brought about by a destruction of water structure, upon which a larger number of basic sites on the water molecules are exposed for bonding with protons. In the vicinity of the pure solvents, the acidity function rises steeply, presumably due to replacement of hydronium ions with the corresponding nonaqueous oxonium ions. The curve in Figure 1 represents an estimate of  $\log m\gamma_{\text{H}}$  from the data of Braude and Stern for 0.1 M solutions of HCl plotted as a function of ethanol-water composition in the form  $(-H^0 - \log C_{\text{HCl}})$ , where  $C$  is the molarity of the acid. Our own estimates of  $\log m\gamma_{\text{H}}$  from the last column of Table IV are shown as individual points. The two sets of estimates show good coincidence up to about 50 wt % ethanol, after which our calculated values of  $\log m\gamma_{\text{H}}$  continue to decrease steadily, while the acidity function proceeds through its previously mentioned minimum followed by a steep rise. While the observed discrepancy could be due to the failure of either function to describe adequately the behavior of the medium effect for the proton in alcohol-rich media, it is most likely the failure of the Stokes hydration model. The latter presumes solvation by water molecules throughout the solvent range and was not meant to be applied in alcohol-rich solvents where it is likely to become in-

creasingly erroneous due to solvation of ions by ethanol or by both ethanol and water. Furthermore, values of  $\log m\gamma_{\text{H}}$  estimated by other independent methods<sup>29,30</sup> also show a steep rise in the region close to 100% ethanol, similar to that experienced by the  $-H^0$  function.

If for the sake of discussion we assume that  $-H^0$  does reflect the true behavior of the medium effect for the proton over the entire ethanol-water range, it is possible to calculate  $\log m\gamma_{\text{H}}$  for 100% ethanol from eq 14. For 0.1 M HCl,  $\alpha$  is 0.26 ( $K_{\text{diss}} = 9 \times 10^{-3}$ ),<sup>31</sup> and  ${}_s\gamma_{\pm\text{HCl}}$ , as an estimate of  ${}_s\gamma_{\text{H}}$ , is about 0.35.<sup>3</sup> Introducing into eq 14 these values as well as the density of ethanol to convert from molarity to molality, we obtain  $\log m\gamma_{\text{H}} = 1.5$ , and (from the last column of Table III)  $\log m\gamma_{\text{K}} = 2.5$ . Previous estimates for the medium effects of  $\text{H}^+$  and  $\text{K}^+$  ions in ethanol are, respectively, 3.9 and 4.0<sup>32</sup> and 2.5 and 4.1.<sup>33</sup> Both pairs are, of course, internally inconsistent, since the experimentally observed value of  $\log m\gamma_{\text{K}} - \log m\gamma_{\text{H}} = 1.0$ .

The variation of  ${}_sE^{\circ}_{\text{K}}$  with ethanol-water composition can now be analyzed in terms of the interplay between the individual medium effects of the potassium ion and of the proton. The conventional standard potential of potassium  ${}_sE^{\circ}_{\text{K}}$ , which is really  ${}_sE^{\circ}_{\text{K}} - {}_sE^{\circ}_{\text{H}}$  is directly related to the difference in the standard free energies of  $\text{K}^+$  and  $\text{H}^+$  ion in nonaqueous solvents and in water (cf. eq 10 and 12). Because  $\log m\gamma_{\text{K}}$  rises steadily with increasing ethanol content ( ${}_sG^{\circ}_{\text{K}}$  increases) while  $\log m\gamma_{\text{H}}$  (and  ${}_sG^{\circ}_{\text{H}}$ ) decreases, the standard potential of potassium becomes increasingly positive with respect to its aqueous value. It probably reaches a maximum somewhere between 90 and 100 wt % ethanol, just prior to the steep rise in  ${}_sE^{\circ}_{\text{H}}$  observed in several of the cited studies. The sudden increase in the free energy of the proton in the region near anhydrous ethanol brings  ${}_sE^{\circ}_{\text{K}}$  again close to its aqueous counterpart  ${}_wE^{\circ}_{\text{K}}$ .

*Acknowledgment.* Research supported in part by the National Science Foundation under Grant GP-6553 and through the NSF Undergraduate Research Participation Program.

(29) B. Gutbezahl and E. Grunwald, *J. Amer. Chem. Soc.*, **75**, 559, 565 (1953).

(30) V. V. Aleksandrov and N. A. Izmaylov, *Zh. Fiz. Khim.*, **32**, 404 (1958).

(31) I. T. Oiwa, The Science Reports of the Tohoku University, Series I, Vol. XLI, No. 2, Oct 1957.

(32) N. A. Izmaylov, *Dokl. Akad. Nauk SSSR*, **149**, 1364 (1963).

(33) N. Bjerrum and E. Larsson, *Z. Phys. Chem. (Leipzig)*, **127**, 358 (1927).

## Activation of Hydrogen at 79°K by Supported Copper<sup>1a</sup>

by J. E. Benson,<sup>1b</sup> Arden B. Walters,<sup>1c</sup> and M. Boudart<sup>1d</sup>

Department of Chemical Engineering, Stanford University, Stanford, California 94305 (Received June 24, 1968)

A new catalyst containing 500 ppm of copper on magnesium oxide has been found to activate molecular hydrogen at 79°K as evidenced by its ability to catalyze the H<sub>2</sub>-D<sub>2</sub> exchange at that temperature at a rate per surface atom comparable to that measured on metallic nickel. This catalyst is poisoned by adsorption of hydrogen at higher temperature. The nature of the surface sites responsible for the exchange is discussed.

### Introduction

Active catalytic centers associated with electronic defects induced by irradiation of silica gel with aluminum impurities were discovered by Kohn<sup>2</sup> and studied in detail by various workers.<sup>3-5</sup> Similar centers have been investigated by Lunsford and Leland<sup>6,7</sup> on magnesia with iron impurities. Several workers,<sup>8-10</sup> whose results have remained unpublished, have also described a catalyst which resembles those of Kohn and Lunsford in its unexpected ability to catalyze the hydrogen-deuterium exchange at liquid nitrogen temperature as well as in its deactivation by hydrogen adsorbed at higher temperatures. The catalyst consisted of 5 mol % copper supported on magnesia, activated without irradiation by reduction and evacuation at high temperature. In view of the recent findings with irradiated catalysts, it became imperative to confirm and expand the previous results with special attention to the absence of impurities such as nickel that might be introduced during the preparation of the catalysts.

### Experimental Section

All chemicals used were of high purity. The gases used were hydrogen (produced electrolytically) and deuterium (99.5% D<sub>2</sub>, obtained from the Matheson Co.). Both hydrogen and deuterium were purified by diffusion through palladium alloys prior to their use. Grade A helium was obtained from General Dynamics. Catalysts containing 5.0 and 0.05 mol % copper on magnesia were prepared by impregnating Mallinckrodt analytical reagent grade magnesia with a cupric nitrate solution prepared by dissolving ASARCO copper metal (99.999+ % Cu, <1 ppm of Ni) in Baker and Adamson reagent grade nitric acid (<0.05 ppm of Ni). A simple Pyrex flow system was used for the activation and reaction. The powder catalysts were protected from grease and other contaminants by liquid nitrogen traps on the upstream and the downstream sides of the catalyst chamber. Following impregnation, the catalysts were calcined in air at 673°K. Then they were activated *in situ*. The 5.0 mol % Cu-MgO catalysts were reduced for 24 hr in hydrogen flowing at a space velocity of 0.020 sec<sup>-1</sup> at temperatures from 575 to 750°K and

then evacuated to 10<sup>-5</sup> torr for at least 12 hr at the reduction temperatures before the exchange reaction was studied at temperatures from 79 to 373°K. The 0.05 mol % Cu-MgO catalyst was similarly activated at 733°K.

Approximately equimolar mixtures of hydrogen and deuterium were passed over the thermostated catalysts at atmospheric pressure. The gas mixtures were analyzed gas chromatographically by the method of Fujita and Kwan.<sup>11</sup> The column, immersed in liquid nitrogen, was packed with 100-200 mesh alumina impregnated with 10 wt % MnCl<sub>2</sub>. Helium at a flow of 150 ml/min was used as the carrier gas. The separated isotopes were oxidized to the corresponding isotopic water molecules in a CuO column at 853°K to increase the sensitivity of detection in an Aerograph A90-P3 gas chromatograph connected to a Honeywell-Brown recorder equipped with an integrator. The amount of each isotopic component was taken from the area of each recorded peak. The chromatographic system was calibrated for H<sub>2</sub> and D<sub>2</sub> by sampling equal amounts of pure H<sub>2</sub> and D<sub>2</sub> separately, and for HD by equilibrating H<sub>2</sub>-D<sub>2</sub> mixtures over a 0.6% Pt-Al<sub>2</sub>O<sub>3</sub> catalyst at room temperature.

### Results and Discussion

The previous studies<sup>8-10</sup> showed that the unusual activity of the Cu-MgO catalyst for the H<sub>2</sub>-D<sub>2</sub> ex-

(1) (a) This work was supported by the National Science Foundation under Grant No. NSF GK 2208; (b) Department of Chemistry, Dickinson College, Carlisle, Pa. 17013; (c) National Science Foundation Graduate Fellow; (d) to whom correspondence should be addressed.

(2) H. W. Kohn, *J. Phys. Chem.*, **63**, 966 (1959).

(3) H. W. Kohn and E. H. Taylor, "Actes du Deuxieme Congres International de Catalyse, Paris, 1960," Vol. II, Editions Technip, Paris, 1961, p 1461.

(4) H. W. Kohn, *J. Catal.*, **2**, 208 (1963).

(5) Y. A. Meeshchenko and G. K. Borekov, *Kinet. Katal.*, **6**, 842 (1965).

(6) J. H. Lunsford and T. W. Leland, Jr., *J. Phys. Chem.*, **66**, 2591 (1962).

(7) J. H. Lunsford, *ibid.*, **68**, 2312 (1964).

(8) M. Alei, Jr., Ph.D. Dissertation, Princeton University, 1951.

(9) M. L. Snow, Ph.D. Dissertation, Princeton University, 1956.

(10) J. P. Manges, Jr., A.B. Dissertation, Gettysburg College, 1964.

(11) K. Fujita and T. Kwan, *Japan Analyst*, **12**, 15 (1963).

change in the region of 100°K was a consequence of suitable reduction and evacuation. Our study of the 5.0 mol % Cu-MgO catalyst has verified these findings. Moreover, the activity was increased even further by long evacuation following reduction. These results are presented in Table I. *The most active catalyst, activated at 750°K, equilibrated the H<sub>2</sub>-D<sub>2</sub> mixture at 115°K.*

**Table I:** Conversion (HD)/(HD)<sub>equil</sub> × 100 for Equimolar H<sub>2</sub>-D<sub>2</sub> Mixtures over 5.13 g of 5% Cu-MgO<sup>a</sup>

Reaction temp, °K	Conversion %			
	Catalyst pretreatment temperatures			
	575°K		750°K	
	A	B	A	B
79	3	3	12	35
115	...	...	94	100
173	4	29	...	94
273	36	48	100	98
373	96	100	...	100

<sup>a</sup> Pressure, 1 atm; reactor volume, 11 cc; H<sub>2</sub>-D<sub>2</sub> flow, 9.5 μmol/sec; space velocity, 0.020 sec<sup>-1</sup> (for gas at NTP); catalyst pretreatment: A, reduced and cooled to reaction temperature in flowing H<sub>2</sub>; B, outgassed after reduction.

A slight dip in conversion with increasing temperature due to the deactivation of the catalysts by hydrogen was observed in this study and in the previous unpublished work. The results presented in Table II demonstrate that exposure to hydrogen at higher temperatures deactivates the catalyst for the exchange at liquid nitrogen temperature but that this activity can be restored by high-temperature evacuation for suitably long periods of time.

**Table II:** Conversion (HD)/(HD)<sub>equil</sub> × 100 for Equimolar H<sub>2</sub>-D<sub>2</sub> Mixtures over 5.13 g of 5% Cu-MgO<sup>a</sup>

Successive conditions of treatment of catalyst prior to run	Temp, °K	% conversion at 79°K
		Reduction and outgas
Flowing H <sub>2</sub> , 1 hr	373	28
Flowing H <sub>2</sub> , 3 hr	466	~0
Outgas 6 hr	477	~0
Outgas 10 hr	638	3
Outgas 18 hr	747	38

<sup>a</sup> Pressure, 1 atm; reactor volume 11 cc; H<sub>2</sub>-D<sub>2</sub> flow, 9.5 μmol/sec; space velocity, 0.020 sec<sup>-1</sup> (for gas at NTP).

A magnesia sample treated with the same chemicals used in preparing the Cu-MgO catalysts was studied to discover if impurities other than copper were responsible for the activity of the 5.0 mol % Cu-MgO catalyst. Activated by reduction and evacuation at

780°K, the magnesia yielded negligible conversion at 77°K and a conversion of only 60% at 273°K at a space velocity of 0.013 sec<sup>-1</sup>. This demonstrates that copper is essential to the catalytic activity observed for the Cu-MgO catalysts at low temperatures.

To see whether dilution of the copper on the magnesia support changes its activity per copper atom, we decided to reduce drastically the amount of copper used. A sample of 0.05 mol % Cu-MgO catalyst was activated at 733°K. The exchange reaction was studied at a space velocity of 0.010 sec<sup>-1</sup>. A conversion of 17% was obtained at liquid nitrogen temperature. Thus the catalyst, containing one hundred times less copper, was about one-fourth as active as the 5.0 mol % Cu-MgO catalyst. A conversion of 91% was observed at 117°K. After exposure to flowing H<sub>2</sub>-D<sub>2</sub> mixtures at 211°K, the 77°K conversion dropped to 2%.

From these data a turnover number of 1.1 molecules of HD per minute per Cu atom in the sample was calculated for the 0.05 mol % Cu-MgO catalyst at liquid nitrogen temperature. By contrast, a turnover number of 5 × 10<sup>-9</sup> min<sup>-1</sup> for copper foil at 77°K was calculated from the data of Mikovsky, *et al.*,<sup>12</sup> by using the reported activation energy to extrapolate from 600 to 77°K. This demonstrates that metallic copper cannot be active for the exchange reaction at liquid nitrogen temperature. For metallic nickel, an excellent catalyst for the H<sub>2</sub>-D<sub>2</sub> exchange reaction, a turnover number of 2.2 min<sup>-1</sup> was calculated at 1 atm from the data of Eley and Norton<sup>13</sup> for a clean nickel wire at liquid nitrogen temperature. Thus, per surface metal atom, our active catalyst is practically as active as bulk nickel for the exchange reaction at liquid nitrogen temperature.

In analogy with the catalytic center of Kohn and Lunsford, we propose that the anomalous catalytic activity observed in this work is due to an intermediate state of reduction of copper stabilized in the magnesia matrix at or near the surface. Quite clearly, copper metal is totally inactive at low temperatures. If, as is reasonable, adsorption of hydrogen requires *two* adjacent sites, it is unlikely that Cu<sup>+</sup>(d<sup>10</sup>) or Cu<sup>2+</sup>(d<sup>9</sup>) *alone* can account for the observed results. Instead, we assume that the reduction of Cu<sup>2+</sup> ions leads to Cu<sup>+</sup> ions and OH<sup>-</sup> ions. Some of the latter, especially after evacuation of this partially reduced system at high temperature for long periods of time would then lead, by loss of hydrogen, to an O<sup>-</sup> center, a positive hole trapped in the vicinity of a Cu<sup>+</sup> ion. We ascribe the low-temperature activity of the Cu-MgO system to such V-centers, which are completely analogous to

(12) R. J. Mikovsky, M. Boudart, and H. S. Taylor, *J. Amer. Chem. Soc.*, **76**, 3814 (1954).

(13) D. D. Eley and P. R. Norton, *Discussions Faraday Soc.*, **41**, 135 (1966).

those first demonstrated by Kohn<sup>2,3</sup> and Meeshchenko and Boreskov<sup>5</sup> in the case of irradiated silica gel with aluminum impurities and by Lunsford<sup>7</sup> in the case of irradiated magnesia with iron impurities. In particular, the poisoning of the active sites by high-temperature adsorption of hydrogen receives a common explanation: with homolytic adsorption of H<sub>2</sub> on Cu<sup>+</sup>O<sup>-</sup>, the dual center becomes (CuH)<sup>+</sup>(OH)<sup>-</sup> and is inactivated. It is suggested that at low temperatures H<sub>2</sub> is adsorbed in heterolytic manner on the same center to yield (CuH)(OH) reversibly.<sup>14</sup>

The identification of another electronic defect associated with a catalytically active site would be of particular importance for further development of the electronic theory of catalysis. Work now in progress is directed toward such an identification. It includes

more detailed studies on hydrogen poisoning, further studies of the role played by the copper by means of electron paramagnetic resonance spectroscopy, and a search for the particular electronic defect responsible for the catalytic activity observed for the Cu-MgO system.

*Acknowledgment.* Valuable discussions of their unpublished work with Drs. Alei and Snow in Sir Hugh Taylor's laboratory and with Dr. Manges are gratefully acknowledged. This work was supported by the National Science Foundation under Grant NSF GK 2208.

(14) R. L. Burwell, Jr., and C. J. Loner, "Proceedings of the Third International Congress on Catalysis, Amsterdam, 1964," Vol. II, North-Holland Publishing Co., Amsterdam, 1965, p. 804.

## Apparent Molal Expansibilities of Some Divalent Chlorides in Aqueous Solution at 25°

by Frank J. Millero

Contribution No. 975 from Institute of Marine Sciences, University of Miami, Miami, Florida 33149  
(Received June 24, 1968)

The apparent molal volumes,  $\phi_v$ , of dilute aqueous MgCl<sub>2</sub>, CaCl<sub>2</sub>, SrCl<sub>2</sub>, and BaCl<sub>2</sub> solutions have been determined at 1° intervals from 20 to 30° from precision density measurements. The apparent molal expansibilities,  $\phi_E$ , have been calculated from the apparent molal volumes at various temperatures and have been equated to the infinite-dilution partial molal expansibilities ( $\phi_E^0 = \bar{E}^0$ ). The  $\bar{E}^0$ 's of the divalent chlorides increase in the order MgCl<sub>2</sub> < CaCl<sub>2</sub> < SrCl<sub>2</sub>  $\approx$  BaCl<sub>2</sub>. The  $\bar{E}^0$ 's of these salts were divided into their ionic components,  $\bar{E}^0(\text{ion})$ , by assigning a value for  $\bar{E}^0(\text{Cl}^-) = 0.046$  ml/mol deg. The  $\bar{E}^0$ 's of the divalent cations can be represented by the equation  $\bar{E}^0(\text{ion}) = -0.034(Z^2/r) + 0.092$  ml/mol deg. The  $\bar{E}^0$ 's of the divalent cations and other monovalent cations and anions are discussed by dividing  $\bar{E}^0(\text{ion})$  into the following components:  $\bar{E}^0(\text{int})$ , the intrinsic expansibility;  $\bar{E}^0(\text{elect})$ , the electrostriction expansibility; and  $\bar{E}^0(\text{struct})$ , the structural expansibility. The  $\bar{V}^0$ 's and  $\bar{E}^0$ 's of ions in solution are also qualitatively examined by describing the hydration of an ion by the Frank and Wen model.

### Introduction

The partial molar volume of salts at infinite dilution,  $\bar{V}_0$ , in aqueous solutions have frequently been used to obtain a better understanding of solute-solvent interactions.<sup>1-13</sup> The  $\bar{V}^0$ 's of salts have been shown to be additive within experimental error;<sup>14</sup> however, the separation of the  $\bar{V}^0$ 's of salts into their ionic components,  $\bar{V}^0(\text{ion})$ , cannot normally be made by direct experimental methods.<sup>15</sup> Once  $\bar{V}^0$  of one ion is estimated by some correlation or curve-fitting method (by assuming some simple model for solute-solvent interactions), the  $\bar{V}^0$ 's of the other ions are fixed. Muker-

jee<sup>16</sup> has recently summarized the various estimates of  $\bar{V}^0$  of a proton, and it is generally agreed that  $\bar{V}^0(\text{H}^+)$  is about -4.5 ml/mol at 25° in aqueous solution.

- (1) T. J. Webb, *J. Amer. Chem. Soc.*, **48**, 2589 (1926).
- (2) H. M. Evjen and F. Zwicky, *Phys. Rev.*, **33**, 860 (1929).
- (3) J. D. Bernal and R. H. Fowler, *J. Chem. Phys.*, **1**, 515 (1933).
- (4) O. Redlich and J. Bigeleisen, *Chem. Rev.*, **30**, 171 (1942).
- (5) L. G. Hepler, *J. Phys. Chem.*, **61**, 1426 (1957).
- (6) P. Mukerjee, *ibid.*, **65**, 740 (1961).
- (7) S. W. Benson and C. S. Copeland, *ibid.*, **67**, 1194 (1963).
- (8) J. Padova, *J. Chem. Phys.*, **39**, 1552 (1963).
- (9) E. Whalley, *ibid.*, **38**, 1400 (1963).

Various workers<sup>5-13</sup> have attempted to divide  $\bar{V}^0(\text{ion})$  into two components

$$\bar{V}^0(\text{ion}) = \bar{V}^0(\text{int}) + \bar{V}^0(\text{elect}) \quad (1)$$

where  $\bar{V}^0(\text{int})$  is the intrinsic volume of the ion including void space and  $\bar{V}^0(\text{elect})$  is the decrease in volume due to electrostriction. It has been shown for some ions ( $\text{Li}^+$ ,  $\text{F}^-$ ,  $\text{Be}^{2+}$ ,  $\text{Mg}^{2+}$ , and  $\text{R}_4\text{N}^+$ , for example) that another term may be necessary,<sup>13,17-19</sup>  $\bar{V}^0(\text{struct})$ , the volume change due to changes in the structure of water (*i.e.*, changes in the ratio of "ice-like" to "non-icelike" forms of water). Thus  $\bar{V}^0(\text{ion})$  can be expressed by the equation

$$\bar{V}^0(\text{ion}) = \bar{V}^0(\text{int}) + \bar{V}^0(\text{elect}) + \bar{V}^0(\text{struct}) \quad (2)$$

Since the various components of eq 2 may be small when compared with the absolute size of the ion (excluding void effects), it is difficult to determine the individual components of  $\bar{V}^0(\text{ion})$  or to separate them. By looking at the effect of temperature on  $\bar{V}^0(\text{ion})$ , it is possible to solve this problem. Upon differentiation of eq 2 with respect to temperature,  $d\bar{V}^0(\text{ion})/dT = \bar{E}^0(\text{ion})$ , one obtains the partial molal expansibility of an ion

$$\bar{E}^0(\text{ion}) = \bar{E}^0(\text{int}) + \bar{E}^0(\text{elect}) + \bar{E}^0(\text{struct}) \quad (3)$$

where  $\bar{E}^0(\text{int})$  is the expansibility due to void-space changes (assuming the intrinsic size of the ion does not change with temperature),  $\bar{E}^0(\text{elect})$  is the expansibility due to electrostriction changes, and  $\bar{E}^0(\text{struct})$  is the expansibility due to changes in the structure of water.

In recent papers<sup>18-20</sup> we have measured the apparent molal volume,  $\phi_v$ , of a number of dilute aqueous salt solutions as a function of temperature. From these apparent molal volumes we have calculated the apparent molal expansibilities ( $\phi_E = d\phi_v/dT$ ) and have equated them to the infinite-dilution apparent molal expansibility (the partial molal expansibility,  $\phi_E^0 = \bar{E}^0$ ). The  $\bar{E}^0$ 's of the salts have been divided into their ionic components,  $\bar{E}^0(\text{ion})$ , by assuming that  $\bar{E}^0(\text{H}^+) = 0.000^{18}$  and  $-0.012$  ml/mol deg;<sup>19</sup> the results of this division have been discussed by comparing the terms of eq 3.

In this paper are reported the  $\phi_E$ 's of dilute aqueous  $\text{MgCl}_2$ ,  $\text{CaCl}_2$ ,  $\text{SrCl}_2$ , and  $\text{BaCl}_2$  at 25°, calculated from precision density measurements made at 1° intervals from 20 to 30°. The results will be discussed by comparing  $\bar{E}^0(\text{Mg}^{2+})$ ,  $\bar{E}^0(\text{Ca}^{2+})$ ,  $\bar{E}^0(\text{Ba}^{2+})$ , and  $\bar{E}^0(\text{Sr}^{2+})$  with the  $\bar{E}^0$ 's obtained for other ions.

### Experimental Section

All the salts used were reagent grade Baker Analyzed chemicals and were used without further purification. The salts were dried in a vacuum desiccator at 70° for at least 1 week before use. The solutions were made by weight with doubly distilled water, degassed to

prevent the formation of bubbles on the magnetic float.

The magnetic float densitometer used to make the density measurements has been described elsewhere.<sup>21</sup> The densitometer was on the bottom of a constant-temperature bath that was controlled to better than  $\pm 0.001^\circ$  with a Hallikainen thermoregulator. The temperature of the bath was initially set and subsequently was read to within  $\pm 0.002^\circ$  with a Melabs platinum resistance thermometer.

### Results

The densities of dilute  $\text{MgCl}_2$ ,  $\text{CaCl}_2$ ,  $\text{SrCl}_2$ , and  $\text{BaCl}_2$  aqueous solutions have been measured at 1° intervals from 20 to 30° with a magnetic float densitometer. The apparent molal volumes,  $\phi_v$ 's, were calculated from the densities by using the equation

$$\phi_v = \frac{1000(d^0 - d)}{d d^0 m} + \frac{M}{d} \quad (4)$$

where  $d^0$  is the density of pure water,<sup>22</sup>  $d$  is the density of the solution,  $M$  is the molecular weight of the solute, and  $m$  is the molality of the solution (mol/1000 g of water). The apparent molal expansibilities,  $\phi_E$ , for the various solutions were calculated from  $\phi_v$  at various temperatures ( $\phi_E = d\phi_v/dT$ ). The average apparent molal expansibilities and the average deviations from the mean are given in Table I. Although these  $\phi_E$  values were not made as a function of concentration, we have equated these  $\phi_E$  values to the infinite-dilution partial molal expansibilities,  $\phi_E = \bar{E}^0$ . Since  $\phi_E$  does not vary considerably with concentration<sup>23,24</sup> and the measurements were made on dilute solutions, the differences between  $\phi_E$  and  $\bar{E}^0$  are well within the experi-

(10) J. Padova, *J. Chem. Phys.*, **40**, 691 (1964).

(11) B. E. Conway, R. E. Verrall, and J. E. Desnoyers, *Z. Phys. Chem.* (Leipzig), **230**, 157 (1965).

(12) J. E. Desnoyers, R. E. Verrall, and B. E. Conway, *J. Chem. Phys.*, **43**, 243 (1965).

(13) E. Glueckauf, *Trans. Faraday Soc.*, **61**, 914 (1965).

(14) A. M. Couture and K. J. Laidler, *Can. J. Chem.*, **34**, 1209 (1956).

(15) R. Zana and E. Yeager, *J. Phys. Chem.*, **70**, 954 (1966); **71**, 521 (1967), reported the first estimates of the  $\bar{V}^0$ 's of ions based on a direct experimental method using an ultrasonic technique.

(16) P. Mukerjee, *J. Phys. Chem.*, **70**, 2708 (1966).

(17) F. J. Millero, *ibid.*, **71**, 4567 (1967).

(18) F. J. Millero and W. Drost-Hansen, *J. Chem. Eng. Data*, **13**, 330 (1968).

(19) F. J. Millero and W. Drost-Hansen, *J. Phys. Chem.*, **72**, 1758 (1968).

(20) F. J. Millero, W. Drost-Hansen, and L. Korson, *ibid.*, **72**, 2251 (1968).

(21) F. J. Millero, *Rev. Sci. Instrum.*, **38**, 1441 (1967).

(22) L. W. Tilton and J. L. Taylor, *J. Res. Nat. Bur. Stand.*, **18**, 204 (1937).

(23) H. S. Harned and B. B. Owen, "The Physical Chemistry of Electrolyte Solutions," American Chemical Society Monograph No. 137, Reinhold Publishing Corp., New York, N. Y., 1958.

(24) F. Franks and H. T. Smith, *Trans. Faraday Soc.*, **63**, 2586 (1967).

**Table I:** Apparent Molal Expansibilities of MgCl<sub>2</sub>, CaCl<sub>2</sub>, SrCl<sub>2</sub>, and BaCl<sub>2</sub> Aqueous Solutions at 25°

Salt	Concn., <i>m</i>	Apparent molal expansibility, <sup>a</sup> ml/mol deg
MgCl <sub>2</sub>	0.06083	-0.013 ± 0.009
CaCl <sub>2</sub>	0.06200	0.050 ± 0.017
SrCl <sub>2</sub>	0.04243	0.082 ± 0.020
BaCl <sub>2</sub>	0.07482	0.080 ± 0.029

<sup>a</sup> It should be kept in mind that an error of 1 ppm in the density at concentrations of ~0.05 *m* corresponds to an error of ±0.02 ml/mol in  $\phi_v$  or ±0.04 ml/mol deg in  $\phi_E$ . Since all the measurements were made with the same apparatus, the relative comparison of  $\phi_E$  is probably more accurate than the average deviations indicate.

mental error (0.009–0.03 ml/mol deg). We know of few other expansibility data for the divalent salts or ions at 25° that can be used to compare with our results. Noyes<sup>25</sup> lists values for  $\bar{E}^0(\text{Mg}^{2+})$ ,  $\bar{E}^0(\text{Sr}^{2+})$ , and  $\bar{E}^0(\text{Ba}^{2+})$  (respectively, equal to 0.004, 0.12, and 0.18 ml/mol deg) where  $\bar{E}^0(\text{Cl}^-) = 0$  and  $\bar{E}^0(\text{H}^+) = 0$ . These values were calculated from the tabulated and graphical information of Fajans and Johnson.<sup>26</sup> Since  $\bar{E}^0(\text{HCl}) = 0.034$  ml/mol deg and not 0 at 25°, the results are not very reliable, but they do agree with our results within the combined experimental errors. Dunn<sup>27</sup> has recently measured  $\bar{V}^0(\text{CaCl}_2)$  and  $\bar{V}^0(\text{BaCl}_2)$  at 0.05, 5.0, 15°, and the  $\bar{E}^0$ 's extrapolated from these results (to 25°) agree within experimental error with our results for these salts ( $\bar{E}^0(\text{CaCl}_2) \cong 0.08$  ml/mol deg and  $\bar{E}^0(\text{BaCl}_2) \cong 0.11$  ml/mol deg). The  $\bar{E}^0$ 's of the divalent chlorides were divided into their ionic components,  $\bar{E}^0(\text{ion})$ , by assigning a value for  $\bar{E}^0(\text{Cl}^-) = 0.046$  ml/mol deg.<sup>19</sup> Table II lists the  $\bar{E}^0(\text{ion})$  for these divalent cations and other ions along with the literature references<sup>18–20, 23</sup> and crystal radii.<sup>28</sup>

## Discussion

The values of  $\bar{E}^0$  of the divalent ions (given in Table II) vary with the crystal radius (or the radius of the ion in solution) unlike values of  $\bar{V}^0(\text{elect})$  of these ions.<sup>6</sup> The apparently constant electrostriction for the divalent ions (and other polyvalent ions)<sup>6</sup> is due to the other terms of eq 3,  $\bar{V}^0(\text{int})$  and  $\bar{V}^0(\text{struct})$ , masking the effects of  $\bar{V}^0(\text{elect})$ . The variation of the  $\bar{E}^0$ 's of the divalent cations (as a function of crystal radius) is in opposite order to the  $\bar{E}^0$ 's of the monovalent cations. Thus the effect of temperature on the hydration of divalent and monovalent cations is different. Also,  $\bar{E}^0(\text{ion})$  appears to be a much more sensitive probe of ion-solvent interactions than  $\bar{V}^0(\text{ion})$ .

If one assumes that the  $\bar{E}^0$ 's of the divalent cations (Mg<sup>2+</sup>, Ca<sup>2+</sup>, Sr<sup>2+</sup>, and Ba<sup>2+</sup>) are mainly due to the electrostrictive expansibility, one would expect  $\bar{E}^0$  of these ions to be proportional to  $Z^2/r$  (where *r* is the

**Table II:** Partial Molal Expansibility of Ions in Aqueous Solution at 25°

Ion	$r$ (crystal radius), <sup>a</sup> Å	$\bar{E}^0(\text{ion})$ , ml/mol deg	Ref
H <sup>+</sup>	...	-0.012	<i>b</i>
Li <sup>+</sup>	0.60	-0.014	<i>c</i>
Na <sup>+</sup>	0.95	0.032	<i>c</i>
K <sup>+</sup>	1.33	0.023	<i>c</i>
Rb <sup>+</sup>	1.48	0.016	<i>c</i>
Cs <sup>+</sup>	1.69	0.012	<i>c</i>
NH <sub>4</sub> <sup>+</sup>	1.48	-0.028	<i>d</i>
Me <sub>6</sub> N <sup>+</sup>	3.47	0.033	<i>d</i>
Et <sub>4</sub> N <sup>+</sup>	4.00	0.054	<i>d</i>
Pr <sub>4</sub> N <sup>+</sup>	4.52	0.095	<i>d</i>
Bu <sub>4</sub> N <sup>+</sup>	4.94	0.177	<i>d</i>
Mg <sup>2+</sup>	0.65	-0.105	<i>e</i>
Ca <sup>2+</sup>	0.99	-0.042	<i>e</i>
Sr <sup>2+</sup>	1.13	-0.010	<i>e</i>
Ba <sup>2+</sup>	1.35	-0.012	<i>e</i>
F <sup>-</sup>	1.36	0.035	<i>c</i>
Cl <sup>-</sup>	1.81	0.046	<i>c</i>
Br <sup>-</sup>	1.95	0.050	<i>f</i>
I <sup>-</sup>	2.16	0.069	<i>c</i>
NO <sub>3</sub> <sup>-</sup>	2.64	0.100	<i>c</i>
SO <sub>4</sub> <sup>2-</sup>	2.90	0.107	<i>g</i>

<sup>a</sup> The Pauling crystal radii as quoted in E. R. Nightingale, Jr., *J. Phys. Chem.*, **63**, 1381 (1959). <sup>b</sup> Calculated from  $\bar{E}^0(\text{HCl})$  listed in ref 23 by assuming  $\bar{E}^0(\text{Cl}^-) = 0.046$  ml/mol deg.<sup>19</sup> <sup>c</sup> Calculated from the  $\bar{E}^0$ 's of the salts listed in ref 18 by assuming  $\bar{E}^0(\text{Cl}^-) = 0.046$  ml/mol deg.<sup>19</sup> <sup>d</sup> Calculated from the  $\bar{E}^0$ 's of the salts listed in ref 19. <sup>e</sup> Calculated from the  $\bar{E}^0$ 's of the salts listed in Table I by assuming  $\bar{E}^0(\text{Cl}^-) = 0.046$  ml/mol deg. <sup>f</sup> Recalculated from  $\bar{E}^0(\text{KBr})$  given in ref 18 by using the data above 25° and comparing the nearly constant difference obtained between the values listed in ref 23 and ref 18. <sup>g</sup> Calculated from  $\bar{E}^0(\text{Na}_2\text{SO}_4)$  given in ref 20.

crystal radius in ångströms). Figure 1 shows a plot of  $\bar{E}^0$  for the divalent ions (listed in Table II) vs.  $Z^2/r$ . The slope of this line is found to be equal to 0.034 Å ml/mol deg and the intercept equal to 0.092 ml/mol deg. The value obtained for the slope agrees very well with the theoretical value (0.027 Å ml/mol deg) obtained by Noyes<sup>25</sup> by differentiating the Drude-Nernst<sup>29</sup> equation with respect to temperature

$$\bar{E}^0(\text{elect}) = \frac{d\bar{V}^0(\text{elect})}{dt} = \frac{-d\left[1 \left(\frac{d \ln D}{dP}\right)\right] e^2 Z^2}{2r} \quad (5)$$

The positive intercept indicates that there is a positive contribution to the  $\bar{E}^0$  of the divalent ions similar to nonelectrolytes and other ions. At present it is not

(25) R. M. Noyes, *J. Amer. Chem. Soc.*, **86**, 971 (1964).

(26) K. Fajans and O. Johnson, *ibid.*, **64**, 668 (1942).

(27) L. A. Dunn, *Trans. Faraday Soc.*, in press.

(28) The Pauling crystal radii as quoted by E. R. Nightingale, Jr., *J. Phys. Chem.*, **63**, 1381 (1959).

(29) P. Drude and W. Nernst, *Z. Phys. Chem. (Frankfurt am Main)*, **15**, 79 (1894).

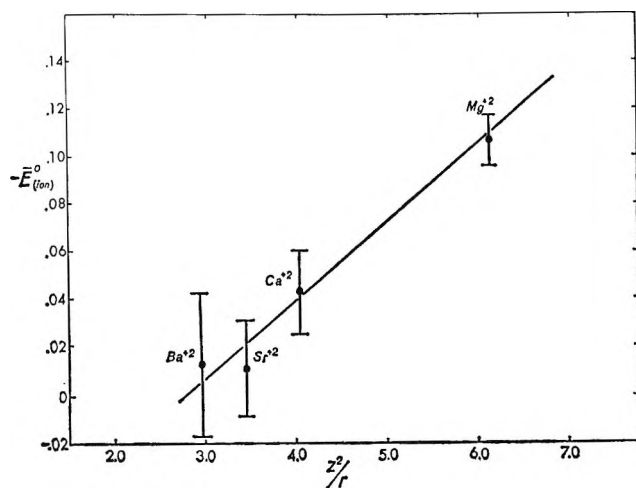


Figure 1. Partial molal expansibility of some divalent ions as a function of  $Z^2/r$ , where  $Z$  is the charge on the ion and  $r$  is the crystal radius in ångströms.

possible to separate this positive  $\bar{E}^0$  effect (*i.e.*,  $\bar{E}^0(\text{int}) + \bar{E}^0(\text{struct})$ ) or say that it is not a function of the size of the ion. The curve can be made to pass through zero by adjusting  $\bar{E}^0(\text{Cl}^-)$  to a value of 0.092 ml/mol deg. This value for  $\bar{E}^0(\text{Cl}^-)$ , however, appears to be quite high compared with other estimates.<sup>18,19,25</sup> This division would also cause  $\bar{E}^0$  of almost all the cations in Table II to be negative (except  $\text{Et}_4\text{N}^+$ ,  $\text{Pr}_4\text{N}^+$ , and  $\text{Bu}_4\text{N}^+$ ) and all the anions to be positive, which seems unreasonable.

The  $\bar{E}^0$ 's of the simple monovalent cations and anions vary with size or radius in an inverse order (Table I). Thus, although various workers have been successful in treating the ion-solvent interactions of these simple monovalent ions by a common relationship, the  $\bar{E}^0$  results indicate that (1) the effect of ions on the structure of water (over and above the electrostrictive region) is very important and should not be neglected and (2) the effect of the ions on the structure of water is different for cations and anions of similar size and is not a smooth function of crystal radius or the charge on the ion.

Water is one of the few solvent systems where the  $\bar{E}^0$ 's of monovalent salts and ions have positive values at room temperatures. At temperatures above 50–70°, however, the  $\bar{E}^0$ 's of salts and ions are negative<sup>30</sup> in water, as predicted from the simple continuum model. The  $\bar{V}^0$ 's of salts are also in their predicted order at temperatures above 50° (*i.e.*, as a function of  $r^3$ ). It appears as though the structure of water (that is thought to exist at room temperatures) accounts for the positive  $\bar{E}^0$  and that at high temperatures the positive effect disappears. The exact form of the  $\bar{E}^0$  due to the structure of water for various ions is quite complicated, and it is impossible at this time to predict the relationship of  $\bar{E}^0$  to the intrinsic properties of the ions. Until more is known about the structure of water at

room temperatures, the division of  $\bar{E}^0$ 's or  $\bar{V}^0$ 's of ions into various components may be entirely arbitrary.

Another qualitative approach to the division of the  $\bar{V}^0$ 's and  $\bar{E}^0$ 's of ions into individual components can be developed by describing the hydration of an ion in solution by the Frank and Wen model.<sup>31</sup> From this model the  $\bar{V}^0$  of an ion can be viewed as being due to the following four components: (1) the intrinsic volume of the ion,  $\bar{V}^0(\text{int})$ ; (2) the electrostricted volume,  $\bar{V}^0(\text{elect})$ , due to the water firmly attached to the ion; (3) the disordered volume,  $\bar{V}^0(\text{disord})$ , due to the disordered region surrounding the electrostricted region of the ion; and (4) the caged volume due to the formation of structured or "caged" water around the ion (this region is important for ions that have a hydrocarbon portion or possibly for highly charged ions). The effect of temperature on these various regions can likewise be divided into four regions: (1) the intrinsic expansibility,  $\bar{E}^0(\text{int})$ , which is the volume change due to the expansion of the ion (this term is probably very small and can be neglected for normal ions); (2) the electrostriction expansibility,  $\bar{E}^0(\text{elect})$ , which is due to changes in the electrostricted region; (3) the disordered expansibility,  $\bar{E}^0(\text{disord})$ , which is due to changes in the disordered region; and (4) the "caged" expansibility,  $\bar{E}^0(\text{caged})$ , which is due to the changes in the "caged" or highly structured water around hydrocarbon portion of an ion (or possibly around highly electrostricted ions where the disordered region is very small).

The  $\bar{V}^0(\text{int})$  of the ion is equal to the volume of the ion calculated from the crystal radius, and if it is assumed that the ion is hard sphere,  $\bar{V}^0(\text{int}) = 2.52r^3$ , where  $r$  is in ångströms.  $\bar{E}^0(\text{int})$  is positive and very small for normal ions; however, it may be large for ions with hydrocarbon portions or simple hydrocarbon nonelectrolytes.

The  $\bar{V}^0(\text{elect})$  and  $\bar{E}^0(\text{elect})$  regions immediately surrounding an ion appear to be predictable in sign and order of magnitude from the simple continuum model or modifications to this model for dielectric saturation effects.  $\bar{V}^0(\text{elect})$  and  $\bar{E}^0(\text{elect})$  are both negative and proportional to  $Z^2/r$ .

The  $\bar{V}^0(\text{disord})$  and  $\bar{E}^0(\text{disord})$  region appears to be different for cations and anions of the same size, owing to the different orientation of the water molecules in the first electrostricted region. The size of the disordered region depends on the temperature and magnitude of the electrostriction region (*i.e.*,  $Z^2/r$ ). For ions with a large electrostriction region (large  $Z^2/r$ ) the disordered region is very small or nonexistent; however, for ions with a small electrostriction region (small  $Z^2/r$  like the large monovalent ions) this region is very

(30) A. J. Ellis, *J. Chem. Soc.*, 1579 (1966); 660 (1967).

(31) H. Frank and W. Y. Wen, *Discussions Faraday Soc.*, 24, 133 (1967).



important. The disordered region appears to become less important at high temperatures, causing the maximum in  $\bar{V}^0$  of the simple monovalent salts near  $50^\circ$ .<sup>30</sup> At low temperatures or near room temperature the  $\bar{V}^0$  of the disordered region accounts for the  $\bar{V}^0$ 's of the large monovalent ions appearing to be larger in solutions than the crystal volume normally attributed to void-space effects. The  $\bar{E}^0$  of the disordered region accounts for the large positive values for the monovalent ions at room temperatures and the differences between the cation and anion  $\bar{E}^0$  dependence on size. The  $\bar{V}^0$ - (disord) and  $\bar{E}^0$  (disord) are both positive and become less important at high temperatures or as the structure of water is broken.

The  $\bar{V}^0$  and  $\bar{E}^0$  of the caged region which is important for ions with hydrocarbon tails (or possibly highly charged ions) has been discussed elsewhere.<sup>19</sup> The  $\bar{V}^0$  (caged) is negative and increases in magnitude with the size of the hydrocarbon portion of the molecule. This region may also exist for highly charged ions and may be the cause of the constant  $\bar{V}^0$  (elect) observed by Mukerjee.<sup>6</sup> The  $\bar{E}^0$  (caged) is positive and also increases in magnitude with size of the hydrocarbon portion of the ion. This positive contribution of  $\bar{E}^0$  (caged) may be the cause of the  $\bar{E}^0$ 's of the divalent cations appearing to be too large. Since  $\bar{E}^0$  (disord) can also cause the same positive effect, it cannot be stated with certainty which effect causes the positive contribution to the  $\bar{E}^0$ 's of the divalent ions.

In conclusion, the experimental results of the  $\bar{V}^0$ 's and the  $\bar{E}^0$ 's of ions indicate that solute-solvent interactions are very dependent upon the structure of water. After the structure of water is broken down (*i.e.*, at high temperatures), the solute-solvent interactions appear to be normal (or predictable in magnitude and sign by a simple model). By saying that the structure of water is broken down it is not meant that water exists as only monomers but that one structured form responsible for the anomalous thermodynamic behavior<sup>32</sup> disappears at high temperatures. Accurate measurements of the  $\bar{V}^0$ 's of solutes (and other thermodynamic data) in water are needed at temperatures above  $50^\circ$ . From these data it may be possible to obtain a better understanding of the effects of the structure of water and the changes in structure caused by ions at lower temperatures.

*Acknowledgment.* The author wishes to thank Dr. W. Drost-Hansen for his helpful comments and Dr. L. A. Dunn who made his manuscript available prior to publication. This work was supported by Grant 14-01-001-310 from the Office of Saline Water and the Office of Naval Research Contract NONR 40008(02)-B7895R.

(32) For example, the temperature coefficient of the isothermal compressibility of water: G. S. Kell and E. Whalley, *Phil. Trans. Roy Soc. (London)*, **258**, 565 (1965).

## Electronic Oscillator Strength of CF<sub>2</sub>

by A. P. Modica

Avco Space Systems Division, Wilmington, Massachusetts (Received June 24, 1968)

A shock tube and samples of C<sub>2</sub>F<sub>4</sub>, CF<sub>2</sub>Cl<sub>2</sub>, and CF<sub>4</sub> in argon diluent were used to prepare CF<sub>2</sub> species for spectroscopic study. Absorption spectra of these shocked mixtures, taken with a Hilger medium quartz spectrograph, show a series of absorption bands from 2250 to 3000 Å corresponding to those of the CF<sub>2</sub> radical. In the region of strongest absorption (2400–2500 Å) the bands appear to overlap completely. Absorption coefficients of the observed band system were determined at various wavelengths with a low-resolution radiometer. Integration of the absorption coefficients gave from theory electronic oscillator strengths of  $f_{\text{abs}}^e = 0.034$  (C<sub>2</sub>F<sub>4</sub> data, 1804°K) 0.032 (CF<sub>2</sub>Cl<sub>2</sub> data, 2085°K), and 0.024 (CF<sub>4</sub> data, 2878°K). The uncertainty in these  $f$ -number values is estimated to be  $\pm 10\%$ .

### Introduction

The 2500-Å emission band system of the CF<sub>2</sub> radical was first observed and reported by Venkateswarlu.<sup>1</sup> Absorption<sup>2–6</sup> and microwave<sup>7</sup> spectra of CF<sub>2</sub> have shown that the molecule is in a singlet ground state, <sup>1</sup>A<sub>1</sub>. The electronic oscillator strength of this band system has been estimated to be 0.01 to within a factor of 2 from a measured absorption coefficient at 2488 Å.<sup>8</sup> Currently, the CF<sub>2</sub> electronic oscillator strength is particularly useful in radiative heat transfer and optical diagnostic problems associated with fluorocarbon chemistry in rocket combustion and reentry ablation. Therefore, it has become of interest to obtain an improved value of the  $f$  number from measurements of the absorption coefficient over the entire band system.

### Experimental Measurements

Absorption spectra of shock-heated argon mixtures containing 1% fluorocarbon were photographed on Eastman Kodak 103-0 plates with a Hilger medium quartz spectrograph (Figure 1). A xenon flash lamp was timed with the passage of the shock wave across the entrance slit (200 μ) of the spectrograph, and multiple exposures totaling 600 μsec were required to obtain spectra. Photographic plates were analyzed with a Jarrell-Ash microdensitometer (Model 2310). The ratio of the per cent transmission of the absorbing gas flash lamp spectra to that of the flash lamp spectra alone was taken to be the relative transmission of the absorbing gas sample. Absorption coefficients for different wavelengths in the band system were determined from spectrophotometric measurements, using an Engis SO502 grating monochromator (30-Å triangular band pass at half-peak-height) and a 1P-28 photomultiplier detector to monitor incident and transmitted light intensities. Output from a xenon-mercury arc lamp served as the source of ultraviolet light. Details of the shock tube and optical setup are given elsewhere.<sup>9</sup>

### Ultraviolet Absorption

Argon gas mixtures of 1% C<sub>2</sub>F<sub>4</sub>, CF<sub>2</sub>Cl<sub>2</sub>, and CF<sub>4</sub> were shocked to temperatures around 1804 ± 23 (C<sub>2</sub>F<sub>4</sub> experiments), 2085 ± 45 (CF<sub>2</sub>Cl<sub>2</sub> experiments), and 2878 ± 49°K (CF<sub>4</sub> experiments). Thermochemical equilibrium calculations<sup>10</sup> (Tables I–III) showed that under the experimental conditions chosen for study the parent fluorocarbon molecules were virtually all dissociated to CF<sub>2</sub> radicals and halogen atoms. The absorption spectrum (Figure 2) obtained from these shock-heated fluorocarbon molecules was seen to consist of a series of diffused bands extending from about 2250 to 3000 Å. The locations of these bands are found to closely coincide with those of the well-known CF<sub>2</sub> ultraviolet absorption bands.<sup>4</sup> It is believed from other experimental evidence that the spectrum observed in the present study is virtually due to only CF<sub>2</sub> species. Spectrophotometric measurements of the parent fluorocarbons before and after shock heating indicated a lack of absorption in the 2250–3000-Å region. The absorption coefficient measured at 2536 Å in this work is found to be similar to that deduced from ultraviolet absorption in the pyrolysis of CF<sub>3</sub>H,<sup>11</sup> for which gas there is gas chromatographic evidence<sup>12</sup> indicating CF<sub>2</sub> and HF are produced in splitting the molecule. Studies of the thermal dissociation of CF<sub>3</sub>

- (1) P. Venkateswarlu, *Phys. Rev.*, **77**, 676 (1950).
- (2) R. K. Laird, E. B. Andrews, and R. F. Barrow, *Trans. Faraday Soc.*, **46**, 803 (1950).
- (3) D. E. Mann and B. A. Thrush, *J. Chem. Phys.*, **33**, 1372 (1960).
- (4) A. M. Bass and D. E. Mann, *ibid.*, **36**, 3501 (1962).
- (5) B. A. Thrush and J. J. Zwolenik, *Trans. Faraday Soc.*, **59**, 582 (1963).
- (6) D. E. Milligan, D. E. Mann, M. E. Jacox, and R. A. Mitsch, *J. Chem. Phys.*, **41**, 1199 (1964).
- (7) F. X. Powell and D. R. Lide, Jr., *ibid.*, **45**, 1067 (1966).
- (8) F. W. Dalby, *ibid.*, **41**, 2297 (1964).
- (9) A. P. Modica and J. E. LaGraff, *ibid.*, **43**, 3383 (1965).
- (10) J. J. Warga, *Soc. Ind. Appl. Math.*, **11**, 594 (1963).
- (11) A. P. Modica and J. E. LaGraff, *J. Chem. Phys.*, **44**, 3375 (1966).
- (12) E. Tschuikow-Roux, *ibid.*, **42**, 3639 (1965).

**Table I:** Equilibrium Composition of a 1:100 C<sub>2</sub>F<sub>4</sub>-Ar Mixture at 1.3 Atm Total Pressure<sup>a</sup>

Temp, °K	Mole fraction of species						
	Ar	C <sub>2</sub> F <sub>4</sub>	CF <sub>4</sub>	CF <sub>3</sub>	CF <sub>2</sub>	F <sub>2</sub>	F
1700	0.98	0.50 × 10 <sup>-3</sup>	0.20 × 10 <sup>-15</sup>	0.20 × 10 <sup>-9</sup>	0.19 × 10 <sup>-1</sup>	0.21 × 10 <sup>-27</sup>	0.79 × 10 <sup>-13</sup>
1800	0.98	0.18 × 10 <sup>-3</sup>	0.14 × 10 <sup>-16</sup>	0.63 × 10 <sup>-10</sup>	0.19 × 10 <sup>-1</sup>	0.26 × 10 <sup>-27</sup>	0.12 × 10 <sup>-12</sup>
1900	0.98	0.71 × 10 <sup>-4</sup>	0.13 × 10 <sup>-17</sup>	0.23 × 10 <sup>-10</sup>	0.19 × 10 <sup>-1</sup>	0.32 × 10 <sup>-27</sup>	0.18 × 10 <sup>-12</sup>

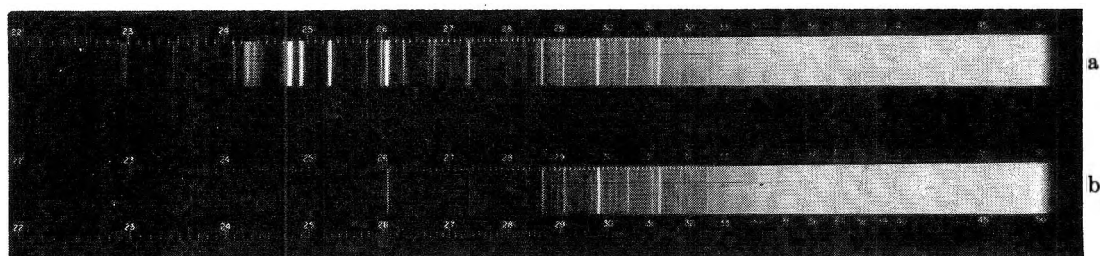
<sup>a</sup> "JANAF thermochemical Tables," Dow Chemical Co., Midland Mich., 1966, and  $\Delta H_f(\text{CF}_3) = -104$  kcal/mol (A. P. Modica, *J. Chem. Phys.* **48**, 3283 (1968)) were used in equilibrium calculation.

**Table II:** Equilibrium Composition of a 1:100 CF<sub>2</sub>Cl<sub>2</sub>-Ar Mixture at 2.3 Atm of Total Pressure

Temp, °K	Mole fraction of species								
	Ar	CF <sub>2</sub> Cl <sub>2</sub>	CF <sub>4</sub>	CF <sub>3</sub>	CF <sub>2</sub>	Cl <sub>2</sub>	Cl	F <sub>2</sub>	F
2000	0.97	0.25 × 10 <sup>-8</sup>	0.65 × 10 <sup>-15</sup>	0.43 × 10 <sup>-9</sup>	0.97 × 10 <sup>-2</sup>	0.12 × 10 <sup>-2</sup>	0.17 × 10 <sup>-1</sup>	0.19 × 10 <sup>-23</sup>	0.14 × 10 <sup>-10</sup>
2100	0.97	0.74 × 10 <sup>-7</sup>	0.64 × 10 <sup>-29</sup>	0.49 × 10 <sup>-16</sup>	0.97 × 10 <sup>-2</sup>	0.66 × 10 <sup>-3</sup>	0.18 × 10 <sup>-1</sup>	0.16 × 10 <sup>-36</sup>	0.49 × 10 <sup>-17</sup>
2200	0.97	0.23 × 10 <sup>-7</sup>	0.21 × 10 <sup>-32</sup>	0.10 × 10 <sup>-17</sup>	0.97 × 10 <sup>-2</sup>	0.37 × 10 <sup>-3</sup>	0.19 × 10 <sup>-1</sup>	0.0	0.29 × 10 <sup>-18</sup>

**Table III:** Equilibrium Composition of a 1:100 CF<sub>4</sub>-Ar Mixture at 2.3 Atm of Total Pressure

Temp, °K	Mole fraction of species						
	Ar	C <sub>2</sub> F <sub>4</sub>	CF <sub>4</sub>	CF <sub>3</sub>	CF <sub>2</sub>	F <sub>2</sub>	F
2800	0.97	0.12 × 10 <sup>-6</sup>	0.19 × 10 <sup>-3</sup>	0.52 × 10 <sup>-3</sup>	0.90 × 10 <sup>-2</sup>	0.20 × 10 <sup>-6</sup>	0.19 × 10 <sup>-1</sup>
2900	0.97	0.88 × 10 <sup>-7</sup>	0.56 × 10 <sup>-4</sup>	0.31 × 10 <sup>-3</sup>	0.94 × 10 <sup>-2</sup>	0.16 × 10 <sup>-6</sup>	0.19 × 10 <sup>-1</sup>
3000	0.97	0.64 × 10 <sup>-7</sup>	0.16 × 10 <sup>-4</sup>	0.18 × 10 <sup>-3</sup>	0.95 × 10 <sup>-2</sup>	0.13 × 10 <sup>-6</sup>	0.19 × 10 <sup>-1</sup>

**Figure 1.** The high-temperature absorption spectra of CF<sub>2</sub>: (a) xenon flash lamp; (b) shocked 1:100 C<sub>2</sub>F<sub>4</sub>-Ar gas mixture.

radicals<sup>13</sup> show that these species do not absorb in the 2250–3000-Å region. Finally, in accordance with the equilibrium calculations, it was observed that for each of the fluorocarbon mixtures the absorption coefficient varied slightly (10%) with a change in temperature of  $\pm 100^\circ\text{K}$ . If species other than CF<sub>2</sub> had been responsible for the absorption, larger changes in the absorption coefficients would have been noticed because of the relatively large variations in concentration for a  $\pm 100^\circ\text{K}$  change in temperature.

The absorption coefficient  $\epsilon_r$  of the CF<sub>2</sub> radical was obtained from Beer's law according to

$$\ln \frac{I_0}{I} = \epsilon_r L [\text{CF}_2] = \epsilon_r L \rho_{21} [X] = \ln \frac{H}{H-h} \quad (1)$$

where  $I_0$  and  $I$  are the intensities of the incident and transmitted light beam, respectively;  $K$  is the optical path across the absorbing gas;  $\epsilon_r$  is the absorption coefficient, in l./mol cm;  $[\text{CF}_2]$  is the CF<sub>2</sub> species concentration,  $\rho_{21}$  is the product of the shock density ratio; and  $[X]$  is the stoichiometric concentration of the unshocked fluorocarbon to be completely dissociated. Experimentally the light intensity is measured by the detector output displayed on a Tektronix 535 oscilloscope. The incident beam produces the deflection ( $H$ ) immediately after the run and  $h$  is that from CF<sub>2</sub> absorption. An oscillogram record of CF<sub>2</sub> ultraviolet absorption is shown in Figure 3. Measurements were

(13) A. P. Modica, *J. Chem. Phys.*, **48**, 3283 (1968).

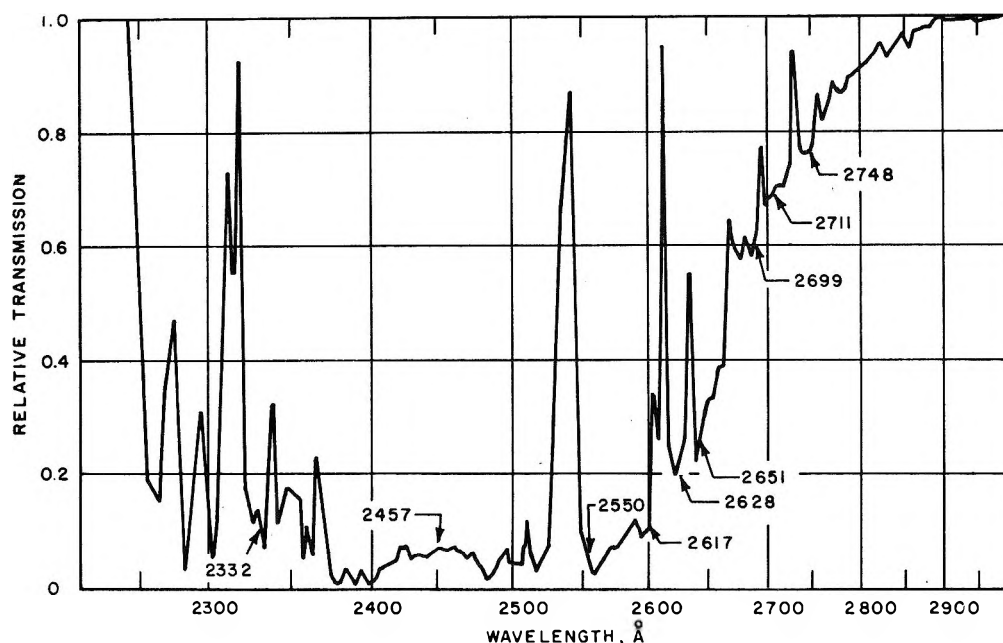


Figure 2. Analysis of the absorption spectrogram from a shock-heated 1:100  $C_2F_4$ -Ar gas mixture. The arrows show some wavelengths of known  $CF_2$  absorption bands.<sup>4</sup>

Table IV:  $CF_2$  Absorption Coefficient

$\lambda$ , Å	$\lambda$ , $cm^{-1}$	$10^{-3}\epsilon_{\nu}$ , l./mol cm		
		$2878 \pm 49^\circ K$	$2085 \pm 45^\circ K$	$1804 \pm 23^\circ K$
2150	46,511	$0.32 \pm 0.04$		
2180	45,871			$0.29 \pm 0.04$
2225	44,943		$0.50 \pm 0.02$	
2235	44,742			$0.59 \pm 0.00$
2250	44,444	$0.67 \pm 0.07$		
2300	43,478	$0.88 \pm 0.07$	$1.18 \pm 0.09$	$1.39 \pm 0.09$
2350	42,553	$1.22 \pm 0.11$		
2380	42,016		$2.14 \pm 0.04$	
2390	41,841			$2.62 \pm 0.28$
2400	41,666	$1.60 \pm 0.16$		
2450	40,816	$1.68 \pm 0.02$		
2482	40,290	$1.87 \pm 0.28$		
2537	39,416	$1.59 \pm 0.17$		$2.29 \pm 0.09$
2600	38,461	$1.33 \pm 0.02$		$2.38 \pm 0.10$
2652	37,707	$1.14 \pm 0.10$	$1.24 \pm 0.18$	$1.31 \pm 0.03$
2700	37,037	$0.88 \pm 0.04$	$1.03 \pm 0.06$	$1.08 \pm 0.05$
2750	36,363	$0.75 \pm 0.02$		$0.76 \pm 0.01$
2804	35,663	$0.55 \pm 0.01$	$0.53 \pm 0.03$	$0.45 \pm 0.01$
2893	33,566	$0.33 \pm 0.01$	$0.28 \pm 0.01$	$0.22 \pm 0.01$
2967	33,704	$0.21 \pm 0.01$		$0.10 \pm 0.01$

made from the steady absorption level where the chemical relaxation period is completed and the gas is characterized by a constant temperature and density. The shock temperature and density ratios were obtained by solving the Rankine-Hugoniot equations with the measured shock velocity and JANAF thermochemical data of the appropriate species. Absorption coefficients of the  $CF_2$  radical were determined for concentrations between  $0.9 \times 10^{-4}$  and  $1.7 \times 10^{-4}$  mol/l. The experimental results of the study are given in Table IV.

### Theoretical Interpretation

An expression for the electronic oscillator strength of a molecular band system can be derived from considerations analogous to those for atomic line absorption. Following Herzberg,<sup>14</sup> the only difference between the intensity of an electronic transition of a molecule and that of an electronic transition in an atom is that in the molecule the total intensity is distributed over a

(14) G. Herzberg in "Spectra of Diatomic Molecules," D. Van Nostrand Co., Inc., New York, N. Y., 1950, pp 381-383.

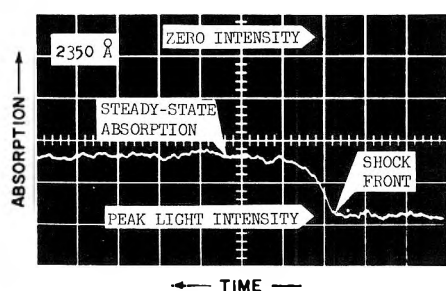


Figure 3. The ultraviolet light absorption behind the shock wave into a 1:100 CF<sub>4</sub>-argon gas mixture (shock temperature, 2850°K; [CF<sub>2</sub>] =  $9.45 \times 10^{-6}$  mole/l.; writing, 20  $\mu$ sec between vertical lines).

large number of lines or over a continuous spectrum. For an electronic transition in absorption, the electronic oscillator strength is related to the integrated molar absorption coefficient ( $\epsilon_\nu$ , l./mol cm) by

$$f_{\text{abs}}^e = \frac{mc^2 1000}{\pi N e^2} \int \epsilon_\nu d\nu \quad (2)$$

$$= 1.877 \times 10^{-9} \int \epsilon_\nu d\nu$$

where  $m$  and  $e$  are the electronic mass and charge ( $4.802 \times 10^{-10}$  esu),  $c$  is the speed of light, and  $N$  is Avogadro's number. To evaluate the oscillator strength of the CF<sub>2</sub> absorption band, the experimental absorption coefficients were least-squares fitted with a fourth-order polynomial of the form

$$\epsilon_\nu = a_0 + a_1\nu^1 + a_2\nu^2 + a_3\nu^3 + a_4\nu^4 \quad (3)$$

This procedure was adopted in order to cope with the statistical scatter in the data and permit numerical integration of the absorption coefficients with wavelength. The solid lines in Figure 4 are the results of the fits. In Table V, the oscillator strength of this work is presented along with the value estimated by Dalby.

**Table V:** Electronic Oscillator Strength of the CF<sub>2</sub>(<sup>1</sup>B<sub>1</sub> ← <sup>1</sup>A<sub>1</sub>) Band System

Ref	Temp, °K	$f_{\text{abs}}^e$
a	2875	0.024
	2085	0.032
	1804	0.034
b	298	$0.014 \pm 0.006$

<sup>a</sup> This work; integration over wavelength interval 33,000–47,000 cm<sup>-1</sup>. <sup>b</sup> F. W. Dalby, *J. Chem. Phys.*, **41**, 2297 (1964).

## Discussion

The sources of error inherent to the present type of spectroscopy study have been considered extensively in a previous paper.<sup>15</sup> Uncertainties in the recording

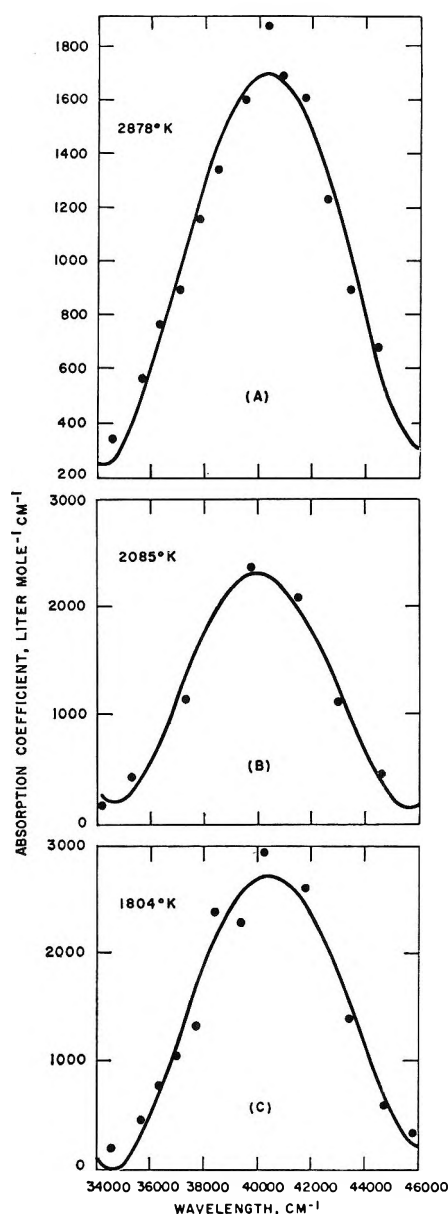


Figure 4. Variation of the CF<sub>2</sub> absorption coefficient with wavelength and temperature. The solid lines are fourth-order least-squares fits of data.

and measurement of the absorption oscillograms contribute less than 1% error to the experimental oscillator strength. Light emission from the shocked gases did not occur; hence the absorption measurements were free from this interference. Data were taken from the oscillogram records after the steady-state absorption was reached, where the temperature and density are constant and readily calculated from the thermodynamic properties of the dissociated gas mixture. The uncertainty in the measured shock velocity introduced a  $\pm 20^\circ$  error in the calculated shock temperature and an error of less than 1% in the calculated density.

(15) J. A. Harrington, A. P. Modica, and D. R. Libby, *J. Chem. Phys.*, **44**, 3380 (1966).

Since the data were analyzed for conditions close to the shock front, boundary-layer effects on the shock temperature and density would have been unimportant. Absorption by species other than  $\text{CF}_2$  in the gas mixture would seem rather unlikely, based on arguments presented earlier in the text. Absorption coefficients for a given wavelength were averaged from measurements taken within a  $100^\circ$  temperature interval. This averaging amounted to about a 5% uncertainty in the absorption coefficients for wavelengths of strongest absorption and less for the other wavelengths in the band system. Theoretically, the oscillator strength is independent of temperature, since the energy of the total absorption band is constant. In the present study the absorption  $f$  number was found to decrease by about 30% for a decrease in temperature of around  $1000^\circ\text{K}$ . Aside from the possibility of experimental error, the lower  $f$  numbers at the higher temperatures may have resulted from the broadening of the absorption band to wavelengths below  $2250 \text{ \AA}$ , where the radiometer and light source could not provide accurate optical measurements.

The high-temperature absorption spectrum reported

here is believed to be that of the singlet ground state of  $\text{CF}_2$  and not its triplet state,  $^3\text{B}_1$ . Because of extensive overlap of rotational states which apparently takes place at high temperatures, it cannot be resolved from the spectra obtained that splitting of the vibrational bands did occur indicating that the triplet state might be responsible for some of the absorption. However, Simons<sup>16</sup> has estimated that the  $\text{CF}_2$  triplet is about 45 kcal above the singlet ground state, which would make the number of molecules in the triplet state less than a factor of  $10^{-3}$  at the temperatures considered in this study. Hence, it can be assumed that any contributions to the absorption spectra by the triplet state would be insignificant.

*Acknowledgment.* The support of this research by the Ballistic Systems Division, United States Air Force, under Contract AF04(694)-687, ABRES program, is gratefully acknowledged. The author wishes to thank J. A. Harrington for his comments on the interpretation of the experimental data.

(16) J. P. Simons, *Nature*, 205, 1308 (1965).

## Effects of Matrix Polarity on the Optical and Electron Spin Resonance

Spectra of Trapped Electrons in Organic Glasses<sup>1</sup>

by Alfred Ekstrom and John E. Willard

*Department of Chemistry, University of Wisconsin, Madison, Wisconsin (Received June 25, 1968)*

Trapped electrons produced by  $\gamma$  irradiation of 13 organic glasses at 77°K have optical absorption maxima (eV) and esr line widths which increase smoothly with increasing polarity of the matrix molecules, from 3-methylpentane to glycerol, consistent with a model in which the electrons are trapped in preexisting cavities in the matrix, the size of cavities which stabilize the electrons decreasing with increasing polarity. Trapped electrons in mixtures of alcohols in the glassy state show only one optical absorption maximum. This shifts from the energy characteristic of the first alcohol to that of the second as the mole fraction of the second is increased, indicating that the alcohol molecules are homogeneously mixed, and that each trapping site is composed of several molecules. Trapped electrons in mixtures of normal propanol and 3MP in the glassy state show two electron absorption peaks, one characteristic of each pure species, with preference for trapping in the alcohol phase, indicating aggregation of like molecules.

## Introduction

Considerable evidence is available on the properties of trapped electrons in both polar and nonpolar organic matrices<sup>2</sup> as observed by visible-infrared absorption,<sup>3</sup> esr,<sup>3d,3f,4</sup> electrical conductivity,<sup>5</sup> and luminescence measurements,<sup>6</sup> but there is relatively limited evidence as to the physical nature of the trapping sites.

It appears plausible that the same type of forces may be responsible for stable trapping in the solid state at 77°K as are responsible for the relatively unstable "solvation" of electrons in liquids at 300°K.<sup>3d,3e</sup> Jortner<sup>7</sup> has proposed a hypothesis for the stabilization of electrons in liquids, in which the electron is regarded as creating a cavity in the liquid due to the short-range repulsion between the electron and the electrons of the medium. The electron is stabilized by the polarization of the molecules in the surrounding liquid. For polar molecules the trapping energy increases and the cavity size decreases with increasing polarity. In qualitative agreement with this hypothesis, the absorption maxima of the solvated electron in a series of liquid alcohols at 25°<sup>8</sup> and glassy alcohols at 77°K<sup>3e</sup> show a red shift with decreasing dielectric constant of the alcohol. It might be expected that the line width of the esr signal of the electron would decrease with decreasing polarity of the medium, that is, with increasing minimum size of the trapping cavities and consequent decreasing interaction of the electron with the nuclei of the cavity walls. Such an effect seems to hold for several  $\gamma$ -irradiated alcohols compared to ethers and for electrons prepared by the deposition of sodium in a few alcohols of different polarity.<sup>3d</sup>

This paper extends the available data on the optical and esr spectra of trapped electrons in  $\gamma$ -irradiated organic glasses covering a range in polarity from 3-methylpentane (3MP) to glycerol. It examines the

correlation between the static dielectric constants, the visible-infrared absorption maxima, and the esr line widths, and between the absorption spectra of solvated electrons in the liquid state and trapped electrons in the glassy state. The properties of the electrons trapped in mixtures of components of differing polarity have also been studied.

## Experimental Section

All materials were of reagent grade quality, whose purity was checked by gas chromatography as being

(1) This work has been supported in part by the U. S. Atomic Energy Commission under Contract AT(11-1)-1715 and by the W. F. Vilas Trust of the University of Wisconsin.

(2) For recent reviews of this subject, see: (a) W. H. Hamill, "Ionic Processes in  $\gamma$ -Irradiated Organic Solids at  $-196^{\circ}\text{C}$ ," a chapter in "Radical Ions," L. Kevan, Ed., John Wiley and Sons, Inc., New York, N. Y., 1968; (b) J. E. Willard, "Radiation Chemistry of Organic Solids," a chapter in "Fundamentals of Radiation Chemistry," P. Ausloos, Ed., John Wiley and Sons, Inc., New York, N. Y., 1968.

(3) (a) D. W. Skelly and W. H. Hamill, *J. Chem. Phys.*, **44**, 2891 (1966); (b) J. Lin, K. Tsuji, and F. Williams, *J. Amer. Chem. Soc.*, **90**, 2766 (1968); (c) P. J. Dyne and O. A. Miller, *Can. J. Chem.*, **43**, 2696 (1965); (d) J. Blandamer, L. Shields, and M. C. R. Symons, *J. Chem. Soc.*, 1127 (1965); (e) B. G. Ershov, I. E. Makarov, and A. K. Pikaev, *Khim. Vysokikh Energii*, **1**, 472 (1967); *High Energy Chem.*, **1**, 414 (1967); (f) J. E. Bennett, B. Milne, and A. Thomas, *J. Chem. Soc.*, 1393 (1967).

(4) (a) K. Tsuji, H. Yoshida, and K. Hayashi, *J. Chem. Phys.*, **46**, 810 (1967); (b) M. Shirom, R. F. C. Claridge, and J. E. Willard, *ibid.*, **47**, 286 (1967); (c) K. Tsuji and F. Williams, *J. Amer. Chem. Soc.*, **89**, 1526 (1967); (d) C. Chachaty and E. Hayon, *J. Chim. Phys.*, **61**, 1115 (1964); (e) D. R. Smith and J. J. Pieroni, *Can. J. Chem.*, **43**, 2141 (1965).

(5) B. Wiseall and J. E. Willard, *J. Chem. Phys.*, **46**, 4387 (1967).

(6) (a) K. Funabashi, P. J. Herley, and M. Burton, *ibid.*, **43**, 3939 (1965); (b) D. W. Skelly and W. A. Hamill, *ibid.*, **43**, 3497 (1965).

(7) (a) J. Jortner, *ibid.*, **30**, 839 (1959); (b) J. Jortner and S. A. Rice, *Advances in Chemistry Series*, No. 50, American Chemical Society, Washington, D. C., 1965, p 7; (c) D. C. Walker, *Quart. Rev.*, **21**, 79 (1967); (d) J. Jortner, *Radiation Res. Suppl.*, **4**, 24 (1964); (e) K. Fueki, *J. Chem. Phys.*, **44**, 3140 (1966).

(8) (a) M. C. Sauer, S. Arai, and L. M. Dorfman, *ibid.*, **42**, 708 (1965); (b) S. Arai and M. C. Sauer, *ibid.*, **44**, 2297 (1966).

greater than 99.9%. The alcohols were further distilled from 2,4-dinitrophenylhydrazine sulfuric acid solution to ensure the absence of ketonic impurities. Methyltetrahydrofuran (MTHF), methylcyclohexane (MCHx), and 3-methylpentane (3MP) were purified as previously described.<sup>9</sup> Degassing of the purified samples was accomplished by repeated freeze-pump-thaw cycles and included direct pumping on the liquid to ensure removal of CO<sub>2</sub>. All experiments were made with glassy rather than crystalline samples unless otherwise specified. Isopropyl alcohol at a concentration of 1 mol % was present in all samples of CH<sub>3</sub>OH to prevent crystallization.

Irradiations were made with a cobalt-60 source at a dose rate of  $0.8\text{--}2.0 \times 10^{18}$  eV g<sup>-1</sup> min<sup>-1</sup>, the total dose being, typically,  $2.4 \times 10^{19}$  eV g<sup>-1</sup>. During the irradiation the samples were immersed in liquid nitrogen and positioned reproducibly adjacent to a cobalt-60 source.

Samples for optical examination were contained in flat, high-purity quartz cells,  $2 \times 0.5$  cm, with a normal path length of 1 mm. On completion of irradiation, they were transferred to an optical dewar for spectroscopic measurements, these operations being carried out in complete darkness to avoid bleaching of the trapped electrons. A Cary 14 spectrophotometer, modified to pass the infrared analyzing beam through the monochromator before passing through the reaction cell, was used. The esr measurements were made as previously described<sup>9</sup> at a microwave power of *ca.* 0.01 mW. The esr line width measurements on the trapped electrons in alcohols were reproducible to  $\pm 1$  G.

## Results

The optical absorption spectra at 77°K of trapped electrons in ten  $\gamma$ -irradiated alcohol glasses observed in this work are all similar in shape to the spectra of solvated electrons in the liquid alcohols,<sup>8</sup> but are somewhat narrower and are shifted 100–200 nm toward shorter wavelengths. This is illustrated in Figure 1 by the spectra in ethanol. The absorption spectra of solvated electrons in liquid alcohols shift to shorter wavelength with decreasing temperature<sup>8</sup> but do not show the decrease in the width of the absorption band observed when the electrons are trapped in a glass.

The photon energy at the wavelength of maximum optical absorption by trapped electrons in  $\gamma$ -irradiated organic glasses at 77°K increases with increasing polarity of the matrix molecules, as shown in Table I and Figure 2 and reported earlier for a series of alcohols.<sup>3a</sup> This trend holds over a wide range from compounds which are essentially nonpolar to highly polar compounds. It is analogous to the trend<sup>8</sup> of the absorption maxima for the solvated electron in liquid alcohols (Table I).

Paralleling the shift in the optical absorption maximum of the trapped electron with polarity of the matrix, there is a continuous variation in the line width of

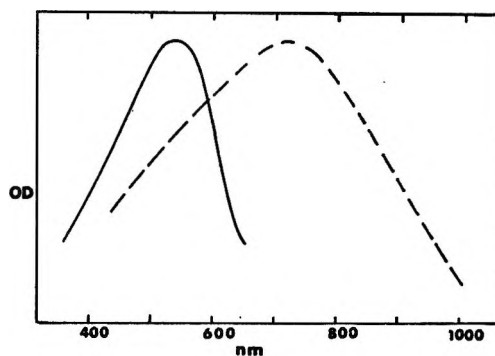


Figure 1. Comparison of the absorption spectra of the solvated electron in liquid ethanol<sup>8</sup> (---) and the trapped electron in glassy ethanol at 77°K (—).

Table I: Absorption Maxima and Esr Line Widths for Electrons in Media of Different Polarity

	300°K		77°K		<i>R</i> <sub>0</sub> <sup>e</sup> au
	<i>D</i> <sub>s</sub> <sup>a</sup>	<i>E</i> <sub>max</sub> <sup>b</sup> eV photon <sup>-1</sup>	<i>E</i> <sub>max</sub> <sup>c</sup> eV photon <sup>-1</sup>	$\Delta H$ <sup>d</sup> G	
Glycerol	42.5	2.35	2.50		1.40
Ethylene glycol	37.7	2.14	2.41	15	1.46
Methyl alcohol	32.6	1.96	2.38	14	1.48
Ethyl alcohol	24.5	1.77	2.28	12	1.50
<i>n</i> -Propyl alcohol	20.1	1.67	2.22	12	1.53
Isopropyl alcohol	18.6	1.51	1.92	10	1.65
<i>n</i> -Butyl alcohol	17.8	1.82	2.21	8	1.53
Isobutyl alcohol	15.8		1.76	9	1.69
<i>n</i> -Pentyl alcohol	13		2.18	7	1.51
<i>t</i> -Butyl alcohol	10.9		1.75 <sup>f</sup>		1.73
Methyltetrahydrofuran	4.6		0.99	4.2	2.29
Diethyl ether	4.3		0.89	3.6	2.42
3-Methylpentane	2.0		0.75	3.0	2.64
Methylcyclohexane	2.0		0.73	3.0	2.67

<sup>a</sup> Static dielectric constant. <sup>b</sup> Absorption maximum of "solvated" electron, ref 8. <sup>c</sup> Absorption maximum of "trapped" electron. <sup>d</sup> Esr line width. <sup>e</sup> Square potential well radius. Calculated from  $E_{1s} \rightarrow E_{2p} = 1.05\pi^2/2R_0^2$ , ref 3d. <sup>f</sup> Value taken from ref 3f.

its esr singlet. The esr spectra are illustrated in Figure 3 and the relationship between the line widths and the energies of the optical absorption maxima is shown in Figure 4.

When two alcohols such as ethylene glycol and isopropyl alcohol or ethyl alcohol and isobutyl alcohol are mixed in various proportions, frozen to the glassy state at 77°K, and  $\gamma$ -irradiated, the spectra of the trapped electrons produced show absorption maxima which vary continuously with change in composition, shifting toward shorter wavelength with increasing concentration of the more polar component (Figures 5 and 6). This observation is analogous to the shifts in absorption

(9) M. Shirom and J. E. Willard, *J. Phys. Chem.*, **72**, 1702 (1968).



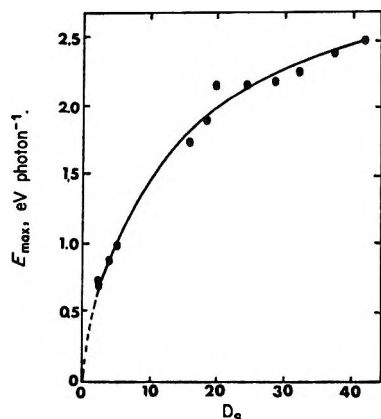


Figure 2. Variation of energy per photon at the absorption maximum of the trapped electron with the dielectric constant of the medium.

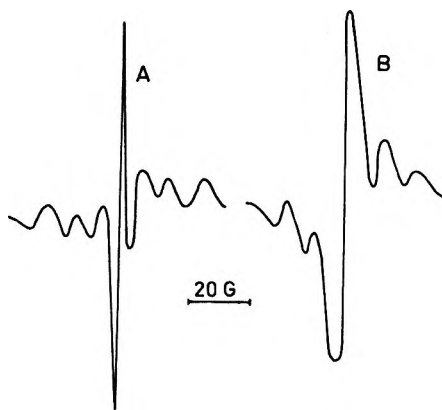


Figure 3. Comparison of esr spectra of the trapped electron in glassy MCHx (A) and ethanol (B).

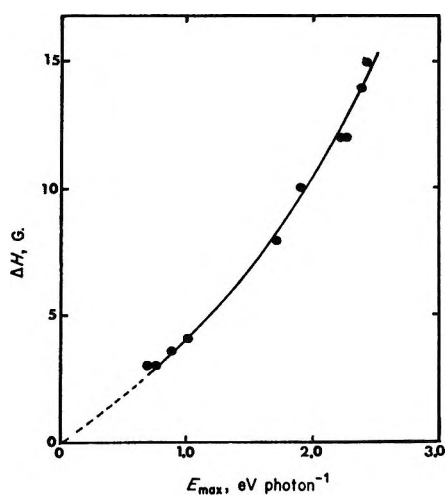


Figure 4. ESR line width ( $\Delta H$ ) vs. the optical absorption maximum (eV) for the trapped electron in a series of  $\gamma$ -irradiated organic glasses at 77°K.

spectra observed in a series of liquid alcohol mixtures<sup>8</sup> and in glassy ethylene glycol-water and glycerol-water mixtures.<sup>10</sup>

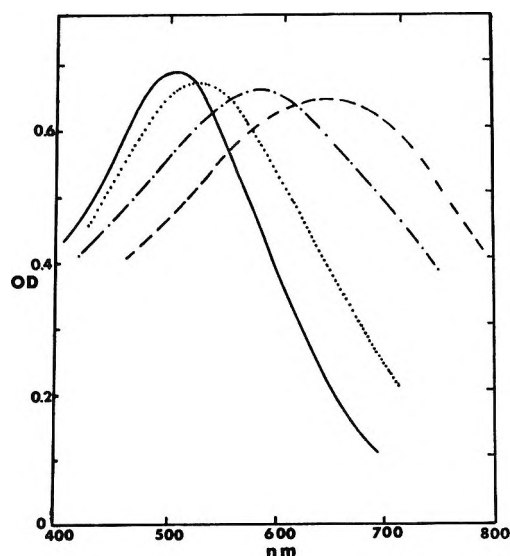


Figure 5. Effect of matrix composition on the absorption spectrum of the trapped electron in ethylene glycol-isopropyl alcohol mixtures: —, pure ethylene glycol; ---, pure isopropyl alcohol; ·····, 0.4 mf isopropyl alcohol in ethylene glycol; —·—, 0.7 mf isopropyl alcohol in ethylene glycol.

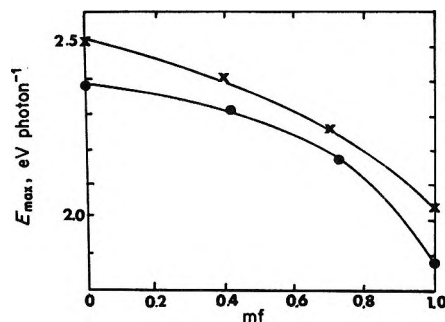


Figure 6. Effect of matrix composition on the energy of the photon at the absorption maximum of the trapped electron: X, ethylene glycol-isopropyl alcohol mixtures; ●, ethyl alcohol-isobutyl alcohol mixtures.

In contrast to the mixtures of two alcohols or alcohols and water,  $\gamma$ -irradiated glassy mixtures of *n*-propyl alcohol with 3MP show two absorption peaks attributable to trapped electrons, one characteristic of *n*-propyl alcohol and one characteristic of 3MP (Figure 7). Similarly,  $\gamma$ -irradiated glassy mixtures of MTHF and ethyl alcohol have been reported<sup>11</sup> to yield two absorption peaks, one characteristic of each pure component.

Figure 8 shows the change in concentration of trapped electrons in methylcyclohexane glass at 77°K as a function of  $\gamma$  dose, as measured by infrared absorption at 1600 nm. This confirms earlier results,<sup>12</sup> obtained

(10) B. G. Ershov, I. E. Makarov, and A. K. Pikaev, *Khim. Vysokikh Energii*, **1**, 404 (1967); *High Energy Chem.*, **1**, 355 (1967).

(11) L. Shields, *J. Phys. Chem.*, **69**, 3186 (1965).

(12) M. Shirom and J. E. Willard, *J. Amer. Chem. Soc.*, **90**, 2184 (1968).

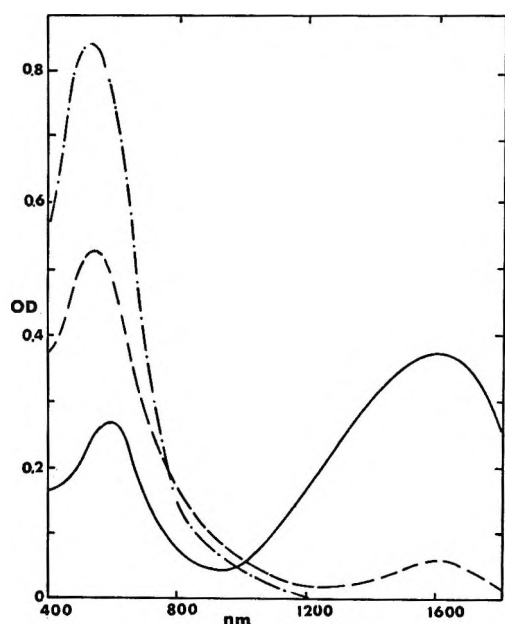


Figure 7. Effect of matrix composition on the absorption spectrum of the trapped electron in *n*-propyl alcohol-3-methylpentane mixtures: —, pure *n*-propyl alcohol; ---, 0.3 mf *n*-propyl alcohol in 3-methylpentane; — · —, 0.1 mf *n*-propyl alcohol in 3-methylpentane.

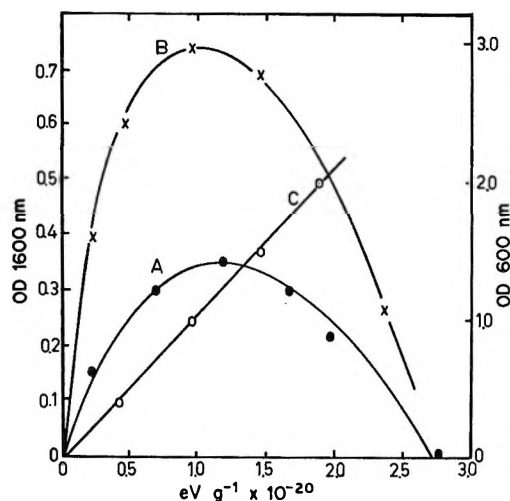


Figure 8. The effect of  $\gamma$  dose at 77°K on the concentration of trapped electrons in (A) pure MCHx, (B) MCH + 5.0% 2-methylpentene-1, and (C) ethanol. The absorption in MCHx was measured at 1600 nm (scale at left) and in ethanol at 600 nm (scale at right).

by esr measurements and with less precise infrared techniques, which demonstrate that only a limited number of electron trapping sites are available in the glassy hydrocarbon matrix. Curve B of Figure 8 shows that the enhanced electron population known to be obtained in the presence of 2-methylpentene-1<sup>5,13</sup> is also subject to removal by products of the irradiation, and that the electron trapping sites are destroyed or preempted. Similar experiments on glassy ethanol at

77°K show no decrease in  $G(e^-)$  up to at least  $2 \times 10^{20}$  eV g<sup>-1</sup> (curve C), indicating that, as in the case of methyltetrahydrofuran,<sup>12</sup> more electron trapping sites are available than in the hydrocarbons or that the entity which removes trapped electrons in the hydrocarbons is not available to do so in the alcohol.

Incidental to these studies, it was noted that bleaching of the trapped electrons in alcohols, and particularly in methanol, resulted in a significant increase in the free-radical signal which underlies the electron singlet. This effect was absent in the case of nonpolar matrices, as previously reported.<sup>9</sup>

### Discussion

The compounds used as matrices in the present investigation are all characterized by a negative electron affinity, and so have no vacant orbitals capable of accommodating an additional electron. Consequently, the stabilized electrons cannot be considered as localized on any particular molecule but must be stabilized by some other mechanism. This is further confirmed by the absence of hyperfine splitting of the electron esr signal.

The similarity between the visible-infrared spectra of solvated electrons in liquid alcohols and of trapped electrons in glassy alcohols suggests that the environment of the electrons is similar in the two cases.

However, the electron lifetimes in the glasses at 77°K are of the order of minutes to days as compared to microseconds in the liquids. This is, plausibly, the result of the fact that the stabilizing configuration of solvating molecules in the liquid is transitory, because it is subject to rapid disruption by thermal motions, whereas in the glass at 77°K trapping occurs in relatively stable voids frozen into the matrix.

It is probable that reorientation of matrix dipoles under the influence of an electron is too slow a process to assist electron trapping.<sup>14,15</sup> If this is the case, the electrons must be trapped in the alcohols in preexisting cavities which have configurations of favorably oriented dipoles determined by the molecular dimensions of the alcohols and the nature of the polymeric aggregates resulting from hydrogen bonding. Compounds which have the highest static dielectric constant in the liquid phase apparently form cavities capable of the most stable trapping.

There is evidence that even in the nonpolar hydrocarbon glasses, trapping occurs only in preexisting voids. The concentration of trapped electrons in hydrocarbon glasses previously investigated<sup>12</sup> and further examined in the present work (Figure 8) passes through a maximum and then decreases with increasing dose, indicating that the number of trapping sites is

(13) J. B. Gollivan and W. H. Hamill, *J. Chem. Phys.*, **44**, 2378 (1966).

(14) L. Kevan, *Progr. Solid State Chem.*, **2**, 321 (1965).

(15) R. Schiller, *J. Chem. Phys.*, **47**, 2281 (1967).

limited, and that these become filled and subsequently removed or populated by nonparamagnetic non-ir-absorbing species. Consistent with the conclusion that preexisting voids are required is the fact that trapping of electrons and positive charge does not occur nearly as effectively in organic crystals as in the corresponding glasses which, because of their random structure, may be expected to have a higher concentration of voids.<sup>16</sup> This is true despite the fact that electrons and positive charge can be chemically trapped in the crystals by additives such as biphenyl<sup>17</sup> when the latter are present at concentrations as low as  $10^{-3}$  mf. The yield,  $G(\text{biphenylide})$ , is about 1, indicating that charge migrates extensively in the crystals without finding physical trapping sites. In the absence of scavengers it eventually encounters a positive ion and is neutralized.

The Jortner theory, developed for liquid systems, assumes that the dipole orientation required for solvation occurs as a result of the presence of the electron. In the application of the theory to the glassy systems it must be assumed that the portion of the trapping interaction which is due to permanent dipoles is the result of configurations existing in the trapping matrix prior to the arrival of the electron.

In terms of the Jortner theory,<sup>7</sup> the radii of the trapping voids may be estimated using the assumption that the energy per photon at the wavelength of maximum absorption is equal to the energy of the  $E_{1s} \rightarrow E_{2p}$  transition in a square potential well which is equal to  $1.05\pi^2/2R_0^2$ , where  $R_0$  is the cavity radius. As noted earlier,<sup>3e</sup> the radii so obtained for the glasses listed in Table I increase progressively with decreasing polarity of the matrix. The increasing esr line width with increasing polarity is consistent with this theory, if broadening of the esr line is attributable<sup>14,18</sup> to interaction of the electron with the nuclear magnetic moments of the hydrogen atoms in the cavity wall. That such interaction is important is demonstrated by the fact that the line width of the trapped electron signal is 6 G in  $\text{C}_2\text{H}_5\text{OD}$ ,<sup>19</sup> as compared to 12 G in  $\text{C}_2\text{H}_5\text{OH}$ , as a result of the lower nuclear magnetic moment of D than of H.

The fact that the  $\lambda_{\text{max}}$  values and the esr line widths of the hydrocarbons fall in a consistent sequence, as a function of polarity, with those of the alcohols, is strong evidence that polarity rather than more specific features of the trapping species are dominating, and adds qualitative support to the applicability of the Jortner model to electron trapping in glasses.

The curves of Figures 2 and 4, as drawn, extrapolate to the origin. This is consistent with the fact that the transition energy,  $E_{1s} \rightarrow E_{2p} = 1.05\pi^2/2R_0^2$ , approaches

zero as  $R_0$  becomes very large. An electron in a very large or infinite cavity is essentially a free electron. Such a free electron would be expected in an environment of zero polarizability. Similarly, a free electron would be expected to exhibit a "zero" esr line width, consistent with the trend of the extrapolation of Figure 4.

A further interesting aspect of Figure 2 is that the value of the transition energy appears to approach a limiting value with increasing dielectric constant of the medium. Such a behavior may be expected if the radius of the cavities suitable for trapping electrons approaches a limiting value.

In *n*-propyl, *n*-butyl, and *n*-pentyl alcohols the transition energies are somewhat higher than the general trend but the branched isomers of these compounds give consistent values, suggesting that the linear molecules orient in such a way as to provide smaller cavities with greater trapping stability.<sup>3f</sup>

The observation that electrons in mixtures of alcohols (Figure 5) give only one absorption peak, the maximum of which shifts to the red as the mole fraction of the less polar component increases, suggests random intermolecular hydrogen bonding of the two alcohols to provide traps of polarity intermediate between those of either pure alcohol. The results confirm the concept that the electron is not trapped by an individual alcohol molecule but is contained by a group of molecules, the absorption energy being related to the composition of the whole group, as is also the case for solvated electrons in liquid alcohols.<sup>8</sup>

The absorption spectra of the electron trapped in *n*-propyl alcohol-3-methylpentane mixtures (Figure 7) show that the electron is preferentially trapped in an environment of *n*-propyl alcohol molecules, even at low *n*-propyl alcohol concentrations. As a result of their ability to form hydrogen bonds, alcohols are extensively aggregated in the form of dimers, trimers, and tetramers in a nonpolar solvent, even at very low alcohol concentrations, and this aggregation would be expected to be enhanced at low temperatures. These aggregates presumably form suitable traps for the electron, and are present in a sufficient concentration to compete favorably with those formed by 3MP molecules.

(16) M. A. Bonin, J. Lin, K. Tsuji, and F. Williams, *Advances in Chemistry Series*, No. 82 American Chemical Society, Washington, D. C., 1968, Vol. II, p 269.

(17) A. Ekstrom and J. E. Willard, unpublished results.

(18) P. N. Moorthy and J. J. Weiss, *Advances in Chemistry Series*, No. 50, American Chemical Society, Washington, D. C., 1965, p 180.

(19) D. R. Smith and J. J. Pieroni, *Can. J. Chem.*, **45**, 2723 (1967).

## Radical Decay Kinetics in Organic Glasses. Spatial Effects and Isotope Effects<sup>1</sup>

by William G. French and John E. Willard

Department of Chemistry, University of Wisconsin, Madison, Wisconsin 53706 (Received July 1, 1968)

Radical decay kinetics show that 3-methylpentyl radicals produced by  $\gamma$  irradiation of 3-methylpentane (3MP) glass at 77°K disappear by combination at random with other radicals in the matrix rather than by geminate recombination or intraspur or intratrack combination. By contrast, 3-methylpentyl radicals produced by hydrogen abstraction by hot hydrogen atoms formed by photolysis of HI in 3MP glass decay much faster and by a process which is first order in dose rather than second order. This indicates that the mechanism of decay is combination of each radical with the geminate iodine atom left by the hot hydrogen atom which produced the radical. It is shown that the rate of decay of methyl radicals produced from methyl halides in organic glasses at 77°K may be either first order in dose and exponential with time ("pure" first order) or first order in dose and not exponential with time ("composite" first order) depending on the matrix. The pure or composite first-order processes must occur by geminate recombination, with the rate-determining process being the thermal relaxation of geometrical constraints placed on the radicals by the matrix. Of great interest is the observation that the rates of radical decay in perdeuterated 3MP and in perdeuterated methylcyclohexane glasses at 77°K are very much slower than in the protiated matrices but approach the rates in the latter as the temperature is increased.

### Introduction

The kinetics of disappearance of free radicals formed in organic solids by photolysis or radiolysis depend on the proximity and geometry with which radical partners are trapped. Methyl radicals produced from methyl halides in glassy 3-methylpentane (3MP) by photodissociation or dissociative electron attachment decay by a "pure"<sup>2</sup> first-order process.<sup>3-5</sup> Since the thermalized radicals at 77°K do not abstract hydrogen from the 3MP,<sup>3,5</sup> the first-order decay must result from recombination of geminate partners trapped in the parent cage. The half-life (16 min at 77°K) is independent of whether the partner of the methyl radical is I, produced by photodissociation, or I<sup>-</sup>, Br<sup>-</sup>, or Cl<sup>-</sup>, produced by dissociative electron capture, and is the same for CD<sub>3</sub> as CH<sub>3</sub>, indicating that the rate-determining step is achievement of the necessary configuration of the radical for reaction, against the constraining forces of the rigid lattice. Ethyl radicals produced from ethyl halides by dissociative electron capture in 3MP or methyltetrahydrofuran (MTHF) glass at 77°K decay by "composite" first-order processes.<sup>6</sup> This indicates either geminate recombination or combination of each radical with another radical produced in the same radiation "track." If it is geminate recombination, which seems most probable,<sup>6</sup> the radicals must be produced with a variety of orientations which have varying probability per unit time of thermal reorientation to achieve the reactive configuration. Thus a knowledge of the decay kinetics and decay rates of trapped species can be informative about their spatial distribution in a matrix and about the constraints which the matrix exerts on them.

In this paper we have used decay kinetics to answer the following questions. (1) Do the 3-methylpentyl radicals observable by esr in  $\gamma$ -irradiated 3MP glass

disappear primarily by combination with other radicals produced in the same track or by random combination with radicals from other tracks? (2) Do 3-methylpentyl radicals formed by hydrogen abstraction by hot H atoms from the photolysis of HI in 3MP glass combine with the geminate iodine atom? (3) Do trapped CH<sub>3</sub> radicals decay by pure first-order kinetics in all matrices, as they do in 3MP? (4) Does deuteration of a radical or deuteration of a matrix influence radical yields, decay kinetics, or decay rates?

### Experimental Methods

The methods of reagent purification, degassing,  $\gamma$  irradiation, and esr measurements used in the work of this paper are similar to those described previously.<sup>3,5</sup> The perdeuterated compounds used all had greater than 99.8% chemical purity, as shown by gas chromatographic analysis, and greater than 99% deuteration,

(1) This work was supported in part by U. S. Atomic Energy Commission Contract AT(11-1)-1715, by the W. F. Vilas Trust of the University of Wisconsin, and by a Public Health Service Fellowship (F1-GM-28,853) from the National Institute of General Medical Sciences.

(2) We use the term "pure" first-order decay for a decay process for which a plot of the logarithm of the concentration of the decaying species vs. time is linear, and the term "composite" first-order decay for a process for which this plot is not linear but has a shape which is independent of the radiation dose (*i. e.* of the initial concentration of the decaying species). For "composite" first-order decay the plots for samples which have received different doses are superimposable after normalization for dose.

(3) R. F. C. Claridge and J. E. Willard, *J. Amer. Chem. Soc.*, **87**, 4992 (1965).

(4) D. W. Skelly, R. G. Hayes, and W. H. Hamill, *J. Chem. Phys.*, **43**, 2795 (1965).

(5) M. Shirom and J. E. Willard, *J. Phys. Chem.*, **72**, 1702 (1968).

(6) Intratrack combination is excluded because an identical decay is observed with radicals resulting from photoionization of TMPD in a glass containing ethyl chloride. In this case no radiation "tracks" are produced.

as shown by mass spectrometry. Temperatures of samples in the Varian esr cavity were maintained within  $\pm 1^\circ\text{K}$  in the range from 78 to  $110^\circ\text{K}$ , using a Varian variable-temperature device arranged to pass the flowing nitrogen through an additional coil immersed in liquid nitrogen. Temperatures were measured with a thermocouple placed in the cold nitrogen stream at a point 1 cm before it encountered the sample, with the reference junction in liquid  $\text{N}_2$  assumed to be at  $77.0^\circ\text{K}$ .

## Results

*Spatial Effects. Decay of 3-Methylpentyl Radicals Produced by  $\gamma$ -Irradiation of 3MP Glass.* The most probable mechanisms for production of 3-methylpentyl radicals<sup>7-9</sup> during  $\gamma$  irradiation of 3MP glass are decomposition of an excited 3MP molecule ( $\text{C}_6\text{H}_{14} \rightsquigarrow \text{C}_6\text{H}_{13} + \text{H}$ ) and proton transfer from a 3MP ion ( $\text{C}_6\text{H}_{14}^+ + \text{C}_6\text{H}_{14} \rightarrow \text{C}_6\text{H}_{13} + \text{C}_6\text{H}_{15}^+$ ). Neither process is expected to provide a geminate partner with which the radical can combine.<sup>10</sup> Therefore, radicals must disappear by combination with other radicals. Figure 1 shows that the decay kinetics are second order over at least the first 85% of decay. A similar slope is obtained independent of the initial dose (and hence the initial radical concentration). Thus the decay is second order with respect to dose as well as with respect to time. This is significant since radical decay by intraspur or intratrack combination might approximate second order with respect to time during the initial stages of decay but would be first order with respect to dose. Thus radicals produced by the  $\gamma$  irradiation of 3MP at  $77^\circ\text{K}$  have essentially as high a probability of combining with radicals from other tracks as with those from the parent spur. The measurements of Figure 1 were made at  $87^\circ\text{K}$  in order to obtain a conveniently rapid decay rate. Similar second-order decay has been observed at  $77^\circ\text{K}$  by M. Vlatkovic of our laboratory on a sample with a higher radical concentration produced by a dose of  $1.2 \times 10^{21}$  eV  $\text{g}^{-1}$  and measured over a period of 100 hr during which 85% of the radicals decayed.

*Decay of 3-Methylpentyl Radicals Produced by Hot H Atoms from HI.* Photolysis of HI with  $2537\text{\AA}$  radiation produces hot H atoms with up to 1.8 eV of kinetic energy.<sup>11</sup> In solid 3MP at  $77^\circ\text{K}$  these abstract hydrogen atoms with a quantum yield of about 0.2,<sup>12</sup> forming 3-methylpentyl radicals.<sup>13</sup> If the iodine atom from a photodissociated HI molecule is trapped in proximity to the radical formed by the hot H atom, it might be expected that radical decay would occur by  $\text{C}_6\text{H}_{13}\text{I}$  formation from these geminate partners. This predicted geminate combination is confirmed by the kinetics of decay shown in Figure 2. Rather than the second-order decay found for random combination of radicals, these data indicate a composite first-order decay which is much faster. This was demonstrated in two experiments differing by a factor of 2 in initial concentration. Data for the decay of 3-methylpentyl radicals produced

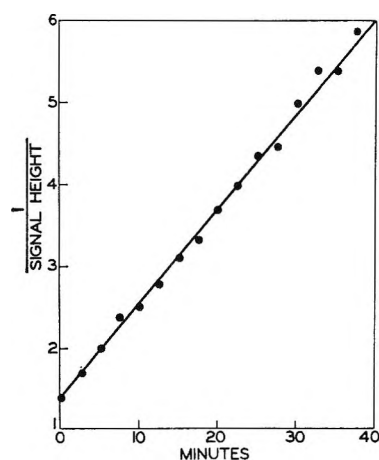


Figure 1. Second-order decay of 3-methylpentyl radicals in  $\gamma$ -irradiated ( $2 \times 10^{19}$  eV  $\text{g}^{-1}$ ) 3-methylpentane at  $87^\circ\text{K}$ .

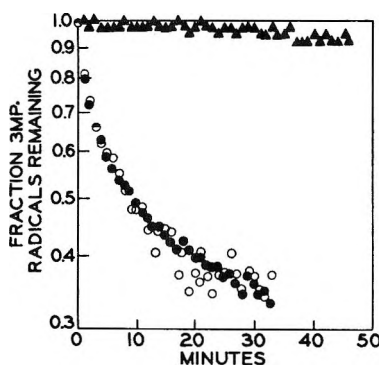


Figure 2. Decay of 3-methylpentyl radicals formed by photolysis and by radiolysis of 3-methylpentane containing  $8 \times 10^{-3}$  mf HI ( $77^\circ\text{K}$ ): ●, 2 min of uv photolysis; ○, 1 min of uv photolysis; ▲, 5 min of  $\gamma$  irradiation. The initial concentrations of radicals after 2 min of photolysis, 1 min of photolysis, and 5 min of  $\gamma$  irradiation were in the ratio 2:1:2.

by  $\gamma$  irradiation of a 3MP-HI glass, identical with that used for the photolysis experiments, are included in Figure 2 to illustrate the dramatic difference in decay characteristics. The decay of radicals from the HI photolysis cannot be attributed to reaction with HI,

(7) The esr spectrum of 3-methylpentyl radicals in 3MP glass at  $77^\circ\text{K}$  has been previously reported by several investigators.<sup>8</sup> The predominant radical is the secondary 3-methylpentyl radical,<sup>9</sup> whether formation is by  $\gamma$  irradiation, hot-atom attack, or photosensitization.

(8) J. E. Willard in "Fundamentals of Radiation Chemistry," P. Ausloos, Ed., John Wiley & Sons, Inc., New York, N. Y., 1968, Chapter 9.

(9) D. H. Henderson, Ph.D. Thesis, University of Wisconsin, 1968.

(10) Hydrogen atoms have never been observed in hydrocarbon glasses at  $77^\circ\text{K}$ , presumably because they diffuse readily and combine with each other or radicals. If the proton-transfer process is responsible for radical formation, it is exothermic and not reversible.

(11) R. M. Martin and J. E. Willard, *J. Chem. Phys.*, **40**, 3007 (1964).

(12) J. R. Nash, R. R. Williams, and W. H. Hamill, *J. Amer. Chem. Soc.*, **82**, 5974 (1960).

(13) S. Aditya and J. E. Willard, *ibid.*, **88**, 229 (1966).

since it has been shown that the rate is unchanged by changing the HI concentration from  $10^{-2}$  to  $10^{-3}$  M.<sup>13</sup> The fact that this decay is much faster than that of radicals produced by dissociative electron capture (with the exception of  $\text{CH}_3$  radicals) prompts the speculation that hydrogen abstraction does not disorient the trapped radical from its reactive configuration as much as dissociative electron capture.

*Composite First-Order Decay of Methyl Radicals in Hydrocarbon Glasses.* It is a striking fact that 90% or more of methyl radicals formed by dissociative electron capture in 3MP at 77°K show pure first-order decay kinetics,<sup>3</sup> indicating that each radical is retained in the parent cage with its geminate partner and that in each case the configuration is very similar. To determine whether this behavior of methyl radicals from methyl halides is dependent on the matrix, we have investigated their decay in a variety of organic glasses. Figure 3 shows the decay in 2-methylpentane (2MP) and in methylcyclohexane (MCHx). Decay in 2MP is slower than in 3MP and that in MCHx is slower than in 2MP. The decay in 2MP is shown to be composite first order by the superimposability of the curves for two doses, after normalization for dose. The shape of the MCHx curve and of the curves for all other matrices listed in Table I, except 3MP, is also typical of composite first-order decay. Table I lists the times required for the decay of the first 50% of the radicals in several of the matrices studied. These decay times are independent of whether the geminate partner of the  $\text{CH}_3$  radical is  $\text{I}^-$  or  $\text{Cl}^-$  in all of the matrices for which this test was made.

*Isotope Effects.* Consistent with earlier observations on  $\text{CD}_3$ ,<sup>3</sup> our results show that the decay rates of  $\text{CD}_3$  radicals and  $\text{CH}_3\text{CD}_2$  radicals formed from alkyl halides in 3MP at 77°K by dissociative electron capture are indistinguishable from the rates of  $\text{CH}_3$  and  $\text{C}_2\text{H}_5$ .

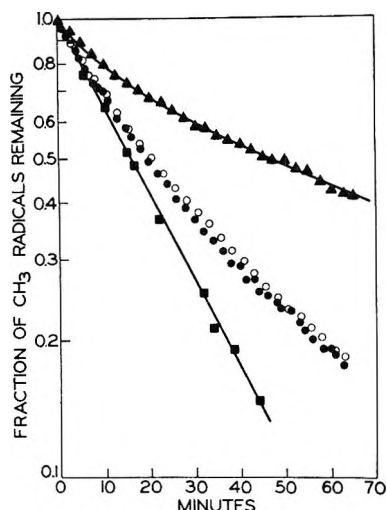


Figure 3. Decay of  $\text{CH}_3$  radicals in  $\gamma$ -irradiated hydrocarbon glasses containing  $10^{-2}$  mf  $\text{CH}_3\text{Cl}$  (77°K): ●, 2MP (2-min  $\gamma$  dose); ○, 2MP (10-min  $\gamma$  dose); ■, 3MP; ▲, MCHx.

Table I:  $\text{CH}_3$  Decay in Hydrocarbon Glasses at 77°K

Matrix	Half-life, <sup>a</sup> min	Viscosity, $\rho^b$
3-Methylpentane	16	$2 \times 10^{12}$
3-Methylpentane- $d_{14}$	150	$2 \times 10^{12}$
2-Methylpentane	27	$2 \times 10^{13}$
3-Methylhexane	45	$3 \times 10^{18}$
4-Methylheptane	36	$2 \times 10^{25}$
Methylcyclohexane	60	$1 \times 10^{18}$
Ethylcyclohexane	50	$4 \times 10^{22}$
2-Methyltetrahydrofuran	10	$4 \times 10^{20}$

<sup>a</sup> Time required for decay of first 50% of the radicals. <sup>b</sup> A. C. Ling and J. E. Willard, *J. Phys. Chem.*, **72**, 1918, 3349 (1968).

By contrast, if perdeuterated rather than protiated 3MP glass is used as the matrix, the half-life of  $\text{CH}_3$  at 77°K is increased from 16 to 150 min and that of  $\text{C}_2\text{H}_5$  from 300 to 1500 min. The half-life of  $\text{CH}_3$  radicals in MCHx glass at 77°K is 60 min, while in MCHx- $d_{14}$  it is greater than 1 day.

The above decay processes are pure or composite first order. To examine the effect of deuteration on a second-order process, we have  $\gamma$ -irradiated 3MP- $d_{14}$  glass. Both the yield of  $\text{C}_6\text{D}_{13}$  radicals ( $G(\text{C}_6\text{D}_{13})$ ) at 77°K and the rate constants for their decay at 83°K and above are the same, within experimental error, as the values for  $\text{C}_6\text{H}_{13}$  radicals formed by the irradiation of protiated 3MP.

The effects of temperature on the decay rates of methyl and ethyl radicals produced by dissociative electron capture in both protiated and deuterated 3MP glass are shown in Figure 4. Similar data for methyl radicals in MCHx are shown in Figure 5. The rates for the protiated and deuterated systems approach each other as the temperature is raised. Figure 4 also shows the variation of the second-order rate constant for the decay of 3-methylpentyl radicals in protiated and deuterated 3MP glass as a function of temperature, and indicates the rate of change of viscosity with temperature.

## Discussion

The results presented have answered the four questions posed in the Introduction: (1) 3-methylpentyl radicals produced by the  $\gamma$  radiolysis of 3MP glass disappear primarily by random combination with radicals from other tracks; (2) 3-methylpentyl radicals produced by abstraction of H by hot hydrogen atoms from the photolysis of HI in 3MP glass decay primarily by combination with the geminate iodine atom; (3) methyl radicals produced by dissociative electron capture in some organic glasses decay by composite first-order kinetics in contrast to the pure first-order kinetics observed in 3MP; and (4) deuterated radicals decay at the same rate as their protiated analogs. The yields of 3-methylpentyl radicals from the radiolysis

of 3MP- $d_{14}$  and 3MP- $h_{14}$  are the same. The decay rates of radicals by geminate combination in 3MP- $d_{14}$  at 77°K are much slower than in the protiated compounds but approach the rates in the protiated compounds as the temperature is increased, while decay by random combination at 83°K and above<sup>14</sup> is unaffected by isotopic substitution. These conclusions are discussed further below.

The fact that 3-methylpentyl radicals produced by  $\gamma$  irradiation of 3MP glass at 77°K disappear at a rate proportional to the square of the total radical concentration indicates that the average separation of the radicals within the spurs is sufficiently great so that the probability of intraspur radical encounters is negligible. The slowness of decay of the 3-methylpentyl radicals produced by  $\gamma$  irradiation as compared with radicals produced in juxtaposition to a geminate partner must result from the slowness of diffusion. For 3-methylpentyl radicals produced<sup>5</sup> with  $G = 1.6$  and a dose of  $10^{19}$  eV  $g^{-1}$ , the concentration before any decay would be  $1.5 \times 10^{-4}$  M, and the average distance of separation, if randomly distributed, would be 200 Å. Assuming random distribution and a reaction on every radical-radical encounter, it may be estimated from the second-order rate constant,  $k$ , indicated by the data of Figure 1 that the diffusion constant of the radicals at 87°K is  $2 \times 10^{-15}$  cm<sup>2</sup>/sec ( $k = 1.7 \times 10^{-21}$  ml molecule<sup>-1</sup> sec<sup>-1</sup> =  $4\pi\rho D$ ; the diameter,  $\rho$ , of the 3MP molecule is taken as 7 Å). This value is within about one order of magnitude of the diffusion coefficient,  $D = 2 \times 10^{-16}$ , calculated from the Stokes-Einstein equation,  $D = kT/6\pi\eta r$ ; if the radius of the 3MP molecule is 3.5 Å, the viscosity<sup>15</sup> at 87°K is  $10^8$  P and  $k$  is the Boltzmann constant.

The viscosities<sup>15</sup> of 3MP at 77 and 87°K are  $10^{12.5}$  and  $10^8$ . Within the accuracy of measurement the viscosity of perdeuterated 3MP is the same as that of the protiated compound.<sup>16</sup> Thus it is to be expected, as observed at 83°K, that the second-order decay constant should be nearly the same in the two media.

The fact that radicals produced by photolysis of HI in 3MP glass decay by combination with the geminate iodine atom is consistent with the expectation that abstraction by hot hydrogen atoms occurs primarily from 3MP molecules in the walls of the parent cage. Competing with the abstraction process are deactivation of the excited HI (or primary recombination) and cage escape accompanied by thermalization of the H atom. Previous evidence<sup>12,13</sup> shows that the ratio of HI stabilization to abstraction to thermalization is about 0.7:0.2:0.1.

The decay of CH<sub>3</sub> radicals from dissociative capture processes in organic glasses cannot be the result of H abstraction from the matrix.<sup>3,5</sup> Likewise, neither type of 3-methylpentyl radical decay reported here can be the result of H abstraction. Such abstraction would follow first-order kinetics rather than the second order

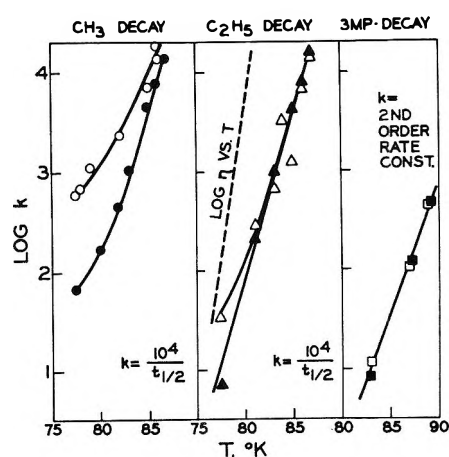


Figure 4. Temperature dependence of radical decay rates in 3-methylpentane (O,  $\Delta$ ,  $\square$ ) and 3MP- $d_{14}$  ( $\bullet$ ,  $\blacktriangle$ ,  $\blacksquare$ ). Methyl and ethyl radicals formed by  $\gamma$  irradiation ( $2 \times 10^{19}$  eV  $g^{-1}$ ) of glasses which contained  $10^{-2}$  mf CH<sub>3</sub>Cl and C<sub>2</sub>H<sub>5</sub>Cl, respectively. 3-Methylpentyl radicals formed by  $2 \times 10^{19}$  eV  $g^{-1}$  irradiation of 3MP glasses.

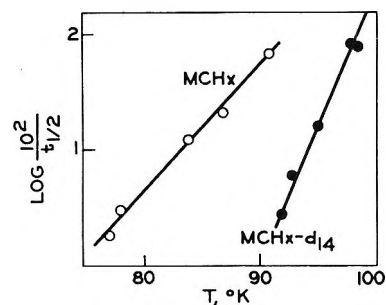


Figure 5. Temperature dependence of CH<sub>3</sub> radical decay rates in methycyclohexane and MCHx- $d_{14}$  glasses. CH<sub>3</sub> radicals formed by  $\gamma$  irradiation ( $2 \times 10^{19}$  eV  $g^{-1}$ ) of MCHx containing  $10^{-2}$  mf CH<sub>3</sub>Cl.

observed in  $\gamma$ -irradiated 3MP. Therefore, H abstraction must be slower than second-order radical-radical combination at the concentrations tested. Consequently, the faster radical disappearance observed in the HI photolysis experiments cannot be due to H abstraction. H abstraction is also eliminated by activation energy considerations and by the fact that it would replace each radical removed by a new radical, thus yielding no decrease in radical concentration. Experimentally the total radical concentration decreases.

Pure first-order decay of 100% of the radicals in a system of the type discussed here implies that every radical is trapped with its geminate partner in its parent-solvent envelope. The fact that half-lives for re-

(14) This decay has been followed to 85% completion on samples which had received  $\gamma$  doses of  $10^{19}$  eV  $g^{-1}$ . The decay rates at 77°K of radicals produced by  $2 \times 10^{20}$  eV  $g^{-1}$   $\gamma$  irradiation of protiated and of deuterated 3MP were followed to 25% decay and found to be identical with each other.

(15) A. C. Ling and J. E. Willard, *J. Phys. Chem.*, **72**, 1918 (1968).

(16) A. C. Ling and J. E. Willard, *ibid.*, **72**, 3349 (1968).

combination of such highly reactive fragments are minutes or longer but are the same for each of several different geminate partners<sup>9</sup> indicates that the rate-determining step in the decay is a rearrangement of the radical structure or position against constraints placed upon it by the surrounding matrix molecules. With methyl radicals this may involve rearrangement from the planar structure to a more favorable geometry for combination with the partner. Similar changes must be required for other radicals, but the necessary geometry for reaction is achieved with less frequency because of their greater complexity. These changes are made possible by the random thermal motions of the matrix molecules in the cage wall. If some of the radicals are trapped in quite different configurations than others, their probability, per unit time, of reorientation to the reactive configuration may be different. Where two or more or a spectrum of such probabilities exist, the decay kinetics will be composite first order. If some radicals escaped by as much as one molecular diameter from the geminate partner, there is a possibility that they will escape the geminate partner completely, in which case they would be expected to contribute to a long-lived second-order tail on the composite first-order curve.

The absence of an esr signal from the iodine atoms formed from the photodissociation of methyl iodide and of HI in the systems described here is not unexpected, since the 18-line spectrum of <sup>127</sup>I observable in the gas phase<sup>17</sup> is not observed in 3MP glass,<sup>18</sup> presumably because of line broadening. Likewise, it is not surprising that no esr signal is observed for the paramagnetic species RX<sup>-</sup>, formed by geminate recombination of radicals with halide ions split off by dissociative electron capture, since halogen-containing radicals give broad spectra<sup>19</sup> with correspondingly low intensities of the individual lines relative to those of alkyl radicals.

The fact that the methyl radical esr signal when an I atom is the geminate partner is indistinguishable from that when I<sup>-</sup> is the partner indicates that any line broadening from dipolar interaction in the radical pair R·I· is small compared with other line broadening effects in the solid.

As would be expected, the rates of radical decay in glassy matrices have positive temperature coefficients (Figure 4). These have a different value than the temperature coefficient of viscosity. Other evidence that radical decay rates are not directly related to viscosity includes the widely different decay rates of radicals in 3MP-*h*<sub>14</sub>, and 3MP-*d*<sub>14</sub>, which have similar viscosity, and the lack of correlation between decay rates and viscosity in other systems, as, for example, in a comparison of

the decay rates in 3MP and MTHF, which are given in Table I.

We have avoided presenting the data in an Arrhenius-type plot or stating an "activation energy" because doing so does not seem meaningful in a temperature range where the viscosity is changing very rapidly and other relaxation processes of importance to the radical reactions are occurring simultaneously.

The differences between the 3MP-*d*<sub>14</sub> molecule and 3MP-*h*<sub>14</sub> molecule which may conceivably contribute to the difference in their effects on radical decay rates are the rotational moments of inertia, the rotational moments of inertia of the methyl groups, and the vibrational frequencies. The data of Figures 4 and 5 indicate that the differences between the deuterated and nondeuterated matrices decrease with temperature and, with 3MP, become unobservable at 85°K. At this temperature the viscosity is down to  $2 \times 10^8$  P,<sup>15,16</sup> and, as indicated by Figure 4, diffusion of radicals occurs relatively readily. It is of interest to note that we find that the rate of decay of trapped electrons in 3MP-*d*<sub>14</sub> at 77°K is similar to that in 3MP-*h*<sub>14</sub>, although the decay is composite first order and there is strong evidence that each electron combines with a predestined positive ion.<sup>8</sup>

Effects of deuteration on free-radical decay have previously been observed for CD<sub>3</sub> in CD<sub>3</sub>OH (presumably polycrystalline), CH<sub>3</sub> + CD<sub>3</sub> in CH<sub>3</sub>OH + CD<sub>3</sub>OH,<sup>20</sup> C<sub>2</sub>D<sub>5</sub> and CD<sub>3</sub> in C<sub>2</sub>D<sub>5</sub>OH, and (C<sub>2</sub>D<sub>5</sub>)<sub>2</sub>O,<sup>21</sup> with radicals produced by photosensitization processes. The half-life of ethyl radicals produced by  $\gamma$  irradiation of ethyl iodide at 77°K increases from 6 hr to 12 days when glassy C<sub>2</sub>D<sub>5</sub>I rather than C<sub>2</sub>H<sub>5</sub>I is used, and in polycrystalline samples it increases from 3 weeks to 3 months as a result of a deuteration.<sup>22</sup> In the case of the alcohols and ethers, the slower rates in the deuterated systems have been attributed to the higher activation energy for abstraction of D than of H from the secondary position. Because of the low temperature, H atom abstraction is unexpected, unless the activation energy is unexpectedly low. The question of the mechanism of decay in these systems should therefore be subjected to further critical scrutiny.

(17) S. Aditya and J. E. Willard, *J. Chem. Phys.*, **44**, 833 (1966).

(18) S. Aditya and J. E. Willard, *J. Amer. Chem. Soc.*, **88**, 229 (1966).

(19) (a) R. Eglund and J. E. Willard, *J. Phys. Chem.*, **71**, 4158 (1967); (b) H. W. Fenrick and J. E. Willard, *J. Amer. Chem. Soc.*, **88**, 412 (1966).

(20) P. J. Sullivan and W. J. Koski, *ibid.*, **85**, 384 (1963); **86**, 159 (1964).

(21) H. S. Judekeis and S. Siegel, *J. Chem. Phys.*, **43**, 3625 (1965).

(22) H. J. Fenrick, Ph.D. Thesis, University of Wisconsin, 1966.



# Homolytic Hydroxylation of Naphthalene in Oxygenated Aqueous Solutions by $\gamma$ Radiolysis at Higher Temperatures<sup>1</sup>

by I. Balakrishnan and M. P. Reddy

National Chemical Laboratory, Poona-8, India (Received June 26, 1968)

$G$  values for naphthol formation in the  $\gamma$  radiolysis of naphthalene dissolved in oxygenated water in sealed tubes rise from 0.28 to 1.44 over the temperature range 55–120° and thereafter fall. The solubilities of naphthalene and of oxygen in water appear to be the two major controlling factors. The temperature dependence of the ratio of  $\alpha$ - and  $\beta$ -naphthols in the product is discussed briefly in the light of what is known of the mechanism of homolytic substitution in aromatic hydrocarbons.

## Introduction

The radiolysis of aqueous solutions of organic compounds provides information, on the one hand, regarding the fundamental processes of the radiation chemistry of water, and, on the other, regarding homolytic reactions involving the hydrogen and hydroxyl radicals.<sup>2</sup> Studies of homolytic hydroxylation of benzene by this method indicate yields of phenolic compounds of the order of  $G(\text{OH})$  of water.<sup>3–5</sup> Naphthalene is known to be 24 times as susceptible as benzene to homolytic phenylation,<sup>6</sup> and yet the yield of naphthol in the radiolysis of its aqueous solution is only 0.01 of the phenol yield for benzene solution. The low solubility of naphthalene in water ( $\sim 10^{-4} M$ ) is evidently the cause of this anomaly. Addition of organic liquids to improve its solubility does not help, since the additive diverts the OH radicals from naphthalene and seems to reduce the yields still further.<sup>7</sup> As a last resort the oxygenated system containing only water and excess naphthalene was pressurized by heating in a sealed tube and irradiated.  $G$  values of the expected order were thus obtained, as will be described below.

## Experimental Section

**Materials.** Triply distilled water, resublimed May and Baker "naphthalene scales," and pure oxygen from heated permanganate crystals were used. A 1-kCi <sup>60</sup>Co  $\gamma$ -radiation source was used for the irradiations, on the basis of the 15.6 value for the Fricke dosimeter. The dose rate was  $4.7 \times 10^{16}$  eV/ml min. The analyses were done using a Perkin-Elmer 350 spectrophotometer.

**Procedures.** A mixture of 0.20 g of naphthalene and 50 ml of water was sealed off in a heavy-walled Pyrex bulb after replacing all of the air in solution with pure oxygen. The bulb was put into a furnace and after it had attained the required temperature ( $\pm 2^\circ$ ) the furnace was lowered into the radiation field. After irradiation, the bulb was taken out, cooled in air for 0.5 hr, and opened.

Naphthalene was removed by ether extraction after

making the solutions alkaline. The naphthol product was coupled in alkaline medium (pH  $\sim 13$ ) with *p*-nitrobenzenediazonium chloride and estimated spectrophotometrically according to a method reported recently.<sup>8</sup>

## Results

Figure 1 summarizes the results. Three features stand out. The naphthol formation is linear in dose and the total yield rises from 0.29 to 1.44 over the range 55–130°. Thereafter the linearity is lost and the yield drops. Up to 130° the proportion of  $\beta$ -naphthol in the product drops steadily and thereafter rises, particularly sharply beyond 150°. Three runs, at 152, 160, and 170°, respectively, clearly confirm these trends in that they indicate a further drop in the total yield and a large increase in the proportion of  $\beta$ -naphthol.

Some of the available data<sup>9–12</sup> on the temperature dependence of the solubility in water, of benzene and naphthalene, to be used in the discussion below, are listed in Table I.

The values of the yields are given in Table II.

(1) Communication No. 1153 from National Chemical Laboratory, Poona, India.

(2) G. Stein, *Discussions Faraday Soc.*, **12**, 232 (1952).

(3) (a) G. Stein and J. Weiss, *J. Chem. Soc.*, 3245 (1949); (b) T. J. Sworski, *J. Chem. Phys.*, **20**, 1817 (1952).

(4) G. R. Freeman and A. B. Van Cleave, *Can. J. Chem.*, **31**, 448 (1953).

(5) P. V. Phung and M. Burton, *Radiation Res.*, **7**, 199 (1957).

(6) D. H. Hey and G. H. Williams, *Discussions Faraday Soc.*, **14**, 216 (1953).

(7) N. B. S. N. Rao, P. S. Rao, and M. P. Reddy, *Indian J. Chem.*, **4**, 244 (1966).

(8) I. Balakrishnan and M. P. Reddy, *ibid.*, **6**, 257 (1968).

(9) R. L. Bohon and W. F. Claussen, *J. Am. Chem. Soc.*, **73**, 1571 (1951).

(10) A. N. Guseva and E. I. Parnov, *Vestn. Mosk. Univ., Ser. II, Khim.*, **18** (4), 80 (1963); *Chem. Abstr.*, **59**, 13392b (1963).

(11) H. Cerfontain, *Rec. Trav. Chim.*, **84**, 491 (1965).

(12) N. C. Deno and C. Perizzolo, *J. Am. Chem. Soc.*, **79**, 1345 (1957).

Table I

	Temp, °C					
	25	35	42.8	217	117	147
Concn of C <sub>6</sub> H <sub>6</sub> , 10 <sup>-3</sup> M	23 (19 in 5% H <sub>2</sub> SO <sub>4</sub> )	24.3	25.6			
Concn of C <sub>10</sub> H <sub>8</sub> , 10 <sup>-5</sup> M	27 (16 in 0.8 N H <sub>2</sub> SO <sub>4</sub> ) (8.8 in 40% H <sub>2</sub> SO <sub>4</sub> )	42	57	3800	~530 <sup>a</sup>	~1000 <sup>a</sup>

<sup>a</sup> Computed from the Klapeyron graph based upon the rest.

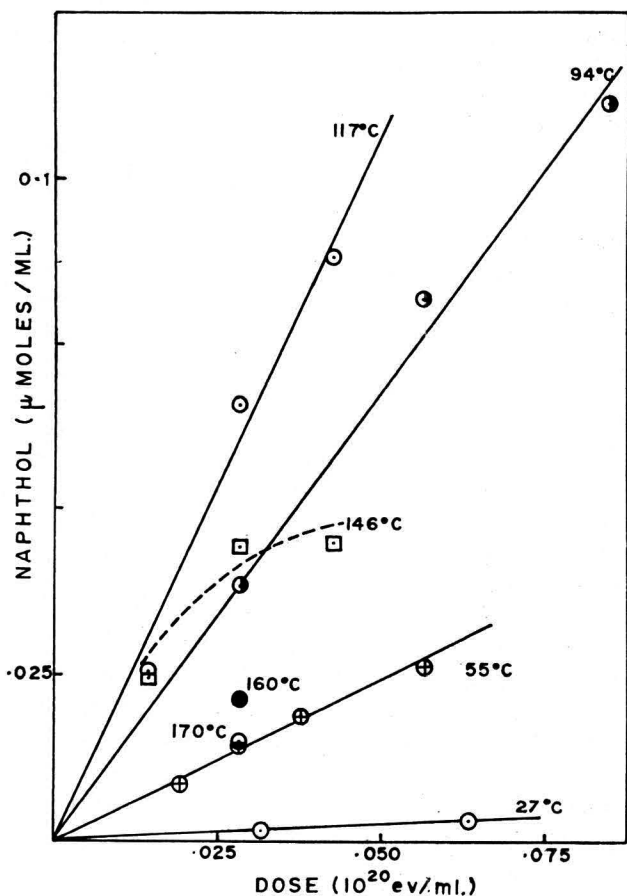


Figure 1. Total naphthol yield as a function of temperature.

## Discussion

The  $\gamma$  radiolysis of water produces H, OH, and hydrated electrons. As they diffuse out of the "spurs" in which they are formed, a portion combines to produce the "molecular" products H<sub>2</sub>, H<sub>2</sub>O<sub>2</sub>, and H<sub>2</sub>O. In the absence of an adequate concentration of solute (the critical value,<sup>13</sup> of course, being dependent on the nature of the solute and hence on the efficiency of the specific "scavenging" reaction) a chain reaction involving the "molecular" products and the radicals that escape recombination in the spurs



sets in and vastly diminishes the ultimate yield of the products.

*Mechanism of Radiolytic Hydroxylation of Aromatic Hydrocarbons.* Earlier work<sup>3a,14,15</sup> on the aqueous benzene system has established the following basic features of the mechanism. In the absence of oxygen, the H and OH mainly add to benzene to form the radicals C<sub>6</sub>H<sub>7</sub>· and C<sub>6</sub>H<sub>6</sub>(OH)· which eventually lead to diphenyl derivatives of varying degree of saturation<sup>16</sup> by combination among themselves. Disproportionation, occurring to a small extent, results in a low yield (~0.3) of phenol.

When oxygen is present in the system, the H and e<sub>aq</sub><sup>-</sup> add swiftly to O<sub>2</sub> to form HO<sub>2</sub> and O<sub>2</sub><sup>-</sup>, which at room temperature are removed as H<sub>2</sub>O<sub>2</sub> via HO<sub>2</sub> + HO<sub>2</sub> → H<sub>2</sub>O<sub>2</sub> + O<sub>2</sub>, without reacting with benzene.<sup>5</sup> Because of the low rate constant of this reaction, an appreciable local concentration of HO<sub>2</sub> radicals is established in the periphery of the spur in the ultimate stage of its expansion. When the concentration of benzene is below a critical value, HO<sub>2</sub> might begin to compete with it for OH radicals via OH + HO<sub>2</sub> → H<sub>2</sub>O + O<sub>2</sub> and cut down the G(phenol). Such a competition is the most plausible explanation for a concentration dependence of G(phenol) observed in the radiolysis of aqueous benzene, to be described later in this discussion. The possibility of occurrence of the above reaction in the aqueous H<sub>2</sub>-O<sub>2</sub> system, as contrasted with the aqueous lactic acid and ethanol systems, has been discussed earlier by Allen.<sup>13</sup>

When the concentration of benzene is adequate, the presence of oxygen enhances the yield of phenol, the species that count in its formation being OH and O<sub>2</sub>. Scheme I summarizes the main known facts of the mechanism of hydroxylation of an aromatic hydrocarbon by reaction with OH, together with some speculation (steps IV and V, in dotted lines) regarding other possible reactions. The molecule chosen for the illustration is naphthalene but the evidence for the individual steps is drawn largely from studies of the aqueous

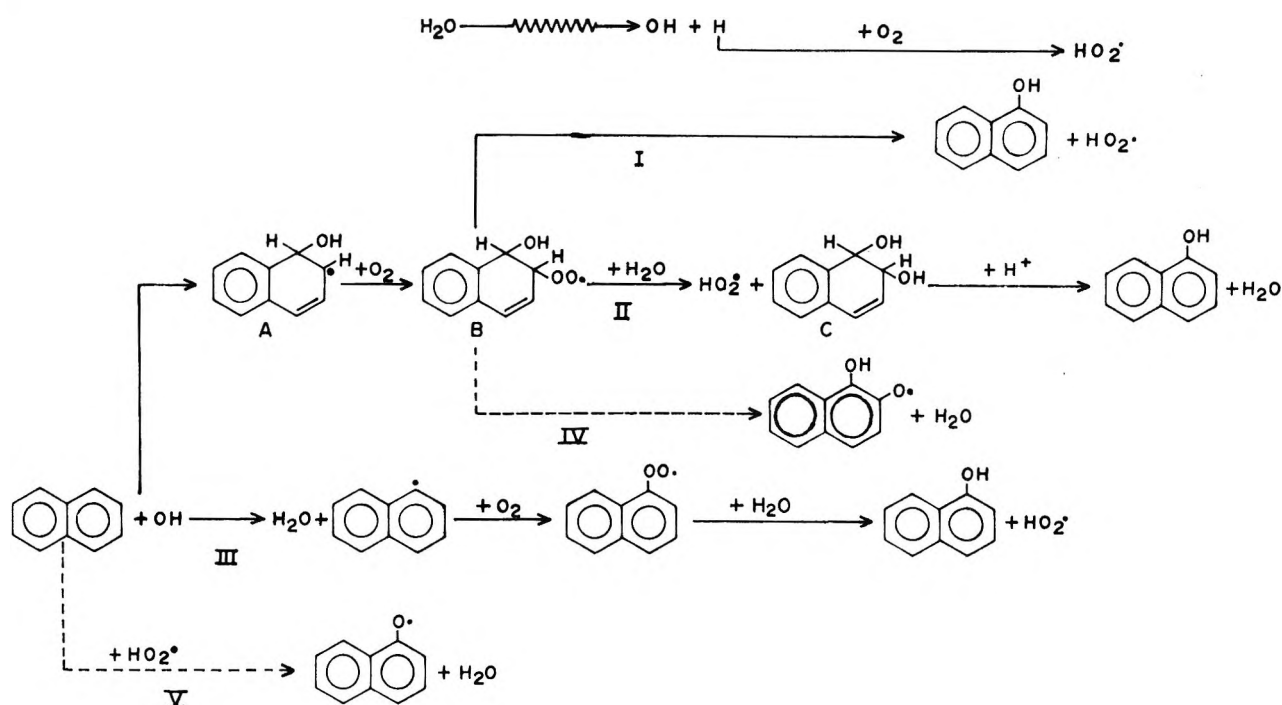
(13) A. O. Allen, "The Radiation Chemistry of Water and Aqueous Solutions," D. Van Nostrand Co., Inc., New York, N. Y., 1961, pp 30, 45, 46.

(14) J. H. Baxendale and D. Smithies, *J. Chem. Soc.*, 779 (1959).

(15) H. C. Christensen, Aktiebolaget Atomenergi, Stockholm, AE-142, p 35, 1964, and AE-193, p 10, 1965; *Chem. Abstr.*, **61**, 12829h (1964); **63**, 10896g (1965).

(16) E. V. Barelko, *et al.*, Proceedings of the First All-Union Conference on Radiation Chemistry, Vol. II, Moscow, 1957, p 84; *Dokl. Akad. Nauk SSSR*, **136**, 143 (1961).

Scheme I



benzene system. The mechanism of OH attack on naphthalene cannot be too different from that in the case of benzene.

Successive addition of OH and O<sub>2</sub> to the aromatic species, leading to the equivalent of species A and B, was suggested by Proskurnin,<sup>16</sup> Waters,<sup>17</sup> and Dorfman.<sup>18</sup> Step I, which is a fast, unimolecular reaction, was observed by Dorfman<sup>19</sup> in the case of benzene. Boyland and Booth<sup>20</sup> proved that the glycol, C, gives α-naphthol exclusively upon warming with acid. Sworski<sup>21</sup> originally advanced for the aqueous benzene system the equivalent of path III. Since it totally ignores the well-known addition of OH to aromatics, this mechanism could account, at best, for a small part only of the phenol formed.

Step IV speculates about a reaction plausible at higher temperature. Ebert and Land<sup>22</sup> observed that phenol reacts with OH from radiolyzed water to yield the phenoxy radical. If one visualizes this as the result of elimination of water from a radical intermediate formed by initial attachment of OH to phenol, then it is possible to see how a phenoxy-type radical could be formed from naphthalene *via* species B by an analogous process and result, at higher temperature, in polyhydric phenols.

Step V suggests a plausible alternative source (other than OH attack) from which phenolic compounds could come, particularly at higher temperatures.

*Temperature Dependence of Naphthol Formation.* The three main features of the effect of temperature on naphthol formation could be briefly correlated with the facts of the radiolysis of the aqueous benzene system on

the one hand, and, on the other, with what is known about homolytic substitution in naphthalene.

In the first place, there is a sharp rise in naphthol yield in going from 27 to 55° and then a slow rise up to 130°, both clearly attributable to the increase in solubility of naphthalene. If factors of mechanism of reaction do play a role in this, one would expect a similar trend, even in the range 27–55°, in the aqueous benzene system, which is not found (*cf.* Table II), whereas an effect similar to the above is found<sup>3a</sup> if the concentration of benzene is lowered below 10<sup>-3</sup> M. Further, upon the introduction of sulfuric acid, known to reduce the solubility of naphthalene (*cf.* entry 3 in Table II and the solubility values quoted earlier), the yield of naphthol again drops sharply. Thus, it is clear that in the concentration range 2–5 × 10<sup>-4</sup> M naphthalene sees only a small fraction of the hydroxyl radicals emerging from the spurs because of competition from HO<sub>2</sub> as described earlier.

It is a telling fact that the highest naphthol yield attained is almost equal to  $G(\text{phenol}) = 1.54$  established in a study of the aqueous benzene system conducted along with the present (to be submitted shortly) in which it was proved that a fraction of the total num-

(17) W. A. Waters, *Discussions Faraday Soc.*, **14**, 247 (1953).

(18) L. M. Dorfman, R. E. Bühler, and I. A. Taub, *J. Chem. Phys.*, **36**, 549 (1962).

(19) L. M. Dorfman, I. A. Taub, and R. E. Bühler, *ibid.*, **36**, 3051 (1962).

(20) J. Booth and E. Boyland, *Biochem. J.*, **44**, 361 (1949).

(21) T. J. Sworski, *Radiation Res.*, **1**, 231 (1954).

(22) E. J. Land and M. Ebert, *Trans. Faraday Soc.*, **63**, 1181 (1967).

Table II: Yields of Naphthol at Various Temperatures

Temp, °C	Dose, 10 <sup>19</sup> × eV/ml	[β-naphthol], %	G(total naphthol)	G(phenol)
27		20-30	0.025 ± 0.003	1.54 ± 0.045
55		7-12	0.28 ± 0.019	~1.4
55 (0.8 N H <sub>2</sub> SO <sub>4</sub> )			Below level of detection	
94		4-8	0.81 ± 0.035	
117		~0	1.28 ± 0.13	
130	2.82	~0	1.44	
146	1.41	10.9	1.05	
	2.82	7	0.94	
	4.23	5.9	0.46	
152	0.47	38.0	0.77	
160	2.82	46.0	0.46	
170	2.82	75.0	0.32	

<sup>a</sup> These are only apparent and not initial (true) *G* values.

ber of OH radicals attack benzene to convert it into open-chain oxidized product<sup>13,23,24</sup> with an enhanced consumption of oxygen. *G*(-O<sub>2</sub>) even at room temperature is 5.3.<sup>5</sup>

A second feature of the temperature effect is the drop in naphthol yield at ~140° and above. This is accompanied by a marked departure from linearity, so much so that what are reported are not true but only apparent *G* values. Now such a departure indicates either a product effect or depletion of reactant. The absence of a product effect in the 94 and 117° runs, in which much larger concentrations of naphthol and other products are built up in the course of the reaction, eliminates the first of these two possibilities. The reactant most likely to be depleted is oxygen. In the aqueous benzene system, at room temperature, for *G*(phenol) = 1.54, *G*(-O<sub>2</sub>) = 5.3,<sup>5</sup> and so, for an oxygen solubility of 1.2 × 10<sup>-3</sup> *M* at 27°, depletion occurs at ~0.13 × 10<sup>20</sup> eV/ml. The solubility at 100° drops to 7.6 × 10<sup>-4</sup> *M*. At 120-130° when the naphthol yield is ≈ *G*(phenol) at 27° for aqueous benzene, depletion should occur at ~0.06 × 10<sup>20</sup> eV/ml if the solubility is ~6 × 10<sup>-4</sup> *M* at 120°. Christensen<sup>15</sup> has established that the *G*(phenol) for aqueous benzene gets nearly trebled somewhere in the temperature range 100-200°, and the phenol formation begins to depart from linearity from 150° on, even as the initial (true) *G* value rises sharply. Evidently therefore the mechanism of hydroxylation changes considerably at this stage and phenol begins to be formed from other sources besides OH (*cf.* step V in the diagram, for instance). The *G*(-O<sub>2</sub>) should go up at least by the same factor, while the solubility of oxygen must continue to diminish. Clearly, therefore, the formation of naphthol would be expected to depart from linearity even for a dose of ~0.02 × 10<sup>20</sup> eV/ml at some temperature not far above 130°. This is the most likely and the simplest explanation for such a departure reported here.

*Homolytic Substitution in Naphthalene.* The third and most interesting feature of the temperature effect is the variation of the ratio of the α and β isomers in the product. In general, the α isomer is favored<sup>25,26</sup> as required by theory<sup>6</sup> and in harmony with earlier findings.<sup>27</sup> Starting at a relatively high 20-30% at 27° the β content drops to ~5% at 94° and nearly vanishes in the range 120-130°. Homolytic hydroxylation by other means<sup>27</sup> and phenylation<sup>28,29</sup> also yields 20 and 17-20% β isomer, respectively, at room temperature. However, phenylation at ~80° reduces the β isomer content<sup>30</sup> to 10%. On the strength of the present results it is suggested that this difference observed by earlier workers is not accidental but is evidence of a temperature dependence of the path of homolytic substitution.

Past 140° the β-isomer content rises sharply, indicating a change in the mechanism of hydroxylation, as discussed earlier, and naphthol formation by other means besides OH attack.

The mechanisms of aromatic homolytic substitution

(23) J. Goodman and J. Steigman, *J. Phys. Chem.*, **62**, 1020 (1958).

(24) M. Daniels, G. Scholes, and J. Weiss, *J. Chem. Soc.*, 832 (1956).

(25) The higher *G*<sub>β</sub> values in ref 7 were based upon the absorption at 225 mμ, much of which has since been proved to be due to an unknown alkali-soluble material other than naphthol. The *G*<sub>α</sub> values and the trend of the temperature effect, however, are essentially correct. The metal ion effect was actually due to interaction between the oxidized form of the ions and an organic radical otherwise yielding naphthol, long after the depletion of oxygen. It was an instance of the third of the three stages of metal ion action described lately.<sup>28a</sup> Because of erratic behavior, the iodine complex method for α-naphthol<sup>28b</sup> has also been abandoned.

(26) (a) R. Broszkiewicz, Institute of Nuclear Research Report No. 579-XVII-C, Warsaw, 1964, p 89; *Chem. Abstr.*, **63**, 17363d (1964).

(b) P. S. Rao, N. B. S. N. Rao, and M. P. Reddy, *Indian J. Chem.*, **3**, 408 (1965).

(27) E. Boyland and P. Sims, *J. Chem. Soc.*, 2966 (1953).

(28) B. A. Marshall and W. A. Waters, *ibid.*, 381 (1959).

(29) R. Huisgen and G. Sorge, *Ann. Chem.*, **566**, 162 (1950).

(30) R. Möhlau and R. Berger, *Chem. Ber.*, **26**, 1196 (1893).

advanced hitherto<sup>17</sup> have not satisfactorily explained how the H atom is removed from the intermediate addition complex. We venture to suggest that reaction I (in the diagram) observed and formulated by Dorf-

man<sup>19</sup> is valid for all homolytic attack on aromatics and that homolytic substitution in general would be found to be meager, if not nonexistent, when oxygen is strictly excluded.

## Polymer Studies by Gel Permeation Chromatography. IV. The Degradation of Polystyrene by Ultrasonics and by Benzoyl Peroxide

by William B. Smith and Harold W. Temple

Department of Chemistry, Texas Christian University, Fort Worth, Texas 76129 (Received June 26, 1968)

The degradation of narrow range molecular weight samples of polystyrene has been carried out by ultrasonic radiation and by benzoyl peroxide decomposition. The changes in molecular weight distribution have been followed as a function of time. For ultrasonic degradation the change in distribution clearly showed a preferential breaking near the center of the molecule. For the peroxide degradations, the curves were those resulting from random attack along the polymer chains. Under the conditions used here, about  $6 \times 10^3$  peroxide molecules decomposed for every polymer bond broken. A correlation of these data with extent theories is given, and a simple model for calculating the change in distribution is described.

The degradation of polymer molecules by the action of heat, light, ultrasonic radiation, and various chemical reagents has proven to be a subject of great practical importance and equal theoretical interest. While many studies on polymer degradation have appeared, these have often suffered from the difficulties of characterizing the polymeric products which so often plague workers in the macromolecular field.

The development of gel permeation chromatography has provided the polymer chemist with a valuable tool for arriving at rapid, accurate molecular weight distributions, and we have taken advantage of it to achieve a deeper insight of the details of vinyl polymerization.<sup>1</sup>

While the studies of ultrasonic degradation are many, there is no agreement to date on the theory to be applied to the process nor any overwhelming experimental evidence that would allow one to decide among the various theories or to describe a better one. Experimentally, it is observed that the rate of disappearance of a polymer with a given degree of polymerization (DP) is first order. The reaction order is truly more complex, however, since the rate constant is a function of the gross polymer concentration and the chain length of the species undergoing degradation.<sup>2</sup>

The latter point has excited particular interest. It is agreed that for a given system there is some minimum chain length, characterized by  $DP_e$ , below which no

degradation occurs. Above this minimum value Schmid<sup>3</sup> proposed that the experimental rate was a linear function of the degree of polymerization as follows:  $k_i = K(DP_i - DP_e)$ , where  $K$  is a true rate constant. Jellinek and White<sup>4</sup> proposed a more complex model which was simplified for computational purposes to  $k_i = K(DP_i - 1)$ . Arguing from considerations of the energetics of the shock waves produced during the cavitation process, Gooberman<sup>5</sup> derived a proportionality of  $k_i$  to  $DP_i \exp(2.8)$ . Ovenall and coworkers<sup>6</sup> returned to the Schmid postulation.

The above workers have considered also the distribution of products from the fragmented molecules. In the Jellinek model all bonds in molecules greater than  $DP_e$  are equally apt to break. Ovenall, *et al.*,<sup>6</sup> assumed that bonds with  $DP_e/2$  units from either end of the chain would not break, while an equal probability

(1) (a) W. B. Smith, J. A. May, and C. W. Kim, *J. Polym. Sci., Part A-2*, **4**, 365 (1966); (b) J. A. May and W. B. Smith, *J. Phys. Chem.*, **72**, 216 (1968); (c) J. A. May and W. B. Smith, *ibid.*, **72**, 2993 (1968).

(2) G. Gooberman and J. Lamb, *J. Polym. Sci.*, **42**, 35 (1960).

(3) G. Schmid, *Z. Phys. Chem.*, **A186**, 113 (1939).

(4) H. H. G. Jellinek and G. White, *J. Polym. Sci.*, **6**, 745 (1951).

(5) G. Gooberman, *ibid.*, **42**, 25 (1960).

(6) (a) D. W. Ovenall, G. W. Hastings, and P. E. M. Allen, *ibid.*, **33**, 207 (1958); (b) P. E. M. Allen, G. M. Burnett, G. W. Hastings, H. W. Melville, and D. M. Ovenall, *ibid.*, **33**, 213 (1958); (c) D. W. Ovenall, *ibid.*, **42**, 455 (1960).

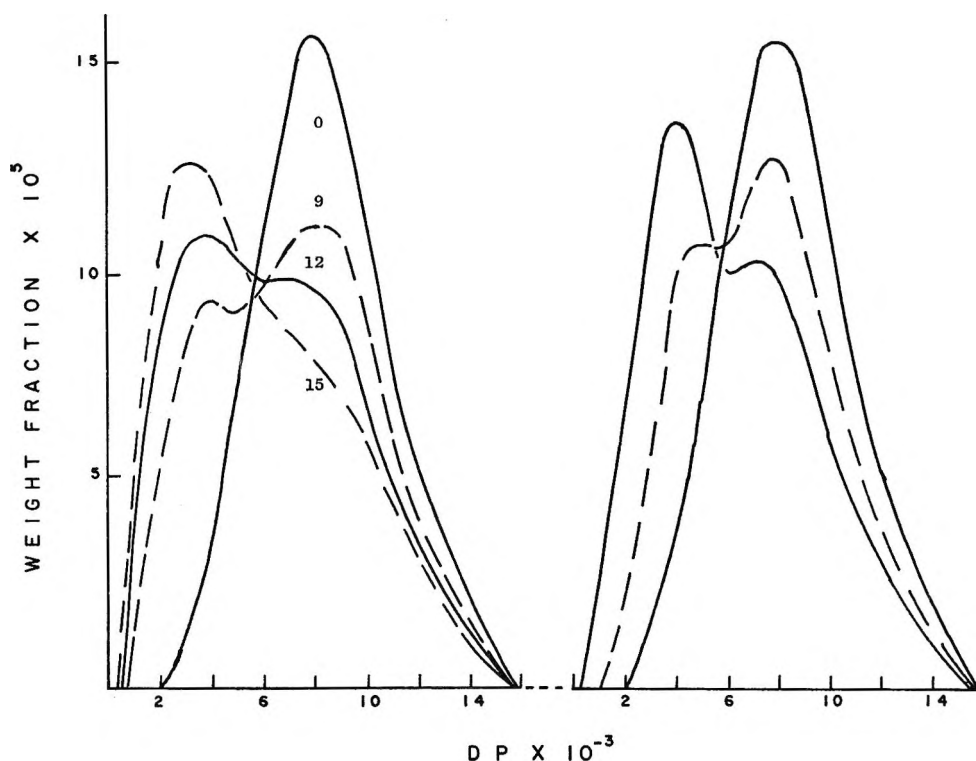


Figure 1. Comparison of actual (left) and theoretical (right) distribution curves for ultrasonically degraded polystyrene ( $M_w = 860,000$ ). The times are in minutes.

existed for rupture along the center segment. Goberman and Lamb<sup>2</sup> determined the distribution of material for a sample of degraded polystyrene using a turbidometric technique and concluded that rupture preferentially occurred near the center of the molecules.

We have now examined in detail the change in molecular weight distribution for the ultrasonic degradation of a number of polystyrene samples. Coupled with results from the literature, it is evident that the process cannot be described as random scission. In order to provide examples where random cleavage should prevail, the degradation of polystyrene with benzoyl peroxide has been studied also.

### Experimental Section

*Ultrasonic Degradations.* Ultrasonic energy was provided by a Brownwill Biosonik probe<sup>7</sup> operating at 20 kHz and with a manufacturer's rated output of 48 W with the probe submerged about 0.8 cm. The reaction vessel was a glass cylinder 2 in. in diameter and 6 in. deep cooled in an ice bath throughout the irradiation process. The temperature in the reaction vessel was maintained at  $15 \pm 3^\circ$ .

Most studies were carried out using narrow-range polystyrene samples (Pressure Chemical Co., Pittsburgh, Pa.) as follows, for  $M_w$ - $M_n$  and their ratio, respectively: A, 867,000-773,000, 1.12; B, 411,000-392,000, 1.05; C, 267,000-247,000 (Dow Chemical S-108), 1.08; and D, 98,200-96,200, 1.02. Several samples of broad-range polystyrene were also prepared

by the bulk polymerization of styrene at  $60^\circ$  with benzoyl peroxide.

Samples were made up to the appropriate concentration in tetrahydrofuran (THF) freshly distilled from

Table I: Change in Molecular Parameters with Time for the Ultrasonic Degradation of Polystyrene A ( $M_w = 867,000$ )

Time, min	$M_w$	$M_n$	$M_w/M_n$
0	841,300	763,200	1.10
2	816,000	711,000	1.15
4	795,900	661,400	1.20
8	779,000	624,000	1.25
12	719,400	559,800	1.29
14	661,400	472,000	1.40
16	650,800	483,500	1.35
20	629,900	458,000	1.37
30	553,900	394,500	1.40
60	344,300	248,500	1.38
120	218,400	156,200	1.40
180	171,000	130,500	1.31
240	140,800	103,200	1.36
300	125,800	94,500	1.33
600	85,800	67,400	1.27
Time, hr			
37	39,000	33,000	1.18
88	27,800	23,800	1.17

(7) Brownwill Scientific, Rochester, N. Y.

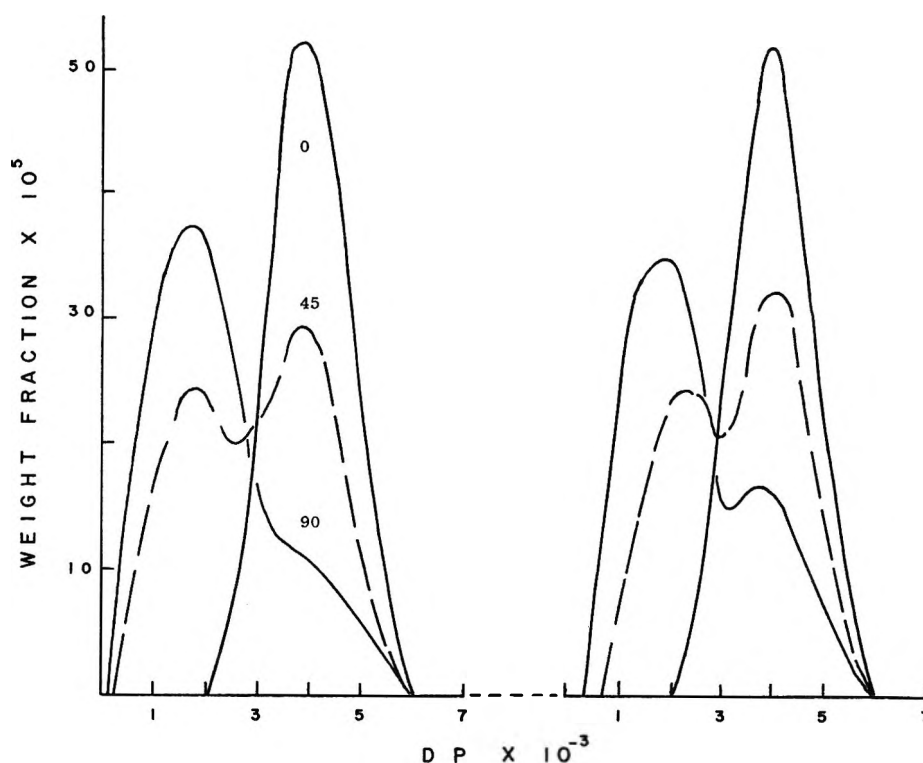


Figure 2. Comparison of actual (left) and theoretical (right) distribution curves for ultrasonically degraded polystyrene ( $M_w = 411,000$ ). The times are in minutes.

potassium hydroxide. The cell was filled, cooled while flushing with nitrogen, and then irradiated. Aliquots were withdrawn from time to time, diluted with THF to about 0.2% (w/v), and chromatographed as previously described.<sup>1b</sup> Molecular weights and replot curves of weight fraction *vs.* degree of polymerization were also obtained as before.<sup>1b</sup>

Typical results for a run using sample A made up to 20 g/l. are given in Table I. The replotted gpc results for a series of samples are shown in Figures 1 and 2.

Rates for the degradation were determined by two different methods. The height of replotted gpc curves (as in Figures 1 and 2) is the weight fraction of that species. Using a series of concentrations of the various narrow-range samples it was possible to follow the course of the degradation by following the change in peak height as a function of time. It was found that the rate of change was first order for about the first 50% of the degradation of the original material. Peak heights from the replotted curves (method A) or from normalized gpc curves gave equally good results as tabulated in Table II.

In another type of experiment a broader molecular weight range sample was chosen. The gpc replot curves were used, and the change in height was followed at various points on the curve above the molecular weight of the original maximum. First-order changes in weight fraction were noted throughout the early stages in the reaction. The rate increased above that

Table II: First-Order Rate Constants for Polystyrene Degradation from Replot Curves (A) or Gpc Curves (B)

DP <sup>a</sup>	Polymer concn g/l.	10 <sup>4</sup> k, min <sup>-1</sup>	
		Method A	Method B
7980	19	32	28
7980	10	38.5	44
7980	5	87.4	89.8
3865	20	6.4	6.3
3865	10	15.1	16.3
3865	5	29.2	30.6
2470	20	5.3	5.2
2470	10	7.0	7.4
935	20	0.6	0.5

<sup>a</sup> Degree of polymerization at distribution maximum for samples A-D in descending order.

expected in the latter stages of the decomposition. Typical results are shown in Figure 3 for a sample characterized by  $M_w = 433,200$  and  $M_w/M_n = 1.71$ .

**Peroxide Degradations.** With the exception of one series of runs in toluene, all determinations were carried out in benzene freshly distilled from sodium. Solutions of polymer and benzoyl peroxide, (BZO)<sub>2</sub>, were made up at room temperature, and 15-ml aliquots were sealed in ampoules after a thorough series of degassing cycles. Kinetic runs were made in an oil bath at  $60.0 \pm 0.01^\circ$ . Samples were pulled at various times, and the polymer was precipitated by pouring it into 700 ml of methanol containing a small amount of hydroquinone. The

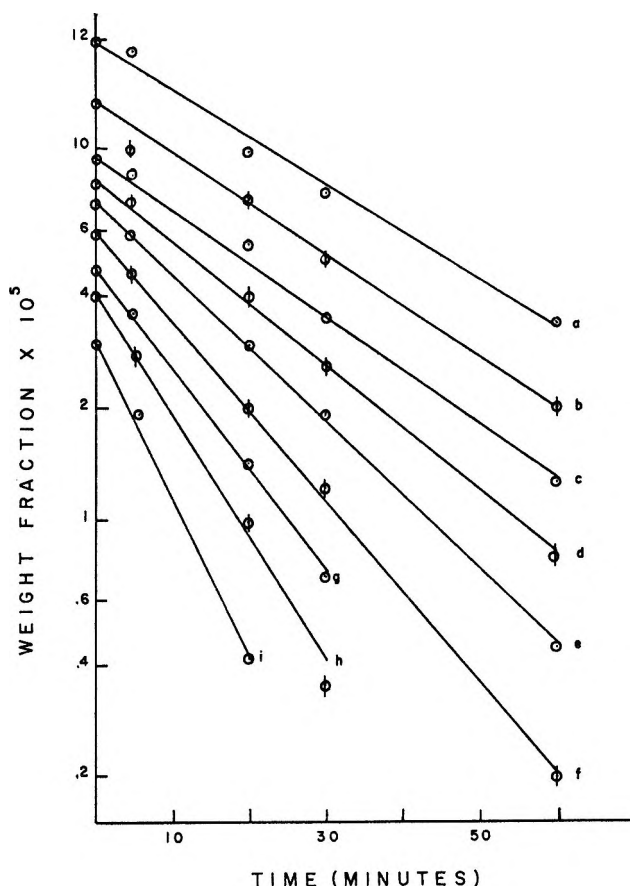


Figure 3. First-order rate plots taken from gpc curves for ultrasonically degraded polystyrene ( $M_w = 433,200$ ,  $M_w/M_n = 1.71$ ); curve,  $10^{-3}DP$ , and  $10^3k$  ( $\text{min}^{-1}$ ), respectively: a, 4.5, 14.3; b, 5.0, 24.7; c, 5.5, 32.6; d, 6.0, 37.5; e, 6.5, 45.4; f, 7.0, 53.0; g, 7.5, 64.0; h, 8.0, 93.1; i, 9.0, 97.4

collected sample was vacuum dried at  $50^\circ$ . Weight losses ranged from 3 to 10%.

The rate of polymer degradation was followed by the change in peak height of the gpc replot curves as described above. The rates were first order, and the graphically derived rate constants are given in Table III.

In another series of studies the rate of benzoyl per-

Table III: Rates Constants for Benzoyl Peroxide Degradation of Polystyrene<sup>a</sup>

[Peroxide], g/100 ml	$10^3k$ , $\text{min}^{-1}$	Remarks
1.00	0.057	$60^\circ$ , toluene
2.02	0.16	$60^\circ$ , benzene
2.01	0.12	$60^\circ$ , benzene
4.00	0.28	$60^\circ$ , benzene
4.00	0.27	$60^\circ$ , benzene
6.00	0.39	$60^\circ$ , benzene
4.00	5.5	$80^\circ$ , benzene

<sup>a</sup> Sample A (degree of polymerization at peak 7980) at 1.0 g/100 ml.

oxide disappearance both in the presence and in the absence of polystyrene was determined. The unreacted benzoyl peroxide was determined by transferring the benzene solution from the reaction ampoule to a flask attached to a condenser. Glacial acetic acid (5 ml) was added plus *ca.* 10 g of potassium iodide. The mixture was refluxed for 5–10 min and cooled, and the liberated iodine was titrated with standard thiosulfate. Decomposition rates for the peroxide were first order, and the rate constants were determined graphically. Decompositions of benzoyl peroxide (40 g/l.) were determined in benzene solution of polystyrene samples A and D (10 g/l. each). Rate constants of peroxide disappearance for each case were determined as  $0.014 \text{ hr}^{-1}$  at  $60^\circ$  and  $0.20 \text{ hr}^{-1}$  at  $80^\circ$ .

The number of polymer molecule bonds broken after a given time can be calculated from

$$B_t = \frac{n_0(DP_0 - DP_t)}{DP_t} \quad (1)$$

where  $n_0$  is the number of polymer molecules of initial  $DP_0$  which degrade to  $DP_t$  after time  $t$ .<sup>6b</sup> Typical results (Table IV) for the decomposition of polystyrene under conditions described above for sample A gave the following results, where the entry for benzoyl peroxide is the number of molecules decomposed as calculated from the above rate data.

Table IV: The Degradation of Polystyrene (Sample A) with Benzoyl Peroxide in Benzene at  $60^\circ$

Time, hr	$10^{-5}M_w$	$M_w/M_n$	$10^{-10}B_t^a$	No. of (BZO) <sub>2</sub> molecules $\times 10^{-20}^a$
0	8.4	1.1	...	...
20	6.9	1.3	4.5	3.7
30	6.5	1.6	9.6	5.3
46	5.8	1.5	11.5	7.2
96	4.9	1.6	18.1	11.1

<sup>a</sup> Bonds broken per 15-ml sample of solution.

## Discussion

In order to obtain a detailed picture of what occurs during the ultrasonic degradation of a polymer, narrow molecular weight range samples of polystyrene in tetrahydrofuran have been degraded, and the gpc data have been obtained after various times have been replotted on a scale linear in units of DP (Figures 1 and 2). A previous observation of Gooberman and Lamb<sup>2</sup> has been amply confirmed, as it is clear from these examples that there is a high preference for molecular rupture near the center of each molecule. Thus those models which hypothesize random scission over the whole of the molecular length are clearly in error.

The rate of disappearance of polystyrene as measured



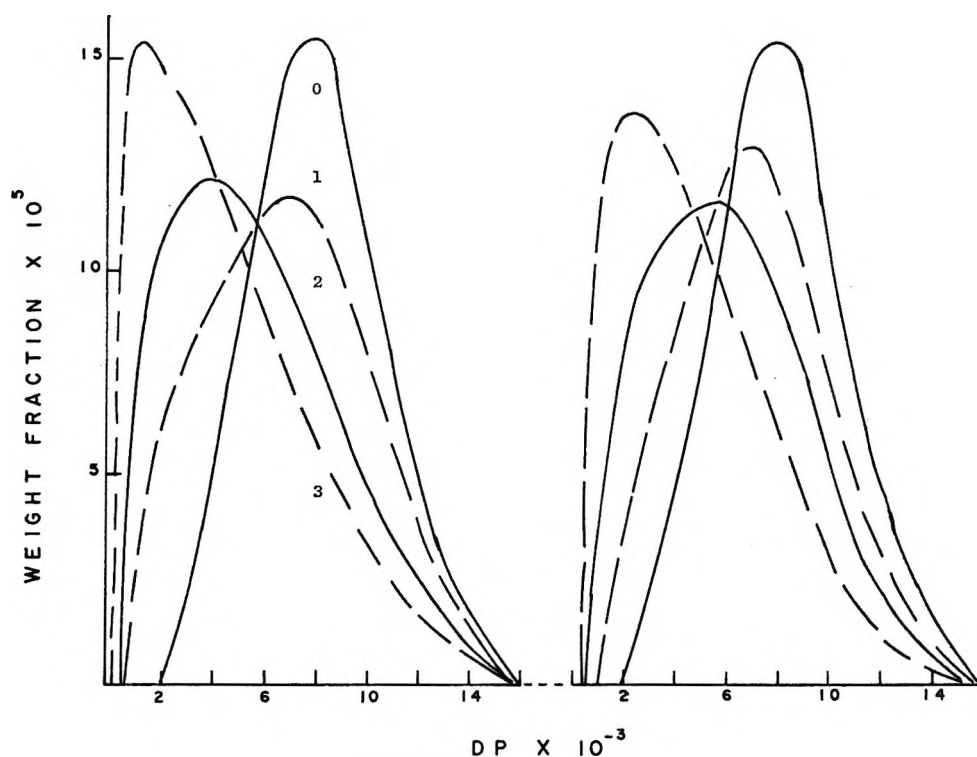


Figure 4. Comparison of actual (left) and theoretical (right) distribution curves for the degradation of polystyrene ( $M_w = 860,000$ ) with benzoyl peroxide at  $80^\circ$ . The times are in hours.

either from normalized gpc curves or the replotted curves at the peak height was first order over the early stages of the reaction. The first-order rates for a series of narrow polystyrenes are given in Table II. Several points may be made regarding these data. First, the variation in rate constant with the degree of polymerization is linear. While not shown, a plot of  $k_1$  vs.  $DP_i$  for each of the three concentrations gave lines with intercepts around 800–1000. The 88-hr sample noted in the Experimental Section (Table I) had a  $DP_n$  of around 240, suggesting that the kinetically derived value of  $DP_0$  must be somewhat too high.

Figure 3 shows the rate plots and constants taken from the gpc replot curves for a broad molecular weight sample. The curves were followed at various  $DP$ 's above the peak, the assumption being that all degradation products would fall at  $DP$ 's below the peak. As noted, first-order behavior was observed. Furthermore, the rate constants give an excellent linear plot vs.  $DP_i$ . However, the intercept for zero rate would give a  $DP_0$  value of 3700. This result is clearly too high. While the exact reason for this is not clear, it is evident that such rate studies are best carried out using narrow-range samples following the rate of disappearance of material at the peak where the change in height is maximum.

As evidenced in Table II, the reaction order for ultrasonic degradation is pseudo first order. With increasing concentration the rate constant decreases in a non-linear fashion. Over the range studied here the con-

centration vs. rate curves are approximately parabolic. Gooberman and Lamb<sup>2</sup> have made rather similar observations and have attributed the decrease in rate with increasing polymer concentration as due to the buildup of polymer networks and to increased viscosity which slow down the rate of cavity collapse and decrease the shock wave pressures.

Many studies have been carried out on the degradation of polystyrene by peroxides in the presence of air, though the degradation by benzoyl peroxide alone has received only cursory study.<sup>8</sup> Montgomery and Winkler<sup>8</sup> noted that the degradation proceeded to a far greater extent when oxygen was present. In view of the potential mechanistic complications of the reaction with oxygen, we chose to carry out the degradation in the absence of oxygen.

The disappearance of benzoyl peroxide in benzene solutions of polystyrene was kinetically first order, and the rate was independent of the molecular weight of the polymer. The rate of polystyrene disappearance was followed from the change in the peak of the gpc replot curves as described above. The disappearance of polymer was pseudo first order, and the rate constants are listed in Table III where the dependence of peroxide concentration can be seen.

The number of bonds broken as a function of time for one sample were calculated from eq 1 and are listed in

(8) D. S. Montgomery and C. A. Winkler, *Can. J. Res.*, **B28**, 407, 416, 429 (1950).

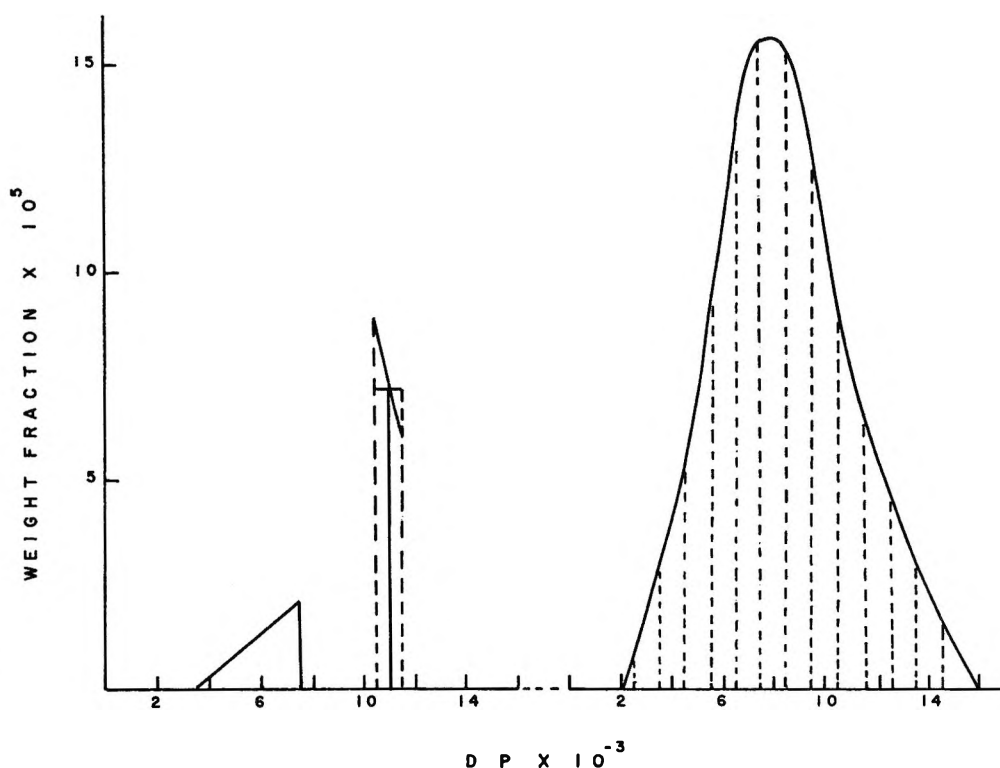


Figure 5. Illustration of how a gpc replot curve was sectioned (right) and how the area of a zone was estimated and replotted (left).

Table IV along with the number of peroxide molecules decomposed as ascertained from the rate data. It is evident that the rupture of each polymer bond requires the reaction of about  $6 \times 10^3$  peroxide molecules. An increase in the concentration of peroxide enhanced the rate of polymer degradation in a linear fashion, while the efficiency of the scission process remained the same. Similar results follow on increasing the temperature from 60 to 80°, in that the rates of both peroxide and polymer disappearance are increased about 20-fold while the degradation efficiency remains about the same.

The change in molecular weight distribution during the course of the peroxide degradation (see Figure 4) is quite different from that observed during the ultrasonic degradation (Figures 1 and 2). The initial distribution broadens but at no time shows the double maxima observed in the ultrasonic degradations. During the course of considering the nature of these changes in distribution, we developed the following rather simple model to allow a calculation of the change. Three factors of the over-all problem may be seen.

First, the change in the rate of degradation with chain length must be known. This matter can be handled using the data in Table II, which indicates that for a given concentration the change in  $k_i$  is linear in  $DP_i$ . From such a plot the values for any  $k_i$  can be determined.

Second, the region of chain breaking within each molecule that degrades must be known. The Jellinek<sup>4</sup>

model calls for random degradation over the entire chain length, while the Ovenall<sup>6</sup> model excludes the region of  $DP_0/2$  from the rupture process. The calculation described below indicated that neither of these models reproduced the experimental curves.

Finally, the mode of distributing the breaks within the region where bond breaking can occur must be elucidated.

According to either model above the probability distribution of breaks is random. In considering a molecule with  $DP = 8000$  and  $DP_0$  around 800, it would make little difference if the distribution were considered to occur over the whole molecule or if the end regions of 400 were excluded. Furthermore, as concluded earlier, there is a marked preference for rupture near the center of the molecule. Thus one should perhaps consider a Gaussian-type distribution of breaks across the allowed region. Since this type of break pattern would pose computational difficulties, some simplifying assumptions have been introduced, as seen below.

The replotted gpc curve was first sectioned into vertical zones of  $\Delta DP = 1000$  (Figure 5). The area within each zone was approximated by a rectangle as shown and as described previously.<sup>1b</sup> These areas were taken as proportional to the amount of material having the average DP of the zone, and the amount of material decomposed during a small increment of time was then calculated from the first-order rate law and the appropriate value of  $k_i$  from the linear plot of the data in Table II. In starting a plot of the new distri-

bution curve the first act was to subtract the appropriate amount (areas) of degraded material from their original rectangles giving a new series of rectangles with smaller heights.

Next it was necessary to redistribute the degraded material. As can be seen in Figure 5, when material having an average DP of 11,000 is degraded in such a way that random degradation occurs over the interval of chain length between DP = 3500 and 7500, the redistributed material will appear as a triangle of area equal to the area of the amount of original material lost and spread over the interval 3500-7500.

The only question left to be decided is the size and relationship to DP of this center interval where the random degradation is to be allowed. Since the rate constants vary in a linear fashion with DP, it seemed reasonable that the size of the rupture interval should also. For purposes of calculation it was decided that  $DP_0$  should be taken as 1000; *i.e.*, no degradation occurs below this value, and the rupture zone is zero. This obvious oversimplification should be important only in the latter stages of the degradation. The rupture zone at DP = 5500 was chosen by trial and error as 2000, and all species from 1000 up were scaled to rupture proportionally.<sup>9</sup> This material was then distributed on the new plot as described above, the total contributions of rectangles and the various triangles were summed, and a smooth distribution curve was drawn very much as described previously.<sup>1b</sup>

The results of this type of calculation are shown in Figures 1 and 2 for two of the polystyrene runs. As can be seen, the simple model described above seems to account quite well for the observed behavior. Curves calculated with the assumption that the rupture zone included everything within  $DP_0/2$  from the ends did not show the double maxima of the experimental curves.

The process described above was used to calculate curves for the peroxide decomposition. However, since it is reasonable that degradation proceeds with equal probability along the chain, completely random degradation was assumed. The results are shown in Figure 4. Again it is seen that the simple model proves a remarkably close picture of the change in molecular distribution for this type of degradation.

*Acknowledgment.* This research was generously supported by funds from the Texas Christian University Research Foundation and the Dow Chemical Co. Grateful acknowledgment is extended to both groups. We also thank Dr. E. L. Secrest for many helpful discussions.

(9) With a rupture zone of 3000 at DP = 5500, the curves tended to approximate random degradation. A zone of 1000 produced results closely matching the calculations with a zone of 2000 for low molecular weight polystyrene but produced a more sharply peaked distribution for the high molecular weight samples.

## Association in Mixed Alkali Halide Vapors

by J. Guion,<sup>1</sup> D. Hengstenberg, and M. Blander

Science Center, Aerospace and Systems Group, North American Rockwell Corporation,  
Thousand Oaks, California 91360 (Received July 1, 1968)

Vapor density measurements on the six binary alkali halide mixtures NaBr–KBr, NaBr–RbBr, NaBr–CsBr, KBr–CsBr, NaCl–CsCl, and KCl–CsCl, were made in a liquid gold isotensoscope. Association constants for the vapor species NaKBr<sub>2</sub>, NaRbBr<sub>2</sub>, NaCsBr<sub>2</sub>, KCsBr<sub>2</sub>, NaCsCl<sub>2</sub>, and KCsCl<sub>2</sub> calculated from these measurements did not fit a relation derived from simple conformal theory (eq 2). Our preliminary calculations indicate that interactions not included in the conformal theory as cation–cation and anion–anion van der Waals interactions and high-order terms due to the ion-induced dipole interactions are probably significant. The energetic factors involved in forming these molecules appear to be more complex than we anticipated. This implies that the analogous factors in molten salt mixtures are also more complex and difficult to understand than is presently believed.

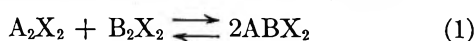
### Introduction

In this paper we present vapor density measurements of the six binary alkali halide vapor mixtures, NaBr–KBr, NaBr–RbBr, NaBr–CsBr, KBr–CsBr, NaCl–CsCl, and KCl–CsCl. The vapor densities are consistent with the presence of alkali halide dimer molecules in the vapor as well as with the vapor species NaKBr<sub>2</sub>, NaRbBr<sub>2</sub>, NaCsBr<sub>2</sub>, KCsBr<sub>2</sub>, NaCsCl<sub>2</sub>, and KCsCl<sub>2</sub>. From our measurements we derive association constants for these six species, which are compared with a function of the interionic distances predicted from dimensional considerations.

The thermodynamic study of compounds formed in vapors of ionic salts can provide data which will aid in understanding the fundamental interactions between ions. Because of the relative simplicity of the vapor species formed, one might expect that with association constants for a sufficient number of systems one would be able to unravel the different types of interactions which are significant in forming these associated molecules.

In this paper we will give a preliminary discussion of this point. Many studies of one-component alkali halides have been made<sup>2–5</sup> and have been discussed theoretically.<sup>2,3,6</sup> These studies have given considerable insight into the significant interactions between ions. Few binary alkali halide mixtures have been studied quantitatively.<sup>2,7,8</sup> Of the six systems we have investigated, the two binary chloride systems NaCl–CsCl and KCl–CsCl have been investigated previously.<sup>8</sup>

One of the purposes of this work was to test the validity of a relation derived in a dimensional analysis of associations in binary vapors.<sup>6</sup> For the equilibrium



the theory led to the relation

$$RT \ln (K/4) = M \left( \frac{1}{d_{AX}} - \frac{1}{d_{BX}} \right)^2 \quad (2)$$

where  $M$  is a function of temperature and of the anion. Mass spectrometric data for binary fluoride mixtures fitted eq 2 with  $M \approx 100$ . In this paper, we will compare our experimental results on chloride or bromide mixtures with this expression and with computer calculations of the energetics of these equilibria.

Because of an apparent discrepancy in the dimerization constants for NaBr,<sup>3,5</sup> we have repeated the measurements of Datz, Smith, and Taylor on NaBr, since these constants are necessary in our calculations.

### Experimental Method

Our apparatus and technique were similar to those of Datz, Smith, and Taylor,<sup>3</sup> and our modifications of this method have been described previously.<sup>4a,9</sup> A small weighed sample of salt is placed in a thermostated fused silica vessel of known volume which is connected to one side of a U tube containing liquid gold. The salt is completely vaporized at a fixed temperature and exerts a pressure on the liquid gold in one arm of the U tube. The liquid gold levels are equalized by introducing argon into the other arm of the U tube. The pressure

(1) On leave from the Laboratoire D'Electrochimie et de Chimie Physique du Corps Solide, Strasbourg University, Strasbourg, France. Partial support was obtained in a grant from the North Atlantic Treaty Organization.

(2) S. H. Bauer and R. F. Porter in "Molten Salt Chemistry," M. Blander, Ed., Interscience Publishers, New York, N. Y., 1964.

(3) S. Datz, W. T. Smith, Jr., and E. H. Taylor, *J. Chem. Phys.*, **34**, 558 (1961).

(4) (a) K. Hagemark, M. Blander, and E. B. Luchsinger, *J. Phys. Chem.*, **70**, 276 (1966); (b) K. Hagemark and D. Hengstenberg, *ibid.*, **71**, 3337 (1967).

(5) I. G. Murgulescu and L. Topor, *Rev. Chim., Acad. Rep. Populaire Roumaine.*, **11**, 1353 (1966).

(6) M. Blander, *J. Chem. Phys.*, **41**, 170 (1964).

(7) (a) R. C. Schoonmaker and R. F. Porter, *ibid.*, **30**, 283 (1959); (b) T. A. Milne and H. M. Klein, *ibid.*, **33**, 1628 (1960).

(8) (a) A. V. Tarasov, L. A. Kuligina, G. I. Novikov, *Vestn. Leningr. Univ., Ser. Fiz. Khim.*, **115** (1966); (b) A. V. Tarasov, A. B. Pospelov, G. I. Novikov, *ibid.*, **101** (1965).

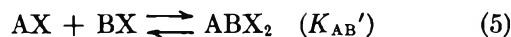
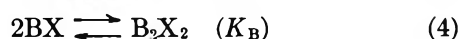
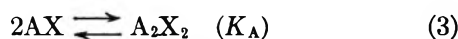
(9) K. Hagemark, D. Hengstenberg, and M. Blander, *J. Phys. Chem.*, **71**, 1819 (1967).

of argon is measured and is equal to the pressure exerted by the salt. The deviations from ideal gas behavior are related to association of salt molecules so that one may derive association constants from these measurements.<sup>3</sup>

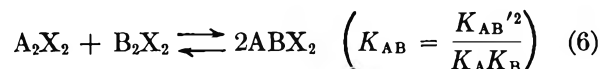
The sources of starting materials and their stated purities are: NaCl and KCl; Baker Analyzed reagent, 99.9%; CsCl, Penn Rare Metals Division, Kawecki Chemical Co., 99.9%; NaBr and KBr, Mallinckrodt Analyzed reagent, 99.9%; and RbBr and CsBr, Electronic Space Products, Inc., 99.87%. The salts were dehydrated under vacuum at moderate temperatures below the melting points. We used single crystals which yielded more reproducible results than powder. These were grown in an argon atmosphere from melts of dried salts and were stored over P<sub>2</sub>O<sub>5</sub> in a vacuum desiccator. The originally clear NaBr crystals developed a fogged surface in storage at room temperature, probably due to water adsorption. Washing with dry methyl alcohol and storage at 180° eliminated this difficulty. No difficulties were encountered with the other salts.

### Thermodynamic Calculations

For a binary mixture of the salts AX and BX, we consider the equilibria



and



where the units of the association constants  $K_A$ ,  $K_B$ , and  $K_{AB}'$  are liter per mole. The presence of significant amounts of other species, such as trimers, can be ascertained from the internal consistency of the data at different pressures and mole fractions of the two components and from mass spectrometric data.<sup>7</sup> In general, the measurements were made at pressures low enough so that trimers were not significant.

If the only significant deviations from ideal gas behavior are due to associations, then the total pressure is the sum of the partial pressures of all vapor species

$$p = \sum p_i = p_{AX} + p_{A_2X_2} + p_{BX} + p_{B_2X_2} + p_{ABX_2} \quad (7)$$

where the partial pressure, in millimeters, of a species  $i$  is given by

$$p_i = \frac{n_i R^* T}{V} \quad (8)$$

and where  $n_i$  is the number of moles of  $i$ ,  $V$  is in liters,  $T$  is in degrees Kelvin, and  $R^*$  is 62.360 l. mm mol<sup>-1</sup> deg<sup>-1</sup>.  $n_{AX}^T$  and  $n_{BX}^T$  are the total number of moles

of AX and BX sealed into the vessel and are related to the values of  $n_i$  by the expressions

$$n_{AX}^T = n_{AX} + 2n_{A_2X_2} + n_{ABX_2} \quad (9)$$

$$n_{BX}^T = n_{BX} + 2n_{B_2X_2} + n_{ABX_2}$$

If we define the "ideal partial pressures" of AX and BX,  $p_{AX}^{id}$  and  $p_{BX}^{id}$ , as the partial pressures these salts would have if they behaved ideally, then

$$p_{AX}^{id} = p_{AX} + 2p_{A_2X_2} + p_{ABX_2} = \frac{n_{AX}^T R^* T}{V} \quad (10)$$

$$p_{BX}^{id} = p_{BX} + 2p_{B_2X_2} + p_{ABX_2} = \frac{n_{BX}^T R^* T}{V} \quad (11)$$

then upon substituting for  $p_{A_2X_2}$  and  $p_{B_2X_2}$  from the expressions for the association constants  $K_A$  and  $K_B$

$$K_A = R^* T (p_{A_2X_2} / p_{AX}^2) \quad (12)$$

$$K_B = R^* T (p_{B_2X_2} / p_{BX}^2) \quad (13)$$

we obtain from combining eq 7 and 10–13

$$p_{AX} + p_{BX} = 2p - (p_{AX}^{id} + p_{BX}^{id}) \quad (14)$$

$$p - p_{AX}^{id} =$$

$$p_{BX} + (K_B / R^* T) p_{BX}^2 - (K_A / R^* T) p_{AX}^2 \quad (15)$$

When solved for  $p_{BX}$ , we obtain the quadratic equation

$$\begin{aligned} [(K_B - K_A) / R^* T] p_{BX}^2 + \{ (2K_A / R^* T) \times \\ [2p - (p_{AX}^{id} + p_{BX}^{id})] + 1 \} p_{BX} - \\ (K_A / R^* T) [2p - (p_{AX}^{id} + p_{BX}^{id})]^2 = 0 \end{aligned} \quad (16)$$

From eq 10, 11, and 14–16 and our measured values of  $n_{AX}^T$ ,  $n_{BX}^T$ ,  $V$ ,  $T$ , and  $p$ , in addition to known values of  $K_A$  and  $K_B$ , we can calculate  $p_{AX}$  and  $p_{BX}$ . From these we may calculate  $p_{A_2X_2}$  and  $p_{B_2X_2}$  using eq 12 and 13. Using these partial pressures we may calculate  $p_{ABX_2}$  from eq 10 or 11 and thus obtain  $K_{AB}'$  and  $K_{AB}$ , where

$$K_{AB}' = R^* T (p_{ABX_2} / p_{AX} p_{BX}) \quad (17)$$

$$K_{AB} = \frac{p_{ABX_2}^2}{p_{A_2X_2} p_{B_2X_2}} \quad (18)$$

**Table I:** Values of  $A_i$  and  $B_i$  in the Equation  $\log K_i = A_i + (B_i/T)$  Used to Calculate the Dimerization Constants,  $K_i$ , of the Salt  $i$

Salt	$A_i$	$B_i$	Ref
NaBr	-3.808	9,374	3
KBr	-3.407	8,378	4a
RbBr	-3.126	7,716	4b
CsBr	-2.226	6,072	4b
NaCl	-3.698	10,499	3
KCl	-3.434	9,014	3
CsCl	-3.044	7,586	3

Table II: Data Calculated from Vapor Density Measurements on the Six Binary Mixtures, NaBr-KBr, NaBr-RbBr, NaBr-CsBr,

$10^4 \rho$ , mol/l.	$T$ , °K	$P_{KNaBr_2}$	$P_{KBr}$	$P_{K_2Br_2}$	$P_{NaBr}$	$P_{Na_2Br_2}$	Log $K'$
NaBr-KBr							
3.737 (58.1% KBr)	1327	4.438	11.131	1.207	6.604	0.950	3.699
	1338	3.875	11.849	1.204	7.210	0.983	3.578
	1351	3.951	12.168	1.094	7.447	0.889	3.565
	1363	3.154	13.099	1.109	8.257	0.941	3.311
4.471 (78.6% KBr)	1349	2.801	20.442	3.160	4.565	0.343	3.402
	1355	3.656	20.246	2.896	3.954	0.238	3.586
	1366	2.541	21.575	2.909	4.958	0.327	3.306
	1367	3.128	21.247	2.790	4.498	0.266	3.446
	1378	2.384	22.344	2.735	5.215	0.313	3.245
	1387	3.013	22.396	2.493	4.791	0.237	3.385
4.302 (50.0% KBr)	1397	2.749	23.099	2.383	5.110	0.239	3.307
	1350	3.943	12.016	1.079	10.546	1.806	3.418
	1360	3.744	12.440	1.034	11.014	1.738	3.365
	1378	3.950	12.760	0.892	11.491	1.518	3.365
	1382	3.811	12.970	0.882	11.713	1.503	3.335
	1399	3.734	13.457	0.792	12.311	1.356	3.294
4.623 (57.0% KBr)	1353	4.576	14.583	1.537	9.390	1.404	3.450
	1354	4.301	14.813	1.568	9.592	1.447	3.408
	1355	4.448	14.746	1.536	9.530	1.411	3.427
	1361	4.525	14.904	1.468	9.658	1.345	3.426
	1369	4.470	15.224	1.401	9.928	1.287	3.402
	1378	4.064	15.833	1.373	10.459	1.231	3.324
	1383	4.342	15.795	1.295	10.413	1.195	3.358
	1392	4.170	16.224	1.240	10.785	1.151	3.316
1396	3.815	16.628	1.248	11.146	1.173	3.253	
$10^4 \rho$ , mol/l.	$T$ , °K	$P_{NaRbBr_2}$	$P_{RbBr}$	$P_{Rb_2Br_2}$	$P_{NaBr}$	$P_{Na_2Br_2}$	Log $K'$
NaBr-RbBr							
5.539 (76.1% RbBr)	1340	4.408	24.598	3.104	5.535	0.565	3.432
	1348	3.727	25.545	3.076	6.152	0.630	3.300
	1355	4.183	25.657	2.884	5.938	0.538	3.365
	1356	3.965	25.867	2.901	6.114	0.563	3.326
	1366	3.798	26.576	2.762	6.399	0.545	3.279
	1380	3.175	27.834	2.628	7.098	0.565	3.141
5.107 (57.5% RbBr)	1390	3.619	28.071	2.419	6.915	0.476	3.208
	1352	4.438	17.536	1.390	10.425	1.721	3.311
	1363	4.603	17.798	1.277	10.693	1.579	3.313
	1364	4.304	18.065	1.303	10.914	1.624	3.269
	1374	4.023	18.632	1.251	11.428	1.576	3.209
	1380	4.170	18.719	1.189	11.530	1.492	3.221
4.887 (62.0% RbBr)	1389	4.316	18.901	1.108	11.722	1.384	3.227
	1394	3.741	19.531	1.126	12.273	1.430	3.133
	1328	5.084	16.751	1.638	7.717	1.281	3.513
	1341	4.514	17.672	1.585	8.420	1.290	3.404
	1346	4.457	17.906	1.544	8.593	1.261	3.386
	1357	4.207	18.511	1.470	9.053	1.219	3.327
	1368	3.915	19.043	1.404	9.545	1.183	3.262
	1383	3.631	19.909	1.305	10.142	1.113	3.191
3.767 (48.4% RbBr)	1384	3.907	19.726	1.268	9.975	1.064	3.234
	1328	3.711	10.177	0.604	8.946	1.721	3.528
	1340	3.568	10.529	0.569	9.412	1.633	3.478
	1354	3.012	11.258	0.561	10.194	1.604	3.346
	1361	2.877	11.506	0.545	10.502	1.561	3.306
	1379	2.533	12.135	0.505	11.290	1.447	3.201
1382	2.322	12.371	0.509	11.523	1.454	3.147	
$10^4 \rho$ , mol/l.	$T$ , °K	$P_{NaCsBr_2}$	$P_{CsBr}$	$P_{Cs_2Br_2}$	$P_{NaBr}$	$P_{Na_2Br_2}$	Log $K'$
NaBr-CsBr							
3.914 (68.4% CsBr)	1334	3.264	17.456	0.775	5.723	0.652	3.434
	1338	3.371	17.466	0.750	5.716	0.618	3.450
	1349	3.067	18.002	0.726	6.111	0.614	3.370
	1359	3.138	18.187	0.681	6.222	0.562	3.371

KBr-CsBr, NaCl-CsCl, and KCl-CsCl<sup>a</sup>

$10^4 \rho$ , mol/l.	$T$ , °K	$P_{NaCsBr_2}$	$P_{CsBr}$	$P_{Cs_2Br_2}$	$P_{NaBr}$	$P_{Na_2Br_2}$	Log $K'$
NaBr-CsBr							
	1363	2.502	18.838	0.707	6.753	0.630	3.223
	1367	2.678	18.783	0.680	6.691	0.588	3.259
	1371	2.801	18.772	0.658	6.664	0.556	3.282
	1385	2.664	19.226	0.616	6.988	0.516	3.234
	1392	2.581	19.463	0.597	7.160	0.498	3.206
4.521	1307	5.426	15.442	0.769	6.568	1.224	3.640
(60.8%	1330	4.922	16.453	0.713	7.449	1.163	3.520
CsBr)	1330	4.484	16.825	0.746	7.717	1.248	3.457
	1339	4.991	16.617	0.673	7.631	1.087	3.517
	1355	5.139	16.877	0.607	7.921	0.957	3.512
	1370	5.116	17.250	0.560	8.284	0.869	3.486
	1375	4.697	17.733	0.568	8.695	0.901	3.417
	1393	4.435	18.383	0.529	9.298	0.830	3.353
	1395	4.720	18.173	0.509	9.131	0.782	3.393
	1410	4.291	18.903	0.489	9.783	0.753	3.310
4.507	1306	3.898	20.933	1.426	4.140	0.493	3.564
(75.4%	1314	4.355	20.861	1.319	3.927	0.399	3.639
CsBr)	1322	3.661	21.701	1.330	4.522	0.476	3.488
	1329	3.240	22.290	1.320	4.916	0.513	3.389
	1346	4.031	22.229	1.135	4.559	0.355	3.202
	1348	3.911	22.397	1.133	4.676	0.364	3.497
	1353	3.791	22.663	1.112	4.829	0.365	3.466
	1367	3.512	23.360	1.052	5.218	0.358	3.390
	1370	3.511	23.458	1.035	5.256	0.350	3.386
	1391	3.573	24.071	0.920	5.453	0.292	3.373
$10^4 \rho$ , mol/l.	$T$ , °K	$P_{KCsBr_2}$	$P_{CsBr}$	$P_{Cs_2Br_2}$	$P_{KBr}$	$P_{K_2Br_2}$	Log $K'$
KBr-CsBr							
3.658	1314	2.095	14.237	0.614	8.628	0.846	3.146
(58.6%	1322	1.928	14.544	0.597	8.918	0.822	3.088
CsBr)	1353	1.774	15.295	0.507	9.660	0.674	2.988
	1364	1.578	15.679	0.486	10.025	0.642	2.931
	1366	1.767	15.548	0.470	9.911	0.614	2.990
	1385	1.712	15.949	0.424	10.296	0.538	2.954
	1390	1.569	16.170	0.419	10.502	0.531	2.904
4.865	1322	3.325	17.163	0.832	11.769	1.431	3.133
(55.2%	1360	2.978	18.424	0.693	13.175	1.160	3.017
CsBr)	1371	2.437	19.166	0.685	13.899	1.143	2.893
	1394	2.279	19.857	0.612	14.670	0.993	2.833
	1400	2.565	19.741	0.577	14.604	0.923	2.890
	1406	2.293	20.123	0.572	14.980	0.912	2.824
	1429	2.351	20.591	0.502	15.515	0.772	2.817
4.867	1329	3.669	12.565	0.419	15.198	2.198	3.202
(42.3%	1342	2.737	13.621	0.441	16.367	2.194	3.012
CsBr)	1351	2.536	13.961	0.429	16.894	2.110	2.957
	1369	3.336	13.554	0.348	17.095	1.767	3.090
	1403	2.590	14.801	0.317	18.956	1.507	2.907
	1428	2.497	15.290	0.279	19.928	1.286	2.863
$10^4 \rho$ , mol/l.	$T$ , °K	$P_{KCsCl_2}$	$P_{CsCl}$	$P_{Cs_2Cl_2}$	$P_{KCl}$	$P_{K_2Cl_2}$	Log $K'$
NaCl-CsCl							
4.746	1368	2.941	10.820	0.435	8.152	7.383	3.454
(36.1%	1379	2.377	11.491	0.440	8.814	7.437	3.305
CsCl)	1382	2.531	11.408	0.421	8.929	7.331	3.331
	1392	2.023	12.018	0.423	9.563	7.363	3.184
	1417	1.723	12.689	0.372	10.992	7.034	3.038
3.983	1339	2.490	18.187	1.657	3.254	1.762	3.546
(72.1%	1350	2.390	18.680	1.559	3.488	1.733	3.490
CsCl)	1365	2.059	19.486	1.455	3.889	1.750	3.364
	1381	2.214	19.933	1.298	4.144	1.601	3.363
	1382	2.230	19.955	1.288	4.158	1.589	3.365
	1396	2.242	20.418	1.176	4.427	1.497	3.334
	1424	2.178	21.362	0.987	5.008	1.336	3.257

Table II (Continued)

$10^4 p$ , mol/l.	$T$ , °K	$P_{KCsCl_2}$	$P_{CsCl}$	$P_{K_2Cl_2}$	$P_{KCl}$	$P_{K_2Cl_2}$	Log $K'$
4.647 (69.1% CsCl)	1352	2.777	20.587	1.855	4.272	2.529	3.425
	1363	2.669	21.132	1.746	4.569	2.484	3.371
	1385	2.291	22.316	1.564	5.247	2.432	3.228
	1406	1.759	23.553	1.421	6.002	2.415	3.038
	1428	1.769	24.355	1.235	6.603	2.208	2.877
KCl-CsCl							
4.930 (66.2% CsCl)	1353	3.543	20.394	1.801	7.968	1.273	3.265
	1363	3.061	21.176	1.754	8.519	1.290	3.159
	1380	3.274	21.707	1.554	8.806	1.129	3.169
	1390	3.436	21.971	1.443	8.934	1.035	3.181
	1397	3.679	22.043	1.357	8.927	0.954	3.212
	1412	3.860	22.444	1.219	9.125	0.843	3.220
3.882 (70.8% CsCl)	1423	3.604	23.044	1.159	9.547	0.817	3.163
	1337	2.795	17.113	1.498	5.300	0.685	3.410
	1350	2.557	17.754	1.408	5.664	0.667	3.331
	1381	2.609	18.752	1.148	6.096	0.535	3.294
	1388	2.489	19.071	1.109	6.287	0.525	3.255
	1396	2.612	19.219	1.042	6.306	0.482	3.273
3.026 (53.7% CsCl)	1418	2.771	19.739	0.891	6.473	0.397	3.283
	1327	2.024	10.240	0.596	6.919	1.321	3.374
	1349	2.011	10.645	0.511	7.438	1.164	3.330
	1367	2.002	10.958	0.451	7.846	1.044	3.298
	1384	2.090	11.155	0.395	8.148	0.923	3.298
	1401	2.081	11.424	0.351	8.498	0.827	3.273
1425	2.081	11.775	0.297	8.954	0.703	3.244	

<sup>a</sup>  $p$  is in millimeters.

The values of the dimerization constants we used were calculated from the equation

$$\log K_i = A_i + (B_i/T) \quad (19)$$

where  $A_i$  and  $B_i$  are given in Table I.

### Experimental Results

The necessary values for the dimerization constants of all the salts in our mixtures are available.<sup>3,4</sup> Because of the apparent discrepancy in the data for NaBr,<sup>3</sup> we have repeated the measurements for this salt at three different densities. As has been previously discussed,<sup>3,4</sup> the dimerization constants were calculated from the relations

$$P_{AX} = 2p - p_{AX}^{id}$$

$$P_{A_2X_2} = p^{id} - p$$

$$K_A = R^*T(p_{A_2X_2}/p_{AX}^2)$$

The agreement with the reported values of Datz, Smith, and Taylor<sup>3</sup> for  $\log K_A$  was good ( $\pm 0.1$ ) and there appears to be no discrepancy in the values reported in ref 3. NaBr exhibits the largest deviations from the predictions of the dimensional theory of any salt which has been measured.<sup>6</sup> The data of Murgulescu and Topor<sup>5</sup> are in agreement with these results.

The measurements for the binary systems NaBr-KBr, NaBr-RbBr, NaBr-CsBr, KBr-CsBr, NaCl-KCl, and NaCl-CsCl are given in Table II. For each binary system, we made at least three independent series of

measurements at different compositions. Values of  $\log K_{AB}$  calculated from  $K_{AB}'$  appear to be constant at different compositions within an uncertainty of  $\pm 0.15$  and also differ little at different temperatures. Because of the relatively narrow range of temperatures and the small temperature dependence, we could not establish a temperature dependence for  $K_{AB}$ . This means that, within experimental error, the energy of forming the mixed compound from the monomers (eq 5) is the average of the energy of dimerization of the two monomers.

In all cases, except for the mixture of NaCl with CsCl, the values of  $K_{AB}/4$  are greater than unity. A value of  $K_{AB}/4$  greater than unity indicates that the tendency to form  $ABX_2$  is stronger than the "average" for the two dimers  $A_2X_2$  and  $B_2X_2$ . The experimental errors in  $K_{AB}$  arise not only from errors in our measurements but also from errors in the dimerization constants of the two salts. We estimate that the cumulative errors in  $RT \ln (K_{AB}/4)$  are about  $\pm 1$  kcal. Consequently,  $K_{AB}/4$  for the NaCl-CsCl system may be close to unity. In Figure 1 are plotted our measured values of  $RT \ln (K_{AB}/4)$  vs.  $[(1/d_1) - (1/d_2)]^2$ . The values for the fluorides which have been measured in the mass spectrometer<sup>7</sup> lie close to a line plotted in the figure.

### Discussion

It can be seen in Figure 1 that the values of  $RT \ln (K_{AB}/4)$  for the bromides are larger than for the fluorides or chlorides. If only coulomb interactions in-



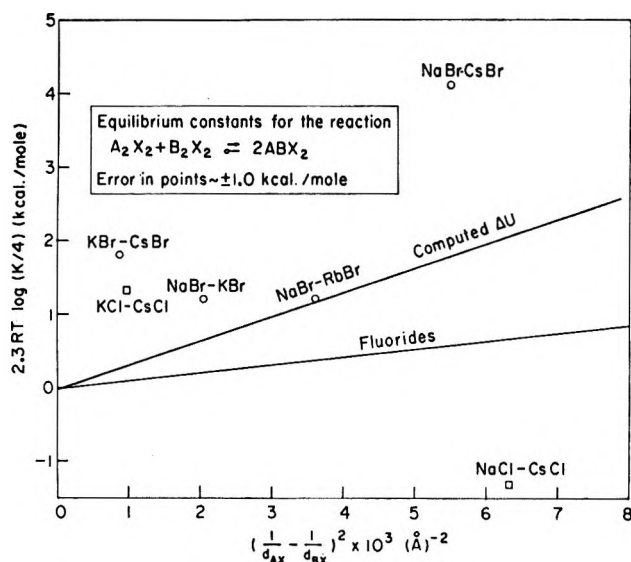


Figure 1. Plot of  $RT \ln (K_{AB}/4)$  vs.  $[(1/d_{AX}) - (1/d_{BX})]^2$  for six binary mixtures. The line labeled  $\Delta U$  represents the coulombic energy change given in Table III which was calculated from the simple model.

fluenced the magnitude of  $K_{AB}/4$ , then there should be no difference between bromides, chlorides, and fluorides in a plot such as in Figure 1. Consequently, the differences indicate that other interactions are significant. Since vapor molecules are simple, fairly accurate calculations of the energetics are feasible. Thus, by comparing such calculations with our measurements, it is hoped that, in the future, we may gain insight into the magnitude of those interionic interactions which are important in mixtures. The implications of such calculations are significant not only for salt vapors but also in understanding the relative importance of different interactions in molten salt mixtures where simple calculations are not feasible.

Some of the types of interactions which need to be considered may be deduced from previous calculations of the energies of formation of monomeric alkali halides and of the energies of association of the dimer molecules which have been made by several authors.<sup>10</sup> The general conclusion reached by most of these authors is that the three most significant interactions are the coulombic attractions and repulsions, the soft-core repulsion between ions, and the ion-induced dipole interactions. In ref 10c and d, the ion-induced dipole interactions were taken into account by the simple artifice of softening the repulsive potential. Because of the low coordination number of vapor molecules, the van der Waals (dispersion) interactions are relatively small in the monomers but may be significant in dimers.

A preliminary idea of the influence of the coulomb interactions and the soft-core repulsions on  $K_{AB}$  may be gauged by comparison of the data with calculations which include only these two interactions. Consider

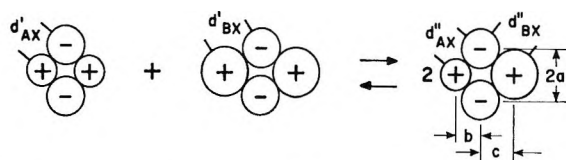


Figure 2. The model used in the calculations given in Table III.

the equilibrium shown in Figure 2. The energy change for this equilibrium was calculated taking into account only coulomb interactions and a repulsion representing the two extreme cases: (a) the soft inverse power potential  $k/r^8$  and (b) a hard-core repulsion. The energy change is

$$\Delta U_{AB} = 2U_{AB} - U_A - U_B \quad (20)$$

where  $U_{AB}$  is the potential energy of the mixed alkali halide molecule,  $U_A$  that of one dimer, and  $U_B$  that of the other. If the pair potential for the  $A^+$  and  $X^-$  ions is written as

$$U = -\frac{e^2}{d_{AX}} + \frac{ke^2}{d_{AX}^8} = \frac{-e^2}{d_{AX}} \left(1 - \frac{1}{8}\right) \quad (21)$$

where from the minimization of  $U$ ,  $k = (d_{AX}^7/8)$  and  $d_{AX}$  is the internuclear distance for the monomer, then for the dimer  $A_2X_2$

$$\begin{aligned} (U_{AX}/e^2) &= \frac{-2.586(0.8750)}{d_{AX}'} = \\ &= \frac{-2.586(0.8750)}{1.064307d_{AX}} = \frac{-2.126}{d_{AX}} \quad (22) \end{aligned}$$

and for  $B_2X_2$

$$(U_{BX}/e^2) = \frac{-2.126}{d_{BX}} \quad (23)$$

where  $d_{BX}$  is the internuclear distance for the monomer  $BX$ . The factor 1.064 which is calculated by minimizing  $U_{AX}$  arises because of the lengthening of the cation-anion distances in the dimer as compared with the monomer. For the mixed compound

$$\begin{aligned} \frac{U_{AB}}{e^2} &= -\frac{2}{d_{AX}''} - \frac{2}{d_{BX}''} + \frac{1}{b+c} + \\ &= \frac{1}{2a} + \frac{2k}{(d_{AX}'')^8} + \frac{2k'}{(d_{BX}'')^8} \quad (24) \end{aligned}$$

where  $k' = (d_{BX}^7/8)$ . Core repulsions between ions of like sign were assumed to be negligible. Minimizing  $U_{AB}$  with respect to the three variables  $a$ ,  $b$ , and  $c$

(10) (a) E. S. Rittner, *J. Chem. Phys.*, **19**, 1030 (1951); (b) C. T. O'Konski and W. I. Higuchi, *ibid.*, **23**, 1175 (1955); (c) L. Pauling, *Proc. Nat. Acad. Sci., India*, **A25** (1956); (d) T. A. Milne and D. Cubicciotti, *J. Chem. Phys.*, **29**, 846 (1958); (e) J. Berkowitz, *ibid.*, **29**, 1386 (1958); (f) G. M. Rothberg, *ibid.*, **34**, 2069 (1961); (g) Y. P. Varshni and R. C. Shukla, *ibid.*, **35**, 582 (1961).

**Table III:** Energies for the Equilibrium  $A_2X_2 + B_2X_2 \rightleftharpoons 2ABX_2$  Calculated from the Model in Figure 2 Utilizing the Anion-Cation Pair Potential  $U = -(e^2/r) + (ke^2/r^8)$

Salt pair	$d_{AX}$	$d_{BX}$	$a$	$b$	$c$	$d_{AX''}$	$d_{BX''}$	$10^3(\Delta U/e^3)$	$10^3[(1/d_{AX}) - (1/d_{BX})]^2$
NaBr-KBr	2.5020	2.8207	1.9941	1.7454	2.2655	2.6501	3.0181	-1.941	2.039
NaBr-RbBr	2.5020	2.9447	2.0330	1.6934	2.4154	2.6459	3.1571	-3.509	3.610
NaBr-CsBr	2.5020	3.0722	2.0707	1.6409	2.5700	2.6420	3.3004	-5.430	5.503
KBr-CsBr	2.8207	3.0722	2.2125	2.0136	2.4241	2.9917	3.2820	-0.893	0.842
NaCl-CsCl	2.3606	2.9062	1.9559	1.5450	2.4341	2.4925	3.1225	-5.901	6.325
KCl-CsCl	2.6666	2.9062	2.0923	1.9028	2.2939	2.8281	3.1048	-0.960	0.956

led to three nonlinear equations which, when combined with the conditions

$$a^2 + b^2 = (d_{AX''})^2 \quad (25)$$

$$a^2 + c^2 = (d_{BX''})^2 \quad (26)$$

were solved on a computer. The results are given in Table III for the salt pairs studied for the case in which the core repulsion was represented by a very soft inverse eighth power term.

These calculations of  $\Delta U_{AB}$ , in effect, are the same as  $-RT \ln (K_{AB}/4)$  at 0°K. The temperature dependence is unknown. Consequently, a direct comparison with our data is not possible. However, it is probable that the temperature coefficients are not very large, so that these calculations can provide us with considerable information.

There are two points to be noted in these calculations.

a.  $\Delta U$  when plotted *vs.* the parameter  $[(1/d_{AX}) - (1/d_{BX})]^2$ , which is suggested by the dimensional theory used to derive eq 2, yields an essentially linear plot. This linearity lends confidence in the validity of the derivation of eq 2 for coulomb attractions and a soft repulsion. Within small limits

$$\Delta U = -330 \left( \frac{1}{d_{AX}} - \frac{1}{d_{BX}} \right)^2 \text{ kcal/mol} \quad (27)$$

which is plotted in Figure 1.

A similar calculation for hard-core ions leads to a result which is smaller than this by about 9%. This relative insensitivity to the softness of the cores is an important result.

b. When  $d_{AX}' < d_{BX}'$ , then in the mixed compound  $d_{AX}' > d_{AX}''$  and  $d_{BX}' < d_{BX}''$  (*i.e.*, the short interionic distances get shorter and the long ones longer).

Although these idealized classical calculations are for the energetics at 0°K, they are significant as a point of departure. The bromides lie above the line representing eq 27. This difference is, at least in part, related to the ion-induced dipole interactions. Calculation of the square of the electric intensity vectors,  $E^2$ , for the ions using the data in Table III indicates that the changes in  $E^2$  on the anions are negative and approximately proportional to the parameter  $[(1/d_{AX}) - (1/d_{BX})]^2$ . Thus, to first order, the polarization of

the anions leads to a term of the form of eq 2, and the parameter  $M$  in eq 2 is more positive for salts with more polarizable anions. If the induced-dipole energy may be represented by  $(\alpha E^2/2)$ , where  $\alpha$  is a constant, then we find as a first-order approximation  $M \sim 330[1 + 0.3\alpha_{\text{anion}}]$  kcal/mol, where  $\alpha$  is given in  $10^{-24} \text{ cm}^3$ . This expression, of course, does not take into account the changes in internuclear distances which result from the inclusion of the polarization interactions. The magnitude of this interaction is, relatively, very large and leads to significant changes in the interionic distances. For example, the strong tendency of the more polarizable anions to be stabilized in regions of high field intensity leads to configurations in which the anion-anion distances are increased and the cation-cation distances are decreased. These changes will stabilize the dimers as well as the mixed compound. Our preliminary calculations show that, in general, the dimers are stabilized more than the mixed compound. Consequently, although the first-order contribution to  $M$  is positive, the change of the configuration of the molecules leads to higher order terms which are negative and may be large enough to lead to a net negative contribution to  $\log (K/4)$  from the ion-induced dipole terms. Further calculations of this and of the influence of temperature will be necessary for a quantitative evaluation.

Another interaction which may be of importance is the van der Waals (dispersion) interaction. A calculation of the magnitude of these interactions using parameters given by Mayer<sup>11</sup> shows that the cesium-cesium interactions in cesium halide dimers and the halogen-halogen interactions in lithium and sodium halide dimers are significant and in reactions such as reaction 1 may lead to significant (*e.g.*,  $\sim 1-3$  kcal/mol) positive contributions to the energy changes in the fluoride systems in which LiF or NaF is one component and in the NaCl-CsCl system. These positive contributions result from the change of next neighbor cations of the cesium halide dimers and an increase in the distances between anions in the lithium and sodium halides in the other cases. The magnitudes of these van der Waals effects are very sensitive to the details of the calculation and are most sensitive to the softness

(11) J. E. Mayer, *J. Chem. Phys.*, **1**, 327 (1933).

of the core repulsions. A precise determination of this possibility must await more detailed calculations now in progress.

The results for binary fluoride systems reported by Schoonmaker and Porter<sup>12</sup> and for the NaCl–CsCl system lie below the measured values of  $RT \log (K/4)$  for the bromides. The higher order polarization terms and the van der Waals interaction terms are undoubtedly important for at least a part of these differences. In addition, a calculation of the influence of temperature will be needed to correlate the absolute values of  $-\Delta U$  with  $RT \ln (K/4)$  and thus go further than our present discussion of the relative contributions to these quantities.

These conclusions are significant not only in understanding the energetics in salt vapors but also in understanding the corresponding effects in molten salt mixtures. Kleppa and Holm<sup>13</sup> have observed a difference between the heats of mixing in fluoride and bromide mixtures analogous to the one discussed here. We are now carrying out detailed calculations on the vapor molecules which we hope will aid in understanding the relative importance of different ionic interactions, especially of the higher order polarization and the anion–anion van der Waals interactions which have not been discussed previously.

### Conclusions

We may therefore conclude the following.

a. Contributions to  $RT \ln (K_{AB}/4)$  from the coulomb and ion-induced anion dipole interactions, to first order, depend upon the size parameters according to the relation

$$RT \ln (K_{AB}/4) = M \left( \frac{1}{d_{AX}} - \frac{1}{d_{BX}} \right)^2$$

where  $M$  is positive and is more positive the larger the polarizability of the anion.

b. The ion-induced anion dipole interactions are so large that terms higher than first order are very significant, especially for polarizable anions in salts where  $d$  is small. These higher order terms lead to increased anion–anion distances and decreased cation–cation distances and generally make a negative contribution to  $RT \log (K_{AB}/4)$ .

c. For lithium and sodium halides, the separation of next nearest neighbor anions is larger in the mixed compound than in the dimer which leads to significant negative contributions to  $RT \ln (K_{AB}/4)$  from van der Waals interactions. This contribution has not been discussed previously and may have analogies in molten salt mixtures.

d. For rubidium and cesium halides, the change of next nearest neighbor cations generally leads to significant negative contributions to  $RT \ln (K_{AB}/4)$  in a manner analogous to molten salt mixtures.<sup>14,15</sup>

A general conclusion is that the energetic factors involved in forming these molecules are much more complex than we anticipated. This implies that the analogous factors in molten salt mixtures are also more complex and difficult to understand than is presently believed.

*Acknowledgments.* The authors wish to thank Stephen T. Imrich and Dr. Jerome Spanier of this laboratory who carried out the computer solution of the nonlinear equations obtained from the model.

(12) R. C. Schoonmaker and R. F. Porter, *J. Chem. Phys.*, **30**, 283 (1959).

(13) O. J. Kleppa and J. Holm, to be submitted for publication.

(14) M. Blander, *J. Chem. Phys.*, **36**, 1092 (1962); **37**, 172 (1962).

(15) J. Lumsden, *Discussions Faraday Soc.*, **32**, 138 (1961).

Spectra of Gaseous Protio- and Deuteriooxalic Acids<sup>1</sup>

by Bruce M. Pava and Fred E. Stafford

*Department of Chemistry and The Materials Research Center, Northwestern University, Evanston, Illinois 60201 (Received July 1, 1968)*

The ir spectra from 400 to 4000  $\text{cm}^{-1}$  were obtained for gaseous oxalic acid and oxalic acid- $d_2$ . These are consistent with a chelated structure for the gaseous molecules. The carbonyl stretching frequencies of the dicarbonyl species  $\text{X}(\text{CO})_2\text{Y}$  correlate with the electronegativities of X and Y, as do the  $\text{C}=\text{O}$  stretching frequencies in the  $\text{XCOY}$  system.

## Introduction

In the spectra of  $\alpha$ -alkoxy and  $\alpha$ -keto carboxylic acids in dilute solutions, two OH stretching frequencies appear in the 3400–3600  $\text{cm}^{-1}$  region. The higher frequency band was assigned to the free form; it appears between 3500 and 3550  $\text{cm}^{-1}$ . The lower frequency band, 3400–3500  $\text{cm}^{-1}$ , was assigned to the proton-chelated form. It was found that the lower frequency band appears only when a five-membered internally hydrogen bonded ring can be formed.<sup>2</sup>

The ir spectra of pyruvic acid (PA), methylpyruvic acid (MPA), dimethylpyruvic acid (DMPA), and trimethylpyruvic acid (TMPA) have been studied also in the gas phase at approximately 100°. Two bands due to OH stretching modes were found in the 3400–3600  $\text{cm}^{-1}$  region. The higher frequency band always appeared between 3560 and 3575  $\text{cm}^{-1}$ . The lower frequency band appeared between 3440 and 3470  $\text{cm}^{-1}$ . In the spectrum of trimethylpyruvic acid- $d$ , two OD stretching bands were observed at 2559 and 2636  $\text{cm}^{-1}$ . Again, the higher frequency bands were assigned to the nonchelated structure; the lower frequency bands were assigned to the chelated structure<sup>3</sup> (Table I).

**Table I:** The OH Absorption Frequencies of Gaseous Pyruvic Acid, Methylpyruvic Acid, Dimethylpyruvic Acid, and Trimethylpyruvic Acid at 100°<sup>a</sup>

Acid	Frequency, $\text{cm}^{-1}$	
	Nonchelated	Chelated
PA	3573	3465
MPA	3574	3463
DMPA	3570	3458
TMPA	3560	3441

<sup>a</sup> Reference 3.

Oxalic acid also has a proton-accepting group  $\alpha$  to the carboxyl group. Although the condensed phase has been extensively studied,<sup>4,5</sup> particularly with respect to hydrogen bonding, only electron diffraction results<sup>6</sup> are reported for the vapor. This lack of data is probably due to the thermal decomposition of oxalic

acid. The purpose of this work is to determine the ir spectrum of gaseous oxalic acid to help deduce its structure.

## Experimental Section

The anhydrous oxalic acid was purchased from the Fisher Chemical Co. The anhydrous deuterated oxalic acid was prepared by repeatedly dissolving oxalic acid in  $\text{D}_2\text{O}$  and evaporating under vacuum.

Because of the toxicity of oxalic acid, precautions were taken to keep it out of the air and off the body.

Spectra were obtained using a 1-m mullite cell with KBr windows. A side arm permitted the cell to be evacuated and refilled with argon. A Thermac, R. I. Controls, Minneapolis, Minn., was used to regulate the temperature and a Beckman IR-9 spectrometer was used to obtain the spectra. All spectra were taken in single-beam operation with the internal chopper.<sup>7</sup>

A cycle consisted of recording spectra at room temperature, next at a series of selected higher temperatures, and then again at room temperature. Every experiment was recycled at least once.

## Data and Results

The spectra of gaseous oxalic acid and oxalic acid- $d_2$  were first observed at approximately 105°. At higher temperatures, white deposits sometimes coated the ends of the cell. Decomposition, at approximately 140°, was evidenced by the appearance of bands due to carbon monoxide and formic acid as well as by the reduction in intensity of the bands that were assigned to oxalic acid. The frequencies of the observed bands are in Table II and Figure 1.

(1) Supported by the U. S. Army Research Office, Durham, N. C., and the National Science Foundation through an undergraduate research grant.

(2) M. Oki and M. Hirota, *Nippon Kagaku Zasshi*, **81**, 855 (1960).

(3) A. Schellenberger, W. Beer, and G. Oehme, *Spectrochim. Acta*, **21**, 1345 (1965).

(4) R. G. Delaplane and J. A. Ibers, *J. Chem. Phys.*, **45**, 3451 (1966), and earlier references.

(5) J. Reynolds and S. Sternstein, *ibid.*, **41**, 47 (1964).

(6) S. Shibata and M. Kimura, *Bull. Chem. Soc. Jap.*, **27**, 485 (1954).

(7) S. M. Chackalackal and F. E. Stafford, *J. Amer. Chem. Soc.*, **88**, 723 (1966).

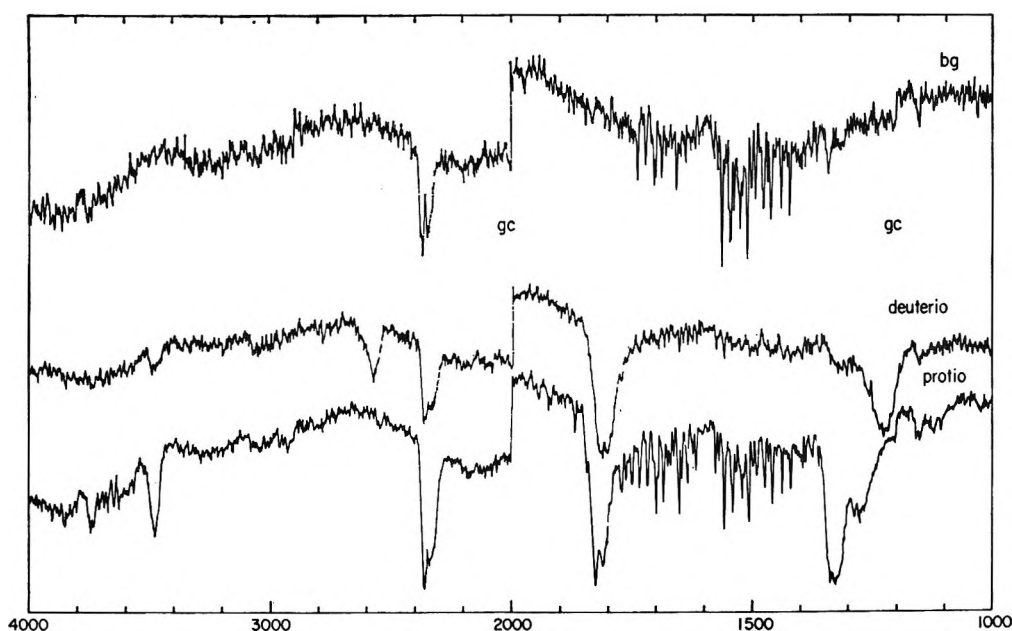


Figure 1. The ir spectra of oxalic acid and oxalic acid- $d_2$  (bg, background; gc, grating change). No features were observed between 1000 and 400  $\text{cm}^{-1}$ . Note the scale change at 2000  $\text{cm}^{-1}$ .

**Table II:** Ir Absorption Frequencies of Gaseous Oxalic Acid and Oxalic Acid- $d_2$ , 110–140 $^{\circ}\text{a}$

Frequency, $\text{cm}^{-1}$		Assignments
3485 sh	2575 sh	O—H(D) str
1830 vs	1820 vs	C=O str
1810 vs	1800 vs	
1325 s	1220 vs	...
1240 br		...

<sup>a</sup> sh, sharp; vs, very strong; s, strong; br, broad; str, stretch.

Only one OH and only one OD stretching band were found for oxalic acid and oxalic acid- $d_2$ . The observed OH and OD stretching frequencies correspond in shape, location, and relative intensity to those assigned to the proton-chelated structure of pyruvic acid<sup>3</sup> (Table I).

For compounds of the type XCOY (X, Y = F, OH, Cl, CH<sub>3</sub>, H, etc.), it is known that the carbonyl stretching frequency<sup>8–10</sup> varies systematically with the electronegativity<sup>11</sup> of X and Y, as discussed by Kagarise.<sup>12</sup> This relationship is shown by the open circles in Figure 2. That this correlation can be extended successfully to symmetric molecules of the type X(CO)<sub>2</sub>X is shown by the filled circles. In addition, the frequencies for the two carbonyls of CH<sub>3</sub>(CO)<sub>2</sub>OH correlate well if each is treated individually using, respectively, the electronegativities of CH<sub>3</sub> and OH (half-filled circles). The frequencies shown in Figure 2 are for oxalic acid and oxalic acid- $d_2$ , as well as for glyoxal,<sup>13</sup> oxalyl chloride,<sup>14</sup> and methyl oxalate.

A very weak feature which may be a Q branch some-

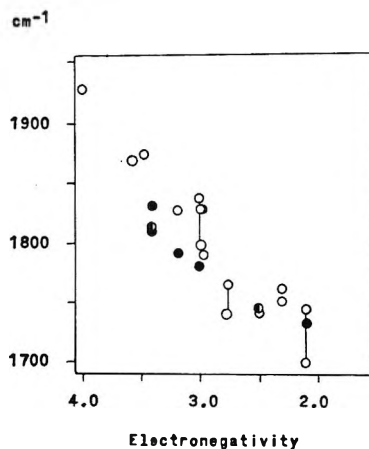


Figure 2. Carbonyl frequency ( $\text{cm}^{-1}$ ) vs. average electronegativity<sup>11</sup> for gaseous XCOY (open circles), X(CO)<sub>2</sub>X (filled circles), and CH<sub>3</sub>COCOOH (half-filled circles); see the text. Points for isotopically substituted molecules (e.g., -OH and -CD) are connected by vertical lines and demonstrate the weakness of using frequencies for such a correlation. See the text. The data are from Nakamoto,<sup>8</sup> Bellamy<sup>9</sup> (pp 135, 155, 165–67, 179), and Herzberg.<sup>10</sup> Data concerning the X(CO)<sub>2</sub>Y systems are from B. D. Saksena and R. E. Kagarise, *J. Chem. Phys.*, 19, 987 (1951), R. K. Harris, *Spectrochim. Acta*, 20, 1129 (1964), and this work.

(8) K. Nakamoto, "Infrared Spectra of Inorganic and Coordination Compounds," John Wiley & Sons, Inc., New York, N. Y., 1963.

(9) L. J. Bellamy, "The Infrared Spectra of Complex Molecules," John Wiley & Sons, Inc., New York, N. Y., 1958.

(10) G. Herzberg, "Infrared and Raman Spectra," D. Van Nostrand Co., Inc., Princeton, N. J., 1945.

(11) A. L. Allred, *J. Inorg. Nucl. Chem.*, 17, 215 (1961).

(12) R. E. Kagarise, *J. Amer. Chem. Soc.*, 77, 1377 (1955).

(13) R. K. Harris, *Spectrochim. Acta*, 20, 1129 (1964).

(14) B. D. Saksena and R. E. Kagarise, *J. Chem. Phys.*, 19, 987 (1951).

times appeared in the oxalic acid spectrum at  $1817\text{ cm}^{-1}$  between the two prominent branches of the C=O stretching band. Low resolution and strong background, however, prevented assigning it to the oxalic acid spectrum. Another similar feature appeared in the oxalic acid- $d_2$  spectrum at  $1808\text{ cm}^{-1}$ . This band also was too weakly resolved to be assigned to the spectrum of oxalic acid- $d_2$ .

### Discussion

The OH stretching bands of oxalic acid and oxalic acid- $d_2$  are consistent with a predominantly chelated structure. Although only one absorption frequency was found for the OH stretch in oxalic acid, a weaker one at a higher frequency could have been hidden by the water vapor background. In the oxalic acid- $d_2$  spectrum, however, this background was at a minimum, and the intensity of the second band, if present, was 5% or less of the chelated band intensity.

The assumption of a chelated structure for the two oxalic acids helps explain the planarity of the gaseous oxalic acid molecule deduced by Shibata and Kimura from electron diffraction data.<sup>6</sup> Electron resonance structures, as invoked to explain the planarity of glycer-aldehyde, oxalyl chloride, and butadiene, also help to explain this planar structure.

In Figure 2, the three vertical lines connect points for isotopically substituted molecules in which X and Y are H, F and D, F; H, OH and D, OH; and H, H and D, D. Quite clearly the CO frequency depends on the mass as

well as the electronegativity of X and Y. Overend and Scherer<sup>15</sup> have shown that the Urey-Bradley C=O force constants are sensibly constant at  $12.7 \pm 0.1$  mdyn/Å, as are the corresponding C=O bond distances for Cl<sub>2</sub>CO, F<sub>2</sub>CO, and Br<sub>2</sub>CO. They have also offered an explanation for the observed variation of frequency. Subsequently  $k(\text{CO})$  in H<sub>2</sub>CO has been reported<sup>16</sup> to be  $12.6 \pm 0.2$  mdyn/Å. Shirk and Pimentel have shown that  $k(\text{CO})$  in HCO, FCO, and ClCO also are relatively insensitive to the electronegativity of the attached atom.

The case of the X<sub>2</sub>CO thus seems to be qualitatively different from those of X<sub>3</sub>PO<sup>17</sup> and XSO<sub>2</sub>Y,<sup>18</sup> where the -PO and -SO<sub>2</sub> frequencies seem to be insensitive to the masses of X and Y and where the change in MO force constants can be attributed to the coming into play of the 3d orbitals.

*Acknowledgments.* The assistance of Dr. Brian G. Ward and Mr. Robert Delaplane is gratefully acknowledged. Acquisition of the infrared spectrometer was made possible by a National Science Foundation Institutional Facilities Grant.

(15) J. Overend and J. R. Scherer, *J. Chem. Phys.*, **32**, 1296 (1960).

(16) J. S. Shirk and G. C. Pimentel, *J. Amer. Chem. Soc.*, **90**, 3349 (1968).

(17) S. M. Chackalackal and F. E. Stafford, *ibid.*, **88**, 4823 (1966), and references cited therein.

(18) M. Spoliti, S. M. Chackalackal, and F. E. Stafford, *ibid.*, **89**, 1092 (1967), and references cited therein.

# Spectra of Metal $\beta$ -Ketoenolates. The Electronic Spectrum of Monomeric Nickel(II) Acetylacetonate and the Infrared Spectra of Matrix-Isolated Acetylacetonates of Cobalt(II), Nickel(II), Copper(II), and Zinc(II)

by J. P. Fackler, Jr.,<sup>1</sup> M. L. Mittleman, H. Weigold, and G. M. Barrow

Department of Chemistry, Case Western Reserve University, Cleveland, Ohio 44106 (Received July 5, 1968)

The ultraviolet electronic spectra of several nickel(II)  $\beta$ -ketoenolates in  $\text{CHCl}_3$  and hydrocarbon solvents are described and are shown to be consistent with the assignment of Cotton and Wise for the  $\sim 233$ - and  $\sim 268$ - $\mu$  bands. The vapor ultraviolet spectrum of nickel(II) acetylacetonate also shows these same bands, as expected for a planar species. The infrared spectra of  $\text{CO}_2$  matrix-isolated acetylacetonates of copper(II), nickel(II), cobalt(II), and zinc(II) are reported between 650 and 2200  $\text{cm}^{-1}$ . These spectra suggest the existence of similar (planar) structures for the nickel(II) and copper(II) monomeric species and similar (tetrahedral) structures for the zinc(II) and cobalt(II) complexes. Since previous infrared studies of metal acetylacetonates have ignored the fact that the anhydrous complexes are polymeric, it is fortunate that only minor differences exist between the spectra of the matrix-isolated copper(II) complex, the complex which has received the greatest study, and the crystalline material.

## Introduction

Numerous metal acetylacetonates are known to exist as oligomers in the solid state or in solutions of weakly coordinating solvents.<sup>2</sup> As a result, the early investigations<sup>3</sup> of the spectral properties of many of these complexes were subject to reinterpretation.<sup>4,5</sup> Since monomeric species of these acetylacetonates either were not known or are difficult to achieve, it has been assumed that the stereochemistry and spectra exhibited by the complex obtained from the ligand 1,1,6,6-tetramethylheptanedione (dipivaloylmethane, H-DPM), where the bulky *t*-butyl groups prevent polymerization, would be essentially the same as for the anhydrous monomeric acetylacetonate. Some evidence has been presented to support this view for the complexes of nickel(II),<sup>5</sup> cobalt(II),<sup>4</sup> copper(II),<sup>6</sup> and zinc(II).<sup>7</sup>

Dipivaloylmethane complexes of cobalt(II) and zinc(II),<sup>7</sup> among other bivalent metal ions,<sup>8</sup> have a  $\text{MO}_4$  stereochemistry which is essentially tetrahedral, while the copper(II) and nickel(II) complexes<sup>6</sup> display a planar  $\text{MO}_4$  structure. The acetylacetonate complexes of all four bivalent metal ions are polymeric. Only copper(II) acetylacetonate<sup>9</sup> displays a stereochemistry in the crystalline phase which is even grossly similar to that of the DPM analog. Oligomeric nickel(II) and cobalt(II) acetylacetonates can be made to dissociate<sup>4,5</sup> at least partially in hydrocarbon solvents so some physical properties of the monomer can be deduced and compared with the DPM species. However, few studies have been conducted with these acetylacetonates under conditions which greatly reduce or eliminate oligomers.

While Shibata<sup>10</sup> has indicated that nickel(II) acetylacetonate,  $\text{Ni}(\text{acac})_2$ , is planar in the gas phase, the results seemed sufficiently inaccurate to make them questionable. Thus we considered it desirable to verify this configuration for the gas-phase molecule by an alternate technique. By studying the ultraviolet spectrum of  $\text{Ni}(\text{acac})_2$  and other nickel(II)  $\beta$ -ketoenolates at very low concentrations in hydrocarbon solvents and by comparing these spectra with the ultraviolet spectrum of  $\text{Ni}(\text{acac})_2$  in the gaseous phase, we have been able to confirm the fact that monomeric  $\text{Ni}(\text{acac})_2$  is indeed planar. Furthermore, some interesting features of the ultraviolet spectra have been uncovered.

In addition to electronic spectral studies of  $\text{Ni}(\text{acac})_2$ , we have examined the infrared spectra of the cobalt(II), nickel(II), copper(II), and zinc(II) complexes under conditions suggestive of the presence of only monomers. Since low vapor pressures for the gaseous species pro-

(1) Author to whom correspondence should be addressed.

(2) (a) J. P. Fackler, Jr., *Progr. Inorg. Chem.*, **7**, 361 (1965); *Advances in Chemistry Series*, No. 62, American Chemical Society, Washington, D. C., 1966, p 580; (b) F. A. Cotton and R. Eiss, *J. Amer. Chem. Soc.*, **90**, 38 (1968).

(3) G. Maki, *J. Chem. Phys.*, **28**, 651 (1961); **29**, 162 1129 (1959); A. D. Liehr and C. J. Ballhausen, *J. Amer. Chem. Soc.*, **81**, 538 (1959); R. H. Holm and F. A. Cotton, *ibid.*, **80**, 5658 (1958).

(4) F. A. Cotton and R. H. Soderberg, *Inorg. Chem.*, **3**, 1 (1964).

(5) J. P. Fackler, Jr., and F. A. Cotton, *J. Amer. Chem. Soc.*, **82**, 5005 (1960); **83**, 2818, 3775 (1961).

(6) F. A. Cotton and J. J. Wise, *Inorg. Chem.*, **5**, 1200 (1966).

(7) F. A. Cotton and J. S. Wood, *ibid.*, **3**, 245 (1964).

(8) J. P. Fackler, Jr., D. G. Holah, D. A. Buckingham, and J. T. Henry, *ibid.*, **4**, 920 (1965).

(9) L. Dahl, *Mol. Phys.*, **5**, 169 (1962).

(10) S. Shibata, *Bull. Chem. Soc. Jap.*, **30**, 753 (1957).

duce monomers,<sup>11</sup> we have deposited these species in a carbon dioxide matrix held at 77°K and have studied their spectra over the 650–2000-cm<sup>-1</sup> region.

### Experimental Section

*Preparation of Compounds.* All the compounds were prepared by standard methods described in the literature<sup>1</sup> and were purified by vacuum sublimation. The sublimation was effected at 116–120° for the zinc(II) compound, 130–135° for the cobalt(II) compound, 195–200° for the copper(II) compound, and 230–235° for the nickel(II) compound.

The matrix gas, carbon dioxide, used was Matheson Coleman instrument grade purified by repeated distillation from an acetone–Dry Ice bath. No water bands were observed in a matrix of carbon dioxide purified by this method.

Solvents used were spectral grade when available. The hydrocarbons *n*-decane and *n*-undecane were shaken with 20% fuming H<sub>2</sub>SO<sub>4</sub> until no further coloration of the acid layer was seen and then they were distilled. Spectral grade CHCl<sub>3</sub> was shaken with H<sub>2</sub>SO<sub>4</sub>(c), dilute NaOH, and water and was distilled from phosphoric anhydride to remove the ethanol stabilizer.

*Spectral Measurements.* Infrared spectra were recorded on a Beckman IR-7 spectrophotometer, wavelength calibrated with polystyrene and CO<sub>2</sub>. Electronic spectra at various temperatures were recorded with a Beckman DK-2 spectrophotometer using a thermostated high-temperature cell holder. The vapor spectrum of nickel(II) acetylacetonate was obtained using a 6-cm quartz cell wrapped with a heating jacket. Approximately 50 mg of the complex was sealed into an unheated Pyrex side arm on the cell which was heated to ~190° and evacuated overnight. After cooling, crystals of the complex were tapped into the cell under vacuum. A background spectrum was recorded on the Beckman DU spectrophotometer, and then the cell was heated to record the vapor spectrum of the complex at 190 ± 10°.

*Matrix Isolation.* The glass cryostat used was of the double-Dewar design.<sup>12</sup> The temperature of the copper block and of the cold window could be monitored with copper–constantan thermocouples. CsBr was used for the window material. The Knudsen cell, constructed of Type 2020 carbon from Stackpole Carbon, was heated by wrapping the glass jacket with a heating tape. A constant check on the temperature of the cell was kept using an iron–constantan thermocouple. The temperature of the Knudsen cell during spray-on of the acetylacetonates was 27–31° for zinc, 84° for cobalt, 130–135° for copper, and 170–174° for nickel. Spray-on times were in the range of 6–10 hr, the carbon dioxide being deposited at a rate of approximately 0.5 mmol/hr. The design of the spray-on apparatus, together with the lack of knowledge of the vapor pres-

sure of the species, did not allow us to calculate the matrix-to-complex ratio, M:A. However, from a comparison of the intensity of the absorption bands and a knowledge of the amount of CO<sub>2</sub> deposited, the M:A ratio for some of the complexes was estimated to have been varied by a factor of about 5 without any detectable difference being observed in the spectra of the species in the matrix.

*Molecular Complexity of Zinc(II) Acetylacetonate in Benzene.* The molecular weight of zinc(II) acetylacetonate, mp 129–131°,<sup>13</sup> was determined in benzene at concentrations up to 0.06 M using a Mechrolab osmometer. The average molecular weight obtained was 285 (calcd, 263). The ultraviolet spectrum in decane shows a peak at 292 mμ, ε 2.1 × 10<sup>4</sup> l. mol<sup>-1</sup> cm<sup>-1</sup>, which obeys Beer's law to a concentration of ~10<sup>-3</sup> M, the maximum allowable concentration with which an ultraviolet spectrum could be obtained using 0.1-mm cells.

### Results and Discussion

*Electronic Spectra of Nickel(II) Complexes.* The electronic spectrum in the ultraviolet region for the Ni(DPM)<sub>2</sub> and Cu(DPM)<sub>2</sub> complexes has been discussed recently by Cotton and Wise.<sup>14</sup> These authors concluded that the electronic transition which occurs near 233 mμ (~43,000 cm<sup>-1</sup>) largely corresponds to a σ<sub>L</sub>→3d<sub>xy</sub> (ligand-to-metal) charge transfer, based on molecular orbital calculations.<sup>15</sup> The transition near 268 mμ (~37,300 cm<sup>-1</sup>) is assigned to the π<sub>L</sub>→π<sub>L</sub>\* transition expected in this region. These bands are labeled I and II, respectively.

The electronic spectra in the ultraviolet region for five anhydrous β-ketoenolates of nickel(II) in CHCl<sub>3</sub> and hydrocarbon solvents are presented in Table I. These results lead us independently to make<sup>16</sup> assignments for bands I and II similar to the assignments of Cotton and Wise.<sup>14</sup> Furthermore, the shifts we have observed (Table I) in band I with changes in the ligand agree quite well with changes to be expected for a σ<sub>L</sub>→metal charge transfer. In accord with earlier spectral studies on β-ketoenolates of copper(II),<sup>17</sup> a σ<sub>L</sub>→metal charge-transfer band would be expected to shift to lower energy in the order Ni(acac)<sub>2</sub> > Ni(DIBM)<sub>2</sub> > Ni(DPM)<sub>2</sub>. The magnitude of the shift

(11) K. D. Carlson, J. P. Fackler, F. Kohl, and M. Uy, unpublished mass spectroscopic results; see also C. G. MacDonald and J. S. Shannon, *Aust. J. Chem.*, **19**, 1545 (1966).

(12) J. Rogers, M.S. Thesis, Case Institute of Technology, 1965.

(13) G. Rudolph and M. C. Henry, *Inorg. Chem.*, **3**, 1317 (1964).

(14) F. A. Cotton and J. J. Wise, *ibid.*, **6**, 917 (1967).

(15) F. A. Cotton, C. B. Harris, and J. J. Wise, *ibid.*, **6**, 909 (1967); F. A. Cotton and J. J. Wise, *ibid.*, **6**, 915 (1967).

(16) M. Middleman, M.S. Thesis, Case Institute of Technology, 1965.

(17) J. P. Fackler, Jr., F. A. Cotton, and D. W. Barnum, *Inorg. Chem.*, **2**, 97 (1963); J. P. Fackler, Jr. and F. A. Cotton, *ibid.*, **2**, 102 (1963).



**Table I:** Ultraviolet Spectra of Some  $\beta$ -Ketoenolate Complexes of Nickel(II)

Complex <sup>a</sup>	Solvent	Concn, <i>M</i>	Temp, °C	$\lambda$ , <i>m</i> $\mu$ ; log $\epsilon$		
				O <sub>b</sub>	II	I
Ni(acac) <sub>2</sub>	C <sub>8</sub> H <sub>12</sub>	7.0 × 10 <sup>-4</sup>	25	298; 4.34		
			71	298; 4.04 <sup>b</sup>	265; 4.04 <sup>c</sup>	223; 3.88 <sup>c</sup>
Ni(acac) <sub>2</sub>	CHCl <sub>3</sub>	10 <sup>-4</sup>	25	298; 4.34	265; 4.44	228
Ni(DPM) <sub>2</sub>	C <sub>11</sub> H <sub>24</sub>	10 <sup>-3</sup>	25		265; 4.61	233; 4.43
Ni(DPM) <sub>2</sub>	CHCl <sub>3</sub>	10 <sup>-3</sup>	25		268; 4.76	233
Ni(DIBM) <sub>2</sub> <sup>a</sup>	C <sub>10</sub> H <sub>22</sub>	10 <sup>-4</sup>	25	304; 4.25 <sup>b</sup>	268; 4.20 <sup>c</sup>	232; 3.97 <sup>c</sup>
			71			
Ni(DIBM) <sub>2</sub> <sup>a</sup>	CHCl <sub>3</sub>	10 <sup>-4</sup>		304; 3.86	268; 4.52	234; 4.34
Ni(3-CH <sub>3</sub> acac) <sub>2</sub>	C <sub>8</sub> H <sub>12</sub>	2.7 × 10 <sup>-3</sup>	25	313; 4.10 <sup>b</sup>	263; 4.32 <sup>c</sup>	223; 4.23 <sup>c</sup>
			71			
Ni(3-CH <sub>3</sub> acac) <sub>2</sub>	CHCl <sub>3</sub>	1.6 × 10 <sup>-3</sup>	25		263; 4.41	224; 4.30
Ni(3-Cl-acac) <sub>2</sub>	C <sub>8</sub> H <sub>12</sub>	5.0 × 10 <sup>-4</sup>	25	322; 4.30 <sup>b</sup>	263 <sup>c</sup>	
			71 <sup>d</sup>			
Ni(3-Cl-acac) <sub>2</sub>	CHCl <sub>3</sub>	1.7 × 10 <sup>-3</sup>	25	320; 4.43	263; 4.52	
Ni(3-Ph-acac) <sub>2</sub>	C <sub>8</sub> H <sub>12</sub>	3.9 × 10 <sup>-3</sup>	25	316; 4.15 <sup>b</sup>	271; 4.23 <sup>c</sup>	
			71			
Ni(3-Ph-acac) <sub>2</sub>	CHCl <sub>3</sub>	2.4 × 10 <sup>-4</sup>	25		271; 4.54	

<sup>a</sup> acac, acetylacetonate; HDIBM, diisobutylmethane; HDMP, dipivaloylmethane; H(3-CH<sub>3</sub>acac), 3-methyl-2,4-pentanedione; H(3-Cl-acac), 3-chloro-2,4-pentanedione; H(3-Ph-acac), 3-phenyl-2,4-pentanedione. <sup>b</sup> Intensity decreases with heating. <sup>c</sup> Intensity increases with heating. <sup>d</sup> Decomposes with heating.

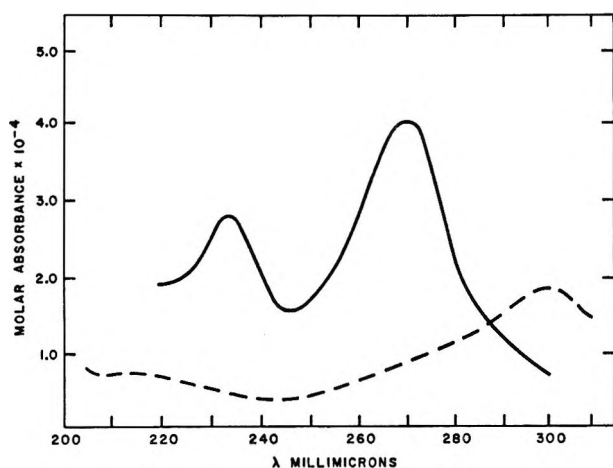


Figure 1. The ultraviolet spectrum of Ni(DPM)<sub>2</sub>: —, Ni(DPM)<sub>2</sub> in undecane; ---, Ni(DPM)<sub>2</sub> in methanol.

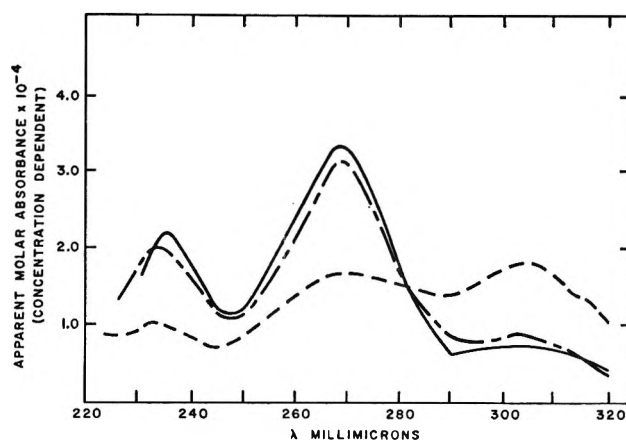


Figure 2. The ultraviolet spectrum of Ni(DIBM)<sub>2</sub>: —, Ni(DIBM)<sub>2</sub> in chloroform; ---, Ni(DIBM)<sub>2</sub> in decane (25°); - · - ·, Ni(DIBM)<sub>2</sub> in decane (71°).

even appears to be about the same for the copper(II) and nickel(II) complexes.

The band labeled O<sub>b</sub> in Table I corresponds to the  $\pi \rightarrow \pi^*$  transition in the "ionic," six-coordinate, pseudo-octahedral (paramagnetic) nickel(II) complexes where the coordination about the metal arises from either polymerization or adduct interaction. As readily seen in Figure 1, dissolution of Ni(DPM)<sub>2</sub> in the coordinating solvent methanol, a solvent well known to produce a pseudo-octahedral, paramagnetic nickel(II) dipivaloylmethane complex,<sup>18</sup> produces a spectrum wherein the principal ultraviolet band appears near 300 *m* $\mu$ . Hence we can confidently assume that the band labeled O<sub>b</sub> in Table I is associated with the polymeric  $\beta$ -ketoenolate species.

The disappearance of the O<sub>b</sub> band for Ni(3-CH<sub>3</sub>acac)<sub>2</sub> and Ni(3-Ph-acac)<sub>2</sub> in CHCl<sub>3</sub> as opposed to its presence in a hydrocarbon solvent and the observation in Figure 2 that the spectra of Ni(DIBM)<sub>2</sub> in decane at 71° and CHCl<sub>3</sub> at room temperature are nearly identical clearly shows a dependence of the polymerization of the complex on the solvent. Ni(DIBM)<sub>2</sub> has been known to exhibit a monomer-oligomer equilibrium in cyclohexane which is temperature dependent.<sup>5</sup> Thus chloroform interacts with the complex specifically to reduce the degree of polymerization at a given temperature.<sup>19</sup> This increased monomer formation in CHCl<sub>3</sub> is presumably associated with the ability of the CHCl<sub>3</sub> to

(18) P. E. Rakita, S. J. Kopperl, and J. P. Fackler, Jr., *J. Inorg. Nucl. Chem.*, **30**, 2139 (1968).

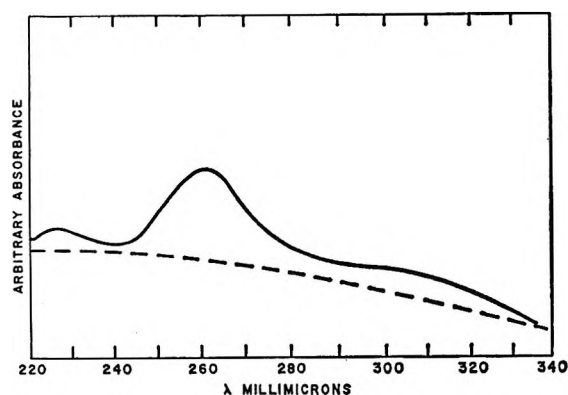


Figure 3. The vapor ultraviolet spectrum of  $\text{Ni}(\text{acac})_2$ : —,  $190 \pm 10^\circ$ ; --- background (before heating).

hydrogen bond<sup>20</sup> with the monomer more effectively than with the polymer.

From the results discussed above, it is quite apparent that the ultraviolet spectrum of  $\text{Ni}(\text{acac})_2$  in the vapor phase at  $190^\circ$ , Figure 3, corresponds with the spectrum expected for a monomeric planar  $\beta$ -ketoenolate complex of nickel(II). Recognizing the likelihood that a tetrahedral  $\text{NiO}_4$  system would be paramagnetic and thus undoubtedly give rise to a significantly different ultraviolet spectrum (no tetrahedral  $\text{NiO}_4$  species with  $\beta$ -ketoenolates have been observed or are suggested for monomeric species in solution), the ultraviolet bands observed near 260 and 225  $\mu$  clearly substantiate the presence of a planar configuration in the gas-phase, monomeric  $\text{Ni}(\text{acac})_2$  species.<sup>10</sup>

**Infrared Spectra.** The energies of the spectral bands found in the region of 650–2000  $\text{cm}^{-1}$  in a carbon dioxide matrix at  $77^\circ\text{K}$ , in a warmed matrix at room temperature, and in the polymeric material at  $77^\circ\text{K}$  are given in Tables II–V for the four complexes investigated. The band positions reported by Nakamoto, *et al.*,<sup>21</sup> for the complexes in a KBr pellet are included for comparison. The infrared spectrum of the copper complex has come under thorough investigation by two independent groups. Nakamoto, *et al.*,<sup>21</sup> and Mikami, *et al.*,<sup>22</sup> have assigned all the spectral bands found for this compound in the solid state on the basis of normal coordinate analyses. The results obtained by these two groups are quite similar, but one must consider the results of the latter group to be the more reliable, as in their study the whole molecule was considered in the normal coordinate treatment (a  $D_{2h}$  symmetry being assigned to the complex), whereas Nakamoto, *et al.*,<sup>21</sup> based their calculations on a 1:1 complex (symmetry  $C_{2v}$ ). Also, Mikami, *et al.*,<sup>22</sup> considered all the atoms in their treatment, while Nakamoto, *et al.*,<sup>21</sup> included only the skeletal atoms in their coordinate analysis. Both groups fitted their analyses to the spectrum of the polymeric  $\text{Cu}(\text{acac})_2$  species, which, fortunately, is not significantly different from that of the monomer.

In comparing the infrared spectra taken at low tem-

Table II: Infrared Absorption Bands for Bis(acetylacetonato)copper(II) ( $\text{cm}^{-1}$ )

In $\text{CO}_2$ matrix	At $77^\circ\text{K}^a$ (not in matrix)	At room temp <sup>b</sup>	KBr pellet (room temp)
1629 w			
1582 s	1579 s	1580 s	1580 s
	1557 s	1554 s	1554 s
1531 s	1531 s	1531 s	1534 s
		1518 sh, s	
1462 m	1467 m	1458 m	1464 m
1426 m	1417 sh, s		
1406 s	1410 s	1413 s	1415 s
1358 m	1354 m	1356 m	1356 m
1280 m	1277 m	1276 m	1274 m
1260 w	1260 w	1261 w	
1246 sh, w			
1196 w	1191 w	1190 w	1190 w
1028 m	1023 m	1021 m	1020 m
1022 sh, m			
942 m	938 w	936 w	937 w
808 w	805 w	805 w	
		784 sh, m	
779 w	782 m	780 m	781 m
	687 w	687 w	684 w
		652 w	654 w

<sup>a</sup> Complex deposited from vapor without the  $\text{CO}_2$  matrix.

<sup>b</sup> Complex in a  $\text{CO}_2$  matrix warmed up to room temperature (w, weak; s, strong; m, medium; sh, shoulder).

peratures (*viz.*  $77^\circ\text{K}$ ) with those at room temperature, one expects to find a sharpening up of the bands in the low-temperature spectrum owing to the decreased population of the higher vibrational states of the molecule. Hence bands at room temperature may well be resolved as doublets at  $77^\circ\text{K}$ . If one considers only the CH bands of the copper complex, it is seen that the absorbances found at 1415, 1020, and 781  $\text{cm}^{-1}$  in the solid state are split when the complex is placed into a carbon dioxide matrix at  $77^\circ\text{K}$ . Further, except for the 1020- $\text{cm}^{-1}$  band which is only weakly split in the matrix, this splitting is seen in the spectrum of the vapor-deposited complex<sup>23</sup> at  $77^\circ\text{K}$ . The spectra will be discussed individually for each of the four title compounds.

**Bis(acetylacetonato)copper(II).** For the copper complex most bands appear at similar energies in both the matrix-isolated species and the sprayed-on solid at room temperature.<sup>23</sup> There are some exceptions, but

(19) Red solutions of  $\text{Ni}(\text{DIBM})_2$  and  $\text{Ni}(\text{3-Ph-acac})_2$ , a color typical of the diamagnetic planar species, can be achieved in mixed hydrocarbon-chloroform solvents at concentrations and temperatures where the absence of  $\text{CHCl}_3$  would cause the solutions to appear green (the six-coordinate species tend to be green or blue-green).

(20) T. S. Davis and J. P. Fackler, Jr., *Inorg. Chem.*, **5**, 242 (1966).

(21) K. Nakamoto, P. J. McCarthy, and A. E. Martell, *J. Am. Chem. Soc.*, **83**, 1272 (1961), and references cited within.

(22) M. Mikami, I. Nakagawa, and T. Shimamouchi, *Spectrochim. Acta*, **23**, 1037 (1967).

(23) Vapor deposition of the complexes on the window at room temperature presumably gives the polymeric species, as this is the technique used to grow single crystals of the complexes for X-ray studies.

**Table III:** Infrared Absorption Bands for Bis(acetylacetonato)nickel(II) ( $\text{cm}^{-1}$ )

In $\text{CO}_2$ matrix (77°K)	At 77°K <sup>a</sup> (not in matrix)	At room temp <sup>b</sup>	KBr pellet (room temp)
1626 w	1617 sh, w		
1572 s	1570 s	1588 s	1598 s
1564 sh, w		1572 sh, s	
1533 s	1527 s	1517 s	1514 s
1461 w	1460 m	1450 m	1453 m
1428 m	1424 m		
1399 s	1391 s	1393 s	1398 s
1362 m	1358 m	1368 s	1367 s
1293 w	1289 w		
1264 w	1263 w	1262 m	1261 m
1252 sh, w			
1194 w	1192 w	1196 w	1198 w
1087 sh, w			
1036 m	1020 m	1020 m	1020 m
1023 m			
955 m	927 m	927 m	929 m
945 m			
808 m	778 m	777 m	
782 m	765 sh, m	764 w	764 w
693 m	674 w	673 w	
		656 w	666 w

<sup>a</sup> See footnote a, Table II. <sup>b</sup> See footnote b, Table II.

**Table IV:** Infrared Absorption Bands for Bis(acetylacetonato)zinc(II) ( $\text{cm}^{-1}$ )

In $\text{CO}_2$ matrix (77°K)	At 77°K <sup>a</sup> (not in matrix)	At room temp <sup>b</sup>	KBr pellet (room temp)
1579 s	1589 s	1597 s	1592 s
1528 s	1524 s	1528 s	1523 s
1457 m	1456 m	1463 sh	1464 sh
1427 m	1423 m	1450 m	
1390 s	1397 } s	1402 s	1394 s
	1383 } sh, s		
1363 m	1362 s	1375 } s	1361 s
		1367 } s	
1267 } m	1268 m	1263 s	1264 s
1263 } m			
1198 w	1198 w	1207 } w	1197 w
		1197 } w	
1021 m	1017 m	1019 m	1019 m
931 m	925 m	928 m	927 m
777 } m	773 w	807 } w	769 w
766 } m		788 } w	
728 } w			
717 } w			

<sup>a</sup> See footnote a, Table II. <sup>b</sup> See footnote b, Table II.

these arise as discussed above owing to the observation of a doublet instead of the unresolved singlet. Certainly the spectrum of the matrix-isolated species and that of the compound at 77°K are very similar, the absorption bands for the two species being in general within five wave numbers of each other. This fact tends to confirm the hypothesis of Mikami, *et al.*,<sup>22</sup> that even though the copper complex is not planar and

because the acetylacetonate ligand molecules do have  $C_{2v}$  symmetry, the absorption bands of the complex may be discussed assuming a molecule of  $D_{2h}$  symmetry. However, in the matrix-isolated species, a weak band is found at  $1629\text{ cm}^{-1}$  which has not been accounted for by either Mikami, *et al.*,<sup>22</sup> or Nakamoto, *et al.*,<sup>21</sup> This band is also observed for the nickel complex in a carbon dioxide matrix and in the cobalt complex as a shoulder. It is absent in the zinc(II) complex. Further, in the copper complex, the strong band at  $1554\text{ cm}^{-1}$  is found only for the polymeric and not for the matrix-isolated species. Nakamoto, *et al.*,<sup>21</sup> assigned this band and the one at  $1534\text{ cm}^{-1}$  to a mode consisting of 75% C=O stretch and 25% C=C stretch, but they indicated that they do not have a ready explanation why this band should be split. Mikami, *et al.*,<sup>22</sup> did not attempt to assign this band. It therefore appears probable, since this band is not found in the matrix-isolated species, that the distortion of the complex from planarity, owing to intermolecular interactions, may be sufficient to cause this band to split. The spectra obtained in this work also differ from those measured by Nakamoto, *et al.*,<sup>21</sup> in that we have observed an additional weak band at  $1260\text{ cm}^{-1}$ . This band is of similar energy for the polymeric species and for the matrix-isolated molecule. From the coordinate analyses, the band at  $1274\text{ cm}^{-1}$  has been assigned to a  $B_{1u}$  transition arising from a C=C stretch (28%) and a C-CH<sub>3</sub> stretch (50%) mode. The  $1260\text{-cm}^{-1}$  band is tentatively considered to result from the splitting of the  $1274\text{-cm}^{-1}$  band, the complex having a symmetry lower than  $D_{2h}$ . Absorptions are also found on the high-energy side of the  $1028\text{-cm}^{-1}$  band. The shape of this band varies on changing the temperature and also on going from polymer to monomer at liquid nitrogen temperature. Mikami, *et al.*,<sup>22</sup> assigned a band at  $1055\text{ cm}^{-1}$  (not observed by us or Nakamoto, *et al.*<sup>21</sup>) to a CH<sub>3</sub> degenerate rocking mode.

*Bis(acetylacetonato)nickel(II)*. The general features of the spectrum of this planar, monomeric complex in the carbon dioxide matrix are very similar to that of the matrix-isolated copper species, which undoubtedly has a very similar structure. It is of interest to note that the  $1582\text{-cm}^{-1}$  band of the copper complex has been shifted  $10\text{ cm}^{-1}$  to lower energies in the matrix-isolated nickel complex, whereas the  $1531\text{-cm}^{-1}$  band is nearly of the same energy in both the copper and nickel species. Since the  $1582\text{-cm}^{-1}$  band is predominantly due to the C=C stretching mode, whereas the  $1531\text{-cm}^{-1}$  band is associated predominantly with a C=O stretching mode, the change in the energy of the  $1582\text{-cm}^{-1}$  band may possibly reflect a difference in the electronic properties of the structure of the two complexes. Differences in the  $\pi \rightarrow \pi^*$  transitions of the isomorphous Ni(DPM)<sub>2</sub> and Cu(DPM)<sub>2</sub> have been noted.<sup>6</sup> Also, the  $1582\text{-cm}^{-1}$  band in the copper complex is quite insensitive to the temperature of the complex or

whether it is matrix isolated, but the band in the nickel complex is extremely sensitive to these conditions. Thus, as reported by Nakamoto, *et al.*,<sup>21</sup> the band appears at 1598  $\text{cm}^{-1}$  in a KBr pellet. It is shifted to lower energies (1588  $\text{cm}^{-1}$ ) in the pure complex at room temperature and then is further displaced to 1570  $\text{cm}^{-1}$  when cooled to 77°K. The shoulder at 1564  $\text{cm}^{-1}$  is considered to arise from the overlap of the two adjacent strong high-energy bands. The splitting of the band around 1028  $\text{cm}^{-1}$  observed for the copper complex is much more prominent in the nickel complex. Further, the band around 950  $\text{cm}^{-1}$  is split into a doublet, the maxima occurring at energies of 954 and 945  $\text{cm}^{-1}$ .

*Bis(acetylacetonato)zinc(II)*. In the absence of polymerization, it is found that in general the tetra-coordinate zinc(II) complexes are tetrahedral.<sup>7</sup> For the complex observed here, one expects the monomer to be tetrahedral. The species formed on vaporization of this complex was isolated in a carbon dioxide matrix. The infrared spectrum of the matrix-isolated species was found to compare closely with that of the copper complex, except that in the zinc spectrum no splitting of the 1020- $\text{cm}^{-1}$  band was observed. Further, the CH out-of-plane bending mode is shifted to lower energies in the zinc complex. This band still exists as a doublet, the band maxima lying at 777 and 766  $\text{cm}^{-1}$ . Based on the infrared spectrum in the region investigated alone, it is not possible to deduce *a priori* the symmetry of the matrix-isolated species (however, see the discussion for  $\text{Co}(\text{acac})_2$ ).

The infrared spectrum is dependent upon the physical conditions under which the investigation is made. As is found for the nickel complex, the absorption band arising from the predominantly C=C stretching mode is shifted 16  $\text{cm}^{-1}$  to lower energies from the solid at room temperature to the matrix-isolated species. A second band which does exhibit a very large shift on cooling is that band found at 1450  $\text{cm}^{-1}$  at room temperature. Makami, *et al.*,<sup>22</sup> assigned this band, for the copper complex, to a  $\text{CH}_3$  degenerate deformation (out of plane). It is noted that this band was not observed by Nakamoto, *et al.*,<sup>21</sup> in the KBr pellet of this complex nor in the nickel and copper complexes. The doublet (CH out-of-plane bending) near 800  $\text{cm}^{-1}$  is a doublet at room temperature, a singlet at 77°K, and again a doublet in the matrix-isolated species. Furthermore, the energies of these bands vary appreciably. The room-temperature doublet at 788, 807  $\text{cm}^{-1}$  is a singlet at 773  $\text{cm}^{-1}$  for the

polymer cooled to 77°K. These bands appear at 766 and 777  $\text{cm}^{-1}$  for the matrix-isolated complex.

*Bis(acetylacetonato)cobalt(II)*. Tetracoordinated cobalt(II) has been shown to exist in both square-planar and tetrahedral configurations.<sup>4</sup> A  $\text{CoO}_4$  system such as is found in the monomer of this complex is expected to be tetrahedral ( $D_{2d}$ ).<sup>4</sup> An essentially tetrahedral arrangement of the oxygens about the cobalt is found for  $\text{Co}(\text{DPM})_2$ .<sup>7</sup> The infrared absorption spectrum of the matrix-isolated species is very similar to that found for the corresponding zinc(II) complex. The only band to show an appreciable energy shift is the  $\text{CH}_3$  degenerate deformation band found at 1390  $\text{cm}^{-1}$  for the zinc complex and 1402  $\text{cm}^{-1}$  for the cobalt species. The doublet near 800  $\text{cm}^{-1}$  in the matrix-isolated species is also present in the polymeric species at 77°K but is absent in the room-temperature spectrum. A further point of interest is that the band at 1080  $\text{cm}^{-1}$  for the polymer at 77°K, which might be assigned to the  $\text{CH}_3$  degenerate rocking mode according to the results of Makami, *et al.*,<sup>21</sup> on the copper complex, was absent in the matrix-isolated species. (See Table V.)

**Table V:** Infrared Absorption Bands for  $\text{Bis}(\text{acetylacetonato})\text{cobalt}(\text{III})$  ( $\text{cm}^{-1}$ )

In $\text{CO}_2$ matrix (77°K)	At 77°K <sup>a</sup> (not in matrix)	At room temp <sup>b</sup>	KBr pellet (room temp)
1615 sh			
1584 s	1588 s	1589 s	1610 s
1524 s	1518 s	1512 s	1513 s
1463 m	1461 m	1450 sh	1461 sh
1428 m	1421 m		
1402 s	1396 s	1395 s	1398 s
1364 m	1358 s	1362 s	1366 s
1265 m	1258 m	1256 m	1261 m
1198 w	1196 w	1193 w	1199 w
	1080 w		
1010 m	1018 m	1017 m	1020 m
929 m	924 m	922 m	931 m
776 } m	807 w		
766 } m	771 w	768 w	767 w
731 } w			
713 } w			

<sup>a</sup> See footnote a, Table II; <sup>b</sup> See footnote b, Table II.

*Acknowledgments.* We are pleased to acknowledge the support of the National Science Foundation, GP-2850, for these studies.

## Catalytic Polarographic Current of a Metal Complex.<sup>1</sup> IV. Effect of the Electrode Double Layer on the Ni(II)-*o*-Phenylenediamine Prewave<sup>2</sup>

by Lowell R. McCoy, Harry B. Mark, Jr.,

*Department of Chemistry, University of Michigan, Ann Arbor, Michigan 48104*

and Lucien Gierst

*Department of Chemistry, Free University of Brussels, Brussels, Belgium (Received July 8, 1968)*

A study of the Ni(II)-*o*-phenylenediamine prewave has shown that a pronounced double-layer effect is observed when measurements are made of polarographs obtained with various types and concentrations of supporting electrolytes. The effect on the prewave is qualitatively consistent with theoretical predictions when the concentration of the electrolyte is not so high as to invalidate the assumptions employed in the theoretical treatment. The results of this investigation support the existence of a surface-controlled chemical reaction involving an adsorbed ligand and the nickel ion diffusing to the electrode. The conclusion by Tur'yan and Malyavinskaya that the chemical rate-limiting reaction involves the formation of an electroactive Ni(II)-*o*-phenylenediamine complex in the bulk of the solution well beyond the influence of the electrode double layer is therefore incorrect. A quantitative analysis of the relationship between the height of the prewave and the potential of the outer Helmholtz plane indicates that the charge on the electroactive species in the rate-determining step is +1 rather than +2 as expected from the charge of the hexaaquonickel ion. The reason for this disagreement may lie in the adsorption behavior of the ligand.

A number of investigators<sup>2,3-7</sup> have reported the appearance of prewaves during the polarographic reduction of Ni(II) in the presence of complexing agents such as pyridine, *o*-phenylenediamine, ethylenediamine, triethylenetetramine, chloride ion, etc. These prewaves can arise several hundred millivolts positive to the main reduction wave of Ni(H<sub>2</sub>O)<sub>6</sub><sup>2+</sup>. The height of the prewave varies directly with the concentrations of ligand and nickel ion. Shifts of the entire Ni(II) wave to more positive potentials in the presence of certain anions of the supporting electrolytes such as chloride and thiocyanate and large excesses of pyridinium salts have been recognized for some time and have been used as an analytical method of separating the nickel wave from that of other metal ions having similar half-wave potentials, *i.e.*, cobalt.<sup>8</sup> In these cases the complexing agent is present in great excess with respect to the nickel ion concentration, and no separate prewave can be distinguished.

From a study of the prewave obtained with Ni(II) and *o*-phenylenediamine,<sup>2a,2b,4</sup> it was concluded that the mechanism involved a rate-limiting chemical reaction between the hexaaquonickel ion and the adsorbed ligand in the sequence shown in eq 1 and 2. The adsorbed ligand is cyclically regenerated by the electrochemical reduction of the adsorbed complex. This view has been disputed by Tur'yan and Malyavinskaya,<sup>9</sup> who stipulated that the electroactive complex is formed in the bulk of the solution in a rate-limiting homogeneous reaction between the hexaaquonickel ion and the regenerated ligand diffusing outward from the electrode surface. These writers supported their con-

clusion by a calculation of a reaction layer thickness based on an estimated equilibrium constant for the Ni(II)-ligand complex.

Gierst<sup>10</sup> has shown that the observed rate of an electrode process will be affected by the state of the electrode double layer where the reaction layer thickness for a rate-limiting chemical reaction is small relative to the thickness of the diffuse layer. A surface reaction involving an adsorbed ligand must fulfil this condition. Conversely, Tur'yan and Malyavinskaya<sup>9</sup> state that their calculated reaction layer thickness ( $3 \times 10^{-4}$  cm) precludes any double-layer effect. As the structure of the electrode double layer can be varied at

(1) This research was supported in part by grants from the National Science Foundation, Grants No. GP-4620 and GP-6425, and the U. S. Army Office of Research, Durham, N. C., No. DA-31-124-ARO-D-284.

(2) For other papers of this series see: (a) H. B. Mark, Jr. and C. N. Reilley, *J. Electroanal. Chem.*, **4**, 189 (1962); (b) H. B. Mark, Jr., *ibid.*, **7**, 276 (1964); (c) H. B. Mark, Jr., L. R. McCoy, E. Kirowa-Eisner, and H. C. MacDonald, Jr., *J. Phys. Chem.*, **72**, 1083 (1968).

(3) H. B. Mark, Jr. and C. N. Reilley, *Anal. Chem.*, **35**, 195 (1963).

(4) H. B. Mark, Jr., *ibid.*, **35**, 940 (1964); *J. Electroanal. Chem.*, **8**, 253 (1964).

(5) Ya I. Tur'yan and G. G. Serova, *Zh. Fiz. Khim.*, **31**, 1976 (1957); Ya. I. Tur'yan, *Dokl. Akad. Nauk SSSR*, **148**, 848 (1962); *Zh. Fiz. Khim.*, **39**, 257 (1965).

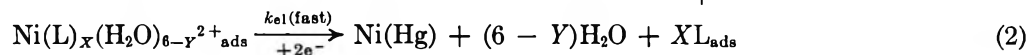
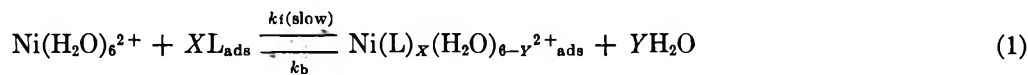
(6) I. V. Nelson and R. T. Iwamoto, *J. Electroanal. Chem.*, **6**, 234 (1963).

(7) D. C. Olson, *Anal. Chem.*, **39**, 1785 (1967).

(8) I. M. Kolthoff and J. J. Lingane, "Polarography," 2nd ed, Vol. II, Interscience Publishers, New York, N. Y., 1952, p 486.

(9) Ya I. Tur'yan and O. N. Malyavinskaya, *Elektrokhimiya*, **2**, 1185 (1966); *Sov. Electrochem.*, **2**, 1082 (1966).

(10) L. Gierst, *Trans. Symp. Electrode Processes*, 109 (1959).



will by changing the nature and/or concentration of the supporting electrolyte, a study of the effects of these variables on the observed height of the prewave thus offers an experimental method of resolving this question.

This paper will present the detailed results of such a study of the Ni(II)-*o*-phenylenediamine (OPDA) system.<sup>11</sup> The prewaves produced by this combination arise at potentials well separated from the main hexa-aquonickel wave, permitting calculations to be made with minimum interference or overlap from the main hexa-aquo wave. Also the  $pK_{a_2}$  of this ligand<sup>12</sup> ( $pK_{a_2} = 4.5$ ) permits measurements to be made in a reasonably broad pH range (6.5–7.5) where little of the Ni(II) is present as the hydroxyl complex, and yet the ligand exists almost wholly in its nonprotonated form in this range.<sup>3,4</sup>

### Experimental Methods

The methods and procedures employed in making the polarograms were generally the same as those reported previously<sup>2,3,4</sup> with a few exceptions. The drop time of the dropping mercury electrode (dme) was controlled mechanically at  $4.0 \pm 0.05$  sec.<sup>13</sup> No maximum suppressors such as the  $\text{Ca}^{2+}$  ion, used in the previous investigations,<sup>2,3,4</sup> were used here as they would complicate the double-layer studies. A three-electrode polarograph with a scan rate of 100 mV/min was employed.<sup>13</sup>

The supporting electrolytes and ligand solutions were prepared from triple-distilled water and analytical reagents. The latter were further purified where necessary by standard practices.<sup>13</sup> As the ligand (*o*-phenylenediamine) solutions are unstable in the presence of air, these were prepared using aliquots of deaerated electrolyte solution. Storage of the ligand solutions for prolonged periods was found to be feasible if these were frozen immediately after preparation and thawed just prior to use.

The pH of the polarographic solutions were adjusted to  $7.0 \pm 0.5$  where necessary by the addition of an acid or base corresponding to the cation or anion of the specific supporting electrolyte. The pH was monitored continuously during the course of the polarographic measurements, as some drifting was evident in dilute solutions of unbuffered reagents. The temperature of the solution in the polarographic cell was maintained at  $25 \pm 0.1^\circ$ .

### Qualitative Effect of the Type and Concentration of the Supporting Electrolyte

Where an electrochemical reaction is preceded by a surface rate-limiting chemical reaction involving an uncharged ligand, Gierst<sup>10</sup> has shown that the following expression describes the relationship between the "apparent" and "true" velocities of the reaction

$$v^* = v_0 \exp\left(-\frac{ZF}{RT}\psi^0\right) \quad (3)$$

In eq 3,  $v^*$  is the apparent velocity of the reaction calculated from the wave height where the surface concentration of a charged reactant is subject to perturbation by the electrode double layer;  $v_0$  is the true velocity that would be obtained in the absence of any effect from the double layer;  $Z$  is the charge of the reactant; and  $\psi^0$  is the potential of the outer Helmholtz plane.<sup>10</sup> The symbols,  $F$ ,  $R$ , and  $T$  have their usual electrochemical significance. For a preelectron-transfer association reaction taking place in the bulk of the solution,  $v_0$  is given by

$$v_0 = [\text{L}]^X \sqrt{DKk_t} \quad (4)$$

where  $[\text{L}]$  is the ligand concentration,  $D$  is the diffusion coefficient for the hexa-aquonickel ion,  $X$  is the stoichiometric coefficient of the ligand,  $K$  is the formation equilibrium constant for the Ni(II)-ligand complex, and  $k_t$  is the forward reaction rate constant. As this relationship has been derived for the case of a homogeneous equilibrium reaction of the type described by Tur'yan and Malyavinskaya,<sup>9</sup> it is not directly applicable to the proposed surface-reaction mechanism.<sup>2,3,4</sup> The quantity  $\sqrt{DKk_t}$  may be calculated from the ratio of the observed prewave height to the diffusion-limiting height, using a relationship derived by Koutecky.<sup>14</sup> Where a double-layer effect exists, however,  $v^*$  rather than  $v_0$  will be obtained by this process. The calculated value of  $v^*$  will then vary with  $\psi^0$  in the manner shown in eq 3. The quantity,  $Z$ , is expected to be  $+2$  for the hexa-aquonickel ion, and  $\psi^0$  will be negative over the electrode potential range of the prewave. Under otherwise identical conditions,  $v^*$  and therefore the prewave height will decrease as  $\psi^0$  becomes less nega-

(11) See ref 2c for a preliminary communication of part of the results of this study.

(12) R. T. Morrison and R. N. Boyd, "Organic Chemistry," Allyn and Bacon, Inc., Boston, 1959, p 544.

(13) L. R. McCoy, Ph.D. Thesis, University of Michigan, Ann Arbor, Mich., 1967; L. R. McCoy, H. B. Mark, Jr., and L. Gierst, unpublished results, 1967.

(14) J. Koutecky, *Coll. Czech. Chem. Commun.*, **18**, 597 (1953).

tive. At these electrode potentials, the Gouy-Chapman relationship shows that  $\psi^0$  will decrease as the concentration of the supporting electrolyte is increased.<sup>15</sup> Also for a given supporting electrolyte concentration, the choice of an electrolyte whose ions are specifically adsorbed will result in a more (anion adsorption) or less (cation adsorption) negative value of  $\psi^0$  than would be obtained for an electrolyte whose ions are not adsorbed. Thus measurement of polarograms obtained with various types and concentrations of electrolytes and with invariant reactant concentrations affords a ready means of observing the effect, if any, of the electrode double layer on the prewave.

In the study of the effect of variation of the concentration of the supporting electrolyte, lithium salts were used. The  $\text{Li}^+$  ion is the least specifically adsorbed cation available and its effects on  $\psi^0$  as a function of concentration are known.<sup>10</sup> Lithium perchlorate and lithium nitrate were the preferred electrolytes in these investigations, as neither anion is specifically adsorbed to a significant degree at electrode potentials of concern to the prewave region at moderate concentrations<sup>10,16</sup> and neither forms stable complexes and/or ion pairs with the  $\text{Ni(II)}$  cation.<sup>13,16</sup>

Prewaves obtained using a series of concentrations of lithium perchlorate are shown in Figure 1. Within the concentration range shown here, attenuation of both the prewave and the main hexaaquonickel wave with increasing electrolyte concentration is evident. The same results were obtained where lithium nitrate or lithium acetate were employed as the supporting electrolytes. When the concentration of these electrolytes exceeded 0.5 *M*, however, the opposite effect was produced, and the prewave either became static or began to rise in height with an increasing concentration of electrolyte. Prewaves obtained with the more concentrated solutions are shown in Figures 2 and 3.

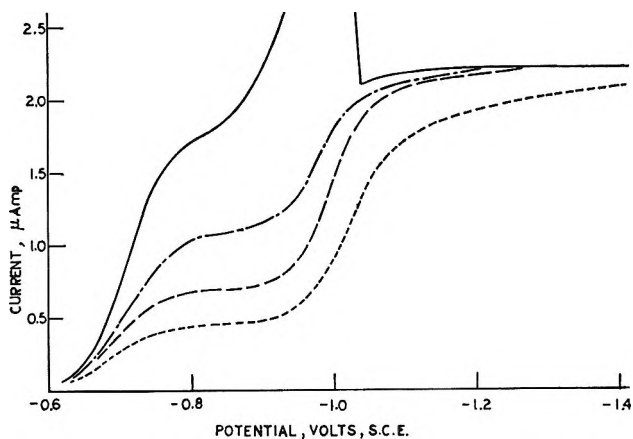


Figure 1. The effect of varying concentrations of lithium perchlorate upon the prewave height (low-concentration range,  $5 \times 10^{-4} M \text{ Ni}^{2+}$ ,  $1.6 \times 10^{-4} M \text{ OPDA}$ ): —, 0.05 *M*  $\text{LiClO}_4$ ; ---, 0.1 *M*  $\text{LiClO}_4$ ; — · —, 0.2 *M*  $\text{LiClO}_4$ ; · · ·, 0.5 *M*  $\text{LiClO}_4$ .

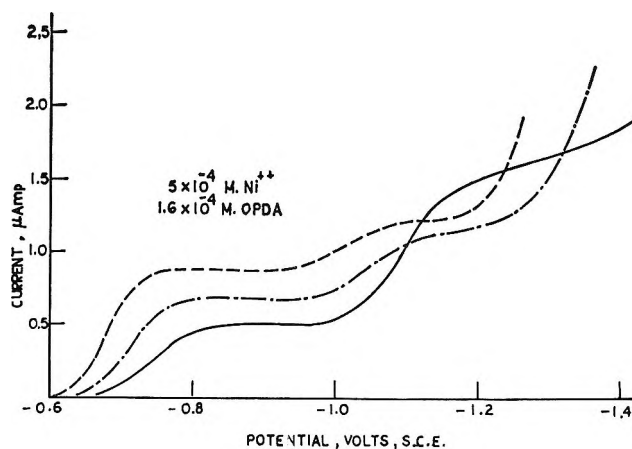


Figure 2. The effect of varying concentrations of lithium nitrate upon the prewave height (high-concentration range,  $5 \times 10^{-4} M \text{ Ni}^{2+}$ ,  $1.6 \times 10^{-4} M \text{ OPDA}$ ): —, 1.0 *M*  $\text{LiNO}_3$ ; ---, 3.0 *M*  $\text{LiNO}_3$ ; — · —, 5.0 *M*  $\text{LiNO}_3$ .

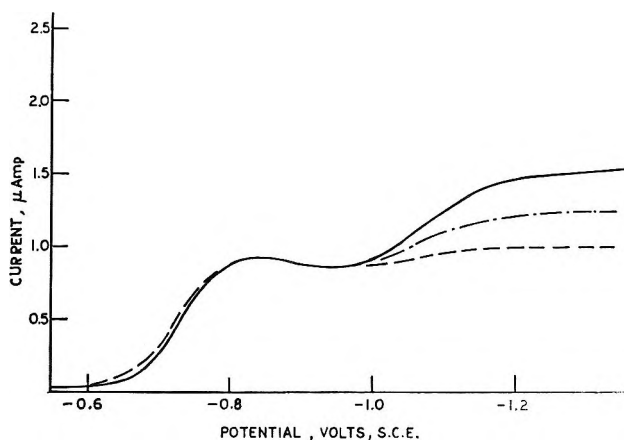


Figure 3. The effect of varying concentrations of lithium acetate upon the prewave height (high-concentration range,  $5 \times 10^{-4} M \text{ Ni}^{2+}$ ,  $1.6 \times 10^{-4} M \text{ OPDA}$ ): —, 1.0 *M*  $\text{LiC}_2\text{H}_3\text{O}_2$ ; ---, 2.0 *M*  $\text{LiC}_2\text{H}_3\text{O}_2$ ; — · —, 4.0 *M*  $\text{LiC}_2\text{H}_3\text{O}_2$ .

Coincident with the reversal of the trend of wave height with electrolyte concentration, a rather pronounced shift of both the prewave and main wave toward more positive potentials was observed in both lithium perchlorate and lithium nitrate. Dandoy and Gierst<sup>17</sup> have noted this effect in the case of the hexaaquonickel wave alone, attributing the phenomenon to changing activity of the reactant ion in these very concentrated solutions.

In the concentrations  $\leq 0.5 M$ , the observed changes in prewave height are therefore in accordance with the anticipated double-layer effect upon a surface reaction. At higher concentrations, the reverse is true. Interpretation of the results obtained in the latter case is

(15) P. Delahay, "Double Layer and Electrode Kinetics," Interscience Publishers, New York, N. Y., 1965, p 42.

(16) L. Gierst, private communication, 1966.

(17) J. Dandoy and L. Gierst, *J. Electroanal. Chem.*, 2, 116 (1961).

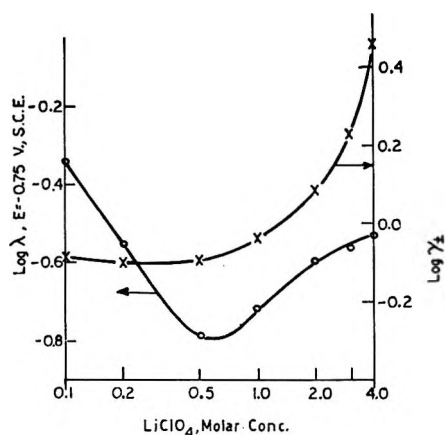


Figure 4. The dependence of the rate parameter,  $\lambda$ , and the mean ionic activity coefficient upon the concentration of lithium perchlorate.

subject to a number of uncertainties. These include pronounced activity changes for both reactants, an increase in specific adsorption of the electrolyte anion, salting out effects on the ligand,<sup>16</sup> a possible increase in the equilibrium concentration of less highly aquated nickel ions (regarded by Dandoy and Gierst<sup>17</sup> as the electroactive species in the absence of the ligand), and, perhaps, an increasingly dubious applicability of classical double-layer theory. That activity effects may play a major role in the more concentrated electrolyte is indicated by Figure 4, where the change in the observed rate,  $v^*$  (shown here as  $\lambda$ , defined below), and the mean ion activity coefficient,  $\gamma_{\pm}$ , appear as functions of the concentration of this electrolyte. The concentration at which the prewave height reverses its trend is roughly coincident with an accelerating rise in  $\gamma_{\pm}$  with concentration. The static behavior of the prewave in higher concentrations of lithium acetate may be attributed to the fact that the acetate ion forms a moderately stable ( $pK_{st} = 1.0$ ) complex with the nickel cation.<sup>18,19</sup>

The experiments described above were performed with electrolytes whose anions are subject only to limited degrees of specific adsorption.<sup>10,16</sup> The effect of changes in the electrode double layer on the prewave characteristics may also be studied by employing electrolytes whose anions are subject to different degrees of specific adsorption. The halogen salts offer a convenient group of electrolytes for this purpose. Values of  $\psi^0$ , obtained by Grahame and Soderberg<sup>20</sup> in 0.1 *M* solutions of KI, KBr, KCl, and NaF, are shown in Figure 5.<sup>21</sup> The disparity in the values of  $\psi^0$  at electrode potentials from  $-0.6$  to  $-0.9$  V arises from the fact that the specific adsorption of these anions is different and decreases in the order  $I \gg Br > Cl > F$ . At an electrode potential of  $-0.9$  V, desorption of the anions is nearly complete, and the values of  $\psi^0$  are the same for all of these salts. In view of the earlier discussion, a greater prewave height should result from more negative values of  $\psi^0$ . The polarographic results obtained with

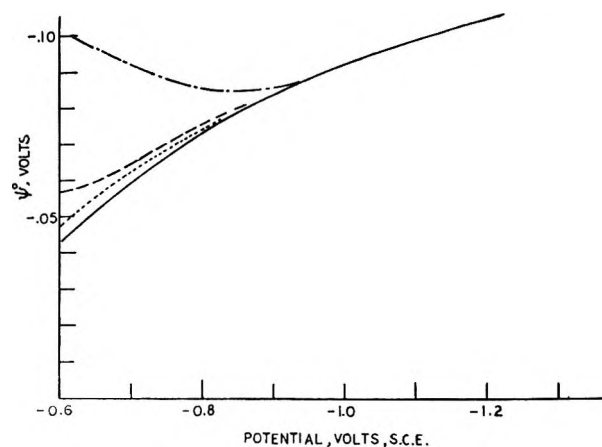


Figure 5. Variation of the outer Helmholtz potential,  $\psi^0$ , with the electrode potential in 0.1 *N* solutions of potassium halides: —, KF; ---, KCl; - · - ·, KBr; · · · ·, KI.

0.1 *M* solutions of the lithium halides are shown in Figure 6, where it may be seen that the prewave heights are in the order predicted by the  $\psi^0$  values for these salts. The same order is retained also in 1.0 *M* solutions.<sup>13</sup> The prewave obtained with lithium iodide is particularly interesting, as desorption of the anion at more negative electrode potentials results in the appearance of a pronounced "hump" in the prewave.

The effect of changes in the electrode double layer on the prewave was also investigated by varying the cation of the supporting electrolyte. Although  $Ca^{2+}$  is not specifically adsorbed, values of  $\psi^0$  for a 1:2 electrolyte will be significantly lower than those pertaining to a 1:1 electrolyte at the same concentration. Values of  $\psi^0$  for the former type have been calculated by Grahame.<sup>22</sup> The result of substituting calcium nitrate for lithium nitrate as the supporting electrolyte on the prewave height is shown in Figure 7. The decrease in prewave height is consistent with a decrease in  $\psi^0$ . Tetraalkylammonium ions are specifically adsorbed and thus also decrease values of  $\psi^0$ .<sup>23,24</sup> A comparison

(18) L. G. Sillén and A. E. Martell, "Stability Constants of Metal-Ion Complexes," The Chemical Society, Burlington House, London, 1964, p 366.

(19) The polarographic study of Ni(II) and Ni(II)-complex systems of this type shows numerous anomalous characteristics which cannot be explained in terms of the  $\psi^0$  effect treatment given in this paper. Part of these anomalies appear to result from the formation of Ni(II)-acetate complexes in the bulk of the solution. Also, it appears from double-layer capacitance studies that the acetate ion, although not specifically adsorbed to an appreciable extent,<sup>16</sup> affects the surface excess of the adsorbed ligand (H. B. Mark, Jr., H. C. MacDonald, Jr., and E. Kirowa-Eisner, unpublished results, 1968).

(20) D. C. Grahame and B. A. Soderberg, Technical Report No. 14 to the Office of Naval Research, Amherst College, Amherst, Mass., Feb (1954).

(21) The electrode potential scale used here has been changed to sce rather than the nhe scale used by Grahame.

(22) D. C. Grahame, *J. Chem. Phys.*, **21**, 1054 (1953).

(23) J. Koryta, *Electrochim. Acta*, **6**, 67 (1962).

(24) A. N. Frumkin, *Advan. Electrochem. Electrochem. Eng.*, **1**, 95 (1961).



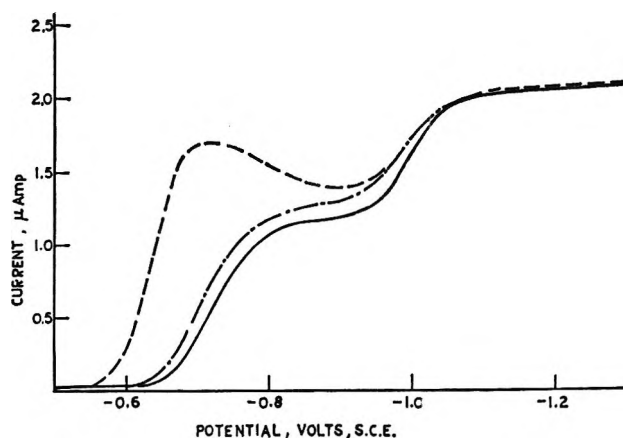


Figure 6. The effect of anion adsorption upon the shape and amplitude of the prewave (0.1 *N* solutions of lithium halides,  $5 \times 10^{-4}$  *M*  $\text{Ni}^{2+}$ ,  $1.6 \times 10^{-4}$  *M* OPDA): —, LiCl; ---, LiBr; - · - ·, LiI.

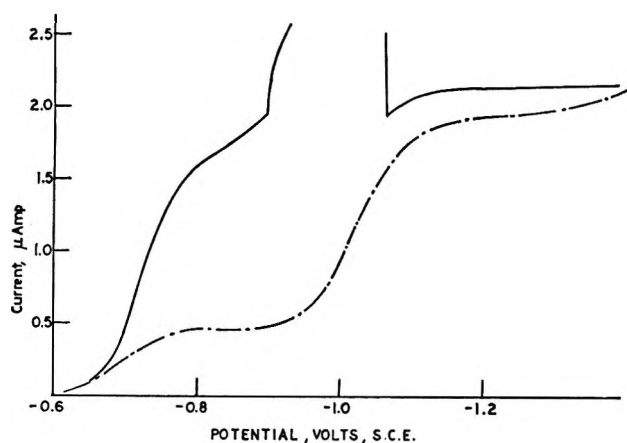


Figure 7. Comparison of prewaves obtained in 0.1 *N* solutions of lithium and calcium nitrate ( $5 \times 10^{-4}$  *M*  $\text{Ni}^{2+}$ ,  $1.6 \times 10^{-4}$  *M* OPDA): —,  $\text{LiNO}_3$ ; ---,  $\text{Ca}(\text{NO}_3)_2$ .

of the prewaves obtained in 0.1 *M* solutions of lithium acetate and tetramethylammonium acetate appears in Figure 8. Interpretation of this result requires some caution, however, as adsorption of this cation may also decrease the reaction rate by a reduction in the effective electrode area. If adsorption of the ligand does occur, the cation competes for electrode surface area and may reduce the surface concentration of the reacting species. Studies of the effect of the alkali metal cations on the rates of other electrode reactions have shown that these produce an effect akin to that of cation adsorption, increasing in the order Li, Na, K, and Cs.<sup>17</sup> Figure 9 shows the polarograms obtained with lithium, potassium, and cesium nitrate supporting electrolytes. The results are again consistent with a double-layer effect on a surface-rate-limiting reaction.

Qualitatively, the results obtained in these investigations with a wide variety of concentrations and types of electrolytes are consistent with a pronounced double-layer effect on the prewave and clearly invalidate the

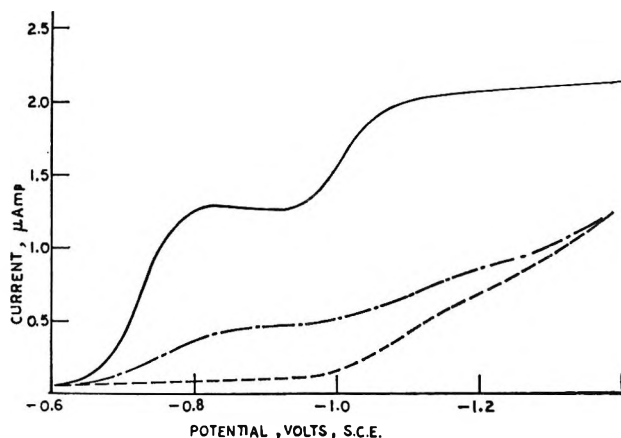


Figure 8. The effect of cation adsorption upon prewave height: —, 0.1 *N* lithium acetate; ---, 0.1 *N* tetramethylammonium acetate; - · - ·, without OPDA.

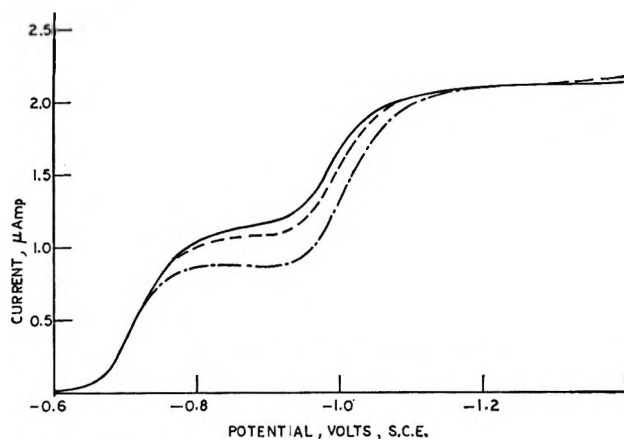


Figure 9. The effect of the alkali metal cations upon the height of the prewave (0.1 *N* nitrate solutions): —,  $\text{LiNO}_3$ ; ---,  $\text{KNO}_3$ ; - · - ·,  $\text{CsNO}_3$ .

concept of a rate-limiting "bulk" chemical reaction as proposed by Tur'yan and Malyavinskaya.<sup>9</sup>

#### Quantitative Analysis of the Prewave

It should be possible to verify quantitatively the mechanism described in reactions 1 and 2 using eq 3 and 4. Some modification of eq 4 will be required first, however, if the reaction does involve an adsorbed ligand. The ligand concentration,  $[L]$ , in eq 4 is defined in terms of a volume concentration. This difficulty can be avoided if the assumption is made that near-equilibrium coverage of the adsorbed ligand is attained quickly within the life of the drop. The surface concentration of the adsorbed species can then be effectively regarded as a time-invariant quantity. While this is ordinarily a dangerous assumption in view of the known slow attainment of equilibrium coverage by many adsorbed organic molecules, sufficient evidence was at hand to permit such an assumption as a reasonable first-order approximation at the concentration of OPDA used in the polarographic measurements.<sup>13,19</sup> If Koutecky's

relationships<sup>14</sup> for a heterogeneous electrochemical reaction are written in somewhat modified form<sup>25</sup>

$$\frac{i}{i_d} = F(\lambda) \quad (5)$$

$$i = nFAk_{th} \left[ C^0 \frac{\sqrt{7/3} F(\lambda)}{\sqrt{\pi \lambda}} \right] \quad (6)$$

The quantity in brackets in eq 6 represents the surface concentration of the reactant species at time  $t$ . In the context of reaction 2, it may be equated with the surface concentration of the hexaaquonickel ion at the electrode surface. With the assumption that  $[L]_{ads}$  is virtually a constant over the life of the drop,  $k_{th}$ , the normal heterogeneous rate constant, can then be replaced by  $k_f[L]_{ads}^x$ , where  $k_f$  is the forward chemical reaction rate constant for reaction 1. The quantity  $\lambda$  in eq 5 is then defined as

$$\lambda = \frac{k_f[L]_{ads}^x \sqrt{t}}{\sqrt{D}} \quad (7)$$

The quantity  $\lambda$  calculated from the height of the prewave, is, however, clearly subject to the effect of the electrode double layer as shown in the previous section. The reaction velocity,  $v_0$ , in eq 3 is now defined for a surface reaction as

$$v_0 = k_f[L]_{ads}^x \quad (8)$$

The apparent velocity,  $v^*$ , then becomes

$$v^* = \frac{\sqrt{D}}{\sqrt{t}} \lambda \quad (9)$$

These equations may then be combined in the form of eq 3 to give

$$\lambda = \frac{k_f[L]_{ads}^x \sqrt{t}}{\sqrt{D}} \exp\left(-\frac{ZF}{RT}\psi^0\right) \quad (10)$$

The above relationships have been derived on the basis that the rate of the electrode process is controlled wholly by the forward rate of the chemical reaction. They may be strictly applied therefore only to data taken at electrode potentials that are sufficiently negative to the rising portion of the prewave to ensure that the rate of the charge-transfer reaction exceeds the chemical rate. Inspection of Figures 1, 3, and 6-9 suggests that the applicable electrode potential ranges from about  $-0.8$  to  $-0.9$  V sce. At electrode potentials more negative than  $-0.9$  V, serious interference from the main hexaaquonickel wave is encountered.

If a Henry's law relationship is assumed to exist between the surface concentration of the ligand and its bulk concentration (at low ligand concentrations), eq 10 may be written as

$$\lambda = \frac{k_f(K_h[L]^0)^x \sqrt{t}}{\sqrt{D}} \exp\left(-\frac{ZF}{RT}\psi^0\right) \quad (11)$$

where  $[L]^0$  is the bulk ligand concentration and  $K_h$  is the Henry's law constant. The stoichiometric coefficient,  $X$ , may then be evaluated through a series of measurements of the prewave height as a function of the ligand concentration in the same supporting electrolyte. If  $\lambda$  is calculated at the same electrode potential in each case and if the adsorbed ligand surface concentration is not so large as to cause  $\psi^0$  to differ significantly from that of the electrolyte itself, the exponential term becomes a constant. At a constant time of current measurement, eq 11 then becomes simply

$$\log \lambda = \text{constant} + X \log [L]^0 \quad (12)$$

The results obtained in such an experiment are shown in Figure 10. The slope of the curves at lower ligand concentrations clearly indicates a 1:1 combining ratio for the ligand and the hexaaquonickel ion. The result is evidently not critically dependent on the choice of electrode potential. The deviation from linearity suggests that either a deviation from Henry's law occurs or adsorption of the ligand is great enough to cause a significant change in  $\psi^0$  as the concentration increases. It should be noted also that eq 12 would apply equally well to a bulk chemical reaction having a reaction layer thickness well within the diffuse zone of the double layer. In this instance, the Henry's law approximation would not be involved, and greater rigor would be expected from the relationship. In a nega-

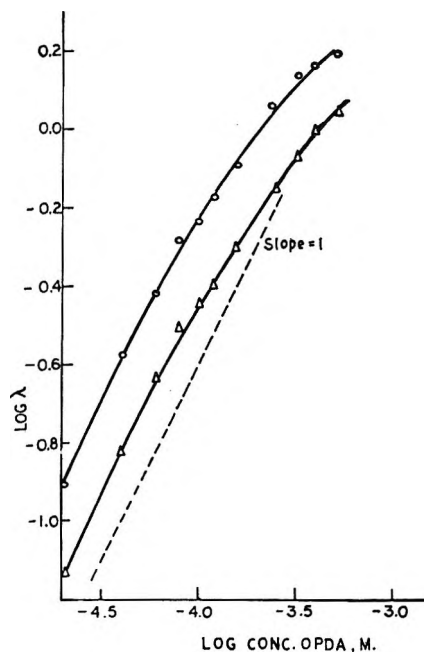


Figure 10. The dependence of the rate parameter,  $\lambda$ , upon the bulk concentration of OPDA (0.1  $N$  lithium perchlorate solutions,  $5 \times 10^{-4} M Ni^{2+}$ ):  $\circ$ —,  $-0.85$  V sce;  $\triangle$ —,  $-0.75$  V sce.

(25) The original relationship derived by Koutecky<sup>14</sup> was written in terms of the symbol  $\chi$ ;  $\lambda$  used here equals  $\sqrt{7/12}\chi$ .

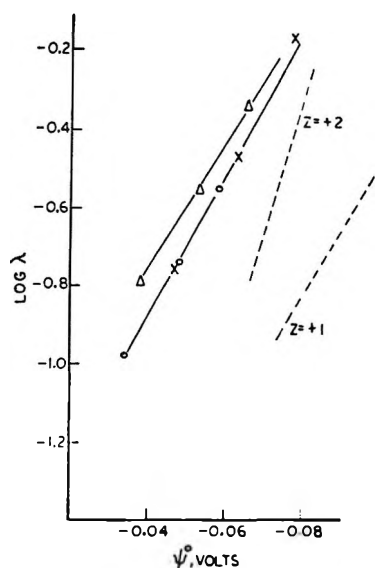


Figure 11. Dependence of the rate parameter,  $\lambda$ , upon  $\psi^0$  in 0.1 *N* lithium perchlorate solutions ( $5 \times 10^{-4}$  *M*  $\text{Ni}^{2+}$ ,  $1.6 \times 10^{-4}$  *M* OPDA): —○—, -0.70 V; —Δ—, -0.75 V; —×—, -0.85 V.

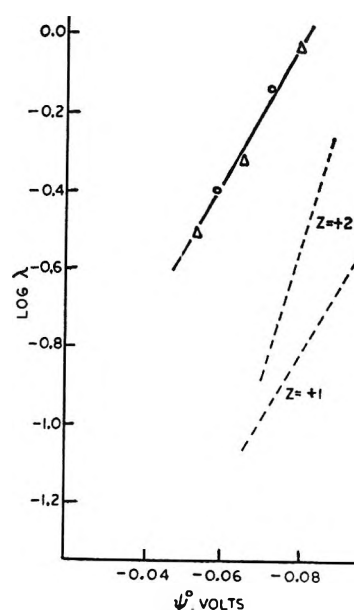


Figure 12. The dependence of the rate parameter,  $\lambda$ , upon  $\psi^0$  in 0.1 *N* lithium nitrate solutions ( $5 \times 10^{-4}$  *M*  $\text{Ni}^{2+}$ ,  $1.6 \times 10^{-4}$  *M* OPDA): —Δ—, -0.75 V; —○—, -0.80 V.

tive sense, the observed deviation from linearity argues against this possibility. Unfortunately, changes in  $\psi^0$  by adsorbed ligand, even if this species did not participate in the electrochemical reaction, could also produce the curvature noted in Figure 10.

If the experimental conditions involve changing  $\psi^0$  through the use of a range of concentrations of supporting electrolyte at constant reactant concentrations, eq 10 may be employed to determine the dependence of  $\lambda$  on this variable. If  $[\text{L}]_{\text{ads}}$  is reasonably insensitive to a range of electrolyte concentrations, it may be regarded as substantially constant under these conditions, and eq 10 is reduced to

$$\log \lambda = \text{constant} - \frac{ZF}{2.3RT} \psi^0 \quad (13)$$

The results of such experiments using lithium perchlorate and lithium nitrate are shown in Figures 11 and 12. In both instances, the values of  $\psi^0$  were taken from Russell's<sup>26</sup> tables after correction of the electrode potentials shown there to sce. It has therefore been assumed that anion adsorption is negligible in both instances. While this assumption is untenable at higher concentrations of these electrolytes, the data of Payne<sup>27</sup> and Wroblowa, *et al.*,<sup>28</sup> offer assurance that errors from this source are minor in the potential region of the prewave and at the electrolyte concentrations ( $\leq 0.5$  *M*) employed here. Figures 11 and 12 include only the data calculated at this lower concentration range of supporting electrolyte, where the predictions of the double-layer theory were found to be qualitatively obeyed in the previous section. While a

linear relationship between  $\log \lambda$  and  $\log \psi^0$  is observed in these cases, the slopes of the lines do not conform to a reaction involving an uncharged ligand and the hexa-aquonickel with a charge  $Z = +2$ . Dotted lines have been included on these figures with slopes equal to  $ZF/2.3RT$ , where  $Z$  equals +1 and +2. To the extent that  $Z$  must be an integer, the experimental results agree more closely with a reactant charge of +1. The results obtained by Dandoy and Gierst<sup>17</sup> in experiments involving the hexa-aquonickel ion alone have shown that the electroactive species has a +2 charge as expected. The cause of this difference could lie either in the behavior of the ligand or in the assumptions employed in the development of the relationship presented above. Of the latter, the treatment of  $[\text{L}]_{\text{ads}}$  as a constant with respect to both time and electrolyte concentration is certainly suspect. On the other hand, experimental evidence obtained from differential capacitance measurements indicates that the errors introduced by these assumptions are not great enough to account for this charge value.<sup>13,19</sup> This capacitance evidence does suggest, however, that adsorption of *o*-phenylenediamine may involve the coadsorption of the electrolyte anion. This aspect of this problem will be discussed in a subsequent paper.

(26) C. D. Russell, *J. Electroanal. Chem.*, **6**, 486 (1963).

(27) R. Payne, private communication of unpublished results to L. R. McCoy, 1966.

(28) H. Wroblowa, Z. Kovac, and J. O'M. Bockris, *Trans. Faraday Soc.*, **61**, 1523 (1965).

## Brillouin Spectra of Dilute Solutions and the Landau-Placzek Formula

by George A. Miller and Ching S. Lee

*School of Chemistry, Georgia Institute of Technology, Atlanta, Georgia 30332 (Received July 8, 1968)*

The intensity ratio of central to side peaks has been measured in the Brillouin spectra of several dilute solutions. The solvents, chosen for their known deviation from the Landau-Placzek formula, were benzene, carbon tetrachloride, water, and ethylene glycol, with toluene included as a "normal" liquid. The concentration dependence of the intensity ratio was shown to be affected by a deviation from the Landau-Placzek relation. If one wishes to determine activity coefficients of binary solutions by measuring intensity ratios, careful consideration must be given to these deviations.

The resolving of the Brillouin spectrum or fine structure of Rayleigh scattering offers an interesting new approach to the study of the intensity of light scattered by solutions. Since concentration fluctuations contribute to the unshifted central component of the scattered light, one can substitute the intensity of the Doppler-shifted side peaks for that of the incident beam as a reference. Then the Rayleigh ratio or the turbidity is replaced by the ratio of the intensities of the central peak to the two side peaks as the experimental quantity to be determined. One of us has developed the relationship of this ratio to concentration for binary solutions<sup>1</sup> from the standard thermodynamic theory of light scattering. In the simplest form the result reduces to the well-known Landau-Placzek (LP) formula  $J = \gamma - 1$  for a pure liquid, where  $J$  is the intensity ratio and  $\gamma$  is the ratio of heat capacities at constant pressure and constant volume. However, for many liquids the LP formula is not an accurate one.

Light-scattering intensity measurements provide a tool for studying the nonideality of solutions or, as is more common, for determining the weight-average molecular weight of polymers in solution. In either case, if the Brillouin spectrum approach is to be used, it is necessary to be able to treat those instances in which the pure solvent does not obey the LP formula. With this in mind, we have measured intensity ratios for several deviant liquids with small amounts of a second component dissolved in them. The solvents studied were toluene (normal liquid), benzene and carbon tetrachloride (internally relaxing liquids), water (liquid with very small thermal expansion), and ethylene glycol (structurally relaxing liquid). The concentrations of the solute did not exceed 10 mol % and were much less for the more nonideal solutions studied; hence we were working always within or close to the Henry's law region of ideality. In what follows, we discuss the relevance of these measurements to the LP formula.

In most accurate form, the thermodynamic theory yields, for an ideal, binary solution, having a solute mole fraction of  $x_2$ <sup>1</sup>

$$J = \frac{\frac{T}{C_p} \left( \frac{\partial n}{\partial T} \right)^2 + \frac{x_1 x_2}{RT} \left( \frac{\partial n}{\partial x_2} \right)^2}{\frac{T}{C_v} \left( 1 - \frac{1}{\gamma} \right) \left( \frac{\partial n}{\partial T} \right)^2 + \frac{2T\alpha}{\beta_T C_v} \left( \frac{\partial n}{\partial T} \right) \left( \frac{\partial n}{\partial P} \right) + \frac{1}{v\beta_S} \left( \frac{\partial n}{\partial P} \right)^2} \quad (1)$$

where  $T$  is the absolute temperature,  $P$  is the pressure,  $n$  is the refractive index,  $R$  is the gas constant,  $\alpha$  is the thermal expansivity,  $v$  is the molar volume, and  $\beta_T$  and  $\beta_S$  are the two compressibilities. The partial differentiation always concerns the triad  $P$ ,  $T$ , and  $x_2$ . A good assumption for many liquids is that

$$\frac{\partial n}{\partial P} \cong -\frac{\beta_T}{\alpha} \left( \frac{\partial n}{\partial T} \right) \quad (2)$$

which leads to the simplified form

$$J = (\gamma - 1) + (\gamma - 1)Kx_1x_2 \quad (3)$$

where

$$K = \frac{C_p}{RT^2} \frac{(\partial n / \partial x_2)^2}{(\partial n / \partial T)^2}$$

Equations 1 and 3 may be thought in an approximate way to arise from the equation

$$J = \frac{(\text{entropy fluctuation term}) + (\text{concentration fluctuation term})}{(\text{pressure fluctuation term})}$$

We will take eq 3 as representing the behavior of a "normal" solution. Deviations from normal behavior may result first of all from the incorrectness of the assumption implied in eq 2, in which case the full eq 1 must be used. Then there will be cases where the solution is a relaxing fluid for which the simple thermodynamic theory is inadequate. For discussing deviant behavior of various kinds, we can write a slightly more general form of equation for the intensity ratio

(1) G. A. Miller, *J. Phys. Chem.*, **71**, 2305 (1967).

$$J = A + BKx_1x_2 \quad (4)$$

If we consider dilute solutions, then the coefficients  $A$ ,  $B$ , and  $K$ , which are actually concentration dependent, will be essentially the values at infinite dilution. Except for the refractive index increment which occurs in  $K$ , these coefficients will depend only on the properties of the pure solvent to a good approximation.

First, we will consider the error involved in introducing eq 2. Coumou, Mackor, and Hijmans<sup>2</sup> have studied this problem in relation to total isotropic light scattering. They introduced the parameter

$$x = 1 + \frac{\beta_T(\partial n/\partial T)}{\alpha(\partial n/\partial P)}$$

which becomes zero if eq 2 holds exactly. Equation 1 may be rewritten in terms of  $x$  by means of a factor

$$f = \frac{2x}{1-x} + \frac{\gamma x^2}{(1-x)^2}$$

to give a form of eq 4 in which

$$A = B = \frac{\gamma - 1}{1 + f\gamma} \cong \frac{\gamma - 1}{1 + 2\gamma x} \quad (5)$$

For many organic solvents,  $x$  is typically 0.01–0.05,<sup>2</sup> which means that  $A$  and  $B$  are some 2–10% less than  $\gamma - 1$ . For water,  $x$  is negative, and  $A$  and  $B$  are about 50% greater than  $\gamma - 1$  at 25°. At 4° the density of water goes through a maximum, and the above formulation in terms of  $x$  may not be used. Instead we have  $\alpha = \gamma - 1 = 0$ , and eq 1 becomes

$$J = \frac{\frac{T}{C_p} \left(\frac{\partial n}{\partial T}\right)^2 + \frac{x_1x_2}{RT} \left(\frac{\partial n}{\partial T}\right)^2}{\frac{1}{v\beta_s} \left(\frac{\partial n}{\partial P}\right)^2}$$

Formally, this fits eq 4 with

$$A = B = \frac{Tv\beta_s}{C_p} \left(\frac{\partial n/\partial T}{\partial n/\partial P}\right)^2 \quad (6)$$

However, in the complete coefficient of the concentration term,  $\partial n/\partial T$  is cancelled out, *i.e.*

$$BK = \frac{v\beta_s}{RT} \left(\frac{\partial n/\partial x_2}{\partial n/\partial P}\right)^2$$

which, we will see, allows us to ignore the probably rapid change of  $\partial n/\partial T$  with concentration in aqueous solutions at 4°.

Next, we will consider relaxation effects. In a relaxing liquid the spontaneously generated sound waves, as represented by the pressure fluctuation term, transfer energy to nonpropagating modes of energy, thereby decreasing the intensity of the side peaks and enhancing that of the central peak.<sup>3,4</sup> The summed intensity of these peaks remains the same as that predicted by thermodynamic theory. Let  $R$  be the value of  $J$  for a

pure liquid, as given by thermodynamic theory.  $R$  will be approximately equal to  $\gamma - 1$  but is given more precisely by the formulas discussed above. Let  $J_0$  be the experimental intensity ratio of the pure liquid. The effect of a relaxation process will be that  $J_0 > R$ ; the intensity of the side peaks will be multiplied by the factor  $(R + 1)/(J_0 + 1)$  and that of the central peak by the factor  $J_0(R + 1)/R(J_0 + 1)$ . For dilute solutions in which the solvent is a relaxing liquid, the intensity ratio is given, thus, by eq 4 with

$$A = J_0; \quad B = R(J_0 + 1)/(R + 1) \quad (7)$$

In some cases the component of the central peak contributed by the relaxation process may be broad enough to appear to contribute partly to the intensity of the side peaks. Therefore, a reasonably consistent procedure should be used to determine the relative intensities of the three peaks, such that the relaxation component contributes the same amount to the side peaks at different concentrations.

Examples of liquids in which the relaxation is with internal modes of energy are carbon tetrachloride<sup>5</sup> and benzene.<sup>6–8</sup> In viscous liquids, such as ethylene glycol and glycerol,<sup>4,9</sup> the relaxation occurs with structural or intermolecular modes of energy. We find eq 7 quite inadequate for glycol solutions. Since no theoretical treatment of Brillouin scattering from viscous solutions is available, we must consider the coefficient  $B$  to be unpredictable for such solutions.

Water is an interesting case experimentally, because  $J_0$  is very small and difficult to measure in the face of small contributions from dust and instrument scattering. Values of  $J_0$  calculated by thermodynamic theory agree as well as can be expected with experiment.<sup>10</sup> Since there are no relaxation effects here, we can assume that  $A = B$  for aqueous solutions. With the proper choice of solute, large values of  $J$  may be obtained from relatively dilute solutions. Therefore,  $B$  may be measured more accurately than  $A$ . At 4°, where  $J_0$  is truly miniscule ( $4 \times 10^{-4}$ ),  $B$  is still a readily measurable quantity.

Our assumption about the limiting behavior of  $A$  and  $B$  warrants additional comment. In the limit of

(2) D. J. Coumou, E. L. Mackor, and J. Hijmans, *Trans. Faraday Soc.*, **60**, 1539 (1964).

(3) C. J. Montrose, V. A. Solov'yev, and T. A. Litovitz, *J. Acoust. Soc. Amer.*, **43**, 117 (1968).

(4) D. A. Pinnow, S. J. Candau, J. T. LaMacchia, and T. A. Litovitz, *ibid.*, **43**, 131 (1968).

(5) W. S. Gornall, G. I. A. Stegeman, B. P. Stoicheff, R. H. Stolen, and V. Volterra, *Phys. Rev. Lett.*, **17**, 297 (1966).

(6) J. L. Hunter, E. F. Carome, H. D. Hardy, and J. A. Bucaro, *J. Acoust. Soc. Amer.*, **40**, 313 (1966).

(7) C. L. O'Connor and J. P. Schlupf, *ibid.*, **40**, 663 (1966).

(8) E. F. Carome and S. P. Singal, *ibid.*, **41**, 1371 (1967).

(9) D. H. Rank, E. M. Kiess, and U. Fink, *J. Opt. Soc. Amer.*, **56**, 163 (1966).

(10) C. L. O'Connor and J. P. Schlupf, *J. Chem. Phys.*, **47**, 31 (1967).

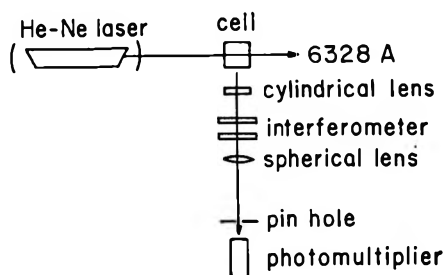


Figure 1. Schematic of light-scattering apparatus.

infinite dilution, the derivatives  $\partial A/\partial x_2$  and  $\partial B/\partial x_2$  will not be zero except by accident. The value of  $B$  obtained from a determination of  $J$  in dilute solutions, even if extrapolated to  $x_2 = 0$ , will contain an unwanted increment,  $(\partial A/\partial x_2)/K$ . This error may be kept small by choosing a solute-solvent pair with a large refractive index increment.

### Experimental Section

Brillouin spectra were recorded at a scattering angle of approximately  $90^\circ$  as shown in Figure 1. A Perkin-Elmer Model 6320 He-Ne laser provided 10-mW radiation at 6328 Å with a half-width of about  $0.025 \text{ cm}^{-1}$  ( $0.010 \text{ Å}$ ). The sample was contained in a standard square turbidity cell made by the Phoenix Precision Instrument Co. The cell was surrounded by a close fitting, electrically heated aluminum block for temperature control. The scattered light was gathered with a cylindrical lens of 10-cm focal length, which served to collimate the light parallel to the horizontal plane only. Thus the original scattering angle of a ray was preserved as it passed through the lens. The scattered light was analyzed with a piezoelectrically driven, scanning Fabry-Perot interferometer. A simplified sketch of the interferometer is shown in Figure 2. The actual mounting resembled that of the magnetically driven interferometers described by Fork, *et al.*<sup>11</sup> The 95% reflectant mirrors gave a finesse of about 60. Light emerging from the interferometer was focused by a 50-cm focal length lens onto a pinhole. The central spot of the interferometer ring system was then gathered by an EMI 9592-B photomultiplier with an S-10 response. The signal was amplified through a Schoeffel M-600 photometer and was displayed on an X-Y recorder. The mirror spacing,  $d$ , was set at 10.67 mm, giving a free spectral range of  $0.48 \text{ cm}^{-1}$  and an over-all instrumental half-width of about  $0.032\text{--}0.042 \text{ cm}^{-1}$  (arising from the laser line width, the interferometer finesse, and the size of the pinhole).

The voltage drive for the interferometer consisted of a stabilized 350-V power supply coupled with a 10-turn, 250,000-ohm Helipot driven by the multispeed output of a synchronous motor. The same ramp voltage provided the signal for the X axis of the recorder. Thus the piezoelectric element of the interferometer remained

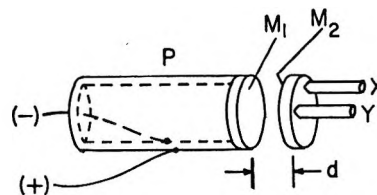


Figure 2. Simplified diagram of scanning Fabry-Perot interferometer showing piezoelectric ceramic tube (P), multilayer dielectric mirrors ( $M_1$ ,  $M_2$ ), micrometer adjustment for parallelism (X, Y). Mirror spacing ( $d$ ) is adjustable.

the only real source of possible nonlinearity in the frequency axis of the recorded spectrum.

The solutions were made from commercially available reagents without further purification. The benzene, toluene, carbon tetrachloride, glycerol, and ethylene glycol were Fisher Certified reagents. The naphthalene was Eastman Highest Purity, recrystallized from alcohol. The water was ordinary distilled.

Organic solutions were made dust free by a single filtration through a Millipore filter of  $0.22\text{-}\mu$  pore size under a slight excess pressure of nitrogen. The turbidity cell was first washed free of dust with the condensing vapors of boiling carbon tetrachloride, and the solution to be studied was then filtered immediately into the cell. Aqueous solutions required repeated filtration (about six times) to remove dust. Some of this dust came from the walls of the cell and could not be removed by steaming, hence the main purpose of repeated filtration was to wash the dust from the cell. Using this fairly well standardized procedure on water gave a good indication of how much dust remained on the average in the solutions. The glycol solutions required two to three filtrations. Naphthalene dissolved in glycol only upon heating the mixture to about  $80^\circ$ . The most concentrated solution was definitely supersaturated at  $25^\circ$ .

The index of refraction of the solvents as a function of temperature and of the solutions as a function of composition was determined on an Abbé-type Bausch and Lomb precision refractometer, using the laser as the illuminating source.

### Results

A representative selection of recorder traces of the Brillouin spectra of the various solutions is given in Figures 3-7. Some variation in finesse of the interferometer due to slight misalignment is to be observed. The occasional spikes were caused by a dust particle passing through the incident light beam. Undoubtedly, small amounts of finer dust together with a trace of instrumental scattering added perhaps a few per cent to the intensity of the central peak in all our experi-

(11) R. L. Fork, D. R. Herriott, and H. Kogelnik, *Appl. Opt.*, **3**, 1471 (1964).

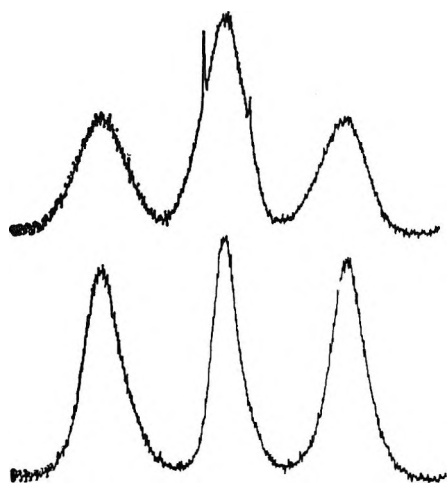


Figure 3. Spectrum of light scattered at  $25^\circ$  from toluene (lower curve) and a solution of 100 g of naphthalene/kg of toluene.

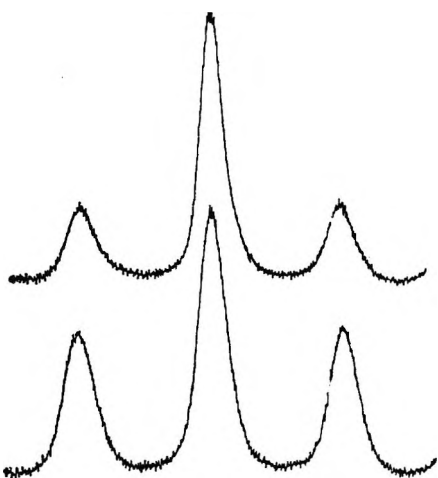


Figure 4. Spectrum of light scattered at  $25^\circ$  from benzene (lower curve) and a solution of 200 g of naphthalene/kg of benzene.

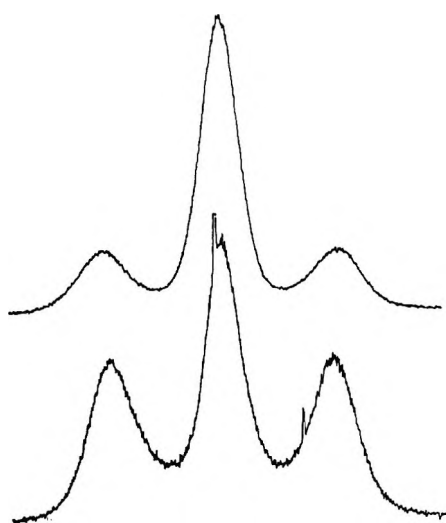


Figure 5. Spectrum of light scattered at  $25^\circ$  from carbon tetrachloride (lower curve) and a solution of 100 g of naphthalene/kg of carbon tetrachloride.

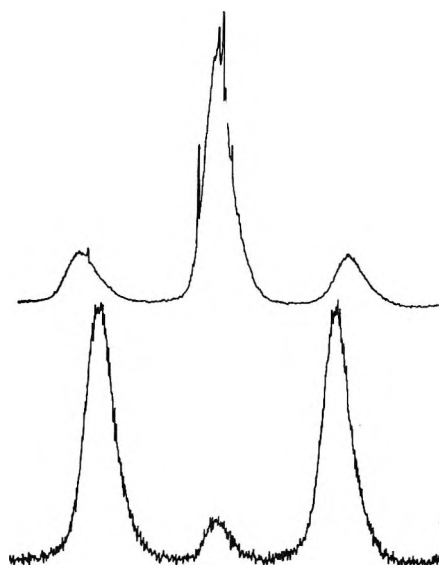


Figure 6. Spectrum of light scattered at  $25^\circ$  from water (lower curve) and a solution of 300 g of glycerol/kg of water.

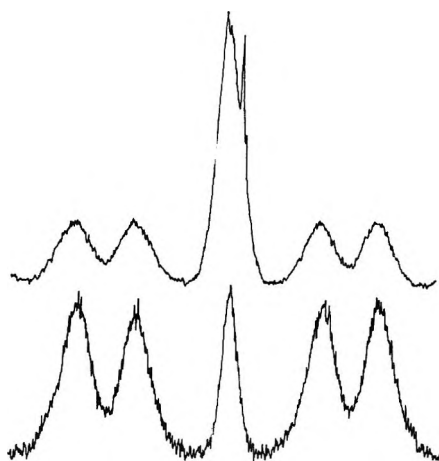


Figure 7. Spectrum of light scattered at  $25^\circ$  from ethylene glycol (lower curve) and a solution of 15 g of naphthalene/kg of ethylene glycol.

ments. However, our method of following the concentration dependence of  $J$  minimizes these sources of error, since, to the degree to which they were constant from one solution to the next, they were cancelled out. By the same token we did not try to identify the true base line of our Brillouin spectra and correct for overlap of adjacent peaks. Rather, we drew our base line through the minimum points on the trace between successive orders and divided the central peak from the Brillouin peaks by vertical lines at the minimum where they overlap. The areas marked off were then measured with a planimeter. The test of this method was that it produces intensity ratios in reasonable agreement with previously published values. This was indeed the case even for carbon tetrachloride where the internal-relaxation component is broad enough to produce severe

**Table I:** Experimental Intensity Ratios,  $J$ 

Wt of solute (g)/ wt of solvent (kg)	Solvent-solute						
	$C_7H_8-C_{10}H_8$ (25°)	$C_8H_8-C_{10}H_8$ (25°)	$CCl_4-C_{10}H_8$ (25°)	$H_2O-C_8H_8O_2$		$C_2H_6O_2-C_{10}H_8$	
				4°	25°	25°	50°
0	0.432	0.890	0.752	0.140	0.140	0.297	0.206
5						0.705	
10						1.136	
15						1.630	0.884
20		0.982					
25	0.515		1.091				
40		1.070					
50	0.644		1.383		0.700		
60		1.143					
75	0.724		1.594				
80		1.238					
100	0.836	1.325	1.809		1.016		
150					1.567		
200		1.560		1.940	1.855		
250				2.210	1.988		
300				2.440	2.330		

**Table II:** Solvent Parameters

Liquid	Temp, °C	$C_p$ , cal/mol deg	$-10^4(\partial n/\partial T)$	$\gamma - 1$	$\alpha$	$R$
Toluene	25	38.25 <sup>a</sup>	5.51 <sup>f</sup>	0.36 <sup>g</sup>	0.015 <sup>i</sup>	0.35
Benzene	25	32.52 <sup>b</sup>	6.27 <sup>f</sup>	0.43 <sup>g</sup>	0.046 <sup>i</sup>	0.38
Carbon tetrachloride	25	31.49 <sup>c</sup>	5.74 <sup>f</sup>	0.45 <sup>g</sup>	0.028 <sup>i</sup>	0.42
Water	4	18.101 <sup>d</sup>	0.1717 <sup>d</sup>	0	( $-\infty$ )	$3.71 \times 10^{-4}$ <sup>i</sup>
Water	25	17.993 <sup>d</sup>	0.978 <sup>d</sup>	0.0106 <sup>d</sup>	-0.158 <sup>d</sup>	0.0145
Ethylene glycol	25	35.6 <sup>e</sup>	2.572 <sup>f</sup>	0.140 <sup>h</sup>		
Ethylene glycol	50	37.1 <sup>e</sup>	2.659 <sup>f</sup>	0.183 <sup>h</sup>		

<sup>a</sup> J. S. Burlew, *J. Amer. Chem. Soc.*, **62**, 696 (1940). <sup>b</sup> G. D. Oliver, M. Eaton, and H. M. Huffman, *ibid.*, **70**, 1502 (1948). <sup>c</sup> J. F. G. Hicks, J. G. Hooley, and C. C. Stephenson, *ibid.*, **66**, 1064 (1944). <sup>d</sup> Reference 10. <sup>e</sup> G. C. Parks and K. K. Kelly, *J. Amer. Chem. Soc.*, **47**, 2089 (1925); M. B. Neumann and I. A. Kuryankin, *J. Gen. Chem. USSR*, **2**, 317 (1932); I. B. Rabinovich and P. N. Nikolaev, *Dokl. Akad. Nauk SSSR*, **142**, 1335 (1962). <sup>f</sup> Measured in this laboratory at 6328 Å. <sup>g</sup> Values at 20° from H. Z. Cummins and R. W. Gammon, *J. Chem. Phys.*, **44**, 2785 (1966); the temperature variation is not more than 0.2%/deg. <sup>h</sup> Calculated from  $\gamma - 1 = T\alpha^2 v_s^2 / C_p$  using data from various sources: temperature dependence of density, "International Critical Tables," Vol. III, McGraw-Hill Book Co., Inc., New York, N. Y., 1933, p 112; sound velocity, ref 9; and heat capacity, footnote e. <sup>i</sup> Reference 2. <sup>j</sup> Calculated from data in ref 10 using eq 6.

overlap with Brillouin components. For ethylene glycol the Brillouin components of successive orders overlapped so much that it was necessary to measure the area of two Brillouin peaks combined.

The experimental intensity ratios (Table I) were plotted against  $x_1x_2$  (Figures 8 and 9) in accordance with eq 4. The coefficient  $B$  was calculated from the limiting slope, as estimated visually. The quantities needed to calculate the limiting value of  $K$  in dilute solutions ( $K_0$ ) are listed in Tables II and III. Also, values of  $B = (J - J_0)/K_0x_1x_2$  were calculated for each solution and extrapolated to zero concentration for comparison. (See Table IV.) We have included these latter plots for the aqueous solutions (Figures 10 and 11) to show that the dust problem was rather severe in this case. For the other systems studied the values

of  $B$  obtained by the two kinds of plots agreed to better than 5%.

Table II includes the intensity ratio,  $R$ , calculated from thermodynamic theory. For the first three solvents, we used values of  $\alpha$  determined by Coumou, Mackor, and Hijmans, which are based on values of  $\partial n/\partial T$  and  $\partial n/\partial P$  at 5460 Å. For water we were able to use values of these derivatives at the laser wavelength. We were unable to calculate  $R$  for ethylene glycol for lack of a value of  $\partial n/\partial P$ .

Table III lists our experimental values of  $A$  (i.e.,  $J_0$ ) and  $B$  and the calculated values of  $B$ . For the non-aqueous systems,  $B$  was calculated by eq 7. Toluene behaved very nearly like a normal liquid. With carbon tetrachloride there is a 10% discrepancy between the calculated and measured values of  $B$ . The overlap



**Table III:** Solution Parameters

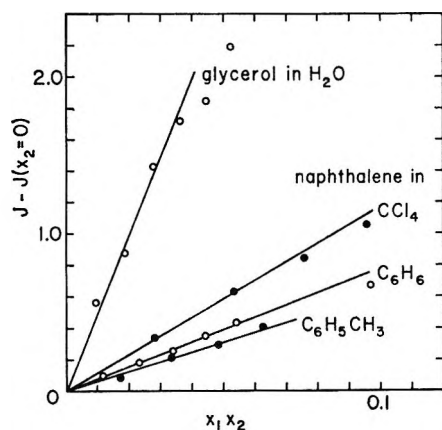
Solvent	Solute	Temp, °C	$\partial n / \partial x_1^a$	$K_0$
Toluene	Naphthalene	25	0.1502	16.10
Benzene	Naphthalene	25	0.1768	14.68
Carbon tetra- chloride	Naphthalene	25	0.2217	26.6
Water	Glycerol	4	0.611	$1.502 \times 10^6$
Water	Glycerol	25	0.580	$3.585 \times 10^3$
Ethylene glycol	Naphthalene	25	0.400	489
Ethylene glycol	Naphthalene	50	0.410	499

<sup>a</sup> Measured in this laboratory at 6328 Å.

**Table IV:** Intensity Ratio Coefficients

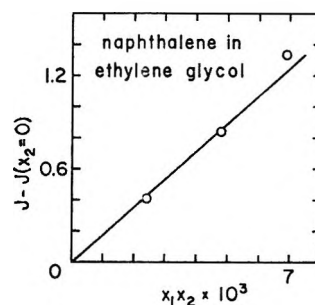
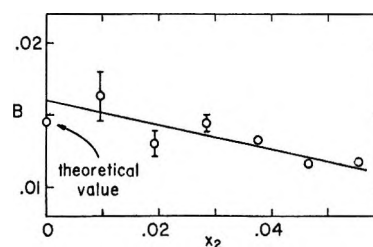
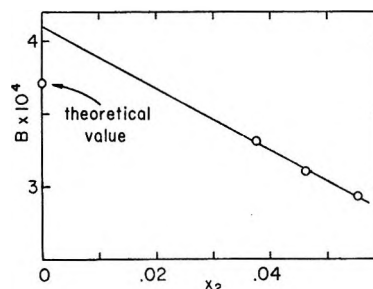
Solvent-solute	Temp, °C	Exptl		B (calcd)
		A	B	
$C_7H_8-C_{10}H_8$	25	0.432	0.37	0.37
$C_6H_6-C_{10}H_8$	25	0.890	0.52	0.52
$CCl_4-C_{10}H_8$	25	0.752	0.47	0.52
$H_2O-C_3H_8O_3$	4		$4.1 \times 10^{-4}$ <sup>a</sup>	$3.71 \times 10^{-4}$
$H_2O-C_3H_8O_3$	25		0.0138, <sup>b</sup> 0.0160 <sup>c</sup>	0.0145
$C_2H_6O_2-C_{10}H_8$	25	0.297	0.37	0.16 <sup>d</sup>
$C_2H_6O_2-C_{10}H_8$	50	0.206	0.20	0.19 <sup>d</sup>

<sup>a</sup> From the zero intercept in Figure 11. <sup>b</sup> From the limiting slope in Figure 8. <sup>c</sup> From the zero intercept in Figure 10. <sup>d</sup> Assuming  $R = \gamma - 1$ .

**Figure 8.** Excess intensity ratio of solutions at 25°.

between the central and side peaks was greatest here because of the broadness of the relaxation component. By our method, some of the intensity of this component was included in the side peaks, and, unless this apportionment was the same at all concentrations, a systematic error may have been introduced. Benzene, on the other hand, fit quite well our treatment of relaxation, and in our benzene spectra there was very little overlap.

For water we assumed no relaxation; *i.e.*,  $A = B = R$ . The agreement with experiment is quite good, al-

**Figure 9.** Excess intensity ratio of solutions at 25°.**Figure 10.** Intensity ratio coefficient for the concentration term of dilute aqueous glycerol at 25°.**Figure 11.** Intensity ratio coefficient for the concentration term of dilute aqueous glycerol at 4°.

though we were not able to reduce the dust problem to insignificance. It must be admitted that, at 4°,  $K$  is very concentration dependent, since small amounts of glycerol destroy the density maximum and greatly increase  $\partial n / \partial T$ . In fact we estimate that  $K$  decreases by one order of magnitude over the concentration range considered. However, in the product  $BK$ , the term  $\partial n / \partial T$  is much less dominant and we could use  $K_0$  to get a fictitious value of  $B$  which varied slowly with concentration and extrapolated readily to the true value at infinite dilution. Our data, nevertheless, are limited, because with our experimental setup we had difficulty operating at 4°.

To obtain an estimated value of  $B$  for ethylene glycol we assumed that  $R$  was equal to  $\gamma - 1$ . At 50° we got normal nonviscous behavior with  $A \cong B \cong \gamma - 1$ . At 25° the concentration fluctuation term was enhanced even more than the entropy fluctuation term; *i.e.*,  $B > A > \gamma - 1$ . Our treatment of relaxation appears to be inapplicable to viscous solutions.

### Conclusions

The intensity ratio of a real binary system follows the general form

$$J = A + BKRTx_1/(\partial\mu_2/\partial x_2)$$

Activity coefficients or the excess free energy can be extracted from the concentration dependence of  $\partial\mu_2/\partial x_2$ . To obtain the latter from experimental values of  $J$ , one must know the concentration dependence of the coefficients  $A$ ,  $B$ , and  $K$ . For a normal solution these may be obtained from a few subsidiary experiments.<sup>1</sup> If either component of the solution deviates significantly from the LP formula, some assumptions must be made about  $A$  and  $B$ . Each system will present its own problems, but some generalizations are possible at this point. The role of  $A$  is minimized by choosing systems with large excess scattering. Conversely, one can study the concentration dependence of  $A$  if the excess scattering is so small that any reasonable estimate of  $B$  will suffice. In a solution of two miscible liquids, at least one of which undergoes internal relaxation,  $B$  will probably not be much different from  $\gamma - 1$ . The limiting values of  $B$  may be determined experimentally, and the concentration dependence of  $\gamma - 1$  will serve as a good guide to the concentration dependence of  $B$ . In aqueous solutions  $A$  is negligibly small and the limiting value of  $B$  may be calculated. The important terms in the concentration dependence of  $B$  are perhaps  $\alpha$  and  $\partial n/\partial T$ , and it may be permissible to assume that  $\beta_T$  and  $\partial n/\partial P$  are concentration independent.

The determination of the molecular weight ( $M_2$ ) of polymers in solutions by light scattering is carried out

normally in very dilute solutions. If we let  $c$  be, say, grams of polymer per kilogram of solvent, then eq 4 becomes

$$J = J_0 + BK'M_2c$$

where

$$K' = \frac{C_p'}{RT^2} \left( \frac{\partial n/\partial c}{\partial n/\partial T} \right)^2$$

and  $C_p'$  is the heat capacity of 1 kg of solvent. Since the determination of  $M_2$  is directly affected by any uncertainty in the limiting value of  $B$ , it would be advisable to measure  $B$  using several solutes of known molecular weight. These need not be previously characterized polymers but, rather, simple compounds of low molecular weight like the ones used in the present study.

It has been tacitly assumed here that it is not generally practicable to separate the relaxation peak from the rest of the Brillouin spectrum, since this requires a fortuitous relaxation time plus higher resolution and a perfectly aligned interferometer. Indeed such a separation has been achieved with carbon tetrachloride and greatly simplifies the analysis, because addition of the relaxation intensity to that of the side peaks instead of the central peak gives a value of  $J$  equal to  $\gamma - 1$ .<sup>5</sup> Treated thusly, internally relaxing solutions would become normal ones.

*Acknowledgment.* This research was supported by a grant from the National Science Foundation (GP-4027).

# The Solubility of Helium, Nitrogen, Argon, and Ethane in N-Methylacetamide, a High Dielectric Solvent without Anomalous Structural Effects<sup>1,2</sup>

by R. H. Wood and D. E. DeLaney

Department of Chemistry, University of Delaware, Newark, Delaware 19711 (Received July 8, 1968)

The solubilities of helium, nitrogen, argon, and ethane in N-methylacetamide (NMA) have been measured from 35 to 70° and values of the free energy, heat, and entropy of solution have been calculated. A Barclay-Butler plot of  $\Delta H_v$  vs.  $\Delta S_v$  indicates that NMA unlike water behaves as a normal polar solvent toward nonpolar gases. The application of regular-solution theory gives values of the solubility which are far too low. The hypothesis that nonpolar solutes dissolve in NMA without disrupting the linear hydrogen-bonded chains of solvent molecules can explain both the solubility of inert gases in NMA and the fact that NMA dissolves large quantities of many nonpolar solutes.

## Introduction

The present measurements represent a small step in the investigation of the structure and thermodynamics of N-methylacetamide (NMA) solutions. It is known that the structure of the water molecules plays an important role in determining the properties of aqueous solutions and that thermodynamic measurements are a useful way of investigating structural effects.<sup>3-11</sup> Thus it seems reasonable that a knowledge of the structure of NMA and how this is affected by solutes will be useful for an understanding of NMA solutions.

In the crystalline state, the NMA molecules are hydrogen bonded together into long linear chains<sup>12</sup> with the nitrogen and oxygen atoms *trans* to each other. Infrared, Raman, dipole moment, and dielectric constant measurements indicate the presence in the pure liquid of long chains of molecules in the *trans* position.<sup>13-19</sup> In addition, the dipole moment of a chain increases substantially with chain length.<sup>13, 14, 16, 18</sup> The solubilities of nonpolar gases in NMA reported here can be explained by the hypothesis that small amounts of nonpolar solutes dissolve in NMA without appreciably disrupting the hydrogen-bonded chains of NMA molecules.

## Experimental Section

The details of the gas solubility measuring apparatus are given elsewhere.<sup>20</sup> Basically, the apparatus consisted of a gas buret and a solvent buret connected by a three-way capillary stopcock. A known amount of gas was quantitatively transferred to a known volume (about 100 ml) of degassed solvent, and the total pressure and volume of the system were observed when equilibrium was reached. Measurements at several temperatures were made and then the system was returned to the lowest temperature to check the initial

reading. Constant-temperature water circulating through a water jacket controlled the temperatures of the solvent and gas burets. Degassing was checked by measuring the vapor pressure of the solvent and by compressing the vapor and looking for a residual gas bubble. The observed solubility did not change after 3 hr of equilibration, but for safety at least 12 hr

(1) This work was supported by a grant from the National Science Foundation which is gratefully acknowledged.

(2) Presented at the 155th National Meeting of the American Chemical Society, San Francisco, Calif., April 1968.

(3) D. D. Eley, *Trans. Faraday Soc.*, **32**, 1281, 1421 (1939).

(4) H. S. Frank and M. W. Evans, *J. Chem. Phys.*, **13**, 507 (1945).

(5) W.-Y. Wen and H. S. Frank, *Discussions Faraday Soc.*, **24**, 133 (1957).

(6) D. N. Glew, *J. Phys. Chem.*, **66**, 605 (1962).

(7) L. A. D'Orazio and R. H. Wood, *ibid.*, **67**, 1435 (1963).

(8) G. Némethy and H. A. Scheraga, *J. Chem. Phys.*, **36**, 3382, 3401 (1962); **41**, 680 (1964); *J. Phys. Chem.*, **66**, 1773 (1962).

(9) A. Ben-Naim and S. Baer, *Trans. Faraday Soc.*, **59**, 2735 (1963); **60**, 1736 (1964).

(10) A. Ben-Naim, *J. Chem. Phys.*, **42**, 1512 (1965); **45**, 1848 (1966); *J. Phys. Chem.*, **69**, 1922, 3240, 3245 (1965); **71**, 448, 1137 (1967).

(11) A. Ben-Naim and M. Egel-Thal, *ibid.*, **69**, 3250 (1965).

(12) J. L. Katz and B. Post, *Acta Crystallogr.*, **13**, 624 (1960).

(13) S. Mizushima, T. Simanout, S. Nagakura, K. Kuratani, M. Isuboi, H. Baba, and O. Fujioka, *J. Amer. Chem. Soc.*, **72**, 3490 (1950).

(14) G. Leader and J. F. Gormley, *ibid.*, **73**, 5731 (1951).

(15) M. Davies and D. K. Thomas, *J. Phys. Chem.*, **60**, 767 (1956).

(16) R. Linn and W. Dannhauser, *ibid.*, **67**, 1805 (1963).

(17) I. M. Klotz and J. S. Franzen, *J. Amer. Chem. Soc.*, **84**, 3461 (1962).

(18) S. J. Bass, W. I. Nathan, R. M. Meighan, and R. H. Cole, *J. Phys. Chem.*, **68**, 509 (1964).

(19) L. A. Planche, H. B. Thompson, and M. T. Rogers, *ibid.*, **69**, 1482 (1965).

(20) D. E. DeLaney, M.S. Thesis, University of Delaware, Newark, Del., 1968.

was allowed for equilibration. In addition, approach to equilibrium from undersaturation and supersaturation gave identical results.

The solvent was recrystallized three times in a dry-box and typically had a water content of 0.04 mol % after a run. The helium, nitrogen, and argon were all high purity grade (99.99%) and the ethane was CP grade (99.0%).

Duplicate runs checked to within 0.5% for low solubilities (3 ml of gas/100 ml, of solvent) and within 0.1% for high solubilities (100 ml of gas/100 ml of solvent). As an additional check, the solubility of argon in water was measured at 25°. The result ( $\alpha = 31.05$ ) agrees nicely with the value of Ben-Naim<sup>9</sup> ( $\alpha = 31.21$ ).

### Results and Discussion

The experimental results were fit by the method of least squares to the equation

$$\ln X_2 = (a/T) + b \ln T + c \quad (1)$$

where  $X_2$  is the mole fraction of gas in the solvent when the partial pressure of gas is 1 atm. The smoothed values at 5° intervals are given in Table I and the constants of the equation are given in Table II. The heat, free energy, entropy, and change in heat capacity on solution were calculated (Table III) by the equations

$$\Delta G = -RT \ln X_2$$

$$\Delta H = -aR + bRT$$

$$\Delta S = (\Delta H - \Delta G)/T$$

$$\Delta C_p = bR$$

The results in Table I show that the larger nonpolar gases are much more soluble in NMA than they are in water. This seems to be a general characteristic of NMA, because Dawson, Berger, Vaughn and Eckstrom<sup>21</sup> have shown that unlike water, NMA will dissolve large amounts of nonpolar liquids. For instance, the following dissolve to an extent greater than 30 wt % in NMA: dioxane, cyclohexane, toluene, pyridine, and naphthalene. If NMA solutions are compared with typical nonpolar solvents, the solu-

**Table I:** Solubilities of Helium, Nitrogen, Argon, and Ethane in N-Methylacetamide (35–70°) from Least-Squares Fit

T, °C	Mole fraction $\times 10^4$ (at 1 atm)			
	Helium	Nitrogen	Argon	Ethane
35.00	0.557	2.461	4.444	41.91
40.00	0.591	2.492	4.456	39.63
45.00	0.626	2.523	4.466	37.52
50.00	0.663	2.554	4.476	35.57
55.00	0.699	2.583	4.483	33.76
60.00	0.738	2.613	4.490	32.07
65.00	0.776	2.641	4.494	30.50
70.00	0.816	2.669	4.498	29.03

**Table II:** Constants in Eq 1

	Helium	Nitrogen	Argon	Ethane
<i>a</i>	-1152.5	-245.7	-399.4	352.7
<i>b</i>	0 <sup>a</sup>	0 <sup>a</sup>	-1.12	-2.32
<i>c</i>	-6.0579	-7.514	-0.0278	6.704

<sup>a</sup> This was set equal to zero, since including this term did not appreciably help the least-squares fit.

**Table III:** Mole Fraction Solubility ( $\times 10^4$ ), Free Energy, Enthalpy, and Entropy of Solution of Helium, Nitrogen, Argon, and Ethane in N-Methylacetamide at 35°

Gas	$10^4 X_2$	$\Delta G$ , kcal/ mol <sup>a</sup>	$\Delta H$ , kcal/ mol <sup>a</sup>	$\Delta S$ , cal/deg mol	$\Delta C_p$ , <sup>a</sup> cal/ deg mol
He	0.557	6.00	2.3	-12.0	0
N <sub>2</sub>	2.461	5.09	0.5	-14.9	0
Ar	4.444	4.73	0.1	-15.0	-2
C <sub>2</sub> H <sub>6</sub>	41.91	3.35	-2.1	-17.8	-5

<sup>a</sup> The estimated 95% confidence limits are:  $\Delta G$ , about 0.01 kcal/mol;  $\Delta H$ , about 0.1 kcal/mol; and  $\Delta C_p$ , about 10 cal/deg mol.

bilities in Table I are a little lower than those observed for nonpolar solvents.

Frank and Evans<sup>4</sup> used a Barclay-Butler Plot<sup>22</sup> of  $\Delta S_v$  vs.  $\Delta H_v$  to show that nonpolar solutes in water created much more structure in the solvent than would be expected on the basis of the heat of interaction. This ability of a nonpolar solute to structure the water molecules around it has a very important influence on the properties of aqueous solutions.<sup>3-11</sup> A Barclay-Butler plot of the present results on NMA solutions is shown in Figure 1. This plot shows that nonpolar solutes in NMA do not have an unusual effect on the structure of the solutions. The line marked nonpolar in Figure 1 is Frank's<sup>23</sup> modification of the Barclay-Butler correlation. It shows how the entropy of vaporization and heat of vaporization of nonpolar solutes in nonpolar solvents are related. The data for NMA are only slightly higher than what would be expected for a nonpolar solute in a nonpolar solvent. The slightly high entropy of vaporization shown by NMA solutions is a characteristic of many somewhat polar solvents. In contrast, the line marked water shows the very high entropies of vaporization of aqueous solutions of nonpolar gases. This means that the nonpolar solutes do not appreciably affect the structure of

(21) L. R. Dawson, J. E. Berger, J. W. Vaughn, and H. Eckstrom, *J. Phys. Chem.*, **67**, 281 (1963).

(22) I. M. Barclay and J. A. V. Butler, *Trans. Faraday Soc.*, **34**, 1445 (1938).

(23) H. S. Frank, *J. Chem. Phys.*, **13**, 493 (1945).

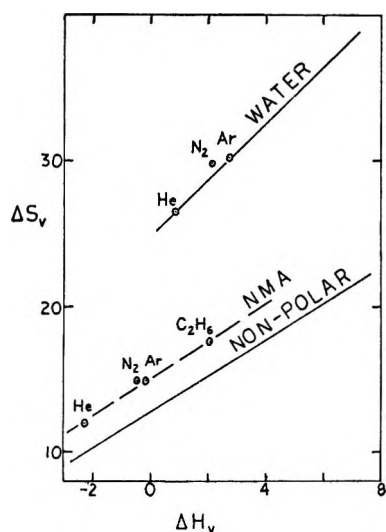


Figure 1. Heat of vaporization vs. entropy of vaporization for gases in water, NMA, and nonpolar solvents.

NMA solutions and that the anomalous effects in water are not present in NMA solutions.

Another effect of the water structure around nonpolar solutes is to produce a very large increase in the heat capacity of the solutions.<sup>3-6</sup> Table IV shows that the change in heat capacity upon dissolving these gases in NMA is very small compared with the results for aqueous solutions. This reinforces the conclusion that these solutes do not affect the structure of the solvent.<sup>5-7</sup>

Table IV: Change in Heat Capacity on Dissolving Gases in N-Methylacetamide

Gas	$\Delta C_p$ , cal/deg	
	NMA	H <sub>2</sub> O <sup>a</sup>
He	0	24
N <sub>2</sub>	0	41
Ar	-2	38
C <sub>2</sub> H <sub>6</sub>	-5	66

<sup>a</sup> Values from D. N. Glew and E. A. Moelwyn-Hughes, *Discussions Faraday Soc.*, 15, 150 (1953).

The solubility of nonpolar gases in nonpolar liquids can be roughly predicted by applying the equations for a regular solution<sup>24</sup> to the liquefied gas.<sup>25</sup> The resulting equation is

$$-\log X_2 = -\log X_2^i + 0.4343(\bar{V}_2/RT)(\delta_1 - \delta_2)^2 + \log(\bar{V}_2/V_1) + 0.4343[1 - (\bar{V}_2/V_1)] \quad (2)$$

where  $X_2^i$  is the "ideal solubility"<sup>25</sup> and  $\delta$  is the solubility parameter.<sup>24</sup> When this is done for NMA solutions, the predicted solubilities are  $1/10^{-1}/16$  times the experimental solubilities.<sup>26</sup>

A very simple model will explain all of the properties

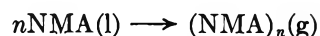
of NMA solutions discussed above. The model assumes that when small amounts of a nonpolar solute are dissolved in NMA the chains of NMA molecules are not appreciably disrupted but that the solute fits in between the chains. Thus toward a nonpolar solute, NMA behaves like a linear (but not rigid) polymer. The solute molecules are in contact with the nonpolar sides of the NMA polymer so that NMA behaves like a relatively nonpolar liquid toward these solutes. This explains why NMA dissolves so much ethane and why hydrocarbons are so soluble in it. In addition, the lack of any unusual entropy effects is also expected. Naturally, this assumption fails when polar solutes are introduced. The solubility of electrolytes in NMA is undoubtedly due to the solvation of the ions by the NMA. It is these two possible ways of interacting with solutes that explains why NMA is a good solvent for both electrolytes and nonpolar solutes.

The above model can be made somewhat more quantitative by applying eq 2 to the NMA polymer. If an  $n$ -mer is assumed, the equation for the solubility becomes

$$-\log X_2^0 = -\log X_2^i + 0.4343(\bar{V}_2/RT)(\delta_1 - \delta_2)^2 + \log(\bar{V}_2/V_1^0) - 0.4343[1 - (\bar{V}_2/nV_1^0)] \quad (3)$$

where the superscript zero represents monomer values, and we have used  $V_1 = nV_1^0$  and  $X_2 \simeq nX_2^0$ .

There is very little difference between eq 2 and 3. If anything, eq 3 predicts a lower solubility than eq 2 by a factor of 3 or so. However, there is a large difference in the solubility parameter  $\delta = ((\Delta H_v - RT)/V_1)^{1/2}$ . The appropriate solubility parameter for the  $n$ -mer is calculated from  $\Delta H_v$  for the process



If the heat of hydrogen bonding in the gas phase is known, then it can be shown that the appropriate solubility parameter is

$$\delta_1 = \{(\delta_1^0)^2 + [(n-1)/n](\Delta H(\text{HB}) + RT)/V_1\}^{1/2}$$

where  $\Delta H(\text{HB})$  is the heat of forming a hydrogen bond in the gas phase.

Unfortunately the heat of hydrogen bonding in the gas phase is not known. If the calculation is reversed, the gas solubility data are explained by a solubility parameter of  $9.3 \pm 0.3$  and a chain length ( $n$ ) of 15. This requires a gas-phase heat of hydrogen bonding of  $-6.5$  kcal/mol, which is the correct order of magnitude. The reported values of the heat of hydrogen bonding

(24) J. H. Hildebrand and R. L. Scott, "The Solubility of Non-electrolytes," 3rd ed, Reinhold Publishing Corp., New York, N. Y., 1950, p 240.

(25) J. Chr. Gjaldbaek and J. H. Hildebrand, *J. Amer. Chem. Soc.*, 71, 3147 (1949).

(26) The heat of vaporization of NMA,  $\Delta H_v = 13,290$  kcal/mol, was obtained from L. R. Dawson, W. H. Zuber, and H. C. Eckstrom, *J. Phys. Chem.*, 69, 1335 (1965).

are  $-3.6$  kcal/mol in benzene,<sup>27</sup>  $-4.2$  kcal/mol in carbon tetrachloride,<sup>28</sup> about  $-8$  kcal/mol in solid NMA,<sup>29</sup> and  $-4.5$  kcal/mol in liquid NMA.<sup>30</sup>

The model is crude enough that good agreement is not expected and the only conclusion is that the correction for the heat of hydrogen bonding is of approximately the right magnitude to explain the results. For quantitative predictions, the experimental solubility parameter  $\delta = 9.3$  should be used.

At high concentrations of nonpolar solute, the hydrogen-bonded chains will break apart and this will have to be taken into account. Appropriate theories are available<sup>31-33</sup> but there are no data to test them.

*Acknowledgment.* The authors thank Professor Carl A. von Frankenberg and Mr. Jonathan P. Hopkins for helpful discussions.

(27) M. Davis and D. K. Thomas, *J. Phys. Chem.*, **60**, 767 (1956).

(28) I. M. Klotz and J. S. Franzen, *J. Amer. Chem. Soc.*, **84**, 3461 (1962).

(29) M. Davis in "Hydrogen Bonding," D. Hadzi, Ed., Pergamon Press Inc., New York, N. Y., 1959, p 393.

(30) R. Lin and W. Dannhauser, *J. Phys. Chem.*, **67**, 1805 (1963).

(31) A. V. Tobolsky and P. J. Blatz, *J. Chem. Phys.*, **13**, 379 (1945).

(32) P. J. Flory, *ibid.*, **14**, 49 (1945).

(33) O. Redlick and A. T. Kister, *ibid.*, **15**, 849 (1947).

## Thermodynamics of Ionization of Deuterium Oxide

by Robert N. Goldberg<sup>1</sup> and Loren G. Hepler<sup>2</sup>

*Department of Chemistry, Carnegie-Mellon University, Pittsburgh, Pennsylvania (Received July 9, 1968)*

Heats of neutralization of HCl (in H<sub>2</sub>O) with NaOH (in H<sub>2</sub>O) and of DCl (in D<sub>2</sub>O) with NaOD (in D<sub>2</sub>O) have been measured calorimetrically. Heats of dilution of NaOD (in D<sub>2</sub>O) have also been measured. Results of these measurements have been combined with other heat of dilution data to yield standard heats of ionization of H<sub>2</sub>O and D<sub>2</sub>O at 298°K. The results are  $\Delta H^\circ = 13,350$  cal/mol for H<sub>2</sub>O and  $\Delta H^\circ = 14,488$  cal/mol for D<sub>2</sub>O. This  $\Delta H^\circ$  for H<sub>2</sub>O is in excellent agreement with results of several other calorimetric investigations but is smaller than a value derived from the variation of the ionization constant of H<sub>2</sub>O with temperature. Our calorimetric  $\Delta H^\circ$  for D<sub>2</sub>O is larger than the value derived from variation of the ionization constant of D<sub>2</sub>O with temperature. Standard states and concentration scales for aqueous solutions are discussed, followed by calculation of free energies and entropies of ionization of H<sub>2</sub>O and D<sub>2</sub>O.

### Introduction

Just as knowledge of thermodynamics of ionization of H<sub>2</sub>O is important for many aspects of chemistry involving acids and bases in ordinary water, knowledge of thermodynamics of ionization of D<sub>2</sub>O is important for this solvent. Since many earlier workers have also shown that comparison of thermodynamics of reactions taking place in H<sub>2</sub>O with thermodynamics of analogous reactions taking place in D<sub>2</sub>O can lead to useful information about solutes and the structures of aqueous solutions, it is clear that reliable and directly comparable data for ionization of H<sub>2</sub>O and D<sub>2</sub>O should be available.

For H<sub>2</sub>O we have equilibrium constants for ionization at several temperatures that permit calculation of  $\Delta G^\circ$ ,  $\Delta H^\circ$ , and  $\Delta S^\circ$  of ionization. Values of  $\Delta H^\circ$  derived from calorimetric measurements are also available. For D<sub>2</sub>O there are equilibrium constants at several temperatures but no calorimetric investigation of the enthalpy of ionization. Since there are important dis-

crepancies between the equilibrium and calorimetric data for H<sub>2</sub>O, we have undertaken the calorimetric investigation of the enthalpy of ionization of D<sub>2</sub>O that is described in this paper. Results of our measurements are presented along with detailed comparison with enthalpies calculated from equilibrium data of earlier investigators. We also discuss in detail the important question of standard states for solutions in H<sub>2</sub>O and D<sub>2</sub>O.

### Experimental Section

The calorimeter used in this investigation and an earlier investigation of water-triethylamine mixtures<sup>3</sup> consisted of a dewar vessel (capacity  $\sim 300$  ml) from Sears and Roebuck. This inexpensive vessel, which

(1) This paper is based on part of the Ph.D. Thesis of R. N. Goldberg, Carnegie-Mellon University, 1968.

(2) Some of the calculations and writing of this paper have been done at the University of Louisville.

(3) G. L. Bertrand, J. W. Larson, and L. G. Hepler, submitted for publication.

was recommended to us by Professor Robert Wood of the University of Delaware, is constructed of very thin glass. It therefore has low heat capacity and did not cause serious thermal lags in our measurements. A bright chrome-plated copper flange was fastened to the top of this dewar with epoxy resin.

The calorimeter environment consisted of a large cylindrical aluminum block that was donated to us by J. A. Nock of the Alcoa Research Laboratories for an earlier calorimetric investigation of molten salts.<sup>4</sup> Two cavities have been machined in the block to accommodate two dewars, but only one of these cavities was used in the present work. The 25-kg block sat in a constant-temperature bath that was controlled to 0.005°.

A bright chrome-plated copper lid for the dewar could be bolted to the flange that was attached with epoxy glue to the dewar, with a Teflon gasket placed between the flange and lid. This calorimeter lid was permanently fastened with Tru-bore ground-glass tubing from Ace Glass and epoxy resin to a larger lid of aluminum that covered the hole in the aluminum block without quite touching the block. This aluminum lid was itself fastened with thin-walled Monel tubes to a larger aluminum plate that could be securely mounted above the large block and constant-temperature bath.

Shafts for the glass stirrer and the sample introduction device slid through the Tru-bore tubes connecting the lid to the plate above. The stirrer was driven at 350 rpm by a small synchronous motor. Calorimetric samples were contained in small glass bulbs that were fastened to the end of the rod sliding through the Tru-bore tube. Gentle finger pressure on the top of the rod caused the bulb to break on a three-fingered glass prong attached to the heater coil described below. After the sample was broken and finger pressure released, a small spring caused the rod to return to its initial position. Careful experiments with water in both bulb and dewar showed that the heat effect associated with introduction of samples was  $0.003 \pm 0.007$  cal.

The calibration heater was contained in a glass spiral made of 6-mm Pyrex tubing that was filled with mineral oil and epoxied to the copper lid. This coil was so placed that the stirrer passed through its center. The calibration heater consisted of a 300-ohm coil of bifilarly wound no. 40 manganin wire. Leads of no. 30 copper wire were silver-soldered to the heater. Resistance of the heater was determined by comparison with a 100-ohm standard resistor. Power for the heater was supplied by a Kepco Model ABC 40-0.5 dc power supply that was connected to a dummy heater in a circuit similar to that previously described.<sup>5</sup> Two aged 100-ohm thermistors from Yellow Spring Instrument Co. were connected in parallel and contained in a straight Pyrex tube filled with mineral oil and epoxied to the copper lid. Leads to the thermistors were no. 26

manganin wire. Resistance changes were determined with a Leeds and Northrup G-2 Mueller bridge maintained at 35° and a Keithley Model 150B amplifier. In an effort to minimize noise, all wires were carefully shielded and appropriate points were connected to a common ground. The thermistors were calibrated against an NBS-calibrated mercury-in-glass thermometer and were periodically checked at 25.00° against this same thermometer.

All H<sub>2</sub>O used was purified by distillation from a tin-lined still and was degassed just prior to use to remove dissolved carbon dioxide. A solution of hydrochloric acid from Baker Chemical Co. was used to prepare a stock solution of HCl. This solution was analyzed by precipitation of silver chloride.<sup>6</sup> The average deviation of seven determinations made at different times through the course of the calorimetric measurements was 0.02%. A carbonate-free solution of sodium hydroxide was prepared<sup>6</sup> from NaOH pellets from Baker Chemical Co. and analyzed by titration with the already standardized HCl solution. Repeated testing of this solution with barium chloride showed no detectable carbonate.

Deuterium oxide of stated isotopic purity 99.8+‰ was loaned to us by the U. S. Atomic Energy Commission. Solutions of DCl and NaOD in D<sub>2</sub>O were obtained from the Stohler Isotope Co. and diluted to the desired concentrations with D<sub>2</sub>O that had been previously degassed. The average deviation of seven analyses of the DCl solution by precipitation of AgCl was 0.02% and repeated testing of the NaOD solution with barium chloride confirmed the absence of carbonate.

The heat of neutralization measurements for H<sub>2</sub>O and D<sub>2</sub>O solutions were carried out identically in an effort to make the difference in the two resulting  $\Delta H^\circ$  values as significant as possible. All measurements were carried out with an excess of base so that presence of traces of carbonate could not cause appreciable error.

A semimicrobalance sensitive to 10<sup>-5</sup> g was used for all weighings. Calibrated weights were used, and appropriate vacuum corrections were made.

A weighed amount of stock acid solution was added to the calorimetric dewar, to which a weighed amount of degassed water (H<sub>2</sub>O or D<sub>2</sub>O) had been previously added. Stock solution of base was injected with a Teflon syringe into a weighed thin-walled glass sample bulb, which was sealed with a torch, weighed, and tied to the sample introduction rod with thread.

At least 1 hr was allowed for the calorimeter to approach thermal equilibrium after it was assembled and placed in the aluminum block in the constant-temper-

(4) T. Hu, H. C. Ko, and L. G. Hepler, *J. Phys. Chem.*, **68**, 387 (1964).

(5) W. F. O'Hara, C. H. Wu, and L. G. Hepler, *J. Chem. Educ.*, **38**, 512 (1961).

(6) E. H. Swift, "Introductory Quantitative Analysis," Prentice-Hall, Inc., New York, N. Y., 1950.

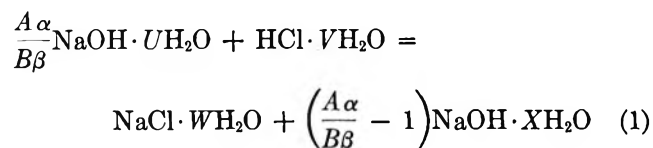
ature bath. During this time the dewar and its contents were brought to  $25.00 \pm 0.10^\circ$  by means of the internal calibration heater. The reaction was then initiated by breaking the bulb. After a suitable period, the dewar and its contents were cooled to below  $25^\circ$  and slowly brought back to  $25.00^\circ$ . Then the system was calibrated by using the heater to bring about a temperature rise nearly identical with that caused by the reaction. All  $\Delta H$  values were therefore obtained in terms of the defined calorie equal to 4.184 J.

Heat of dilution measurements for NaOD in  $D_2O$  were also made. For these measurements a known amount of degassed  $D_2O$  was placed in the dewar and 1 drop of NaOD solution was added. Solutions of NaOD in  $D_2O$  were placed in the sample bulbs. Two dilution measurements with NaOH in  $H_2O$  yielded results in good agreement with heats calculated from data cited in Parker's tabulation.<sup>7</sup>

In all cases the assigned reaction temperature was  $25.0^\circ$ .<sup>8</sup>

### Results

We describe the reaction of NaOH with HCl in  $H_2O$  with the equation



A similar equation may be written for the reaction of NaOD with DCl in  $D_2O$ , except that every H in eq 1 is replaced by a D. In both cases the following definitions hold:  $A$  = mass in grams of basic solution in the sample bulb;  $\alpha$  = concentration (moles of NaOH or NaOD/g of solution) of basic solution in the bulb;  $B$  = mass in grams of acidic solution added to the dewar;  $\beta$  = concentration (moles of HCl or DCl/g of solution) of acidic solution added to water in the dewar;  $C$  = mass in grams of water ( $H_2O$  or  $D_2O$ ) added to the dewar. The coefficients  $U$ ,  $V$ ,  $W$ , and  $X$  in eq 1 can be related to the measured quantities  $A$ ,  $B$ ,  $C$ ,  $\alpha$ , and  $\beta$  by

$$U = \frac{1 - \alpha M_b}{\alpha M_w}$$

$$V = \frac{C + (1 - \beta M_a)B}{\beta B M_w}$$

$$W = \frac{A\alpha U}{B\beta} + V + 1$$

$$X = \frac{W}{\frac{A\alpha}{B\beta} - 1}$$

In these equations  $M_b$ ,  $M_a$ , and  $M_w$  are the molecular weights of base (NaOH or NaOD), acid (HCl or DCl), and water ( $H_2O$  or  $D_2O$ ).

The measured heat of neutralization is represented by  $\Delta h$  and the molar heat of reaction represented by  $\Delta H_N$  is calculated as  $\Delta H_N = \Delta h/B\beta$ . The standard heat of neutralization represented by  $\Delta H_N^\circ$  is calculated from  $\Delta H_N$  by means of

$$\Delta H_N^\circ = \Delta H_N + \frac{A\alpha}{B\beta} \Phi_L(\text{NaOH} \cdot U\text{H}_2\text{O}) + \Phi_L(\text{HCl} \cdot V\text{H}_2\text{O}) - \Phi_L\left(\text{NaCl} \cdot \frac{WX}{W+X} \text{H}_2\text{O}\right) - \left(\frac{A\alpha}{B\beta} - 1\right) \Phi_L\left(\text{NaOH} \cdot \frac{WX}{W+X} \text{H}_2\text{O}\right) = \Delta H_N + \Delta H_{\text{cor}} \quad (2)$$

In this equation heats of dilution are represented by  $\Phi_L$ , the negative of the integral heat of dilution to infinite dilution. Replacing each hydrogen in eq 2 with deuterium makes it applicable to the heat of neutralization of DCl with NaOD in  $D_2O$ .

The results of our measurements with HCl and NaOH in  $H_2O$  and calculations based on eq 2 are given in Table I. Heat of dilution data were taken from Parker's tabulation.<sup>7</sup> The average result of our 15 measurements (no measurements discarded) is  $\Delta H_N^\circ = -13,350$  cal/mol with the average deviation from this value being 25 cal/mol. Uncertainties due to random and systematic errors in our calorimetric measurements ( $\sim 15$  cal/mol), analyses of reagents ( $\sim 7$  cal/mol), and heats of dilution ( $\sim 15$  cal/mol) lead to a total uncertainty of about  $\pm 25$  cal/mol in our  $\Delta H_N^\circ$  value.

In order to obtain the standard heat of neutralization from measured heats of neutralization in  $D_2O$  it is necessary to have heat of dilution data for NaCl, DCl, and NaOD in  $D_2O$ . Recent measurements by Wood<sup>9</sup> have yielded  $\Delta\Phi_L = \Phi_{LH}(\text{NaCl in } H_2O) - \Phi_{LD}(\text{NaCl in } D_2O) = 53.6m' - 7.11m'^2$ , while Wu and Friedman<sup>10</sup> have reported  $\Delta\Phi_L = (34 \pm 5)m'$  where  $m'$  is aquamolality (moles of solute per 55.51 mol of solvent). The discrepancy between these  $\Delta\Phi_L$  values is less than 1 cal/mol when applied to our measurements in which  $m' < 0.04$ . Gary, Bates, and Robinson<sup>11</sup> have calculated  $\bar{L}$  values for DCl in  $D_2O$  from results of their emf measurements at several temperatures. Their  $\bar{L}$  values lead us to  $\Delta\Phi_L \cong 40m'$ . Because  $m' < 0.04$  for the DCl solutions used in our neutralization measurements, the error introduced by an error of 25 in the constant will be no more than 1 cal/mol.

(7) V. B. Parker, "Thermal Properties of Aqueous Uni-univalent Electrolytes," Report NSRDS-NBS 2, U. S. National Bureau of Standards, U. S. Government Printing Office, Washington, D. C., 1965.

(8) F. D. Rossini, "Experimental Thermochemistry," Interscience Publishers, New York, N. Y., 1956.

(9) R. Wood, personal communication, 1968.

(10) Y. Wu and H. L. Friedman, *J. Phys. Chem.*, **70**, 166 (1966).

(11) R. Gary, R. G. Bates, and R. A. Robinson, *ibid.*, **68**, 1186 (1964).



**Table I:** Heats of Neutralization of NaOH with HCl in H<sub>2</sub>O

Run no.	HCl, <sup>a</sup> g	NaOH, <sup>b</sup> g	-Δ <i>h</i> , cal	-Δ <i>H</i> <sub>N</sub> , cal/mol	<i>U</i> <sup>c</sup>	<i>V</i> <sup>c</sup>	<i>W</i> <sup>c</sup>	<i>X</i> <sup>c</sup>	Δ <i>H</i> <sub>cor</sub> , cal/mol	-Δ <i>H</i> <sub>N</sub> <sup>c</sup> , cal/mol
1	7.98691	4.86371	104.36	13,326	24.73	2087	2119	7,585	-16	13,342
2	6.58521	3.75487	85.864	13,298	24.73	2519	2550	12,880	-10	13,308
3	7.20691	4.03148	94.446	13,366	24.73	2307	2337	13,332	-7	13,373
4	5.20974	2.92452	68.251	13,361	24.73	3170	3200	17,838	-11	13,372
5	6.24873	3.49274	81.891	13,366	24.73	2652	2683	15,383	-9	13,375
6	7.59243	4.24496	99.232	13,330	24.73	2192	2222	12,723	-6	13,336
7	6.01309	3.38810	78.640	13,338	24.73	2754	2784	15,147	-10	13,348
8	7.06846	3.89257	92.528	13,351	24.73	2351	2381	15,166	-5	13,356
9	11.36834	6.33247	148.11	13,288	24.73	1482	1512	8,880	+2	13,286
10	7.30291	4.13707	95.707	13,366	24.73	2277	2308	12,132	-8	13,374
11	9.39748	5.23980	123.11	13,361	24.73	1782	1812	10,566	-2	13,363
12	8.03204	4.51980	105.22	13,361	24.73	2075	2106	11,552	-7	13,368
13	8.14321	4.56479	106.05	13,282	24.73	2048	2079	11,691	-6	13,288
14	9.14440	5.11294	119.74	13,355	24.73	1830	1860	10,642	-3	13,358
15	5.93701	3.30448	77.948	13,390	24.73	2788	2818	16,638	-9	13,398

<sup>a</sup> HCl solution contains  $9.8049 \times 10^{-4}$  mol of HCl/g of solution. <sup>b</sup> NaOH solution contains  $2.060 \times 10^{-3}$  mol of NaOH/g of solution. <sup>c</sup> To the HCl in the dewar was added 286.7 g of H<sub>2</sub>O. Molecular weights used were: HCl, 36.451; NaOH, 39.997; H<sub>2</sub>O, 18.01534.

**Table II:** Heat of Dilution Measurements for NaOD in D<sub>2</sub>O

Run no.	NaOD, <sup>a</sup> g	Δ <i>h</i> , cal	NaOD, mol	Δ <i>H</i> , cal/mol	<i>m</i> ' <sub>i</sub>	<i>m</i> ' <sub>f</sub> <sup>b</sup>	$\frac{[\Phi_{LH}(m'_f) - \Phi_{LH}(m'_i) - \Delta H]/(m'_f - m'_i)}$
1	8.09099	5.534	0.018116	305.5	2.741	0.0621	74.3
2	7.64274	5.227	0.017112	305.5	2.741	0.0588	74.8
3	6.79760	4.584	0.015220	301.2	2.741	0.0524	74.2
4	6.91481	4.644	0.015482	300.0	2.741	0.0533	73.6
5	6.20055	0.897	0.007273	123.3	1.370	0.0251	79.3
6	4.97573	0.752	0.005837	128.8	1.370	0.0202	87.0
7	4.72760	0.693	0.005545	125.0	1.370	0.0192	84.9
8	5.28790	0.791	0.006203	127.5	1.370	0.0214	85.2
9	6.18670	1.798	0.009398	191.3	1.801	0.0324	78.6
10	9.53483	3.049	0.014483	210.5	1.801	0.0494	83.4
11	7.77811	2.311	0.011815	195.6	1.801	0.0405	78.0
12	6.78045	2.151	0.010300	208.8	1.801	0.0354	87.3
13	7.71688	3.880	0.014762	262.8	2.308	0.0507	77.2
14	6.86983	3.468	0.013142	263.9	2.308	0.0452	79.1
15	7.49869	3.728	0.014345	259.9	2.308	0.0493	76.3

<sup>a</sup> NaOD solutions contain  $2.239 \times 10^{-3}$  mol of NaOD/g of solution in runs 1-4,  $1.173 \times 10^{-3}$  mol of NaOD/g of solution in runs 5-8,  $1.519 \times 10^{-3}$  mol of NaOD/g of solution in runs 9-12, and  $1.913 \times 10^{-3}$  mol of NaOD/g of solution in runs 13-15. <sup>b</sup> In all runs 316.8 g of D<sub>2</sub>O was contained in the dewar.

Since there are no heat of dilution data available for NaOD in D<sub>2</sub>O, we have measured heats that correspond to the dilution represented by

$$\text{NaOD}(m'_i) = \text{NaOD}(m'_f) \quad (3)$$

A measured enthalpy change (Δ*h*) for a dilution divided by the number of moles of NaOD gives the molar heat represented by

$$\Delta H = \Phi_{LD}(m'_f) - \Phi_{LD}(m'_i) \quad (4)$$

The results of our measurements are put into convenient form by way of

$$\Delta \Phi_L = \Phi_{LH} - \Phi_{LD} = k_1 m' + k_2 m'^2 \quad (5)$$

that is combined with (4) to give

$$\frac{\Phi_{LH}(m'_f) - \Phi_{LH}(m'_i) - \Delta H}{m'_f - m'_i} = k_1 + k_2(m'_f + m'_i) \quad (6)$$

Our data that are reported in Table II have been used in constructing a graph. ( $\Phi_{LH}(m'_f) - \Phi_{LH}(m'_i)$ ) was calculated from Parker's<sup>7</sup> tabulation) of the left side of eq 6 against ( $m'_f + m'_i$ ), from which we have obtained  $k_1 = 95.2 \pm 6$  and  $k_2 = -7.5 \pm 2$ .

The results of our heat of neutralization measurements with DCl and NaOD in D<sub>2</sub>O and calculations based on the "D" version of eq 2 are given in Table III.

Table III: Heats of Neutralization of NaOD with DCl in D<sub>2</sub>O

Run no.	DCl, <sup>a</sup> g	NaOH, <sup>b</sup> g	-Δh, cal	-ΔH <sub>N</sub> , cal/mol	U <sup>c</sup>	V <sup>c</sup>	W <sup>c</sup>	X <sup>c</sup>	ΔH <sub>cor</sub> , cal/mol	-ΔH <sub>N</sub> <sup>o</sup> , cal/mol
1	8.76665	4.08040	125.381	14,238	20.25	1844	1866	49,802	-219	14,457
2	8.28172	4.26321	118.605	14,257	20.25	1949	1973	13,385	-254	14,511
3	10.21102	5.28211	146.649	14,297	20.25	1590	1614	10,547	-253	14,550
4	10.24028	5.28464	146.465	14,239	20.25	1585	1610	10,710	-252	14,491
5	11.38303	5.86407	162.553	14,216	20.25	1431	1455	9,815	-250	14,466
6	10.28157	5.25795	147.495	14,281	20.25	1579	1603	11,461	-248	14,529
7	9.13561	4.68810	130.632	14,235	20.25	1771	1795	12,483	-251	14,486
8	10.96777	5.65333	156.613	14,215	20.25	1483	1508	10,124	-250	14,465
9	7.57431	3.91172	108.297	14,234	20.25	2127	2151	14,231	-256	14,490
10	8.00506	4.08115	114.307	14,215	20.25	2015	2039	14,949	-251	14,466
11	8.78927	4.48347	125.533	14,219	20.25	1839	1863	13,599	-250	14,469
12	10.00779	5.09665	143.731	14,298	20.25	1621	1645	12,173	-247	14,545
13	10.07512	5.12539	143.672	14,196	20.25	1611	1635	12,206	-247	14,443
14	9.91121	5.07376	141.579	14,221	20.25	1636	1651	11,718	-249	14,470
15	11.31769	5.78835	161.911	14,242	20.25	1439	1463	10,451	-247	14,489

<sup>a</sup> DCl solution contains  $1.0045 \times 10^{-3}$  mol of DCl/g of solution. <sup>b</sup> NaOD solution contains  $2.239 \times 10^{-3}$  mol of NaOD/g of solution. <sup>c</sup> To the DCl in the dewar was added 316.8 g of D<sub>2</sub>O. Molecular weights used were: DCl, 37.469; NaOD, 41.005; D<sub>2</sub>O, 20.031.

We have taken care to present our data in such form that they can be used for further calculations when better heat of dilution data become available. The average result of our 15 measurements (no measurements discarded) is  $\Delta H^\circ = -14,488$  cal/mol with the average deviation from this value being 24 cal/mol. Estimated uncertainties due to calorimetric errors in the heat of neutralization measurements ( $\sim 15$  cal/mol), analyses of reagents ( $\sim 10$  cal/mol), and heats of dilution ( $\sim 40$  cal/mol) lead to a total uncertainty of about  $\pm 45$  cal/mol in our  $\Delta H_N^\circ$  value.

### Discussion

Previous careful calorimetric measurements by Vanderzee and Swanson<sup>12</sup> and by Hale, Izatt, and Christensen<sup>13</sup> have led these workers to report  $\Delta H^\circ = 13,336 \pm 18$  and  $13,340 \pm 20$  cal/mol for ionization of H<sub>2</sub>O at 298°K. They<sup>12,13</sup> have also reviewed earlier calorimetric investigations leading to  $\Delta H^\circ$  values ranging from 13,320 to 13,369 cal/mol. Parker's<sup>7</sup> consideration of the results of Vanderzee and Swanson<sup>12</sup> along with the results of earlier investigations led her to recommend  $\Delta H^\circ = 13,345 \pm 25$  cal/mol. Our average  $\Delta H^\circ$  for H<sub>2</sub>O is thus in excellent agreement with results of a number of earlier investigators.

Covington, Robinson, and Bates<sup>14</sup> have recalculated the results of earlier emf measurements that led to ionization constants for H<sub>2</sub>O at several temperatures and have derived  $\Delta H^\circ = 13,526$  cal/mol for the heat of ionization at 298°K. Although there is no certain explanation of the difference between this value and the calorimetric results, the weight of evidence suggests that the "best"  $\Delta H^\circ$  value is very close to 13.34 kcal/mol as derived from calorimetry.

Covington, Robinson, and Bates<sup>14</sup> have made careful measurements on emf cells without liquid junctions in

order to determine the ionization constant of D<sub>2</sub>O at several temperatures. They have reported  $pK_m = 14.955$  and  $pK_c = 14.869$  at 25°, where the subscripts *m* and *c* indicate "molality scale" (moles of solute/kg of solvent) and "molarity scale" (moles of solute/l. of solution), respectively. The relation between the *pK* values on these "scales" or choices of solute standard states is

$$pK_c = pK_m - 2 \log \rho \quad (7)$$

in which  $\rho$  represents the density of the solvent. As pointed out later, it is also useful to know the ionization constant on the *aquamolality* scale (moles of solute/55.51 mol of solvent). When D<sub>2</sub>O is the solvent, the "reference" mass of solvent is 1.112 kg and we have

$$pK_{m'} = pK_m - 2 \log 1.112 = pK_m - 0.092 \quad (8)$$

in which the subscript *m'* indicates the "aquamolality scale." We therefore have  $pK_{m'} = 14.863$  from the work of Covington, Robinson, and Bates.<sup>14</sup>

Covington, Robinson, and Bates<sup>14</sup> have compared their *pK* values with corresponding results of earlier workers. More recently, measurements by Pentz and Thornton<sup>15</sup> at 25° led to  $pK_c = 14.86$ . For further calculations of free energies of ionization of D<sub>2</sub>O we use the *pK* values from Covington, Robinson, and Bates<sup>14</sup> that are given in the paragraph above.

Covington, Robinson, and Bates<sup>14</sup> have used their  $pK_m$  values at several temperatures with the van't

(12) C. E. Vanderzee and J. A. Swanson, *J. Phys. Chem.*, **67**, 2608 (1963).

(13) J. D. Hale, R. M. Izatt, and J. J. Christensen, *ibid.*, **67**, 2605 (1963).

(14) A. K. Covington, R. A. Robinson, and R. G. Bates, *ibid.*, **70**, 3820 (1966).

(15) L. Pentz and E. R. Thornton, *J. Am. Chem. Soc.*, **89**, 6931 (1967).

Hoff equation in calculating  $\Delta H^\circ = 14,311$  cal/mol for ionization of  $D_2O$  at  $25^\circ$ . Wynne-Jones<sup>16</sup> has used emf cells with liquid junction to obtain  $pK_c$  at three temperatures and has reported  $\Delta H^\circ = 14,420$  cal/mol for ionization of  $D_2O$  at  $25^\circ$ . This value, which was calculated from  $dpK_c/dT$ , requires correction as follows. Differentiation of eq 7 with respect to  $T$  and combination with the van't Hoff equation gives

$$\Delta H^\circ = \Delta H^\circ_{WJ} - (2)(2.303)RT^2 \left( \frac{d \log \rho}{dT} \right) \quad (9)$$

in which  $\Delta H^\circ_{WJ}$  represents the value calculated by Wynne-Jones<sup>16</sup> from  $d \ln K_c/dT$ . We use densities of  $D_2O$  from Schrader and Wirtz<sup>17</sup> to obtain  $\Delta H^\circ = 14,492$  cal/mol from the work of Wynne-Jones<sup>16</sup> on ionization of  $D_2O$ . It should be understood that  $\Delta H^\circ$  values on the various "scales" are identical, but it is necessary to include the effect of temperature on the density of the solvent as in eq 9 when  $K$  values based on volume of solution (molarity, rather than molality, aquamolality, or mole fraction) are used with the van't Hoff equation for calculation of  $\Delta H^\circ$ .

Our calorimetric  $\Delta H^\circ = 14,488$  cal/mol for ionization of  $D_2O$  at  $298^\circ K$  is 177 cal/mol larger than the  $\Delta H^\circ = 14,311$  cal/mol derived by Covington, Robinson, and Bates<sup>14</sup> from their  $pK_m$  values at several temperatures. In this connection it is interesting to note that the "best" calorimetric  $\Delta H^\circ$  for ionization of  $H_2O$  is about 180 cal/mol *smaller* than the  $\Delta H^\circ$  recalculated by Covington, Robinson, and Bates<sup>14</sup> from  $pK$  values for  $H_2O$  at several temperatures.

The difference between the independent  $\Delta H^\circ$  values from our work and from Covington, Robinson, and Bates<sup>14</sup> is larger than the sum of reasonable estimates of the uncertainties. Since both investigations have been carried out with considerable care, only further measurements can tell which of these  $\Delta H^\circ$  values is "best." Although the  $\Delta H^\circ$  value calculated from work of Wynne-Jones<sup>16</sup> is in excellent agreement with our calorimetric results for  $D_2O$  (14,492 and 14,488 kcal/mol), our estimate of the uncertainty to be associated with the  $\Delta H^\circ$  from Wynne-Jones is sufficiently large that his value may also be regarded as agreeing well with that from Covington, Robinson, and Bates<sup>14</sup> and cannot necessarily be regarded as independent confirmation of our work.

We have used the results cited by Covington, Robinson, and Bates<sup>14</sup> at  $298^\circ K$  to calculate the  $\Delta G^\circ$  values

given in Table IV. These  $\Delta G^\circ$  values have been combined with our calorimetric  $\Delta H^\circ$  for  $D_2O$  and our selection of the "best"  $\Delta H^\circ$  for  $H_2O$  to yield the tabulated  $\Delta S^\circ$  values. The  $\Delta H^\circ$  and  $\Delta S^\circ$  values in parentheses are derived entirely from Covington, Robinson, and Bates.<sup>14</sup>

Table IV: Thermodynamics of Ionization of  $H_2O$  and  $D_2O$  at  $298^\circ K^a$

Parameter	$H_2O$	$D_2O$
$\Delta G^\circ_m$	19,095	20,403
$\Delta G^\circ_{m'}$	19,095	20,278
$\Delta G^\circ_c$	19,099	20,286
$\Delta H^\circ$	13,340 (13,526) <sup>b</sup>	14,488 (14,311) <sup>b</sup>
$\Delta S^\circ_m$	-19.30 (-18.68) <sup>c</sup>	-19.84 (-20.43) <sup>c</sup>
$\Delta S^\circ_{m'}$	-19.30 (-18.68) <sup>c</sup>	-19.42 (-20.01) <sup>c</sup>
$\Delta S^\circ_c$	-19.32 (-18.69) <sup>c</sup>	-19.45 (-20.04) <sup>c</sup>

<sup>a</sup>  $\Delta G^\circ$  and  $\Delta H^\circ$  values are in cal/mol and  $\Delta S^\circ$  values are in gibbs/mol, where 1 gibbs = 1 cal/deg. <sup>b</sup>  $\Delta H^\circ$  values given in parentheses are those reported by Covington, Robinson, and Bates.<sup>14</sup> <sup>c</sup>  $\Delta S^\circ$  values given in parentheses are those based on our tabulated  $\Delta G^\circ$  values and on the  $\Delta H^\circ$  values from Covington, Robinson, and Bates.<sup>14</sup>

It is our opinion that the most meaningful theoretical comparisons of  $\Delta G^\circ$  and  $\Delta S^\circ$  of ionization for  $D_2O$  and  $H_2O$  should be made on the aquamolality, mole fraction, or molarity scales, rather than on the molality scale. These comparisons would then be in terms of equal numbers of moles of water or equal volumes rather than in terms of equal masses.

*Acknowledgments.* We are pleased to thank Dr. G. L. Bertrand, who largely designed and built the calorimetric apparatus used in this investigation. We are also grateful to Dr. Robert Wood for helpful comments on calorimeter construction and for his kindness in giving us the results of his unpublished heat of dilution measurements. Dr. A. K. Covington, Dr. R. A. Robinson, and Dr. R. G. Bates kindly informed us of their results before their paper was published. We also thank the Atomic Energy Commission for lending us  $D_2O$  and the National Science Foundation and the Department of Chemistry, Carnegie-Mellon University, for their financial support of part of this research.

(16) W. F. K. Wynne-Jones, *Trans. Faraday Soc.*, **32**, 1397 (1936).

(17) R. Schrader and K. Wirtz, *Z. Naturforsch.*, **6a**, 220 (1951).

## Potentials of Cells with Liquid Junctions

by William H. Smyrl<sup>1</sup> and John Newman

*Inorganic Materials Research Division, Lawrence Radiation Laboratory, and  
Department of Chemical Engineering, University of California, Berkeley, California 94720 (Received July 11, 1968)*

The potential of cells with liquid junctions is affected by diffusion of ions in the junction region. From the laws of diffusion, concentration profiles and values of potentials have been calculated for several different junctions without the assumption of activity coefficients equal to 1. The results have been compared to existing experimental data, and the results of the calculations of others. The magnitude of the diffusion effect has been calculated also for cases where it is desirable that the effect be negligible, as with an electrode of the second kind.

### Introduction

The only cells used in electrochemical studies which are strictly without liquid junction are those used to study the thermodynamic properties of alloys. In addition there are cells in which the effect of diffusion in the liquid junction is negligible, for example, a cell with an electrode of the second kind involving a solid salt which is only very slightly soluble. The theoretical analysis of the potential of cells with liquid junctions has been of interest to workers who wish to derive thermodynamic values from such cells by correcting for the effect of diffusion. Some of the basic problems of liquid junctions have been treated adequately (Taylor,<sup>2a</sup> Guggenheim,<sup>2b</sup> and Wagner<sup>3</sup>), and we give here an alternate discussion which emphasizes the quantitative treatment of the transport phenomena. In addition, we shall present a method, with examples, of the calculation of the effect of diffusion on cell potentials without the assumption of ideal-solution behavior and activity coefficients equal to unity.

We shall attempt to give a clear definition of what is meant by liquid junction potentials and to give a clear treatment of the diffusion phenomena. The expression of cell potentials involves a consideration of electrode equilibria. However, the final result generally requires a knowledge of the concentration profiles and of the effect of diffusion. Therefore, we begin with the treatment of transport in electrolytic solutions and of the determination of the concentration profiles.

### Transport in Electrolytic Solutions

The difference of the electrochemical potential,  $\mu_i$ , of an ion between two points (or phases) is the work of transferring 1 gram-ion reversibly at constant temperature and volume from one point (or phase) to the other.<sup>4</sup> If we regard  $c_i \nabla \mu_i$  as the driving force per unit volume for diffusion and migration of species  $i$ , neutral species included (where  $\nabla \mu_i$  is the gradient of the electrochemical potential of species  $i$ ), and  $K_{ij}(\mathbf{v}_j - \mathbf{v}_i)$  is the drag force exerted on species  $i$  by species  $j$  by virtue of their relative motion, then a force balance leads to the multicomponent diffusion equation

$$c_i \nabla \mu_i = \sum_j K_{ij}(\mathbf{v}_j - \mathbf{v}_i) \quad (1)$$

The coefficient  $K_{ij}$  is taken to be independent of the velocity difference  $\mathbf{v}_j - \mathbf{v}_i$ , but it may be a function of temperature, pressure, and composition of the solution. The velocity  $\mathbf{v}_j$  is the average or macroscopic velocity of species  $j$ .

Instead of  $K_{ij}$ , one can define a transport coefficient  $\mathcal{D}_{ij}$  having the dimensions of a diffusion coefficient

$$K_{ij} = RT \frac{c_i c_j}{c_T \mathcal{D}_{ij}} \quad (2)$$

where  $c_T$  is the total concentration of the solution. This also serves the goal of accounting for much of the composition dependence of the coefficients  $K_{ij}$ . Equation 1 has been discussed elsewhere (see, for example, Newman<sup>5</sup>).

In this force balance,  $K_{ij} = K_{ji}$  or  $\mathcal{D}_{ij} = \mathcal{D}_{ji}$  by Newton's third law of motion. This is equivalent to the assumption frequently made in treatments of irreversible thermodynamics. Compare Onsager,<sup>6</sup> who wrote the equation in the form

$$-\nabla \mu_i = \sum_k R_{ik}(c_k v_k - c_k v_i) \quad (3)$$

In applications it is frequently desirable to use this equation in an inverted form. Toward this end it is to be noted that there are only  $n - 1$  independent velocity differences and  $n - 1$  independent gradients of electrochemical potentials in a solution with  $n$  species. Therefore, eq 1 can be expressed as

$$c_i \nabla \mu_i = \sum_j M_{ij}(\mathbf{v}_j - \mathbf{v}_o) \quad (4)$$

(1) School of Pharmacy, University of California, San Francisco, Calif.

(2) (a) P. B. Taylor, *J. Phys. Chem.*, **31**, 1478 (1927); (b) E. A. Guggenheim, *ibid.*, **33**, 842 (1929).

(3) C. Wagner, *Advan. Electrochem. Electrochem. Eng.*, **4**, 1 (1966).

(4) E. A. Guggenheim, "Thermodynamics," North-Holland Publishing Co., Amsterdam, The Netherlands, 1959, p 374.

(5) J. Newman, *Advan. Electrochem. Electrochem. Eng.*, **5**, 87 (1967).

(6) L. Onsager, *Ann. N. Y. Acad. Sci.*, **46**, 241 (1945).

where  $\mathbf{v}_o$  is the velocity of any one of the species and where

$$M_{ij} = K_{ij} \quad (i \neq j)$$

$$M_{ij} = K_{ij} - \sum_k K_{ik} \quad (i = j)$$

It further follows that  $M_{ij} = M_{ji}$ . Bearing in mind that there are  $n - 1$  independent equations of the form of eq 4, one can invert this equation to read

$$\mathbf{v}_j - \mathbf{v}_o = - \sum_{k \neq 0} L_{jk} c_k \nabla \mu_k \quad (j \neq 0) \quad (5)$$

where the matrix  $L^o$  is the inverse of the submatrix  $M^o$

$$L^o = (M^o)^{-1} \quad (6)$$

and where the submatrix  $M^o$  is obtained from the matrix  $M$  by deleting the row and the column corresponding to the species  $o$ . The inverse matrix  $L^o$  is also symmetric, that is

$$L_{ij}^o = L_{ji}^o \quad (7)$$

It is to be expected that the  $R_{ij}$ 's and the  $\mathfrak{D}_{ij}$ 's will be less composition dependent than the  $L_{ij}^o$ 's.

Certain combinations of the  $L_{ij}^o$ 's are related to measurable transport properties and have particular significance in the treatment of cells with liquid junctions. The current density is related to the fluxes of ionic species as follows

$$\mathbf{i} = F \sum_i z_i \mathbf{N}_i = F \sum_i z_i c_i \mathbf{v}_i = F \sum_i z_i c_i (\mathbf{v}_i - \mathbf{v}_o) \quad (8)$$

Substitution of eq 5 yields

$$\mathbf{i} = -F \sum_{i \neq 0} z_i c_i \sum_{k \neq 0} L_{ik} c_k \nabla \mu_k \quad (9)$$

In a solution of uniform composition

$$\nabla \mu_k = z_k F \nabla \Phi \quad (10)$$

where  $\nabla \Phi$  is the gradient of the electric potential. Equation 9 becomes in this case

$$\mathbf{i} = -F^2 \nabla \Phi \sum_{i \neq 0} z_i c_i \sum_{k \neq 0} L_{ik} z_k c_k \quad (11)$$

Comparison with Ohm's law, also applicable in this case

$$\mathbf{i} = -\kappa \nabla \Phi$$

allows us to identify the conductivity

$$\kappa = F^2 \sum_{i \neq 0} \sum_{k \neq 0} L_{ik} z_i c_i z_k c_k \quad (12)$$

Although the  $L_{ik}$ 's depend upon the reference velocity chosen, the conductivity,  $\kappa$ , is invariant with respect to this choice.

Next we can identify the transference numbers. Again, for a solution of uniform composition, eq 10 is valid and eq 5 becomes

$$\mathbf{v}_j - \mathbf{v}_o = -F \nabla \Phi \sum_{k \neq 0} L_{jk} z_k c_k \quad (13)$$

For this case of uniform composition, the species flux is related to the current density and the transference number by the expression

$$t_j \mathbf{i} = z_j F c_j (\mathbf{v}_j - \mathbf{v}_o) = -t_j^o \kappa \nabla \Phi \quad (14)$$

Comparison shows that the transference number  $t_j^o$  of species  $j$  with respect to species  $o$  is given by

$$t_j^o = \frac{z_j c_j F^2}{\kappa} \sum_{k \neq 0} L_{jk} z_k c_k \quad (15)$$

It is to be noted that the transference number has been defined as the fraction of the current carried by an ion in a solution of uniform composition. In a solution in which there are concentration gradients, the transference number is still a transport property related to the  $L_{ij}^o$ 's by eq 15, but it no longer represents the fraction of current carried by an ion. A different choice of the reference species will change the  $L_{ij}$ 's and hence the transference numbers with respect to a common reference species.

Equation 9 is applicable even in a nonuniform solution, and it can be rewritten in terms of the conductivity and the transference numbers, since  $L_{ij}^o = L_{ji}^o$

$$\frac{F}{\kappa} \mathbf{i} = - \sum_i \frac{t_i^o}{z_i} \nabla \mu_i \quad (16)$$

As already noted, a different choice of reference species will change the transference numbers, but eq 16 still applies. However, it is apparent from eq 15 that the ratio  $t_j^o/z_j$  is not zero even for a neutral species. While the reference velocity can be chosen arbitrarily to be that of any one of the species, charged or uncharged, it is usually taken to be the velocity of the solvent. In this case there is no problem if there are no other neutral components, since the ratio  $t_i^o/z_i$  is always zero for the reference species.

Equation 16 also has the same form if other reference velocities, such as the mass-average velocity or the molar-average velocity, are used. Again, care should be exercised since the ratio  $t_i/z_i$  is then not zero for neutral species.

Equation 16 is quite useful in the calculation of the potential of cells with liquid junctions. In the cases of interest the current density is supposed to be zero, but eq 16 also allows one to estimate the effect of the passage of small amounts of current. Equation 16 is generally useful only if the concentration profiles in the liquid junction are known. These are determined not from eq 16 but from the laws of diffusion (eq 1) and the method of forming the junction.

### Determination of Concentration Profiles

Several models of liquid junctions are popular, and to these we add one more.

a. *Free-Diffusion Junction.* At time zero the two solutions are brought into contact to form an initially sharp boundary in a long, vertical tube. The solutions

are then allowed to diffuse into each other, and the thickness of the region of varying concentration increases with the square root of time. Even if the transport properties are concentration dependent and the activity coefficients are not unity, the potential of a cell containing such a junction should be independent of time.

*b. Restricted-Diffusion Junction.* The concentration profiles are allowed to reach a steady state by one-dimensional diffusion in the region between  $x = 0$  and  $x = L$ , in the absence of convection. The composition  $x = 0$  is that of one solution and at  $x = L$  is that of the other solution. The potential of a cell containing such a junction is independent of  $L$  (as well as time). The condition of no convection is usually not specified (*i.e.*, zero solvent velocity or zero mass-average velocity, etc.).

*c. Continuous-Mixture Junction.* At all points in the junction, the concentrations (excluding, we suppose, that of the solvent) are assumed to be linear combinations of those of the solutions at the ends of the boundary. This assumption obviates the problem of calculating the concentration profiles by the laws of diffusion.

*d. Flowing Junction.* In some experiments the solutions are brought together and allowed to flow side by side for some distance. It is sometimes supposed that observed potentials should approximate those given by a free-diffusion boundary.

*e. Electrode of the Second Kind.* To these we add the region of varying composition produced when a sparingly soluble salt is brought into contact with a solution containing a common ion. We might use a model similar to the free-diffusion junction if we imagine the salt to be introduced at the bottom of a vertical tube containing the solution. The sparingly soluble salt will then diffuse up the tube, and the concentration at the bottom will be governed by the solubility product.

The concentration profiles in cases a, b, and e are governed by the laws of diffusion (eq 1). We propose to treat solutions so dilute that, in eq 1, we can neglect the interaction of the diffusing species with the other components except the solvent

$$c_i \nabla \mu_i = RT \frac{c_i c_o}{c_T \mathcal{D}_{oi}} (\mathbf{v}_o - \mathbf{v}_i) = RT \frac{c_i}{\mathcal{D}_{oi}} (\mathbf{v}_o - \mathbf{v}_i) \quad (17)$$

or

$$\mathbf{N}_i = c_i \mathbf{v}_i = - \frac{c_i \mathcal{D}_{oi}}{RT} \nabla \mu_i + c_i \mathbf{v}_o \quad (18)$$

However, the activity coefficients will not be assumed to be unity.

The electrochemical potential,  $\mu_i$ , of an ionic species depends not only on the composition of the phase but also on the electrical state of the phase. For computational purposes it is convenient to express all the electro-

chemical potentials in terms of one electrical variable. One way to do this is to use the electrochemical potential for one ionic species,  $\mu_n$ , as a reference

$$\mu_i = \mu_i - \frac{z_i}{z_n} \mu_n + \frac{z_i}{z_n} \mu_n \quad (19)$$

The combination  $\mu_i - (z_i \mu_n / z_n)$  is then the chemical potential of a neutral combination of ions and is independent of the electrical state, depending only on the local composition.

However, this choice is not convenient, particularly when the concentration of species  $n$  goes to zero. Another possibility is to express the electrochemical potential of species  $n$  as

$$\mu_n = RT \ln c_n + z_n F \Phi + \mu_n^\theta \quad (20)$$

The potential  $\Phi$  then has some of the characteristics of the commonly used electrostatic potential and, in fact, has exactly the same properties in infinitely dilute solutions where the activity coefficients of all neutral combinations become equal to 1. At higher concentrations, the quasi-electrostatic potential,  $\Phi$ , is of course arbitrary in the sense that it depends on the designation of the reference species  $n$ .

In contrast, the electrochemical potential of species  $n$ , or  $\mu_n / z_n F$ , behaves more like the potential of a reference electrode reversible to species  $n$ . In a solution of uniform composition, both of these potentials behave like the commonly used electrostatic potential and, in fact, satisfy Laplace's equation

$$\nabla^2 \Phi = 0 \quad (21)$$

Now the chemical potential of a neutral combination can be expressed in terms of a well-defined combination of activity coefficients

$$\mu_i - \frac{z_i}{z_n} \mu_n = \mu_i^\theta - \frac{z_i}{z_n} \mu_n^\theta + RT \ln c_i - \frac{z_i RT}{z_n} \ln c_n + RT \left( \ln f_i - \frac{z_i}{z_n} \ln f_n \right) \quad (22)$$

For the activity coefficients we shall use Guggenheim's expression<sup>7</sup> for dilute solutions of several electrolytes

$$\ln f_i - \frac{z_i}{z_n} \ln f_n = -\alpha z_i (z_i - z_n) \frac{I^{1/2}}{1 + I^{1/2}} + 2 \sum_j \left( \beta_{ij} - \frac{z_i}{z_n} \beta_{nj} \right) c_j \quad (23)$$

where

$$I = 1/2 \sum_j z_j^2 c_j \quad (24)$$

is the ionic strength,  $c_j$  is in moles per liter, and for aqueous solutions  $\alpha = 1.171$  (l./mol)<sup>1/2</sup> at 25°. The values of the coefficients  $\beta_{ij}$  are tabulated by Guggenheim and are zero unless species  $i$  and  $j$  are ions of

(7) See ref 4, p 357.

opposite charge. We shall use these expressions with concentrations instead of molalities, as used by Guggenheim.

Finally, then, the electrochemical potential of an ionic species is expressed as

$$\mu_i = RT \ln c_i + z_i F \Phi + \mu_i^0 + RT \left\{ -\alpha z_i (z_i - z_n) \times \frac{I^{1/2}}{1 + I^{1/2}} + 2 \sum_j \left( \beta_{ij} - \frac{z_i}{z_n} \beta_{nj} \right) c_j \right\} \quad (25)$$

To determine the concentration profiles in liquid junctions involves solving the diffusion eq 18 in conjunction with eq 25 and with the material balance equation

$$\frac{\partial c_i}{\partial t} = -\nabla N_i \quad (26)$$

the electroneutrality equation

$$\sum_i z_i c_i = 0 \quad (27)$$

and the condition of zero current. In a following section we illustrate how to use the concentration profiles or the values of  $\Delta\Phi$  to calculate cell potentials. Substitution of eq 18 and 25 into eq 26 yields an equation describing diffusion, migration, and convection of an ionic species but including the activity coefficients in the driving force

$$\frac{\partial c_i}{\partial t} + \nabla \cdot (c_i \mathbf{v}_0) = \mathcal{D}_{oi} \nabla^2 c_i + \frac{z_i F \mathcal{D}_{oi}}{RT} \nabla \cdot (c_i \nabla \Phi) - \alpha z_i (z_i - z_n) \mathcal{D}_{oi} \nabla \cdot \left( c_i \nabla \frac{I^{1/2}}{1 + I^{1/2}} \right) + 2 \mathcal{D}_{oi} \sum_j \left( \beta_{ij} - \frac{z_i}{z_n} \beta_{nj} \right) \nabla \cdot (c_i \nabla c_j) \quad (28)$$

This equation applies to solutions so dilute that interactions except with the solvent in the multicomponent diffusion equation can be ignored and eq 23 can be used for the activity coefficients.

This problem can be solved numerically for the various models of the liquid junction. In the case of restricted diffusion, the equations are already ordinary differential equations. For free diffusion and for an electrode of the second kind, the similarity transformation  $Y = y/\sqrt{t}$  reduces the problem to ordinary differential equations. These coupled, nonlinear, ordinary differential equations can readily be solved by the method of Newman.<sup>8</sup> The equations can be linearized about a trial solution, producing a series of coupled, linear differential equations. In finite difference form these give coupled, tridiagonal matrices which can be solved on a high-speed, digital computer. The nonlinear problem can then be solved by iteration.

## Numerical Results

We present here calculated values of  $\Delta\Phi$  for the several models for the junctions between solutions of various compositions. No detailed concentration profiles will be given, since the potentials of cells with liquid junctions can be calculated directly from the tabulated values of  $\Delta\Phi$ , without further reference to the concentration profiles, as indicated in the next section. The tabulation of the values of  $\Delta\Phi$ , rather than the potentials of complete cells, is convenient because these values relate to the junction itself, whereas more than one combination of electrodes is possible for a given junction. In addition to  $\Delta\Phi$ , only thermodynamic data are needed to calculate potentials of complete cells, the entire effect of the transport phenomena being included in  $\Delta\Phi$ .

The value of  $\Delta\Phi$  depends upon the choice of the reference ion  $n$ . In each case this is the last ion for a given junction in the tables. For infinitely dilute solutions,  $\Delta\Phi$  becomes independent of this choice and, furthermore, depends only on the ratios of concentrations of the ions in the end solutions. Solutions of zero ionic strength ( $f_i = 1$ ) are indicated by an asterisk, but the concentrations are given nonzero values so that these ratios will be clear. These junctions also provide a basis for comparison with more concentrated solutions, to indicate the effect of the activity coefficients.

Table I gives values of  $\Delta\Phi$  for the continuous-mixture, restricted-diffusion, and free-diffusion junctions. Table II gives values of  $\Delta\Phi$  for an electrode of the second kind, where AgCl, with a solubility product of  $10^{-10}$  (mol/l.)<sup>2</sup>, diffuses into hydrochloric acid solutions of various concentrations. For solutions of zero ionic strength, the values of  $\Delta\Phi$  for the continuous-mixture and restricted-diffusion junctions agree with the values calculated by the methods of Henderson<sup>9</sup> and Planck,<sup>10</sup> respectively. In Figures 1-6 are presented the results of more extensive calculations on the HCl-KCl junction.

## Cells with Liquid Junction

Once the concentration profiles are known for a liquid junction region, it is then possible to calculate the effect of the nonuniform composition on the cell potential. This effect is considered in the following subsections for cells of increasingly complex liquid junctions. It will always be assumed that the electrodes are in equilibrium with the adjacent solutions and that regions of nonuniform composition lie outside the immediate vicinity of the electrodes.

The procedure then involves first the treatment of electrode equilibria, in the manner of Guggenheim.<sup>11</sup>

(8) J. Newman, *Ind. Eng. Chem., Fundamentals*, **7**, 514 (1968).

(9) P. Henderson, *Z. Phys. Chem. (Leipzig)*, **59**, 118 (1907); **63**, 325 (1908).

(10) M. Planck, *Ann. Phys. Chem.*, **39**, 161 (1890); **40**, 561 (1890).

**Table I:** Values of  $\Delta\Phi$  for Various Junctions and Various Models at 25<sup>o</sup>a

Ion	Soln 1	Soln 2	$\Phi_1 - \Phi_2$ , mV		
			Free diffusion	Restricted diffusion	Continuous mixture
H <sup>+</sup>	0.2	0.1	...	...	-10.31
Cl <sup>-</sup>	0.2	0.1	...	...	-11.43*
K <sup>+</sup>	0.2	0.1	...	...	1.861 (2.05) <sup>b</sup>
Cl <sup>-</sup>	0.2	0.1	...	...	0.335*
K <sup>+</sup>	0	0.01	-33.50	-32.65	-33.75
H <sup>+</sup>	0.02	0	-34.67*	-33.80*	-34.95*
Cl <sup>-</sup>	0.02	0.01			
K <sup>+</sup>	0	0.1	-27.31, (-27.08), <sup>c</sup> (-28.25, 18°), <sup>d</sup> (-28.3), <sup>e</sup> -26.69*	-27.45	-27.47 (-28.10, 18°) <sup>d</sup>
H <sup>+</sup>	0.1	0		-26.85*	-26.85*
Cl <sup>-</sup>	0.1	0.1			
K <sup>+</sup>	0	0.2	-27.92	-28.04	-28.09
H <sup>+</sup>	0.2	0	-26.69*	-26.85*	-26.85*
Cl <sup>-</sup>	0.2	0.2			
K <sup>+</sup>	0	0.2	-22.58	-23.03	-22.31
H <sup>+</sup>	0.1	0	-20.24*	-20.74*	-19.96*
Cl <sup>-</sup>	0.1	0.2			
K <sup>+</sup>	0	0.05	-20.70	-21.09	-20.23
H <sup>+</sup>	0.02	0	-18.50*	-18.97*	-18.02*
Cl <sup>-</sup>	0.02	0.05			
K <sup>+</sup>	0	0.1	-18.02	-17.89	-16.84
H <sup>+</sup>	0.02	0	-14.05*	-14.12*	-12.90*
Cl <sup>-</sup>	0.02	0.1			
K <sup>+</sup>	0	0.1	-15.91	-14.99	-14.04
H <sup>+</sup>	0.01	0	-10.85*	-10.30*	-9.09*
Cl <sup>-</sup>	0.01	0.1			
K <sup>+</sup>	0	0.1	-27.24, (-27.98) <sup>f</sup>	-27.38	-27.40
H <sup>+</sup>	0.09917	0	-26.60*	-26.77*	-26.76*
Cl <sup>-</sup>	0.09917	0.1			
K <sup>+</sup>	0	0.1			
H <sup>+</sup>	0.09917	0	-27.39	-27.48	-27.55
NO <sub>3</sub> <sup>-</sup>	0	0.05	-26.53*	-26.62*	-26.70*
Cl <sup>-</sup>	0.09917	0.05			
K <sup>+</sup>	0.1	0.1	-0.157	-0.157	-0.157
NO <sub>3</sub> <sup>-</sup>	0.05	0	-0.423*	-0.423*	-0.423*
Cl <sup>-</sup>	0.05	0.1			
Na <sup>+</sup>	0.1	0			
H <sup>+</sup>	0	0.05	28.58	29.64	28.10
ClO <sub>4</sub> <sup>-</sup>	0	0.05	26.72*	27.90*	26.22*
Cl <sup>-</sup>	0.1	0			
Na <sup>+</sup>	0.1	0			
H <sup>+</sup>	0	0.1	32.83	33.50	33.05
ClO <sub>4</sub> <sup>-</sup>	0	0.1	32.35*	33.11*	32.57*
Cl <sup>-</sup>	0.1	0			
Na <sup>+</sup>	0.2	0			
H <sup>+</sup>	0	0.2	33.29	33.88	33.53
ClO <sub>4</sub> <sup>-</sup>	0	0.2	32.35*	33.11*	32.57*
Cl <sup>-</sup>	0.2	0			
Na <sup>+</sup>	0.05	0			
H <sup>+</sup>	0	0.1	38.77	38.31	39.26
ClO <sub>4</sub> <sup>-</sup>	0	0.1	39.96*	39.58*	40.48*
Cl <sup>-</sup>	0.05	0			



Table I (Continued)

Ion	Soln 1	Soln 2	$\Phi_1 - \Phi_2$ , mV		
			Free diffusion	Restricted diffusion	Continuous mixture
Cu <sup>2+</sup>	0	0.1			
Ag <sup>+</sup>	0.2	0			
NO <sub>3</sub> <sup>-</sup>	0.2	0	-6.22*	-6.22*	-6.22*
ClO <sub>4</sub> <sup>-</sup>	0	0.2			

<sup>a</sup> Values for  $f_1 = 1$  are indicated by an asterisk. The last ion is the reference ion. Experimental values are given in parentheses. <sup>b</sup> T. Shedlovsky and D. A. MacInnes, *J. Amer. Chem. Soc.*, **59**, 503 (1937). <sup>c</sup> J. B. Chloupek, V. Z. Kanes, and B. A. Danesova, *Collect. Czech. Chem. Commun.*, **5**, 469, 527 (1933). <sup>d</sup> E. A. Guggenheim and A. Unmack, *Kgl. Danske Videnskab. Selskab, Mat-Fys. Medd.*, **10**, 1 (1931). <sup>e</sup> D. C. Grahame and J. I. Cummings, Office of Naval Research Technical Report No. 5, 1950. <sup>f</sup> N. P. Finkelstein and E. T. Verdier, *Trans. Faraday Soc.*, **53**, 1618 (1957).

Table II: Values of  $\Delta\Phi$  for an Ag-AgCl Electrode in HCl Solutions at 25°<sup>a</sup>

	[HCl] (bulk), M					
	10 <sup>-4</sup>	5 × 10 <sup>-5</sup>	2 × 10 <sup>-5</sup>	10 <sup>-6</sup>	5 × 10 <sup>-6</sup>	2 × 10 <sup>-6</sup>
$\Phi_0 - \Phi_{\infty}$ , mV	0.0198	0.0737	0.359	0.915	1.780	3.21
$c_{\text{Cl}^-}^0/c_{\text{Cl}^-}^{\infty}$	1.00961	1.0392	1.200	1.604	2.539	5.499
$(\mu_{\text{Cl}^-}^{\infty} - \mu_{\text{Cl}^-}^0)/F$ , mV	-0.226	-0.914	-4.32	-11.22	-22.16	-40.58

<sup>a</sup> Chloride is the reference electrode, and  $\beta$  values are taken to be zero.

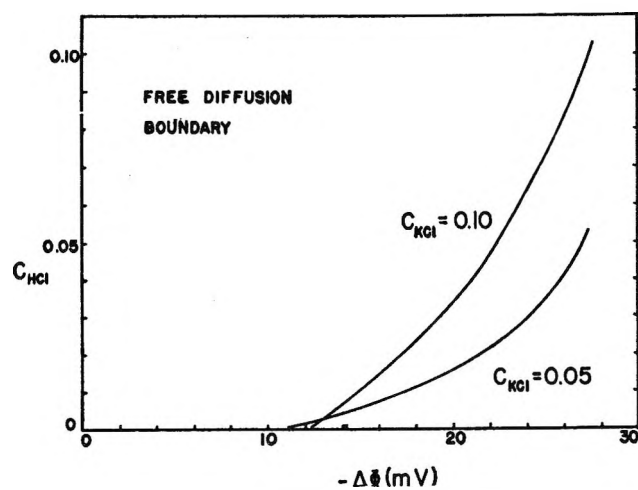


Figure 1.  $-\Delta\Phi$  (mV) for free-diffusion boundary between HCl and KCl, calculated for two different concentrations of KCl.

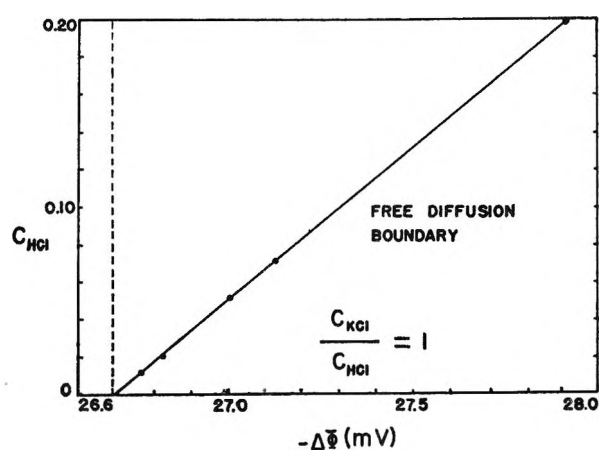


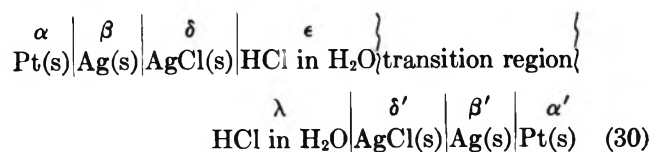
Figure 2. Calculated values of  $-\Delta\Phi$  (mV) for free-diffusion boundary between HCl and KCl, at a constant ratio of  $C_{\text{KCl}}$  to  $C_{\text{HCl}}$ . The dashed line represents the (constant) ideal-solution calculation, the solid line includes activity coefficient corrections.

This allows the expression of the cell potential in terms of a difference in the electrochemical potential of ions in the solutions adjacent to the two electrodes. The evaluation of this difference involves the integration of eq 16 across the junction region. This equation can be rewritten in the form

$$\frac{1}{z_j} \nabla \mu_j = - \sum_i \frac{t_i^0}{z_i} \left[ \nabla \mu_i - \frac{z_i}{z_j} \nabla \mu_j \right] - \frac{F}{\kappa} \mathbf{i} \quad (29)$$

The sum on the right now involves only the gradients of electrochemical potentials of neutral combinations of ions and can be determined from a knowledge of the concentration profiles.

a. *Cell with a Single Electrolyte of Varying Concentration.* Cells containing a single electrolyte whose concentration varies with location in the cell constitute the simplest of the so-called cells with transference. An example is



(11) See ref 4, p 382.

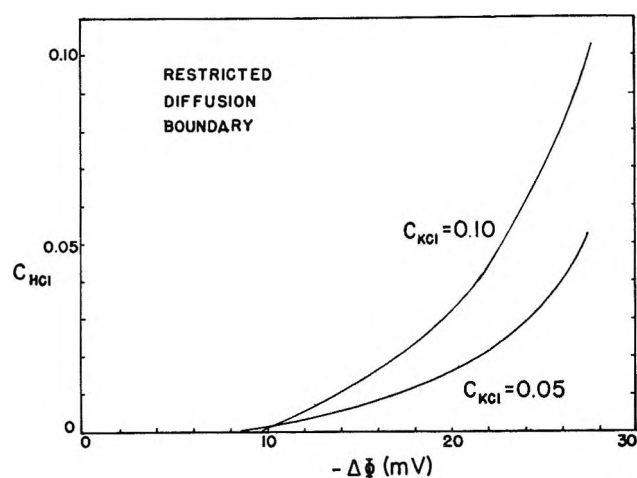


Figure 3. Results for the restricted-diffusion boundary HCl-KCl, given for two different concentrations of KCl.

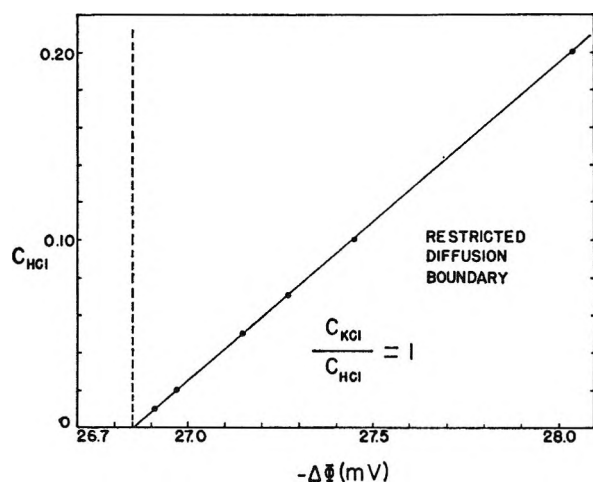


Figure 4. Results for the restricted-diffusion boundary HCl-KCl, for a constant ratio of  $C_{\text{KCl}}$  to  $C_{\text{HCl}}$ . The dashed line represents the ideal-solution calculation, the solid line includes activity coefficient corrections.

where the platinum leads and the silver-silver chloride electrodes have identical compositions on both sides of the cell. In the transition region or liquid junction, the concentration of HCl varies from the value in the  $\epsilon$  phase to that in the  $\lambda$  phase.

At both electrodes there is equilibrium among the  $\alpha$ ,  $\beta$ ,  $\delta$ , and  $\epsilon$  phases, for example

$$\mu_{\text{Cl}^-}^{\delta} = \mu_{\text{Cl}^-}^{\epsilon}; \quad \mu_{\text{Ag}^+}^{\delta} = \mu_{\text{Ag}^+}^{\beta}; \quad \mu_{e^-}^{\alpha} = \mu_{e^-}^{\beta} \quad (31)$$

Combination of these relations with the definitions of the chemical potentials of the neutral silver and silver chloride, for example

$$\mu_{\text{Ag}}^{\beta} = \mu_{\text{Ag}^+}^{\beta} + \mu_{\text{e}^-}^{\beta}; \quad \mu_{\text{AgCl}}^{\delta} = \mu_{\text{Ag}^+}^{\delta} + \mu_{\text{Cl}^-}^{\delta} \quad (32)$$

yields an expression for the cell potential

$$-F(\psi^{\alpha} - \psi^{\alpha'}) = \mu_{e^-}^{\alpha} - \mu_{e^-}^{\alpha'} = \mu_{\text{Ag}}^{\beta} - \mu_{\text{AgCl}}^{\delta} + \mu_{\text{Cl}^-}^{\epsilon} - \mu_{\text{Ag}}^{\beta'} + \mu_{\text{AgCl}}^{\delta'} - \mu_{\text{Cl}^-}^{\lambda} \quad (33)$$

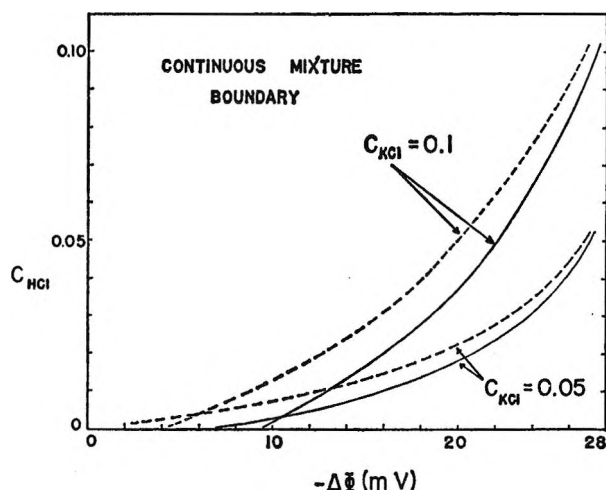


Figure 5. Values of  $-\Delta\Phi$  (mV) for the continuous-mixture boundary. The dashed line corresponds to the Henderson calculation; the solid line includes activity coefficient corrections.

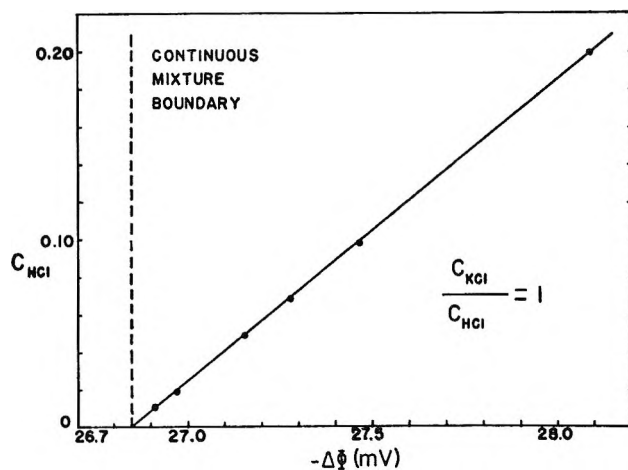


Figure 6. Continuous-mixture boundary calculations for a constant ratio of  $C_{\text{KCl}}$  to  $C_{\text{HCl}}$ . The dashed line is the ideal-solution calculation, the solid line includes activity coefficient corrections.

since the difference in electrochemical potential of electrons in the two leads is related to the cell potential as indicated. Since the electrodes are of identical composition, the expression for the cell potential reduces to

$$-F(\psi^{\alpha} - \psi^{\alpha'}) = \mu_{\text{Cl}^-}^{\epsilon} - \mu_{\text{Cl}^-}^{\lambda} \quad (34)$$

This difference in the electrochemical potentials of chloride ions can be evaluated with the aid of eq 29, which becomes in this case

$$\frac{\partial \mu_{\text{Cl}^-}}{\partial x} = t_{\text{H}^+}^{\circ} \frac{\partial \mu_{\text{HCl}}}{\partial x} \quad (35)$$

Equation 34 becomes

$$-F(\psi^{\alpha} - \psi^{\alpha'}) = \int_{\lambda}^{\epsilon} t_{\text{H}^+}^{\circ} d\mu_{\text{HCl}} \quad (36)$$

On the other hand, one could express the difference in

electrochemical potentials of chloride ions in terms of the quasi-electrostatic potential  $\Phi$  based on chloride ions as the reference ion

$$-F(\psi^\alpha - \psi^{\alpha'}) = -F(\Phi^\epsilon - \Phi^\lambda) + RT \ln (c_{\text{Cl}^-}^\epsilon / c_{\text{Cl}^-}^\lambda) \quad (37)$$

As shown in eq 36, the cell potential is independent of the method of forming the junction for the case of a single electrolyte of varying concentration; that is, the integral is independent of the detailed form of the concentration profile. From measured cell potentials, eq 36 may be used to determine activity coefficients if the transference number is known, or it may be used to determine the transference number if the activity coefficient is known. Both types of determination are common practice.

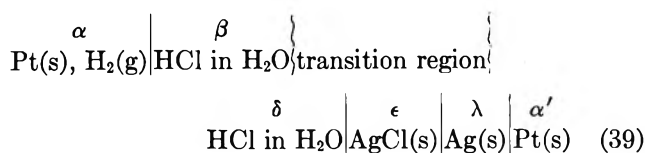
From the tabulated values of  $\Delta\Phi$  (which tabulation requires prior knowledge of the transference number and the activity coefficient) one can calculate the cell potential from eq 37. For example, for  $c_{\text{HCl}}^\epsilon = 0.2 M$  and  $c_{\text{HCl}}^\lambda = 0.1 M$  we obtain  $-(\psi^\alpha - \psi^{\alpha'}) = 28.11 \text{ mV}$ .

If the silver-silver chloride electrodes were replaced by hydrogen electrodes, the expression for the potential of such a cell would become

$$-F(\psi^\alpha - \psi^{\alpha'}) = \mu_{\text{HCl}}^\lambda - \mu_{\text{HCl}}^\epsilon + \mu_{\text{Cl}^-}^\epsilon - \mu_{\text{Cl}^-}^\lambda \quad (38)$$

for identical partial pressures of hydrogen over the two electrodes. Equations 34 and 38 thus show the relation between the potentials of two cells with the same liquid junction but different electrodes.

*b. Cell with Two Electrolytes, One of Nearly Uniform Concentration.* With an electrode of the second kind, as used in the previous example, the solubility of the sparingly soluble salt will, strictly speaking, lead to diffusion of this salt from the electrode. At high concentrations of the other electrolyte, the solubility of the sparingly soluble salt is depressed and the effect on the cell potential is expected to be small. However, this effect becomes more important as the concentration of the second electrolyte is decreased. For the cell



it is assumed that the two platinum electrodes are of identical composition and that the two solutions  $\beta$  and  $\delta$  differ in the concentration of AgCl, phase  $\delta$  being saturated. The transition region, in the model used here, is formed by contacting the solution  $\beta$  with the solid AgCl, and a diffusion layer develops by free diffusion into a stagnant medium. The concentrations of AgCl and HCl in phase  $\delta$ , adjacent to the solid surface, are determined by the laws of diffusion and the conditions of

saturation of AgCl and zero flux of hydrogen ions into the solid phase.

From the conditions of phase equilibria at the electrodes and the definitions of the chemical potentials of neutral species, the cell potential can be written

$$-F(\psi^\alpha - \psi^{\alpha'}) = \frac{1}{2}\mu_{\text{H}_2}^\alpha - \mu_{\text{HCl}}^\beta - \mu_{\text{Ag}}^\lambda + \mu_{\text{AgCl}}^\epsilon + (\mu_{\text{Cl}^-}^\beta - \mu_{\text{Cl}^-}^\delta) \quad (40)$$

If the chemical potentials of hydrogen and HCl are expressed as

$$\mu_{\text{H}_2} = \mu_{\text{H}_2}^\theta + RT \ln p_{\text{H}_2}$$

and

$$\mu_{\text{HCl}} = \mu_{\text{HCl}}^\theta + 2 RT \ln c_{\text{HCl}} f_{\text{HCl}}$$

then the standard cell potential,  $E^\circ$ , can be identified as a collection of thermodynamic quantities

$$FE^\circ = \frac{1}{2}\mu_{\text{H}_2}^\theta - \mu_{\text{HCl}}^\theta - \mu_{\text{Ag}}^\theta + \mu_{\text{AgCl}}^\theta \quad (41)$$

and the cell potential becomes

$$-F(\psi^\alpha - \psi^{\alpha'}) = FE^\circ + \frac{1}{2}RT \ln p_{\text{H}_2}^\alpha - 2RT \ln c_{\text{HCl}}^\beta f_{\text{HCl}}^\beta + (\mu_{\text{Cl}^-}^\beta - \mu_{\text{Cl}^-}^\delta) \quad (42)$$

For the evaluation of the difference  $\mu_{\text{Cl}^-}^\beta - \mu_{\text{Cl}^-}^\delta$ , eq 29 becomes in the absence of current

$$\nabla \mu_{\text{Cl}^-} = t_{\text{H}^+} \nabla \mu_{\text{HCl}} + t_{\text{Ag}^+} \nabla \mu_{\text{AgCl}} \quad (43)$$

Integration gives

$$\mu_{\text{Cl}^-}^\beta - \mu_{\text{Cl}^-}^\delta = \int_\delta^\beta t_{\text{H}^+} \frac{\partial \mu_{\text{HCl}}}{\partial x} dx + \int_\delta^\beta t_{\text{Ag}^+} \frac{\partial \mu_{\text{AgCl}}}{\partial x} dx \quad (44)$$

The evaluation of these integrals requires a knowledge of the concentration profiles, as well as the transference numbers and thermodynamic properties as functions of the concentrations. For high concentrations of HCl,  $\nabla \mu_{\text{HCl}}$  and  $t_{\text{Ag}^+}$  approach zero, and the term  $\mu_{\text{Cl}^-}^\beta - \mu_{\text{Cl}^-}^\delta$  may be neglected in comparison to the other terms in eq 42.

The difference in electrochemical potentials of the chloride ion can be expressed in terms of the quasi-electrostatic potentials (referred to the chloride ion), differences of which are given in Table II

$$\mu_{\text{Cl}^-}^\beta - \mu_{\text{Cl}^-}^\delta = F(\Phi^\delta - \Phi^\beta) + RT \ln (c_{\text{Cl}^-}^\beta / c_{\text{Cl}^-}^\delta) \quad (45)$$

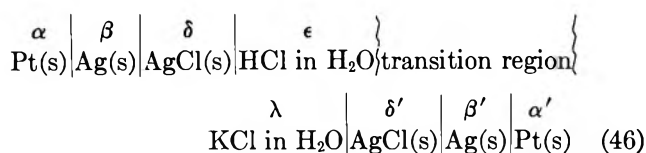
For a bulk HCl concentration of  $10^{-4} M$ , one obtains  $(\mu_{\text{Cl}^-}^\beta - \mu_{\text{Cl}^-}^\delta)/F = 0.0198 - 0.2457 = -0.226 \text{ mV}$ . This small error is not of much practical significance, since very few measurements have been made in this range of concentration.

Thus it is seen that the effect of the solubility of the slightly soluble salt will be to cause the potential of the

chloride electrode to be more negative with respect to the other electrode than would otherwise be the case. Hence the measured potential of the above cell will be lower than if silver chloride were more insoluble. Smyrl and Tobias<sup>12</sup> have discussed several nonaqueous systems where the effect is much larger in more concentrated solutions, since the effect becomes important for bulk concentrations on the order of the square root of the solubility product. The problem arises because the determination of standard cell potentials involves an extrapolation to infinite dilution. Smyrl and Tobias took the diffusion coefficients to be equal (hence  $\Delta\Phi = 0$ ) and assumed that the concentration of the second electrolyte is uniform up to the surface of the sparingly soluble salt.

*c. Cells with Two Electrolytes, Both of Varying Concentration.* Cells of this type may still be divided into two groups according to whether or not the two electrolytes have an ion in common. A junction between  $\text{CuSO}_4$  and  $\text{ZnSO}_4$  is an example where there is a common ion; a junction between  $\text{NaCl}$  and  $\text{HClO}_4$  is an example where there is not. The former class will be discussed first.

Consider the cell



The cell potential is again given by eq 34. The effect of the nonzero solubility of  $\text{AgCl}$ , discussed in subsection b, will be ignored here. In this case, however, eq 29 becomes

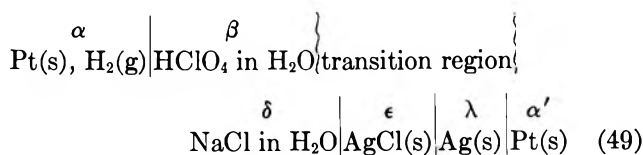
$$\nabla\mu_{\text{Cl}^-} = t_{\text{H}^+} \nabla\mu_{\text{HCl}} + t_{\text{K}^+} \nabla\mu_{\text{KCl}} \quad (47)$$

and integration gives

$$\mu_{\text{Cl}^-}^{\epsilon} - \mu_{\text{Cl}^-}^{\lambda} = \int_{\lambda}^{\epsilon} \left[ t_{\text{H}^+} \frac{\partial\mu_{\text{HCl}}}{\partial x} + t_{\text{K}^+} \frac{\partial\mu_{\text{KCl}}}{\partial x} \right] dx \quad (48)$$

Here, as with eq 44 and in contrast to eq 36, the integral depends on the detailed form of the concentration profiles in the junction region. As in the preceding examples, the cell potential can again be expressed in terms of the quasi-electrostatic potential, referred to the chloride ion, eq 37, and the values of  $\Delta\Phi$  in Table I allow the cell potential to be calculated. By means of the various models, the detailed form of the concentration profiles has already been taken into account in the tabulated values of  $\Delta\Phi$ .

Many cells of practical importance contain two electrolytes of varying concentration with no common ion. Such a cell is



From the conditions of phase equilibria at the electrodes and the definitions of the chemical potentials of neutral species, the cell potential can be written

$$-F(\psi^{\alpha} - \psi^{\alpha'}) = \frac{1}{2}\mu_{\text{H}_2}^{\alpha} - \mu_{\text{Ag}}^{\lambda} + \mu_{\text{AgCl}}^{\epsilon} - (\mu_{\text{H}^+}^{\beta} + \mu_{\text{Cl}^-}^{\delta}) \quad (50)$$

The cell potential is again related to the thermodynamic properties of electrically neutral components, but a new term has appeared. Instead of the difference of electrochemical potential of a single ion between the two solutions, there is now a combination of electrochemical potentials of two ions. This more complicated situation can be analyzed if the ionic strength does not go to zero anywhere in the junction (as must also be the case with the junctions treated earlier). Choose some solution in the junction and denote it as I. The quantities  $\mu_{\text{Cl}^-}^{\delta} - \mu_{\text{Cl}^-}^{\text{I}}$  and  $\mu_{\text{H}^+}^{\beta} - \mu_{\text{H}^+}^{\text{I}}$  are both well defined if the intermediate solution I has nonzero concentrations of both ions  $\text{Cl}^-$  and  $\text{H}^+$ . The cell potential can be written, then

$$-F(\psi^{\alpha} - \psi^{\alpha'}) = \frac{1}{2}\mu_{\text{H}_2}^{\alpha} - \mu_{\text{Ag}}^{\lambda} + \mu_{\text{AgCl}}^{\epsilon} - (\mu_{\text{H}^+}^{\beta} - \mu_{\text{H}^+}^{\text{I}}) - (\mu_{\text{Cl}^-}^{\delta} - \mu_{\text{Cl}^-}^{\text{I}}) - \mu_{\text{HCl}}^{\text{I}} \quad (51)$$

The electrochemical potential differences in eq 51 can now be related through eq 29 to integrals of transference numbers multiplied by gradients of chemical potentials of neutral combinations. The integrals can be evaluated from the concentration profiles in the junction along with the concentration dependence of the transport and thermodynamic properties. The cell potential is, of course, independent of the choice of the intermediate solution I.

In this case it may be particularly convenient to use the quasi-electrostatic potential, here referred to the chloride ion. This allows one to write

$$\mu_{\text{H}^+}^{\beta} + \mu_{\text{Cl}^-}^{\delta} = \mu_{\text{HCl}}^{\delta} + RT \ln c_{\text{H}^+}^{\beta} c_{\text{Cl}^-}^{\delta} + F(\Phi^{\beta} - \Phi^{\delta}) + RT \ln (f_{\text{H}^+}^{\beta} f_{\text{Cl}^-}^{\delta}) \quad (52)$$

The last term in eq 52 is well defined, although it is somewhat unusual. Here  $f_{\text{H}^+}^{\beta} f_{\text{Cl}^-}^{\delta}$  represents the activity coefficient of hydrogen ions referred to chloride ions in a solution of vanishing chloride concentration. According to eq 23, this term would be given by

$$\ln f_{\text{H}^+}^{\beta} f_{\text{Cl}^-}^{\delta} = \frac{-2\alpha I^{1/2}}{1 + I^{1/2}} + 2(\beta_{\text{HClO}_4} + \beta_{\text{HCl}}) c_{\text{H}^+}^{\beta} \quad (53)$$

where  $I$  now refers to the ionic strength in solution  $\beta$ . This procedure is justified by the fact that it is no

(12) W. H. Smyrl and C. W. Tobias, *Electrochim. Acta*, **13**, 1581 (1968).

longer necessary to select an intermediate solution in the junction.

The cell potential can now be written

$$-F(\psi^\alpha - \psi^{\alpha'}) = FE^\circ + \frac{1}{2}RT \ln p_{H_2}^\alpha - RT \ln c_{H^+}^\beta c_{Cl^-}^\delta + F(\Phi^\delta - \Phi^\beta) - RT \ln f_{H^+}^\beta f_{Cl^-}^\beta \quad (54)$$

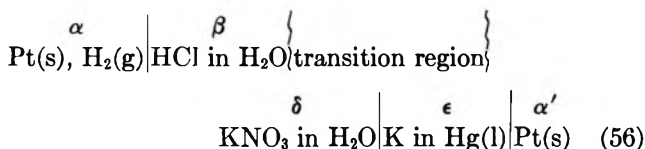
where the standard cell potential has been identified

$$FE^\circ = \frac{1}{2}\mu_{H_2}^\theta - \mu_{Ag}^\theta + \mu_{AgCl}^\theta - \mu_{HCl}^\theta \quad (55)$$

A determination of the standard cell potential by means of this cell would be affected by the uncertainties in the values of  $\Delta\Phi$  and  $f_{H^+}^\beta f_{Cl^-}^\beta$ , a problem which is avoided with the cell discussed in subsection b. If  $E^\circ$  is known from measurements with that cell, any uncertainty in the calculated value of  $\Delta\Phi$  will cause a consequent uncertainty in any value of  $f_{H^+}^\beta f_{Cl^-}^\beta$  obtained from measurements on the present cell. This discussion reveals some of the difficulties involved in the use of such cells for thermodynamic measurements.

We could check the calculated value of  $\Delta\Phi$  in Table I by subtracting from the cell potential the standard cell potential and the terms in activity coefficients and concentrations. The potentials of such cells have not been measured.

The cell



is very similar to that of the previous example but differs in that both electrodes involve phase equilibria of cations. Again, from the phase equilibria and the relevant thermodynamic identities, the cell potential may be written

$$\begin{aligned} -F(\psi^\alpha - \psi^{\alpha'}) &= \frac{1}{2}\mu_{H_2}^\alpha - \mu_K^\epsilon + \mu_{K^+}^\delta - \mu_{H^+}^\beta \\ &= \frac{1}{2}\mu_{H_2}^\alpha - \mu_K^\epsilon + (\mu_{K^+}^\delta - \mu_{K^+}^I) - (\mu_{H^+}^\beta - \mu_{H^+}^I) + (\mu_{K^+}^I - \mu_{H^+}^I) \end{aligned} \quad (57)$$

where I denotes an intermediate solution where both  $K^+$  and  $H^+$  ions are present. The quantities  $\mu_{K^+}^\delta - \mu_{K^+}^I$  and  $\mu_{H^+}^\beta - \mu_{H^+}^I$  can be related through eq 29 to integrals of transference numbers multiplied by gradients of chemical potentials of neutral combinations. The last term in eq 57 is well defined and is given by

$$\mu_{K^+}^I - \mu_{H^+}^I = \mu_{KCl}^I - \mu_{HCl}^I$$

To demonstrate the usefulness of tabulated values of  $\Delta\Phi$ , let the quasi-electrostatic potential be based on the chloride ion. Equation 57 can be rewritten

$$\begin{aligned} -F(\psi^\alpha - \psi^{\alpha'}) &= \frac{1}{2}\mu_{H_2}^\alpha - \mu_K^\epsilon + \mu_{KCl}^\theta - \mu_{HCl}^\theta + RT \ln (c_{K^+}^\delta / c_{H^+}^\beta) + \\ &RT \ln (f_{K^+}^\delta f_{Cl^-}^\delta / f_{H^+}^\beta f_{Cl^-}^\beta) + F(\Phi^\delta - \Phi^\beta) \end{aligned} \quad (58)$$

Any uncertainty in  $\Delta\Phi$  and  $f_{K^+}^\delta f_{Cl^-}^\delta$  would be reflected in the uncertainty in a derived value of a standard cell potential. Thus the use of such a cell to determine standard cell potentials is justified only if the junction is well characterized and if the thermodynamic properties of one of the end solutions are well known.

Other cells could be analyzed, but the analysis would involve only the principles and procedures which have been used above.

### Discussion

The analysis of the cells in the previous section revealed the relation between measured cell potentials and the thermodynamic and transport properties of the materials in the cells. For cells with liquid junctions, the cell potential depends on the concentration profiles in the liquid junction and the transport and thermodynamic properties of the junction region, in addition to the standard cell potential and the composition of activity coefficients of the end solutions. Alternatively, for the junction one could specify the concentration profiles, the value of  $\Delta\Phi$  which characterizes the junction, and the ion to which  $\Phi$  is referred. Once single junctions have been characterized, the behavior of combinations of these junctions in other cells, *e.g.*, cells with salt bridges, may be predicted.

Calculations for several single junctions have been made, and the results are given in Table I. The only one of the junctions for which our calculations may be compared with other calculations and with experimental results is the 0.1 M HCl-0.1 M KCl junction. MacInnes and Longworth<sup>13</sup> have made calculations for this junction of the free-diffusion type and reported a value of 28.19 mV to compare with 27.31 mV of the present study. Spiro<sup>14</sup> has discussed cells with liquid junctions, including salt bridges, for junctions of constant ionic strength across the junction and of the continuous-mixture type and has included activity coefficient corrections. For this HCl-KCl junction, Spiro calculated 29.07 mV, and we calculate 27.47 mV. The experimental results are given in Table I.

MacInnes and Longworth used eq 29 and the known activity coefficients and transference numbers for this junction and an assumed concentration profile to make their calculation. It is not clear whether the difference between their results and ours is due to our assumption about activity coefficients, our assumption about the ionic diffusion coefficients, or their assumption about the concentration profile.

(13) D. A. MacInnes and L. G. Longworth, *Cold Spring Harbor Symp. Quant. Biol.*, **4**, 18 (1936).

(14) M. Spiro, *Electrochim. Acta*, **11**, 569 (1966).

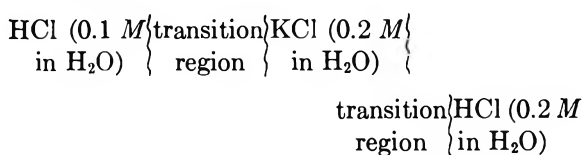
It is known<sup>15</sup> that  $D_{\text{OCl}}$  varies by 17% across the 0.1  $M$  KCl-HCl junction, whereas it is the same in both solutions at infinite dilution. Their use of experimental data on transference numbers takes this variation of  $D_{\text{OCl}}$  into account, but our treatment does not. On the other hand, they have assumed a concentration profile in order to make their calculations which will certainly lead to some error. It is not possible at present to estimate the relative importance of these differences, but it is gratifying that the two treatments agree so well.

Spiro calculates about the same activity coefficient correction (0.55 mV) as we do (0.62 mV), but his calculation neglecting activity coefficients ( $-28.52$  mV) is higher than ours by about 1.7 mV. The major differences in the results are caused by different assumptions about the ionic diffusion coefficients. We have assumed the ionic diffusion coefficients to be constant throughout the junction and have used the values corresponding to infinite dilution in making the Henderson calculation. Spiro has used the Lewis and Sargent equation and has utilized conductivity data for the 0.1  $M$  solutions. The restrictions in the use of the Lewis and Sargent equation lead one to conclude that this is not a valid way to correct for the variation of  $D_{\text{OCl}}$  mentioned earlier. The restrictions come about in the following way. The Lewis and Sargent equation is derived from the Henderson equation, which in turn is derived with an assumption that the ionic diffusion coefficients are constant across the junction. Thus one must use data consistent with this assumption. The conductivity data used by Spiro do not fulfill this requirement.

Since the results reported here for the other junctions may not be compared to experimental data, we can only propose that they are at least as accurate as for the HCl-KCl junction.

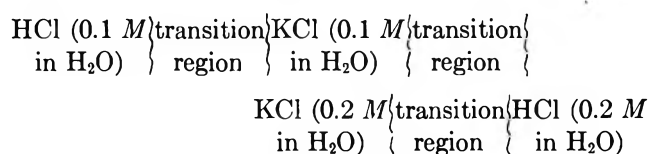
The variation of the ionic diffusion coefficients across the junction may be important for the junctions containing hydrogen ion, but less important for the others. It will be necessary to make the comparison with experimental data to verify this. The comparison must be made also before calculations are made at higher concentrations—the concentration region where the junction might be used as part of salt bridges.

A salt bridge is often used to separate two electrolytic solutions and sometimes the stated purpose is "to eliminate liquid junction potentials." We should now be in a position to evaluate whether this purpose is achieved, if we could define the liquid junction potential which is supposed to be eliminated. Such a salt bridge might be



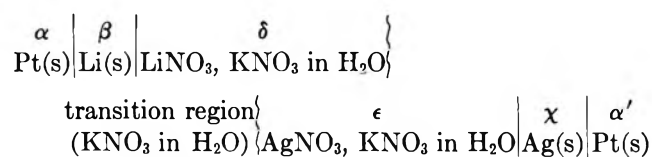
It seems clear that the salt bridge does not make the value of  $\mu_{\text{Cl}^-}$  equal in the two hydrochloric acid solutions. The value of  $\Delta\Phi$  (referred to the chloride ion) for this combination of junctions is 5.78 mV if the junctions are of the continuous-mixture type. This can be compared with the value  $\Delta\Phi = 10.31$  mV for a single, direct junction between 0.1 and 0.2  $M$  HCl solutions.

If the transference numbers of KCl were equal to 0.5 and if departures of activity coefficients from unity could be ignored, the liquid junction potential of the combination of two junctions of the salt bridge should decrease as the concentration of KCl increases. If one insists on using salt bridges, one might consider as an alternative the series of junctions



for which  $\Delta\Phi = 1.24$  mV and for which the value of  $\Delta\Phi$  would approach zero as all the concentrations were reduced in proportion if the transference numbers of KCl were 0.5.

Although cells with salt bridges are not useful for determining activity coefficients, they are useful for determining standard cell potentials. A cell which is particularly appropriate for such studies, but which has not been utilized extensively, is one in which the electrolyte of the salt bridge is present throughout. An example of this cell is



in which  $\text{KNO}_3$  is present throughout the cell at the same concentration. The transition region contains concentration gradients of both  $\text{LiNO}_3$  and  $\text{AgNO}_3$ . The cell potential may be expressed as

$$-F(\psi^\alpha - \psi^{\alpha'}) = \mu_{\text{Li}^\beta} - \mu_{\text{LiNO}_3^\delta} - \mu_{\text{Ag}^\chi} + \mu_{\text{AgNO}_3^\epsilon} - \mu_{\text{NO}_3^-^\epsilon} + \mu_{\text{NO}_3^-^{\epsilon'}}$$

We adopt the following approximations which essentially fix the range of concentrations

$$\begin{array}{l} t_{\text{Ag}^\chi} = 0 \\ t_{\text{Li}^\beta} = 0 \\ c_{\text{Ag}^\chi} = c_{\text{Li}^\beta} \ll c_{\text{K}^\alpha} \\ (c_{\text{Ag}^\chi})^{1/2} = (c_{\text{Li}^\beta})^{1/2} \ll c_{\text{K}^\alpha}^{1/2} \end{array}$$

The expression for the cell potential becomes

$$-F(\psi^\alpha - \psi^{\alpha'}) = FE^\circ + 2RT(\beta_{\text{AgNO}_3} - \beta_{\text{LiNO}_3})c_{\text{NO}_3^-}$$

(15) T. W. Chapman, Ph.D. Thesis, University of California, Berkeley, Calif., 1967.

Thus the measured cell potential should be a linear function of  $c_{\text{NO}_3^-}$ . As  $c_{\text{NO}_3^-} \rightarrow 0$ , the standard cell potential may be determined from the intercept. It would not be necessary to extrapolate to the low concentrations which are necessary for cells without transference.

### Conclusions

A general treatment of the effect of diffusion on the electrical potential of cells with liquid junctions has been given. It was found that such cells have a potential which is related to a difference (or sum) of the electrochemical potential of an ion (or ions). It has been shown that this characteristic combination of electrochemical potentials can be determined from a knowledge of the concentration profiles and the transport and thermodynamic properties in the junction region. From the laws of diffusion, the concentration profiles have been calculated and values of  $\Delta\Phi$  have been determined for several different junctions without the assumption of activity coefficients equal to 1. These results have been applied to specific cells. Such an analysis has made it possible to determine the magnitude of the diffusion effect in cases where it is desirable that the effect be negligible.

The cell potential can still be obtained from contributions of various phase boundaries and liquid junctions if certain conventions are adopted. This procedure makes simpler the tabulation of the properties of electrochemical cells.

*Acknowledgment.* This work was supported by the United States Atomic Energy Commission under Contract No. W-7405-eng-48.

### Appendix. Nomenclature

$c_i$	Concentration of species $i$ (mol/cm <sup>3</sup> )
$D_{i,j}$	Diffusion coefficient for interaction of species $i$ and $j$ (cm <sup>2</sup> /sec)
$E^\circ$	Standard cell potential (V)
$f_i$	Activity coefficient
$F$	Faraday's constant (C/equiv)
$i$	Current density (A/cm <sup>2</sup> )
$I$	Ionic strength (mol/l.)
$K_{i,j}$	Friction coefficient
$L_{i,j}^\circ$	Interaction coefficient
$M_{i,j}$	Interaction coefficient
$N_i$	Flux of species $i$ (mol/cm <sup>2</sup> sec)
$p$	Pressure (dyn/cm <sup>2</sup> )
$R$	Universal gas constant (J/mol deg)
$R_{i,j}$	Interaction coefficient
$t$	Time (sec)
$t_i^\circ$	Transference number of species $i$ with respect to species $o$
$T$	Absolute temperature (°K)
$v_i$	Velocity of species $i$ (cm/sec)
$x$	Distance (cm)
$z_i$	Charge number of species $i$
$\alpha$	Debye-Hückel constant ((l./mol) <sup>1/2</sup> )
$\beta_{i,j}$	Constant, independent of concentration (l./mol)
$\kappa$	Conductivity (mho/cm)
$\mu_i$	Electrochemical potential of species $i$ (J/mol)
$\Phi$	Electric potential or quasi-electrostatic potential (V)
$\psi$	Potential of an electrode (V)

# A Shock Tube Study of the Pyrolysis of Propylene. Kinetics of the Vinyl-Methyl Bond Rupture

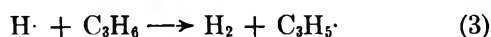
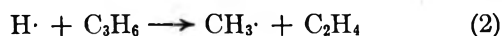
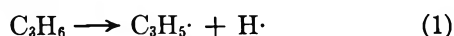
G. A. Chappell and H. Shaw

Esso Research and Engineering Company, Central Basic Research Laboratory, Linden, New Jersey 07036  
(Received July 12, 1968)

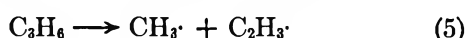
The pyrolysis of propylene was investigated in the temperature range of 1100–1650°K with reaction times of approximately 1 msec in a shock tube. The unimolecular rate constant for the vinyl-methyl bond rupture was determined to be  $k_5 = 10^{16.1} \exp(-85,800/RT)$  sec<sup>-1</sup>. This value was obtained by calculating the initial production of methyl and vinyl radicals from the product spectrum. The bond dissociation energy for the vinyl-methyl bond is  $88 \pm 2$  kcal at 298°K. Alternately, the enthalpy of formation of the vinyl radical is  $61 \pm 2$  kcal mol<sup>-1</sup> at 298°K. Assuming that the rate constant for methyl-vinyl radical combination is  $10^{10 \pm 1}$  l. mol<sup>-1</sup> sec<sup>-1</sup>, the entropy of the vinyl radical is  $55 \pm 4$  cal mol<sup>-1</sup> deg<sup>-1</sup> at 298°K.

## Introduction

The pyrolysis of propylene has been investigated by many workers. Kallend, Purnell, and Shurlock<sup>1</sup> give a comprehensive review of existing information. Some of the steps in the decomposition mechanism propylene have been assumed to be



This accounts for the observed equal yields of ethylene and methane. Reaction 2 occurs when the hydrogen atom adds to the middle carbon atom of propylene and the vibrationally excited normal propyl radical, thus produced, decomposes. Falconer, Rabinovitch, and Cvetanović<sup>2</sup> showed that only  $6 \pm 1\%$  of the hydrogen atom additions at 298°K produce *n*-propyl radicals. On the other hand, Jackson and McNesby<sup>3</sup> showed that the isopropyl radical decomposes primarily into propylene and a hydrogen atom, while a maximum of only 7% cracks into methyl radicals and ethylene at about 800°K with no temperature trend. Since Bellinge and Gowenlock<sup>4</sup> found no evidence for the isomerization of the isopropyl radical at about 700°K, we are left to speculate that at high temperatures step 2 is much less important than step 3. Since step 3 is not the precursor to both ethylene and methane, one may propose another initiation reaction which involves the rupture of the vinyl-methyl bond. Both Kallend,<sup>1</sup> *et al.*, and Steacie<sup>5</sup> do propose that the initiation step is



The bond dissociation energy at 298°K,  $DH^\circ(\text{C}_2\text{H}_3\text{-CH}_2)$ , has not been determined directly but has been inferred as 92 kcal mol<sup>-1</sup>,<sup>6</sup> while the bond energy  $DH^\circ$

( $\text{C}_3\text{H}_5\text{-H}$ ) has been inferred as 85 kcal mol<sup>-1</sup>.<sup>6</sup> One would thus assume that reaction 1 is favored kinetically. This may not be the case if the entropies of reaction are different. Since entropies affect the preexponential factor in the Arrhenius expression and if reaction 5 has a larger preexponential than reaction 1, then at high temperatures reaction 5 will be the predominant initiation reaction.

The bond dissociation energy  $DH^\circ(\text{CH}_3\text{-C}_2\text{H}_3)$  has not been measured directly because the pyrolysis of propylene is influenced by surface reactions.<sup>1,7</sup> However, shock tube techniques should prove fruitful in determining  $DH^\circ(\text{CH}_3\text{-C}_2\text{H}_3)$  because the short reaction times would minimize surface effects.

## Experimental Section

Reactant mixtures consisting of 0.870 mol % propylene in argon were pyrolyzed in a 3-in. (i.d.) stainless steel single-pulse shock tube. The low-pressure or reactant section was 12 ft long and the high-pressure or driver section was 6 ft long. The tube was attached at the high-pressure end to a vacuum tank having a volume of 30 ft<sup>3</sup>. The two sections of the shock tube and the tank were all separated by diaphragms made of Alclad aluminum, Type 2024-T3, 0.016 in. thick. The diaphragm dividing the two shock tube sections had two perpendicular, centered scribe lines of 0.007 in. in depth milled into the side facing the low-pressure

(1) A. S. Kallend, J. H. Purnell, and B. C. Shurlock, *Proc. Roy. Soc.*, **A300**, 120 (1967).

(2) W. E. Falconer, B. S. Rabinovitch, and R. J. Cvetanović, *J. Chem. Phys.*, **39**, 40 (1963).

(3) W. M. Jackson and J. R. McNesby, *ibid.*, **36**, 2272 (1962).

(4) B. H. M. Bellinge and B. G. Gowenlock, *J. Chem. Soc.*, 3252 (1962).

(5) E. W. R. Steacie, "Atomic and Free Radical Reactions," Vol. 1, Reinhold Publishing Corp., New York, N. Y., 1954.

(6) S. W. Benson, *J. Chem. Educ.*, **42**, 502 (1965).

(7) J. A. Kerr, *Chem. Rev.*, **66**, 465 (1966).



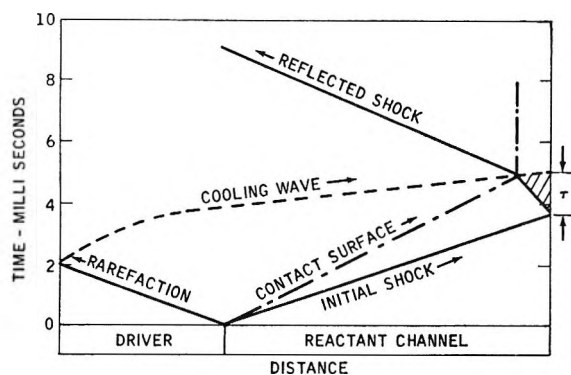


Figure 1. An idealized wave diagram for the shock tube.

end. This diaphragm ruptured with a  $175 \pm 10$ -psi pressure drop. The diaphragm separating the driver section from the vacuum tank was also scribed but to a depth of 0.006 in. An externally actuated plunger ruptured the second diaphragm.

Figure 1 depicts an idealized wave diagram which shows the reaction zone to be the triangular area initiated by the reflected shock wave and terminated by the cooling wave. Our real diagrams do not indicate any marked deviation from this figure. The effective reaction time behind the reflected shock wave for a given portion of reactant is dependent upon its location with respect to the end plate of the shock tube. As shown in Figure 1, the reactant at the end plate is exposed to the reaction environment for  $\tau$  seconds, while the reactant at the intersection of the cooling and reflected shock waves has zero contact time. The products, being thoroughly mixed prior to analysis, reflect an average reaction time at the particular temperature of the experiment. The first-order rate constant ( $k_5$ ) may be calculated by means of the expression<sup>9</sup>

$$F = \frac{1}{k_5 \tau} (1 - e^{-k_5 \tau})$$

where  $F$  is the fraction remaining of the original starting material and  $\tau$  is the maximum reaction time as described above.

The velocities and pressures of the incident shock, reflected shock, and expansion waves were measured at three points along the reactant section by quartz pressure transducers positioned on the end plate, 6 in. from the end plate, and 3 ft from the end plate, respectively. The transducer signals were displayed on two Tectronix oscilloscopes, types 585A and 545B. The traces were photographed using Polaroid cameras. The reaction temperatures were calculated from the incident shock velocity using the ideal gas law. These results were corrected for the endothermicity of the reaction and also for heat capacity changes due to the small amount of hydrocarbon present. In our experiments the pressure behind the reflected shock wave was approximately 13 atm in all runs.

Following a run the samples were withdrawn from the stock tube by means of a vacuum line, and the constituents were analyzed on a Beckman GC-5 gas chromatograph equipped with hydrogen flame ionization and thermal conductivity detectors. A 10-ft Porapak Q column was used to separate the products. The reactant mixture contained 0.25 mol % xenon for material balance determinations. The propylene was Phillips research grade, the xenon was Matheson research grade, the helium was Matheson high-purity grade, and the argon was Linde high-purity dry grade. Since chromatographic analysis of all gases indicated less than 0.1% impurities, these were used as received.

## Results

The shock tube experiments were carried out over the temperature range of 1100–1650°K with an average reaction time of 1 msec. In Table I we list the moles of product per 100 mol of propylene in the feed. Although we did not analyze for all our products in each experiment, we found substantial evidence for the production of ethane, butadiene, 1-butene, 1,4-pentadiene, and 1,5-hexadiene in trace amounts.

The unimolecular rate constant for propylene cracking can be expressed implicitly as

$$\frac{(P)_0 - \Delta(P)}{(P)_0} = \frac{1}{k_5 \tau} (1 - e^{-k_5 \tau}) \quad (\text{I})$$

where  $(P)_0$  is the initial concentration of propylene and  $\Delta(P)$  is the change in the concentration of propylene due *only* to decomposition *via* reaction 5. The quantity  $\Delta(P)$  can be evaluated for any single reaction path in which the resulting products are dependent on the initiation step and there are no *other* ways of producing these products. In the case of methyl radicals produced from step 5 we have

$$\Delta(P) = (\text{CH}_3) + 2(\text{C}_2\text{H}_5) + (1-\text{C}_4\text{H}_9) \quad (\text{II})$$

Similarly for vinyl radicals we obtain

$$\Delta(P) = (\text{C}_2\text{H}_3) + (\text{C}_2\text{H}_4) + 2(\text{C}_4\text{H}_6) + (\text{C}_5\text{H}_7) \quad (\text{III})$$

We solved eq I by iteration for  $k_5$  after calculating  $\Delta(P)$  from eq II or III and our product yields (Table I). Figure 2 shows the Arrhenius plot of  $k_5$  as determined from a vinyl radical and a methyl radical balance (eq III and II, respectively). The least-squares equation is

$$k_5 = 10^{16.07 \pm 0.40} e^{-(85840 \pm 237)/RT} \text{ sec}^{-1} \quad (\text{IV})$$

## Discussion

The over-all decomposition of propylene is not understood.<sup>7</sup> We have obtained the Arrhenius expression for the initiating vinyl-methyl bond split. Although other initiating reactions are possible and were men-

(8) V. Kevorkian, C. E. Heath, and M. Boudart, *J. Phys. Chem.*, **64**, 964 (1960).

Table I: Propylene Pyrolysis Data

No. of run	Temp, °K	$\tau$ , msec	Moles of product/100 mol of initial propylene										Initial press., <sup>a</sup> Torr
			CH <sub>4</sub>	C <sub>2</sub> H <sub>6</sub>	C <sub>2</sub> H <sub>4</sub>	C <sub>2</sub> H <sub>2</sub>	C <sub>2</sub> H <sub>6</sub>	C <sub>2</sub> H <sub>4</sub>	C <sub>3</sub> H <sub>6</sub>	C <sub>3</sub> H <sub>8</sub>	C <sub>3</sub> H <sub>4</sub>	C <sub>3</sub> H <sub>10</sub>	
235	1140	1.95	0.06	...	0.05	0.01	97.9	0.07	...	...	...	...	600
237	1160	2.00	0.06	...	0.05	0.03	97.5	...	...	...	...	...	580
238	1200	1.80	0.14	...	0.12	...	93.6	0.06	...	...	...	...	570
236	1205	1.81	0.27	...	0.31	0.07	93.7	0.30	...	...	...	...	575
234	1310	1.25	...	0.11	3.60	0.80	86.8	2.70	...	...	...	...	525
206	1340	1.15	9.9	0.80	8.10	2.30	63.2	7.50	0.70	...	...	...	490
204	1390	1.30	16.1	1.20	15.9	5.60	63.4	13.9	1.20	...	0.60	...	490
229	1410	1.31	...	1.40	15.5	6.20	62.4	14.9	...	...	...	...	500
201	1460	1.38	43.8	1.60	19.8	29.0	15.2	15.5	3.30	0.20	0.20	3.90	400
217	1520	1.57	50.5	0.14	24.0	65.8	2.40	3.70	1.10	0.90	...	4.90	350
211	1650	1.60	54.2	0.10	12.7	83.9	1.50	2.00	0.60	1.60	...	...	300

<sup>a</sup> The initial pressure is that of the total reactant mixture prior to shocking. The final or reaction pressure behind the reflected shock wave is 13 atm in all experiments.

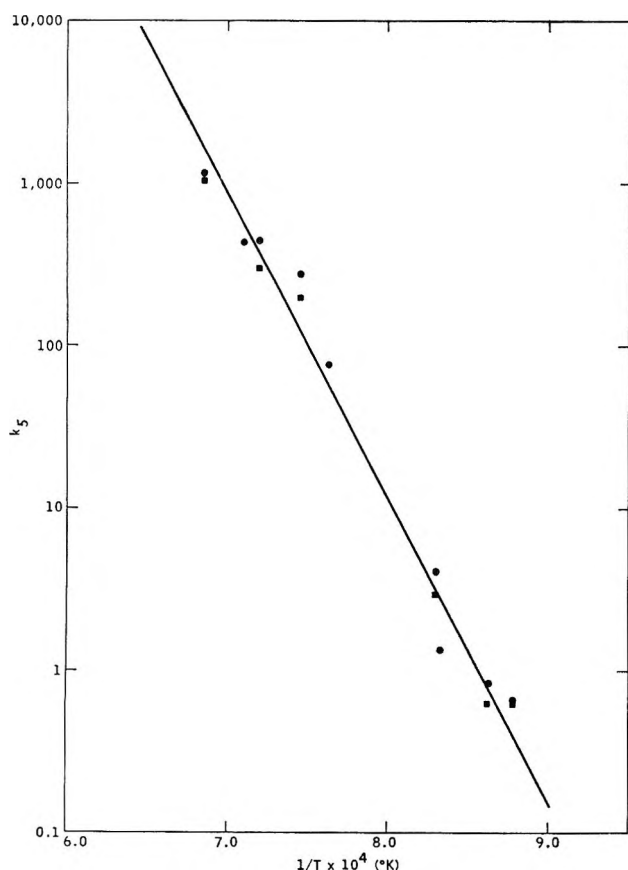


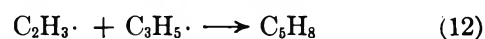
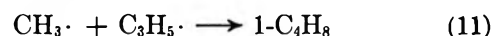
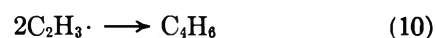
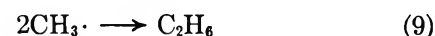
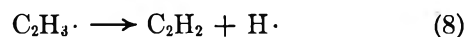
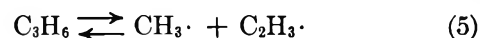
Figure 2. Propylene pyrolysis: ■, methyl radical balance; ●, vinyl radical balance.

$$k_5^{\text{m}} = 10^{16.07 \pm 0.40} e^{(-86.84 \pm 2.37)/RT}$$

tioned in the Introduction, we present data to support our contention that step 5 predominates under our conditions. In the review by Kallend *et al.*,<sup>1</sup> data were presented which indicated that propylene cracks by a complex free-radical sequence with a chain length of 50 in the temperature range 800–1000°K. Some of these conclusions are not valid under shock

tube conditions at higher temperatures and pressures with millisecond residence times. Our data indicate no significant influence from a free-radical chain in agreement with Sakakibara's<sup>9</sup> flow pyrolysis data at similar temperatures.

Our results are consistent with the reaction sequence



Although the series of reactions listed above is incomplete with respect to the over-all thermal decomposition of propylene, all reasonable steps governing the formation and disappearance of the methyl and vinyl radicals are included. The possible reaction between hydrogen atoms and propylene was discussed in the Introduction. If we assume: (a) only 6% of the hydrogen atom addition occurs to produce *n*-C<sub>3</sub>H<sub>7</sub>·; (b) a maximum of 7% of the isopropyl radicals decompose into ethylene and methyl radicals; and (c) isopropyl radicals do not isomerize under our conditions, then we must infer that ethylene and methane are primarily produced by reactions 6 and 7. We found that the experimental ratio of acetylene to ethylene was 10–40 times greater than that predicted using Kozlov and Knorre's data<sup>10</sup> on ethylene pyrolysis. The larger ratios were observed at the lower temperatures. We must therefore assume that ethylene is not the precursor

(9) Y. Sakakibara, *Bull. Chem. Soc. Jap.*, **37**, 1262, 1268 (1964).

(10) G. I. Kozlov and V. G. Knorre, *Combust. Flame*, **6**, 253 (1962).

sor to acetylene in this case. It would seem more likely that acetylene is produced by cracking the vinyl radical rather than by cracking ethylene. Although we did not analyze for all our products in each experiment, we still found significant indications that the radical combination reactions 9-12 do occur. It would be difficult to account for these products in any other manner. Based on all the above factors, we believe that the mechanism presented accounts for the observed yields of products and that other reactions leading to these products may be neglected to a first approximation.

Our calculations are based on the assumption that the methyl-vinyl radical combination occurs with zero activation energy and that the vinyl radical behaves like an alkyl radical. This assumption is supported by the data and calculations of Simons, Rabinovitch, and Dorer.<sup>11</sup> The excellent agreement between the methyl and vinyl radical balances serves as an internal check on the consistency of our argument.

We have assumed that our value for  $k_5$  is at the high-pressure limit because the reaction pressure was 13 atm. This assumption is supported by the calculations of Rabinovitch and Setser,<sup>12</sup> which showed that under our experimental conditions  $k/k_\infty$  is greater than 0.8 for the thermal activation of ethane, propane, and butane.

The bond dissociation energy ( $DH^\circ$ ) may be determined from the observed activation energy assuming the back reaction ( $k_{-5}$ ) requires zero energy. The enthalpy of the reaction at 1300°K is  $\Delta H_{\text{react},1300} = E_{\text{act}} + RT = 88 \pm 2 \text{ kcal mol}^{-1}$ . We used the thermodynamic data shown in Table II to correct the enthalpy of reaction to 298°K. We found the correction to be negligible; thus  $DH^\circ(\text{CH}_3\text{-C}_2\text{H}_3)$  is  $88 \pm 2 \text{ kcal mol}^{-1}$ . The values for  $DH^\circ(\text{CH}_3\text{-C}_2\text{H}_3)$  previously reported by Benson<sup>6</sup> and Kerr<sup>7</sup> are in good agreement with our value.

One can alternatively calculate the standard heat of formation of the vinyl radical from the measured activation energy. This value is  $61 \pm 2 \text{ kcal mol}^{-1}$ . Our  $\Delta H_f^\circ(\text{C}_2\text{H}_3)$  compares quite favorably with the values that Benson<sup>6</sup> and Kerr<sup>7</sup> quoted based on thermal techniques and mass spectrometric techniques.<sup>13</sup>

For the purpose of calculating the entropy of the vinyl radical we assumed that the methyl-vinyl recombination rate constant ( $k_{-5}$ ) is the same as the rate constant for the methyl radical dimerization. In order to bracket the actual value of the rate constant we let  $k_{-5} = 10^{10 \pm 1} \text{ l. mol}^{-1} \text{ sec}^{-1}$ . This value is in agreement with the methyl radical dimerization rate constant at approximately our midrange temperature.<sup>14</sup> Using this value of  $k_{-5}$  we calculate the entropy of the vinyl

Table II: Thermodynamic Data<sup>a</sup>

	CH <sub>3</sub> ·	C <sub>2</sub> H <sub>3</sub> ·	C <sub>2</sub> H <sub>2</sub>	C <sub>2</sub> H <sub>4</sub>	C <sub>3</sub> H <sub>6</sub> <sup>†</sup>
$\Delta H_{f,298}$ , kcal mol <sup>-1</sup>	31.94	63 ± 2 <sup>b</sup>	54.19	12.50	4.88
$\Delta H_{f,1300}$ , kcal mol <sup>-1</sup>	29.69	61 ± 2 <sup>c</sup>	53.13	8.77	-0.42

<sup>a</sup> All data are from the "JANAF Thermochemical Tables," Dow Chemical Co., Midland, Mich., 1963, except as noted.

<sup>b</sup> Reference 6. <sup>c</sup> We used the following expression to estimate this quantity:  $\Delta H_{f,1300}(\text{C}_2\text{H}_3\cdot) = \Delta H_{f,298}(\text{C}_2\text{H}_3\cdot) + \frac{1}{2}[\Delta H_{f,1300}(\text{C}_2\text{H}_2) - \Delta H_{f,298}(\text{C}_2\text{H}_2) + \Delta H_{f,1300}(\text{C}_2\text{H}_4) - \Delta H_{f,298}(\text{C}_2\text{H}_4)]$ .

<sup>†</sup> Project 44 Tables, American Petroleum Institute, Pittsburgh, Pa., 1952.

radical as  $78 \pm 4 \text{ cal mol}^{-1} \text{ deg}^{-1}$  at 1300°K. When we apply the same calculational technique for entropy change as we used to estimate the enthalpy change for the vinyl radical in going from 1300 to 298°K, then  $S^\circ = 55 \pm 4 \text{ cal mol}^{-1} \text{ deg}^{-1}$ .

We have shown in this paper that shock tube techniques can be used to obtain kinetic and thermodynamic data for a system which does not lend itself to direct analysis using more conventional methods.

*Acknowledgment.* We are grateful to Mr. S. S. Kasegrande for his excellent experimental assistance and to Dr. F. H. Field for helpful discussions.

(11) J. W. Simons, B. S. Rabinovitch, and F. H. Dorer, *J. Phys. Chem.*, **70**, 1076 (1966).

(12) B. S. Rabinovitch and D. W. Setser, *Advan. Photochem.*, **3**, 1 (1964).

(13) A. G. Harrison and F. P. Lossing, *J. Amer. Chem. Soc.*, **82**, 519 (1960); F. W. Lampe and F. H. Field, *ibid.*, **81**, 3238 (1959).

(14) H. Shaw and S. Toby, *J. Phys. Chem.*, **72**, 2337 (1968).

## Hydrogen Bonding between Adsorbed Gases and Surface

### Hydroxyl Groups on Silica

by W. Hertl and M. L. Hair

*Research and Development Laboratories, Corning Glass Works, Corning, New York 14830 (Received July 12, 1968)*

The isosteric heats of adsorption of 23 compounds on the 3750-cm<sup>-1</sup> surface hydroxyl group on silica have been determined spectroscopically. Comparison of these heats ( $\Delta H$ ) with the observed frequency shifts ( $\Delta\nu$ ) of the hydroxyl band show that the compounds studied can be divided into two groups: (i) those in which  $\Delta H$  is constant and in which  $\Delta\nu$  increases with decreasing ionization potential and (ii) those in which  $\Delta H$  is a function of  $\Delta\nu$  and of the location of the lone-pair electrons in the adsorbing molecule ( $\Delta H(\text{kcal}) = 0.455(\Delta\nu\text{cm}^{-1})^{1/2} + k$ ). The constant  $k$  has a value of 3.0 kcal when the lone-pair electrons involved in the hydrogen bonding are in a p orbital and a value of -2.3 kcal when they are in sp<sup>2</sup> or sp<sup>3</sup> hybrid orbitals. Direct correlations are also observed between the integrated areas of the perturbed hydroxyl bands, the frequency of this band, and the amount of free hydroxyl covered. For compounds in the series in which the frequency shift is a function of the heat of adsorption, a decreasing frequency shift is observed with increasing temperature. Electrostatic interaction probably plays an important part in this hydrogen bonding, but there are other factors which contribute together or individually to the strengths of the H bonds and to the observed frequency shifts.

#### Introduction

When physical adsorption takes place on the surface of silica, it is observed that the band in the infrared spectrum attributed to the freely vibrating hydroxyl group is perturbed to lower frequencies. In many cases the interaction between the adsorbate molecule and the freely vibrating surface hydroxyl group is very specific and adsorption occurs on that site preferentially to other groups on the surface, such as adjacent, hydrogen-bonded hydroxyls.<sup>1</sup> Previous work on the physical adsorption of molecules on silica has attempted to correlate the observed frequency shift with physical parameters such as polarizability,<sup>2</sup> quadrupole moment,<sup>3</sup> ionization potential,<sup>4</sup> and heat of adsorption.<sup>5</sup> Of these approaches, only the latter shows any success in correlating differing groups of compounds and Kiselev has proposed that the shift in frequency of the free silanol vibration is directly proportional to the heat of adsorption on the hydroxyl groups.<sup>5</sup> In the past, these heats have been determined calorimetrically by investigating surfaces both with and without surface silanol groupings.

By spectroscopically determining the amount of coverage of the freely vibrating groups on silica, it is possible to obtain the isotherms for adsorption on these groups only, independent of any other adsorption which may take place. From these isotherms, measured at various temperatures, the isosteric heat of adsorption can be calculated. While inherently not so accurate as calorimetric methods, this method has the distinct advantage that it defines precisely the surface site on which adsorption is taking place. This paper describes the results obtained from measuring the iso-

stemic heats of adsorption of 23 compounds on the freely vibrating hydroxyl group of silica and enables the adsorbate molecules to be separated into three distinct series based on their molecular structure. By the use of an electronic curve resolver, several overlapping bands have been isolated and more accurate data for frequency shifts have been obtained. A complete analysis is given of the perturbed peaks obtained when the following molecules are adsorbed on silica: (CH<sub>3</sub>)<sub>2</sub>CO, CH<sub>3</sub>CHO, NH<sub>3</sub>, C<sub>6</sub>H<sub>6</sub>, and C<sub>6</sub>H<sub>14</sub>.

#### Experimental Section

A self-supporting pressed silica disk (Cabot Co., Cab-O-Sil, 150-m<sup>2</sup>/g surface area) was placed within a cylindrical furnace mounted in a Perkin-Elmer 421 spectrophotometer (the spectral slit width at 3700 cm<sup>-1</sup> was 1.6 cm<sup>-1</sup>). The furnace was connected to a conventional glass vacuum rack, and the silica disks were preheated to 800° in air in order to remove all water and hydrogen-bonded hydroxyl groups.

To obtain the adsorption isotherm, various pressures of the desired reagent were admitted to the cell, and the change in peak intensity of the band due to the freely vibrating hydroxyl group was measured. The ratio of the peak intensity of this band in the presence

(1) M. L. Hair, "Infrared Spectroscopy in Surface Chemistry," Marcel Dekker, Inc., New York, N. Y., 1967.

(2) R. S. McDonald, *J. Amer. Chem. Soc.*, **79**, 850 (1957).

(3) G. J. C. Fronsdorff and G. L. Kington, *Trans. Faraday Soc.*, **55**, 1173 (1959).

(4) M. R. Basila, *J. Chem. Phys.*, **35**, 1151 (1961); M. R. Basila, E. L. Saier, and L. R. Cousins, *J. Amer. Chem. Soc.*, **87**, 1665 (1965).

(5) G. A. Galkin, A. V. Kiselev, and V. I. Lygin, *Russ. J. Phys. Chem.*, **41**, 20 (1967).

**Table I:** Isothermic Heats of Adsorption on Silica, Observed Hydroxyl Band Frequency Shifts, and Ionization Potentials

Compd	$-\Delta H_{\text{ads}}^{\text{a}}$ (isosteric), kcal/mol	$\Delta\nu$ , $\text{cm}^{-1}$	Ionization potential, eV
1. $\text{SiCl}_4$	$5.4 \pm 0.3$	$25 \pm 5$	11.6
2. $\text{CHCl}_3$	$5.6 \pm 0.3$	$45 \pm 4$	11.42
3. $\text{CCl}_4$	$6.0 \pm 0.5$	$45 \pm 3$	11.47
4. $\text{CH}_2\text{SiCl}_3$	$6.5 \pm 1.0$	57	...
5. $(\text{CH}_3)_2\text{SiCl}_2$	$7.8 \pm 0.8$	90	...
6. $(\text{CH}_3)_3\text{SiCl}$	$8.7 \pm 0.4$	$135 \pm 10$	...
7. $\text{CS}_2$	$6.9 \pm 0.3$	$60 \pm 5$	10.4
9. $\text{CH}_3\text{CHO}$	$10.5 \pm 1.0$	$280 \pm 10$	...
10. $(\text{CH}_3)_2\text{CO}$	$12 \pm 1.5$	$395 \pm 15$ (at $25^\circ$ ) $345 \pm 20$ (at $100^\circ$ )	9.69
11. $\text{CH}_3\text{Si}(\text{OCH}_3)_3$	$6.0 \pm 0.1$	$363 \pm 7$	...
12. $(\text{CH}_3)_2\text{Si}(\text{OCH}_3)_2$	$6.7 \pm 0.3$	$403 \pm 8$	...
13. $(\text{C}_2\text{H}_5)_2\text{O}$	$7.9 \pm 0.2$	$460 \pm 20$	9.6
14. $(\text{CH}_3)_3\text{SiOCH}_3$	$8.3 \pm 0.1$	$477 \pm 8$	...
15. $\text{NOCl}$	3.7	178, 195	...
16. $\text{NH}_3$	$8.9 \pm 0.2$	580 (at $90^\circ$ ) 675 (at $25^\circ$ )	10.16
17. $\text{C}_5\text{H}_5\text{N}$ (pyridine)	$10.8 \pm 1.0$	$765 \pm 50$	9.7
18. $(\text{C}_2\text{H}_5)_3\text{N}$	$11.0 \pm 1.2$	$975 \pm 50$	7.50
19. <i>n</i> -Pentane	$5.7 \pm 0.4$	30	10.58
20. $\text{CH}_3\text{Cl}$	...	25	10.7
21. <i>n</i> -Heptane	...	45	10.34
22. Cyclohexane	$6.4 \pm 0.6$	45	10.06
23. Benzene	$5.6 \pm 1.0$	$120 \pm 10$	9.2
24. $\text{CH}_3\text{I}$	$6.0 \pm 1.0$	$125 \pm 20$	9.1
25. Toluene	...	127	8.81
26. Xylene	$6.2 \pm 0.3$	$155 \pm 5$	8.45-8.60
27. <i>n</i> -Hexane	...	30	10.43

<sup>a</sup> The error limits for the heats of adsorption are estimated.

of the gas to the peak intensity under vacuum gives the fraction of hydroxyl groups remaining uncovered ( $1 - \theta$ ). The quantity  $\theta$  is the fraction of hydroxyl groups covered at any given pressure of added gas. With each reagent this procedure was repeated at three or more temperatures. A new value of the peak intensity under vacuum was obtained at each temperature, since the peak intensity decreases slightly with increasing temperature. The spectrum of the perturbed hydroxyl band was also recorded. In the case of reagents where the adsorption bands due to the gas phase overlapped the band due to the perturbed hydroxyl band, a compensating cell was mounted in the reference beam in order to cancel out the absorption due to the gas phase.

## Results

**Heat of Adsorption.** From the isotherms obtained at several temperatures, the heat of adsorption was calculated as follows. The pressures required to give exactly the same degree of physical coverage at various temperatures were determined to give the adsorption isostere. A plot of  $\log P(\theta = \text{constant})$  vs.  $1/T$  was then made. The slope of the resultant straight line is proportional to the isosteric heat of adsorption. For each compound, plots were made at various coverages

and, in all cases, were found to be linear and parallel up to a coverage of about  $\theta = 0.5$  or  $0.6$ . Beyond  $\theta = 0.6$  deviations occurred. These could be due either to mutual repulsion of the adsorbed molecules or to errors in the calculation, since at high coverages the isotherm is almost flat and it is difficult to obtain the precise pressure for a given  $\theta$ . It should be noted here that  $\theta$  refers to coverage of the surface hydroxyl group and that the enthalpy change measured is the isosteric heat of adsorption of the molecule *on the freely vibrating hydroxyl groups*.

The measured enthalpy changes are listed in Table I, together with the observed frequency shifts and literature values for the ionization potentials of the compounds. In obtaining these ionization potentials from the literature, no attempt has been made to distinguish which were the "best" values.

**Frequency Shift and Intensity.** The perturbed peaks obtained when physical adsorption takes place on silica were resolved on an electronic curve resolver (Du Pont Model 310 curve resolver). Two typical analyses are shown in Figures 1 and 2 (benzene and acetone). Both the observed band and the individually resolved bands are shown. Also shown in the figures are the gas-phase spectra taken without the silica present. It should be

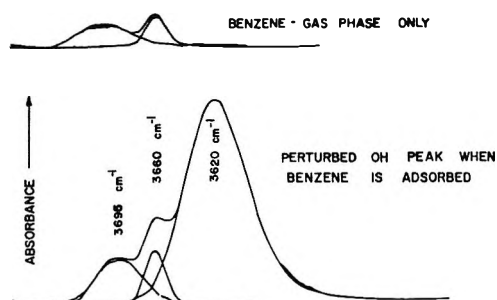


Figure 1. Resolution of perturbed hydroxyl band due to benzene adsorption.

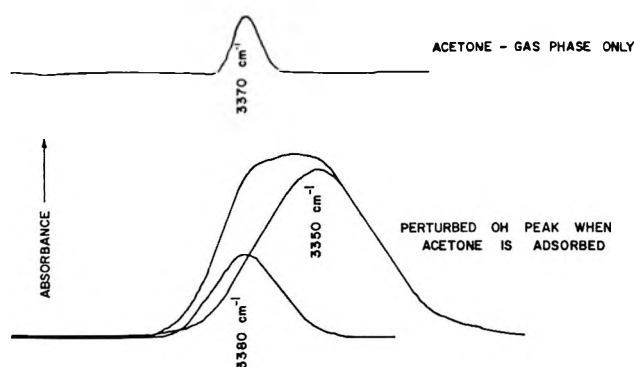


Figure 2. Resolution of perturbed hydroxyl band due to acetone adsorption.

noted that overtone bands occur in the gas-phase spectrum in the same frequency region where the perturbed hydroxyl group band appears. The net effect of this superimposition is to create an initial observation that the frequency shift changes with increased coverage. With the exception of the benzene adsorption, this appears to be untrue.

In any accurate analysis of the perturbed bands, therefore, these gas-phase overtones (and the overtones from the gaseous molecules which have adsorbed on the silica) must be subtracted from the perturbed peak.

From each spectrum the following information was obtained: (a) the shape of the peak due solely to the perturbed hydroxyl, (b) the integrated area under this peak, and (c) the position of the peak (*i.e.*, the frequency). Except for the aromatic compounds, all the perturbed peaks resolved were found to consist of a single, symmetrical Gaussian band. In the case of the aromatic hydrocarbons, the Gaussian band was skewed.

## Discussion

**Band Shape.** Gas-phase infrared absorption bands are normally Lorentzian in shape. Examination of an expanded spectrum of the band at  $3750\text{ cm}^{-1}$ , attributed to the freely vibrating surface silanol group, shows that it can be satisfactorily accounted for by the superimposition of two symmetrical Lorentzian peaks whose maxima are separated by less than  $5\text{ cm}^{-1}$ . After physical adsorption and interaction between the ad-

sorbate and the hydroxyl group, the perturbed peaks are all fitted by a single Gaussian peak. This is taken as an indication that the adsorbed molecules show a distribution of energies; *i.e.*, there is a Boltzmann distribution, suggesting that the thermal kinetic energy modulates the precise adsorption interaction energy. The perturbed peaks, with the exception of those due to aromatic hydrocarbons, are symmetrical in shape.

**Frequency Shifts.** The adsorption studied here takes place on a freely vibrating surface hydroxyl group and is thus a form of hydrogen bonding. It is of some interest then to comment briefly on the available theories of hydrogen bonding. Pimentel and McLellan<sup>6</sup> have reviewed earlier spectroscopic studies of hydrogen bonding, most of which dealt with hydrogen bonding in solutions. It was generally noted that the O-H stretching mode was shifted to lower frequencies, the half-width of the perturbed peak was broadened, and the integrated intensity of the perturbed peak was many times larger than that of the unperturbed peak. Correlations have been found between the observed hydroxyl frequency shift and various other parameters, such as the band half-width, the integrated intensity, Hammett's  $\sigma$  function, the length of the H-B bond, the heat of formation of the hydrogen bond, and others.<sup>6</sup> These correlations only hold, however, within restricted classes of compounds. Of particular interest is the approximately linear relationship which is observed between  $\Delta\nu$  and  $\Delta H$ —a relationship that is only approximately true out to about  $\Delta\nu = 500\text{ cm}^{-1}$ , after which gross deviations are observed.

In a study of adduct formation with the hydroxyl group of phenol, Purcell and Drago<sup>7</sup> have correctly pointed out that the enthalpy change for the interaction of phenol with a Lewis base consists of two contributions. These are (i) the change in the phenol O-H bond energy and (ii) the bond energy involved in forming the new hydrogen bond between the phenol and the base; *i.e.*

$$\Delta H = \delta E_{\text{O-H}} + E_{\text{H-B}}$$

Unfortunately, H-B vibrations are normally observed below  $200\text{ cm}^{-1}$  and are not readily susceptible to observation with solids.

It is now believed that hydrogen bonding is due primarily to electrostatic interaction. The electrostatic model, however, does not explain the following two important points:<sup>8</sup> (i) the increase in the intensity of the ir absorption band, which is many fold in excess of that explainable by the electrostatic model, and (ii) the absence of a correlation between hydrogen-bond strengths and molecular dipole moments. The expla-

(6) G. C. Pimentel and A. L. McLellan, "The Hydrogen Bond," W. H. Freeman and Co., San Francisco, Calif., 1960.

(7) K. F. Purcell and R. S. Drago, *J. Amer. Chem. Soc.*, **89**, 2874 (1967).

(8) C. A. Coulson, quoted in ref 6, p 233.

nations offered for these behaviors are lumped together by attributing some covalent character to the H bond. In brief, one may say that there is no one theory of H bonding which explains all the experimental phenomena.

Basila has studied the physical adsorption of methylbenzenes and chloromethanes on silica.<sup>4</sup> He considered the hydrogen bonding on the freely vibrating groups to be a special case of charge-transfer interaction and the observed frequency shift to be a measure of the strength of the interaction. In this case, the strength of the interaction of a series of donor molecules with a given acceptor should be related to the ionization potential of the donors. Within any one homologous series (the benzenes or the chloromethanes), he found a nonlinear correlation between the ionization potential of the donor and the frequency shift of the hydroxyl group, but no relationship was found between different series of compounds.

More recently, Kiselev, *et al.*,<sup>5</sup> have studied the relationship between the observed frequency shifts of the hydroxyl groups on silica and both the ionization potentials and the heats of adsorption of the adsorbates. From their data they concluded that the ionization potential cannot serve as a measure of the effect of electron-donor properties in the specific interactions of molecules differing markedly in electronic structure. By calorimetrically measuring the heat of adsorption ( $Q$ ) of various molecules on hydroxylated and dehydroxylated silica, they concluded that the differential heat between these two quantities was the heat of specific adsorption on the hydroxyl groups. A reasonably linear plot was obtained of  $\Delta Q$  vs.  $\Delta\nu$  for shifts up to 500  $\text{cm}^{-1}$ .

The heats of adsorption and  $\Delta\nu$  values obtained in this work are given in Table I. These show that, within a given homologous series, there is a monotonic rise in the frequency shift with a rise in the heat of adsorption (compounds 1-6, 9-10, 11-14, and 15-18). With the hydrocarbons and methyl halides (compounds 19-26), no such relationship holds. The heats of adsorption are all the same within experimental error, although the frequency shifts do vary over a wide range. Thus, in this series, there is a contribution to the frequency shift which does not show up in the heat of adsorption.

Comparing the values of the ionization potentials of the nonhydrocarbon compounds with the frequency shifts or heats of adsorption shows that there is no correlation between these parameters. However, for the hydrocarbons, where the heat of adsorption is approximately constant, there is a correlation between the frequency shift and the ionization potential. This is shown in Figure 3.

The adsorbates used in this study can be immediately separated into two classes of compounds: (i) those in which the frequency shift increases with increasing heat of adsorption and (ii) those in which the heat of adsorp-

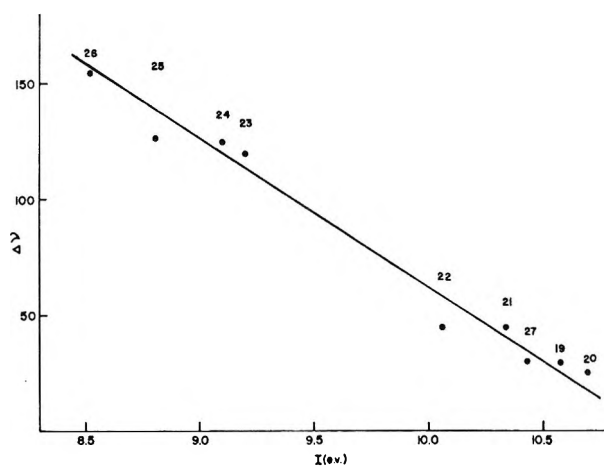


Figure 3. Comparison of frequency shifts and ionization potentials for the series of hydrocarbon adsorbates on silica.

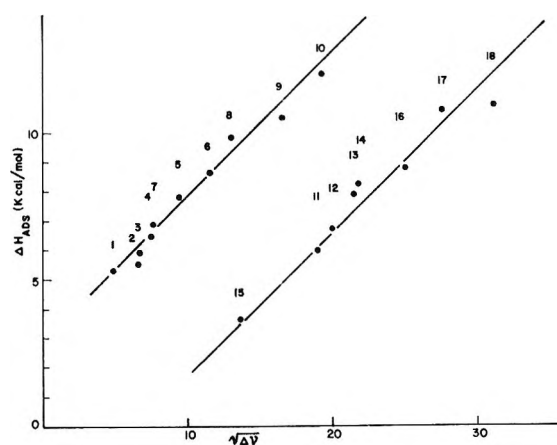


Figure 4. Isosteric heats of adsorption of compounds adsorbed on silica as a function of  $(\Delta\nu)^{1/2}$ .

tion is approximately constant and thus independent of the frequency shift.

In Figure 4, the heats of adsorption of compounds 1-18 are plotted as a function of  $(\Delta\nu)^{1/2}$ . The plot gives two good linear relationships (upper-curve compounds 1-10 and lower-curve compounds 11-18). Since the adsorbing sites (the OH groups) are the same for all the measurements, it seems likely that this difference can be traced to electronic differences in the adsorbing molecules. One striking difference between the molecules in the upper and lower curves is apparent. In the upper set, the lone-pair electrons are all located in p orbitals, whereas in the lower set, the lone-pair electrons are all located in hybrid orbitals ( $sp^2$  or  $sp^3$ ). Thus, for a given heat of adsorption, a low shift is observed when p-orbital electrons are available for H bonding and a large shift is observed when hybrid orbital electrons are used for H bonding.

"The most noticeable distinction between a hybrid orbital and its component s, p, . . . orbitals is that the hybrid no longer possesses central symmetry. . . the

centre of mean position of a hybrid may be at some distance from the nucleus."<sup>9</sup> In hybrid orbitals, then, the atomic dipole can be quite large and, in the case of carbon, can contribute as much as 2.2 D. As suggested above, the theory of hydrogen bonding is incomplete. However, if we assume the hydrogen bond is principally due to electrostatic interaction, then the process taking place is as follows. As the lone-pair electron orbital of the adsorbing molecule approaches the surface hydroxyl group, the electrostatic interaction distorts the hydrogen 1s orbital. This causes the O-H stretching vibration frequency to be lowered. The amount of electrostatic interaction will determine the magnitude of the frequency shift and will be greater in the case of a hybrid orbital than in the case of a p orbital. The over-all heat of adsorption which is measured will be determined by the amount of this electrostatic interaction plus contributions due to other interactions with the hydroxyl groups. The factor causing the observed frequency shift is thus only one of several effects which contribute to the over-all heat of adsorption. This must be so, since the magnitude of the shift in the case of the hydrocarbons is independent of the over-all heat of adsorption.

On the basis of these results, it appears that adsorbates on silica can be divided into two groups: (i) those in which the heat of adsorption is constant ( $6.0 \pm 0.4$  kcal/mol) and in which the frequency shift can be given in terms of the ionization potential

$$\Delta\nu(\text{cm}^{-1}) = \frac{10.9 - I(\text{eV})}{0.015} \quad (1)$$

and (ii) those in which the heat of adsorption is a function of the frequency shift and of the location of the lone-pair electrons responsible for the H bonding. These heats are given by the equation

$$\Delta H(\text{kcal}) = 0.455(\Delta\nu\text{cm}^{-1})^{1/2} + (\text{constant}) \quad (2)$$

When the electrons responsible for the H bonding are located in p orbitals, the constant is equal to 3.0; when the electrons are located in  $sp^2$  or  $sp^3$  hybrid orbitals, the constant is equal to  $-2.3$ .

For compounds in the first series the dependence of the shift on ionization potential indicates a charge-transfer interaction, as proposed by Basila.<sup>4</sup> However, in the second series, the lack of this dependence makes a charge-transfer mechanism unlikely, and, in this case, the shift must be attributed mainly to electrostatic interaction. However, since there is a nonzero intercept, there must be other contributions to  $\Delta\nu$ .

The choice of a relationship based on  $(\Delta\nu)^{1/2}$  is difficult to justify on theoretical grounds. It should be pointed out, however, that the linear relationships which have been predicted and then observed, in solution chemistry, are useful only when  $\Delta\nu < 500 \text{ cm}^{-1}$ . Above this value, gross deviations occur which cannot

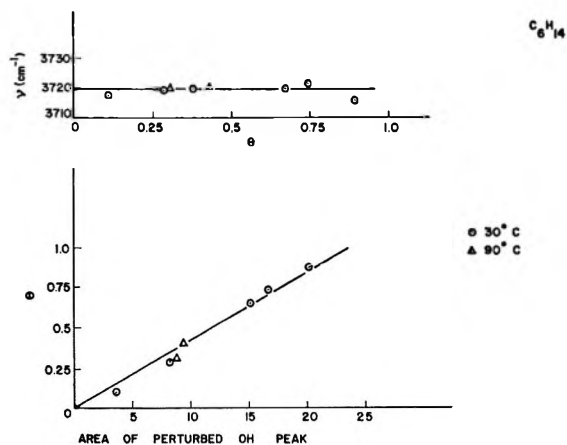


Figure 5. (Top) effect of coverage ( $\theta$ ) on the frequency of the perturbed hydroxyl group during hexane adsorption; (bottom) effect of coverage on the area of the perturbed hydroxyl peak.

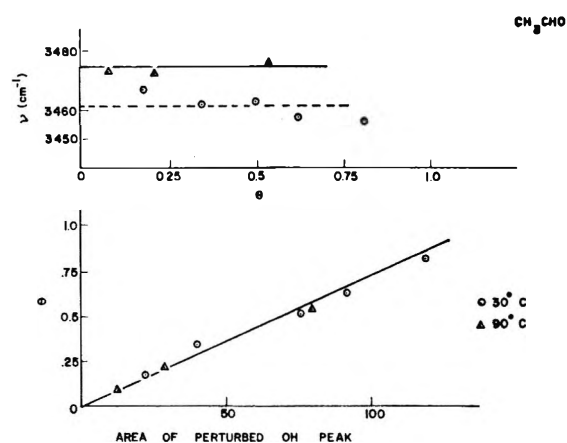


Figure 6. (Top) effect of coverage ( $\theta$ ) on the frequency of the perturbed hydroxyl group during acetaldehyde adsorption; (bottom) effect of coverage on the area of the perturbed hydroxyl peak.

be understood in terms of our present knowledge of hydrogen bonding and which are usually ignored.

*Intensity, Frequency, and Temperature.* The results of measurements made on the perturbed OH bands following adsorption of hexane, acetaldehyde, ammonia, and benzene are shown in Figures 5–8.

The lower part of each figure shows the area of the perturbed peak as a function of the fraction of freely vibrating hydroxyl groups consumed when adsorption takes place. Except for benzene the plots are linear and pass through the origin. The upper plots of Figures 5, 6, and 8 show the frequency of the perturbed peak as various fractions of the free hydroxyl group are consumed. With the possible exception of benzene, the position of the perturbed peak does not change with coverage at any given temperature. However, in the case of the nonhydrocarbon compounds, there is a

(9) C. A. Coulson, "Valence," Oxford University Press, London, 1968, p 207.



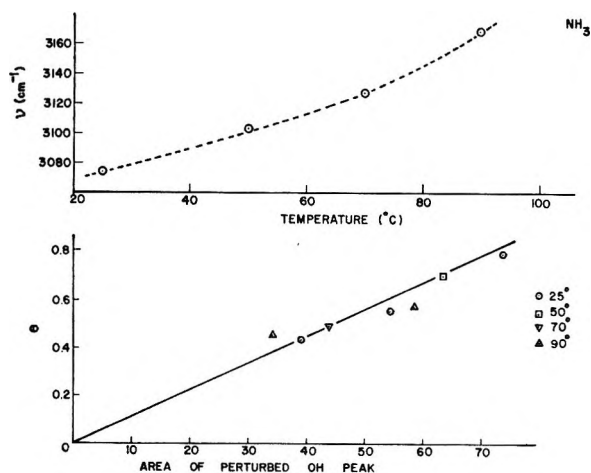


Figure 7. (Top) ammonia adsorption position of the perturbed hydroxyl peak of various temperatures; (bottom) effect of coverage on the area of the perturbed hydroxyl peak.

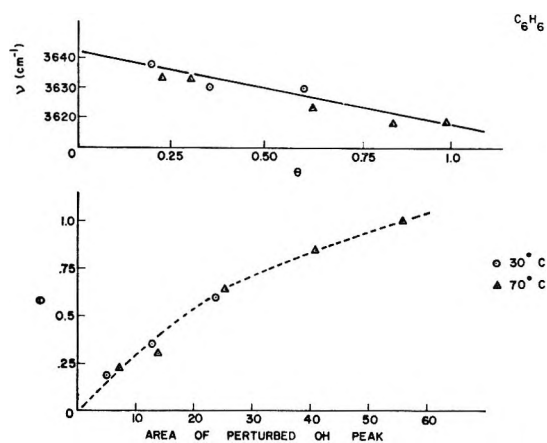


Figure 8. (Top) effect of coverage ( $\theta$ ) on the frequency of the perturbed hydroxyl group during benzene adsorption; (bottom) effect of coverage on the area of the perturbed hydroxyl peak.

change in the frequency shift at different temperatures. This is best illustrated in Figure 7 (top) for ammonia, where the frequency of the perturbed OH band is plotted for various temperatures; the frequency increases by about  $100\text{ cm}^{-1}$  over the range from 30 to  $90^{\circ}$ . In the case of hydrocarbon compounds no significant shift was noted with change in temperature.

With the exception of the aromatic hydrocarbons, the perturbed bands were all symmetrical and Gaussian. The measured areas (normalized for the amount of free OH consumed) are plotted in Figure 9 against the observed frequency shift. It is seen that the intensities increase linearly with increasing wave number shift out to about  $700\text{ cm}^{-1}$ , beyond which deviations from the straight line occur. The linear relationship between  $\Delta\nu$  and the integrated absorption intensity has been observed in studies of hydrogen bonding in solution. The existence of this linear relationship in this work demonstrates a confidence in the use of the electronic

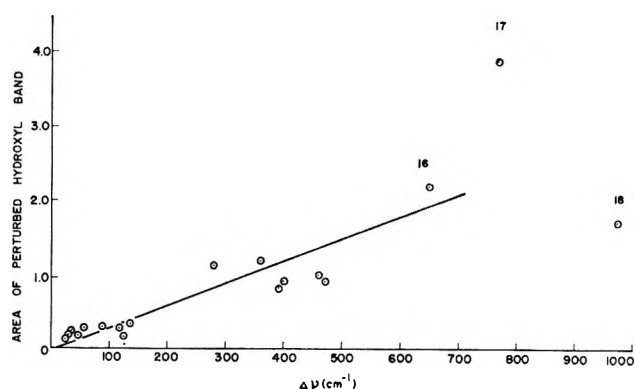


Figure 9. Areas of perturbed hydroxyl bands as a function of frequency shift.

curve resolver in analyzing the data obtained. Measurements made before resolving the spectra gave a random scatter instead of the expected relationship. It should be noted that this simple linear relationship was not observed with benzene, which throughout these experiments gave anomalous results.

With increasing temperature, acetone, acetaldehyde, and ammonia all cause a decreasing frequency shift for the perturbed hydroxyl band. These compounds fall in the group in which the heat of adsorption can be described in terms of the observed frequency shift. Thus the heat of physical adsorption falls off with increasing temperature. This effect is very often noted in physical adsorption. The magnitude of the change in the observed shift and the change in heat to which this corresponds can be calculated from eq 2, which was determined from the average  $\Delta H - \Delta\nu$  data of a large number of compounds. These results are given in Table II. By using the observed frequency shift at various temperatures one has a very sensitive estimate of this change in heat of adsorption. In the case of the compounds in which the frequency shift is a function of the ionization potential and independent of the heat of adsorption (benzene and hexane), the shift is independent of temperature in the range reported.

Table II

Compd	Change in shift, $\text{cm}^{-1}$ (temp range, $^{\circ}\text{C}$ )	Change in heat, kcal
Acetone	50 (25-100)	0.6
Acetaldehyde	15 (30-90)	0.2
Ammonia	100 (25-90)	0.9

Except for benzene, the observed shifts are independent of the degree of physical coverage, showing that over the range of coverages studied there is not appreciable lateral interaction.

Benzene shows anomalous behavior compared with

the other compounds. Thus the linear relationship between the amount of OH consumed and the area of the perturbed peak is not obeyed, and the frequency of the perturbed OH peak decreases with increasing surface coverage.<sup>4</sup> This increase in frequency shift with increasing coverage is somewhat strange. Since benzene belongs to the series of compounds in which the shifts are independent of the heat of adsorption, it seems unreasonable to attribute this to changes in the heat of adsorption due to coverage. Moreover, the shift is in the opposite direction. If, however, it can be attributed to a change in the ionization potential, this would indicate that the ionization potential of adsorbed benzene decreases by about 0.4 eV as its coverage of the surface hydroxyl group increases.

*Acknowledgment.* The authors wish to acknowledge the able assistance of Miss Ethel Herritt in the experimental work.

#### Addendum

An anonymous reviewer has suggested that ketone adducts of Lewis acids have C–O–X bond angles near

120° (where X is the first atom of the Lewis acid). In view of this, he suggests that the lone pairs in C=O groups are sp<sup>2</sup> hybrids rather than pure p states. This view can be reconciled with the two lines in Figure 4 by assuming that in compounds 7–10 it is the double bond that is involved in hydrogen bonding rather than the lone-pair electrons on oxygen or sulfur. The referee suggests that the work of Fritzsche<sup>10</sup> on phenol bonding to ketones in CCl<sub>4</sub> solution supports this supposition.

This comment has obvious validity. However, the authors would like to emphasize the incomplete theoretical state of hydrogen bonding and the difficulties of explaining hydrogen-bonded interactions in terms of Lewis acid adducts where strong orbital overlap occurs. Both Coulson<sup>11</sup> and Ballhausen and Gray<sup>12</sup> in their discussions of carbonyl groups and formaldehyde, respectively, refer to the existence of pure p states on the carbonyl oxygen atom.

(10) H. Fritzsche, *Acta Chim. Acad. Sci. Hung.*, **40**, 31 (1964).

(11) Reference 8, p 185.

(12) C. J. Ballhausen and H. B. Gray, "Molecular Orbital Theory," W. A. Benjamin, Inc., New York, N. Y., 1964, p 85.

## NOTES

### A Proposed Viscosity–Concentration Equation beyond Einstein's Region

by S. P. Moulik

*Department of Physical Chemistry, Jadavpur University, Calcutta, India (Received May 22, 1968)*

Rigid particles suspended in a continuous medium will interfere with the stream lines of flow pattern and the suspension should have a higher viscosity than the medium. From hydrodynamic considerations Einstein<sup>1</sup> was the first to treat this problem in the case of rigid spheres suspended in a continuum. His results for dilute suspensions may be expressed by

$$\eta/\eta_0 = 1 + 2.5\phi \quad (1)$$

where  $\eta$  is the absolute viscosity of the suspension,  $\eta_0$  that of the medium, and  $\phi$  the volume fraction occupied by the particles. In the above equation the volume fraction  $\phi$  must be taken to include the volume of any solvent immobilized on the surface of the solute particle.

The volume fraction may then be expressed by  $\phi = cV_h$ , where  $c$  is the concentration ( $M$ ) and  $V_h$  is the molar volume of the solute including attached solvent ( $M^{-1}$ ). Thus eq 1 can be modified to

$$\eta/\eta_0 = 1 + 2.5cV_h = 1 + Kc \quad (2)$$

where  $2.5V_h = K = \text{constant}$ .

This viscosity relation of Einstein is restricted to the dilute domain of solute concentration and consequently neglects the solvent–solute interaction. Jones and Dole<sup>2</sup> formulated an empirical equation which can account for both solute–solute electrostatic interaction and solvent–solute interaction. According to Merker and Scott<sup>3</sup> it is the difference between the microscopic and macroscopic viscosities, depending on the solvent–solute interaction, that determines the various values of Einstein's constant for different solute–solvent systems.

To deal with viscosity of concentrated solutions, Suryanarayana and Venkatesan<sup>4</sup> empirically formulated

(1) A. Einstein, *Ann. Physik*, **19**, 289 (1906); **34**, 591 (1911).

(2) G. Jones and M. Dole, *J. Amer. Chem. Soc.*, **51**, 2950 (1929).

(3) R. L. Merker and M. J. Scott, *J. Colloid Sci.*, **19**, 245 (1964).

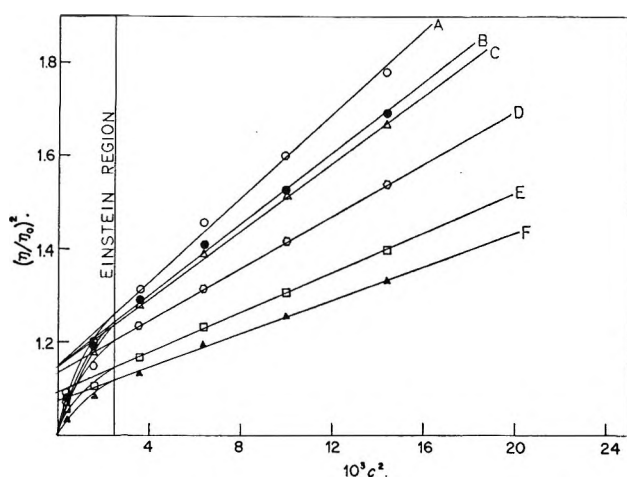


Figure 1. Plot of  $(\eta/\eta_0)^2$  vs.  $c^2$  for tetrakis(trimethylsilyl)methane in different solvents:<sup>3</sup> A, hexane; B, pentane; C, heptane; D, tetrahydrofuran; E, toluene; F, benzene.

an equation and confirmed its validity for some electrolytes. For concentrated solutions the flow patterns around neighboring particles can no longer be treated as independent. From such consideration Vand<sup>5</sup> developed an equation which can explain the experimental results in a far better way. However, even deviation from this equation is not uncommon and has been observed by the present author in many systems.

### The Proposed Equation

In a differential form Einstein's eq 2 can be written as

$$\frac{d(\eta/\eta_0)}{dc} = K \quad (3)$$

This is only true for dilute solutions, and the upper concentration limit to which it is valid may vary from solute to solute. We shall now define a term,  ${}^uE_c$ , called the "upper concentration limit of Einstein behavior." This is the maximum concentration up to which eq 3 is valid. It has been empirically observed by the author, in many cases (both electrolytes and nonelectrolytes), that above this "upper concentration limit of Einstein behavior" eq 4 holds instead of eq 3.

$$\frac{\Delta(\eta/\eta_0)}{\Delta c} \left( \frac{\eta/\eta_0}{c} \right) = \text{constant} = K' \quad (4)$$

In this equation  $\Delta(\eta/\eta_0)$  represents the change in viscosity for a change in experimental concentration  $\Delta c$ . For a small change eq 4 can be written as

$$\frac{d(\eta/\eta_0)}{dc} \left( \frac{\eta/\eta_0}{c} \right) = K' \quad (5)$$

Integration of the above gives

$$(\eta/\eta_0)^2 = I + K'c^2 \quad (6)$$

where  $I$  is the integration constant.

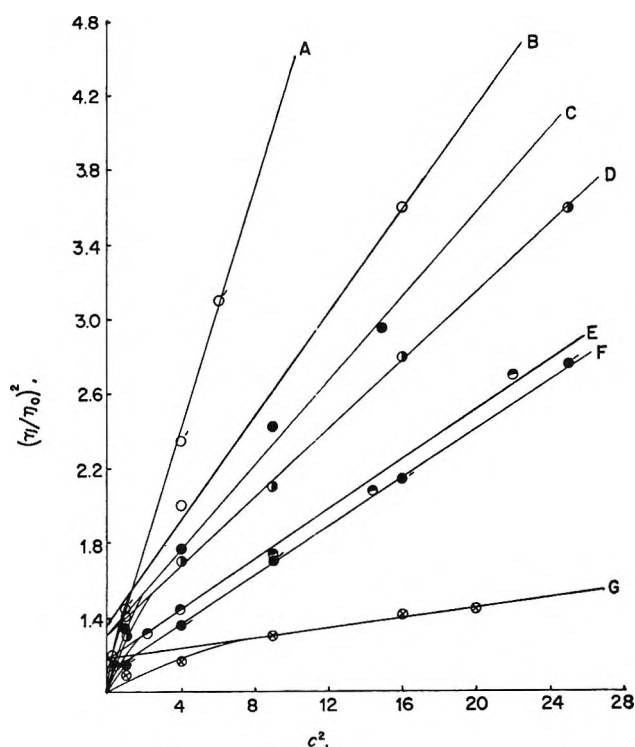


Figure 2. Plot of  $(\eta/\eta_0)^2$  vs.  $c^2$  for various electrolytes in water: A,  $K_2CrO_4$ ;<sup>8</sup> B,  $H_2SO_4$ ;<sup>8</sup> C,  $ClCH_2CO_2H$ ;<sup>7</sup> D,  $LiCl$ ;<sup>7</sup> E,  $LiBr$ ;<sup>6</sup> F,  $AgNO_3$ ;<sup>7</sup> G,  $KCl$ .<sup>7</sup>

### Results and Discussion

The integration constant or the intercept of eq 6 becomes equal to the relative viscosity value at zero concentration, *i.e.*, the solvent relative viscosity which is 1. However, as discussed before, eq 6 should not hold at concentrations below  ${}^uE_c$ . So extrapolation of results, plotted according to this equation, to zero concentration has little physical meaning. In Figures 1, 2, and 3 plots are shown for a number of solutes. In these figures the curved portion of each individual straight line, in the lower concentration ranges, represents the Einstein region of viscosity-concentration behavior, *i.e.*, the valid domain of eq 3. In this zone the system does not obey eq 6 and the curved plot approaches the limiting value of 1. To decide upon the correct value of the boundary between these two equations, that is the value of  ${}^uE_c$ , a knowledge of measured viscosity, both at lower and higher concentration, is required. We see from the figures that extrapolation of the linear portion of each curve to zero concentrations always offers an intercept greater than 1. From the  ${}^uE_c$  concept this value of the intercept can be shown to be

$$(\eta/\eta_0)^2_{\text{at } c = {}^uE_c} - K'({}^uE_c)^2 = M$$

Equation 6 can then be rewritten as

(4) C. V. Suryanarayana and V. K. Venkatesan, *Trans. Faraday Soc.*, **54**, 1709 (1958); *Monatsh.* **89**, 824 (1958).

(5) V. Vand, *J. Phys. Colloid Chem.*, **52**, 314 (1948).

$$(\eta/\eta_0)^2 = M + K'c^2 \quad (7)$$

Data used in the above illustrations have been taken from the literature.<sup>3,6-9</sup> Equation 6 or 7 has been tested for many solutes. In Table I the names of the solutes, other than those described in the illustrations, with their corresponding upper limits of tested concentra-

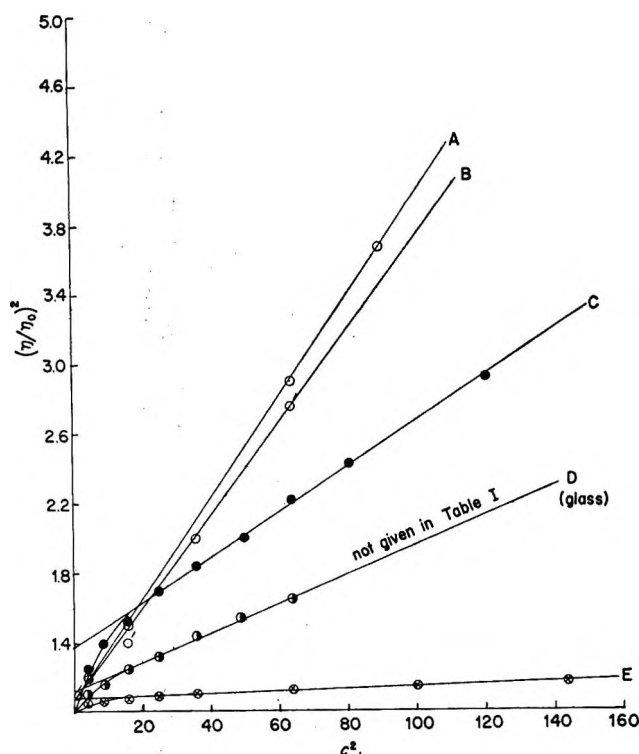


Figure 3. Plot of  $(\eta/\eta_0)^2$  vs.  $c^2$  for some solutes in water: A, urea;<sup>8</sup> B, urea;<sup>9</sup> C, HCl;<sup>8</sup> D, glass; E,  $\text{NH}_4\text{OH}$ .<sup>8</sup>

Table I

Solute	Max exptl concn, M	Concn validity of eq 9, upper limit, M	Ref
$\text{CuSO}_4$	1.68	1.68	7
HCl	12.84	12.84	8
KF	6.45	6.45	7
KI	6.00	6.00	7
$\text{K}_2\text{Cr}_2\text{O}_7$	1.76	1.76	7
$\text{MnCl}_2$ (water-alcohol)	2.50	2.50	7
$\text{LiClO}_3$	19.03	4.55	7
NaBr	7.00	5.00	7
NaCl	5.00	5.00	7
NaI	4.94	4.94	7
$\text{NaNO}_3$	9.27	9.27	7
$\text{Na}_2\text{SO}_4$	1.71	1.71	7
$\text{NH}_4\text{OH}$	12.00	12.00	8
Tetrakis(trimethylsilyl)methane	0.12	0.12	3
Urea	8.00	8.00	8
Urea	9.44	9.44	9

tions are furnished. The wide variety of examples warranting use of such an equation can be emphasized.

*Acknowledgment.* This work has been supported by Federal Water Pollution Control Administration Grant No. WP00783 in the laboratory of Dr. M. Bier, VA Hospital, Tucson, Ariz.

(6) G. Jones and J. H. Cohn, *J. Amer. Chem. Soc.*, **62**, 338 (1940).

(7) E. A. Guggenheim, J. C. Mayer, and F. C. Tompkins, Ed., "International Encyclopedia of Physical Chemistry and Chemical Physics," Vol. 3, Pergamon Press Inc., New York, N. Y., 1965, Topic 16.

(8) "International Critical Tables," Vol. 5, National Research Council, McGraw-Hill Book Co., Inc., New York, N. Y., 1929.

(9) H. B. Bull, K. Breese, G. L. Ferguson, and C. A. Swenson, *Arch. Biochem. Biophys.*, **104**, 297 (1964).

### Gas-Phase Photolysis of Mixtures of Cyclohexane with Benzene and with Nitrous Oxide at 1470 Å

by Robert R. Hentz and Ronald J. Knight

Department of Chemistry and the Radiation Laboratory,<sup>1</sup>  
University of Notre Dame, Notre Dame, Indiana 46556  
(Received May 31, 1968)

Energy transfer from neutral excited cyclohexane molecules apparently is not involved appreciably in the mechanism of radiation-induced luminescence from dilute solutions of scintillators ( $\leq 10^{-2} M$ ) in liquid cyclohexane.<sup>2,3</sup> However, such a process may contribute to the "protective" effect of benzene on cyclohexane in radiolysis of their mixtures in both the liquid<sup>4</sup> and gas<sup>5</sup> phases, particularly at higher benzene concentrations.<sup>6</sup> In a previous study,<sup>7</sup> quantum yields were determined in gas-phase photolysis of benzene and of cyclohexane with the Xe resonance lamp. Such a study was undertaken as a prelude to study of the mixtures because, as was noted, photolysis of the mixtures with the Xe resonance lamp should permit assessment of the role of *single*<sup>8</sup> excited cyclohexane molecules (and an

(1) The Radiation Laboratory of the University of Notre Dame is operated under contract with the U. S. Atomic Energy Commission. This is AEC Document No. COO-38-611.

(2) M. Burton, *Mol. Cryst.*, **4**, 61 (1968).

(3) R. R. Hentz and R. J. Knight, *J. Phys. Chem.*, **72**, 1783 (1968).

(4) J. P. Manion and M. Burton, *ibid.*, **56**, 560 (1952); J. F. Merklin and S. Lipsky, *ibid.*, **68**, 3297 (1964).

(5) J. M. Ramaradhy and G. R. Freeman, *Can. J. Chem.*, **39**, 1769 (1961); J. Blachford and P. J. Dyne, *ibid.*, **42**, 1165 (1964); L. M. Theard, *J. Phys. Chem.*, **69**, 3292 (1965).

(6) Contribution of such a process in liquid radiolysis and photolysis is suggested by: J. Y. Yang, F. M. Servedio, and R. A. Holroyd, *J. Chem. Phys.*, **48**, 1331 (1968); R. A. Holroyd, *J. Phys. Chem.*, **72**, 759 (1968).

(7) R. R. Hentz and S. J. Rzad, *ibid.*, **71**, 4096 (1967).

(8) The term "single excited molecules" is used to make a distinction from collective excitations which could be involved in the liquid.

estimate of their lifetime) in the "protective" effect. In the present study, hydrogen quantum yields have been determined in gas-phase photolysis of cyclohexane-benzene and cyclohexane-N<sub>2</sub>O mixtures with the Xe resonance lamp.

Phillips research grade cyclohexane, specified as 99.98% pure with 2,4-dimethylpentane as the major impurity, and Air Reduction CO<sub>2</sub> were used without purification. Fisher Certified benzene and Matheson Co. N<sub>2</sub>O were purified as described previously.<sup>3,7</sup> Mixtures were prepared on a vacuum line free of mercury and grease. The required amount of each component was condensed from a calibrated volume, filled to the necessary pressure, into the photolysis cell cold finger at 77°K. The photolysis cell was warmed to ensure complete mixing. After photolysis the cold finger was immersed in liquid nitrogen and noncondensable gases were pumped through cold traps at 77°K and collected for analysis by gas chromatography.<sup>3</sup>

The 3-l. photolysis cell and the construction and operation of the Xe lamps have been described.<sup>7</sup> Only the Xe resonance lines are detected below 2500 Å with the intensity at 1295 Å (9.5 eV) about 2% of that at 1470 Å (8.4 eV). In the previous study,<sup>7</sup> use of  $\phi(\text{CO}) = 1.0$  for the CO<sub>2</sub> actinometer<sup>9</sup> gave  $\phi(\text{H}_2) = 0.74 \pm 0.02$  for the Xe-lamp photolysis of cyclohexane over the range 1-70 torr. This result was confirmed in the present work using N<sub>2</sub>O at 6 torr as the actinometer with  $\phi(\text{N}_2) = 1.4$ .<sup>10</sup> Lamp intensities were determined in each experiment with 6 torr of N<sub>2</sub>O or 1 torr of cyclohexane and were usually about  $2 \times 10^{15}$  quanta sec<sup>-1</sup>. Because of the nonlinear decrease in intensity during photolysis,<sup>7</sup> owing to polymer formation on the lamp window, quantum yields were calculated from the geometric mean of intensities measured before and after a photolysis; the intensity decrease was minimized by photolysis for only 1 min. All photolyses were at room temperature.

Quantum yields of hydrogen were measured in Xe-lamp photolysis of cyclohexane-benzene mixtures at 1 and 70 torr and of cyclohexane-N<sub>2</sub>O mixtures at 70 torr. Results are presented in Figure 1 in which  $\phi(\text{H}_2)$ <sup>11</sup> is plotted as a function of the fraction of light  $F_C$  absorbed by cyclohexane, given by  $F_C = \epsilon_C P_C / (\epsilon_C P_C + \epsilon_B P_B)$ , where  $\epsilon$  denotes an extinction coefficient,  $P$  a partial pressure, the subscript C cyclohexane, and the subscript B benzene or N<sub>2</sub>O. Values of 408,<sup>12</sup> 159,<sup>12</sup> and 110<sup>13</sup> atm<sup>-1</sup> cm<sup>-1</sup> were used as the decadic extinction coefficients of cyclohexane, benzene, and N<sub>2</sub>O, respectively, at 25°.

In the absence of any kind of interaction between the mixture components, hydrogen quantum yields should conform to the straight line  $\phi = \phi_B + (\phi_C - \phi_B)F_C$ . Such behavior is evident in Figure 1, except for  $F_C > 0.8$  in cyclohexane-benzene mixtures at 70 torr.<sup>14</sup> The broken curve in Figure 1 has been calculated with the assumption that energy transfer from excited cyclo-

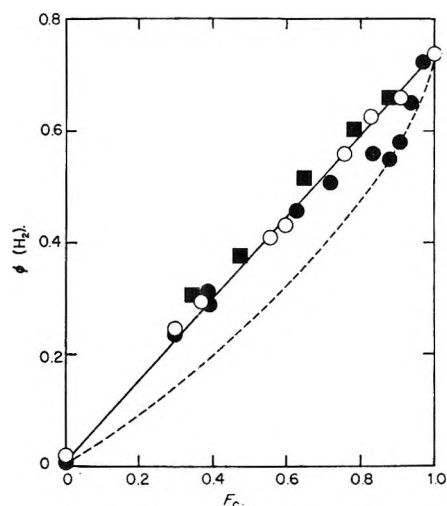


Figure 1.  $\phi(\text{H}_2)$  in Xe-lamp photolysis of cyclohexane mixtures vs.  $F_C$ , the fraction of 1470-Å light absorbed by cyclohexane: O, *c*-C<sub>6</sub>H<sub>12</sub>-C<sub>6</sub>H<sub>6</sub> at 1 torr; ●, *c*-C<sub>6</sub>H<sub>12</sub>-C<sub>6</sub>H<sub>6</sub> at 70 torr; ■, *c*-C<sub>6</sub>H<sub>12</sub>-N<sub>2</sub>O at 70 torr. The broken curve is calculated as described in the text.

hexane, *c*-C<sub>6</sub>H<sub>12</sub>\*<sup>\*</sup>, to benzene is indeed responsible for the deviations from linearity at 70 torr. Equation 1,

$$\phi = 0.74F_C k / (k + Z) \quad (1)$$

in which  $k$  represents the specific decay rate of *c*-C<sub>6</sub>H<sub>12</sub>\*<sup>\*</sup> and  $Z$  its collision frequency<sup>15</sup> with benzene ( $1.28 \times 10^7$  sec<sup>-1</sup> at 1 torr of benzene), was fitted to the most divergent points by use of  $1/k \equiv \tau = 6.6 \times 10^{-10}$  sec. Obviously, such a calculated curve is not consistent with the observations. Inclusion of a term in eq 1 for induced dissociation of *c*-C<sub>6</sub>H<sub>12</sub>\*<sup>\*</sup> on each collision with *c*-C<sub>6</sub>H<sub>12</sub>, with fitting to the most divergent points, gives a curve even less compatible with the observations. Furthermore, the identical behavior of  $\phi(\text{H}_2)$  in cyclohexane-benzene mixtures at 1 and 70 torr for  $F_C < 0.8$  precludes a detectable energy-transfer process from

(9) B. H. Mahan, *J. Chem. Phys.*, **33**, 959 (1960).

(10) J. Y. Yang and F. M. Servidio, *ibid.*, **47**, 4817 (1967).

(11) With pure benzene, some hydrogen is generated from polymer that is deposited on the window during photolysis. Correction for such a contribution gives  $\phi_B(\text{H}_2)$ , for  $F_C = 0$  in Figure 1, equal to  $\sim 0.02$  at 1 torr and  $\sim 0.007$  at 70 torr as upper limits (compare 0.03 at 1 torr and 0.015 at 66 torr in ref 7).

(12) Values for cyclohexane and benzene were obtained by S. Lipsky with a high-pressure Ar lamp at 1467 Å and were privately communicated.

(13) M. Zelikoff, K. Watanabe, and E. C. Y. Inn, *J. Chem. Phys.*, **21**, 1643 (1953).

(14) Each quantum yield in this region represents the average of a number of experiments; therefore, the deviation from linearity is considered significant.

(15) Collision frequencies were calculated using 6.1, 5.3, and 3.9 Å as the collision diameters of *c*-C<sub>6</sub>H<sub>12</sub>, C<sub>6</sub>H<sub>6</sub>, and N<sub>2</sub>O, respectively; cf., J. O. Hirschfelder, C. F. Curtiss, and R. B. Bird, "Molecular Theory of Gases and Liquids," John Wiley & Sons, Inc., New York, N. Y., 1954, p 1111.

that state of cyclohexane initially excited, regardless of any uncertainty in the extinction coefficient ratio.

A value of  $\phi(\text{H}) = 0.07$  has been estimated<sup>7</sup> from reported yields of HD in Xe-lamp photolysis of 1:1 mixtures of *c*-C<sub>6</sub>H<sub>12</sub> and *c*-C<sub>6</sub>D<sub>12</sub>.<sup>16</sup> For  $k(\text{H} + \text{C}_6\text{H}_6 \rightarrow \text{C}_6\text{H}_7)$ <sup>17</sup> =  $3.7 \times 10^7 \text{ M}^{-1} \text{ sec}^{-1}$  and  $k(\text{H} + \text{c-C}_6\text{H}_{12} \rightarrow \text{H}_2 + \text{c-C}_6\text{H}_{11}) \approx 10^6 \text{ M}^{-1} \text{ sec}^{-1}$ , 96% of the H atoms would be scavenged by benzene at  $X_C$  (mole fraction of cyclohexane) = 0.61, which corresponds to  $F_C = 0.8$  in Figure 1. The data for *c*-C<sub>6</sub>H<sub>12</sub>-C<sub>6</sub>H<sub>6</sub> mixtures at 70 torr can be made consistent with homogeneous competition for the small yield of H atoms by use of a smaller extinction coefficient ratio than that used in obtaining Figure 1; however, for such a case, the larger values of  $\phi(\text{H}_2)$  at 1 torr in mixtures with  $X_C > 0.61$  (corresponding to  $F_C > 0.8$  in Figure 1) are not understandable.

Holroyd<sup>6</sup> has presented evidence for energy transfer from excited cyclohexane molecules to N<sub>2</sub>O in liquid cyclohexane. The work of Holroyd suggested study of the photolysis of *c*-C<sub>6</sub>H<sub>12</sub>-N<sub>2</sub>O mixtures in the gas phase to eliminate possible complications associated with H atom reactions. Because  $k(\text{H} + \text{N}_2\text{O})$ <sup>18</sup>  $\approx 10^4 \text{ M}^{-1} \text{ sec}^{-1}$ , essentially all H should react with cyclohexane over the range of N<sub>2</sub>O concentrations used in the present study. Thus the results for *c*-C<sub>6</sub>H<sub>12</sub>-N<sub>2</sub>O mixtures in Figure 1 unambiguously establish that energy transfer from excited cyclohexane to a potential acceptor is not detectable in the gas phase at 70 torr.

Regardless then of the lack of complete understanding of deviations from linearity for  $F_C > 0.8$  in *c*-C<sub>6</sub>H<sub>12</sub>-C<sub>6</sub>H<sub>6</sub> mixtures at 70 torr, there is no evidence of energy transfer from that state of cyclohexane initially excited. Consequently, assuming that energy transfer will occur on every collision of *c*-C<sub>6</sub>H<sub>12</sub>\* with C<sub>6</sub>H<sub>6</sub> or N<sub>2</sub>O, an upper limit can be estimated for the lifetime  $\tau$  of *c*-C<sub>6</sub>H<sub>12</sub>\* from eq 1.<sup>19</sup> For a maximum possible error in  $\phi(\text{H}_2)$  of 10%, absence of a detectable deviation from linearity requires that  $k/(k + Z) = \phi/0.74F_C > 0.9$ . Substitution for  $Z$  of values at 70 torr corresponding to  $F_C = 0.3$  in *c*-C<sub>6</sub>H<sub>12</sub>-C<sub>6</sub>H<sub>6</sub> mixtures and to  $F_C = 0.35$  in *c*-C<sub>6</sub>H<sub>12</sub>-N<sub>2</sub>O mixtures gives  $\tau < 1.5 \times 10^{-10} \text{ sec}$  and  $\tau < 1.8 \times 10^{-10} \text{ sec}$ , respectively.

From present results, then, it is concluded that  $\tau(\text{c-C}_6\text{H}_{12}^*) < 0.2 \text{ nsec}$ . Such an estimate is consistent with that of  $\tau < 0.3 \text{ nsec}$  derived from scintillator decay-time studies in liquid cyclohexane.<sup>2</sup> For  $\tau < 0.2 \text{ nsec}$ , the results of Holroyd, *et al.*,<sup>6</sup> require specific rates of transfer from *c*-C<sub>6</sub>H<sub>12</sub>\* in the liquid to benzene and N<sub>2</sub>O of  $k_t > 1.6 \times 10^{10} \text{ M}^{-1} \text{ sec}^{-1}$  and  $k_t > 3.4 \times 10^{10} \text{ M}^{-1} \text{ sec}^{-1}$ , respectively.

(16) R. D. Doepker and P. Ausloos, *J. Chem. Phys.*, **42**, 3746 (1965).

(17) M. C. Sauer and B. Ward, *J. Phys. Chem.*, **71**, 3971 (1967).

(18) M. Schiavello and G. G. Volpi, *J. Chem. Phys.*, **37**, 1510 (1962).

(19) For  $F_C < 0.7$ ,  $\tau$  is increased by less than 10% by inclusion of a term for *c*-C<sub>6</sub>H<sub>12</sub>\* dissociation induced by collision with *c*-C<sub>6</sub>H<sub>12</sub>.

## The Vapor-Phase Infrared Spectra of the Niobium Oxotrihalides, NbOCl<sub>3</sub>, NbOBr<sub>3</sub>, and NbOI<sub>3</sub>

by Carl O. Schulz and Fred E. Stafford

Department of Chemistry and The Materials Research Center,  
Northwestern University Evanston, Illinois 60201  
(Received June 10, 1968)

The frequency of the metal-oxygen (M-O) stretching vibration in main group element gaseous oxides, hydroxides, and oxohalides can be correlated with substituent electronegativity.<sup>1,2</sup> It is expected that similar correlations can be used for predicting frequencies in transition metal oxides, hydroxides, and oxohalides.<sup>2</sup>

Both the main group and transition group V elements give rise to a series of isostructural oxohalides of the type MOX<sub>3</sub>. Condensed- and vapor-phase spectra have been observed<sup>3-9</sup> for many of the phosphorus and vanadium oxohalides (see Table I). Since heavier members of a series often behave differently from the first member, it is of interest to extend this series by observing the infrared spectra of the gaseous niobium and tantalum oxohalides and to determine how the metal-oxygen stretching vibration frequency varies with the nature of the substituents and central metal atom. This was not possible by conventional infrared techniques, since the tantalum and niobium compounds polymerize in the condensed phase.

**Table I:** Metal-Oxygen Stretching Vibration Frequencies in Group V Oxohalides and Monoxides

Compd	Frequencies, cm <sup>-1</sup>		
	P	V	Nb
F <sub>3</sub> MO	1418 <sup>a</sup>	1058 <sup>a</sup>	
Cl <sub>3</sub> MO	[1290] <sup>c</sup>	[1035] <sup>d</sup>	999 <sup>f</sup>
Br <sub>3</sub> MO	[1261] <sup>c</sup>	[1025] <sup>e</sup>	994 <sup>f</sup>
I <sub>3</sub> MO			986 <sup>f</sup>
MO	(1231) <sup>g</sup>	(1012) <sup>g</sup>	(989) <sup>h</sup>

<sup>a</sup> Reference 3. <sup>b</sup> Reference 4. <sup>c</sup> Reference 5. <sup>d</sup> Reference 6. <sup>e</sup> Reference 7. <sup>f</sup> This study. <sup>g</sup> Reference 8, gas-phase band spectra. <sup>h</sup> Reference 9, gas-phase band spectra.

(1) S. M. Chackalackal and F. E. Stafford, *J. Amer. Chem. Soc.*, **88**, 4823 (1966).

(2) M. Spoliti, S. M. Chackalackal, and F. E. Stafford, *ibid.*, **89**, 1092 (1967).

(3) H. Selig and H. H. Claassen, *J. Chem. Phys.*, **44**, 1404 (1966).

(4) M. Delwalle and F. Francois, *Compt. Rend.*, **220**, 817 (1945).

(5) H. Gerding and M. Van Driel, *Rec. Trav. Chim. Pays-Bas*, **61**, 419 (1942).

(6) F. A. Miller and L. R. Cousins, *J. Chem. Phys.*, **26**, 329 (1957).

(7) F. A. Miller and W. K. Baer, *Spectrochim. Acta*, **17**, 114 (1961).

(8) G. Herzberg, "Spectra of Diatomic Molecules," D. Van Nostrand Co., Inc., Princeton, N. J., 1950.

(9) U. Uhler, *Arkiv Fysik*, **8**, 265 (1954).

Infrared spectra ( $4000\text{--}400\text{ cm}^{-1}$ ) were obtained with a Beckman IR-9 spectrometer modified<sup>10</sup> to accommodate an external light source and a 1-m long, gas diffusion barrier, high-temperature cell.

All attempts to generate the desired gaseous oxohalide were performed *in situ* using one or more of three different methods. These were: fusing the metal pentoxide ( $\text{M}_2\text{O}_5$ ) with the lithium halide; vaporizing the metal pentahalide ( $\text{MX}_5$ ) in an oxygen atmosphere; and heating a sample of the metal pentahalide covered with a layer of the metal pentoxide.

The compounds  $\text{Nb}_2\text{O}_5$ ,  $\text{Ta}_2\text{O}_5$ ,  $\text{NbCl}_5$ , and  $\text{TaCl}_5$  were obtained from City Chemical Corp., New York, N. Y.;  $\text{NbBr}_5$ ,  $\text{NbI}_5$ , and  $\text{TaF}_5$  from Alfa Inorganics, Inc., Beverly, Mass.;  $\text{NbF}_5$  from Chemical Procurements Laboratories, Inc., College Point, N. Y.; and  $\text{TaBr}_5$  from Research Inorganic Chemicals Corp., Sun Valley, Calif. All were used as received.

The cells were baked out at  $200\text{--}400^\circ$  under vacuum. Samples were placed in the sample holder and were transferred to the cells in a dry argon atmosphere. After observation of a background spectrum at ambient temperature, the cell was heated by means of a mullite tube furnace controlled by a Thermac proportional temperature controller (R. I. Inc., Minneapolis, Minn.). In addition to absorption spectra, emission spectra were obtained by operating the spectrometer on the internal chopper.

Crude vapor pressure information was obtained by observing changes in the spectrum as the cell was cooled and reheated. When each run was completed, the cell was evacuated and the new background spectrum was observed. Only those bands which appeared and disappeared at temperatures consistent with reported reaction temperatures and/or vapor pressure data were assigned to the  $\text{MOX}_3$  species. Additional evidence for these assignments was provided by the appearance of appropriately colored sublimates at the cold cell ends while the bands were being observed. The frequencies of transitions attributed to  $\text{MOX}_3$  species and the conditions under which they were observed are summarized in Table II.

Early attempts to observe the vapor-phase spectra of the niobium and tantalum oxohalides were complicated by the appearance of three separable systems of absorption bands whose frequencies, band contours, and tem-

peratures of appearance were independent of the sample, sample holder, and filler gas. These bands were, however, dependent on the cell material, appearing in stainless steel, nickel, and monel cells but not appearing in mullite ( $2\text{Al}_2\text{O}_3\text{--SiO}_2$ ) cells with glass ends. All three of these band systems disappeared on pumping the cell and would not reappear until the temperature of the cell had been raised above the previous maximum. In those cases where absorption bands attributed to the oxohalide of interest were observed in conjunction with these independent band systems, careful pumping eliminated the independent band systems selectively, permitting observation of a clean spectrum of the oxohalide. Further characterization of the band carriers is being undertaken.

Both  $\text{NbOCl}_3$  and  $\text{NbOBr}_3$  were readily generated in the cell by heating the pentahalide in an oxygen atmosphere or mixed with  $\text{Nb}_2\text{O}_5$ .  $\text{NbOI}_3$ , on the other hand, was prepared only by heating a sample of  $\text{NbI}_5$  covered with a layer of  $\text{Nb}_2\text{O}_5$ .

The absorption bands centered at  $450$  and  $999\text{ cm}^{-1}$  attributed to  $\text{NbOCl}_3$  began to appear at temperatures as low as  $175^\circ$  and were observed as emission bands at  $250^\circ$ . Appearance of these bands was accompanied by formation of a yellow sublimate at the ends of the cell. This sublimate probably corresponds to a mixture of  $\text{NbCl}_5$  (yellow) and  $\text{NbOCl}_3$  (white).<sup>11</sup>

The absorption band centered at  $994\text{ cm}^{-1}$  attributed to  $\text{NbOBr}_3$  began to appear at  $250^\circ$  and was observed as an emission band at  $275^\circ$ ; at  $225^\circ$  a bright yellow solid began to condense at the ends of the cell. At temperatures above  $250^\circ$  this condensate turned orange. The yellow condensate probably corresponds to sublimed  $\text{NbBr}_5$ , whereas the orange color probably results from the sublimation of orange-brown  $\text{NbOBr}_3$ .<sup>11</sup>

The absorption band centered at  $986\text{ cm}^{-1}$  attributed to  $\text{NbOI}_3$  began to appear at  $350^\circ$  and was observed as an emission band at  $550^\circ$ . Formation of  $\text{NbOI}_3$  was accompanied by decomposition of some of the reactant to molecular iodine, which masked any other sublimate which may have been formed.

All attempts to observe vapor-phase spectra of  $\text{NbOF}_3$ ,  $\text{TaOF}_3$ ,  $\text{TaOCl}_3$ ,  $\text{TaOBr}_3$ , and  $\text{TaOI}_3$  were unsuccessful. There is only meager evidence for the existence of the first two in either the vapor or the solid phase.<sup>12-14</sup> The last three have been characterized in the solid phase, and  $\text{TaOCl}_3$  has been observed

**Table II:** Observed Ir Frequencies in Absorption and Emission for  $\text{NbOX}_3$

Compd	Frequencies, <sup>a</sup> $\text{cm}^{-1}$
$\text{NbOCl}_3$	(991, 999, 1007) (P, Q, R), $\sim 450^b$
$\text{NbOBr}_3$	(988, 994, 1001) (P, Q, R)
$\text{NbOI}_3$	(980, 986, 993) (P, Q, R)

<sup>a</sup> Reproducibility of the absorption and emission frequencies  $\pm 1\text{ cm}^{-1}$ . <sup>b</sup> Possibly due to  $\text{NbCl}_5$ .

(10) S. M. Chackalackal and F. E. Stafford, *J. Amer. Chem. Soc.*, **88**, 723 (1966).

(11) F. Fairbrother, "The Chemistry of Niobium and Tantalum," Elsevier Publishing Co., New York, N. Y., 1967, Chapter 4.

(12) S. Andersson and A. Astrom, *Acta Chem. Scand.*, **19**, 2136 (1965).

(13) H. Schäfer, D. Bauer, W. Beckmann, R. Gerken, H-G. Niedervarenholz, K-J. Nieuhues, and H. Scholz, *Naturwissenschaften*, **51**, 241 (1964).

(14) K. F. Zmbov and J. L. Margrave, *J. Phys. Chem.*, **72**, 1099 (1958).

in the vapor phase, but their relative instability<sup>15</sup> made observation of their spectra impossible by our techniques.

By analogy to the phosphorus and vanadium oxotrihalides, the niobium oxotrihalides are expected to have a trigonal pyramid structure of symmetry  $C_{3v}$  in the vapor phase. Molecules of this symmetry give rise to six infrared-active fundamental vibrations. The vibration  $\nu_1$  corresponds to the metal-oxygen stretching vibration. Being of symmetry class  $a_1$ , it exhibits P, Q, and R branches. It is to this mode that we attribute the bands observed between 986 and 1000  $\text{cm}^{-1}$ .

The band at 450  $\text{cm}^{-1}$  in the spectra of the vapors in the Nb-Cl-O systems can be attributed to  $\nu_4$ , the metal-chlorine stretching vibration of  $\text{NbOCl}_3$ , or to  $\text{NbCl}_5$ , which gives rise to an absorption band at 444  $\text{cm}^{-1}$  when observed in a nitrogen matrix at 5° K.<sup>16</sup>

In Table I the known metal-oxygen stretching vibration frequencies for the phosphorus, vanadium, and niobium oxohalides and monoxides are presented. In contrast to the phosphorus case, the metal-oxygen stretching frequencies in the niobium oxotrihalides seem to be nearly independent of the halogen substituents, decreasing by only 13  $\text{cm}^{-1}$  in going from the oxotrichloride to the oxotriiodide. Substituent effects on the metal-oxygen stretching frequency become less important in going from main group to transition element oxohalides and in going from lighter to heavier central metal elements. This conclusion is supported by data in a similar investigation of gaseous group VI oxohalides.<sup>17</sup>

*Acknowledgment.* This work was supported by the U. S. Army Research Office, Durham, N. C. Dr. B. G. Ward and Miss H. V. Taylor performed some of the initial experiments.

(15) H. Schäfer and E. Sibbing, *Z. Anorg. Allgem. Chem.*, **305**, 341 (1960).

(16) R. D. Werder, R. A. Frey, and Hs. H. Gunthard, *J. Chem. Phys.*, **47**, 4159 (1967).

(17) B. G. Ward and F. E. Stafford, *Inorg. Chem.*, **7**, 2569 (1968).

## Some Comments on Cohesion

### Energies of Liquids

by Vojtech Fried and Garry B. Schneier

Department of Chemistry, Brooklyn College of the City University of New York, Brooklyn, New York 11210 (Received June 24, 1968)

The solution of many theoretical problems in chemistry requires knowledge of the cohesion energy of liquids. The energy-volume-temperature relations present an especially severe and sensitive test for a theory of liquids.

The cohesion energy as a function of volume has been studied by many investigators;<sup>1,2</sup> over a small volume range the following form is employed

$$U_C = \frac{-a}{V^n} \quad (1)$$

where  $U_C$  is the cohesion energy,  $V$  is the molar volume, and  $a$  and  $n$  are constants dependent upon the nature of the particular liquid and upon the temperature. It was shown experimentally that, for a number of liquid substances, the exponent  $n$  has a value close to unity over a limited range of temperatures.<sup>1-3</sup> For a uniformly expanded model, Benson<sup>4</sup> derived a value of  $n = 2$ , but a value of 5.3 resulted in better agreement with experiment. For perfect liquids and hydrocarbons in the normal liquid range, Scott<sup>5</sup> found a value for  $n$  equal to about 1.5 for nonisothermal conditions (along the vapor-liquid equilibrium curve).

In this connection, we present our recently found results for normal aliphatic hydrocarbons ( $C_4$ - $C_{15}$ ) and for carbon tetrachloride, tetrachloroethylene, benzene, thiophene, and pyridine. As is evident from Figure 1 (curve a), the change of the cohesion energy of hexane with temperature is more pronounced at temperatures near the melting point. This can be partially explained in terms of the more "solidlike" structure of liquids at these temperatures. A similar curve was obtained for the exponent  $n$  as a function of temperature (Figure 1, curve b), with the only exception that  $n$  reaches a constant value in a certain temperature range ( $T_r =$

**Table I:** Cohesion Energies Calculated from Experimental Data and from the Group Contributions

Sub- stance	$-10^{-4}U_C, \text{ J mol}^{-1}$				$\omega^b$
	$T_r = 0.6$		$T_r = 0.7$		
	Exptl <sup>a</sup>	Calcd	Exptl <sup>a</sup>	Calcd	
$C_4$	2.137	2.190	1.927	1.998	0.201
$C_5$	2.522	2.534	2.255	2.288	0.252
$C_6$	2.881	2.878	2.571	2.579	0.298
$C_7$	3.241	3.222	2.885	2.869	0.352
$C_8$	3.592	3.566	3.192	3.160	0.395
$C_9$	3.941	3.909	3.486	3.450	0.440
$C_{10}$	4.283	4.253	3.772	3.741	0.479
$C_{11}$	4.613	4.597	4.058	4.031	0.521
$C_{12}$	4.953	4.941	4.338	4.322	0.560
$C_{13}$	5.289	5.285	4.617	4.612	0.602
$C_{14}$	5.617	5.629	4.881	4.903	0.641
$C_{15}$	5.955	5.973	5.153	5.193	0.680

<sup>a</sup> The uncertainty is  $\pm 2$  in the last figure. <sup>b</sup> Pitzer's acentric factor.

(1) J. H. Hildebrand and R. L. Scott, "The Solubility of Nonelectrolytes," Reinhold Publishing Corp., New York, N. Y., 1950, p 97.

(2) J. H. Hildebrand and R. L. Scott, "Regular Solutions," Prentice-Hall, Inc., Englewood Cliffs, N. J., 1962, p 76.

(3) H. Benninga and R. L. Scott, *J. Chem. Phys.*, **23**, 1911 (1955).

(4) S. W. Benson, *ibid.*, **15**, 367 (1947).

(5) R. L. Scott, unpublished data, cited in ref 1, p 101.



**Table II:** Vapor Pressure and Molar Volume of the Liquid Substances as Functions of Temperature

Substance	Antoine eq			$V = a + bt + ct^2$		
	A	-B	C	a	b	10 <sup>c</sup>
C <sub>4</sub>	6.83209	946.90	240.0	96.75	0.1696	3.707
C <sub>5</sub>	6.85221	1064.63	232.0	111.79	0.1639	2.946
C <sub>6</sub>	6.87776	1171.530	224.37	127.19	0.1670	4.282
C <sub>7</sub>	6.90240	1268.115	216.900	143.01	0.1620	4.714
C <sub>8</sub>	6.92377	1355.126	209.517	158.83	0.1721	3.855
C <sub>9</sub>	6.93520	1428.817	201.621	175.67	0.1536	5.249
C <sub>10</sub>	6.95367	1501.268	194.480	192.25	0.1531	5.377
C <sub>11</sub>	6.97674	1572.477	188.022	210.59	0.1224	6.898
C <sub>12</sub>	6.98059	1625.928	180.311	229.21	0.0954	8.031
C <sub>13</sub>	6.98870	1677.43	172.90	250.24	0.0455	9.657
C <sub>14</sub>	6.9957	1725.46	165.75	269.30	0.0318	9.952
C <sub>15</sub>	7.0017	1768.82	158.60	287.14	0.0314	9.943
CCl <sub>4</sub>	6.88853	1217.165	227.00	94.25	0.1084	1.975
C <sub>2</sub> Cl <sub>4</sub>	7.21511	1531.460	232.379	100.28	0.0951	1.384
Benzene	6.89745	1206.350	220.237	86.59	0.1067	1.097
Thiophene	6.95926	1246.038	221.354	77.13	0.0942	...
Pyridine	6.90374	1293.969	206.321	78.61	0.0904	...

0.6–0.7). Similar behavior has been observed for all the other aforementioned substances. This constant value of  $n$ , for each hydrocarbon, is plotted against the number of carbons in the molecule,  $n_C$ , in Figure 2 (curve *a*). The average value of  $n$ , for all the hydrocarbons, is  $1.42 \pm 0.04$ , which is very close to the value given by Scott.<sup>5</sup> The small fluctuations result probably from the inaccuracy of the experimental data. Although the acentric force field changes with  $n_C$  in the hydrocarbon series (as is evident from Table I, where Pitzer's acentric factors are given), the value of  $n$  is not affected by it. The values of the exponent  $n$  for carbon tetrachloride, tetrachloroethylene, benzene, thiophene, and pyridine, under the same conditions, are the following: 1.38, 1.40, 1.53, 1.63, and 1.89, respectively. As is evident from Figure 2 (curve *b*), the value of the constant  $a$  increases with  $n_C$ . The constant  $a$  depends on temperature very strongly; nevertheless, in the limited temperature range ( $T_r = 0.6$ – $0.7$ ) the change is less than  $\pm 3\%$ . This is a very important fact, because as a consequence of it the radial distribution function might also be considered as temperature independent in the given temperature interval (so far considered acceptable only for a very simple potential model). Values of  $a$  and  $n$  for eq 1 were obtained by solving two simultaneous equations over a small increment of temperature. Over this temperature interval,  $a$  and  $n$  were assumed to be constant. This process was repeated throughout the entire liquid range and it was found that from  $T_r = 0.6$  to  $0.7$ ,  $a$  and  $n$  were only slightly temperature dependent. Finally in Figure 3 the exponent  $n$  is plotted as a function of the dipole moment. For the substances studied,  $n$  increases with the polarity of the liquids. The rate of increase is, however, not uniform, and  $n$  seems to approach a constant value at higher dipole moments.

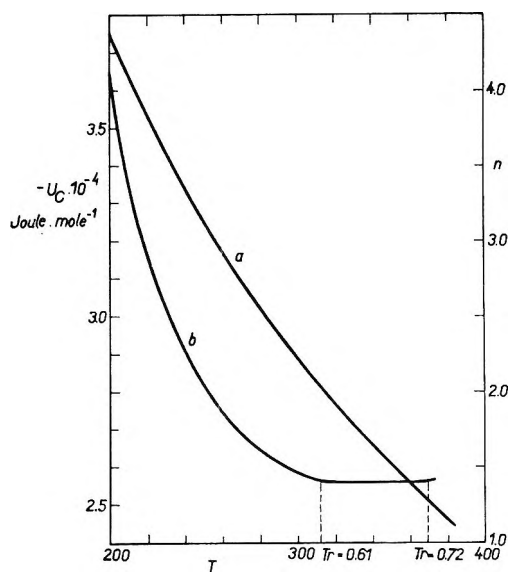


Figure 1. (a) The cohesion energy of hexane as a function of the temperature; (b) the exponent  $n$  of hexane as a function of the temperature.

The cohesion energy at pressures approaching zero was calculated from the relation

$$\begin{aligned}
 -U_C &= \Delta U_{\text{vap}} + \Delta U^* \\
 &= [RT - P^0(V_1 - B)] \times \\
 &\quad \left[ T \frac{d \ln P^0}{dT} - 1 \right] + P^0 T \frac{dB}{dT} \quad (2)
 \end{aligned}$$

where  $P^0$  is the saturated vapor pressure at temperature  $T$ ,  $V_1$  is the molar volume of the liquid substance, and  $B$  is the second virial coefficient.  $\Delta U_{\text{vap}}$  represents the change of the internal energy associated with the vaporization of 1 mol of a liquid at a constant tem-

perature and a pressure equal to the saturated vapor pressure at this temperature.  $\Delta U^*$  denotes the change of the internal energy associated with the change of the pressure from its saturated value to a pressure approaching zero. Pola'k,<sup>6</sup> in his basic work on cohesion energies, found that for a great number of liquids the value of  $\Delta U^*$  represents about 0.8–1.2% of the total value of the cohesion energy at the normal boiling point.

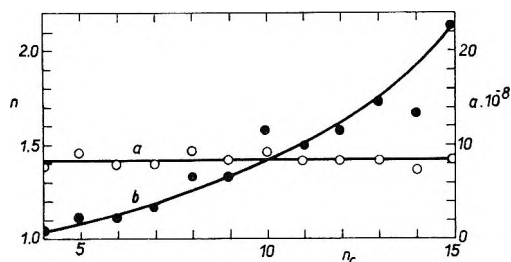


Figure 2. (a) The exponent  $n$  as a function of the number of carbons,  $n_c$ , in the molecule; (b) the constant  $a$  as a function of the number of carbons,  $n_c$ , in the molecule.

The experimental data necessary to calculate the cohesion energies (*i.e.*, saturated vapor pressures and molar volumes of the liquids as functions of temperature), except those for carbon tetrachloride, tetrachloroethylene, *n*-nonane, and pyridine, have been taken from the literature.<sup>7–11</sup> All the data are summarized in Table II. The virial coefficient was calculated from Pitzer's equation.<sup>12</sup>

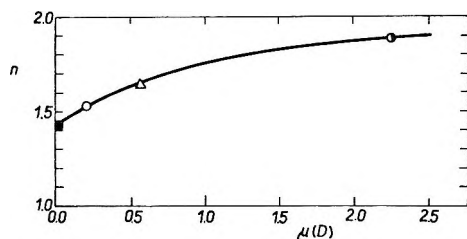


Figure 3. The exponent  $n$  as a function of the dipole moment: ●, hydrocarbons, carbon tetrachloride, tetrachloroethylene; ○, benzene; △, thiophene; ◐, pyridine.

The values of the cohesion energies calculated from eq 2 are accurate enough, as has been proved by comparing the experimental (calorimetric) data on heat of vaporization with the values calculated from the modified eq 2. It was found that the difference is less than 0.15% in the normal liquid range.

The vapor pressure and molar volumes of carbon tetrachloride, tetrachloroethylene, *n*-nonane, and pyridine have been measured in our laboratory.

Fisher spectroanalyzed substances were purified by the usual methods until their physical constants were in agreement with the literature values.<sup>7–10</sup> The vapor pressure was measured by a dynamic method in which two ebulliometers were connected in parallel in the measuring systems. One of the ebulliometers contained water and the other the substance to be measured. From the boiling point of water, the corresponding vapor pressure of the substance was found. Single-stem pycnometers of about 10-ml capacity were used for density measurement. The data are reported in Table II.

As is well known, the increment of the cohesion energy per  $\text{CH}_2$  group inserted is not constant for the paraffin series at constant temperature. Some of the conditions under which the  $\text{CH}_2$  increment might be expected to be constant are discussed by Meyer and Wagner.<sup>13</sup>

From the values of the cohesion energies obtained, the  $\text{CH}_2$ ,  $\text{CH}_3$ ,  $\text{CH}$ , and  $\text{C-C}$  increments of the cohesion energy were calculated at two reduced temperatures ( $T_r = 0.6$  and  $0.7$ ). The cohesion energy, calculated from the average values of these increments, is in a very good agreement with the cohesion energy calculated from the experimental data, as is evident from Table I. The following values (Joules per mole) have been found for the different group contributions to the cohesion energy:  $T_r = 0.6$ ;  $U_C = 2(U_C)_{\text{CH}_3} + (n_c - 2)(U_C)_{\text{CH}_2} = -15020 - 3439(n_c - 2)$ ;  $U_C = (n_c - 1)(U_C)_{\text{C-C}} + (2n_c + 2)(U_C)_{\text{CH}} = 2353(n_c - 1) - 2896(2n_c + 2)$ ;  $T_r = 0.7$ ;  $U_C = 2(U_C)_{\text{CH}_3} + (n_c - 2)(U_C)_{\text{CH}_2} = -14166 - 2905(n_c - 2)$ ;  $U_C = (n_c - 1)(U_C)_{\text{C-C}} + (2n_c + 2)(U_C)_{\text{CH}} = 2725(n_c - 1) - 2815(2n_c + 2)$ .

The observations reported in this note on cohesion energies of liquids may be helpful in the development of theories of liquids and liquid solutions (especially theories based on the radial distribution function).

(6) J. Pola'k, *Collect. Czech. Chem. Commun.*, **31**, 1483 (1966).

(7) J. Timmermans, "Physico-Chemical Constants of Pure Organic Compounds," Elsevier Publishing Co., Amsterdam, The Netherlands, 1950.

(8) "Selected Values of Properties of Hydrocarbons and Related Compounds," American Petroleum Institute Research Project 44, Carnegie Press, Pittsburgh, Pa., 1953.

(9) R. R. Dreisbach, "Physical Properties of Chemical Compounds," *Advances in Chemistry Series*, No. 15, 22, and 29, American Chemical Society, Washington, D. C., 1955, 1959, 1961.

(10) T. E. Jordan, "Vapor Pressure of Organic Compounds," Interscience Publishers, New York, N. Y., 1954.

(11) G. Waddington, J. W. Knowlton, D. W. Scott, G. D. Oliver, S. S. Todd, W. N. Hubbard, J. C. Smith, and H. M. Huffman, *J. Amer. Chem. Soc.*, **71**, 797 (1949).

(12) K. S. Pitzer and R. F. Curl, *ibid.*, **79**, 2369 (1957).

(13) E. F. Meyer and R. E. Wagner, *J. Phys. Chem.*, **70**, 3162 (1966).

## Acidic Sites on Mordenite. An Infrared Study of Adsorbed Pyridine

by F. R. Cannings

The British Petroleum Company, Limited,  
British Petroleum Research Centre,  
Sunbury-on-Thames, Middlesex, England  
(Received June 24, 1968)

Parry<sup>1</sup> and Basila, *et al.*,<sup>2</sup> have used pyridine to elucidate acid-site structures on the surfaces of alumina and silica-alumina. In particular, they were able to differentiate between adsorption centers that were either Brønsted or Lewis acid in character. The relevant information was obtained from the 1700–1440-cm<sup>-1</sup> range of the infrared spectrum and arises from variations in the position of one of the “in-ring” vibrations of the chemisorbed pyridine, indicating the presence of either pyridinium ions or coordinately bound pyridine.

We have extended this work to an examination of the surface of mordenite. The changes in the spectrum of adsorbed pyridine and acid-site numbers after evacuation of the sample at temperatures up to 600° are consistent with the scheme proposed by Hall and co-workers<sup>3</sup> to account for the formation of defect sites on decationated zeolites.

Sodium mordenite was obtained from the Norton Co., Worcester, Mass. It was leached with dilute sulfuric acid to give an aluminum content of 5.05 wt %, a sodium content of 0.94 wt %, and a BET surface area of 385 m<sup>2</sup>/g. A 13-mm diameter disk weighing 6.5 mg/cm<sup>2</sup> was formed at 10 tons/cm<sup>2</sup> and was examined in a Grubb-Parsons GS2 infrared spectrometer, using ancillary equipment and techniques already reported.<sup>4</sup> The successive treatments of the disk are described in Table I, and absorbances, calculated from maximum band heights, are quoted therein. All spectra were run at 25°.

### Results and Discussion

The spectrum of pyridine retained by mordenite after evacuation at 500° is shown in Figure 1. Bands at 1623, 1496, and 1455 cm<sup>-1</sup> are typical of pyridine coordinated to a Lewis acid site (Lpy). The additional feature to note in the spectrum is the peak at 1462 cm<sup>-1</sup>. The appearance of a band at this wave number can be interpreted as arising from a second distinct type of Lewis acid site, of greater coordinating power than that characterized by the band at 1455 cm<sup>-1</sup>. This conforms with the regular transition in wave number value for the 19b vibration of pyridine adsorbed in a progressively stronger manner, commencing with physisorbed pyridine (1440 cm<sup>-1</sup>), to H-bonded pyridine (1446 cm<sup>-1</sup>), to coordinated pyridine (1455 cm<sup>-1</sup>). The strength of attachment of the pyridine to the surface is

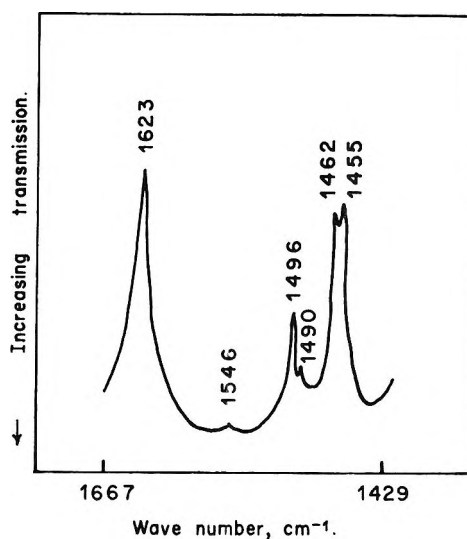


Figure 1. Spectrum of pyridine adsorbed on mordenite after pyridine dosing at 25° and evacuating at 500° (see Table I).

indicated by the relative ease of removal upon evacuation and calcination.

The generation of the 1462-cm<sup>-1</sup> band occurred with mordenite after evacuation above 300°. In Figure 1, the separation into two definite absorption bands is clear, and approximately equal numbers of the two forms of Lpy are detected (given equal extinction coefficients).

An assessment of the numbers of acid sites present on the specimen after calcination up to a temperature of 600° was also undertaken. This was possible with a knowledge of the relative extinction coefficients of bands at 1546 and 1455 cm<sup>-1</sup>, typical of Brønsted and Lewis species, respectively. A satisfactory conversion factor for calculating numbers on one arbitrary scale, namely, Lpy, was obtained in a previous investigation.<sup>5</sup> The use of the band at 1490 cm<sup>-1</sup>, as outlined by Basila and Kantner,<sup>6</sup> is not suitable, as only Brønsted pyridine (Bpy) produces a band at this wave number. The corresponding vibration for Lewis pyridine occurs at 1496 cm<sup>-1</sup>. (Refer to Figure 1.)

Table I lists the absorbances of the 1546-, 1462-, and 1455-cm<sup>-1</sup> bands, calculated on the Lpy scale, and these values are taken to be equal to the relative number of acid sites of each type present on the disk. It shows, for example, that after calcination at 500° and

- (1) E. P. Parry, *J. Catal.*, **2**, 371 (1963).
- (2) M. R. Basila, T. R. Kantner, and K. H. Rhee, *J. Phys. Chem.*, **68**, 3197 (1964).
- (3) J. B. Uytterhoeven, L. G. Christner, and W. K. Hall, *ibid.*, **69**, 2117 (1965).
- (4) F. R. Cannings, *J. Phys. Chem.*, **72**, 1072 (1968).
- (5) When pyridine adsorbed on a silica-alumina was contacted with water vapor, a complete interconversion of Lewis to Brønsted acid sites was observed. From the respective absorbances of the 1455- and 1546-cm<sup>-1</sup> bands, a conversion factor of 2.61 was observed. More details will be given in a future publication.
- (6) M. R. Basila and T. R. Kantner, *J. Phys. Chem.*, **70**, 1681 (1966).

**Table I:** Absorbances of Pyridine Retained by Mordenite after a 1-Hr Evacuation at the Quoted Temperature<sup>a,b</sup>

Temp of evacuation, °C	Absorbance				Total absorbance omitting the 1462-cm <sup>-1</sup> band	Total absorbance including twice the absorbance of the 1462-cm <sup>-1</sup> band
	—1546 cm <sup>-1</sup> — (Bpy)	1462 cm <sup>-1</sup>	—1455 cm <sup>-1</sup> — (Lpy)			
25 <sup>c</sup>	0.76		0.05		0.81	0.81
200		0.67		0.11	0.78	0.78
25 <sup>d</sup>	0.80		0.04		0.84	0.84
300		0.53	sh	0.13	0.66	0.66
25 <sup>d</sup>	0.82		0.02		0.84	0.84
400		0.28	~0.15	0.20	0.48	0.78
25 <sup>d</sup>	0.67		0.03		0.70	0.70
25 <sup>e</sup>	0.80		0.03		0.83	0.83
500		0.01	0.20	0.22	0.23	0.63
25 <sup>d</sup>	0.45		0.03		0.48	0.48
25 <sup>f</sup>	0.54		0.04		0.58	0.58
25 <sup>e</sup>	0.63		0.03		0.66	0.66
25 <sup>e</sup>	0.57		0.05		0.62	0.62
600		Nil	0.09	0.12	0.12	0.30
25 <sup>d</sup>	0.09		0.03		0.12	0.12
25 <sup>e</sup>	0.26		0.04		0.30	0.30

<sup>a</sup> The values were obtained after successive treatments of the disk. <sup>b</sup> Brønsted pyridine at 1546 cm<sup>-1</sup> and Lewis pyridine at 1455 cm<sup>-1</sup> are calculated on the same scale. <sup>c</sup> The sample after pyridine and water vapor dosing (each at *ca.* 3 torr) for 72 hr and then evacuation. <sup>d</sup> The sample after pyridine and water vapor dosing (each at *ca.* 3 torr) for 5 min and then evacuation. <sup>e</sup> The sample after pyridine and water vapor dosing (each at *ca.* 3 torr) for 16 hr and then evacuation. <sup>f</sup> The sample after pyridine and water vapor dosing (each at *ca.* 3 torr) for 1 hr and then evacuation.

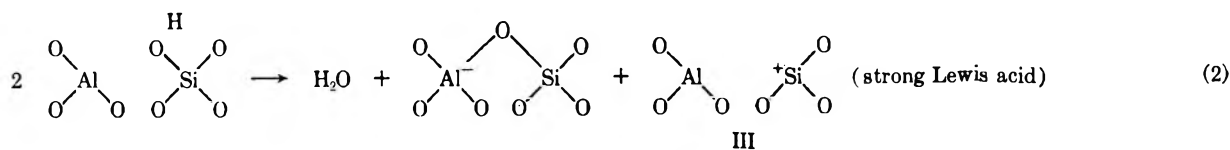
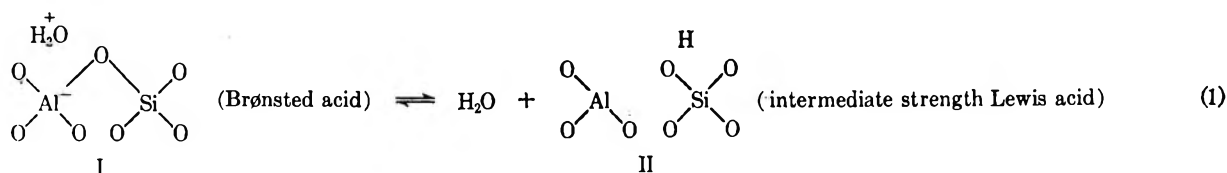
subsequent equilibration with pyridine and water vapor at 25°, mordenite has lost some 25% of the total number of acid sites present at lower temperatures. So a system exists where the total number of intermediate strength Lewis acid plus Brønsted acid sites decreases while some very strong Lewis sites have been formed during the preceding calcination. The number of the latter produced appears less than the quantity of the former lost.

The chemical reaction proposed by Hall and coworkers<sup>3</sup> to explain their observations of changes in calcined X and Y zeolites can also account for the transformations we have noted. The assumption must be made that some sites having structure II (eq 1) behave as intermediate strength Lewis acids and that they retain their identity upon adsorbing pyridine, producing a band at 1455 cm<sup>-1</sup>. Reduction in over-all acid site numbers occurs on disproportionation along the path outlined by eq 2.

Structure III represents a strong Lewis acid and one site only is produced from two of intermediate strength. The apparent loss of acid sites upon calcination could be accounted for in this way.

The close agreement between calculated acid site population after high-temperature evacuation, when this total includes twice the absorbance of the 1462-cm<sup>-1</sup> band (final column of Table I) and the number detected on subsequent equilibration with pyridine and water vapor at 25° supports this mechanism. The reason for the large decrease in acidity upon calcination at 600° is not known, but it may indicate major structural changes.

The mechanism of the reverse reaction for eq 2 is not fully understood. From our work, it appears likely that the change is slow and that the initial product of combination of structure III with excess water is a single Brønsted site. The increase of total acidity of mordenite from 0.48 unit after 5 min to 0.62 unit after



72 hr of contact with pyridine and water vapor following evacuation at 500° may be a function of this slow site rearrangement. Total acidity alters little after 16 hr of dosing, and the value obtained after this time is regarded as a correct final measure.

*Acknowledgment.* Permission to publish this paper has been given by The British Petroleum Co., Ltd.

### An Apparatus for Degassing Liquids by Vacuum Sublimation

by T. N. Bell, E. L. Cussler, K. R. Harris, C. N. Pepela, and Peter J. Dunlop<sup>1</sup>

*Department of Physical and Inorganic Chemistry, University of Adelaide, Adelaide, South Australia 5001 (Received June 28, 1968)*

The precision of vapor pressure and virial coefficient measurements depends in part upon the efficiency with which the liquid systems are degassed. Most methods described in the literature are repetitive and consequently often tedious and time consuming. A common procedure<sup>2</sup> is that of freezing the liquid, pumping away the noncondensable gases, melting, and refreezing, the process being continued until some experimental parameter is constant. Experience in this laboratory has shown that up to 20 such cycles are necessary with aqueous systems.<sup>3</sup> Hermsen and Prausnitz<sup>4</sup> have described a method whereby their materials were "refluxed for several days... at low pressure," and Cruickshank and Cutler<sup>5</sup> described another involving "several vacuum redistillations."

The method reported in this paper is similar to the technique of "freeze drying,"<sup>6</sup> and usually one cycle is sufficient to completely degas aqueous systems and pure hydrocarbons. The apparatus (see Figure 1) consists of a Pyrex glass dewar, the vacuum chamber being the vapor pressure cell. The material to be degassed is frozen, either in the cell itself or in the detachable sampling bulb. (This is also used to sample mixtures for analysis at the end of a run without breaking the vacuum in the system.) The cell is then evacuated and a suitable freezing mixture is placed in the central compartment of the dewar. The frozen liquid slowly sublimates onto the cold glass surface, while noncondensable gases are continuously pumped away (less than 5% of the sample is lost in this process). These gases do not seem to redissolve unless the sublimate thaws. This was found to occur with *n*-heptane and its mixtures with benzene when the deposit was thick; in these cases anomalous vapor pressure measurements were noted with only one degassing (up to 0.2 torr too high). The effect was prevented in the case of *n*-

heptane by keeping the distilling liquid at about 0°, but in addition it was found necessary to degas the mixtures two or three times to obtain reproducible results. The hydrocarbons were always degassed in the presence of sodium wire.

The results of static measurements of the vapor pressures of water, benzene, *n*-hexane, *n*-heptane, *n*-octane, and cyclohexane samples degassed in this manner are given in Table I, together with literature values.

**Table I:** Vapor Pressures at 25° of Several Hydrocarbons and Water

	Vapor pressure, torr		Ref
	This work	Lit.	
Benzene	95.15 ± 0.03	95.18 ± 0.04	<i>b</i>
		95.15 ± 0.05	<i>c</i>
		95.17	<i>d</i>
		95.04 ± 0.08	<i>e</i>
		95.03 ± 0.04	<i>f</i>
Cyclohexane	97.59 ± 0.03	95.14 ± 0.03	<i>g</i>
		97.58 ± 0.04	<i>b</i>
		97.81 ± 0.04	<i>h</i>
<i>n</i> -Hexane	151.16 ± 0.02	97.41 ± 0.03	<i>f</i>
		151.26 ± 0.04	<i>b</i>
		151.05 <sup>a</sup>	<i>i</i>
<i>n</i> -Heptane	45.79 ± 0.02	45.72 ± 0.04	<i>b</i>
		45.64 <sup>a</sup>	<i>i</i>
<i>n</i> -Octane	13.97 ± 0.02	13.98 <sup>a</sup>	<i>b</i>
Water	23.755 ± 0.003	23.753	<i>j</i>

<sup>a</sup> Extrapolated using the Antoine equation. <sup>b</sup> C. B. Willingham, W. J. Taylor, J. N. Pignocco, and F. D. Rossini, *J. Res. Nat. Bur. Stand.*, **35**, 219 (1945); F. D. Rossini, K. S. Pitzer, R. L. Arnett, and G. C. Pimental, "Selected Values of Physical and Thermodynamic Properties of Hydrocarbons," Carnegie Press, Pittsburgh, Pa., 1953. <sup>c</sup> Reference 4. <sup>d</sup> R. H. Stokes, Department of Physical and Inorganic Chemistry, University of New England, Armidale, New South Wales, private communication. <sup>e</sup> Reference 2b. <sup>f</sup> D. H. Everett and F. L. Swinton, *Trans. Faraday Soc.*, **59**, 2476 (1963). <sup>g</sup> W. J. Gaw and F. L. Swinton, *ibid.*, **64**, 637 (1968). <sup>h</sup> Reference 5. <sup>i</sup> I. Brown, *Aust. J. Sci. Res.*, **A5**, 530 (1952). <sup>j</sup> F. G. Keyes, *J. Chem. Phys.*, **15**, 602 (1947).

Samples which were degassed more than the minimum number of times stated above gave identical results within the experimental error. A sample of 40 ml of liquid takes from 1 to 2 hr to be degassed. The alkanes were allowed to melt in the sampling cell during the process, but, as mentioned above, it was only

(1) To whom all correspondence should be addressed.

(2) *E.g.*, (a) J. B. Gilmour, J. O. Zwicker, J. Katz, and R. L. Scott, *J. Phys. Chem.*, **71**, 3259 (1967); (b) G. Kortüm and W. Vogel, *Z. Elektrochem.*, **62**, 40 (1958).

(3) H. D. Ellerton, Ph.D. Thesis, University of Adelaide, 1966.

(4) R. W. Hermsen and J. M. Prausnitz, *Chem. Eng. Sci.*, **18**, 485 (1963).

(5) A. J. B. Cruickshank and A. J. B. Cutler, *J. Chem. Eng. Data*, **12**, 326 (1967).

(6) M. Dixon and E. C. Webb, "Enzymes," Longmans, Green and Co., Ltd., London, 1958, p 13.

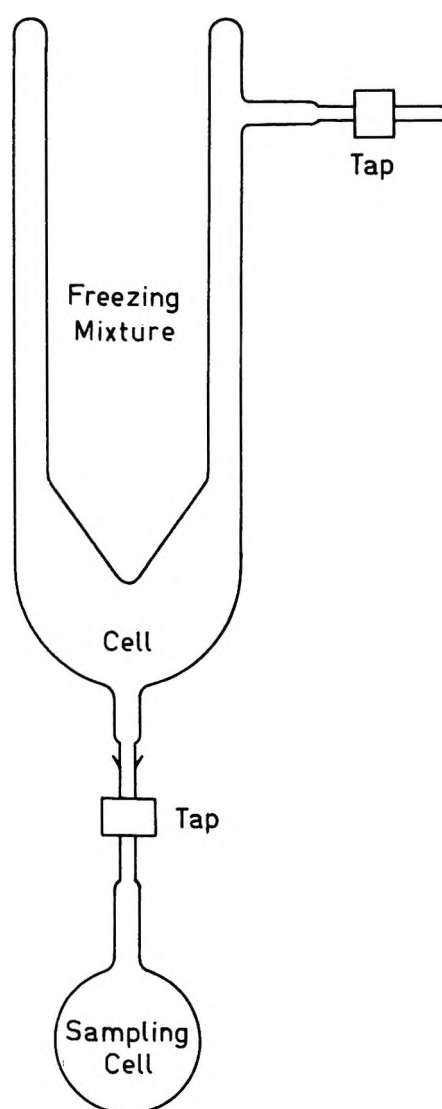


Figure 1. Diagram of the cell used for degassing organic liquids and solutions. The cell used for aqueous systems (*e.g.*, a sodium chloride solution) did not have the bottom tap and sampling cell.

necessary to slow the rate of distillation of *n*-heptane. The sublimation of water and benzene was accelerated by warming the containing vessel. All measurements were made at  $25.000 \pm 0.002^\circ$ . The method has also been used to degas aqueous solutions<sup>7</sup> containing non-volatile solutes, *e.g.*, sodium chloride, and to provide degassed liquid samples for second virial coefficient measurements.<sup>8</sup>

### Experimental Section

**Materials.** The hydrocarbons, with the exception of *n*-octane, were obtained from the Ajax Chemical Co., Ltd., Auburn, New South Wales. The *n*-octane was supplied by the Aldrich Chemical Co., Inc., Milwaukee, Wis. Benzene and cyclohexane were purified by treatment with concentrated sulfuric acid, followed by washing with water, bicarbonate solution,

and again with water. The dried product was distilled through a dry, 1-m column with an evacuated jacket. The column was packed with stainless steel helices approximately  $4 \times 4$  mm and was fitted with a reflux head. That fraction which showed negligible impurity on analysis by gas phase chromatography was collected and stored over sodium wire. The alkanes were similarly treated using chlorosulfonic acid<sup>9</sup> as the sulfonating agent. The densities of the pure hydrocarbons together with literature values are given in Table II. These were measured, at  $25.000 \pm 0.002^\circ$ , in triplicate, in single-stem pycnometers with volumes of approximately  $30 \text{ cm}^3$ . The precision of these density measurements is believed to be  $\pm 10^{-5} \text{ g cm}^{-3}$ .

Table II: Density Data at  $25^\circ$  for Several Hydrocarbons

	Density, $\text{g cm}^{-3}$		
	This work	Lit. <sup>9</sup>	Mol % impurity
Benzene	0.87368	0.87368	<0.001
Cyclohexane	0.77389	0.77389	<0.005
<i>n</i> -Hexane	0.65479	0.65479	<0.001
<i>n</i> -Heptane	0.67949	0.67949	<0.001
<i>n</i> -Octane	0.69854	0.69846	<0.005

Deionized rain water was distilled once to give a product which had a conductance of less than  $10^{-6} \text{ ohm}^{-1} \text{ cm}^{-1}$ . There was no noticeable difference between the vapor pressure of a freshly distilled sample and that of one which had been allowed to stand in air. However, it was observed that the latter sublimed more rapidly. Only one cycle was required to degas each sample.

**Vapor Pressure Measurements.** An Edwards' Speedivac, two-stage, oil diffusion pump and an Edwards' Model E02 Speedivac vapor diffusion pump were mounted in series to evacuate the system. The latter pump was separated with a 2-in. viton O ring, butterfly valve from a 316 stainless steel, internally polished manifold in which Pirani and ionization gauge heads were mounted. A similar 1-in. valve separated the manifold from a vapor trap. The cell and the manometer could be isolated from one another and from the vapor trap by Nupro brass or stainless steel bellows valves.<sup>10</sup> The valves were connected to the glass sections of the apparatus by means of Swagelok fittings<sup>11</sup> with Teflon ferrules and Kovar metal-glass seals. A pressure of  $10^{-6}$  torr was maintained in the manifold, and the leak rate in the cell, when isolated from the pump, was less than  $10^{-3}$  torr/hr.

(7) This work will be reported in a future publication.

(8) M. L. Martin and P. J. Dunlop, submitted for publication.

(9) A. F. Shepard, A. L. Henne, and T. Midgely, Jr., *J. Amer. Chem. Soc.*, **53**, 1948 (1931).

(10) Obtainable from Nupro Co., Cleveland, Ohio 44110.

(11) Obtainable from Crawford Fittings, Niagara Falls, Ontario.

Quadruply distilled mercury was used as a manometer fluid for the hydrocarbon measurements, and either Apiezon B oil ( $d^{25} 0.86993 \pm 10^{-5} \text{ g cm}^{-3}$ ) or Dow Corning, silicone 704 oil ( $d^{25} 1.06201 \pm 10^{-5} \text{ g cm}^{-3}$ ) was used for those with water. The oils were continuously stirred and degassed in a bulb fitted to the side of the manometer. After the sample and manometer had been degassed, the system was isolated from the pumps and placed in a large thermostat which had a glass window as one side. The menisci were separately illuminated by two fluorescent lamps fitted with shields and slits 1 cm in width. Reflected light effects were minimized by fitting the mercury manometer with similar slits. The distances between the menisci were measured with respect to a calibrated invar scale<sup>12</sup> situated in the plane of the manometer arms. To take readings a Gaertner telescope with a very small depth of focus was mounted on a cathetometer stand. Distances between the scale marks and the menisci were measured by means of a micrometer screw gauge attached to the telescope. The apparatus frame to which the invar scale was attached was kinematically suspended<sup>13</sup> in the water bath and thus it was possible to adjust the scale to a vertical position by means of a sensitive level. The telescope was set in a horizontal position using the artificial horizon produced by the two menisci in the manometer. The measured pressures were corrected to standard conditions.<sup>14</sup>

A freezing mixture of Dry Ice and ethanol was used for measurements with benzene and with aqueous solutions, and liquid nitrogen was used for all other compounds. It was found that with a liquid nitrogen freezing mixture it was impossible to degas water with a single sublimation.

*Acknowledgment.* This project was supported by the Australian Research Grants Committee. C. N. P. is grateful to the Commonwealth Scholarship and Fellowship Plan for an award, during the tenure of which this work was done.

(12) Calibrated by the Metrology Section, South Australian Railways, Islington.

(13) J. Strong, "Procedures in Experimental Physics," Prentice Hall, Inc., Englewood Cliffs, N. J., 1938, p 585.

(14) G. K. Burgess, *J. Res. Nat. Bur. Stand.*, **1**, 635 (1928).

## Phase Separation in the Palladium-Hydrogen System

by Y. Ebisuzaki and M. O'Keeffe

Department of Chemistry, Arizona State University,  
Tempe, Arizona 85281 (Received July 1, 1968)

Phase equilibria in metal-hydrogen systems are very frequently described in terms of the model originally

proposed by Lacher<sup>1</sup> and its subsequent refinements.<sup>2,3</sup> The essential feature of this theory is that it is postulated that there are short-range (strictly nearest neighbor) attractive interactions between dissolved hydrogens. The heat of solution of  $x$  g-atom of hydrogen/mol of metal is then written

$$\Delta H = Ax + Bx^2 + \text{constant} \quad (1)$$

where  $A$  and  $B$  are constants.  $2B/z$  is the energy of interaction per pair of hydrogens, where, in turn,  $z$  is the number of nearest neighbor positions of a given hydrogen.

In its simplest form, the theory now assumes an ideal entropy of mixing. It is then predicted that two solid phases of different compositions can coexist below a critical temperature,  $T_c = B/2R$ , where  $R$  is the gas constant. If the critical temperature and composition are used as adjustable parameters, it is possible to describe adequately the composition of the hydride as a function of temperature and hydrogen pressure. However, as discussed below, there are physical reasons for rejecting this model of hydrogen in metals. It is our purpose here to outline an alternative approach to the description of such systems.

### Hydrogen in Metals

There are several features of hydrogen in metals that bear examination.

(a) There is good evidence<sup>4</sup> that hydrogen dissolves in transition metals as a proton, with the proton charge strongly screened by the conduction electrons of the metal. In a first approximation, the screened potential of the proton at a distance  $r$  may be taken to be the form<sup>4,5</sup>

$$V(r) = (q/r) \exp(-\lambda r) \quad (2)$$

where  $q$  is the proton charge, and the screening parameter,  $\lambda$ , is given by

$$\lambda = (4\pi q^2 N)^{1/2} \quad (3)$$

where  $N$  is the density of electronic states at the Fermi energy. The interaction energy between two protons a distance  $\Delta r$  apart will then be<sup>5</sup>

$$\Delta E = (q^2/\Delta r) \exp(-\lambda \Delta r) \quad (4)$$

For hydrogen in a metal such as palladium, one calculates, according to eq 3 and 4, that  $\Delta E < 1 \text{ cal mol}^{-1}$ ; this is several orders of magnitude smaller than the value of  $2B/z$  necessary to explain the observed behavior of the palladium-hydrogen system. More im-

(1) J. R. Lacher, *Proc. Roy. Soc.*, **A161**, 525 (1937).

(2) G. G. Libowitz, "The Solid State Chemistry of Binary Metal Hydrides," W. A. Benjamin, Inc., New York, N. Y., 1965.

(3) F. A. Lewis, "The Palladium-Hydrogen System," Academic Press, New York, N. Y., 1967.

(4) Y. Ebisuzaki and M. O'Keeffe, *Progr. Solid State Chem.*, **4**, 187 (1967).

(5) J. M. Ziman, *Advan. Phys.*, **13**, 89 (1964).

portantly,  $\Delta E$  has the wrong sign, that is to say, that eq 4 predicts that neighboring hydrogens will naturally repel each other.

These conclusions remain generally valid even when a more sophisticated form of the screened potential, such as discussed by Blandin and Déplanté,<sup>6</sup> is used in place of eq 2.

(b) A second point is that the heat of solution of hydrogen in a metal or alloy depends strongly on the density of states at the Fermi energy,<sup>4,7</sup> a quantity that will, in turn, vary with the valence electron:atom ratio of the alloy. Solution of hydrogen in palladium contributes one electron per hydrogen to the d band of the metal with a consequent change in the Fermi energy density of states, in a way strictly analogous to the effect of allowing palladium with silver. It is anticipated, therefore, that the heat of solution of hydrogen in palladium will be strongly composition dependent.

### The Palladium-Hydrogen System

The two observations made above lead to the following considerations with respect to the palladium-hydrogen and related systems.

(a) As the energy of interaction between two hydrogens is expected to be much less than  $RT$  (at or above room temperature), the configuration entropy of the solution is expected to be close to the ideal-solution value.

(b) The heat of solution of hydrogen will be composition dependent. We write, therefore, the partial molar free energy of hydrogen in the solution  $\text{PdH}_x$

$$\mu_{\text{H}} = \bar{H}_{\text{H}} - T\bar{S}_{\text{H}} = \Delta\bar{H}(x) + RT \ln [x/(1-x)] + \frac{1}{2}\mu^0(\text{H}_2) \quad (5)$$

where the constant term  $\frac{1}{2}\mu^0(\text{H}_2)$  depends on the choice of standard state for hydrogen and is of no consequence in this context.  $\Delta\bar{H}(x)$  is the composition-dependent heat of solution of 1 g-atom of hydrogen in  $\text{PdH}_x$ .

In order to estimate  $\Delta\bar{H}(x)$  we make use of the observation<sup>4,8</sup> that to a good approximation the heat of solution of hydrogen in an alloy depends only on the valence electron:atom ratio of the alloy and not on the chemical identity of its minor constituent. Brodowsky and Poeschel<sup>9</sup> have made very accurate measurements of the heat of solution in a series of alloys,  $\text{Pd}_{1-x}\text{Ag}_x$ , with the results shown in Figure 1. For the reasons just given we use these data as a measure of  $\Delta\bar{H}(x)$ .

### Evaluation of the Critical Constants

From eq 5 and the condition for a critical point at  $x = x_c$ , viz.

$$\partial\mu/\partial x = \partial^2\mu/\partial x^2 = 0; \quad x = x_c \quad (6)$$

one readily derives

$$\frac{(\partial^2\Delta\bar{H}/\partial x^2)/(\partial\Delta\bar{H}/\partial x)}{(1-2x)/x(x-1)}; \quad x = x_c \quad (7)$$

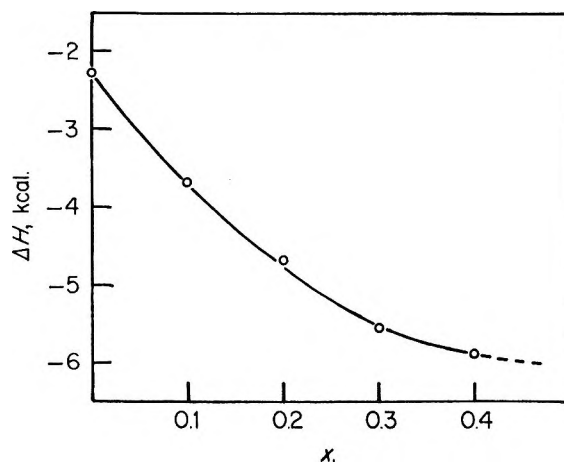


Figure 1. The heat of solution per gram-atom of hydrogen in the alloys  $\text{Pd}_{1-x}\text{Ag}_x$  (data of Brodowsky and Poeschel<sup>9</sup>).

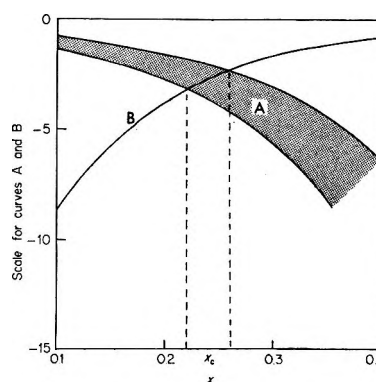


Figure 2. Curve A:  $(\partial^2\Delta\bar{H}/\partial x^2)/(\partial\Delta\bar{H}/\partial x)$ ; curve B:  $(1-2x)/x(x-1)$  as a function of  $x$  in  $\text{PdH}_x$ . The intersection of the two curves is the solution of eq 7.

In Figure 2 we have plotted separately as a function of  $x$  the left-hand side of eq 7 as derived from the data of Figure 1 by graphical differentiation and the right-hand side of the same equation. It may be seen that, although there is considerable error in obtaining  $\partial^2\Delta\bar{H}/\partial x^2$  from the experimental data, it is nevertheless possible to locate fairly precisely the critical composition at  $x_c = 0.24 \pm 0.02$ , in very good agreement with the experimental value<sup>2,3</sup> of  $x_c = 0.27$ .

The critical temperature,  $T_c$ , may likewise be evaluated from eq 5 and 6 as

$$\partial\Delta\bar{H}/\partial x = RT_c/x(x-1); \quad x = x_c \quad (8)$$

Using the critical composition already determined, one finds in this way that  $T_c = 680 \pm 100^\circ\text{K}$ , in fair enough

(6) A. Blandin and J. L. Déplanté, *J. Phys. Radium*, **23**, 609 (1962).

(7) H. Schnabl, *Ber. Bunsenges. Phys. Chem.*, **68**, 549 (1964).

(8) Y. Ebisuzaki and M. O'Keeffe, *Phil. Mag.*, **14**, 867 (1966).

(9) H. Brodowsky and E. Poeschel, *Z. Phys. Chem. (Frankfurt am Main)*, **44**, 143 (1965).



agreement with the experimental<sup>2,3</sup> value of  $T_c = 570^\circ\text{K}$ .

A further check is possible on the validity of the assumption that  $\Delta H$  is given accurately by the data of Figure 1. At room temperature the composition of the hydrogen-rich phase in equilibrium with the metal-rich phase is  $\text{PdH}_{0.6}$ . The integral heat of formation, per gram-atom of hydrogen, of  $\text{PdH}_{0.6}$  will be

$$\Delta H_t = (1/0.6) \int_0^{0.6} \Delta \bar{H}(x) dx \quad (9)$$

Numerical integration of the area under the curve in Figure 1 gives  $\Delta H_t = -5.0$  kcal, in very good agreement with the experimental (calorimetric) value of  $\Delta H_t = -4.8$  kcal mol<sup>-1</sup>.<sup>10</sup>

### Concluding Remarks

The excellent agreement with experiment of the approach to the palladium-hydrogen system outlined above leads us to believe that the basic assumptions are well founded. These assumptions are that the configurational entropy of the solution has the ideal value and that to an excellent approximation the heat of solution of hydrogen contains no contributions from the hydrogen-hydrogen interactions but depends only on the valence electron:atom ratio of the compound. Using these assumptions, the critical constants for the Pd-H system can be predicted using only experimental data obtained with very dilute solutions of hydrogen in palladium-silver alloys.

Finally, it is interesting to note that it is probable that hydrogen-hydrogen interactions, although weak, are repulsive. One would anticipate, therefore, that at a sufficiently low temperature there will be an order-disorder transition in a hydride of suitable composition. It is tempting to interpret the specific heat anomaly observed<sup>11</sup> in  $\beta$ -Pd-H at  $55^\circ\text{K}$  in these terms. One might suppose that the vacant and ordered sites would order as in  $\text{CuAu}$  ( $\text{L}_1$  type) or  $\text{Cu}_3\text{Au}$  ( $\text{L}_2$  type), although the establishment of long-range order would be hindered by the low mobility of hydrogen at these temperatures. In this connection, low-temperature neutron diffraction experiments with hydrides of the ideal composition  $\text{PdH}_{0.5}$  or  $\text{PdH}_{0.75}$  would be very interesting.

*Acknowledgment.* This work was supported by the Air Force Office of Scientific Research, Office of Aerospace Research, United States Air Force, under AFOSR Grant No. AF-AFOSR-68-1371.

(10) D. M. Nace and J. G. Aston, *J. Amer. Chem. Soc.*, **79**, 3619 (1957).

(11) D. M. Nace and J. G. Aston, *ibid.*, **79**, 3623 (1957).

## Mass Spectra and Sublimation

### Pressures of $\text{IF}_7$ and $\text{IOF}_5$

by C. J. Schack, D. Pilipovich,  
S. N. Cohz, and D. F. Sheehan

*Research Division, Rocketdyne, a Division of North American Rockwell Corporation, Canoga Park, California 91304*  
(Received July 5, 1968)

Several recent papers<sup>1-3</sup> have dealt with the preparation and properties of  $\text{IF}_7$  and  $\text{IOF}_5$ . While these articles have helped to clarify some of the earlier discrepancies with regard to the properties of  $\text{IF}_7$  and  $\text{IOF}_5$ , some inaccuracies still persist. For example, the reported vapor pressures<sup>3</sup> and/or sublimation pressures of these compounds are incorrect. The vapor pressure-temperature relationship of  $\text{IF}_7$  has been corrected<sup>1</sup> but that of  $\text{IOF}_5$  has not. We wish to report the sublimation pressure-temperature data and also the characteristic mass spectra of  $\text{IF}_7$  and  $\text{IOF}_5$ .

### Experimental Section

*Materials.* Iodine pentafluoride (Matheson Co.) and  $\text{F}_2$  were heated at  $150^\circ$  in monel or stainless steel cylinders for several hours. Partial purification of the  $\text{IF}_7$  was achieved by vacuum fractionation on a vacuum line constructed of stainless steel and equipped with Teflon U traps. Final purification of  $\text{IF}_7$  was accomplished by treatment with  $\text{KF}$  to remove  $\text{HF}$  and  $\text{IF}_5$ , followed by additional fractional condensations. No  $\text{HF}$  was detectable by near-infrared spectroscopy.<sup>4</sup> This method generally gave  $\text{IF}_7$  contaminated with 1-2% of  $\text{IOF}_5$ . However, the product on occasion was found to be completely free of  $\text{IOF}_5$  or any other detectable impurity and comprised the material used for the measurements.

Iodine oxide pentafluoride was prepared by condensing  $\text{IF}_7$  over  $\text{SiO}_2$  (Cab-O-Sil) at  $-196^\circ$  in stainless steel cylinders, warming to ambient temperature over several hours, and allowing the reaction to proceed overnight. If the reaction cylinder was warmed too rapidly, sufficient heat was generated to decompose most of the  $\text{IOF}_5$  to  $\text{IF}_5$  and  $\text{O}_2$ . Vacuum fractionation, treatment with  $\text{KF}$ , and an additional fractionation served to purify the product. No impurities were detected by gas chromatography,<sup>4</sup> infrared spectroscopy, and near-infrared spectroscopy.

*Sublimation-Vapor Pressure Measurements.* The pressures over solid or liquid  $\text{IF}_7$  or  $\text{IOF}_5$  were measured

(1) H. Selig, C. W. Williams, and G. J. Moody, *J. Phys. Chem.*, **71**, 2739 (1967).

(2) D. F. Smith and G. M. Begun, *J. Chem. Phys.*, **43**, 2001 (1965).

(3) N. Bartlett and L. E. Levchuk, *Proc. Chem. Soc.*, 242 (1963).

(4) V. H. Dayan and B. C. Neale, *Advances in Chemistry Series*, No. 54, American Chemical Society, Washington, D. C., 1966, p 223.

with Heise bourdon-tube-type gauges, 0–1500-mm scale graduated in 2-mm divisions and capable of readings to 1 mm. A thermocouple was used to determine the temperature of the slush baths. Solid  $\text{IF}_7$  gave the following sublimation pressures (in mm) over the temperature range  $-80$  to  $0^\circ$ :  $193.4^\circ\text{K}$ , 6;  $209.4^\circ\text{K}$ , 15;  $218.1^\circ\text{K}$ , 25;  $243.7^\circ\text{K}$ , 113;  $261.8^\circ\text{K}$ , 316; and  $273.2^\circ\text{K}$ , 567. The sublimation pressure–temperature relationship is described by the equation  $\log P(\text{mm}) = 11.2319 - (3046.93/T) + (197,769/T^2)$ . The heat of sublimation is 6.0 kcal/mol. Solid  $\text{IOF}_5$  gave the following sublimation pressures (in mm) over the temperature range  $-78$  to  $0^\circ$ :  $195.1^\circ\text{K}$ , 3;  $226.3^\circ\text{K}$ , 46;  $50.5^\circ\text{K}$ , 228;  $262.8^\circ\text{K}$ , 464; and  $273.2^\circ\text{K}$ , 824. The vapor pressure of  $\text{IOF}_5$  was checked at  $5.3^\circ$  (1044 mm) and  $13.4^\circ$  (1398 mm). Values calculated from the Bartlett and Levchuk equation<sup>3</sup> for these temperatures are 2140 and 3090 mm, respectively. The sublimation pressure–temperature relationship is described by the equation  $\log P(\text{mm}) = 8.9874 - (1659.4/T)$ . The heat of sublimation is 7.6 kcal/mol. The samples of  $\text{IF}_7$  and  $\text{IOF}_5$  were tensiometrically homogeneous, and vapor density measurements at approximately 1000 mm indicated no association for either compound.

**Mass Spectra.** A CEC 21-103C mass spectrometer was used to obtain the mass spectra. The inlet system of the instrument was modified by eliminating both the micromanometer and a 3-l. expansion volume. Reproducible mass cracking patterns were obtained using an ionizing current of 10.5 A and an ionizing voltage of 70 eV. The inlet system was considered passivated when a stable pattern was obtained for  $\text{IF}_5^+$ .<sup>5</sup>

## Results and Discussion

The sublimation pressures of solid  $\text{IF}_7$  and  $\text{IOF}_5$  were determined over the temperature range  $-78$ – $0^\circ$ . The earlier data of Bartlett did not specify a temperature range, but no agreement was found with values calculated from the reported equations<sup>3</sup> above or below the melting point. Measurements employing liquid  $\text{IF}_7$  gave vapor pressure readings in excellent agreement with those calculated from the more recent equation<sup>1</sup> of Selig, *et al.* In the case of liquid or solid  $\text{IOF}_5$ , pressure measurements were obtained that were somewhat less than half the values calculated.<sup>3</sup> These results corroborate the earlier qualitative observation of Smith and Begun.<sup>2</sup> Since the accuracy of the measured density of liquid  $\text{IOF}_5$ <sup>1</sup> was dependent on the incorrect vapor pressure data, it would appear that the reported densities will be in error.

Stable mass cracking patterns of  $\text{IF}_7$  and  $\text{IOF}_5$  were obtained and are shown in Tables I and II. The spectral patterns are normalized to the most intense peak. Parent ions were observed with the reference,  $\text{IF}_5^+$ , and  $\text{IOF}_5^+$  but not with  $\text{IF}_7$ . Recombination reactions were not

observed, and thus no species such as  $\text{IF}_x\text{O}_2^+$  were noted. The intensity of the  $m/e$  203 peak ( $\text{IF}_4^+$ ) is at first somewhat surprising, inasmuch as no oxygen is contained in the ion. However, a commonality of bond cleavage due to electron bombardment and thermal initiation is expected, and for  $\text{IOF}_5$  the thermal degradation involves the rupture of the IO bond.<sup>6</sup> Thus intense peaks due to the ionized partners of this bond scission ( $\text{IF}_x^+$ ) are not extraordinary. The occurrence of appreciable thermal decomposition of  $\text{IOF}_5$  within

Table I: Mass Spectrum of  $\text{IF}_7$

$m/e$	Intensity relative to $\text{IF}_4^+$	Ion	$m/e$	Intensity relative to $\text{IF}_4^+$	Ion
260	...	$\text{IF}_7^+$	184	7.50	$\text{IF}_3^+$
241	73.68	$\text{IF}_6^+$	165	6.45	$\text{IF}_2^+$
222	19.34	$\text{IF}_5^+$	146	35.13	$\text{IF}^+$
203	100.00	$\text{IF}_4^+$	127	50.26	$\text{I}^+$

Table II: Mass Spectrum of  $\text{IOF}_5$

$m/e$	Intensity relative to $\text{IF}_4^+$	Ion	$m/e$	Intensity relative to $\text{IF}_4^+$	Ion
238	32.05	$\text{IOF}_5^+$	181	17.95	$\text{IOF}_2^+$
222	2.60	$\text{IF}_5^+$	165	10.14	$\text{IF}_2^+$
219	17.40	$\text{IOF}_4^+$	162	9.04	$\text{IOF}^+$
203	100.00	$\text{IF}_4^+$	146	28.77	$\text{IF}^+$
200	4.38	$\text{IOF}_3^+$	143	12.19	$\text{IO}^+$
184	21.92	$\text{IF}_3^+$	127	48.25	$\text{I}^+$

the instrument to give  $\text{IF}_5^+$  is excluded by the low relative intensity of the  $\text{IF}_5^+$  peak coupled with the high relative intensity of the other  $\text{IF}_x^+$  peaks. Some  $\text{IF}_x\text{O}^+$  impurities were found in the  $\text{IF}_7$  (3–4%) owing to the reaction of  $\text{IF}_7$  with glass portions of the inlet system. No iodine oxide fluorides were observed with  $\text{IF}_5$ . Only very minor quantities of impurities generated in the mass spectrometer ( $\text{SiF}_4$  and  $\text{COF}_2$ ) were found, and these could not be confused with mass-charge values of iodine-containing ions.

**Acknowledgment.** We wish to acknowledge support for this work by the Office of Naval Research, Power Branch.

(5) A. P. Irsa and L. Friedman, *J. Inorg. Nucl. Chem.*, **6**, 77 (1958).

(6) C. J. Schack and D. Pilipovich, unpublished results, this laboratory.

## The Diffusion of Gases in Nonpolar Liquids.

### The Open-Tube Method

by Lorna Bennett, Wing Y. Ng, and John Walkley

Department of Chemistry, Simon Fraser University,  
Burnaby 2, British Columbia, Canada (Received July 8, 1968)

Hildebrand<sup>1</sup> has recently made use of the diaphragm method for the measurement of the diffusion of gases in nonpolar solvents. This is a pseudo-steady-state method and relies upon measuring the change in volume of the gas in equilibrium with the saturated solution above the diaphragm. The gas in the solution diffuses through a diaphragm of macroscopic size holes into the bulk solvent of essentially infinitely dilute solute concentration. This method is often lengthy, and the conditions which give rise to a steady-state system are sometimes difficult to attain. We now report some measurements of the diffusion of gases in nonpolar solvents using an open-tube method. This method is a nonsteady-state one and has the advantage that a value of both the diffusion coefficient and the interfacial resistance can be measured.

### Theory

The solution for Fick's law of linear diffusion, *viz.*, using the usual definition of terms

$$J_x = -D \frac{\partial c}{\partial x} \quad (1)$$

$$\frac{\partial c}{\partial t} = D \frac{\partial^2 c}{\partial x^2} \quad (2)$$

and satisfying the conditions that  $C = C_0$  if  $x = 0$  and  $t > 0$ ,  $C = 0$  if  $x > 0$  and  $t = 0$ , is

$$C = C_0 \operatorname{erfc}(x/2\sqrt{Dt}) \quad (3)$$

where  $C_0$  is the saturation solubility of the solute and  $\operatorname{erfc}(y)$  is the complement of the error function. Thus the volume of gas dissolved at time  $t$  in a previously degassed solvent is given as

$$V = \frac{2RTA}{P} C_0 \sqrt{\frac{Dt}{\pi}} \quad (4)$$

where  $A$  is the cross-sectional area of the cell and  $P$  and  $T$  are the pressure and temperature, respectively, of the gas. Experiments show that the observed  $V$  vs.  $\sqrt{t}$  curve is displaced from that expected using eq 4. It is seen that the slope of the curve rapidly approaches, as a limiting value, that expected from eq 4. The basic equation for mass transfer across an interface<sup>2</sup> is

$$J_{x=0} = -D \left( \frac{\partial c}{\partial x} \right)_{x=0} = -\alpha(C_s - C_0) \quad (5)$$

where  $\alpha$  is the reciprocal of the interfacial resistance and  $C_s$  is the concentration of the solute at the interface. Combining eq 5 with eq 1 and 2, the solution now becomes<sup>3</sup>

$$C = C_0 \operatorname{erfc}(x/2\sqrt{Dt}) - e^{hx+h^2Dt} \operatorname{erfc}\left(\frac{x}{2\sqrt{Dt}} + h\sqrt{Dt}\right) \quad (6)$$

where  $h = \alpha/D$ . The volume of gas crossing the interface is given by

$$V = \frac{RTA}{Ph} \left[ e^{h^2Dt} \operatorname{erfc}(h\sqrt{Dt}) - 1 + 2h\sqrt{\frac{Dt}{\pi}} \right] \quad (7)$$

where  $P$  is the partial pressure of the gas and  $R$  is the gas constant. It is seen from eq 7 that the limiting behavior will be given by an equation identical with eq 4, hence giving a value of  $D$ . By curve fitting eq 7 to the complete set of data (from  $t = 0$ ), a value of  $D$  and  $h$  can be found. It is found that these two values of  $D$  are in good agreement.

### Experimental Section

The apparatus used was similar to that of Houghton, *et al.*<sup>4</sup> The diffusion cell was a uniform tube of 24 cm<sup>2</sup> in cross-sectional area and 25 cm long. The average diffusion length for 200 min (the duration of a typical run) was less than 2 cm. The volume of gas diffusing into the solvent was measured with a calibrated manometer. After filling the diffusion cell with the degassed solvent, a good thermal equilibrium was established by keeping the cell thermostated (to  $\pm 0.01^\circ$ ) for at least 24 hr prior to allowing gas into the cell above the solvent. Solvents were spectroquality reagents supplied by Matheson Coleman and Bell, and the gases were research grade, supplied by Matheson.

### Results and Discussion

Figure 1 shows the experimental  $V$  vs.  $\sqrt{t}$  curve for  $N_2$  in  $C_6H_6$ . The dotted line shows the expected relationship in the absence of interfacial resistance. Owing to the nature of eq 7,  $D$  may be estimated from the limiting slope of the experimental curve. The expected relationship between  $V$  and  $\sqrt{t}$ , as given by eq 7, is also shown in Figure 1 for various values of  $h$ . In no experiment is it found possible to reproduce the data at the beginning of a run ( $t \rightarrow 0$ ). This is undoubtedly due to a time lag in setting up the gas-vapor equilibrium above the solvent.

(1) M. Ross and J. H. Hildebrand, *J. Chem. Phys.*, **40**, 2397 (1964); K. Nakanishi, E. M. Voigt, and J. H. Hildebrand, *ibid.*, **42**, 1860 (1965).

(2) J. T. Davies and E. K. Rideal, "Interfacial Phenomena," 2nd ed, Academic Press, New York, N. Y., 1963, Chapter 7.

(3) H. S. Carslaw and J. C. Jaeger, "Conduction of Heat in Solids," 2nd ed, Oxford University Press, London, 1959, Chapter 2.

(4) G. Houghton, A. S. Kesten, J. E. Funk, and J. Coull, *J. Phys. Chem.*, **65**, 649 (1961).

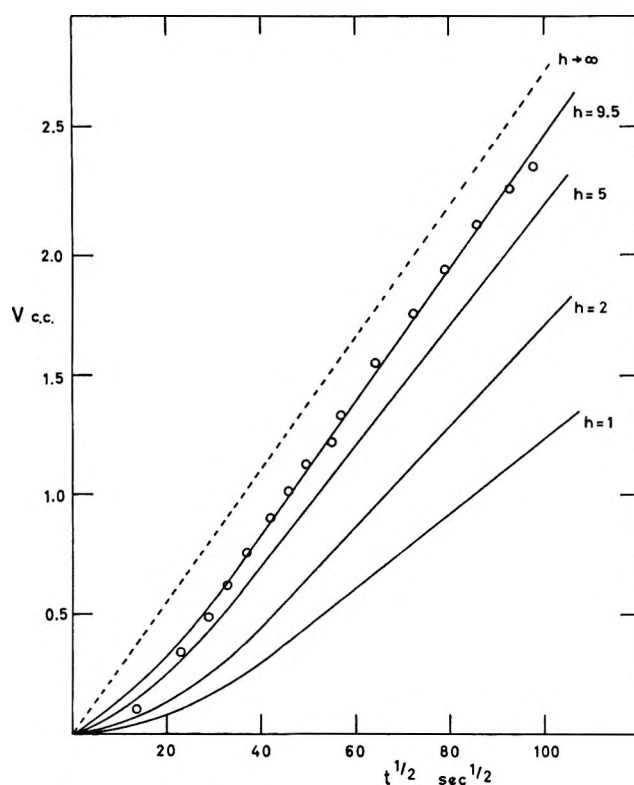


Figure 1. Diffusion of nitrogen gas in benzene at 25° ( $D = 7.23 \text{ cm}^2 \text{ sec}^{-1}$ ): O, experimental results; ---, eq 4 (no interfacial resistance).

The  $D$  and  $h$  values for several gas-solvent systems are given in Table I together with the  $D$  values obtained using the Hildebrand diaphragm method. It is seen that, in general, good agreement between the two  $D$  values exists. It is seen from Table I that the  $D$

Table I: Diffusion Coefficients and Permeability Values at 25°

System	$10^6 D, \text{ cm}^2 \text{ sec}^{-1}$			$h, \text{ cm}^{-1}$
	Diaphragm method	From the slope	Least-squares fit of eq 7	
Ar- $\text{CCl}_4$	(3.63) <sup>a</sup>	3.71	3.73	11.3
$\text{N}_2$ - $\text{CCl}_4$	(3.42) <sup>a</sup>	3.63	3.79	8.1
Ar- $\text{C}_6\text{H}_6$	11.2	...	...	...
$\text{N}_2$ - $\text{C}_6\text{H}_6$	6.93	7.20	7.23	9.5

<sup>a</sup> Reference 1.

value for argon in benzene is anomalously high when measured by the diaphragm method. No sensible value of  $D$  could be obtained from the open-tube method for this system. From the data obtained it would appear that this system behaves as if the flux at the interface were constant. Such a condition is incompatible with eq 7, and as such no value of  $D$  or of  $\alpha$  can be obtained from the data.

Data for this open-tube method have not previously been analyzed by curve fitting to eq 7. We are unable to comment upon the  $h$  values with the limited data available. It is pertinent to note, however, that the linear portion of the curve is only strongly dependent upon  $h$ , for small  $h$  values, *i.e.*, less than 15. This method is excellent for measuring the diffusion coefficient  $D$  and this coefficient, unlike  $h$ , is not sensitive to interfacial impurity.

### Quantum Yield of the Photonitrosation of Cyclohexane

by Hajime Miyama, Noriho Harumiya,

Basic Research Laboratories, Toyo Rayon Company, Ltd.,  
Tebiro, Kamakura, Japan

Yoshikazu Ito, and Shigeru Wakamatsu

Nagoya Laboratory, Toyo Rayon Company, Ltd.,  
Tebiro, Kamakura, Japan (Received July 10, 1968)

The photonitrosation of cyclohexane is one of the important processes of synthesizing caprolactam.<sup>1</sup> However, not much is known about the quantum yield of this reaction. A value of 0.7 was obtained by Torimitsu, *et al.*,<sup>2</sup> in the wavelength range 365–560  $\text{m}\mu$ , and a value of 1.48 was obtained by Baumgartner, *et al.*<sup>3</sup> The latter value was later corrected to 0.87 (420  $\text{m}\mu$ ) and 0.68 (580  $\text{m}\mu$ ).<sup>4</sup> Fukuzawa and Miyama<sup>5</sup> obtained, under a flash lamp, 0.65 in the range 360–505  $\text{m}\mu$ . The accuracy of most of these values cannot be estimated because the oxime hydrochloride produced does not dissolve in cyclohexane, and the scattering of the incident light by suspended oxime particles becomes marked as the reaction proceeds. Therefore, in order to obtain a more reliable value without being disturbed by the light scattering, we used an integrating sphere in the wavelength range 365–589  $\text{m}\mu$ .

The integrating sphere<sup>6</sup> made from mild steel has a diameter of 1.3 m and its inside wall is coated with white paint, containing barium sulfate as a main component, in order to obtain uniformly reflected light (the reflectance is about 90%). The reaction vessel is a Pyrex

(1) Y. Ito, *Bull. Chem. Soc. Jap.*, **29**, 227 (1956); E. Müller and H. Metzger, *Chem. Ber.*, **87**, 1282 (1954).

(2) S. Torimitsu, S. Wakamatsu, and Y. Ito, unpublished work.

(3) P. Baumgartner, A. Seschamps, and C. Roux-Guerraz, *Compt. Rend.*, **259**, 4021 (1964).

(4) A. Deschamp, Ph.D. Thesis, Faculty of Science, University of Paris, 1966.

(5) D. Fukuzawa and H. Miyama, *J. Phys. Chem.*, **72**, 371 (1968).

(6) B. J. Hisdak, *J. Opt. Soc. Amer.*, **55**, 1122 (1965). The theoretical details of the integrating sphere were described in the references cited in this paper.

cylinder 16 cm in diameter and 20 cm long and has a 3.7-l. capacity. It is clamped to the holder through a Pyrex plate and Teflon gaskets and is equipped with an inlet and exit for the gas mixture and a water jacket to keep the reaction temperature constant. As a light source, high-pressure mercury lamps of 2 kW were used. To obtain nearly monochromatic light, one or two Toshiba glass filters were used with an aqueous solution of copper sulfate to cut out light above 700  $m\mu$ . In order to measure the intensity ratio of the absorbed light to the incident light, a photocell with a millivoltmeter was used. In front of the photocell, a baffle plate, to prevent the effect of the direct incident light, and an opal glass, to obtain a uniformly diffuse light, were placed. Actually, the above-described ratio was obtained by measuring the light intensities before and after the introduction of light-absorbing nitrosyl chloride gas. At 365  $m\mu$ , the absolute intensity of the incident light in front of the reaction vessel was measured by a potassium ferrioxalate actinometer,<sup>7</sup> which was placed in the reaction vessel instead of in the reacting mixture. Light intensities at other wavelengths were measured by a thermopile (with a potentiometer) which was located between the filter and the reaction vessel and was calibrated at 365  $m\mu$  by the above-described actinometer. Other details were the same as in the previous article,<sup>5</sup> except that the blowing rate of nitrosyl chloride was 200 ml/min and that of hydrochloric acid 1000 ml/min; the concentration of nitrosyl chloride in the reaction mixture was 0.3–0.5 wt %.

(A preliminary experiment showed that the change of nitrosyl chloride concentration in this concentration range did not affect the quantum yield.)

The results of measurements at 365, 435, 535, and 578  $m\mu$  are shown in Table I. Here, more than 99% of the incident light was absorbed by the reaction system at 365, 435, and 535  $m\mu$ , but about 80% of the incident light was absorbed at 578 and 589  $m\mu$ . Therefore, at longer wavelengths, the measurement of absorbance was less accurate and the effect of light scattering was considered to be more marked. In order to examine this effect, in two runs at longer wavelengths, 10 vol % of chloroform was added to the reaction system to dissolve the oxime hydrochloride produced.

The over-all experimental error involved in the measurement of the quantum yield was estimated to be  $\pm 15\%$ , that is,  $\pm 6.5\%$  due to the error of calibrating the thermopile at 365  $m\mu$ ,  $\pm 2.5\%$  due to that of reading the thermopile,  $\pm 2\%$  due to that of the oxime analysis,  $\pm 2\%$  due to the instability of the light source and the filter, and  $\pm 2\%$  due to the dark reaction correction.

According to Table I, the addition of chloroform seems to increase the quantum yield, although this is not conclusive because of the experimental error. Within this experimental error, the quantum yield of photonitrosation of cyclohexane is about 0.72, independent of the wavelengths. Even if this large experimental error is taken into account, the quantum yield does not exceed unity. Therefore, our experimental result suggests, as in the previous article,<sup>5</sup> that the present reaction proceeds not *via* chain mechanism.

Table I

Wave-length, <sup>a</sup> $m\mu$	Temp, $^{\circ}\text{C}$	$10^5 \times$ rate of oxime production, mol. l. <sup>-1</sup> min <sup>-1</sup>	$10^5 \times$ absorbed light quantity, einsteins l. <sup>-1</sup> min <sup>-1</sup>	Quantum yield
365	21	1.05	1.47	0.72
	19	0.93	1.35	0.69
	15	1.26	1.63	0.78
	17	1.12	1.67	0.67
435	17	0.86	1.07	0.80
	17	0.87	1.07	0.81
	15.5	0.93	1.32	0.70
	14.5	0.99	1.29	0.76
535	16.5	2.36	3.17	0.75
	16.5	2.27	3.08	0.74
	18	2.30	3.05	0.75
578	15.5	1.79	2.55	0.70 <sup>b</sup>
	17.7	1.22	2.01	0.61
	18	1.20	1.90	0.63
589	16.5	5.56	8.20	0.67
	16.5	5.60	8.04	0.70 <sup>b</sup>
				Av 0.72

<sup>a</sup> The contribution of the intensities of other lines and the background was less than 4%, except at 589  $m\mu$  where the intensity of 578  $m\mu$  was ca. 12%. <sup>b</sup> In these runs, 10 vol % of chloroform was added.

(7) C. A. Parker, *Proc. Roy. Soc.*, **A220**, 104 (1953).

## Electron Magnetic Resonance Spectra of MnCl<sub>2</sub>—LiCl—KCl Eutectic Mixtures<sup>1</sup>

by Terry B. Swanson<sup>2</sup>

*Department of Chemistry, Stanford University, Stanford, California*  
(Received July 15, 1968)

In the present study solid mixtures of MnCl<sub>2</sub> in the LiCl–KCl eutectic have been studied by electron magnetic resonance (emr) and also in some cases by X-ray diffraction. The concentration of MnCl<sub>2</sub> in the mixtures has been varied and the emr spectra has been recorded as a function of the concentration. Several different resonances have been observed and some have been identified as to their origin.

(1) This research was supported in part by the Advanced Research Projects Agency of the Department of Defense through the Center for Materials Research at Stanford University.

(2) Fairchild Semiconductor Research and Development, Palo Alto, Calif.

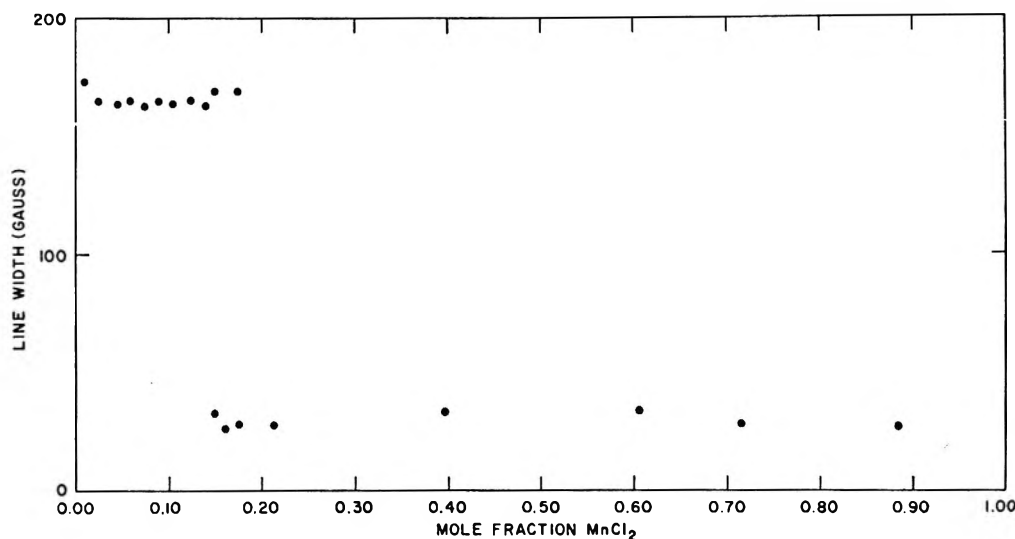


Figure 1. The emr line width vs. mole fraction of  $\text{MnCl}_2$  in the  $\text{LiCl-KCl}$  eutectic at  $25^\circ$ .

### Experimental Section

The emr spectra were obtained with a Varian X-band spectrometer operating near 9.5 Gcps. A sample of aqueous  $\text{VO}(\text{ClO}_4)_2$  was used for magnetic field sweep calibration. Resonance line widths refer to the full width at points of maximum slope and are obtained from the experimentally observed first-derivative curves.

In all instances in this investigation reagent grade materials were used without further purification. Samples containing various quantities of  $\text{MnCl}_2$  in the  $\text{LiCl-KCl}$  eutectic, prepared by weighing out the proper quantities of the anhydrous materials, were sealed under vacuum into 1-mm i.d. quartz sample tubes.

The high-temperature emr spectra were obtained through the use of a cavity system which had been described in detail elsewhere.<sup>3</sup>

### Results and Discussion

Shown in Figure 1 are the room-temperature emr line widths obtained from samples containing various amounts of  $\text{MnCl}_2$  in the  $\text{LiCl-KCl}$  eutectic. Sample preparation consisted of weighing out the proper quantities of  $\text{MnCl}_2$  and eutectic, vacuum drying at  $\sim 200^\circ$ , melting under vacuum, and quenching in air. Quenching in air refers to the rapid removal of the heat source used to keep the sample in the molten state and subsequent solidification of the melt without external influence. For samples containing between 0.06 and 0.15 mol fraction of  $\text{MnCl}_2$  ( $X$ ), one observes only a single resonance line whose width is  $\sim 175$  G. Beginning near  $X = 0.15$  a relatively narrow line of width 25 G is observed. In the region  $X = 0.15-0.175$  both resonance lines are observable, the spectrum appearing as a narrow line superimposed on a broader one. Above  $X = 0.18$  only the resonance of width 25 G is observable. This is not to say, however, that the broader resonance is nonexistent. On the contrary, the broader line may

well exist but is unobservable because of the much greater peak height of the 25-G resonance. The 25-G resonance is the only one seen in the region  $X = 0.18-0.89$ .

At room temperature a six-line hyperfine pattern was observed superimposed on the 175-G resonance for  $\text{MnCl}_2$  concentrations between  $X = 0.06$  and 0.12 (the lowest concentration investigated). The spectrum of a 0.0575 mol fraction sample of  $\text{MnCl}_2$  has been investigated over the temperature interval  $300-575^\circ\text{K}$ . It has been noted that as the temperature is raised the intensity of the hyperfine pattern increased relative to that of the 175-G line. The separation between the individual hyperfine lines is about 91 G.

The six-line hyperfine pattern arises from "isolated"  $\text{Mn}^{2+}$  ions in the  $\text{LiCl-KCl}$  lattice. "Isolated" refers to  $\text{Mn}^{2+}$  ions not in close proximity to other  $\text{Mn}^{2+}$  ions. The hyperfine structure arises, of course, because of interaction between the 3d electrons and the nucleus (spin of  $5/2$ ) of  $^{55}\text{Mn}$ . The separation observed here agrees fairly well with the values reported by others.<sup>4-6</sup> Dissolution of manganese compounds with increasing sample temperature is responsible for the observed increase in intensity of the hyperfine pattern upon sample heating. This process increases the concentration of "isolated"  $\text{Mn}^{2+}$  ions.

The origin of the 175-G line is not clear at this time. However, it does not arise from  $\text{MnCl}_2$  as such, since the emr spectrum of pure  $\text{MnCl}_2$  gives a resonance approximately 900 G in breadth. Nevertheless, con-

(3) T. B. Swanson, Ph.D. Dissertation, Stanford University, Stanford, Calif., 1965.

(4) L. Yarmus, M. Kukk, and B. R. Sundheim, *J. Chem. Phys.*, **40**, 33 (1964).

(5) J. Brown, Ph.D. Dissertation, University of California, Berkeley, Calif., 1961.

(6) L. S. Singer and M. C. Haun, *Bull. Amer. Phys. Soc.*, **7**, 200 (1962).

siderable exchange narrowing is indicated, thereby implying a reasonably close approach of  $Mn^{2+}$  ions. Brown<sup>5,7</sup> has seen a similar resonance ( $\sim 170$  G) and has attributed it to "exchange-narrowed manganese clusters." The nature of any such cluster is unknown at the present time.

The origin of the 25-G resonance has become clear in the course of this work. A similar resonance has been noted in several previous studies<sup>6-10</sup> and has been suggested as being due to  $K_4MnCl_6$ <sup>9</sup> but has not been positively identified. An X-ray analysis of two samples, one  $X = 0.137$  and the other  $X = 0.175$ , has been carried out. Comparison with previous work on  $K_4MnCl_6$ <sup>11</sup> showed that the sample containing the higher  $MnCl_2$  concentration ( $X = 0.175$ ) definitely contains  $K_4MnCl_6$ . Furthermore, none of the  $K_4MnCl_6$  X-ray lines showed up in the powder pattern obtained from the  $X = 0.137$  sample. These results, along with those shown in Figure 1, indicate that  $K_4MnCl_6$  is indeed responsible for the 25-G resonance. This conclusion is further substantiated by comparison with previous work involving emr and magnetic susceptibility measurements on pure  $K_4MnCl_6$ .<sup>12</sup> In this case a room-temperature line width of 23 G is observed. A calculation of the expected exchange-narrowed line width for  $K_4MnCl_6$  gives a value of 30 G. The calculation is based on the dipolar linewidth, which can be calculated from the known crystal structure of  $K_4MnCl_6$ , along with a value of the exchange integral obtained from the experimentally observed Weiss constant in conjunction with the Weiss molecular field relationship.

Brown<sup>5,7</sup> has discounted the possibility that  $K_4MnCl_6$  is responsible for the 25-G line on the basis of her observation that a mixture of LiCl and  $MnCl_2$  ( $X = 0.02$ ) also gave the 25-G line. This has been carefully checked and no narrow resonance has been found for a vacuum-dried mixture of LiCl and  $MnCl_2$  ( $X = 0.02$ ) prepared in the manner used by Brown. In addition, for a quenched sample containing a 4:1 mole ratio of LiCl: $MnCl_2$ , we have observed a resonance whose width is 730 G and definitely not 25 G. We must therefore, disagree with Brown as to the origin of the 25-G emr absorption.

There was some indication from previous work<sup>5,7</sup> that vacuum drying of  $MnCl_2$  in the LiCl-KCl eutectic could form the species responsible for the 25-G line. To check this indication, a  $X = 0.142$  sample of  $MnCl_2$  in LiCl-KCl eutectic was prepared in the following manner. The sample was prepared by weighing out and then grinding together, with mortar and pestle, the proper quantities of previously vacuum dried  $MnCl_2$  and eutectic. The sample was then placed in the emr sample container and evacuated but was not dried under vacuum. Observation of the spectrum showed a line 575 G in breadth. Upon this line was superimposed a very faint line of indeterminable width. Four samples were then prepared in a manner analogous to

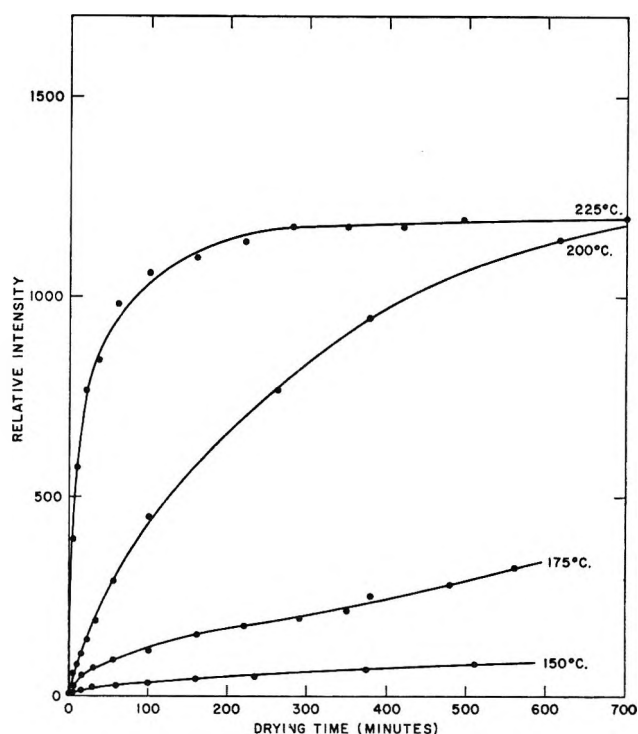


Figure 2. The emr relative intensity vs. vacuum drying time for 0.142 mol. fraction of  $MnCl_2$  in the LiCl-KCl eutectic. Drying temperatures were 150, 175, 200, and 225°.

the first. The four separate samples were then vacuum dried at four different temperatures (150, 175, 200, and 225°) and their emr spectra were observed after various drying times. The height of the narrow component grew relative to that of the broader component until the broader component could no longer be seen. However, the width remained constant at 25 G. Figure 2 shows the relative intensity (taken as the height of the narrow component) as a function of the total drying time at four different temperatures. The rate of increase of the intensity of the narrow component is seen to depend strongly on the drying temperature. However, one can see that at least in the cases of the runs at 200 and 225° the intensities approach the same value at long drying times. The runs at 150 and 175° have not proceeded far enough at the maximum drying time to ascertain whether they too will approach the same intensity. In addition to the samples which were dried, two control samples were prepared. One sample was sealed onto the vacuum line and was pumped on continuously but was not heated. The other was merely evacuated,

(7) J. Brown, *J. Phys. Chem.*, **67**, 2524 (1963).

(8) P. A. Forrester and E. E. Schneider, *Proc. Phys. Soc.*, **B69**, 833 (1956).

(9) G. D. Watkins, *Phys. Rev.*, **113**, 79 (1959).

(10) K. G. Bansiger and E. E. Schneider, *J. Appl. Phys.*, **33**, 383 (1962).

(11) X-Ray Powder Data File, Sets 1-5 Revised, American Society for Testing and Materials, Philadelphia, Pa., 1960.

(12) T. B. Swanson, V. W. Laurie, and W. Duffy, Jr., submitted for publication.

sealed, and left at room temperature. Both were examined at 600 min and were found to be as they were at zero time (immediately after preparation). No increase in the intensity of the 25-G component was noted. The sample which was evacuated, sealed, and left at room temperature was observed again after several weeks and again no change was noted.

From the data shown in Figure 2 one is led to the conclusion that the formation of  $K_4MnCl_6$  in samples containing  $MnCl_2$  ( $X = 0.142$ ) in  $LiCl$ - $KCl$  eutectic is accomplished quite readily by vacuum drying at relatively low temperatures ( $200^\circ$ ) and for short times (a few hours). This is in contrast with Brown's<sup>5,7</sup> conclusion that formation of  $K_4MnCl_6$  during the vacuum drying process is improbable.

*Acknowledgment.* The author wishes to thank Mr. G. Martin, Center for Materials Research, Stanford University, for obtaining the X-ray powder patterns.

### Ion Exchange in Molten Salts. III. The Ion-Exchange Properties of Sodium Zeolite A in Molten $NaNO_3$ . The Exchange with Calcium and Strontium Cations

by M. Liquornik<sup>1</sup> and Y. Marcus<sup>2</sup>

Soreq Nuclear Research Center, Israel Atomic Energy Commission, Yavne, Israel (Received July 17, 1968)

In the first paper of this series,<sup>3</sup> dealing with the exchange of sodium for monovalent ions in molten salts, it was pointed out that owing to the relatively high temperature involved, an inorganic exchanger, such as the synthetic crystalline zeolite Linde 4A, must be used. The work is extended in this paper to the alkaline earth ions, the choice of ions being reduced to calcium and strontium because of the apparent instability of magnesium and barium zeolites. Molten sodium nitrate was used as a solvent, as it has a common cation with the zeolite.

#### Experimental Section

Analytically pure nitrates were used, without further purification.  $NaNO_3$  and  $Sr(NO_3)_2$  were dried at  $150^\circ$  for at least 24 hr. Anhydrous calcium nitrate was prepared from  $Ca(NO_3)_2 \cdot 4H_2O$  by removing the water of crystallization under vacuum at about  $130^\circ$  overnight. After this treatment, the salt cake was broken up in a mortar and was dried in air at  $300^\circ$ . The dehydrated  $Ca(NO_3)_2$  was handled in a drybox. Solutions of calcium nitrate-sodium nitrate were heated to  $330^\circ$  for at least 24 hr, and no change in weight or appearance could be detected. The treatment of the

zeolite, the experimental procedure, and the analytical methods have been given.<sup>3</sup>

Concentrations in either phase are expressed as mole fractions, as suggested by Blander<sup>4</sup> (Temkin's activities), rather than as equivalent fractions

$$N_{Ca(NO_3)_2} = \frac{n_{Ca(NO_3)_2}}{n_{Ca(NO_3)_2} + n_{NaNO_3}} \quad (1)$$

where  $n_i$  is the number of moles. The zeolite in contact with molten sodium nitrate gives an occlusion compound of the composition  $Na_{22}[A \cdot 10NO_3]$ , *i.e.*,  $Na_{22}[(SiO_2AlO_2)_{12}(NO_3)_{10}]$ .<sup>5</sup> Mole fractions in the zeolite were based on the presence of 22  $Na^+$  ions, which, in principle at least, are available for exchange, and not on the exchange capacity, which was not determined and probably cannot be determined isothermally in the case of the alkaline earth nitrates. Thus  $\bar{N}_{Ca} = \bar{n}_{Ca}/22$ , where  $\bar{n}_{Ca}$  is the number of moles of Ca found per formula weight of zeolite.

#### Results

The ion-exchange properties of the zeolite with solutions of calcium or strontium nitrates in molten sodium nitrate were investigated at  $330^\circ$ . The concentration of the minor component was varied from very dilute solutions of  $10^{-3}$  to  $10^{-4}$  mol fraction to 0.04-0.06 mol fraction. The exchange isotherms thus obtained are presented in Figure 1.

It should be noted that after the exchange of eight  $Na^+$  cations with four  $Ca^{2+}$  cations, there is an increase in the number of occluded nitrate anions as further calcium enters the zeolite, and this is a function of the concentration of calcium nitrate in the solution. Comparing the three arbitrarily selected compositions of the zeolite from the exchange isotherm, Figure 1 (given in

Table I

Com- position	No. of ions/formula wt of zeolite			
	$Ca^{2+}$	$Na^+$	$NO_3^-$	$SiAlO_4$
1	2.8	16.5	10.1	12.0
2	4.1	14.3	10.5	12.0
3	7.3	11.0	13.7	12.0

Table I), it is found that the difference between 1 and 2 roughly corresponds to the exchange between one  $Ca^{2+}$  ion and two  $Na^+$  ions, with due allowance for analytical errors. However, subtracting 2 from 3, one

(1) Taken from a part of the Ph.D. thesis submitted by M. L. to the Hebrew University, Jerusalem, 1967.

(2) Department of Inorganic and Analytical Chemistry, The Hebrew University, Jerusalem.

(3) M. Liquornik and Y. Marcus, *J. Phys. Chem.*, **72**, 2885 (1968).

(4) M. Blander in "Molten Salt Chemistry," M. Blander, Ed., Interscience Publishers, New York, N. Y., 1964, p 127.

(5) M. Liquornik and Y. Marcus, *Israel J. Chem.*, **6**, 115 (1968).



obtains  $3.2\text{Ca}^{2+}$ ,  $-3.3\text{Na}^+$ ,  $3.2\text{NO}_3^-$ , which suggests the exchange between  $\text{Na}^+$  and  $\text{CaNO}_3^+$ .

On the contrary, in the exchange of sodium with strontium there is no change in the occlusion as the exchange proceeds; the total number of cationic equivalents per mole of zeolite remains constant at  $21.7 \pm$

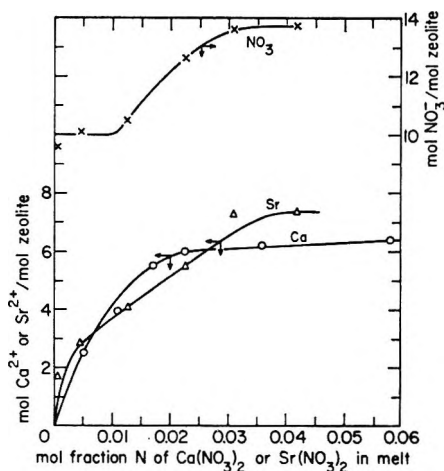


Figure 1. The exchange isotherms for the systems NaA and molten solutions of  $(\text{Na}, 1/2\text{Ca})\text{NO}_3$  ( $\circ$ ) or  $(\text{Na}, 1/2\text{Sr})\text{NO}_3$  ( $\Delta$ ) at  $330^\circ$  and the occlusion isotherm of  $\text{NO}_3^-$  from the  $(\text{Na}, 1/2\text{Ca})\text{NO}_3$  melt.

0.6, which is not different from the 22.0 expected. It is, however, interesting to note that more than 12 g-atoms of sodium was exchanged with strontium per mole of zeolite, in fact  $12.80 \pm 0.08$  mol. The experiments with strontium were limited to low concentrations because of the limitations imposed by the phase diagram.

## Discussion

The occlusion of additional nitrate ions is a function of the calcium ion concentration in the solution. It is suggested that the exchange reaction as well as the occlusion proceeds through the ion pair  $\text{CaNO}_3^+$ , since the rather voluminous calcium nitrate molecule should not find space in the already sodium filled zeolite. The ionic radii of sodium and calcium are quite close; therefore,  $\text{CaNO}_3^+$  should have the same volume and dimensions as the  $\text{NaNO}_3$  ion pair and should be able to move freely in the zeolite channel system. The assumed  $\text{CaNO}_3^+$  may also explain the clearing of room in the zeolite cage for the additional occlusion.

According to the model<sup>6</sup> for the occluded sodium zeolite, the ions can be grouped into three categories: (a) four  $\text{Na}_I\text{NO}_3\text{Na}^+$  groups, (b) four  $\text{Na}_I^+$  ions, and (c) four  $\text{Na}_{II}\text{NO}_3\text{Na}^+$  groups which are coordinated pairwise with two  $\text{Na}^+\text{NO}_3^-$  ion pairs.

The four  $\text{Na}_I\text{NO}_3\text{Na}^+$  groups in this model are

the only positions where two  $\text{Na}^+$  ions are available on the spot for exchanging with one  $\text{Ca}^{2+}$  ion, without necessitating (a) bridging of two zeolite positions by the  $\text{Ca}^{2+}$  ion or (b) disturbing the coordination between the  $\text{Na}_{II}\text{NO}_3\text{Na}^+$  group and the  $\text{Na}^+\text{NO}_3^-$  ion pairs. The replacement of the two sodium ions of the  $\text{Na}_I\text{NO}_3\text{Na}^+$  group by one  $\text{Ca}^{2+}$  ion produces some space which enables the zeolite to accept more nitrate groups. The fact that the exchange beyond the first four calcium ions proceeds by exchanging one  $\text{Na}^+$  ion for one  $\text{CaNO}_3^+$  ion pair suggests that the remaining four  $\text{Na}_I^+$  ions are now exchanged, and the zeolite reaches the composition  $8\text{Ca}_I\text{NO}_3^+$ ,  $4\text{Na}_{II}\text{NO}_3\text{Na}^+$ ,  $2\text{NaNO}_3$ ,  $12(\text{SiAlO}_4)$ .

The exchange with the larger strontium ion seems to proceed according to the same pattern as with calcium, but after a loading of four strontium cations in the zeolite no additional occlusion of nitrate molecules occurs. This can be explained either by steric reasons or by the nonexistence of such an entity as  $\text{SrNO}_3^+$  in the melt.

Kleppa's enthalpy-of-mixing,  $\Delta H^M$ , measurements for calcium and strontium nitrates in sodium nitrate<sup>6,7</sup> show that the former has higher deviations from ideality and is more stabilized in the solution:  $\Delta H^M/X = 5.0$  kcal/mol for calcium and 10.5 kcal/mol for strontium, where  $X$  is the mole fraction of the alkaline earth nitrate. The field of the strontium ion ( $z/r^2 = 1.2 \text{ \AA}^{-2}$ ) is indeed similar to that of sodium ( $1.0 \text{ \AA}^{-2}$ ), so that only calcium (with a field of  $1.8 \text{ \AA}^{-2}$ ) would be expected to organize the anions in the sodium nitrate melt to form an ion pair,  $\text{CaNO}_3^+$ , and not strontium. This view is strengthened by recent Raman work.<sup>8</sup>

A difference in behavior between calcium and strontium toward the sodium zeolite A was found also in aqueous solutions. Sherry and Walton<sup>9</sup> found that while the calcium ions are strongly bound to the lattice oxygens, only half of the strontium ions are so bound; the remainder float in the zeolite water.

The isotherms in Figure 1 do not show a significant difference in the selectivity of the zeolite for calcium and strontium in the dilute range. The initial slope, however, shows great preference for the divalent ions over sodium in this range.

*Acknowledgment.* The support of the Israel Atomic Energy Commission is gratefully acknowledged. The authors wish to thank the members of the analytical department for their support and Miss Nili Abel for her technical assistance.

(6) O. J. Kleppa and L. S. Hersh, *Discussions Faraday Soc.*, **32**, 99 (1961).

(7) O. J. Kleppa, *J. Phys. Chem.*, **66**, 1668 (1962).

(8) R. E. Hester and K. Krishnan, *J. Chem. Phys.*, **47**, 1747 (1967).

(9) H. S. Sherry and H. F. Walton, *J. Phys. Chem.*, **71**, 1457 (1967).

## The Formation of the $S_2O_4^-$ Free Radical in Dimethylformamide<sup>1</sup>

by R. G. Rinker

*Department of Chemical and Nuclear Engineering, University of California, Santa Barbara, California 93106*

and S. Lynn

*Department of Chemical Engineering, University of California, Berkeley, California 94720 (Received July 17, 1968)*

It has been shown previously<sup>2,3</sup> that reactions involving the oxidation and disproportionation of the dithionite ion,  $S_2O_4^{2-}$ , in aqueous solutions of sodium dithionite,  $Na_2S_2O_4$ , occur *via* detectable free-radical intermediates. In particular, the  $SO_2^-$  radical ion and its protonated forms appear to play a major role in the several steps leading from reactant  $S_2O_4^{2-}$  to stable products such as  $SO_4^{2-}$ ,  $SO_3^{2-}$ , and  $S^{2-}$ .

A limited amount of work was done by Hodgson<sup>4</sup> on the direct identification of free  $SO_2^-$  in aqueous solutions. He obtained a single but rather weak esr signal for  $SO_2^-$  in solutions of  $Na_2S_2O_4$  containing ice crystals. The low resolution of Hodgson's measurements provided little information about the detailed structure of the radical anion.

More recent work<sup>5,6</sup> confirmed the existence of  $SO_2^-$  from esr measurements and in addition measured its equilibrium concentration at 25° in aqueous solutions  $5 \times 10^{-3} M$  in  $Na_2S_2O_4$ . Under those conditions, the concentration of  $SO_2^-$  was  $1.8 \times 10^{-6} M$ . This value along with Cermák's<sup>7</sup> polarographic information and similar information from Fischer's<sup>8</sup> chronopotentiometric measurements was used to obtain a value of the monomerization rate constant which at 25° was found to be  $40 \text{ sec}^{-1}$ .

In studies related to the preparation of sodium dithionite in nonaqueous media,<sup>9</sup> it was found that the reduction of sulfur dioxide by sodium amalgam,  $Na(Hg)$ , in dry amide solvents and in dimethyl sulfoxide occurred *via* free-radical intermediates. In dimethylformamide (DMF) and other homologs containing no protons directly bonded to the amide group, the radical ion was unusually stable. This was apparent from its high steady-state concentration, which, in turn, was indicated by the bright blue color imparted to the solvent.

Previous investigators<sup>10-12</sup> studying the formation of  $Na_2S_2O_4$  in nonaqueous solvents have worked primarily with aliphatic alcohols and glycol ethers. The appearance of colored radical intermediates was not reported.

It was therefore important to the over-all study<sup>9</sup> to confirm and at least partially characterize the blue radical in DMF by direct measurement. To the authors' knowledge, no other work has been done on

the direct measurement of  $SO_2^-$  in nonaqueous systems.

Samples of the stabilized blue radical for esr analysis were prepared by contacting a measured quantity of  $SO_2$  with half the stoichiometric amount of  $Na(Hg)$  in a nonoxidizing, dry atmosphere. The  $SO_2$  was dissolved in dry DMF containing less than 15 ppm of  $H_2O$ , and its concentration was 0.5 *M*. The concentration of sodium in the amalgam was 0.05 wt %.

The blue radical began forming immediately upon contact of the two liquids, which were agitated by gentle swirling to avoid dispersion of the amalgam. With the reaction only partially completed, an aliquot of the DMF phase was withdrawn and injected into 1-mm diameter Pyrex tubes. The sample tubes were then sealed, inserted into the cavity of the spectrometer, and scanned. The exposed volume of each sample was 0.05 cm.<sup>3</sup> Sample tubes containing aqueous saturated solutions of  $Na_2S_2O_4$  in 0.1 *M*  $NaOH$  were also scanned for comparison with nonaqueous systems so as to aid in identifying the blue radical.

To calibrate the esr instrument, a  $Cr^{3+}$  standard in  $MgO$  was attached to one of the unknown samples. The standard contained  $1.63 \times 10^{16}$  spins corrected for traces of  $^{53}Cr$ .

For the samples containing the blue radical in DMF, a single, primary absorption band was obtained. The band was slightly asymmetric, and its width at half-peak height was 3 G. The location of the band was nearly the same as that found for  $SO_2^-$  in water,<sup>5</sup> giving a *g* value of 2.006.

Using the  $Cr^{3+}$  standard as a basis, the steady-state concentration of the blue radical was estimated to be  $10^{-3} M$ , which was nearly three orders of magnitude higher than the maximum  $SO_2^-$  concentration in water at the same temperature, 25°.

The blue radical slowly deteriorated by disproportionation in the sealed tubes. Its half-life for a second-order

(1) This work was done while R. G. R. was spending a sabbatical year at the Western Research Laboratories of the Dow Chemical Co. at Pittsburg, Calif.

(2) R. G. Rinker, T. P. Gordon, D. M. Mason, R. R. Sakaida, and W. H. Corcoran, *J. Phys. Chem.*, **64**, 573 (1960).

(3) R. G. Rinker, S. Lynn, D. M. Mason, and W. H. Corcoran, *Ind. Eng. Chem. Fund.*, **4**, 282 (1965).

(4) W. G. Hodgson, A. Neaves, and C. A. Parker, *Nature*, **178**, 589 (1956).

(5) R. G. Rinker, T. P. Gordon, D. M. Mason, and W. H. Corcoran, *J. Phys. Chem.*, **63**, 302 (1959).

(6) S. Lynn, R. G. Rinker, and W. H. Corcoran, *ibid.*, **68**, 2363 (1964).

(7) V. Cermák, *Chem. Zvesti*, **8**, 714 (1954).

(8) O. Fischer, O. Dracka, and E. Fischerová, *Coll. Czech. Chem. Commun.*, **25**, 323 (1960).

(9) R. G. Rinker and S. Lynn, unpublished data.

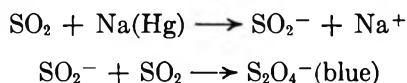
(10) Z. Krzesz, British Patent 786, 212, (Nov 13, 1957); *Chem. Abstr.*, **52**, 7631h (1958).

(11) W. P. Wang and K. S. Chia, *Chemistry (Taipei)*, **29** (1960); *Chem. Abstr.*, **55**, 2327h (1961).

(12) Ethyl Corp., British Patent 717,207, (Oct 20, 1954); *Chem. Abstr.*, **49**, 3489d (1955).

disproportionation was dependent not only on its initial concentration but also on the initial molar ratio of  $\text{SO}_2:\text{Na}$  in the  $\text{SO}_2$ -amalgam reaction. When that ratio was 2/1, the half-life of the blue radical was a maximum. At an initial radical concentration level of  $5 \times 10^{-3} M$ , the half-life was found to be approximately 100 hr at  $25^\circ$ .

Additional observations included conductance measurements and extensive stoichiometric measurements which are described in detail elsewhere.<sup>9</sup> It was found that the radical was charged and contained at least two  $\text{SO}_2$  units, giving an empirical formula of  $\text{S}_2\text{O}_4^-$ . The over-all reactions leading to the stabilized blue radical in DMF were postulated to be



At high resolution, the esr scans revealed hyperfine interactions. There were a total of four splittings or five absorption bands, which included the single primary band and four relatively weak interaction bands. These were attributed to hyperfine interaction in the natural-occurring isotope,  $^{33}\text{S}$ . The bands were too small to have any further quantitative significance. Further work in which  $^{33}\text{S}$  is added to the system is under way.

In summary, it is significant to point out that many inorganic radical ions are short-lived, and in water  $\text{SO}_2^-$  is no exception. Therefore, it was unusual and certainly unexpected to find that its stability was greatly increased in DMF. Explanations could include the absence of  $\text{H}^+$  and  $\text{OH}^-$  in the DMF, the solvent "cage" effects, and the existence of resonance structures.

### Crystal Structure Effect in the $\gamma$ Radiation of *p*-Dichlorobenzene

by F. K. Milia and E. K. Hadjoudis

Nuclear Research Center "Democritos," Athens, Greece  
(Received July 19, 1968)

It has been shown<sup>1</sup> that the measurement of the intensity of the nuclear quadrupole resonance lines can give a measure of isomorphous impurities in low concentration or impurities produced in the solid phase by irradiation with  $\gamma$  rays. In the light of the above work and in order to find a relation between the radiosensitivity and the molecular structure, Depireux<sup>2</sup> irradiated crystals of *p*-dichloro-, *p*-dibromo-, and *p*-diiodobenzene with  $^{60}\text{Co}$   $\gamma$  rays. The advantages of this method have been discussed by Duchesne,<sup>3</sup> who

used it for the study of some homologous series of organic crystals containing halogens.

In the present work, using  $\gamma$  rays, we investigate the influence of the crystal structure on the radiosensitivity with the difference that we use two different crystalline modifications of the same compound, namely, of *p*-dichlorobenzene which is known to exist in at least three different polymorphic phases.<sup>4</sup> For the present study we used the triclinic  $\beta$  form which is stable at about  $40^\circ$  and the monoclinic  $\alpha$  form which is stable around  $20^\circ$ .

This method of studying the crystal-structure effect is preferable because there is no change in the character of the C-X bond, the rupture of which is the most probable action of the  $\gamma$  radiation, and we avoid the additional factor, namely, the difference in the covalent radii of halogen X (Cl, 0.99 Å; Br, 1.14 Å; and I, 1.33 Å) which enters the previous investigations.

### Experimental Section

The spectrometer used in this work is an externally quenched superregenerative oscillator of the type described by Dean and Pollak,<sup>5</sup> with the modification that we used a voltage-dependent capacitor instead of their vibrating condenser and gave a signal:noise ratio of about 20. The sample was placed in a sealed tube; the coil of the oscillator was immersed in a thermostat bath which maintained the temperature constant to within  $0.2^\circ$ . The *p*-dichlorobenzene sample was Carlo Erba analytical grade recrystallized twice from alcohol. The  $\alpha$  and the  $\beta$  forms were prepared in each case from a solution<sup>6</sup> at 20 and  $40^\circ$ , and the resulting solid materials were kept sealed at these temperatures for more than 24 hr. X-Ray powder photographs on a Debye-Scherrer camera of radius 5.7 cm with Cu  $K\alpha$  radiation agreed with those reported before<sup>4b</sup> and thus verified that the samples were in the  $\alpha$  and the  $\beta$  form. The X-ray camera during these measurements was placed in an air thermostat which maintained the temperature at 20 and  $40^\circ$ , respectively. A 2117-Ci<sup>60</sup>Co  $\gamma$  ray source which accommodated 24 source "pencils" each containing 5 cobalt-60 slugs was used. During the irradiations the samples were held at 20 and  $40^\circ$ , respectively, by circulating water from a thermostat which maintained the temperature constant within  $0.2^\circ$ .

(1) (a) J. Duchesne and A. Monfils, *C. R. Acad. Sci. Paris*, **238**, 1801 (1954); (b) J. Duchesne, *Arch. Sci. (Geneva)*, **10**, 257 (1957); (c) A. Monfils and D. Grosjean, *Physica*, **22**, 541 (1956); (d) R. Baer and C. Dean, *J. Chem. Phys.*, **31**, 1690 (1959).

(2) J. Depireux, *Bull. Acad. Roy. Belg.*, **43**, 751 (1957).

(3) J. Duchesne, *Arch. Sci. (Geneva)*: **II**, 310 (1958).

(4) (a) G. A. Jeffrey and J. McVeagh, *J. Chem. Phys.*, **23**, 1165 (1955); (b) G. S. R. Krishna Murti and S. N. Sen, *Indian J. Phys.*, **30**, 242 (1956); (c) C. Dean and E. Linstrand, *J. Chem. Phys.*, **24**, 1114 (1956).

(5) C. Dean and M. Pollak, *Rev. Sci. Instrum.*, **29**, 630 (1958).

(6) A. I. Kitaigorodskii, Yn. V. Mnyukh, and Yn. G. Asadov, *Sov. Phys. Doklady*, **8**, 127 (1963).

A measurement of the  $\alpha$  form has also been carried out at 25° to detect any temperature dependence. We measured the height of the nuclear quadrupole resonance lines for the  $\alpha$  and  $\beta$  form before and after the  $\gamma$  radiation with a dose of  $1.1 \times 10^8$  R. In order to avoid instrumental variations the height of the line of the sample under study was always compared with that of a standard sample measured afterward.

### Results and Discussion

We found that the height of the nuclear quadrupole resonance line corresponding to the  $\alpha$  form decreased by about 21% and that of the  $\beta$  form by about 10% for the same dose of irradiation. This difference in the radio sensitivity cannot, probably, be due to a temperature effect (since the measurement of the  $\alpha$  form at 25° showed no difference from that at 20°); hence it can only be attributed to a difference in the crystal structures of the two forms. In the triclinic<sup>7</sup> arrangement all the molecules are parallel; the monoclinic arrangement is achieved by pivoting the molecules in every second layer along  $a$  about their respective centers in the  $ab$  plane followed by a translation of  $b/2$ . The intermolecular contacts of  $\text{Cl} \cdots \text{Cl}$  is 3.46 Å for the  $\beta$  form and 3.85 Å for the  $\alpha$  form.<sup>8</sup> The resulting structure of the  $\alpha$  phase is more open, and, consequently, the chlorine atoms freed from the rupture of the C-Cl bond can migrate more easily and in larger quantities into the space between the molecular planes than in the  $\beta$  form. Another reason for the greater stability of the  $\beta$  form lies in the fact that in this structure the  $\text{Cl} \cdots \text{Cl}$  intermolecular contacts are shorter than in the  $\alpha$  form. These results confirm the fact that purely crystallographic factors can affect radioresistance in the solid state.

Work is in progress at liquid nitrogen temperature where a third phase has been reported<sup>9</sup> and in other polymorphic systems also.

*Acknowledgment.* We wish to thank Mr. M. Voudouris for his valuable contribution in the development of the instrumentation and for technical assistance.

(7) J. Honstý and J. Clastre, *Acta Crystallogr.*, **10**, 695 (1957).

(8) U. Croatto, S. Bezzi, and E. Bua, *ibid.*, **5**, 825 (1952).

(9) D. E. Woessner and H. S. Gutowsky, *J. Chem. Phys.*, **39**, 440 (1963).

### The Effect of Neighboring Magnetic Anisotropy on NH Proton Chemical Shifts

by B. M. Fung

Contribution No. 372 from the Department of Chemistry, Tufts University, Medford, Massachusetts 02155  
(Received August 2, 1968)

The effect of the magnetic anisotropy of a neighboring group on the proton chemical shift of acetylene, hydro-

gen halides, several binary hydrogen compounds, and hydrocarbons has been studied.<sup>1-3</sup> We wish to discuss briefly the application of the theory of neighboring magnetic anisotropy on the NH proton chemical shift on several compounds upon protonation and coordination to Co(III).

For dilute solutions of ammonia and amines in dimethyl sulfoxide (DMSO), the NH proton chemical shift did not change with concentration. This indicated that the self-association between the solute molecules was not appreciable. Therefore the data can be treated by considering only 1:1 amine-solvent complexes. For dilute solutions of diamagnetic salts in the same solvent, the effect of ion pairing on chemical shift is not very important<sup>4</sup> and will be neglected.

The replacement of a hydrogen by a methyl group causes the NH proton signal to move downfield. The change in the series of ammonia, methylamine, and dimethylamine was fairly regular (Table I). For ethylenediamine, which has two functional groups, the NH proton signal lay between those of the primary and the secondary amines. Pyrrolidine is a secondary cyclic amine. Its NH proton signal appeared at considerably lower field than a similar open-chain secondary amine, dimethylamine. The shift is larger than that in open-chain and cyclic alkanes. In the alkanes, the anisotropy of the C-C bond in the  $\beta$  position is responsible for the difference in shielding.<sup>3</sup> It is possible that in amines the anisotropy of the C-C bond is enhanced by the neighboring nitrogen atom, which has a lone pair of electrons. Other structural differences between the two kinds of amine may also contribute to the difference in chemical shift.

Upon protonation, the NH proton resonance experienced a large downfield shift of about 6.5 ppm for ammonia and the open-chain amines. For pyrrolidine, the change was considerably smaller (Table I). The <sup>14</sup>N coupling ( $J_{\text{NH}} = 52.0 \pm 0.5$  Hz) showed up only for the most symmetrical ammonium ion; the NH proton in all other ions appeared as a slightly broadened singlet. The downfield shift of the NH proton is probably caused by three main factors: decrease in electron density, reduction of magnetic anisotropy due to increased symmetry, and enhanced hydrogen bonding with the solvent. For ammonia, if we consider a 0.25 positive charge being added to each hydrogen in forming the ammonium ion, the contribution to the local diamagnetic shielding would be  $-5.35 \times 10^{-6}$ .

(1) J. A. Pople, *Proc. Roy. Soc.*, **A239**, 550 (1951).

(2) H. M. McConnell, *J. Chem. Phys.*, **27**, 226 (1957).

(3) A. A. Bothner-By and C. Naar-Colin, *Ann. N. Y. Acad. Sci.*, **70**, 333 (1958).

(4) J. C. Fanning and R. S. Drago, *J. Amer. Chem. Soc.*, **90**, 3987 (1968).

(5) J. A. Pople, W. G. Schneider, and H. J. Bernstein, "High-Resolution Nuclear Magnetic Resonance," McGraw-Hill Book Co., Inc., New York, N. Y., 1959, p 175.

**Table I:** The NH Proton Chemical Shift of Ammonia and Some Amines Dissolved in Dimethyl Sulfoxide

	$\delta$ (from TMS), ppm	$\Delta\delta$ (from free base), ppm	
		Protonation <sup>a</sup>	Coordination to Co(III)
Ammonia	$-0.63 \pm 0.02$	$-6.45 \pm 0.02$	$-2.80 \pm 0.02^b$
Methylamine	$-1.09 \pm 0.02$	$-6.34 \pm 0.02$	
Ethylenediamine	$-1.26 \pm 0.02$	$-6.52 \pm 0.02^c$	$-4.30 \pm 0.02^d$
Dimethylamine	$-1.45 \pm 0.02$	$-6.67 \pm 0.02$	
Pyrrolidine	$-2.28 \pm 0.04$	$-6.07 \pm 0.04$	

<sup>a</sup> Perchlorate salts. <sup>b</sup> Hexaamminecobalt(III). <sup>c</sup> Diprotonated. <sup>d</sup> Tris(ethylenediamine)cobalt(III), averaged for axial and equatorial protons: B. M. Fung, *J. Amer. Chem. Soc.*, **89**, 5788 (1967).

The removal of the neighbor anisotropy changes the shielding by  $-0.25 \times 10^{-6}$ .<sup>1</sup> These two factors account for the bulk part of the observed downfield shift. For the effect of hydrogen bonding, the ammonium ion is expected to be a better proton donor than ammonia; however, the contribution to the deshielding of proton is difficult to estimate. A downfield shift of the order of 1 ppm does not seem too unreasonable in the highly basic solvent, DMSO. The argument can be extended to explain the protonation of the open-chain amines. The NH proton of pyrrolidine has a smaller downfield shift upon protonation. As a result, the over-all NH proton chemical shifts (from tetramethylsilane (TMS)) for dimethylammonium ion and pyrrolidinium ion (*ca.* 0.2 ppm) do not differ very much. The bonding of the lone electron pair to a proton apparently makes the systems behave more like normal alkanes.

When coordinated to Co(III), the protons of ammonia experienced a downfield shift of  $-2.80$  ppm (Table I). The main cause for this is again the decrease of electron density around the hydrogen atom. Cotton and Haas estimated that about 87% of the positive charges in the complex are distributed to the ligands.<sup>6</sup> From this estimation it may be considered that a positive charge of 0.14 is added to each hydrogen in forming the hexaammine cobalt(III) ion; then the proton shielding is decreased by  $3.0 \times 10^{-6}$ .<sup>5</sup> The contribution of magnetic anisotropy is probably not very large: although Co(III) has low-lying excited states, it is octahedrally symmetrical in the hexaammine complex. There may also be a small effect due to the increase of hydrogen bonding between the NH proton and the solvent.

Upon coordination to Co(III), the NH protons in ethylenediamine move to a considerably lower field than those in ammonia. The charge distribution in the two complexes is expected to be very much the same. The effect of neighbor anisotropy, however, would be quite different, which may be the cause of further deshielding for ethylenediamine. First, the symmetry of the complex is lowered from  $O_h$  to  $D_3$  in the trisene complex. The low-lying excited states of the complex may then have significant contribution to the magnetic anisotropy of the cobalt-nitrogen bond. Second, ethylene-

diamine is a bidentate ligand which forms a five-membered ring with the cobalt atom. The Co-N bond for ethylenediamine cannot rotate freely as it does for ammonia. The effect on the average anisotropy seen by the hydrogen is similar to the case of C-C bonds in aliphatic compounds. Estimated from the data in Table I,  $\Delta\chi_{Co-N}$  is probably one order of magnitude greater than  $\Delta\chi_{C-C}$ . This may also be the cause of the larger chemical shift (*ca.* 0.67 ppm) between the axial and equatorial NH protons<sup>7</sup> in the chelate than the shift between the CH protons (*ca.* 0.40 ppm) in cyclohexane. The difference in the NH proton chemical shift of ammonia and ethylenediamine was also observed for *cis*- and *trans*-[Co(en)<sub>2</sub>(NH<sub>3</sub>)<sub>2</sub>]<sup>3+</sup>,<sup>8</sup> which contains both kinds of ligand in the same molecule. This fact indicates that the effect of ring formation is the more important one.

Jolly, *et al.*, found that, in a number of cobalt(III)-pentaammine complexes, the ammonia molecule *trans* to the sixth ligand (X) has a higher field proton chemical shift than the ammonia molecules *cis* to X.<sup>9</sup> They showed that the effect is additive by studying the proton resonance of several cobalt(III)-tetraammine complexes. This effect can be readily explained by the difference in the magnetic anisotropy of the Co-X bond as seen by the protons in *trans* and *cis* positions. The length of the vector connecting the protons and the center of the Co-X bond is larger for the *trans* position than the *cis* position. However, the angle ( $\theta$ ) between this vector and the Co-X bond of usual bond distance is such that, during the rotation of the ammonia molecules about the Co-N bond,  $(3 \cos^2 \theta - 1)$  stays constant for the *trans*-protons but changes sign for the *cis*-protons. Therefore, on the average the contribution of the magnetic anisotropy to the shielding of both kinds of proton are of the same order. Interesting enough, for X = NO<sub>2</sub><sup>-</sup>, there is no difference in the chemical shift for the two kinds of protons. This is

(6) F. A. Cotton and T. E. Haas, *Inorg. Chem.*, **3**, 1004 (1964).

(7) B. M. Fung, *J. Am. Chem. Soc.*, **89**, 5788 (1967).

(8) S. T. Spees, Jr., L. J. Durham, and A. M. Sargeson, *ibid.*, **5**, 2103 (1966).

(9) W. L. Jolly, A. D. Harris, and T. S. Briggs, *ibid.*, **4**, 1064 (1965).

probably because the Co-X bond in that case is not too different from the other Co-N bonds, as far as the hydrogen atoms are concerned.

### Experimental Section

All chemicals were analytical grade. Dimethyl sulfoxide was dried over calcium hydride for 24 hr or more and was vacuum distilled over Molecular Sieve 3A.

Ammonia, methylamine, and dimethylamine were passed through a 9-ft column packed with Molecular Sieve 3A into DMSO to make up solutions. The concentration was determined by diluting the DMSO solution with water and titrating with standard HCl solution. Pyrrolidine and ethylenediamine were directly weighed for making up solutions in DMSO. The concentrations of the amines were 0.1–1.0 *N*; in this range the NH proton chemical shift of each amine did not change with the concentration within experimental error.

The perchlorate salts were prepared by passing the corresponding gases (ammonia, methylamine, and dimethylamine) or adding the liquid amines (pyrrolidine and ethylenediamine) to solutions of perchloric acid in ethanol, filtering, washing with ether, and drying under vacuum. The cobalt(III) complexes were prepared according to standard procedure<sup>10</sup> and were recrystallized from water. The concentrations of the salt solutions were 0.2–0.5 *N*. The proton nmr spectra of these solutions did not change with concentration. Proton nmr spectra were taken with a Varian A-60A spectrometer at 35°.

*Acknowledgment.* This work is supported by the National Institutes of Health.

(10) W. C. Fernelius, *Inorg. Syn.*, 2, 221 (1946).

### Conductance of Thallous Nitrate in Dioxane-Water Mixtures at 25°

by Alessandro D'Aprano<sup>1</sup> and Raymond M. Fuoss

*Sterling Chemistry Laboratory, Yale University,  
New Haven, Connecticut 06520 (Received August 5, 1968)*

Ion association in aqueous solutions of the alkali halides is undetectable by conductance at concentrations less than about 0.04 *N*, but if the range of concentration is extended to 0.1 *N* (the upper limit of applicability of the present theory), association constants of the order of unity are found.<sup>2</sup> Nitrates have been assumed to be more highly associated than halides. In order to test this assumption, we have measured the conductance of a series of nitrates in dioxane-water

mixtures at 25°. Here we present the results for thal-  
lous nitrate. In water, the association constant was  
found to be  $3.2 \pm 0.1$ , with a limiting conductance of  
146.20. From the latter, the single-ion conductance of  
the thal-  
lous ion is 74.75, in excellent agreement with an  
earlier value<sup>3</sup> of 74.71.

### Experimental Section

Fischer's Purified grade of thal-  
lous nitrate was dried  
for 24 hr at 100°; portions were then weighed in plati-  
num boats on the microbalance to make the initial  
solutions for the conductance determinations. Dilu-  
tions were made by weight and were calculated to  
volume concentrations  $c$  (equiv/l.) =  $\rho_0(1 + \gamma w)$ ,  
where  $\rho_0$  is the solvent density and  $w$  is the weight  
concentration of the salt (equiv/kg of solution). For  
thal-  
lous nitrate in water,  $\gamma = 0.232$ , from a density of  
1.035 g/ml at  $w = 0.1638$ . For solvent mixtures 2, 3, and  
4,  $\gamma = 0.212, 0.190, \text{ and } 0.141$ , respectively. For mix-  
tures 5–8, where the concentrations were less than 0.007,  
we used  $\gamma = 0.14$ . Water was laboratory supply  
distilled water, boiled vigorously and then cooled under  
nitrogen; its conductance was  $(1-2) \times 10^{-6}$  mho. Di-  
oxane was refluxed under nitrogen over potassium hy-  
droxide at least 24 hr and was then distilled under nitro-  
gen from silver nitrate just before use. (It had been  
found that dioxane distilled from potassium hydroxide  
still contained a trace impurity, undetectable by vapor-  
phase chromatography, which reduces silver and  
thal-  
lous nitrate solutions to give colloidal or mirror  
metal.)

Viscosities of the solvents were determined in an  
Ubbelohde viscometer whose water flow time was 473.1  
sec. Dielectric constants were determined at 1 Mc.<sup>4</sup>  
Four conductance cells were used, with constants  $5.1313$   
 $\pm 0.0001, 0.85696 \pm 0.00002, 0.51361 \pm 0.00004,$  and  
 $0.14464 \pm 0.00001$ . The first three were calibrated  
using potassium chloride solutions.<sup>5</sup> The fourth was  
calibrated by comparison with the second and third,  
using 0.0024 *N* tributylammonium pictrate in 2-  
propanol. The conductance bridge and general tech-  
nique were as described by Lind and Fuoss.<sup>4</sup> Solvent  
properties are summarized in Table I, where the  $\rho$  is  
the density,  $D$  is the dielectric constant,  $100\eta$  is the  
viscosity in centipoises, and  $\sigma_0$  is the solvent conduc-  
tance. The conductance data are summarized in  
Table II, where  $c$  (equiv/l.) is concentration and  $\Lambda$   
( $\text{cm}^{-2} \text{ ohm}^{-1} \text{ equiv}^{-1}$ ) is equivalent conductance.

(1) On leave of absence from the University of Palermo, Palermo, Italy.

(2) R. M. Fuoss and K. L. Hsia, *Proc. Nat. Acad. Sci. U. S.*, **57**, 1550; **58**, 1818 (1967).

(3) R. A. Robinson and C. W. Davies, *J. Chem. Soc.*, **139**, 574 (1937).

(4) J. E. Lind, Jr., and R. M. Fuoss, *J. Phys. Chem.*, **65**, 999 (1961).

(5) J. E. Lind, Jr., J. J. Zwolenik, and R. M. Fuoss, *J. Amer. Chem. Soc.*, **81**, 1557 (1959).

**Table I:** Solvent Properties

Sys-tem no.	Wt % dioxane	$\rho$ , g/ml	$D$	100 $\eta$ , cP	10 $^6\sigma_0$ , mho
1	0.0	0.99707	78.54	0.8903	1.68
2	7.8	1.0039	71.89	1.046	0.52
3	16.0	1.0109	64.49	1.210	0.55
4	36.2	1.0264	47.60	1.674	0.48
5	52.5	1.0343	33.60	1.960	0.13
6	59.2	1.0361	27.96	2.014	0.25
7	70.0	1.0369	18.95	1.953	0.122
8	76.4	1.0362	14.34	1.810	0.107

**Table II:** Conductance of Thallous Nitrate in Dioxane-Water Mixtures at 25°

10 $^4c$	$\Lambda$	10 $^4c$	$\Lambda$
$D = 78.54$			
56.370	138.438	7.211	60.528
97.110	135.866	11.792	59.392
155.385	133.019	17.982	58.190
224.598	130.291	24.999	57.088
322.34	127.167	34.855	55.816
438.60	124.142	46.319	54.608
644.36	119.756	69.513	52.718
$D = 71.89$			
39.204	122.001	2.7519	56.123
66.071	119.940	4.3712	55.324
103.978	117.764	6.650	54.383
151.812	115.619	9.301	53.464
211.177	113.465	12.962	52.411
287.46	111.136	16.616	51.509
420.91	107.858	25.351	49.714
$D = 64.49$			
62.667	104.068	1.3330	47.726
94.016	102.334	2.1763	46.302
128.629	100.748	3.2159	44.876
175.854	98.986	4.6545	43.298
232.352	97.219	6.737	41.492
350.94	94.265	9.312	39.742
$D = 47.60$			
16.773	75.858	1.0511	39.817
27.241	74.717	2.0150	36.647
40.153	73.599	2.6780	34.880
59.360	72.252	3.5200	33.237
83.616	70.888	4.6963	31.361
110.507	69.647	6.6832	29.009
160.351	67.780		
$D = 33.60$			
$D = 27.96$			
$D = 18.95$			
$D = 14.34$			

**Discussion**

Equivalent conductance depends on concentration through an equation with three parameters:  $\Lambda_0$ , the limiting conductance;  $a$ , the center-to-center contact distance between the spheres which represent the ions; and  $K_A$ , the association constant. Symbolically

$$\Lambda = \gamma(\Lambda_0 - \Delta\Lambda)[1 + (\Delta X/X)]/[1 + (3\phi/2)] \quad (1)$$

where  $\gamma$  is the ratio of the free-ion concentration to the stoichiometric,  $\Delta\Lambda$  is the electrophoretic term,  $\Delta X/X$  is the relaxation field (limiting value at low concentrations,  $-\alpha c^{1/2}$ ), and the term in the denominator allows for the detour effect. An explicit expansion of eq 1 is available.<sup>2,6</sup> Defining  $\delta\Lambda$  by

$$\delta\Lambda = \Lambda(\text{calcd}) - \Lambda(\text{obsd}) \quad (2)$$

the standard deviation is given by

$$\sigma^2 = \Sigma \delta\Lambda_j^2 / (n - 3) \quad (3)$$

where  $n$  is the number of data points. In order to determine the three parameters from the data, eq 1 is written in the form

$$\Lambda = \Lambda_0(c; \Lambda_0 + x, \bar{d} + y, K_A + z) \quad (4)$$

where  $\Lambda_0$ ,  $\bar{d}$ , and  $K_A$  are preliminary estimates of the parameters and  $x = \Delta\Lambda_0$ ,  $y = \Delta\bar{d}$ , and  $z = \Delta K_A$  are increments in their values which are chosen to satisfy the equations which minimize the standard deviation

$$\partial\sigma^2/\partial x = 0; \quad \partial\sigma^2/\partial y = 0; \quad \partial\sigma^2/\partial z = 0 \quad (5)$$

The calculation is an iterative process of successive approximations, which can be programmed for an electronic computer.

Our preferred method of analyzing the data is to give the computer a sequence of  $\bar{d}$  values and ask for the pairs of values of  $\Lambda_0$  and  $K_A$  which will minimize  $\sigma^2$  for each value of  $\bar{d}$ . Then  $\sigma$  is plotted against  $\bar{d}$ . Ideally, a curve with a sharp minimum will result, which locates the desired contact distance. Then from plots of  $K_A$  and of  $\Lambda_0$  against the corresponding  $\bar{d}$  values, the association constant and limiting conductance are interpolated, to correspond to that value of  $\bar{d}$  which minimizes  $\sigma$ . An example is shown by curve 1 in Figure 1 for thallous nitrate in water (system 1 of Table I). The  $\sigma$ - $\bar{d}$  curve has a sharp minimum at  $\bar{d} = 7.8$  where  $\sigma = 0.020 \Lambda$  unit. At  $\bar{d} = 7.0$ ,  $\sigma = 0.078$ , and at  $\bar{d} = 8.5$ ,  $\sigma = 0.092$ ; both of these values of  $\sigma$  are well beyond the experimental error.

The analysis of the data for the other systems is not so unambiguous, as shown by the other seven curves of Figure 1, which are numbered to correspond to the system numbers of Table I. For  $D = 71.89$  and 64.49, minima appear at 7.0 and 8.0, respectively, but they are not as sharp as the one in the water curve. At  $D = 47.60$ , the  $\sigma$ - $\bar{d}$  curve actually shows a slight maximum, but the entire variation in  $\sigma$  as  $\bar{d}$  goes from 5.0 to 9.0 is only 0.010  $\Lambda$  unit; within the experimental error, the  $\sigma$ - $\bar{d}$  curve is flat. In other words, any value of  $\bar{d}$  between 5.0 and 9.0 will reproduce the observed data within  $\pm 0.04 \Lambda$  unit, if the corresponding  $K_A$  and  $\Lambda_0$  values are used. The change of  $K_A$  with  $\bar{d}$  for system 4 is shown as the lower curve in Figure 2 (ordinate scale to left);  $\Lambda_0$  does not change very much

(6) Y. C. Chiu and R. M. Fuoss, *J. Phys. Chem.*, in press.

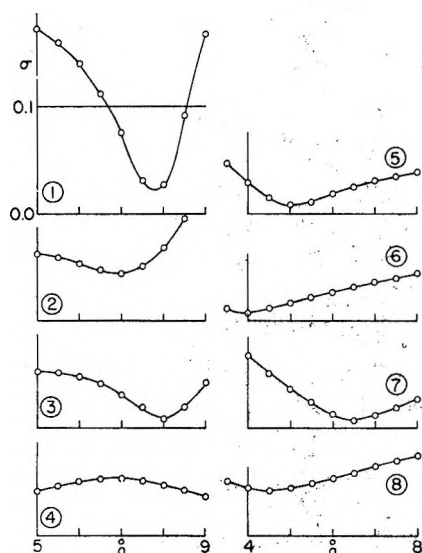


Figure 1. The method for the determination of the minimizing contact distance.

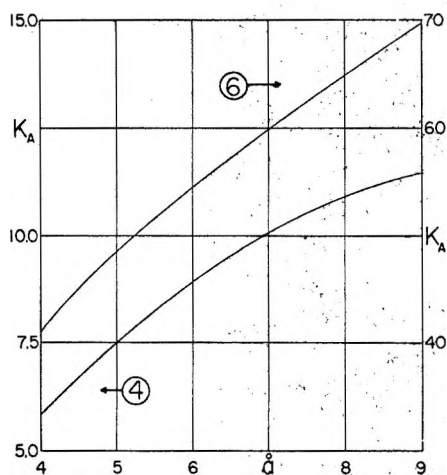


Figure 2. The values of the minimizing association constants for a range of  $\bar{d}$  values.

(79.792 at  $\bar{d} = 4.0$  to 79.866 at  $\bar{d} = 9.0$ ). It is easy to see what the difficulty is: an increase in  $\bar{d}$  increases conductance through the higher terms in electrophoresis and relaxation, while an increase in  $K_A$  decreases conductance by decreasing  $\gamma$  at a given concentration. Around  $D = 50$ , for any  $\bar{d}$  value in a reasonable range, the pair of values of  $\bar{d}$  and  $K_A$  which minimize  $\sigma$  have opposing effects on conductance which almost exactly compensate each other, and so we get a band of solutions instead of a unique solution as we did for the water case. For  $D > 50$ , the long-range terms involving  $\bar{d}$  control and the system of equations (5) can be solved for the three parameters.

For  $D < 50$ , the balance between  $\kappa\bar{d}$  effects and  $K_A$  effects is again upset;  $K_A$  now dominates the change of conductance with concentration, and the minimum reappears. However, the nature of the curves has also changed. The minima now are broad and shallow.

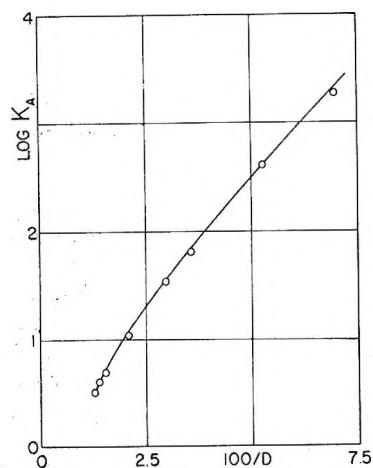


Figure 3. The dependence of association constants on the dielectric constant.

In other words,  $\bar{d}$  can again be chosen over a fairly wide range without changing  $\sigma$  by more than a few hundredths of a unit, if matching values of  $\Lambda_0$  and  $K_A$  are chosen. As an example, the minimizing  $K_A$  values for system 6 ( $D = 27.96$ ) are shown as the upper curve (ordinates to the right) of Figure 2. This insensitivity of  $\sigma$  to  $\bar{d}$  at lower dielectric constants might be expected; most of the conductance change with concentration is due to  $\gamma$ , and when  $K_A$  is large, a small change in it will therefore compensate a relatively large change due to a change in the contact distance.

A self-consistent set of parameters for all the data can be obtained by setting  $\bar{d} = 8.0$ , the average of the values found for the three systems of highest dielectric constant, and using the values of  $K_A$  and  $\Lambda_0$  for the other systems which minimize  $\sigma$  for  $\bar{d} = 8.0$ . These constants are summarized in Table III.

A plot of  $\log K_A$  against the reciprocal dielectric constant is shown in Figure 3. As in the case of the alkali halides, there is distinct curvature at the water-rich end; presumably, energy and entropy terms in  $K_A$  due to differences in interaction between solvent and ions and ion pairs as the structure of the solvent is changed from hydrogen-bonded water to an essentially unstructured water-dioxane mixture are responsible.

Table III: Derived Constants for  $\bar{d} = 8.0$

System no.	$\Lambda_0$	$K_A$	$\sigma$
1	146.195	3.2	0.028
2	128.02	4.0	0.068
3	111.64	4.9	0.008
4	79.90	10.9	0.047
5	64.17	35.0	0.038
6	58.82	65	0.043
7	51.70	408	0.026
8	47.44	1850	0.074



Below a dielectric constant of about 40, the curve approximates linearity, showing that the factor  $\exp(\epsilon^2/aDkT)$  in the association constant<sup>7</sup> is now the significant variable. The slope of the linear portion gives an  $\delta$  value of 5.35; as seen in Figure 1, this value of  $\delta$  would also give values of  $\sigma$  within experiment error and is in fact nearer to the minima of Figure 1 than 8.0. This choice of  $\delta$  for the range of low dielectric constants would, of course, force agreement between the values of  $a$  for both the association constant and for the long-range  $\kappa a$  terms, but it would involve two values (8.0 for  $D > 50$  and 5.35 for  $D < 50$ ) for the parameter. For the alkali halides, we found<sup>2</sup> that one value of the parameter sufficed for the entire range.

The single-ion conductance for thallium can be obtained from our value of  $\Lambda_0 = 146.195$  for  $\text{TlNO}_3$  in water at 25°. Using<sup>6</sup>  $\Lambda_0(\text{KCl}) = 149.93$  and Longworth's<sup>8</sup> value of 0.4906 for the limiting transference number of potassium,  $\lambda_0(\text{K}^+) = 73.56$ , where  $\lambda_0(\text{NO}_3^-) = 71.44$  from<sup>9</sup>  $\Lambda_0(\text{KNO}_3) = 144.998$ . Combining this with our  $\Lambda_0(\text{TlNO}_3)$ , we find  $\lambda_0(\text{Tl}^+) = 74.75$ , in excellent agreement with the value of 74.71 reported by Robinson and Davies,<sup>3</sup> which is based on their conductance data for thallos acetate and MacInness and Shedlovsky's results<sup>10</sup> for sodium acetate and chloride. Robinson and Davies calculated an association constant of 2.0 for thallos nitrate in water at 25°, using earlier data.<sup>11</sup> Nair and Nancollas<sup>12</sup> obtained  $K_A = 2.15$  from the solubility of thallos iodate in solutions of potassium nitrate. Our value, based on conductance, is 3.2. Finally, from the conductance data of Jones and Schumb,<sup>13</sup> we obtain  $K_A = 3.0 \pm 0.5$ , with  $\delta = 6.0$ ,  $\Lambda_0 = 147.15$ , and  $\sigma = 0.19$ . These conductances average about 0.65% high compared with our values and the value of  $\lambda_0(\text{Tl}^+)$  obtained by Robinson and Davies, and the points scatter by about  $\pm 0.1\%$ . The association constant is, however, determined by the shape of the conductance curve rather than by its absolute value (which is determined by  $\Lambda_0$ ); that is, if plotted using  $\Lambda/\Lambda_0$  as the ordinate, the data of Jones and Schumb would be distributed within  $\pm 0.1\%$  around our conductance curve, giving the same value for the association constant of thallos nitrate in water at 25°.

**Acknowledgment.** The authors acknowledge the support of this work by the Office of Saline Water, U. S. Department of The Interior, under Contract No. 14-01-0001-1308.

- (7) R. M. Fuoss, *J. Amer. Chem. Soc.*, **80**, 5059 (1958).
- (8) L. G. Longworth, *ibid.*, **54**, 2741 (1932).
- (9) L. D. McKenzie, unpublished observation in this laboratory.
- (10) D. A. MacInness and T. Shedlovsky, *ibid.*, **54**, 1429 (1932).
- (11) W. C. Bray and W. J. Winninghof, *ibid.*, **33**, 1663 (1911).
- (12) V. S. K. Nair and G. H. Nancollas, *J. Chem. Soc.*, 318 (1957).
- (13) G. Jones and W. C. Schumb, *Proc. Amer. Acad. Arts Sci.*, **56**, 199 (1921).

## The Thermochemistry of the Gas-Phase Equilibrium $2\text{CH}_3\text{I} \rightleftharpoons \text{CH}_4 + \text{CH}_2\text{I}_2$ .

### The Heat of Formation of $\text{CH}_2\text{I}_2$ <sup>1</sup>

by Shozo Furuyama,<sup>2</sup> David M. Golden, and Sidney W. Benson

*Department of Thermochemistry and Chemical Kinetics, Stanford Research Institute, Menlo Park, California 94025 (Received August 7, 1968)*

In 1965, Golden, Walsh, and Benson<sup>3</sup> studied the thermochemistry of the gas-phase equilibrium  $\text{CH}_3\text{I} + \text{HI} \rightleftharpoons \text{CH}_4 + \text{I}_2$  and determined the heat of formation ( $\Delta H^\circ$ ) of  $\text{CH}_3\text{I}$ . They also showed in that study that  $\Delta H_f^\circ(\text{CH}_2\text{I}_2(\text{g})) \geq 21.6$  kcal/mol. In this paper, we report the determination of  $\Delta H_f^\circ(\text{CH}_2\text{I}_2(\text{g}))$  from a study of the gas-phase equilibrium  $2\text{CH}_3\text{I} \rightleftharpoons \text{CH}_4 + \text{CH}_2\text{I}_2$ .

### Experimental Section

Phillips research grade methane (99.9% pure) and Mallinckrodt reagent grade, resublimed, iodine were used. Eastman methyl iodide and methylene iodide were used after purification by distillation under vacuum. Eastman iodoform was purified by recrystallization in methanol and by resublimation under vacuum and was used for calibration purposes. Purities of iodomethanes were determined to be greater than 99.5% by nmr measurements. Visible and uv absorption data for these materials are summarized in Table I.

**Table I:** Uv and Visible Spectrophotometric Data for Iodine and Iodomethanes

Compd	$\lambda_{\text{max}}$	$10^{-2}a_c^c$		
		450 $\mu\mu$	350 $\mu\mu$	300 $\mu\mu$
$\text{I}_2^a$	500	1.15	...	0.07
$\text{CH}_3\text{I}^a$	260	...	0.0026	0.200
$\text{CH}_2\text{I}_2^a$	295 vs, 250 m	...	1.80	8.25
$\text{CHI}_3^b$	340 vs, 300 vs, 270 s	...	15.2	14.5

<sup>a</sup> Measurements were done in the gas phase at 250–300°.

<sup>b</sup> This was measured in methanol solution at room temperature.

<sup>c</sup> The decadic molar extinction coefficient ( $M^{-1} \text{cm}^{-1}$ ), which is calculated by  $a_c = a_p T / (1.6 \times 10^{-2} l)$ , where  $a_p$  is the extinction coefficient in torr units and  $l$  is the optical path length of the reaction vessel ( $\sim 20$  cm).

(1) This work was supported in part by Grant No. AP-00353-04, Public Health Service, Division of Air Pollution, National Institutes of Health.

(2) Postdoctoral research associate.

(3) D. M. Golden, R. Walsh, and S. W. Benson, *J. Amer. Chem. Soc.*, **87**, 4053 (1965).

**Table II:** Equilibrium Data for  $2\text{CH}_3\text{I} \rightleftharpoons \text{CH}_4 + \text{CH}_2\text{I}_2$ 

Temp., °C	Time, hr	Torr										$\Delta H^\circ_T,^a$ kcal/ mol	$\Delta H^\circ_{298},^{b,c}$ kcal/ mol	
		(CH <sub>4</sub> ) <sub>0</sub>	(CH <sub>3</sub> I) <sub>0</sub>	(CH <sub>2</sub> I <sub>2</sub> ) <sub>0</sub>	(I <sub>2</sub> ) <sub>0</sub>	(CH <sub>4</sub> ) <sub>e</sub>	(CH <sub>3</sub> I) <sub>e</sub>	(CH <sub>2</sub> I <sub>2</sub> ) <sub>e</sub>	(I <sub>2</sub> ) <sub>e</sub>	$\Delta(\text{I}_2)$	$\Delta p$			10 <sup>3</sup> K
332.8	24	87.4	71.7	1.41	11.60	86.8	67.6	0.766	14.30	2.7	1.8	1.45	4.27	3.9
331.3	70	54.0	51.3	0	11.81	54.5	44.1	0.485	15.00	3.2	2.1	1.36	4.35	4.0
332.1	30	78.0	103.8	0	14.45	79.3	95.4	1.28	17.50	3.0	2.2	1.10	4.61	4.3
331.6	30	103.7	102.4	2.17	12.64	102.6	93.4	0.906	16.24	3.6	1.0	1.09	4.62	4.3
331.7	28	106.4	209.7	0	14.35	108.4	194.8	2.00	19.60	5.2	2.5	0.571	5.39	5.1
279.2	170	85.0	78.2	0	22.3	85.2	77.7	0.178	22.3	0	1.0	0.252	5.78	5.5
277.3	150	191.3	125.8	0.35	8.15	191.1	123.4	0.198	9.38	1.2	0.6	0.248	5.81	5.5

<sup>a</sup>  $\Delta S^\circ = -1.36$  (332°) and  $-1.38$  (278°) were used (see ref 3 and 4). <sup>b</sup>  $\Delta H^\circ_{298} = \Delta H^\circ_T + 10^{-3}\overline{\Delta C_p^\circ}_{298-T}$ ;  $\overline{\Delta C_p^\circ} = (\Delta C_{p^\circ_{298}} + \Delta C_{p^\circ_T})/2$ . <sup>c</sup>  $\overline{\Delta C_p^\circ} = 1.1$  cal/mol deg was used (see ref 3 and 4).

The slightly modified Cary 15 spectrophotometer, adapted for use with a quartz reaction vessel situated in an Al block oven, has been described in detail previously.<sup>3</sup>

The equilibrium constant for the reaction  $2\text{CH}_3\text{I} \rightleftharpoons \text{CH}_4 + \text{CH}_2\text{I}_2$  was measured in the usual way.<sup>3</sup> Several preliminary experiments showed that the rate of the reaction was very slow below 300°, while decomposition of methylene iodide was very rapid above 350°. Measurements were thus done only at 332 and 278°. About 50–200 torr of  $\text{CH}_3\text{I}$  and  $\text{CH}_4$  were introduced into the reaction vessel, with 8–22 torr of iodine as a catalyst. In some cases, 0.3–2.2 torr of  $\text{CH}_2\text{I}_2$  was introduced initially along with the  $\text{CH}_3\text{I}$  and  $\text{CH}_4$ , and equilibrium was approached from the reverse direction. After absorption in the 300–400- $\mu$  region became constant, the pressure of iodine was monitored by the absorption at 450  $\mu$ . In all of the experiments, iodine pressure increased by several torr. The approximate pressure of  $\text{CH}_2\text{I}_2$  was determined from the absorption at 350  $\mu$ , since most of the absorption at this wavelength was due to  $\text{CH}_2\text{I}_2$  (see Table I). Pressures of  $\text{CH}_4$  and  $\text{CH}_3\text{I}$  were then determined by the relations  $(\text{CH}_4) = (\text{CH}_4)_0 + \Delta(\text{CH}_2\text{I}_2)$  and  $(\text{CH}_3\text{I}) = (\text{CH}_3\text{I})_0 - 2\Delta(\text{I}_2) - 2\Delta(\text{CH}_2\text{I}_2)$ .  $2\Delta(\text{I}_2)$  comes from the decomposition of  $\text{CH}_2\text{I}_2$  or  $\text{CH}_3\text{I}$  during the reaction mentioned above. (One of the present authors suggested that the decomposition may be  $2\text{CH}_2\text{I}_2 \rightleftharpoons \text{C}_2\text{H}_4 + 2\text{I}_2$ .<sup>4</sup>  $\text{C}_2\text{H}_4$  was not identified by glpc in one run, but the fact that  $\Delta(\text{I}_2) \approx 2\Delta p$  (see Table II) supports the above suggestion. If this is the case,  $(\text{CH}_4)_e$  should be  $(\text{CH}_4)_0 + \Delta(\text{CH}_2\text{I}_2) + \Delta(\text{I}_2)$ . Whatever the mode of the decomposition,  $(\text{CH}_4)_e$  was determined with a precision of 6%, since  $\Delta(\text{I}_2)$  was less than 6% of  $(\text{CH}_4)_e$  in any experiment.) Finally,  $(\text{CH}_2\text{I}_2)_e$  was determined accurately by subtracting the calculated  $(\text{OD})_{\text{I}_2}$ 's and  $(\text{OD})_{\text{CH}_3\text{I}}$ 's from the observed OD's at 340, 320, 310, and 300  $\mu$ , where  $(\text{OD})_{\text{I}_2}$  and  $(\text{OD})_{\text{CH}_3\text{I}}$  are optical densities of iodine and methyl iodide. The precision of this measurement was  $\pm 3\%$ . (As one can see from Table I,  $\text{CHI}_3$  also has very strong absorptions at 350–300  $\mu$ , and it was feared that a precise determination of  $(\text{CH}_2\text{I}_2)$  would be

disturbed by even a small amount of  $\text{CHI}_3$ . However, the equilibrium constant of  $2\text{CH}_2\text{I}_2 \rightleftharpoons \text{CH}_3\text{I} + \text{CHI}_3$  was estimated as  $10^{-2.0}$  at 332° (see the Discussion), which means that  $(\text{CHI}_3)_e/(\text{CH}_2\text{I}_2)_e$  would be  $\sim 10^{-4}$  in this experiment. This did not disturb the determination of  $(\text{CH}_2\text{I}_2)_e$ .)

## Results and Discussion

Five experiments were made at 332° and two were made at 278°. The equilibrium constants obtained at 332° agreed well with each other with one exception. Those obtained at 278° agreed well. It is very imprecise to determine a "second-law value" of  $\Delta H^\circ$  and  $\Delta S^\circ$  from a plot of the logarithm of the equilibrium constants vs.  $1/T$ , because the equilibrium constants were measured at only two different temperatures. "Third-law values" of  $\Delta H^\circ$  were determined from combinations of the equilibrium constants obtained here with  $\Delta S^\circ$ , which was calculated from the entropies of the compounds in the JANAF Tables<sup>5</sup> and in the table of Gelles and Pitzer.<sup>6</sup>  $\Delta H^\circ_T$  thus obtained is summarized in Table II. Using  $\overline{\Delta C_p^\circ} = 1.1$  gibbs/mol,  $\Delta H^\circ_{298} = \Delta H^\circ_T + 10^{-3}\overline{\Delta C_p^\circ}_{298-T}$  was determined as  $4.7 \pm 0.07$  kcal/mol, where  $\overline{\Delta C_p^\circ}$  is  $(\Delta C_{p^\circ_{298}} + \Delta C_{p^\circ_T})/2$ .  $\Delta H^\circ_{298}(\text{CH}_2\text{I}_2) = 29.2 \pm 1.0$  kcal/mol was obtained from the  $\Delta H^\circ_{298}$  determined here, and  $\Delta H^\circ_{298}(\text{CH}_4) = -17.9$  kcal/mol<sup>5</sup> and  $\Delta H^\circ_{298}(\text{CH}_3\text{I}) = 3.3$  kcal/mol.<sup>3</sup> This not only is consistent with the previous estimation<sup>2</sup> but also agrees satisfactorily with the value, 27 kcal/mol, tabulated in the most recent National Bureau of Standards table.<sup>7</sup> (This table gives neither a reference for the error limits nor for the data source. However, it may be guessed that this comes from the combination of  $\Delta H^\circ(\text{CH}_2\text{I}_2)$  in the liquid phase with the

(4) S. W. Benson, *J. Chem. Phys.*, **38**, 1945 (1963).

(5) "JANAF Interim Thermochemical Tables," D. R. Stull, Ed., Dow Chemical Company, Midland, Mich., 1963.

(6) E. Gelles and K. S. Pitzer, *J. Amer. Chem. Soc.*, **75**, 5259 (1953).

(7) "Selected Values of Chemical Thermodynamic Properties," National Bureau of Standards Technical Note 270-3, U. S. Department of Commerce, Washington, D. C.

Table III<sup>a</sup>

	$\Delta H_f^\circ$	$\Delta(\Delta H_f^\circ)$	$\Delta[\Delta(\Delta H_f^\circ)]$
CH <sub>4</sub>	-17.9		
CH <sub>3</sub> I	3.3	21.2	4.7
CH <sub>2</sub> I <sub>2</sub>	29.2	25.9	(4.7)
CHI <sub>3</sub>	(59.8)	(30.6)	(4.7)
CI <sub>4</sub>	(95.1)	(35.3)	

<sup>a</sup>  $\Delta H_f^\circ$  is the value (in kcal/mol) at 298°K; the values in parenthesis are estimated values.

heat of vaporization. We estimate the errors of such a determination to be in excess of 1 kcal/mol.)

(CH<sub>2</sub>I<sub>2</sub>)<sub>e</sub>, determined by using various OD's in the range 300–350 mμ, was self-consistent. This further indicates that CHI<sub>3</sub> which would absorb in these regions could be disregarded in the present experimental

condition. To ensure this, an equilibrium study of the reaction  $2\text{CH}_2\text{I}_2 \rightleftharpoons \text{CH}_3\text{I} + \text{CHI}_3$  was tried at 300°. Unfortunately, it failed completely, owing to the rapid decomposition of CH<sub>2</sub>I<sub>2</sub> and/or CHI<sub>3</sub>.  $\Delta H_f^\circ(\text{CHI}_3)$  was not determined here, but the double-difference-of- $\Delta H_f^\circ$  treatment (Table III) may allow a rough estimation of it.

Using  $\Delta H_f^\circ(\text{CHI}_3) = 59.8$  kcal/mol and  $\Delta S^\circ = S^\circ(\text{CH}_3\text{I}) + S^\circ(\text{CHI}_3) - 2S^\circ(\text{CH}_2\text{I}_2) = \Delta(-R \ln \sigma)$  (where  $\sigma$  is the symmetry number),  $K = (\text{CH}_3\text{I}) \cdot (\text{CHI}_3) / (\text{CH}_2\text{I}_2)^2$  is estimated to be  $10^{-2.0}$  at 332°, which means that (CHI<sub>3</sub>)<sub>e</sub> / (CH<sub>2</sub>I<sub>2</sub>)<sub>e</sub> was usually around  $10^{-4}$  in this experiment. This is too small to affect the measurement of CH<sub>2</sub>I<sub>2</sub>.

It is interesting to note from Table III that the substitution of I for H in the methane series is accompanied by quite large nonlinear effects. That is, the second-order differences  $\Delta[\Delta(\Delta H_f^\circ)]$  of 4.7 kcal/mol are quite large. The approximation of additivity of bond energies, which is based on a zero value of the second-order differences, would predict  $\Delta H_f^\circ$  values with very large errors if applied to this series.

## COMMUNICATIONS TO THE EDITOR

### On Carbonyl Carbon-13 Hyperfine Splitting in Free Radicals and the Possible Nonplanarity of Certain Ketyls

*Sir:* The evaluation of semiempirical parameters to reproduce the <sup>13</sup>C hyperfine splitting constant (hfsc) from the carbonyl carbon of a free radical within the framework of the Karplus-Fraenkel<sup>1</sup> theory has been a subject of recent interest. The splitting is calculated from

$$a_{C=O}^C = Q_{C\rho C}^C + Q_{CO\rho C}^C + Q_{OC\rho O}^C + Q_{C'\rho C'}^C \quad (1)$$

where  $Q_C^C$  is a parameter including both spin polarization of the 1s electrons on the carbonyl carbon and of the  $\sigma$  bonds of any attached carbon atoms,  $Q_{CO}^C$  and  $Q_{OC}^C$  account for spin polarization of the carbon-oxygen bond by spin on carbon and oxygen, respectively, and  $Q_{C'}^C$  reflects the effects of spin delocalized on any of the attached carbon atoms. Strauss and Fraenkel<sup>2</sup> placed limiting values on the carbonyl parameters, while Das and Venkataraman<sup>3</sup> arrived at two sets of parameters, depending on the sign of the carbonyl <sup>13</sup>C hfsc of *p*-benzosemiquinone in ethanol. Strom and Russell<sup>4</sup> observed a 4.9-G splitting in cyclohexane-1,2-semidione,

which they attributed to the carbonyl carbon. From an evaluation of spin densities, they concluded that the Das and Venkataraman parameters of opposite sign were correct and, furthermore, that values of  $Q_{CO}^C = 10$ ,  $Q_{OC}^C = -5$  G correlated carbonyl <sup>13</sup>C splitting in three radicals rather well. Recently, however, it was found that <sup>13</sup>C hfs from carbons  $\alpha$  to the carbonyl in aliphatic semidiones is of the order of 4–5 G, while carbonyl <sup>13</sup>C splitting is 0–1 G.<sup>5</sup> The 4.9-G splitting observed by Strom and Russell<sup>4,6</sup> undoubtedly arose from the carbon  $\alpha$  to the carbonyl, and no conclusions as to carbonyl parameters should be drawn from that study.

Values for  $Q_{CO}^C$  and  $Q_{OC}^C$  have recently been obtained by Das and Fraenkel<sup>7</sup> in a more satisfying manner.

(1) M. Karplus and G. K. Fraenkel, *J. Chem. Phys.*, **35**, 1312 (1961).

(2) H. L. Strauss and G. K. Fraenkel, *ibid.*, **35**, 1738 (1961).

(3) M. R. Das and B. Venkataraman, *ibid.*, **35**, 2262 (1961).

(4) E. T. Strom and G. A. Russell, *ibid.*, **41**, 1514 (1964).

(5) G. A. Russell and G. R. Underwood, *J. Phys. Chem.*, **72**, 1074 (1968).

(6) The 5.0-G <sup>13</sup>C hfsc attributed by Ward to the carbonyl carbon in tetramethyl-1,3-cyclobutanedione ketyl (R. L. Ward, *J. Chem. Phys.*, **36**, 2230 (1962)) probably arises from the quaternary carbon.

(7) M. R. Das and G. K. Fraenkel, *ibid.*, **42**, 1350 (1965).

Their treatment did not entail any assumption of a constant value of  $Q_{C-H}^H$ , although correctness of all the pertinent Karplus-Fraenkel parameters was assumed. Das and Fraenkel obtained values for  $Q_{CO}^C$  and  $Q_{OC}^C$  of 17.7 and  $-27.1$  G, respectively. We wish to point out that these parameters will not reproduce the 49–53-G<sup>5,8</sup> carbonyl  $^{13}C$  hfsc in hexamethylacetone ketyl and to suggest that the ketyl deviates from pure  $sp^2$  hybridization, *i.e.*, is nonplanar at the carbonyl carbon.

The carbonyl  $^{13}C$  hfsc in hexamethylacetone ketyl within the Karplus-Fraenkel formulation, neglecting the small amount of spin delocalized by hyperconjugation, is calculated as

$$a_{C=O}^C = Q_{C\rho C}^C + 17.7\rho_C - 27.1\rho_O \quad (2)$$

For this radical,  $Q_C^C$  consists of the spin polarization parameter for the 1s electrons on carbon,  $S^C = -12.7$  G,<sup>1</sup> and spin polarization parameters involving the two carbonyl carbon-*t*-butyl carbon bonds,  $Q_{C-t-bu}^C$ . An estimate of the latter can be obtained by making the plausible assumption that spin polarization involving a carbonyl carbon-quaternary carbon bond is not very different from that involving an  $sp^2$  hybridized carbon-methyl carbon bond. If one uses a value of 13.57 G for  $Q_{C-t-bu}^C$ , derived from the  $^{13}C$  methyl splitting in ethyl radical,<sup>9</sup> a value of 14.44 G is obtained for  $Q_C^C$ .

Next, it is necessary to evaluate the spin density within the carbonyl function. This can be done in several ways. To a first approximation, it can be assumed that the spin density in hexamethylacetone ketyl is about the same as that in acetone ketyl. Bennett, *et al.*,<sup>10</sup> estimate the carbonyl spin density in the latter as 0.66 ( $a_{CH_3}^H = 16.4$  G). Using values of  $Q_{C-CH_3}^H$  of 20.0<sup>11,12</sup> or 26.87 G,<sup>13</sup> carbon spin densities of 0.82 and 0.61, respectively, can be calculated. Russell and Underwood<sup>5</sup> suggest that the  $^{13}C$  splitting of the quaternary carbon in hexamethylacetone ketyl might be equal to the 7.7-G methyl carbon splitting. Experimental verification of this approximate equality in di-*t*-butyl nitroxide<sup>14</sup> gives credence to this suggestion. We can then evaluate  $\rho_C$  from the parameter  $Q_{C-t-bu}^C$ , and arrive at a value of 0.57. Certainly one can say that  $\rho_C$  is in the range 0.55–0.80. Using (2), a value of 14.44 for  $Q_C^C$ , and the extreme spin densities, one calculates  $a_{C=O}^C = 5.48$  G with  $\rho_C = 0.55$  and  $a_{C=O}^C = 20.29$  G with  $\rho_C = 0.8$ . Compared to the experimental values of 49–53 G, the calculated spin densities give values of  $a_{C=O}^C$  factors of 2.5–9.5 too small.<sup>15</sup>

We feel that the disagreement between calculated and experimental results indicates *nonplanarity* at the carbonyl carbon of hexamethylacetone ketyl with the unpaired electron in an orbital having some *s* character. For an odd electron in an  $sp^3$  hybrid orbital of carbon, the predicted  $^{13}C$  hfsc is 300 G.<sup>16</sup> Thus, only a small amount of *s* character is needed for a sizeable effect on the  $^{13}C$  splitting. A similar interpretation has been

put forth for the rather large  $^{13}C$  hfscs observed in the fluorinated methyl radicals.<sup>17,18</sup>

In view of the highly alkylated nature of hexamethylacetone ketyl, a plausible explanation for slight deviation of the ketyl from planarity might lie in steric effects. The conformer of minimum energy is that in which the methyl groups are staggered. However, when the *t*-butyl groups rotate about the carbonyl carbon, unless the rotational motion is coordinated in a cogwheel fashion, methyl groups must become eclipsed. These steric repulsions could be relieved by a slight rotation of *one* of the quaternary carbons from the plane determined by the other quaternary carbon, the carbonyl carbon, and the oxygen. Such a rotation would increase steric interactions between the rotated quaternary carbon and the oxygen, but an energy minimum might lie a few degrees from planarity. It would be of interest to measure the carbonyl  $^{13}C$  splitting in acetone ketyl, where these steric effects are no longer present, and in hexafluoroacetone ketyl,<sup>19</sup> where delocalization of spin *via*  $p-\pi$  conjugation should favor planarity.

(8) N. Hirota and S. I. Weissman, *J. Amer. Chem. Soc.*, **82**, 4424 (1960).

(9) R. W. Fessenden, *J. Phys. Chem.*, **71**, 74 (1967). The positive sign is assigned on theoretical grounds (ref 2).

(10) J. E. Bennett, B. Mile, and A. Thomas, *J. Chem. Soc.*, **A**, 298 (1968).

(11) B. L. Barton and G. K. Fraenkel, *J. Chem. Phys.*, **41**, 1455 (1964).

(12) E. T. Strom, G. A. Russell, and R. Konaka, *ibid.*, **42**, 2033 (1965).

(13) R. W. Fessenden and R. H. Schuler, *ibid.*, **39**, 2147 (1963).

(14) R. Briere, H. Lemaire, and A. Rassat, *ibid.*, **48**, 1429 (1968).

(15) A referee has commented that a  $Q_C^C$  of  $\sim 21$  G can be derived from the  $\alpha$   $^{13}C$  hfs in ethyl radical. The referee further states that although this can give a calculated  $a_{C=O}^C$  as high as 28 G, this is still nearly a factor of 2 less than the experimental value.

(16) T. Cole, H. O. Pritchard, N. R. Davidson, and H. M. McConnell, *Mol. Phys.*, **1**, 406 (1958).

(17) R. W. Fessenden and R. H. Schuler, *J. Chem. Phys.*, **43**, 2704 (1965).

(18) While this manuscript was being reviewed, work was published (J. E. Bennett and L. H. Gale, *Trans. Faraday Soc.*, **64**, 1174 (1968)) in which it was concluded that ketyls of carboxylic acids are nonplanar.

(19) E. G. Janzen and J. L. Gerlock, *J. Phys. Chem.*, **71**, 4577 (1967);  $^{13}C$  splitting is presently being sought, private communication from E. G. Janzen.

MOBIL RESEARCH AND DEVELOPMENT CORPORATION  
FIELD RESEARCH LABORATORY  
DALLAS, TEXAS 75221

E. THOMAS STROM

RECEIVED MAY 24, 1968

### The Measurement of Rotary Power and Rotary Dispersion Using Polarized Rayleigh Scattering of Laser Radiation

*Sir:* The property of optical rotation in solution has long been a matter of concern in those areas where

stereochemical and other structural information is desired.<sup>1</sup> The object of this communication is to report a novel technique for the determination of optical rotatory power and circular birefringence in solution and in other optically active media in which no internal axis is specified.

Using expressions for the electric field of a laser beam incident on a medium which is circularly birefringent such that differential refractive index is

$$\Delta n = n_R - n_L \quad (1)$$

it is possible to show that the *intensity* scattered into the direction  $\theta$ , measured from the azimuth in the plane perpendicular to the direction of propagation,  $z$ , is given by<sup>2</sup>

$$I(\theta, z) \propto 1 - E_0 \cos(\Delta\gamma + k\Delta n z + 2\theta) \quad (2)$$

where  $k = 2\pi/\lambda$ ,  $\Delta\gamma$  is a difference in phase factors, and  $E_0$  is a combination of right and left circular plane wave amplitude factors.  $E_0$  has the unit magnitude for linearly polarized light for any value of  $\theta$ ; however, this quantity does change signs for the two cases.

Equation 2 indicates that as polarized light proceeds into an optically active medium, the  $z$  and  $k$  dependence combine to produce a nodal pattern in the observed Rayleigh scattering, with period  $\Delta z = \lambda/\Delta n$ . This makes it possible to determine rapidly precise values of the circular birefringence for pure transparent solids, liquids, and solutions. It is also clearly possible to determine optical rotatory dispersion using this technique over the range of available laser wavelengths.

Figure 1 indicates the nodal pattern observed in a sample of bulk polymerized polystyrene with an He-Ne laser. The nodal spacing shown corresponds to a circular birefringence of  $2.24 \times 10^{-5}$ . The birefringence in this case is due to the polymerization of polystyrene in the form of helical aggregates. The analogous value in quartz is  $6.0 \times 10^{-5}$  at  $7620 \text{ \AA}$ .

Figure 2 indicates the same effect in an aqueous solution of (+)- $\beta$ -maltose as the He-Ne laser traverses a 1.5-m path. The concentration for this figure was  $1.50 \text{ g/cm}^3$ . The birefringence,  $\Delta n$ , has been shown to have values in the range  $(3.3\text{--}4.8) \times 10^{-6}$  in the wavelength range  $4500\text{--}6328 \text{ \AA}$ , exhibiting a positive plain dispersion curve.<sup>1</sup> The value of the specific rotary power may be obtained directly at a given wavelength by dividing  $180^\circ$  by the product of the nodal spacing at the given wavelength and concentration. Also, the presently available laser wavelengths make it possible to determine fully dispersion curves over the visible region, and with minor revisions in the detection system ultraviolet and infrared dispersion curves may also be obtained.

This technique has the advantage over previous methods of eliminating path-length uncertainties in the measurement of rotatory power and rotatory dispersion. In cases where it is applicable, the technique also elimi-

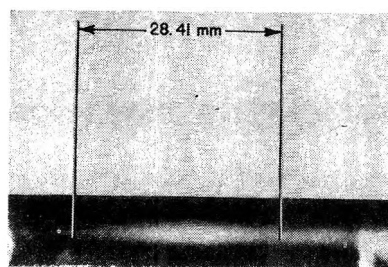


Figure 1. Intensity modulation of Rayleigh scattering in bulk polymerized polystyrene. The viewing angle,  $\theta$ , is  $90^\circ$ .

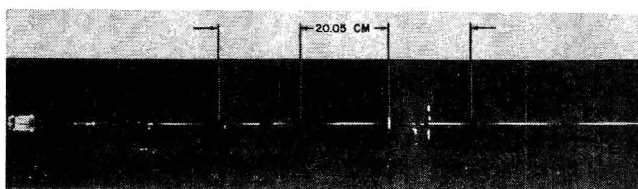


Figure 2. Intensity modulation of Rayleigh scattering in an aqueous solution of D-(+)- $\beta$ -maltose contained in a 2-m tube. The photograph was taken with a viewing angle of  $90^\circ$ .

nates the need for elaborate stabilized light sources, filters, monochromators, and detectors. In addition, precision in calculated birefringence values on the order of parts per 10,000 are, by comparison with other methods, relatively easily obtained.

(1) C. Djerassi, "Optical Rotatory Dispersion," McGraw-Hill Book Co., Inc., New York, N. Y., 1960.

(2) J. N. Gayles and A. W. Lohmann, to be published in *Applied Optics*. This later work will deal in detail with the derivation of the scattering formula.

IBM RESEARCH LABORATORY  
SAN JOSE, CALIFORNIA 95114

J. N. GAYLES  
A. W. LOHMANN

RECEIVED JULY 5, 1968

### Interpretation of the High-Resolution Electron Spin Resonance Spectrum of the 2,4,5-Triphenylimidazolyl Radical

*Sir:* The esr spectrum of the 2,4,5-biphenylimidazolyl radical (Figure 1) has been reported by Ueda<sup>1</sup> and it consists of 47 lines each having a line width of about 0.3 G. The radical may be expected to give up to 6750 lines, which suggests that each observed line consists of a number of overlapping, unresolved lines. Ueda<sup>1</sup> has proposed an interpretation based on splittings from the *ortho*, *para*, *ortho'*, and *meta* protons only and no splitting from the nitrogen atoms. The calculated line spectrum gives moderately good agreement with the observed spectrum, assuming that each peak in the observed spectrum corresponds to one line in the line spectrum. If Ueda's interpretation is plotted out as a spectrum complete with line-shape function, using a

(1) H. Ueda, *J. Phys. Chem.*, **68**, 1304 (1964).

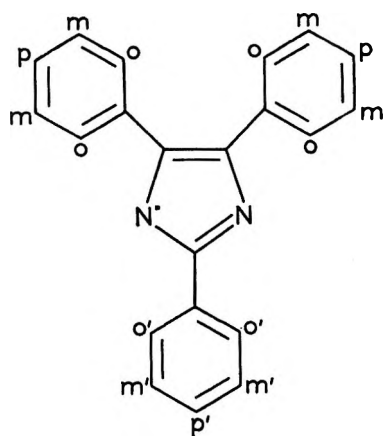


Figure 1.

computer program written for this purpose, it is clear that the interpretation is incorrect.

In order to obtain an improved interpretation, several deuterated compounds based on the 2,4,5-triphenylimidazolyl radical were prepared and their esr spectra recorded. The spectrum of 2,4,5-trideuteriophenylimidazolyl contained five partially resolved lines, corresponding to a nitrogen splitting constant of about 1.63 G. To indicate the relative magnitudes of the different proton splittings in the phenyl rings, a McLachlan<sup>2</sup> calculation was performed using the following parameters:  $h_N = 0.5 k_{CN} = 1.0 \lambda 1.2$ . Molecular models showed that the 4- and 5-phenyl rings were twisted out of coplanarity with the imidazolyl ring. The resonance integral between the rings was set to  $0.76\beta$  corresponding to an angle of twist of about  $41^\circ$ . The spin densities calculated by this method are given in Table I, together with the

Table I

	<i>ortho</i>	<i>meta</i>	<i>para</i>	<i>ortho'</i>	<i>meta'</i>	<i>para'</i>
Spin density	0.0427	-0.0167	0.045	0.0679	-0.0265	0.072
Splitting, G	1.01	0.38	1.07	1.61	0.63	1.71

calculated splittings assuming a  $Q$  of 23.7 G. With the nitrogen splitting constant at 1.44 G, spectra were computed for varying  $Q$  values. It was then found that the best fit with number, intensity, and separation of lines was with a slightly higher proportion of the spin density on the *para'* proton; the splittings (in gauss) are: *ortho*, 1.45; *meta*, 0.55; *para*, 1.52; *ortho'*, 2.33; *meta'*, 0.92; and *para'*, 2.98. The line shape used was 100% gaussian and the line width at half-power for any line was set at 0.15 G. The observed and theoretical spectra are shown in Figure 2. As a further test of the correctness of this interpretation, esr spectra were calculated for the 2-deuteriophenyl-4,5-diphenylimidazolyl, the 2-phenyl-4,5-dideuteriophenylimidazolyl,

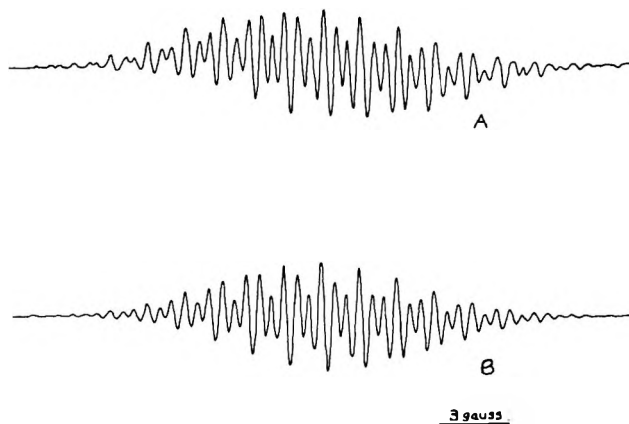


Figure 2. A is the experimental spectrum; B is the simulated spectrum.

and the fully deuterated material. The deuterium splittings were obtained by reducing the proton splittings by a factor of 6.514 and setting the nuclear spin to 1. The experimental and theoretical plots were in good agreement.

The splittings suggest that the parameters used in the preliminary McLachlan calculation are capable of improvement; it is hoped to find parameters which will give a good fit with the spectrum of this compound and with the spectra of substituted compounds.

(2) A. D. McLachlan, *Mol. Phys.*, **3**, 233 (1960).

DEPARTMENT OF CHEMISTRY  
UNIVERSITY OF NOTTINGHAM  
NOTTINGHAM, ENGLAND

M. A. J. WILKS  
M. R. WILLIS

RECEIVED JULY 8, 1968

### Effect of Dimer Formation on the Triplet States of Organic Dyes<sup>1</sup>

*Sir:* Under appropriate conditions most organic dyes will dimerize or form higher aggregates in solution. Although there have been many experimental<sup>2-12</sup> and

(1) This work was supported by a grant from the U. S. Public Health Service (No. GM 10449) and by an Aerospace Corporation Advanced Study Grant (R. W. C.).

(2) (a) Th. Förster and E. König, *Z. Elektrochem.*, **61**, 344 (1957); (b) L. V. Levshin and V. K. Gorshkov, *Opt. Spektrosk.*, **10**, 401 (1961).

(3) L. A. Ignat'eva, L. V. Levshin, T. D. Osipova, and Y. M. Polukhin, *ibid.*, **13**, 219 (1962).

(4) K. L. Arvan and N. E. Zaitseva, *ibid.*, **11**, 38 (1961).

(5) G. P. Gurinovich and T. I. Stelkova, *Biofizika*, **8**, 229 (1963).

(6) L. V. Levshin and I. S. Lonskaya, *Opt. Spektrosk.*, **11**, 148 (1961).

(7) L. V. Levshin and E. G. Baranova, *ibid.*, **6**, 31 (1959).

(8) L. V. Levshin and V. G. Bocharov, *ibid.*, **10**, 330 (1961).

(9) V. G. Bocharov and L. V. Levshin, *Izv. Akad. Nauk SSSR, Ser. Fiz. (Bull. Acad. Sci., Phys. Ser.)*, **27**, 591 (1963).

(10) L. V. Levshin, *ibid.*, **29**, 1299 (1965).

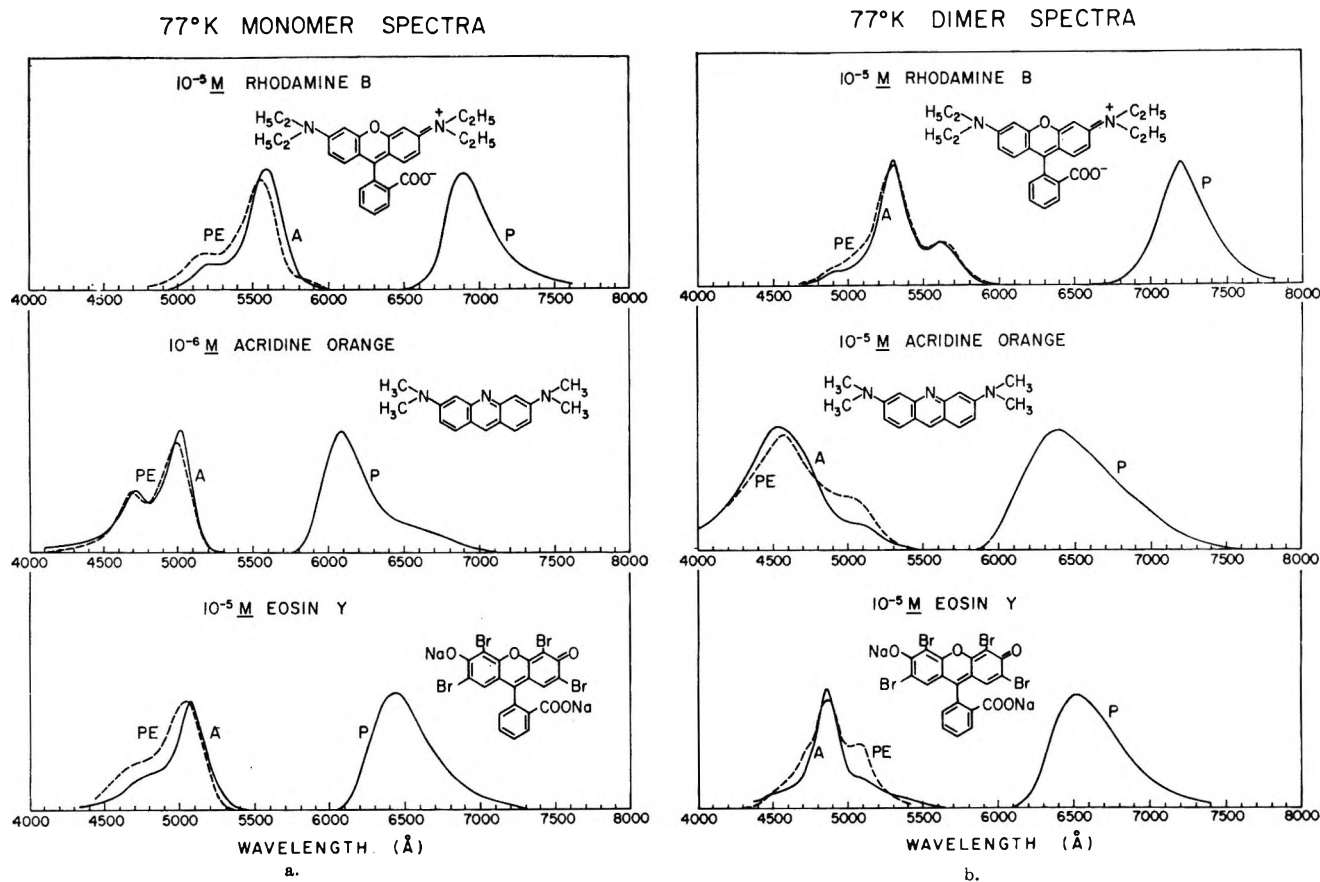


Figure 1. a, Spectral properties of dye monomers at 77°K; absorption (A), phosphorescence (P), and phosphorescence excitation (PE) spectra; solvents, 1:1 ethanol:water containing 10 M LiBr. The phosphorescence emission spectra were measured using an RCA 7265 photomultiplier. b, Spectral properties of dye dimers at 77°K; absorption (A), phosphorescence (P), and phosphorescence excitation (PE) spectra; solvents, aqueous solution with 10 M LiBr (Rhodamine B, acridine Orange), or 10 M LiCl (Eosin Y). For comparison with the direct absorption spectra, the PE spectra have been corrected for the wavelength dependence of the intensity of the exciting light. The phosphorescence emission spectra have not been corrected for the spectral response of the photomultiplier.

theoretical<sup>13-17</sup> studies of dimerization effects on excited singlet state properties, little is known about the effects of dimerization on the triplet state properties of dyes. There are several reports of dye phosphorescence which are attributed to dimer emission,<sup>18,19</sup> but the evidence is more suggestive than conclusive. In this communication we present the first unambiguous experimental evidence for *both* monomer and dimer phosphorescence from three organic dyes, describe the conditions used to obtain these emission spectra, and use these data to obtain information regarding intermolecular interactions in the triplet state.

The 77°K monomer absorption spectra of the three dyes presented in Figure 1a were obtained using dilute ( $10^{-6}$  to  $10^{-5}M$ ) solutions in aqueous 10 M LiCl or LiBr to which ethanol was added in order to suppress dimer formation. The 77°K dimer absorption spectra shown in Figure 1b were obtained using aqueous salt solutions without ethanol. Comparison of our low-temperature spectra with previously published and assigned 300°K spectra<sup>2a,20,21</sup> confirms our assignment of the low-temperature monomer and dimer spectra.

We obtained monomer and dimer phosphorescence emission spectra for these dyes (see Figure 1) by excitation of solutions known to contain primarily monomers or dimers. While we chose experimental conditions favorable to the observation of either monomer or dimer phosphorescence emission, we felt, for several reasons, that it was necessary to prove that the emission spectra were authentic. First of all these dyes are

- (11) L. V. Levshin and D. M. Akbarova, *Zh. Prikl. Spektros.*, **2**, 43 (1965).
- (12) L. V. Levshin and D. M. Akbarova, *ibid.*, **3**, 326 (1965).
- (13) E. G. McRae and M. Kasha, *J. Chem. Phys.*, **28**, 721 (1958).
- (14) E. G. McRae and M. Kasha, Bulletin 10, Institute of Molecular Biophysics, U. S. Atomic Energy Commission, July 1963.
- (15) M. Kasha, H. R. Rawls, and M. A. El Bayoumi, Bulletin 30, Institute of Molecular Biophysics, U. S. Atomic Energy Commission, Sept 1966.
- (16) J. N. Murrell and J. Tanaka, *Mol. Phys.*, **7**, 363 (1964).
- (17) E. G. McRae, *Aust. J. Chem.*, **14**, 329 (1961).
- (18) Y. V. Morozov, *Biofizika*, **8**, 388 (1963).
- (19) G. S. Levinson, W. T. Simpson, and Curtis, *J. Amer. Chem. Soc.*, **79**, 4314 (1957).
- (20) V. Zanker, *Z. Phys. Chem. (Leipzig)*, **199**, 225 (1952).
- (21) V. Zanker, *ibid.*, **200**, 250 (1952).

difficult to purify. Secondly, identification of the emitting species is complicated by the fact that the phosphorescence from one species (monomer or dimer) is generally much brighter than the other. Finally, apparent changes in phosphorescence spectra accompanying changes in the dye concentration or solvent might be due to experimental artifacts (re-absorption effect?). To eliminate these possible complications and to establish the identity of the emitting species, we simply measured the phosphorescence excitation (PE) spectra of *optically dilute* samples.<sup>22,23</sup> In the PE measurements the intensity of phosphorescence is monitored at the peak of the phosphorescence while the wavelength of the exciting light is continuously varied throughout the region in which the sample absorbs. Since the PE spectrum obtained under these conditions is essentially identical with the true absorption spectrum of the *phosphorescing* species, comparison of the PE spectrum with the known monomer or dimer absorption spectrum serves to identify the phosphorescing species. This comparison is shown in Figure 1a and 1b and convincingly establishes that the spectra reported here are authentic monomer or dimer phosphorescence spectra.<sup>24</sup>

From these data it is evident that with Eosin Y and Rhodamine B (i) the shape of the phosphorescence spectrum is the same for both the monomer and dimer, and (ii) the dimer phosphorescence is red shifted only 100–200 Å relative to the monomer. We conclude from (i) that the intermolecular separation is the same in both the ground and excited triplet states of these dimers (change much less than  $\sim 0.1$  Å judging from studies on pyrene excimers<sup>25</sup>) and from (ii) that the lowering in energy accompanying dimerization is only 300–500  $\text{cm}^{-1}$  greater for the triplet state than for the ground state. Conclusion ii also applies to Acridine Orange, but the observed change in the shape of the phosphorescence emission spectrum accompanying dimerization suggests that there is a significant change in the intermolecular separation upon excitation of the Acridine Orange dimers.

When PE measurements are combined with measurements of the relative intensities of monomer and dimer phosphorescence, it may also be possible to evaluate the effect of dimerization on various nonradiative processes in these dyes.<sup>13</sup>

(22) A. Marchetti and D. R. Kearns, *J. Amer. Chem. Soc.*, **89**, 768 (1967).

(23) D. R. Kearns and W. A. Case, *ibid.*, **88**, 5087 (1966).

(24) The "extra" long wavelength peaks in the dimer PE spectra of Acridine Orange and Eosin Y (5000 and 5100 Å, respectively) were shown to be due to excitation of residual monomers.

(25) J. B. Birks, Paper presented at 4th Molecular Crystal Symposium, July 9–12, 1968, Enschede, Netherlands.

DEPARTMENT OF CHEMISTRY  
UNIVERSITY OF CALIFORNIA  
RIVERSIDE, CALIFORNIA 92502

RICHARD W. CHAMBERS  
DAVID R. KEARNS

RECEIVED AUGUST 16, 1968

### Correlation of $\Delta H$ and $\Delta S$ for the Association of the Rare Earth(III) Ions with Fluoride<sup>1</sup>

*Sir:* In the extensive literature on the stabilities of rare earth complexes in solution, the absence of fundamental relationships representing their behavior is disappointing. Moeller, *et al.*,<sup>2</sup> attributed this situation to the concentration of effort on relatively complicated organic and polydentate ligands before the behavior of simple ligands was well understood. An important contribution has recently been made toward alleviating this deficiency by Walker and Choppin,<sup>3</sup> who reported stability and calorimetric data on the first stepwise association reactions of the tripositive rare earths cations with fluoride ion. Walker and Choppin pointed out the irregular variation with the atomic number ( $Z$ ) of the  $\Delta H$  and  $\Delta S$  associated with complex formation. They accounted for the differences in the variation of  $\Delta H$  for fluoride complexes and the variation of  $\Delta H$  for acetate complexes in terms of the greater amount of covalent character in bonding of the acetate ion to the rare earths. They attributed the relatively large  $\Delta S$  values associated with the formation of the fluoride complexes to a "dehydration" of the fluoride ion on complexing.

Linear correlations of enthalpy changes with entropy changes were first pointed out in 1938 by Barclay and Butler<sup>4</sup> for a number of vaporization processes. A similar but limited correlation of enthalpy and entropy changes has been made with early data for some ion-pair-formation reactions by Duncan and Kepert,<sup>5</sup> and more recently Kazakov, *et al.*,<sup>6</sup> have reported such a correlation for  $\Delta H^\ddagger$  and  $\Delta S^\ddagger$  of activation among various reactions involving actinide ions, but no attempts have been reported to test such a correlation for an extended series of cations with a single, simple ligand for which wide variations in  $\Delta H$  and  $\Delta S$  exist.

We wish to point out the very striking linear correlation which exists between  $\Delta H$  and  $\Delta S$  for the rare earth-fluoride complexes,  $\text{LnF}^{2+}$  (Figure 1). Over the relatively wide ranges of enthalpy and entropy changes involved, the following expression represents the  $\Delta S$  and  $\Delta H$  values of Walker and Choppin within experimental error

(1) Research sponsored by the U. S. Atomic Energy Commission under contract with the Union Carbide Corp.

(2) T. Moeller, D. F. Martin, L. C. Thompson, R. Ferrus, G. R. Feistel, and W. J. Randall, *Chem. Rev.*, **65**, 1 (1965).

(3) J. B. Walker and G. R. Choppin in "Lanthanide/Actinide Chemistry," P. R. Fields and T. Moeller, Ed., *Advances in Chemistry Series*, No. 71, American Chemical Society, Washington, D. C., 1967, pp 127–138.

(4) I. M. Barclay and J. A. V. Butler, *Trans. Faraday Soc.*, **34**, 1445 (1938).

(5) J. F. Duncan and D. L. Kepert in "The Structure of Electrolytic Solutions," W. J. Hamer, Ed., John Wiley and Sons, Inc., New York, N. Y., 1959, pp 380–400.

(6) V. P. Kazakov, B. I. Peshchevitskii, and A. M. Erenburg, *Radiokhimiya*, **6**, 291 (1964).

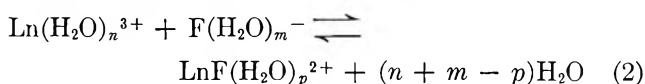


$$\Delta H(\text{kcal/mol}) = -2.38 + 0.246\Delta S \quad (1)$$

The experimental  $\log K$  for the 1:1 rare earth fluoride complexes increase with  $Z$  from 2.6 to 3.6.  $\Delta H$  is positive, however, varying from 4.0 to 9.6 kcal/mol, and it is the large positive value of  $\Delta S$  which accounts for the stability of these complexes.

The correlation between  $\Delta H$  and  $\Delta S$  is the more remarkable in view of the variations with  $Z$  of both  $\Delta H$  and  $\Delta S$ . The following trends, pointed out by Walker and Choppin, can be seen in Figure 1. In going from  ${}_{57}\text{La}^{3+}$  to  ${}_{62}\text{Sm}^{3+}$  (atomic numbers are written as subscripts to aid the reader), both  $\Delta H$  and  $\Delta S$  become more positive; then from  ${}_{63}\text{Eu}^{3+}$  to  ${}_{66}\text{Dy}^{3+}$  both become less positive; and finally from  ${}_{67}\text{Ho}^{3+}$  to  ${}_{71}\text{Lu}^{3+}$  both become more positive again.

The complexing reaction in general can be written



where  $n$ ,  $m$ , and  $p$  are unspecified hydration numbers. The number of water molecules liberated by complex formation ( $n + m - p$ ) should be at least 2, since  $\text{F}^-$  ion would displace at least one water from  $\text{Ln}(\text{H}_2\text{O})_n^{3+}$  and would give up at least one hydrate water of its own in forming the complex. Actually, the number of water molecules liberated should be considerably higher because of the reduction in outer-sphere hydration which ought to accompany the reaction of a trivalent cation with a monovalent anion to produce a divalent cationic complex. Thus it is reasonable that  $\Delta S$  and  $\Delta H$  values accompanying such a reaction are positive.

However, the changes in  $\Delta S$  and  $\Delta H$  as one proceeds through the series require a more detailed interpretation. Their steady increase with  $Z$  early in the rare earth series would suggest either (1) that the strength of the ion-dipole  $\text{Ln}^{3+}-\text{OH}_2$  bond increases more rapidly than does the strength of the ion-ion  $\text{Ln}^{3+}-\text{F}^-$  bond (*i.e.*, initially a fixed number of hydrate water molecules are bound increasingly more strongly relative to the fluoride ion as  $Z$  increases), or (2) that an increasing amount of water is liberated by complex formation as  $Z$  increases. In either case, the reversal in the upward trends of  $\Delta S$  and  $\Delta H$  beginning at  $\text{Gd}^{3+}$  and extending to  $\text{Dy}^{3+}$  could indicate a decrease in the amount of water released by complex formation. In the first case, this would suggest a decrease in the hydration number of the cation  $\text{Ln}(\text{H}_2\text{O})_n^{3+}$ , induced by the decrease in ion size, begun at about  $\text{Gd}^{3+}$  and completed at  $\text{Dy}^{3+}$ . In the second instance, wherein the hydration number of both  $\text{Ln}^{3+}$  and  $\text{LnF}^{2+}$  are viewed as being more variable, the reversal could indicate simply that the hydration number of  $\text{Ln}^{3+}$  decreases relative to that of  $\text{LnF}^{2+}$ .

Spedding,<sup>7</sup> *et al.*, have pointed out that the partial molal volumes of the rare earth chlorides show a break

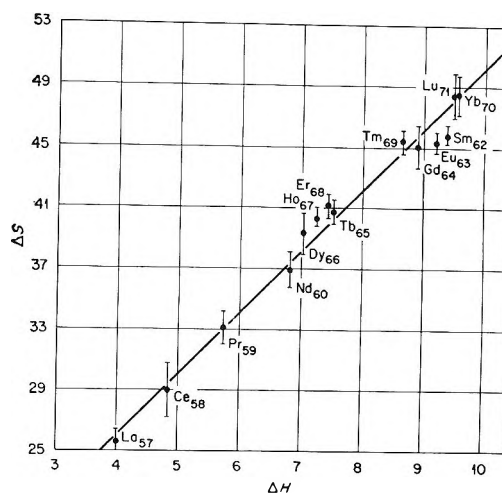


Figure 1. The change in enthalpy vs. the change in entropy for the formation of the 1:1 complex between the rare earths and fluoride.<sup>3</sup>

equivalent to about 8 ml/mol between  $\text{Nd}^{3+}$  and  $\text{Tb}^{3+}$  superimposed on the regular decrease of  $\bar{V}_2$  with  $Z$ . They have attributed this behavior to a reduction in hydration number of  $\text{Ln}^{3+}$  near the center of the series. Grenthe<sup>8</sup> and Edelin De La Praudiere, *et al.*,<sup>9</sup> similarly have invoked changes in hydration to account for the variation of  $\Delta S$  and  $\Delta H$  values associated with the formation of rare earth complexes with carboxylated ligands.

Although many have been inclined to attribute trends in the stability of rare earth complexes to ligand-field effects, there is no compelling evidence at the present time that ligand field effects are significant. The ligand field effects in the first transition series are large because the d electrons are external in the ions, but in the rare earths shielding by the  $5s^25p^6$  octet should make ligand field effects produced by the f electrons very small.<sup>1</sup>

(7) F. H. Spedding, M. J. Pikal, and B. O. Ayers, *J. Phys. Chem.*, **70**, 2440 (1966).

(8) I. Grenthe, *Acta Chem. Scand.*, **18**, 293 (1964).

(9) P. L. Edelin De La Praudiere and L. A. K. Staveley, *J. Inorg. Nucl. Chem.*, **26**, 1713 (1964).

REACTOR CHEMISTRY DIVISION  
OAK RIDGE NATIONAL LABORATORY  
OAK RIDGE, TENNESSEE 37830

R. E. MESMER  
C. F. BAES, JR.

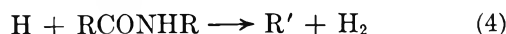
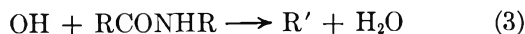
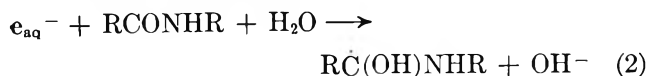
RECEIVED AUGUST 22, 1968

### On the Radiation-Induced Reduction of Amide and Peptide Functions in Aquoorganic Systems<sup>1</sup>

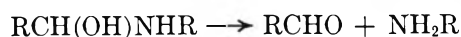
*Sir:* In the  $\gamma$  radiolysis of neutral, oxygen-free solutions of peptides such as N-acetylglycine and N-acetylalanine, the labile products of the radiation-induced step<sup>2,3</sup>



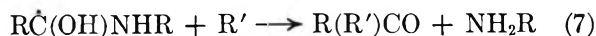
are removed through reactions of the type<sup>4,5</sup>



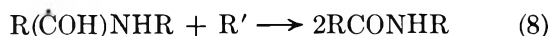
In subsequent chemistry the radical reactions which lead to net reductive cleavage of the amide linkage through intermediate formation of Schiff-type derivatives



and



(where reactions 6 and 7 show only the over-all stoichiometry for purposes of simplicity) occur in low yield. We find, for example, that the combined yield of carbonyl products ( $\text{RCO}$ )<sub>2</sub>, RCHO, and R(R')CO in neutral solutions of N-acetylglycine and N-acetylalanine corresponds to  $G(>\text{CO}) \leq 0.2$ .<sup>4b</sup> The indirect evidence is that a reconstitution reaction with the stoichiometry



represents an important path for removal of the radical species derived from  $\text{RCONHCH}(\text{R})\text{COO}^-$  through reactions 2-4.

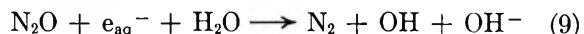
By formulating reaction 8 as a major termination reaction in the radiolysis of these systems we have assumed that the C=O linkage of the carboxylate group of the acylamino acid does not compete effectively as a trap for  $e_{\text{aq}}^-$ . This would seem to be a valid assumption, since the rate constants for reaction of  $e_{\text{aq}}^-$  with acetylglycine and acetylalanine ( $\text{RCONHCHRCOO}^-$ ) are of the order,<sup>4a</sup>  $k \sim 10^8 \text{ M}^{-1} \text{ sec}^{-1}$ , whereas for reactions of  $e_{\text{aq}}^-$  with the simple fatty acids ( $\text{RCOO}^-$ ) the rates are low,<sup>6</sup>  $k < 10^6 \text{ M}^{-1} \text{ sec}^{-1}$ .

However, the most appropriate model compounds for study of reactions 2-8 are, of course, those in which the C=O group of the amide function represents the only locus of unsaturation.

Accordingly, we have investigated the analogs of reactions 2-8 in oxygen-free solutions of acetamide and of N-ethylacetamide under  $\gamma$  radiolysis. Because of the relative simplicity of the chemistry of the aqueous acetamide system, we have been able on the basis of stoichiometric considerations to substantiate wholly the validity of the proposed reaction scheme given in eq

1-8. We report here a brief description of the experimental findings.<sup>7</sup>

To establish the locus of OH attack on acetamide and to eliminate any contribution of the back-reaction 8, we make use of the fact that dissolved  $\text{N}_2\text{O}$  converts  $e_{\text{aq}}^-$  to OH *via*<sup>8,9</sup>



where  $k_9 = 5.6 \times 10^9 \text{ M}^{-1} \text{ sec}^{-1}$ .

The data of Table I, column 1, show that the OH radicals formed *via* reactions 1 and 9 react preferentially at the methyl group of acetamide to yield the radicals  $\dot{\text{C}}\text{H}_2\text{CONH}_2$  which subsequently dimerize to give  $G(\text{succinamide}) = 2.6 \simeq (G_{\text{OH}} + G_{e_{\text{aq}}^-} + G_{\text{H}})/2$ . That the H atom also reacts with acetamide to yield  $\dot{\text{C}}\text{H}_2\text{CONH}_2$  is shown by the data obtained with 0.25 M acetamide at pH 1 (Table I, column 2). In acidic solution  $e_{\text{aq}}^-$  is converted to H *via*



where  $k_{10} = 2.3 \times 10^{10} \text{ M}^{-1} \text{ sec}^{-1}$ . Hence at pH 1 we find  $G(\text{H}_2) = 3.8 \simeq G_{\text{H}} + G_{e_{\text{aq}}^-} + G_{\text{H}_2}$ , and  $G(\text{succinamide}) = 2.5 \simeq (G_{\text{OH}} + G_{e_{\text{aq}}^-} + G_{\text{H}})/2$ . The yield of carbonyl products is essentially zero in solutions containing the electron scavengers  $\text{H}^+$  and  $\text{N}_2\text{O}$ .

**Table I:** Product Yields in the  $\gamma$  Radiolysis of Oxygen-Free Solutions of Acetamide<sup>a</sup>

Product	G value		
	pH 7 (+0.02 M N <sub>2</sub> O)	pH 1	pH 7
Succinamide	2.6	2.5	0.3
Acetaldehyde	<0.05	<0.05	0.1
Other carbonyls <sup>b</sup>	<0.05	<0.05	~0.03
Hydrogen	<i>c</i>	3.8	0.9

<sup>a</sup> 0.25 M. <sup>b</sup> Acetone plus biacetyl. <sup>c</sup> Not measured.

(1) This work was done under the auspices of the United States Atomic Energy Commission.

(2) (a) A. O. Allen, *Radiat. Res. Suppl.*, **4**, 54 (1964); (b) E. J. Hart and R. L. Platzman, *Mech. Radiobiol.*, **1**, 93 (1961); (c) C. S. Hochanadel and R. Casey, *Radiat. Res.*, **25**, 198 (1965).

(3) Recent measurements<sup>2c</sup> of the 100-eV yields for reaction 1 give  $G_{\text{OH}} = 2.59$ ,  $G_{e^-} = 2.58$ ,  $G_{\text{H}} = 0.55$ ,  $G_{\text{H}_2} = 0.45$ , and  $G_{\text{H}_2\text{O}_2} = 0.72$ .

(4) (a) R. L. Willix and W. M. Garrison, *Radiat. Res.*, **32**, 452 (1967); (b) M. A. J. Rodgers, H. A. Sokol, and W. M. Garrison, *J. Amer. Chem. Soc.*, **90**, 795 (1968); (c) W. M. Garrison, *Curr. Topics Radiat. Res.*, **4**, 45 (1968); (d) H. L. Atkins, W. Bennett-Corniea, and W. M. Garrison, *J. Phys. Chem.*, **71**, 772 (1967).

(5) (a) For purposes of simplicity, we use the general formulation RCONHR to represent both the primary amide and the monosubstituted primary amide (peptide); (b) in the radiolysis of N-acetylglycine and N-acetylalanine, OH and H attack occur at CH linkage of the main chain; *i.e.*,  $\text{R}' = \text{RCONH}\dot{\text{C}}(\text{R})\text{COOH}$ .<sup>4c</sup>

(6) For a recent compilation of rate data, see M. Anbar and P. Neta, *J. Appl. Radiat. Isotopes*, **17**, 493 (1967).

(7) Experimental procedures and analytical methods used in this work have been described in ref 4.

(8) F. S. Dainton and D. B. Peterson, *Proc. Roy. Soc.*, **A267**, 443 (1962).

(9) Rate constants,  $k_2$ , for reaction of  $e_{\text{aq}}^-$  with acetamide and N-ethylacetamide are  $1.7 \times 10^7$  and  $2 \times 10^7 \text{ M}^{-1} \text{ sec}^{-1}$ , respectively.<sup>4a,b</sup>

**Table II:** Effect of Cysteine (RSH) on the  $\gamma$ -Ray-Induced Reduction of Acetamide and N-Ethylacetamide in Oxygen-Free Solution

Amide solution (1 M, pH7) <sup>a</sup>	[RSH], M	G(CH <sub>3</sub> CHO)
Acetamide	None	~0.1
Acetamide	$4 \times 10^{-4}$	2.4 <sup>b</sup>
N-Ethylacetamide	None	<0.05
N-Ethylacetamide	$4 \times 10^{-4}$	2.8 <sup>c</sup>

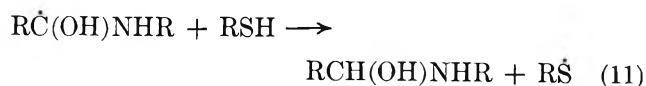
<sup>a</sup> Since the rate constant for reaction of cysteine with  $e_{aq}^-$  corresponds to  $k = 2 \times 10^{10} M^{-1} \text{sec}^{-1}$ ,<sup>8</sup> it was necessary in this series of experiments to increase the amide concentration to 1 M to ensure the preferential scavenging of  $e_{aq}^-$  by RCONHCHR. Concentrations of RSH much below  $4 \times 10^{-4} M$  are experimentally impracticable because of excessive depletion of the mercaptan during radiolysis. <sup>b</sup> This yield is dose dependent and the value 2.4 represents the extrapolated yield at zero dose. <sup>c</sup> At dosages below  $2.5 \times 10^{18} \text{eV/g}$ .

If now we examine product yields in evacuated, 0.25 M acetamide solutions at pH 7 we find, as shown in Table I, column 3, that succinamide is produced in a quite low yield ( $G(\text{succinamide}) \simeq 0.3$ ). The combined yield of carbonyl products is also low, with  $G(>\text{CO}) < 0.2$ . Detailed analytical probes of this relatively simple system have failed to reveal any other organic products in significant yield.

Since we know from the rate data that both  $e_{aq}^-$  and OH are quantitatively scavenged by acetamide in 0.25 M solution at pH 7, we are led to conclude that radical termination in this system occurs almost exclusively through the reconstitution reaction 8.

Direct substantiating evidence for the occurrence of such reaction in neutral solutions of amides and peptides

has also been obtained. We find that certain labile organic compounds, notably the thiols, RSH, are effective at low concentrations in blocking the back-reaction 8 by virtue of the H atom transfer reaction



which leads in turn to the cleavage of the amide (peptide) linkage



As indicated in Table II, acetaldehyde appears as the major product with  $G(\text{CH}_3\text{CHO}) \simeq 2.5$  in solutions of acetamide and N-ethylacetamide containing the thiol cysteine.

It is to be noted that the thiols, because of their marked reactivity, are ordinarily found to act as protective agents in the radiolysis of aqueous systems.<sup>10</sup> Of interest from both the chemical and biological standpoint is the present finding that RSH at low concentrations induces a very striking enhancement in the radiolytic lability of the amide (peptide) linkage. A detailed report of this work is in preparation.

*Acknowledgment.* We thank H. A. Sokol for assistance in developing the analytical methods.

(10) For example, see A. O. Allen, "Radiation Chemistry of Water and Aqueous Solutions," D. Van Nostrand Co., Inc., Princeton, N. J., 1961.

LAWRENCE RADIATION LABORATORY  
UNIVERSITY OF CALIFORNIA  
BERKELEY, CALIFORNIA 94720

JOHN HOLIAN  
WARREN M. GARRISON

RECEIVED SEPTEMBER 5, 1968

# ADDITIONS AND CORRECTIONS

1967, Volume 71

**Karlheinz K. Brandes and R. J. Gerdes:** The Influence of 1,4-Dioxane and Tetrahydrofuran as Solvents upon the Stability and the Solvation of Negative Ions of the Potassium Compounds of Naphthalene and Anthracene.

Pages 512 and 513. A mathematical error has been found in the calculation of the molar conductances. The molar conductivities in Table I must be multiplied by  $10^3$ . In Figures 6 and 7, the value of 3.00 has to be added to  $\log \Lambda_c$ . The molar enthalpies of dissociation and conclusions are not affected by these corrections.—K. K. BRANDES.

**Akira Takahashi, Tadayo Kato, and Mitsuru Nagasawa:** The Second Virial Coefficient of Polyelectrolytes.

Page 2002. In the Experimental Section, the third sentence should read, "... isopropyl alcohol, was dissolved in 5 l. of aqueous 0.6 N NaOH solution which contains 35% ethyl alcohol and ..."—AKIRA TAKAHASHI.

**Edward K. C. Lee:** Benzene Photosensitization of Cyclopentanone and Cyclopentanone-2-*t*.

Page 2807. Numerical values of  $N^c$  listed in the seventh column of Table II for series B runs should be multiplied by 10 and series C runs by 100. However, the corresponding quantum yields of PA in the last column of Table II are correct.

Page 2811 and 2812. Captions for Figures 1-3 have been left out inadvertently, and they should read as follows: Figure 1. Variation of sensitized decomposition quantum yield *vs.* cyclopentanone pressure (benzene pressure = 2.5 mm). Figure 2. Quenching of benzene fluorescence by cyclopentanone: series A (O) and series B (●) in Table III (benzene pressure = 2.5 mm). Figure 3. Variation of sensitized rearrangement quantum yield *vs.* cyclopentanone pressure: series A (●), series B (O), and series C (Δ) in Table II.—EDWARD K. C. LEE.

1968, Volume 72

**Donald R. Scott and F. A. Matsen:**  $d^2$  and  $d^8$  Configurations in an Axial Model Field.

Page 16. The word "changes" in line 14 of the first paragraph should read "charges."

Page 17. The expression in braces in the second column is a 6-*j* symbol.

Page 19. In the first paragraph on line 8 the sentence should read spin *triplet*. In the second sentence of the third paragraph the magnetic moment should read  $2.86 \pm 0.10$  B.M.—D. R. SCOTT.

**A. Chughtai, R. Marshall, and G. H. Nancollas:** Complexes in Calcium Phosphate Solutions.

Page 209. The following corrections should be made.

$$T_p - 2T_M + [Cl^-] - [K^+] - \frac{[Na^+] - [H^+]}{\frac{[H^+]f_1^2}{k_{1a}} - \frac{k_{2a}}{[H^+]f_2}}$$

$$-\log f_z = Az^2[I^{1/2}/(1 + I^{1/2}) - 0.3I]$$

$$[HPO_4^{2-}]^2 \left[ \frac{K + [H^+]f_2^2}{k_{2a}} \left( 1.0 + \frac{[H^+]^2 f_1^2 f_2}{k_{1a} k_{2a}} + \frac{[H^+]f_z}{k_{2a}} \right) \right] + [HPO_4^{2-}] \left( \frac{2[H^+]^2 f_1^2 f_2}{k_{1a} k_{2a}} + \frac{[H^+]f_z}{k_{2a}} - (T_P - T_M) \frac{K + [H^+]f_2^2}{k_{2a}} \right) + 2T_M - 2T_P - [Cl^-] + [H^+] + [Na^+] + [K^+] = 0$$

Page 210

$$I = 0.5 \left\{ [HPO_4^{2-}] \left( 8.0 + \frac{2[H^+]^2 f_1^2 f_2}{k_{1a} k_{2a}} + \frac{4[H^+]f_z}{k_{2a}} \right) + 2[Cl^-] + 2T_M - 2T_P \right\}$$

GEORGE H. NANCOLLAS

**D. D. Deshpande and L. G. Bhatgadde:** Sound Velocities, Adiabatic Compressibilities, and Free Volumes in Aniline Solutions.

Page 261. In this paper the excess adiabatic compressibility of the aniline-dioxane system has been reported as *positive*. It has been noticed that this was a calculation error and the sign of the excess compressibility is *negative*. The magnitude remains unaltered.—D. D. DESHPANDE.

**A. J. Dandy:** Sorption of Vapors by Sepiolite.

Page 337. In Figure 2, the right-hand ordinate should read:  $2 + \log x$  ( $x$  in g) (curve 3).—A. J. DANDY.

**Ralph F. Krause, Jr., and Thomas B. Douglas:** The Vapor Pressure, Vapor Dimerization, and Heat of Sublimation of Aluminum Fluoride, Using the Entrainment Method.

Page 476. In the first column, the last line should read, "... 1-6 mg..." instead of "... 11-16 mg..."—RALPH F. KRAUSE, JR.

**Pill-Soon Song:** Electronic Structure and Photochemistry of Flavins. IV.  $\sigma$ -Electronic Structure and the Lowest Triplet Configuration of a Flavin.

Page 538. The bottom half of the eigenvectors in Table I should be replaced with the accompanying table (*i.e.*, eigenvectors for LEMO). None of the discussion and conclusions will be affected by this correction.

Table I

	2s	2p <sub>x</sub>	2p <sub>y</sub>	2p <sub>z</sub>	2f <sub>z<sup>2</sup></sub>
LEMO 1	0.00(0.00)	0.00(0.00)	0.00(0.00)	0.275(0.083)	-0.210
2	0.00(0.00)	0.00(0.00)	0.00(0.00)	0.124(0.202)	-0.141
3	0.00(0.00)	0.00(0.00)	0.00(0.00)	0.054(0.181)	-0.056
4	0.00(0.00)	0.00(0.00)	0.00(0.00)	-0.201(-0.385)	0.213
5	0.00(0.00)	0.00(0.00)	0.00(0.00)	-0.307(-0.251)	0.289
6	0.00(0.00)	0.00(0.00)	0.00(0.00)	0.050(0.181)	-0.072
7	0.00(0.00)	0.00(0.00)	0.00(0.00)	0.185(0.182)	-0.259
8	0.00(0.00)	0.00(0.00)	0.00(0.00)	-0.148(-0.180)	0.169
9	0.00(0.00)	0.00(0.00)	0.00(0.00)	0.194(0.358)	-0.266
10	0.00(0.00)	0.00(0.00)	0.00(0.00)	0.577(0.574)	-0.508
11	0.00(0.00)	0.00(0.00)	0.00(0.00)	-0.290(-0.240)	0.255
12	0.00(0.00)	0.00(0.00)	0.00(0.00)	-0.372(-0.409)	0.416
13	0.00(0.00)	0.00(0.00)	0.00(0.00)	0.086(-0.102)	-0.009
14	0.00(0.00)	0.00(0.00)	0.00(0.00)	-0.084(-0.159)	0.187
15	0.00(0.00)	0.00(0.00)	0.00(0.00)	-0.174(-0.107)	0.184
16	0.00(0.00)	0.00(0.00)	0.00(0.00)	0.273(0.177)	-0.270
1s					
1	0.00(0.00)				
2	0.00(0.00)				
3	0.00(0.00)				
4	0.00(0.00)				
5	0.00(0.00)				
6	0.00(0.00)				

PILL-SOON SONG

R. E. Coffman, D. L. Lyle, and D. R. Mattison: Small Tunneling Effect in the Electron Paramagnetic Resonance Spectrum of Cu<sup>2+</sup>-CaO at 1.2°K.

Page 1392. Equation 1 should read

$$g_1 = g_{\perp} \tag{1a}$$

$$g_2 = (g_{\parallel}^2 \cos^2 \theta + g_{\perp}^2 \sin^2 \theta)^{1/2} \tag{1b}$$

$$g_3 = (g_{\parallel}^2 \sin^2 \theta + g_{\perp}^2 \cos^2 \theta)^{1/2} \tag{1c}$$

R. E. COFFMAN

Sidney M. Selis: Kinetics of Electrode Processes in Molten Salts. II. The Influence of Solvent Anions and Cations on the Molybdenum-Molybdenum(III) Electrode.

Page 1443. Reference 7 should read: (7) A. Klemm, "Molten Salt Chemistry," M. Blander, Ed., Interscience Publishers, New York, N. Y., 1964, pp 564, 565, 567.

Page 1445. References 15 and 16 should read, respectively: (15) M. Blander in ref 7, pp 226, 227; (16) S. H. Bauer and R. F. Porter in ref 7, p 642.—SIDNEY M. SELIS.

Ivan Haller: Thermal Isomerization of Hexafluorobicyclo-[2.2.0]hexa-2,5-diene.

Page 2885. In column 1, line 6, the word "reduces" should be replaced by "increases." As the remainder of the paragraph was based on the correct facts and not on the erroneous wording, the conclusions remain valid.—IVAN HALLER.

# AUTHOR INDEX to Volume 72, 1968

- ABRAMSON, F. P., AND FUTRELL, J. H. On the Reaction Complex of the  $C_3H_6^+-C_3H_6$  Ion-Molecule Reaction... 1826  
 ABRAMSON, F. P., AND FUTRELL, J. H. Ionic Reactions in Unsaturated Compounds. III. Propylene and the Isomeric Butenes... 1994  
 ABRAMSON, F. P. See Futrell, J. H., 1071  
 ACHE, H. J., AND WOLF, A. P. The Effect of Radiation on the Reactions of Recoil Carbon-11 in the Nitrogen-Oxygen System... 1988  
 ADAMS, D. G. See Fraenkel, G., 944  
 ADAMS, R. N. See Nelson, R. F., 740, 4336  
 ADAMSON, A. W. Response to "Comments on Temperature Dependence of Contact Angle and of Interfacial Free Energies in the Naphthalene-Water-Air System"... 2284  
 ADAMSON, A. W. See Chiang, A., 3827; Jones, J. B., 646; Perumareddi, J. R., 414; Spees, S. T., Jr., 1822  
 AFFSPRUNG, H. E. See Gregory, M. D., 1748; Grigsby, R. D., 2465; Johnson, J. R., 3223  
 AGRAWAL, M. C., AND MUSHRAN, S. P. Oxidation of Thiourea and Thioacetamide by Alkaline Hexacyanoferrate(III)... 1497  
 AHLUWALIA, J. C. See Subramanian, S., 2525  
 AHMAD, S. I. See Shukla, J. P., 1013  
 AHNELL, J. E. See Munro, D. F., 2682  
 AKITA, K., AND KASE, M. Relationship between the DTA Peak and the Maximum Reaction Rate... 906  
 ALBERINO, L. M., AND GRAESSLEY, W. W. Cross-linking of Polystyrene by High-Energy Radiation. II. Molecular Weight Changes in the Pregel Region... 4229  
 ALBRECHT, A. C. See Cadogan, K. D., 929  
 ALBRIGHT, J. G. Equations for the Description of Isothermal Diffusion in Multicomponent Systems Containing Pairs of Chemically Equivalent Components... 11  
 ALDRICH, R. G., AND KELLER, D. V., JR. A Sessile Drop Study of Liquid-Solid Adhesion for the System Indium(1)-Aluminum Using Ultrahigh Vacuum Techniques... 1092  
 ALEI, M., JR., AND FLORIN, A. E. Proton Magnetic Resonance Studies of Proton Exchange in Ethylenediamine-Water and Ammonia-Water Systems... 550  
 ALEXANDER, L. E. See Ganis, P., 3997; Northolt, M. G., 2838  
 ALGAR, B. E. See Stevens, B., 2582, 3468, 3794  
 ALLAMAN, L. See Coleman, J. S., 2605  
 ALLARD, K., MAELAND, A., SIMONS, J. W., AND FLANAGAN, T. B. Application of the Electron-Donation Model for Hydrogen Absorption to Palladium-Rich Alloys. Hydrogen-Gold-Palladium... 136  
 ALLEN, A. O. See Capellos, C., 4265; Rao, K. N., 2181; Schmidt, W. F., 3730  
 ALLENDOERFER, R. D., SMITH, G., AND WALTER, R. I. The  $A_2B_2$  Aromatic Proton Nuclear Magnetic Resonance Spectra of *para*-Substituted Anilines, Diphenylamines, and Triphenylamines... 1217  
 ALLENDORF, H. D. See Rosner, D. E., 4159  
 ALLOU, A. L., JR. See Mandelkern, L., 309  
 ALLRED, A. L., AND BUSH, LEE W. Electron Spin Resonance Spectra of Polyphenyl Anion Radicals... 2238  
 ALLRED, A. L. See Meyer, J. M., 3043  
 AL-THANNON, A., PETERSON, R. M., AND TRUMBORE, C. N. Studies in the Aqueous Radiation Chemistry of Cysteine. I. Deaerated Acidic Solutions... 2395  
 ALTUG, I., AND HAIR, M. L. Porous Glass as an Ionic Membrane... 599  
 ALTUG, I., AND HAIR, M. L. The Ion-Selective Properties of Sintered Porous Glass Membranes... 2976  
 AMATA, C. D. See Ludwig, P. K., 3725  
 AMEY, R. L. The Extent of Association in Liquid Dimethyl Sulfoxide... 3358  
 ANACKER, E. W. Comments on the Paper "Solubilization of a Water-Insoluble Dye as a Method for Determining Micellar Molecular Weights" by Hans Schott... 379  
 ANDERSON, J. H., AND PARKS, G. A. The Electrical Conductivity of Silica Gel in the Presence of Adsorbed Water... 3662  
 ANDREWS, L., AND CARVER, T. G. Infrared Spectral Evidence for Trihalomethyl lithium and -sodium Compounds in Solid Argon... 1743  
 ANSON, F. C. Analysis of the Ionic Composition of the Diffuse Double Layer in Mixed Electrolytes by Charge-Step Chronocoulometry... 727  
 ANTONIAK, C. E. See Marks, G. W., 1117  
 APPIANO, A. See Zecchina, A., 1471  
 APPLGATE, K. R. See Parker, R. C., 3177  
 ARENDS, M. See Wilkening, V. G., 185  
 ARMSTRONG, D. A. See Wilkening, V. G., 185  
 ARMSTRONG, R. D., PORTER, D. F., AND THIRSK, H. R. The Passivation of Mercury in Sulfide Ion Solutions... 2300  
 ARNOLD, D. R. See Meisels, G. G., 3061  
 ARNOLD, S. J., BROWNLEE, W. G., AND KIMBELL, G. H. Light Emission from Shock-Heated Carbon Disulfide-Argon Mixtures... 4344  
 ARTHUR, J. C., JR. See Bains, M. S., 2250  
 ASAI, K. See Ise, N., 1366  
 ASMUS, K.-D., AND FENDLER, J. H. The Reaction of Sulfurhexafluoride with Hydrated Electrons... 4285  
 ASMUS, K.-D., AND TAUB, I. A. Spectrum and Kinetics of the Hydroxynitromethane Anion Radical in Pulse-Irradiated Alkaline Nitromethane Solutions... 3382  
 ASSAAD, F. F. See Helmy, A. K., 2358  
 ASSARSSON, P., AND EIRICH, F. R. Properties of Amides in Aqueous Solution. I. A. Viscosity and Density Changes of Amide-Water Systems. B. An Analysis of Volume Deficiencies of Mixtures Based on Molecular Size Differences (Mixing of Hard Spheres)... 2710  
 ATTWOOD, D. A Light-Scattering Study of the Effect of Temperature on the Micellar Size and Shape of a Non-ionic Detergent in Aqueous Solution... 339  
 AUSLOOS, P., REBBERT, R. E., AND LIAS, S. G. Gas-Phase Photolysis of Cyclohexane in the Photoionization Region... 3904  
 AVRAMI, L. See Pai Verneker, V. R., 778  
 AYLMORE, L. A. G. See Olejnik, S., 241  
 BAAS, G. See Maatman, R., 97  
 BACCANARI, D. P., YEVITZ, M. M., AND SWAIN, H. A., JR. The Measurement of the Vapor Pressures of Carbon-14-Labeled Dodecanoic Acid from 20 to 30° Using a Modified Knudsen Effusion Method... 2243  
 BACK, R. A. See Choudhary, G., 2289  
 BADDOUR, R. F., MODELL, M., AND HEUSSER, U. K. Simultaneous Kinetic and Infrared Spectral Studies of Carbon Monoxide Oxidation on Palladium under Steady-State Conditions... 3621  
 BAES, C. F., JR. See Mesmer, R. E., 4720  
 BAINS, M. S., ARTHUR, J. C., JR., AND HINOJOSA, O. An Electron Spin Resonance Study of Intermediates Formed in  $Fe^{2+}-H_2O_2$  and  $Ce^{4+}-H_2O_2$  Systems in the Presence of  $Ti^{4+}$  Ions... 2250  
 BAIRD, M. E. Relationships between the Two Types of Frequency-Temperature Representation of Dielectric Relaxation Data... 1462  
 BALAKRISHNAN, I., AND REDDY, M. P. Homolytic Hydroxylation of Naphthalene in Oxygenated Aqueous Solutions by  $\gamma$  Radiolysis at High Temperatures... 4609  
 BALDWIN, W. H. See Raridon, R. J., 925  
 BALFOUR, F. W., AND FAGLEY, T. F. The Kinetics of the Rearrangement of 2',4'-Dinitro-2-aminodiphenyl Ether in Methyl Alcohol-Carbon Tetrachloride Solutions... 1300  
 BALZANI, V., AND CARASSITI, V. Photochemistry of Some Square-Planar and Octahedral Platinum Complexes... 383  
 BANEWICZ, J. J., MAGUIRE, J. A., AND SHIH, P. S. The Electrical Conductance of Tetraethylammonium Perchlorate in Valeronitrile... 1960  
 BÄR, F. See Smith, W. H., 369

- BARANETZKY, W. See Mukherjee, L. M., 3410
- BARANOWSKI, B., AND CUKROWSKI, A. S. The Complete Macroscopic Characteristic of Isothermal Diffusion in Binary Systems of Neutral Components. . . . . 1831
- BARD, A. J. See Maloy, J. T., 4348; Valenzuela, J. A., 286
- BAR-ELI, K. H. See Gabor, G., 153
- BARET, J. F. Kinetics of Adsorption from a Solution. Role of the Diffusion and of the Adsorption-Desorption Antagonism. . . . . 2755
- BARGER, H. J., JR., AND COLEMAN, A. J. Hydrogen-Deuterium Exchange of Propane on a Fuel-Cell Electrode. . . . . 2285
- BARIEAU, R. E. The Interpretation of Heat Capacity Measurements through Two-Component, Liquid-Liquid Critical Regions. . . . . 4079
- BARONE, G., CRESCENZI, V., AND VITAGLIANO, V. Potassium Chloride Conductance in Aqueous Solutions of a Structure-Forming Nonionic Solute, Hexamethylenetetramine. . . . . 2588
- BARRETT, E. J. See Hoyer, H. W., 4312
- BARROW, G. M., AND DATTA, P. The Relation of Rotation-Like Absorptions to Vibrational Band Contours of Molecules in Liquids. . . . . 2259
- BARROW, G. M. See Fackler, J. P., Jr., 4631
- BARTHOLOMEW, R. F., AND DONIGIAN, D. W. Kinetics of the Reaction  $\text{NO}_2(\text{g}) + \text{I}^-$  in Molten Alkali Metal Nitrates. . . . . 3545
- BARTLEY, B. H., HABGOOD, H. W., AND GEORGE, Z. M. Tracer Studies of the Isomerization of Cyclopropane over a Deuterated Zeolite Catalyst. . . . . 1689
- BASKIN, L. S. Electric Conductance and pH Measurements of Isoionic Salt-Free Bovine Mercaptalbumin Solutions. An Evaluation of Root-Mean-Square Proton Fluctuations. . . . . 2958
- BATES, R. G. See Hetzer, H. B., 2081
- BATTINO, R. Thermodynamics of Binary Solutions of Nonelectrolytes with 2,2,4-Trimethylpentane. IV. Vapor-Liquid Equilibrium (35-75°) and Volume of Mixing (25°) with Carbon Tetrachloride. . . . . 4503
- BATTINO, R. See Washington, E. L., 4496
- BATTLES, J. E., GUNDERSEN, G. E., AND EDWARDS, R. K. A Mass Spectrometric Study of the Rhenium-Oxygen System. . . . . 3963
- BAUMGARTNER, N. See Blatz, P. E., 2690
- BAUSHER, L. P. See Haake, P., 2213
- BAXENDALE, J. H., AND RODGERS, M. A. J. Electrons, Ions, and Excited States in the Pulse Radiolysis of Dioxane. . . . . 3849
- BEAR, J. L., AND LIN, C.-T. The Kinetics of Formation of Nickel Malonate and Nickel Succinate Complexes. . . . . 2026
- BEAUCHAMP, J. L. See Bowers, M. T., 3599
- BECK, A. See Turner, D. J., 2831
- BECKER, C. A. L., MEEK, D. W., AND DUNN, T. M. Crystal Field-Spin Orbit Treatment in  $d^1$  and  $d^9$  Trigonal Bipyramidal Complexes. . . . . 3588
- BECKER, R. S., AND KOLC, J. Photochromism: Spectroscopy and Photochemistry of Pyran and Thiopyran Derivatives. . . . . 997
- BELARDO, E. V. See Daniels, M., 389
- BELL, T. N., CUSSLER, E. L., HARRIS, K. R., PEPELA, C. N., AND DUNLOP, P. J. An Apparatus for Degassing Liquids by Vacuum Sublimation. . . . . 4693
- BELL, W. K., AND BROWN, L. F. A Multilayer Model for the Surface Transport of Adsorbed Gases. . . . . 2365
- BEN-NAIM, A. Solubility and Thermodynamics of Solution of Argon in the Water-Ethylene Glycol System. . . . . 2998
- BENNETT, L., NG, W. Y., AND WALKLEY, J. The Diffusion of Gases in Nonpolar Liquids. The Open-Tube Method. . . . . 4699
- BENSASSON, R. See Ottolenghi, M., 3774
- BENSON, G. C., AND SINGH, J. Excess Properties of Some Aromatic-Alicyclic Systems. III. Analysis of  $H^E$  and  $V^E$  Data in Terms of the Theory of Flory. . . . . 1345
- BENSON, G. C. See Singh, J., 1939
- BENSON, J. E., WALTERS, A. B., AND BOUDART, M. Activation of Hydrogen at 79°K by Supported Copper. . . . . 4587
- BENSON, S. W., AND SPOKES, G. N. Very Low Pressure Pyrolysis. III. *t*-Butyl Hydroperoxide in Fused Silica and Stainless Steel Reactors. . . . . 1182
- BENSON, S. W. See Furuyama, S., 3204, 4713; O'Neal, H. E., 1866
- BERAN, P., AND BRUCKENSTEIN, S. A Rotating Disk Electrode Study of the Catalytic Wave Produced by the Reduction of Iodine in the Presence of Iodate. . . . . 3630
- BERG, J. C. See Cramer, L. R., 3686
- BERGER, P. A., AND ROTH, J. F. Electron Spin Resonance Studies of Carbon Dispersed on Alumina. . . . . 3186
- BERLIN, E., AND PALLANSCH, M. J. Densities of Several Proteins and L-Amino Acids in the Dry State. . . . . 1887
- BERNDT, A. F., AND DIESTLER, D. J. On the Slope of the Liquidus and Solidus Curves at the Melting Point of a Congruently Melting Compound. . . . . 2263
- BERNSTEIN, H. J. See Rummens, F. H. A., 2111
- BERONTUS, P., AND JOHANSSON, H. Isotopic Exchange between *p*-Nitrobenzyl Chloride and Chloride Ions as Studied by Electrodeposition. . . . . 713
- BERTOZZI, G., AND SOLDANI, G. Surface Tension of Liquid Cadmium Chloride-Alkali Chloride Systems. . . . . 353
- BERTRAND, G. L., LARSON, J. W., AND HEPLER, L. G. Thermochemical Investigations of the Water-Triethylamine System. . . . . 4194
- BERTRAND, L., FRANKLIN, J. A., GOLDFINGER, P., AND HUYBRECHTS, G. The Point of Attack of a Chlorine Atom on Trichloroethylene. . . . . 3926
- BHATGADDE, L. G. See Deshpande, D. D., 261
- BHATTACHARYYA, S. N., AND MUKHERJEE, A. Excess Thermodynamic Functions of Some Binary Nonelectrolyte Mixtures. I. Measurements of Excess Gibbs Free Energy, Enthalpies, and Volumes of Mixing. . . . . 56
- BHATTACHARYYA, S. N., MITRA, R. C., AND MUKHERJEE, A. Excess Thermodynamic Functions of Some Binary Nonelectrolyte Mixtures. II. Analyses of  $g^E$ ,  $h^E$ , and  $v^E$  Data in Terms of a Generalized Quasi-Lattice Theory. . . . . 63
- BIEDERMAN, D. L. See Murty, H. N., 746
- BIEGLER, T. Composition of Electrodesorbed Methanol. . . . . 1571
- BIELSKI, B. H. J., FREEMAN, J. J., AND GEBICKI, J. M. Electron Spin Resonance of Nitrogen Dioxide in Frozen Solutions. . . . . 1721
- BIELSKI, B. H. J., AND SCHWARZ, H. A. The Absorption Spectra and Kinetics of Hydrogen Sesquioxide and the Perhydroxyl Radical. . . . . 3836
- BIELSKI, B. H. J. See Fajer, J., 1281
- BINET, D. J., GOLDBERG, E. L., AND FORSTER, L. S. Energy Transfer and Quenching of Triplet States by Chromium(III) Complexes. . . . . 3017
- BINSCH, G., AND ROBERTS, J. D. Nitrogen-15 Magnetic Resonance Spectroscopy. Coupling Constants in Hydrogen Cyanide. . . . . 4310
- BIRKHAHN, R. H. See Muller, N., 583
- BJORKLUND, S., FILIPESCU, N., MCAVOY, N., AND DEGNAN, J. Correlation of Molecular Structure with Fluorescence Spectra in Rare Earth Chelates. I. Internal Stark Splitting in Tetraethylammonium Tetrakis(dibenzoylmethido)europate(III). . . . . 970
- BLAIR, R. C., AND MUNIR, Z. A. Vapor Pressure and Heats of Sublimation of Calcium Nitride. . . . . 2434
- BLAIS, M. See Pai Verneker, V. R., 774
- BLANC, J., AND ROSS, D. L. A Procedure for Determining the Absorption Spectra of Mixed Photochromic Isomers Not Requiring Their Separation. . . . . 2817
- BLANCHARD, J., AND NAIRN, J. G. The Binding of Cholates and Glycocholate Anions by Anion-Exchange Resins. . . . . 1204
- BLANDAMER, M. J., FOSTER, M. J., HIDDEN, N. J., AND SYMONS, M. C. R. Ultrasonic Relaxation in 3,3-Diethylpentane and Its Relation to That in Alkylammonium Ions. . . . . 2268
- BLANDER, M. See Guion, J., 2086, 4620
- BLANK, B. A. H., AND SEARCY, A. W. The Rate of Sublimation of Magnesium Nitride from Effusion Cells and from Free Surfaces *in Vacuo* and in Argon and Nitrogen Gases. . . . . 2241
- BLASCO, P. A. See Martire, D. E., 3489
- BLEARS, D. J., DANYLUK, S. S., AND BOCK, E. Motional Properties of Polycrystalline Tetramethylammonium Bromide. . . . . 2269
- BLATZ, L. A., AND WALDSTEIN, P. Low-Frequency Raman Spectra of Aqueous Solutions of Formates and Acetates. . . . . 2614
- BLATZ, P. E., BAUMGARTNER, N., AND DEWHURST, S. The Spectra of Polyene-Iodine Complexes. . . . . 2690
- BLAUER, J. A. The Kinetics of Dissociation of Hydrogen Fluoride behind Incident Shock Waves. . . . . 79
- BLAUER, J. A., AND SOLOMON, W. C. The Thermal Dissociation of Oxygen Difluoride. I. Incident Shock Waves. . . . . 2307
- BLAUER, J. A. See Solomon, W. C., 2311
- BLOOM, H., AND HASTIE, J. W. Transpiration Vapor Pressure Measurements for the Molten Salt Systems  $\text{PbCl}_2 + \text{CsCl}$  and  $\text{CdCl}_2 + \text{CsCl}$ . . . . . 2361
- BLOOM, H., AND HASTIE, J. W. Mass Spectrometry of

- the Vapors over  $\text{PbCl}_2 + \text{ACl}$  Mixtures ( $A = \text{Na, K, Rb, or Cs}$ ). I. Thermodynamic Studies. . . . . 2706
- BLOOM, H., HASTIE, J. W., AND MORRISON, J. D. Ionization and Dissociation of the Alkali Halides by Electron Impact. . . . . 3041
- BLOOR, J. E., AND BREEN, D. L. Valence Shell Calculations on Polyatomic Molecules. II. CNDO SCF Calculations on Monosubstituted Benzenes. . . . . 716
- BLOUNT, H. N., AND HERMAN, H. B. Chronopotentiometric Measurements of Chemical Reaction Rates. II. Kinetics and Mechanism of the Dehydration of *p*-Hydroxyphenylhydroxylamine. . . . . 3006
- BOCK, E. See Blears, D. J., 2269
- BOEYENS, J. C. A. See Kruger, G. J., 2120
- BONNER, O. D. Solute-Solvent Interactions in Aqueous Media. . . . . 2512
- BONNER, O. D., RUSHING, C., AND TORRES, A. L. The Osmotic and Activity Coefficients of Some Bolaform Electrolytes. . . . . 4290
- BONNER, O. D., AND WOOLSEY, G. B. The Effect of Solutes and Temperature on the Structure of Water. . . . . 899
- BONOLI, L., AND WITHERSPOON, P. A. Diffusion of Aromatic and Cycloparaffin Hydrocarbons in Water from 2 to 60°. . . . . 2532
- BORGARDT, F. G. See Marshall, H. P., 1513
- BORNONG, B. J. See Martin, P., Jr., 4172
- BOSTON, C. R., JAMES, D. W., AND SMITH, G. P. The Ultraviolet Spectrum of the Nitrate Ion in Molten Mixtures of Alkali Metal Nitrates. . . . . 293
- BOTHNER-BY, A. A. See Cox, R. H., 1642, 1646
- BOTTINGA, Y. Calculation of Fractionation Factors for Carbon and Oxygen Isotopic Exchange in the System Calcite-Carbon Dioxide-Water. . . . . 800
- BOTTINGA, H. Hydrogen Isotope Equilibria in the System Hydrogen-Water. . . . . 4338
- BOUDART, M. See Benson, J. E., 4587; Delgass, W. N., 3563
- BOURÉNE, M. See Meaburn, G. M., 3920
- BOWDEN, M. J., AND O'DONNELL, J. H. Radiation-Induced Solid-State Polymerization of Derivatives of Methacrylic Acid. IV. Electron Spin Resonance Spectra of Barium Methacrylate Dihydrate. . . . . 1577
- BOWERS, M. T., ELLEMAN, D. D., AND BEAUCHAMP, J. L. Ion Cyclotron Resonance of Olefins. I. A Study of the Ion-Molecule Reactions in Electron-Impacted Ethylene. . . . . 3599
- BOYD, G. E., LARSON, Q. V., AND LINDENBAUM, S. Heat Capacity Changes in Ion-Exchange Reactions. The Exchange of Tetra-*n*-butylammonium with Sodium Ion in Cross-Linked Polystyrenesulfonate. . . . . 2651
- BRASWELL, E. Evidence for Trimerization in Aqueous Solutions of Methylene Blue. . . . . 2477
- BRAUSSE, G., MAYER, A., NEDETZKA, T., SCHLECT, P., AND VOGEL, H. Water Adsorption and Dielectric Properties of Lyophilized Hemoglobin. . . . . 3098
- BREBRICK, R. F. Tellurium Vapor Pressure and Optical Density at 370-615°. . . . . 1032
- BREDIG, M. A. See Dworkin, A. S., 1277, 1892
- BREEN, D. L. See Bloor, J. E., 716
- BREESE, K. See Bull, H. B., 1817
- BREITER, M. W. Adsorption and Oxidation of Carbon Monoxide on Platinized Platinum Electrodes. . . . . 1305
- BRESLOW, R. See Kispert, L. D., 4276
- BREY, W. S., JR., SCOTT, K. N., AND WHITMAN, D. R. Temperature Dependence of Nuclear Magnetic Resonance Coupling Constants and Chemical Shifts of the Vinyl Halides and Some Vinyl Ethers. . . . . 4351
- BREY, W. S., JR., AND WILLIAMS, H. P. Dielectric Properties of Ice and Water Clathrates. . . . . 49
- BREY, W. S., JR. See Porter, D. M., 650
- BRINCKMAN, F. E. See Johannesen, R. B., 660
- BRINTON, R. K. The Gaseous Photolysis of the Methylene-cycloalkanes. . . . . 321
- BROADUS, J. D., AND VAUGHAN, J. D. Dipole Moments of 1-Alkylpyrazoles in Nonpolar and Polar Solvents. . . . . 1005
- BROADWATER, T. L. See Evans, D. F., 1037
- BROCK, J. R. Some New Modes of Aerosol Particle Motion: Photodiffusiophoresis. . . . . 747
- BRONSKILL, M. J., AND HUNT, J. W. A Pulse-Radiolysis System for the Observation of Short-Lived Transients. . . . . 3762
- BRONSTEIN, H. R. See Dworkin, A. S., 1892
- BROOKS, J. M., AND DEWALD, R. R. Absorption Spectra of the Alkali Metals in Hexamethylphosphoramide. . . . . 2655
- BROWN, G. H. See DeSando, R. J., 1088
- BROWN, L. F. See Bell, W. K., 2365
- BROWNLEE, W. G. See Arnold, S. J., 4344
- BRUCKENSTEIN, S. See Beran, P., 3630
- BRUNNER, R. S. See Oberth, A. E., 845
- BRUMBERGER, H., AND SMITH, W. H. Kinetics of the Gas-Phase Reactions of Diborane with Methylphosphines and Trimethylamine. . . . . 3340
- BRUMMER, S. B. See Taylor, A. H., 2856
- BRYANT, J. T. See Pritchard, G. O., 1603
- BRYNESTAD, J., AND SMITH, G. P. Isobestic Points and Internally Linear Spectra Generated by Changes in Solvent Composition Temperature. . . . . 296
- BUCHANAN, A. S., AND McRAE, J. A. Mercury-Photosensitized Decomposition of Acetaldehyde. Evidence for a Two-Quantum Process. . . . . 3052
- BUDDENBAUM, W. E. See Huang, T. T.-S., 4431
- BUFALINI, M., AND TODD, J. E. Formation of Hydrogen in the Photolysis of Diborane at 1849 Å. . . . . 3367
- BULL, H. B., AND BREESE, K. Temperature Coefficients of Protein Partial Volumes. . . . . 1817
- BUNDSCHUH, J. E., AND LI, N. C. Nuclear Magnetic Resonance Studies of Proton-Exchange Kinetics of *N*-Methylacetamide and *N*-Acetylglycine *N*-Methylamide. . . . . 1001
- BURKHART, M. J. See Sullivan, J. C., 2675
- BURNHAM, D. A., AND EYRING, L. Phase Transformations in the Praseodymium Oxide-Oxygen System: High-Temperature X-Ray Diffraction Studies. . . . . 4415
- BURNHAM, D. A., EYRING, L., AND KORDIS, J. High Temperature X-Ray Diffraction Studies of the Terbium Oxide-Oxygen and Mixed Cerium Terbium Oxide-Oxygen Systems. . . . . 4424
- BUROW, D. F., AND LAGOWSKI, J. J. Metal-Ammonia Solutions. II. Internal Reflection Spectroscopy of Alkali Metal-Ammonia Solutions. . . . . 169
- BUSH, LEE W. See Allred, A. L., 2238
- BUTLER, J. N. Solubility and Complex Formation Equilibria of Silver Chloride in Anhydrous Dimethylformamide. . . . . 3288
- BUTLER, J. N. See Cogley, D. R., 1017, 4568; Huston, R., 4263; Synnott, J. C., 2474
- CABLE, M. A Note on the Dissolving of Stationary Spheres, Especially Gas Bubbles. . . . . 3356
- CADENHEAD, D. A., AND EVERETT, D. H. The Sintering of Porous Glass: Benzene Adsorption by Heat-Treated Porous Glasses. . . . . 3201
- CADENHEAD, D. A., AND WAGNER, N. J. Low-Temperature Hydrogen Adsorption on Copper-Nickel Alloys. . . . . 2775
- CADMAN, P., AND POLANYI, J. C. Production of Electronically Excited Atoms. II.  $\text{H} + \text{HI} \rightarrow \text{H}_2 + \text{I}^*(^2\text{P}_{1/2})$ . . . . . 3715
- CADOGAN, K. D., AND ALBRECHT, A. C. Detailed Studies of a One-Electron, Two-Proton Ionization in a Rigid Organic Solution at 77°K. . . . . 929
- CAMERON, A. M. See Choudhary, G., 2289
- CANNINGS, F. R. An Infrared Study of Hydroxyl Groups on Sepiolite. . . . . 1072
- CANNINGS, F. R. Acidic Sites on Mordenite: An Infrared Study of Adsorbed Pyridine. . . . . 4691
- CANTU, A. A. See Matsen, F. A., 21
- CAPELLOS, C., AND ALLEN, A. O. Ionization of Liquids by Radiation Studies by the Method of Pulse Radiolysis. I. Solutions of  $\text{N,N,N',N'}$ -Tetramethyl-*p*-phenylenediamine in Hydrocarbons. . . . . 4265
- CAPWELL, R. J., JR., AND ROSENBLATT, G. M. Entropy and Thermodynamic Functions of  $\text{As}_4(\text{g})$ . . . . . 4327
- CARABETTA, R., AND KASKAN, W. E. The Oxidation of Sodium, Potassium, and Cesium in Flames. . . . . 2483
- CARASSITI, V. See Balzani, V., 383
- CARLSON, K. D. See Uy, O. M., 1611
- CARMAN, C. J., AND KROENKE, W. J. Electron Spin Resonance of  $\alpha$ -Chromia-Alumina Solid Solutions. . . . . 2562
- CARMAN, P. C. Intrinsic Mobilities and Independent Fluxes in Multicomponent Isothermal Diffusion. I. Simple Darken Systems. . . . . 1707
- CARMAN, P. C. Intrinsic Mobilities and Independent Fluxes in Multicomponent Isothermal Diffusion. II. Complex Darken Systems. . . . . 1713
- CARON, A. P., RAGLE, J. L., YORKE, M. E., AND YEH, H. The Powder Patterns and Lattice Constants of Ammonia-boron Trifluoride and Ammonium Tetrafluoroborate. . . . . 556
- CARONE, P. F. See Martire, D. E., 3489
- CARSON, S. D. See Rosenberg, H. M., 3531
- CARTER, J. L. See Khoobiar, S., 1682
- CARUSO, J. A., AND POPOV, A. I. A Potentiometric Study of Acid-Base Equilibria in 1,1,3,3-Tetramethylguanidine. . . . . 918



- CARVER, T. G. See Andrews, L., 1743
- CASTELLANO, S. See Williamson, M. P., 175
- CATER, E. D., AND STEIGER, R. P. Vaporization, Thermodynamics, and Dissociation Energy of Lanthanum Monosulfide. II. . . . . 2231
- CAVASINO, F. P. A Temperature-Jump Study of the Kinetics of the Formation of the Monosulfato Complex of Iron(III). . . . . 1378
- CAVELL, E. A. S., AND KNIGHT, P. C. On the Analysis of Dielectric Dispersion Data into Two Relaxation Regions. . . . . 1656
- CERCEK, B. Activation Energy for the Mobility of the Hydrated Electron. . . . . 2279
- CERCEK, B. Substituent Effects in Cyclohexadienyl Radicals as Studied by Pulse Radiolysis. . . . . 3832
- CERCEK, B., AND EBERT, M. Activation Energies for Reactions of the Hydrated Electron. . . . . 766
- CERUTTI, P. See Larson, J. W., 2902
- CHAFFEE, R. G. See Stark, F. O., 2750
- CHAMBERS, R. W., AND KEARNS, D. R. Effect of Dimer Formation on the Triplet States of Organic Dyes. . . . . 4718
- CHAN, S. C. See Lin, Y. N., 1932
- CHANDROSS, E. A., AND VISCO, R. E. On Preannihilation Electrochemiluminescence and the Heterogeneous Electrochemical Formation of Excited States. . . . . 378
- CHANG, E. T., AND GOKCEN, N. A. Thermodynamic Properties of Gases in Propellants. III. Equilibria in  $N_2H_4-1,1-N_2H_2(CH_3)_2$  and He (or  $N_2$ )- $N_2H_4-1,1-N_2H_2(CH_3)_2$  Systems. . . . . 2556
- CHANG, E. T., GOKCEN, N. A., AND POSTON, T. M. Thermodynamic Properties of Gases in Propellants. II. Solubilities of Helium, Nitrogen, and Argon Gas in Hydrazine, Methylhydrazine, and Unsymmetrical Dimethylhydrazine. . . . . 638
- CHANG, H. L., AND CUSTARD, H. C. Ion Exchange of Montmorillonite at High Pressures. . . . . 4340
- CHANG, P. C., AND GATZ, C. R. Kinetic Isotope Effects: Approximate Calculations. . . . . 2602
- CHANTOONI, M. K., JR. See Kolthoff, I. M., 2270
- CHAPMAN, I. D. The Effect of Temperature on Dielectric Properties of Water-in-Oil Emulsions. . . . . 33
- CHAPPELL, G. A., AND SHAW, H. A Shock Tube Study of the Pyrolysis of Propylene. Kinetics of the Vinyl Carbon-Carbon Bond Rupture. . . . . 4672
- CHATTORAJ, D. K. Reply to the Comments on "Gibbs Equation for Polyelectrolyte Adsorption". . . . . 1835
- CHEN, E. See Wentworth, W. E., 2671
- CHEN, Y., AND ORTUNG, W. H. Observation of a Minimum in the Kerr Constants of Light and Heavy Water Near 30°. . . . . 3069
- CHENG, W. J., AND SZWARC, M. Studies of Gas-Phase Reactions of  $CF_3$  Radical with Methylchlorosilanes. . . . . 494
- CHEERNICK, C. L. See Schreiner, F., 1162
- CHIANG, A., AND ADAMSON, A. W. Photochemistry of Aqueous  $Cr(CN)_6^{3-}$ . . . . . 3827
- CHIGNELL, D. A., AND GRATZER, W. B. Solvent Effects on Aromatic Chromophores and Their Relation to Ultraviolet Difference Spectra of Proteins. . . . . 2934
- CHIU, Y.-C., AND FUOSS, R. M. Conductance of the Alkali Halides. XII. Sodium and Potassium Chlorides in Water at 25°. . . . . 4123
- CHIU, Y.-C., AND GENSHAW, M. A. A New Method for Studying Ion Adsorption. . . . . 4325
- CHOI, S. U. See Kwun, O. C., 3148
- CHOUDHARY, G., CAMERON, A. M., AND BACK, R. A. The Photolysis and Pyrolysis of Succinimide Vapor. . . . . 2289
- CHOW, L. C. See Martire, D. E., 3489
- CHRISTENSEN, J. J. See Izatt, R. M., 1208, 2720
- CHRISTIAN, S. D. See Gregory, M. D., 1748; Grigsby, R. D., 2465; Johnson, J. R., 3223
- CHUGHTAI, A., MARSHALL, R., AND NANCOLLAS, G. H. Complexes in Calcium Phosphate Solutions. . . . . 208
- CHURCH, J. A., AND DRESKIN, S. A. On the Kinetics of Color Development in the Landolt ("Iodine Clock") Reaction. . . . . 1387
- CIANI, F., CICOGNA, G., AND MAESTRO, M. A Semi-empirical Model for Simple Liquids. . . . . 1510
- CICOGNA, G. See Ciani, F., 1510
- CLARK, W. G. See Newton, T. W., 4333
- CLARKE, J. K. A., FARREN, G. M., AND RUBALCAVA, H. E. Infrared Absorption at 21  $\mu$  of Carbon Monoxide Adsorbed on Silica-Supported Platinum. . . . . 327
- CLARKE, J. K. A., FARREN, G. M., AND RUBALCAVA, H. E. Infrared Absorption at 21  $\mu$  of Carbon Monoxide Adsorbed on Silica-Supported Platinum. . . . . 2688
- CLEGG, R. M. See Hammaker, R. M., 1837
- CLEMENA, G. See Jhon, M. S., 4155
- CLEVER, H. L. See Schmidt, R. L., 1529
- CLIFFORD, A. A. See Favelukes, C. E., 962
- CLINCKEMAILLIE, G. G. See Kenney, D. J., 410
- COBB, C. M., AND WALLIS, E. B. The Absorption of Iodine by Perylene. . . . . 2986
- COBURN, R. A., AND DUDEK, G. O. Spectroscopic Studies of Isotopically Substituted 2-Pyridones. . . . . 1177
- COBURN, R. A., AND DUDEK, G. O. Spectroscopic Studies of Isotopically Substituted 4-Pyridones. . . . . 3681
- COBURN, T. T. See Harmon, K. M., 2950
- COCIVERA, M. Nuclear Magnetic Resonance Study of Proton Exchange Involving Methyl-Substituted Pyridinium Salts in Methanol. . . . . 2515
- COCIVERA, M. Nuclear Magnetic Resonance Study of Proton Exchange Involving Methyl-Substituted Pyridinium Salts in Water. . . . . 2520
- CODELL, M., GISSER, H., WEISBERG, J., AND IYENGAR, R. D. Electron Spin Resonance Study of Hydroperoxide on Zinc Oxide. . . . . 2460
- COFFMAN, R. E., LYLE, D. L., AND MATTISON, D. R. Small Tunneling Effect in the Electron Paramagnetic Resonance Spectrum of  $Cu^{2+}-CaO$  at 1.2°K. . . . . 1392
- COGLEY, D. R., AND BUTLER, J. N. The Activity of Lithium in Lithium Amalgams. . . . . 1017
- COGLEY, D. R., AND BUTLER, J. N. Kinetics of the  $Li(Hg)-Li^+$  Reaction in Dimethyl Sulfoxide. . . . . 4568
- COHEN, A. O., AND MARCUS, R. A. On the Slope of Free Energy Plots in Chemical Kinetics. . . . . 4249
- COHEN, J. I. See Cohen, S. G., 3782
- COHEN, S. G., AND COHEN, J. I. Photoreduction of Aminobenzophenones in Nonpolar Media. Effects of Tertiary Amines. . . . . 3782
- COHN, J. Theory of the Radial Distribution Function. . . . . 608
- COHZ, S. N. See Schack, C. J., 4697
- COLE, D. L. See Holmes, L. P., 301
- COLEMAN, A. J. See Barger, H. J., Jr., 2285
- COLEMAN, C. F. Properties of Organic-Water Mixtures. VIII. Dielectric Constants of *N,N*-Dialkylamides Containing Water. . . . . 365
- COLEMAN, J. S., GEORGE, P., ALLAMAN, L., AND JONES, L. H. Stepwise Formation of Cyanide Complexes of Copper(I) in Anion Exchangers. . . . . 2605
- COLTHARP, M. T., AND HACKERMAN, N. The Surface of a Carbon with Sorbed Oxygen on Pyrolysis. . . . . 1171
- CONDER, J. R. See Langer, S. H., 4020
- CONTI, F., DELOGU, P., AND PISTOIA, G. Influence of the Solvent Structure on Ion-Pair Association. . . . . 1396
- CONTI, F., AND PISTOIA, G. Ion-Pair Association of Strong Electrolytes in Binary Mixtures of Polar Solvents: Alkaline Perchlorates in Methanol-Methyl Cyanide Mixtures. . . . . 2245
- CONWAY, B. E., AND LALIBERTÉ, L. H.  $H_2O-D_2O$  Isotope Effect in Partial Molal Volume of Alkali Meta. and Tetraalkylammonium Salts. . . . . 4317
- COOK, R. L. See Harris, N. H., 3326
- COPELAND, B. K. W. See Levy, J. B., 3168
- COPELAND, J. L., AND SEIBLES, L. Thermodynamics of High-Temperature High-Pressure Solutions. Argon in Molten Sodium Nitrate. . . . . 603
- CORDES, H. F. The Preexponential Factors for Solid-State Thermal Decomposition. . . . . 2185
- CORDES, H. F., AND SMITH, S. R. The Thermal Decomposition of Solid Alkali Perchlorates. . . . . 2189
- CORDIER, P., AND GROSSWEINER, L. I. Pulse Radiolysis of Aqueous Fluorescein. . . . . 2018
- CORRIN, M. L., AND NELSON, J. A. Energetics of the Adsorption of Water Vapor on "Pure" Silver Iodide. . . . . 643
- COSTANTINO, L., CRESCENZI, V., AND VITAGLIANO, V. Differential Diffusion Coefficients of Hexamethylenetetramine Aqueous Solutions. . . . . 149
- COTTON, D. J. A Theory of Interfacial Tension of Two-Phase Ternary Liquid Systems. . . . . 4139
- COURTNEY, W. G. Reexamination of Homogeneous Nucleation and Condensation of Water. . . . . 421
- COURTNEY, W. G. Condensation of Water in a Cloud Chamber. . . . . 433
- COVINGTON, A. K., LILLEY, T. H., AND ROBINSON, R. A. Excess Free Energies of Aqueous Mixtures of Some Alkali Metal Halide Salt Pairs. . . . . 2759
- COX, R. A., AND CVETANOVIĆ, R. J. The Reaction of Methylene with Carbon Monoxide. . . . . 2236
- COX, R. H., AND BOTHNER-BY, A. A. Proton Nuclear Magnetic Resonance Spectra of Di- and Trisubstituted Pyrazines and Their Cations. . . . . 1642

- COX, R. H., AND BOTHNER-BY, A. A. Proton Nuclear Magnetic Resonance Spectra of Monosubstituted Pyrazines. . . . . 1646
- COX, R. H. See Smith, S. L., 198
- COYLE, T. D. See Johannesen, R. B., 660
- CRAIG, N. C., HU, T., AND MARTYN, P. H. Elimination of Difluoromethylene from Chemically Activated 1,1,2,2-Tetrafluorocyclopropane. . . . . 2234
- CRAMAROSSA, F., MOLINARI, E., AND RORO, B. Rates of Reactions of Oxygen Atoms with Solid and Liquid Sulfur (and Selenium). . . . . 84
- CRAMER, L. R., AND BERG, J. C. The Effect of Micelles on the Kinetics of the Cannizzaro Reaction. . . . . 3686
- CRAWFORD, B., JR. See Favelukes, C. E., 962; Fujiyama, T., 2174
- CRESCENZI, V. See Barone, G., 2588; Costantino, L., 149
- CRISS, C. M., HELD, R. P., AND LUKSHA, E. Thermodynamic Properties of Nonaqueous Solutions. V. Ionic Entropies: Their Estimation and Relationship to the Structure of Electrolytic Solutions. . . . . 2970
- CRISS, C. M., AND LUKSHA, E. Thermodynamic Properties of Nonaqueous Solutions. IV. Free Energies and Entropies of Solvation of Some Alkali Metal Halides in N,N-Dimethylformamide. . . . . 2966
- CRONAN, C. L. See Schneider, F. W., 4563; Wittstruck, T. A., 4243
- CROWTHER, P. See Lamprecht, G. J., 1439
- CUBICCIOTTI, D. See Johnson, J. W., 1664, 1669; Keneshea, F. J., 1272
- CUKROWSKI, A. S. See Baranowski, B., 1831
- CUNDALL, R. B., EVANS, G. B., GRIFFITHS, P. A., AND KEENE, J. P. The Pulse Radiolysis of Benzene-Biacetyl Solutions. . . . . 3871
- CURTHOYS, G. See Elkington, P. A., 3475
- CUSSLER, E. L. See Bell, T. N., 4693; Skinner, J. F., 1057
- CUSTARD, H. C. See Chang, H. L., 4340
- CVETANOVIĆ, R. J. See Cox, R. A., 2236
- CYVIN, S. J. See Hagen, G., 1446, 1451
- DAHMS, H. Electronic Conduction in Aqueous Solution. . . . . 362
- DAINTON, F. S., PENG, C. T., AND SALMON, G. A. Transient Species in the Radiolysis of Solutions of Stilbene. . . . . 3801
- DANDY, A. J. Sorption of Vapors by Sepiolite. . . . . 334
- DANESI, P. R., MAGINI, M., AND SCIBONA, G. Vapor Pressure Lowering and Light Scattering in Benzene Solutions of Alkylammonium Salts. . . . . 3437
- DANIELS, M., MEYERS, R. V., AND BALARDO, E. V. Photochemistry of the Aqueous Nitrate System. I. Excitation in the 300-m $\mu$  Band. . . . . 389
- DANNHAUSER, W. See Johari, G. P., 3273
- DANTZLER, E. M., KNOBLER, C. M., AND WINDSOR, M. L. Interaction Virial Coefficients in Hydrocarbon Mixtures. . . . . 676
- DANYLUK, S. S. See Blears, D. J., 2269
- DANZIGER, R. M., HAYON, E., AND LANGMUIR, M. E. Pulse-Radiolysis and Flash-Photolysis Study of Aqueous Solutions of Simple Pyrimidines. Uracil and Bromouracil. . . . . 3842
- D'APRANO, A., AND FUOSS, R. M. Conductance of Thallous Nitrate in Dioxane-Water Mixtures at 25°. . . . . 4710
- DARLAK, J. O. See Spencer, H. E., 2384
- DARLEY, P. E. See Matwiyoff, N. A., 2659
- DARNELL, A. J., AND GREYSON, J. The Effect of Structure-Making and -Breaking Solutes on the Temperature of Maximum Density of Water. . . . . 3021
- DARNELL, A. J., AND GREYSON, J. The Temperature of Maximum Density of Heavy Water Solutions. . . . . 3032
- DARNELL, A. J., AND MCCOLLUM, W. A. Phase Diagrams of the Bismuth Trihalides at High Pressure. . . . . 1327
- DARWENT, B. DEB. See Penzhorn, R. D., 1639
- DAS, B. See Rao, K. S., 1223
- DATTA, P. See Barrow, G. M., 2259
- DAVIES, G. A., PONTER, A. B., AND SINGH, S. An Analysis of the Particle Size Distribution of Ammonium Chloride Formed by Rhythmic Precipitation of Ammonia and Hydrogen Chloride. . . . . 4320
- DAVIS, J. C. See Grinstead, R. R., 1630
- DAVIS, J. C., JR. See Murphy, R. A., 3111
- DAWSON, W. R., AND WINDSOR, M. W. Fluorescence Yields of Aromatic Compounds. . . . . 3251
- DAYAGI, S. See Fraenkel, G., 953
- DEAN, R. R. See Fraenkel, G., 944
- DE BOER, C. See Kispert, L. D., 4276
- DEGN, H., AND HIGGINS, J. The Existence of Homogeneous Oscillating Reactions. . . . . 2692
- DEGNAN, J. See Bjorklund, S., 970
- DE IASI, R. See Steigman, J., 1132
- DE KÖRÖSY, F. An Asymmetry-Potential Effect across Gradient Permselective Membranes. . . . . 2591
- DELAHAY, P. See Susbilles, G. G., 841
- DELANEY, D. E. See Wood, R. H., 4651
- DELGASS, W. N., BOUDART, M., AND PARRAVANO, G. Mössbauer Spectroscopy of Supported Gold Catalysts. . . . . 3563
- DELLA MONICA, M., JANNELLI, L., AND LAMANNA, U. Physicochemical Properties of Sulfolane. . . . . 1068
- DELLA MONICA, M. D., AND LAMANNA, U. Solvation Numbers of Some Ions in Sulfolane by Conductance Measurements. . . . . 4329
- DELLA MONICA, M., LAMANNA, U., AND SENATORE, L. Transport Numbers and Ionic Conductances in Sulfolane at 30°. . . . . 2124
- DELOGU, P. See Conti, F., 1396
- DEO, A. V. See Low, M. J. D., 2371
- DE PALMA, D. See Scott, R., 3192
- DESANDO, R. J., AND BROWN, G. H. An X-Ray Study of Formamide and Solutions of Potassium Iodide in Formamide. . . . . 1088
- DESHPANDE, D. D., AND BHATGADDE, L. G. Sound Velocities, Adiabatic Compressibilities, and Free Volumes in Aniline Solutions. . . . . 261
- DEVLIN, J. P. See Ware, B., 3970
- DEVONSHIRE, R., AND WEISS, J. J. Nature of the Transient Species in the Photochemistry of Negative Ions in Aqueous Solution. . . . . 3815
- DEWALD, R. R., AND ROBERTS, J. H. The Conductance of Dilute Solutions of Sodium in Liquid Ammonia at -33.9, -45, and -65°. . . . . 4224
- DEWALD, R. R., AND TSINA, R. V. A Kinetic Study of the Reactions of Water and *t*-Butyl Alcohol with Sodium in Liquid Ammonia. . . . . 4520
- DEWALD, R. R. See Brooks, J. M., 2655
- DEWHURST, S. See Blatz, P. E., 2690
- DHINGRA, R. C., AND POOLE, J. A. The Fluorescence of Protonated Azulenoid Systems. . . . . 4577
- DIAMOND, R. M. See Turner, D. J., 2831, 3504
- DI BELLO, L. M., MCDEVITT, H. M., AND ROBERTI, D. M. The Temperature Variation of the Dipole Moment of *o*-Dimethoxybenzene. . . . . 1405
- DI CARLO, E. N., LOGAN, T. P., AND STRONSKI, R. E. An Investigation of the Electrical Polarizations of Several Molecules Which Have Been Assigned Anomalous Dipole Moments. . . . . 1517
- DICKS, L. See Lamprecht, G. J., 1439
- DIESEN, R. W. Kinetics of the Reaction of Fluorine with Difluoramino Radicals and the Dissociation of Fluorine. . . . . 108
- DIESTLER, D. J. See Berndt, A. F., 2263
- DILL, A. J., ITZKOWITZ, L. M., AND POPOVYCH, O. Standard Potentials of Potassium Electrodes and Activity Coefficients and Medium Effects of Potassium Chloride in Ethanol-Water Solvents. . . . . 4580
- DILRENZO, J. V., AND SCHNEIDER, R. F. Chlorine Nuclear Quadrupole Resonance in (C<sub>2</sub>H<sub>5</sub>)<sub>4</sub>NAsCl<sub>6</sub>. . . . . 761
- DITMARS, W. E., JR., AND VAN WINKLE, Q. A Comparative Study of Pheophytin *a* and Pheophytin *b* Monolayers. . . . . 39
- DOBROW, J. See Steigman, J., 3424
- DOEPKER, R. D. Vacuum Ultraviolet Photolysis of the C<sub>4</sub>H<sub>6</sub> Isomers. I. 1,3-Butadiene. . . . . 4037
- DOGLIOTTI, L., AND HAYON, E. Flash Photolysis Study of Sulfite, Thiocyanate, and Thiosulfate Ions in Solution. . . . . 1800
- DONALDSON, G. W., AND JOHNSTON, F. J. The Radiolysis of Colloidal Sulfur. . . . . 3552
- DONDES, S. See Liuti, G., 1081
- DONIGIAN, D. W. See Bartholomew, R. F., 3545
- DOREMUS, R. H. Ion Exchange with a Two-Phase Glass. . . . . 2665
- DOREMUS, R. H. Electrical Potentials of Glass Electrodes in Molten Salts. . . . . 2877
- DORFMAN, L. M. See Wander, R., 2946
- DOUGLAS, T. B. See Krause, R. F., Jr., 475, 3444
- DRAGANIĆ, Z. D., MIČIĆ, O. I., AND NENADOVIĆ, M. T. The Radiolysis of Some Heavy Water Solutions at pD 1.3-13. . . . . 511
- DRENNAN, G. A., AND MATULA, R. A. The Pyrolysis of Tetrafluoroethylene. . . . . 3462
- DRESKIN, S. A. See Church, J. A., 1387
- DRISCOLL, J. N., AND WARNECK, P. Primary Processes in the Photolysis of SO<sub>2</sub> at 1849 Å. . . . . 3736
- DROST-HANSEN, W. See Millero, F. J., 1758, 2251
- DUBROW, R., HATZENBUHLER, D., MARX, W., ZAHORIAN, E., AND WILSON, D. J. Application of the WKB Method to the Dynamics of Anharmonic Oscillators. . . . . 2489

- DUDA, J. L., AND VRENTAS, J. S. Mathematical Analysis of Dropping Mercury Electrode. I. Solution of Diffusion Equation for Variable Mercury Flow Rate. . . . . 1187
- DUDA, J. L., AND VRENTAS, J. S. Mathematical Analysis of Dropping Mercury Electrode. II. Prediction of Time Dependence of Mercury Flow Rate. . . . . 1193
- DUDEK, E. P. See Swett, V. C., 1244
- DUDEK, G. O. See Coburn, R. A., 1177, 3681
- DUERKSEN, W. K. See Tamres, M., 966
- DUISMAN, J. A., AND GIAUQUE, W. F. Thermodynamics of the Lead Storage Cell. The Heat Capacity and Entropy of Lead Dioxide from 15 to 318°K. . . . . 562
- DU MEZ, M. See Maatman, R., 97
- DUNLOP, P. J. See Bell, T. N., 4693
- DUNN, T. M. See Becker, C. A. L., 3588
- DURIGON, D. D. See Sandler, Y. L., 1051
- DUVALL, J. J., AND JENSEN, H. B. Reactions in the Cobalt-60 Irradiation of Pyridine and Methylpyridines. . . . . 4528
- DWORKIN, A. S., AND BREDIG, M. A. Diffuse Transition and Melting in Fluorite and Anti-Fluorite Type of Compounds: Heat Content of Potassium Sulfide from 298 to 1260°K. . . . . 1277
- DWORKIN, A. S., BRONSTEIN, H. R., AND BREDIG, M. A. Miscibility of Liquid Metals with Salts. VIII. Strontium-Strontium Halide and Barium-Barium Halide Systems. . . . . 1892
- DYKE, M., AND SASS, R. L. The Crystal Structure of Dipotassium Tetranitroethide. . . . . 266
- EATON, D. R., AND SUART, S. R. Electron Spin Resonance Studies of the Photooxidation and Reduction of Cobalt Complexes. . . . . 400
- EATOUGH, D. See Izatt, R. M., 1208, 2720
- EBERHARDT, M. K. Steric Effect in the Radiolysis of *cis* and *trans*-1,2-Dimethylcyclohexane. . . . . 4509
- EBERHART, J. G., AND GRUETTER, E. N. Estimation of the High-Temperature Entropy of Solids by the Entropy Correspondence Principle. . . . . 1825
- EBERLY, P. E., JR. High-Temperature Infrared Spectroscopy of Pyridine Adsorbed on Faujasites. . . . . 1042
- EBERT, M. See Cercek, B., 766
- EBISUZAKI, Y., AND O'KEEFE, M. Phase Separation in the Palladium-Hydrogen System. . . . . 4695
- ECKSTROM, H. C. See Smith, W. H., 369
- EDING, H. See Keneshea, F. J., 1272
- EDWARDS, R. K. See Battles, J. E., 3963; Macur, G. J., 1047
- EIBEN, K., AND FESSENDEN, R. W. Electron Spin Resonance Studies of Radiolytically Produced Radicals in Aqueous Nitroalkane Solutions. . . . . 3387
- EICK, H. A. See Haschke, J. M., 1697, 4235
- EIRICH, F. R. See Assarsson, P., 2710
- EISENMAN, G. See Walker, J. L., Jr., 978
- ETTEL, M. J. Concentration Fluctuations in Dilute Polymer Solutions. I. A Theoretical Treatment of Flow-Time Fluctuations in a Capillary Viscometer. . . . . 448
- EKSTROM, A., AND WILLARD, J. E. Effects of Matrix Polarity on the Optical and Electron Spin Resonance Spectra of Trapped Electrons in Organic Glasses. . . . . 4599
- ELIASON, R. See Kreevoy, M. M., 1313
- ELKANA, Y. Differentiation between Tryptophan Residues in Proteins. . . . . 3654
- ELKINGTON, P. A., AND CURTHOYS, G. Infrared Spectral Shifts and Heats of Adsorption of Vapors on Silica Gel. . . . . 3475
- ELLEMAN, D. D. See Bowers, M. T., 3599
- ELLISON, R. See Fontijn, A., 3701
- EMERSON, J., REEVES, R., AND HARTECK, P. Chemiluminescent Emission in Gaseous Reactions at Low Concentrations. . . . . 3721
- EMMERSON, P. T., AND WILLSON, R. L. Pulse Radiolysis of Aqueous Solutions of Thymine and Triacetoneamine N-Oxyl. . . . . 3669
- EPSTEIN, J., AND MOSHER, W. A. Magnesium Ion Catalysis of Isopropyl Methylphosphonofluoridate. The Charge Effect in Metal Ion Catalysis. . . . . 622
- ERB, R. A. The Wettability of Gold. . . . . 2412
- ERIKSSON, L. E. G. See Hyde, J. S., 4269
- ESPINO, R. L., JONES, J. P., REID, R. C., AND STRANDBERG, M. W. P. Interruption and Evaporation Effects for the Reaction of Atomic Hydrogen with Solid Olefins at 77°K. . . . . 3689
- EVANS, D. F., AND BROADWATER, T. L. The Conductance of the Trialkylsulfonium Iodides in Water, Methanol, and Acetonitrile at 10 and 25°. . . . . 1037
- EVANS, D. F., AND GARDAM, P. Transport Processes in Hydrogen-Bonding Solvents. I. The Conductance of Tetraalkylammonium Salts in Ethanol and Propanol at 25°. . . . . 3281
- EVANS, G. B. See Cundall, R. B., 3871
- EVANS, H. B., JR., TARPLEY, A. R., AND GOLDSTEIN, J. H. Nuclear Magnetic Resonance Spectra of Mono- and Disubstituted Benzenes Containing OH, SH, NH<sub>2</sub>, and COOH. . . . . 2552
- EVERETT, D. H. See Cadenhead, D. A., 3201
- EYRING, E. M. See Holmes, L. P., 301
- EYRING, H. See Miles, D. W., 1483; Zandler, M. E., 2730
- EYRING, L. See Burnham, D. A., 4415, 4424; Kordis, J., 2030, 2044
- EZELL, J. B., AND GILKERSON, W. R. Investigation of the Validity of Several Approximations in Measurements of Cation-Ligand Association Constants by a Conductance Method. . . . . 144
- FABIAN, J., MEHLHORN, A., AND ZAHRADNIK, R. Semi-empirical Calculations on Sulfur-Containing Heterocycles. . . . . 3975
- FACKLER, J. P., JR., MITTLEMAN, M. L., WEIGOLD, H., AND BARROW, G. M. Spectra of Metal  $\beta$ -Ketoenolates. The Electronic Spectrum of Monomeric Nickel(II) Acetylacetonate and the Infrared Spectra of Matrix-Isolated Acetylacetonates of Cobalt(II), Nickel(II), Copper(II), and Zinc(II). . . . . 4631
- FAGLEY, T. F. See Balfour, F. W., 1300
- FAJER, J., BIELSKI, B. H. J., AND FELTON, R. H. Electronic and Electron Spin Resonance Spectra of the Perfluoro-2,1,3-benzoselenadiazole Anion Radical. . . . . 1281
- FANNING, J. E., JR. See Klein, N., 880
- FARREN, G. M. See Clark, J. K. A., 327, 2688
- FAVELUKES, C. E., CLIFFORD, A. A., AND CRAWFORD, B., JR. Vibrational Intensities. XVIII. Infrared Band Shapes for Some Liquid Methyl Iodide Bands. . . . . 962
- FEBER, R. C. See Herrick, C. C., 1102
- FELBER, B. J., HODNETT, E. M., AND PURDIE, N. Divalent Transition Metal Complexes of Hydrolyzed Ethylene-Maleic Anhydride Copolymer. . . . . 2496
- FELDMAN, L. H., HERZ, A. H., AND REGAN, T. H. pH Dependence of Electronic and Nuclear Magnetic Resonance Spectra of Isomeric Cyanine Dyes. . . . . 2008
- FELDMANN, T., AND TREININ, A. I<sup>-</sup> Photosensitized Reactions in Metaphosphate Glass. . . . . 3768
- FELTON, R. H. See Fajer, J., 1281
- FENDLER, J. H. See Asmus, K.-D., 4285
- FESSENDEN, R. W. See Eiben, K., 3387
- FEUER, P. Lattice Anharmonicity and the Thermal Accommodation Coefficient. . . . . 3573
- FICALORA, P. J., HASTIE, J. W., AND MARGRAVE, J. L. Mass Spectrometric Studies at High Temperatures. XXVII. The Reactions of Aluminum Vapor with S<sub>2</sub>(g), Se<sub>2</sub>(g), and Te<sub>2</sub>(g). . . . . 1660
- FIELDEN, E. M. See Hart, E. J., 577
- FILIPESCU, N., AND MUSHKUSH, G. W. Lanthanide Ions as Sensitive Probes in Organic Photochemistry. I. Collisional Sensitization of Fluorescence by Triplet Donors. . . . . 3516
- FILIPESCU, N., AND MUSHKUSH, G. W. Lanthanide Ions as Sensitive Probes in Organic Photochemistry. II. Photoreduction of *p,p'*-Dimethoxybenzophenone in Isopropyl Alcohol. . . . . 3522
- FILIPESCU, N. See Bjorklund, S., 970
- FINEGOLD, H. Nuclear Magnetic Resonance Studies of Weak Intermolecular Forces: Medium Effects in Saturated Heterocyclic Rings. . . . . 3244
- FISCHER, E. See Gabor, G., 3266
- FISCHER, J. See Krumpelt, M., 506
- FLANAGAN, T. B. See Allard, K., 136
- FLAUTT, T. J. See Lawson, K. D., 2058, 2066
- FLEISCHER, E. B., SUNG, N., AND HAWKINSON, S. The Crystal Structure of Benzophenone. . . . . 4311
- FLETCHER, A. N. Fluorescence Emission Band Shift with Wavelength of Excitation. . . . . 2742
- FLETCHER, A. N., AND HELLER, C. A. The Alcohol Self-Association Dimer and the Absorption Band(s) near 1.53  $\mu$ m. . . . . 1839
- FLORIN, A. E. See Alei, M., Jr., 550
- FLORIN, R. E., SICILIO, F., AND WALL, L. A. The Paramagnetic Species from Titanous Salts and Hydrogen Peroxide. . . . . 3154
- FONTIJN, A., AND ELLISON, R. Formation of Electronically Excited Species in Nitrogen Atom-Oxygen Atom Recombination Reactions Catalyzed by Carbon Compounds: NO(A<sup>2</sup> $\Sigma$ , B<sup>2</sup>II) and O(<sup>4</sup>S). . . . . 3701

- FORCHIONI, A., AND WILLIS, C. The Photolysis of Carbon Suboxide in the Presence of Hydrogen. . . . . 3105
- FORSÉN, S. See Lindman, B., 2805
- FORSLIND, E. See Lindman, B., 2805
- FORSTER, D., AND WEISS, V. W. An Electron Paramagnetic Resonance Study of Cupric Ion Tetrahedrally Coordinated by Nitrogen Atoms. . . . . 2669
- FORSTER, L. S. See Binet, D. J., 3017; Nishimoto, K., 914
- FORSYTH, A. C. See Verneker, V. R. P., 111
- FOSS, G. D., AND PITT, D. A. Calorimetric Studies of Bis(fluoroxy)perfluoromethane. . . . . 3512
- FOST, D. See Stern, J. H., 3053
- FOSTER, M. J. See Blandamer, M. J., 2268
- FOWKES, F. M. Comments on "The Calculation of Cohesive and Adhesive Energies," by J. F. Padday and N. D. Uffindell. . . . . 3700
- FRAENKEL, G., ADAMS, D. G., AND DEAN, R. R. Nuclear Magnetic Resonance and Ultraviolet Spectroscopy of Phenylmagnesium Bromide, Phenyllithium, and Pyridine. . . . .
- FRAENKEL, G., DAYAGI, S., AND KOBAYASHI, S. Nuclear Magnetic Resonance and Ultraviolet Spectroscopy of Substituted Aromatic Organometallic Compounds of Lithium, Magnesium, and Calcium. . . . . 953
- FRAME, G. M., II. See Moorhead, E. D., 3684
- FRANKEL, L. S. A Nuclear Magnetic Resonance Investigation of Paramagnetic Relaxation in Viscous Solutions. . . . . 736
- FRANKLIN, J. A. See Bertrand, L., 3926
- FRANKS, F., QUICKENDEN, M. J., RAVENHILL, J. R., AND SMITH, H. T. Volumetric Behavior of Dilute Aqueous Solutions of Sodium Alkyl Sulfates. . . . . 2668
- FREEMAN, C. G., AND PHILLIPS, L. F. Kinetics of Chlorine Oxide Reactions. I. The Reaction of Oxygen Atoms with Cl<sub>2</sub>O. . . . . 3025
- FREEMAN, C. G., AND PHILLIPS, L. F. Kinetics of Chlorine Oxide Reactions. II. The Reaction of Nitrogen Atoms with Cl<sub>2</sub>O. . . . . 3028
- FREEMAN, C. G., AND PHILLIPS, L. F. Kinetics of Chlorine Oxide Reactions. III. The Reaction of Hydrogen Atoms with Cl<sub>2</sub>O. . . . . 3031
- FREEMAN, C. G. See Grady, Q. J. F., 743
- FREEMAN, G. R. See Robinson, M. G., 1394, 1780; Russell, J. C., 808, 816
- FREEMAN, J. J. See Bielski, B. H. J., 1721
- FREI, Y. F. See Gabor, G., 3266
- FREIBERG, M., RON, A., AND SCHNEPP, O. The Low-Frequency Spectra of Lithium Halide Molecular Species. . . . . 3526
- FRENCH, W. G., AND WILLARD, J. E. Radical Decay Kinetics in Organic Glasses. Spatial Effects and Isotope Effects. . . . . 4604
- FRICKE, H. See Sehested, K., 626
- FRIED, V., AND SCHNEIER, G. B. Some Comments on Cohesion Energies of Liquids. . . . . 4688
- FRIEDEL, R. A. See Retcofsky, H. L., 290, 2619
- FRIEDMAN, H. L. See Haugen, G. R., 4549; Rasiaiah, J. C., 3352
- FRIPIAT, J. J., LEONARD, A., AND MENDELUVICI, E. Structural Features of Some Water *n*-Alkylamine Complexes. . . . . 1808
- FRITSCH, J. M. See Seo, E. T., 1829
- FROMMER, M. A., AND MILLER, I. R. Adsorption of DNA at the Air-Water Interface. . . . . 2862
- FROMMER, M. A. See Miller, I. R., 1834
- FROST, A. A. A Floating Spherical Gaussian Orbital Model of Molecular Structure. III. First-Row Atom Hydrides. . . . . 1289
- FUJIMORI, E. See Sherman, G., 4345
- FUJITA, H. See Kobatake, Y., 1752; Okita, K., 278; Yanagida, T., 1265; Yuasa, M., 2871
- FUJIYAMA, T., AND CRAWFORD, B., JR. Vibrational Intensities. XXI. Some Band Shapes and Intensities in Liquid Hexafluorobenzene. . . . . 2174
- FUKUI, K. See Taniguchi, H., 1926
- FUKUZAWA, K., AND MIYAMA, H. Quantum Yield of Photonitrosation of Cyclohexane under a Flash Lamp. . . . . 371
- FULLER, E. L., JR., HOLMES, H. F., SECOY, C. H., AND STUCKEY, J. E. Heats of Immersion in the Thorium Oxide-Water System. III. Variation with Specific Surface Area and Outgassing Temperature. . . . . 573
- FULLER, E. L., JR. See Holmes, H. F., 2095, 2293
- FUNG, B. M. The Effect of Neighboring Magnetic Anisotropy on NH Proton Chemical Shifts. . . . . 4708
- FUOSS, R. M. See Chiu, Y.-C., 4123; D'Aprano, A., 4710; Skinner, J. F., 1057
- FURUYAMA, S., GOLDEN, D. M., AND BENSON, S. W. The Thermochemistry of the Gas-Phase Equilibria *trans*-1,2-Diiodoethylene  $\rightleftharpoons$  Acetylene + I<sub>2</sub> and *trans*-1,2-Diiodoethylene  $\rightleftharpoons$  *cis*-1,2-Diiodoethylene. . . . . 3204
- FURUYAMA, S., GOLDEN, D. M., AND BENSON, S. W. The Thermochemistry of the Gas-Phase Equilibrium 2CH<sub>3</sub>I  $\rightleftharpoons$  CH<sub>4</sub> + CH<sub>2</sub>I<sub>2</sub>. The Heat of Formation of CH<sub>2</sub>I<sub>2</sub>. . . . . 4713
- FUTRELL, J. H., ABRAMSON, F. P., AND TIERNAN, T. O. On the Reaction of D<sub>2</sub><sup>+</sup> with Cyclohexane. . . . . 1071
- FUTRELL, J. H., AND TIERNAN, T. O. Ionic Reactions of Unsaturated Compounds. I. Polymerization of Acetylene. . . . . 158
- FUTRELL, J. H. See Abramson, F. P., 1826, 1994; Tiernan, T. O., 3080
- GABOR, G., AND BAR-ELI, K. H. Conformational Isomerism of 1,1'-Disubstituted Azo Compounds. . . . . 153
- GABOR, G., FREI, Y. F., AND FISCHER, E. Tautomerism and Geometric Isomerism in Arylazophenols and Naphthols. IV. Spectra and Reversible Photoreactions of *m*- and *p*-Hydroxyazobenzene. . . . . 3266
- GALLEGOS, E. J. Mass Spectrometry and Ionization Energies of Some Condensed-Ring Aromatic and Heterocyclic Compounds. . . . . 3452
- GANIS, P., TEMUSSI, P. A., NORTHOLT, M. G., AND ALEXANDER, L. E. The Crystal Structure of Racemic  $\alpha,\alpha'$ -Dimethylglutaric Acid. . . . . 3997
- GARBER, H. K. See Larson, J. W., 2902
- GARDAM, P. See Evans, D. F., 3281
- GARFINKEL, H. M. Ion-Exchange Equilibria between Glass and Molten Salts. . . . . 4175
- GARGRAVE, W. E. See Redlich, O., 3045
- GARLAND, J. F., AND SCHROEDER, J. W. Rate of Hydrogen Diffusion in Room-Temperature Irradiated Quartz. . . . . 2277
- GARNETT, J. L. See Hodges, R. J., 1673
- GARRISON, W. M. See Holian, J., 4723; Rodgers, M. A. J., 758
- GATZ, C. R. See Chang, P. C., 2602
- GAY, D. L., AND WHALLEY, E. Solvolysis of Benzyl Chloride in Glycerol-Water Mixtures: Relation between Activation Parameters and Thermal Expansivity. . . . . 4145
- GAYLES, J. N., AND LOHMANN, A. W. The Measurement of Rotary Power and Rotary Dispersion Using Polarized Rayleigh Scattering of Laser Radiation. . . . . 4716
- GEBICKI, J. M. See Bielski, B. H. J., 1721
- GEERTSEMA, A. See Maatman, R., 97
- GENSHAW, M. A. See Chiu, Y.-C., 4325
- GEORGE, R. See Coleman, J. S., 2605
- GEORGE, Z. M. See Bartley, B. H., 1689
- GERARDI, G. J. See Holleran, E. M., 3559
- GERHOLD, G. A., AND MILLER, E. Temperature Dependence of the Solvent Stark Effect. . . . . 2737
- GERLOCK, J. L., AND JANZEN, E. G. Electron Spin Resonance of Perfluorocyclobutanone Ketyl. Long-Range Fluorine Coupling. . . . . 1832
- GERSHON, H. See Schulman, S. G., 3297, 3372, 3692
- GIAUQUE, W. F. See Duisman, J. A., 562
- GIBALDI, M. See Gillap, W. R., 2218, 2222
- GIBBONS, R. M. Quantum Deviations from the Principle of Corresponding States. . . . . 2567
- GIDDINGS, J. C., KUCERA, E., RUSSELL, C. P., AND MYERS, M. N. Statistical Theory for the Equilibrium Distribution of Rigid Molecules in Inert Porous Networks. Exclusion Chromatography. . . . . 4397
- GERST, L. See McCoy, L. R., 4637
- GILKERSON, W. R. See Ezell, J. B., 144
- GILLAP, W. R., WEINER, N. D., AND GIBALDI, M. Ideal Behavior of Sodium Alkyl Sulfates at Various Interfaces. Thermodynamics of Adsorption at the Air-Water Interface. . . . . 2218
- GILLAP, W. R., WEINER, N. D., AND GIBALDI, M. Ideal Behavior of Sodium Alkyl Sulfates at Various Interfaces. Thermodynamics of Adsorption at the Oil-Water Interface. . . . . 2222
- GILSON, D. F. R. See Tsau, J., 4082
- GISSER, H. See Codell, M., 2460
- GLASS, J. E. Adsorption Characteristics of Water-Soluble Polymers. I. Poly(vinyl alcohol) and Poly(vinylpyrrolidone) at the Aqueous-Air Interface. . . . . 4450
- GLASS, J. E. Adsorption Characteristics of Water-Soluble Polymers. II. Poly(ethylene oxide) at the Aqueous-Air Interface. . . . . 4459
- GLOVER, D. J. Reactions of Tetranitromethane with Hydroxide Ion and Nitrite Ion. . . . . 1402

- GODSCHALK, W. Mathematical Formulation of Rotor Deceleration Experiments in Ultracentrifugation..... 498
- GOKCEN, N. A. See Chang, E. T., 638, 2556
- GOLDBERG, E. L. See Binet, D. J., 3017
- GOLDBERG, R. N., AND HEPLER, L. G. Thermodynamics of Ionization of Deuterium Oxide..... 4654
- GOLDEN, D. M. See Furuyama, S., 3204, 4713
- GOLDFINGER, P. See Bertrand, L., 3926
- GOLDSTEIN, J. H. See Evans, H. B., Jr., 2552; Loemker, J. E., 991; Rattet, L. S., 2954
- GOLDSTEIN, L. See Van Heuvelen, A., 481
- GOLDWHITE, H., AND ROWSELL, D. G. The Nuclear Magnetic Resonance Spectrum of Chloromethylphosphine.. 2666
- GONDO, Y., AND MAKI, A. H. Paramagnetic Resonance Study of the Triplet States of Various Aromatic Nitrogen Heterocycles, Biphenyl, and Acenaphthene..... 3215
- GOODENOW, J. M. See Tamres, M., 966
- GOPAL, R., AND SIDDIQI, M. A. The Variation of Partial Molar Volume of Some Tetraalkylammonium Iodides with Temperature in Aqueous Solutions..... 1814
- GOPALAN, M. See Mandelkern, L., 309
- GOPALAN, T. V., AND KADABA, P. K. Dielectric Relaxation in Pure Chloroform..... 3676
- GORDON, S. See Meaburn, G. M., 1592
- GORZYNSKI, C. S., JR. See Maycock, J. N., 4015
- GOTTLIEB, C. See Zuehlke, R. W., 1425
- GOTTSCHALL, W. C., JR., AND TOLBERT, B. M. The Solid-State Radiation Chemistry of Selected Transition Metal Chelates of Glycine and Alanine..... 922
- GOUGH, S. R., AND PRICE, A. H. Dielectric Study of the Molecular Complexes Formed between Triethylamine and Acetic and Monochloroacetic Acid..... 3347
- GRADY, Q. J. F., FREEMAN, C. G., AND PHILLIPS, L. F. Reaction of Oxygen Atoms with ICN..... 743
- GRAESSLEY, W. W. See Alberino, L. M., 4229
- GRAHAM, D. M., AND HIKIDA, T. Hg( $6^3P_1$ )-Photosensitized Isomerization of Octafluorobutene-2..... 3328
- GRANT, E. H., KEFFE, S. E., AND TAKASHIMA, S. The Dielectric Behavior of Aqueous Solutions of Bovine Serum Albumin from Radiowave to Microwave Frequencies..... 4373
- GRANTHAM, L. F., AND YOSIM, S. J. Electrical Conductivity of Liquid and Saturated Vapor of BiCl<sub>3</sub> and HgCl<sub>2</sub> to Their Critical Temperatures..... 762
- GRANZOW, A., HOFFMAN, M. Z., LICHTIN, N. N., AND WASON, S. K. Production of N<sub>2</sub>(A<sup>3</sup> $\Sigma$ ) and CO(a<sup>3</sup> $\pi$ ) by Hg( $^1P_1$ ) Photosensitization; Pressure Dependence of 2537-Å Emission..... 1402
- GRANZOW, A., HOFFMAN, M. Z., LICHTIN, N. N., AND WASON, S. K. Production of N<sub>2</sub>(A<sup>3</sup> $\Sigma_u^+$ ) and CO(a<sup>3</sup> $\pi$ ) by Hg( $^1P_1$ ) Photosensitization: Evidence from 2537-Å Mercury Scintillation..... 3741
- GRATZER, W. B. See Chignell, D. A., 2934
- GRAVES, R. E. See Newmark, R. A., 4299
- GREEN, M. E., AND YAFUSO, M. A Study of the Noise Generated during Ion Transport across Membranes... 4072
- GREENBERG, E., AND HUBBARD, W. N. Fluorine Bomb Calorimetry. XXIII. The Enthalpy of Formation of Carbon Tetrafluoride..... 222
- GREGORY, M. D., AFFSPRUNG, H. E., AND CHRISTIAN, S. D. Dielectric Study of the Hydration of Cyclohexylamine in Benzene..... 1748
- GREGORY, N. W. See Passchier, A. A., 2697; Rice, D. W., 3361, 4524
- GREINER, N. R. Hydroxyl Radical Kinetics by Kinetic Spectroscopy. III. Reactions with H<sub>2</sub>O<sub>2</sub> in the Range 300–458°K..... 406
- GREYSON, J. See Darnell, A. J., 3032, 3021
- GRIFFIN, C. E. See Williamson, M. P., 175, 2678
- GRIFFITH, O. H. See Waggoner, A. S., 4129
- GRIFFITHS, P. A. See Cundall, R. B., 3871
- GRIGSBY, R. D., CHRISTIAN, S. D., AND AFFSPRUNG, H. E. Hydration of N-Methylacetamide in Carbon Tetrachloride..... 2465
- GRIMISON, A., AND SIMPSON, G. A. Spectrophotometric Identification of  $\gamma$ -Radiolytic Intermediates in a New Halogenic Glassy Matrix..... 1776
- GRINSTEAD, R. R., AND DAVIS, J. C. Base Strengths of Amine-Amine Hydrochloride Systems in Toluene..... 1630
- GROENWEGHE, L. C. D. See Moedritzer, K., 4380
- GROSSWEINER, L. I., AND RODDE, A. F., JR. Chemiluminescent Reactions of Fluorescein Dyes in Aqueous Solution..... 756
- GROSSWEINER, L. I. See Cordier, P., 2018; Rodde, A. F., Jr., 3337
- GROTH, W. E., SCHURATE, U., AND SCHINDLER, R. N. The Photolysis of Ammonia at 2062 Å in the Presence of Propane..... 3914
- GRUETTER, E. N. See Eberhart, J. G., 1825
- GRUNWALD, E., AND HALEY, J. F., JR. Acid Dissociation Constant of Trifluoroacetic Acid in Water Measured by Differential Refractometry..... 1944
- GRYGORCEWICZ, C., AND LAURENCE, G. S. The Exchange Reaction of Pentafluoroethyl Iodide with Iodine..... 1811
- GUADAGNO, J. R., AND FOOL, M. J. Investigation of Liquid Palladium-Tin Alloys..... 2535
- GUIDELLI, R. Influence of Heterogeneous Chemical Reactions upon Potentiostatic Current-Time Curves..... 3535
- GUIDELLI, R. See Piccardi, G., 2782
- GUILBAULT, G. G. See Kagan, M. R., 2867
- GUION, J., BLANDER, M., HENGSTENBERG, D., AND HAGEMARK, K. Thermodynamic Treatment and Electromotive Force Measurements of the Ternary Molten Salt Systems Silver Chloride-Sodium Chloride-Potassium Chloride and Silver Chloride-Sodium Chloride-Cesium Chloride..... 2086
- GUION, J., HENGSTENBERG, D., AND BLANDER, M. Association in Mixed Alkali Halide Vapors..... 4620
- GUNDERSEN, G. E. See Battles, J. E., 3963
- GÜNTARD, H. H. See Halonbrenner, R., 3929
- GUSTAFSON, R. L., AND LIPIO, J. A. Binding of Divalent Metal Ions by Cross-Linked Polyacrylic Acid..... 1502
- GÜSTEN, H. See Malan, O. G., 1457
- GUTMANN, H., LEWIN, M., AND PERLMUTTER-HAYMAN, B. The Ultraviolet Absorption Spectra of Chlorine, Bromine, and Bromine Chloride in Aqueous Solution..... 3671
- HAAKE, P., AND BAUSER, L. P. Thiazolium Ions and Related Heteroaromatic Systems. II. The Acidity Constants of Thiazolium, Oxazolium, and Imidazolium Ions..... 2213
- HABGOOD, H. W. See Bartley, B. H., 1689; Watanabe, Y., 3066
- HACKERMAN, N. See Coltharp, M. T., 1171
- HADJOUUDIS, E. K. See Milia, F. K., 4707
- HAGEMARK, K. Thermodynamics of Ternary Systems. The Quasi-Chemical Approximation..... 2316
- HAGEMARK, K. See Guion, J., 2086
- HAGEN, G., AND CYVIN, S. J. Tentatively Standardized Symmetry Coordinates for Vibrations of Polyatomic Molecules. VI. Naphthalene and Biphenyl Models... 1451
- HAGEN, G., AND CYVIN, S. J. Mean Amplitudes of Vibration of Comparatively Large Molecules. I. Isotopic Naphthalenes..... 1446
- HAGOPIAN, A. K. E., AND JOHNSEN, R. H. The Reaction of Thermal Hydrogen Atoms with Frozen Organic Substrates..... 1949
- HAHN, S. J. See Miles, D. W., 1483
- HAIR, M. L. See Altug, I., 599, 2976; Hertl, W., 4676
- HALEY, J. F., JR. See Grunwald, E., 1944
- HALL, W. K. See Hightower, J. W., 4555
- HALLADA, C. J., TSGIDINOS, G. A., AND HUDSON, B. S. Molybdovanadophosphoric Acids and Their Salts. II. Investigation of Solution Properties..... 4304
- HALLER, I. Thermal Isomerization of Hexafluorobicyclo-[2.2.0]hexa-2,5-diene..... 2882
- HALONBRENNER, R., HUBER, J. R., WILD, U., AND GÜNTARD, H. H. A Flash-Photolysis Study of Chromyl Chloride..... 3929
- HALPERN, A. M., AND WEISS, K. The Photochemistry of Charge-Transfer Systems. I. Complexes of Iodine with Amines..... 3863
- HALSTEAD, C. J. See Thrush, B. A., 3711
- HAMADA, F., WUNDERLICH, B., SUMIDA, T., HAYASHI, S., AND NAKAJIMA, A. Density and Heat of Fusion of Folded-Chain Polyethylene Crystals..... 178
- HAMILL, W. H. See Louwrier, P. W. F., 3878
- HAMILTON, F. J. See Smith, G. H., 3567
- HAMMAKER, R. M., CLEGG, R. M., PATTERSON, L. K., RIDER, P. E., AND ROCK, S. L. Hydrogen-Bonded Dimers and the 2.86- $\mu$  Band in Alcohols..... 1837
- HAMMAKER, R. M., PATTERSON, L. K., AND LIN, K. C. Spin-Spin Coupling in Di-*t*-butylcarbinol. An Alternate Interpretation..... 4346
- HAMMES, G. G., AND PACE, C. N. Ultrasonic Absorption Measurements in Aqueous Solutions of Glycine, Diglycine, and Triglycine..... 2227
- HAMMOND, G. S. See Murov, S., 3797
- HAMMOND, P. R. Studies on Complexes. XIII. Another

- Spectrophotometric Equilibrium Equation, a Simple, Versatile Apparatus Designed for Its Use, and the Application to Some Charge-Transfer Interactions. . . . . 2272
- HANANIA, G. I. H., IRVINE, D. H., AND SHURAYH, F. R. Reduction Potentials of Complex Ions. The Tris(pyridine-2-aldoxime)iron(III)-Tris(pyridine-2-aldoxime)-iron(II) System. . . . . 1355
- HANSEN, W. N. See Probst, A., 2576
- HAQUE, I., AND WOOD, J. L. The Reaction Products of  $\gamma$ -Picoline and Iodine. . . . . 2438
- HAQUE, R. Nuclear Magnetic Resonance Study of Micelle Formation in Sodium Perfluorocaprylate and -propionate 3056
- HARDGROVE, G. L., TEMPLETON, L. K., AND TEMPLETON, D. H. Crystal and Molecular Structures of Three Dihalobenzocyclobutenes. . . . . 668
- HARE, C. R. See Sleight, T. P., 2207
- HARMON, K. M., AND COBURN, T. T. Carbonium Ion Salts. XII. Thermodynamic and Infrared Spectral Studies on Hydroxytropenylium Halide Hydrates. . . . . 2950
- HARRIS, K. R. See Bell, T. N., 4693
- HARRIS, N. H., AND COOK, R. L. Solid-State Reactions of  $\text{SrCo}_3 + \text{TiO}_2$ . . . . . 3326
- HARRISON, A. G. See Myher, J. J., 1905
- HART, E. J., AND FIELDEN, E. M. Reaction of the Deuterated Electron  $e_d^-$ , with  $e_d^-$ , D, OD, and  $\text{D}_2\text{O}$ . . . . . 577
- HARTECK, P. See Emerson, J., 3721; Liuti, G., 1031
- HARTLAND, S. The Radius of the Draining Film beneath a Drop Approaching a Plane Interface. . . . . 318
- HARUMIYA, N. See Miyama, H., 4700
- HASCHKE, J. M., AND EICK, H. A. The Vaporization of Ytterbium Dicarbide. . . . . 1697
- HASCHKE, J. M., AND EICK, H. A. The Vaporization Thermodynamics of Trieuropium Tetroxide. . . . . 4235
- HASEGAWA, H. See Hirasawa, R., 2541; Taniguchi, H., 1926
- HASKELL, R. W., HOLLINGER, H. B., AND VAN NESS, H. C. The Chemical Model as Applied to Associated Liquid Solutions. The Ethanol-Heptane System. . . . . 4534
- HASSAN, M. N. See Helmy, A. K., 2358
- HASTIE, J. W., HAUGE, R., AND MARGRAVE, J. L. Infrared Vibrational Properties of  $\text{GeF}_2$ . . . . . 4492
- HASTIE, J. W. See Bloom, H., 2361, 2706, 3041; Ficalora, P. J., 1660; Hauge, R. H., 3510
- HATANO, H. See Taniguchi, H., 1926
- HATZENBUHLER, D. See Dubrow, R., 2489
- HAUGE, R. H., HASTIE, J. W., AND MARGRAVE, J. L. Ultraviolet Absorption Spectra of Gaseous  $\text{SnF}_2$  and  $\text{PbF}_2$ . . . . . 3510
- HAUGE, R. See Hastie, J. W., 4492
- HAUGEN, G. R., AND FRIEDMAN, H. L. The Gibbs Free Energy of Transfer of the Alkali Perrenates and Perchlorates between Pure Water and Pure Nitromethane. . . . . 4549
- HAWARD, R. N., AND PARKER, B. M. The Internal Pressure of Simple Liquids. . . . . 1842
- HAWKINSON, S. See Fleischer, E. B., 4311
- HAYAMIZU, K. See Yamamoto, O., 822
- HAYASHI, S. See Hamada, F., 178
- HAYON, E. See Danziger, R. M., 3842; Dogliotti, L., 1800; Huber, J. R., 3820
- HEINTZ, E. A. See Murty, H. N., 746
- HELD, R. P. See Criss, C. M., 2970
- HELLEMANS, L., AND JONCKHEERE, C. Kinetics of the Chlorination of Mercuric Chloride in Acetone at a Solid Surface. . . . . 2154
- HELLER, C. A. See Fletcher, A. N., 1839
- HELMY, A. K., ASSAAD, F. F., HASSAN, M. N., AND SADEK, H. Apparent and Partial Molal Volumes of Na-Kaolin and NaCl in Kaolin Suspensions. . . . . 2358
- HEMMES, P., AND PETRUCCI, S. Ultraviolet and Ultrasonic Absorption Spectral Studies of the Association of  $\text{CuSO}_4$  and  $\text{Cu}(\text{en})_2\text{S}_2\text{O}_3$  in Water at  $25^\circ$ . . . . . 3986
- HENGSTENBERG, D. See Guion, J., 2086, 4620
- HENSLEY, A. L., JR. See Peri, J. B., 2926
- HENTZ, R. R., AND KNIGHT, R. J. The Mechanism of Radiation-Induced Luminescence from Scintillators in Cyclohexane. . . . . 1783
- HENTZ, R. R., AND KNIGHT, R. J. Gas-Phase Photolysis of Mixtures of Cyclohexane with Benzene and with Nitrous Oxide at  $1470 \text{ \AA}$ . . . . . 4684
- HENTZ, R. R., AND RZAD, S. J. Gas-Phase Radiolysis of Benzene. . . . . 1027
- HENTZ, R. R., AND SHERMAN, W. V. The Mechanism of Hydrogen Formation in the  $\gamma$  Radiolysis of 1,4-Dioxane and Its Mixtures with Water. . . . . 2635
- HEPLER, L. G. See Bertrand, G. L., 4194; Goldberg, R. N., 4654; Hill, J. O., 3695; Larson, J. W., 2902
- HERMAN, H. B. See Blount, H. N., 3006
- HERMANN, A. See Stern, J. H., 364
- HERRICK, C. C., AND FEBER, R. C. Vaporization Studies on Arsenic. . . . . 1102
- HERRON, J. T., AND HUIE, R. E. On the Reaction of Atomic Nitrogen with Carbon Dioxide. . . . . 2235
- HERRON, J. T., AND HUIE, R. E. Arrhenius Parameters for the Reactions of Atomic Nitrogen with Some Olefins and Acetylenes. . . . . 2538
- HERSH, L. S. Ionic Membranes. I. Surface Sulfonic Acid Groups on Porous Glass: a Potentiometric Study. . . . . 2195
- HERTL, W. Mechanism of Gaseous Siloxane Reaction with Silica. I. . . . . 1248
- HERTL, W. Mechanism of Gaseous Siloxane Reaction with Silica. II. . . . . 3993
- HERTL, W., AND HAIR, M. L. Hydrogen Bonding between Adsorbed Gases and Surface Hydroxyl Groups on Silica. . . . . 4676
- HERZ, A. H. See Feldman, L. H., 2008
- HETZER, H. B., ROBINSON, R. A., AND BATES, R. G. Dissociation Constants of Piperazinium Ion and Related Thermodynamic Quantities from  $0$  to  $50^\circ$ . . . . . 2081
- HEUSSER, U. K. See Baddour, R. F., 3621
- HIDDEN, N. J. See Blandamer, M. J., 2268
- HIGGINS, J. See Degn, H., 2692
- HIGHTOWER, J. W., AND HALL, W. K. Tracer Studies of Acid-Catalyzed Reactions. VIII. Langmuir Kinetics in Cycloalkane Isomerization over Silica-Alumina. . . . . 4555
- HIKIDA, T. See Graham, D. M., 3328
- HILDEBRAND, J. H. A Criticism of the Term "Hydrophobic Bond". . . . . 1841
- HILL, J. O., WORSLEY, I. G., AND HEPLER, L. G. Calorimetric Determination of the Distribution Coefficient and Thermodynamic Properties of Bromine in Water and Carbon Tetrachloride. . . . . 3695
- HILTNER, P. A. See Slabaugh, W. H., 4295
- HINDMAN, J. C., SVIRNICKAS, A., AND WOOD, M. Deuteron Spin-Lattice Relaxation of  $\text{D}_2\text{O}$  in Organic Solvents. . . . . 4188
- HINOJOSA, O. See Bains, M. S., 2250
- HIRASAWA, R., MUKAIBO, T., HASEGAWA, H., ODAN, N., AND MARUYAMA, T. Study on the Kinetics of Fast Electrode Processes with Pulse Technique and Electron Spin Resonance Methods. . . . . 2541
- HIROHARA, H. See Ise, N., 4543
- HIROTA, K., KERA, Y., AND TERATANI, S. Carbon Monoxide Oxidation with an Oxygen Tracer over a Vanadium Pentoxide Catalyst. . . . . 3133
- HIROTA, K., AND NIWA, Y. The Fragmentation of Skeletal Bonds of Cyclic Alkanes in Mass Spectra. . . . . 5
- HIROTA, K., UEDA, T., KITAYAMA, T., AND ITOH, M. Self-Exchange Reaction of Deuterium in Monodeuterio-toluene Catalyzed by Nickel and Platinum. . . . . 1976
- HISATSUNE, I. C. Estimation of the Isomerization Rate of Nitrous Acid. . . . . 269
- HODGES, R. J., AND GARNETT, J. L. The Kinetics of Hydrogen Isotope Exchange in Benzene Using a Homogeneous Platinum Catalyst. . . . . 1673
- HODNETT, E. M. See Felber, B. J., 2496
- HOECKER, F. See Zimbrick, J., 3277
- HOFFMAN, M. Z. See Granzow, A., 1402, 3741
- HOLIAN, J., AND GARRISON, W. M. On the Radiation-Induced Reduction of Amide and Peptide Functions in Aqueous Systems. . . . . 4723
- HOLLERAN, E. M. The Reduced Equation of State of Argon and Xenon. . . . . 1230
- HOLLERAN, E. M., AND GERARDI, G. J. Corresponding States of Argon and Methane. . . . . 3559
- HOLLINGER, H. B. See Haskell, R. W., 4534
- HOLLOWAY, H. E., NAUMAN, R. V., AND WHARTON, J. H. Absorptions and Fluorescences of 2-Phenylnaphthalene, 2'-Methyl-2-phenylnaphthalene, and 1-Fluoro-2-phenylnaphthalene. Spectroscopic Evidence for the Equilibrium Conformation of the Lowest Excited States. . . . . 4468
- HOLLOWAY, H. E., NAUMAN, R. V., AND WHARTON, J. H. The Electronic Structure and Spectra of 2-Phenylnaphthalene. Ground- and Excited-State Potential Energies as Functions of Molecular Conformation. . . . . 4474
- HOLMES, H. F., FULLER, E. L., JR., AND SECoy, C. H. Heats of Immersion in the Thorium Oxide-Water System. IV. Variation of the Net Differential Heat of Adsorption with Specific Surface Area. . . . . 2095
- HOLMES, H. F., FULLER, E. L., JR., AND SECoy, C. H.

- Gravimetric Adsorption Studies of Thorium Oxide. III. Adsorption of Water on Porous and Nonporous Samples. 2293
- HOLMES, H. F. See Fuller, E. L., Jr., 573
- HOLMES, L. P., COLE, D. L., AND EYRING, E. M. Kinetics of Aluminum Ion Hydrolysis in Dilute Solutions. 301
- HOLROYD, R. A. The Reaction of Nitrous Oxide with Excited Molecules in the Radiolysis and Photolysis of Liquid Alkanes. 759
- HOPKINS, P. D., AND STOFFER, R. L. Isobutane Chemisorption on Synthetic Faujasites. 3345
- HORNE, R. A., JOHNSON, D. S., AND YOUNG, R. P. The Electrical Conductivity of 0.10 M Potassium Chloride Water-Alcohol Solutions under Hydrostatic Pressure. 866
- HORNE, R. A., AND YOUNG, R. P. A Low-Temperature, High-Pressure Hydrate of *n*-Tetrabutylammonium Halides. 376
- HORNE, R. A., AND YOUNG, R. P. The Electrical Conductivity of Aqueous Tetraalkylammonium Halide Solutions under Hydrostatic Pressure. 1763
- HORNE, R. A., AND YOUNG, R. P. The Pressure Dependence, Specific Volume, and Suggested Structure of Hydrophobic Hydration. 2694
- HORSMA, D. A., AND NASH, C. P. Solutions of N-Substituted Amino Acids. III. The Influence of Solvent on the Tautomeric Equilibrium. 2351
- HOU, K. C. See Palmer, H. B., 348
- HOYER, H. W., SANTORO, A. V., AND BARRETT, E. J. Determination of Critical Temperature by Differential Thermal Analysis. 4312
- HU, T. See Craig, N. C., 2234
- HUANG, T., AND SPENCE, J. T. The Oxidation of Hydrazine by Molybdenum(VI). 4198
- HUANG, T., AND SPENCE, J. T. The Molybdenum(VI)-Catalyzed Oxidation of Hydrazine by Methylene Blue. 4573
- HUANG, T. T.-S., KASS, W. J., BUDDENBAUM, W. E., AND YANKWICH, P. E. Anomalous Temperature Dependence of Kinetic Carbon Isotope Effects and the Phenomenon of Crossover. 4431
- HUBBARD, W. N. See Greenberg, E., 222
- HUBER, J. R., AND HAYON, E. Flash Photolysis in the Vacuum Ultraviolet Region of the Phosphate Anions  $\text{H}_2\text{PO}_4^-$ ,  $\text{HPO}_4^{2-}$ , and  $\text{P}_2\text{O}_7^{4-}$  in Aqueous Solutions. 3820
- HUBER, J. R. See Halonbrenner, R., 3929
- HUDSON, B. S. See Hallada, C. J., 4304
- HUEBERT, B. J., AND MARTIN, R. M. Gas-Phase Far-Ultraviolet Absorption Spectrum of Hydrogen Bromide and Hydrogen Iodide. 3046
- HUIE, R. E. See Herron, J. T., 2235, 2538
- HUNG, G. W. See Messer, C. E., 3958
- HUNT, J. W. See Bronskill, M. J., 3762
- HUSTON, R., AND BUTLER, J. N. The Standard Potential of the Lithium Electrode in Aqueous Solutions. 4263
- HUYBRECHTS, G. See Bertrand, L., 3926
- HYDE, J. S., RIST, G. H., AND ERIKSSON, L. E. G. Endor of Methyl, Matrix, and  $\alpha$  Protons in Amorphous and Polycrystalline Matrices. 4269
- HYDE, J. S. See Kispert, L. D., 4276
- IKEDA, R., NAKAMURA, D., AND KUBO, M. Pure Quadrupole Resonance of Nitrogen-14 in Some Metal Cyano Complexes. 2982
- IKEDA, R., ONDA, S., NAKAMURA, D., AND KUBO, M. Nuclear Quadrupole Resonance of Nitrogen-14 in Some Pyridine Derivatives. 2501
- IKEDA, T., AND YOSHIOKA, H. New Method for Determining Magnetic Susceptibility and Magnetic Moment. 4392
- IMAI, H., ONO, Y., AND KEIL, T. Adsorption of 1,1-Diphenyl-2-picrylhydrazyl on Solid Acid Catalysts. 46
- INAGAKI, H. See Kotaka, T., 829
- IRVINE, D. H. See Hanania, G. I. H., 1355
- ISE, N., AND ASAI, K. Mean Activity Coefficient of Polyelectrolytes. IX. Activity Coefficients of Polyethylenesulfonates of Various Gegenions. 1366
- ISE, N., HIROHARA, H., MAKINO, T., AND SAKURADA, I. Ionic Polymerization under an Electric Field. XII. Living Anionic Polymerization of Styrene in the Binary Mixtures of Benzene and Tetrahydrofuran. 4543
- ISE, N., AND OKUBO, T. Mean Activity Coefficient of Polyelectrolytes. VIII. Osmotic and Activity Coefficients of Polystyrenesulfonates of Various Gegenions. 1361
- ISE, N., AND OKUBO, T. Mean Activity Coefficient of Polyelectrolytes. X. Activity Coefficients of Polyphosphates of Various Gegenions. 1370
- ISHIDA, H. See Tsubomura, H., 367
- ISHIDA, K. Stochastic Approach to Nonequilibrium Thermodynamics of First-Order Chemical Reactions. II. Open Systems. 92
- ITO, Y. See Miyama, H., 4700
- ITOH, M. See Hirota, K., 1976
- ITZKOWITZ, L. M. See Dill, A. J., 4580
- IWAMOTO, R. T. See Kemula, A., 1334, 2764
- IWASAKI, M., TORIYAMA, K., AND OHMORI, T. Trapped Electrons in  $\gamma$ -Irradiated Polycrystalline *n*-Hydrocarbons Studied by Electron Spin Resonance Spectroscopy. 4347
- IWASAKI, M. See Sakurai, T., 1491
- IYENGAR, R. D. See Codell, M., 2460
- IZATT, R. M., EATOUGH, D., AND CHRISTENSEN, J. J. Calorimetric Determination of  $\log K^{\circ}$ ,  $\Delta H^{\circ}$ , and  $\Delta S^{\circ}$  Values for the Interaction at 25° of Thiourea with  $\text{Hg}(\text{CN})_2$  in Water-Ethanol Solvents. 2720
- IZATT, R. M., EATOUGH, D., SNOW, R. L., AND CHRISTENSEN, J. J. Computer Evaluation of Entropy Titration Data. Calorimetric Determination of  $\log \beta_1$ ,  $\Delta S^{\circ}$ , and  $\Delta S^{\circ}$  Values for the Silver(I)- and Copper(II)-Pyridine Systems. 1208
- JACOBS, P. See Uyterhoeven, J. B., 1768
- JACOBS, P. W. M., AND RUSSELL-JONES, A. Sublimation of Ammonium Perchlorate. 202
- JAMES, D. W. The Rate of Oxidation of Nitrite Ions in Dilute Solutions of Sodium Nitrite in Molten Lithium Perchlorate. 876
- JAMES, D. W., AND MARSHALL, R. C. An Electron Spin Resonance Study of the Dinitrogen Tetroxide-Nitrogen Dioxide System. 2963
- JAMES, D. W. See Boston, C. R., 293
- JANATA, J., AND MARK, H. B., JR. The Reduction of Aromatic Hydrocarbons. II. Polarographic Study of the Effect of Proton Donors. 3616
- JANNELLI, L. See Della Monica, M., 1068
- JANZEN, E. G. See Gerlock, J. L., 1832
- JARVIS, N. L., AND SCHEIMAN, M. A. Surface Potentials of Aqueous Electrolyte Solutions. 74
- JASTER, W. See Safrany, D. R., 518, 3305, 3318, 3323
- JAYE, F. C. See Solomon, W. C., 2311
- JENSEN, H. B. See Duvall, J. J., 4528
- JHON, M. S., CLEMENA, G., AND VAN ARTSDALEN, E. R. The Significant Structure and Properties of Molten Mercuric Halides. 4155
- JINDAL, M. R. See Malik, W. U., 3612
- JOHANNESSEN, R. B., BRINCKMAN, F. E., AND COYLE, T. D. Nuclear Magnetic Resonance Studies of Inorganic Fluorides. V. Fluorosilanes. 660
- JOHANNSSON, O. K. See Stark, F. O., 2750
- JOHANSSON, H. See Beronius, P., 713
- JOHARI, G. P., AND DANNHAUSER, W. Dielectric Study of Intermolecular Association in Sterically Hindered Octanol Isomers. 3273
- JOHNS, L. E., JR. A Further Note on the Rate of Dissolving of Spherical Gas Bubbles. 3357
- JOHNSEN, R. H. See Hagopian, A. K. E., 1949
- JOHNSON, B. M. See Langer, S. H., 4020
- JOHNSON, D. S. See Horne, R. A., 866
- JOHNSON, G. R. A., AND REDPATH, J. L. Electron Capture Processes in Irradiated Gaseous  $\text{HCl}$ . 765
- JOHNSON, I. See Krumpelt, M., 506
- JOHNSON, J. D. Applications of McLachlan's Theory to Physical Adsorption. 3697
- JOHNSON, J. R., KILPATRICK, P. J., CHRISTIAN, S. D., AND AFFSPRUNG, H. E. The Hydration of Pyridine in Organic Solvents. 3223
- JOHNSON, J. S. See Rush, R. M., 767
- JOHNSON, J. S., JR., AND RUSH, R. M. Osmotic Coefficients of Tungstosilicic Acid. 360
- JOHNSON, J. S., JR. See Shor, A. J., 2200
- JOHNSON, J. W., SILVA, W. J., AND CUBICCIOTTI, D. The Critical Temperature and Coexistence Curve for Aluminum Bromide. 1664
- JOHNSON, J. W., SILVA, W. J., AND CUBICCIOTTI, D. The Vapor Pressure and Enthalpy of Vaporization of Molten Aluminum Bromide to the Critical Point. 1669
- JOHNSTON, F. J. See Donaldson, G. W., 3552
- JONAS, V. See Neuman, R. C., Jr., 2469
- JONCKHEERE, C. See Helemans, L., 2154
- JONES, A., MORRIS, E. R., AND THYNNE, J. C. J. The Thermal Decomposition of Dimethyl Azodiformate. 2677
- JONES, J. B., AND ADAMSON, A. W. Temperature Dependence of Contact Angle and of Interfacial Free Energies in the Naphthalene-Water-Air System. 646

- JONES, J. P. See Espino, R. L., 3689  
 JONES, L. H. See Coleman, J. S., 2605  
 JONES, W. E. See Madhavan, N., 1812  
 JOY, A. S. See Kini, K. A., 2127  
 JOYNER, T. B. The Thermal Decomposition of Solid *cis*-Diazidotetraamminecobalt(III) Azide. . . . . 703  
 JOYNER, T. B. The Thermal Decomposition of Solid Hexaamminecobalt(III) Azide: The Cobalt(II) Reaction. . . . . 4386  
 JULIEN, L. M., AND PERSON, W. B. Contact Charge-Transfer Spectra of Iodine in Some Hydrocarbon Solvents. . . . . 3059
- KACMAREK, A. J. See Solomon, I. J., 2262  
 KADABA, P. K. See Gopalan, T. V., 3676  
 KAGAN, M. R., AND GUILBAULT, G. G. Ion-Mobility Measurements of Inorganic and Organic Phosphorus Compounds. . . . . 2867  
 KALANTAR, A. H. Isotropic Rotational Relaxation of Photoselected Emitters and Systematic Errors in Emission Decay Times. . . . . 2801  
 KALANTAR, A. H. See Martin, T. E., 2265  
 KALE, J. D., AND TIMMONS, R. B. The Kinetics of the Reaction of Trifluoromethyl Radicals with Hydrogen Sulfide. . . . . 4239  
 KALFOGLOU, N., AND SZWARC, M. The Heat and Entropy of Dissociation of Carbonium Ion Pairs. . . . . 2233  
 KANELLOPOULOS, A. See Lykourezos, P. A. P., 2330  
 KARP, S. Homogeneous Chemical Kinetics with the Rotating Disk Electrode. The ECE Mechanism. . . . . 1082  
 KASE, M. See Akita, K., 906  
 KASKAN, W. E. See Carabetta, R., 2483  
 KASS, W. J. See Huang, T. T.-S., 4431  
 KATAKIS, D., AND KONSTANTATOS, J. Decomposition of Aqueous Perchlorates by Radiation. . . . . 2054  
 KATAKIS, D. See Lykourezos, P. A. P., 2330  
 KATO, T., MIYASO, K., AND NAGASAWA, M. Light-Scattering Measurements of Poly( $\alpha$ -methylstyrene). The Effect of Molecular Weight Heterogeneity on the Second Virial Coefficient. . . . . 2161  
 KAUFMANN, W. See Nemethy, G., 1842  
 KAWAHARA, K. See Okita, K., 278  
 KE, C. H. See Nishimura, S., 1297  
 KEARNS, D. R. See Chambers, R. W., 4718  
 KEBARLE, P. See Searles, S. K., 742  
 KEEFE, S. E. See Grant, E. H., 4373  
 KEENAN, A. G., NOTZ, K., AND WILCOX, F. L. Pyrex Membrane Potential in Binary Nitrate Melts. . . . . 1085  
 KEENE, J. P. See Cundall, R. B., 3871  
 KEII, T. See Imai, H., 46; Ono, Y., 2851  
 KEITH, A. D. See Waggoner, A. S., 4129  
 KELLER, D. V., JR. See Aldrich, R. G., 1092  
 KELLNER, J. D. The Viscosity of Molten Bismuth-Bismuth Halide Solutions. . . . . 1737  
 KELLY, J. J. See Mukherjee, L. M., 3410  
 KEMP, T. J., ROBERTS, J. P., SALMON, G. A., AND THOMPSON, G. F. Pulse Radiolysis of Solutions of Amines of Low Ionization Potential. . . . . 1464  
 KEMULA, A., AND IWAMOTO, R. T. Molecular Addition Compounds of Tin(IV) Chloride with Ethyl Esters of Dicarboxylic Acids in Benzene and Methylene Chloride. . . . . 1334  
 KEMULA, A., AND IWAMOTO, R. T. Interactions in Benzene. Investigation of Collision Complexes of Free and of Coordinated Monoethyl, Diethyl, and Cyanoethyl Esters and Benzene by Nuclear Magnetic Resonance Spectroscopy. . . . . 2764  
 KENESHEA, F. J., CUBICCIOTTI, D., WITHERS, G., AND EDING, H. Enthalpy and Entropy Increments above 298°K and a  $\Sigma$ -Plot Treatment of Vaporization Data for Niobium Pentachloride. . . . . 1272  
 KENNEY, D. J., CLINCKEMAILLIE, G. G., AND MICHIELS, C. L. Ligand Substitution Reactions of Hexacyanoferrate(III) and Azide Induced by Flash Photolysis. . . . . 410  
 KENNEY, J. T., AND POWELL, F. X. Raman Spectra of Fused Indium and Bismuth Chlorides. . . . . 3094  
 KERA, Y. See Hirota, K., 3133  
 KERR, G. T. Chemistry of Crystalline Aluminosilicates. IV. Factors Affecting the Formation of Zeolites X and B. . . . . 1385  
 KERR, G. T. Chemistry of Crystalline Aluminosilicates. V. Preparation of Aluminum-Deficient Faujasites. . . . . 2594  
 KERR, G. T., AND SHIPMAN, G. F. The Reaction of Hydrogen Zeolite Y with Ammonia at Elevated Temperatures. . . . . 3071
- KERTES, A. S., AND MARKOVITS, G. Activity Coefficients, Aggregation, and Thermodynamics of Tridodecylammonium Salts in Nonpolar Solvents. . . . . 4202  
 KEVAN, L. See Koob, R. D., 3808; Sokolowska, A., 253; Zimbrick, J., 3277  
 KHOBIAR, S., CARTER, J. L., AND LUCCHESI, P. J. The Electronic Properties of Aluminum Oxide and the Chemisorption of Water, Hydrogen, and Oxygen. . . . . 1682  
 KILPATRICK, P. J. See Johnson, J. R., 3223  
 KILROY, W. P. See Schulman, S. G., 3372  
 KIMBELL, G. H. See Arnold, S. J., 4344  
 KIMMEL, P. I., AND STRAUSS, H. L. The Electronic Spectrum of the Cyclooctatetraenyl Radical Anion. . . . . 2813  
 KING, C. M. See O'Malley, J. A., 3584  
 KINI, K. A., MANSER, R. M., AND JOY, A. S. The Surface Area of Silicate Minerals by the BET Method Using the Adsorption of Xenon at  $-78^\circ$ . . . . . 2127  
 KIROWA-EISNER, E. See Mark, H. B., Jr., 1083  
 KISPERT, L. D., HYDE, J. S., DE BOER, C., LAFOLLETTE, D., AND BRESLOW, R. Combined Electron-Nuclear Double Resonance and Electron Paramagnetic Resonance Techniques in a Study of Some Low-Symmetry Triphenylmethyl Derivatives. . . . . 4276  
 KISTAKOWSKY, G. B., AND WALTER, T. A. Photolysis of Ketene by 2139-Å Radiation. . . . . 3952  
 KITAYAMA, T. See Hirota, K., 1976  
 KLASSEN, N. V. The Argon-Sensitized Radiolysis of Methane and Ethane in the Liquid Phase. . . . . 1076  
 KLEIN, G. W. See Spittler, E. G., 1432  
 KLEIN, N., TRUMBORE, C. N., FANNING, J. E., JR., AND WARNER, J. W. Reactions of the Hydrated Electron in Alkaline Solution. . . . . 880  
 KLEIN, R., AND SCHEER, M. D. Mechanism of O(<sup>3</sup>P) Addition to Condensed Films. II. Propene, 1-Butene, and Their Mixtures. . . . . 616  
 KLEMENT, W., JR. Thermodynamics of the  $\lambda$  Transition in Sodium Nitrate. . . . . 1294  
 KLENERT, M. See Niemann, E.-G., 3766  
 KNIGHT, A. R. See Steer, R. P., 2145  
 KNIGHT, P. C. See Cavell, E. A. S., 1656  
 KNIGHT, R. J. See Hentz, R. A., 1783, 4684  
 KNOBLER, C. M. See Dantzler, E. M., 676  
 KNOZINGER, H., SCHEGLILA, A., AND WATSON, A. M. The Dehydration of Alcohols over Alumina. VIII. The Ether Formation from the Deuterated Methanols CH<sub>3</sub>OH, CD<sub>3</sub>OH, CH<sub>3</sub>OD, and CD<sub>3</sub>OD. . . . . 2770  
 KOBATAKE, Y., YUASA, M., AND FUJITA, H. Studies of Membrane Phenomena. VI. Further Study of Volume Flow. . . . . 1752  
 KOBATAKE, Y. See Yuasa, M., 2871  
 KOBAYASHI, S. See Fraenkel, G., 953  
 KOBAYASHI, T., UYEDA, N., AND SUITO, E. The *n*-Donor Complex Formation and Polymorphic Transformation of Zinc Phthalocyanine in Organic Suspension Media. . . . . 2446  
 KOHL, F. J. See Uy, O. M., 1611  
 KOLC, J. See Becker, R. S., 997  
 KOLTHOFF, I. M., AND CHANTOONI, M. K., JR. Autoprotolysis of Constant of Acetonitrile. . . . . 2270  
 KONSTANTATOS, J. See Katakis, D., 2054  
 KOOB, R. D., AND KEVAN, L. Energy Transfer in Radiolysis of Rare Gas-Propane Liquid Mixtures. . . . . 3808  
 KORDIS, J., AND EYRING, L. Some Tensimetric Studies in the Mixed Ceria-Terbia System. . . . . 2030  
 KORDIS, J., AND EYRING, L. A Tensimetric Study of the Terbia and Praseodymia Systems and the Mixed Praseodymia-Terbia System. . . . . 2044  
 KORDIS, J. See Burnham, D. A., 4424  
 KORSON, L. See Millero, F. J., 2251  
 KOSKI, W. S. See Munro, D. F., 2682  
 KOTAKA, T., MURAKAMI, Y., AND INAGAKI, H. Dilute Solution Properties of Styrene-Methyl Methacrylate Random Copolymers. . . . . 829  
 KRAMER, A. See Maatman, R. W., 104  
 KRAUS, K. A. See Marcinkowsky, A. E., 1201; Raridon, R. J., 925; Shor, A. J., 2200  
 KRAUSE, R. F., JR., AND DOUGLAS, T. B. The Vapor Pressure, Vapor Dimerization, and Heat of Sublimation of Aluminum Fluoride, Using the Entrapment Method. . . . . 475  
 KRAUSE, R. F., JR., AND DOUGLAS, T. B. The Heats of Formation of AlCl<sub>2</sub> and AlCl<sub>2</sub>F from Subliming AlF<sub>3</sub> in the Presence of AlCl<sub>3</sub> Vapor. . . . . 3444  
 KREEVOY, M. M., AND ELIASON, R. The Brønsted  $\alpha$  and Isotope Effects for Vinyl Ether Hydrolysis. . . . . 1313



- KREGLEWSKI, A. A Semiempirical Treatment of Properties of Fluid Mixtures. II. Estimation of the Effects of Molecular Sizes in Fluids and Fluid Mixtures . . . . . 1897
- KREGLEWSKI, A. On the Critical and Pseudocritical Pressure of Binary Mixtures . . . . . 2280
- KRIEGER, I. M. Reply to Communication by M. Cable . . . . . 3357
- KROENKE, W. J. See Carman, C. J., 2562
- KRUGER, G. J., AND BOEYENS, J. C. A. The Crystal and Molecular Structure of 1,2,3,4-Tetrabromo-1,2,3,4-diphthaloylcyclobutane . . . . . 2120
- KRUMPELT, M., FISCHER, J., AND JOHNSON, I. The Reaction of Magnesium Metal with Magnesium Chloride . . . . . 506
- Kubo, M. See Ikeda, R., 2501, 2982
- KUBOKAWA, Y., AND MIYATA, H. Desorption of Cumene from Silica-Alumina Catalysts . . . . . 356
- KUCERA, E. See Giddings, J. C., 4397
- KUHLMANN-WILSDORF, D. See Vermaak, J. S., 4150
- KULEVSKY, N., AND REINEKE, W. Thermodynamic Values for the Dimerization of 2-Pyridone and 2-Thio-pyridone . . . . . 3339
- KUNIMITSU, D. K., WOODY, A. Y., STIMSON, E. R., AND SCHERAGA, H. A. Thermodynamic Data from Fluorescence Spectra. II. Hydrophobic Bond Formation in Binary Complexes . . . . . 856
- KUNTZ, R. R. See Volkert, W. A., 3394
- KUPPERMAN, A., RICE, J. K., AND TRAJMAR, S. Low-Energy, High-Angle Electron-Impact Spectrometry . . . . . 3894
- KUWANA, T. See Srinivasan, V. S., 1144
- KWUN, O. C., AND CHOI, S. U. Kinetics of the Bromine-Exchange Reaction of Gallium Bromide with Ethyl Bromide in 1,2,4-Trichlorobenzene and in Nitrobenzene . . . . . 3148
- LABHART, H. See von Salis, G. A., 752
- LACEFIELD, R. M. See Stark, F. O., 2750
- LAFFOLLETTE, D. See Kispert, L. D., 4276
- LAGOWSKI, J. J. See Burow, D. F., 169; Rounsaville, J. F., 1111; Quinn, R. K., 1374
- LAHAYE, J. See Palmer, H. B., 348
- LAKSHMINARAYANAI AH, N. Reply to "Comment on 'Current Dependence of Water Transport in Cation-Exchange Membranes'" . . . . . 3699
- LAKSHMINARAYANAI AH, N., AND SUBRAHMANYAN, V. Current Dependence of Water Transport in Cation-Exchange Membranes . . . . . 1253
- LAKSHMINARAYANAI AH, N. See Subrahmanyam, V., 4314
- LAL, M. See Wilkening, V. G., 185
- LALIBERTE, L. H. See Conway, B. E., 4317
- LAMANNA, U. See Della Monica, M., 1068, 2124, 4329
- LAMPE, F. W. See Tewarson, A., 3261
- LAMPRECHT, G. J., DICKS, L., AND CROWTHER, P. A Study of the Solubility of Metals in Liquid Sodium. II. The System Sodium-Lead . . . . . 1439
- LANG, R. P. Molecular Complexes of Iodine with Tetramethylurea and Tetramethylthiourea . . . . . 2129
- LANGER, S. H., JOHNSON, B. M., AND CONDER, J. R. Gas-Liquid Chromatographic Study of the Thermodynamics of Solution of Some Aromatic Compounds. III. Solutions and Associative Interaction with Tetrachloroterephthalate Esters . . . . . 4020
- LANGMUIR, M. E. See Danziger, R. M., 3842
- LARDON, M. See Sharp, J. H., 3230
- LARHER, Y. Bidimensional Condensation in Adsorbed Layers . . . . . 1847
- LARSON, J. W., CERUTTI, P., GARBER, H. K., AND HEPLER, L. G. Electrode Potentials and Thermodynamic Data for Aqueous Ions. Copper, Zinc, Cadmium, Iron, Cobalt, and Nickel . . . . . 2902
- LARSON, J. W. See Bertrand, G. L., 4194
- LARSON, Q. V. See Boyd, G. E., 2651
- LAURENCE, G. S. See Grygorowicz, C., 1811
- LAVELLE, J. A. Comments on "Temperature Dependence of Contact Angle and of Interfacial Free Energies in the Naphthalene-Water-Air System" . . . . . 2283
- LAW, S. L., AND McDONALD, R. L. Solvation of Extracted Complex Metal Acids. IV. The  $\text{HAuCl}_4$ -Nitrobenzene System . . . . . 1617
- LAWSON, K. D., AND FLAULT, T. J., Mesomorphic Phases. II. Proton and Deuterium Magnetic Resonance Studies of the Dimethyldodecylamine Oxide-Deuterium Oxide System . . . . . 2066
- LAWSON, K. D., MABIS, A. J., AND FLAULT, T. J. Mesomorphic Phases. I. X-Ray Studies of the Dimethyldodecylamine Oxide-Deuterium Oxide System . . . . . 2058
- LAZARTIC, J. See Stern, J. H., 3053
- LEBEL, J., MICHAUD, P., AND OUELLET, C. Inhibition by  $\text{C}_2\text{O}_2$  of the Explosive Combustion of  $\text{CO}$  . . . . . 3678
- LECALVÉ, J. See Meaburn, G. M., 3920
- LEDBETTER, J. W., JR. Substituent Effects on the Tautomerism of Schiff Bases . . . . . 4111
- LEE, C. S. See Miller, G. A., 4644
- LEE, G. A. See Markgraf, J. H., 2276
- LÉONARD, A. See Fripiat, J. J., 1808
- LEONHARDT, H. R. See Livingston, R., 2254
- LE ROY, D. J. See Ridley, B. A., 1844
- LEVISON, S. A., AND MARCUS, R. A. Kinetics of Ferrocyanide Reduction of Quinones . . . . . 358
- LEVY, J. See Morrow, J. L., 885
- LEVY, J. B., AND COPELAND, B. K. W. The Kinetics of the Hydrogen-Fluorine Reaction. III. The Photochemical Reaction . . . . . 3168
- LEVY, R. M. An X-Ray Study of the Participation of the Bulk Phase of Cobalt Oxide in Oxidation Catalysis . . . . . 2609
- LEWIN, M. See Gutmann, H., 3671
- LEYTE, J. C., ZUIDERWEG, L. H., AND VAN REISEN, M. A Spectroscopic Study of Binuclear Copper Complexes in Aqueous Poly(methacrylic acid) Solutions . . . . . 1127
- LI, N. C. See Bundschuh, J. E., 1001; Nishimura, S., 1297, 2908
- LIAS, S. G. See Ausloos, P., 3904
- LIBUŠ, W., PUCHALSKA, D., AND SZUCHNICKA, T. Coordination Disproportionation Equilibria in Solution. II. Cobaltous Chloride and Zinc Chloride in Acetonitrile . . . . . 2075
- LICHTIN, N. N. See Granzow, A., 1402, 3741; Titani, Y., 526
- LIDDIARD, V. C. See Prout, E. G., 2281
- LIETZKE, M. H., AND O'BRIEN, H. A., JR. Electromotive Force Studies in Aqueous Solutions at Elevated Temperatures. X. The Thermodynamic Properties of  $\text{HCl-KCl}$ ,  $\text{HCl-RbCl}$ ,  $\text{HCl-CsCl}$ ,  $\text{HCl-MgCl}_2$ ,  $\text{HCl-CaCl}_2$ ,  $\text{HCl-SrCl}_2$ , and  $\text{HCl-AlCl}_3$  Mixtures . . . . . 4408
- LIETZKE, M. H., AND STOUGHTON, R. W. Electromotive Force Studies in Aqueous Solutions at Elevated Temperatures. IX. The Thermodynamic Properties of Hydrochloric Acid-Gadolinium Chloride Mixtures . . . . . 257
- LILENFELD, H. See Steigman, J., 1132
- LILLEY, T. H. See Covington, A. K., 2759
- LIN, C.-T. See Bear, J. L., 2026
- LIN, J., AND WILLIAMS, F. Electron Spin Resonance Study of the Neopentyl Radical from the Radiolysis of Solid Neopentane in the Presence of Nitrous Oxide . . . . . 3707
- LIN, K. C. See Hammaker, R. M., 4346
- LIN, Y. N., CHAN, S. C., AND RABINOVITCH, B. S. Energy Transfer in Thermal Methyl Isocyanide Isomerization. Incremental and Relative Cross Sections of Hydrocarbons . . . . . 1932
- LIN, Y. N., AND RABINOVITCH, B. S. Energy Transfer in Thermal Methyl Isocyanide Isomerization. Dilution Effects at Low Pressure . . . . . 1726
- LIND, J. E., JR. See Morrison, G., 3001
- LINDENBAUM, S. Osmotic Coefficients of Aqueous Solutions of Tri-*n*-alkylsulfonium Halides at 25° . . . . . 212
- LINDENBAUM, S. See Boyd, G. E., 2651
- LINDERSTRØM-LANG, C. U., AND VASLOW, F. The Isotope Effect on the Vapor Pressures of  $\text{H}_2\text{O-C}_2\text{H}_5\text{OH}$  and  $\text{D}_2\text{O-C}_2\text{H}_5\text{OD}$  Mixtures . . . . . 2645
- LINDMAN, B., FORSEN, S., AND FORSLIND, E. Nuclear Quadrupole Relaxation of  $^{79}\text{Br}$  in Aqueous Solutions of Quaternary Ammonium Bromides . . . . . 2805
- LING, A. C., AND WILLARD, J. E. Viscosities of Some Organic Glasses Used as Trapping Matrices . . . . . 1918
- LING, A. C., AND WILLARD, J. E. Viscosities of Some Organic Glasses Used as Trapping Matrices. II . . . . . 3349
- LIQUORNIK, M., AND MARCUS, Y. Ion Exchange in Molten Salts. I. The Ion-Exchange Properties of Sodium Zeolite A in Molten  $\text{NaNO}_3$ ; Exchange Reactions with Alkali Metal, Thallium, and Silver Cations . . . . . 2885
- LIQUORNIK, M., AND MARCUS, Y. Ion Exchange in Molten Salts. III. The Ion-Exchange Properties of Sodium Zeolite A in Molten  $\text{NaNO}_3$ . The Exchange with Calcium and Strontium Cations . . . . . 4704
- LIRIO, J. A. See Gustafson, R. L., 1502
- LIUTI, G., DONDES, S., AND HARTECK, P. The Reaction of Nitrogen Atoms with  $\text{N}_2\text{O}_2$  . . . . . 1081
- LIVINGSTON, R., AND LEONHARDT, H. R. An Attempted Kinetic Study of Chemiluminescent Electron-Transfer Reactions . . . . . 2254
- LOEMKER, J. E., READ, J. M., AND GOLDSTEIN, J. H. Nuclear Magnetic Resonance Analyses and Parameters for Some Monohalobstituted Fluorobenzenes . . . . . 991

- LOGAN, T. P. See Di Carlo, E. N., 1517  
 LOHMANN, A. W. See Gayles, J. N., 4716  
 LOSENICKY, Z. Thermal Conductivity of Binary Liquid Solutions..... 4308  
 LOSSING, F. P. See Shapiro, J. S., 1552  
 LOSURDO, A. See Wirth, H. E., 751  
 LOUWRIER, P. W. F., AND HAMILL, W. H. Positive Charge Migration in  $\gamma$ -Irradiated Organic Solids and Trapping by Alkanes at 77°K..... 3878  
 LOW, M. J. D., AND RAMAMURTHY, P. Infrared Study of the Surface Properties of Phosphoric Acid Impregnated Silica..... 3161  
 LOW, M. J. D., RAMASUBRAMANIAN, N., RAMAMURTHY, P., AND DEO, A. V. Infrared Spectrum, Surface Reaction, and Polymerization of Adsorbed Hydrogen Cyanide on Porous Glass..... 2371  
 LOW, M. J. D. See McManus, J. C., 2378  
 LUCCHESI, P. J. See Khoobiar, S., 1682  
 LUDWIG, P. K., AND AMATA, C. D. Liquid Benzene Luminescence Quenching by Carbon Tetrachloride. Consideration of the Presence of Solvent Excimers in the Interpretation of the Observed Rates of Quenching.... 3725  
 LUISI, P. L., AND PINO, P. Conformational Properties of Optically Active Poly- $\alpha$ -olefins in Solution..... 2400  
 LUKSHA, E. See Criss, C. M., 2966, 2970  
 LUNSFORD, J. H. Surface Interactions of Zinc Oxide and Zinc Sulfide with Nitric Oxide..... 2141  
 LUNSFORD, J. H. Surface Interactions of NaY and Decationated Y Zeolites with Nitric Oxide as Determined by Electron Paramagnetic Resonance Spectroscopy..... 4163  
 LURIA, M., AND TREININ, A. The Photochemistry of NCS<sup>-</sup> in Solution..... 305  
 LYKOUREZOS, P. A. P., KANELLOPOULOS, A., AND KATAKIS, D. Radiolysis of Aqueous Chromium and Vanadium in Their +2 and +3 Oxidation States..... 2330  
 LYLE, D. L. See Coffman, R. E., 1392  
 LYNN, S. See Rinker, R. G., 4706  
 LYONS, L. E., MORRIS, G. C., AND WARREN, L. J. Electron Affinities and the Electron-Capture Method for Aromatic Hydrocarbons..... 3677
- MAATMAN, R., GEERTSEMA, A., VERHAGE, H., BAAS, G., AND DU MEZ, M. Electrolytes in High Surface Area Systems. I. The Reaction between Lithium Chloride-Acetone Solutions and Silica Gel, an Unusual Addition Reaction..... 97  
 MAATMAN, R. W., AND KRAMER, A. Electrolytes in High Surface Area Systems. II. The Reaction between Aqueous Dichromate and Silica Gel..... 104  
 MABIS, A. J. See Lawson, K. D., 2058  
 MACDONALD, H. C., JR. See Mark, H. B., Jr., 1083  
 MACGILLIVRAY, A. D., AND SWIFT, J. D. On the Variational Principle for the Poisson-Boltzmann Equation... 3575  
 MACINTYRE, F. BUBBLES: A Boundary-Layer "Microtome" for Micron-Thick Samples of a Liquid Surface... 589  
 MACKAY, L. D. See Schrier, E. E., 733  
 MACKNIGHT, W. J., MCKENNA, L. W., READ, B. E., AND STEIN, R. S. Properties of Ethylene-Methacrylic Acid Copolymers and Their Sodium Salts: Infrared Studies.. 1122  
 MACUR, G. J., EDWARDS, R. K., AND WAHLBECK, P. G. Measurement of Activities in Gallium-Indium Liquid Alloys..... 1047  
 MADHAVAN, N., AND JONES, W. E. The Rate of Reaction of Active Nitrogen with Perfluorobutene-2..... 1812  
 MAELAND, A. See Allard, K., 136  
 MAESTRO, M. See Ciani, F., 1510  
 MAGINI, M. See Danesi, P. R., 3437  
 MAGUIRE, J. A. See Banewicz, J. J., 1960  
 MAHLMAN, H. A. See Matthews, R. W., 3704  
 MAKAY, K. See Uytterhoeven, J. B., 1768  
 MAKI, A. H. See Gondo, Y., 3215  
 MAKINO, T. See Ise, N., 4543  
 MALAN, O. G., GÜSTEN, H., AND SCHULTE-FROHLINDE, D.  $\gamma$ -Radiation-Induced *cis-trans* Isomerization of Stilbenes in Liquid Naphthalene..... 1457  
 MALIK, W. U., AND JINDAL, M. R. Hydrogen Ion Equilibria of Soybean Protein..... 3612  
 MALONEY, K. M., AND RABINOVITCH, B. S. Heterogeneous Activation in Thermal Unimolecular Reaction.. 4483  
 MALOY, J. T., PRATER, K. B., AND BARD, A. J. Electrogenerated Chemiluminescence. II. The Rotating-Ring-Disk Electrode and the Pyrene-N,N,N',N'-Tetramethyl-*p*-phenylenediamine System..... 4348
- MALTENIEKS, O. See Scott, D. R., 3354  
 MANDELKERN, L., ALLOU, A. L., JR., AND GOPALAN, M. The Enthalpy of Fusion of Linear Polyethylene..... 309  
 MANI, I. See Sauer, M. C., Jr., 3856  
 MANSER, R. M. See Kini, K. A., 2127  
 MARCINKOWSKY, A. E., PHILLIPS, H. O., AND KRAUS, K. A. Properties of Organic-Water Mixtures. VII. Self-Diffusion Coefficients of Na<sup>+</sup> in Ethylene Glycol-Water and Glycerol-Water Mixtures at 25°..... 1201  
 MARCUS, R. A. Theoretical Relations among Rate Constants, Barriers, and Brønsted Slopes of Chemical Reactions..... 891  
 MARCUS, R. A. See Cohen, A. O., 4249; Levison, S. A., 358  
 MARCUS, Y. See Liquornik, M., 2885, 4704  
 MARGRAVE, J. L. See Ficalora, P. J., 1660; Hauge, R. H., 3510; Hastie, J. W., 4492; Zmbov, K. F., 1099  
 MARICLE, D. L. See Zweig, A., 377  
 MARK, H. B., JR., MCCOY, L. R., KIROWA-EISNER, E., AND MACDONALD, H. C., JR. Evidence for the Formation of a Surface Complex as the Rate-Determining Step in the Polarographic Reduction of Certain Nickel(II)-Organic Amine Complexes. Effect of the Structure of the Electrical Double Layer..... 1083  
 MARK, H. B., JR. See Janata, J., 3616; McCoy, L. R., 4637; Prostack, A., 2576  
 MARK, J. E. A Thermochemical Test of Interatomic Potential Functions for Hydrocarbons..... 2941  
 MARKGRAFT, J. H., LEE, G. A., AND SKINNER, J. F. The Electric Dipole Moment and Conformation of Acetyl Sulfide..... 2276  
 MARKOVITS, G. See Kertes, A. S., 4202  
 MARKS, G. W., AND ANTONIAK, C. E. Dielectric Properties of Polycrystalline Barium Trititanate and Barium Tetratitanate..... 1117  
 MARSHALL, H. P., BORGARDT, F. G., AND NOBLE, P., JR. Thermal Decomposition of Some Polynitroalkanes.... 1513  
 MARSHALL, R. See Chughtai, A., 208  
 MARSHALL, R. C. See James, D. W., 2963  
 MARSHALL, W. L. See Quist, A. S., 684, 1536, 1545, 2100, 3122  
 MARSTON, A. L. See Siddall, T. H., III, 2135  
 MARTIN, P., JR., AND BORNONG, B. J. Surface Dipole Moments of Adsorbed Organic Films on Chromium.... 4172  
 MARTIN, R. B. See Morlino, V. J., 2661  
 MARTIN, R. M. See Huebert, B. J., 3046  
 MARTIN, T. E., AND KALANTAR, A. H. Observed Phosphorescence Lifetimes and Glass Relaxation at 77°K... 2265  
 MARTIN, W. J., AND MCGEE, H. A., JR. Pyrolysis and Energetics of Halocarbons in Cryochemical Studies of Divalent Carbon..... 738  
 MARTIRE, D. E., BLASCO, P. A., CARONE, P. F., CHOW, L. C., AND VICINI, H. Thermodynamics of Solutions with Liquid-Crystal Solvents. I. A Gas-Liquid Chromatographic Study of Cholesteryl Myristate..... 3489  
 MARTIRE, D. E., AND RIEDL, P. A Thermodynamic Study of Hydrogen Bonding by Means of Gas-Liquid Chromatography..... 3478  
 MARTY, P. H. See Craig, N. C., 2234  
 MARUYAMA, T. See Hirasawa, R., 2541; Taniguchi, H., 1926  
 MARX, W. See Dubrow, R., 2489  
 MASLOV, P. G. The Semiempirical Method for the Calculation of Some Parameters for High-Resolution Nuclear Magnetic Resonance Spectra..... 1414  
 MASTERTON, W. L., AND SEILER, H. K. Apparent and Partial Molal Volumes of Water in Organic Solvents... 4257  
 MATHESON, R. A. Formation Constants of Some 2:2 and 3:3 Ion Pairs..... 3330  
 MATSEN, F. A., AND CANTU, A. A. Spin-Free Quantum Chemistry. V. Spin Density..... 21  
 MATSEN, F. A. See Scott, D. R., 16  
 MATSUO, T. Studies of the Solvent Effects on the Chemical Shifts in Nuclear Magnetic Resonance Spectroscopy. V. A Model for the Benzene Solutions of Polar Molecules..... 1819  
 MATSUSHITA, S. See Nakata, T., 458  
 MATTHEWS, R. W., MAHLMAN, H. A., AND SWORSKI, T. J. Oxidation of Cerium(III) in Sulfuric Acid Solutions Induced by Cobalt-60  $\gamma$  Radiation..... 3704  
 MATTISON, D. R. See Coffman, R. E., 1392  
 MATULA, R. A. The Thermal Decomposition of Perfluoropropene..... 3054  
 MATULA, R. A. See Drennan, G. A., 3462  
 MATWIYOFF, N. A., AND DARLEY, P. E. Direct Detection

- of the Hexaquoocobalt(II) Ion in Aqueous Solutions by Proton Magnetic Resonance Spectroscopy . . . . . 2659
- MATWIYOFF, N. A. See Movius, W. G., 3063; Zeltmann, A. H., 121
- MAY, J. A., JR., AND SMITH, W. B. Polymer Studies by Gel Permeation Chromatography. II. The Kinetic Parameters for Styrene Polymerizations . . . . . 216
- MAY, J. A., JR., AND SMITH, W. B. Polymer Studies by Gel Permeation Chromatography. III. Polymerization Initiated by Azobisisobutyronitrile . . . . . 2993
- MAYCOCK, J. N., AND PAI VERNEKER, V. R. Kinetics and Mechanism of the Thermal Decomposition of Nitronium Perchlorate . . . . . 4004
- MAYCOCK, J. N., PAI VERNEKER, V. R., AND GORZYNSKI, C. S., JR. Effects of Intentional Impurities on the Thermal Stability of Nitronium Perchlorate . . . . . 4015
- MAYCOCK, J. N. See McCarty, M., Jr., 4009; Pai Verneker, V. R., 2798
- MAYER, A. See Brause, G., 3098
- MAYER, S. W., AND SCHIELER, L. Computed Activation Energies and Rate Constants for Forward and Reverse Transfers of Hydrogen Atoms . . . . . 236
- MAYER, S. W., AND SCHIELER, L. Activation Energies and Rate Constants Computed for Reactions of Oxygen with Hydrocarbons . . . . . 2628
- MAZAC, C. J. See Simons, J. W., 749
- MCAVOY, N. See Bjorklund, S., 970
- MCCAIN, D. C., AND MYERS, R. J. Electron Paramagnetic Resonance Studies of Complex Ion Formation between  $Mn^{2+}$  and  $F^-$ ,  $Cl^-$ ,  $Br^-$ ,  $I^-$ , or  $SO_4^{2-}$  . . . . . 4115
- MCCARTY, M., JR., MAYCOCK, J. N., AND PAI VERNEKER, V. R. Thermal Decomposition of  $LiAlH_4$  . . . . . 4009
- MCCOLLUM, W. A. See Darnell, A. J., 1327
- MCCOY, L. R., MARK, H. B., JR., AND GIERST, L. Catalytic Polarographic Current of a Metal Complex. IV. Effect of the Electrode Double Layer on the Ni(II)-o-Phenylenediamine Prewave . . . . . 4637
- MCCOY, L. R. See Mark, H. B., Jr., 1083
- MCCRARY, G. E. See Newton, T. W., 4333
- MCDÉVITT, H. M. See DiBello, L. M., 1405
- MCDONALD, G. N. See Schreiner, F., 1162
- MCDONALD, R. L. See Law, S. L., 1617
- MCDONNELL, J. See Russell, G. A., 1386
- MCGEE, H. A., JR. See Martin, W. J., 738
- MCGEE, T. H. The Photolysis of Cyclobutanone . . . . . 1621
- MCHALE, E. T., AND VON ELBE, G. The Explosive Decomposition of Chlorine Dioxide . . . . . 1849
- MCINTYRE, J. D. E., AND SALOMON, M. Kinetic Isotope Effects in the Hydrogen Electrode Reaction . . . . . 2431
- MCKENNA, L. W. See MacKnight, W. J., 1122
- MCKENZIE, A. See Thrush, B. A., 3711
- MCKINNON, A. J., AND TOBOLSKY, A. V. Structure and Properties of Poly- $\gamma$ -benzyl-L-glutamate Cast from Dimethylformamide . . . . . 1157
- MCMANUS, J. C., AND LOW, M. J. D. Interactions of Propionic and Acetic Acids with Germania . . . . . 2378
- MCPHERSON, W. G., AND MEYERS, E. A. The Crystal Structures of Bismuth Halide Complex Salts. II. Bis(piperidinium) Pentabromobismuthate(III) . . . . . 532
- MCPHERSON, W. G., AND MEYERS, E. E. The Crystal Structures of Bismuth Halide Complex Salts. III. Tris(dimethylammonium) Hexabromobismuthate(III),  $[(CH_3)_2NH_2]_3BiBr_6$  . . . . . 3117
- MCRÆE, J. A. See Buchanan, A. S., 3052
- MEABURN, G. M., AND GORDON, S. Pulse Radiolysis of Ammonia Gas—Rate of Disappearance of the  $NH^{\cdot 2}$  Radical . . . . . 1592
- MEABURN, G. M., PERNER, D., LECALVE, J., AND BOURENE, M. A Pulsed-Radiolysis Study of Atomic Oxygen Reactions in the Gas Phase . . . . . 3920
- MEANY, J. E. See Pocker, Y., 655
- MEARES, P., AND THAIN, J. F. The Thermodynamics of Cation Exchange. VI. Selectivity and Activity Coefficients in Moderately Concentrated Solutions . . . . . 2789
- MEEHAN, E. J., AND MILLER, J. K. Complex Refractive Index of Colloidal Silver Bromide in the Near-Ultraviolet . . . . . 1523
- MEEHAN, E. J., AND MILLER, J. K. Kinetics of Formation and Growth of Colloidal Silver Bromide Particles. III. Experiments at Short Reaction Times . . . . . 2168
- MEEK, D. W. See Becker, C. A. L., 3588
- MEHLHORN, A. See Fabian, J., 3975
- MEISELS, G. G., AND ARNOLD, D. R. Tropylium Ion Formation in the Mass Spectra of Stereoisomeric Penta-cyclo[8.2.1.1<sup>4,7</sup>.0<sup>2,8</sup>.0<sup>3,6</sup>]tetradecanes . . . . . 3061
- MEISELS, G. G., AND TIBBALS, H. F. Higher Order Ion-Molecule Reactions. I. Theoretical Basis . . . . . 3746
- MENDELOVICI, E. See Fripiat, J. J., 1808
- MENON, P. G. The Pressure at the Maximum in Adsorption Isotherms at High Pressures . . . . . 2695
- MENZINGER, M., AND WOLFGANG, R. Recoil-Tritium Reactions in the Solid Phase: Absolute Yields and Phase Effects . . . . . 1789
- MESMER, R. E., AND BAES, C. F., JR. Correlation of  $\Delta H$  and  $\Delta S$  for the Association of the Rare Earth(III) Ions with Fluoride . . . . . 4720
- MESSER, C. E., AND HUNG, G. W. Dissociation Pressures in the System  $LaH_2-LaH_3$ , 250–450° . . . . . 3958
- MEYER, J. M., AND ALLREI, A. L.  $\pi$  Bonding by Germanium and the Ultraviolet Spectra of Some Phenylgermanes . . . . . 3043
- MEYER, R. T. Flash Photolysis and Time-Resolved Mass Spectrometry. II. Decomposition of Methyl Iodide and Reactivity of  $I(^2P_{1/2})$  Atoms . . . . . 1583
- MEYERS, E. A. See McPherson, W. G., 532, 3117; Schweikert, W. W., 1561
- MEYERS, R. V. See Daniels, M., 389
- MEYERSTEIN, D., AND MULAC, W. A. Reductions by Monovalent Zinc, Cadmium, and Nickel Cations . . . . . 784
- MEYERSTEIN, D. See Rabani, J., 1599
- MICHAUD, P. See Lebel, J., 3678
- MICHELIS, C. L. See Kenney, D. J., 410
- MICIC, O. I. See Draganić, Z. D., 511
- MICKEWICH, D., AND TURKEVICH, J. Methyl Radicals in Aqueous Solution as Studied by Electron Spin Resonance Spectroscopy . . . . . 2703
- MILES, D. W., HAHN, S. J., ROBINS, R. K., ROBINS, M. J., AND EYRING, H. Vicinal Effects on the Optical Activity of Some Adenine Nucleosides . . . . . 1483
- MILIA, F. K., AND HADJOUDES, E. K. Crystal Structure Effect in the  $\gamma$  Radiation of *p*-Dichlorobenzene . . . . . 4707
- MILLER, E. See Gerhold, G. A., 2737
- MILLER, G. A., AND LEE, C. S. Brillouin Spectra of Dilute Solutions and the Landau-Placzek Formula . . . . . 4644
- MILLER, I. R., AND FROMMER, M. A. Comments on "Gibbs Equation for Polyelectrolyte Adsorption," by D. K. Chattoraj . . . . . 1834
- MILLER, I. R. See Frommer, M. A., 2862
- MILLER, J. K. See Meehan, E. J., 1523, 2168
- MILLER, K. W. The Solubility of Fluorocarbon Gases in Cyclohexane . . . . . 2248
- MILLER, R. J. See Overman, A. R., 155
- MILLER, R. L. See Sharp, J. H., 3335
- MILLERO, F. J. Relative Viscosity and Apparent Molal Volume of *N*-Methylpropionamide Solutions at Various Temperatures . . . . . 3209
- MILLERO, F. J. Apparent Molal Expansibilities of Some Divalent Chlorides in Aqueous Solution at 25° . . . . . 4589
- MILLERO, F. J., AND DROST-HANSEN, W. Apparent Molal Volumes of Ammonium Chloride and Some Symmetrical Tetraalkylammonium Chlorides at Various Temperatures . . . . . 1758
- MILLERO, F. J., DROST-HANSEN, W., AND KORSON, L. Relative Viscosity and Apparent Molal Volume of Aqueous Sodium Sulfate at Various Temperatures . . . . . 2251
- MILNE, G. S., AND STEEL, C. The Gas-Phase Oxidation of Photochemically Generated Isopropyl Radicals . . . . . 3754
- MINAGAWA, Y. See Tanaka, I., 2684
- MINTER, C. C. Thermal Conductivity of Binary Mixtures of Gases. I. Hydrogen-Helium Mixtures . . . . . 1924
- MITRA, R. C. See Bhattacharyya, S. N., 63
- MITTLEMAN, M. L. See Fackler, J. P., Jr., 4631
- MIYAMA, H., AND HARUMIYA, N. Quantum Yield of the Photolysis of Cyclohexane . . . . . 4700
- MIYAMA, H. See Fukuzawa, K., 371
- MIYASO, K. See Kato, T., 2161
- MIYATA, H. See Kubokawa, Y., 356
- MIYAZAKI, T. See Tanno, K., 3496
- MÖBIUS, K., AND PLATO, M. Comment on "Electron Paramagnetic Resonance Spectra of the Naphthacene Trianion and the 5,12-Naphthacenequinone Anion Radicals" . . . . . 1830
- MODELL, M. See Baddour, R. F., 3621
- MODICA, A. P. Electronic Oscillator Strength of  $CF_2$  . . . . . 4594
- MODRITZER, K., GROENWEGHE, L. C. D., AND VAN WAZER, J. R. Multicomponent Equilibria in Exchange of Substituents between the Dimethylsilicon and Dimethylgermanium Moieties . . . . . 4380
- MOLINARI, E. See Cramarossa, F., 84
- MOMI, R. K., AND NACHTRIEB, N. H. Nuclear Magnetic

- Resonance in Thallium Borate Glasses. I. The Thallium-205 Chemical Shift. . . . . 3416
- MONTAGUE, D. C., AND ROWLAND, F. S. Singlet Methylenes in the Photolysis of Mercury-Ketene-Butene Systems. . . . . 3705
- MOORHEAD, E. D., AND FRAME, G. M., II. A Measurement of the Heterogeneous Rate Constant for the Thiocyanate-Catalyzed Polarographic Reduction of Trivalent Gallium. . . . . 3684
- MORGAN, L. O. See Zeltmann, A. H., 121
- MORI, Y. See Takita, S., 4360; Tanaka, I., 2684
- MORLINO, V. J., AND MARTIN, R. B. Proton Magnetic Resonance Spectra of DL- and LL-Phenylalanylvalines. . . . . 2661
- MORRIS, E. R., AND THYNNE, J. C. J. Intramolecular Elimination Reactions in the Photolysis of Fluoroaldehydes. . . . . 3351
- MORRIS, E. R. See Jones, A., 2677
- MORRIS, G. C. See Lyons, L. E., 3677
- MORRISON, G., AND LIND, J. E., JR. Friction Constants for Fused Salts. . . . . 3001
- MORRISON, J. D. See Bloom, H., 3041
- MORROW, J. I., AND LEVY, J. Implications and Use of Spectral Shifts in Polymerization Studies of Metal Ions. . . . . 885
- MOŚCIŃSKI, J., AND SUSKI, L. Radiometric Determination of the Volume Change on Mixing in the Liquid Cadmium-Cadmium Chloride System. . . . . 441
- MOSER, H. C. See Shores, R. D., 1
- MOSHER, W. A. See Epstein, J., 622
- MOULIK, S. P. A Proposed Viscosity-Concentration Equation beyond Einstein's Region. . . . . 4682
- MOVIUS, W. G., AND MATWIYOFF, N. A. Magnetic Resonance Studies of Outer-Sphere Ion-Pair Formation in N,N-Dimethylformamide Solutions of Aluminum(III) Halides. . . . . 3063
- MUKAIBO, T. See Hirasawa, R., 2541
- MUKHERJEE, A. See Bhattacharyya, S. N., 56, 63
- MUKHERJEE, L. M., KELLY, J. J., BARANETZKY, W., AND SICA, J. Equilibria in Pyridine. I. Determination of Absolute  $pK$  Values of Several Uncharged Acids and Investigation of a Few Typical Acid-Salt Mixtures. . . . . 3410
- MULAC, W. A. See Meyerstein, D., 784
- MULLER, N., AND BIRKHAHN, R. H. Investigation of Micelle Structure by Fluorine Magnetic Resonance. II. Effects of Temperature Changes, Added Electrolyte, and Counterion Size. . . . . 583
- MUNIR, Z. A. See Blair, R. C., 2434
- MUNRO, D. F., AHNELL, J. E., AND KOSKI, W. S. Negative-Ion Mass Spectra of Some Boron Hydrides. . . . . 2682
- MURAKAMI, Y., AND TAKAGI, M. Stability Order in Metal Chelate Compounds. V. Bivalent Metal Complexes of 2-Pyridylmethyl Phosphate. . . . . 116
- MURAKAMI, Y. See Kotaka, T., 829
- MUROV, S., AND HAMMOND, G. S. Mechanisms of Photochemical Reactions in Solution. LVI. A Singlet-Sensitized Reaction. . . . . 3797
- MURPHY, R. A., AND DAVIS, J. C., JR. A Proton Magnetic Resonance Study of Hydrogen Bonding in Aliphatic Secondary Amines. . . . . 3111
- MURTY, H. N., BIEDERMAN, D. L., AND HEINTZ, E. A. The Determination of Activation Energies in Solid-State Kinetic Processes. . . . . 746
- MUSHRAN, S. P. See Agrawal, M. C., 1497
- MUSHRUSH, G. W. See Filipescu, N., 3516, 3522
- MYERS, C. See Russell, G. A., 1386
- MYERS, D. C., AND SCHMIDT-BLEEK, F. Low-Conversion Radiolysis of Methane Containing Traces of Oxygen and Olefins. . . . . 1475
- MYERS, M. N. See Giddings, J. C., 4397
- MYERS, R. J. See McCain, D. C., 4115
- MYHER, J. J., AND HARRISON, A. G. Ion-Molecule Reactions in Propyne and Allene. . . . . 1905
- MYLONAKIS, S. G. See Seltzer, S., 754
- NACHTRIEB, N. H. See Momii, R. K., 3416
- NAGASAWA, M. See Kato, T., 2161; Noda, I., 2890
- NAIRN, J. G. See Blanchard, J., 1204
- NAKAJIMA, A. See Hamada, F., 178
- NAKAMURA, D. See Ikeda, R., 2501, 2982
- NAKATA, T., AND MATSUSHITA, S. Infrared Studies of Intermediates of the Ammonia Synthesis on Iron. . . . . 458
- NANCOLLAS, G. H. See Chughtai, A., 208
- NARA, K. See Wen, W.-Y., 1137, 3048
- NASH, C. P. See Horsma, D. A., 2351
- NAUMAN, R. V. See Holloway, H. E., 4468, 4474
- NEDETZKA, T. See Brausse, G., 3098
- NEECE, G. A., AND SQUIRE, D. R. On the Tait and Related Empirical Equations of State. . . . . 128
- NELSON, J. A. See Corrin, M. L., 643
- NELSON, R. F., AND ADAMS, R. N. The Anion and Cation Radicals of N,N-Dimethyl-p-nitroaniline. . . . . 740
- NELSON, R. F., AND ADAMS, R. N. Electrochemical and Electron Paramagnetic Resonance Investigation of Nitrotriphenylamine Reductions. . . . . 4336
- NELSON, R. F. See Seo, E. T., 1829
- NEMETHY, G., SCHERAGA, H. A., AND KAUFMANN, W. Comments on the Communication "A Criticism of the Term 'Hydrophobic Bond'" by Joel H. Hildebrand. . . . . 1842
- NENADOVIĆ, M. T. See Dragani, Z. D., 511
- NETA, P. See Wander, R., 2946
- NEUMAN, R. C., JR., SNIDER, W., AND JONAS, V. Concentration Dependence of the Nuclear Magnetic Resonance Spectral Properties of Some N,N-Dimethylamides and -thioamides. . . . . 2469
- NEWMAN, J. See Smyrl, W. H., 4660
- NEWMARK, R. A., AND GRAVES, R. E. Internal Rotation in Liquid 1,2-Difluorotetrahydroethane. . . . . 4299
- NEWTON, T. W., MCCRARY, G. E., AND CLARK, W. G. The Chloride Catalysis of the Np(III)-Fe(III) Reaction in Aqueous Acid Solutions. . . . . 4333
- NG, W. Y. See Bennett, L., 4699
- NICHOLLS, D., SUTPHEN, C., AND SZWARC, M. Dissociation of Lithium and Sodium Salts in Ethereal Solvents. . . . . 1021
- NICHOLSON, R. S. See Olmstead, M. L., 1650
- NIEMANN, E.-G., AND KLENERT, M. A New Flash-Photolysis System for the Investigation of Fast Reactions. . . . . 3766
- NISHIMOTO, K., AND FORSTER, L. S. SCFMO Calculations of Heteroatomic Systems with Variable- $\beta$  Approximation. III. Electronic Spectra of Anions of Hydroxyaromatics. . . . . 914
- NISHIMURA, S., KE, C. H., AND LI, N. C. Studies of Chloroform as Hydrogen Donor to Some Organophosphorus Compounds and Long-Chain Tertiary Alkylamines. . . . . 1297
- NISHIMURA, S., AND LI, N. C. Infrared Studies of Amine Complexes with Some Organophosphorus Compounds. . . . . 2908
- NIWA, Y. See Hirota, K., 5
- NOBILIONE, J. M. See Stern, J. H., 1064, 3937
- NOBLE, P., JR. See Marshall, H. P., 1513
- NODA, I., YAMADA, Y., AND NAGASAWA, M. The Rate of Shear Dependence of the Intrinsic Viscosity of Monodisperse Polymer. . . . . 2890
- NOGGLE, J. H. The Study of the Hindered Rotation of Methyl Groups Using Nuclear Magnetic Resonance. . . . . 1324
- NORTHOLT, M. G., AND ALEXANDER, L. E. The Crystal Structure of 1,8-Diazacyclotetradecane-2,7-dione, a Cyclic Monomeric Model of Nylon 66. . . . . 2838
- NORTHOLT, M. G. See Ganis, P., 3997
- NORTHROP, D. A. Possible Error in the Calibration of Knudsen Cells by Mercury Effusion. . . . . 4323
- NOTZ, K. See Keenan, A. G., 1085
- OBERTH, A. E., AND BRUENNER, R. S. The Effect of Hydrogen Bonding on the Kinetics of the Urethane Reaction. . . . . 845
- O'BRIEN, H. A., JR. See Lietzke, M. H., 4408
- OCCHIENA, G. See Zecchina, A., 1471
- O'CONNELL, J. P., AND PRAUSNITZ, J. M. Analytical Potential Models and the Properties of Noble Gases. . . . . 632
- ODAN, N. See Hirasawa, R., 2541
- O'DONNELL, J. H. See Bowden, M. J., 1577
- OGILVIE, J. F. On the Purported Infrared Absorption at  $21 \mu$  of Carbon Monoxide Adsorbed on Silica-Supported Platinum. . . . . 2688
- OGRYZLO, E. A., AND PEARSON, A. E. Excitation of Violanthrone by Singlet Oxygen. A Chemiluminescence Mechanism. . . . . 2913
- OHMORI, T. See Iwasaki, M., 4347
- OHNISHI, S. See Taniguchi, H., 1926
- O'KEEFE, M. See Ebisuzaki, Y., 4695
- OKITA, K., TERAMOTO, A., KAWAHARA, K., AND FUJITA, H. Light Scattering and Refractometry of a Monodisperse Polymer in Binary Mixed Solvents. . . . . 278
- OKUBO, T. See Ise, N., 1361, 1370
- OKUTSU, E. See Tanaka, I., 2684
- OLEJNIK, S., AYLMOORE, L. A. G., POSNER, A. M., AND QUIRK, J. P. Infrared Spectra of Kaolin Mineral-Dimethyl Sulfoxide Complexes. . . . . 241
- OLMSTEAD, M. L., AND NICHOLSON, R. S. Influence of Double-Layer Charging in Chronopotentiometry. . . . . 1650

- OLSON, D. H. X-Ray Evidence for Residual Water in Calcined Divalent Cation Faujasite-Type Zeolites. . . . 1400
- OLSON, D. H. Crystal Structure of the Zeolite Nickel Faujasite. . . . 4366
- OLSON, D. H., AND SHERRY, H. S. An X-Ray Study of Strontium-Sodium Ion Exchange in Linde X. An Example of a Two-Phase Zeolite System. . . . 4095
- O'MALLEY, J. A., OWENS, C., SCHMID, C., QUIMBY, D., AND KING, C. M. The Vapor Pressure of *p*-Xylene and Solutions of Tetra-*n*-pentylammonium Thiocyanate in *p*-Xylene. . . . 3584
- ONDA, S. See Ikeda, R., 2501
- O'NEAL, H. E., AND BENSON, S. W. The Biradical Mechanism in Small Ring Compound Reactions. . . . 1866
- O'NEIL, J. R. Hydrogen and Oxygen Isotope Fractionation between Ice and Water. . . . 3683
- ONO, Y., AND KEII, T. Photolysis of Alcohols Adsorbed on Alumina as Studied by Electron Spin Resonance. . . . 2851
- ONO, Y. See Imai, H., 46
- OREF, I., AND RABINOVITCH, B. S. The Experimental Evaluation of  $k_{\infty}$  in Unimolecular Reaction Systems. . . . 4488
- ORNELLAS, D. L. The Heat and Products of Detonation of Cyclotetramethylenetetranitramine, 2,4,6-Trinitrotoluene, Nitromethane, and Bis[2,2-dinitro-2-fluoroethyl]formal. . . . 2390
- ORTTUNG, W. H. Anisotropy of Proton Fluctuations and the Kerr Effect of Protein Solutions. Theoretical Considerations. . . . 4058
- ORTTUNG, W. H. Anisotropy of Proton Fluctuations in Proteins. Calculations for Simple Models. . . . 4066
- ORTTUNG, W. H. See Chen, Y., 3069
- OTTOLENGHI, M., AND BENSASSON, R. A Mixed Triplet-Excimer Intermediate in the Photooxidation of *N,N'*-Diphenyl-*p*-phenylenediamine by the Diimine. . . . 3774
- OTTOLENGHI, M., AND RABANI, J. Photochemical Generation of Nitrogen Dioxide in Aqueous Solutions. . . . 593
- OUELLET, C. See Lebel, J., 3678
- OVERMAN, A. R. Transient Convective Diffusion in Capillaries. . . . 3286
- OVERMAN, A. R. Convective Diffusion across a Porous Diaphragm. . . . 4168
- OVERMAN, A. R., AND MILLER, R. J. Convective Diffusion in Capillaries. . . . 155
- OWENS, B. B. See Topol, L. E., 2106
- OWENS, C. See O'Malley, J. A., 3584
- PACE, C. N. See Hammes, G. G., 2227
- PADDAY, J. F. Metachromasy of a Thiocarbocyanine Dye in Aqueous Solution: The Formation of Dimers and Trimers. . . . 1259
- PADDAY, J. F., AND UFFINDELL, N. D. The Calculation of Cohesive and Adhesive Energies from Intermolecular Forces at a Surface. . . . 1407
- PADDAY, J. F., AND UFFINDELL, N. D. Reply to Comments of F. M. Fowkes on "The Calculation of Cohesive and Adhesive Energies". . . . 3700
- PADNOS, N. Analysis of Experimental Term Energies. . . . 2335
- PADOVA, J. Ion-Solvent Interaction. VI. A Thermodynamic Approach to Preferential Solvation in Mixed Solvents. . . . 796
- PAI VERNEKER, V. R. Photodecomposition of Solid Metal Azides. . . . 1733
- PAI VERNEKER, V. R., AND AVRAMI, L. Study of the Explosive Behavior of Barium Azide. . . . 778
- PAI VERNEKER, V. R., AND BLAIS, M. Photodecomposition of Aqueous Solutions of Barium Azide. . . . 774
- PAI VERNEKER, V. R., AND MAYCOCK, J. N. The Photochemical Decomposition of Silver Perchlorate. . . . 2798
- PAI VERNEKER, V. R. See Maycock, J. N., 4004, 4015; McCarty, M., 4009
- PALLANSCH, M. J. See Berlin, E., 1887
- PALMER, H. B., LAHAYE, J., AND HOU, K. C. On the Kinetics and Mechanism of the Thermal Decomposition of Methane in a Flow System. . . . 348
- PAN, C. New Forms of McKay-Perring Equations. . . . 2548
- PAPAIIOANNOU, C. G. See Walling, C., 2260
- PARKER, B. M. See Haward, R. N., 1842
- PARKER, C. A., AND SHORT, G. D. Comment on the Electroluminescence from Phenanthrene Solutions. . . . 3071
- PARKER, R. C., SLUTSKY, L. J., AND APPLGATE, K. R. Ultrasonic Absorption and the Kinetics of Conformational Change in Poly-L-lysine. . . . 3177
- PARKS, G. A. See Anderson, J. H., 3662
- PARRAVANO, G. See Delgass, W. N., 3563
- PARTHASARATHY, A. See Wiewiorowski, T. K., 1890
- PASSCHIER, A. A., AND GREGORY, N. W. Evidence for Molecular Dimers,  $(I_2)_2$ , in Iodine Vapor. . . . 2697
- PATTERSON, L. K. See Hammaker, R. M., 1837, 4346
- PAUL, R. See Tschuikow-Roux, E., 375
- PAVA, B. M., AND STAFFORD, F. E. Infrared Spectra of Gaseous Protio- and Deuteriooxalic Acids. . . . 4628
- PEARSON, A. E. See Ogryzlo, E. A., 2913
- PENG, C. T. See Dainton, F. S., 3801
- PENZHORN, R. D., AND DARWENT, B. DEB. The Reaction of Hydrogen Atoms with Hydrogen Iodide. . . . 1639
- PEPELA, C. N. See Bell, T. N., 4693
- PERI, J. B. The Effect of Fluoride on Surface "Acid" Sites on  $\gamma$ -Alumina and Silica-Alumina. . . . 2917
- PERI, J. B., AND HENSLEY, A. L., JR. The Surface Structure of Silica Gel. . . . 2926
- PERLMUTTER-HAYMAN, B. See Gutmann, H., 3671
- PERNER, D. See Meaburn, G. M., 3920
- PERONA, M. J. See Pritchard, G. O., 3352
- PERSON, W. B. See Julien, L. M., 3059
- PERUMAREDDI, J. R., AND ADAMSON, A. W. Photochemistry of Complex Ions. V. The Photochemistry of Some Square-Planar Platinum(II) Complexes. . . . 414
- PERUMAREDDI, J. R. See Spees, S. T., Jr., 1822
- PETERSON, R. M. See Al-Thannon, A., 2395
- PETRAKIS, L. Quadrupolar Relaxation of Aluminum-27 Nuclear Magnetic Resonance in Aluminum Alkyls. . . . 4182
- PETRAKIS, L., AND SWIFT, H. E. Aluminum-27 Nuclear Magnetic Resonance of Trialkylaluminum Complexes. . . . 546
- PETRUCCI, S. See Hammes, P., 3986
- PFLUG, H. D. See Singh, J., 1939
- PHILLIPS, H. O. See Marcinkowsky, A. E., 1201
- PHILLIPS, L. Comment on "Evidence for Nitrogen Trioxide in the Combustion of a Double-Base Propellant". . . . 2279
- PHILLIPS, L. F. See Freeman, C. G., 3025, 3028, 3031; Grady, Q. J. F., 743
- PICCARDI, G., AND GUIDELLI, R. The Voltammetric Behavior of the Aqueous System  $I^- - I_2 - ICl - Cl^-$  on Smooth Platinum. . . . 2782
- PIERCE, C. The Hill Equation for Adsorption on Uniform Surfaces. . . . 1955
- PIERCE, C. The Universal Nitrogen Isotherm. . . . 3673
- PILIPOVICH, D. See Schack, C. J., 4697
- PINO, P. See Luisi, P. L., 2400
- PISTOIA, G. See Conti, F., 1396, 2245
- PITT, D. A. See Foss, G. D., 3512
- PLATFORD, R. F. Isopeistic Measurements on the System Water-Sodium Chloride-Magnesium Chloride at 25°. . . . 4053
- PLATO, M. See Möbius, K., 1830
- POCKER, Y., AND MEANY, J. E. The Reversible Hydration of 2- and 4-Pyridinecarboxaldehydes. II. General Acid-Base and Metal Ion Catalysis. . . . 655
- PODDER, S. K. See Schneider, F. W., 4563
- POLANYI, J. C. See Cadman, P., 3715
- PONTER, A. B. See Davies, G. A., 4320
- POOL, M. J. See Guadagno, J. R., 2535
- POOLE, J. A. See Dhingra, R. C., 4577
- POPOV, A. I. See Caruso, J. A., 918; Wehman, T. C., 4031
- POPOVYCH, O. See Dill, A. J., 4580
- PORTER, D. F. See Armstrong, R. D., 2300
- PORTER, D. M., AND BREY, W. S., JR. Nuclear Magnetic Resonance Studies of Hydrogen Bonding. II. The Pyrrole-Dimethyl Sulfoxide System. . . . 650
- POSNER, A. M. See Olejnik, S., 241
- POSTON, T. M. See Chang, E. T., 638
- POWELL, F. X. See Kenney, J. T., 3094
- PRATER, K. B. See Maloy, J. T., 4348
- PRASUNITZ, J. M. See O'Connell, J. P., 632; Rigby, M., 330
- PRICE, A. H. See Gough, S. R., 3347
- PRINCEN, H. M. Contact Angles and Transition Regions in Soap Films. . . . 3342
- PRITCHARD, G. O., AND BRYANT, J. T. The Photolysis of 1,3-Difluoro- and 1,1,3,3-Tetrafluoroacetone at Low Pressure. . . . 1603
- PRITCHARD, G. O., AND PERONA, M. J. A Reply to "Intramolecular Elimination Reactions in the Photolysis of Fluoroaldehydes". . . . 3352
- PRITCHARD, H. O. See Shaw, D. H., 1403, 2693
- PROSTAK, A., MARK, H. B., JR., AND HANSEN, W. N. Simultaneous Electrochemical and Internal-Reflection Spectrometric Measurements Using Gold-Film Electrodes. . . . 2576
- PROUT, E. G., AND LIDDIARD, V. C. The Thermal Decomposition of Lithium Azide. . . . 2281

- PUCHALSKA, D. See Libus, W., 2075  
 PURDIE, N. See Felber, B. J., 2496
- QUEE, M. J. Y., AND THYNNE, J. C. J. The Pressure Dependence of the Decomposition of the Isopropoxyl Radical . . . . . 2824  
 QUICKENDEN, M. J. See Franks, F., 2668  
 QUICKERT, K. A. See Ridley, B. A., 1844  
 QUIMBY, D. See O'Malley, J. A., 3584  
 QUINLAN, K. P. Light-Induced Proton Ejection and Electron Transfer in the Zinc Tetrphenylporphyrin-Benzoquinone System . . . . . 1797  
 QUINN, R. K., AND LAGOWSKI, J. J. Metal-Ammonia Solutions. III. Spectroscopy of Quaternary Ammonium Radicals . . . . . 1374  
 QUIRK, J. P. See Olejnik, S., 241  
 QUIST, A. S., AND MARSHALL, W. L. Electrical Conductances of Aqueous Sodium Chloride Solutions from 0 to 800° and at Pressures to 4000 Bars . . . . . 684  
 QUIST, A. S., AND MARSHALL, W. L. The Independence of Isothermal Equilibria in Electrolyte Solutions on Changes in Dielectric Constant . . . . . 1536  
 QUIST, A. S., AND MARSHALL, W. L. Electrical Conductances of Aqueous Hydrogen Bromide Solutions from 0 to 800° and at Pressures to 4000 Bars . . . . . 1545  
 QUIST, A. S., AND MARSHALL, W. L. Electrical Conductances of Aqueous Sodium Bromide Solutions from 0 to 800° and at Pressures to 4000 Bars . . . . . 2100  
 QUIST, A. S., AND MARSHALL, W. L. Ionization Equilibria in Ammonia-Water Solutions to 700° and to 4000 Bars of Pressure . . . . . 3122
- RABANI, J., AND MEYERSTEIN, D. Pulse Radiolytic Studies of the Competition  $H + H$  and  $H + Ferricyanide$ . The Absolute Rate Constants . . . . . 1599  
 RABANI, J. See Ottolenghi, M., 593  
 RABINOVITCH, B. S. See Lin, Y. N., 1726, 1932; Maloney, K. M., 4483; Oref, I., 4488; Ring, D. F., 191  
 RABINOVITCH, E. See Singhal, G. S., 3941  
 RAGLE, J. L. See Caron, A. P., 556; Yeh, H. J. C., 3688  
 RAKINTZIS, N. T., AND STEIN, G. Radical Yield in  $\gamma$ -Irradiated Aqueous Alkaline Solutions of Fremy's Salt . . . . . 1011  
 RAMAKRISHNA, V. See Suri, S. K., 1555, 3073  
 RAMAMURTHY, P. See Low, M. J. D., 2371, 3161  
 RAMASUBRAMANIAN, N. See Low, M. J. D., 2371  
 RANBY, B. See Takakura, K., 164  
 RANEY, J. See Solomon, I. J., 2262  
 RAO, K. N., AND ALLEN, A. O. The Radiation Chemistry of Acetamide . . . . . 2181  
 RAO, K. S., AND DAS, B. Varietal Differences in Gelatin, Egg Albumin, and Casein in Relation to Sorption-Desorption Hysteresis with Water . . . . . 1223  
 RARIDON, R. J., BALDWIN, W. H., AND KRAUS, K. A. Properties of Organic-Water Mixtures. VI. Activity Coefficients of Sodium Chloride in Saturated Water-Pyridine Mixtures at 5 and 25° . . . . . 925  
 RASAIHA, J. C., AND FRIEDMAN, H. L. Charged Square-Well Model for Ionic Solutions . . . . . 3352  
 RASMUSSEN, O. L. See Sehested, K., 626  
 RASTOGI, R. P., AND SINGH, N. B. Solid-State Reactivity of Picric Acid and Substituted Hydrocarbons . . . . . 4446  
 RATTET, L. S., WILLIAMSON, A. D., AND GOLDSTEIN, J. H. Dependence of  $sp^3$  Geminal Coupling Constants in Acetal and Some Haloacetals on Solvent and Concentration . . . . . 2954  
 RAVENHILL, J. R. See Franks, F., 2668  
 RAYNES, W. T. See Rummens, F. H. A., 2111  
 READ, B. E. See MacKnight, W. J., 1122  
 READ, J. M. See Loemker, J. E., 991  
 REBBERT, R. E. See Ausloos, P., 3904  
 REDDY, M. P. See Balakrishnan, I., 4609  
 REDINGTON, R. L., AND REDINGTON, T. E. Infrared Evidence for  $FHF^-$  in Annealed  $LiF-HX$  Films . . . . . 2456  
 REDINGTON, T. E. See Redington, R. L., 2456  
 REDLICH, O., AND GARGRAVE, W. E. Reaction Rate and Dissociation of Sulfuric Acid . . . . . 3045  
 REDMOND, T. F., AND WAYLAND, B. B. Dimerization of Nitrogen Dioxide in Solution: a Comparison of Solution Thermodynamics with the Gas Phase . . . . . 1626  
 REDMOND, T. F., AND WAYLAND, B. B. Comments on the Planarity of Dinitrogen Tetroxide . . . . . 3038  
 REDPATH, J. L. See Johnson, G. R. A., 765  
 REEVES, R. See Emerson, J., 3721  
 REGAN, T. H. See Feldman, L. H., 2008
- REID, R. C. See Espino, R. L., 3689  
 REINEKE, W. See Kulevsky, N., 3339  
 RETCOFSKY, H. L., AND FRIEDEL, R. A. Carbon-13 Nuclear Magnetic Resonance Studies of 3-Substituted Pyridines . . . . . 290  
 RETCOFSKY, H. L., AND FRIEDEL, R. A. Carbon-13 Nuclear Magnetic Resonance Studies of 2-Substituted Pyridines . . . . . 2619  
 RICE, D. W., AND GREGORY, N. W. Vaporization Characteristics of Zinc Chloride, Bromide, and Iodide . . . . . 3361  
 RICE, D. W., AND GREGORY, N. W. Vaporization Equilibria in the Sodium Chloride-Zinc Chloride System . . . . . 4524  
 RICE, J. K. See Kuppermann, A., 3894  
 RICE, O. K. See Wu, E.-C., 542  
 RIDER, P. E. See Hammaker, R. M., 1837  
 RIDLEY, B. A., QUICKERT, K. A., AND LE ROY, D. J. Comment on "Quantum Theoretical Treatment of Equilibrium Chemical Rate Processes" . . . . . 1844  
 RIEDL, P. See Martire, D. E., 3478  
 RIGBY, M., AND PRAUSNITZ, J. M. Solubility of Water in Compressed Nitrogen, Argon, and Methane . . . . . 330  
 RING, D. F., AND RABINOVITCH, B. S. Triplet Methylene Radical Reaction with *cis*-Butene-2 . . . . . 191  
 RINKER, R. G., AND LYNN, S. The Formation of  $S_2O_4$  Free Radical in Dimethylformamide . . . . . 4706  
 RIST, G. H. See Hyde, J. S., 4269  
 RIZZO, F. E., AND SMITH, J. V. Coulometric Titration of Wustite . . . . . 485
- ROBERTI, D. M. See DiBello, L. M., 1405  
 ROBERTS, J. D. See Binsch, G., 4310  
 ROBERTS, J. H. See Dewald, R. R., 4224  
 ROBERTS, J. P. See Kemp, T. J., 1464  
 ROBINS, M. J. See Miles, D. W., 1483  
 ROBINS, R. K. See Miles, D. W., 1483  
 ROBINSON, M. G., AND FREEMAN, G. R. The Radiolysis of Liquid Nitrous Oxide . . . . . 1394  
 ROBINSON, M. G., AND FREEMAN, G. R. The Radiolysis of Cyclohexane in the Presence of Deuterated Olefins. The Involvement of the Olefins in Hydrogen Formation . . . . . 1780  
 ROBINSON, R. A. See Covington, A. K., 2759; Hetzer, H. B., 2081  
 ROCK, S. L. See Hammaker, R. M., 1837  
 RODDE, A. F., JR., AND GROSSWEINER, L. I. Cobalt-60 Radiolysis of Aqueous Eosin . . . . . 3337  
 RODDE, A. F., JR. See Grossweiner, L. I., 756  
 RODGERS, A. S. Kinetics of Fluorination. III. The Unimolecular Decomposition of Chemically Activated *sec*-2,3-Dichloroperfluorobutyl Radicals . . . . . 3400  
 RODGERS, A. S. Kinetics of Fluorination. IV. The Unimolecular Decomposition of Chemically Activated *sec*-1,4-Dichloroperfluorobutyl Radicals . . . . . 3407  
 RODGERS, M. A. J., AND GARRISON, W. M. Excited-Molecule Reactions in the Radiolysis of Peptides in Concentrated Aqueous Solution . . . . . 758  
 RODGERS, M. A. J. See Baxendale, J. H., 3849  
 ROE, R.-J. Surface Tension of Polymer Liquids . . . . . 2013  
 ROGERS, J. W., AND WATSON, W. H. Electron Spin Resonance Study of Some Trifluoromethylnitrobenzene Anion Radicals . . . . . 68  
 ROGERS, M. T., AND RYAN, J. A. Chlorine Nuclear Quadrupole Resonance Study of Some Molecular Adducts of Phosphorus Oxychloride . . . . . 1340  
 ROIO, B. See Cramarossa, F., 84  
 RON, A. See Freiberg, M., 3526  
 ROSENBERG, H. M., AND CARSON, S. D. Electronic Properties of Perfluorocarbons. Fluorescence and Phosphorescence in Perfluorobiphenyl, Perfluoronaphthalene, and Perfluorotoluene . . . . . 3531  
 ROSENBLATT, G. M. See Capwell, R. J., Jr., 4327  
 ROSNER, D. E., AND ALLENDORF, H. D. Kinetics of Elemental Boron Chlorination by Chlorine Atoms and Chlorine Molecules . . . . . 4159  
 ROSS, D. L. See Blanc, J., 2817  
 ROTH, J. F. See Berger, P. A., 3186  
 ROUNSAVILLE, J. F., AND LAGOWSKI, J. J. Spectroscopy of Alkali Metals in Fused Alkali Metal Salts . . . . . 1111  
 ROWLAND, F. S. See Montague, D. C., 3705; Smail, T., 1845; Tang, Y.-N., 707; Ting, C. T., 763; Tominaga, T., 1399; Wai, C. M., 3049  
 ROWSELL, D. G. See Goldwhite, H., 2666  
 RUBALCAVA, H. E. See Clarke, J. K. A., 327, 2688  
 RUFF, I. Extension of the "Band Model" to the Inner-Sphere Mechanism of Electron-Transfer Reactions . . . . . 1792  
 RUMMENS, F. H. A., RAYNES, W. T., AND BERNSTEIN, H. J. Medium Effects in Nuclear Magnetic Resonance. V.

- Liquids Consisting of Nonpolar, Magnetically Isotropic Molecules . . . . . 2111
- RUSAKOWICZ, R., AND TESTA, A. C. A Comparison of Quinine Bisulfate and 9,10-Diphenylanthracene as Fluorescence Standards . . . . . 793
- RUSAKOWICZ, R., AND TESTA, A. C. 2-Aminopyridine as a Standard for Low-Wavelength Spectrofluorimetry . . . . . 2680
- RUSH, R. M., AND JOHNSON, J. S. Isopiestic Measurements of the Osmotic and Activity Coefficients for the Systems  $\text{HClO}_4\text{-LiClO}_4\text{-H}_2\text{O}$ ,  $\text{HClO}_4\text{-NaClO}_4\text{-H}_2\text{O}$ , and  $\text{LiClO}_4\text{-NaClO}_4\text{-H}_2\text{O}$  . . . . . 767
- RUSH, R. M. See Johnson, J. S., Jr., 360; Wu, Y. C., 4048
- RUSHING, C. See Bonner, O. D., 4290
- RUSSELL, C. P. See Giddings, J. C., 4397
- RUSSELL, G. A., McDONNELL, J., AND MYERS, C. Aliphatic Semidiones. IX. Hyperfine Splittings by Nitrogen Atoms Attached to a Paramagnetic Center . . . . . 1386
- RUSSELL, G. A., AND UNDERWOOD, G. R. Aliphatic Semidiones. VIII. Hyperfine Splitting by Oxygen and Carbon Atoms in Semidiones . . . . . 1074
- RUSSELL, J. C., AND FREEMAN, G. R. Reactions of the Primary Reducing Species in the Radiolysis of Liquid 2-Propanol . . . . . 808
- RUSSELL, J. C., AND FREEMAN, G. R. The Yields of the Primary Reducing Species in the Radiolysis of Liquid Ethanol . . . . . 816
- RUSSELL-JONES, A. See Jacobs, P. W. M., 202
- RYAN, J. A. See Rogers, M. T., 1340
- RZAD, S. J., AND SCHULER, R. H. Dose and Concentration Dependence of Hydrogen Transfer in the Radiolysis of Dilute Solutions of Cyclopropane in *n*-Hexane and Cyclohexane . . . . . 228
- RZAD, S. J., AND WARMAN, J. M. The Formation of Phenol and Nitrogen by a Negative Ion-Molecule Chain Reaction on Irradiation of Gaseous Benzene-Nitrous Oxide Mixtures . . . . . 3013
- RZAD, S. J. See Hentz, R. R., 1027
- SADEK, H. See Helmy, A. K., 2358
- SAFRANY, D. R., AND JASTER, W. Reactions of Hydrocarbons with Mixtures of Active Nitrogen and Hydrogen Atoms. I. "Normal" Reactions; Reactions of Alkenes and Alkanes . . . . . 518
- SAFRANY, D. R., AND JASTER, W. Reactions of Hydrocarbons with Mixtures of Active Nitrogen and Hydrogen Atoms. II. "Anomalous" Reactions: the Reactions of Cyanogen, Hydrogen Cyanide, and Acetylene . . . . . 3305
- SAFRANY, D. R., AND JASTER, W. The Effect of Additives upon the Reaction of Cyanogen with Active Nitrogen: Reactions of Carbon Atoms, CN Radicals, and the Chemiluminescent Reaction of  $\text{C}_2\text{N}$  Radicals with Atomic Oxygen . . . . . 3318
- SAFRANY, D. R., AND JASTER, W. Reactions of Hydrocarbons with Mixtures of Active Nitrogen and Hydrogen Atoms. III. The Reactions of Methylacetylene and Allene . . . . . 3323
- SAKURADA, I. See Ise, N., 4543
- SAKURAI, T., AND IWASAKI, M. Kinetics and Mechanism of the Reaction between Bromine Trifluoride Vapor and Uranium Tetrafluoride . . . . . 1491
- SALMON, G. A. See Dainton, F. S., 3801; Kemp, T. J., 1464
- SALOMON, M. See McIntyre, J. D. E., 2431
- SAMUEL, D., AND SILVER, B. L. Isotopic Oxygen Exchange and Hydrolysis in Dialkylphosphonates . . . . . 1809
- SANCER, K. M. Electron Spin Resonance Line Width of the Hexaquochromic Ion as a Criterion of Outer-Sphere Coordination Interactions . . . . . 1317
- SANDBLOM, J. P. See Walker, J. L., 978
- SANDHU, H. S. Thermal Decomposition of Azoethane . . . . . 1857
- SANDLER, Y. L., AND DURIGON, D. D. Isotopic Exchange Powder . . . . . 1051
- SANTORO, A. V. See Hoyer, H. W., 4312
- SASS, R. L. See Dyke, M., 266
- SATO, H. See Tsubomura, H., 367
- SAUER, M. C., JR., AND MANI, I. Pulsed Radiolysis of Liquid Cyclohexane and *n*-Hexane. I. Yield of Hydrogen Atoms Measured by the Cyclohexadienyl Radical Absorption in Solutions Containing Benzene. II. Absorption Spectra and Reactions of Cyclohexyl and Hexyl Radicals . . . . . 3856
- SAXENA, M. C. See Shukla, J. P., 1013
- SCATCHARD, G. See Wu, Y. C., 4048
- SCHACK, C. J., PILIPOVICH, D., COHZ, S. N., AND SHEEHAN, D. F. Mass Spectra and Sublimation Pressures of  $\text{IF}_7$  and  $\text{IOF}_4$  . . . . . 4697
- SCHAEER, M. D. See Klein, R., 616
- SCHIEGLILA, A. See Knözinger, H., 2770
- SCHIEIMAN, M. A. See Jarvis, N. L., 74
- SCHERAGA, H. A. See Kunimitsu, D. K., 856; Némethy, G., 1842
- SCHIELER, L. See Mayer, S. W., 236, 2528
- SCHINDLER, R. N. See Groth, W. E., 3914
- SCHLECT, P. See Bräusse, G., 3098
- SCHMIDT, C. See O'Malley, J. A., 3584
- SCHMIDT, R. L., AND CLEVER, H. L. Thermodynamics of Binary Liquid Mixtures by Rayleigh Light Scattering . . . . . 1529
- SCHMIDT, W. F., AND ALLEN, A. O. Yield of Free Ions in Irradiated Liquids; Determination by a Clearing Field . . . . . 3730
- SCHMIDT-BLEEK, F. See Myers, D. C., 1475
- SCHNEIDER, F. W., CRONAN, C. L., AND PODDER, S. K. Cooperative Binding to a One-Dimensional Lattice. The Amylose-Iodine-Iodide Complex . . . . . 4563
- SCHNEIDER, R. F. See DiLorenzo, J. V., 761
- SCHNEIER, G. B. See Fried, V., 4688
- SCHNEPP, O. See Freiberg, M., 3526
- SCHOONHEYDT, R. See Uytterhoeven, J. B., 1768
- SCHOTT, H. Reply to Comments on the Paper "Solubilization of a Water-Insoluble Dye as a Method for Determining Micellar Molecular Weights," and Remarks on Molecular Weight Determination of Charged Micelles by Light Scattering . . . . . 380
- SCHOTT, H. N. See Wagner, P. J., 3702
- SCHOTTE, W. Prediction of Heats of Formation . . . . . 2422
- SCHREINER, F., McDONALD, G. N., AND CHERNICK, C. L. The Vapor Pressure and Melting Points of Xenon Difluoride and Xenon Tetrafluoride . . . . . 1162
- SCHRIER, E. E., AND MACKAY, L. D. The Effect of Salts of Organic Acids and Bases on the Thermal Transition of Ribonuclease . . . . . 733
- SCHROEDER, J. W. See Garland, J. F., 2277
- SCHULER, R. H. See RZAD, S. J., 228
- SCHULMAN, S. G., AND GERSHON, H. Intramolecular Hydrogen Bonding in the Lowest Excited Singlet States of Some Substituted Salicylic Acids . . . . . 3297
- SCHULMAN, S. G., AND GERSHON, H. The Absence of Fluorescence in 5-Nitro-8-quinolinol . . . . . 3692
- SCHULMAN, S. G., KILROY, W. P., AND GERSHON, H. Mixed Ligand Chelates of Copper(II) with 8-Quinolinol and Arylhydroxycarboxylic Acids. I. Electronic Absorption Spectra . . . . . 3372
- SCHULTE-FROHLINDE, D. See Malan, O. G., 1457; Vacek, K., 2686
- SCHULZ, C. O., AND STAFFORD, F. E. The Vapor Phase Infrared Spectra of the Niobium Oxotrihalides  $\text{NbOCl}_3$ ,  $\text{NbOBr}_3$ , and  $\text{NbOI}_3$  . . . . . 4686
- SCHURATH, U. See Groth, W. E., 3914
- SCHWARZ, A. Calorimetric Determination of the Heat of the Sodium-Lithium Ion-Exchange Reaction in Anhydrous Methanol . . . . . 789
- SCHWARZ, H. A. See Bielski, B. H. J., 3836
- SCHWEIKERT, W. W., AND MEYERS, E. A. The Crystal Structure of the Triphenylphosphine Sulfide-Iodine Addition Complex . . . . . 1561
- SCIBONA, G. See Danesi, P. R., 3437
- SCOTT, D. R., AND MALTENIEKS, O. Experimental Method for Determining the Intersystem Crossing Rate Constant from Lowest Excited Singlet to Lowest Triplet State . . . . . 3354
- SCOTT, D. R., AND MATSEN, F. A.  $d^2$  and  $d^8$  Configurations in an Axial Model Field . . . . . 16
- SCOTT, K. N. See Brey, W. S., Jr., 4351
- SCOTT, R., DE PALMA, D., AND VINOGRADOV, S. Proton-Transfer Complexes. I. Preferential Solvation of *p*-Nitrophenol-Amine Complexes in Nonaqueous-Solvent Mixtures . . . . . 3192
- SEARCY, A. W. See Blank, B. A. H., 2241; Skinner, H. B., 3375
- SEARLES, S. K., AND KEARLE, P. Ion-Solvent-Molecule Interactions in the Gas Phase. Enthalpies and Entropies for the Reactions  $\text{NH}_4^+(\text{NH}_3)_{n-1} + \text{NH}_3 = \text{NH}_4^+(\text{NH}_3)_n$  . . . . . 742
- SEARS, J. T., AND SUTHERLAND, J. W. Radiolytic Formation and Decomposition of Ozone . . . . . 1166
- SECOY, C. H. See Fuller, E. L., 573; Holmes, H. F., 2095, 2293
- SEHESTED, K., RASMUSSEN, O. L., AND FRICKE, H. Rate Constants of OH with  $\text{HO}_2$ ,  $\text{O}_2$ , and  $\text{H}_2\text{O}_2^+$  from

- Hydrogen Peroxide Formation in Pulse-Irradiated Oxygenated Water..... 626
- SEIBLES, L. See Copeland, J. L., 603
- SEIGEL, L. Thermal Conductivity and Diffusion Parameter: Critical-Point Behavior..... 4316
- SEILER, H. K. See Masterton, W. L., 4257
- SELIS, S. M. Kinetics of Electrode Processes in Molten Salts. II. The Influence of Solvent Anions and Cations on the Molybdenum-Molybdenum(III) Electrode..... 1442
- SELTZER, S., AND MYLONAKIS, S. G. The Effect of Temperature on Magnetically Nonequivalent Protons in an Asymmetric Azo Compound..... 754
- SENATORE, L. See Monica, M. D., 2124
- SEO, E. T., FRITSCH, J. M., AND NELSON, R. F. Electron Paramagnetic Resonance Spectra of the Naphthacene Trianion and the 5,12-Naphthacenequinone Anion Radicals..... 1829
- SEVILLA, M. D., AND VINCOW, G. Electron Spin Resonance Spectroscopy of the Xanthyl Free Radicals. I. Xanthyl Radical: a Planar Diphenylmethyl..... 3635
- SEVILLA, M. D., AND VINCOW, G. Electron Spin Resonance Spectroscopy of the Xanthyl Free Radicals. II. 9-Phenylxanthyl: Spatial Configuration..... 3641
- SEVILLA, M. D., AND VINCOW, G. Electron Spin Resonance Spectroscopy of the Xanthyl Free Radicals. III. 9-Alkylxanthyls: Torsional Oscillation of the Alkyl Groups..... 3647
- SHAPIRO, J. S., AND LOSSING, F. P. Free Radicals by Mass Spectrometry. XXXVII. The Ionization Potential and Heat of Formation of Dichlorocarbene..... 1552
- SHARP, J. H., AND LARDON, M. Spectroscopic Characterization of a New Polymorph of Metal-Free Phthalocyanine..... 3230
- SHARP, J. H., AND MILLER, R. L. Kinetics of the Thermal  $\alpha \rightarrow \beta$  Polymorphic Conversion in Metal-Free Phthalocyanine..... 3335
- SHAW, D. H., AND PRITCHARD, H. O. Homogeneous Periodic Reactions..... 1403
- SHAW, D. H., AND PRITCHARD, H. O. Homogeneous Periodic Reactions..... 2693
- SHAW, H., AND TOBY, S. The Photochemistry of Gaseous Acetone..... 2337
- SHAW, H. See Chappell, G. A., 4672
- SHEEHAN, D. F. See Schack, C. J., 4697
- SHERMAN, G., AND FUJIMORI, E. Effect of Water on Chlorophyll-Quinone Interactions in the Solid State... 4345
- SHERMAN, W. V. Radical-Initiated Chain Dehalogenation of Alkyl Halides in Alkaline Alcoholic Solution..... 2287
- SHERMAN, W. V. See Hentz, R. R., 2635
- SHERRY, H. S. The Ion-Exchange Properties of Zeolites. IV. Alkaline Earth Ion Exchange in the Synthetic Zeolites Linde X and Y..... 4086
- SHERRY, H. S. See Olson, D. H., 4095
- SHIDA, S. See Tanno, K., 3496
- SHIDA, T. Electron Spin Resonance and Optical Studies of *t*-Butyl Peroxide Ion Produced by  $\gamma$  Irradiation..... 723
- SHIDA, T. Disulfide Ions Products in  $\gamma$ -Irradiated Organic Glasses at  $-196^\circ$ . A Photochromism of the Anion... 2597
- SHIH, P. S. See Banewicz, J. J., 1960
- SHIMURA-KAMBE, Y. Temperature Dependence of the Limiting Viscosity Number of the Solutions of Acrylonitrile-Styrene Copolymers in Dimethylformamide... 4104
- SHINE, H. J., AND SULLIVAN, P. D. Complete Proton and Naturally Occurring  $^{35}\text{S}$  Hyperfine Splittings in the Thianthrene Cation Radical..... 1390
- SINGH, N. B. See Rastogi, R. P., 4446
- SINGH, S. See Davies, G. A., 4320
- SINGHAL, G. S., WILLIAMS, W. P., AND RABINOWITZ, E. Fluorescence and Absorption Studies on Chlorophyll *a* *in Vitro* at  $77^\circ$ ..... 3941
- SHIPMAN, G. F. See Kerr, G. T., 3071
- SHIROM, M., AND WILLARD, J. E. Radical Production by  $\gamma$  Irradiation of 3-Methylpentane, Methyltetrahydrofuran, and Methylcyclohexane Glasses at  $77^\circ\text{K}$  with and without Alkyl Halide Solutes..... 1702
- SHOR, A. J., KRAUS, K. A., SMITH, W. T., JR., AND JOHNSON, J. S., JR. Hyperfiltration Studies. XI. Salt Rejection Properties of Dynamically Formed Hydrated Zirconium(IV) Oxide Membranes..... 2200
- SHORES, R. D., AND MOSER, H. C. Reactions of Tritium Atoms Produced by Electron Impact on  $\text{T}_2$  with Solid Propene and Propane..... 1
- SHORT, G. D. See Parker, C. A., 3071
- SHUKLA, D. D. See Shukla, J. P., 1013
- SHUKLA, J. P., AHMAD, S. I., SHUKLA, D. D., AND SAXENA, M. C. Study of Dielectric Relaxation in Benzene Solutions of Some Hydroxy- and Methoxybenzaldehydes... 1013
- SHURAYH, F. R. See Hanania, G. I. H., 1355
- SICA, J. See Mukherjee, L. M., 3410
- SICILIO, F. See Florin, R. E., 3154
- SIDDALL, T. H., III, STEWART, W. E., AND MARSTON, A. L. Proton Magnetic Resonance and Infrared Studies of the *cis* and *trans* Isomers of a Monosubstituted Formanilide..... 2135
- SIDDIQI, M. A. See Gopal, R., 1814
- SIECK, L. W. Continuum Emission from Xenon in the Vapor Phase Induced by Absorption of 1470-Å Radiation..... 3129
- SILVA, W. J. See Johnson, J. W., 1664, 1669
- SILVER, B. L. See Samuel, D., 1809
- SIMONS, J. W., MAZAC, C. J., AND TAYLOR, G. W. Intramolecular Comparison of the Insertion into the C-H Bonds of Alkanes by Singlet Methylene Radicals..... 749
- SIMONS, J. W. See Allard, K., 136
- SIMPSON, G. A. See Grimison, A., 1776
- SIMS, L. B. See Wettaw, J. F., 3440
- SINGH, J., PFLUG, H. D., AND BENSON, G. C. Molar Excess Enthalpies and Volumes of Benzene-Isomeric Xylene Systems at  $25^\circ$ ..... 1939
- SINGH, J. See Benson, G. C., 1345
- SINGH, N. B. See Rastogi, R. P., 4446
- SIODA, R. E. Electrolytic Oxidation of 9,10-Diphenylanthracene and Properties of Its Free Radical Cation and Anion..... 2322
- SKIBBA, M. See Zuehlke, R. W., 1425
- SKINNER, H. B., AND SEARCY, A. W. The Vapor Pressure, the Heat of Sublimation, and the Evaporation Coefficient of Praseodymium Trifluoride..... 3375
- SKINNER, J. F., CUSSLER, E. L., AND FUOSS, R. M. Pressure Dependence of Dielectric Constant and Density of Liquids..... 1057
- SKINNER, J. F. See Markgraf, J. H., 2276
- SLABAUGH, W. H., AND HILTNER, P. A. The Swelling of Alkylammonium Montmorillonites..... 4295
- SLATEN, B. L. See Wiewiorowski, T. K., 1890
- SLEIGHT, T. P., AND HARE, C. R. The Spectrum of the Hexachloroiridium(IV) Ion..... 2207
- SLUTSKY, L. J. See Parker, R. C., 3177
- SMALL, T., AND ROWLAND, F. S. The Primary Isotope Effect for the Replacement of H vs. D by Energetic Tritium Atoms..... 1845
- SMITH, G. See Allendoerfer, R. D., 1217
- SMITH, G. H., AND HAMILTON, F. J. Etherate Formation in Organoaluminum Compounds. Complex-Formation Tendency in a Series of Trialkylaluminum, Dialkylaluminum Chloride, Alkylaluminum Dichloride, and Aluminum Chloride Aryl Etherates..... 3567
- SMITH, G. P. See Boston, C. R., 293; Brynestad, J., 296
- SMITH, H. T. See Franks, F., 2668
- SMITH, J. V. See Rizzo, F. E., 485
- SMITH, S. L., AND COX, R. H. Solvent-Dependent H-H Couplings in Hexachlorobicyclo[2.2.1]heptenes..... 198
- SMITH, S. R. See Cordes, H. F., 2189
- SMITH, W. B., AND TEMPLE, H. W. Polymer Studies by Gel Permeation Chromatography. IV. The Degradation of Polystyrene by Ultrasonics and by Benzoyl Peroxide..... 4613
- SMITH, W. B. See May, J. A., Jr., 216, 2993
- SMITH, W. H., ECKSTROM, H. C., AND BÄR, F. Interpretation of Infrared Spectra of Chemisorbed Hydrogen and Deuterium..... 369
- SMITH, W. H. See Brumberger, H., 3340
- SMITH, W. T., JR. See Shor, A. J., 2200
- SMYRL, W. H., AND NEWMAN, J. Potentials of Cells with Liquid Junctions..... 4660
- SNELSON, A. Infrared Spectra of the Beryllium Halides... 250
- SNIDER, W. See Neuman, R. C., 2469
- SNOW, R. L. See Izatt, R. M., 1208
- SNOWDEN, B. S., JR. See Woessner, D. E., 1139
- SNYDER, L. R. Interactions Responsible for the Selective Adsorption of Nonionic Organic Compounds on Alumina. Comparisons with Adsorption on Silica... 489
- SOKOLOWSKA, A., AND KEVAN, L. Energy Transfer in Radiolysis of Rare Gas-C<sub>2</sub>F<sub>4</sub> Liquid Mixtures..... 253
- SOLDANI, G. See Bertozzi, G., 353
- SOLOMON, I. J., KACMAREK, A. J., AND RANEY, J. The Reaction of Oxygen Difluoride and Sulfur Trioxide. Transfer of the OF Radical..... 2262
- SOLOMON, W. C., BLAUER, J. A., AND JAYE, F. C. The



- Thermal Dissociation of Oxygen Difluoride. II. Static Reactor. . . . . 2311
- SOLOMON, W. C. See Blauer, J. A., 2307
- SONG, P.-S. Electronic Structure and Photochemistry of Flavins. IV.  $\sigma$ -Electronic Structure and the Lowest Triplet Configuration of a Flavin. . . . . 536
- SPALDING, G. E. Diffusion Potential Decay Accompanying Transient-State Diffusion of Electrolytes in Ideal Solutions. . . . . 272
- SPEES, S. T., JR., PERUMAREDDI, J. R., AND ADAMSON, A. W. Crystal Field Energy Levels for Various Symmetries. . . . . 1822
- SPENCE, J. T. See Huang, T., 4198, 4573
- SPENCER, H. E., AND DARLAK, J. O. Lead Bromide Photochemistry: Reduction of Lead Ion and Oxidation of Leucocrysal Violet. . . . . 2384
- SPENCER, J. N., AND VOIGT, A. F. Thermodynamics of the Solution of Mercury Metal. I. Tracer Determination of the Solubility in Various Liquids. . . . . 464
- SPENCER, J. N., AND VOIGT, A. F. Thermodynamics of the Solution of Mercury Metal. II. The Free-Volume Theory. . . . . 471
- SPENCER, J. N., AND VOIGT, A. F. Thermodynamics of the Solubility of Mercury Metal. III. Dimethylcyclohexanes and Alcohols as Solvents. . . . . 1913
- SPERLING, L. H. See Tobolsky, A. V., 345
- SPEROS, D. M., AND WOODHOUSE, R. L. Realization of Quantitative Differential Thermal Analysis. II. A Solid-Gas Reaction. . . . . 2846
- SPITTLER, E. G., AND KLEIN, G. W. The Hg(<sup>1</sup>P<sub>1</sub>)-Photosensitized Decomposition of Cyclobutane. . . . . 1432
- SPOKES, G. N. See Benson, S. W., 1182
- SPURLING, T. H. See Storvick, T. S., 1821
- SQUIRE, D. R. See Neece, G. A., 128
- SRINIVASAN, V. S., AND KUWANA, T. Internal Reflectance Spectroscopy at Optically Transparent Electrodes. . . . . 1144
- STAFFORD, F. E. See Pava, B. M., 4628; Schulz, C. O., 4686
- STARK, F. O., JOHANNSON, O. K., VOGEL, G. E., CHAFFEE, R. G., AND LACEFIELD, R. M. The Interactions between Trialkylsilanes and E-Glass or Aerosil Surfaces. Reactions of Trimethylsilanol, Trimethylchlorosilane, and Hexamethyldisilazane. . . . . 2750
- STEEL, C. See Milne, G. S., 3754
- STEELHAMMER, J. C. See Wentworth, W. E., 2671
- STEER, R. P., AND KNIGHT, A. R. Reactions of Thyl Radicals. IV. Photolysis of Methanethiol. . . . . 2145
- STEIGER, R. P. See Cater, E. D., 2231
- STEIGMAN, J., DE IASI, R., LILENFELD, H., AND SUSSMAN, D. Acid-Base Reactions in Concentrated Aqueous Quaternary Ammonium Salt Solutions. III. Dicarboxylic Acids. . . . . 1132
- STEIGMAN, J., AND DOBROW, J. The Interaction of Antagonistic and Cooperative Electrolytes in Water at 25°. A Hypothesis Concerning Anion-Exchange Resins. . . . . 3424
- STEIN, G. See Rakintzis, N. T., 1011
- STEIN, R. S. See MacKnight, W. J., 1122
- STERN, J. H., AND HERMANN, A. Solute-Solvent Interactions: Ethyl Acetate in Water. . . . . 364
- STERN, J. H., LAZARTIC, J., AND FOST, D. Thermodynamics of Aqueous Mixtures of Electrolytes and Nonelectrolytes. V. Enthalpies of Transfer in the Limiting Region at 25°. . . . . 3053
- STERN, J. H., AND NOBILIONE, J. Thermodynamics of Aqueous Mixtures of Electrolytes and Nonelectrolytes. IV. Transfer of Hydrochloric Acid from Water to Aqueous Acetic Acid at 25°. . . . . 1064
- STERN, J. H., AND NOBILIONE, J. M. Thermodynamics of Aqueous Mixtures of Electrolytes and Nonelectrolytes. VI. Transfer of Hydrochloric Acid from Water to Aqueous Ethylene Glycol at 25°. . . . . 3937
- STERN, K. H. Membrane Potentials and Ion Selectivity of Fused Silica in Molten Salts. . . . . 1963
- STERN, K. H. Ion Diffusion into Fused Silica from Molten Salts. . . . . 2256
- STEVENS, B., AND ALGAR, B. E. The Photoperoxidation of Unsaturated Organic Molecules. I. Relaxation and Oxygen-Quenching Parameters of the Sensitizer Singlet State. . . . . 2582
- STEVENS, B., AND ALGAR, B. E. The Photoperoxidation of Unsaturated Organic Molecules. II. The Autoperoxidation of Aromatic Hydrocarbons. . . . . 3468
- STEVENS, B., AND ALGAR, B. E. The Photoperoxidation of Unsaturated Organic Molecules. III. Autoperoxidation in Polymer Films. . . . . 3794
- STEWART, W. E. See Siddall, T. H., III, 2135
- STIMSON, E. R. See Kunimitsu, D. K., 856
- STOFFER, R. L. See Hopkins, P. D., 3345
- STORVICK, T. S., AND SPURLING, T. H. On the Kihara Core Model for Polar Molecules. . . . . 1821
- STOUGHTON, R. W. See Lietzke, M. H., 257
- STRANDBERG, M. W. P. See Espino, R. L., 3689
- STRAUSS, H. L. See Kimmel, P. I., 2813
- STRAUSS, U. P. See Varoqui, R., 2507
- STROM, E. T. On Carbonyl Carbon-13 Hyperfine Splitting in Free Radicals and the Possible Nonplanarity of Certain Ketyls. . . . . 4715
- STRONSKI, R. E. See Di Carlo, E. N., 1517
- STUCKEY, J. E. See Fuller, E. L., Jr., 573
- STURM, G. P., JR., AND WHITE, J. M. The Photochemical Decomposition of Methanethiol. Hot Hydrogen Atom Reaction with Deuterium. . . . . 3679
- SUART, S. R. See Eaton, D. R., 400
- SUBRAHMANYAN, V., AND LAKSHMINARAYANAIAH, N. A Rapid Method for the Determination of Electrical Conductance of Ion-Exchange Membranes. . . . . 4314
- SUBRAHMANYAN, V. See Lakshminarayanaiah, N., 1253
- SUBRAMANIAN, S. Comment on "A Low-Temperature, High-Pressure Hydrate of *n*-Tetrabutylammonium Halides". . . . . 2694
- SUBRAMANIAN, S., AND AHLUWALIA, J. C. Standard Partial Molal Heat Capacities of Sodium Tetraphenylboron in Aqueous Solution from 0 to 90°. . . . . 2525
- SUDMEIER, J. L. Analysis of Proton Magnetic Resonance Spectra of *trans*-2,5-Dimethylpiperazine and Its Hydrochlorides. Effect of Amine Substituents on Chemical Shifts and Coupling Constants. . . . . 2344
- SUGISHIMA, K. See Tsubomura, H., 367
- SUITO, E. See Kobayashi, T., 2446
- SULLIVAN, J. C., AND BURKHART, M. J. A Kinetic Study of the System <sup>234</sup>Np(V)·Cr(III)-<sup>239</sup>Np(V). . . . . 2675
- SULLIVAN, P. D. See Shine, H. J., 1390
- SUMIDA, T. See Hamada, F., 178
- SUNG, N. See Fleischer, E. B., 4311
- SURI, S. K., AND RAMAKRISHNA, V. Adsorption from Solution on a Free Liquid Surface and on an Inert Solid. . . . . 1555
- SURI, S. K., AND RAMAKRISHNA, V. Surface Tension of Some Binary Liquid Mixtures. . . . . 3073
- SUSBIELLES, G. G., AND DELAHAY, P. Diffuse Double Layer of Weak Electrolytes with Field Dissociation. . . . . 841
- SUSKI, L. See Mościński, J., 441
- SUSSMAN, D. See Steigman, J., 1132
- SUTHERLAND, J. W. See Sears, J. T., 1166
- SUTPHEN, C. See Nicholls, D., 1021
- SVIRMICKAS, A. See Hindman, J. C., 4188
- SWAIN, H. A., JR. See Baccanari, D. P., 2243
- SWANSON, T. B. Electron Magnetic Resonance Spectra of MnCl<sub>2</sub>-LiCl-KCl Eutectic Mixtures. . . . . 4701
- SWETT, V. C., AND DUDEK, E. P. An Electron Paramagnetic Resonance Study of the Bonding in Copper Complexes. . . . . 1244
- SWIFT, H. E. See Petrakis, L., 546
- SWIFT, J. D. See MacGillivray, A. D., 3375
- SWORSKI, T. J. See Matthews, R. W., 3704
- SYMONS, M. C. R. See Blandamer, M. J., 2268
- SYNNOTT, J. C., AND BUTLER, J. N. The Mean Activity Coefficient of Sodium Sulfate in Aqueous Sodium Sulfate-Sodium Chloride Electrolytes. . . . . 2474
- SZUCHNICKA, T. See Libuś, W., 2075
- SZWARC, M. See Cheng, W. J., 494; Kalfoglou, N., 2233; Nicholls, D., 1021
- TAKAGI, M. See Murakami, Y., 116
- TAKAKURA, K., AND RANBY, B. Studies of Free-Radical Species from the Reactions of Titanium(III) Ions with Hydrogen Peroxide. . . . . 164
- TAKASHIMA, S. See Grant, E. H., 4373
- TAKITA, S., MORI, Y., AND TANAKA, I. The Acetylene-Photosensitized Reaction of Methane at 1470 Å. . . . . 4360
- TAMRES, M., DUERKSEN, W. K., AND GOODENOW, J. M. Vapor-Phase Charge-Transfer Complexes. II. The 2I<sub>2</sub> = I<sub>4</sub> System. . . . . 966
- TANAKA, I., MORI, Y., MINAGAWA, Y., AND OKUTSU, E. Photolysis of Methylene Blue by a Giant-Pulse Ruby Laser. . . . . 2684
- TANAKA, I. See Takita, S., 4360
- TANCREDI, T. See Temussi, P. A., 3581
- TANG, Y.-N., AND ROWLAND, F. S. Some Upper Limits for the Single-Step Double-Displacement Reaction in Recoil Tritium Systems. . . . . 707

- TANIGUCHI, H., FUKUI, K., OHNISHI, S., HATANO, H., HASEGAWA, H., AND MARUYAMA, T. Free-Radical Intermediates in the Reaction of the Hydroxyl Radical with Amino Acids. . . . . 1926
- TANNO, K., SHIDA, S., AND MIYAZAKI, T. Reactions of Ions in the Radiolysis of Liquid Isobutane, Isopentane, and 2,3-Dimethylbutane. . . . . 3496
- TARPLEY, A. R. See Evans, H. B., Jr., 2552
- TAUB, I. A. See Asmus, K.-D., 3382
- TAYLOR, A. H., AND BRUMMER, S. B. The Adsorption and Oxidation of Hydrocarbons on Noble Metal Electrodes. VII. Oxidative Adsorption of Methane on Platinum Electrodes. . . . . 2856
- TAYLOR, G. W. See Simons, J. W., 749
- TEMPLE, H. W. See Smith, W. B., 4613
- TEMPLETON, D. H. See Hardgrove, G. L., 668
- TEMPLETON, L. K. See Hardgrove, G. L., 668
- TEMUSSI, P. A., AND TANCREDI, T. The Mechanism of Isomerization of Methyl Nitrite. . . . . 3581
- TEMUSSI, P. A. See Ganis, P., 3997
- TENNANT, W. C. The Action of Lead Monoxide as an Inorganic Photosensitizer. . . . . 1078
- TERAMOTO, A. See Okita, K., 278; Yanagida, T., 1265
- TERATANI, S. See Hirota, K., 3133
- TESTA, A. C. See Rusakowicz, R., 793, 2680; Weisstuch, A., 1982
- TEARSON, A., AND LAMPE, F. W. The Krypton-Radiosensitized Reaction of Deuterium Atoms with Ethylene. 3261
- THAIN, J. F. See Meares, P., 2789
- THIRSK, H. R. See Armstrong, R. D., 2300
- THOMPSON, G. F. See Kemp, T. J., 1464
- THOMPSON, R. C. The Oxidation of Chlorine Dioxide by Cobalt(III) in Perchlorate Solution. . . . . 2642
- THRUSH, B. A., HALSTEAD, C. J., AND MCKENZIE, A. Chemiluminescence in Gases: Reactions Yielding Electronically Excited Sulfur Dioxide. . . . . 3711
- THYNNE, J. C. J. See Jones, A., 2677; Morris, E. R., 3351; Quee, M. J. Y., 2824
- TIBBALS, H. F. See Meisels, G. G., 3746
- TIEN, H. T. The Thermodynamics of Bimolecular (Black) Lipid Membranes at the Water-Oil-Water Biface. . . . . 2723
- TIEN, H. T. Photoelectric Effects in Thin and Bilayer Lipid Membranes in Aqueous Media. . . . . 4512
- TIERNAN, T. O., AND FUTRELL, J. H. Ionic Reactions in Unsaturated Compounds. II. Ethylene. . . . . 3080
- TIERNAN, T. O. See Futrell, J. H., 158, 1071
- TIMMONS, R. B. See Kale, J. D., 4239
- TING, C. T., AND ROWLAND, F. S. High Internal Excitation Energies of Products Following Energetic Substitution of Tritium for Hydrogen in Methyl Isocyanide. 763
- TITANI, Y., AND LICHTIN, N. N. Reactions of Active Nitrogen with Organic Substrates. VII. Molecular Origins of Products of Reaction with Propene. II. . . . . 526
- TOBOLSKY, A. V., AND SPERLING, L. H. Volume Dependence of the Equation of State for Rubber Elasticity: Poly(dimethyl siloxane). . . . . 345
- TOBOLSKY, A. V. See McKinnon, A. J., 1157
- TOBY, S. See Shaw, H., 2337
- TODD, J. E. See Bufalini, M., 3367
- TOKIWA, F. Solubilization Behavior of Sodium Dodecylpolyoxyethylene Sulfates in Relation to Their Polyoxyethylene Chain Lengths. . . . . 1214
- TOKIWA, F. Solubilization Behavior of a Polyoxyethylene Sulfate Type of Surfactant in Connection with the Micellar Charge. . . . . 4331
- TOLBERT, B. M. See Gottschall, W. C., Jr., 922
- TOMBALAKIAN, A. S. Phenomenological Coefficients for Volume Flow across an Ion-Exchange Membrane. . . . . 1566
- TOMBALAKIAN, A. S. Comment on "Current Dependence of Water Transport in Cation-Exchange Membranes". . . . . 3698
- TOMINAGA, T., AND ROWLAND, F. S. Estimation of Bond Dissociation Energies of N-H Bonds by Correlation with HT Yields from Recoil Tritium Abstraction. . . . . 1399
- TOPOL, L. E., AND OWENS, B. B. Thermodynamic Studies in the High-Conducting Solid Systems RbI-AgI, KI-AgI, and NH<sub>4</sub>I-AgI. . . . . 2106
- TORIYAMA, K. See Iwasaki, M., 4347
- TORRES, A. L. See Bonner, O. D., 4290
- TOU, J. C., AND WAHRHAFTIG, A. L. A Modified VWJ Equation for Calculating the Totality of States of a Collection of Harmonic Oscillators. . . . . 3034
- TRAJMAR, S. See Kuppermann, A., 3894
- TREININ, A. See Feldmann, T., 3768; Luria, M., 305
- TRUMBORE, C. N. See Al-Thannon, A., 2395; Klein, N., 880
- TSAU, J., AND GILSON, D. F. R. Polymorphism in *n*-Alkylammonium Halides. A Differential Scanning Calorimetric Study. . . . . 4082
- TSCHUIKOW-ROUX, E. Critical Bond Length in Radical Combination and Unimolecular Dissociation Reactions. 1009
- TSCHUIKOW-ROUX, E., AND PAUL, R. Comment on "Fast Reactions of Polar Molecules in Processes with No Activation Energy". . . . . 375
- TSIGIDINOS, G. A. See Hallada, C. J., 4304
- TSINA, R. V. See Dewald, R. R., 4520
- TSUBOMURA, H., YAMAMOTO, N., SATO, H., YOSHINAGA, K., ISHIDA, H., AND SUGISHIMA, K. Experimental Determination of the Electronic Absorption Spectrum Ascribable to the O<sub>2</sub><sup>-</sup> Ion Adsorbed on Porous Glass. . . . . 367
- TSUJI, K., AND WILLIAMS, F. Comparison of Photo- and  $\gamma$ -Induced Ionization Processes in the Condensed Phase by Means of Electron Spin Resonance Spectroscopy. . . . . 3884
- TURKEVICH, J. See Mickewich, D., 2703
- TURNER, D. J., BECK, A., AND DIAMOND, R. M. The Extraction of Tetraheptylammonium Fluoride and the Solvation of the Fluoride Ion. . . . . 2831
- TURNER, D. J., AND DIAMOND, R. M. The Extraction of Perchloric Acid by 1-Decanol. . . . . 3504
- UEDA, T. See Hirota, K., 1976
- UFFINDELL, N. D. See Padday, J. F., 1407, 3700
- UMBERGER, J. Q. Solution Kinetics *via* Fluorescence Quenching—Transient and Solvent Effects. . . . . 1350
- UNDERWOOD, G. R. See Russell, G. A., 1074
- URRY, D. W. Circular-Dichroism Pattern of Methylpyrrolidone Can Resemble That of the  $\alpha$  Helix. . . . . 3035
- UY, O. M., KOHL, F. J., AND CARLSON, K. D. Dissociation Energy of PN and Other Thermodynamic Properties for the Vaporization of P<sub>3</sub>N<sub>5</sub>. . . . . 1611
- UYEDA, N. See Kobayashi, T., 2446
- UYTTERHOEVEN, J. B., JACOBS, P., MAKAY, K., AND SCHOONHEYDT, R. The Thermal Stability of Hydroxyl Groups in Decationated Zeolites X and Y. . . . . 1768
- VACEK, K., AND SCHULTE-FROHLINDE, D. The Kinetics of the Reaction of Trapped Hydrogen Atoms in Sulfuric Acid Glasses. . . . . 2686
- VALENZUELA, J. A., AND BARD, A. J. Electron Spin Resonance Spectrum of Tetrakis(*p*-methoxyphenyl)-ethylene Cation Radical. . . . . 286
- VAN ARTSDALEN, E. R. See Jhon, M. S., 4155
- VAN HEUVELEN, A., AND GOLDSTEIN, L. Electron Paramagnetic Resonance and Optical Studies of the Oxidation of Aniline by Copper(II) Acetate. . . . . 481
- VAN HOOK, W. A. Vapor Pressures of the Isotopic Waters and Ices. . . . . 1234
- VAN NESS, H. C. See Haskell, R. W., 4534
- VAN REISEN, M. See Leyte, J. C., 1127
- VAN WAZER, J. R. See Moedritzer, K., 4380
- VAN WINKLE, Q. See Ditmars, W. E., Jr., 39
- VAROQUI, R., AND STRAUSS, U. P. Comparison of Electrical Transport Properties of Anionic Polyelectrolytes and Polysoaps. . . . . 2507
- VASLOW, F. See Linderström-Lang, C. U., 2645
- VAUGHAN, J. D. See Broadus, J. D., 1005
- VEERAVAGU, P. See Wiley, R. H., 2417
- VERHAGE, H. See Maatman, R., 97
- VERMAAK, J. S., AND KUHLMANN-WILSDORF, D. Measurement of the Average Surface Stress of Gold as a Function of Temperature in the Temperature Range 50–985°. . . . . 4150
- VERNEKER, V. R. P., AND FORSYTH, A. C. Mechanism for Controlling the Reactivity of Lead Azide. . . . . 111
- VERSINO, C. See Zecchina, A., 1471
- VICINI, H. See Martire, D. E., 3489
- VIJH, A. K. Electrolytic Hydrogen Evolution Reaction on Aluminum in Acidic Solutions. . . . . 1148
- VILK, P. See Willi, A. V., 3142
- VINCOW, G. See Sevilla, M. D., 3635, 3641, 3647
- VINOGRADOV, S. See Scott, R., 3192
- VISCO, R. E. See Chandross, E. A., 378
- VISSERS, D. R. The Sorption of Orthophosphate on Crystalline Metal Oxides. . . . . 3236
- VITAGLIANO, V. See Barone, G., 2588; Costantino, L., 149
- VOGEL, G. E. See Stark, F. O., 2750
- VOGEL, H. See Brause, G., 3098
- VOIGT, A. F. See Spencer, J. N., 464, 471, 1913

- VOIGT, E. M. Absorption Maxima of the Visible Band of Iodine in Different Groups of Solvents..... 3300
- VOLKERT, W. A., AND KUNTZ, R. R. The Reactions of Hydrogen Atoms in Aqueous Solutions. Some Amino Acids..... 3394
- VON ELBE, G. See McHale, E. T., 1849
- VON SALIS, G. A., AND LABHART, H. On the Temperature Dependence of the Viscosity of Organic Glasses..... 752
- VRENTAS, J. S. See Duda, J. L., 1187, 1193
- WADE, W. H., AND WHALEN, J. W. Pendular-Ring Condensation on Teflon Powders..... 2898
- WAGGONER, A. S., KEITH, A. D., AND GRIFFITH, O. H. Electron Spin Resonance of Solubilized Long-Chain Nitroxides..... 4129
- WAGNER, N. J. See Cadenhead, D. A., 2775
- WAGNER, P. J., AND SCHOTT, H. N. The Inefficiency of Triplet Energy Transfer from Ketones to Trivalent Rare Earth Ions..... 3702
- WAHLBECK, P. G. See Macur, G. J., 1047
- WAHRHAFTIG, A. L. See Tou, J. C., 3034
- WAI, C. M., AND ROWLAND, F. S. The Substitution of Energetic Chlorine Atoms for Hydrogen Atoms in Butyl Chlorides..... 3049
- WAKAMATSU, S. See Miyama, H., 4700
- WALDSTEIN, P. See Blatz, L. A., 2614
- WALKER, D. C. An Efficient and Highly Selective Radiation-Induced Isomerization in the Crystalline State.... 3772
- WALKER, J. L., JR., EISENMAN, G., AND SANDBLOM, J. P. Electrical Phenomena Associated with the Transport of Ions and Ion Pairs in Liquid Ion-Exchange Membranes. III. Experimental Observations in a Model System.... 978
- WALKER, J. Q. See Wolf, C. J., 3457
- WALKLEY, J. See Bennett, L., 4699
- WALL, L. A. See Florin, R. E., 3154
- WALLING, C., AND PAPAIOANNOU, C. G. Bond Dissociation Energies of *t*-Butyl Hypohalites..... 2260
- WALLIS, E. B. See Cobb, C. M., 2986
- WALTER, R. I. See Allendoerfer, R. D., 1217
- WALTER, T. A. See Kistiakowsky, G. B., 3952
- WALTERS, A. B. See Benson, J. E., 4587
- WALTON, J. C. Reply to Comment on "Fast Reactions of Polar Molecules in Processes with No Activation Energy" by E. Tschuikow-Roux and R. Paul..... 375
- WANDER, R., NETA, P., AND DORFMAN, L. M. Pulse Radiolysis Studies. XII. Kinetics and Spectra of the Cyclohexadienyl Radicals in Aqueous Benzoic Acid Solution..... 2946
- WARD, A. T. Crystal-Field Splitting of Fundamentals in the Raman Spectrum of Rhombic Sulfur..... 744
- WARD, A. T. Raman Spectroscopy of Sulfur, Sulfur-Selenium, and Sulfur-Arsenic Mixtures..... 4133
- WARD, J. W. The Nature of Sites Formed on Zeolites by Addition of Water..... 2689
- WARD, J. W. A Spectroscopic Study of the Surface of Zeolite Y. II. Infrared Spectra of Structural Hydroxyl Groups and Adsorbed Water on Alkali, Alkaline Earth, and Rare Earth Ion-Exchanged Zeolites..... 4211
- WARE, B., WILLIAMSON, K., AND DEVLIN, J. P. An Infrared Study of Internal-Rotational Barriers in Solid  $\pi$  Complexes of Methylbenzenes. I. Hexamethylbenzene-Tetracyanoethylene..... 3970
- WARMAN, J. M. The Reaction of O<sup>-</sup> with Alcohols in Gas-Phase Radiolysis..... 52
- WARMAN, J. M. See Rzd, S. J., 3013
- WARNECK, P. See Driscoll, J. N., 3736
- WARNER, J. W. See Klein, N., 880
- WARREN, L. J. See Lyons, L. E., 3677
- WARSHAWSKY, I. Absorption Spectra of Sodium-Ammonia Mixtures in the Gas Phase..... 3334
- WASHINGTON, E. L., AND BATTINO, R. Thermodynamics of Binary Solutions of Nonelectrolytes with 2,2,4-Trimethylpentane. III. Volumes of Mixing with Cyclohexane (10-80°) and Carbon Tetrachloride (10-80°)... 4496
- WASON, S. K. See Granzow, A., 1402, 3741
- WATANABE, Y., AND HABGOOD, H. W. Spectroscopic Evidence for Brønsted Acidity in Partially Dehydrated Group Ia Forms of Zeolites X and Y..... 3066
- WATSON, A. M. See Knözinger, H., 2770
- WATSON, J. A., JR. See Zandler, M. E., 2730
- WATSON, W. H. See Rogers, J. W., 68
- WAYLAND, B. B. See Redmond, T. F., 1626, 3038
- WEHMAN, T. C., AND POPOV, A. I. Electrical Conductance Studies in Anhydrous Formic Acid Solutions.. 4031
- WEIGOLD, H. See Fackler, J. P., Jr., 4631
- WEINER, N. D. See Gillap, W. R., 2218, 2222
- WEISBERG, J. See Codell, M., 2460
- WEISS, J. J. See Devonshire, R., 3815
- WEISS, K. See Halpern, A. M., 3863
- WEISS, V. W. See Forster, D., 2669
- WEISSTUCH, A., AND TESTA, A. C. A Fluorescence Study of Aminopyridines..... 1982
- WEN, W.-Y., AND NARA, K. Volume Changes on Mixing Solutions of Alkali Halides and Symmetrical Tetraalkylammonium Halides. II. Effects of Deuterium Oxide and Temperature..... 1137
- WEN, W.-Y., NARA, K., AND WOOD, R. H. Volume Changes on Mixing Solutions of Potassium Halides and Symmetrical Tetraalkylammonium Halides. Evidence for Cation-Cation Interaction. A Correction and Further Comments..... 3048
- WENTWORTH, W. E., CHEN, E., AND STEELHAMMER, J. C. Determination of Electron Affinities of Radicals and Bond Dissociation Energies by Electron-Attachment Studies at Thermal Energies—Electron Affinity of Acetate Radical..... 2671
- WETTAW, J. F., AND SIMS, L. B. Carbon-13 Kinetic Isotope Effect in the Thermal Isomerization of Methyl Isocyanide..... 3440
- WHALEN, J. W. See Wade, W. H., 2898
- WHALLEY, E. See Gay, D. L., 4145
- WHARTON, J. H. See Holloway, H. E., 4468, 4474
- WHEELER, R. On Radical Recombination Rates in SO<sub>2</sub>-Doped Flames..... 3359
- WHITE, J. M. See Sturm, G. P., Jr., 3679
- WHITMAN, D. R. See Brey, W. S., Jr., 4351
- WHITTINGTON, S. G., AND WILLIAMS, P. J. The Treatment of End Effects in a Markov Chain Model of the Configurational Properties of Long-Chain Molecules... 372
- WIEWIOWSKI, T. K., PARTHASARATHY, A., AND SLATEN, B. L. Molten Sulfur Chemistry. V. Kinetics of Chemical Equilibration in Pure Liquid Sulfur..... 1890
- WILCOX, F. L. See Keenan, A. G., 1085
- WILD, U. See Halonbrenner, R., 3929
- WILEY, R. H., AND VEERAVAGU, P. Focused, Coherent Radiation (Laser)-Induced Degradation of Aromatic Compounds..... 2417
- WILKENING, V. G., LAL, M., ARENDS, M., AND ARMSTRONG, D. A. The Cobalt-60  $\gamma$  Radiolysis of Cysteine in Deaerated Aqueous Solutions at pH Values between 5 and 6..... 185
- WILKS, M. A. J., AND WILLIS, M. R. Interpretation of the High-Resolution Electron Spin Resonance Spectrum of the 2,4,5-Triphenylimidazolyl Radical..... 4717
- WILLARD, J. E. See Ekstrom, A., 4604; French, W. G., 4599; Ling, A. C., 1918, 3349; Shirom, M., 1702; Wong, P. K., 2623
- WILLI, A. V., WON, C. M., AND VILK, P. Kinetics and Mechanism of the Decarboxylation of Anthranilic Acid in Aqueous Solution..... 3142
- WILLIAMS, F. See Lin, J., 3707; Tsuji, K., 3884
- WILLIAMS, H. P. See Brey, W. S., Jr., 49
- WILLIAMS, P. J. See Whittington, S. G., 372
- WILLIAMS, W. P. See Singhal, G. S., 3941
- WILLIAMSON, A. D. See Rattet, L. S., 2954
- WILLIAMSON, K. See Ware, B., 3970
- WILLIAMSON, M. P., CASTELLANO, S., AND GRIFFIN, C. E. The Proton Magnetic Resonance Spectra of Diethyl Vinylphosphonate and Substituted Vinylphosphonates. 175
- WILLIAMSON, M. P., AND GRIFFIN, C. E. Some Observations on the Proton Magnetic Resonance Spectrum of Tetraethyl Ethylenebisphosphonate..... 2678
- WILLIAMSON, M. P., AND GRIFFIN, C. E. Three- and Four-Bond <sup>31</sup>P-<sup>1</sup>H Coupling Constants and Geminal Proton Nonequivalence in Ethyl Esters of Phosphorus Acids. 4043
- WILLIS, C. See Forchioni, A., 3105
- WILLIS, M. R. See Wilks, M. A. J., 4717
- WILLSON, R. L. See Emmerson, P. T., 3669
- WILSON, D. J. See Dubrow, R., 2489
- WINDSOR, M. L. See Dantzler, E. M., 676
- WINDSOR, M. W. See Dawson, W. R., 3251
- WIRTH, H. E., AND LOSURDO, A. Solubility of Benzene in Concentrated Aqueous Solutions of Tetraalkylammonium Bromides..... 751
- WITHERS, G. See Keneshea, F. J., 1272
- WITHERSPOON, P. A. See Bonoli, L., 2532
- WITKIN, J., AND WOLFGANG, R. Reaction of Recoil Tritium with Methylsilanes..... 2631
- WITTSTUCK, T. A., AND CRONAN, J. F. Nuclear Magnetic Resonance Studies of the Competition between

- Inter- and Intramolecular Hydrogen Bonding. I. Determination of Equilibrium Constants. . . . . 4243
- WOESSNER, D. E., AND SNOWDEN, B. S., JR. The Effect of Impurities on the Spin-Lattice Relaxation of Ammonium Chloride. . . . . 1139
- WOLF, A. P. See Ache, H. J., 1988
- WOLF, C. J., AND WALKER, J. Q. Radiolysis of Liquid and Solid Dimethylmercury. . . . . 3457
- WOLFGANG, R. See Menzinger, M., 1789; Witkin, J., 2631
- WON, C. M. See Willi, A. F., 3142
- WONG, P. K., AND WILLARD, J. E. Evidence for Electron Migration during  $\gamma$  Irradiation of Silica Gel: Reactions of Adsorbed Electron Scavengers. . . . . 2623
- WOOD, J. L. See Haque, I., 2438
- WOOD, M. See Hindman, J. C., 4188
- WOOD, R. H., AND DELANEY, D. E. The Solubility of Helium, Nitrogen, Argon, and Ethane in N-Methylacetamide, a High Dielectric Solvent without Anomalous Structural Effects. . . . . 4651
- WOOD, R. H. See Wen, W.-Y., 3048
- WOODHOUSE, R. L. See Speros, D. M., 2846
- WOODY, A. Y. See Kunimitsu, D. K., 856
- WOOLSEY, G. B. See Bonner, O. D., 899
- WORSLEY, I. G. See Hill, J. O., 3695
- WU, E.-C., AND RICE, O. K. The Photolysis of Perfluoroazomethane. . . . . 542
- WU, S. Estimation of the Critical Surface Tension for Polymers from Molecular Constitution by a Modified Hildebrand-Scott Equation. . . . . 3332
- WU, Y. C. Viscosity of Mixtures of Electrolyte Solutions. 2663
- WU, Y. C., RUSH, R. M., AND SCATCHARD, G. Osmotic and Activity Coefficients for Binary Mixtures of Sodium Chloride, Sodium Sulfate, Magnesium Sulfate, and Magnesium Chloride in Water at 25°. I. Isopiestic Measurements on the Four Systems with Common Ions. 4048
- WUNDERLICH, B. See Hamada, F., 178
- YAFUSO, M. See Green, M. E., 4072
- YAMADA, Y. See Noda, I., 2890
- YAMAMOTO, N. See Tsubomura, H., 367
- YAMAMOTO, O., AND HAYAMIZU, K. Proton Magnetic Resonance Studies of Mixed Aluminum Alkyls. I. Aluminum Trialkyls. . . . . 822
- YANAGIDA, T., TERAMOTO, A., AND FUJITA, H. Studies of Concentrated Polymer Solutions by the Fluorescence Polarization Method. II. Polyacrylamide in Water. 1265
- YANKWICH, P. E. See Huang, T. T.-S., 4431
- YANNOPOULOS, L. N. The Thermodynamics of the Vanadium Pentoxide (Solid or Liquid)-Water Vapor System. 3293
- YAO, S. J., AND ZWOLINSKI, B. J. Quantum Theoretical Treatment of Equilibrium Chemical Rate Processes. . . . 373
- YAO, S. J., AND ZWOLINSKI, B. J. Reply to "Comment on 'Quantum Theoretical Treatment of Equilibrium Chemical Rate Processes'" . . . . . 1845
- YEH, H. See Caron, A. P., 556
- YEH, H. J. C., AND RAGLE, J. L. Nuclear Magnetic Resonance Dynamic Determination of Boron-Fluorine Internuclear Distances in Alkali Metal Fluoroborates. . 3688
- YEVITZ, M. M. See Baccanari, D. P., 2243
- YORKE, M. E. See Caron, A. P., 556
- YOSHINAGA, K. See Tsubomura, H., 367
- YOSHIOKA, H. See Ikeda, T., 4392
- YOSIM, S. J. See Grantham, L. F., 762
- YOUNG, R. P. See Horne, R. A., 376, 866, 1763, 2694
- YUASA, M., KOBATAKE, Y., AND FUJITA, H. Studies of Membrane Phenomena. VII. Effective Charge Densities of Membrane. . . . . 2871
- YUASA, M. See Kobatake, Y., 1752
- ZAHORIAN, E. See Dubrow, R., 2489
- ZAHRADNIK, R. See Fabian, J., 3975
- ZANDLER, M. E., WATSON, J. A., JR., AND EYRING, H. Application of Significant Structure Theory to the Correlation of Thermodynamic Properties of CO<sub>2</sub>, COS, and CS<sub>2</sub> in Terms of the Respective Molecular Parameters. . . . . 2730
- ZECCHINA, A., VERSINO, C., APPIANO, A., AND OCCHIENA, G. Infrared Study of Benzene Adsorption on Aerosil. . 1471
- ZELTMANN, A. H., MATWIYOFF, N. A., AND MORGAN, L. O. Nuclear Magnetic Resonance of Oxygen-17 and Chlorine-35 in Aqueous Hydrochloric Acid Solutions of Cobalt(II). I. Line Shifts and Relative Abundances of Solution Species. . . . . 121
- ZEVOS, N. The Radiolysis of Aqueous Solutions of Cobalt Complexes. . . . . 1506
- ZIMBRICK, J., HOECKER, F., AND KEVAN, L. Spatial Distribution of Trapped Radicals in  $\gamma$ -Irradiated Ethylene Glycol Dimethacrylate Polymers. . . . . 3277
- ZMBOV, K. F., AND MARGRAVE, J. L. Mass Spectrometric Studies at High Temperatures. XXII. The Stabilities of Tantalum Pentafluoride and Tantalum Oxytrifluoride 1099
- ZSAKÓ, J. Kinetic Analysis of Thermogravimetric Data. 2406
- ZUEHLKE, R. W., SKIBBA, M., AND GOTTLIEB, C. Sorption and Magnetic Susceptibility Studies on Metal-Free-Radical Systems: Nitric Oxide on Palladium. . . . . 1425
- ZUIDERWEG, L. H. See Leyte, J. C., 1127
- ZWEIG, A., AND MARICLE, D. L. On the Mechanism of Preannihilative Electrochemiluminescence. . . . . 377
- ZWOLINSKI, B. J. See Yao, S. J., 373, 1845

# SUBJECT INDEX to Volume 72, 1968

- Absorption, I<sub>2</sub> by perylene, 2986  
 Acetaldehyde, photosens. decompn., 3052  
 Acetal and haloacetals, sp<sup>3</sup> geminal coupling, 2954  
 Acetamide, radiochem., 2181  
 Acetate radical, electron affinity, 2671  
 Acetone, photochem., 2337  
 Acetonitrile, autoprotolysis, 2270  
 Acetylene, photolysis, 4360; polymerization, 158; rx. w/ I<sub>2</sub>, 3204  
 N-Acetylglucine, N-methylamide and N-methylacetamide, H<sup>+</sup> exch. kinetics, 1001  
 Acetyl sulfide, conformation and dipole moment, 2276  
 Acrylonitrile-styrene copolymers, in DMF, limiting viscosity no., 4104  
 Activation energies, solid-state kinetic processes, 746  
 Adenine nucleosides, optical activity, 1483  
 Adhesion, liq.-solid, In(1)-Al, 1092  
 Adhesive and cohesive energies, calcd., 3700  
 Adsorption, see also absorption, chemisorption, and sorption; alkanes on Teflon, 2898; benzene on Aerosil, 1471; benzene by porous glass, 3201; from binary soln., 1555; CCl<sub>4</sub> on graphite, 1955; CO<sub>2</sub> and CO on  $\gamma$ -alumina and silica-alumina, 2917; CO on Pt electrodes, 1305; 1,1-diphenyl-2-picrylhydrazyl on solid acid catalysts, 46; DNA at H<sub>2</sub>O-air interface, 2863; gases on silica, 4676; H<sub>2</sub> on Au-Pd, 136; H<sub>2</sub> on Cu-Ni, 2775; high-press. isotherms, 2695; H<sub>2</sub>O on lyophilized hemoglobin, 3098; H<sub>2</sub>O on ThO<sub>2</sub>, 2095, 2293; hydrocarbons on alkylammonium montmorillonites, 4295; ion, new method for studying, 4325; NO on NaY and decationated Y zeolites, 4163; nonionic organics on Al<sub>2</sub>O<sub>3</sub> and SiO<sub>2</sub>, 489; NO on ZnO and ZnS, 2141; organics on Cr, 4172; organic vapors on silica gel, 3475; O<sub>2</sub> on Spheron-6, 1171; oxidative, CH<sub>4</sub> on Pt, 2856; phys., McLachlan's theory and, 3697; polyelectrolyte, Gibbs eq., 1834, 1835; poly(ethylene oxide) at aq.-air interface, 4459; poly(vinyl alcohol) and poly(vinyl pyrrolidone) at aq.-air interface, 4450; pyridine on faujasites, 1042; pyridine on mordenite, 4691; sodium alkyl sulfates at air-water interface, 2218; sodium alkyl sulfates at oil-water interface, 2222; from soln., kinetics, 2755; universal N<sub>2</sub> isotherm., 3673; Xe on silicate minerals, 2127  
 Aerosil, benzene ads., 1471  
 Aerosol particle motion, photodiffusiophoresis, 747  
 Alcohols, on alumina, photolysis, 2851; hydrogen-bonded dimers, 1837, 1839; rxs. w/ O<sup>-</sup>, 52  
 Alkali metal fluoroborates, B-F bond lengths, 3688  
 Alkali metal halides, aq., conductance, 4123; in N,N-dimethylformamide, thermo. data, 2966; ionization and disocn., 3041; molten, Mo-Mo(III) electrode in, 1442  
 Alkali metal halide salt pairs, aq., thermo. data, 2759  
 Alkali metal halide vapors, mixed, association, 4620  
 Alkali metal-NH<sub>3</sub>, internal refl. spec., 169  
 Alkali metals, in fused alk. met. salts, visible spectra, 1111; visible-ir spec. in hexamethylphosphoramide, 2655  
 Alkaline perchlorates, in CH<sub>3</sub>OH-CH<sub>3</sub>CN, 2245  
 Alkali perchlorates, solid, therm. decomp., 2189  
 Alkali perhenates and perchlorates, free energy of trans. between H<sub>2</sub>O and CH<sub>3</sub>NO<sub>2</sub>, 4549  
 Alkanes, cyclic, mass spectral fragmentation, 5  
 n-Alkanes, surface tensions, 1407  
 n-Alkanes-H<sub>2</sub>O, interfacial tensions, 1407  
 n-Alkylammonium halides, polymorphism, 4082; thermo. data, 4082  
 Alkylammonium salts, in benzene, vapor press. and light scattering, 3437  
 Alkyl halides, dehalogenation, 2287  
 1-Alkylpyrazoles, dipole moments, 1005  
 9-Alkylxanthyl radicals, torsional osc. of alkyl gps., 3647  
 Alumina, ads. of nonionic organics, 489  
 $\gamma$ -Alumina and silica-alumina, F<sup>-</sup> effect on "acid" sites, 2917  
 Aluminosilicates, Al-deficient faujasites, 2594; zeolite X and B form., 1385  
 Aluminum alkyls, <sup>27</sup>Al nmr quadrupolar relaxation, 4182  
 Aluminum bromide, critical data, 1664; thermo. data, 1664, 1669  
 Aluminum fluoride, thermo. data, 475  
 Aluminum halides, mixed, thermo. data, 3444  
 Aluminum(III) halides, in N,N-dimethylformamide, 3063  
 Aluminum ion, hydrolysis kinetics, 301  
 Aluminum oxide, electronic properties, 1682  
 Aluminum trialkyls, nmr study, 822  
 Aluminum vapor, rxs. w/ S<sub>2</sub>(g), Se<sub>2</sub>(g), Te<sub>2</sub>(g), 1660  
 Amide and peptide functions, radiation-induced redn., 4721  
 Amides, aq., soln. properties, 2710  
 Amine-amine hydrochloride, base strengths in toluene, 1630  
 Amines, aliphatic sec., hydrogen bonding, 3111; radiolysis, 1464  
 Amino acids, rxs. w/ H atoms in aq. solns., 3394  
 Amino acid tautomeric equil. solv. effect, 2351  
 Aminobenzophenones, photoreduction in nonpolar media, 3782  
 Aminopyridines, fluorescence study, 1982  
 Ammonia, pulse radiolysis, 1592; syn. on Fe, 458  
 Ammonia boron trifluoride and NH<sub>4</sub>BF<sub>4</sub>, powder patterns and lattice constants, 556  
 Ammonia-H<sub>2</sub>O, proton exchange, 550  
 Ammonia-propane, photolysis, 3914  
 Ammonium chloride, by rhythmic precipitation, particle size dist., 4320; spin-lattice relaxn., 1139; and sym. tetraalkylammonium chlorides, molal volumes, 1758  
 Ammonium perchlorate, sublimation kinetics, 202  
 Amylose-I<sub>2</sub>-I<sup>-</sup> complex, one-dimensional lattice cooperative binding, 4563  
 Analytic potential models, and noble gas properties, 632  
 Anharmonic oscillators, dynamics, 2489  
 Aniline, oxidn. by Cu(II) acetate, 481  
 Anilines, para-subst., nmr, 1217  
 Aniline solutions, adiabatic compressibilities, 261  
 Anion-exchange resins, binding of cholate and glycocholate anions, 1204; dist. coeffs. of anions, 3424  
 Anion exchangers, Cu(I)-CN<sup>-</sup> complexes in, 2605  
 Anthranilic acid, aq., decarboxylation, 3142  
 Aqueous media, solute-solvent interactions, 2512  
 Argon, redn. eq. of state, 1230  
 Argon-H<sub>2</sub>O-ethylene glycol, thermo. data, 2998  
 Argon and methane, corresponding states, 3559  
 Argon-NaNO<sub>3</sub>(l), thermo. data, 603  
 Aromatic-alicyclic sys., excess thermo. props., 1345  
 Aromatic and heterocyclic cpds., cond.-ring, ionization energies, 3452  
 Aromatic hydrocarbons, autooxidation, 3468; electron affinities, 3677; fluorescence yields, 3251; laser-induced degradation, 2417; proton-donor effect on electrochem. redn., 3616; solns. and assoc. interaction w/ tetrachloroterephthalate esters, 4020  
 Arsenic, thermo. data, 1102, 4327  
 Asymmetry-potential effect, across gradient permselective membranes, 2591  
 Azoethane, therm. decomp., 1857  
 Azulenoid sys., protonated, fluorescence, 4577  
 Barium azide, aq., photodecomp., 774; explosion, 778  
 Barium-barium halide systems, miscibility, 1892  
 Barium methacrylate dihydrate, esr, 1577  
 Barium tri- and tetra-titanate, dielectric prop., 1117  
 Benzene, luminescence quenching by CCl<sub>4</sub>, 3725; radiolysis, 1027; solns. of polar molecules, 1819  
 Benzene-biacetyl solutions, pulse radiolysis, 3871  
 Benzene-cyclohexane solution, surface free energy, 1555  
 Benzene-N<sub>2</sub>O, radiolysis, 3013  
 Benzenes, monosubst., CNDO SCF calc., 716; subst., nmr, 2552  
 Benzene-xylenes, thermo. data, 1939  
 Benzophenone, crystal structure, 4311  
 Benzyl chloride, solvolysis in glycerol-H<sub>2</sub>O, 4145  
 Beryllium halides, ir spectra, 250  
 Bifluoride ion, in LiF-HX films, 2456  
 Binary mixtures, critical and pseudocritical press., 2280; surface tension, 3073  
 Biphenyl, model sym. coords., 1451  
 Bis(fluoroxy)perfluoromethane, thermo. data, 3512  
 Bismuth-bismuth halide solutions, viscosity, 1737  
 Bismuth chloride, molar conductance, 762  
 Bismuth trihalides, phase diagrams to 36 kbars, 1327  
 Bispyridinium pentabromobismuthate(III), crystal structure, 532  
 (1) Index prepared by Dr. Jack Opdyke, University of San Diego, College for Men, San Diego, Calif.

- Bolaform electrolytes, osmotic and activity coeffs., 4290  
 Bond energies, N-H bonds, 1399  
 Bonding, Cu(II) complexes, 1244  
 Bond lengths, B-F, alkali metal fluoroborates, 3688  
 Boron, rxs. w/ Cl and Cl<sub>2</sub>, 4159  
 Boron hydrides, mass spectra, 2682  
 Bovine mercaptalbumin, aq., net valence charge, 2958  
 Bovine serum albumin, dielectric behavior, 4373  
 Brillouin spectra, dilute solns., 4644  
 Bromine, in H<sub>2</sub>O and CCl<sub>4</sub>, thermo. data, 3695  
 Bromine trifluoride(g), rx. w/ UF<sub>4</sub>, 1491  
*p*-Bromophenacyl hirsutate, efficient radioisomerization, 3772  
 1,3-Butadiene, photolysis, 4037  
*t*-Butyl hydroperoxide, pyrolysis, 1182  
*t*-Butyl hypohalites, thermo. data, 2260
- Cadmium-CdCl<sub>2</sub> liquid system, thermo. data, 441  
 Cadmium chloride-alkali chloride system, liq. surface tensions, 353  
 Calcium carbonate, decomp., 2846  
 Calcium nitride, thermo. data, 2434  
 Calcium phosphate, aq., complex formation, 208  
 Cannizzaro reaction, effect of micelles, 3686  
 Carbon, dispersed on alumina, 3186; divalent, cryochemical studies, 738; pyrolyzed Spheron-6 surface, 1171  
 Carbon-11, recoil, rx. w/ N<sub>2</sub>-O<sub>2</sub> sys., 1988  
 Carbon disulfide-Ar, shock-heated, light emission, 4344  
 Carbon monoxide, explosive combustion, 3O<sub>2</sub> inhibition, 3678; (a<sup>3</sup>π), Hg(<sup>1</sup>P<sub>1</sub>) photosens. prod., 3741; on Pt, 21-μ ir ads., 327; oxid. on Pd, 3621; oxid. on Pt electrodes, 1305; oxid. over V<sub>2</sub>O<sub>5</sub>, 3133; rx. w/ methylene, 2236  
 Carbon suboxide-H<sub>2</sub>, photolysis, 3105  
 Carbon tetrafluoride, thermo. data, 222  
 Carbonium ion pairs, thermo. data, 2233  
 Catalysis, metal ion, 622  
 Catalysts, supported gold, spectroscopic study, 3563  
 Cation exchange, thermo. data, 2789  
 Cation-exchange membranes, electroosmosis, 1253  
 Cation mobility, ligand assn. effect, 144  
 Cell potentials, w/ liq. junction, 4660  
 Ceria-terbia system, tensiometric study, 2030  
 Cerium(III), radiation ind. oxid. in aq. H<sub>2</sub>SO<sub>4</sub>, 3704  
 CF<sub>2</sub> radical, electronic oscillator strength, 4594  
 Charge density, effect. membrane, 2871  
 Chemiluminescence, electrogenerated, 4348; electron-trans. rxs., 2254; I\*, 3715; in gases, 3711, 3721  
 Chemiluminescent reactions, aq. fluorescein dyes, 756  
 Chemisorption, isobutane on faujasites, 3345; H<sub>2</sub>O, H<sub>2</sub>, O<sub>2</sub> on Al<sub>2</sub>O<sub>3</sub>, 1682; H<sub>2</sub>O on sepiolite, 1072  
 Chlorides, aq. divalent, molal expansibilities, 4589  
 Chlorine atoms, point of attack on C<sub>2</sub>HCl<sub>3</sub>, 3926; energetic, subst. for H ats. in butyl chlorides, 3049  
 Chlorine dioxide, explosive decomp., 1849  
 Chloroform, dielectric relaxation, 3676; hydrogen donor to organosphosphorus cpds. and tertiary alkylamines, 1297  
 Chloromethylphosphine, nmr, 2666  
 Chlorophyll, spectroscopic study at 77°K, 3941  
 Chlorophyll-quinone interactions, solid state, H<sub>2</sub>O effect, 4345  
 Cholate and glycocholate anions, on Dowex 1 resins, 1204  
 Cholesteryl myristate, glpc study, 3489  
 Chromatography, statistical theory for exclusion, 4397  
 α-Chromia-alumina solid solns., esr, 2562  
 Chromium(II)-(III), aq., radiolysis, 2330  
 Chromium(III) complexes, triplet state quenching, 3017  
 Chromophores, aromatic, solv. effect on uv spectra, 2934  
 Chromyl chloride, flash-photolysis, 3929  
 Chronopotentiometry, double-layer charging, 1650  
 Circular dichroism, methylpyrrolidone, 3035  
 Cobalt(III), oxid. of ClO<sub>2</sub>, 2642  
 Cobalt complexes, aq., radiolysis, 1506; photochemistry, 400  
 Cobalt oxide, oxid. catalysis, 2609  
 Cohesive and adhesive energies, calc., 3700  
 Cohesive energies, liquids, 4688  
 Complexes, amines w/ organosphosphorus comps., 2908; chg. trans., I<sub>2</sub> ↔ I<sub>4</sub>, 966; trigonal bipyramidal, crystal field-spin orbit treatment, 3588  
 Complex ion formation, between Mn<sup>2+</sup> and F<sup>-</sup>, Cl<sup>-</sup>, Br<sup>-</sup>, I<sup>-</sup>, SO<sub>4</sub><sup>2-</sup>, esr study, 4115  
 Complex ions, red. potentials, 1355  
 Condensation, H<sub>2</sub>O, 433  
 Conductance, AgClO<sub>4</sub> in sulfolane, 2124; aq. bovine mercaptalbumin, 2958; aq. HBr, 1545; aq. KCl-hexamethylenetetramine, 2588; aq. NaBr to 4000 bars, 2100; aq. NaCl 0 to 800°, to 4000 bars, 684; aq. soln., electronic, 362; aq. tetraalkylammonium halides to 4000 kg/cm<sup>2</sup>, 1763; 1:1 electrolytes in HCO<sub>2</sub>H, 4031; ion-exch. membranes, 4314; KCl-H<sub>2</sub>O-alcohol, 866; liq. and vap. BiCl<sub>3</sub> and HgCl<sub>2</sub>, 762; NaCl and KCl in H<sub>2</sub>O, 4123; Na in NH<sub>3</sub>(l), 4224; NH<sub>4</sub>-H<sub>2</sub>O solns. to 4000 bars and 700°, 3122; silica gel w/ ads. H<sub>2</sub>O, 3662; tetraalkylammonium salts in ethanol and propanol, 3281; tetraethylammonium perchlorate in valeronitrile, 1960; TiNO<sub>2</sub> in dioxane-H<sub>2</sub>O, 4710; trialkylsulfonium iodides in H<sub>2</sub>O, CH<sub>3</sub>OH, and CH<sub>3</sub>CN, 1037  
 Conductivity, therm. binary liq. sons., 4308; therm. critical-point behavior, 4316; therm., H<sub>2</sub>-He mixs., 1924  
 Conformational properties, opt. act. poly-α-olefins in sol., 2400  
 Contact angles, naphthalene-H<sub>2</sub>O-air sys., 646  
 Continuum emission, xenon vapor, 3129  
 Convective diffusion, capillary, 155  
 Copper, tetrahedral, esr, 2669  
 Copper(II)-CaO, esr at 1.2°K, 1392  
 Copper(II) mixed ligand chelates, elect. ads. spectra, 3372  
 Copper(II)-poly(methacrylic acid), aq., spectro. study, 1127  
 Copper complexes, bonding, 1244  
 Copper on MgO, H<sub>2</sub> activation at 79°K, 4587  
 Copper sulfate and Cu(en)<sub>2</sub>S<sub>2</sub>O<sub>3</sub>, aq., association, 3986  
 Coulometric titration, wustite, 485  
 Critical regions, liquid-liquid, heat capacity meas. through, 4079  
 Critical temperature, by dta, 4312  
 Cryoscopic behavior, sulfolane, 1068  
 Crystal-field energy levels, 1822  
 Crystal-field interactions, NO on NaY and decationated Y zeolites, 4163  
 Crystal structure, benzophenone, 4311; bispiperidinium pentabromobismuthate(III), 532; ((CH<sub>2</sub>)<sub>2</sub>NH<sub>2</sub>)<sub>3</sub>BiBr<sub>6</sub>, 3117; 1,8-diazacyclotetradecane-2,7-dione, 2838; dihalobenzocyclobutenes, 668; dipotassium tetranitroethide, 266; NH<sub>3</sub>BF<sub>3</sub> and NH<sub>4</sub>BF<sub>4</sub>, 556; racemic α,α'-dimethylglutaric acid, 3997; 1,2,3,4-tetrabromo-1,2,3,4-diphthaloylcyclobutane, 2120; tetraethylammonium tetrakis(dibenzoylmethido)europate(III), 970; triphenylphosphine sulfide-iodine complex, 1561; zeolite nickel faujasite, 4366  
 Current-time curves, potentiostatic, theoretical, 3535  
 Cyanine dyes, isomeric, nmr and electronic spectra, 2008  
 Cycloalkanes, isomerization over silica-alumina, 4555  
 Cyclobutane, Hg(<sup>1</sup>P<sub>1</sub>)-photosens. decomp., 1432  
 Cyclobutanone, photolysis, 1621  
 Cyclohexadienyl radicals, in aq. benzoic acid, 2946; substituent effects, 3832  
 Cyclohexane, photolysis, 3904; photonitrosation, 371; photonitrosation quantum yield, 4700; rx. w/ D<sub>2</sub><sup>+</sup>, 1071; scintillator luminescence in, 1783; pulse radiolysis, 3856  
 Cyclohexane-benzene and -N<sub>2</sub>O, photolysis, 4684  
 Cyclohexane-deuterated olefins, radiolysis, 1780  
 Cyclohexylamine, hydration in benzene, 1748  
 Cyclooctatetraenyl radical anion, electronic spectrum, 2813  
 Cyclopropane, isomerization, 1689; radiolysis in *n*-hexane and cyclohexane, 228  
 Cysteine, aq., radiolysis, 185, 2395
- Decomposition, therm., dimethyl azodiformate, 2677  
 Degassing apparatus, liquids, 4693  
 Density, anhydrous proteins and L-amino acids, 1887  
 Detonation, cyclooctamethylenetetranitramine, 2,4,6-trinitrotoluene, nitromethane, and bis(2,2-dinitro-2-fluoroethyl)formal, 2390  
 Deuterated electron, rx. w/ e<sub>a</sub><sup>-</sup>, D, OD, and D<sub>2</sub>O, 577  
 Deuterium, self-exch. rx. in monodeuteriotoluene, 1976  
 Deuterium atms, rx. w/ ethylene, 3261  
 Deuterium oxide, ionization thermodynamics, 4654  
 1,8-Diazacyclotetradecane-2,7-dione, crystal structure, 2838  
*cis*-Diazidotetraamminecobalt(III) azide, therm. decomposition, 703  
 N,N-Dialkylamides, aq., dielectric consts., 365  
 Dialkylphosphonates, hydrolysis and isotopic O exch., 1809  
 Diborane, photolysis, 3367; rxs. w/ methylphosphines and trimethylamine, 3340  
 Di-*t*-butylcarbinol, spin-spin coupling, 4346  
 Dicarboxylic acids, in aq. tetra-*n*-butylammonium bromide, 1132  
*p*-Dichlorobenzene, crystal structure effect on radiosensitivity, 4707  
 Dichlorocarbene, IP and heat of form., 1552  
*sec*-2,3-Dichloroperfluorobutyl rad., unimol. decomp., 3400  
*sec*-1,4-Dichloroperfluorobutyl rad., unimol. decomp., 3407  
 Dichromate, aq., rx. w/ silica gel, 104  
 Dielectric constants, H<sub>2</sub>O-in-oil emulsions, 33; liq., press. and dens. dependence, 1057; N,N-dialkylamides-H<sub>2</sub>O, 365  
 Dielectric dispersion data, analysis, 1656  
 Dielectric properties, BaTi<sub>3</sub>O<sub>7</sub>, BaTi<sub>4</sub>O<sub>9</sub>, 1117; bovine serum

- albumin, 4373; ice and water clathrates, 49; lyophilized hemoglobin, 3098  
 Dielectric relaxation, chloroform, 3676; data representation, 1462; hydroxy- and methoxybenzaldehydes, 1013  
 3,3-Diethylpentane, ultrasonic relax., 2268  
 Differential thermal analysis, critical temp. determination by, 4312; quantitative, solid-gas rx., 2846; rx. kinetics, 906  
 Diffusion, aromatic and cycloparaffin hydrocarbons in H<sub>2</sub>O, 2532; convective, capillary, 155; convective, porous diaphragm, 4168; critical-point behavior, 4316; gases in non-polar liqs., 4699; hexamethylenetetramine in H<sub>2</sub>O, 149; H<sub>2</sub> in irradiated quartz, 2277; isothermal, multicomponent complex dark sys., 1713; isothermal, multicomponent simple dark sys., 1707; isothermal, multicomponent systems, 11; isothermal, neutral binary sys., 1831; self-, Na<sup>+</sup> in ethylene glycol-H<sub>2</sub>O, 1201; transient convective, in capillaries, 3286  
 Diffusion double layer, ionic composition in mixed electrolytes, 727  
 Diffusion potential, decay in ideal electrolyte sols., 272  
 Difluoramino radicals, rx. w/ F<sub>2</sub>, 108  
 1,3-Difluoro- and 1,1,3,3-tetrafluoroacetone, photolysis, 1603  
 Difluoromethylene, elimination from 1,1,2,2-tetrafluorocyclopropane, 2234  
 1,2-Difluorotetrachloroethane, internal rotation, 4299  
 Dihalobenzocyclobutenes, crystal and mol. structure, 668  
 Dimer formation, effect on triplet states of organic dyes, 4718  
 1,1'-Dimethoxyazobenzene, photoisomerization, 153  
*o*-Dimethoxybenzene, dipole moment *vs.* T, 1405  
*p,p'*-Dimethoxybenzophenone, photoreduction, 3522  
 N,N-Dimethylamides and -thioamides, nmr, 2469  
 Dimethyl azodiformate, therm. decomp., 2677  
 9,10-Dimethyl-1,2-benzanthracene, autoperoxidation in polymer films, 3794  
*cis*- and *trans*-1,2-Dimethylcyclohexane, radiolysis, 4509  
 $\alpha,\alpha'$ -Dimethylglutaric acid, racemic, crystal structure, 3997  
 Dimethylmercury, radiolysis, 3457  
 N,N-Dimethyl-*p*-nitroaniline, anion and cation radical, 740  
*trans*-2,5-Dimethylpiperazine and hydrochlorides, nmr, 2344  
 Dimethylsilicon and dimethylgermanium moieties, exchange of substituents between, 4380  
 Dimethyl sulfoxide, liq. assn., 3358  
 2',4'-Dinitro-2-aminodiphenyl ether, rearrangement in CH<sub>3</sub>OH-CCl<sub>4</sub>, 1300  
 Dioxane, pulse radiolysis, 3849  
 1,4-Dioxane,  $\gamma$ -radiolysis, 2635  
 9,10-Diphenylanthracene, electrolytic oxid., 2322  
 N,N'-Diphenyl-*p*-phenylenediamine and -diimine, photolysis, 3774  
 1,1-Diphenyl-2-picrylhydrazyl, ads. on solid acid catalysts, 46  
 Dipole moments, 1-alkylpyrazoles, 1005; cyclohexylamine, cyclohexylamine-H<sub>2</sub>O, H<sub>2</sub>O, 1748; N,N-di-*n*-butyl- $\beta$ -amino-propionic acid in seven solvs., 2351; *o*-dimethoxybenzene, 1405; electric, acetyl sulfide, 2276; surface, organic films on Cr, 4172  
 Dipotassium tetranitroethide, crystal structure, 266  
 Disulfide ions, in  $\gamma$ -irradiated organic glasses, 2597  
 DNA, ads. at air-H<sub>2</sub>O interface, 2862  
 Dodecanoic acid, <sup>14</sup>C-labeled, vap. press., 2243  
 Double layer, diffuse, weak electrolytes, 841  
 Double-layer charging, chronopotentiometry, 1650  
 Drop, fluid draining film radius, 318  
 Dropping Hg electrode, diffusion eqn. for var. Hg flow, 1187; math. analysis, 1187; time depend. of Hg flow, 1193
- Electrical transport properties, anionic polyelectrolytes and polysoaps, 2507  
 Electric polarizations, molecules w/ anomalous dipole moments, 1517  
 Electrochemical measurements, simultaneous internal reflect. spec., 2576  
 Electrochemical reduction, aromatic hydrocarbons, proton donor effect, 3616  
 Electrode processes, coupled w/ heterogeneous chem. rxs., 3535; fast, kinetics, 2541  
 Electrodes, optically transparent, visible IRS, 1144  
 Electroluminescence, preannihilative, mech., 377, 378  
 Electrolyte-nonelectrolyte, aq., thermo. data, 3053  
 Electrolytes, antagonistic-cooperative interaction, 3424; aq., surface potentials, 74; diffusion in ideal solutions, 272; mixtures, aq., viscosities, 2663; weak, diffuse double layer, 841  
 Electron, aq., rxs. in alkaline soln., 880; hydrated, mobility, 2279  
 Electron affinities, acetate rad., 2671; aromatic hydrocarbons, 3677  
 Electronic conduction, aq. soln., 362  
 Electronic properties, perfluorocarbons, 3531  
 Electronically excited atoms, I\* production, 3715  
 Electron-impact spectrometry, low-energy, high-angle, 3894  
 Electron-transfer reactions, "band model," inner-sphere extension, 1792; kinetics, 891  
 Electroosmosis, current depend., 1253  
 Electroosorption, CH<sub>3</sub>OH, 1571  
 Endor, triphenylmethyl derivatives, 4276; triphenylmethyl and tris(*p*-tolyl)methyl rads., 4269  
 Energy transfer, thermal CH<sub>3</sub>NC isom., 1932  
 Eosin, aq., radiolysis, 3337  
 Equation of state, rubber elasticity, volume dependence, 345  
 Equilibria, isothermal, in electrolyte solns., 1536  
 Esr, aliphatic semidiones, 1386; aromatic nitrogen heterocycles, biphenyl, acenaphthene, 3215; barium methacrylate dihydrate, 1577; *t*-butyl peroxide ions, 723; carbon on alumina, 3186; carbonyl <sup>13</sup>C hyperfine splitting in free rads., 4715;  $\alpha$ -chromia-alumina solid solns., 2562; complex ion formation between Mn<sup>2+</sup> and F<sup>-</sup>, Cl<sup>-</sup>, Br<sup>-</sup>, I<sup>-</sup>, SO<sub>4</sub><sup>2-</sup>, 4115; Cu(II)-CaO at 1.2°K, 1392; N,N-dimethyl-*p*-nitroaniline anion and cation rad., 740; free-rad. intermeds. in rx. of OH rad. w/ amino acids, 1926; hexaquochromic ion, 1317; HO· and HO<sub>2</sub>· rads., 164; hydroperoxide on ZnO, 2460; intermediates in Fe<sup>2+</sup>-H<sub>2</sub>O<sub>2</sub>-Ti<sup>4+</sup> and Ce<sup>4+</sup>-H<sub>2</sub>O<sub>2</sub>-Ti<sup>4+</sup> sys., 2250; irradiated aq. nitroalkane solns., 3387; MnCl<sub>2</sub>-LiCl-KCl eutectic, 4701; naphthacene trianion and 5,12-naphthacene-quinone anion rads., 1829, 1380; nitroxides, solubilized long-chain, 4129; NO<sub>2</sub> in frozen solns., 1721; N<sub>2</sub>O-NO<sub>2</sub> sys., 2963; NO on ZnO and ZnS, 2141; perfluoro-2,1,3-benzoselenadiazole anion rad., 1281; perfluorocyclobutanone ketyl, 1832; polyphenyl anion rads., 2238; semidiones, 1074; tetrahedral cupric ion, 2669; tetrakis(*p*-methoxyphenyl)ethylene cation rad., 286; thianthrene cation rad., 1390; 2,4,5-triphenylimidazolyl rad., 4717; triphenylmethyl derivatives, 4276; trifluoromethylnitrobenzene anion rads., 68; xanthyl rads., 3635, 3641, 3647  
 Ethanol, radiolysis, 816  
 Ethanol-heptane system, chemical model, 4534  
 Etherate formation, organoaluminum cpds., 3567  
 Ethyl acetate-H<sub>2</sub>O, solute-solv. interactions, 364  
 Ethylene, electron-impacted, ion-mol. rxs., 3599; ionic rxs. in, 3080  
 Ethylenediamine-H<sub>2</sub>O, proton exchange, 550  
 Ethylene glycol dimethacrylate polymers,  $\gamma$ -irradiated trapped rad. dist., 3277  
 Ethylene-maleic anhydride copolymer, hydrolyzed, metal complexes, 2496  
 Ethylene-methacrylic acid copolymers, and their Na salts, film ir study, 1122  
 Ethyl esters, interaction w/ benzene, 2764; of phosphorus acids, nmr, 4043  
 Explosive behavior, barium azide, 778  
 Extraction, HClO<sub>4</sub> by 1-decanol, 3504; tetraheptylammonium fluoride, 2831
- Fast reactions, flash-photolysis, 3766  
 Faujasites, Al-deficient, 2594; isobutane chemisorption on, 3345  
 Ferrocyanide, quinone reduction, 358  
 Fluid mixtures, molecular size effect, 1897  
 Fluorescein, aq., pulse radiolysis, 2018; aq. dyes, chemiluminescent rxs., 756  
 Fluorescence, absence in 5-nitro-8-quinolinol, 3692; aminopyridines, 1982; aromatic cpds., 3251; band shift w/ excitation shift, 2742; chlorophyll at 77°K, 3941; lanthanide ions in organic solvs., 3516; 2-phenylnaphthalenes, 4468; protonated azulenoic systems, 4577; soln., quenching-transient and solv. effects, 1350; standard, quinine bisulfate *vs.* 9,10-diphenylanthracene, 793; tetraethylammonium tetrakis(dibenzoyl-methido)europate(III), 970  
 Fluorine, dissn., 108  
 Fluoroaldehydes, photolysis, 3351, 3352  
 Fluorobenzenes, monohalosubstituted, nmr, 991  
 Fluorocarbon gases, solubility in cyclohexane, 2248  
 Fluorosilanes, nmr study, 660  
 Formates and acetates, aq., Raman spectra, 2614  
 Formic acid, anhydrous, 1:1 electrolytes in, 4031  
 Fractionation factors, isotopic exchange, calcite-CO<sub>2</sub>-H<sub>2</sub>O, 800  
 Free ion, liq.-yield det., 3730  
 Friction constants, fused salts, 3001  
 Fuel-cell electrode, H-D exchange of propane, 2285
- Gallium(III), SCN<sup>-</sup> cat. polarographic red., 3684  
 Gallium bromide-ethyl bromide, bromine exch. rx., 3148  
 Gallium-In system, activities, 1047

- Gas bubbles, rate of dissolving, 3356, 3357, 3357  
 Gases, ads., surface transport, 2365  
 Germania, propionic and acetic acid sorption, 2378  
 Germanium fluoride, ir spectra, 4492  
 Gibbs equation, polyelectrolyte ads., 1834, 1835  
 Glass, porous, ionic membranes, 2195  
 Glass electrodes, in molten salts, 2877  
 Glasses, organic, temp. dependence of viscosity, 752  
 Glycine, diglycine, triglycine, ultrasonic ads., 2227  
 Glycine and alanine, trans. metal chelates, radiation chem., 922  
 Gold, surface stress to 985°, 4150; wettability, 2412  
 Gold catalysts, supported, spectroscopic study, 3563
- Halocarbons, pyrolysis and energetics, 738  
 Halogens, aq., uv spectra, 3671  
 Halomethanes, binary liq. mixs., thermol data, 1529  
 Harmonic oscillators, totality of states, 3034  
 Heat capacity measurements, through liq.-liq. critical regions, 4079  
 Heats of formation, prediction, 2422  
 Hemoglobin, lyophilized, H<sub>2</sub>O ads. and dielectric props., 3098  
 Heterocycle rings, sat., nmr study, 3244  
 Heterocycles, S-containing, semiempirical calcs., 3975  
 Heterogeneous activation, therm. unimol. rxs., 4483  
 Hexaamminecobalt(III) azide, therm. decomp., 4386  
 Hexaquochromic ion, outer-sphere coord. interactions, 1317  
 Hexaquo cobalt(II) ion, aq., nmr detection, 2659  
 Hexachlorobicyclo[2.2.1]heptenes, solv.-dep. H-H couplings, 198  
 Hexacyanochromium(III) ion, aq., photoaquation, 3827  
 Hexacyanoferrate(III)-N<sub>3</sub><sup>-</sup>, photochemistry, 410  
 Hexafluorobenzene, liq., ir spectrum, 2174  
 Hexafluorobicyclo[2.2.0]hexa-2,5-diene, therm. isom., 2882  
 Hexamethylbenzene-tetracyanoethylene complexes, methyl group rotation barriers, 3970  
 Hexamethylenetetramine, aq., differential diffusion coefficients, 149  
*n*-Hexane, pulse radiolysis, 3856  
 Hill equation, ads. on uniform surfaces, 1955  
 Homogeneous oscillating reactions, existence, 2692, 2693  
 Hydrated electron, *E<sub>s</sub>*'s for rxs., 766  
 Hydrazine, Mo(VI)-catalyzed oxidn. by methylene blue, 4573; oxidn. by Mo(VI), 4198  
 Hydrazine-1,1-N<sub>2</sub>H<sub>2</sub>(CH<sub>3</sub>)<sub>2</sub> and He(or N<sub>2</sub>)-N<sub>2</sub>H<sub>4</sub>-1,1-N<sub>2</sub>H<sub>2</sub>(CH<sub>3</sub>)<sub>2</sub> systems, equilibria, 2556  
 Hydrides, first-row atom, FSGO model of structure, 1289  
 Hydrocarbons, aromatic, phosphorescence lifetimes and glass relaxn., 2265; interatomic pot. functs., 2941; mixtures, interaction virial coefficients, 676  
*n*-Hydrocarbons, polycrystalline, trapped electrons, 4347  
 Hydrochloric acid, in aq. salt solns., 4408; trans. from H<sub>2</sub>O to aq. ethylene glycol, 3937; trans. from H<sub>2</sub>O to HAc, 1064  
 Hydrochloric acid-CdCl<sub>2</sub>, thermo. data, 257  
 Hydrogen, activation by Cu on MgO, 4587; ads. on Au-Pd, 136; ads. on Cu-Ni, 2775; chemisorbed, ir spectra, 369; electrolytic evolution rx. on Al, 1148  
 Hydrogen atoms, gas-phase transfer between elements 1-19, 236; rx. w/ aq. ferricyanide, 1599; rx. w/ Cl<sub>2</sub>O, 3031; rx. w/ solid olefins, 3689; rx. in H<sub>2</sub>SO<sub>4</sub> glasses, 2686; thermal, rx. w/ frozen organic substrates, 1949  
 Hydrogen bonding, in ads. on silica, 4676; alcohol dimers, 1837, 1839; glpc study, 3478; inter- and intramolecular, competition, 4243; singlet-state salicylic acids, 3297  
 Hydrogen bromide, aq., conductance 0 to 800°, to 4000 bars, 1545; uv spectrum, 3046  
 Hydrogen chloride and DCl, far-ir spectra, 2259  
 Hydrogen chloride-SF<sub>6</sub>, radiolysis, 765  
 Hydrogen cyanide, ads. on glass, rxs., 2371; <sup>15</sup>N nmr, 4310  
 Hydrogen-deuterium exch., fuel-cell electrode, 2285  
 Hydrogen electrode rx., kinetic isotope effects, 2431  
 Hydrogen fluoride, dissn. behind incident shock waves, 79  
 Hydrogen-fluorine, photochem., 3168  
 Hydrogen-He mixs., therm. conductivity, 1924  
 Hydrogen iodide, rx. w/ H atoms, 1639; uv spectrum, 3046  
 Hydrogen isotope exch., benzene, 1673  
 Hydrogen and nitrogen, active atoms, rxs. w/ CH<sub>3</sub>C<sub>2</sub>H and CH<sub>2</sub>-CCH<sub>2</sub>, 3323; active atoms, rxs. w/ (CN)<sub>2</sub>, HCN, C<sub>2</sub>H<sub>2</sub>, 3305; mixs., rxs. w/ alkenes and alkanes, 518  
 Hydrogen sesquioxide and perhydroxyl radical, decay kinetics, 3836  
 Hydrogen-water, hydrogen isotope equilibria, 4338  
 Hydrogen zeolite Y, rx. w/ NH<sub>3</sub>, 3071  
 Hydroperoxide on ZnO, esr study, 2460  
 Hydrophobic bond, term criticism, 1841, 1842  
 Hydrophobic bond formation, thermo. data, 856  
 Hydrophobic hydration, *n*-tetrabutylammonium halides, 2694, 2695
- Hydroxyaromatic anions, SCFMO calc., 914  
*m*- and *p*-Hydroxyazobenzene, photoisomerization, 3266  
 Hydroxy- and methoxybenzaldehydes, dielectric relaxation, 1013  
 Hydroxyl groups, decationated zeolites X and Y, 1768  
 Hydroxyl radical, rx. w/ amino acids, 1926  
 Hydroxyl radical-H<sub>2</sub>O<sub>2</sub>, photochemistry, 406  
*p*-Hydroxyphenylhydroxylamine, dehydration, 3006  
 Hydroxytropylium halide hydrates, thermo. and ir study, 2950  
 Hysteresis, H<sub>2</sub>O sorption-desorption, 1223
- Ice, dielectric properties, 49  
 Indium(1)-aluminum, liq.-solid adhesion, 1092  
 Indium and bismuth chlorides, Raman spectra, 3094  
 Interfacial tension, two-phase ternary liq. sys., 4139  
 Internal reflection spectra, alkali metal-NH<sub>3</sub>, 169; and simult. electrochem. meas., 2576  
 Internal-rotation barriers, solid  $\pi$  complexes of methylbenzenes, 3970  
 Intersystem crossing, singlet-triplet, 3354  
 Iodate, rx. w/ I<sup>-</sup>, 3630  
 Iodide, photosensitized rxs., 3768  
 Iodine, abs. by perylene, 2986; chg. trans. spec. in hydrocarbons, 3059; rx. w/  $\gamma$ -picoline, 2438; vap. phase I<sub>2</sub> formation, 966, 2697; visible ads. max. in many solvs., 3300  
 Iodine-amine complexes, flash photolysis, 3863  
 Iodine cyanide, rx. w/ O, 743  
 Iodine-tetramethylurea and -tetramethylthiourea, mol. complexes, 2129  
 Ion diffusion, into fused silica, 2256  
 Ion exchange, alk. earth ions by zeolites, 4086; in molten salts, 2885; Linde X zeolite, X-ray study, 4095; sodium zeolite A in molten salts, 4704; w/ two-phase glass, 2665  
 Ion-exchange equilibria, glass w/ molten salts, 4175  
 Ion-exchange membrane, liquid, model system test, 978; volume flow, 1566  
 Ionic membranes, phenylsulfonate gps. on porous glass, 2195; porous glass as, 599  
 Ionic reactions, acetylene, 158  
 Ionic solutions, charged square-well model, 3352  
 Ion mobility, organic and inorganic phosphorus cpds., 2867  
 Ion-molecule reactions, C<sub>3</sub>H<sub>6</sub><sup>+</sup>-C<sub>2</sub>H<sub>6</sub>, 1826; higher order, theo. basis, 3746; in propylene and isomeric butenes, 1994; in propyne and allene, 1905  
 Ion-pair association, solv. structure effect, 1396  
 Ion pairs, 2:2 and 3:3, form. consts., 3330  
 Ions, aq. neg., photolysis, 3815; aq., thermo. data, 2902  
 Ion-selective properties porous glass membranes, 2976  
 Ion-solvent-molecule interactions, gas phase, 742  
 Ion transport, membrane, 4072
- Ir spectra, ads. HCN, 2371; beryllium halides, 250; chemisorbed H<sub>2</sub> and D<sub>2</sub>, 369; CH<sub>4</sub>(l), 962; CO on Pt, 327; CO on Pt-SiO<sub>2</sub>, 2688, 2688; ethylene-methacrylic acid copolymers and their Na salts, 1122; GeF<sub>2</sub>, 4492; HCl and DCl, 2259; hexachloroiridium(IV) ion, 2207; intermediates in NH<sub>3</sub> syn. on Fe, 458; isotopically subst. 2-pyridones, 1177; kaolin mineral-dimethyl sulfoxide complexes, 241; lithium halides, far-ir, 3526; liq. hexafluorobenzene, 2174; metal  $\beta$ -ketoenolates, 4631; NbOCl<sub>3</sub>, NbOBr<sub>3</sub>, NbOI<sub>3</sub>, 4686; OH gps. and H<sub>2</sub>O on Y zeolites, 4211; oxalic acids, protio- and deuterio-, 4628; phthalocyanine, 3230; trihalomethyl lithium and sodium cpds. in Ar(s), 1743  
 Iron(III) monosulfato complex, formation, 1378  
 Iron(III)-Np(III), aq rx., 4333  
 Irreversible thermodynamics, first-order chem. rxs. in closed sys., 92; isothermal diffusion in multicomponent systems, 11, 1707, 1713  
 Isoalloxazine, MO calcs., 536  
 Isobutane, isopentane, 2,3-dimethylbutane, radiolysis, 3496  
 Isopropoxyl radical, decomp., 2824  
 Isopropyl methylphosphonofluoridate, hydrolysis, 622  
 Isopropyl radicals, gas-phase oxid., 3754  
 Isosbestic points, and no. of rx. parameters, 296  
 Isotope effect, H<sub>2</sub>O-D<sub>2</sub>O, alkali metal and tetraalkylammonium salt thermol data, 4317  
 Isotopic exchange, calcite-CO<sub>2</sub>-H<sub>2</sub>O, 800; *p*-nitrobenzyl chloride-<sup>38</sup>Cl<sup>-</sup>, 713
- Kaolin mineral-dimethyl sulfoxide complexes, ir spectra, 241  
 Kerr constants, H<sub>2</sub>O and D<sub>2</sub>O at 30°, 3069  
 Kerr effect, protein solns, 4058  
 Ketene, photolysis, 3952  
 Ketene-butene-mercury, photolysis, 3705  
 Ketones, triplet energy trans. to rare earth ions, 3702  
 Ketyls, possible nonplanarity, 4715  
 Kihara core model, polar molecules, 1821



- Kinetic data, see also photolysis and radiolysis; active N rx. w/ perfluorobutene-2, 1812; Al<sup>3+</sup> hydrolysis, 301; aq. Np(III)-Fe(III) rx., 4333; azoethane therm. decomp., 1857; B rx. w/ Cl and Cl<sub>2</sub>, 4159; benzyl chloride solvolysis in glycerol-H<sub>2</sub>O, 4145; B<sub>2</sub>H<sub>6</sub> rx. w/ methylphosphines and trimethylamine, 3340; BrF<sub>3</sub> rx. w/ UF<sub>4</sub>, 1491; *t*-butyl hydroperoxide pyrolysis, 1182; <sup>13</sup>C kinetic isotope effect in CH<sub>3</sub>NC isom., 3440; C<sub>2</sub>F<sub>4</sub>I exch. rx. w/ I<sub>2</sub>, 1811; CH<sub>3</sub> rxs. in aq. soln., 2703; CH<sub>4</sub>, term. decomp., 348; CH<sub>3</sub>NC isomerization, 1726; CH<sub>3</sub>NO<sub>2</sub> isomerization, 3581; ClO<sub>2</sub> explosive decomp., 1849; ClO<sub>2</sub> oxid. by Co(III), 2642; C(NO<sub>2</sub>)<sub>4</sub> rx. w/ NO<sub>2</sub><sup>-</sup> and OH<sup>-</sup>, 1402; Co oxid. on Pd, 3621; Co oxid. on V<sub>2</sub>O<sub>5</sub>, 3133; chemiluminescent electron-trans. rxs., 2254; chlorination of HgCl<sub>2</sub> in acetone, 2154; cobalt oxide in oxid. catalysis, 2609; colloidal AgBr growth, 2168; color dev. in Landolt "clock" rx., 1387; cumene desorption from SiO<sub>2</sub>-Al<sub>2</sub>O<sub>3</sub>, 356; cycloalkanes isom. over silica-alumina, 4555; cyclopropane isom., 1689; decarboxylation of aq. anthranilic acid, 3142; *sec*-1,4-dichloroperfluorobutyl rads., decomp., 3407; *sec*-2,3-dichloroperfluorobutyl rads., decomp., 3400; 2',4'-dinitro-2-aminodiphenyl ether rearrangement in CH<sub>3</sub>OH-CCl<sub>4</sub>, 1300; 9,10-diphenylanthracene, electro. oxid., 2322; dissn. of F<sub>2</sub>, 108; dissn. of HF behind incident shock waves, 79; H<sub>2</sub> evolution on Al, 1148; <sup>1</sup>H-<sup>2</sup>H exchange in benzene, 1673; H ats. in H<sub>2</sub>SO<sub>4</sub> glasses, 2686; 324 H at. transfers between elements 1-19, 236; H at. rxs. w/ solid olefins, 3689; H at. rx. w/ Cl<sub>2</sub>O, 3031; H at. rx. w/ aq. ferricyanide, 1599; gas-phase rxs. of CF<sub>3</sub> w/ methylchlorosilanes, 494; GaBr<sub>3</sub>-CH<sub>3</sub>CH<sub>2</sub>Br bromine exch., 3148; Fe(III) monosulfato complex form., 1378; fast electrode processes, 2541; F<sub>2</sub> rx. w/ NF<sub>2</sub>, 108; ether form. from deuterated methanols, 2770; electron-impacted ethylene ion-mol. rxs., 3599; e<sub>aq</sub><sup>-</sup> rx. w/ e<sub>aq</sub><sup>-</sup>, D, OD, and D<sub>2</sub>O, 577; e<sub>aq</sub><sup>-</sup> rxs. in alkaline soln., 880; H<sub>2</sub>O and *t*-butyl alcohol rxs. w/ Na in NH<sub>3</sub>(1), 4520; H<sub>2</sub>O<sub>2</sub> rxs. w/ titanous salts, 3154; hexaamminecobalt(III) azide decomp., 4386; hexafluorobicyclo(2.2.0)hexa-2,5-diene therm. isom., 2882; hydration of 2- and 4-pyridine-carboxaldehydes, 655; hydrazine oxid. by methylene blue, Mo(VI) catalyzed, 4573; hydrazine oxid. by Mo(VI), 4198; hydrogen sesquioxide rad. and perhydroxyl rad. decay, 3836; hydrolysis of isopropyl methylphosphonofluoridate, 622; *p*-hydroxyphenylhydroxylamine dehyd., 3006; iodate rx. w/ I<sup>-</sup>, 3630; ionic rxs. in ethylene, 3080; ion-mol. rxs. in propyne and allene, 1905; isomerization of HNO<sub>2</sub>, 269; isopropoxyl rad. decomp., 2824; isotopic O exch. on Pt, 1051; kinetic isotope effect, 2602; LiAlH<sub>4</sub> therm. decomp., 4009; Li(Hg)-Li<sup>+</sup> rx. in DMSO, 4568; LiN<sub>3</sub> therm. decomp., 2281; N-methylacetamide, N-acetylglycine N-methylamide H<sup>+</sup> exch., 1001; methylene rx. w/ CO, 2236; *cis-trans*-*o*-methylformanilide equilibrium, 2135; micelle effect on Cannizzaro rx., 3686; Mo-Mo(III) electrode in molten salts, 1442; N at. rx. w/ Cl<sub>2</sub>O, 3028; N at. rx. w/ CO<sub>2</sub>, 2235; N at. rxs. w/ olefins and acetylenes, 2538; NO<sub>2</sub> (aq.) disproportionation, 593; NO<sub>2</sub>(g) rx. w/ I<sup>-</sup> in molten alkali metal nitrates, 3545; NO<sub>2</sub><sup>-</sup> oxid. in NaNO<sub>2</sub>-LiClO<sub>4</sub>, 876; NO<sub>2</sub>ClO<sub>4</sub> therm. decomp., 4004, 4015; <sup>237</sup>Np(V)-Cr(III)-<sup>239</sup>Np(V) sys., 2675; nickel malonate and nickel succinate complex form., 2026; *p*-nitrobenzyl chloride-<sup>36</sup>Cl isotopic exchange, 713; O at. rx. w/ Cl<sub>2</sub>O, 3035; O at. rx. w/ S(s), S(l), Se(s), and Se(l), 84; O(<sup>3</sup>P) addn. to propene, butene, and propene-butene films, 616; OH rx. w/ HO<sub>2</sub>, O<sub>2</sub><sup>-</sup>, and H<sub>2</sub>O<sub>2</sub><sup>+</sup>, 626; oxalic acid-<sup>13</sup>C decomp., 4431; oxid. of Na, K, Cs in flames, 2483; oxygen rx. w/ hydrocarbons, 2628; perfluoropropene decomp., 3054; photoperoxidation of unsat. organics, 2582; phthalocyanine α → polymorphic conv., 3335; picric acid rx. w/ subst. hydrocarbons, solid state, 4446; polystyrene degradation by ultrasonics and by benzoyl peroxide, 4613; propylene pyrolysis, 4672; pyridinium salts in CH<sub>3</sub>OH, H<sup>+</sup> exch., 2515; pyridinium salts in H<sub>2</sub>O, H<sup>+</sup> exch., 2520; quinones, ferrocyanide redn., 358; rad. decay in organic glasses, 4604; rxs. of e<sub>aq</sub><sup>-</sup>, 766; rxs. of α-PbN<sub>6</sub>, 111; rxs. of siloxane w/ SiO<sub>2</sub>, 1248; reductions by Zn<sup>+</sup>, Cd<sup>+</sup>, Ni<sup>+</sup>, 784; S<sub>8</sub> ring-chain equilib., 1890; SCN<sup>-</sup> cat. red. of Ga(III), 3684; SF<sub>6</sub> rx. w/ e<sub>aq</sub><sup>-</sup>, 4285; siloxane rxs. w/ silica, 3993; slope of free energy plots, 4249; small ring cpd. rxs., 1866; SrCO<sub>3</sub> rx. w/ TiO<sub>2</sub>, 3326; styrene and methyl methacrylate polym., 2993; styrene polym. in an electric field, 4543; tetrafluoroethylene pyrolysis, 3462; therm. decomp. of *cis*-diazidotetraamminecobalt(III) azide, 703; therm. decomp. of polynitroalkanes, 1513; therm. decomp. of solid alkali perchlorates, 2189; therm. dissn. of OF<sub>2</sub>, 2307, 2311; therm. H at. rx. w/ frozen organic substrates, 1949; thiourea and thioacetamide oxid. by alk. hexacyanoferrate(III), 1497; trifluoromethyl rad. rx. w/ H<sub>2</sub>S, 4239; urethane rx., 845; vinyl ether hydrolysis, 1313
- Kinetic isotope effect, malonic acid decarbox., 2602; <sup>13</sup>C, anomalous temp. dependence and crossover, 4431; H<sub>2</sub> electrode rx., 2431
- Kinetic processes, solid-state, E<sub>n</sub>'s, 746
- Kinetics, ads. from soln., 2755; biradical mech. in small ring cpd. rxs., 1866; disocn. rxs., 1009; dta peak and max. rx. rate, 906; ECE mech., 1082; electron trans. rxs., 1792; equil. chem. rate processes, 373; fast rxs. w/ no act. energy, 375; hetero. activation in therm. unimol. rxs., 4483; nonequil. thermo. of first-order rxs. in closed sys., 92; oxygen rx. w/ hydrocarbons, 2628; rxs. w/ resonance splitting, 891; solid-state therm. decomp., 2185; soln., fluorescence quenching—transient and solv. effects, 1350; styrene polymerization, 216; thermogravimetric analysis, 2406; unimol. rx. sys., 4483, 4488
- Knudsen cells, calibration by Hg effusion, 4323
- Landau-Placzek formula, Brillouin spectra of dil. solns., 4644
- Lanthanum-hydrogen sys., dissoc. press. 250-450°, 3958
- Lanthanum monosulfide, thermo. data, 2231
- Lead azide, reactivity control, 111
- Lead bromide, photochem., 2384
- Lead chloride-ACl mixtures (A = Na, K, Rb, Cs), thermo. data, 2706
- Lead chloride-CsCl and CdCl<sub>2</sub>-CsCl, vapor press., 2361
- Lead dioxide, thermo. data, 562
- Lead storage cell, thermol. data, 562
- Light scattering, poly- $\alpha$ -methylstyrene, monodisperse, in mixed solvents, 278
- Liquid junctions, potentials of cells w/, 4660
- Liquid solutions, binary, therm. conductivity, 4308
- Lithium aluminum hydride, therm. decomp., 4009
- Lithium amalgam-Li<sup>+</sup> electrode, in LiCl-DMSO, 4568
- Lithium azide, therm. decomp., 2281
- Lithium chloride, rx. w/ silica gel in acetone, 97
- Lithium electrode, std. pot. in aq. solns., 4263
- Lithium fluoride-HX films, FHF<sup>-</sup>, 2456
- Lithium halides, far-ir spectra, 3526
- Lithium in Li-Hg, activity coeff., 1017
- Liquids, simple, internal press., 1842; simple, semiempirical model, 1510
- Luminescence, benzene, 3725; emission decay time errors, 2801; scintillators in cyclohexane, 1783
- Magnesium nitride, thermo. data, 2241
- Magnesium, rx. w/ MgCl<sub>2</sub>, 506
- Magnetic moments, determination, new method, 4392
- Magnetic susceptibility, determination, new method, 4392; NO on Pd, 1425
- Manganous chloride in LiCl-KCl eutectic, esr, 4701
- Markov chain model, end effects, 372
- Mass spectra, acetylene, 158; aromatic and heterocyclic cond.-ring cpds., 3452; boron hydrides, 2682; fragmentation of cyclic alkanes, 5; IF<sub>7</sub>, IOF<sub>5</sub>, 4697; pentacyclopentadecanes, 3061
- McKay-Perring equations, new forms, 2548
- Membrane potential, Pyrex, in MNO<sub>3</sub>-AgNO<sub>3</sub> (M = Li, Na, K), 1085
- Membrane potentials, fused SiO<sub>2</sub> in molten salts, 1963
- Membranes, cation-exch., H<sub>2</sub>O transport, 3698, 3699; effective chg. dens., 2871; grad. permselective, asymmetry potential, 2591; hydrous Zr(IV) oxide, 2200; ion-exchange, conductance determination, 4314; ion transport across, 4072; lipid, photoelectric effects in aq. media, 4512; oxid. collodion, volume flow, 1752; porous glass, ion-selective props., 2976
- Mercuric chloride, chlorination in acetone, 2154; molar conductance, 762
- Mercuric halides, molten, thermo. data, 4155
- Mercury, in 17 solvents, thermo. data, 464, 471; passivation in aq. S<sub>2</sub><sup>2-</sup>, 2300; solubility in dimethylcyclohexanes and alcohols, 1913
- Metachromasy, aq. thiocarbocyanine dye, 1259
- Metal azides, photodecomp., 1733
- Metal cyano complexes, <sup>14</sup>N nqr, 2982
- Metal ions, divalent, binding by polyacrylic acid, 1502; polymerization studies, 885
- Metal  $\beta$ -ketoenolates, spectra, 4631
- Metalocenes, axial field model calc., 16
- Metaphosphate glass, I<sup>-</sup> photosens. rxs., 3768
- Methane, acetylene photosensitized decomp., 4360; oxidative ads. on Pt, 2856; therm. decomp., 348; w/ trace O<sub>2</sub>, olefin, radiolysis, 1475
- Methanethiol, photolysis, 2145, 3679
- Methanol, electro sorbed, 1571
- Methanols, deuterated, ether form., 2770
- N-Methylacetamide, He, N<sub>2</sub>, Ar, and ethane solubility in, 4651; hydration in CCl<sub>4</sub>, 2465; H<sup>+</sup> exch. kinetics, 1001
- Methylcyclohexane-fluorobenzene, thermo. data, 56, 63
- Methylene, rx. w/ CO, 2236

- Methylene blue, aq., trimerization, 2477; laser photolysis, 2684  
 Methylene cycloalkanes, gaseous photolysis, 321  
 Methylene radical, triplet, rx. w/ *cis*-butene-2, 191  
*o*-Methylformamide, *cis-trans* equilib., 2135  
 Methyl groups, hindered rotation study, 1324  
 Methyl iodide, flash photolysis, 1583; ir band shapes, 962  
 Methyl isocyanide, <sup>13</sup>C effect in therm. isom., 3440; rx. w/ T\*, 763; therm. isom., 1726; therm. isom., energy trans., 1932  
 Methyl methacrylate-styrene random copolymers, dil. soln. props., 829  
 Methyl nitrite, isom. mechanism, 3581  
*N*-Methylpropionamide solutions, viscosity and molal vols., 3209  
 Methylpyrrolidone, circular dichroism, 3035  
 Methyl radical, rx. in aq. soln., 2703  
 Methylsilanes, rx. w/ recoil <sup>3</sup>H, 2631  
 Micelle, aq. heptaoxyethylene glycol monohexadecyl ether, 339  
 Micelles, mol. wt. detn., 379, 380; sodium perfluorocaprylate and -propionate, 3056; structure by <sup>19</sup>F nmr, 583  
 Microtome, liquid surface sampling, 589  
 MO calculations, CNDO SCF, monosubst. benzenes, 716; FSGO model of first-row hydrides, 1289; hydroxyaromatic anions, 914; isoalloxazine, 536; SCF, 2-phenylnaphthalenes, 4474; sulfur-containing heterocycles, 3975  
 Model field calc., axial, d<sup>2</sup> and d<sup>8</sup> configurations, 16  
 Molybdenum-Mo(III) electrode, in molten salts, 1442  
 Molybdovanadophosphoric acids and salts, soln. properties, 4304  
 Monodeuteriotoluene, <sup>2</sup>H self-exch. rx., 1976  
 Monodisperse polymer, intrinsic visc., 2890  
 Monomolecular films, phenophytin *a* and phenophytin *b*, 39  
 Montmorillonite, high press. ion exch., 4340  
 Montmorillonites, alkylammonium, swelling, 4295  
 Mordenite, acidic sites, 4691  
 Morse and Fues oscillators, dynamics, 2489  
 Multilayer flow model, ads. gases, 2365
- Naphthacene, solv. Stark effect, 2737  
 Naphthacene trianion and 5,12-naphthacenequinone anion rads., esr, 1829, 1830  
 Naphthalene, model sym. coords., 1451  
 Naphthalene-H<sub>2</sub>O-air system, contact angles, 646; interfacial free energies, 2283, 2284  
 Naphthalene-O<sub>2</sub>-H<sub>2</sub>O, radiolysis, 4609  
 Naphthalenes, isotopic, harmonic-vib. analysis, 1446  
 Neopentane(s)-nitrous oxide, radiolysis, 3707  
 Ni(II)-*o*-phenylenediamine, polarographic prewave, 4637  
 Nickel malonate and succinate complexes, formation, 2026  
 Nickel(II)-organic amine complexes, polarographic red., 1083  
 Niobium oxotrihalides, ir spectra, 4686  
 Niobium pentachloride, thermo. data, 1272  
 Nitrate, aq., photochem., 389  
 Nitrate ion, uv spectrum, 293  
 Nitric oxide, ads. on ZnS and ZnO, 2141; esr study on NaY and decationated Y zeolites, 4163; on Pd, sorption and mag. susceptibility, 1425  
 Nitrite ion, oxid. in NaNO<sub>2</sub>-LiClO<sub>4</sub>, 876  
 Nitroalkanes, radiolysis, 3387  
 Nitrobenzene-HAuCl<sub>4</sub> sys., aq. HCl-benzene distribution, 1617  
 Nitrogen, active, rx. w/ perfluorobutene-2, 1812; active, rx. w/ propene, 526; ads. isotherm, universal, 3763; (A<sup>2</sup>Σ<sup>+</sup>), Hg(<sup>1</sup>P<sub>1</sub>) photosens. prod., 3741  
 Nitrogen atoms, active, rx. w/ (CN)<sub>2</sub>, 3381; rx. w/ olefins and acetylenes, 2538; rx. w/ Cl<sub>2</sub>O, 3028; rx. w/ CO<sub>2</sub>, 2235; rx. w/ N<sub>2</sub>O<sub>5</sub>, 1081  
 Nitrogen atom-oxygen atom recombination reactions, catalyzed by carbon cpds., 3701  
 Nitrogen-CO-Hg, photolysis, 1402  
 Nitrogen dioxide, aq., photochemical generation, 593; dimerization in soln., 1626; esr in frozen solns., 1721; rx. w/ I<sup>-</sup> in molten alkali metal nitrates, 3545  
 Nitrogen and hydrogen, active ats., rx. w/ CH<sub>3</sub>C<sub>2</sub>H and CH<sub>2</sub>CCH<sub>2</sub>, 3323; active ats., rx. w/ (CN)<sub>2</sub>, HCN, C<sub>2</sub>H<sub>2</sub>, 3305; at. mixs., rx. w/ alkenes and alkanes, 518  
 Nitrogen-hydrogen bonds, dissociation energies, 1399  
 Nitrogen tetroxide, planarity, 3038  
 Nitrogen trioxide, double-base propellant combustion, 2279  
 Nitromethane, radiolysis in alkaline solns., 3382, 3387  
 Nitronium perchlorate, therm. decomp. 4004, 4015  
*p*-Nitrophenol-amine complexes, in nonaq. solvs., 3192  
 5-Nitro-8-quinolinol, absence of fluorescence, 3692  
 Nitrosodisulfonate, aq., radiochem., 1011  
 Nitrotriphenylamines, red. at Pt, 4336  
 Nitrous acid, unimolecular isomerization, 269  
 Nitrous oxide, liq., radiolysis, 1394  
 Nitroxides, solubilized long-chain, esr, 4129
- Nmr, acetal and haloacetals, 2954; aluminum trialkyls, 822; chloromethylphosphine, 2666; (CH<sub>3</sub>)<sub>3</sub>NBr, 2269; di-*t*-butylcarbinol, 4346; *trans*-2,5-dimethylpiperazine and hydrochlorides, 2344; ethyl esters in benzene, 2764; ethyl esters of phosphorus acids, 4043; ethylenediamine-H<sub>2</sub>O and NH<sub>3</sub>-H<sub>2</sub>O, 550; hexachlorobicyclo(2.2.1)heptenes, 198; fluorosilanes, 660; high-resolution, semiempirical treatment, 1414; in nonpolar, magnetically isotropic mol. 2111; isomeric cyanine dyes, 2008; isotopically subst. 2-pyridones, 1177; medium effects, 2111; methyl gp. hindered rotation study, 1324; monohalogenated fluorobenzenes, 991; NH<sub>4</sub>Cl spin-lattice relax., 1139; *N,N*-dimethylamides and -thioamides, 2469; neighboring magnetic anisotropy effect on N-H chem. shifts, 4708; organometallics of Li, Mg, Ca, 953; DL- and LL-phenylalanylvalines, 2661; α-phenylethylazo-2-propane, 754; phenylmagnesium bromide, phenyllithium, pyridine, 944; polar molecules in benzene, 1819; pyrazines and their cations, 1642, 1646; saturated heterocyclic rings, 3244; *para*-subst. anilines, diphenylamines, triphenylamines, 1217; subst. benzenes, 2552; tetraethyl ethylenebisphosphonate, 2678; vinyl halides and vinyl ethers, 4351; vinylphosphonates, 175; <sup>2</sup>H, D<sub>2</sub>O in organic solvents, 4188; <sup>1</sup>H and <sup>27</sup>Al, Al(III) halides in *N,N*-dimethylformamide, 3063; <sup>27</sup>Al, aluminum alkyls, 4182; <sup>27</sup>Al, trialkylaluminum complexes, 546; <sup>79</sup>Br, aq. quaternary ammonium bromides, 2805; <sup>13</sup>C, 2-subst. pyridins, 2619; <sup>13</sup>C, 3-subst. pyridines, 290; <sup>19</sup>F, 1,2-difluorotetrachloroethane, 4299; <sup>19</sup>F, micelle structure, 583; <sup>15</sup>N, HCN, 4310; <sup>17</sup>O and <sup>35</sup>Cl, aq. HCl-Co(II), 121; <sup>205</sup>Tl, thallium borate glasses, 3416  
 Noble gases, potential models and properties, 632  
 Nonaqueous ionic solns., thermo. data, 2970  
 Nonionic detergent, aq., micellar size and shape, 339  
 Norbornadiene and quadricyclene, fluorescence quenching, 3797  
 Nqr, <sup>36</sup>Cl, (C<sub>2</sub>H<sub>5</sub>)<sub>3</sub>NAsCl<sub>6</sub>, 761; <sup>36</sup>Cl, phosphorus oxychloride mol. adducts, 1340; <sup>14</sup>N, metal cyano complexes, 2982; <sup>14</sup>N, pyridine derivs., 2501  
 Nucleation, homo. vapor phase, 421
- Octafluorobutene-2, Hg(6<sup>3</sup>P<sub>1</sub>)-photosensitized isom., 3328  
 Octanol, intermolecular assn., 3273  
 Optical activity, adenine nucleosides, 1483  
 Organic dyes, triplet states, dimer formation effect, 4718  
 Organic glasses, photo- and γ-induced ionization, 3884; rad. decay kinetics, 4604; radiolysis, 1702; trapped electrons, 4599; viscosities, 1918, 3349  
 Organic solids, γ-irradiated, positive chg. migration, 3878  
 Organic vapors, ads. on silica gel, 3475  
 Organoaluminum cpds., etherate formation, 3567  
 Organometallics of Li, Mg, Ca, nmr and uv spectra, 953  
 Orthophosphate, sorption on crystalline metal oxides, 3236  
 Oscillator strength, electronic, CF<sub>2</sub>, 4594  
 Osmotic coefficients, aq. tri-*n*-alkylsulfonium halides, 212  
 Oxalic acid-<sup>13</sup>C, decomp., 4431  
 Oxalic acids, protio- and deuterio-, ir spectra, 4628  
 Oxidation, aniline by Cu(II) acetate, 481; flame, Na, K, Cs, 2483  
 Oxygen, ads. on Spheron-6, 1171; isotopic exch. on Pt, 1051; (<sup>3</sup>P), addn. to propene, butene, and propene-butene films, 616; photosens. adn. to unsat. organics, 2852; singlet, violanthrone excitation, 2913  
 Oxygen atoms, gas phase rx., 3920; rx. w/ Cl<sub>2</sub>O, 3025; rx. w/ ICN, 743; rx. w/ (S(s), S(l), Se(s), Se(l), 84  
 Oxygen difluoride, rx. w/ SO<sub>3</sub>, 2262; thermal dissn. 2307, 2311  
 Ozone, radiolytic form. and decomp., 1166
- Palladium-hydrogen system, phase separation, 4695  
 Paramagnetic relaxation, viscous solutions, 736  
 Pentacyclotetradecanes, mass spec., 3061  
 Pentafluoroethylene iodide, exch. rx. w/ I<sub>2</sub>, 1811  
 Peptides, aq., radiolysis, 758  
 Perchlorates, aq., radiochem., 2054  
 Perchloric acid, extraction by 1-decanol, 3504  
 Perfluoro-2,1,3-benzoselenadiazole anion radical, electronic and esr spectra, 1281  
 Perfluoroazomethane, photolysis, 542  
 Perfluorocarbons, electronic props., 3531  
 Perfluorocyclobutanone ketyl, esr, 1832  
 Perfluoroethane-rare gas liquid mixtures, radiolysis, 253  
 Perfluoropropene, therm. decomp., 3054  
 Periodic reactions, homogeneous, 1403  
 Phenanthrene solution, electrochemiluminescence, 3071  
 DL-, LL-Phenylalanylvalines, nmr, 2661  
 Phenylamine, nmr, 1217  
 α-Phenylethylazo-2-propane, nmr, 754  
 Phenylgermanes, π bonding, 3043  
 Phenyllithium, nmr and uv spectra, 944

- Phenylmagnesium bromide, nmr and uv spectra, 944  
 2-Phenylnaphthalenes, electronic spectra, 4468, 4474  
 9-Phenylxanthyl radical, spatial config., 3641  
 Pheophytin *a* and *b*, monolayers, 39  
 Phosphate anions, aq., photolysis, 3820  
 Phosphorescence, aromatic hydrocarbons, 2265  
 Phosphorus compounds, organic and inorganic, ion mobilities, 2867  
 Phosphorus-nitrogen system, thermo. data, 1611  
 Phosphorus oxychloride molecular adducts,  $^{35}\text{Cl}$  nqr, 1340  
 Photochemistry, aq. nitrate, 389; cobalt complexes, 400; hexacyanoferrate(III)- $\text{N}_3^-$ , 410;  $\text{OH}-\text{H}_2\text{O}_2$ , 406; organic, lanthanide ions as probes, 3516, 3522; platinum complexes, 383; platinum(II) complexes, 414  
 Photochromic isomers, ads. spectra w/ o separation, 2817  
 Photoelectric effects, lipid membranes in aq. media, 4512  
 Photoionization,  $\text{N,N,N',N'}$ -tetramethyl-*p*-phenylenediamine, 929  
 Photolysis, acetaldehyde-Hg, 3052; acetone, 2337; acetylene, 4360;  $\text{AgClO}_4$ , 2798; alcohols on alumina, 2851; alkane- $\text{N}_2\text{O}$ , 759; aromatic hydrocarbons- $\text{O}_2$  sensitizer, 3468; aq.  $\text{Ba}(\text{N}_3^-)_2$ , 774; aq.  $\text{Cr}(\text{CN})_6^{3-}$ , 3827; aq. neg. ions, 3815; aq. phosphate anions, 3820; aq. pyrimidines, 3842; aq. sulfur polyvalent anions 1800; azoisopropane, 3754; benzil-Cr(III), 3017; 1,3-butadiene, 4037; *cis*-butene-2-*n*-butane-diazomethane- $\text{O}_2$  mixtures, 749;  $\text{C}_8\text{O}_2-\text{H}_2$ , 3105;  $\text{CH}_3\text{I}$ , 1583;  $\text{CH}_3\text{SiH}_3$ -*n*-butane-diazomethane- $\text{O}_2$ , 749;  $\text{CrO}_2\text{Cl}$ , 3929; cyclobutanone, 1621; cyclohexane, 3904; cyclohexane w/ benzene and w/  $\text{N}_2\text{O}$ , 4684; cyclohexane-nitrosyl chloride, 4700; diazomethane-*cis*-butene-2- $\text{N}_2$ , 191; diborane, 3367; 1,3-difluoro- and 1,1,3,3-tetrafluoroacetone, 1603; 1,1'-dimethoxyazobenzene, 153; *p,p'*-dimethoxybenzophenone, 3522;  $\text{N,N'}$ -diphenyl-*p*-phenylenediamine, 3774; flash, fast rxs., 3766; fluoroaldehydes, 3351, 3352; Hg-cyclobutane, 1432; Hg-ketene-butene, 3705;  $\text{HI}-\text{I}_2-\text{CO}_2$ , 1639; *m*- and *p*-hydroxyazobenzene, 3266; iodine-amine complexes, 3863; ketene, 3952; laser, aromatic cpds., 2417; metal azides, 1733; methanethiol, 2145, 3679; methylene blue, 2684; methylenecycloalkanes, 321  $\text{N}_2-\text{CO}-\text{Hg}$ , 1402;  $\text{N}_2-\text{CO}$ , 3741;  $\text{NCS}_2$ , 305;  $\text{NH}_3$ -propane, 3914;  $\text{NO}_2$ (aq) formation by, 593;  $\text{NOCl}$ -cyclohexane, 371;  $\text{O}_2-\text{F}_2-\text{N}_2-\text{H}_2$ , 3168;  $\text{O}_2$ -unsat. organics, 2582; octafluorobutene-2-Hg, 3328;  $\text{OF}_2-\text{SO}_2$ , 2262; organic glasses, 3884;  $\text{PbBr}_2$ , 2384;  $\text{PbO}$  as photosensitizer, 1078; perfluoroazomethane, 542; pyran and thiopyran derivatives, 997;  $\text{SO}_2$ , 3736; succinimide, 2289;  $\text{N,N,N',N'}$ -tetramethyl-*p*-phenylenediamine, 929; xenon, 3129  
 Photooxidation,  $\text{N,N'}$ -diphenyl-*p*-phenylenediamine, 3774  
 Photoperoxidation, autoperoxidation of 9,10-dimethyl-1,2-benzanthracene, 3794  
 Photoreduction, aminobenzophenones in nonpolar media, 3782  
 Photoselected emitters, emission decay time errors, 2801  
 Phthalocyanine, metal-free, spectro. characterization, 3230  
 Phthalocyanine,  $\alpha \rightarrow \beta$  polymorphic conv., 3335  
 $\gamma$ -Picoline, rx. w/  $\text{I}_2$ , 2438  
 Picric acid, solid state rxs. w/ subst. hydrocarbons, 4446  
 Piperazinium ion, aq., therm. data, 2081  
 Platinum(II), square-planar complexes, photochemistry, 414  
 Platinum complexes, octahedral, square planar, photochemistry, 383  
 Poisson-Boltzmann equation, variation principle for, 3575  
 Polar molecules, Kihara core model, 1821  
 Polarization, molar, benzene solns. of molecules w/ anomalous dipole moments, 1517  
 Polarographic prewave, Ni(II)-*o*-phenylenediamine, 4637  
 Polyacrylamide, conc. aq. soln. properties, 1265  
 Polyacrylic acid, divalent metal ion binding, 1502  
 Polyatomic molecules, standard sym. coords. for vib., 1451  
 Poly- $\gamma$ -benzyl-L-glutamate, properties, 1157  
 Polyelectrolytes and polysoaps, anionic, electrical trans. props., 2507  
 Polyene-iodine complexes, spectra, 2690  
 Polyethylene crystals, folded chain, density and heat of fusion 178  
 Polyethylene, linear, enthalpy of fusion, 309  
 Polyethylenesulfonates of various gegenions, activity coeffs., 1366  
 Poly-L-lysine, aq., conformational change kinetics, 3177  
 Poly(methacrylic acid)-Cu(II), aq., spectro. study, 1127  
 Poly- $\alpha$ -methylstyrene, monodisperse, in mixed solvs., thermo. data, 278  
 Poly( $\alpha$ -methylstyrene)s in cyclohexane, light-scattering data, 2161  
 Polymer, liqs., surface tension, 2013  
 Polymerization, styrene and methyl methacrylate, 2993  
 Polymers, critical surface tension estimation, 3332  
 Polymer solutions, concentration fluctuations, 448  
 Polymorphic transformation, zinc phthalocyanine, 2446  
 Polynitroalkanes, therm. decomp., 1513  
 Poly- $\alpha$ -olefins, opt. act., conformational props. in solr., 2400  
 Polyoxyethylene sulfate type surfactant, solubilization behavior, 4331  
 Polyphenyl anion radicals, esr, 2238  
 Polyphosphates of various gegenions, activity coeffs., 1370  
 Polystyrene, degradation by ultrasonics and by benzoyl peroxide, 4613; radiation-cross-linking properties, 4229  
 Polystyrenesulfonate, cross-linked, tetra-*n*-butylammonium exch. w/  $\text{Na}^+$ , 2651  
 Polystyrenesulfonates of various gegenions, osmotic and activity coeffs., 1361  
 Polystyrenesulfonic acid ion-exchange membrane, volume flow, 1566  
 Porous diaphragm, convective diffusion across, 4168  
 Porous glass, as ionic membrane, 599  
 Potassium chloride, activities in ethanol- $\text{H}_2\text{O}$ , 4580  
 Potassium chloride- $\text{H}_2\text{O}$ -alcohol, conductivity, 866  
 Potassium electrode, std. potentials in ethanol- $\text{H}_2\text{O}$ , 4580  
 Potassium sulfide, thermo. data, 1277  
 Potential functions, interatomic, thermochem. test, 2341  
 Praseodymia, tensiometric study, 2044  
 Praseodymium oxide-oxygen system, phase transformations, 4415  
 Praseodymium trifluoride, thermo. data, 3375  
 2-Propanol, radiolysis, 808  
 Propene, rx. w/ active N, 526  
 Propylene and isomeric butenes, ion-mol. rxs., 1994  
 Propylene, pyrolysis, 4672  
 Proteins, aq., partial vols., 1817; tryptophan residue differentiation, 3654  
 Proteins and L-amino acids, densities, 1887  
 Protein solutions, proton fluctuation anisotropy, 4058, 4066  
 Proton exchange, ethylenediamine- $\text{H}_2\text{O}$  and  $\text{NH}_3-\text{H}_2\text{O}$ , 550  
 Proton fluctuations, anisotropic, protein solns., 4058, 4066  
 Pyran and thiopyran derivatives, photochromism, 997  
 Pyrazines and their cations, nmr, 1642, 1646  
 Pyrene- $\text{N,N,N',N'}$ -tetramethyl-*p*-phenylenediamine system, chemiluminescence, 4348  
 Pyrex, membrane pot. in  $\text{MNO}_3-\text{AgNO}_3$  ( $\text{M} = \text{Li}, \text{Na}, \text{K}$ ), 1085  
 Pyridine, ads. on faujasites, 1042; hydration in org. solvs., 3223; ionic equilibria in, 3410; nmr and uv spectra, 944  
 Pyridine and methylpyridines, radiolysis, 4528  
 Pyridines,  $^{14}\text{N}$  nqr, 2501; 2-subst.,  $^{13}\text{C}$  nmr, 2619; 5-subst.,  $^{13}\text{C}$  nmr, 290  
 2- and 4-Pyridinecarboxaldehydes, reversible hydration, 655  
 Pyridinium salts, in  $\text{CH}_3\text{OH}$ ,  $\text{H}^+$  exch., 2515; in  $\text{H}_2\text{O}$ ,  $\text{H}^+$  exch., 2520  
 2-Pyridone and 2-thiopyridone, dimerization, 3339  
 2-Pyridones, isotopically subst., nmr, ir, 1177  
 4-Pyridones, isotopically subst., spectro. study, 3681  
 2-Pyridylmethyl phosphate-bivalent metal complexes, stability order, 116  
 Pyrimidines, aq., radiolysis and photolysis, 3842  
 Pyrolysis, succinimide, 2289  
 Pyrrole-dimethyl sulfoxide system, hydrogen bonding, 650  
 Quantum chemistry, spin-free, spin density, 21  
 Quartz, irradiated,  $\text{H}_2$  diffusion, 2277  
 Quaternary ammonium bromides,  $^{79}\text{Br}$  nmr line widths, 2805  
 Quaternary ammonium radicals, in  $\text{NH}_3$ , uv-visible-ir spectra, 1374  
 Radial distribution function, theory, 608  
 Radical recombination reactions, crit. bond length, 1009  
 Radiolysis, acetamide, 2181; air-sat. aq.  $\text{HClO}_4$ , 3836; alkane- $\text{N}_2\text{O}$ , 759; alkane- $\text{N}_2\text{O}$ -alcohol, 52; alkyl and aromatic disulfides in glasses, 2597; amides and peptides in equo-organic sys., 4721; amines, 1464; aq. amino acids, 3394; aq. Co complexes, 1506; aq.  $\text{Cr}^{2+}$ ,  $\text{Cr}^{3+}$ ,  $\text{V}^{2+}$ , and  $\text{V}^{3+}$ , 2330; aq. cysteine, 185, 2395; aq. eosin, 3337; aq. fluorescein, 2018; aq. nitrosodisulfonate, 1011; aq.  $\text{N}_2\text{O}$ -benzoic acid, 2946; aq. peptides, 758; aq. perchlorates, 2054; aq. perchloric acid-ferricyanide, 1599; aq. pyrimidines, 3842; aq.  $\text{SF}_6$ , 4285; aq. thymine and triacetoneamine N-oxyl, 3669; benzene, 1027; benzene-biacetyl solns., 3871; benzene- $\text{N}_2\text{O}$ , 3013; *p*-bromophenacyl hirsutate, 3772;  $\text{CCl}_3\text{F}-\text{CF}_2\text{BrCF}_2\text{Br}$ , 50:50 mix., 1776; Ce(III) in aq.  $\text{H}_2\text{SO}_4$ , 3704;  $\text{CH}_4(\text{l})-\text{Ar}$ , 1076;  $(\text{CH}_3)_2\text{Hg}$ , 3457;  $\text{CH}_3\text{NO}_2$  in alkaline solns., 3382, 3387;  $\text{CH}_4-\text{O}_2$ -olefins, 1475;  $\text{CO}_2$ ,  $\text{N}_2\text{O}$ ,  $\text{CO}$ , 3920; colloidal S, 3552; cyclohexane-deuterated olefins, 1780; cyclopropane in *n*-hexane and cyclohexane, 228; di-*t*-butyl peroxide, 723; *p*-dichlorobenzene, crystal structure effect, 4707; *cis*- and *trans*-1,2-dimethylcyclohexane, 4509;

- dioxane, 3849; 1,4-dioxane, aq. 1,4-dioxane, 2635; D<sub>2</sub>-ethylene-Kr, 3261; D<sub>2</sub>O, 511; ethane(1)-Ar, 1076; ethanol, 816; ethylene glycol dimethacrylate polymers, 3277; free ion, yield in liq., 3730; HCl-SF<sub>6</sub>, 765; *n*-hexane, cyclohexane, 3856; isobutane, isopentane, 2,3-dimethylbutane, 3496; metal chelates of glycine and alanine, 922; methyl halides, 2287; 3-methylpentane, methyltetrahydrofuran, methylcyclohexane; glasses, 1702; 10-MeV proton, N<sub>2</sub>-O<sub>2</sub> sys., 1988; mixed Freons, 1776; naphthalene-O<sub>2</sub>-H<sub>2</sub>O, 4609; neopentane(s)-nitrous oxide, 3707; NH<sub>3</sub>, 1592; N<sub>2</sub>O(l), 1394; N<sub>2</sub>-O<sub>2</sub>, 1081; N<sub>2</sub>O-cyclohexane, 1783; O<sub>2</sub>, 1166; organic glasses, 3884, 4599, 4604; organic solids, 3878; oxygenated H<sub>2</sub>O, 626; polycrystalline *n*-hydrocarbons, 4347; polystyrene, 4229; 2-propanol, 808; pulse, cyclohexadienyl radicals by, 3832; pulse, short-lived transients, 3762; pyridine and methylpyridines, 4528; rare gas-C<sub>2</sub>F<sub>6</sub>(l), 253; rare gas-propane liq. mixs., 3808; silica gel, 2623; stilbene, 3801; stilbenes, 1457; *N,N,N',N'*-tetramethyl-*p*-phenylenediamine in hydrocarbons, 4265
- Raman spectra, aq. formates and acetates, 2614; fused BiCl<sub>3</sub>, InCl<sub>3</sub>, InCl<sub>3</sub>, 3094; rhombic S, 744; S, S-Se, S-As, 4133
- Rare earth(III) ions, assn. w/ F<sup>-</sup>, 4720
- Rare gas-propane liq. mixs., radiolysis, 3808
- Recoil tritium systems, single-step double-displacement rx., 707
- Reduction, by Zn<sup>+</sup>, Cd<sup>+</sup>, Ni<sup>+</sup>, 784
- Reduction potentials, complex ions, 1355
- Refractive index, complex, colloidal AgBr, 1523
- Rhenium-oxygen sys., thermo. data, 3963
- Ribonuclease, transition temp., salt effect, 733
- Rotary power and dispersion, meas. using polarized Rayleigh scattering of laser radiation, 4716
- Rotating disk electrode, homo. chem. kinetics, 1082
- Salicylic acids, substituted, ads. spectra pH dependence, 3297
- Salt mixtures, aq. binary, thermo. data, 4048, 4053; ternary thermo. data, 2086
- Salts, fused, friction consts., 3001; Li and Na, in ethereal solvs., 1021; molten, glass electrode potentials, 2877; molten, ion exch., 2885
- Schiff bases, substituent effects on tautomerism, 4111
- Semidiones, aliphatic, N atom hyperfine splittings, 1386; esr, 1074
- Sepiolite, ir study, 1072; vapor sorption, 334
- Silica, fused, ion diffusion from molten salts, 2256; fused, membrane potentials in fused salts, 1963; H<sub>3</sub>PO<sub>4</sub> impregnated, surface props., 3161
- Silica-Al<sub>2</sub>O<sub>3</sub>, cumene desorption, 356
- Silica gel, w/ ads. H<sub>2</sub>O, conductivity, 3662;  $\gamma$ -irradiation, 2623; surface struct., 2926
- Silicate minerals, surface area, 2127
- Siloxane, rx. w/ silica, 3993
- Siloxane(g), rxs. w/ SiO<sub>2</sub>, 1248
- Silver(I)- and Cu(II)-pyridine systems, aq., thermo. data, 1208
- Silver bromide, colloidal, complex ref. ind., 1523; colloidal partical growth, 2168
- Silver chloride, in binary and ternary molten salt sys., 2086; solubility and complex formn. in dimethylformamide, 3288
- Silver iodide-RgI, -KI, and -NH<sub>4</sub>I solid systems, thermo. data, 2106
- Silver perchlorate, conductance in sulfolane, 2124; photochem., 2798
- Singlet-sensitized reaction, photochem., mech., 3797
- Soap films, contact angles and trans. regions, 3342
- Sodium alkyl sulfates, ads. at air-water interface, 2218; ads. at oil-H<sub>2</sub>O interface, 2222; aq., thermo. data, 2668
- Sodium bromide, aq., conductance to 4000 bars, 2100
- Sodium chloride, aq., conductances, 684
- Sodium chloride-H<sub>2</sub>O-pyridine, activity coeffs., 925
- Sodium chloride-MgCl<sub>2</sub>-H<sub>2</sub>O, isopiestic meas., 4048, 4053
- Sodium chloride-ZnCl<sub>2</sub> system, vaporization equilibria, 4524
- Sodium dodecylpolyoxyethylene sulfates, solubilization, 1214
- Sodium ion, self-diffusion in ethylene glycol-H<sub>2</sub>O, glycerol-H<sub>2</sub>O, 1201
- Sodium ion-Li<sup>+</sup> ion exch., thermo. data, 789
- Sodium-kaolin and NaCl in kaolin suspension, partial molal vols., 2358
- Sodium-NH<sub>3</sub>, gas, ads. spectra, 3334
- Sodium in NH<sub>3</sub>(l), conductance, 4224
- Sodium nitrate,  $\lambda$  transition, 1294
- Sodium-Pb, thermo. data, 1439
- Sodium perfluorocaprylate and propionate, micelle form., 3056
- Sodium sulfate-NaCl-H<sub>2</sub>O, thermo. data, 2474
- Sodium tetraphenylboron, aq., thermo. data, 2525
- Sodium zeolite A, in molt. NaNO<sub>3</sub>, 2885
- SO<sub>2</sub>-doped flames, rad. recomb., 3359
- Solids, high-temp. entropy estimate, 1825
- Solubility, benzene in aq. tetraalkylammonium bromides, 751
- Solubilization, polyoxyethylene sulfate type surfactant, 4331; sodium dodecylpolyoxyethylene sulfates, 1214
- Solute-solvent interactions, aq. media, 2512
- Solvation, preferential, thermodynamics, 796
- Sorption, NO on Pd, 1425; orthophosphate on crystalline metal oxides, 3236; propionic and acetic acids on germania, 2378; trialkylsilanes by E-glass or aerosil, 2750; vapor by sepiolite, 334
- Sorption-desorption, H<sub>2</sub>O on gelatin, egg albumin, casein, 1223
- S<sub>2</sub>O<sub>4</sub><sup>-</sup> radical, formation in dimethylformamide, 4706
- Soybean protein, H<sup>+</sup> equilibria, 3612
- Spectrofluorimetry, low-wavelength, 2-aminopyridine as standard, 2680
- Spin density, spin-free quantum chem., 21
- Stannic fluoride and PbF<sub>2</sub>, gases, uv spectra, 3510
- Stark effect, solv., temp. depend., 2737
- Stilbene, radiolysis, 3801
- Stilbenes, radiolytic *cis-trans* isom., 1457
- Strontium carbonate, rx. w/ TiO<sub>2</sub>, 3326
- Strontium-Sr halide systems, miscibility, 1892
- Structure, see crystal structure; aq. hexamethylenetetramine, 2588; dihalobenzyccyclobutenes, 668; H<sub>2</sub>O, 899, 3032; H<sub>2</sub>O-*n*-alkylamine complexes, 1808; H<sub>2</sub>O solutions, 3021; liq., formamide, formamide-KI, 1088; liq. Pd-Sn, 2535; mesomorphic phases, 2058; molecular, first-row atom hydrides, 1289; molecular, 1,2,3,4-tetrabromo-1,2,3,4-diphthaloylcyclobutane, 2120; N<sub>2</sub>O<sub>4</sub>, 3038; poly- $\gamma$ -benzyl-L-glutamate, 1157; surface, silica gel, 2926
- Styrene, polymerization in an electric field, 4543; polymerization kinetics, 216
- Styrene-methyl methacrylate random copolymers, dil. soln. props., 829
- Sublimation kinetics, NH<sub>4</sub>ClO<sub>4</sub>, 202
- Sulfide ion, aq., Hg passivation, 2300
- Sulfolane, cryoscopic behavior, 1068; solvation nos. of some ions in, 4329
- Sulfur, colloidal, radiolysis, 3552; liq., ring-chain equil., 1890; rhombic, raman spectrum, 744; S-Se, S-As, Raman spectra, 4133
- Sulfur dioxide, photolysis, 3736; rxs. yielding excited, 3711
- Sulfur hexafluoride, rx. w/ e<sub>aq</sub><sup>-</sup>, 4285
- Sulfur polyvalent anions, aq., photolysis, 1800
- Surface, liquid, jet drop sampling, 589
- Surface potentials, aq. electrolytes, 74
- Surface properties, H<sub>3</sub>PO<sub>4</sub>-impregnated SiO<sub>2</sub>, 3161
- Surface stress, Au, 50-985°, 4150
- Surface tension, binary mixtures, 3073; critical, polymer estimation, 3332
- Swelling, alkylammonium montmorillonites, 4295
- Symposium, photo- and radiochemistry, 3709
- Tait equation, and related eq. of state, 128
- Tantalum pentafluoride, rx. w/ Ta<sub>2</sub>O<sub>5</sub>, 1099
- Tautomerism, of Schiff bases, substituent effects, 4111
- Teflon, pendular-ring cond., 2898
- Tellurium, vapor press., 1032
- Terbia, tensiometric study, 2044
- Terbia-praseodymia system, tensiometric study, 2044
- Terbium oxide-O<sub>2</sub> and mixed cerium, terbium oxide-O<sub>2</sub> system, phase transformations, 4424
- Term energies, experimental, analysis, 2335
- Tetraalkylammonium bromides-aqueous KBr, vol. changes on mixing, 1137
- Tetraalkylammonium halides, aq., conductivities to 4000 kg/cm<sup>3</sup>, 1763; potassium halides, aq., vols. of mixing, 3048
- Tetraalkylammonium iodides, aq., partial molal vols., 1814
- Tetraalkylammonium salts, conductance in ethanol and propanol, 3281
- Tetra-*n*-butylammonium bromide, aq., acid-base rxs. in, 1132
- n*-Tetrabutylammonium halides, hydrophobic hydration, 2694, 2695; low-temp., high-pressure hydrate, 376
- Tetrachloroethanes, Cl-photosensitized ox., 3926
- Tetraethyl ethylenebisphosphonate, nmr, 2678
- Tetraethylammonium perchlorate, conductance in valeronitrile, 1960
- Tetraethylammonium tetrakis(dibenzoylmethiodo)europate(III), structure, 970
- 1,1,2,2-Tetrafluorocyclopropane, difluoromethylene elimin., 2234
- Tetrafluoroethylene, pyrolysis, 3462
- Tetraheptylammonium fluoride, extraction, 2831
- Tetrakis(*p*-methoxyphenyl)ethylene cation rad., esr, 286
- Tetramethylammonium bromide, motional properties, 2269
- N,N,N',N'*-Tetramethyl-*p*-phenylenediamine, photoionization, 929; radiolysis in hydrocarbons, 4265

- Tetranitromethane, rx. w/  $\text{NO}_2^-$  and  $\text{OH}^-$ , 1402  
 Thallium-205, nmr, 3416  
 Thallous nitrate, conductance in dioxane- $\text{H}_2\text{O}$ , 4710  
 Thermal accommodation coefficient, lattice anharmonicity and, 3573  
 Thermal decomposition, solid-state, 2185  
 Thermodynamic data, acetonitrile autoprotolysis, 2270; acetylene rx. w/  $\text{I}_2$ , 3204; acid-base equilib. in 1,1,3,3-tetramethylguanidine, 918; Ag(I)- and Cu(II)-pyridine aq. sys., 1208; AgCl in dimethylformamide, 3288; AlBr<sub>3</sub>, 1664, 1669; AlClF<sub>2</sub>, AlCl<sub>2</sub>F, 3444; AlF<sub>3</sub>, 475; Al(g), rx. w/  $\text{S}_2$ (g),  $\text{Se}_2$ (g),  $\text{Te}_2$ (g), 1660; alkali met. halides in N,N-dimethylformamide, 2966; alkali metal and tetraalkylammonium salts in  $\text{H}_2\text{O}$  and  $\text{D}_2\text{O}$ , 4317; alkali perchlorates and perchlorates trans. between  $\text{H}_2\text{O}$  and  $\text{CH}_3\text{NO}_2$ , 4549; alkaline perchlorates in  $\text{CH}_3\text{OH}-\text{CH}_3\text{CN}$ , 2245; *n*-alkane surfaces, *n*-alkane- $\text{H}_2\text{O}$  interfaces, 1407; alkanes on Teflon, 2898; *n*-alkylammonium halides, 4082; alkylammonium salts in benzene, 3437; amine-amine hydrochloride sys. in toluene, 1630; amylose- $\text{I}_2$ - $\text{I}^-$  complex, 4563; aniline solutions, 261; aq. alk. met. halide salt pairs, 2759; aq. amides, 2710; aq. calcium phosphate, 208; aq.  $\text{CuSO}_4$  and  $\text{Cu}(\text{en})_2\text{S}_2\text{O}_3$ , 3986; aq. dichromate rx. w/ silica gel, 104; aq. divalent chlorides, 4589; aq. electrolyte-nonelectrolyte, 3053; aq. HCl-Co(II), 121; aq.  $\text{I}^-$ - $\text{I}_2$ - $\text{ICl}$ - $\text{Cl}^-$ -Pt, 2782; aq. ions, 2902; aq. methylene blue, 2477; aq. molybdovanadophosphoric acids and salts, 4304; aq. NaCl, 684; aq.  $\text{Na}_2\text{SO}_4$ , 2251; aq.  $\text{Na}_2\text{SO}_4$ -NaCl, 2474; aq.  $\text{NH}_4\text{Cl}$  and sym. tetraalkylammonium chlorides, 1758; aq. piperazinium ion, 2081; aq. proteins, 1817; aq. tetraalkylammonium halides-KX, 3048; aq. tetraalkylammonium iodides, 1814; aq. sodium alkyl sulfates, 2668; aq. sodium tetraphenylboron, 2525; aq. thiocarbocyanine dye, 1259; aq. thiazolium and related ions, 2213; aq. tri-*n*-alkylsulfonium halides, 212; aq. trifluoroacetic acid, 1944; aq. tungstosilicic acid, 360; aromatic-acyclic sys., 1345; aromatic cpds. in tetrachloroterephthalate esters, 4020; Ar, Xe, 1230; Ar and  $\text{CH}_4$ , 3559; Ar- $\text{H}_2\text{O}$ -ethylene glycol, 2998; Ar in  $\text{NaNO}_3$ (l), 603; As, 1102;  $\text{As}_4$ (g), 4327; assn. in mixed alkali halide vapors, 4620; benzene in aq. tetraalkylammonium bromides, 751; benzene on porous glass, 3201; benzene-cyclohexane soln. surface, 1555; benzene-xylenes, 1939; bidimensional cond. in ads. layers, 1847; bimol. lipid membranes at  $\text{H}_2\text{O}$ -oil- $\text{H}_2\text{O}$  biface, 2723; binary liq. halomethane mixs., 1529; binary solns. of dioxane, benzene, cyclohexane, nitrobenzene, 3073; bismuth trihalides to 36 kbars, 1327; bivalent metal complexes of 2-pyridylmethyl phosphate, 116; bolaform electrolytes, 4290; Br<sub>2</sub> in  $\text{H}_2\text{O}$  and  $\text{CCl}_4$ , 3695; *t*-butyl hypohalites, 2260;  $\text{Ca}_3\text{N}_2$ , 2434; carbonium ion pairs, 2233; cation exch., 2789; cation-ligand assn., 144;  $\text{CCl}_2$ , 1552;  $\text{CCl}_4$  on graphite, 1955; Cd-CdCl<sub>2</sub> liq. sys., 44; CdCl<sub>2</sub>-alkali chloride sys., 353; ceria-terbia sys., 2030;  $\text{CF}_4$ (g), 222; charge-trans. interactions, 2272;  $\text{CHCl}_3$  as hydrogen donor, 1297;  $\text{CH}_2\text{I}_2$ (g) and rx. w/  $\text{CH}_4$ (g), 4713; cholesteryl myristate, 3489; <sup>14</sup>C-labeled dodecanoic acid, 2243;  $\text{CoCl}_2$  and  $\text{ZnCl}_2$  in acetonitrile, 2075;  $\text{CO}_2$ , COS,  $\text{CS}_2$ , 2730; cohesive energies of liqs., 4688; Cu(I)- $\text{CN}^-$  complexes in anion exchangers, 2605; cyclohexane-isooctane and  $\text{CCl}_4$ -isooctane, 4496, 4503; cyclotetramethylenetetranitramine, 2,4,6-trinitrotoluene, nitromethane, and bis(2,2-dinitro-2-fluoroethyl)formal detonation, 2390; dicarboxylic acids in aq. tetra-*n*-butylammonium bromide, 1132; diffusion double layer in mixed electrolytes, 727; divalent metal ions bound by polyacrylic acid, 1502;  $\text{D}_2\text{O}$ , 4654; 1:1 electrolytes in  $\text{HCO}_2\text{H}$ , 4031; ethanol-heptane sys., 4534; ethyl acetate- $\text{H}_2\text{O}$ , 364;  $\text{Eu}_3\text{O}_4$ (s), 4235; exch. of substituents between  $(\text{CH}_3)_2\text{Si}$  and  $(\text{CH}_3)_2\text{Ge}$  moieties, 4380; fluorocarbon gases in cyclohexane, 2248; bis(fluoroxy)perfluoromethane, 3512; fused  $\text{SiO}_2$  in molten salts, 1963; Ga-In sys., 1047; gas ads. on silica, 4676;  $\text{H}^+$  equil. of soybean protein, 3612;  $\text{H}_2$  ads. on Ni-Cu, 2775;  $\text{H}_2$ - $\text{H}_2\text{O}$  hydrogen isotope equilibria, 4338;  $\text{H}_2$ -Pd-Au, 136; HCl in aq. salt solns., 4408; HCl trans. from  $\text{H}_2\text{O}$  to aq. ethylene glycol, 3937; HCl trans.,  $\text{H}_2\text{O}$  to HAc, 1064; HCl-GdCl<sub>3</sub>, 257; HClO<sub>4</sub> extraction by 1-decanol, 3504; HClO<sub>4</sub>-LiClO<sub>4</sub>- $\text{H}_2\text{O}$ , 767; HClO<sub>4</sub>-NaClO<sub>4</sub>- $\text{H}_2\text{O}$ , 767;  $\text{H}_2\text{O}$  ads. on AgI, 643;  $\text{H}_2\text{O}$  in  $\text{N}_2$ , Ar,  $\text{CH}_4$ , 20-100 atm, 330;  $\text{H}_2\text{O}$  in organic solvents, 4257;  $\text{H}_2\text{O}$  on ThO<sub>2</sub>, 2293;  $\text{H}_2\text{O}$ -triethylamine sys., 4194;  $\text{H}_2\text{O}-\text{C}_2\text{H}_5\text{OH}$ ,  $\text{D}_2\text{O}-\text{CH}_3\text{OD}$ , 2645;  $\text{H}_2\text{SO}_4$  aq., 562; He,  $\text{N}_2$ , Ar in hydrazine, methylhydrazine, and unsymmetrical dimethylhydrazine, 638; Hg in dimethylcyclohexanes and alcohols, 1913; Hg in 17 solvents, 464, 471; harmonic oscillators, 3034; high-press. ads., 2695; hydrocarbon mixtures, 676; hydrocarbons, 2941; hydrogen bonding, 3478; hydrogen bonding in aliphatic sec. amines, 3111; inter- and intramolecular hydrogen bonding, 4243; hydrophobic bond formation, 856; hydroxytropenylum halide hydrates, 2950; ( $\text{I}_2$ )<sub>2</sub>, 2697;  $\text{IF}_7$ ,  $\text{IOF}_3$ , 4697; iodine-tetramethylurea and -tetramethylthiourea mol. complexes, 2129; ion exch. of zeolites, 4086; ion exch. rxs., 2651; ion exch. w/ 2-phase glass, 2665; ion-pair assn., 1396; 2:2 and 3:3 ion pairs, 3330; ionic equilibria in pyridine, 3410;  $\text{I}_2$  on perylene, 2986; isotherm. equil. in electrolyte solns., 1536; isotopic waters and ices, 1234; KCl in ethanol- $\text{H}_2\text{O}$ , 4580; Knudsen cell calibration, 4323;  $\text{K}_2\text{S}$ , 1277;  $\text{LaH}_2$ - $\text{LaH}_3$ , 3958; LaS, 2231; Li electrode in aq. solns., 4263; Li in Li-Hg, 1017; Li and Na salts in ethereal solvs., 1021; LiCl-acetone-silica gel, 97; LiClO<sub>4</sub>-NaClO<sub>4</sub>- $\text{H}_2\text{O}$ , 767; linear polyethylene, 309; liq. Pd-Sn, 2535; mercuric halides, 4155; metal complexes of hydrolyzed ethylene-maleic anhydride copolymer, 2496; metal ion polymerization, 885; N-methylacetamide in  $\text{CCl}_4$ , 2465; methylcyclohexane-fluorobenzene, 56, 63; N-methylpropionamide solns., 3209; Mg-MgCl<sub>2</sub>, 506;  $\text{Mg}_3\text{N}_2$ , 2241; molten  $\text{PbCl}_2$ -CsCl and  $\text{CdCl}_2$ -CsCl, 2361; molten salts, 2877; molten salt ion exchange w/ glass, 4175; Montmorillonite ion exch., 4340;  $\text{N}_2$  ads., universal isotherm., 3673; NaCl,  $\text{Na}_2\text{SO}_4$ ,  $\text{MgSO}_4$ ,  $\text{MgCl}_2$  aq. binary mixtures, 4048, 4053; NaCl and KCl in  $\text{H}_2\text{O}$ , 4123; NaCl- $\text{H}_2\text{O}$ -pyridine, 925; NaCl-ZnCl<sub>2</sub> sys., 4524; Na-Li ion-exch., 789; Na in  $\text{NH}_3$ (l), 4224; Na-kaolin and NaCl in kaolin susp., 2358; Na-Pb, 1439; naphthalene- $\text{H}_2\text{O}$ -air sys., 646, 2283, 2284; NbCl<sub>5</sub>, 1272;  $\text{NH}_3$ - $\text{H}_2\text{O}$  solns., to 700° and 4000 bars, 3122;  $\text{N}_2\text{H}_4$ -1,1- $\text{N}_2\text{H}_2(\text{CH}_3)_2$  and He(or  $\text{N}_2$ )- $\text{N}_2\text{H}_4$ -1,1- $\text{N}_2\text{H}_2(\text{CH}_3)_2$  sys., 2556;  $\text{NH}_4^+(\text{NH}_3)_{n-1} + \text{NH}_3$ , 742; nitrobenzene-HAuCl<sub>4</sub>-aq. HCl-benzene sys., 1617; nonaq. ionic solns., 2970; nonionic organics on  $\text{Al}_2\text{O}_3$  and  $\text{SiO}_2$ , 489;  $\text{N}_2\text{O}_4$ - $\text{NO}_2$  sys., 2963;  $\text{NO}_2$ - $\text{N}_2\text{O}$ -solv. sys., 1626; *p*-nitrophenol-amine complexes in nonaq. solvs., 3192; octanol intermol. assn., 3273; organic vapors on silica gel, 3475; organophosphorus comp.-amine complexes, 2908;  $\text{PbCl}_2$ -ACl (A = Na, K, Rb, Cs), 2706;  $\text{PbO}_2$ , 562; Pd- $\text{H}_2$  sys., 4395; PN,  $\text{P}_3\text{N}_5$ , 1611; PrF<sub>3</sub>, 3375; perchlorates in sulfolane, 4329; polyethylene crystals, 178; poly(ethylene oxide) ads. at aq.-air interface, 4459; poly(vinyl alcohol) and poly(vinyl pyrrolidone) at aq.-air interface, 4450; polyethylenesulfonates of various gegenions, 1366; poly- $\alpha$ -methylstyrene, monodisperse, in mixed solvents, 278; poly( $\alpha$ -methylstyrene) in cyclohexane, 2161; polymer liqs., 2013; polyphosphates of various gegenions, 1370; polystyrenesulfonates of various gegenions, 1361;  $\text{PrO}_x$ - $\text{O}_2$  sys., 4415; pyridine hyd. in org. solvs., 3223; 2-pyridone and 2-thiopyridone, 3339; pyrrole-dimethyl sulfoxide sys., 650; rare earth(III) ions w/  $\text{F}^-$ , 4720; RbI-AgI, KI-AgI,  $\text{NH}_4\text{I}$ -AgI, 2106; rhenium-oxygen sys., 3963; ribonuclease- $\text{H}_2\text{O}$ -organic salts, 733; sessile drop, 318; siloxanes on silica, 3993; Sn(IV) chloride cpds. w/ ethyl esters of dicarboxylic acids, 1334; sodium alkyl sulfates at air-water interface, 2218; sodium alkyl sulfates at oil-water interface, 2222; Sr-Sr halide, Ba-Ba halide sys., 1892; swollen rubbers, 345; TaF<sub>5</sub> rx. w/  $\text{Ta}_2\text{O}_5$ , 1099; Te, 1032; terbia, praseodymia, praseodymia-terbia, 2044; terbium oxide- $\text{O}_2$  and mixed cerium, terbium oxide- $\text{O}_2$  sys., 4424; ternary molten salt sys., 2086; tetraalkylammonium bromide-aq. KBr, 1137; tetraethylammonium perchlorate in valeronitrile, 1960;  $\text{ThO}_2$ - $\text{H}_2\text{O}$ , 573, 2095; thiourea- $\text{Hg}(\text{CN})_2$ - $\text{H}_2\text{O}$ -EtOH, 2720; toluene-fluorobenzene, 56, 63;  $\lambda$  transition  $\text{NaNO}_3$ , 1294; tridodecylammonium salts in nonpolar solvs., 4202; vapors on sepiolite, 334; various gases in N-methylacetamide, 4651; various liq. densities, 1057;  $\text{V}_2\text{O}_5$ - $\text{H}_2\text{O}$  sys., 3293; water-ice isotope fractionation, 3683;  $\text{XeF}_2$ ,  $\text{XeF}_4$ , 1162; *p*-xylene and tetra-*n*-pentylammonium thiocyanate solns., 3584; YbCl<sub>2</sub>, 1697; zinc halides, 3361  
 Thermodynamics, bimol. lipid membranes at  $\text{H}_2\text{O}$ -oil- $\text{H}_2\text{O}$  biface, 2723; binary mixtures, 2280;  $\text{CO}_2$ , COS,  $\text{CS}_2$  by signif. struct. theory, 2730; congruently melting cpds., 2263; equilib. rate processes, 1844, 1845; excess props. of aromatic-alicyclic sys., 1345; exclusion chromatography, 4397; fluid mixtures, 1897; heats of formation, 2422; Hg in 17 solvents, 464, 471; McKay-Perring eqs., 2548; nucleation, homo. vapor phase, 421; preferential solvation, 796; quantum devs. from corresp. states, 2567; radial distribution function, 608; simple liq. model, 1510; simple liquids, 1842; solids, high-temp. entropy, 1825; spectrophotometric equil. eq., 2272; Tait eq. and related eqs., 128; ternary liq. two-phase system interfaces, 4139; tertiary systems, 2316; variation principle for Poisson-Boltzman eq., 3575  
 Thermogravimetric data, kinetic analysis, 2406  
 Thiocarbocyanine dye, aq., metachromasy, 1259  
 Thianthrene cation radical, <sup>1</sup>H and <sup>35</sup>S hyperfine splitting, 1390  
 Thiazolium and related ions, aq. equilibria, 2213  
 Thiocyanate ion, in soln., photochemistry, 305  
 Thiourea, interaction w/  $\text{Hg}(\text{CN})_2$  in  $\text{H}_2\text{O}$ -EtOH, 2720  
 Thiourea and thioacetamide, oxidn. by alk. hexacyanoferrate-(II), 1497  
 Thorium oxide- $\text{H}_2\text{O}$ , thermo. data, 573, 2095

- Thymine and triacetoneamine N-oxyl, aq., radiolysis, 3669  
 Tin(IV) chloride, cpds. w/ ethyl esters of dicarboxylic acids, 1334  
 Titanium(III) ions, rxs. w/  $H_2O_2$ , 164  
 Titanous salts, rxs. w/  $H_2O_2$ , 3154  
 Toluene-fluorobenzene, thermo. data, 56, 63  
 Transients, short-lived, observation, 3762  
 Trialkylaluminum complexes,  $^{27}Al$  nmr study, 546  
 Trialkylsilanes, rxs. w/ E-Glass or aerosil surfaces, 2750  
 Tri-*n*-alkylsulfonium halides, osmotic coefficients, 212  
 Trialkylsulfonium iodides, conductance in  $H_2O$ ,  $CH_3OH$ , and  $CH_3CN$ , 1037  
 Trichloroethylene, Cl-photosensitized oxidn., 3926  
 Tridodecylammonium salts, in nonpolar solvs., 4202  
 Triethylamine, molecular complexes w/ acetic and monochloroacetic acid, 3347  
 Trieuropium tetroxide, thermo. data, 4235  
 Trifluoroacetic acid, aq., thermo. data, 1944  
 Trifluoromethylnitrobenzene anion radicals, esr, 68  
 Trifluoromethyl radicals, rxs. w/ methylchlorosilanes, 494; rx. w/  $H_2S$ , 4239  
 Trigonal-bipyramidal complexes,  $d^1$  and  $d^9$ , crystal field-spin orbit treatment, 3588  
 Trihalomethyl lithium and sodium compounds, in Ar(s), 1743  
 2,2,4-Trimethylpentane-cyclohexane and  $-CCl_4$ , thermo. data, 4496, 4503  
 2,4,5-Triphenylimidazolyl radical, esr, 4717  
 Triphenylmethyl derivatives, esr and endor, 4276  
 Triphenylmethyl and tris(*p*-tolyl)methyl radicals, endor spectra, 4269  
 Triphenylphosphine sulfide-iodine complex, crystal structure, 1561  
 Triplet states, aromatic nitrogen heterocycles, biphenyl, acenaphthene, 3215  
 Tris(dimethylammonium) hexabromobismuthate(III), crystal structure, 3117  
 Tritium, recoil-, rx. w/ methylsilanes, 2631; recoil-, single-step double-displacement rxs., 707; recoil-, solid phase rxs., 1789; recoil-, subst. in  $CH_3NC$ , 763  
 Tritium atoms, energetic, H vs. D replacement, 1845; rx. w/ solid propene and propane, 1  
 Tropylium ion, in mass spec., 3061  
 Tryptophan residues, differentiation in proteins, 3654  
 Tungstosilicic acid, osmotic coeff., 360
- Ultracentrifugation, rotor deceleration, 498  
 Ultrasonic absorption, aq. poly-L-lysine, 3177  
 Ultrasonic adsorption, aq. glycine, diglycine, triglycine, 2227  
 Ultrasonic relaxation, 3,3-diethylpentane, 2268  
 Unimolecular dissociation reactions, crit. bond length, 1009  
 Unimolecular reaction systems, kinetics, 4483, 4488  
 Urethane reactions, uncatalyzed, kinetics, 845  
 Uv spectra, aq. halogens, 3671; aromatic chromophores, 2934; cyclooctatetraenyl rad. anion, 2813; HBr and HI, 3046; *m*- and *p*-hydroxyazobenzene, 3266;  $I_2$  in hydrocarbons, 3059; metal  $\beta$ -ketoenolates, 4631;  $NO_3^-$  in molten alkali metal nitrate mixtures, 293; organometallics of Li, Mg, Ca, 953; phenylgermanes, 3043; 2-phenylnaphthalenes, 4468, 4474; proteins, 2934;  $SnF_2(g)$ ,  $PbF_2(g)$ , 3510  
 Uv-visible-ir spectra, quaternary ammonium rads., 1374  
 Uv-visible spectra, chlorophyll at 77°K, 3941; Cu(II) chelates w/ 8-quinolinol and arylhydroxycarboxylic acids, 3372; isomeric cyanine dyes, 2008;  $O_2^-$  on glass, 367; perfluoro-2,1,3-benzoselenadiazole anion radical, 1281; photochromic isomers, 2817; polyene-iodine complexes, 2690
- Vanadium pentoxide- $H_2O$ , thermo. data, 3293  
 Vanadium(II)-vanadium(III), radiolysis, 2330  
 Vibration analysis, harmonic-, isotopic naphthalenes, 1446  
 Vinyl ether, hydrolysis, 1313  
 Vinyl halides and vinyl ethers, nmr spectra, 4351  
 Vinylphosphonates, subst., nmr, 175  
 Violanthrone, excitation by singlet  $O_2$ , 2913  
 Viscometer, capillary, flow-time fluctuations, 448  
 Viscosity, acrylonitrile-styrene copolymers in DMF, 4104; aq. electrolyte mixtures, 2663; aq.  $Na_2SO_4$ , 2251; aq. polyacrylamide, 1265; Bi-Bi halide solns., 1737; conc. dependence beyond Einstein's region, 4682; intrinsic, monodisperse polymer, 2890; organic glasses, 752, 1913, 3349  
 Viscous solutions, paramagnetic relaxation, 736  
 Visible-ir spectra, alkali metals in hexamethylphosphoramide, 2655  
 Visible spectra, alk. mets. in fused alk. met. salts, 1111; iodine in many solvs., 3300; IRS at electrodes, 1144; Na- $NH_3$  gas, 3334; phthalocyanine, 3230  
 Voltammetric behavior, aq.  $I^-I_2-ICl-Cl^-Pt$ , 2782  
 Volume flow, oxid. collodion membranes, 1752
- Water, ads. on AgI, 643; ads. on  $ThO_2$ , 2293; condensation, 421, 433; heavy, radiolysis, 511; heavy,  $^3H$  spin-lattice relaxn. in organic solvents, 4188; Kerr consts., 3069; molal vols. in organic solvs., 4257; nucleation, 421, 433; solubility in comp.  $N_2$ , Ar,  $CH_4$ , 330; structure, 899  
 Water-*n*-alkylamine complexes, structure, 1808  
 Water and *t*-butyl alcohol, rxs. w/ Na in  $NH_3(l)$ , 4520  
 Water clathrates, dielectric properties, 49  
 Water-ethanol and  $D_2O-C_2H_5OD$ , vapor press., 2645  
 Water-ice, isotope fractionation, 3683  
 Water-in-oil emulsions, dielectric properties, 33  
 Water-salts, max. dens. temp., 3032  
 Waters and ices, isotopic, vapor press., 1234  
 Water solutions, structure-making and -breaking solutes, 3021  
 Water transport, cation-exchange membranes, 3698, 3699  
 Water-triethylamine system, thermo. data, 4194  
 Wettability, gold, 2412  
 Wustite, coulometric titration, 485
- Xanthyl radicals, esr study, 3635, 3641, 3647  
 Xenon, red. eq. of state, 1230; vapor, continuum emission, 3129  
 Xenon di- and tetrafluoride, thermo. data, 1162  
 X-Ray study, liq. formamide, liq. formamide-KI, 1088  
*p*-Xylene and tetra-*n*-pentylammonium thiocyanate solns., vapor press., 3584
- Ytterbium dicarbide, thermo. data, 1697
- Zeolite nickel faujasite, crystal structure, 4366  
 Zeolites, divalent cation faujasite-type, residual  $H_2O$ , 1400; group Ia X and Y, Brønsted acidity, 3066;  $H_2O$  addn., 2689; hydrogen Y, rx. w/  $NH_3$ , 3071; Linde X, Sr-Na ion exchange, 4095; Linde X and Y, alk. earth ion exch., 4086; sodium A, in molten salts, 4704; X and B, form, 1385; X and Y decationated, OH group stability, 1768; Y, surface group ir study, 4211  
 Zinc halides, vaporization, 3361  
 Zinc phthalocyanine, polymorphic transformm., 2446  
 Zinc tetraphenylporphyrin-benzoquinone system,  $H^+$  ejection and electron trans., 1797  
 Zirconium(IV) oxide membranes, hydrous, salt-rejection props., 2200